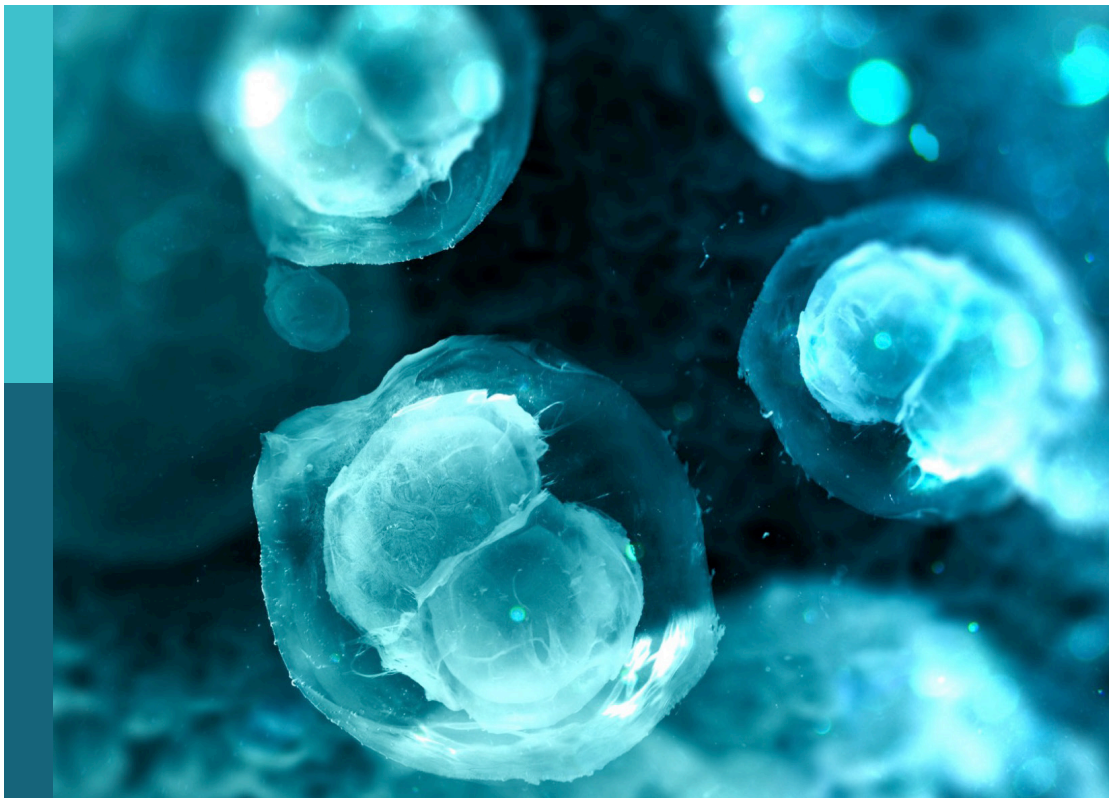
frontiers | Research Topics

Novel insights in RNA modifications: From basic to translational research

Edited by
Huilin Huang, Jianjun Chen, Chengqi Yi, Pengxu Qian and Hengyou Weng

Published in
Frontiers in Cell and Developmental Biology
Frontiers in Genetics



FRONTIERS EBOOK COPYRIGHT STATEMENT

The copyright in the text of individual articles in this ebook is the property of their respective authors or their respective institutions or funders. The copyright in graphics and images within each article may be subject to copyright of other parties. In both cases this is subject to a license granted to Frontiers.

The compilation of articles constituting this ebook is the property of Frontiers.

Each article within this ebook, and the ebook itself, are published under the most recent version of the Creative Commons CC-BY licence. The version current at the date of publication of this ebook is CC-BY 4.0. If the CC-BY licence is updated, the licence granted by Frontiers is automatically updated to the new version.

When exercising any right under the CC-BY licence, Frontiers must be attributed as the original publisher of the article or ebook, as applicable.

Authors have the responsibility of ensuring that any graphics or other materials which are the property of others may be included in the CC-BY licence, but this should be checked before relying on the CC-BY licence to reproduce those materials. Any copyright notices relating to those materials must be complied with.

Copyright and source acknowledgement notices may not be removed and must be displayed in any copy, derivative work or partial copy which includes the elements in question.

All copyright, and all rights therein, are protected by national and international copyright laws. The above represents a summary only. For further information please read Frontiers' Conditions for Website Use and Copyright Statement, and the applicable CC-BY licence.

ISSN 1664-8714
ISBN 978-2-83251-853-3
DOI 10.3389/978-2-83251-853-3

About Frontiers

Frontiers is more than just an open access publisher of scholarly articles: it is a pioneering approach to the world of academia, radically improving the way scholarly research is managed. The grand vision of Frontiers is a world where all people have an equal opportunity to seek, share and generate knowledge. Frontiers provides immediate and permanent online open access to all its publications, but this alone is not enough to realize our grand goals.

Frontiers journal series

The Frontiers journal series is a multi-tier and interdisciplinary set of open-access, online journals, promising a paradigm shift from the current review, selection and dissemination processes in academic publishing. All Frontiers journals are driven by researchers for researchers; therefore, they constitute a service to the scholarly community. At the same time, the *Frontiers journal series* operates on a revolutionary invention, the tiered publishing system, initially addressing specific communities of scholars, and gradually climbing up to broader public understanding, thus serving the interests of the lay society, too.

Dedication to quality

Each Frontiers article is a landmark of the highest quality, thanks to genuinely collaborative interactions between authors and review editors, who include some of the world's best academicians. Research must be certified by peers before entering a stream of knowledge that may eventually reach the public - and shape society; therefore, Frontiers only applies the most rigorous and unbiased reviews. Frontiers revolutionizes research publishing by freely delivering the most outstanding research, evaluated with no bias from both the academic and social point of view. By applying the most advanced information technologies, Frontiers is catapulting scholarly publishing into a new generation.

What are Frontiers Research Topics?

Frontiers Research Topics are very popular trademarks of the *Frontiers journals series*: they are collections of at least ten articles, all centered on a particular subject. With their unique mix of varied contributions from Original Research to Review Articles, Frontiers Research Topics unify the most influential researchers, the latest key findings and historical advances in a hot research area.

Find out more on how to host your own Frontiers Research Topic or contribute to one as an author by contacting the Frontiers editorial office: frontiersin.org/about/contact

Novel insights in RNA modifications: From basic to translational research

Topic editors

Huilin Huang — Sun Yat-sen University Cancer Center (SYSUCC), China
Jianjun Chen — City of Hope National Medical Center, United States
Chengqi Yi — Peking University, China
Pengxu Qian — Zhejiang University, China
Hengyou Weng — Guangzhou Regenerative Medicine and Health Guangdong Laboratory, China

Citation

Huang, H., Chen, J., Yi, C., Qian, P., Weng, H., eds. (2023). *Novel insights in RNA modifications: From basic to translational research*. Lausanne: Frontiers Media SA. doi: 10.3389/978-2-83251-853-3

Table of contents

05 Editorial: Novel insights in RNA modifications: From basic to translational research
Huilin Huang, Chengqi Yi, Pengxu Qian, Hengyou Weng and Jianjun Chen

08 Integrative Analysis of m^{6}A Regulator-Mediated RNA Methylation Modification Patterns and Immune Characteristics in Lupus Nephritis
Huanhuan Zhao, Shaokang Pan, Jiayu Duan, Fengxun Liu, Guangpu Li, Dongwei Liu and Zhangsuo Liu

24 Characterization of Long Non-coding RNAs Modified by m^{6}A RNA Methylation in Skeletal Myogenesis
Shu-Juan Xie, Shuang Tao, Li-Ting Diao, Pan-Long Li, Wei-Cai Chen, Zhi-Gang Zhou, Yan-Xia Hu, Ya-Rui Hou, Hang Lei, Wan-Yi Xu, Wen-Jie Chen, Yan-Wen Peng, Qi Zhang and Zhen-Dong Xiao

42 RNA m^{6}A Demethylase ALKBH5 Protects Against Pancreatic Ductal Adenocarcinoma *via* Targeting Regulators of Iron Metabolism
Rui Huang, Lin Yang, Zhiwen Zhang, Xiaoding Liu, Yi Fei, Wei-Min Tong, Yamei Niu and Zhiyong Liang

58 The Critical Contribution of Pseudouridine to mRNA COVID-19 Vaccines
Pedro Morais, Hironori Adachi and Yi-Tao Yu

67 Comprehensive Analysis of the Transcriptome-Wide m6A Methylation Modification Difference in Liver Fibrosis Mice by High-Throughput m6A Sequencing
Chang Fan, Yanzhen Ma, Sen Chen, Qiumei Zhou, Hui Jiang, Jiafu Zhang and Furong Wu

83 LuHui Derivative, A Novel Compound That Inhibits the Fat Mass and Obesity-Associated (FTO), Alleviates the Inflammatory Response and Injury in Hyperlipidemia-Induced Cardiomyopathy
Ying Yu, Yumiao Pan, Ziyi Fan, Silun Xu, Zhiyuan Gao, Zijing Ren, Jie Yu, Wen Li, Fangtong Liu, Jintao Gu, Ye Yuan and Zhimin Du

98 Integrating m6A Regulators-Mediated Methylation Modification Models and Tumor Immune Microenvironment Characterization in Caucasian and Chinese Low-Grade Gliomas
Wangrui Liu, Chuanyu Li, Yuhao Wu, Wenhao Xu, Shuxian Chen, Hailiang Zhang, Haineng Huang, Shuai Zhao and Jian Wang

114 The Relationship Between the Network of Non-coding RNAs-Molecular Targets and N6-Methyladenosine Modification in Colorectal Cancer
Senxu Lu, Xiangyu Ding, Yuanhe Wang, Xiaoyun Hu, Tong Sun, Minjie Wei, Xiaobin Wang and Huizhe Wu

137 A Broad m6A Modification Landscape in Inflammatory Bowel Disease
Kai Nie, Jun Yi, Yuanyuan Yang, Minzi Deng, Yan Yang, Tianyu Wang, Xuejie Chen, Zhaoyu Zhang and Xiaoyan Wang

152 The Basis and Promise of Programmable RNA Editing and Modification
Nicholas Lo, Xin Xu, Fraser Soares and Housheng Hansen He

162 Diagnostic, Therapeutic, and Prognostic Value of the m^{6}A Writer Complex in Hepatocellular Carcinoma
Zongting Gu, Yongxing Du, Xueping Zhao and Chengfeng Wang

180 Roles of RNA Modifications in Diverse Cellular Functions
Emma Wilkinson, Yan-Hong Cui and Yu-Ying He

206 Improved Methods for Deamination-Based m^{6}A Detection
Huanyu Zhu, Xinhe Yin, Christopher L. Holley and Kate D. Meyer

219 tRNA Function and Dysregulation in Cancer
Tania Gupta, Mark G. Malkin and Suyun Huang

229 The Key Role of RNA Modification in Breast Cancer
Yang Liu, Tong Zhu, Yi Jiang, Jiawen Bu, Xudong Zhu and Xi Gu

242 The Maternal Microbiome Programs the m^{6}A Epitranscriptome of the Mouse Fetal Brain and Intestine
Zhuoyu Xiao, Sun Liu, Zengguang Li, Jinru Cui, Hailan Wang, Zihan Wang, Qihuan Ren, Laixin Xia, Zhijian Wang and Yuan Li

256 The Pivotal Role of Chemical Modifications in mRNA Therapeutics
Albert Liu and Xiao Wang

267 tRNA abundance, modification and fragmentation in nasopharyngeal swabs as biomarkers for COVID-19 severity
Christopher D. Katanski, Hala Alshammary, Christopher P. Watkins, Sihao Huang, Ana Gonzales-Reiche, Emilia Mia Sordillo, Harm van Bakel, Mount Sinai PSP study group, Karen Lolans, Viviana Simon and Tao Pan

frontiers | Frontiers in Cell and Developmental Biology

TYPE Editorial
PUBLISHED 22 February 2023
DOI 10.3389/fcell.2023.1155993

Check for updates

OPEN ACCESS

EDITED AND REVIEWED BY
Michael E. Symonds,
University of Nottingham,
United Kingdom

*CORRESPONDENCE
Huilin Huang,
huanghl1@sysucc.org.cn
Chengqi Yi,
chengqi.yi@pku.edu.cn
Pengxu Qian,
axu@zju.edu.cn
Hengyou Weng,
weng_hengyou@gzlab.ac.cn
Jianjun Chen,
jianchen@coh.org

SPECIALTY SECTION
This article was submitted to Epigenomics and Epigenetics, a section of the journal Frontiers in Cell and Developmental Biology

RECEIVED 01 February 2023
ACCEPTED 14 February 2023
PUBLISHED 22 February 2023

CITATION
Huang H, Yi C, Qian P, Weng H and Chen J (2023), Editorial: Novel insights in RNA modifications: From basic to translational research.
Front. Cell Dev. Biol. 11:1155993.
doi: 10.3389/fcell.2023.1155993

COPYRIGHT
© 2023 Huang, Yi, Qian, Weng and Chen. This is an open-access article distributed under the terms of the Creative Commons Attribution License (CC BY). The use, distribution or reproduction in other forums is permitted, provided the original author(s) and the copyright owner(s) are credited and that the original publication in this journal is cited, in accordance with accepted academic practice. No use, distribution or reproduction is permitted which does not comply with these terms.

Editorial: Novel insights in RNA modifications: From basic to translational research

Huilin Huang[1]*, Chengqi Yi[2,3,4]*, Pengxu Qian[5,6]*, Hengyou Weng[7,8]* and Jianjun Chen[9,10]*

[1]State Key Laboratory of Oncology in South China, Collaborative Innovation Center for Cancer Medicine, Sun Yat-sen University Cancer Center, Guangzhou, China, [2]State Key Laboratory of Protein and Plant Gene Research, School of Life Sciences, Peking University, Beijing, China, [3]Peking-Tsinghua Center for Life Sciences, Peking University, Beijing, China, [4]Department of Chemical Biology, Synthetic and Functional Biomolecules Center, College of Chemistry and Molecular Engineering, Peking University, Beijing, China, [5]Center of Stem Cell and Regenerative Medicine, and Bone Marrow Transplantation Center of the First Affiliated Hospital, Zhejiang University School of Medicine, Hangzhou, China, [6]Liangzhu Laboratory, Zhejiang Engineering Laboratory for Stem Cell and Immunotherapy, Zhejiang University Medical Center, Institute of Hematology, Zhejiang University, Hangzhou, China, [7]Guangzhou Laboratory, Guangzhou, China, [8]State Key Laboratory of Respiratory Diseases, The First Affiliated Hospital, Guangzhou Medical University, Guangzhou, China, [9]Department of Systems Biology, Beckman Research Institute of City of Hope, Monrovia, CA, United States, [10]Gehr Family Center for Leukemia Research, City of Hope Comprehensive Cancer Center, Duarte, CA, United States

KEYWORDS

M^{6}A, epitranscriptome, RNA editing, development, cancer, biomarker, RNA vaccine

Editorial on the Research Topic
Novel insights in RNA modifications: From basic to translational research

Introduction

Chemical modifications add to the diversity of biological macromolecules (e.g., DNA, RNA, and protein) and expand their molecular functions, and the aberrance of such modifications are found as one of the major causes of human diseases and aging (Flavahan et al., 2017; Cavalli and Heard, 2019; Yang et al., 2023). Due to the prominent roles of RNA modifications in human diseases such as cancer and the promise of targeting dysregulated RNA modification machineries in translational medicine (Huang et al., 2020a), the study of RNA modifications (e.g., m^{6}A, m^{1}A, m^{5}C, m^{6}Am, pseudouridine, and A-to-I editing) represents the new Frontier in the epigenetics field.

In this Research Topic on *Novel Insights in RNA Modifications: from Basic to Translational Research*, we aim to publish innovative research from basic science to translational research on RNA modifications. A total of 18 articles were included in this Research Topic, covering the novel methods to detect or modulate RNA modifications, the functions and mechanisms of RNA modifications in physiological processes (e.g., normal cellular functions, skeletal myogenesis and fetal development) and during pathogenesis (e.g., cancer, cadiomyopathy, lupus nephritis, inflammatory bowel disease and liver fibrosis), and the application of RNA modification in disease diagnostics and therapeutics. We summarize and discuss the main findings of these studies in this editorial.

Methodologies for measuring or modulating RNA modifications

The development of reliable m^{6}A profiling methods, such as m^{6}A-seq or MeRIP-seq, a method that uses antibodies to immunoprecipitate methylated RNAs for subsequent sequencing, greatly promotes our understanding of m^{6}A. Recently developed antibody-free techniques, such as DART-seq (Meyer, 2019), m^{6}A-SAC-seq (Hu et al., 2022) and GLORI (Liu et al., 2022), exhibit advantages over antibody-based methods, including requirement of less input RNA and eliminated/reduced cross-reactivity to other modifications, such as DNA 6 mA and RNA m^{6}Am. In this Research Topic, Zhu et al. developed an improved version of *in vitro* DART-seq, which optimizes the APO1-YTH protein to achieve enhanced m^{6}A recognition and allow for m^{6}A mapping in any sample of interest using nanogram amounts of total RNA.

Programmable RNA modification is another powerful method for RNA modification study. Hundreds of m^{6}A sites are often reprogrammed during physiological and pathological processes, making it difficult to dissect the phenotypic outcomes from a single m^{6}A site. The advent of new CRISPR tools allow scientists to install or remove m^{6}A modification at specific loci, showing promise in revealing the physiological or pathological effects of individual m^{6}A mark, especially *in vivo*. In the review article, Lo et al. summarized recent findings on RNA editing and programmable RNA modification with CRISPR, base editors and non-CRISPR related tools, highlighting their future applications for basic and clinical research.

The functions and mechanisms of RNA methylations in physiological processes

Utilizing the m^{6}A sequencing techniques, the profiling of m^{6}A (also known as "epitranscriptome") under various physiological context can be readily characterized, offering an opportunity for revealing the roles of m^{6}A during these processes. Xie et al. characterized the expression and m^{6}A methylation patterns of lncRNAs in mouse myoblasts and differentiated myotubes, uncovering a METTL3/m^{6}A/Brip1os/Tbx2 Axis and the potential role of m^{6}A on the temporal expression regulation of lncRNAs in skeletal myogenesis. Xiao et al. reported that maternal microbiome affects the m^{6}A epitranscriptome of the mouse feral bran and intestine, probably by altering the expression of m^{6}A writers and erasers, implying m^{6}A might serve as a critical regulator for mediating the impact of microbiome to development and disease.

Besides development, RNA modifications have been reported to exert critical roles in a variety of physiological processes. With this regard, Wilkinson et al. summarized the functions and regulation of RNA modifications (e.g., m^{6}A, m^{5}C and m^{1}A) in cellular processes, emphasizing the context-specific roles of RNA modifications during pathogenesis and the recent advances in disease prevention and therapy by targeting RNA modification.

The functions and mechanisms of RNA modifications during pathogenesis

The aberrant regulation and function of RNA modifications is pervasively found in human diseases, particularly in cancer. Huang et al. found m^{6}A demethylase ALKBH5 serves as independent favorable prognostic marker and plays tumor suppressive function by modulating iron metabolism and epithelial-mesenchymal transition (EMT) in pancreatic ductal adenocarcinoma. Moreover, there are three Review articles in this Research Topic focusing on the roles of RNA modifications in cancer. Lu et al. summarized the interaction network of non-coding RNAs (ncRNAs) and their relationship with m^{6}A modification in colorectal cancer (CRC). Gupta et al. focused on the functions of tRNAs, tRNA-derived stress-induced RNAs (tiRNAs) and tRNA-derived fragments (tRFs), as well as their modifications, during tumor development and progression. Liu et al. reviewed recent findings of several common RNA modifications on mRNAs, rRNAs and tRNAs and their regulators in breast cancer.

Besides, RNA modifications emerge as key players in other chronic disease and injury. Yu et al. reported FTO, another m^{6}A demethylase, played a role in hyperlipidemia-induced cardiomyopathy. A novel compound, known as LuHui Derivative, could inhibit FTO and alleviate the inflammatory response and injury in hyperlipidemia-induced cardiomyopathy. Fan et al. revealed the involvement of m^{6}A methylation and its regulator in the development of liver fibrosis, a chronic liver injury that may lead to cirrhosis and even liver cancer, through performing m^{6}A-seq and RNA-seq in liver fibrosis mice. Zhao et al. analyzed the expression of m^{6}A regulators in the glomeruli in lupus nephritis compared with tubulointerstitium and whole kidney tissue, and established an m^{6}A regulator signature that can distinguish lupus nephritis and healthy individuals. Nie et al. found m^{6}A regulators displayed extensive differential expression in the cohorts of inflammatory bowel disease, in which two clusters of consensus clustering exhibit different immune phenotypes and clinical characteristics. These research provide insights that m^{6}A methylation may be associated with the occurrence of these diseases; however, further studies are needed to determine its role.

The application of RNA modifications in translational medicine

It has been anticipated that RNA modifications, similar to DNA methylation, could serve as biomarkers for clinical diagnostics. The integrative analyses by Xu et al. and Gu et al. suggested that m^{6}A regulators may represent promising biomarkers for prediction of prognosis and clinical responses to targeted or immune therapy of low-grade glioma and HCC patients. Katanski et al. performed multiplex small RNA sequencing (MSR-seq) on residual nasopharyngeal swabs to test the idea of utilizing host tRNA properties as biomarkers for the clinical outcome of SARS-CoV-2. They reported that combining tRNA modifications with full-length tRNA abundance and tRNA fragmentation could provide

strong power for the accurate prediction of SARS-CoV-2 infection symposium severity, shedding light on the application of tRNA modification and also potentially other RNA modifications as diagnostic biomarkers.

In clinical practice, RNA modification has become a powerful tool in making mRNA vaccines. Morais et al. reviewed the effect and mechanism of N1-methyl-pseudouridine in the successful invention of mRNA vaccines against SARS-CoV-2. From a broader view, Liu et al. summarized the roles of cap and tail modifications, nucleoside substitutes, and chimeric mRNAs on tuning the properties of mRNAs and discussed the potential of harnessing the efficacy of mRNA drugs through such mRNA modifications.

Conclusion

The studies published in this Research Topic provide a window into the basic and translational research of RNA modifications. We hope the studies and insight provided by the research and review articles in this Research Topic could inspire researchers and bring critical thinking on the field of epitranscriptomics.

Author contributions

All authors listed have made a substantial, direct, and intellectual contribution to the work and approved it for publication.

Funding

This work was supported by the National Key Research and Development Program of China (2020YFA0112403 to HW, 2019YFA0110900 and 2019YFA0802200 to CY, 2022YFA1103500 and 2018YFA0109300 to PQ), the National Natural Science Foundation of China (82173058 to HH, 82270168 to HW, 21825701 and 92153303 to CY, 82222003, 92268117 and 82161138028 to PQ), the U.S. National Institutes of Health (NIH) grants (R01 CA243386 and R01 CA271497 to JC), Guangdong Basic and Applied Basic Research Foundation (2021A1515010425 to HH), the Zhejiang Provincial Natural Science Foundation of China (LR19H080001 to PQ), the Leading Innovative and Entrepreneur Team Introduction Program of Zhejiang (2020R01006 to PQ) and the Guangdong Research Program (2021ZT09Y233 to HW).

Acknowledgments

We would like to express our sincere thanks to the guest editorial team and all the reviewers who participated in the peer-review process of this Research Topic. At the same time, we would like to thank all the authors who contributed to this Research Topic.

Conflict of interest

The authors declare that the research was conducted in the absence of any commercial or financial relationships that could be construed as a potential conflict of interest.

Publisher's note

All claims expressed in this article are solely those of the authors and do not necessarily represent those of their affiliated organizations, or those of the publisher, the editors and the reviewers. Any product that may be evaluated in this article, or claim that may be made by its manufacturer, is not guaranteed or endorsed by the publisher.

References

Cavalli, G., and Heard, E. (2019). Advances in epigenetics link genetics to the environment and disease. *Nature* 571, 489–499. doi:10.1038/s41586-019-1411-0

Flavahan, W. A., Gaskell, E., and Bernstein, B. E. (2017). Epigenetic plasticity and the hallmarks of cancer. *Science* 357, eaal2380. doi:10.1126/science.aal2380

Hu, L., Liu, S., Peng, Y., Ge, R., Senevirathne, C., Harada, B. T., et al. (2022). m^{6}A RNA modifications are measured at single-base resolution across the mammalian transcriptome. *Nat. Biotechnol.* 40, 1210–1219. doi:10.1038/s41587-022-01243-z

Huang, H. L., Weng, H. Y., Deng, X. L., and Chen, J. J. (2020). RNA modifications in cancer: Functions, mechanisms, and therapeutic implications. *Annu. Rev. Canc Biol.* 4, 221–240. doi:10.1146/annurev-cancerbio-030419-033357

Huang, H., Weng, H., and Chen, J. (2020). m^{6}A modification in coding and non-coding RNAs: Roles and therapeutic implications in cancer. *Cancer Cell.* 37, 270–288. doi:10.1016/j.ccell.2020.02.004

Liu, C., Sun, H., Yi, Y., Shen, W., Li, K., Xiao, Y., et al. (2022). Absolute quantification of single-base m6A methylation in the mammalian transcriptome using GLORI. *Nat. Biotechnol.* doi:10.1038/s41587-022-01487-9

Meyer, K. D. (2019). DART-Seq: An antibody-free method for global m^{6}A detection. *Nat. Methods* 16, 1275–1280. doi:10.1038/s41592-019-0570-0

Yang, J. H., Hayano, M., Griffin, P. T., Amorim, J. A., Bonkowski, M. S., Apostolides, J. K., et al. (2023). Loss of epigenetic information as a cause of mammalian aging. *Cell.* 186, 305–326.e27. doi:10.1016/j.cell.2022.12.027

frontiers in Cell and Developmental Biology

ORIGINAL RESEARCH
published: 07 September 2021
doi: 10.3389/fcell.2021.724837

Integrative Analysis of m^{6}A Regulator-Mediated RNA Methylation Modification Patterns and Immune Characteristics in Lupus Nephritis

Huanhuan Zhao[1,2,3,4,5], Shaokang Pan[1,2,3,4,5], Jiayu Duan[1,2,3,4,5], Fengxun Liu[1,2,3,4,5], Guangpu Li[1,2,3,4,5], Dongwei Liu[1,2,3,4,5] and Zhangsuo Liu[1,2,3,4,5]**

[1] Department of Nephrology, The First Affiliated Hospital of Zhengzhou University, Zhengzhou, China, [2] Research Institute of Nephrology, Zhengzhou University, Zhengzhou, China, [3] Research Center for Kidney Disease, Zhengzhou, China, [4] Key Laboratory of Precision Diagnosis and Treatment for Chronic Kidney Disease in Henan Province, Zhengzhou, China, [5] Core Unit of National Clinical Medical Research Center of Kidney Disease, Zhengzhou, China

OPEN ACCESS

Edited by:
Jianjun Chen,
City of Hope National Medical Center,
United States

Reviewed by:
Jianhuang Xue,
City of Hope National Medical Center,
United States
Yu-Ying He,
University of Chicago, United States

***Correspondence:**
Zhangsuo Liu
zhangsuoliu@zzu.edu.cn
Dongwei Liu
liu-dongwei@zzu.edu.cn

Specialty section:
This article was submitted to Epigenomics and Epigenetics, a section of the journal Frontiers in Cell and Developmental Biology

Received: 14 June 2021
Accepted: 05 August 2021
Published: 07 September 2021

Citation:
Zhao H, Pan S, Duan J, Liu F, Li G, Liu D and Liu Z (2021) Integrative Analysis of m^{6}A Regulator-Mediated RNA Methylation Modification Patterns and Immune Characteristics in Lupus Nephritis. Front. Cell Dev. Biol. 9:724837. doi: 10.3389/fcell.2021.724837

Background: There is growing evidence to demonstrate that the epigenetic regulation of immune characteristics, especially for N6-methyladenosine (m^{6}A) RNA methylation. However, how m^{6}A methylation is involved in lupus nephritis (LN) is still unclear. This study aimed to determine the role of m^{6}A RNA methylation and their association with the immune microenvironment in LN.

Methods: In total, 87 glomeruli (73 LN, 14 living healthy donors), 110 tubulointerstitium (95 LN, 15 living healthy donors), and 21 kidney whole tissue samples (14 LN, 7 controls) were included in our research to evaluate the expression levels of m^{6}A regulators. CIBERSORT was used to assess the abundance of infiltrating immunocytes. The m^{6}A regulator gene signature for LN was identified using LASSO-logistic regression and verified with external data. Consensus clustering algorithms were used for the unsupervised cluster analysis of m^{6}A modification patterns in LN. Single-sample gene-set enrichment analysis and gene set variation analysis algorithms were employed to assess the activity of immune responses and other functional pathways. Weighted gene co-expression network analysis and protein-protein interaction networks were used to identify m^{6}A methylation markers. Lastly, the Nephroseq V5 tool was used to analyze the correlation between m^{6}A markers and renal function.

Results: We found that the expression of m^{6}A regulators was more significantly different in the glomeruli in LN compared with tubulointerstitium and whole kidney tissue. We established an m^{6}A regulator signature, comprised of *METTL3*, *WTAP*, *YTHDC2*, *YTHDF1*, *FMR1*, and *FTO*, that can easily distinguish LN and healthy individuals. Two distinct m^{6}A modification patterns based on 18 m^{6}A regulators were determined, with significant differences in m^{6}A regulator expression, immune microenvironment, biological functional pathways, and clinical characteristics. Activated NK cells, most immune responses, and HLA genes had strong correlations with m^{6}A regulators. Seven

m^{6}A markers were identified and demonstrated a meaningful correlation with GFR, indicating that they are potential prognostic biomarkers.

Conclusion: This study emphasized that m^{6}A RNA methylation and the immune microenvironment are closely linked in LN. A better understanding of m^{6}A modification patterns provide a basis for the development of novel therapeutic options for LN.

Keywords: lupus nephritis, epigenetics, m^{6}A RNA methylation, immune characteristics, bioinformatic analysis

INTRODUCTION

Lupus nephritis (LN) is the most common and most serious manifestation of systemic lupus erythematosus (SLE). It is also a major cause of morbidity and mortality in patients with SLE (Anders et al., 2020). Current treatments for LN are often ineffective and have strong adverse effects. In the last 50 years, only one drug has been developed for the treatment of SLE and LN, and other well-designed clinical trials have been unsuccessful (Thanou and Merrill, 2014; Narain and Furie, 2016). It is widely accepted that LN is caused by autoimmune and inflammatory responses owing to the loss of tolerance to endogenous nuclear material, which activates complement, pro-inflammatory pathways, and resident renal cells (Anders et al., 2020). Previously, the immune response to LN was mainly determined from the analysis of blood samples, which does not effectively reflect the immune state of the kidneys. Therefore, further investigation on the immune characteristics, including immune cell infiltration in LN kidney tissue, may be key in revealing its pathological mechanism and providing insight for the development of new immunotherapies for LN.

Genetic susceptibility can partially explain immune dysregulation in LN. Single-egg twins with the same gene only show a disease consistency of around 20–40%, suggesting that in addition to genetic susceptibility, epigenetics influenced by environmental factors also play an important role in SLE (Javierre et al., 2010) RNA methylation has been widely studied in epigenetic research. N6-methyladenosine (m^{6}A) methylation is the most common RNA post-transcriptional modification that regulates gene expression outside of DNA sequences in eukaryotes and plays a key role in diseases progression (Meyer and Jaffrey, 2014; Huang et al., 2018). It is a reversible process mediated by an expanding list of m^{6}A binding proteins ("readers"), adenosine methyltransferases ("writers"), and potential m^{6}A demethylating enzymes ("erasers") (Zaccara et al., 2019).

Current studies have demonstrated that m^{6}A methylation is involved in immune regulation. For example, Han et al. (2019) discovered that the m^{6}A binding protein YTHDF1 prolongs neoantigen-specific immunity through m^{6}A methylation modification of mRNA. YTHDF1 is also involved in antigen cross-presentation and cross-priming of CD8$^+$ T cells. Li et al. (2017) demonstrated that the m^{6}A "writer" protein METTL3 regulates the homeostasis and differentiation of mouse T cells. However, no study has attempted to explore how m^{6}A modification plays a role in LN, and the association between m^{6}A modification and immune characteristics remains to be elucidated. The aim of this study was to clarify the role of m^{6}A RNA methylation modification in LN and explore how m^{6}A affects the immune status of LN.

MATERIALS AND METHODS

Collection and Preprocessing of Data

The research strategy is presented in **Figure 1**. We collected gene expression data of patients with LN and healthy living donors from the Gene Expression Omnibus (GEO) database.[1] Four datasets (GSE32591 (Berthier et al., 2012), GSE69438 (Ju et al., 2015), GSE127797 (Almaani et al., 2019), and GSE112943) were selected in our study. GSE32591 contained 93 samples, which included 47 tubulointerstitium samples (32 LN samples, 15 living healthy donor samples), whereas 46 glomeruli samples (32 LN samples, 14 living healthy donor samples) were obtained from GPL14663 (Affymetrix Genechip HG-U133A). The platform for GSE69438 was GPL11670 (Affymetrix Human Genome U133 Plus 2.0 Array). It contained 42 tubulointerstitium samples, including 16 LN samples. The platform for GSE127797 was GPL24299 (Affymetrix Human Transcriptome Array 2.0), which contained 47 LN tubulointerstitium samples and 41 LN glomeruli samples. GSE127797 was the only dataset that included the pathological classifications of patients with LN. GSE112943 contained 21 whole kidney tissue samples, including 14 LN and 7 control, and sequencing was performed on GPL10558 (Illumina HumanHT-12 V4.0 expression beadchip). We then divided the samples into the glomeruli, tubulointerstitium, and whole kidney tissue for subsequent analysis. In total, 87 glomeruli samples (73 LN, 14 living healthy donors), 110 tubulointerstitium samples (95 LN, 15 living healthy donors), and 21 whole kidney tissues (14 LN, 7 controls) were included in our study to evaluate the expression levels of m^{6}A regulators. All probes were converted into gene symbols, and median gene expression was used to represent the average expression level when multiple probes corresponded to the same gene symbol. We normalized the expression data from different datasets using the robust multi-array average, merged them together, and used the sva library for ComBat Batch correction to remove batch effects (Leek et al., 2012).

m^{6}A RNA Methylation Regulator Detection

The m^{6}A RNA methylation regulator list we used was based on previous publications (Zhao et al., 2017; He et al., 2019; Zaccara et al., 2019). Then, the R package "limma" was applied

[1] http://www.ncbi.nlm.nih.gov/geo/

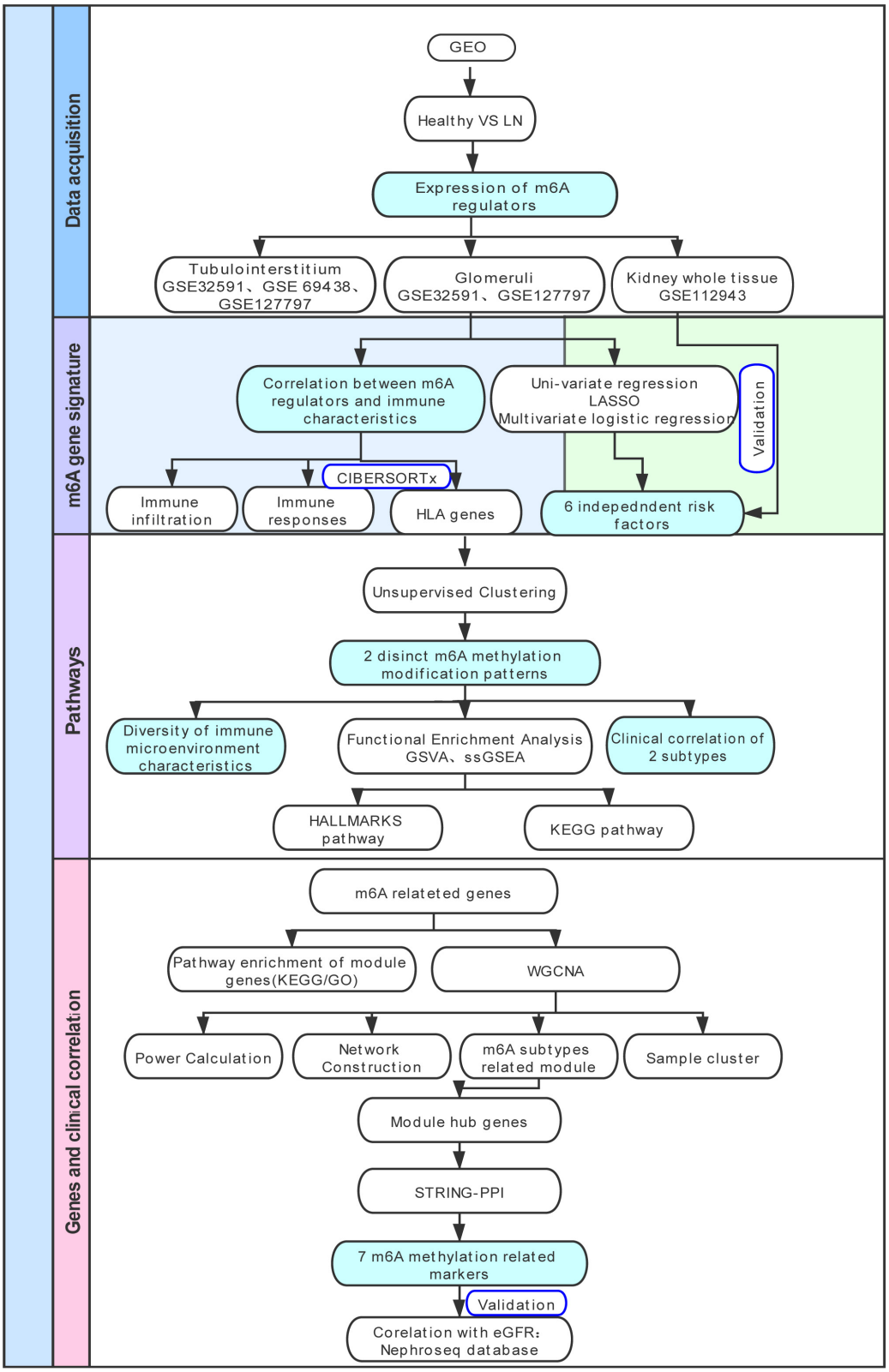


FIGURE 1 | Study flow diagram. GEO, Gene Expression Omnibus; LN, lupus nephritis; HLA, human leukocyte antigen; LASSO, least absolute shrinkage and selection operator; GSVA, gene set variation analysis; ssGSEA, single sample gene set enrichment analysis; KEGG, Kyoto Encyclopedia of Genes and Genomes; GO-BP, Gene Ontology Biological Processes; WGCNA, weighted gene co-expression network analysis; GO, Gene Ontology; PPI, protein-protein interaction.

to determine expression differences of m^{6}A regulators between LN samples and healthy samples (including the glomeruli, tubulointerstitium, and kidney tissues) (Ritchie et al., 2015).

Development and Validation of m^{6}A Regulator Gene Signature for LN

Univariate logistic regression was used to preliminarily screen variables in the identified m^{6}A regulator list, and LASSO regression was used to select the best predictive features while fitting a generalized linear model and avoiding overfitting (Friedman et al., 2010). m^{6}A regulators with non-zero LASSO regression coefficients were included in the multivariate logistic regression (MLR) analysis. The p-value in the MLR was based on the Wald test, and statistical significance was set at $p < 0.05$. Forest plots were drawn using the R package "ggplot2" to visually describe the results of the logistic regression. The receiver operating characteristic curve (ROC) and the average optimism of the area under the curve (AUC) quantified the predicted probabilities of the model. The risk score for each sample was calculated as follows:

$$Risk\ score\ =\ \sum_{i=1}^{n} Coef_i * x_i$$

where $Coef_i$ indicates the coefficients of MLR and x_i is the gene expression value of each m^{6}A regulator.

Correlation Between m^{6}A Regulators and Immune Characteristics

The CIBERSORTx with 1,000 permutations was used to evaluate the abundance of infiltrating immunocytes.[2] The inclusion criterion was as follows: CIBERSORT, $p < 0.05$. We conducted single-sample gene-set enrichment analysis (ssGSEA) to assess immune response activity. We downloaded these gene sets from the ImmPort database (Bhattacharya et al., 2014).[3] Lastly, Spearman correlation analysis was used to determine the correlation between m^{6}A regulators and immune characteristics.

Unsupervised Cluster Analysis of m^{6}A Modification Patterns in LN

Based on 18 identified m^{6}A regulators, unsupervised cluster analysis was performed to determine distinct m^{6}A subtypes using the R package "ConsensusClusterPlus," and the consensus clustering algorithm ran 1,000 times to guarantee the robustness of clustering (Wilkerson and Hayes, 2010). The Kruskal test was used to compare the differences in m^{6}A regulator expression and immune characteristics between subtypes. Principal component analysis was performed with the R package "PCA."

Pathway Enrichment Analysis of the Two m^{6}A Patterns

We downloaded the gene sets "h.all.v7.4.symbols" and "c2.cp.kegg.v7.4.symbols" from the MSigDB database. The gene set variation analysis (GSVA) algorithm was used to calculate the pathway activation score, which was conducted using the R package "GSVA" (Hänzelmann et al., 2013). The R package "limma" was used to compare the differences in pathway activation score between two subtypes, and a p-value < 0.01 was the cut-off criterion (Ritchie et al., 2015).

Identification of m^{6}A Modification Pattern Markers

m^{6}A modification subtypes-related differentially expressed genes (DEGs) between two distinct m^{6}A subtypes ($p < 0.0001$) were defined as m^{6}A related genes. m^{6}A related genes were enriched in biological processes (BP), cellular component (CC), and molecular function (MF) terms in Gene Ontology (GO) and Kyoto Encyclopedia of Genes and Genomes (KEGG) pathways and were visualized with a bubble plot. We performed enrichment analysis with the cut-off criterion of the Q-value at < 0.05, and it was conducted using the "clusterProfiler" package (Yu et al., 2012).

Weighted gene co-expression network analysis (WGCNA) was conducted to identify m^{6}A subtype-related genes and gene modules that characterize the pathways or functions of subtypes based on gene profiles using the WGCNA R package (Langfelder and Horvath, 2008). Correlations between different modules and subgroups were analyzed using Pearson's correlation.

We used the STRING database[4] to construct a protein-protein interaction (PPI) network for genes from the key module of the WGCNA. Visualization was performed using Cytoscape (Szklarczyk et al., 2019).[5]

Clinical Correlation With m^{6}A Pattern Markers

The Nephroseq V5 tool[6] was used to determine the correlation between m^{6}A markers and renal function. We downloaded the expression data of markers and used "ggplot2" to replot the scatter plots.

RESULTS

Landscape of m^{6}A RNA Methylation Regulators in LN

Currently, there are 23 m^{6}A RNA methylation regulators that have been widely studied, including 8 writers, 13 readers, and 2 erasers. **Figure 2A** shows the m^{6}A regulators with functions and crosstalk between regulators and the immune microenvironment. The regulatory interactions of these 23 m^{6}A regulators are shown in **Figure 2B**. First, the m^{6}A regulator gene expression values of glomeruli (GSE32591 and GSE127797), tubulointerstitium (GSE32591, GSE69438, and GSE127797), and whole kidney tissues (GSE112943) of LN and healthy samples were evaluated. The expression of m^{6}A regulators was the most considerably different in the glomeruli between LN and healthy

[2]https://cibersort.stanford.edu/
[3]https://string-db.org/
[4]https://cytoscape.org/
[5]http://v5.nephroseq.org/

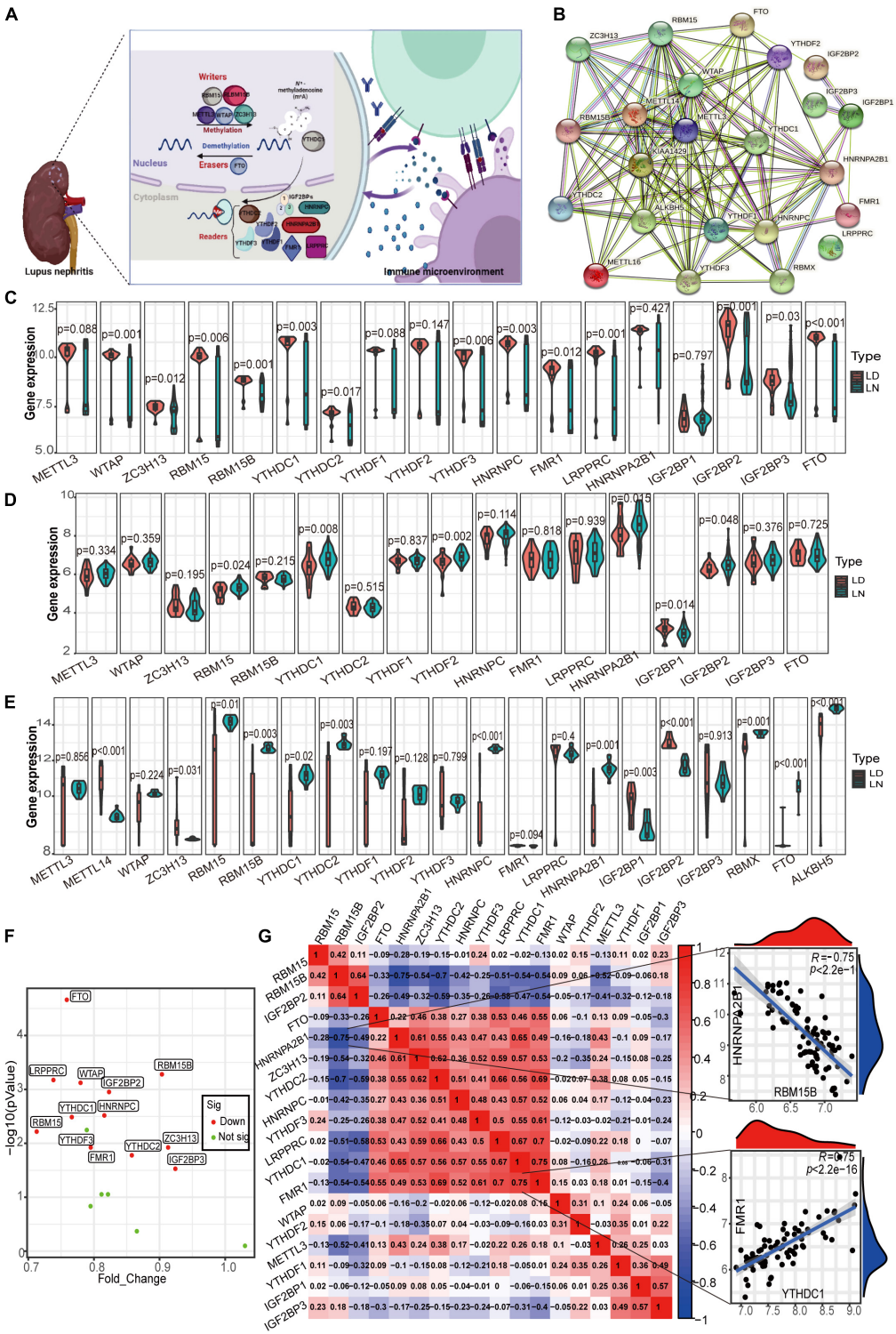


FIGURE 2 | Landscape of m^{6}A RNA methylation regulators in LN. **(A)** m^{6}A RNA methylation modification regulated by m^{6}A "writer," "reader," and "eraser," which is involved in the immune microenvironment of LN. **(B)** Protein-protein interaction (PPI) network composed of 23 m^{6}A regulators. **(C)** Violin plot demonstrating the expression level of 18 m^{6}A regulators in glomeruli between living donor and LN. **(D)** Violin plot demonstrating the expression level of 17 m^{6}A regulators in tubulointerstitium between living donor and LN. **(E)** Violin plot demonstrating the expression level of 21 m^{6}A regulators in kidney whole tissue between living donor and of LN. **(F)** Volcano plot showing a summary of the expression differences of 18 m^{6}A regulators between the healthy and LN patients' glomerular samples. **(G)** Correlations between 18 m^{6}A regulators in LN glomeruli samples. The two respective scatterplots show the two pairs of m^{6}A regulators with the highest correlation, HNRNPA2B1 and RBM15B with the most negative correlation, and YTHDC1 and FMR1 with the most positive correlation.

samples. In total, 18 m^{6}A RNA methylation regulators were identified in the glomeruli (**Figure 2C**). Significant expression differences in the 13 regulators ($p < 0.05$) were observed between LN and healthy samples, including WTAP, RBM15B, LRPPRC, and FTO ($p < 0.001$). Differences in the expression of m^{6}A regulators between LN and healthy samples in the tubulointerstitium were not significant. As shown in **Figure 2D**, only six expressions altered m^{6}A regulators in 17 identified m^{6}A regulators. Significant expression differences in the 13 m^{6}A regulators ($p < 0.05$) were observed among 21 m^{6}A identified regulators in whole kidney tissue (**Figure 2E**). Taken together, the most significant differences in the expression of m^{6}A regulators between LN and healthy samples were observed in the glomeruli. Thus, we selected the glomeruli samples for further detailed analysis.

Interestingly, the expression of all 13 altered m^{6}A regulators was downregulated in LN compared with healthy samples in the glomeruli (**Figure 2F**). The decrease in fold change of *RBM15* was the largest among these genes, whereas the decrease in eraser protein FTO levels was the most statistically significant. Note that there was no significant difference in the expression of the well-studied writer METTL13 between LN and healthy samples. In the correlation analysis for 18 m^{6}A regulators, we observed that close relationships among m^{6}A regulators which means they function together (**Figure 2G**). It contributes to explore the specific mechanism of aberrant m^{6}A modification in LN. **Figure 2G** also shows the two pairs of m^{6}A regulators with the highest positive/negative correlation. The reader HNRNPA2B1 and writer RBM15B were the most negatively correlated, whereas the readers YTHDC1 in the nuclei and FMR1 in the cytoplasm were the most positively correlated.

m^{6}A Regulators Have the Potential to Distinguish Between Healthy and LN Samples

To better understand the contribution of m^{6}A regulators to the progression of LN, we established an m^{6}A regulator gene signature. First, 16 regulators were selected from 18 identified m^{6}A regulators by univariate logistic regression analysis (**Figure 3A**). LASSO regression was performed to further screen the m^{6}A candidates, in which 13 regulators with non-zero coefficients were included in the multivariate logistic regression (**Figures 3B,C**). Finally, multivariate logistic regression analysis demonstrated that *METTL3*, *WTAP*, *YTHDC2*, *YTHDF1*, *FMR1*, and *FTO* were independently associated with LN (**Figure 3D**). It should be noted that the well-studied writer protein METTL3 is an independent risk factor for LN, although its expression does not differ between LN and in healthy samples. How METTL3 plays a role in LN might be an interesting topic for further exploration. For the gene signature model, the AUC for the derivation sets was 0.949, indicating that this model performed well in classifying healthy and LN samples (**Figure 3E**). In the independent external validation set (GSE112943), the AUC was 0.962, which suggests its ability to classify the samples (**Figure 3F**). In addition, **Figure 3G** shows that there was a significant difference in m^{6}A risk scores between LN and healthy samples. The risk scores for LN were noticeably higher than those for healthy samples (**Figure 3G**). The distribution of risk scores and gene profiles based on the six selected m^{6}A regulators is shown in **Figure 3H**. We observed that the expression of WTAP, YTHDC2, and FTO decreased in the high-risk group.

m^{6}A Regulators Are Related to Immune Microenvironment in LN

To further elucidate the relationship between m^{6}A regulators and immune characteristics, we analyzed the correlations between them. Immune characteristics include immune cell infiltration, immune response activity, and Human Leukocyte Antigen (HLA) genes. The abundance of 22 infiltrating immunocytes in the glomeruli of LN was evaluated using the CIBERSORTx algorithm (**Supplementary Figure 1A**). Eosinophils were excluded from the correlation analysis because of the lack of expression in all samples. Several infiltrating immunocytes were correlated with m^{6}A regulators but were mostly weakly correlated (**Figure 4A**). Among all immunocytes, activated NK cells were closely correlated with m^{6}A regulators, and these were most positively correlated with HNRNPA2B1 and most negatively correlated with RBM15B. This indicates that NK-activated cell infiltration in LN is regulated by HNRNPA2B1 and RBM15B. **Supplementary Figure 1B** shows the expression differences of each immune response between LN and healthy samples. Correlation analysis demonstrated that most immune reaction pathways were closely related to m^{6}A regulators (**Figure 4B**). Cytokinesis, inflammation pathway, interferon receptor activity, interferon-mediated signaling pathway, and TGF-β pathway were correlated with most of the 18 m^{6}A regulators, indicating that immune dysregulation in LN is affected by m^{6}A RNA methylation. Both the most positive and negative correlations between regulators and immune reactions were related to the reader protein YTHDC1, indicating that YTHDC1 exerts important functions in the cytokinesis and inflammation pathways in LN. Similarly, HLA genes were closely correlated with m^{6}A regulators (**Figure 4C**). HLA-DRA was most positively correlated with HNRNPA2B1, with a correlation coefficient of 0.67. HLA-F was most negatively correlated with LRPPRC, with a correlation coefficient of –0.61. These indicate that HLA gene expression in LN was affected by m^{6}A regulators. The differences in HLA gene expression between LN and healthy samples were shown in **Supplementary Figure 1C**.

Identification of m^{6}A RNA Methylation Subtypes Based on 18 m^{6}A Regulators in LN and Clinical Correlation of 2 Subtypes

To identify m^{6}A RNA methylation modification patterns of LN, we conducted unsupervised clustering based on the expression similarity of m^{6}A regulators in LN and $k = 2$ seemed to be an adequate selection resulted in 2 distinct subtypes (**Figures 5A–C**). Two m^{6}A subtypes had significantly different populations in PCA (**Figure 5D**). To investigate the relationship between clinical characteristics and m^{6}A subtypes, we used data from GSE127797, including the pathological stages of LN, to create a correlation heatmap. There were

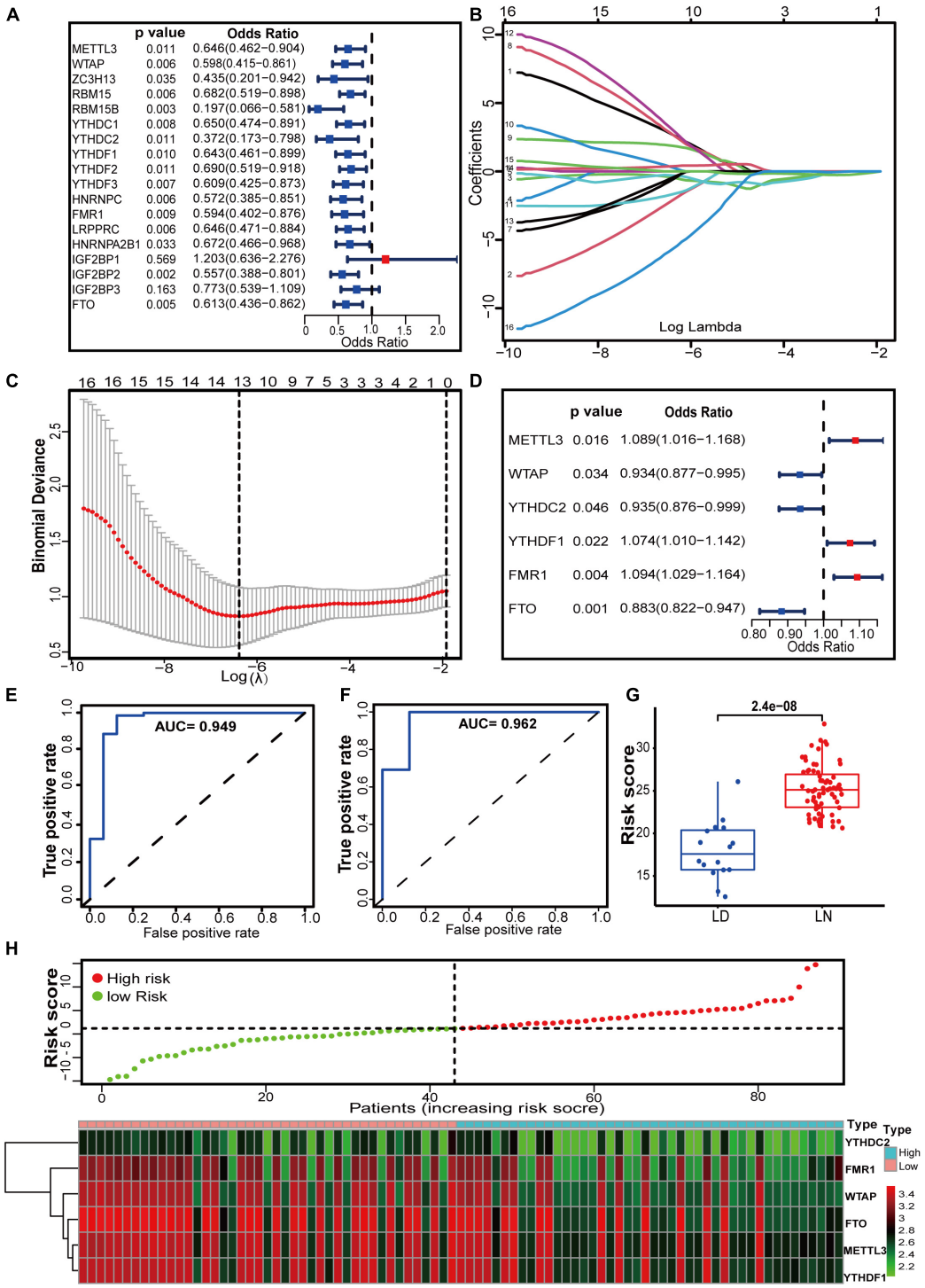


FIGURE 3 | m^{6}A regulators have the potential to distinguish between healthy and LN individuals. **(A)** Univariate logistic regression revealed 16 LN-related m^{6}A regulators ($P < 0.05$). **(B,C)** Feature selection by LASSO regression model. **(B)** By verifying the optimal parameter (lambda) in the LASSO model, the partial likelihood deviance (binomial deviance) curve was plotted vs. log (lambda). Dotted vertical lines were drawn based on 1 SE of the minimum criteria (the 1-SE criteria). **(C)** Thirteen features with non-zero coefficients were selected by optimal lambda. A coefficient profile plot was produced against the log (lambda) sequence in **(B)**. **(D)** Multivariate logistic analysis distinguished six independent risk factors and risk scores for LN were calculated using the LASSO Logistic regression algorithm. **(E,F)** The predictive value of the m^{6}A regulator gene signature in the derivation **(E)** and validation **(F)** sets by calculating the pooled AUC. $0.9 < \text{AUC} \leq 1$ indicates that the gene signature has high accuracy. **(G)** Distribution of risk scores in healthy and LN samples. **(H)** Risk score distribution based on the 6 m^{6}A RNA modification regulator signature and gene expression profiles between our study groups. Patients were divided into high-risk and low-risk groups by the black dotted line, which indicates the median cut-off value.

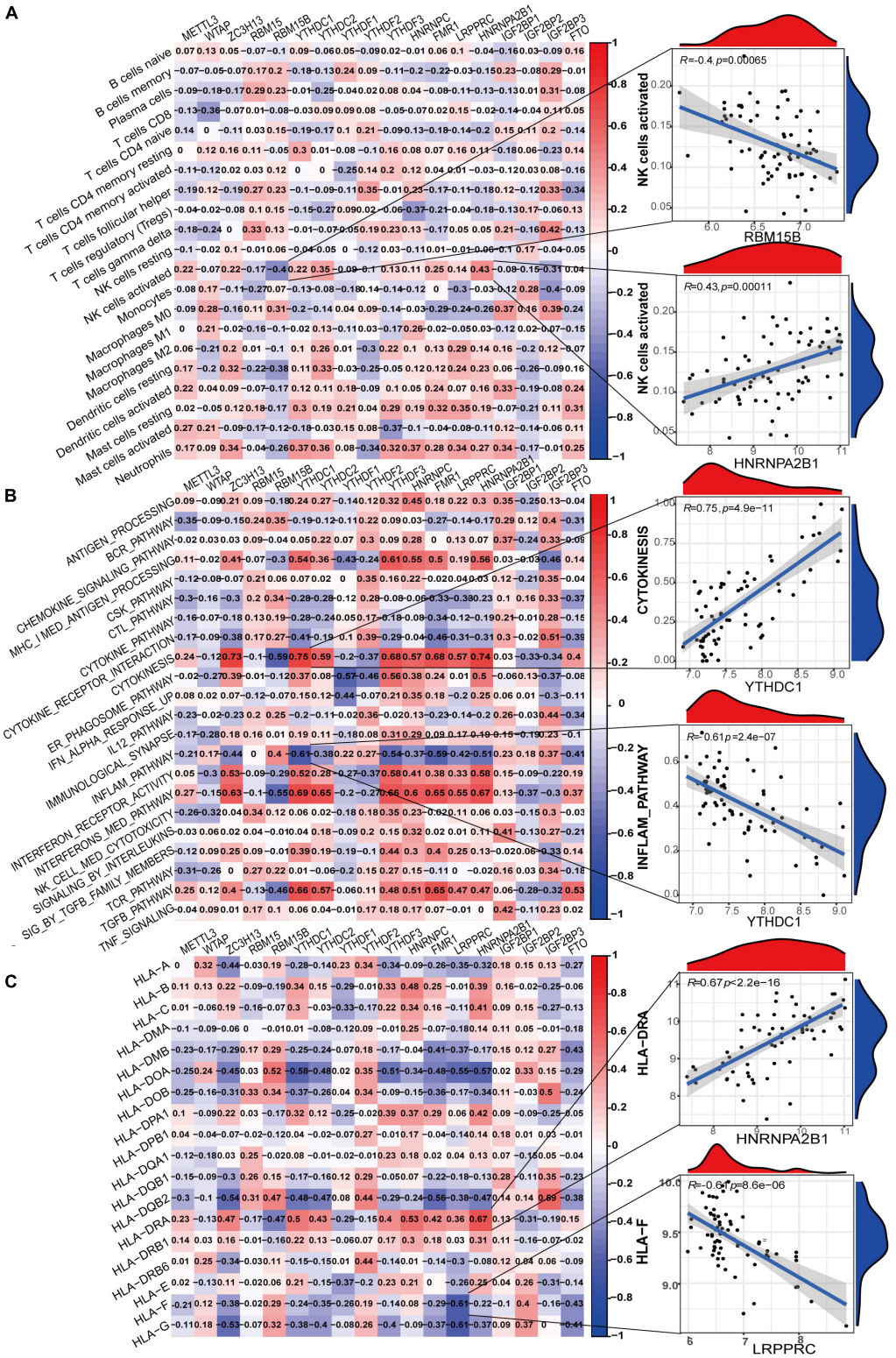


FIGURE 4 | Correlation between m^{6}A regulator expression and immune characteristics in LN. **(A)** Heatmap of the correlations between 18 m^{6}A regulators and 21 immunocytes (eosinophils with no expression were removed in all samples). The two respective scatterplots show the m^{6}A regulator and immunocyte with the highest positive or negative correlation. **(B)** Heatmap of the correlations between 18 m^{6}A regulators and immune response gene sets. The two respective scatterplots show m^{6}A regulators and immune response gene sets with the highest positive or negative correlation. **(C)** Heatmap of the correlations between 18 m^{6}A regulators and 18 HLA genes. The two respective scatterplots show m^{6}A regulators and HLA genes with the highest positive or negative correlation.

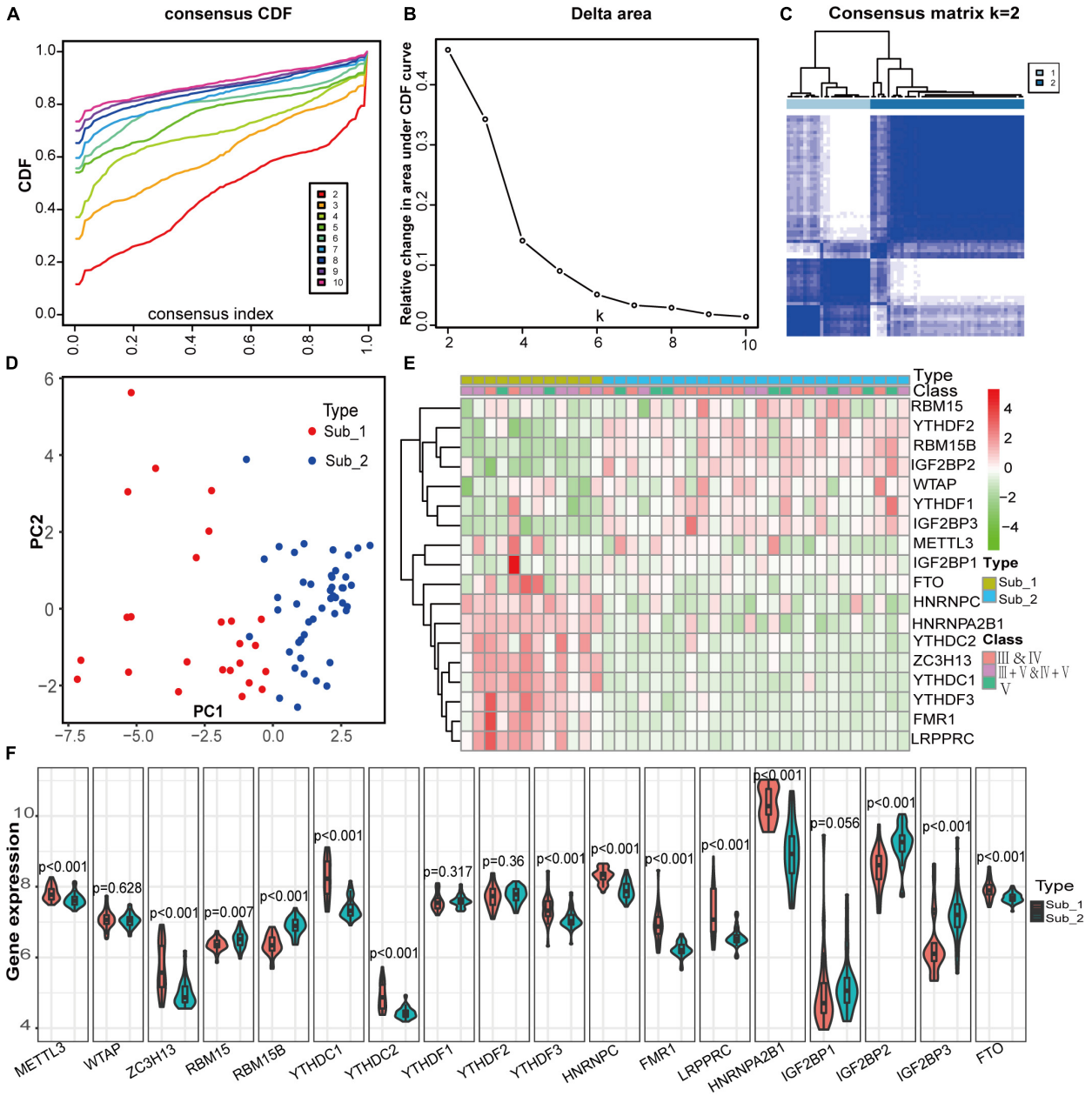


FIGURE 5 | Identification of two distinct m^{6}A modification subtypes in LN and clinical correlation of two subtypes. **(A)** Consensus clustering of cumulative distribution function (CDF) for k = 2–9. **(B)** Elbow plot shows relative change in area under CDF curve. **(C)** Consensus clustering matrix for k = 2. **(D)** Principal component analysis (PCA) of two m^{6}A subtypes in LN. **(E)** Heatmap of the clinical features of two clusters comparing the stages of LN and gene profiles between m^{6}A subtypes in GSE127797. **(F)** The two m^{6}A subtypes exhibit distinct expression statuses of 18 m^{6}A RNA methylation regulators.

38 LN samples, consisting of subtype 1 with 12 samples and subtype 2 with 26 samples. Most patients with mixed proliferative and membranous LN (class III+V and IV+V) belong to subtype 1, whereas most with pure proliferative LN (class III and IV) or pure membranous LN (class V) belong to subtype 2. Significant differences in m^{6}A regulator gene profiles were observed between the two subtypes (**Figures 5E,F**). FTO, HNRNPC, HNRNPA2B1, YTHDC2, ZC3H13, YTHDC1, YTHDF3, FMR1, and LRPPRC were highly expressed in m^{6}A subtype 1, whereas the other regulators were highly expressed in m^{6}A subtype 2.

Immune Characteristics and Biological Functional Characteristics of Two Distinct m^{6}A Subtypes

To further determine the characteristics of the two m^{6}A subtypes, we compared the abundance of infiltrating immune cells, activity

of immune responses and HLA gene expression value between the two distinct m^{6}A subtypes. More infiltrating activated NK cells (p = 0.001), memory resting CD4 T cells (p = 0.009), and activated dendritic cells (p = 0.03) were observed in subtype 1, whereas more plasma cells (p = 0.009), naïve CD4 T cells (p = 0.03), and macrophages M0 (p = 0.003) were observed in subtype 2 (**Figure 6A**). For immune reactions, m^{6}A subtype 1 had a stronger immune response than subtype 2. There were 11 immune reactions, including MHC-I-mediated antigen processing, cytokinesis, and interferon-mediated signaling pathways, which were more active in subtype 1, whereas BCR, CTL, inflammation, and IL-12 pathways were more active in subtype 2 (**Figure 6B**). Different expression levels of HLA genes between the two m^{6}A subtypes were also observed. For example, subtype 1 had a higher expression of HLA-C, HLA-DPA1, and HLA-DRA, whereas subtype 2 had a higher expression of HLA-DOB and HLA-DQB2 (**Figure 6C**). Taken together, m^{6}A modification patterns were shaped with different immune characteristics, suggesting that m^{6}A RNA methylation regulators might play an important role in immune microenvironment regulation in LN. To investigate the biological functional pathways that m^{6}A may affect, we conducted GSVA to assess the enrichment of biological pathways. **Figure 6D** shows the enrichment difference of the HALLMARKS pathways between the two subtypes, indicating that protein secretion and UV-response pathways are more enriched in subtype 1, whereas myogenesis and KRAS signaling pathways are more enriched in subtype 2. Some KEGG pathways, including regulation of autophagy, TGF-β signaling pathway, and antigen processing and presentation were more enriched in subtype 1, whereas other pathways such as cytokine-cytokine receptor interaction, intestinal immune network for IgA production, and the JAK-STAT signaling pathway were more enriched in subtype 2 (**Figure 6E**). It should be noted that the highly enriched pathways in both subtypes both included immune-related pathways.

Identification of m^{6}A Methylation Modification Markers and Clinical Correlation of Markers With Renal Function

To gain further insight into which genes are involved in the biological processes affected by m^{6}A regulators, we identified m^{6}A-related genes, and enrichment analysis of these genes was performed. The top 10 pathways in the BP and GO were mainly RNA or protein modification pathways and immune-related pathways, such as neutrophil degranulation and MHC-I-mediated antigen processing (**Figure 7A**). This confirmed that m^{6}A methylation modification was associated with the immune microenvironment in LN. The KEGG enrichment analysis revealed that m^{6}A modification patterns-related genes were more enriched in protein processing in the endoplasmic reticulum and Salmonella infection pathways (**Figure 7B**). Based on m^{6}A related genes, we performed WGCNA to identify module hub genes (**Figures 7C–E**). Three gene modules were established, including the nonsense gray module, based on their similar expression spectrum (**Figure 7F**). The MEturquoise module genes were most positively correlated with m^{6}A subtype 1 (R^2 = 0.78) (**Figure 7G**), indicating that MEturquoise is a key module. Then, genes in MEturquoise were used to construct the PPI network (**Figure 7H**). If the module membership (MM) of genes in the turquoise module was > 0.8, and their gene significance (GS) was > 0.6, these genes were considered the hub genes of the turquoise module. Finally, we overlapped the central nodes in the PPI and hub genes of the turquoise module, and seven m^{6}A RNA methylation modification markers (CDC5L, CDC40, HNRNPU, NUDT21, PAPOLA, POLR2B, and WBP4) were identified (**Figure 7I**). To further elucidate the roles of these m^{6}A markers in LN, correlation analysis between markers and GFR was carried out in the Nephroseq database (**Figures 8A–G**). Among the seven markers, only CDC40 was positively correlated with GFR, thus, a higher expression of CDC40 indicates better renal function in patients with LN have and may play a protective role against LN. The other six markers, CDC5L, HNRNPU, NUDT21, PAPOLA, POLR2B, and WBP4, were all negatively correlated with GFR, indicating that these genes may aggravate kidney damage in patients with LN.

DISCUSSION

LN is an autoimmune disease characterized by symptoms of inflammation. Immune response dysregulation mediated by genetic and environmental factors leads to the occurrence and development of LN (Anders et al., 2020). Many studies have confirmed that m^{6}A methylation modification exerts critical functions in the development of diseases, especially malignancies. However, little research has been conducted on m^{6}A methylation in LN. Our study is the first to investigate the roles of m^{6}A regulators in LN and reveal the association with m^{6}A methylation modification and immune characteristics. Firstly, significant differences in the expression of most m^{6}A regulators between healthy individuals and LN were observed in the glomeruli. This is mainly because LN is a form of glomerulonephritis. We also identified an m^{6}A regulator gene signature that included *METTL3*, *WTAP*, *YTHDC2*, *YTHDF1*, and *FMR1* after LASSO-logistic regression. LN and healthy samples were easily distinguished, which highlights that m^{6}A methylation modification patterns differ between LN and healthy samples.

Then, we demonstrated a correlation between m^{6}A regulators and immune characteristics. A series of immune reactions were considerably correlated with m^{6}A regulators, especially MHC-I-mediated antigen processing, cytokinesis, inflammation pathway, and interferon-mediated signaling pathway. Most m^{6}A regulators were found to be strongly correlated with the IFN signaling pathway. Recent studies have shown that type I interferon (IFN-I) is an important risk factor for the occurrence and progression of LN (Ding et al., 2021), indicating that m^{6}A methylation modification plays a key role in the development of LN. Most HLA genes were closely correlated with m^{6}A regulators. Studies have identified that HLA-DR3, HLA-DR4, HLA-DR11, and HLA-DR15 can promote or improve kidney damage in LN (Munroe and James, 2015; Iwamoto and Niewold, 2017). For immune cell

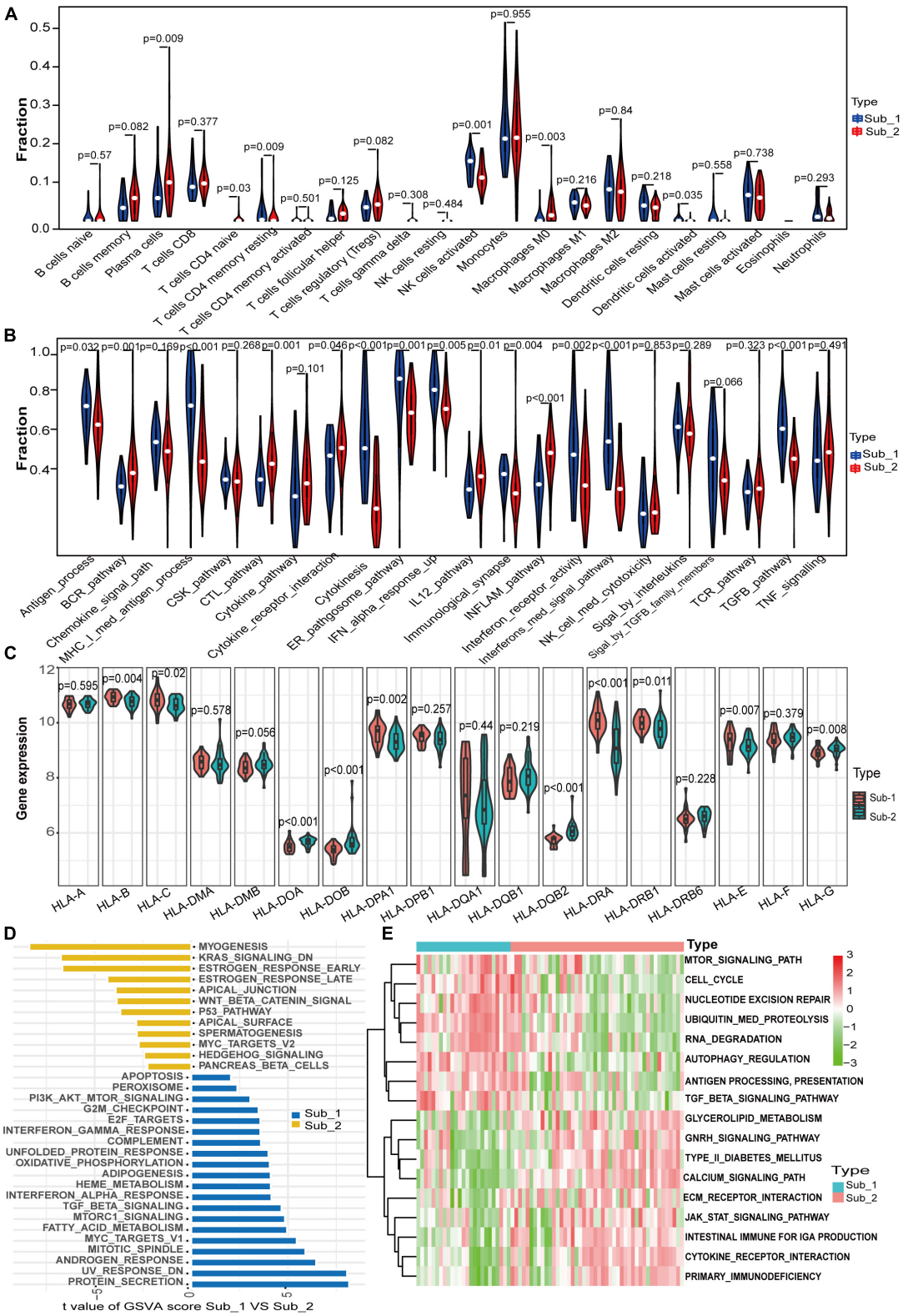


FIGURE 6 | Differences in immune characteristics between m^{6}A subtypes and functional enrichment analysis in two m^{6}A subtypes. **(A)** Differences in abundance of 22 infiltrating immunocytes. **(B)** Differences in the activity of 22 immune response gene sets in two m^{6}A subtypes. **(C)** Expression differences of 18 HLA genes in two m^{6}A subtypes. **(D)** Differences in HALLMARKS pathway enrichment between m^{6}A subtypes. **(E)** KEGG pathways with significant differences in enrichment between m^{6}A subtypes.

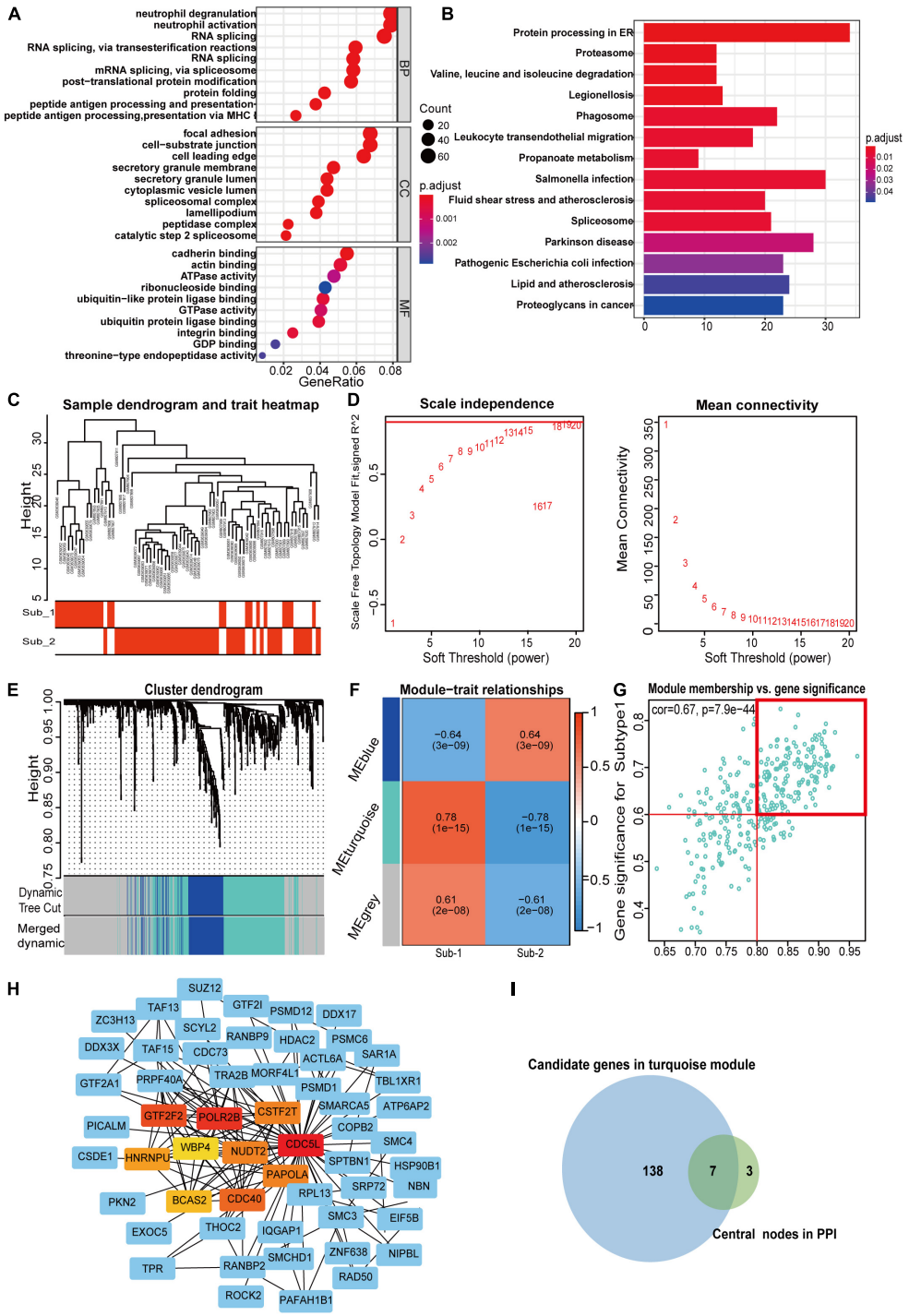


FIGURE 7 | Pathway enrichment analysis of m^{6}A regulator related genes **(A,B)** and identification of m^{6}A methylation pattern markers in LN **(C–I)**. **(A)** Enrichment analysis of GO biological process, cellular component, and molecular function. **(B)** Bubble plot of KEGG enrichment pathways. **(C)** Clustering dendrogram of two m^{6}A modification subtypes in LN. **(D)** Scale-free fitting index analysis and mean connectivity of soft threshold power from 1 to 20. **(E)** Clustering dendrograms for m^{6}A regulator-related genes. According to dynamic tree cutting, the genes were clustered into different modules through hierarchical clustering and merged when the correlation of the modules is > 0.8. Each color represents each module. **(F)** Correlation heatmap between module eigen genes and m^{6}A subtypes. **(G)** Scatter plot of m^{6}A subtype 1 in the turquoise module. In the turquoise module, GS and MM show a very significant correlation, indicating that the genes of the turquoise module are highly related to the m^{6}A modification subtype. The dots in the red box indicate that the module membership of these genes is > 0.8, and their gene significance > 0.6, meaning that these dots are the hub genes of the turquoise module. **(H)** PPI analysis network of m^{6}A methylation-related genes from the turquoise module 10, the central nodes in PPI are marked in red, orange, and yellow. **(I)** Venn diagram of seven m^{6}A modification markers. The central nodes of PPI (green set) were overlapped with the hub genes in the turquoise module (blue set) by weighted correlation network analysis.

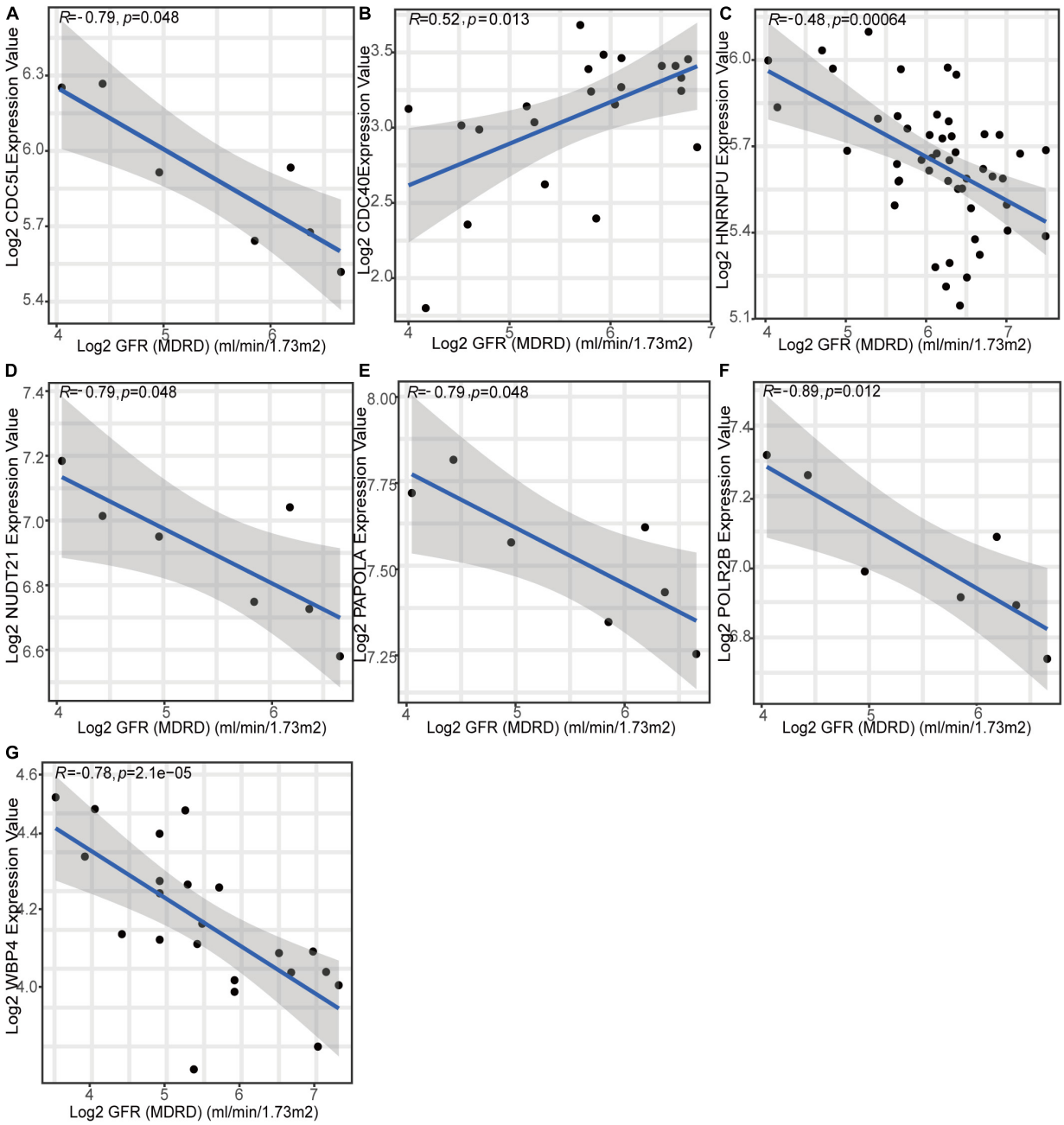


FIGURE 8 | Relationship between seven m^{6}A methylation pattern markers and renal function (glomerular filtration rate).

infiltration, activated NK cells were most strongly correlated with m^{6}A regulators. Activated NK cells were most positively correlated with HNRNPA2B1 and most negatively correlated with RBM15B. NK cells are an important link between the innate and adaptive immune systems. Postól et al. (2008) found that the onset of glomerulonephritis in NZBxNZW (F1) mice (SLE model) can be delayed by long-term depletion of NK cells, indicating that functional defects in NK cells may induce the development of LN (Spada et al., 2015; Segerberg et al., 2019).

However, the overall correlation between various immunocytes and m^{6}A regulators was found to be generally weak. One possible reason for this is the limitations of previous technical tools. The samples collected for RNA sequencing contain very limited immune cells, which might not precisely reflect the abundance of infiltrating immunocytes (Stewart et al., 2020).

In our study, two distinct m^{6}A RNA methylation modification subtypes were identified based on the m^{6}A regulator gene expression profiles using unsupervised clustering. The differences

between the 2 subtypes included the following aspects. As for immune characteristics, m^{6}A subtype 1 of LN was characterized by increased immune response activation and a higher HLA gene expression profile. A higher abundance of infiltrating immune cells was observed in m^{6}A subtype 2, including that of plasma cells, naïve CD4 T cells, M0 macrophages, and dendritic cells. Plasma cells play a key role in the development of SLE and LN (Crickx et al., 2021). A higher abundance of infiltrating T cells, memory resting CD4 T cells, and activated NK cells was found in subtype 1. The deposition of immunoglobulins produced by plasma cells in the glomeruli is the initial trigger for LN. Now, the focus of treatment for LN is targeted B-cell therapy. The two m^{6}A subtypes of LN have the potential to be used to develop targeted immunotherapy.

Additionally, the pathological stages of LN in the two subtypes were also considerably different. Most patients with mixed proliferative and membranous LN (class III+V and IV+V) belong to subtype 1, whereas most with pure proliferative LN (class III and IV) or pure membranous LN (class V) belong to subtype 2. No current research has been conducted to illustrate the relationship between LN classification and immune status. Our results initially suggest that a greater activation of immune reaction pathways occurs in class III+V and IV+V, and a higher abundance of infiltrating plasma cells occurs in class III, IV, and V. In general, class III+V and IV+V have more complicated pathological changes than class III, IV, or V because their lesions are mixed proliferative lesions in class V (Parikh et al., 2020). LN classification is established according to differences in prognosis and is the gold standard for guiding treatment (Levey and Coresh, 2012; Mackay et al., 2019; Mageau et al., 2019). In our study, a strong correlation was observed between LN classification and m^{6}A subtypes. As subtype1 is associated with mixed, complex, and more severe lesions compared with subtype2, uncovering the key differences between the subtypes will contribute to preventing the aggravation of LN. Molecular subtyping is a widely used strategy in malignancies, and targeted treatment plans can be formulated based on different molecular types to improve patient prognosis (Teo et al., 2019). The two m^{6}A modification subtypes of LN have the potential to be considered as an alternative classification of LN. Furthermore, from a functional pathway perspective, genes of m^{6}A subtype 1 are more enriched in the TGF-β signaling pathway, MTOR signaling pathway, and autophagy regulation.

Finally, seven m^{6}A methylation modification markers were identified. CDC5L, HNRNPU, NUDT21, PAPOLA, POLR2B, and WBP4 were negatively correlated with GFR (an indicator of kidney function), whereas CDC40 was positively correlated with GFR. The protein encoded by CDC5L has been shown to be a positive regulator of the G2/M stage of the cell cycle. Zhou et al. (2020) found that CDC5L also regulates cell proliferation and metastasis in lung adenocarcinoma through promoter methylation. POLR2B encodes the second largest subunit of RNA polymerase II (Pol II), which is involved in RNA splicing and modification (Wang et al., 2021). CDC40, HNRNPU, WBP4, NUDT21, and PAPOLA are all involved in precursor mRNA splicing. S-adenosylmethionine (SAM) is a methyl donor for almost all cell methylation events. Scarborough et al. (2021) reported that NUDT21 regulates intracellular SAM levels. As shown, m^{6}A RNA methylation modification plays a key role in mRNA splicing, suggesting that the m^{6}A markers identified in this study are closely related to the m^{6}A modification process. In addition, Fuyuno et al. (2016) proposed that the mutation of the WBP4 locus may lead to the occurrence of inflammatory bowel disease. The nuclear matrix protein HNRNPU is also considered as a nuclear virus dsRNA sensor for DNA and RNA viruses (Lin et al., 2010). m^{6}A markers may be related to immune disorders and inflammatory responses, which again highlights that m^{6}A-regulators can regulate immune characteristics. At present, research on LN mainly focuses on genetics and clinical advances, whereas epigenetic research is rare. There is also almost no research on m^{6}A RNA methylation modification. We took the lead in identifying the role of m^{6}A regulators in LN and exploring their relationship with immune characteristics. The various results in our study indicate that m^{6}A methylation modification is a new direction for research regarding the pathogenesis of LN.

Our study has certain limitations. First, we were unable to obtain more clinical data for each patient, such as sex, age, treatment, and prognosis, for the longitudinal analysis. We could not perform a correlation analysis between m^{6}A patterns, pathological stages, and other clinical characteristics of all samples. Second, we included as many samples as possible in the GEO database that met our requirements, but the sample size was still small (73 LN, 14 living healthy donors). Studies with larger sample sizes are required in the future. Additionally, the expression changes of some identified m^{6}A regulators between LN and healthy samples were small and our findings were mainly obtained through bioinformatics analysis, which is needed to be further verified experimentally. However, the good predictive performance of our identified m^{6}A regulator gene signature was verified using an external data set. The correlation between seven m^{6}A markers identified from GEO data and kidney function was verified using data from the Nephroseq database. We have sufficient reasons to believe that m^{6}A methylation plays an important role in the development of LN.

In summary, we comprehensively assessed the role of m^{6}A methylation in the glomeruli of patients with LN, established an m^{6}A regulators signature that can easily distinguish LN and healthy individuals, and identified two distinct m^{6}A subtypes based on 18 m^{6}A regulators. The two distinct m^{6}A subtypes in LN were determined with significant differences in m^{6}A regulators expression, immune microenvironment, biological functional pathways, and clinical characteristics. We uncovered an association between m^{6}A subtypes and immune characteristics, which can be used to develop targeted immunotherapy. Moreover, seven m^{6}A subtype markers were identified and all of them demonstrated a meaningful correlation with GFR, indicating that they are potential prognostic biomarkers.

DATA AVAILABILITY STATEMENT

The datasets presented in this study can be found in online repositories. The names of the repository/repositories

and accession number(s) can be found in the article/ **Supplementary Material**.

AUTHOR CONTRIBUTIONS

HZ, ZL, and DL conceived the project. HZ analyzed the data, explained the results, drafted the original manuscript, and drew the figures. SP and JD discussed the draft manuscript. FL and GL revised the manuscript. All the authors approved the final version of the manuscript.

FUNDING

This work was supported by the National Science and Technology Major Project of China (Grant No. 2020ZX09201-009), the Innovation Scientists and Technicians Troop Construction Projects of Henan Province (No. 182101510002), and the Excellent Youth Fund Project of Henan Province (No. 202300410363).

ACKNOWLEDGMENTS

We would like to thank all the contributors of the transcriptome sequencing data for this study.

SUPPLEMENTARY MATERIAL

The Supplementary Material for this article can be found online at: https://www.frontiersin.org/articles/10.3389/fcell.2021.724837/full#supplementary-material

REFERENCES

Almaani, S., Prokopec, S. D., Zhang, J., Yu, L., Avila-Casado, C., Wither, J., et al. (2019). Rethinking lupus nephritis classification on a molecular level. *J. Clin. Med.* 8:1524. doi: 10.3390/jcm8101524

Anders, H.-J., Saxena, R., Zhao, M.-H., Parodis, I., Salmon, J. E., and Mohan, C. (2020). Lupus nephritis. *Nat. Rev. Dis. Primers* 6:7.

Berthier, C. C., Bethunaickan, R., Gonzalez-Rivera, T., Nair, V., Ramanujam, M., Zhang, W., et al. (2012). Cross-species transcriptional network analysis defines shared inflammatory responses in murine and human lupus nephritis. *J. Immunol.* 189, 988–1001. doi: 10.4049/jimmunol.1103031

Bhattacharya, S., Andorf, S., Gomes, L., Dunn, P., Schaefer, H., Pontius, J., et al. (2014). ImmPort: disseminating data to the public for the future of immunology. *Immunol. Res.* 58, 234–239. doi: 10.1007/s12026-014-8516-1

Crickx, E., Tamirou, F., Huscenot, T., Costedoat-Chalumeau, N., Rabant, M., Karras, A., et al. (2021). Evolution of kidney antibody secreting cells molecular signature in lupus patients with active nephritis upon immunosuppressive therapy. *Arthritis Rheumatol. (Hoboken, NJ)* 73, 1461–1466. doi: 10.1002/art.41703

Ding, X., Ren, Y., and He, X. I. F. N.-I. (2021). Mediates lupus nephritis from the beginning to renal fibrosis. *Front. Immunol.* 12:676082.

Friedman, J., Hastie, T., and Tibshirani, R. (2010). Regularization paths for generalized linear models via coordinate descent. *J. Stat. Softw.* 33, 1–22.

Fuyuno, Y., Yamazaki, K., Takahashi, A., Esaki, M., Kawaguchi, T., Takazoe, M., et al. (2016). Genetic characteristics of inflammatory bowel disease in a Japanese population. *J. Gastroenterol.* 51, 672–681.

Han, D., Liu, J., Chen, C., Dong, L., Liu, Y., Chang, R., et al. (2019). Anti-tumour immunity controlled through mRNA m 6 A methylation and YTHDF1 in dendritic cells. *Nature* 566, 270–274. doi: 10.1038/s41586-019-0916-x

Hänzelmann, S., Castelo, R., and Guinney, J. (2013). GSVA: gene set variation analysis for microarray and RNA-seq data. *BMC Bioinformatics* 14:7. doi: 10.1186/1471-2105-14-7

He, L., Li, H., Wu, A., Peng, Y., Shu, G., and Yin, G. (2019). Functions of N6-methyladenosine and its role in cancer. *Mol. Cancer* 18:176.

Huang, H., Weng, H., Sun, W., Qin, X., Shi, H., Wu, H., et al. (2018). Recognition of RNA N(6)-methyladenosine by IGF2BP proteins enhances mRNA stability and translation. *Nat. Cell Biol.* 20, 285–295. doi: 10.1038/s41556-018-0045-z

Iwamoto, T., and Niewold, T. B. (2017). Genetics of human lupus nephritis. *Clin. Immunol.* 185, 32–39. doi: 10.1016/j.clim.2016.09.012

Javierre, B. M., Fernandez, A. F., Richter, J., Al-Shahrour, F., Martin-Subero, J. I., Rodriguez-Ubreva, J., et al. (2010). Changes in the pattern of DNA methylation associate with twin discordance in systemic lupus erythematosus. *Genome Res.* 20, 170–179. doi: 10.1101/gr.100289.109

Ju, W., Nair, V., Smith, S., Zhu, L., Shedden, K., Song, P. X. K., et al. (2015). Tissue transcriptome-driven identification of epidermal growth factor as a chronic kidney disease biomarker. *Sci. Transl. Med.* 7:316ra193.

Langfelder, P., and Horvath, S. (2008). WGCNA: an R package for weighted correlation network analysis. *BMC Bioinformatics.* 9:559.

Leek, J. T., Johnson, W. E., Parker, H. S., Jaffe, A. E., and Storey, J. D. (2012). The sva package for removing batch effects and other unwanted variation in high-throughput experiments. *Bioinformatics* 28, 882–883. doi: 10.1093/bioinformatics/bts034

Levey, A. S., and Coresh, J. (2012). Chronic kidney disease. *Lancet* 379, 165–180.

Li, H. B., Tong, J., Zhu, S., Batista, P. J., Duffy, E. E., Zhao, J., et al. (2017). m(6)A mRNA methylation controls T cell homeostasis by targeting the IL-7/STAT5/SOCS pathways. *Nature* 548, 338–342. doi: 10.1038/nature23450

Lin, R. K., Hsieh, Y. S., Lin, P., Hsu, H. S., Chen, C. Y., Tang, Y. A., et al. (2010). The tobacco-specific carcinogen NNK induces DNA methyltransferase 1 accumulation and tumor suppressor gene hypermethylation in mice and lung cancer patients. *J. Clin. Invest.* 120, 521–532. doi: 10.1172/jci40706

Mackay, M., Dall'Era, M., Fishbein, J., Kalunian, K., Lesser, M., Sanchez-Guerrero, J., et al. (2019). Establishing surrogate kidney end points for lupus nephritis clinical trials: development and validation of a novel approach to predict future kidney outcomes. *Arthritis Rheumatol. (Hoboken, NJ)* 71, 411–419. doi: 10.1002/art.40724

Mageau, A., Timsit, J. F., Perrozziello, A., Ruckly, S., Dupuis, C., Bouadma, L., et al. (2019). The burden of chronic kidney disease in systemic lupus erythematosus: a nationwide epidemiologic study. *Autoimmun. Rev.* 18, 733–737. doi: 10.1016/j.autrev.2019.05.011

Meyer, K. D., and Jaffrey, S. R. (2014). The dynamic epitranscriptome: N6-methyladenosine and gene expression control. *Nat. Rev. Mol. Cell Biol.* 15, 313–326. doi: 10.1038/nrm3785

Munroe, M. E., and James, J. A. (2015). Genetics of lupus nephritis: clinical implications. *Semin. Nephrol.* 35, 396–409. doi: 10.1016/j.semnephrol.2015.08.002

Narain, S., and Furie, R. (2016). Update on clinical trials in systemic lupus erythematosus. *Curr. Opin. Rheumatol.* 28, 477–487. doi: 10.1097/bor.0000000000000311

Parikh, S. V., Almaani, S., Brodsky, S., and Rovin, B. H. (2020). Update on lupus nephritis: core curriculum 2020. *Am. J Kidney Dis.* 76, 265–281. doi: 10.1053/j.ajkd.2019.10.017

Postól, E., Meyer, A., Cardillo, F., de Alencar, R., Pessina, D., Nihei, J., et al. (2008). Long-term administration of IgG2a anti-NK1.1 monoclonal antibody ameliorates lupus-like disease in NZB/W mice in spite of an early worsening induced by an IgG2a-dependent BAFF/BLyS production. *Immunology* 125, 184–196. doi: 10.1111/j.1365-2567.2008.02835.x

Ritchie, M. E., Phipson, B., Wu, D., Hu, Y., Law, C. W., Shi, W., et al. (2015). limma powers differential expression analyses for RNA-sequencing and microarray studies. *Nucleic Acids Res.* 43:e47. doi: 10.1093/nar/gkv007

Scarborough, A. M., Flaherty, J. N., Hunter, O. V., Liu, K., Kumar, A., Xing, C., et al. (2021). SAM homeostasis is regulated by CFI(m)-mediated splicing of MAT2A. *Elife* 10:e64930.

Segerberg, F., Lundtoft, C., Reid, S., Hjorton, K., Leonard, D., Nordmark, G., et al. (2019). Autoantibodies to killer cell immunoglobulin-like receptors in patients with systemic lupus erythematosus induce natural killer cell hyporesponsiveness. *Front. Immunol.* 10: 2164.

Spada, R., Rojas, J. M., and Barber, D. F. (2015). Recent findings on the role of natural killer cells in the pathogenesis of systemic lupus erythematosus. *J. Leukoc. Biol.* 98, 479–487. doi: 10.1189/jlb.4ru0315-081rr

Stewart, B. J., Ferdinand, J. R., and Clatworthy, M. R. (2020). Using single-cell technologies to map the human immune system - implications for nephrology. *Nat. Rev. Nephrol.* 16, 112–128. doi: 10.1038/s41581-019-0227-3

Szklarczyk, D., Gable, A. L., Lyon, D., Junge, A., Wyder, S., Huerta-Cepas, J., et al. (2019). STRING v11: protein-protein association networks with increased coverage, supporting functional discovery in genome-wide experimental datasets. *Nucleic Acids Res.* 47, D607–D613.

Teo, W. Y., Sekar, K., Seshachalam, P., Shen, J., Chow, W. Y., Lau, C. C., et al. (2019). Relevance of a TCGA-derived glioblastoma subtype gene-classifier among patient populations. *Sci. Rep.* 9:7442.

Thanou, A., and Merrill, J. T. (2014). Treatment of systemic lupus erythematosus: new therapeutic avenues and blind alleys. *Nat. Rev. Rheumatol.* 10, 23–34. doi: 10.1038/nrrheum.2013.145

Wang, J., Ahimaz, P. R., Hashemifar, S., Khlevner, J., Picoraro, J. A., Middlesworth, W., et al. (2021). Novel candidate genes in esophageal atresia/tracheoesophageal fistula identified by exome sequencing. *Eur. J. Hum. Genet.* 29, 122–130. doi: 10.1038/s41431-020-0680-2

Wilkerson, M. D., and Hayes, D. N. (2010). ConsensusClusterPlus: a class discovery tool with confidence assessments and item tracking. *Bioinformatics* 26, 1572–1573. doi: 10.1093/bioinformatics/btq170

Yu, G., Wang, L. G., Han, Y., and He, Q. Y. (2012). clusterProfiler: an R package for comparing biological themes among gene clusters. *OMICS* 16, 284–287. doi: 10.1089/omi.2011.0118

Zaccara, S., Ries, R. J., and Jaffrey, S. R. (2019). Reading, writing and erasing mRNA methylation. *Nat. Rev. Mol. Cell Biol.* 20, 608–624. doi: 10.1038/s41580-019-0168-5

Zhao, B. S., Roundtree, I. A., and He, C. (2017). Post-transcriptional gene regulation by mRNA modifications. *Nat. Rev. Mol. Cell Biol.* 18, 31–42. doi: 10.1038/nrm.2016.132

Zhou, R. H., Zhang, J. T., Chen, C., Xu, Z. H., Lv, X. B., Ye, L., et al. (2020). Identification of CDC5L as bridge gene between chronic obstructive pulmonary disease and lung adenocarcinoma. *Epigenomics* 12, 1515–1529. doi: 10.2217/epi-2020-0112

Conflict of Interest: The authors declare that the research was conducted in the absence of any commercial or financial relationships that could be construed as a potential conflict of interest.

Publisher's Note: All claims expressed in this article are solely those of the authors and do not necessarily represent those of their affiliated organizations, or those of the publisher, the editors and the reviewers. Any product that may be evaluated in this article, or claim that may be made by its manufacturer, is not guaranteed or endorsed by the publisher.

Copyright © 2021 Zhao, Pan, Duan, Liu, Li, Liu and Liu. This is an open-access article distributed under the terms of the Creative Commons Attribution License (CC BY). The use, distribution or reproduction in other forums is permitted, provided the original author(s) and the copyright owner(s) are credited and that the original publication in this journal is cited, in accordance with accepted academic practice. No use, distribution or reproduction is permitted which does not comply with these terms.

frontiers in Cell and Developmental Biology

ORIGINAL RESEARCH
published: 13 October 2021
doi: 10.3389/fcell.2021.762669

Characterization of Long Non-coding RNAs Modified by m^{6}A RNA Methylation in Skeletal Myogenesis

Shu-Juan Xie[1,2†], Shuang Tao[2†], Li-Ting Diao[2†], Pan-Long Li[2], Wei-Cai Chen[2], Zhi-Gang Zhou[3], Yan-Xia Hu[2], Ya-Rui Hou[2], Hang Lei[2], Wan-Yi Xu[2], Wen-Jie Chen[2], Yan-Wen Peng[2], Qi Zhang[1,2*] and Zhen-Dong Xiao[2*]*

[1] Vaccine Research Institute of Sun Yat-sen University, The Third Affiliated Hospital of Sun Yat-sen University, Guangzhou, China, [2] Biotherapy Center, The Third Affiliated Hospital of Sun Yat-sen University, Guangzhou, China, [3] Department of Orthopedics, First Affiliated Hospital, Jinan University, Guangzhou, China

Proper development of mammalian skeletal muscle relies on precise gene expression regulation. Our previous studies revealed that muscle development is regulated by both mRNA and long non-coding RNAs (lncRNAs). Accumulating evidence has demonstrated that N^6-methyladenosine (m^{6}A) plays important roles in various biological processes, making it essential to profile m^{6}A modification on a transcriptome-wide scale in developing muscle. Patterns of m^{6}A methylation in lncRNAs in developing muscle have not been uncovered. Here, we reveal differentially expressed lncRNAs and report temporal m^{6}A methylation patterns in lncRNAs expressed in mouse myoblasts and myotubes by RNA-seq and methylated RNA immunoprecipitation (MeRIP) sequencing. Many lncRNAs exhibit temporal differential expression, and m^{6}A-lncRNAs harbor the consensus m^{6}A motif "DRACH" along lncRNA transcripts. Interestingly, we found that m^{6}A methylation levels of lncRNAs are positively correlated with the transcript abundance of lncRNAs. Overexpression or knockdown of m^{6}A methyltransferase METTL3 alters the expression levels of these lncRNAs. Furthermore, we highlight that the function of m^{6}A genic lncRNAs might correlate to their nearby mRNAs. Our work reveals a fundamental expression reference of m^{6}A-mediated epitranscriptomic modifications in lncRNAs that are temporally expressed in developing muscle.

Keywords: m^{6}A, lncRNAs, Brip1os, METTL3, skeletal muscle development

OPEN ACCESS

Edited by:
Huilin Huang,
Sun Yat-sen University Cancer Center (SYSUCC), China

Reviewed by:
Zhanpeng Huang,
The First Affiliated Hospital of Sun Yat-sen University, China
Chao Shen,
City of Hope National Medical Center, United States

****Correspondence:***
Zhen-Dong Xiao
xiaozhd@mail2.sysu.edu.cn
Qi Zhang
zhangq27@mail.sysu.edu.cn
Yan-Wen Peng
pengyw@mail.sysu.edu.cn

† These authors have contributed equally to this work

Specialty section:
This article was submitted to Epigenomics and Epigenetics, a section of the journal Frontiers in Cell and Developmental Biology

Received: *22 August 2021*
Accepted: *14 September 2021*
Published: *13 October 2021*

Citation:
Xie S-J, Tao S, Diao L-T, Li P-L, Chen W-C, Zhou Z-G, Hu Y-X, Hou Y-R, Lei H, Xu W-Y, Chen W-J, Peng Y-W, Zhang Q and Xiao Z-D (2021) Characterization of Long Non-coding RNAs Modified by m^{6}A RNA Methylation in Skeletal Myogenesis. Front. Cell Dev. Biol. 9:762669. doi: 10.3389/fcell.2021.762669

INTRODUCTION

Skeletal muscle plays critical roles in the regulation of wider metabolism as well as driving locomotion (Cong et al., 2020). Myogenesis, the development of muscle, is a complex biological process regulated by multiple transcription factors and specific signaling pathways (Bryson-Richardson and Currie, 2008; Bentzinger et al., 2012). Our previous studies showed that non-coding RNAs, including miRNAs and lncRNAs (long non-coding RNAs), play essential roles in skeletal muscle development (Xie et al., 2018; Liu et al., 2021; Tan et al., 2021). LncRNAs are a class of

non-coding RNAs greater than 200 nucleotides in length with limited or no protein-coding capacity that possess complex spatial structures and diverse functions (Chen and Carmichael, 2010; Xie et al., 2021a). Numerous studies have shown that lncRNAs play a significant role in biological functions, such as epigenetic modification, mRNA transcription, splicing, stability and translation (Lan et al., 2021). Functionally, lncRNAs can either act in *cis* by regulating the expression of neighboring genes or in *trans* by regulating the expression of distant genes (Ulitsky and Bartel, 2013). Increasing studies have shown that lncRNAs participate in myogenesis. For example, H19, one of the earliest known imprinted lncRNAs, is strongly repressed after birth in all mouse tissues, but it remains expressed in the skeletal muscle and heart in adults (Milligan et al., 2000), controlling reactivation of the imprinted gene network and alleviating muscular dystrophy (Borensztein et al., 2013; Martinet et al., 2016; Zhang Y. et al., 2020). LncRNA MALAT1 interacts with miRNAs or mRNAs to regulate skeletal muscle maintenance (Yong et al., 2020; Liu et al., 2021). Additionally, several lncRNAs have been reported to shape muscle (Ro et al., 2018; Sweta et al., 2019; Martone et al., 2020), including linc-MD1 (Cesana et al., 2011), lincYY1 (Lu et al., 2013; Zhou et al., 2015), lncRNA Dum (Wang et al., 2015), linc-RAM (Yu et al., 2017; Zhao et al., 2018), muscle-specific lncR-Irm (Sui et al., 2019), lncR-Myoparr (Hitachi et al., 2019), lnc-MyoD (Gong et al., 2015; Lim et al., 2020), and lncMGPF (Lv et al., 2020).

RNA chemical modifications in coding and non-coding RNAs can regulate gene expression without changing the sequence of the RNA molecules via a process referred as "epitranscriptomics" (Helm and Motorin, 2017; Roundtree et al., 2017; Fazi and Fatica, 2019). Greater than 150 RNA modifications have been identified as posttranscriptional regulatory marks in multiple RNA species, including mRNAs, tRNAs, rRNAs, small non-coding RNAs, and lncRNAs (Yang Y. et al., 2018). Among these modifications, N^6-methyladenosine (m^{6}A) is the most common modification in mammalian mRNAs and lncRNAs (Pan, 2013). The effectors in m^{6}A pathways include "writers" and "erasers" that install and remove the methylation, respectively, and "readers" that recognize it (Fu et al., 2014; Meyer and Jaffrey, 2017; Shi et al., 2019). The m^{6}A writer machinery is a methyltransferase complex composed of multiple subunits with a stable core complex formed between methyltransferase-like 3 (METTL3) and methyltransferase-like 14 (METTL14) (Ping et al., 2014). Benefitting from deep sequencing, m^{6}A patterns have been demonstrated to occur in a cell type- and cell state-dependent manner, and the landscape of the m^{6}A methylome has been identified in human and mouse tissues (Liu et al., 2020; Zhang H. et al., 2020).

Given the important function of m^{6}A modification in gene expression, emerging evidence has revealed the critical role of m^{6}A in skeletal muscle regulation (Li et al., 2021). Our recent study elaborated the dynamic m^{6}A methylation of mRNA during skeletal muscle differentiation and revealed the role of METTL3/14-m^{6}A-MNK2-ERK signaling axis in skeletal muscle differentiation and regeneration (Xie et al., 2021b). Besides, another work of us confirmed that the m^{6}A key methyltransferase METTL3 is involved in the biogenesis of muscle-specific miRNAs (Diao et al., 2021a). This finding is consistent with a previous report indicating that METTL3 is sufficient to enhance miRNA maturation in a global and non-cell-type specific manner (Alarcón et al., 2015). Other studies focused on the modification of mRNA by m^{6}A methylation, which is involved in muscle formation, maintaining muscle homeostasis, and musculoskeletal disorders (Zhang W. et al., 2020). Recent studies revealed that METTL3-mediated m^{6}A methylation is essential for muscle stem cell self-renewal (Lin et al., 2020), muscle regeneration (Liang et al., 2021), and muscle stem cell/myoblast state transitions (Gheller et al., 2020). Interestingly, myogenic potential is maintained partly by the Mettl3-mediated stabilization of processed MyoD mRNA through m^{6}A modification of the 5′ untranslated regions (UTR) during proliferative phases (Kudou et al., 2017), and depletion of m^{6}A "eraser" FTO in myoblasts leads to impaired skeletal muscle development (Wang et al., 2017). These data suggested that m^{6}A modification could mediate muscle progenitor cell proliferation and differentiation. It has been demonstrated that m^{6}A lncRNA modification plays roles in different biological processes (Patil et al., 2016; Yang D. et al., 2018; Fazi and Fatica, 2019; Ma et al., 2019; He et al., 2020; Lan et al., 2021). However, little is known about the m^{6}A methylation status of lncRNAs involved in developing skeletal muscle.

In this study, we characterized lncRNAs in mouse myoblasts and differentiated myotubes using RNA sequencing (RNA-seq) and further uncovered abundant m^{6}A sites and specific m^{6}A patterns in these lncRNAs using methylated RNA immunoprecipitation sequencing (MeRIP-seq). Our results reveal the temporal expression profile and m^{6}A methylation status of lncRNAs during skeletal myogenesis. We found that the m^{6}A methylation levels of lncRNAs were positively correlated with their transcriptional abundance. Our data will provide a fundamental reference for further study on the function of lncRNAs.

MATERIALS AND METHODS

Cell Culture

The C2C12 mouse myoblast cell line and HEK-293T cells were purchased from the Cellular Library of the National Collection of Authenticated Cell Cultures (Shanghai, China). The cells were cultured in growth medium (GM)-Dulbecco's modified Eagle's medium (DMEM, Gibco) with 10% fetal bovine serum (FBS, Gibco), 100 U/ml penicillin, and 100 μg/ml streptomycin (1 × penicillin–streptomycin) at 37°C in a humidified chamber supplemented with 5% CO_2. When C2C12 cells reached about 90% confluency, the GM was replaced with differentiation medium (DM)-DMEM containing 2% horse serum (HyClone).

Stable Cell Generation

For METTL3 overexpression, cDNA of mouse METTL3 was cloned into the pKD-CMV-MCS-EF1-PURO (pKD) vector by Gibson Assembly, and pKD-GFP was used as a negative control.

For METTL3 knockdown, the gRNAs downstream of the transcription start sites were used to guide the fusion of inactive Cas9 (dCas9) to the Krüppel-associated box (KRAB) repressor. To generate stable cells, lentiviruses were produced in HEK-293T cells by transfecting vectors together with psPAX.2 and pMD2.G. Lentiviruses were collected and filtered 48 h after transfection and then used to infect target cell lines. Stable cells were selected using the antibiotic puromycin.

All sequences of clone primers used in this study are listed in **Supplementary Table 1**.

Gene Knockdown

To knock down lncRNAs, custom designed siRNAs targeting selected lncRNAs and control siRNAs were synthesized by Shanghai GenePharma Co., Ltd. C2C12 cells were seeded in 12-well plates and transfected with siRNAs using Lipofectamine 2000 (Invitrogen) after the cells reached 30–40% confluency, according to the manufacturer's instructions. The transfected cells were maintained in growth medium for two days, and then cells were harvested for analysis.

All siRNA sequences used in this study are listed in **Supplementary Table 2**.

m^{6}A Dot Blot Assay

RNA dot blotting was performed as previously described with modifications (Chen et al., 2015). Cells were harvested carefully and purified using a Dynabeads mRNA direct kit (Invitrogen, 61012). To avoid RNA degradation, RNase-free tubes and RNase-free water were used. RNA samples were quantified, diluted and incubated at 95°C in a heat block for 3 min to disrupt secondary structures. The tubes were chilled on ice immediately after denaturation for 2 min. The RNA samples were dropped onto the membrane (Amersham Hybond-N $^+$, GE) and allowed to air dry for 5 min. Then, RNA was crosslinked to the membrane with UV light (2 autocrosslink, 150 mJ/cm^2 UV Stratalinker, STRATAGENE). The membrane was washed in TBST (1TBS, 0.1% Tween-20), dyed in methylene blue (Sigma–Aldrich) as a quantitative control, and incubated in blocking buffer containing 5% non-fat dry milk in TBST for 2 h at room temperature. Then, the membrane was incubated with m^{6}A antibody (1:1000, Synaptic Systems, 202-003) at 4°C overnight. The membrane was washed 3 times for 10 min each in TBST and then incubated with HRP-linked secondary anti-rabbit IgG antibody (1:5000, CST, 7074) for 1 h at room temperature. Signals were detected with WesternBright ECL HRP substrate (Advansta). The dots were quantified using ImageJ.

Western Blot

Cells were lysed in ice-cold enhanced RIPA lysis buffer (Shanghai Wansheng Haotian Biological Technology) containing phosphatase inhibitor and protease inhibitor cocktail (Roche). Equivalent total protein extracts were separated by SDS–PAGE and transferred to nitrocellulose membranes (Merck Millipore). The membranes were blocked with 5% non-fat dry milk in TBST for 1 h at room temperature. The following antibodies were used in this study: anti-METTL3 (Proteintech, 15073-1-AP), anti-METTL14 (R&D, HPA038002), anti-MHC (R&D, MAB4470), and anti-GAPDH (CST, 2118). Immunoreactivities were determined using WesternBright ECL HRP substrate (Advansta).

RNA Isolation and Quantitative RT-PCR Assay

Total RNA was extracted from cells with TRIzol reagent (Invitrogen, 15596018). First-strand cDNA for PCR analyses was synthesized with HiScript III RT SuperMix for qPCR (+ gDNA wiper) (Vazyme, R323-01), and quantitative real-time PCR was performed using ChamQ Universal SYBR qPCR Master Mix (Vazyme, Q711-02). The GAPDH gene served as an endogenous control. The qRT-PCR results were analyzed and presented as relative RNA levels of the CT (cycle threshold) values, which were then converted as fold change. The results are presented as the means ± SD.

All primers for qPCR are listed in **Supplementary Table 1**.

RNA Library Construction and Sequencing

Total RNA was isolated and purified using TRIzol reagent (Invitrogen, 15596018) following the manufacturer's procedure. The RNA amount and purity were quantified by a NanoDrop ND-1000 (NanoDrop). RNA integrity was assessed using the Agilent 2100 system with RIN number >7.0 and confirmed by electrophoresis with a denaturing agarose gel.

RNA-seq was performed by BGI Co., Ltd. Briefly, total RNA was used to purify the poly-A containing RNAs using poly-T oligo-attached magnetic beads. Following the purification, the remainder of the RNA was fragmented into small pieces using divalent cations under high temperature. Then, the cleaved RNA fragments were reverse transcribed to create the cDNA library according to the mRNA-Seq sample preparation kit protocol (Illumina). The average insert size for the paired-end libraries was 300 bp (±50 bp). Then, paired-end sequencing was performed on an Illumina NovaSeq^{TM} 6000 (BGI Co., Ltd, Shenzhen, China) following the vendor's recommended protocol.

MeRIP Sequencing

RNA extraction and quality control were performed as previously noted. Poly(A) RNA was purified from 50 μg of total RNA using Dynabeads Oligo (dT) 25-61005 (Thermo Fisher) and fragmented into 100-nucleotide-long oligonucleotides using Magnesium RNA Fragmentation Module (NEB). The cleaved RNA fragments were immunoprecipitated using an anti-m^{6}A affinity purified antibody (Synaptic Systems, 202003). Then, the IP RNA was reverse transcribed to cDNA by SuperScript^{TM} II Reverse Transcriptase (Invitrogen, 1896649) followed by U-labeled second-stranded DNA synthesis. Then, after ligation with the adapter to the A-tailed fragmented DNA, the ligated products were amplified with PCR, and 2 × 150 bp paired-end sequencing (PE150) was performed on an Illumina NovaSeq^{TM} 6000 (LC-Bio Technology CO., Ltd., Hangzhou, China) following the vendor's recommended protocol.

m^{6}A-IP-qPCR

m^{6}A methylated RNA immunoprecipitation was performed as previously described (Diao et al., 2021a). Briefly, 200 μg of total RNA was incubated with 8 μg of m^{6}A-specific antibody (Synaptic Systems, 202003) for 2 h at 4°C with gentle rotation. Then, 50 μl protein A/G magnetic beads were added and incubated for 2 h at 4°C with gentle rotation. Beads were pelleted at 2,500 rpm for 30 s. Then, the supernatant was removed, and the beads are resuspended in 500 μL RIP buffer. The process is repeated for a total of three RIP washes followed by one wash in PBS. Beads were incubated with DNase I for 30 min at 37°C and were then digested by Proteinase K for 2 h at 37°C with rotation. A MicroElute RNA Clean Up Kit (Omega) was used for RNA purification. Purified RNA was reverse transcribed and quantified by real-time RT-PCR.

RNA-Seq Analysis

The sequencing adapters were removed from raw fastq data using cutadapt (Kechin et al., 2017) software, and then clean reads were mapped to the mouse reference genome (mm10) using HISAT2 (Kim et al., 2019). According to reference gene annotation (Ensembl release 102), the raw counts of each gene were calculated using featureCounts (Liao et al., 2014). Raw counts were further normalized as reads per kilobase of genome per million mapped reads (RPKM) using the fpkm function in the DESeq2 (Love et al., 2014) package. Differentially expressed genes were identified using DESeq2 (Love et al., 2014) with adjusted $P \leq 0.05$. LncRNAs were selected for downstream analysis based on gene type.

MeRIP-Seq Analysis

The sequencing adapters were removed from raw fastq data using cutadapt (Kechin et al., 2017) software, and then clean reads were mapped to the mouse reference genome (mm10) using HISAT2 (Kim et al., 2019). Unique mapped reads were selected using samtools (Li et al., 2009) with a mapping quality greater than 30. To visualize read coverage using IGV (Robinson et al., 2011), the bigwig format of mapped reads was generated using deeptools (Ramírez et al., 2014). Mapped reads of IP and input libraries were fed into the exomePeak (Meng et al., 2013) package for calling peaks and identifying distinct peaks, and statistical significance was defined as FDR ≤ 0.05. Called peaks were annotated by intersecting with gene architecture using bedtools (Quinlan and Hall, 2010) and custom Python script. Peaks located at lncRNAs were selected based on gene type for downstream analysis.

Motif Identification and Peak Distribution Among lncRNA Bodies

Sequence motifs enriched in m^{6}A peaks were identified by HOMER (Heinz et al., 2010) with "−len 5,6,7,8 −rna" and other default settings as parameters. An m^{6}A metagene plot was plotted using the Guitar (Cui et al., 2016) package. To investigate the peak distribution of lncRNA exon elements, an in-house Python script was developed to calculate the numbers of peaks located at the first exon, internal exons and last exon. Pie charts were plotted using ggplot2 package.

Relationship Analysis of lncRNA m^{6}A Level and Expression Abundance

Significant differential m^{6}A peaks were integrated with corresponding differential expression data regardless of significance. Based on change orientation, the lncRNAs with significant differential m^{6}A peaks were classified into four groups: hypermethylated and upregulated, hypermethylated and downregulated, hypomethylated and upregulated, and hypomethylated and downregulated. A four-quadrant diagram was generated using the ggplot2 package. To estimate the relationship of lncRNA m^{6}A level and expression abundance, Pearson correlation analysis was performed using R software (version 4.0.3).

Neighbor Gene Analysis of Differentially Expressed lncRNAs

Ten neighboring mRNAs (five upstream and five downstream) of differentially expressed lncRNAs were obtained using an in-house Python script, and mRNAs with significantly different expression (adjusted $P \leq 0.05$) were fed into the clusterProfiler (Yu et al., 2012) package for GO and KEGG analysis. Statistical significance was defined as $p \leq 0.05$. The top 10 most significant terms are shown using dot plots. For genes associated with muscle development, their neighboring lncRNAs were also required to have significant m^{6}A changes. Finally, a set of lncRNAs with expression and m^{6}A alterations related to muscle development were identified.

Visualization Analysis

A heatmap was drawn using the pheatmap package, and other charts that were not specified were drawn using the ggplot2 package.

RESULTS

Dynamic Profile of lncRNAs in Myoblasts and Differentiated Myotubes

We used mouse C2C12 myoblast cells to mimic skeletal muscle differentiation. C2C12 cells constantly proliferate in the presence of serum and begin to differentiate in the absence of serum. After differentiation for 4 days, obvious morphological changes were observed when myocytes fused to form multinucleated myotubes (**Supplementary Figure 1A**), as described in our previous reports (Xie et al., 2018; Tan et al., 2021). Next, RNA dot blotting was performed to investigate the dynamics of m^{6}A RNA modification during myogenesis, and decreased global m^{6}A levels were observed in myotubes that had been differentiated for 4 days (D4) compared to myoblasts (cells on growth medium, GM) (**Figure 1A**). To test whether this change was due to altered expression of m^{6}A methyltransferases or demethylases, we profiled the core components of m^{6}A methyltransferases METTL3, METTL14, and m^{6}A demethylases FTO and ALKBH5

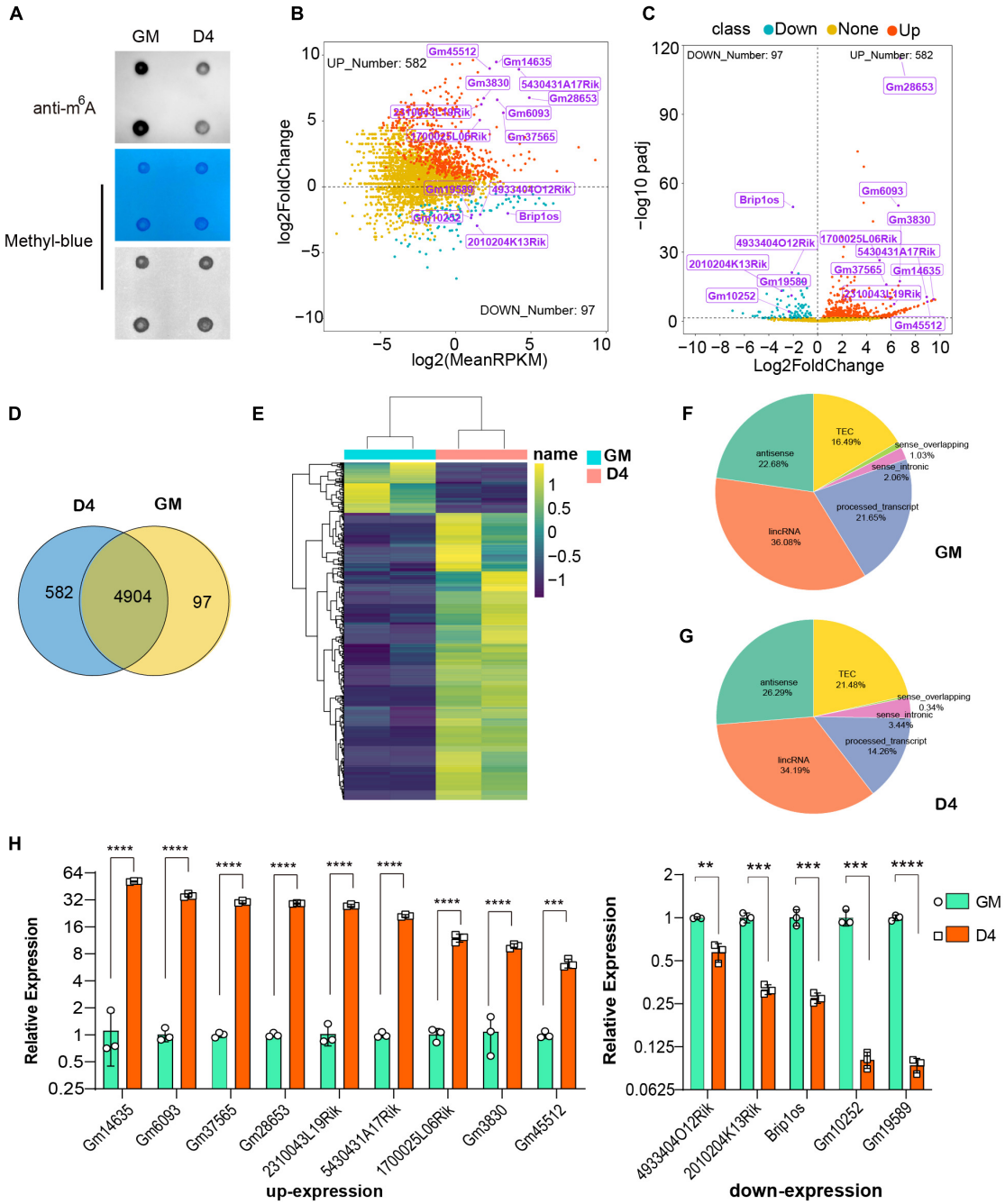


FIGURE 1 | Dynamic profile of lncRNAs in myoblasts and differentiated myotube. **(A)** RNA dot blot assay of m^{6}A methylation levels of C2C12 myoblasts in GM and D4. **(B)** MA plot shows the relationship of expression abundance and fold changes of lncRNAs in myoblasts (GM) and myotube (D4). log2 (MeanRPKM) represents gene expression values, log2Fold Change represents the fold change of lncRNAs at D4 compared to GM. Red dots represent 582 significantly up-regulated lncRNAs at D4 in relation to GM, adjusted $P \leq 0.05$; Green dots, represent 97 significantly down-regulated lncRNAs at D4 in relation to GM, adjusted $P \leq 0.05$; Yellow dots represent lncRNA without significantly differential expression, adjusted $P > 0.05$. Top differentially expressed lncRNAs were marked in purple. **(C)** The volcano plot shows significantly differentially expressed lncRNAs at GM and D4. Red dots represent 582 significantly up-regulated lncRNAs at D4, adjusted $P \leq 0.05$; Green dots, represent 97 significantly down-regulated lncRNAs at D4, adjusted $P \leq 0.05$; Yellow dots represent lncRNA without significantly differential expression, adjusted $P > 0.05$. Top differentially expressed lncRNAs were marked in purple. **(D)** The Venn diagram shows 97 and 582 significantly differentially expressed lncRNAs in GM and D4, and 4904 lncRNAs without significant difference between GM and D4. **(E)** The heatmap shows significantly differentially expressed lncRNAs in GM and D4. Yellow color represents up-regulation in D4, while green color represents down-regulation. Row represents genes, column represents samples, and each cell represents expression value. **(F)** Pie chart show the gene types of lncRNAs up-regulated in GM. **(G)** Pie chart show the gene types of lncRNAs up-regulated in D4. **(H)** Quantitative real-time reverse transcription PCR (qRT-PCR) validated top differently expressed lncRNAs in developing muscle cells. RPKM: Reads Per Kilobase per Million mapped reads. adjusted P: adjusted *p*-value; Data are presented as Mean ± SD; *p* value: $^{**}p < 0.01$, $^{***}p < 0.001$, $^{****}p < 0.0001$.

during C2C12 differentiation. Consistent with the decline in m^{6}A levels, METTL3 and METTL14 protein expression was decreased on D4 and negatively correlated with the myogenic marker MHC (**Supplementary Figure 1B**). However, the demethylases FTO and ALKBH5 had opposite changes during C2C12 differentiation (**Supplementary Figure 1C**), and the upregulation of FTO is consistent with previous report (Wang et al., 2017). These data revealed that m^{6}A and its core methyltransferase decreased during C2C12 differentiation. Such a dynamic change in m^{6}A may contribute to the regulation of muscle genes in myoblasts and myotubes.

In addition to RNA modification, non-coding RNAs, especially long non-coding RNAs (lncRNAs), could represent robust gene expression regulators. To profile the dynamic changes in lncRNAs during C2C12 differentiation, RNA sequencing (RNA-seq) was performed to analyze the expression of lncRNAs in GM and D4. Using bioinformatic analysis, we detected 5,583 lncRNAs expressed in at least one sample. Of these, 679 differentially expressed lncRNAs were identified (adjusted *P* value $\leq$0.05, **Supplementary Table 3**), We found that these differentially expressed genes generally tended to exhibit increased expression (**Figure 1B**). Moreover, the number of upregulated genes was far greater than that of downregulated genes (**Figures 1B,C,E**). We identified 97 and 582 lncRNAs significantly differentially expressed in GM and D4, respectively (**Figure 1D**). The top differentially expressed lncRNAs are marked in purple and are listed in **Table 1**. Among these lncRNAs, the majority were lincRNAs with 36.08% in GM and 34.19% in D4. The second rank was antisense RNA in both GM and D4 samples (**Figures 1F,G**). To validate the RNA-seq results, we performed quantitative real-time reverse transcription PCR (qRT-PCR) for the top nine upregulated and top five downregulated lncRNAs. All tested lncRNAs showed significantly differential expression, which was consistent with the RNA-sequencing results (**Figure 1H**). Of note, the top highly expressed lncRNAs, including Gm14635, Gm28653, 2310043L19Rik and 5430431A17Rik, were also highly expressed in the limb. In particular, Gm28653, which is also known as linc-MD1, is a muscle-specific lncRNA that controls muscle differentiation (Cesana et al., 2011). In addition, lncRNA 1700025l06Rik has the same transcript locus as lincMyod, which is directly activated by MyoD and regulates skeletal muscle differentiation by blocking IMP2-mediated mRNA translation (Gong et al., 2015).

Meanwhile, we analyzed the mRNAs expression pattern of RNA-seq data, and identified 8,817 out of 16,190 differentially expressed mRNAs in D4 versus GM (adjusted *P* value $\leq$0.05, **Supplementary Table 4**). The number of upregulated coding genes was a little less than that of downregulated genes (**Supplementary Figures 2A,B,D**), of which 4483 and 4334 mRNAs significantly differentially expressed in GM and D4, respectively, and 7737 mRNA showed no significantly different expression in both group (**Supplementary Figure 2C**). The distinct difference in the number of genes with significant change between mRNAs and lncRNAs may due to the fact that mRNAs account for the majority of cellular RNA contents. Taken together, our RNA-seq analysis revealed the temporal expression of lncRNAs and mRNAs during myoblast differentiation.

Features of lncRNA m^{6}A Methylation in Undifferentiated and Differentiated Muscle

Given the great importance of m^{6}A methylation and non-coding RNAs in skeletal muscle development (Martone et al., 2020) as well as the altered m^{6}A modification and lncRNA expression profiles in myoblast differentiation, we conducted methylated RNA immunoprecipitation sequencing (MeRIP-seq) in GM and D4 samples to uncover the m^{6}A methylation landscape of lncRNAs. We identified greater than 20 thousand unique peaks from each MeRIP-seq sequencing library (FDR $\leq$ 0.05, **Supplementary Tables 5, 6**). Among them, we found 1383 lncRNA m^{6}A peaks in the GM sample and 1848 lncRNA m^{6}A peaks in the D4 sample (FDR $\leq$ 0.05, **Supplementary Tables 7, 8**). And we also found 5122 significantly differently mRNA peaks in D4 versus GM, of which 2692 mRNA m^{6}A

TABLE 1 | Top differentially expressed lncRNAs in myoblasts and differentiated myotube.

Ensembl_ID	Gene_Name	Expression	log2FoldChange	meanfpkm	padj
ENSMUSG00000087591	Gm14635	Up	9.478458245	6.5058287	2.95E-10
ENSMUSG00000110071	Gm45512	Up	8.979513546	4.7889075	3.66E-09
ENSMUSG00000108322	5430431A17Rik	Up	8.917522207	18.467968	3.13E-11
ENSMUSG00000099906	Gm28653	Up	6.761660182	29.802335	4.47E-115
ENSMUSG00000099465	Gm3830	Up	6.719594193	3.649369	4.34E-18
ENSMUSG00000112963	Gm6093	Up	6.600023017	6.7770027	4.89E-51
ENSMUSG00000101746	2310043L19Rik	Up	6.259516887	3.2733601	3.43E-08
ENSMUSG00000104045	Gm37565	Up	5.616399462	8.984661	1.25E-16
ENSMUSG00000109962	1700025L06Rik	Up	5.062787459	3.0317699	3.23E-27
ENSMUSG00000085208	Brip1os	Down	−2.020791677	11.071526	2.06E-50
ENSMUSG00000097908	4933404O12Rik	Down	−2.110740583	3.1048072	6.83E-22
ENSMUSG00000100798	Gm19589	Down	−2.141593862	2.0967695	7.30E-12
ENSMUSG00000110350	Gm10252	Down	−2.36282624	2.0370561	6.34E-05
ENSMUSG00000063018	2010204K13Rik	Down	−2.962399389	2.6803628	6.84E-14

peaks in the GM sample and 1442 mRNA m^{6}A peaks in the D4 sample (FDR $\leq$ 0.05, **Supplementary Table 9** and **Supplementary Figure 3**). To identify whether m^{6}A peaks share common sequence elements, we analyzed m^{6}A binding motifs using Homer. We detected a significantly enriched consensus motif DRACU within lncRNAs from myoblast GM and myotube D4 (**Figure 2A**). The motif matched the well-validated consensus m^{6}A motif DRACH (where D = A, G or U; R = A or G; H = A, C or U) and was similar to a previous report in lincRNAs (Meyer and Jaffrey, 2017). We explored the distribution of peaks along the lncRNA gene body and found that its density gradually decreased from the transcription initiation site to the transcriptional termination site (**Figure 2B**), which differs from the coding genes (Liu et al., 2015).

We further analyzed the peak distribution of lncRNA exons. We found that m^{6}A peaks were preferentially enriched in the last exon of lncRNAs expressed in GM and D4 samples. In total, 63.69% and 67.25% m^{6}A peaks were identified in the last exon of lncRNAs expressed in GM and D4, respectively. We then analyzed the peak enrichment in each lncRNA. Interestingly, we found that m^{6}A peaks are preferentially enriched in the first exon and internal exon, but not the last exons (**Figures 2C,D**). We then analyzed the numbers of m^{6}A peaks within lncRNAs and identified a median value of 1.0 m^{6}A peaks per lncRNA (**Figure 2E**), and no differences were noted between the GM and D4 data. Furthermore, we performed integrating analysis by coupling MeRIP-seq and RNA-seq data. We mapped m^{6}A peaks to differentially expressed lncRNAs and found that 74 and 83 lncRNAs were significantly hypermethylated in myoblasts (GM) and myotubes (D4), respectively (**Figure 2F**). These data provide a fundamental reference for the m^{6}A epitranscriptome for further study.

Differentially m^{6}A-Modified lncRNAs in Undifferentiated and Differentiated Muscle

To explore the putative function of m^{6}A on lncRNAs, we investigated the correlation between lncRNA transcript abundance and m^{6}A methylation. In total, 123 significantly differentially m^{6}A-methylated lncRNAs were expressed during myogenesis, as shown by RNA-seq. Among these lncRNAs, we identified 34 hypermodified lncRNAs (32 hyper-upregulated and 2 hyper-downregulated) and 14 hypomodified lncRNAs (6 hypo-upregulated and 8 hypo-downregulated) according to the criteria of adjusted $P \leq 0.05$ and FDR ≤ 0.05 (**Figure 3A**). These results indicate a temporal difference in m^{6}A methylation in differentially expressed lncRNAs. To verify the relationship between m^{6}A level changes of lncRNAs and expression changes of lncRNAs, we randomly selected 15 significantly differentially expressed lncRNAs (**Table 2**) and performed qRT-PCR analysis. The results showed that 10 hyper-upregulated lncRNAs increased and 5 hypo-downregulated lncRNAs decreased in D4 (**Figure 3B**). These findings were consistent with sequencing data. It is worth mentioning that lncRNA Brip1os, which is significantly downregulated in D4 samples, as shown in **Figure 1H**, was accompanied by a decline in m^{6}A modification.

To verify the significantly differentially m^{6}A-modified lncRNAs, we used an antibody against m^{6}A and performed RNA immunoprecipitation followed by real-time PCR (m^{6}A-IP-qPCR). As shown in **Figure 3C**, compared to that in the IgG control, most of the lncRNAs in **Figure 3B** were significantly enriched in the m^{6}A group, indicating that these transcripts were m^{6}A enriched. For example, the enrichment of Xist, Ptgs2os2 and Brip1os was elevated up to hundreds of thousands of fold in the m^{6}A group, which is consistent with the MeRIP-seq data that revealed clear m^{6}A peaks around their RNAs (**Figure 3D**). Furthermore, we verified the m^{6}A peaks enrichment of 5 hyper-upregulated and 5 hypo-downregulated lncRNAs in GM and D4. By normalization of each group of Normal IgG, the m^{6}A-IP-qPCR data was consistent with **Figure 3A** (**Figure 3E**). In summary, these results demonstrated that m^{6}A methylation in lncRNAs is involved in myogenesis.

m^{6}A Methylation Levels Were Positively Correlated With the Abundance of lncRNAs

More recently, m^{6}A modification of mRNA was established to influence RNA stability dynamics and translation efficiency, and rapidly accumulating evidence shows significant crosstalk between lncRNA methylation and m^{6}A-mediated epigenetic mechanisms (Kan et al., 2021). We then examined the correlation of lncRNA expression abundance with m^{6}A methylation levels. For lncRNAs with significant expression abundance changes, their m^{6}A levels were positively correlated with their expression levels (R = 0.6, P = 6.8e-6) (**Figure 4A**). However, for lncRNAs without significant transcript abundance changes, no significant correlation was noted between their m^{6}A levels and expression levels (R = 0.21, p = 0.071) (**Figure 4B**). Interestingly, in both GM and D4 samples, lncRNAs with m^{6}A methylation showed higher expression levels than those without m^{6}A methylation (**Figures 4C,D**). Our analysis reveals that m^{6}A methylation levels exhibit a positive correlation with the expression levels of m^{6}A-modified lncRNAs and highlights the importance of m^{6}A methylation in myogenesis-related lncRNAs.

Myogenesis-Related lncRNAs Are Regulated by the m^{6}A Methyltransferase METTL3

To further investigate whether altered m^{6}A modification levels could affect lncRNA expression, we overexpressed METTL3 in C2C12 cells (oe-M3), and GFP-overexpressing cells were used as a negative control (GFP). The real-time PCR and Western blot results validated that METTL3 was successfully overexpressed (**Figures 5A,B**). Then, we assayed the expression levels of six selected lncRNAs in GFP- and METTL3-overexpressing cells. As shown in **Figure 5C**, all 6 lncRNAs, including Brip1os, were significantly upregulated when METTL3 was overexpressed.

To validate the METTL3 overexpression results, we designed two gRNAs downstream of transcription start sites and

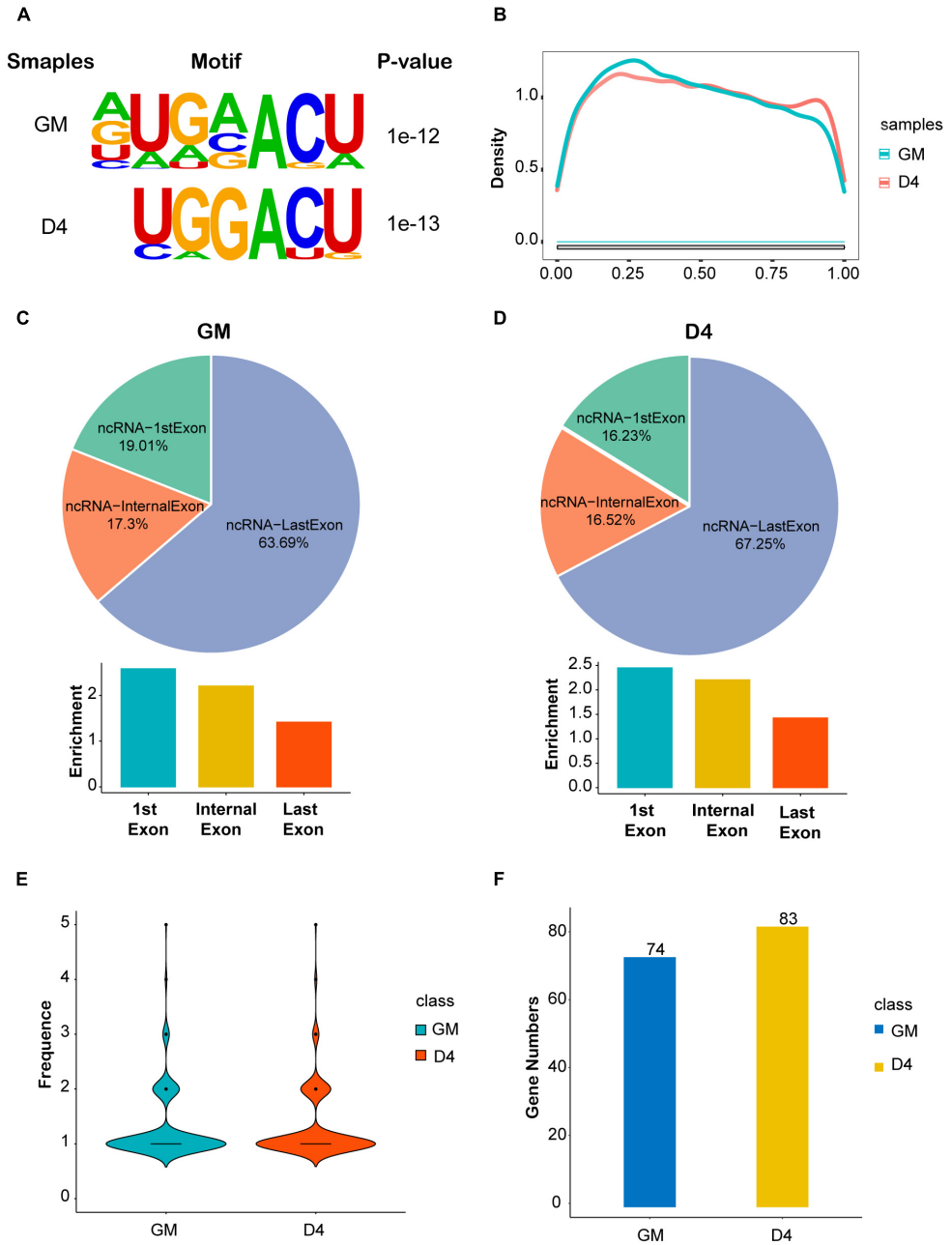


FIGURE 2 | Features of lncRNA m^{6}A methylation in undifferentiated and differentiated muscle. **(A)** The enriched consistent motif of m^{6}A peaks in lncRNAs in GM and D4. **(B)** Metagene profiles of enrichment of all m^{6}A peaks across lncRNAs transcriptome. **(C)** The top: pie charts represent the proportion of m^{6}A peaks in the three regions of lncRNAs at GM. The bottom: histogram represents the relative enrichment of m^{6}A peaks in the three regions of lncRNAs at GM. **(D)** The top: pie charts represent the proportion of m^{6}A peaks in the three regions of lncRNAs at D4. The bottom: histogram represents the relative enrichment of m^{6}A peaks in the three regions of lncRNAs at D4. **(E)** The frequence of m^{6}A Peak Numbers in lncRNAs in GM and D4. **(F)** Bar plot shows the Numbers of m^{6}A methylated lncRNAs in GM and D4. Blue represents 74 hyper-methylated lncRNAs in GM, while yellow represents 83 hyper-methylated lncRNAs in D4.

used them to guide the fusion of inactive Cas9 (dCas9) to the Krüppel-associated box (KRAB) repressor to inhibit the transcription of METTL3 in C2C12 cells. METTL3 mRNA and protein levels were greatly reduced compared to those with control gRNA (**Figures 5D,E**). Then, we assayed the 6 lncRNA expression levels, and qPCR results showed that the expression levels of these lncRNAs decreased when METTL3 was knocked down (**Figure 5F**). Taken together, our results revealed that lncRNA expression is positively correlated with m^{6}A modification levels during myogenesis, and it might be a universal regulation way that m^{6}A modification levels affect lncRNAs abundance.

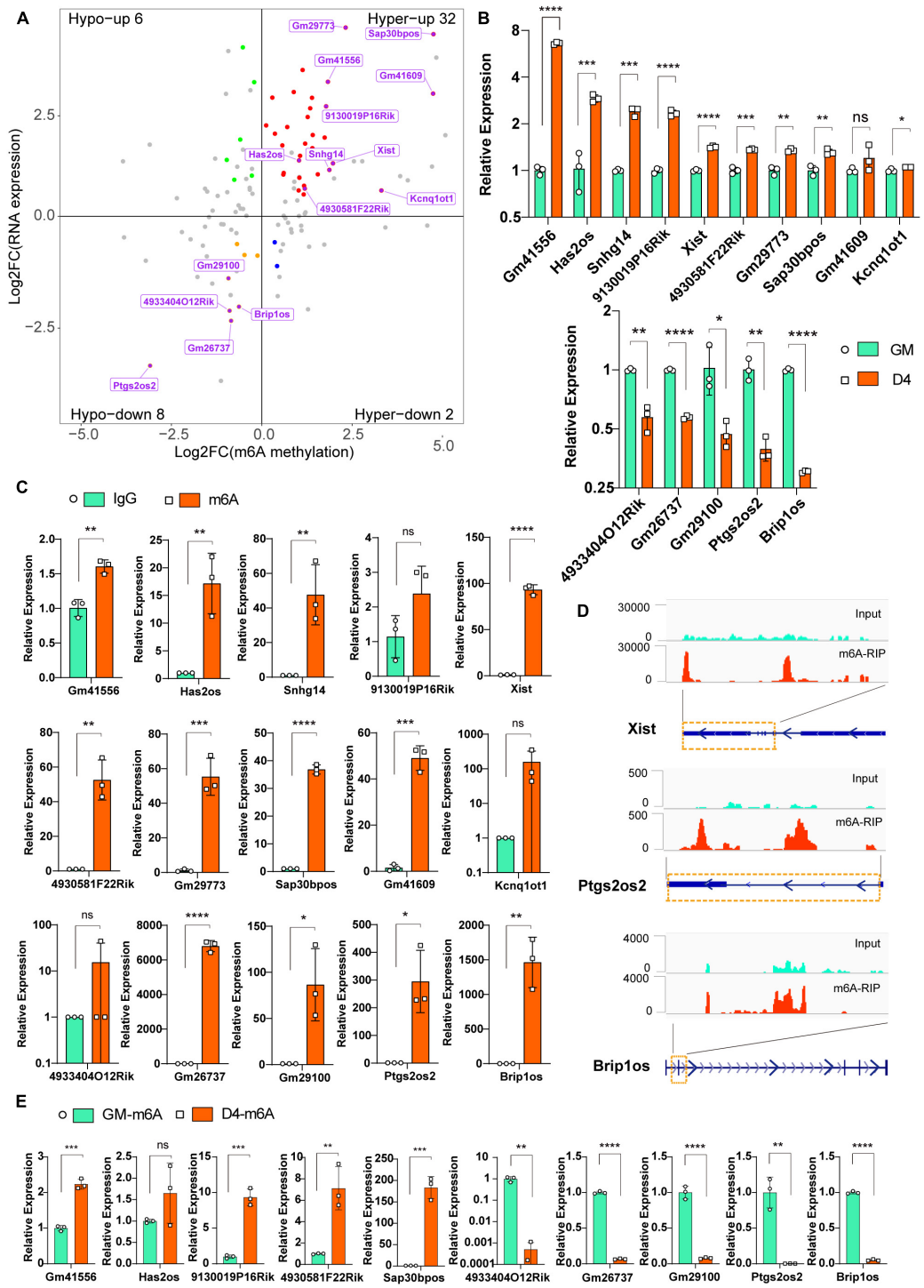


FIGURE 3 | Differentially m^{6}A modified lncRNAs in undifferentiated and differentiated muscle. **(A)** Distribution of genes with a significant change in both the m^{6}A methylation and RNA expression levels before (GM) and after differentiation (D4), different colors were used to identify representative genes. And 15 m^{6}A methylated significantly differently expressed lncRNAs were marked. **(B)** qRT-PCR validated the 15 m^{6}A methylated significantly differently expressed lncRNAs in developing muscle cells. **(C)** Real-time PCR detection of the expression of the 15 m^{6}A methylated significantly differently expressed lncRNAs in immunoprecipitated RNAs. IgG Immunoprecipitation was used as negative control. Quantitative data was represented as Mean ± SD; *p* value: $^*p < 0.05$, $^{**}p < 0.01$, $^{***}p < 0.001$, $^{****}p < 0.0001$. ns, no significant difference. **(D)** Integrative Genomics Viewer (IGV) plots show the m^{6}A peaks of lncRNA Xist, Ptgs2os2 and Brip1os were highly enriched in m^{6}A-RIP data. **(E)** Real-time PCR detection of the expression of the 5 hyper-upregulated and 5 hypo-downregulated lncRNAs in immunoprecipitated RNAs of GM and D4. Data were normalized by IgG Immunoprecipitation. Quantitative data was represented as Mean ± SD; *p* value: $^*p < 0.05$, $^{**}p < 0.01$, $^{***}p < 0.001$, $^{****}p < 0.0001$. ns, no significant difference.

TABLE 2 | Randomly selected 15 altered m^{6}A peaks in myoblasts and differentiated myotube.

Chr	Peak_start	Peak_end	Strand	Ensembl_ID	Gene_Name	RNA-seq_log2FoldChange	RNA-seq_padj	MeRIP-seq_diff.log2.fc	MeRIP-seq_diff.lg.fdr	Gene_Type	Group
11	115946568	115946986	–	ENSMUSG00000087064	Sap30bpos	4.068002111	0.000201133	4.75	−1.71	antisense	Hyper-up
17	70800582	70800823	–	ENSMUSG00000117231	Gm41609	2.740191127	0.003528931	4.74	−1.37	processed_transcript	Hyper-up
7	143257440	143257921	–	ENSMUSG00000101609	Kcnq1ot1	0.575398413	0.013352397	3.31	−1.51	antisense	Hyper-up
8	123899672	123900620	+	ENSMUSG00000110547	Gm29773	4.214800444	4.74E-15	2.32	−3.89	antisense	Hyper-up
X	103469670	103469796	–	ENSMUSG00000086503	Xist	1.181915678	6.27E-20	1.97	−49	lincRNA	Hyper-up
7	59970257	59973787	–	ENSMUSG00000100826	Snhg14	1.035494247	0.000971565	1.87	−6.16	processed_transcript	Hyper-up
17	29059068	29059722	+	ENSMUSG00000117007	Gm41556	3.003943093	0.001225038	1.83	−1.4	lincRNA	Hyper-up
6	54269710	54270309	–	ENSMUSG00000073067	9130019P16Rik	2.455499081	2.29E-06	1.78	−1.7	processed_transcript	Hyper-up
9	35126228	35126888	+	ENSMUSG00000070315	4930581F22Rik	0.617762934	0.032115595	1.19	−5.53	processed_transcript	Hyper-up
15	56694041	56765501	+	ENSMUSG00000086541	Has2os	1.247150122	0.012876036	1.03	−6.52	processed_transcript	Hyper-up
1	150159072	150159782	–	ENSMUSG00000097754	Ptgs2os2	−3.338667012	1.71E-06	−3.09	−2.46	lincRNA	Hypo-down
1	91801436	91801917	–	ENSMUSG00000100980	Gm29100	−1.386873948	0.044030192	−0.922	−1.41	antisense	Hypo-down
5	136933475	136934126	+	ENSMUSG00000097908	4933404O12Rik	−2.110740583	6.83E-22	−0.891	−1.35	lincRNA	Hypo-down
9	44112922	44113191	+	ENSMUSG00000097467	Gm26737	−2.335487486	1.12E-07	−0.849	−1.99	antisense	Hypo-down
11	86209134	86209584	+	ENSMUSG00000085208	Brip1os	−2.020791677	2.06E-50	−0.631	−3.96	antisense	Hypo-down

m^{6}A-Methylated lncRNAs Regulate Nearby mRNAs and Contribute to Muscle Tissue Development

Previous studies have reported that lncRNAs function in various physiological and pathological processes by regulating their adjacent mRNAs, either positively or negatively (Engreitz et al., 2016). Thus, we analyzed the significantly differentially expressed lncRNAs (FDR $\leq$ 0.05) during myogenesis as well as their nearest 10 mRNAs (upstream and downstream 5, respectively, adjusted $P \leq 0.05$). GO analysis of biological processes for these mRNAs showed that 94 mRNAs were related to muscle tissue development (**Figure 6A**, adjusted $P \leq 0.05$). KEGG pathway enrichment analysis showed that the cell cycle and MAPK signaling pathways were significantly enriched (**Figure 6B**, adjusted $P \leq 0.05$), and such results are consistent with our previous studies showing that the JNK/MAPK and P38/MAPK signaling pathways play essential roles in myogenesis (Xie et al., 2018; Liu et al., 2021).

To confirm that m^{6}A-methylated lncRNAs could regulate their adjacent mRNAs, we performed a synthetic analysis of 94 muscle tissue development-related mRNAs and nearby m^{6}A-methylated lncRNAs. Briefly, given that nearby lncRNAs of these 94 mRNAs have significantly different expression, we further estimated m^{6}A difference of these lncRNAs between GM and D4. As a result, seven lncRNAs have a significant m^{6}A difference, and these lncRNAs also correspond to seven mRNAs (**Figure 6C**). Furthermore, mRNA expression of these paired adjacent mRNAs was tested, and qPCR results showed that Pi16, Cdon and Col14a1 were upregulated in D4 samples, consistent with their adjacent lncRNAs Gm41556, 4930581F22Rik, and Has2os, respectively. In contrast, Hdac4, Usp2 and Tbx2 were upregulated, which is an opposite effect compared with that noted in their adjacent lncRNAs (**Figure 6D**). These data indicated two opposite regulatory mechanisms between m^{6}A-methylated lncRNAs and their nearby mRNAs, including positive and retrograde regulation.

Next, we further confirmed the regulation between lncRNAs and their adjacent mRNAs by knocking down corresponding lncRNAs using siRNAs. As shown in **Figure 6E**, when lncRNAs Gm41556, 4930581F22Rik, and Has2os were knocked down, their adjacent mRNAs Pi16, Cdon and Col14a1 were downregulated correspondingly, verifying the positive regulation between these lncRNAs and their nearby mRNAs. In contrast, when lncRNA Brip1os was knocked down, its adjacent mRNA Tbx2 was significantly upregulated, suggesting negative regulation. Taken together, our results showed that knockdown of m^{6}A-methylated lncRNAs impacted the expression of their adjacent mRNAs and suggested that the functional relevance of m^{6}A-methylated lncRNAs by regulating their adjacent mRNAs.

The METTL3/m^{6}A/Brip1os/Tbx2 Axis in Muscle Development

Given that the lncRNA Brip1os exhibits markedly decreased expression and m^{6}A modification levels during myogenesis and a perfectly negative correlation is noted between Brip1os and

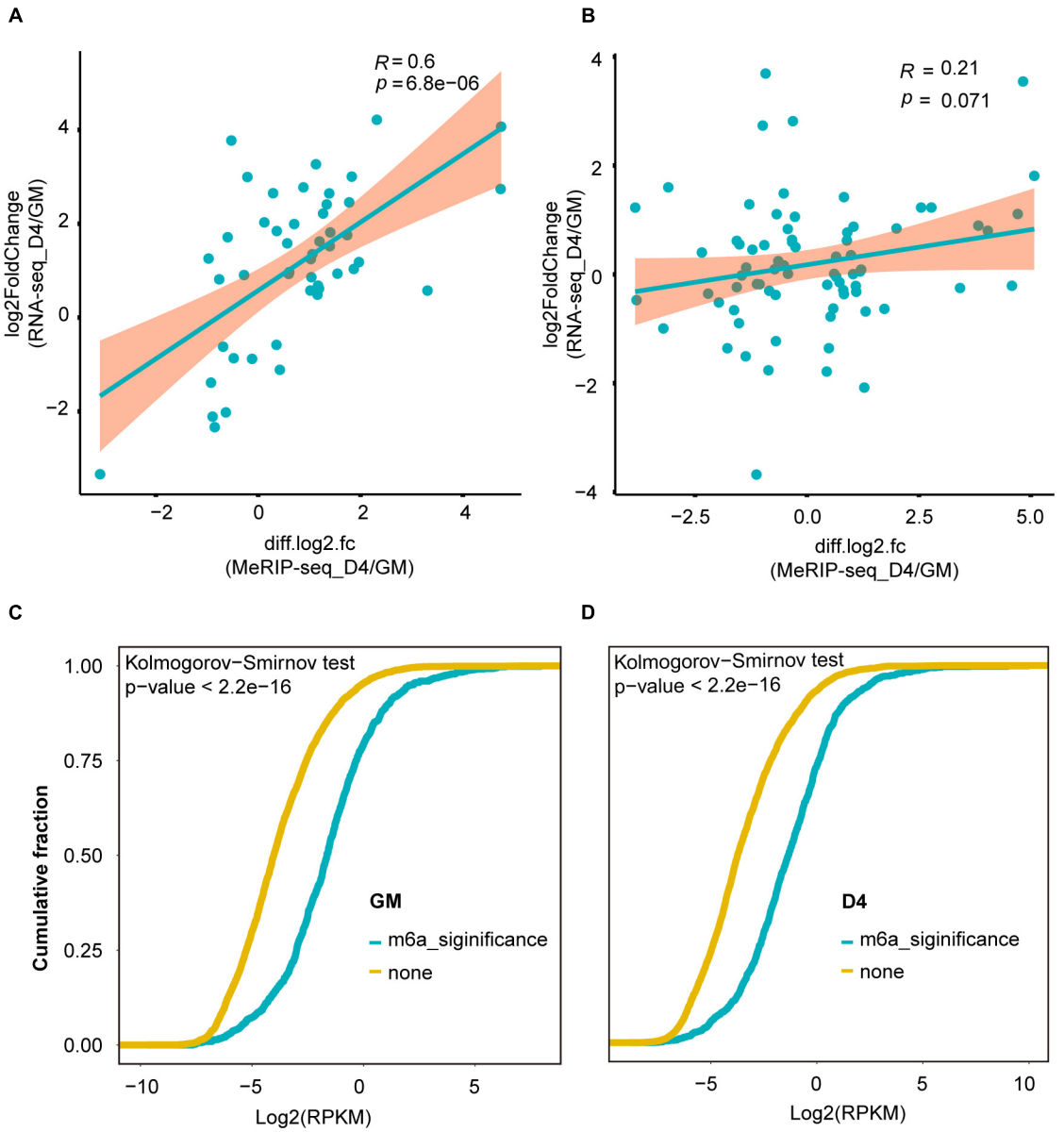


FIGURE 4 | m^{6}A methylation levels were positively correlated with the abundance of lncRNAs. **(A)** Scatter plot shows the positive correlation between m^{6}A levels (significant changes) and expression values of lncRNAs with significantly differential expression between GM and D4, adjusted $P \leq 0.05$. **(B)** Scatter plot shows no correlation between m^{6}A levels (no significant changes) and expression values of lncRNAs without significantly differential expression between GM and D4. **(C)** Cumulative frequency of log2FC for lncRNAs containing m^{6}A or without m^{6}A methylation in GM. Kolmogorov-Smirnov test was used to estimated inter-group difference. **(D)** Cumulative frequency of log2FC for lncRNAs containing m^{6}A or without m^{6}A methylation in D4. Kolmogorov-Smirnov test was used to estimated inter-group difference.

its nearby gene Tbx2, we further clarified their relationship. Brip1os and Tbx2 are both located at chr11qC, and these two transcription units have the same orientation. Brip1os is greater than 10 kb downstream of Tbx2 (359,435 bp) in the genome (**Figure 7A**). We further examined the expression of Tbx2 in muscle development by using single-cell RNA-seq data from Tabula Muris[1] and analyzed the expression levels in skeletal muscle satellite stem cell and smooth muscle cell groups, which could be considered generally representative of undifferentiated myoblasts and differentiated myotubes, respectively. Surprisingly, although there were 439 samples in the skeletal muscle satellite stem cell group and only 42 samples in the smooth muscle cell group, Tbx2 expression levels in the smooth muscle cell group were significantly greater than those in the skeletal muscle satellite stem cell group (**Figure 7B**). Such results implied that Tbx2 was upregulated

[1]http://genome.ucsc.edu

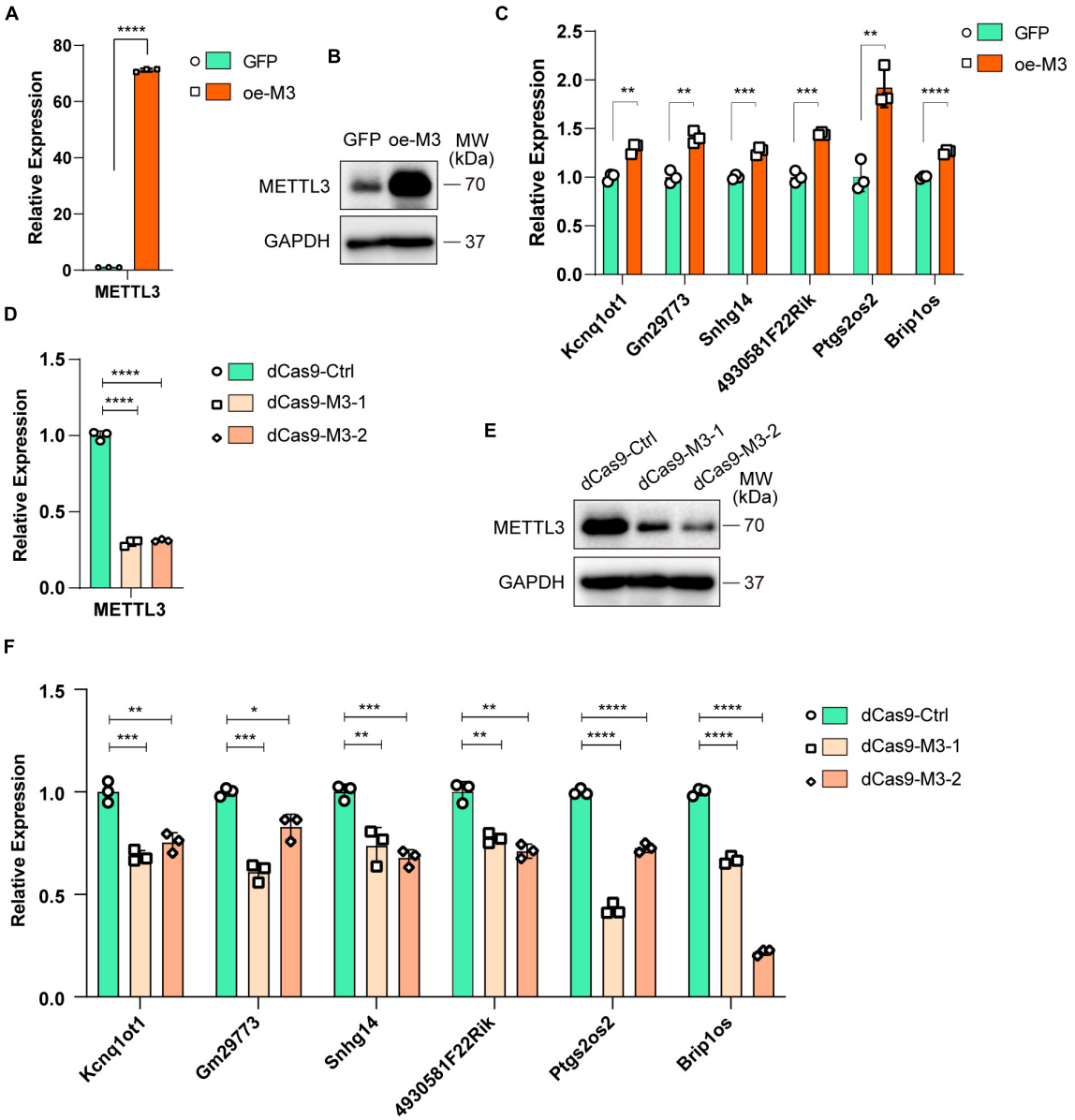


FIGURE 5 | Myogenesis associated lncRNAs are regulated by m^{6}A methyltransferase METTL3. **(A)** qRT-PCR shows the RNA expression level of METTL3 in METTL3-overexpressing C2C12 cells. GFP-overexpressing C2C12 cells as negative control. **(B)** Western blot detected the protein expression levels of METTL3 in METTL3-overexpressing C2C12 cells. **(C)** qRT-PCR shows the expression of myogenesis associated lncRNAs in METTL3-overexpressing C2C12 cells. **(D)** qRT-PCR shows the RNA expression level of METTL3 in METTL3 knockdown C2C12 stable cell lines. A nonsense sequence constructed to dCas9 repressor as negative control. **(E)** Western blot detected the protein expression levels of METTL3 in METTL3 knockdown C2C12 stable cell lines. **(F)** qRT-PCR shows the expression of myogenesis associated lncRNAs when METTL3 was knockdown. Data are presented as Mean ± SD; *p* value: $^*p < 0.05$, $^{**}p < 0.01$, $^{***}p < 0.001$, $^{****}p < 0.0001$.

during skeletal muscle development, which was consistent with our qPCR results.

As shown in **Figure 7C**, Brip1os was highly expressed in two GM samples and decreased in two D4 samples, in which Tbx2 exhibited the opposite trend (Pearson $R = -0.99$, $p = 0.009$). These results confirm their negative correlation with RNA expression. Next, we assessed whether METTL3 affects Tbx2 expression. As shown in **Figure 7D**, the Tbx2 mRNA levels were greatly downregulated when METTL3 was overexpressed. Accordingly, Tbx2 mRNA levels were upregulated when METTL3 was knocked down (**Figure 7E**). These results suggest that Tbx2 could be regulated by METTL3. Taken together, we validated the retrograde regulatory relationship between Brip1os and Tbx2 as well as their responsive reaction to changes in the m^{6}A methyltransferase METTL3.

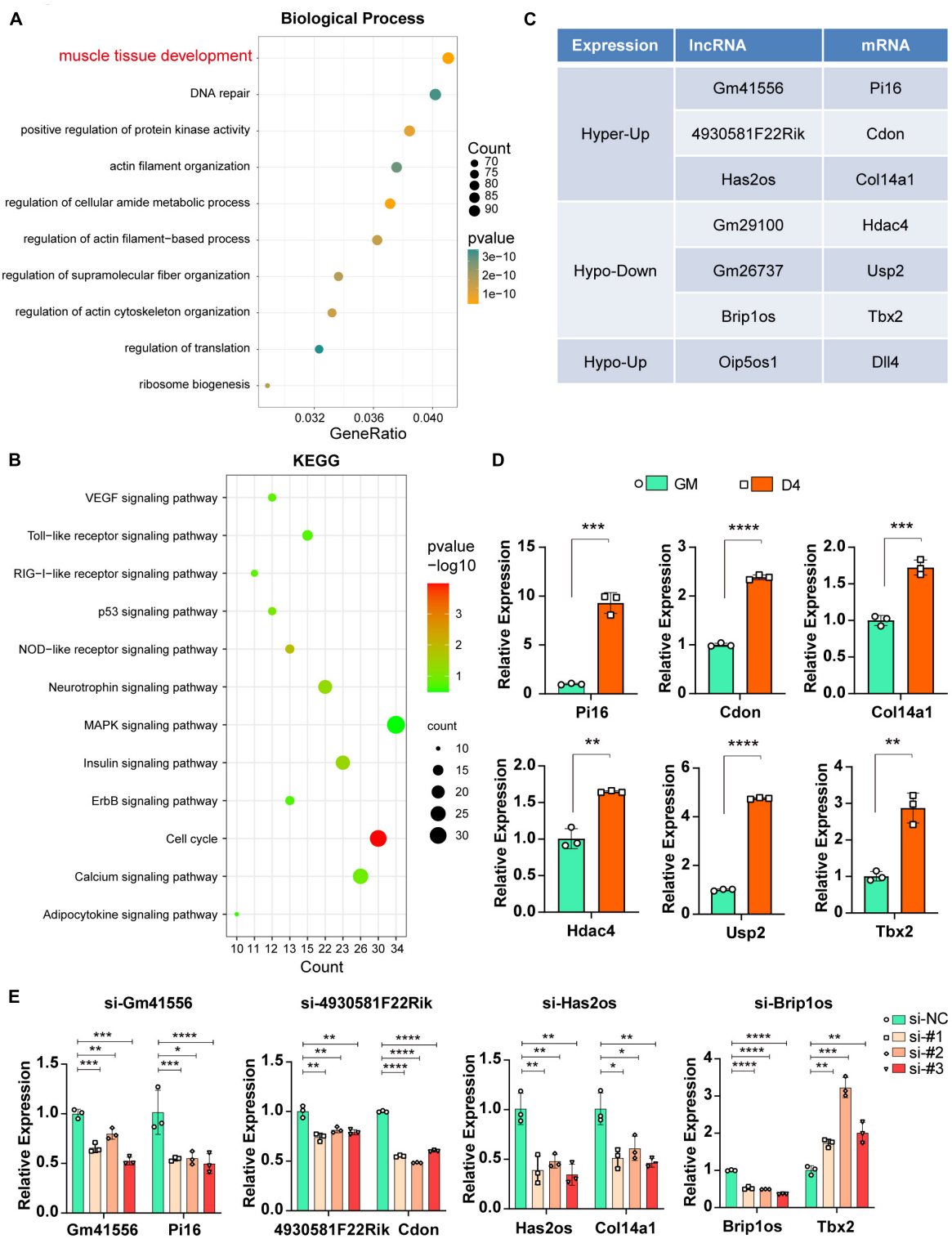


FIGURE 6 | Functional relevance between m^{6}A methylated lncRNAs and their adjacent mRNAs. **(A)** The top ten GO terms of the adjacent mRNAs (adjusted $P \leq 0.05$) that related to differentially expressed lncRNAs in muscle cells. **(B)** The top twelve KEGG pathways of the adjacent mRNAs (adjusted $P \leq 0.05$) that related to differentially expressed lncRNAs in muscle cells. **(C)** Table shows seven pairs of significantly differently expressed and methylated lncRNAs and their adjacent mRNAs in muscle cells. All have a significant threshold of FDR-adjusted *p* value ≤0.05. FDR, False Discovery Rate. **(D)** qRT-PCR shows the adjacent mRNA expression in GM and D4. **(E)** The effects of si-lncRNAs on the RNA expression levels of the corresponding lncRNA and mRNA. Data are presented as Mean ± SD; *p* value: $^*p < 0.05$, $^{**}p < 0.01$, $^{***}p < 0.001$, $^{****}p < 0.0001$.

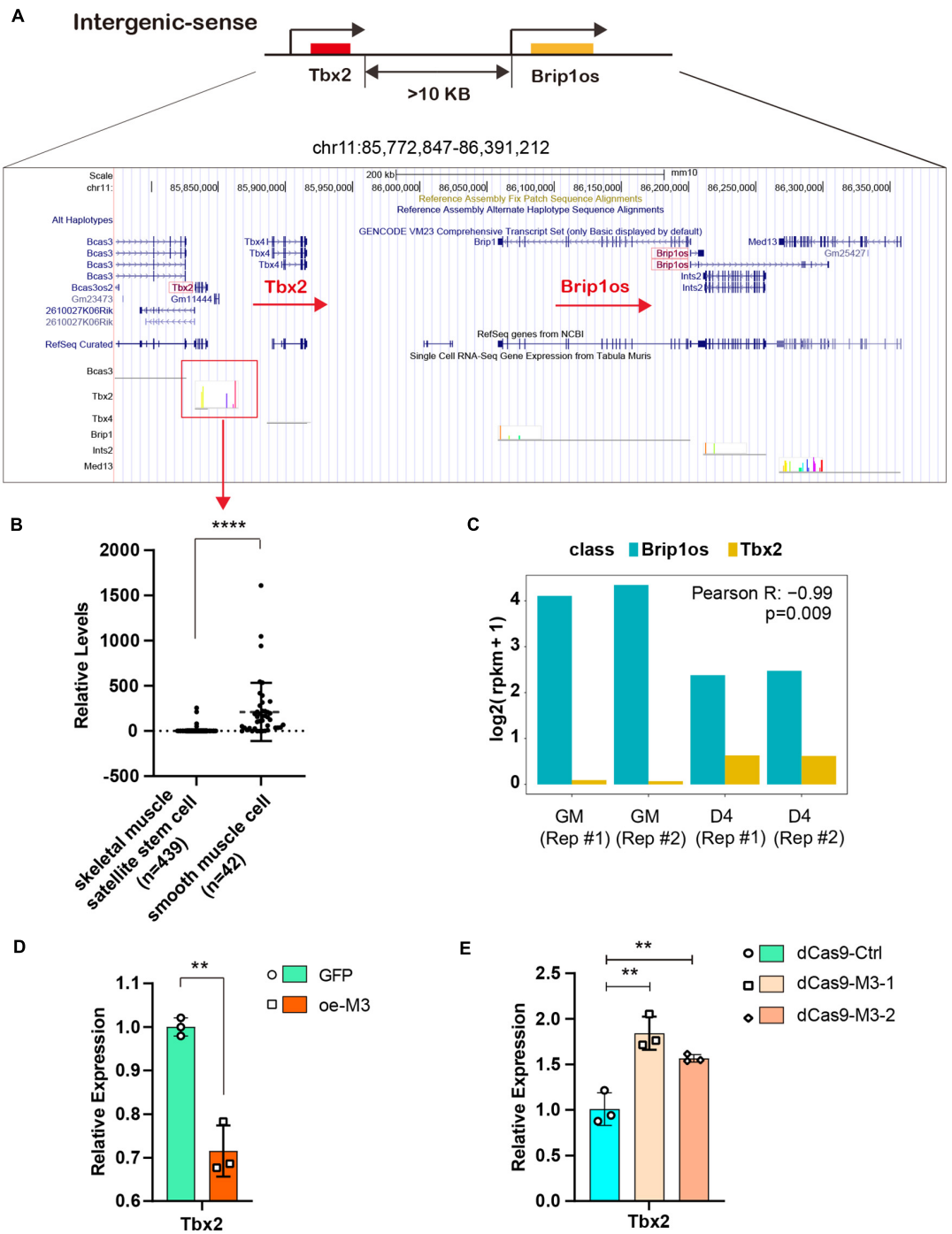


FIGURE 7 | METTL3/m^{6}A/Brip1os/Tbx2 axis in muscle development. **(A)** The genomic location of lncRNA Brip1os and its adjacent mRNA Tbx2. **(B)** Tbx2 expression data from public record of single cell RNA-seq gene expression of Tabula Muris data. **(C)** Brip1os and Tbx2 expression levels in our RNA-seq data. Pearson correlation analysis was performed to estimate expression correlation between two genes. **(D)** qRT-PCR shows the expression of Tbx2 when METTL3 overexpressed. **(E)** qRT-PCR shows the expression of Tbx2 when METTL3 was knockdown. Data are presented as Mean ± SD; *p* value: $^{**}p < 0.01$, $^{****}p < 0.0001$.

DISCUSSION

Skeletal muscle development is precisely regulated in a sophisticated spatiotemporal manner. Our previously identified changes in gene expression and epigenetic modifications during skeletal muscle development have greatly improved our understanding of the mechanism related to myogenesis, including coding gene and non-coding RNA modifications

(Diao et al., 2021a,b), mRNA expression (Tan et al., 2021), miRNA regulation (Xie et al., 2013, 2018), and lncRNA function (Liu et al., 2021). Taking advantage of the sequencing approach and gene annotation, a significant number of lncRNAs have been shown to play crucial roles in skeletal muscle development (Luo et al., 2021). Given the robust function of m^{6}A methylation, the functions of m^{6}A-modified mRNAs in the process of skeletal muscle development have been well studied, and the role of m^{6}A-modified non-coding RNAs has also been appreciated (Li et al., 2021). In the present study, we hypothesized that lncRNAs might also be modified by m^{6}A and participate in skeletal muscle differentiation. In the current study, we provided the first evidence that both the lncRNA transcriptome and m^{6}A epitranscriptome underwent highly dynamic changes throughout mouse skeletal muscle development. Such results are consistent with results from other studies investigating the role of m^{6}A-lncRNA in tissue development, such as those for mouse embryonic stem cell differentiation (Wang et al., 2014). Specifically, we observed that m^{6}A methylation levels of lncRNAs are positively correlated with the transcript abundance of lncRNAs. Moreover, our studies revealed that lncRNAs exhibit pairwise expression correlations with neighboring mRNAs. Our results highlight a potential role of m^{6}A-modified lncRNAs during skeletal muscle development.

LncRNAs are more cell-specific than other RNAs, and their expression models are not completely understood. Given that m^{6}A is a ubiquitous modification in RNAs and regulates gene expression, we systematically identified m^{6}A-modified lncRNAs and uncovered the m^{6}A marks affecting the expression of lncRNAs. Our data showed that for lncRNAs with significant expression abundance changes, their m^{6}A levels were positively correlated with their expression levels. However, for lncRNAs without significant transcript abundance changes, no significant correlation was noted between their m^{6}A levels and expression levels. These results were further verified by overexpression or knockdown of the m^{6}A core methyltransferase METTL3.

Due to the poor conservation of lncRNAs, their function and regulatory mechanisms are not completely understood. It is known that lncRNAs can regulate the expression of neighboring genes by cis-acting mechanisms (Lee, 2012). Mancini-DiNardo et al. clarified that elongation of the Kcnq1ot1 transcript is required for genomic imprinting of neighboring genes (Mancini-DiNardo et al., 2006). Furthermore, Ponjavic et al. noted that spatiotemporal coexpression of ncRNAs and nearby protein-coding genes represents a general phenomenon and presented substantive and predictive criteria for prioritizing lncRNA and mRNA transcript pairs when investigating their biological functions (Ponjavic et al., 2009). This information led us to hypothesize that m^{6}A-methylated lncRNAs regulate nearby mRNAs and contribute to muscle tissue development. This hypothesis was supported by our computational analysis and experimental results. In particular, Brip1os is the most significantly differentially expressed and m^{6}A-modified lncRNA, and its nearby mRNA Tbx2 plays an important function in muscle tissue development. The change in Tbx2 mRNA expression was opposite to that of Brip1os in D4 compared to GM. These findings indicate that they exhibit a retrograde regulatory relationship, which was verified using a public dataset. In addition, it has been known for decades that Tbx (T-Box) genes play crucial roles in limb development (Zhu et al., 2014; Pflugfelder et al., 2017). Further studies on their regulation are warranted. Our analysis provided candidate lncRNAs and mRNAs for further examination of the gene regulation network in muscle development.

The transition from myoblast proliferation to differentiation is accompanied by drastic alterations in the transcriptome. Transcriptional changes influencing muscle status are affected by a number of processes involving DNA, RNA and proteins. This study uncovered the differential expression and m^{6}A methylation status of lncRNAs with temporal-specific expression in developing muscle. Surprisingly, we found no differences in the methylation of lncRNAs that drive myoblast state changes, such as linc-MD1 (Cesana et al., 2011) or lncMyoD (Dong et al., 2020), suggesting that these lncRNAs are not direct targets of dynamic m^{6}A modification. Kcnq1ot1, a differentially expressed and m^{6}A-enriched lncRNA identified in our study, participates in the regulation of genes within the Kcnq1 imprinting domain (Zhang et al., 2014) and controls maternal p57 expression in muscle cells by promoting H3K27me3 accumulation in an intragenic MyoD-binding region (Andresini et al., 2019). Intriguingly, of the top m^{6}A-enriched lncRNA transcripts in GM and in D4, many have not been previously linked to myoblast/myotube function but have been reported to be involved in other cell types. For example, Snhg14 (small nucleolar RNA host gene 14) is expressed at elevated levels among the top ten differentially m^{6}A-enriched lncRNAs in D4 compared to GM. Snhg14 is highly expressed in Parkinson's disease, and silencing Sngh14 mitigated dopaminergic neuron injury by downregulating a-syn by targeting miR-133b (Zhang et al., 2019). In addition, Sngh14 functions as a ceRNA in Ang II-induced cardiomyocytes to sponge both miR-322-5p and miR-384-5p to elevate PCDH17 levels (Long et al., 2020). The function of m^{6}A-modified lncRNAs during skeletal muscle development needs to be further studied.

In summary, we described the expression and m^{6}A methylation profiles of lncRNAs that display temporal expression in mouse myoblasts and differentiated myotubes. Our findings provide new insight into the pivotal regulatory role of m^{6}A-modified lncRNAs in muscle development. Our data uncovered the novel posttranscriptional regulation underlying muscle differentiation and provide a molecular basis for further studies to determine the function and mechanism of m^{6}A-lncRNAs in skeletal muscle development and muscle-related diseases.

DATA AVAILABILITY STATEMENT

The datasets presented in this study can be found in online repositories. The names of the repository/repositories and accession number(s) can be found in the article/**Supplementary Material**.

ETHICS STATEMENT

The animal study was reviewed and approved by the Institutional Animal Care and Use Committee of Sun Yat-sen University.

AUTHOR CONTRIBUTIONS

S-JX, Z-DX, QZ, and Y-WP conceived and designed this project. S-JX, ST, and L-TD performed the experiments with the help of Y-XH, Y-RH, HL and, W-YX. S-JX, W-JC, Z-GZ, P-LL, and W-CC analyzed the data. S-JX, Z-DX, ST, L-TD, Y-WP, and QZ wrote the manuscript. All authors contributed to the article and approved the submitted version.

FUNDING

This work was supported by grants from the Natural Science Foundation of Guangdong Province (2021A1515010477), the National Natural Science Foundation of China (31701116, 81974436, 81900559, 81870449, 81770651, 82170674, and 82170216), the Program for Guangdong Introducing Innovative and Entrepreneurial Teams (2019ZT08Y485), Guangzhou Science and Technology Plan Projects (202102020104), the Key-Area Research and Development Program of Guangdong Province (2019B020236004 and 2019B020235002), and the Guangdong Province Key Laboratory of Malignant Tumor Epigenetics and Gene Regulation (2020B1212060018).

ACKNOWLEDGMENTS

The authors would like to thank Zelin Wang (Shuzhi Biotech, LLC, Guangzhou) who assisted our efforts in analyzing the sequencing data used in this study.

SUPPLEMENTARY MATERIAL

The Supplementary Material for this article can be found online at: https://www.frontiersin.org/articles/10.3389/fcell.2021.762669/full#supplementary-material

REFERENCES

Alarcón, C. R., Lee, H., Goodarzi, H., Halberg, N., and Tavazoie, S. F. (2015). N6-methyladenosine marks primary microRNAs for processing. *Nature* 519, 482–485. doi: 10.1038/nature14281

Andresini, O., Rossi, M. N., Matteini, F., Petrai, S., Santini, T., and Maione, R. (2019). The long non-coding RNA Kcnq1ot1 controls maternal p57 expression in muscle cells by promoting H3K27me3 accumulation to an intragenic MyoD-binding region. *Epigenetics Chromatin* 12:8. doi: 10.1186/s13072-019-0253-1

Bentzinger, C. F., Wang, Y. X., and Rudnicki, M. A. (2012). Building muscle: molecular regulation of myogenesis. *Cold Spring Harb. Perspect. Biol.* 4:a008342. doi: 10.1101/cshperspect.a008342

Borensztein, M., Monnier, P., Court, F., Louault, Y., Ripoche, M. A., Tiret, L., et al. (2013). Myod and H19-Igf2 locus interactions are required for diaphragm formation in the mouse. *Development* 140, 1231–1239. doi: 10.1242/dev.084665

Bryson-Richardson, R. J., and Currie, P. D. (2008). The genetics of vertebrate myogenesis. *Nat. Rev. Genet.* 9, 632–646. doi: 10.1038/nrg2369

Cesana, M., Cacchiarelli, D., Legnini, I., Santini, T., Sthandier, O., Chinappi, M., et al. (2011). A long noncoding RNA controls muscle differentiation by functioning as a competing endogenous RNA. *Cell* 147, 358–369. doi: 10.1016/j.cell.2011.09.028

Chen, L. L., and Carmichael, G. G. (2010). Decoding the function of nuclear long non-coding RNAs. *Curr. Opin. Cell Biol.* 22, 357–364. doi: 10.1016/j.ceb.2010.03.003

Chen, T., Hao, Y. J., Zhang, Y., Li, M. M., Wang, M., Han, W., et al. (2015). m(6)A RNA methylation is regulated by microRNAs and promotes reprogramming to pluripotency. *Cell Stem Cell* 16, 289–301. doi: 10.1016/j.stem.2015.01.016

Cong, X. X., Gao, X. K., Rao, X. S., Wen, J., Liu, X. C., Shi, Y. P., et al. (2020). Rab5a activates IRS1 to coordinate IGF-AKT-mTOR signaling and myoblast differentiation during muscle regeneration. *Cell Death Differ.* 27, 2344–2362. doi: 10.1038/s41418-020-0508-1

Cui, X., Wei, Z., Zhang, L., Liu, H., Sun, L., Zhang, S. W., et al. (2016). Guitar: an R/Bioconductor package for gene annotation guided transcriptomic analysis of RNA-related genomic features. *Biomed. Res. Int.* 2016:8367534. doi: 10.1155/2016/8367534

Diao, L. T., Xie, S. J., Lei, H., Qiu, X. S., Huang, M. C., Tao, S., et al. (2021a). METTL3 regulates skeletal muscle specific miRNAs at both transcriptional and post-transcriptional levels. *Biochem. Biophys. Res. Commun.* 552, 52–58. doi: 10.1016/j.bbrc.2021.03.035

Diao, L. T., Xie, S. J., Yu, P. J., Sun, Y. J., Yang, F., Tan, Y. Y., et al. (2021b). N-methyladenine demethylase ALKBH1 inhibits the differentiation of skeletal muscle. *Exp. Cell Res.* 400:112492. doi: 10.1016/j.yexcr.2021.112492

Dong, A., Preusch, C. B., So, W.-K., Lin, K., Luan, S., Yi, R., et al. (2020). A long noncoding RNA,LncMyoD, modulates chromatin accessibility to regulate muscle stem cell myogenic lineage progression. *Proc. Natl. Acad. Sci.* 117, 32464–32475. doi: 10.1073/pnas.2005868117

Engreitz, J. M., Haines, J. E., Perez, E. M., Munson, G., Chen, J., Kane, M., et al. (2016). Local regulation of gene expression by lncRNA promoters, transcription and splicing. *Nature* 539, 452–455. doi: 10.1038/nature20149

Fazi, F., and Fatica, A. (2019). Interplay between N (6)-methyladenosine (m(6)A) and non-coding RNAs in cell development and cancer. *Front. Cell Dev. Biol.* 7:116. doi: 10.3389/fcell.2019.00116

Fu, Y., Dominissini, D., Rechavi, G., and He, C. (2014). Gene expression regulation mediated through reversible m(6)A RNA methylation. *Nat. Rev. Genet.* 15, 293–306. doi: 10.1038/nrg3724

Gheller, B. J., Blum, J. E., Fong, E. H. H., Malysheva, O. V., Cosgrove, B. D., and Thalacker-Mercer, A. E. (2020). A defined N6-methyladenosine (m^{6}A) profile conferred by METTL3 regulates muscle stem cell/myoblast state transitions. *Cell Death Discov.* 6:95. doi: 10.1038/s41420-020-00328-5

Gong, C., Li, Z., Ramanujan, K., Clay, I., Zhang, Y., Lemire-Brachat, S., et al. (2015). A long non-coding RNA, LncMyoD, regulates skeletal muscle differentiation by blocking IMP2-mediated mRNA translation. *Dev. Cell* 34, 181–191. doi: 10.1016/j.devcel.2015.05.009

He, R. Z., Jiang, J., and Luo, D. X. (2020). The functions of N6-methyladenosine modification in lncRNAs. *Genes Dis.* 7, 598–605. doi: 10.1016/j.gendis.2020.03.005

Heinz, S., Benner, C., Spann, N., Bertolino, E., Lin, Y. C., Laslo, P., et al. (2010). Simple combinations of lineage-determining transcription factors prime cis-regulatory elements required for macrophage and B cell identities. *Mol. Cell* 38, 576–589. doi: 10.1016/j.molcel.2010.05.004

Helm, M., and Motorin, Y. (2017). Detecting RNA modifications in the epitranscriptome: predict and validate. *Nat. Rev. Genet.* 18, 275–291. doi: 10.1038/nrg.2016.169

Hitachi, K., Nakatani, M., Takasaki, A., Ouchi, Y., Uezumi, A., Ageta, H., et al. (2019). *Myogenin* promoter-associated lncRNA *Myoparr* is essential for myogenic differentiation. *EMBO Rep.* 20:e47468. doi: 10.15252/embr.201847468

Kan, R. L., Chen, J., and Sallam, T. (2021). Crosstalk between epitranscriptomic and epigenetic mechanisms in gene regulation. *Trends Genet.* 19:S0168-9525(21)00170-0. doi: 10.1016/j.tig.2021.06.014

Kechin, A., Boyarskikh, U., Kel, A., and Filipenko, M. (2017). cutPrimers: a new tool for accurate cutting of primers from reads of targeted next generation sequencing. *J. Comput. Biol.* 24, 1138–1143. doi: 10.1089/cmb.2017.0096

Kim, D., Paggi, J. M., Park, C., Bennett, C., and Salzberg, S. L. (2019). Graph-based genome alignment and genotyping with HISAT2 and HISAT-genotype. *Nat. Biotechnol.* 37, 907–915. doi: 10.1038/s41587-019-0201-4

Kudou, K., Komatsu, T., Nogami, J., Maehara, K., Harada, A., Saeki, H., et al. (2017). The requirement of Mettl3-promoted MyoD mRNA maintenance in proliferative myoblasts for skeletal muscle differentiation. *Open Biol.* 7:170119. doi: 10.1098/rsob.170119

Lan, Y., Liu, B., and Guo, H. (2021). The role of m^{6}A modification in the regulation of tumor-related lncRNAs. *Mol. Ther. Nucleic Acids* 24, 768–779. doi: 10.1016/j.omtn.2021.04.002

Lee, J. T. (2012). Epigenetic regulation by long noncoding RNAs. *Science* 338, 1435–1439. doi: 10.1126/science.1231776

Li, H., Handsaker, B., Wysoker, A., Fennell, T., Ruan, J., Homer, N., et al. (2009). The sequence alignment/map format and SAMtools. *Bioinformatics* 25, 2078–2079. doi: 10.1093/bioinformatics/btp352

Li, J., Pei, Y., Zhou, R., Tang, Z., and Yang, Y. (2021). Regulation of RNA N6-methyladenosine modification and its emerging roles in skeletal muscle development. *Int. J. Biol. Sci.* 17, 1682–1692. doi: 10.7150/ijbs.56251

Liang, Y., Han, H., Xiong, Q., Yang, C., Wang, L., Ma, J., et al. (2021). METTL3-mediated m^{6}A methylation regulates muscle stem cells and muscle regeneration by notch signaling pathway. *Stem Cells Int.* 2021:9955691. doi: 10.1155/2021/9955691

Liao, Y., Smyth, G. K., and Shi, W. (2014). featureCounts: an efficient general purpose program for assigning sequence reads to genomic features. *Bioinformatics* 30, 923–930. doi: 10.1093/bioinformatics/btt656

Lim, Y. H., Ryu, J., Kook, H., and Kim, Y. K. (2020). Identification of long noncoding RNAs involved in differentiation and survival of vascular smooth muscle cells. *Mol. Ther. Nucleic Acids* 22, 209–221. doi: 10.1016/j.omtn.2020.08.032

Lin, J., Zhu, Q., Huang, J., Cai, R., and Kuang, Y. (2020). Hypoxia promotes vascular smooth muscle cell (VSMC) differentiation of adipose-derived stem cell (ADSC) by regulating Mettl3 and paracrine factors. *Stem Cells Int.* 2020:2830565. doi: 10.1155/2020/2830565

Liu, J., Li, K., Cai, J., Zhang, M., Zhang, X., Xiong, X., et al. (2020). Landscape and regulation of m(6)A and m(6)Am methylome across human and mouse tissues. *Mol. Cell* 77, 426–440.e6. doi: 10.1016/j.molcel.2019.09.032

Liu, N., Dai, Q., Zheng, G., He, C., Parisien, M., and Pan, T. (2015). N6-methyladenosine-dependent RNA structural switches regulate RNA–protein interactions. *Nature* 518, 560–564. doi: 10.1038/nature14234

Liu, S., Xie, S., Chen, H., Li, B., Chen, Z., Tan, Y., et al. (2021). The functional analysis of transiently upregulated miR-101 suggests a "braking" regulatory mechanism during myogenesis. *Sci. China Life Sci.* 64, 1–12. doi: 10.1007/s11427-020-1856-5

Long, Y., Wang, L., and Li, Z. (2020). SP1-induced SNHG14 aggravates hypertrophic response in in vitro model of cardiac hypertrophy via up-regulation of PCDH17. *J. Cell. Mol. Med.* 24, 7115–7126. doi: 10.1111/jcmm.15073

Love, M. I., Huber, W., and Anders, S. (2014). Moderated estimation of fold change and dispersion for RNA-seq data with DESeq2. *Genome Biol.* 15:550. doi: 10.1186/s13059-014-0550-8

Lu, L., Sun, K., Chen, X., Zhao, Y., Wang, L., Zhou, L., et al. (2013). Genome-wide survey by ChIP-seq reveals YY1 regulation of lincRNAs in skeletal myogenesis. *EMBO J.* 32, 2575–2588. doi: 10.1038/emboj.2013.182

Luo, H., Lv, W., Tong, Q., Jin, J., Xu, Z., and Zuo, B. (2021). Functional non-coding RNA during embryonic myogenesis and postnatal muscle development and disease. *Front. Cell Dev. Biol.* 9: 628339. doi: 10.3389/fcell.2021.628339

Lv, W., Jin, J., Xu, Z., Luo, H., Guo, Y., Wang, X., et al. (2020). lncMGPF is a novel positive regulator of muscle growth and regeneration. *J. Cachexia Sarcopenia Muscle* 11, 1723–1746. doi: 10.1002/jcsm.12623

Ma, S., Chen, C., Ji, X., Liu, J., Zhou, Q., Wang, G., et al. (2019). The interplay between m^{6}A RNA methylation and noncoding RNA in cancer. *J. Hematol. Oncol.* 12:121. doi: 10.1186/s13045-019-0805-7

Mancini-DiNardo, D., Steele, S. J. S., Levorse, J. M., Ingram, R. S., and Tilghman, S. M. (2006). Elongation of the Kcnq1ot1 transcript is required for genomic imprinting of neighboring genes. *Gene Dev.* 20, 1268–1282. doi: 10.1101/gad.1416906

Martinet, C., Monnier, P., Louault, Y., Benard, M., Gabory, A., and Dandolo, L. (2016). H19 controls reactivation of the imprinted gene network during muscle regeneration. *Development* 143, 962–971. doi: 10.1242/dev.131771

Martone, J., Mariani, D., Desideri, F., and Ballarino, M. (2020). Non-coding RNAs shaping muscle. *Front. Cell Dev. Biol.* 7:394. doi: 10.3389/fcell.2019.00394

Meng, J., Cui, X., Rao, M. K., Chen, Y., and Huang, Y. (2013). Exome-based analysis for RNA epigenome sequencing data. *Bioinformatics* 29, 1565–1567. doi: 10.1093/bioinformatics/btt171

Meyer, K. D., and Jaffrey, S. R. (2017). Rethinking m(6)A readers, writers, and erasers. *Annu. Rev. Cell Dev. Biol.* 33, 319–342. doi: 10.1146/annurev-cellbio-100616-060758

Milligan, L., Antoine, E., Bisbal, C., Weber, M., Brunel, C., Forne, T., et al. (2000). H19 gene expression is up-regulated exclusively by stabilization of the RNA during muscle cell di€erentiation. *Oncogene* 19, 5810–5816.

Pan, T. (2013). N6-methyl-adenosine modification in messenger and long non-coding RNA. *Trends Biochem. Sci.* 38, 204–209. doi: 10.1016/j.tibs.2012.12.006

Patil, D. P., Chen, C. K., Pickering, B. F., Chow, A., Jackson, C., Guttman, M., et al. (2016). m(6)A RNA methylation promotes XIST-mediated transcriptional repression. *Nature* 537, 369–373. doi: 10.1038/nature19342

Pflugfelder, G. O., Eichinger, F., and Shen, J. (2017). T-Box genes in *Drosophila* limb development. *Curr. Top. Dev. Biol.* 122, 313–354. doi: 10.1016/bs.ctdb.2016.08.003

Ping, X. L., Sun, B. F., Wang, L., Xiao, W., Yang, X., Wang, W. J., et al. (2014). Mammalian WTAP is a regulatory subunit of the RNA N6-methyladenosine methyltransferase. *Cell Res.* 24, 177–189. doi: 10.1038/cr.2014.3

Ponjavic, J., Oliver, P. L., Lunter, G., and Ponting, C. P. (2009). Genomic and transcriptional co-localization of protein-coding and long non-coding RNA pairs in the developing brain. *PLoS Genet.* 5:e1000617. doi: 10.1371/journal.pgen.1000617

Quinlan, A. R., and Hall, I. M. (2010). BEDTools: a flexible suite of utilities for comparing genomic features. *Bioinformatics* 26, 841–842. doi: 10.1093/bioinformatics/btq033

Ramírez, F., Dündar, F., Diehl, S., Grüning, B. A., and Manke, T. (2014). deepTools: a flexible platform for exploring deep-sequencing data. *Nucleic Acids Res.* 42, W187–W191. doi: 10.1093/nar/gku365

Ro, S., Lim, Y.-H., Kwon, D.-H., Kim, J., Park, W. J., Kook, H., et al. (2018). Identification of long noncoding RNAs involved in muscle differentiation. *PLos One* 13:e0193898. doi: 10.1371/journal.pone.0193898

Robinson, J. T., Thorvaldsdóttir, H., Winckler, W., Guttman, M., Lander, E. S., Getz, G., et al. (2011). Integrative genomics viewer. *Nat. Biotechnol.* 29, 24–26. doi: 10.1038/nbt.1754

Roundtree, I. A., Evans, M. E., Pan, T., and He, C. (2017). Dynamic RNA modifications in gene expression regulation. *Cell* 169, 1187–1200. doi: 10.1016/j.cell.2017.05.045

Shi, H., Wei, J., and He, C. (2019). Where, when, and how: context-dependent functions of RNA methylation writers, readers, and erasers. *Mol. Cell* 74, 640–650. doi: 10.1016/j.molcel.2019.04.025

Sui, Y., Han, Y., Zhao, X., Li, D., and Li, G. (2019). Long non-coding RNA Irm enhances myogenic differentiation by interacting with MEF2D. *Cell Death Dis.* 10:181. doi: 10.1038/s41419-019-1399-2

Sweta, S., Dudnakova, T., Sudheer, S., Baker, A. H., and Bhushan, R. (2019). Importance of long non-coding RNAs in the development and disease of skeletal muscle and cardiovascular lineages. *Front. Cell Dev. Biol.* 7:228. doi: 10.3389/fcell.2019.00228

Tan, Y.-Y., Zhang, Y., Li, B., Ou, Y.-W., Xie, S.-J., Chen, P.-P., et al. (2021). PERK signaling controls myoblast differentiation by regulating microRNA networks. *Front. Cell Dev. Biol.* 9:670435. doi: 10.3389/fcell.2021.670435

Ulitsky, I., and Bartel, D. P. (2013). lincRNAs: genomics, evolution, and mechanisms. *Cell* 154, 26–46. doi: 10.1016/j.cell.2013.06.020

Wang, L., Zhao, Y., Bao, X., Zhu, X., Kwok, Y.K.-y, Sun, K., et al. (2015). LncRNA dum interacts with dnmts to regulate Dppa2 expression during myogenic differentiation and muscle regeneration. *Cell Res.* 25, 335–350. doi: 10.1038/cr.2015.21

Wang, X., Huang, N., Yang, M., Wei, D., Tai, H., Han, X., et al. (2017). FTO is required for myogenesis by positively regulating mTOR-PGC-1alpha pathway-mediated mitochondria biogenesis. *Cell Death Dis.* 8:e2702. doi: 10.1038/cddis.2017.122

Wang, Y., Li, Y., Toth, J. I., Petroski, M. D., Zhang, Z., and Zhao, J. C. (2014). N6-methyladenosine modification destabilizes developmental regulators in embryonic stem cells. *Nat. Cell Biol.* 16, 191–198. doi: 10.1038/ncb2902

Xie, S., Zhang, Y., Qu, L., and Xu, H. (2013). A helm model for microRNA regulation in cell fate decision and conversion. *Sci. China Life Sci.* 56, 897–906. doi: 10.1007/s11427-013-4547-4

Xie, S. J., Diao, L. T., Cai, N., Zhang, L. T., Xiang, S., Jia, C. C., et al. (2021a). mascRNA and its parent lncRNA MALAT1 promote proliferation and metastasis of hepatocellular carcinoma cells by activating ERK/MAPK signaling pathway. *Cell Death Discov.* 7:110. doi: 10.1038/s41420-021-00497-x

Xie, S.-J., Lei, H., Yang, B., Diao, L.-T., Liao, J.-Y., He, J.-H., et al. (2021b). Dynamic m^{6}A mRNA methylation reveals the role of METTL3/14-m6A-MNK2-ERK signaling axis in skeletal muscle differentiation and regeneration. *Front. Cell Dev. Biol.* 38, 4755–4772. doi: 10.3389/fcell.2021.744171

Xie, S.-J., Li, J.-H., Chen, H.-F., Tan, Y.-Y., Liu, S.-R., Zhang, Y., et al. (2018). Inhibition of the JNK/MAPK signaling pathway by myogenesis-associated miRNAs is required for skeletal muscle development. *Cell Death Differ.* 25, 1581–1597. doi: 10.1038/s41418-018-0063-1

Yang, D., Qiao, J., Wang, G., Lan, Y., Li, G., Guo, X., et al. (2018). N6-Methyladenosine modification of lincRNA 1281 is critically required for mESC differentiation potential. *Nucleic Acids Res.* 46, 3906–3920. doi: 10.1093/nar/gky130

Yang, Y., Hsu, P. J., Chen, Y. S., and Yang, Y. G. (2018). Dynamic transcriptomic m(6)A decoration: writers, erasers, readers and functions in RNA metabolism. *Cell Res.* 28, 616–624. doi: 10.1038/s41422-018-0040-8

Yong, H., Wu, G., Chen, J., Liu, X., Bai, Y., Tang, N., et al. (2020). lncRNA MALAT1 accelerates skeletal muscle cell apoptosis and inflammatory response in sepsis by decreasing BRCA1 expression by recruiting EZH2. *Mol. Ther. Nucleic Acids* 19, 97–108. doi: 10.1016/j.omtn.2019.10.028

Yu, G., Wang, L. G., Han, Y., and He, Q. Y. (2012). clusterProfiler: an R package for comparing biological themes among gene clusters. *Omics* 16, 284–287. doi: 10.1089/omi.2011.0118

Yu, X., Zhang, Y., Li, T., Ma, Z., Jia, H., Chen, Q., et al. (2017). Long non-coding RNA Linc-RAM enhances myogenic differentiation by interacting with MyoD. *Nat. Commun.* 10:181. doi: 10.1038/ncomms14016

Zhang, H., Shi, X., Huang, T., Zhao, X., Chen, W., Gu, N., et al. (2020). Dynamic landscape and evolution of m^{6}A methylation in human. *Nucleic Acids Res.* 48, 6251–6264. doi: 10.1093/nar/gkaa347

Zhang, H., Zeitz, M. J., Wang, H., Niu, B., Ge, S., Li, W., et al. (2014). Long noncoding RNA-mediated intrachromosomal interactions promote imprinting at the Kcnq1 locus. *J. Cell Biol.* 204, 61–75. doi: 10.1083/jcb.201304152

Zhang, L. M., Wang, M. H., Yang, H. C., Tian, T., Sun, G. F., Ji, Y. F., et al. (2019). Dopaminergic neuron injury in Parkinson's disease is mitigated by interfering lncRNA SNHG14 expression to regulate the miR-133b/α-synuclein pathway. *Aging* 11, 9264–9279. doi: 10.18632/aging.102330

Zhang, W., He, L., Liu, Z., Ren, X., Qi, L., Wan, L., et al. (2020). Multifaceted functions and novel insight into the regulatory role of RNA N(6)-Methyladenosine modification in musculoskeletal disorders. *Front. Cell Dev. Biol.* 8:870. doi: 10.3389/fcell.2020.00870

Zhang, Y., Li, Y., Hu, Q., Xi, Y., Xing, Z., Zhang, Z., et al. (2020). The lncRNA H19 alleviates muscular dystrophy by stabilizing dystrophin. *Nat. Cell Biol.* 22, 1332–1345. doi: 10.1038/s41556-020-00595-5

Zhao, Y., Cao, F., Yu, X., Chen, C., Meng, J., Zhong, R., et al. (2018). Linc-RAM is required for FGF2 function in regulating myogenic cell differentiation. *RNA Biol.* 15, 404–412. doi: 10.1080/15476286.2018.1431494

Zhou, L., Sun, K., Zhao, Y., Zhang, S., Wang, X., Li, Y., et al. (2015). Linc-YY1 promotes myogenic differentiation and muscle regeneration through an interaction with the transcription factor YY1. *Nat. Commun.* 6:10026. doi: 10.1038/ncomms10026

Zhu, B., Zhang, M., Byrum, S. D., Tackett, A. J., and Davie, J. K. (2014). TBX2 blocks myogenesis and promotes proliferation in rhabdomyosarcoma cells. *Int. J. Cancer* 135, 785–797. doi: 10.1002/ijc.28721

Conflict of Interest: The authors declare that the research was conducted in the absence of any commercial or financial relationships that could be construed as a potential conflict of interest.

Publisher's Note: All claims expressed in this article are solely those of the authors and do not necessarily represent those of their affiliated organizations, or those of the publisher, the editors and the reviewers. Any product that may be evaluated in this article, or claim that may be made by its manufacturer, is not guaranteed or endorsed by the publisher.

Copyright © 2021 Xie, Tao, Diao, Li, Chen, Zhou, Hu, Hou, Lei, Xu, Chen, Peng, Zhang and Xiao. This is an open-access article distributed under the terms of the Creative Commons Attribution License (CC BY). The use, distribution or reproduction in other forums is permitted, provided the original author(s) and the copyright owner(s) are credited and that the original publication in this journal is cited, in accordance with accepted academic practice. No use, distribution or reproduction is permitted which does not comply with these terms.

frontiers in Cell and Developmental Biology

ORIGINAL RESEARCH
published: 18 October 2021
doi: 10.3389/fcell.2021.724282

RNA m^{6}A Demethylase ALKBH5 Protects Against Pancreatic Ductal Adenocarcinoma *via* Targeting Regulators of Iron Metabolism

Rui Huang[1†], Lin Yang[2†], Zhiwen Zhang[1], Xiaoding Liu[1], Yi Fei[2], Wei-Min Tong[2], Yamei Niu[2] and Zhiyong Liang[1*]*

[1] Department of Pathology, State Key Laboratory of Complex Severe and Rare Disease, Molecular Pathology Research Center, Peking Union Medical College Hospital, Chinese Academy of Medical Sciences and Peking Union Medical College, Beijing, China, [2] Department of Pathology, Institute of Basic Medical Sciences, Chinese Academy of Medical Sciences and Peking Union Medical College, Beijing, China

Although RNA m^{6}A regulators have been implicated in the tumorigenesis of several different types of tumors, including pancreatic cancer, their clinical relevance and intrinsic regulatory mechanism remain elusive. This study analyzed eight m^{6}A regulators (METTL3, METTL14, WTAP, FTO, ALKBH5, and YTHDF1-3) in pancreatic ductal adenocarcinoma (PDAC) and found that only RNA m^{6}A demethylase ALKBH5 serves as an independent favorable prognostic marker for this tumor. To better understand the molecular mechanism underlying the protective effect conferred by ALKBH5 against pancreatic tumorigenesis, we performed a transcriptome-wide analysis of m^{6}A methylation, gene expression, and alternative splicing (AS) using the MIA PaCa-2 stable cell line with ALKBH5 overexpression. We demonstrated that ALKBH5 overexpression induced a reduction in RNA m^{6}A levels globally. Furthermore, mRNAs encoding ubiquitin ligase FBXL5, and mitochondrial iron importers SLC25A28 and SLC25A37, were identified as substrates of ALKBH5. Mechanistically, the RNA stabilities of *FBXL5* and *SLC25A28*, and the AS of *SLC25A37* were affected, which led to their upregulation in pancreatic cancer cell line. Particularly, we observed that downregulation of FBXL5 in tumor samples correlated with shorter survival time of patients. Owing to FBXL5-mediated degradation, ALKBH5 overexpression incurred a significant reduction in iron-regulatory protein IRP2 and the modulator of epithelial-mesenchymal transition (EMT) SNAI1. Notably, ALKBH5 overexpression led to a significant reduction in intracellular iron levels as well as cell migratory and invasive abilities, which could be rescued by knocking down *FBXL5*. Overall, our results reveal a previously uncharacterized mechanism of ALKBH5 in protecting against PDAC through modulating regulators of iron metabolism and underscore the multifaceted role of m^{6}A in pancreatic cancer.

Keywords: pancreatic ductal adenocarcinoma (PDAC), ALKBH5, RNA m^{6}A methylation, iron metabolism, FBXL5

OPEN ACCESS

Edited by:
Chengqi Yi,
Peking University, China

Reviewed by:
Beisi Xu,
St. Jude Children's Research Hospital, United States
Taiping Chen,
The University of Texas MD Anderson Cancer Center, United States
Ling Xu,
China Medical University, China

****Correspondence:***
Zhiyong Liang
liangzhiyong1220@yahoo.com
Yamei Niu
niuym@ibms.pumc.edu.cn

[†]These authors have contributed equally to this work

Specialty section:
This article was submitted to Epigenomics and Epigenetics, a section of the journal Frontiers in Cell and Developmental Biology

Received: *12 June 2021*
Accepted: *28 September 2021*
Published: *18 October 2021*

Citation:
Huang R, Yang L, Zhang Z, Liu X, Fei Y, Tong W-M, Niu Y and Liang Z (2021) RNA m^{6}A Demethylase ALKBH5 Protects Against Pancreatic Ductal Adenocarcinoma via Targeting Regulators of Iron Metabolism. Front. Cell Dev. Biol. 9:724282. doi: 10.3389/fcell.2021.724282

INTRODUCTION

Pancreatic cancer is a highly malignant carcinoma of the digestive system that affects the global population (Siegel et al., 2021). Pancreatic ductal adenocarcinoma (PDAC) is the most common type of all malignant pancreatic carcinomas. No apparent improvements have been observed in patient survival (Mizrahi et al., 2020), despite the acquisition of knowledge on the genetic and epigenetic dysregulation pathways in pancreatic cancer, and advances in the diagnostic and therapeutic approaches. Further exploration of the molecular mechanism underlying tumor initiation and progression is vital to achieve the final goal of improving the clinical outcomes of patients with pancreatic cancer.

N^6-methyladenosine (m^6A) RNA modification affects all stages of the RNA life cycle and regulates gene expression at the co-transcriptional and post-transcriptional levels (Zhao et al., 2018). m^6A modification modulates various types of physiological processes, including hematopoiesis (Lv et al., 2018), neural development (Ma et al., 2018; Wang et al., 2018; Weng et al., 2018), spermatogenesis (Zheng et al., 2013; Hsu et al., 2017; Lin et al., 2017), adipogenesis (Zhao et al., 2014), osteogenic differentiation (Yu et al., 2020), and other essential processes. On the other hand, dysfunctional m^6A regulators and the resultant fluctuation in m^6A methylation are often observed in various tumors (Huang et al., 2020; Yang et al., 2020). Accumulating evidence has shown that several m^6A regulators exert either promotive or inhibitory effects on the hallmarks of cancer, such as cell proliferation, immune evasion, tumor invasion and metastasis (Barbieri and Kouzarides, 2020). Iron is an essential element for various cellular functions while dysregulation of iron metabolism plays a role in tumor progression and metastasis (Torti and Torti, 2020b). However, the existing knowledge on the crosstalk between m^6A methylation and iron metabolism is extremely limited. Recent study has identified that YTHDF1 accelerates the tumorigenesis of hypopharyngeal squamous cell carcinoma (HPSCC) via the enhancement of iron metabolism (Ye et al., 2020), while the involvement of other m^6A regulators in the control of iron metabolism remains unclear.

Previous studies have reported that METTL3 (Xia et al., 2019), METTL14 (Wang M. et al., 2020; Chen S. et al., 2021), WTAP (Li et al., 2019), FTO (Tang et al., 2019), ALKBH5 (Guo et al., 2020; Tang et al., 2020), YTHDF2 (Chen et al., 2017), and YTHDC1 (Hou et al., 2021) play pivotal roles in regulating the proliferation, metastasis, and chemosensitivity of pancreatic cancer cells. However, the underlying mechanism and clinical relevance of these RNA m^6A regulators remain to be fully elucidated. Although PDAC is the utmost stroma-rich cancer, previous studies were limited to the role of m^6A in tumor cells, while neglecting the difference between the tumor and stroma. Herein, we evaluated the expression of these RNA m^6A regulators in tumor cells and stromal cells and their potential prognostic values for PDAC patients. Furthermore, we focused on ALKBH5 for intensive investigation of its molecular mechanism in protecting against pancreatic cancer.

Abbreviations: AML, acute myelogenous leukemia; AS, alternative splicing; A5SS, alternative 5′ splicing site; A3SS, alternative 3′ splicing site; BCA, bicinchoninic acid; DAB, diaminobenzidine; DMEM, Dulbecco's modified Eagle's medium, DMRs, differentially methylated regions; DTT, dithiothreitol; EDTA, ethylenediaminetetraacetic acid; EMT, epithelial-mesenchymal transition; EV, empty vector; FBS, fetal bovine serum, Fe-S cluster, iron-sulfur cluster; FDR, false discovery rate; Fe-S, iron-sulfur; FFPE, formalin-fixed, paraffin-embedded; GO, Gene Ontology; HPSCC, hypopharyngeal squamous cell carcinoma; HRP, horseradish peroxidase; H&E, hematoxylin and eosin; IHC, immunohistochemical; IJC, inclusion junction counts; IRP2, iron regulatory protein 2; MXE, mutually exclusive exons; m^6A, N^6-methyladenosine; m^6A peaks, m^6A-modified regions; m^6A-seq, methylated RNA immunoprecipitation sequencing; OE, ALKBH5-overexpressing; OS, overall survival; PAAD, pancreatic adenocarcinoma; PCR, polymerase chain reaction; PDAC, pancreatic ductal adenocarcinoma; PFS, progression-free survival; PSI, percent spliced in; PVDF (polyvinylidene fluoride); qPCR, quantitative real-time polymerase chain reaction; RI, retained intron; RIP, RNA immunoprecipitation; RIPA, radioimmunoprecipitation assay buffer; rMATS, replicate multivariate analysis of transcript splicing; RNasin, RNase inhibitor; RPKM, reads per kilobase of transcript per million mapped reads; SD, standard deviation; SJC, skipping junction counts; SDS, sodium dodecyl sulfate; SE, skipped exon; TBS, Tris-buffered saline; TBST, Tris-buffered saline with Tween 20; TCGA, The Cancer Genome Atlas; TMA, tissue microarray.

MATERIALS AND METHODS

Pancreatic Ductal Adenocarcinoma Tissue Samples and Tissue Microarrays

Tissue microarrays [formalin-fixed, paraffin-embedded (FFPE)] of PDAC tumor and normal tissue adjacent to tumors (para-tumor) collected between September 2008 and July 2013, together with corresponding hematoxylin and eosin (H&E)-stained slides, were provided by the Department of Pathology, Peking Union Medical College Hospital (PUMCH, Beijing, China). The specimens were histologically diagnosed by two experienced pathologists and staged according to the 8th edition of the American Joint Committee on Cancer TNM Staging System. Clinical and pathological data, including age, sex, tumor location, lymph node invasion, neural invasion, bile invasion, and tumor TNM stage were extracted from medical records with follow-up period ranging from 2 to 54 months. A total of 63 PDAC tumor and 27 para-tumor samples were included in this study, excluding the samples that fell off from the tissue sections. This study was approved by the PUMCH Ethical Committee (JS-1490), and informed consent was obtained from all patients in accordance with the Declaration of Helsinki.

Immunohistochemical Staining and Evaluation

The PDAC tissue sections (4 μm) were subjected to IHC staining. The sections were deparaffinized with xylene and rehydrated with serial dilutions of ethanol (100, 95, and 75%). Antigen retrieval was performed by heating the sections in a citrate buffer solution (0.01 M, pH = 6.0) at 95°C for 10 min or under high pressure for 2 min 10 s. Subsequently, endogenous peroxidase activity in the tissues was blocked in 3% H_2O_2 at ∼25°C for 10 min. The slides were sequentially incubated with primary antibodies and horseradish peroxidase (HRP)-labeled secondary antibodies

(**Supplementary Table 1**). Finally, the slides were stained with diaminobenzidine (DAB) and counterstained with hematoxylin.

The expression of each individual gene in the normal pancreatic ductal epithelial cells, tumor cells, or stromal cells was scored separately using the H-score. The intensity and percentage of the positive cells were scored independently by two pathologists. The H-score represents the sum of the intensity of each stain (grades 0–3, where 0, 1, 2, and 3 represent negative, weak, moderate, and strong staining) multiplied by the percentages of the cells positive for each marker (0–100%). The final H-score can range from 0 to 300.

Construction of MIA PaCa-2 Stable Cell Line Constitutively Expressing ALKBH5

The human pancreatic cancer cell line MIA PaCa-2 was obtained from the Cell Resource Centre of Peking Union Medical College (Beijing, China). The cells were cultured in high-glucose Dulbecco's modified Eagle's medium (DMEM) (Corning, 10-017-CV) supplemented with 10% fetal bovine serum (FBS) (Corning, 35-010-CV) in an incubator at 37°C in the presence of 5% CO_2. The lentiviruses expressing empty vector (EV) and N-terminal Flag-tagged ALKBH5 (NM_017758) were purchased from OBiO Technology (Shanghai, China). MIA PaCa-2 was transduced with lentiviruses and selected via the limited dilution assay.

Methylated RNA Immunoprecipitation (m^6A-IP) and Sequencing (m^6A-Seq)

The total RNA was extracted from EV and ALKBH5-overexpressing (OE) MIA PaCa-2 cells by using TRIzol™ Reagent (Invitrogen, 15596026), according to the manufacturer's instructions. Poly(A) RNA was isolated from the total RNA using the poly(A) Spin™ mRNA Isolation Kit (NEB, S1560). Poly(A) RNA was fragmented into ∼ 200 nt using RNA Fragmentation Reagents (Ambion, AM8740). A total of 1 μg of fragmented poly(A) RNA was employed for m^6A-IP, which was achieved using the Magna MeRIP™ m^6A Kit (Millipore, 17-10499). Immunoprecipitated RNA was recovered with the RNeasy MinElute® Cleanup Kit (Qiagen, 74204). The cDNA libraries were prepared with the NEBNext® Ultra™ RNA Library Prep Kit for Illumina® (NEB, E7530L). Next-generation sequencing was conducted on the Illumina X Ten platform.

The total RNA purified from the EV and OE MIA PaCa-2 cells was fragmented into ∼100 nt. A total of 10 μg of fragmented total RNA was diluted in 1 × IPP buffer (Tris-HCl, pH = 7.4, 50 mM; NaCl, 750 mM; NP-40, 0.5% vol/vol) and incubated with anti-m^6A antibody. The m^6A-enriched RNAs were eluted in 1 × IPP buffer containing m^6A (BERRY & ASSOCIATES, PR3732) and purified with RNeasy MinElute® Cleanup Kit (Qiagen, 74204). The cDNA libraries were constructed using the SMARTer® Stranded Total RNA-Seq Kit v2 - Pico Input mammalian (Takara, 634414). Next-generation sequencing was conducted on the Illumina NovaSeq 6000 platform.

The m^6A level of a specific gene was detected using m^6A-IP, which was performed with 10 μg of fragmented total RNA (∼400 nt) along with 0.1 fmol of negative and positive spike-in control RNA, unmodified *Cypridina Luciferase* control RNA (*Cluc*) and m^6A-modified *Gaussia luciferase* RNA (*Gluc*), provided within the EpiMark® N^6-methyladenosine Enrichment Kit (NEB, E1610S).

m^6A-Seq Data Analysis

The m^6A-seq data were analyzed in accordance with the procedures described in a previous study (Chang et al., 2017). The clean reads of each sample were mapped against the human genome (version hg38). Only uniquely mapped reads were included in the subsequent analyses. The gene expression levels were evaluated using the reads per kilobase of transcript per million mapped reads (RPKM) values. The genes that were expressed differentially ($|\log_2 FC| > 0.58$, $P < 0.05$) between the EV and OE samples were identified using the *edgeR* (McCarthy et al., 2012) or *DESeq2* R package (Love et al., 2014). The *exomePeak* R package (Meng et al., 2013) was used to identify the RNA m^6A-modified regions (m^6A peaks) in each sample, and HOMER (Heinz et al., 2010) was used to determine the conserved motifs within these regions. We divided the 3′UTR, coding sequence region (CDS), and 5′UTR regions of the longest transcript of each gene into 100 equally sized bins, respectively, to characterize the distribution patterns of m^6A peaks. The percentage of m^6A peaks in each bin was calculated to represent the occupancy of m^6A along with the transcripts. Differentially methylated regions (DMRs) between the EV and OE samples were further identified using *exomePeak* software by taking the cutoff of $|\log_2 FC| > 0.58$ and false discovery rate (FDR) < 0.05. The Gene Ontology (GO) analysis of the differentially expressed or modified genes was conducted based on DAVID online annotation database (Huang da et al., 2009a,b). The visualization of the enriched GO terms was implemented using the *ggplot2* R package.

Detection of Alternative Splicing Events

The input RNA-seq data obtained from the EV and OE samples were utilized to detect alternative splicing (AS) events using the replicate multivariate analysis of transcript splicing (*rMATS*) tool (Shen et al., 2014). This tool enables the detection of 5 types of AS events: alternative 5′ splicing site (A5SS), alternative 3′ splicing site (A3SS), mutually exclusive exons (MXE), retained intron (RI), and skipped exon (SE). It can also identify the AS event that exhibits significant alterations by comparing the inclusion levels between the samples in different conditions. The inclusion levels of each event were quantified by the percent spliced in (PSI) which was calculated according to the inclusion junction counts (IJC) and skipping junction counts (SJC) in each splicing event. The AS events with a FDR < 0.05 and $|\Delta PSI| > 0.2$ and (IJC + SJC) > 12 in the comparison results were considered as significantly dysregulated AS events.

RNA Immunoprecipitation

The MIA PaCa-2 cells were collected and lysed in non-denaturing lysis buffer [Tris-HCl, pH = 7.4, 50 mM; NaCl, 250 mM; Triton X-100, 0.5%; dithiothreitol (DTT), 1 mM; ethylenediaminetetraacetic acid (EDTA), 2 mM; NaF, 1 mM; protease inhibitor cocktail, 1×; RNase inhibitor (RNasin), 0.04 U/mL], followed by bicinchoninic acid (BCA) protein

quantification (Thermo Scientific, 23227). The whole-cell lysates were incubated with the anti-ALKBH5 antibody at 4°C on a rotator for 5 h, followed by the addition of protein A/G magnetic beads (Thermo Scientific, 26162) to the mixture and overnight incubation at 4°C on a rotator. The magnetic beads were sequentially washed in low salt Tris-buffered saline (TBS) (Tris-HCl, pH = 7.4, 50 mM; NaCl, 250 mM; DTT, 1 mM; NaF, 1 mM; protease inhibitor cocktail, 1×; RNasin, 0.04 U/ml) and high salt TBS (Tris-HCl, pH = 7.4, 50 mM; NaCl, 300 mM; DTT, 1 mM; NaF, 1 mM; protease inhibitor cocktail, 1×; RNasin, 0.04 U/mL), followed by treatment with Proteinase K Buffer [Tris-HCl, pH 7.4, 100 mM; NaCl, 150 mM; EDTA, 12.5 mM; sodium dodecyl sulfate (SDS), 2% w/v; proteinase K, 1.2 mg/mL] at 55°C for 30 min. A total of 10 mL of supernatant was subjected to western blot analysis to determine the efficiency of immunoprecipitation. The remaining supernatant was used for RNA purification with the RNeasy MinElute® Cleanup Kit (Qiagen, 74204).

RNA Stability Assay

The EV and OE MIA PaCa-2 cells were used for the RNA stability assay. The cells were seeded onto 48-well plates in triplicate. Actinomycin D (Sigma, A4262) was added to each well after 24 h to achieve a final concentration of 5 μg/mL and incubated for 0, 3, 6, and 9 h. The cells were collected, and total RNA was purified using TRIzol™ Reagent (Invitrogen, 15596026).

Reverse Transcription, Quantitative Real-Time Polymerase Chain Reaction and Polymerase Chain Reaction

The immunoprecipitated RNA, input RNA, and total RNA were reverse-transcribed using the GoScipt™ Reverse Transcription System (Promega, #A5000). The m^{6}A-induced changes in specific genes and ALKBH5-associated RNAs were determined via the qPCR using PowerUp™ SYBR™ Green PCR Master Mix (ABI, A25742) on a qPCR instrument machine (Roche, LightCycler® 480 II). The alternatively spliced products were determined with PCR via 2 × GoldStar MasterMix (CWBIO, CW0929L) and agarose gel (2%) electrophoresis. The primers used in the study are listed in **Supplementary Table 2**.

Western Blot Analysis

The proteins were purified using the radioimmunoprecipitation assay buffer (RIPA) (APPLYGEN, C1053+) and quantified with the BCA assay. Proteins were separated by 8, 10, or 12% SDS-PAGE and transferred to polyvinylidene fluoride (PVDF) membranes (Millipore, ISEQ00010). The membranes were blocked with 10% non-fat milk for 2 h at ∼25°C, followed by overnight incubation with primary antibodies at 4°C. The membranes were washed with Tris-buffered saline with Tween 20 (TBST) buffer (APPLYGEN, B1009) for 10 min and subsequently incubated with the HRP-labeled secondary antibodies using Chemidoc™ Touch Image System (BIO-RAD, 1708370). The antibodies used in this study are listed in **Supplementary Table 1**.

siRNA Transfection

RNA oligos were synthesized by RiboBio Co., Ltd. (Guangzhou, China). The siRNA sequences used are as following: Scramble (SC): 5′-*GGCUCUAGAAAAGCCUAUGC*-3′, si*FBXL5*-1 (KD-1): 5′-*UGCGUAUUGUGGUCACUCA*-3′, si*FBXL5*-2 (KD-2): 5′- *GU UUGCACGAUUUAACUAA*-3′. The siRNAs were transfected into OE MIA PaCa-2 cells with RNAiMax (Invitrogen, 13778150). Forty-eight hours post transfection, cells were collected and proceeded to Western blot analysis, cell migration and invasion assay, and intracellular iron assay.

Cell Migration and Invasion Assays

Cell migration and invasion assays were performed using transwell chambers (8-μm pore size) (Corning Inc., 3422) with or without Matrigel matrix (Corning Inc., 356234). Cells were resuspended with DMEM and seeded into the upper chambers, and the lower chambers were filled with DMEM supplemented with 10% FBS. After ∼16 h, the non-migrating or non-invading cells were wiped off from the membranes, followed by fixation in 37% formaldehyde and staining with 3% crystal violet solution. Images were captured and then the migrated cells were counted.

Intracellular Iron Assay

Cellular iron levels were assayed by using commercial Iron Assay Kit (Colorimetric) (Abcam, ab83366), according to the manufacturer's instructions. Briefly, cells were collected and homogenized in iron assay buffer, the cell lysates were centrifuged at 16,000 × *g* for 10 min to collect the supernatant. Iron probes were added into each sample and incubated at 37°C for 1 h. The absorbance at 593 nm were measured with a colorimetric microplate reader.

Statistical Analysis

Each experiment was performed in triplicate. Data were presented as the mean ± standard deviation (SD). Statistical analyses were conducted using Graphpad Prism 7 (Graphpad Software Inc., San Diego, CA, United States) and SPSS 22.0 (SPSS Inc., Chicago, IL, United States). Differences between the groups were analyzed using Student's *t*-test. The survival status was evaluated using Kaplan–Meier curves and the log-rank test. Cox-regression analyses were used to ascertain the independent prognostic factors for PDAC. Two-tailed *P*-values < 0.05 were considered statistically significant.

RESULTS

Reduced ALKBH5 Expression Correlates With Poor Prognosis of Patients With Pancreatic Ductal Adenocarcinoma

Pancreatic ductal adenocarcinoma is a kind of epithelial tumor arising from pancreatic ductal cells, which is characterized by the extensive proliferation of stromal cells (Lee et al., 2019; Neesse et al., 2019). Even though the roles of several RNA m^{6}A regulators have been identified in pancreatic cancer, their expressions in the tumor cells and stroma cells remain to

be thoroughly explored. Herein, we performed IHC analysis by using the TMAs including 63 samples to detect the *in situ* expression patterns of eight m^6A regulators in the normal pancreatic ductal epithelial cells, PDAC tumor cells, and stroma cells, respectively (**Supplementary Figure 1**). The methyltransferases and demethylases analyzed in this study were mainly located in the nucleus in both normal epithelial cells and tumor cells, while the m^6A-binding protein was located in the cytosol (**Figure 1A**). The tumor cells exhibited a significant increase in the expression of WTAP, YTHDF2, and YTHDF3, but a reduction in the expression of FTO and ALKBH5 compared to the normal epithelial cells in the para-tumor samples. Meanwhile, we found that the expressions of METTL3, METTL14, WTAP, and YTHDF1-3 proteins were significantly lower in the stroma cells than that in the tumor cells (**Figures 1A,B**).

We subsequently performed log-rank test to determine the association between the expression levels of each m^6A regulator and the overall survival (OS) or progression-free survival (PFS) duration to explore the potential clinical relevance of each m^6A regulator in PDAC. ALKBH5 expression in tumor cells exhibited a positive correlation with OS time in patients with PDAC (**Figures 2A,B**). In addition, the decreased expressions of FTO and YTHDF1 in the stroma were predictive of a poor prognosis (**Figures 2C–G**). In contrast, we failed to observe any significant correlation between the expressions of other m^6A regulators (METTL3, METTL14, WTAP, YTHDF2, and YTHDF3) with patient survival (**Figures 2A,C,F** and **Supplementary Figure 2A**). Further univariate and multivariate cox regression analyses showed that out of the eight RNA m^6A regulators, only ALKBH5 was an independent predictive marker for the prognosis of patients with PDAC (**Figures 2H,I** and **Supplementary Figures 2B–E**).

The above-mentioned results collectively illuminate that ALKBH5 is downregulated in PDAC and that, it might be the only m^6A regulator (among the eight RNA m^6A regulators identified in this study) capable of predicting the prognosis independently in patients with PDAC.

m^6A-Seq Reveals Decreased Methylation Level Upon ALKBH5-Overexpression

Next, we generated an MIA PaCa-2 stable cell line constitutively expressing Flag-ALKBH5 for subsequent analyses to unveil the functions and potential targets of ALKBH5 in PDAC. First, we examined the effect of overexpressed ALKBH5 on RNA m^6A methylation at transcriptome-wide level based on m^6A-seq analysis of poly(A) RNA isolated from the EV and OE MIA PaCa-2 cells.

We identified 11,100 and 10,974 m^6A methylation peaks located in the mRNAs in the EV and OE samples, respectively (**Supplementary Table 3**). The m^6A sites were mainly distributed in the GGAC context in both samples (**Figure 3A**) and located in the CDS, with a significant enrichment in the stop codon region (**Figure 3B**), which was consistent with previous studies. We found that the global methylation level decreased significantly ($P < 0.001$) in the OE sample (**Figure 3C**). Using ($|\log_2 FC| > 0.58$, FDR < 0.05) as the criteria, we identified 194 hyper-methylated and 882 hypo-methylated m^6A peaks in the OE sample, which were distributed in 191 and 813 mRNAs, respectively (**Supplementary Table 4**). The substantially greater number of hypo-methylated peaks compared to the hyper-methylated peaks was consistent with the function of ALKBH5 as a demethylase enzyme. Functional enrichment analysis of the genes encoded by differentially methylated mRNAs revealed that the genes regulated by ALKBH5 via RNA methylation participated in various functional pathways. The hypo-methylated RNAs in the OE sample were involved in pathways such as DNA repair, cell division and microtubule cytoskeleton organization (**Figure 3D**). In contrast, the hyper-methylated RNAs in the OE sample were mainly enriched in functions including RNA export, IRE1-mediated unfolded protein response and others. These results imply that ALKBH5 exerts its functions on multiple signaling pathways depending on m^6A methylation in the pancreatic cancer cell line.

We also observed that the expression levels of some genes were altered upon overexpression of ALKBH5, including 89 upregulated and 134 downregulated protein coding genes ($|\log_2 FC| > 0.58$, $P < 0.05$) in the OE MIA PaCa-2 cells (**Supplementary Table 5**). Given the pivotal effects of m^6A methylation in modulating RNA processing, we integrated the RNA methylation and expression data to explore their implications in pancreatic cancer cells. We found that a substantial number of genes harbored both abnormal RNA expression and methylation levels ($|\log_2 FC| > 0.58$) in the OE sample (**Figure 3E**). Only a few were filtered out after taking the significance of difference (P [differential expression] < 0.05 and FDR [differential methylation] < 0.05) into consideration (**Figure 3F**). Given the nature of ALKBH5 as a demethylase, we prioritized these hypo-methylated RNAs for subsequent analyses. Only three of the hypo-methylated mRNAs exhibited significantly lower ($\log_2 FC < -0.58$ and $P < 0.05$) expression levels (hypo_down), while ten RNAs exhibited increased ($\log_2 FC > 0.58$, $P < 0.05$) expression levels (hypo_up) in the OE MIA PaCa-2 cells (**Figure 3F**).

The above-mentioned findings were further validated using another two sets of total RNA-based m^6A-seq using the EV and OE MIA PaCa-2 cells (**Supplementary Figures 3A,B**), followed by differential methylation and expression analyses (**Supplementary Tables 6**, **7**). Most of m^6A methylation regions were hypo-methylated upon ALKBH5-overexpression (**Figure 3G**), consistent with the above-mentioned results. Notably, out of the ten hypo-up RNAs identified in the original sequencing data (**Figure 3F**), only two RNAs (*FBXL5* and *SLC25A28*) exhibited significantly lower methylation levels and higher expression levels in the OE MIA PaCa-2 (**Figure 3H**). The above results implied that ALKBH5 overexpression in pancreatic cancer cells induced the overall demethylation of mRNAs. Importantly, we identified two RNAs, *FBXL5* and *SLC25A28*, as potential substrates of ALKBH5, as evidenced by the simultaneous changes in both methylation and gene expression upon ALKBH5-overexpression.

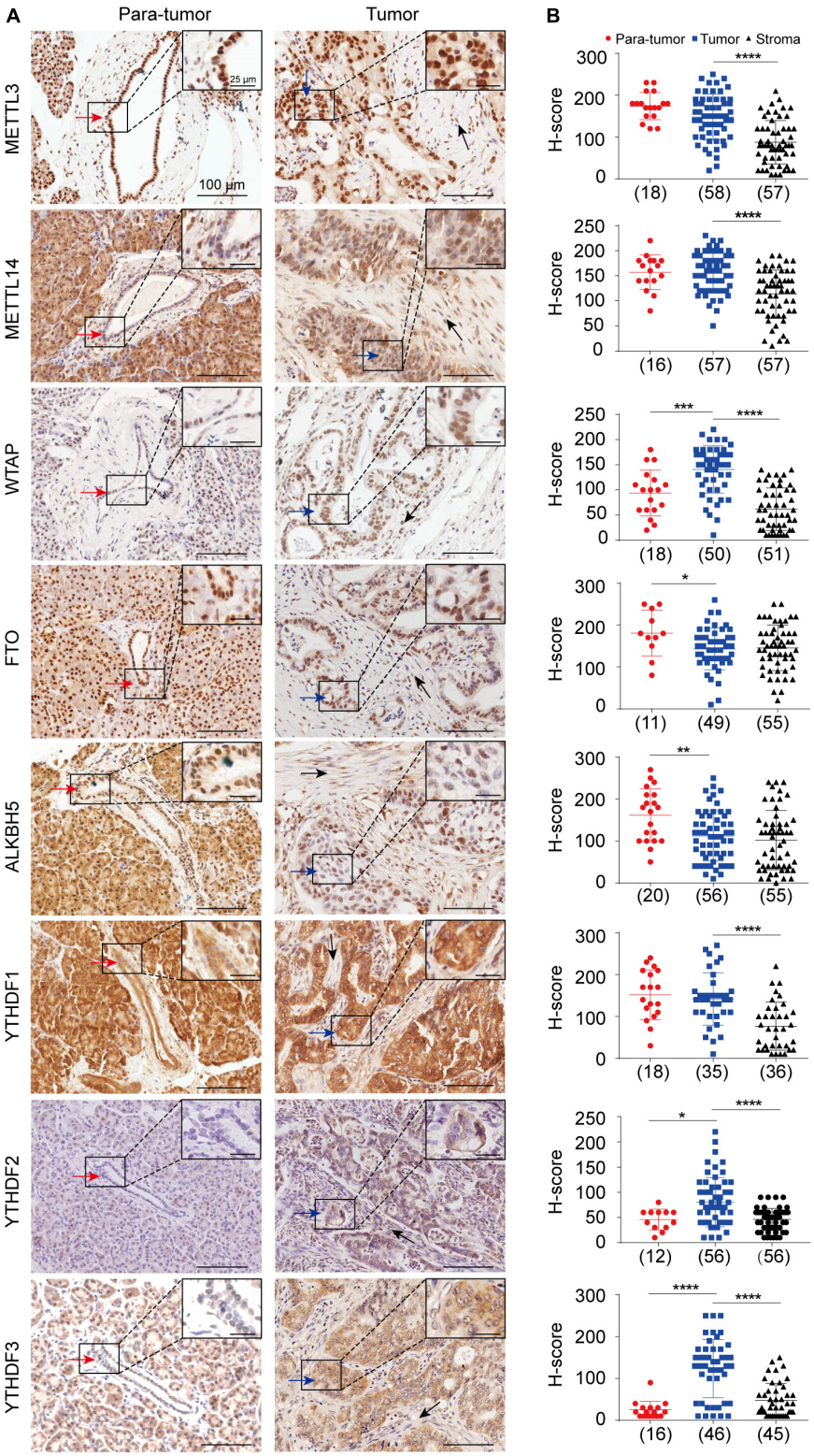


FIGURE 1 | *In situ* protein expression analysis of eight m^{6}A key regulators in pancreatic ductal adenocarcinoma (PDAC). **(A)** Representative immuno-histochemical staining showing the expressions of METTL3, METTL14, WTAP, FTO, ALKBH5, and YTHDF1-3 in normal pancreatic ductal epithelial cells (red arrows) in para-tumor samples, tumor cells (blue arrows), and stromal cells (black arrows) in tumor samples. Enlarged images in the box are shown in the upper right. **(B)** Scatter plots showing the H-scores of each gene in para-tumor, tumor and stroma cells are shown in the right panel. Case numbers are shown in brackets. Scale bars, 100 or 25 μm. *$P < 0.05$, **$P < 0.01$, ***$P < 0.001$, ****$P < 0.0001$.

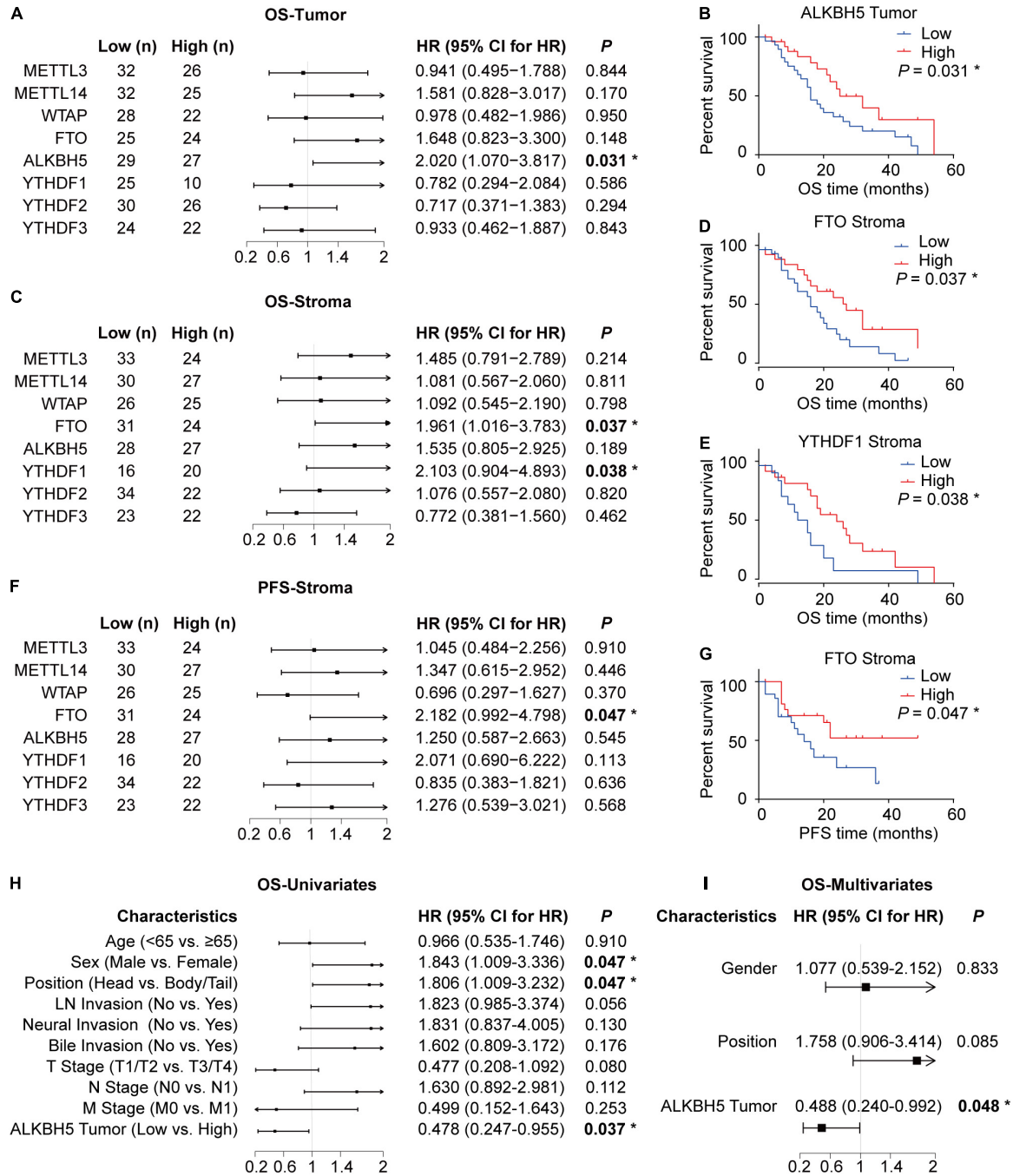


FIGURE 2 | Downregulation of ALKBH5 in PDAC predicts poor prognosis. **(A)** Log-rank analysis of correlation between overall survival (OS) and the expression of each m^{6}A regulator in tumor. **(B,C)** Log-rank analysis of correlation between OS or progression-free survival (PFS) and the expression of m^{6}A regulators in stroma. **(D–G)** Kaplan–Meier analysis of correlation between OS or PFS and ALKBH5, FTO, and YTHDF1 protein expression. **(H,I)** Cox regression analysis for OS in PDAC patients. *$P < 0.05$.

ALKBH5 Regulates RNA Stability of *FBXL5*

We subsequently investigated whether the two genes were regulated as direct downstream targets of ALKBH5 in PDAC. First, we performed gene expression correlation analysis using 178 pancreatic adenocarcinoma (PAAD) samples according to the Cancer Genome Atlas (TCGA) database to explore their correlation with *ALKBH5* (Tang et al., 2017). We found that ALKBH5 exhibited a significantly positive correlation with *FBXL5* ($R = 0.63$, $P < 0.001$) (**Figure 4A**). Therefore, we further investigated the mechanism by which ALKBH5 regulated

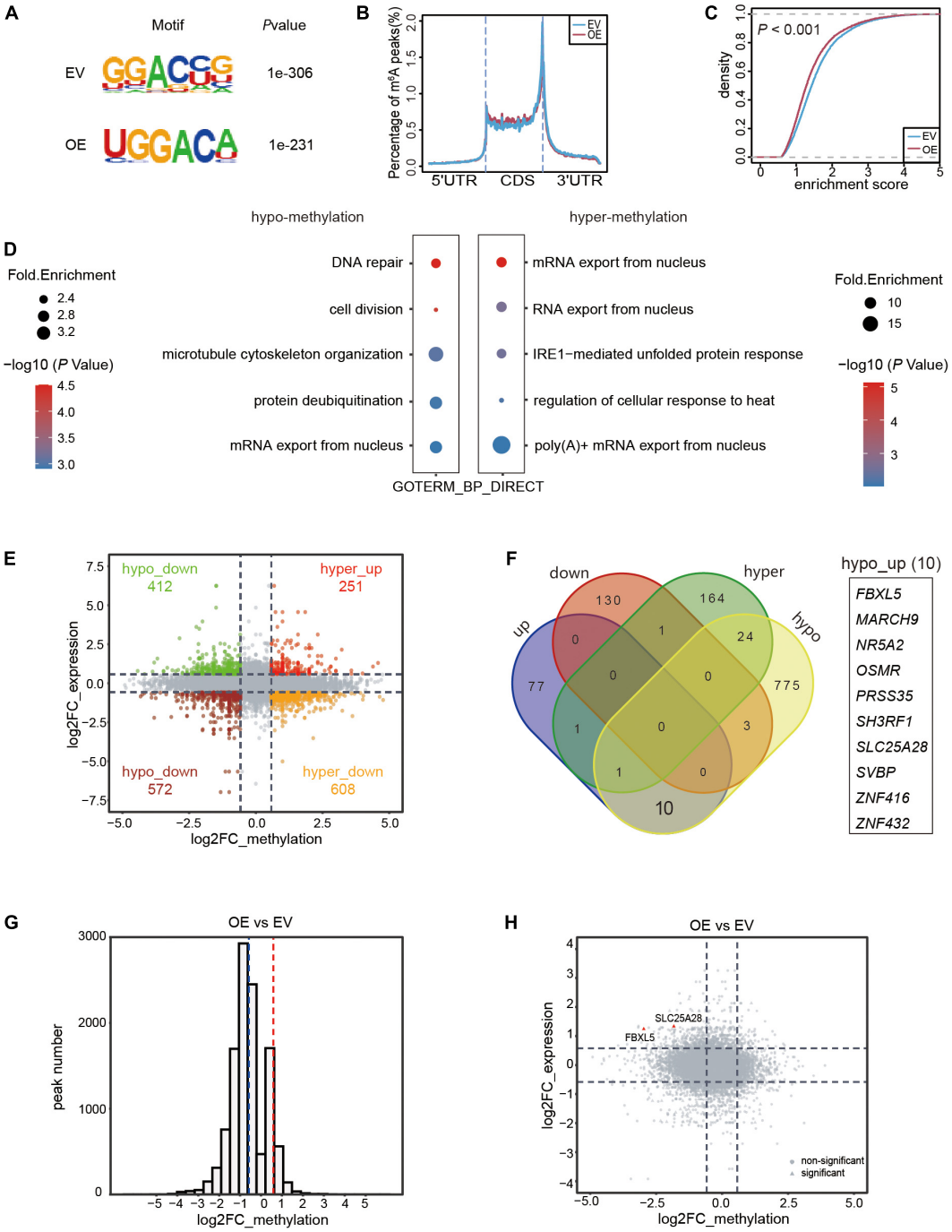


FIGURE 3 | Transcriptome-wide RNA m^{6}A methylation and expression analysis of MIA PaCa-2 stable cell line with ALKBH5 overexpression. **(A)** Top consensus motif of m^{6}A peaks identified in empty vector (EV) or ALKBH5-overexpressing (OE) MIA PaCa-2 cells. **(B)** Normalized distribution of m^{6}A peaks across 5′UTR, CDS, and 3′UTR of mRNAs. **(C)** Cumulative distribution function of log2 enrichment score of m^{6}A modified sites. **(D)** GO term analysis of transcripts with hypo- **(left panel)** and hyper-methylated **(right panel)** m^{6}A sites in OE sample versus EV sample. **(E)** Scatter plot representing the $\log_2$FC of methylation (*x*-axis) and expression (*y*-axis) of each m^{6}A peak in OE versus EV sample. Points with $|\log_2 FC| > 0.58$ in both differential expression and methylation analysis results are highlighted. **(F)** Venn diagram showing the RNAs with significant change in either methylation ($|\log_2 FC| > 0.58$ and FDR < 0.05) or expression ($|\log_2 FC| > 0.58$ and $P < 0.05$) in OE sample. **(G)** Histogram showing the fold changes in m^{6}A enrichment between OE and EV samples from total RNA based m^{6}A data. Dotted lines denote the threshold ($|\log_2 FC| > 0.58$) for filtering differential expression gene. **(H)** Scatter plot showing the distribution of fold changes in methylation (*x*-axis) and expression (*y*-axis) of each RNA in OE versus EV sample. Two RNAs with significantly decreased m^{6}A methylation and increased expression level in OE sample are marked in red. Points in rectangle shape represent significant changes in methylation ($|\log_2 FC| > 0.58$ and FDR < 0.05) and expression ($|\log_2 FC| > 0.58$, $P < 0.05$), while the rest ones are shaped in circle.

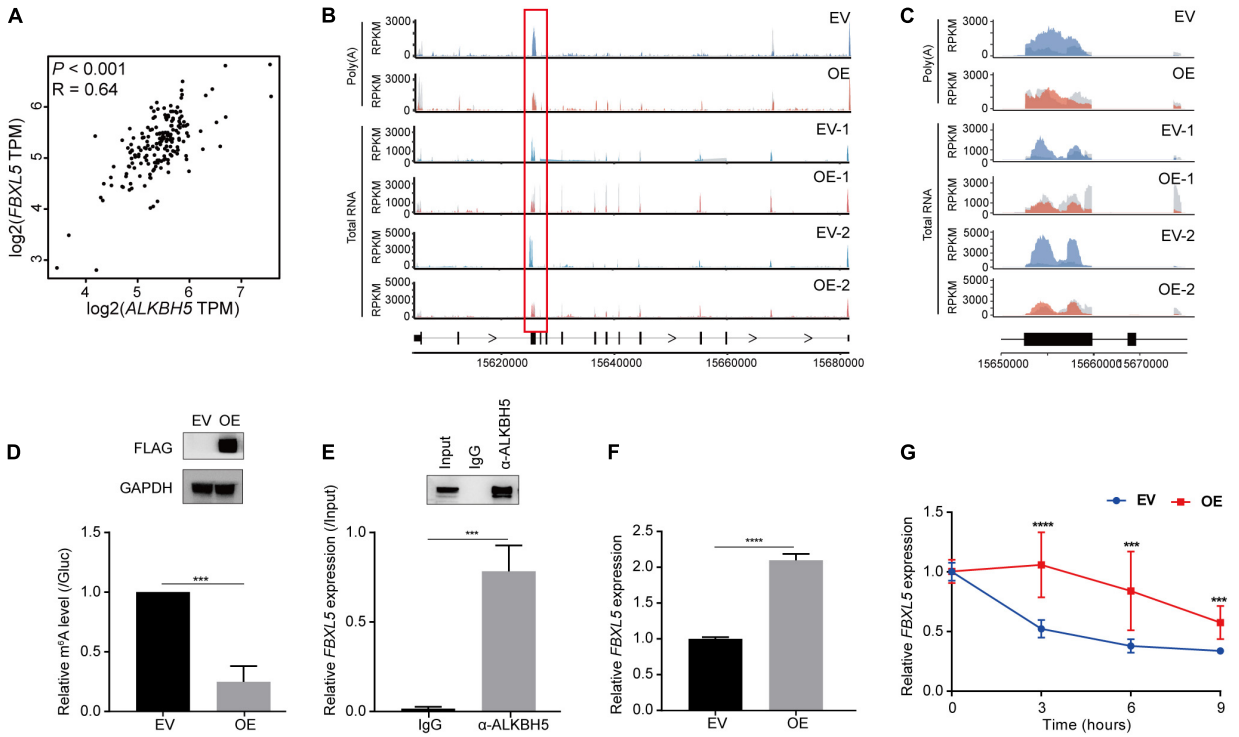


FIGURE 4 | ALKBH5 regulates the stability of *FBXL5* RNA. **(A)** Expression correlation between *ALKBH5* and *FBXL5* across 178 pancreatic adenocarcinoma (PAAD) samples in TCGA database. R, Pearson correlation coefficient. **(B)** Sequencing reads density for input and m^{6}A-IP samples along *FBXL5* transcript in poly(A) RNA- and total RNA-based m^{6}A-seq data. Hypo-methylated peaks are indicated in red rectangles. Gray for input libraries, while blue (EV) or red (OE) for IP libraries. *X*-axis, genomic coordinates; *Y*-axis, normalized number of reads. **(C)** Zoom-in of the hypomethylated region on *FBXL5* transcript. **(D)** m^{6}A-IP-qPCR results showing the methylation changes of *FBXL5* between EV and OE samples. Results of Western blot analysis showing the expression of Flag-ALKBH5 are shown in the upper panel. GAPDH is used as an internal control. **(E)** RIP-qPCR results showing the interaction between ALKBH5 protein and *FBXL5* RNA in MIA PaCa-2 cells. Results of Western blot analysis showing the efficiency of immunoprecipitation are shown in the upper panel. **(F)** RT-qPCR results showing the changes of *FBXL5* expression between EV and OE samples. **(G)** Results of RNA stability assay showing the effect of ALKBH5 overexpression on the decay rate of *FBXL5* RNA. EV, empty vector; OE, ALKBH5 overexpression. ***$P < 0.001$, ****$P < 0.0001$.

FBXL5 RNA dependent on m^{6}A demethylation. According to the above-mentioned results of m^{6}A-seq, ALKBH5 overexpression led to a significant reduction in the m^{6}A levels at the third exon of *FBXL5* in both poly(A) RNA- and total RNA-based data (**Figures 4B,C**), which was consequently validated by m^{6}A-IP-qPCR (**Figure 4D**). Meanwhile, we also detected a physical interaction between the ALKBH5 protein and *FBXL5* RNA (**Figure 4E**). On the basis of positive regulation of ALKBH5 on *FBXL5* expression (**Figure 4F**), we performed an RNA stability assay and found that ALKBH5 overexpression substantially delayed its RNA degradation (**Figure 4G**). In parallel, we also observed significant decrease in the m^{6}A level around the last exon of *SLC25A28* (**Supplementary Figures 4A–C**). Furthermore, ALKBH5 protein interacted with *SLC25A28* RNA (**Supplementary Figure 4D**) and affected its expression and RNA stability as well (**Supplementary Figures 4E,F**). However, despite of the above evidence, *SLC25A28* RNA exhibited a relatively weaker correlation with ALKBH5 in their RNA expression levels in PDAC patients ($R = 0.21$, $P = 0.006$) (**Supplementary Figure 4G**). Taken together, we show here that *FBXL5* and *SLC25A28* RNAs are potential substrate RNAs regulated by ALKBH5 in their RNA stabilities.

ALKBH5 Regulates Alternative Splicing of *SLC25A37*

Besides RNA decay, RNA m^{6}A methylation can also modulate AS of RNAs co-transcriptionally (Zhou et al., 2019). Thus, we utilized *rMATS* to detect the differential utilization of splicing sites for five types of AS events (A5SS, A3SS, MXE, RI, and SE) between the OE and EV samples. We detected varying numbers of AS events (**Supplementary Table 8**), which exhibited significant changes in the OE sample (**Figure 5A**). Considering that some of the differential AS events may be induced by aberrant methylation elicited by ALKBH5 overexpression, we analyzed the RNAs harboring both hypo-methylation and altered AS events after ALKBH5 overexpression (**Figure 5B**). Consequently, seven RNAs were filtered out. By combining with the total RNA-based m^{6}A-seq data (**Supplementary Tables 8**, **9**), we found that only *SLC25A37* exhibited significant changes in its methylation level and AS (**Figure 5C** and **Supplementary Figure 5**). We found that two types of AS (A5SS and A3SS) events occurred within the two hypo-methylated regions in *SLC25A37*, which generated four types of isoforms with different inclusion levels before and after ALKBH5 overexpression (**Figures 5D,E**). Isoform 4# corresponds to the canonical

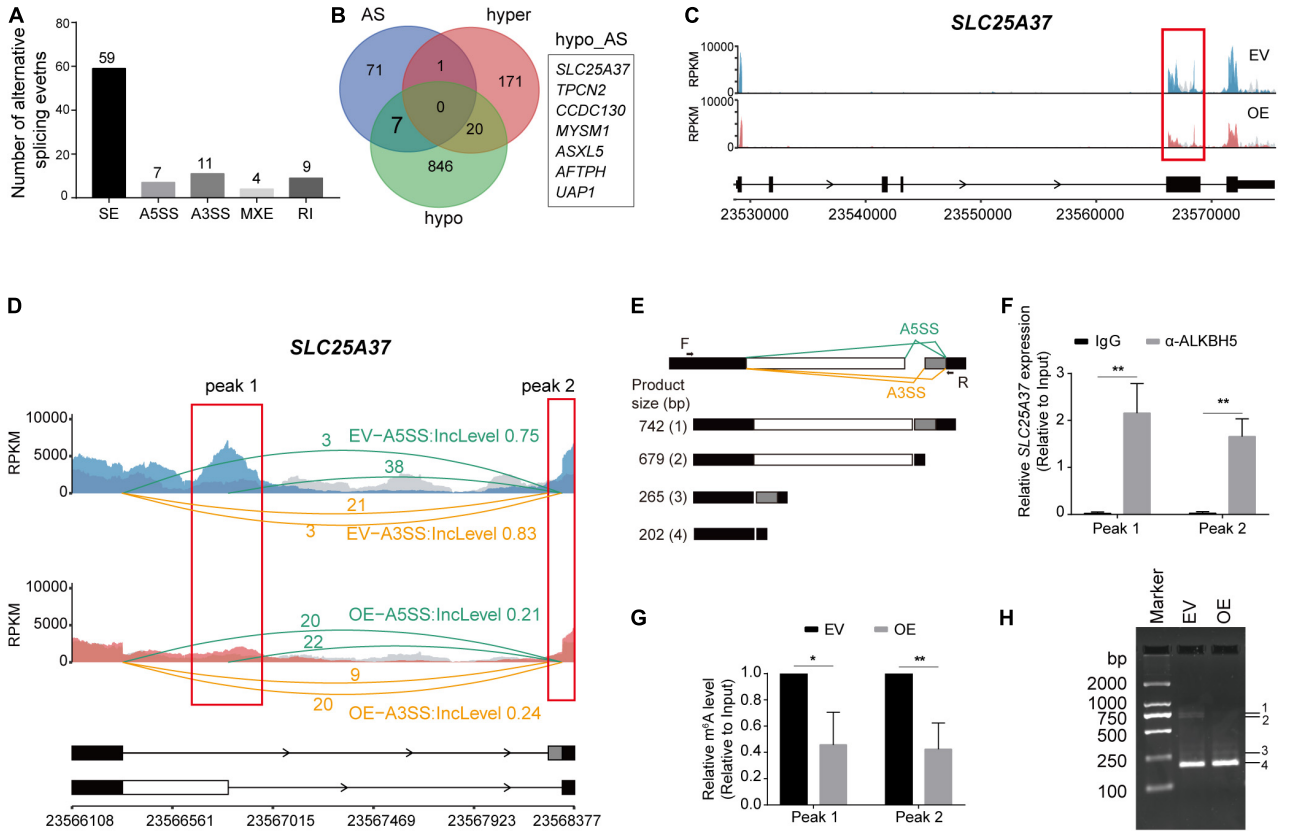


FIGURE 5 | ALKBH5 regulates the alternative splicing events of *SLC25A37* RNA. **(A)** Statistics of the five types of alternative splicing events that are identified as significantly different in OE sample compared with EV sample. The differential alternative splicing events (FDR < 0.05) are identified by *rMATS*. **(B)** Venn plot exhibiting the intersects among the RNAs with hyper-, hypo-methylation peaks or differential alternative splicing events in OE sample. **(C)** Sequencing read density for input and m^{6}A-IP samples along *SLC25A37* transcript. **(D)** Zoom-in of the hypo-methylated region on *SLC25A37* transcript. Sequencing read density of input and m^{6}A-IP libraries along with exon junction read number were indicated. Inclusion levels of A3SS and A5SS events in both samples are recorded. Two concrete m^{6}A peaks (Peak 1 and Peak 2) intersecting with alternative splicing sites are marked with red rectangles. **(E)** Diagram showing the alternative splicing formats of A5SS and A3SS on *SLC25A28* transcript. Black arrows denote the position of PCR primers. Below the figure exhibiting different splicing variants and their molecular weights of PCR products. **(F)** RIP-qPCR results showing the interaction between ALKBH5 protein and *SCL25A37* RNA at the two indicated regions in MIA PaCa-2 cells. **(G)** Results of m^{6}A-RIP-qPCR showing the methylation changes at the two indicated regions between EV and OE samples. **(H)** PCR results showing the size and quantity of four types of transcripts in ALKBH5-overexpressing and control cells. $^*P < 0.05$, $^{**}P < 0.01$.

protein-coding transcript with normal length and function in mitochondrial iron delivery (Wang et al., 2011) (**Supplementary Figure 6**). In contrast, the splicing variants 2# and 3# were characterized by a retained intron, resulting from the A5SS and A3SS, respectively (**Figure 5E**). Notably, the sequence annotations in ENSEMBL (Howe et al., 2021) illuminated that the retained introns of isoforms 2# and 3# had a stop codon, which could generate a truncated mutant of 155 or 159 aa, respectively (**Supplementary Figure 6**). Moreover, an additional splicing variant 1# was also detected, which contained two pieces of retained introns and could have arisen from the concomitance of the A5SS and A3SS events. Similar to isoform 2#, it may be translated into a truncated protein mutant of 155 aa due to the presence of stop codon after the A5SS. We performed RIP-qPCR to detect the interaction between the ALKBH5 protein and *SLC25A37* RNA (**Figure 5F**), followed by m^{6}A-IP-qPCR to confirm the effect of ALKBH5 on its m^{6}A levels within two hypo-methylated regions (**Figure 5G**). Thereafter, we compared the RNA abundance of the four types of isoforms with PCR using a pair of primers capable of amplifying all the transcripts (**Figure 5E**). As shown in **Figure 5H**, we detected an increase in isoform 4#, corresponding to the decrease in isoform 1# and 2#, which was indicative of the presence of more functional transcripts of *SLC25A37* in the OE MIA PaCa-2 cells. Together, we show here that ALKBH5 regulates the RNA splicing of *SLC25A37* in m^{6}A-dependent manner.

ALKBH5 Modulates Iron Metabolism Regulators and Their Downstream Targets

After identifying *FBXL5*, *SLC25A28,* and *SLC25A37* as substrate RNAs of ALKBH5, we further investigated the relevant mechanism associated with pancreatic cancer progression. In line with the effects of ALKBH5 on their RNA stabilities or AS patterns, we detected an elevation in the expressions of

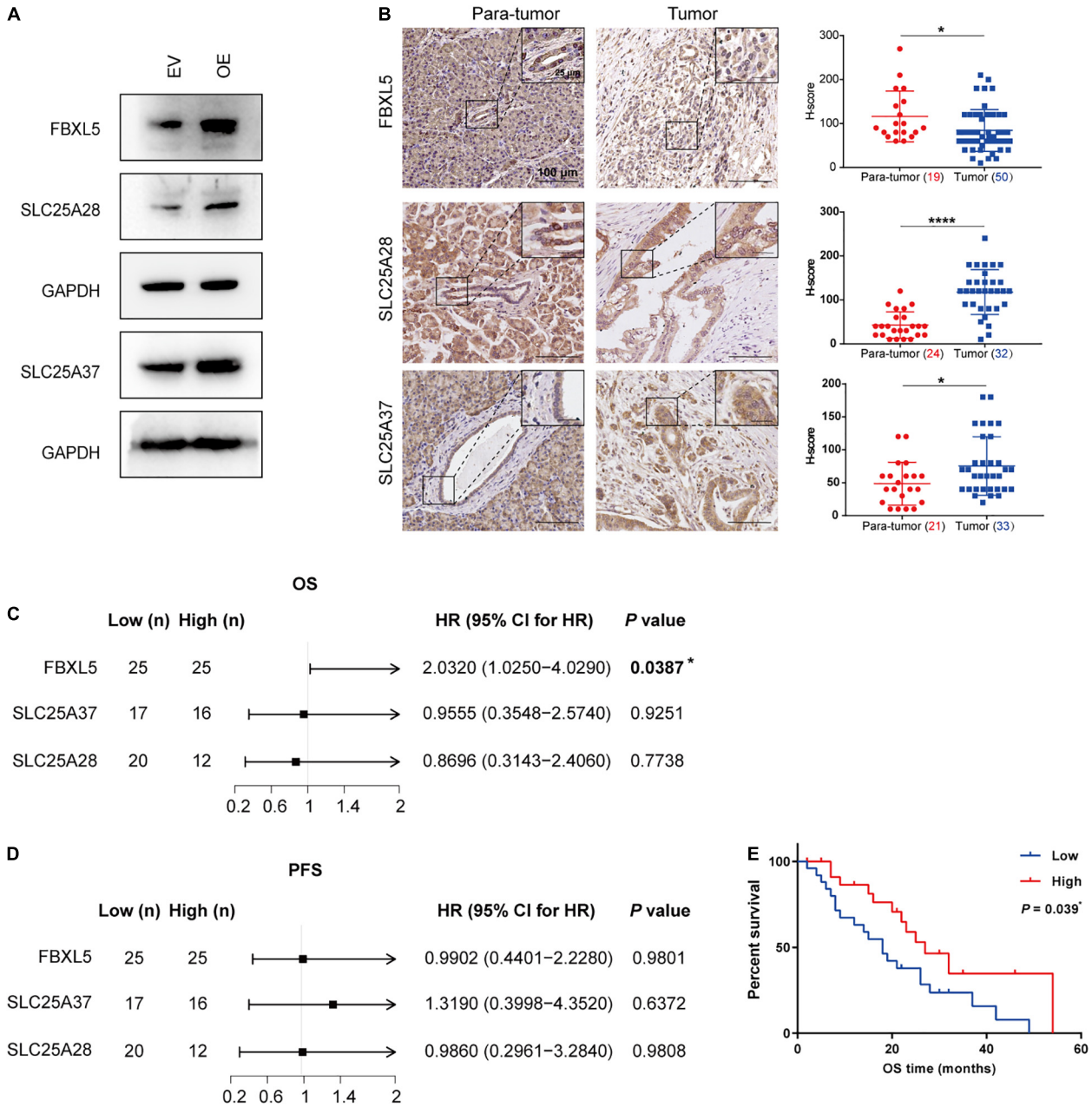


FIGURE 6 | Downregulation of FBXL5 in PDAC predicts poor prognosis. **(A)** Western blot analysis showing the effect of ALKBH5 overexpression on FBXL5, SLC25A28, and SLC25A37. EV, empty vector; OE, ALKBH5-overexpressing cells. GAPDH is used as an internal control. **(B)** Representative images of immunohistochemical staining showing the expressions of FBXL5, SLC25A28, and SLC25A37 in para-tumor and tumor cells. Enlarged images in the box are shown in the upper right. Scatter plots showing the *H*-scores of each gene in para-tumor and tumor cells are shown in the right. Case numbers are shown in brackets. Scale bars, 100 or 25 μm. **(C,D)** Log-rank analysis of correlation between overall survival (OS) or progression-free survival (PFS) and the expression of FBXL5, SLC25A28 and SLC 25A37 in tumors. **(E)** Kaplan–Meier curves for OS of FBXL5 protein expression. $^{*}P < 0.05$, $^{****}P < 0.0001$.

FBXL5 and SLC25A28 proteins in OE sample, as well as the functional protein form of SLC25A37 (**Figure 6A**). Furthermore, we examined their *in situ* protein expressions in tumor samples of PDAC patients. As expected, we observed significant decrease in the expression of FBXL5 protein (**Figure 6B**), which was in agreement with our results obtained *in vitro*. However, both SLC25A28 and SLC25A37 were upregulated in PDAC samples (**Figure 6B**). In addition, log-rank analysis showed that low expression of FBXL5 protein was associated with worse prognosis, while we failed to observe any correlation for SLC25A28 and SLC25A37 proteins (**Figures 6C–E**).

FBXL5 protein plays a role in polyubiquitination and degradation of iron regulatory protein 2 (IRP2) and modulator of epithelial-mesenchymal transition (EMT) SNAI1

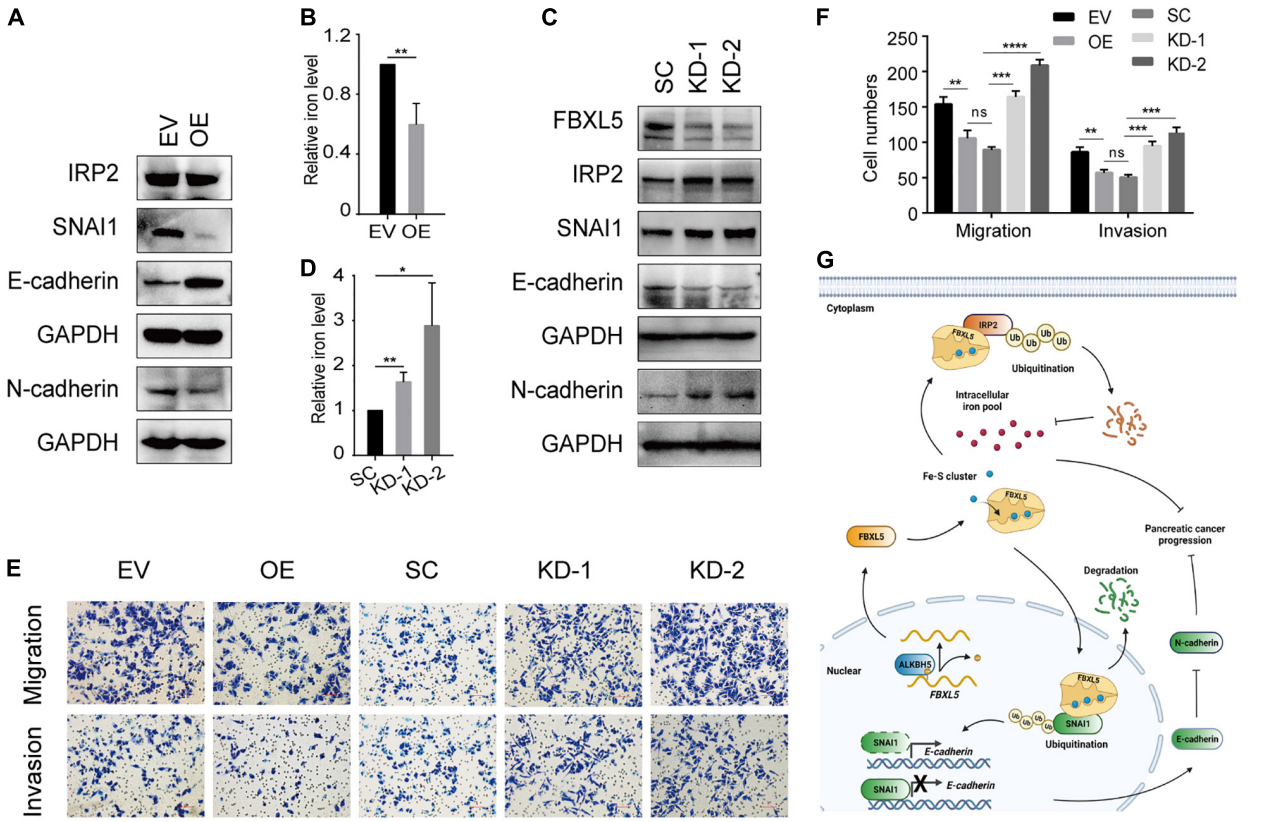


FIGURE 7 | ALKBH5 protects against tumor progression in PDAC by targeting regulators of iron metabolism. **(A)** Western blot analysis showing the expressions of IRP2, SNAI1, E-cadherin, and N-cadherin in ALKBH5-overexpressing cells. EV, empty vector; OE, ALKBH5-overexpressing cells. GAPDH is used as an internal control. **(B)** Intracellular iron assay showing the effect of ALKBH5 overexpression on intracellular iron levels. **(C)** Western blot analysis showing the effect of *FBXL5* knockdown in rescuing the expression of IRP2, SNAI1, E-cadherin, and N-cadherin in ALKBH5-overexpressing cells. SC, scramble control; KD-1, *FBXL5* knockdown-1; KD-2, *FBXL5* knockdown-2. **(D)** Intracellular iron assay showing the effect of *FBXL5* knockdown in restoring intracellular iron levels in ALBKH5-overexpressing cells. **(E)** Cell migration and invasion assays of *FBXL5* knockdown in OE. **(F)** Statistical analysis for the result of transwell assays in **(E)**. Cell numbers per field were presented as the mean ± SD. $^{*}P < 0.05$, $^{**}P < 0.01$, $^{***}P < 0.001$, $^{****}P < 0.0001$. **(G)** Schematic diagram depicting the role of ALKBH5 in attenuating pancreatic tumorigenesis through targeting regulators of iron metabolism. (Created with BioRender.com).

(Vinas-Castells et al., 2014; Wang H. et al., 2020). Accordingly, we found that ALKBH5 overexpression resulted in reduced expression of IRP2 protein (**Figure 7A**) and resultant reduction of intracellular iron levels (**Figure 7B**). ALKBH5-overexpression also led to downregulation of SNAI1, accompanied with upregulation of E-cadherin and downregulation of N-cadherin (**Figure 7A**). Intriguingly, we found that *FBXL5* knockdown rescued the expression of IRP2, SNAI1, and the two EMT markers (**Figure 7C**). Likewise, we observed a robust recovery of intracellular iron accumulation, as well as cell migratory and invasive abilities (**Figures 7D–F**). To validate the above findings, we examined the expression levels of IRP2 and SNAI1 proteins in PDAC samples. In line with downregulation of FBXL5 in tumor cells of PDAC, we found that both IRP2 and SNAI1 were upregulated (**Supplementary Figure 7A**). Notably, log-rank test showed that increased expression of IRP2 in tumor were associated with poor OS, while increased expression of SNAI1 was associated with poor PFS (**Supplementary Figures 7B–E**).

On the basis of the above identified functions of ALKBH5-FBXL5-IRP2/SNAI1 axis in pancreatic cancer cells, we proposed a working model for ALKBH5 in attenuating pancreatic tumorigenesis (**Figure 7G**). As an RNA m^6A demethylase, ALKBH5 induces upregulation of FBXL5 via promoting its RNA stability. Subsequently, FBXL5 triggers the ubiquitination of IRP2 and SNAI1 proteins. IRP2 degradation would protect cells from intracellular iron overload, while downregulated SNAI1 suppresses the EMT process. Consequently, both of these actions contribute to impair tumor progression in ALKBH5-overexpressing cells. Taken together, our results reveal that ALKBH5 attenuates pancreatic cancer progression by targeting the regulators of iron metabolism.

DISCUSSION

The present study analyzed the clinical relevance of eight RNA m^6A regulators based on their protein levels in the tumor and stromal cells in PDAC. We found that ALKBH5 was downregulated in the PDAC tumor cells and served as an independent, favorable prognostic marker. Mechanistically, we

identified that ALKBH5 regulates the RNA stability of *FBXL5* and *SLC25A28*, as well as the AS of *SLC25A37*. Notably, we show here that upon ALKBH5 overexpression, the stabilized *FBXL5* further elicited the downregulation of the IRP2 and SNAI1 proteins, both of which are substrates ubiquitinated by FBXL5 and are crucial drivers of tumor progression.

The PDAC is a complex disease, by virtue of its heterogeneous cancer cell populations and extensive desmoplastic stroma (Neesse et al., 2019; Peng et al., 2019). The active crosstalk between the stromal and tumor cells is crucial in driving tumor progression (Hessmann et al., 2020). To date, the known functions of m^{6}A regulators in PDAC tumorigenesis were limited to tumor cells only, which originate from normal pancreatic ductal epithelial cells and represent only a minority of the tissue mass in PDAC (Lee et al., 2019). Here we analyzed the expression levels of eight RNA m^{6}A regulators in the tumor stroma cells to gain a better understanding of their distinctive characterization. Consequently, we observed a significant difference in the expressions of several RNA m^{6}A regulators between the tumor cells and stromal cells. Particularly, the expression levels of the FTO and YTHDF1 proteins in the stroma were positively correlated with the OS or PFS of PDAC patients. These results suggest that m^{6}A modification has an extensive influence on different components of PDAC tumor tissues, which warrants intensive investigation. It is noteworthy that although previous studies reported that the expressions of METTL3, METTL14, and WTAP exhibited negative correlation with the "patients' OS" (Li et al., 2017; Xia et al., 2019; Wang M. et al., 2020), we did not obtain the same results in this study, probably owing to differences in the respective sizes of the study cohorts.

Intriguingly, out of the eight RNA m^{6}A regulators analyzed in this study, only ALKBH5 served as an independent favorable prognostic factor, suggesting its massive impact in the progression of pancreatic cancer. Mounting evidences state that ALKBH5 plays versatile roles in various cancers. Concretely, ALKBH5 acts as an oncogene in glioblastoma (Zhang et al., 2017), acute myeloid leukemia (Shen et al., 2020), breast cancer (Zhang et al., 2016), and ovarian carcinoma (Jiang et al., 2020), while functioning as a tumor suppressor in lung cancer (Zhang et al., 2021), hepatocellular carcinoma (Chen et al., 2020), and osteosarcoma (Yuan et al., 2021). Moreover, it has also been reported that ALKBH5 exhibits tumor suppressive and chemo-sensitizing effects in pancreatic cancer cells (Guo et al., 2020; Tang et al., 2020). Nevertheless, different from our findings here, they identified *WIF-1* and *PER1* RNAs as key targets of ALKBH5, which further impacts the downstream WNT signaling and ATM-CHK2-P53/CC25C pathway, respectively (Guo et al., 2020; Tang et al., 2020). These studies imply that ALKBH5 disturbs myriad pathways to inhibit pancreatic cancer tumorigenesis.

In order to facilitate an in-depth scrutiny of the regulatory mechanism of ALKBH5 in PDAC, we exploited two types of m^{6}A-seq analyses to identify its substrate RNAs, with respect to RNA stability or AS. We found that ALKBH5 regulated RNA decay of *FBXL5*, *SLC25A28*, and the AS of *SLC25A37*. Intriguingly, all of the three genes are involved in regulating iron metabolism. Iron is essential for diverse biological processes, while dysregulation of iron metabolism may lead to tumor progression and affects the response to therapy (Torti and Torti, 2020a). Although accumulating data implicate the association between m^{6}A and tumor development, knowledge about the crosstalk between m^{6}A and iron metabolism is extremely limited. FBXL5 is a member of the SCF ubiquitin ligase complex that specifically recognizes IRP2 (Wang H. et al., 2020), while FBXL5-IRP2 axis is integral to the control of iron metabolism (Moroishi et al., 2011). Accordingly, we found that in pancreatic cancer cells, ALKBH5-overexpression led to reduction of intracellular iron levels, and this could be restored via *FBXL5* knockdown. Thus, we deduce that the protective role of ALKBH5 in pancreatic cancer is closely related to FBXL5-mediated regulation of iron metabolism. Similarly, studies have reported that FBXL5 also plays a crucial role in tumor suppression in gastric (Wu et al., 2015) and liver cancers (Muto et al., 2019) via the maintenance of iron homeostasis. It has been reported that chronic exposure to excessive iron promotes EMT in pancreatic cancer and carcinogenesis (Bhutia et al., 2020). On the other hand, nuclear FBXL5 protein also functions as a ubiquitin ligase of SNAI1 (Vinas-Castells et al., 2014), which is a key modulator of the EMT and thus involved in multiple kinds of cancers (Moody et al., 2005; Carmichael et al., 2020; Chen R. et al., 2021). Therefore, FBXL5-induced degradation of SNAI1 protein and subsequent EMT changes also contributed to hinder tumor progression of PDAC. Combining the downregulation of FBXL5 in pancreatic cancer samples and its positive correlation with survival, our results indicate that FBXL5, as a downstream target of ALKBH5, plays a vital role in protecting against pancreatic cancer. Notably, significant downregulation of *Fbxl5* was also observed in the testis of *Alkbh5*-deficient mice, while the mechanism remains unknown (Zheng et al., 2013). It is worth to investigate whether ALKBH5-FBXL5 pathway is involved in multiple biological processes. Apart from our observation, a recent study found that YTHDF1 induced HPSCC tumorigenesis depended on iron metabolism (Ye et al., 2020). Given the significantly lower expression of YTHDF1 in the stromal cells and positive correlation with OS of patients with PDAC observed in this study, it will be interesting to determine whether stromal YTHDF1 also exerts an iron-metabolism dependent protective role in pancreatic cancer.

Previous studies reported that patients with erythropoietic protoporphyria (Wang et al., 2011) or myelodysplastic syndrome (Visconte et al., 2015) exhibited a significant decrease in the levels of the normal SLC25A37 isoform, accompanied with an increase in its abnormal isoform encoding a defective protein. Intriguingly, the same two types of isoforms were detected here in the pancreatic cell line. This may explain the reason for the elevated levels of normal SLC25A37 protein observed in the OE MIA PaCa-2 cells. Both SLC25A28 and SLC25A37 were essential for mitochondrial iron delivery and iron-sulfur (Fe-S) cluster synthesis (Kunji et al., 2020). Notably, FBXL5 protein harbors Fe-S clusters, which is indispensable for the recognition of IRP2 and promoting its degradation (Wang H. et al., 2020). Oppositely, defective Fe-S biogenesis caused ubiquitination and degradation of FBXL5, which in turn stabilized IRP2 (Rouault and Maio, 2020). Therefore, our results suggested that the ALKBH5-induced upregulation of

SLC25A28 and SLC25A37 contributed to stabilization of FBXL5 protein. However, despite of positive regulation of ALKBH5 on SLC25A28 and SLC25A37 observed here, we found that these two proteins were overexpressed in the tumor cells of PDAC. We deduce that there may exist complicated mechanism in regulating their gene expressions and functions *in vivo*, which could not be fully characterized through cell line-based studies. For example, an *in vivo* studies by Li et al. (2018) reported that PINK1-PARK2 pathway mediated degradation of SLC25A37 and SLC25A28 proteins via autophagy-dependent pathway, thus preventing from mitochondria iron overload and tumorigenesis of PDAC. Similarly, the relative weaker correlation of RNA expression between *SLC25A28* and *ALKBH5* in tumor samples may also arise from other uncharacterized mechanisms in regulating SLC25A28. Therefore, the regulatory mechanism of SLC25A37 and SLC25A28, and their involvement in iron metabolism deserve intensive investigation.

CONCLUSION

Our study reveals a previously uncharacterized mechanism of ALKBH5 in protecting against pancreatic cancer through modulating regulators of iron metabolism regulators and expanded our understanding of the association between m^{6}A and iron homeostasis. Our results also underscored the multifaceted roles of m^{6}A in pancreatic cancer, thus providing insight for the development of efficient therapeutic strategies for PDAC.

DATA AVAILABILITY STATEMENT

The raw m^{6}A-seq data presented in this study have been deposited in the Genome Sequence Archive in BIG Data Center, Beijing Institute of Genomics (BIG), Chinese Academy of Sciences, under accession number HRA000878 that are accessible at https://bigd.big.ac.cn.

ETHICS STATEMENT

The studies involving human participants were reviewed and approved by the Ethics Committee of the Peking Union Medical College Hospital (JS-1490). The patients/participants provided their written informed consent to participate in this study.

AUTHOR CONTRIBUTIONS

ZL and YN conceived this study and supervised the project. RH, ZZ, XL, and YF modified the methodology and performed the assays. LY analyzed the m^{6}A-seq data. ZL and ZZ performed the clinical analysis. RH and LY wrote the manuscript. ZL, YN, and W-MT revised it. All authors read and approved the final manuscript.

FUNDING

This work was supported by Intergovernmental International Science, Technology and Innovation Cooperation Key Project of the National Key R&D Program (NKP) (Project No. 2017YFE0110300) and National Natural Science Foundation of China (Project No. 82072749). This work was also partially supported by the National Key R&D Program of China (2019YFA0801703).

ACKNOWLEDGMENTS

We thank Chunhui Ma, Yao Zhang, and Mengqi Chang for providing technical assistance. We also thank Jiemin Chen and Junyi Pang for their assistance with IP and IHC; Shenwen Yang, Shangyu Liu, and Chen Wang for their help with survival data analysis.

SUPPLEMENTARY MATERIAL

The Supplementary Material for this article can be found online at: https://www.frontiersin.org/articles/10.3389/fcell.2021.724282/full#supplementary-material

REFERENCES

Barbieri, I., and Kouzarides, T. (2020). Role of RNA modifications in cancer. *Nat. Rev. Cancer* 20, 303–322. doi: 10.1038/s41568-020-0253-2

Bhutia, Y. D., Ogura, J., Grippo, P. J., Torres, C., Sato, T., Wachtel, M., et al. (2020). Chronic exposure to excess iron promotes EMT and cancer via p53 loss in pancreatic cancer. *Asian J. Pharm. Sci.* 15, 237–251. doi: 10.1016/j.ajps.2020.02.003

Carmichael, C. L., Wang, J., Nguyen, T., Kolawole, O., Benyoucef, A., De Maziere, C., et al. (2020). The EMT modulator SNAI1 contributes to AML pathogenesis via its interaction with LSD1. *Blood* 136, 957–973. doi: 10.1182/blood.2019002548

Chang, M., Lv, H., Zhang, W., Ma, C., He, X., Zhao, S., et al. (2017). Region-specific RNA m^{6}A methylation represents a new layer of control in the gene regulatory network in the mouse brain. *Open Biol.* 7:170166. doi: 10.1098/rsob.170166

Chen, J., Sun, Y., Xu, X., Wang, D., He, J., Zhou, H., et al. (2017). YTH domain family 2 orchestrates epithelial-mesenchymal transition/proliferation dichotomy in pancreatic cancer cells. *Cell Cycle* 16, 2259–2271. doi: 10.1080/15384101.2017.1380125

Chen, R., Masuo, K., Yogo, A., Yokoyama, S., Sugiyama, A., Seno, H., et al. (2021). SNAIL regulates gastric carcinogenesis through CCN3 and NEFL. *Carcinogenesis* 42, 190–201. doi: 10.1093/carcin/bgaa133

Chen, S., Yang, C., Wang, Z. W., Hu, J. F., Pan, J. J., Liao, C. Y., et al. (2021). CLK1/SRSF5 pathway induces aberrant exon skipping of METTL14 and Cyclin L2 and promotes growth and metastasis of pancreatic cancer. *J. Hematol. Oncol.* 14:60. doi: 10.1186/s13045-021-01072-8

Chen, Y., Zhao, Y., Chen, J., Peng, C., Zhang, Y., Tong, R., et al. (2020). ALKBH5 suppresses malignancy of hepatocellular carcinoma via m^{6}A-guided epigenetic inhibition of LYPD1. *Mol. Cancer* 19:123. doi: 10.1186/s12943-020-01239-w

Guo, X., Li, K., Jiang, W., Hu, Y., Xiao, W., Huang, Y., et al. (2020). RNA demethylase ALKBH5 prevents pancreatic cancer progression by

posttranscriptional activation of PER1 in an m^{6}A-YTHDF2-dependent manner. *Mol. Cancer* 19:91. doi: 10.1186/s12943-020-01158-w

Heinz, S., Benner, C., Spann, N., Bertolino, E., Lin, Y. C., Laslo, P., et al. (2010). Simple combinations of lineage-determining transcription factors prime cis-regulatory elements required for macrophage and B cell identities. *Mol. Cell* 38, 576–589. doi: 10.1016/j.molcel.2010.05.004

Hessmann, E., Buchholz, S. M., Demir, I. E., Singh, S. K., Gress, T. M., Ellenrieder, V., et al. (2020). Microenvironmental determinants of pancreatic cancer. *Physiol. Rev*. 100, 1707–1751. doi: 10.1152/physrev.00042.2019

Hou, Y., Zhang, Q., Pang, W., Hou, L., Liang, Y., Han, X., et al. (2021). YTHDC1-mediated augmentation of miR-30d in repressing pancreatic tumorigenesis via attenuation of RUNX1-induced transcriptional activation of Warburg effect. *Cell Death Differ*. doi: 10.1038/s41418-021-00804-0 [Epub ahead of print].

Howe, K. L., Achuthan, P., Allen, J., Allen, J., Alvarez-Jarreta, J., Amode, M. R., et al. (2021). Ensembl 2021. *Nucleic Acids Res.* 49, D884–D891. doi: 10.1093/nar/gkaa942

Hsu, P. J., Zhu, Y., Ma, H., Guo, Y., Shi, X., Liu, Y., et al. (2017). Ythdc2 is an N^6-methyladenosine binding protein that regulates mammalian spermatogenesis. *Cell Res.* 27, 1115–1127. doi: 10.1038/cr.2017.99

Huang da, W., Sherman, B. T., and Lempicki, R. A. (2009a). Bioinformatics enrichment tools: paths toward the comprehensive functional analysis of large gene lists. *Nucleic Acids Res.* 37, 1–13. doi: 10.1093/nar/gkn923

Huang da, W., Sherman, B. T., and Lempicki, R. A. (2009b). Systematic and integrative analysis of large gene lists using DAVID bioinformatics resources. *Nat. Protoc.* 4, 44–57. doi: 10.1038/nprot.2008.211

Huang, H., Weng, H., and Chen, J. (2020). m^{6}A modification in coding and non-coding RNAs: roles and therapeutic implications in cancer. *Cancer Cell* 37, 270–288. doi: 10.1016/j.ccell.2020.02.004

Jiang, Y., Wan, Y., Gong, M., Zhou, S., Qiu, J., and Cheng, W. (2020). RNA demethylase ALKBH5 promotes ovarian carcinogenesis in a simulated tumour microenvironment through stimulating NF-kappaB pathway. *J. Cell. Mol. Med*. 24, 6137–6148. doi: 10.1111/jcmm.15228

Kunji, E. R. S., King, M. S., Ruprecht, J. J., and Thangaratnarajah, C. (2020). The SLC25 carrier family: important transport proteins in mitochondrial physiology and pathology. *Physiology* 35, 302–327. doi: 10.1152/physiol.00009.2020

Lee, A. Y. L., Dubois, C. L., Sarai, K., Zarei, S., Schaeffer, D. F., Sander, M., et al. (2019). Cell of origin affects tumour development and phenotype in pancreatic ductal adenocarcinoma. *Gut* 68, 487–498. doi: 10.1136/gutjnl-2017-314426

Li, B. Q., Huang, S., Shao, Q. Q., Sun, J., Zhou, L., You, L., et al. (2017). WT1-associated protein is a novel prognostic factor in pancreatic ductal adenocarcinoma. *Oncol. Lett.* 13, 2531–2538. doi: 10.3892/ol.2017.5784

Li, B. Q., Liang, Z. Y., Seery, S., Liu, Q. F., You, L., Zhang, T. P., et al. (2019). WT1 associated protein promotes metastasis and chemo-resistance to gemcitabine by stabilizing Fak mRNA in pancreatic cancer. *Cancer Lett.* 451, 48–57. doi: 10.1016/j.canlet.2019.02.043

Li, C., Zhang, Y., Cheng, X., Yuan, H., Zhu, S., Liu, J., et al. (2018). PINK1 and PARK2 suppress pancreatic tumorigenesis through control of mitochondrial iron-mediated immunometabolism. *Dev. Cell* 46, 441–455.e8. doi: 10.1016/j.devcel.2018.07.012

Lin, Z., Hsu, P. J., Xing, X., Fang, J., Lu, Z., Zou, Q., et al. (2017). Mettl3-/Mettl14-mediated mRNA N^6-methyladenosine modulates murine spermatogenesis. *Cell Res.* 27, 1216–1230. doi: 10.1038/cr.2017.117

Love, M. I., Huber, W., and Anders, S. (2014). Moderated estimation of fold change and dispersion for RNA-seq data with DESeq2. *Genome Biol.* 15:550. doi: 10.1186/s13059-014-0550-8

Lv, J., Zhang, Y., Gao, S., Zhang, C., Chen, Y., Li, W., et al. (2018). Endothelial-specific m^{6}A modulates mouse hematopoietic stem and progenitor cell development via Notch signaling. *Cell Res.* 28, 249–252. doi: 10.1038/cr.2017.143

Ma, C., Chang, M., Lv, H., Zhang, Z. W., Zhang, W., He, X., et al. (2018). RNA m^{6}A methylation participates in regulation of postnatal development of the mouse cerebellum. *Genome Biol.* 19:68. doi: 10.1186/s13059-018-1435-z

McCarthy, D. J., Chen, Y., and Smyth, G. K. (2012). Differential expression analysis of multifactor RNA-Seq experiments with respect to biological variation. *Nucleic Acids Res.* 40, 4288–4297. doi: 10.1093/nar/gks042

Meng, J., Cui, X., Rao, M. K., Chen, Y., and Huang, Y. (2013). Exome-based analysis for RNA epigenome sequencing data. *Bioinformatics* 29, 1565–1567. doi: 10.1093/bioinformatics/btt171

Mizrahi, J. D., Surana, R., Valle, J. W., and Shroff, R. T. (2020). Pancreatic cancer. *Lancet* 395, 2008–2020. doi: 10.1016/S0140-6736(20)30974-0

Moody, S. E., Perez, D., Pan, T. C., Sarkisian, C. J., Portocarrero, C. P., Sterner, C. J., et al. (2005). The transcriptional repressor Snail promotes mammary tumor recurrence. *Cancer Cell* 8, 197–209. doi: 10.1016/j.ccr.2005.07.009

Moroishi, T., Nishiyama, M., Takeda, Y., Iwai, K., and Nakayama, K. I. (2011). The FBXL5-IRP2 axis is integral to control of iron metabolism in vivo. *Cell Metab.* 14, 339–351. doi: 10.1016/j.cmet.2011.07.011

Muto, Y., Moroishi, T., Ichihara, K., Nishiyama, M., Shimizu, H., Eguchi, H., et al. (2019). Disruption of FBXL5-mediated cellular iron homeostasis promotes liver carcinogenesis. *J. Exp. Med.* 216, 950–965. doi: 10.1084/jem.20180900

Neesse, A., Bauer, C. A., Ohlund, D., Lauth, M., Buchholz, M., Michl, P., et al. (2019). Stromal biology and therapy in pancreatic cancer: ready for clinical translation? *Gut* 68, 159–171. doi: 10.1136/gutjnl-2018-316451

Peng, J., Sun, B. F., Chen, C. Y., Zhou, J. Y., Chen, Y. S., Chen, H., et al. (2019). Single-cell RNA-seq highlights intra-tumoral heterogeneity and malignant progression in pancreatic ductal adenocarcinoma. *Cell Res.* 29:777. doi: 10.1038/s41422-019-0195-y

Rouault, T. A., and Maio, N. (2020). How oxidation of a unique iron-sulfur cluster in FBXL5 regulates IRP2 levels and promotes regulation of iron metabolism proteins. *Mol. Cell* 78, 1–3. doi: 10.1016/j.molcel.2020.03.020

Shen, C., Sheng, Y., Zhu, A. C., Robinson, S., Jiang, X., Dong, L., et al. (2020). RNA demethylase ALKBH5 selectively promotes tumorigenesis and cancer stem cell self-renewal in acute myeloid leukemia. *Cell Stem Cell* 27, 64–80.e9. doi: 10.1016/j.stem.2020.04.009

Shen, S., Park, J. W., Lu, Z. X., Lin, L., Henry, M. D., Wu, Y. N., et al. (2014). rMATS: robust and flexible detection of differential alternative splicing from replicate RNA-Seq data. *Proc. Natl. Acad Sci. U.S.A.* 111, E5593–E5601. doi: 10.1073/pnas.1419161111

Siegel, R. L., Miller, K. D., Fuchs, H. E., and Jemal, A. (2021). Cancer Statistics, 2021. *CA Cancer J. Clin.* 71, 7–33. doi: 10.3322/caac.21654

Tang, B., Yang, Y., Kang, M., Wang, Y., Wang, Y., Bi, Y., et al. (2020). m^{6}A demethylase ALKBH5 inhibits pancreatic cancer tumorigenesis by decreasing WIF-1 RNA methylation and mediating Wnt signaling. *Mol. Cancer* 19:3. doi: 10.1186/s12943-019-1128-6

Tang, X., Liu, S., Chen, D., Zhao, Z., and Zhou, J. (2019). The role of the fat mass and obesity-associated protein in the proliferation of pancreatic cancer cells. *Oncol. Lett.* 17, 2473–2478. doi: 10.3892/ol.2018.9873

Tang, Z., Li, C., Kang, B., Gao, G., Li, C., and Zhang, Z. (2017). GEPIA: a web server for cancer and normal gene expression profiling and interactive analyses. *Nucleic Acids Res* .45, W98–W102. doi: 10.1093/nar/gkx247

Torti, S. V., and Torti, F. M. (2020b). Iron: the cancer connection. *Mol. Aspects Med.* 75:100860. doi: 10.1016/j.mam.2020.100860

Torti, S. V., and Torti, F. M. (2020a). Iron and cancer: 2020 vision. *Cancer Res.* 80, 5435–5448. doi: 10.1158/0008-5472.CAN-20-2017

Vinas-Castells, R., Frias, A., Robles-Lanuza, E., Zhang, K., Longmore, G. D., Garcia de Herreros, A., et al. (2014). Nuclear ubiquitination by FBXL5 modulates snail1 DNA binding and stability. *Nucleic Acids Res.* 42, 1079–1094. doi: 10.1093/nar/gkt935

Visconte, V., Avishai, N., Mahfouz, R., Tabarroki, A., Cowen, J., Sharghi-Moshtaghin, R., et al. (2015). Distinct iron architecture in SF3B1-mutant myelodysplastic syndrome patients is linked to an SLC25A37 splice variant with a retained intron. *Leukemia* 29, 188–195. doi: 10.1038/leu.2014.170

Wang, C. X., Cui, G. S., Liu, X., Xu, K., Wang, M., Zhang, X. X., et al. (2018). METTL3-mediated m^{6}A modification is required for cerebellar development. *PLoS Biol.* 16:e2004880. doi: 10.1371/journal.pbio.2004880

Wang, H., Shi, H., Rajan, M., Canarie, E. R., Hong, S., Simoneschi, D., et al. (2020). FBXL5 regulates IRP2 stability in iron homeostasis via an oxygen-responsive [2Fe2S] cluster. *Mol. Cell* 78, 31–41.e35. doi: 10.1016/j.molcel.2020.02.011

Wang, M., Liu, J., Zhao, Y., He, R., Xu, X., Guo, X., et al. (2020). Upregulation of METTL14 mediates the elevation of PERP mRNA N^6 adenosine methylation promoting the growth and metastasis of pancreatic cancer. *Mol. Cancer* 19:130. doi: 10.1186/s12943-020-01249-8

Wang, Y., Langer, N. B., Shaw, G. C., Yang, G., Li, L., Kaplan, J., et al. (2011). Abnormal mitoferrin-1 expression in patients with erythropoietic protoporphyria. *Exp. Hematol.* 39, 784–794. doi: 10.1016/j.exphem.2011.05.003

Weng, Y. L., Wang, X., An, R., Cassin, J., Vissers, C., Liu, Y., et al. (2018). Epitranscriptomic m^6A regulation of axon regeneration in the adult mammalian nervous system. *Neuron* 97, 313–325.e6. doi: 10.1016/j.neuron.2017.12.036

Wu, W., Ding, H., Cao, J., and Zhang, W. (2015). FBXL5 inhibits metastasis of gastric cancer through suppressing Snail1. *Cell Physiol. Biochem.* 35, 1764–1772. doi: 10.1159/000373988

Xia, T., Wu, X., Cao, M., Zhang, P., Shi, G., Zhang, J., et al. (2019). The RNA m^6A methyltransferase METTL3 promotes pancreatic cancer cell proliferation and invasion. *Pathol. Res. Pract.* 215:152666. doi: 10.1016/j.prp.2019.152666

Yang, L., Wu, S., Ma, C., Song, S., Jin, F., Niu, Y., et al. (2020). RNA m^6A methylation regulators subclassify luminal subtype in breast cancer. *Front. Oncol.* 10:611191. doi: 10.3389/fonc.2020.611191

Ye, J., Wang, Z., Chen, X., Jiang, X., Dong, Z., Hu, S., et al. (2020). YTHDF1-enhanced iron metabolism depends on TFRC m^6A methylation. *Theranostics* 10, 12072–12089. doi: 10.7150/thno.51231

Yu, J., Shen, L., Liu, Y., Ming, H., Zhu, X., Chu, M., et al. (2020). The m^6A methyltransferase METTL3 cooperates with demethylase ALKBH5 to regulate osteogenic differentiation through NF-kappaB signaling. *Mol. Cell. Biochem.* 463, 203–210. doi: 10.1007/s11010-019-03641-5

Yuan, Y., Yan, G., He, M., Lei, H., Li, L., Wang, Y., et al. (2021). ALKBH5 suppresses tumor progression via an m^6A-dependent epigenetic silencing of pre-miR-181b-1/YAP signaling axis in osteosarcoma. *Cell Death Dis.* 12:60. doi: 10.1038/s41419-020-03315-x

Zhang, C., Samanta, D., Lu, H., Bullen, J. W., Zhang, H., Chen, I., et al. (2016). Hypoxia induces the breast cancer stem cell phenotype by HIF-dependent and ALKBH5-mediated m^6A-demethylation of NANOG mRNA. *Proc. Natl. Acad. Sci. U.S.A.* 113, E2047–E2056. doi: 10.1073/pnas.1602883113

Zhang, D., Ning, J., Okon, I., Zheng, X., Satyanarayana, G., Song, P., et al. (2021). Suppression of m^6A mRNA modification by DNA hypermethylated ALKBH5 aggravates the oncological behavior of KRAS mutation/LKB1 loss lung cancer. *Cell Death Dis.* 12:518. doi: 10.1038/s41419-021-03793-7

Zhang, S., Zhao, B. S., Zhou, A., Lin, K., Zheng, S., Lu, Z., et al. (2017). m^6A demethylase ALKBH5 maintains tumorigenicity of glioblastoma stem-like cells by sustaining FOXM1 expression and cell proliferation program. *Cancer Cell* 31, 591–606.e6. doi: 10.1016/j.ccell.2017.02.013

Zhao, B. S., Nachtergaele, S., Roundtree, I. A., and He, C. (2018). Our views of dynamic N^6-methyladenosine RNA methylation. *RNA* 24, 268–272. doi: 10.1261/rna.064295.117

Zhao, X., Yang, Y., Sun, B. F., Shi, Y., Yang, X., Xiao, W., et al. (2014). FTO-dependent demethylation of N^6-methyladenosine regulates mRNA splicing and is required for adipogenesis. *Cell Res.* 24, 1403–1419. doi: 10.1038/cr.2014.151

Zheng, G., Dahl, J. A., Niu, Y., Fedorcsak, P., Huang, C. M., Li, C. J., et al. (2013). ALKBH5 is a mammalian RNA demethylase that impacts RNA metabolism and mouse fertility. *Mol. Cell* 49, 18–29. doi: 10.1016/j.molcel.2012.10.015

Zhou, K. I., Shi, H., Lyu, R., Wylder, A. C., Matuszek, Z., Pan, J. N., et al. (2019). Regulation of co-transcriptional pre-mRNA splicing by m^6A through the low-complexity protein hnRNPG. *Mol. Cell* 76, 70–81.e9. doi: 10.1016/j.molcel.2019.07.005

Conflict of Interest: The authors declare that the research was conducted in the absence of any commercial or financial relationships that could be construed as a potential conflict of interest.

Publisher's Note: All claims expressed in this article are solely those of the authors and do not necessarily represent those of their affiliated organizations, or those of the publisher, the editors and the reviewers. Any product that may be evaluated in this article, or claim that may be made by its manufacturer, is not guaranteed or endorsed by the publisher.

Copyright © 2021 Huang, Yang, Zhang, Liu, Fei, Tong, Niu and Liang. This is an open-access article distributed under the terms of the Creative Commons Attribution License (CC BY). The use, distribution or reproduction in other forums is permitted, provided the original author(s) and the copyright owner(s) are credited and that the original publication in this journal is cited, in accordance with accepted academic practice. No use, distribution or reproduction is permitted which does not comply with these terms.

frontiers in Cell and Developmental Biology

MINI REVIEW
published: 04 November 2021
doi: 10.3389/fcell.2021.789427

The Critical Contribution of Pseudouridine to mRNA COVID-19 Vaccines

Pedro Morais[1]*, *Hironori Adachi*[2] and *Yi-Tao Yu*[2]*

[1]ProQR Therapeutics, Leiden, Netherlands, [2]Department of Biochemistry and Biophysics, Center for RNA Biology, University of Rochester Medical Center, Rochester, NY, United States

The current COVID-19 pandemic is a massive source of global disruption, having led so far to two hundred and fifty million COVID-19 cases and almost five million deaths worldwide. It was recognized in the beginning that only an effective vaccine could lead to a way out of the pandemic, and therefore the race for the COVID-19 vaccine started immediately, boosted by the availability of the viral sequence data. Two novel vaccine platforms, based on mRNA technology, were developed in 2020 by Pfizer-BioNTech and Moderna Therapeutics (comirnaty® and spikevax®, respectively), and were the first ones presenting efficacies higher than 90%. Both consisted of N1-methyl-pseudouridine-modified mRNA encoding the SARS-COVID-19 Spike protein and were delivered with a lipid nanoparticle (LNP) formulation. Because the delivery problem of ribonucleic acids had been known for decades, the success of LNPs was quickly hailed by many as the unsung hero of COVID-19 mRNA vaccines. However, the clinical trial efficacy results of the Curevac mRNA vaccine (CVnCoV) suggested that the delivery system was not the only key to the success. CVnCoV consisted of an unmodified mRNA (encoding the same spike protein as Moderna and Pfizer-BioNTech's mRNA vaccines) and was formulated with the same LNP as Pfizer-BioNTech's vaccine (Acuitas ALC-0315). However, its efficacy was only 48%. This striking difference in efficacy could be attributed to the presence of a critical RNA modification (N1-methyl-pseudouridine) in the Pfizer-BioNTech and Moderna's mRNA vaccines (but not in CVnCoV). Here we highlight the features of N1-methyl-pseudouridine and its contributions to mRNA vaccines.

Keywords: COVID-19, SARS-CoV-2, mRNA, vaccines, RNA modification, pseudouridine, N1-methyl-pseudouridine, lipid nanoparticles

OPEN ACCESS

Edited by:
Chengqi Yi,
Peking University, China

Reviewed by:
Jean-Paul Desaulniers,
Ontario Tech University, Canada
Jia Sheng,
University at Albany, United States

***Correspondence:**
Pedro Morais
PMorais@proqr.com
Yi-Tao Yu
YiTao_Yu@URMC.Rochester.edu

Specialty section:
This article was submitted to Epigenomics and Epigenetics, a section of the journal Frontiers in Cell and Developmental Biology

Received: *04 October 2021*
Accepted: *22 October 2021*
Published: *04 November 2021*

Citation:
Morais P, Adachi H and Yu Y-T (2021) The Critical Contribution of Pseudouridine to mRNA COVID-19 Vaccines. Front. Cell Dev. Biol. 9:789427. doi: 10.3389/fcell.2021.789427

INTRODUCTION

When the COVID-19 pandemic struck in early 2020, there was an urgent need to generate COVID-19 vaccines. At that time, the consensus in the medical field was that a safe and effective vaccine would need at least 12–18 months to be developed (Thorp, 2020). Some even argued that such a timeline was highly optimistic since it would have to be tested in animals first during an exploratory and preclinical phase, and then in three different clinical trial phases to determine efficacy and safety ultimately. Finally, a vaccine candidate would need to go through regulatory review, approval, and manufacturing at an unprecedented scale (Kis et al., 2020) with strict quality controls.

To produce effective vaccines and shorten their production time, developing new vaccine strategies/technologies seemed necessary. One of the emerging new technologies, mRNA

vaccines (Pascolo, 2004; Probst et al., 2007), drew tremendous attention and provided a great deal of hope. This technology made possible a fast pace of discovery and manufacturing, critical features that could be fully utilized in a biotech and pharmaceutical setting (Jackson et al., 2020).

As opposed to the production of, for example, attenuated or inactivated viruses, the production of mRNA vaccines can take only days or weeks to complete (Pascolo, 2021). It can be accomplished by *in vitro* transcription of mRNA, where virtually any mRNA sequence can be produced from a DNA template (Krieg and Melton, 1984; Melton et al., 1984). Further, an mRNA vaccine would provide the cell with the direct instructions for expressing an immunogenic protein of interest *via* cytoplasmic translation. In fact, it was shown 3 decades ago that an mRNA could be directly delivered, *via* injection, to mouse muscle cells for translation (Wolff et al., 1990). However, as with other nucleic acid-based therapeutic modalities, several delivery hurdles of mRNA therapeutics had delayed the emergence of this technology. For instance, an RNA molecule can be degraded by RNases or entrapped by endosomes before reaching the site of action (Wadhwa et al., 2020). In addition, the negatively charged phosphodiester backbone of an RNA makes it difficult to cross biological membranes (Dowdy, 2017).

The solution to this conundrum was to use a shell of lipid nanoparticles (LNPs) to protect the RNA until it reached the site of action. This is conceptually not very far from what was proposed decades ago, when lipids were tested as vehicles to deliver RNA to mammalian cells (Dimitriadis, 1978; Ostro et al., 1978; Malone et al., 1989). Recently, new generations of LNPs were developed and used to deliver patisiran®, an RNAi-based drug approved in 2018, which generated optimism for RNA therapeutics delivery (Hoy, 2018). Indeed, with the approval of patisiran®, there was a mounting belief that LNPs could become enabling technologies for multiple RNA modalities (Adachi et al., 2021). This was a major accomplishment and a scientific breakthrough, and, in fact, current mRNA vaccines are delivered with LNPs that are prepared by mixing four lipids in the presence of ethanol in very specific conditions (Jeffs et al., 2005; Buschmann et al., 2021). LNPs were also critical for the successful delivery of mRNA vaccines *via* intramuscular injection. It is believed that, while muscle cells are not very efficient in the translation of the mRNA encoding the Spike protein, LNPs ultimately carry their cargo to the lymph nodes and are internalized by dendritic cells. The Spike protein is synthesized in these cells from the mRNA template and displayed to other immune system cells (T and B cells) to trigger the immune response (Ruffell, 2021). Without LNPs formulations, the success of mRNA vaccines would not have been possible.

Aside from the delivery problem discussed above, therapeutic mRNA had at least two additional big challenges: 1) the *in vitro* transcribed (IVT) mRNA would be prone to nuclease degradation when injected into animals, and 2) the IVT mRNA would also lead to innate immunogenicity similar to what would happen when infected by a pathogen (Martinon et al., 1993; Hoerr et al., 2000). The answer to these problems came from a well-known RNA modification, pseudouridine (Ψ), which can be used to replace uridine in the IVT mRNA. It is demonstrated that Ψ can enhance RNA stability and, in the meantime, decrease anti-RNA immune response (Karikó et al., 2008). This Ψ-effect is perhaps associated, at least in part, with the fact that Ψ is a naturally occurring modified nucleotide with unique chemical properties and that Ψ is also highly abundant and naturally widespread in virtually all RNAs of all cells (Song et al., 2020).

Both Pfizer-BioNTech and Moderna Therapeutics COVID-19 spike-encoding mRNA vaccines (both with more than 90% of efficacy against COVID-19 symptoms) contain modified Ψs (Nance and Meier, 2021).

In contrast, another COVID-19 mRNA vaccine candidate (developed by Curevac NV), which is based on an unmodified (Ψ-lacking) mRNA encoding the same COVID-19 spike protein and uses the same LNPs as the Pfizer-BioNTech vaccine does (Buschmann et al., 2021), failed to meet expectations (Baker and Dolgin, 2021). The clinical trial test results ultimately revealed only 48% of efficacy against symptomatic disease (Kremsner et al., 2021) for the unmodified mRNA vaccine, suggesting that modified Ψ and use of LNP technology were both critical success factors for platform validation of mRNA (Dolgin, 2021a). In this mini-review, we will emphasize the main features of this RNA modification and a chemically evolved version of it that contribute to the success of COVID-19 mRNA vaccines and the control of the pandemic.

Ψ IS AN ABUNDANT NATURALLY OCCURRING MODIFIED NUCLEOTIDE FOUND IN MANY TYPES OF RNA

Ψ was the first modified ribonucleotide discovered 7 decades ago (Cohn and Volkin, 1951; Davis and Allen, 1957), and it has been found in tRNA, rRNA, snRNA, mRNA, and other types of RNA (Carlile et al., 2014; Lovejoy et al., 2014; Schwartz et al., 2014). Ψ is derived from uridine *via* a base-specific isomerization reaction called pseudouridylation (**Figure 1**), in which the nucleobase rotates 180° around the N3-C6 axis, resulting in the change of nucleobase-sugar bond (from N1-C1′ bond to C5-C1′ bond). The resulting C-C bond allows the nucleobase to rotate more freely (Adachi et al., 2021). In addition, Ψ can provide an extra hydrogen bond donor (in the N1H) in the major groove while keeping the hydrogen bond donor and acceptor (same as in its original uridine) in the Watson-Crick face. While the changes seem subtle (in fact, Ψ can base-pair with adenosine just as uridine does), Ψ can alter RNA structure in a relatively significant way, mainly by improving base-pairing, base stacking, and contributing to making the backbone more rigid (through a network of hydrogen bonding interactions) (Davis, 1995; Charette and Gray, 2000; Newby and Greenbaum, 2001, 2002a, 2002b). As such, RNA pseudouridylation generally stabilizes the RNA. Thus, it is not surprising that the presence of this RNA modification confers distinct biophysical and biochemical properties to the RNA. For example, Ψ favors a C3′-endo conformation in the RNA (Kierzek et al., 2014; Westhof, 2019). Further, it seems that Ψ increases the

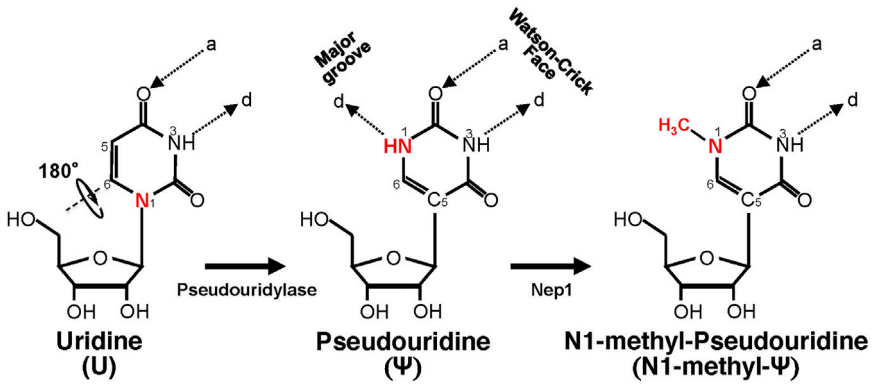


FIGURE 1 | Schematic representation of U-to-Ψ isomerization and additional N1 methylation. Ψ is a rotational isomer of uridine, in which the N-C glycosidic bond is substituted with the C-C bond. The isomerization reaction also creates an extra hydrogen bond donor (-N1H). Ψ can be further methylated at the N1 position by Nep1 (an N1-specific Ψ methyltransferase) to generate N-methyl-Ψ. d, hydrogen bond donor; a, hydrogen bond acceptor.

protection of the RNA against nucleases. A study from Naylor et al. showed that Ψ-containing dinucleotides were more resistant to degradation from snake venom and spleen phosphodiesterases, than the U-containing counterparts (Naylor et al., 1965).

Pseudouridylation can be either catalyzed by stand-alone protein enzymes (pseudouridylases) or by large RNA-Protein complexes called H/ACA box snoRNPs, where the RNA components serve as guides to direct site-specific pseudouridylation (Morais et al., 2021). Since Ψ is highly conserved and known to perform essential functions in the cell, several known diseases are associated with defects in RNA pseudouridylation. Also, because pseudouridylation appears to be irreversible, Ψ is usually excreted from the body. Thus, this RNA modification has drawn attention as a potential biomarker for Alzheimer's disease and certain types of cancer (Morais et al., 2021).

Ψ can be incorporated into RNA transcripts *via in vitro* transcription, where UTP is replaced by ΨTP (Padilla, 2002; Chen et al., 2010; Pardi et al., 2013). It was reported that Ψ-modified transcripts, coding for four transcription factors (KLF4, c-MYC, OCT4, and SOX2), were successfully used to reprogram human cells to pluripotency with great efficiency (Warren et al., 2010). This landmark study indicated the importance of this RNA modification in mRNA platform technologies.

Ψ CAN TRICK THE IMMUNE SYSTEM

Upon entering cells, unmodified IVT mRNA becomes intrinsically immunogenic (Weissman et al., 2000). For many years, this challenge slowed down the development of mRNA therapeutics, especially mRNA-replacement strategies. For instance, it has been shown that when treated with unmodified IVT mRNA, dendritic cells promote a T-cell response (Weissman et al., 2000). The activation of Toll-like receptors (TLRs), concretely TLR3 (a member of the TLRs family), that can recognize double-stranded viral RNA, is one of the mechanisms behind this induction of immune response (Karikó et al., 2004). In another work, it was suggested that single-stranded RNA could also induce an immune response in cells. The authors in that work showed that HIV-derived uridine-rich single-stranded RNA could stimulate, *via* recognition by TLR7 and TLR8, dendritic cells to produce cytokines (Heil, 2004). Later, it was further suggested that TLR7 could recognize uracil repeats in close proximity in the RNA (Diebold et al., 2006). To address this problem, Karikó et al. came up with a brilliant solution. They found that incorporating Ψ, as a replacement of uridine, into the IVT mRNA could suppress this immune response mechanism (Karikó et al., 2005). This discovery revealed another critical facet of Ψ and hinted for the first time that RNA modification might be necessary to establish mRNA as a novel therapeutic modality. However, at the time of this finding, some argued that unmodified mRNA immunotherapeutics would be a better approach than modified mRNA since the RNA itself would act as an adjuvant (Ishii and Akira, 2005).

In a follow-up study published in 2008, Karikó et al. proposed that the inclusion of Ψ would be the crucial step for mRNA to mature as a therapeutic tool, both in gene replacement therapies and in mRNA vaccination (Karikó et al., 2008). They confirmed that unmodified mRNA, as compared to Ψ-modified mRNA, was more immunogenic in mice. However, Karikó et al. also suggested that while Ψ-modified mRNA could be preferable for mRNA vaccines, it would eventually require the co-administration of an adjuvant such as lipopolysaccharide or an immunostimulatory oligo. In this regard, it appears that LNPs played this immunoadjuvant role as both carriers and adjuvants for the approved COVID-19 mRNA vaccines (Alfagih et al., 2020).

Another work from the Karikó/Weissman lab suggested that Ψ-modified mRNA could be more resistant to RNase L-mediated degradation (Anderson et al., 2011). This could be achieved by limiting the activation of 2′-5′-oligoadenylate synthetase, an important enzyme in the innate antiviral response that is usually activated by double-stranded RNA. Because RNase L is a 2′-5′-oligoadenylate synthetase-dependent ribonuclease, the ability of pseudouridylated mRNA to limit the activity of 2′-

5′-oligoadenylate synthetase could provide an advantage to Ψ-modified mRNA over unmodified mRNA (Anderson et al., 2011).

Ψ HAS AN IMPACT ON PROTEIN TRANSLATION

Because of the impact of Ψ on RNA structure, stability, and chemical properties in general, it is not surprising that this RNA modification also affects the translation of mRNA into protein in eukaryotes. For instance, an early work revealed the unusual decoding events provided by Ψ in the mitochondrial tRNA anticodon. The pseudouridylated anticodon could effectively read alternative codons that would otherwise be poorly recognized during translation in mitochondria if the anticodons were not pseudouridylated (Tomita, 1999). Another study suggested that the increased translatability of Ψ-modified mRNA, which was previously observed (Karikó et al., 2008), was due to the fact that unmodified mRNA is more prone to activate, *via* binding, an RNA-dependent protein kinase (PKR) than Ψ-modified mRNA. This PKR is responsible for the phosphorylation of a translation initiation factor 2-alpha (eIF-2α) and ultimately reduces translation efficiency (Anderson et al., 2010).

Ψ also impacts stop codon decoding. The Yu lab showed that nonsense mutations, which create premature termination codons (PTCs), could be suppressed by site-specific pseudouridylation of the uridine of PTCs (UAG, UGA, and UAA) directed by artificial box H/ACA guide RNAs (Karijolich and Yu, 2011; Morais et al., 2020). The identity of the amino acids incorporated in the pseudouridylated PTCs was determined in yeast by immunoprecipitation and mass spectrometry: predominantly phenylalanine/tyrosine at the ΨGA codons and threonine/serine at the ΨAA and ΨAG codons. It was later found that this novel recoding mechanism could happen due to an unusual codon-anticodon base-pairing scheme at the ribosomal decoding center (Fernández et al., 2013).

More recently, it was reported that Ψ is also capable of modulating translatability or sense codon decoding (Eyler et al., 2019). Using either an *Escherichia coli* translation system or human cells (human embryonic kidney cells), the authors demonstrated that Ψ could alter, to a small extent, how ribosomes or codons interact with cognate and near-cognate tRNAs, leading to amino acid substitution. It was suggested that this amino acid substitution mechanism could be a valuable source for adaptation under stress conditions, such as oxidative and temperature stresses.

N1-METHYLATED Ψ BEHAVES BETTER THAN Ψ

Since the finding that Ψ-modification could enable mRNA to resist intrinsic immune responses (Karikó et al., 2005), a search was carried out for Ψ-derivatives that could have improved properties. The amine group (NH) at the N1 position, which provides an extra hydrogen bond donor (created after pseudouridylation) (**Figure 1**), drew particular attention. One N1-modified Ψ-derivative is N1-methyl-Ψ, a naturally occurring modification found in 18S rRNA (Brand et al., 1978) and tRNA in many organisms (Boccaletto et al., 2018). This N1-methylation is catalyzed by N1-specific Ψ methyltransferase Nep1 found in archaea and eukaryotes (Wurm et al., 2010) (**Figure 1**). Potentially N1-methyl-Ψ could be more widespread than reported in human RNA, given that the current standard Ψ-detection (-seq) methods, which rely on the use of CMC-modification followed by primer extension (Morais et al., 2021), may not be able to distinguish N1-methyl-Ψ from Ψ (Svitkin et al., 2017). Possibly, therefore, some Ψs thus identified so far (Schwartz et al., 2014) could actually be N1-methylated Ψs.

In order to understand the biological functions of N1-methyl-Ψ, Parr et al. performed biophysical studies where this modification was compared with Ψ and uridine. They measured the melting temperature of complementary synthetic RNA duplexes in which some uridines were replaced by Ψ or N1-methyl-Ψ (Parr et al., 2020). Both the Ψ- and N1-methyl-Ψ-modified duplexes had higher (and similar) T_m-values than uridine-control duplexes, indicating higher stability provided by increased base pairing and stacking as suggested in previous studies performed with Ψ (Westhof, 2019). However, Ψ contains an extra hydrogen bond donor group (N1H) that contributes to a universal base character, i.e., it can not only pair A but also wobble base-pair with G, U, or C in the context of a duplex (Kierzek et al., 2014). On the other hand, N1-methyl-Ψ has a methyl group instead in the N1-position (**Figure 1**), thus eliminating the extra hydrogen bond donor. Consequently, N1-methyl-Ψ can only use its Watson-Crick face to base-pair with another nucleoside, thus preventing it from wobble-pairing with other nucleotides (G, U, and C). Nonetheless, Ψ and N1-methyl Ψ still share a critical common feature, the C5-C1′ bond, which enables rotation between the nucleobase and the sugar moieties and probably contributes to improving the base-pairing, base-stacking, and duplex stability (Westhof, 2019). It is conceivable that N1-methylated Ψ, which has a higher affinity for pairing with A (similar to Ψ) and is less likely to activate PKR, would be more efficient for translation when compared to uridine. On the other hand, N1-methyl-Ψ remains faithful in coding (more like uridine than Ψ does in pairing) during translation. Finally, N1-methyl-Ψ, which is structurally similar to Ψ, would probably also enable mRNA to evade the immune response.

Indeed, it has been reported that N1-methyl-Ψ diminished the activity of innate immune sensors (Andries et al., 2015) and that N1-methyl-Ψ performed nicely (and even better than Ψ) in improving the translational capacity and reducing cytotoxicity of modified mRNA when tested in several human cell lines, primary human cells, and in animals (intradermal and intramuscular injection in mice) (Andries et al., 2015). Some of the findings were later corroborated by scientists from Moderna Therapeutics (Nelson et al., 2020). Furthermore, another study by Svitkin et al. confirmed the effect of N1-methyl-Ψ on innate immune sensors and demonstrated that N1-methyl-Ψ increased ribosome pausing and thus change the

dynamics of modified mRNA translation by increasing the recruitment or loading of ribosomes (Svitkin et al., 2017). Due to its effectiveness, N1-methyl-Ψ (alone or in conjunction with 5-methylcytidine) was thus proposed to be a new benchmark in RNA modifications for mRNA therapeutics (Andries et al., 2015).

N1-METHYL-Ψ IS USED IN COVID-19 MRNA VACCINES

In 2017 during the development of mRNA vaccine against Zika virus, N1-methyl-Ψ was used and incorporated into two similar mRNA vaccines encoding Zika virus surface proteins. The modified mRNA, encapsulated in LNPs, was designed and then tested to protect against the Zika virus in human cells, mice, and non-human primates (Pardi et al., 2017; Richner et al., 2017). In the following year, further success was obtained with N1-methyl-Ψ-modified mRNA vaccines against HIV-1, Zika, and influenza virus, achieving a sustained antibody response in a preclinical setting (Pardi et al., 2018). A similar example was presented against the Ebola virus in guinea pigs (Meyer et al., 2018). These studies further emphasized the importance of N1-methyl-Ψ for the mRNA vaccine platform technology, as it could provide a reliable way of achieving the sustained and speedy synthesis of the antigenic protein to trigger the desired immune response in a safe manner.

In 2020, Pfizer-BioNTech added N1-methyl-Ψ to their COVID-19 mRNA vaccine candidate (comirnaty® or BNT162b2) coding for the full-length transmembrane S protein "spike." The full sequence of this mRNA vaccine includes the 5′UTR, the coding sequence of the spike protein with two contiguous stop codons, and the 3′UTR (Nance and Meier, 2021). N1-methyl-Ψ was substituted for all uridines throughout the mRNA sequence, including the uridines in the two stop codons. In addition, two amino acid mutations, K986P and V987P (lysine 986 and valine 987 were both changed to proline), were also introduced. These mutations help generate the pre-fusion conformation of the spike protein that is more optimal as an antigen since it more resembles the actual viral protein with which antibodies will interact (Pallesen et al., 2017; Wrapp et al., 2020). In an earlier study of MERS-CoV infection, it was found that the two prolines would stabilize the pre-fusion conformation of the MERS-CoV spike antigen (Pallesen et al., 2017). Antibodies generated against this conformation would block the fusion of the virus and the host protein (CD26), thus offering an ideal solution for MERS-disease vaccine development. This knowledge was incorporated into the development of COVID-19 mRNA vaccine (Pfizer-BioNTech and Moderna) and non-mRNA vaccines as well (J&J and Novavax vaccines) (Kyriakidis et al., 2021).

Massive *in vitro* transcription produced a huge amount of N1-methyl-Ψ-modified SARS CoV-2 (COVID-19) spike mRNA. This vaccine was the first mRNA vaccine fully approved against COVID-19 after showing a good safety profile and 95% protection against disease following a two-dose regimen (intramuscular injection) (Polack et al., 2020; Mullard, 2021).

The Moderna Therapeutics COVID-19 vaccine (spikevax®, or mRNA-1273), also coding for pre-fusion conformation of the spike protein (Corbett et al., 2020), was the second mRNA vaccine to get EAU (emergency approval use) for COVID-19. Spikevax® was also prepared by totally replacing uridines with N1-methyl-Ψ through *in vitro* transcription (Corbett et al., 2020). The spike protein-coding sequence ends with three N1-methyl-pseudouridylated stop codons and is flanked by a 5′UTR and a 3′UTR. This vaccine was shown to prevent COVID-19 disease, including severe illness, with an efficacy of 94% (Baden et al., 2021).

It is worth noting that although the mRNA of both approved vaccines is fully modified (Us are completely substituted with N1-methyl-Ψs), it likely has high coding fidelity, given that N1-methyl-Ψ pairs only with A (unlike Ψ, which can, to some extent, wobble pair with different nucleosides). In addition, two and three contiguous stop codons are placed in the Pfizer and Moderna mRNAs, respectively. Such arrangements ensure that no read-through of modified stop codons will occur (even though a single Ψ-stop codon would allow, to some extent, read-through) (Karijolich and Yu, 2011; Fernández et al., 2013). Also, N1-methyl-Ψ increases translation efficiency, which enables relatively low doses.

MODIFIED VS. UNMODIFIED COVID-19 MRNA VACCINES LEAD TO DIFFERENT OUTCOMES

The intrinsic immunogenicity of non-modified mRNA was once considered a potential advantage for its use in vaccines (Ishii and Akira, 2005) as it would encode the antigen and concomitantly serve as an adjuvant while permitting a low dose. In fact, the unmodified COVID-19 mRNA vaccine candidate in late-stage clinical trials (CVnCoV, developed by Curevac) had a maximum dose of 12 μg. However, the recent CVnCoV vaccine clinical trial results showed only 48% of efficacy against any severity of the disease, (Kremsner et al., 2021).

In light of such results, some argued that this could be due to a dose that was too low to elicit a robust immune response against the disease [higher doses of the unmodified mRNA vaccine appear to be intolerable to patients (Dolgin, 2021a; Cohen, 2021)]. Consistent with this argument, Pfizer-BioNTech and Moderna's mRNA vaccines, which exhibit ~95% high protection rate against COVID-19, come with a much higher dose, by comparison, 30 and 100 μg of modified mRNA each shot, respectively (Pascolo, 2021). Although lower doses (50 and 25 μg) of Moderna's modified mRNA-1273 can still elicit a significant immune response (Chu et al., 2021; Mateus et al., 2021), they remain much higher than the doses of CVnCoV unmodified mRNA vaccine. Interestingly, however, Pfizer-BioNTech just announced that their comirnaty® vaccine, administered with two shots of 10 μg each, is safe and effective in children 5–11 years old (Pfizer, 2021). There is some speculation surrounding the possibility that, although designed for children, this dose is comparable to the dose of the CVnCoV unmodified mRNA vaccine; thus, it would not be the low dose

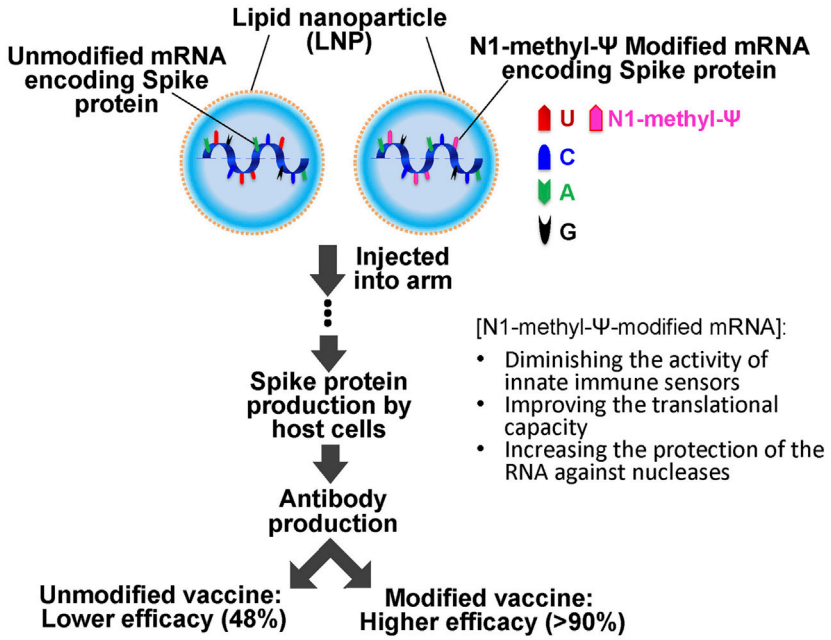


FIGURE 2 | Schematics of SARS-COVID 19 mRNA vaccination. The vaccine consists of unmodified or N-methyl-Ψ-modified mRNA (encoding the SARS-COVID-19 spike protein) and lipid nanoparticles (LNPs). It is injected into the muscle of the upper arm to create an immune response. N-methyl-Ψ-modified mRNA exhibits higher efficacy (more than 90% of efficacy against COVID-19 symptoms) as compared to the unmodified mRNA vaccines (lower than 50%).

that made the unmodified mRNA vaccine relatively ineffective. This hypothesis warrants further study.

It should also be pointed out that the CVnCoV unmodified mRNA vaccine also used an LNP formulation, namely Acuitas ALC-0315, a delivery system identical to that used in the Pfizer-BioNTech modified mRNA vaccine (Buschmann et al., 2021). While Curevac attributed the lower efficacy of CVnCoV to the large number of variants circulating during the clinical trials, this claim has been challenged by the high protection of the Pfizer–BioNTech mRNA vaccine against the alpha, beta and delta variants (92, 75, and 83% respectively) (Abu-Raddad et al., 2021; Sheikh et al., 2021). Given these experimental and clinical trial results, one could argue that RNA modifications are perhaps critical contributors to the success of the mRNA vaccine platform technology (Dolgin, 2021a) (**Figure 2**).

The second-generation of Curevac's COVID-19 vaccine (CV2CoV), currently in preclinical development (Roth et al., 2021), is still a non-chemically modified mRNA, which encodes the full-length spike protein and is encapsulated with LNPs. Compared to the first generation of Curevac COVID-19 unmodified mRNA vaccine, the second-generation unmodified mRNA vaccine consists of coding and non-coding (5′ and 3 UTRs) sequences that have been further engineered to increase translation efficiency and antigen protein production. In a study published before the pandemic, Curevac (and Acuitas) scientists presented data suggesting that the use of unmodified mRNA could be compensated by heavily engineering the sequence of the mRNA to enhance protein expression (erythropoietin) in mice and large animals (Thess et al., 2015). They optimized the codons in the open reading frame and thus improved the stability and translation of the unmodified transcript. Of note is that both Pfizer-BioNTech and Moderna mRNA vaccines are already codon/sequence optimized.

It is possible that the second generation of Curevac's COVID-19 mRNA vaccine, CV2CoV, which has already shown increased levels of neutralizing antibodies in rats (Roth et al., 2021), will enhance the safety and protection profile. The clinical trial results are expected to come in 2022. In the meantime, another unmodified mRNA vaccine (ARCoV), developed by Walvax Biotechnology and Suzhou Abogen Biosciences, is currently in clinical development (Dolgin, 2021b). In addition, Sanofi, a French pharmaceutical company, which recently acquired an unmodified mRNA technology platform from Translate Bio, now a Sanofi company, recently announced the discontinuation of their phase ½ clinical trials of their Sanofi-Translate Bio unmodified COVID-19 mRNA vaccine to focus their efforts instead in their influenza vaccine which is based on modified RNA (Sanofi, 2021). Curevac has also recently withdrawn CVnCoV from the regulatory approval process to focus their efforts instead on their second-generation CV2CoV vaccine clinical development. Moreover, the company stated that it will accelerate the development of modified mRNA vaccine constructs, in collaboration with GlaxoSmithKline, a pharmaceutical company (Curevac, 2021).

Unmodified mRNA is being used in non-COVID-19 clinical trials, particularly for developing new cancer treatments. It has been suggested that the challenge

associated with the activation of an immune response against cancer cells could be better surmounted with the use of unmodified mRNA (with its stronger adjuvant activity) coding for proteins usually present in cancer cells but not in healthy cells, in order to turn a cold tumor into a hot tumor more effectively (Ruffell, 2021). In fact, BioNTech just announced the use of unmodified mRNA encapsulated in a lipoplex delivery formulation, following this concept, for treatment of colorectal cancer patients in phase two trials (BioNTech, 2021).

Regardless, it is clear that RNA modifications, such as Ψ and later N1-methyl-Ψ, have already made a tremendous and timely contribution to generating highly effective (+90%) COVID-19 mRNA vaccines. Pfizer-BioNTech's mRNA vaccine went from first-in-human trials to emergency use authorization in just 8 months (Dolgin, 2021b).

While mutations in COVID-19 are leading to new variants that pose increasing challenges and that require further study of the efficacy of currently approved vaccines, there is no doubt that the developments in biology and chemistry of the most common RNA modification (Ψ) during the last 2 decades have turned out to be game-changing in defining how to end this pandemic.

AUTHOR CONTRIBUTIONS

Conceptualization, PM, and Y-TY; writing: original draft preparation, PM, and Y-TY; writing: review and editing, PM, HA, and Y-TY; funding acquisition, PM and Y-TY. All authors have read and agreed to the published version of the manuscript.

FUNDING

The research performed in the Yu lab was funded by US National Institutes of Health, grants number GM138387 (active until July 2024) and CA241111 (active until July 2021), and the Cystic Fibrosis Foundation, grant CFF YU20G0 (active until April 2022). ProQR Therapeutics and the Cystic Fibrosis Foundation (YU20G0) fund the research performed by PM.

ACKNOWLEDGMENTS

We thank members of the Yu lab for insightful discussions. PM would like to thank Marta Mosquera for the helpful exchange of ideas during the conceptualization of the manuscript.

REFERENCES

Abu-Raddad, L. J., Chemaitelly, H., and Butt, A. A. (2021). Effectiveness of the BNT162b2 Covid-19 Vaccine against the B.1.1.7 and B.1.351 Variants. *N. Engl. J. Med.* 385(2), 187–189. doi:10.1056/NEJMc2104974

Adachi, H., Hengesbach, M., Yu, Y.-T., and Morais, P. (2021). From Antisense RNA to RNA Modification: Therapeutic Potential of RNA-Based Technologies. *Biomedicines* 9, 550. doi:10.3390/biomedicines9050550

Alfagih, I. M., Aldosari, B., AlQuadeib, B., Almurshedi, A., and Alfagih, M. M. (2020). Nanoparticles as Adjuvants and Nanodelivery Systems for mRNA-Based Vaccines. *Pharmaceutics* 13, 45. doi:10.3390/pharmaceutics13010045

Anderson, B. R., Muramatsu, H., Jha, B. K., Silverman, R. H., Weissman, D., and Kariko, K. (2011). Nucleoside Modifications in RNA Limit Activation of 2'-5'-oligoadenylate Synthetase and Increase Resistance to Cleavage by RNase L. *Nucleic Acids Res.* 39, 9329–9338. doi:10.1093/nar/gkr586

Anderson, B. R., Muramatsu, H., Nallagatla, S. R., Bevilacqua, P. C., Sansing, L. H., Weissman, D., et al. (2010). Incorporation of Pseudouridine into mRNA Enhances Translation by Diminishing PKR Activation. *Nucleic Acids Res.* 38, 5884–5892. doi:10.1093/nar/gkq347

Andries, O., Mc Cafferty, S., De Smedt, S. C., Weiss, R., Sanders, N. N., and Kitada, T. (2015). N1-methylpseudouridine-incorporated mRNA Outperforms Pseudouridine-Incorporated mRNA by Providing Enhanced Protein Expression and Reduced Immunogenicity in Mammalian Cell Lines and Mice. *J. Controlled Release* 217, 337–344. doi:10.1016/j.jconrel.2015.08.051

Baden, L. R., El Sahly, H. M., Essink, B., Kotloff, K., Frey, S., Novak, R., et al. (2021). Efficacy and Safety of the mRNA-1273 SARS-CoV-2 Vaccine. *N. Engl. J. Med.* 384, 403–416. doi:10.1056/NEJMoa2035389

Baker, N., and Dolgin, E. (2021). Coronapod: CureVac Disappoints in COVID Vaccine Trial. *Nature*. doi:10.1038/d41586-021-01694-5

BioNTech (2021). BioNTech Expands Clinical Oncology Portfolio with First Patient Dosed in Phase 2 Trial of mRNA-Based Individualized Immunotherapy BNT122 in Colorectal Cancer Patients. Available at: https://investors.biontech.de/news-releases/news-release-details/biontech-expands-clinical-oncology-portfolio-first-patient-dosed (Accessed October 1, 2021).

Boccaletto, P., Machnicka, M. A., Purta, E., Piątkowski, P., Bagiński, B., Wirecki, T. K., et al. (2018). MODOMICS: a Database of RNA Modification Pathways. 2017 Update. *Nucleic Acids Res.* 46, D303–D307. doi:10.1093/nar/gkx1030

Brand, R. C., Klootwijk, J., Planta, R. J., and Maden, B. E. H. (1978). Biosynthesis of a Hypermodified Nucleotide in Saccharomyces Carlsbergensis 17S and HeLa-Cell 18S Ribosomal Ribonucleic Acid. *Biochem. J.* 169, 71–77. doi:10.1042/bj1690071

Buschmann, M. D., Carrasco, M. J., Alishetty, S., Paige, M., Alameh, M. G., and Weissman, D. (2021). Nanomaterial Delivery Systems for mRNA Vaccines. *Vaccines* 9, 65. doi:10.3390/vaccines9010065

Carlile, T. M., Rojas-Duran, M. F., Zinshteyn, B., Shin, H., Bartoli, K. M., and Gilbert, W. V. (2014). Pseudouridine Profiling Reveals Regulated mRNA Pseudouridylation in Yeast and Human Cells. *Nature* 515, 143–146. doi:10.1038/nature13802

Charette, M., and Gray, M. W. (2000). Pseudouridine in RNA: what, where, How, and Why. *IUBMB Life (International Union Biochem. Mol. Biol. Life)* 49, 341–351. doi:10.1080/152165400410182

Chen, C., Zhao, X., Kierzek, R., and Yu, Y.-T. (2010). A Flexible RNA Backbone within the Polypyrimidine Tract Is Required for U2AF 65 Binding and Pre-mRNA Splicing *In Vivo*. *Mol. Cel. Biol.* 30, 4108–4119. doi:10.1128/MCB.00531-10

Chu, L., McPhee, R., Huang, W., Bennett, H., Pajon, R., Nestorova, B., et al. (2021). A Preliminary Report of a Randomized Controlled Phase 2 Trial of the Safety and Immunogenicity of mRNA-1273 SARS-CoV-2 Vaccine. *Vaccine* 39, 2791–2799. doi:10.1016/j.vaccine.2021.02.007

Cohen, J. (2021). What Went Wrong with CureVac's Highly Anticipated New mRNA Vaccine for COVID-19. *Science*. doi:10.1126/science.abk0458

Cohn, W. E., and Volkin, E. (1951). Nucleoside-5′-Phosphates from Ribonucleic Acid. *Nature* 167, 483–484. doi:10.1038/167483a0

Corbett, K. S., Edwards, D. K., Leist, S. R., Abiona, O. M., Boyoglu-Barnum, S., Gillespie, R. A., et al. (2020). SARS-CoV-2 mRNA Vaccine Design Enabled by Prototype Pathogen Preparedness. *Nature* 586, 567–571. doi:10.1038/s41586-020-2622-0

Curevac (2021). CureVac to Shift Focus of COVID-19 Vaccine Development to Second-Generation mRNA Technology. Available at: https://www.curevac.com/en/2021/10/12/curevac-to-shift-focus-of-covid-19-vaccine-development-to-second-generation-mrna-technology/(Accessed October 12, 2021).

Davis, D. R. (1995). Stabilization of RNA Stacking by Pseudouridine. *Nucl. Acids Res.* 23, 5020–5026. doi:10.1093/nar/23.24.5020

Davis, F. F., and Allen, F. W. (1957). Ribonucleic Acids from Yeast Which Contain a Fifth Nucleotide. *J. Biol. Chem.* 227, 907–915. doi:10.1016/S0021-9258(18)70770-9

Diebold, S. S., Massacrier, C., Akira, S., Paturel, C., Morel, Y., and Reis e Sousa, C. (2006). Nucleic Acid Agonists for Toll-like Receptor 7 Are Defined by the Presence of Uridine Ribonucleotides. *Eur. J. Immunol.* 36, 3256–3267. doi:10.1002/eji.200636617

Dimitriadis, G. J. (1978). Translation of Rabbit Globin mRNA Introduced by Liposomes into Mouse Lymphocytes. *Nature* 274, 923–924. doi:10.1038/274923a0

Dolgin, E. (2021a). CureVac COVID Vaccine Let-Down Spotlights mRNA Design Challenges. *Nature* 594, 483. doi:10.1038/d41586-021-01661-0

Dolgin, E. (2021b). The Tangled History of mRNA Vaccines. *Nature* 597, 318–324. doi:10.1038/d41586-021-02483-w

Dowdy, S. F. (2017). Overcoming Cellular Barriers for RNA Therapeutics. *Nat. Biotechnol.* 35, 222–229. doi:10.1038/nbt.3802

Eyler, D. E., Franco, M. K., Batool, Z., Wu, M. Z., Dubuke, M. L., Dobosz-Bartoszek, M., et al. (2019). Pseudouridinylation of mRNA Coding Sequences Alters Translation. *Proc. Natl. Acad. Sci. USA* 116, 23068–23074. doi:10.1073/pnas.1821754116

Fernández, I. S., Ng, C. L., Kelley, A. C., Wu, G., Yu, Y.-T., and Ramakrishnan, V. (2013). Unusual Base Pairing during the Decoding of a Stop Codon by the Ribosome. *Nature* 500, 107–110. doi:10.1038/nature12302

Heil, F., Hemmi, H., Hochrein, H., Ampenberger, F., Kirschning, C., Akira, S., et al. (2004). Species-Specific Recognition of Single-Stranded RNA *via* Toll-like Receptor 7 and 8. *Science* 303, 1526–1529. doi:10.1126/science.1093620

Hoerr, I., Obst, R., Rammensee, H.-G., and Jung, G. (2000). *In Vivo* application of RNA Leads to Induction of Specific Cytotoxic T Lymphocytes and Antibodies. *Eur. J. Immunol.* 30, 1–7. doi:10.1002/1521-4141(200001)30:1<1:aid-immu1>3.0.co;2-#

Hoy, S. M. (2018). Patisiran: First Global Approval. *Drugs* 78, 1625–1631. doi:10.1007/s40265-018-0983-6

Ishii, K. J., and Akira, S. (2005). TLR Ignores Methylated RNA. *Immunity* 23, 111–113. doi:10.1016/j.immuni.2005.08.003

Jackson, N. A. C., Kester, K. E., Casimiro, D., Gurunathan, S., and DeRosa, F. (2020). The Promise of mRNA Vaccines: a Biotech and Industrial Perspective. *npj Vaccin.* 5, 11. doi:10.1038/s41541-020-0159-8

Jeffs, L. B., Palmer, L. R., Ambegia, E. G., Giesbrecht, C., Ewanick, S., and MacLachlan, I. (2005). A Scalable, Extrusion-free Method for Efficient Liposomal Encapsulation of Plasmid DNA. *Pharm. Res.* 22, 362–372. doi:10.1007/s11095-004-1873-z

Karijolich, J., and Yu, Y.-T. (2011). Converting Nonsense Codons into Sense Codons by Targeted Pseudouridylation. *Nature* 474, 395–398. doi:10.1038/nature10165

Karikó, K., Buckstein, M., Ni, H., and Weissman, D. (2005). Suppression of RNA Recognition by Toll-like Receptors: The Impact of Nucleoside Modification and the Evolutionary Origin of RNA. *Immunity* 23, 165–175. doi:10.1016/j.immuni.2005.06.008

Karikó, K., Muramatsu, H., Welsh, F. A., Ludwig, J., Kato, H., Akira, S., et al. (2008). Incorporation of Pseudouridine into mRNA Yields Superior Nonimmunogenic Vector with Increased Translational Capacity and Biological Stability. *Mol. Ther.* 16, 1833–1840. doi:10.1038/mt.2008.200

Karikó, K., Ni, H., Capodici, J., Lamphier, M., and Weissman, D. (2004). mRNA Is an Endogenous Ligand for Toll-like Receptor 3. *J. Biol. Chem.* 279, 12542–12550. doi:10.1074/jbc.M310175200

Kierzek, E., Malgowska, M., Lisowiec, J., Turner, D. H., Gdaniec, Z., and Kierzek, R. (2014). The Contribution of Pseudouridine to Stabilities and Structure of RNAs. *Nucleic Acids Res.* 42, 3492–3501. doi:10.1093/nar/gkt1330

Kis, Z., Kontoravdi, C., Shattock, R., and Shah, N. (2020). Resources, Production Scales and Time Required for Producing RNA Vaccines for the Global Pandemic Demand. *Vaccines* 9, 3. doi:10.3390/vaccines9010003

Kremsner, P. G., Guerrero, R. A. A., Arana, E., Aroca Martinez, G. J., Bonten, M. J. M., Chandler, R., et al. (2021). Efficacy and Safety of the CVnCoV SARS-CoV-2 mRNA Vaccine Candidate: Results from Herald, a Phase 2b/3, Randomised, Observer-Blinded, Placebo-Controlled Clinical Trial in Ten Countries in Europe and Latin America. *SSRN J.* doi:10.2139/ssrn.3911826

Krieg, P. A., and Melton, D. A. (1984). Functional Messenger RNAs Are Produced by SP6in Vitrotranscription of Cloned cDNAs. *Nucl. Acids Res.* 12, 7057–7070. doi:10.1093/nar/12.18.7057

Kyriakidis, N. C., López-Cortés, A., González, E. V., Grimaldos, A. B., and Prado, E. O. (2021). SARS-CoV-2 Vaccines Strategies: a Comprehensive Review of Phase 3 Candidates. *npj Vaccin.* 6, 28. doi:10.1038/s41541-021-00292-w

Lovejoy, A. F., Riordan, D. P., and Brown, P. O. (2014). Transcriptome-Wide Mapping of Pseudouridines: Pseudouridine Synthases Modify Specific mRNAs in *S. cerevisiae*. *PLoS ONE* 9, e110799. doi:10.1371/journal.pone.0110799

Malone, R. W., Felgner, P. L., and Verma, I. M. (1989). Cationic Liposome-Mediated RNA Transfection. *Proc. Natl. Acad. Sci.* 86, 6077–6081. doi:10.1073/pnas.86.16.6077

Martinon, F., Krishnan, S., Lenzen, G., Magné, R., Gomard, E., Guillet, J.-G., et al. (1993). Induction of Virus-specific Cytotoxic T Lymphocytesin Vivo by Liposome-Entrapped mRNA. *Eur. J. Immunol.* 23, 1719–1722. doi:10.1002/eji.1830230749

Mateus, J., Dan, J. M., Zhang, Z., Rydyznski Moderbacher, C., Lammers, M., Goodwin, B., et al. (2021). Low-dose mRNA-1273 COVID-19 Vaccine Generates Durable Memory Enhanced by Cross-Reactive T Cells. *Science* 374, eabj9853. doi:10.1126/science.abj9853

Melton, D. A., Krieg, P. A., Rebagliati, M. R., Maniatis, T., Zinn, K., and Green, M. R. (1984). Efficientin Vitrosynthesis of Biologically Active RNA and RNA Hybridization Probes from Plasmids Containing a Bacteriophage SP6 Promoter. *Nucl. Acids Res.* 12, 7035–7056. doi:10.1093/nar/12.18.7035

Meyer, M., Huang, E., Yuzhakov, O., Ramanathan, P., Ciaramella, G., and Bukreyev, A. (2018). Modified mRNA-Based Vaccines Elicit Robust Immune Responses and Protect Guinea Pigs from Ebola Virus Disease. *J. Infect. Dis.* 217, 451–455. doi:10.1093/infdis/jix592

Morais, P., Adachi, H., Chen, J. L., and Yu, Y.-T. (2021). "Mechanisms and Clinical Applications of RNA Pseudouridylation," in Epitranscriptomics *RNA Technologies*. Editors S. Jurga and J. Barciszewski (Cham: Springer International Publishing), 505–526. doi:10.1007/978-3-030-71612-7_19

Morais, P., Adachi, H., and Yu, Y.-T. (2020). Suppression of Nonsense Mutations by New Emerging Technologies. *IJMS* 21, 4394. doi:10.3390/ijms21124394

Mullard, A. (2021). Pfizer's COVID-19 Vaccine Secures First Full FDA Approval. *Nat. Rev. Drug Discov.* 20, 728. doi:10.1038/d41573-021-00156-x

Nance, K. D., and Meier, J. L. (2021). Modifications in an Emergency: The Role of N1-Methylpseudouridine in COVID-19 Vaccines. *ACS Cent. Sci.* 7, 748–756. doi:10.1021/acscentsci.1c00197

Naylor, R., Ho, N. W. Y., and Gilham, P. T. (1965). Selective Chemical Modifications of Uridine and Pseudouridine in Polynucleotides and Their Effect on the Specificities of Ribonuclease and Phosphodiesterases. *J. Am. Chem. Soc.* 87, 4209–4210. doi:10.1021/ja01096a050

Nelson, J., Sorensen, E. W., Mintri, S., Rabideau, A. E., Zheng, W., Besin, G., et al. (2020). Impact of mRNA Chemistry and Manufacturing Process on Innate Immune Activation. *Sci. Adv.* 6, eaaz6893. doi:10.1126/sciadv.aaz6893

Newby, M. I., and Greenbaum, N. L. (2001). A Conserved Pseudouridine Modification in Eukaryotic U2 snRNA Induces a Change in branch-site Architecture. *RNA* 7, 833–845. doi:10.1017/S1355838201002308

Newby, M. I., and Greenbaum, N. L. (2002a). Investigation of Overhauser Effects between Pseudouridine and Water Protons in RNA Helices. *Proc. Natl. Acad. Sci.* 99, 12697–12702. doi:10.1073/pnas.202477199

Newby, M. I., and Greenbaum, N. L. (2002b). Sculpting of the Spliceosomal branch Site Recognition Motif by a Conserved Pseudouridine. *Nat. Struct. Biol.* 9, 958–965. doi:10.1038/nsb873

Ostro, M. J., Giacomoni, D., Lavelle, D., Paxton, W., and Dray, S. (1978). Evidence for Translation of Rabbit Globin mRNA after Liposomemediated Insertion into a Human Cell Line. *Nature* 274, 921–923. doi:10.1038/274921a0

Padilla, R. (2002). A Y639F/H784A T7 RNA Polymerase Double Mutant Displays superior Properties for Synthesizing RNAs with Non-canonical NTPs. *Nucleic Acids Res.* 30, 138e–138. doi:10.1093/nar/gnf138

Pallesen, J., Wang, N., Corbett, K. S., Wrapp, D., Kirchdoerfer, R. N., Turner, H. L., et al. (2017). Immunogenicity and Structures of a Rationally Designed Prefusion MERS-CoV Spike Antigen. *Proc. Natl. Acad. Sci. USA* 114, E7348–E7357. doi:10.1073/pnas.1707304114

Pardi, N., Hogan, M. J., Naradikian, M. S., Parkhouse, K., Cain, D. W., Jones, L., et al. (2018). Nucleoside-modified mRNA Vaccines Induce Potent T Follicular

Helper and Germinal center B Cell Responses. *J. Exp. Med.* 215, 1571–1588. doi:10.1084/jem.20171450

Pardi, N., Hogan, M. J., Pelc, R. S., Muramatsu, H., Andersen, H., DeMaso, C. R., et al. (2017). Zika Virus protection by a Single Low-Dose Nucleoside-Modified mRNA Vaccination. *Nature* 543, 248–251. doi:10.1038/nature21428

Pardi, N., Muramatsu, H., Weissman, D., and Karikó, K. (2013). "*In Vitro* Transcription of Long RNA Containing Modified Nucleosides," in *Synthetic Messenger RNA and Cell Metabolism Modulation Methods in Molecular Biology*. Editor P. M. Rabinovich (Totowa, NJ: Humana Press), 29–42. doi:10.1007/978-1-62703-260-5_2

Parr, C. J. C., Wada, S., Kotake, K., Kameda, S., Matsuura, S., Sakashita, S., et al. (2020). N 1-Methylpseudouridine Substitution Enhances the Performance of Synthetic mRNA Switches in Cells. *Nucleic Acids Res.* 48, e35. doi:10.1093/nar/gkaa070

Pascolo, S. (2004). Messenger RNA-Based Vaccines. *Expert Opin. Biol. Ther.* 4, 1285–1294. doi:10.1517/14712598.4.8.1285

Pascolo, S. (2021). Synthetic Messenger RNA-Based Vaccines: from Scorn to Hype. *Viruses* 13, 270. doi:10.3390/v13020270

Pfizer (2021). Pfizer and BioNTech Announce Positive Topline Results from Pivotal Trial of COVID-19 Vaccine in Children 5 to 11 Years. Available at: https://www.pfizer.com/news/press-release/press-release-detail/pfizer-and-biontech-announce-positive-topline-results (Accessed September 30, 2021)

Polack, F. P., Thomas, S. J., Kitchin, N., Absalon, J., Gurtman, A., Lockhart, S., et al. (2020). Safety and Efficacy of the BNT162b2 mRNA Covid-19 Vaccine. *N. Engl. J. Med.* 383, 2603–2615. doi:10.1056/NEJMoa2034577

Probst, J., Weide, B., Scheel, B., Pichler, B. J., Hoerr, I., Rammensee, H.-G., et al. (2007). Spontaneous Cellular Uptake of Exogenous Messenger RNA *In Vivo* Is Nucleic Acid-specific, Saturable and Ion Dependent. *Gene Ther.* 14, 1175–1180. doi:10.1038/sj.gt.3302964

Richner, J. M., Himansu, S., Dowd, K. A., Butler, S. L., Salazar, V., Fox, J. M., et al. (2017). Modified mRNA Vaccines Protect against Zika Virus Infection. *Cell* 168, 1114–1125. doi:10.1016/j.cell.2017.02.017

Roth, N., Schön, J., Hoffmann, D., Thran, M., Thess, A., Mueller, S. O., et al. (2021). CV2CoV, an Enhanced mRNA-Based SARS-CoV-2 Vaccine Candidate, Supports Higher Protein Expression and Improved Immunogenicity in Rats. *Immunology*. doi:10.1101/2021.05.13.443734

Ruffell, D. (2021). The Future in an RNA Molecule: from mRNA Vaccines to Therapeutics - an Interview with Drew Weissman. *FEBS Lett.* 595, 2305–2309. doi:10.1002/1873-3468.14190

Sanofi (2021). Sanofi: Press Releases, Tuesday, September 28, 2021. Available at: https://www.sanofi.com/media-room/press-releases/2021/2021-09-28 08-00-00 2304069 (Accessed September 30, 2021).

Schwartz, S., Bernstein, D. A., Mumbach, M. R., Jovanovic, M., Herbst, R. H., León-Ricardo, B. X., et al. (2014). Transcriptome-wide Mapping Reveals Widespread Dynamic-Regulated Pseudouridylation of ncRNA and mRNA. *Cell* 159, 148–162. doi:10.1016/j.cell.2014.08.028

Sheikh, A., McMenamin, J., Taylort, B., and Robertson, C. (2021). SARS-CoV-2 Delta VOC in Scotland: Demographics, Risk of Hospital Admission, and Vaccine Effectiveness. *Lancet* 397(10293), 2461–2462. doi:10.1016/S0140-6736(21)01358-1

Song, B., Tang, Y., Wei, Z., Liu, G., Su, J., Meng, J., et al. (2020). PIANO: A Web Server for Pseudouridine-Site (Ψ) Identification and Functional Annotation. *Front. Genet.* 11, 88. doi:10.3389/fgene.2020.00088

Svitkin, Y. V., Cheng, Y. M., Chakraborty, T., Presnyak, V., John, M., and Sonenberg, N. (2017). N1-methyl-pseudouridine in mRNA Enhances Translation through eIF2α-dependent and Independent Mechanisms by Increasing Ribosome Density. *Nucleic Acids Res.* 45, 6023–6036. doi:10.1093/nar/gkx135

Thess, A., Grund, S., Mui, B. L., Hope, M. J., Baumhof, P., Fotin-Mleczek, M., et al. (2015). Sequence-engineered mRNA without Chemical Nucleoside Modifications Enables an Effective Protein Therapy in Large Animals. *Mol. Ther.* 23, 1456–1464. doi:10.1038/mt.2015.103

Thorp, H. H. (2020). Do us a Favor. *Science* 367, 1169. doi:10.1126/science.abb6502

Tomita, K. (1999). The Presence of Pseudouridine in the Anticodon Alters the Genetic Code: a Possible Mechanism for Assignment of the AAA Lysine Codon as Asparagine in Echinoderm Mitochondria. *Nucleic Acids Res.* 27, 1683–1689. doi:10.1093/nar/27.7.1683

Wadhwa, A., Aljabbari, A., Lokras, A., Foged, C., and Thakur, A. (2020). Opportunities and Challenges in the Delivery of mRNA-Based Vaccines. *Pharmaceutics* 12, 102. doi:10.3390/pharmaceutics12020102

Warren, L., Manos, P. D., Ahfeldt, T., Loh, Y.-H., Li, H., Lau, F., et al. (2010). Highly Efficient Reprogramming to Pluripotency and Directed Differentiation of Human Cells with Synthetic Modified mRNA. *Cell Stem Cell* 7, 618–630. doi:10.1016/j.stem.2010.08.012

Weissman, D., Ni, H., Scales, D., Dude, A., Capodici, J., McGibney, K., et al. (2000). HIV Gag mRNA Transfection of Dendritic Cells (DC) Delivers Encoded Antigen to MHC Class I and II Molecules, Causes DC Maturation, and Induces a Potent Human *In Vitro* Primary Immune Response. *J. Immunol.* 165, 4710–4717. doi:10.4049/jimmunol.165.8.4710

Westhof, E. (2019). Pseudouridines or How to Draw on Weak Energy Differences. *Biochem. Biophysical Res. Commun.* 520, 702–704. doi:10.1016/j.bbrc.2019.10.009

Wolff, J. A., Malone, R. W., Williams, P., Chong, W., Acsadi, G., Jani, A., et al. (1990). Direct Gene Transfer into Mouse Muscle *In Vivo*. *Science* 247, 1465–1468. doi:10.1126/science.1690918

Wrapp, D., Wang, N., Corbett, K. S., Goldsmith, J. A., Hsieh, C.-L., Abiona, O., et al. (2020). Cryo-EM Structure of the 2019-nCoV Spike in the Prefusion Conformation. *Science* 367, 1260–1263. doi:10.1126/science.abb2507

Wurm, J. P., Meyer, B., Bahr, U., Held, M., Frolow, O., Kötter, P., et al. (2010). The Ribosome Assembly Factor Nep1 Responsible for Bowen-Conradi Syndrome Is a Pseudouridine-N1-specific Methyltransferase. *Nucleic Acids Res.* 38, 2387–2398. doi:10.1093/nar/gkp1189

Conflict of Interest: Author PM is Scientific Director (Pseudouridylation Technology) of ProQR Therapeutics.

The remaining authors declare that the research was conducted in the absence of any commercial or financial relationships that could be construed as a potential conflict of interest.

Publisher's Note: All claims expressed in this article are solely those of the authors and do not necessarily represent those of their affiliated organizations, or those of the publisher, the editors and the reviewers. Any product that may be evaluated in this article, or claim that may be made by its manufacturer, is not guaranteed or endorsed by the publisher.

Copyright © 2021 Morais, Adachi and Yu. This is an open-access article distributed under the terms of the Creative Commons Attribution License (CC BY). The use, distribution or reproduction in other forums is permitted, provided the original author(s) and the copyright owner(s) are credited and that the original publication in this journal is cited, in accordance with accepted academic practice. No use, distribution or reproduction is permitted which does not comply with these terms.

frontiers in Cell and Developmental Biology

ORIGINAL RESEARCH
published: 16 November 2021
doi: 10.3389/fcell.2021.767051

Comprehensive Analysis of the Transcriptome-Wide m6A Methylation Modification Difference in Liver Fibrosis Mice by High-Throughput m6A Sequencing

Chang Fan[1,2], Yanzhen Ma[1,2], Sen Chen[1,2], Qiumei Zhou[1], Hui Jiang[1,2,3], Jiafu Zhang[4]* and Furong Wu[5]**

[1]Experimental Center of Clinical Research, The First Affiliated Hospital of Anhui University of Chinese Medicine, Hefei, China, [2]School of Pharmacy, Anhui University of Chinese Medicine, Hefei, China, [3]Key Laboratory of Xin'an Medicine of the Ministry of Education, Anhui University of Chinese Medicine, Hefei, China, [4]Department of Pharmacy, The First Affiliated Hospital of Anhui University of Chinese Medicine, Hefei, China, [5]Department of Pharmacy, The First Affiliated Hospital of USTC, Division of Life Sciences and Medicine, University of Science and Technology of China, Hefei, China*

OPEN ACCESS

Edited by:
Chengqi Yi,
Peking University, China

Reviewed by:
Matthew Wong,
Children's Cancer Institute Australia, Australia
Zhiwen Fan,
Nanjing Drum Tower Hospital, China

***Correspondence:**
Hui Jiang
jianghui@ahtcm.edu.cn
Jiafu Zhang
zyfyzjf@163.com
Furong Wu
Fr13866767052@163.com

Specialty section:
This article was submitted to Epigenomics and Epigenetics, a section of the journal Frontiers in Cell and Developmental Biology

Received: *30 August 2021*
Accepted: *01 November 2021*
Published: *16 November 2021*

Citation:
Fan C, Ma Y, Chen S, Zhou Q, Jiang H, Zhang J and Wu F (2021) Comprehensive Analysis of the Transcriptome-Wide m6A Methylation Modification Difference in Liver Fibrosis Mice by High-Throughput m6A Sequencing. Front. Cell Dev. Biol. 9:767051. doi: 10.3389/fcell.2021.767051

N6-Methyladenosine (m6A), a unique and common mRNA modification method in eukaryotes, is involved in the occurrence and development of many diseases. Liver fibrosis (LF) is a common response to chronic liver injury and may lead to cirrhosis and even liver cancer. However, the involvement of m6A methylation in the development of LF is still unknown. In this study, we performed a systematic evaluation of hepatic genome-wide m6A modification and mRNA expression by m6A-seq and RNA-seq using LF mice. There were 3,315 genes with significant differential m6A levels, of which 2,498 were hypermethylated and 817 hypomethylated. GO and KEGG analyses illustrated that differentially expressed m6A genes were closely correlated with processes such as the endoplasmic reticulum stress response, PPAR signaling pathway and TGF-β signaling pathway. Moreover, a total of 90 genes had both a significant change in the m6A level and mRNA expression shown by joint analysis of m6A-seq and RNA-seq. Hence, the critical elements of m6A modification, including methyltransferase WTAP, demethylases ALKBH5 and binding proteins YTHDF1 were confirmed by RT-qPCR and Western blot. In an additional cell experiment, we also observed that the decreased expression of WTAP induced the development of LF as a result of promoting hepatic stellate cell (HSC) activation. Therefore, this study revealed unique differential m6A methylation patterns in LF mice and suggested that m6A methylation was associated with the occurrence and course of LF to some extent.

Keywords: m6A methylation, m6A-seq, liver fibrosis, HSCs, WTAP

INTRODUCTION

N6-Methyladenosine (M6A) is a posttranscriptional modification found in eukaryotic messenger RNA (mRNA), which is similar to DNA methylation and histone modification and is regulated by a variety of methyltransferases (Bushkin et al., 2019; Gu et al., 2019; Berulava et al., 2020). Methyltransferase complexes are composed of METTL3 (methyltransferase-like 3), METTL14 and their additional linker molecules such as WTAP (Wilms tumor associated protein) and

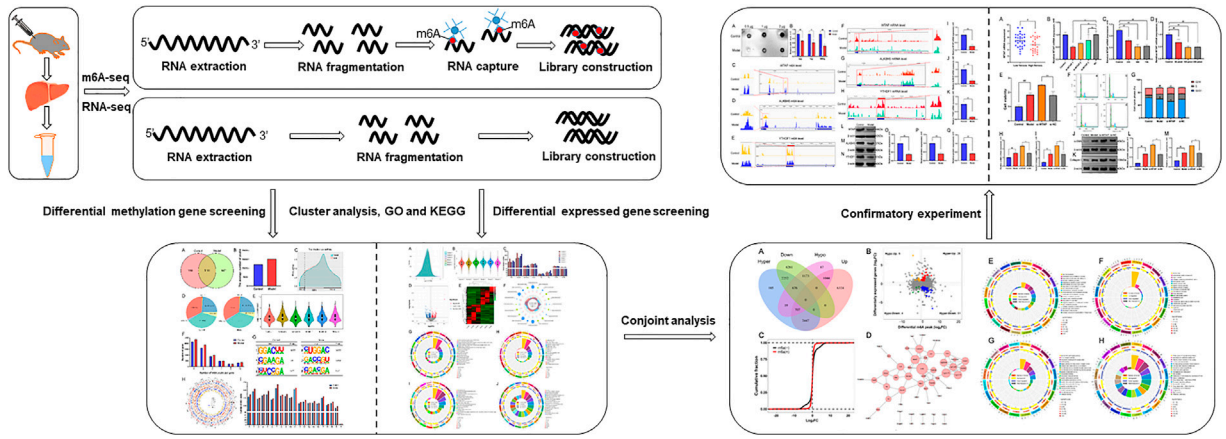


FIGURE 1 | A schematic diagram of m6A-seq and RNA-seq analyses of mice with LF. LF was induced by subcutaneous injection of CCl_4 in mice, and extracted total RNA from liver. Then, RNA was fragmented, and the m6A RNA was separated by immunoprecipitation magnetic beads specifically recognizing m6A sites. Subsequently, the m6A-seq and RNA-seq library were constructed and sequenced.

KIAA1429, which can catalyze mRNA m6A methylation. The m6A methylation site on RNA is recognized by m6A-binding proteins, including YTHDC1/2 (1ap2 containing YTH domain), YTHDF1/2/3 (YTH family proteins 1–2–3) and IGF2BP1/2/3 (insulin-like growth factor 2 mRNA binding protein 1/2/3), which can bind to methylated m6A sites and perform specific functions. In addition, demethyltransferase FTO (fat mass and obesity related protein) and ALKBH5 (alkyl B homolog 5) reduce m6A modified RNA to original RNA (Du et al., 2018; Zhang Z. et al., 2020; Mapperley et al., 2021). The combined action of these methyltransferases makes m6A modification a dynamic and reversible process (Lu et al., 2020). It has been confirmed that m6A modification affects the control of key cellular processes, including RNA stability (Wang et al., 2014), translation efficiency (Wang et al., 2015), secondary structure (Liu et al., 2015), subcellular localization (Meyer and Jaffrey, 2014), splicing and transport (Yang et al., 2018), and plays important roles in a variety of diseases (Zhang B. et al., 2020; Liu et al., 2020).

Liver fibrosis (LF) is defined as excessive deposition of extracellular matrix (ECM) in response to various cases of liver injury, which is a reversible abnormal tissue response, and excessive activation of hepatic stellate cells (HSCs) is central to its pathogenesis (Bataller and Brenner, 2005; Zhang et al., 2017; Smith-Cortinez et al., 2020). LF is the most common pathological consequence of liver diseases and may lead to liver cirrhosis and liver cancer, and even develop into liver failure in severe cases (Wang Q. et al., 2020). Existing studies have found that m6A methylation plays an extremely important role in a variety of physiological and pathological processes of the liver (Lin et al., 2020; Ondo et al., 2021). Zhong et al. (2019) found that the m6A binding protein YTHDF2 can inhibit tumor proliferation and growth by reducing the stability of EGFR mRNA in hepatocellular carcinoma. Ma et al. (2017) found that the methyltransferase METTL14 can inhibit the metastasis of hepatocellular carcinoma by regulating the methylation of microRNAs. However, as a preliminary process in these severe liver diseases, m6A methylation in LF is rarely described.

The purpose of this study was to establish the expression profile of m6A modification in mice with LF and to explore the potential regulatory mechanism of m6A methylation on LF. Therefore, we used m6A-seq and RNA-seq, to analyze the difference in gene methylation modification and mRNA expression levels after LF at the full transcriptional level, and verified the change in methylase expression and its regulatory role in LF (**Figure 1**). In conclusion, this study revealed that RNA m6A methylation can play a key role in the pathogenesis of LF by regulating the mRNA expression level of related transcripts. Moreover, methylase affects the occurrence and development of LF by regulating the process of m6A methylation, which could represent an important factor in the process of LF.

MATERIALS AND METHODS

Animal

SPF male C57 BL/6 mice (6–8 weeks old, 20 ± 2 g) were purchased from the Experimental Animal Center of Anhui Province. All mice were raised in the animal facility of the First Affiliated Hospital of Anhui University of Chinese Medicine with an indoor temperature of 18–22°C and humidity of 40–60%, under 12 h alternate dark/light cycles. All mice were allowed food and water freely. Following 1 week of adaptive feeding, a model of LF was established by subcutaneous injection of 0.01 ml/g 20% carbon tetrachloride (CCl_4) in an olive oil solution in the back flank of the mice twice a week for 12 weeks, as described in our previous study (Fan et al., 2020). The number of samples was three per group for control mice and LF model mice. The experimental design was approved by the Animal Ethics Committee of Anhui University of Chinese Medicine (AHUCM-mouse-2020032).

Histopathological Analysis

Twelve weeks after establishing the model, the mice were sacrificed by cervical dislocation and the liver samples were

taken for histopathological analysis under white light, and hematoxylin and eosin and Masson staining.

Another part of the fresh liver sample was fixed in 2.5% glutaraldehyde and incubated overnight at 4°C. The sample was then fixed in 2% osmium tetroxide for 1 h and dehydrated to 100% through a fractionated series of ethanol (Jiang et al., 2018). Then the sample was embedded in the resin and observed under an electron microscope.

M6A Sequencing and RNA Sequencing

Total RNA was isolated from mouse liver tissue using TRIzol reagent (Invitrogen, United Statesa) according to the manufacturer's protocol. In this study, we used an m6A-specific antibody (Sigma-Aldrich, ABE572) for immunoprecipitation RNA. The m6A RNA-seq service was provided by Shanghai Bohao Biotechnology Corporation (Shanghai, China). Briefly, poly (A) RNA was captured by VAHTS 2X Frag/Prime Buffer. Then one part of the RNA fragment was used to construct the RNA-seq library, and the other part was used for m6A RNA immunoprecipitation through the GenSeqTM m6A-MERIP kit (GenSeq Inc., Cyberjaya, Malaysia), which was used to construct the m6A-seq library. All operations were carried out in accordance with the manufacturer's instructions. RNA input samples without immunoprecipitation and m6A input samples were used for the generation of RNA-seq libraries. The library quality was evaluated with a Bioptic Qsep100 Analyzer (Bioptic lnc., Taiwan, China). Library sequencing was performed on an Illumina NovaSeq instrument with 150 bp paired-end reads.

Sequencing Data Processing

Cutadapt (v2.5.0) was used to trim adapters and filter for sequences, FastQC (www.bioinformatics.babraham.ac.uk/projects/fastqc) was used to analyze the quality of sequencing data, and the sequencing mass distribution, base content distribution and repeated sequencing fragment proportion were obtained (Garsmeur et al., 2018). Then, the remaining reads were aligned to the human ensemble genome GRCh38 (mouse ensemble genome GRCm38) using Hisat2 aligner (v2.1.0) under the following parameters: -rna-strandness RF. m6A peaks were identified using the exomePeak R package (v2.13.2) under the following parameters: "PEAK_CUTOFF_PVALUE = 0.05, PEAK_CUTOFF_FDR = NA, FRAGMENT_LENGTH = 200". Identified m6A peaks with a p value < 0.05 were chosen for the *de novo* motif analysis using homer (v4.10.4) under the following parameters: "-len 6 -rna". M6A-RNA-related genomic features were visualized using the Guitar R package (v1.16.0). We used the HOMER (http://homer.ucsd.edu/homer/ngs/peakMotifs.html) software to analyze the motifs of the m6A peaks (Heinz et al., 2010). The screening of differential m6A peaks was also carried out by the exomePeak R package, and the filtering threshold was p value <0.05, |fold change| > 2. Moreover, Bam files of sequencing results were visualized using IGV (http://software.broadinstitute.org/software/igv/) (Robinson et al., 2011).

GO and KEGG Analyses

Differential methylated genes and mRNAs screened according to the above filtering threshold p value <0.05, |fold change| > 2 were used for Gene Ontology (GO) and Kyoto Encyclopedia of Genes and Genomes (KEGG) analyses (Ashburner et al., 2000). All analyses were performed using the clusterprofile R package (v3.6.0). Then, the top 20 GO terms and pathways were selected for display according to the p value and the degree of enrichment. The figures were generated using OmicShare tools (http://www.omicshare.com/tools).

Protein-Protein Interaction (PPI) Network Analysis

We conducted a joint analysis of genes with differential expression and differential m6A methylation modification and then used the p value and fold change to screen out the genes for PPI analysis. These differentially expressed genes were imported into the STRING database, which contains comprehensive information about interactions between proteins, and was used to determine the interaction relationship between genes (Szklarczyk et al., 2017). The PPI network was constructed based on importing the data into Cytoscape 3.5.1 software, and then, the network was analyzed by Network Analyzer. The genes with interactions with combined scores greater than 0.4 were selected to construct a protein-protein interaction network diagram (Wang X. et al., 2020).

VALIDATION EXPERIMENT

RNA m6A Dot Blot Analysis

A dot blot assay was performed to compare the difference in total m6A levels in liver samples between the control group and the model group. According to the manufacturer's instructions, the total RNA, was isolated from the liver sample with TRIzol (Thermo, 15596018) and the RNA sample was placed on the nitrocellulose filter membrane. The membrane was dried and cross-linked with 200,000 μJ/cm^2 UV twice, washed 3 times with PBST for 5 min each time, and blocked at room temperature for 2 h in 5% skimmed milk. The membrane was transferred to a closed solution containing anti-m6A antibody (ab232905, Abcam) at a dilution of 1: 1,000 and incubated overnight at 4°C. Then, the membrane was rinsed again with PBST for 10 min, sealed in a solution of goat antirabbit IgG combined with HRP (Zs-BIO, ZB-2301) at a dilution of 1: 5,000, incubated at room temperature for 1 h and washed with PBST 3 times. The film was developed with ECL (Western Lightning Plus-ECL, Perkin-Elmer) detection reagent (Thermo, 34094), the signal was detected by chemiluminescence, and the bands were analyzed by ImageJ software.

Isolation and Culture of Primary Mice HSCs

Mice were anesthetized by intraperitoneal injection of pentobarbital sodium and fixed on the operating table. A middle incision of the lower abdomen was used to open the abdominal cavity and exposed the liver and portal vein. Then, the

liver was perfused with preheated HBSS at a uniform speed, the open vein was cut when the liver turned gray, and then 0.05% type IV collagenase perfusion solution was perfused (Nishanth et al., 2013; Kim et al., 2016). After perfusion, the liver was cut out and placed in a Petri dish to clean the liver surface with PBS. Tweezers were used to tear up the liver, and 0.05% type IV collagenase was added to the 37°C incubator to digest the tissue for 30 min, followed by filtering with a 200-mesh strainer. The filtrate was centrifuged at 80, 50 and 40 g gradients, and the cell precipitate was collected. The cells were resuspended in serum containing DMEM and seeded in plates precoated with rat-tail collagen I (Zhang et al., 2012; Vig et al., 2015; Yang et al., 2019). After 4 h, the cell culture medium was replaced with serum-free DMEM to continue culturing, and the results of HSC identification are shown in **Supplementary Figure 1**.

Synthesis and Screening of siRNA and Cell Transfection

To suppress the expression of WTAP, the sequence information of WTAP was obtained from the NCBI database, and the specific WTAP small interference RNA (siRNA) sequence was designed and synthesized according to the full-length sequence information. The specific sequence information is shown in **Supplementary Table 1**. All siRNA sequences were synthesized by Shanghai Jima Biotechnology Co., Ltd. (Shanghai, China). Three dose groups of 50 pmol, 100 and 200 pmol were set for each siRNA to screen the best transfection conditions. The murine HSCs were seeded in 6-well cell culture plates and cultured until the degree of cell fusion reached 60–80% (Wang Z. et al., 2021). Then, WTAP siRNA was transfected into HSCs with Lipofectamine 2000 transfection reagent (Invitrogen). After 24, 48 and 72 h of siRNA transfection, the HSCs were collected and the expression of WTAP was detected by RT-qPCR assay.

Cell Proliferation Assays and Cell Cycle Analysis

The proliferation of HSCs was detected using a CCK-8 assay. In short, HSCs were trypsinized and resuspended in complete medium, and the cell density was adjusted to 1×10^5. HSCs were inoculated into 96-well plates at 100 μl per well and cultured for 72 h in a 37°C incubator. Then, 10 μl CCK-8 reagent (BestBio, BB-4202-01) was added to each well, and cells were cultured for another 1 h. The absorbance of each well at 450 nm was measured using a microplate reader. Cell cycle was analyzed by flow cytometry. The HSCs of each group were collected and added to PI staining solution (BestBio, BB-4104) and incubated. The percentage of HSCs in each stage was detected by flow cytometry, and the data were analyzed by FlowJo software (Tree Star Inc., United Statesa).

RT-qPCR

RT-qPCR was used to detect the expression level of candidate genes. Total RNA from HSCs was extracted with TRIzol (Thermo, 15596018). An ultramicro spectrophotometer was used to determine the concentration and purity of RNA. Then, cDNA reverse transcription and RT-qPCR reactions were performed using the PrimeScript™ RT reagent Kit with gDNA Eraser (TaKaRa, RR047A) and 2×SYBR Green qPCR Master Mix (High ROX) (Servicebio, G3322-05). The primer information is shown in **Supplementary Table 2**. Reactions proceeded using the following conditions: 95°C for 30 s, followed by 40 cycles of 95°C for 15 s and 60°C for 30 s.

Western Blot

Total proteins were obtained from HSCs using the radioimmunoprecipitation assay (RIPA) lysis buffer (Beyotime, P0013B) and PMSF (Biosharp, BL507A). The protein contents of the samples were determined by the bicinchoninic acid method. Twenty micrograms of protein samples were separated by 10% SDS-PAGE and transferred to polyvinylidene fluoride membranes. Following blocking with 5% skim milk for 1 h at room temperature, the membranes were incubated with primary antibodies against WTAP (Affinity, DF3282), YTHDF1 (Affinity, DF3422), ALKBH5 (Affinity, DF2585), α-SMA (Affinity, AF1032), and collagen Ⅰ (Affinity, AF7001) overnight at 4°C. The dilution concentrations of the above antibodies were all 1: 1,000. After washing with TBST, diluted goat-anti-mouse IgG (1: 10,000) antibody (Zs-BIO, ZB-2305) or goat anti-rabbit IgG (1: 3,000) antibody (Zs-BIO, ZB-2301) conjugated with horseradish peroxidase was added, and membranes were incubated for 2 h at room temperature. The membranes were developed with an enhanced chemiluminescence detection kit, and the bands were analyzed by ImageJ software.

Statistical Analysis

The experimental data are presented as the mean ± standard deviation (SD). Statistical analysis was performed by using SPSS 23.0 software. Paired Student's t-tests were used to detect the differences between the two groups. For multiple comparisons, one-way ANOVA was used with Tukey's multiple comparisons test. When the p value was <0.05, the results were considered to be statistically significant.

RESULTS

Pathologic HE Staining, Sirius Red Staining and Transmission Electron Microscopy of the Liver

Liver morphology and the pathological changes in LF mice were observed by white light, HE staining, Masson staining and transmission electron microscopy. As shown in **Figure 2A**, after 12 weeks of CCl_4 induction, the livers of the control group were red and smooth, while the livers of the model group were relatively swollen and rough, and the color was gray and white. In **Figure 2B**, the results of HE staining showed that the structure of the hepatic lobules in the control group was clear, and the hepatocyte cords were in their normal arrangement. In contrast, in the model group there were abundant and large lipid droplets in the cytoplasm of

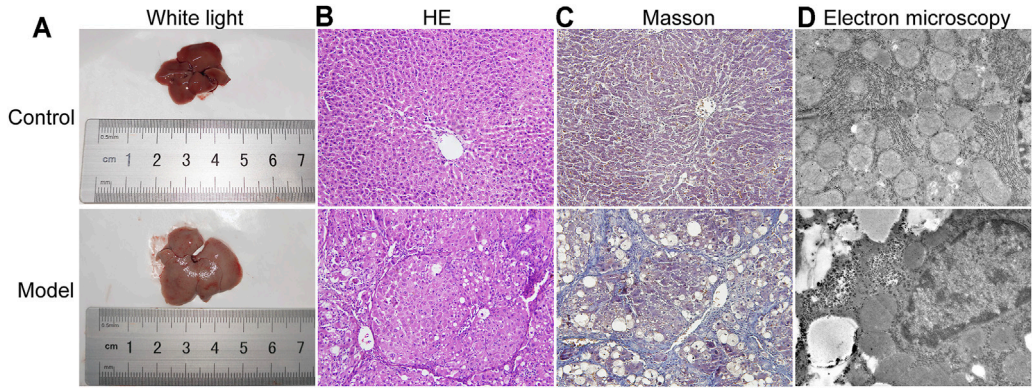


FIGURE 2 | Collected livers were subjected to pathological analysis by white light, HE and Sirius red staining and transmission electron microscopy. **(A)** Liver under white light. **(B)** HE staining (200-fold). **(C)** Sirius Red staining (200-fold). **(D)** Transmission electron microscopy (TEM) analysis (20000-fold).

hepatocytes, severe steatosis, disordered liver tissue structure, obvious hyperplasia of fibrotic tissue, and unclear structure of some hepatic lobules.

In **Figure 2C**, the results of Masson staining showed that there was a large amount of collagen deposition in the liver tissue of the model group compared with the control group. Similarly, obvious changes in the subcellular structure of the liver were observed under an electron microscope (**Figure 2D**). Hepatocytes in the control group were intact and without morphological signs of degeneration or necrosis, while in the model group, the hepatocytes showed abnormal morphological changes, including disappearance of the cell boundary, rupture of the cell membrane, cytoplasmic turbidity, organelle expansion and nuclear shrinkage.

General Description of m6A Methylation Modification in LF

We compared m6A methylation peaks at each site in hepatic tissues from mice with fibrosis. The differences and overlaps in m6A methylation between the individuals are shown by the Venn diagram in **Figure 3A**. We found 6,221 m6A methylation modifier genes in the control group and 6,982 m6A methylation modifier genes in the model group, of which 5,111 m6A methylation modifier genes were common between the two groups. Compared with the control group, 1871 m6A methylation modifier genes appeared, and 1,110 m6A methylation modifier genes disappeared in the model group, indicating that there was a significant difference in the m6A modification pattern after LF. **Figure 3B** shows the level of m6A methylation in different groups. We found an average of 12166 peaks in the control group and 15100 peaks in the model group.

As shown in **Figures 3C,D**, m6A methylation of mRNAs occurred mainly in coding sequences (CDSs) and 3′ untranslated regions (3′UTRs). More specifically, approximately 35.7% of m6A peaks were distributed in the CDS region, and 33% of m6A peaks were distributed in the 3′UTR. The violin diagram (**Figure 3E**) shows the results of the enrichment degree analysis of m6A methylation in each sample. The average logarithmic fold-enrichment of the control group was 4.8, while the average logarithmic fold-enrichment of the model group was 5.3. By means of the distribution of m6A peaks in each gene, we found that approximately 37% of the genes had separate m6A modification sites, and 80% of the genes had one to three m6A modification sites (**Figure 3F**).

Subsequently, we predicted the m6A motif in LF by the mRNA sequence corresponding to m6A methylation peaks. As shown in **Figure 3G**, the most significant mRNA methylation occurred at the RRAC motifs. The analysis of the m6A methylation distribution at different chromosome loci found that the m6A peaks of genes in the model group increased, and the chromosomes with the highest m6A methylation frequency were chromosome 7 with 1,119 m6A methylation peaks, chromosome 11 with 993 m6A methylation peaks and chromosome 2 with 940 m6A methylation peaks (**Figures 3H,I**). By further comparison, we found that there was no significant difference in the distribution number of m6A peaks on chromosomes between the two groups.

Analysis of Differentially Methylated m6A Genes and Their Signaling Pathways

Using the filtering criteria of a p value <0.05 and |fold change| >2, 3,315 genes with differential m6A methylation were identified, of which 2,498 m6A hypermethylated genes and 817 m6A hypomethylated genes were identified (**Figures 4A,B**). We also visually assessed the enrichment degree and fold change of the top 10 hypermethylated genes and top 10 hypomethylated genes (**Figure 4C**), as shown in **Table 1**. Specific information of all differentially methylated m6A genes is presented in **Supplementary file 1**.

Simultaneously, the results of GO and KEGG analyses showed the enrichment of GO functions and pathways of differentially methylated genes. We found 1122 GO terms were significantly enriched in biological processes (**Figure 4D**), 210 GO terms were significantly enriched in cellular components (**Figure 4E**), and 476 GO terms were significantly enriched in molecular functions (**Figure 4F**), especially in the process of transcription, liver

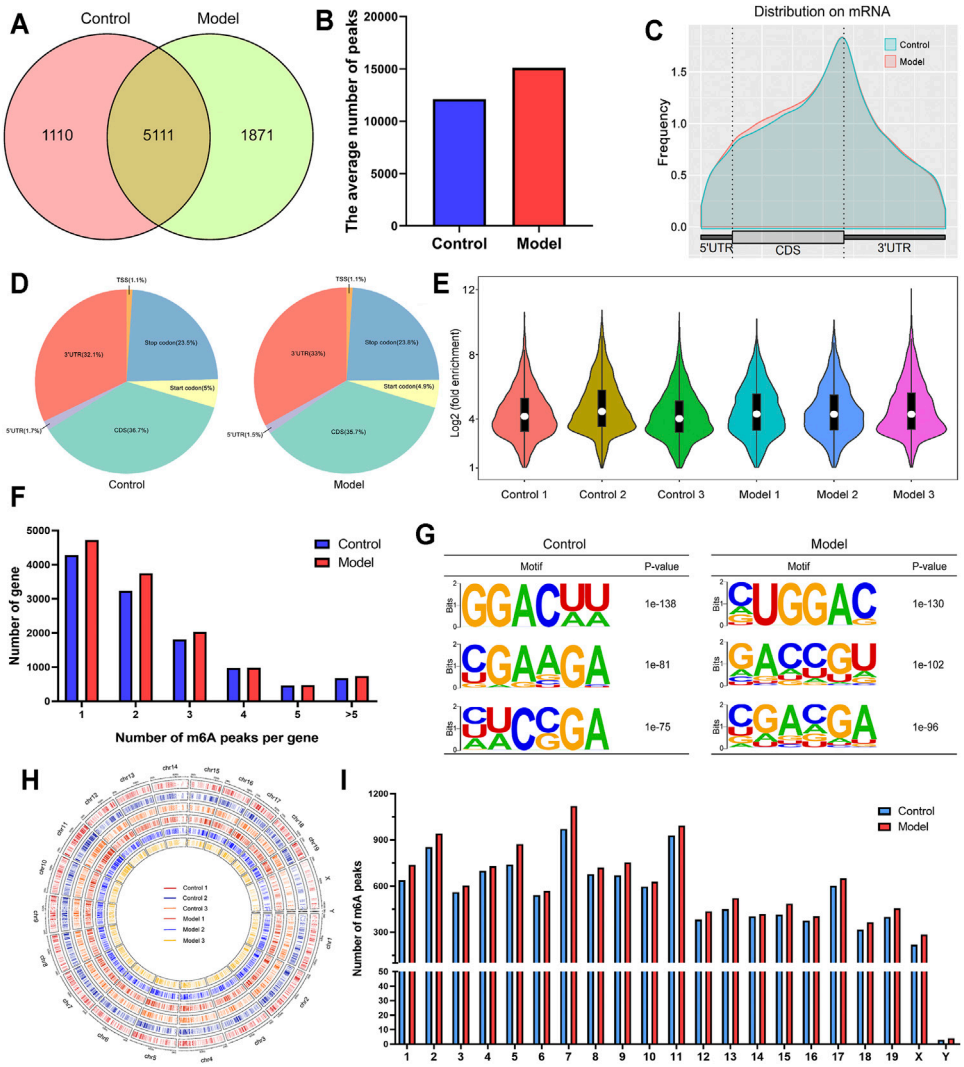


FIGURE 3 | Overview of m6A-modified transcripts in LF mice. **(A)** Venn diagram of m6A-modified genes in the control group and the model group. **(B)** The average number of m6A peaks in each group. **(C)** Density of differential m6A peaks along transcripts. Each transcript was divided into three parts: 5′UTR, CDS, and 3′UTR. **(D)** Pie charts showing the region of m6A peaks in each group. **(E)** Violin plot of the relative abundance of m6A peaks in each group. **(F)** Number of peaks per transcript. **(G)** The most conserved sequence motif of the differential m6A peak region. **(H)** The distribution patterns of m6A peaks in different chromosomes. **(I)** The count of m6A peaks in per chromosome.

development, response of endoplasmic reticulum to unfolded proteins, and protein binding. Similarly, KEGG analysis found that 104 pathways were significantly enriched (**Figure 4G**), especially protein processing in the endoplasmic reticulum, PI3K-Akt signaling pathway and TGF-β signaling pathway. Specific information on the GO and KEGG pathway enrichment analyses is presented in **Supplementary Table 3**.

Description of mRNA Expression and Analysis of Differential Genes in LF

In **Figure 5A**, not only the mRNA distribution and abundance of control samples and LF samples were shown, but also the peak patterns of these samples were visually displayed. The violin diagram in **Figure 5B** demonstrates a similar result; the average logarithmic fold-enrichment of the control group was 1.2, while the average logarithmic fold-enrichment of the model group was 1.3. The gene distribution pattern of the control group was also different from the gene distribution pattern of the model group, but they were distributed mainly in the CDS region and exon region (**Figure 5C**).

Then, similar to the screening of differentially methylated genes, a p value <0.05 and |fold change| > 2 were used as screening criteria, and we found 828 differentially expressed genes, including 398 upregulated genes and 430 downregulated genes (**Figures 5D,E**). Moreover, we also visually compared the expression and corresponding abundance of the top 10 upregulated genes and top 10 downregulated genes

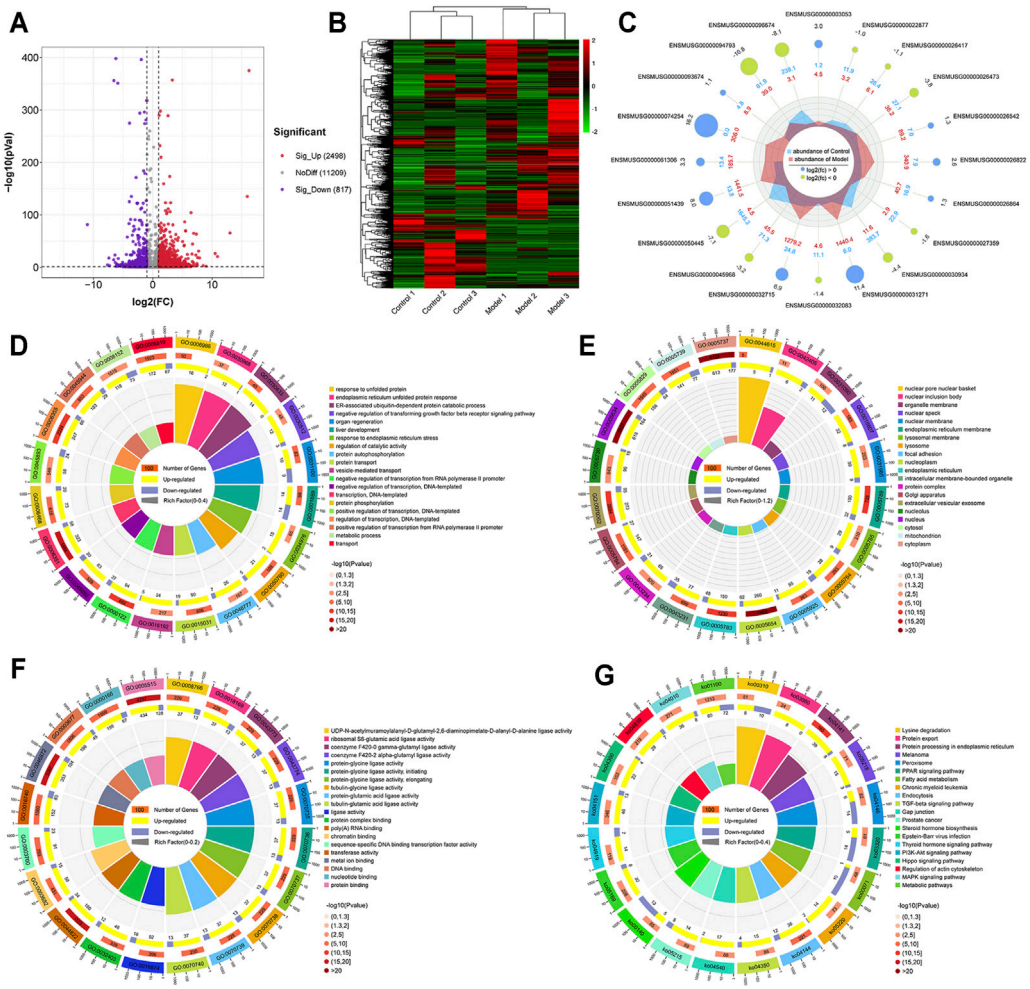


FIGURE 4 | Genes with differential m6A methylation modification in LF. **(A)** Volcano plot representation of microarray data on the differentially expressed m6A methylation genes. The blue and red dots to the left and to the right of the two vertical lines indicate more than a 2-fold change and represent the differentially expressed m6A methylation genes with statistical significance. **(B)** Hierarchical cluster analysis of differentially expressed m6A methylation genes. Hierarchical clustering shows that the differentially expressed m6A methylation genes ultimately cluster into two major branches, including hypermethylated genes, which are labeled in red, and hypomethylated genes, which are labeled in green. The darker the color, the more significant the difference. **(C)** The radar map shows the top 10 most significant hypermethylated genes and top 10 hypomethylated genes. **(D)** GO biological processes enrichment analysis. **(E)** GO cellular component enrichment analysis. **(F)** GO molecular function enrichment analysis. **(G)** KEGG enrichment analysis.

(**Figure 5F**), as shown in **Table 2**. Specific information of all differentially expressed RNAs is presented in **Supplementary File 2**. Meanwhile, the results of GO analysis showed that 376 GO terms were significantly enriched in biological processes (**Figure 5G**), 64 GO terms were significantly enriched in cellular components (**Figure 5H**), and 136 GO terms were significantly enriched in molecular functions (**Figure 5I**), particularly in cellular response to hormone stimulus, proteinaceous extracellular matrix, extracellular matrix structural constituent, and more. Similarly, in **Figure 4J**, the results of KEGG analysis found that 41 pathways were significantly enriched (**Figure 4J**), particularly the metabolism of xenobiotics by cytochrome P450, retinol metabolism, chemical carcinogenesis, and more. Specific information on the GO and KEGG pathway enrichment analyses is presented in **Supplementary Table 4**.

Overview of Transcriptome Profiles and Conjoint Analyses of m6A-Seq and RNA-Seq Data

A conjoint analysis was conducted for m6A-seq and RNA-seq data. We found that a total of 8,299 peaks located on 2,353 genes not only had m6A modification but also had altered mRNA levels (**Figure 6A**). However, not all of them were significant. As shown in **Figure 6B**, by setting the filter conditions of a p value < 0.05 and | fold change| >2, we found 90 genes that commonly had significant differential m6A methylation levels and significant differentially

TABLE 1 | the top 10 hypermethylation genes and top 10 hypomethylation genes.

Gene	ID	Description	Chromosome	Start	End	Sizes	*p* Value	Log_2FC	Class	Hyper/ Hypo
Trib3	ENSMUSG00000032715	tribbles pseudokinase 3	2	152337421	152338619	1,198	0	6.93	exon	Hyper
Cd14	ENSMUSG00000051439	CD14 antigen	18	36725103	36726289	1,186	0	8.02	CDS	Hyper
Serpina7	ENSMUSG00000031271	serine (or cysteine) peptidase inhibitor, clade A (alpha-1 antiproteinase, antitrypsin), member 7	X	139080062	139080331	269	0	11.40	3′UTR	Hyper
Cyp2c29	ENSMUSG00000003053	cytochrome P450, family 2, subfamily c, polypeptide 29	19	39330237	39330446	209	0	3.03	3′UTR	Hyper
Hspa5	ENSMUSG00000026864	heat shock protein 5	2	34775567	34776318	751	0	1.30	CDS	Hyper
Cyp2a4	ENSMUSG00000074254	cytochrome P450, family 2, subfamily a, polypeptide 4	7	26314847	26315088	241	0	16.2	3′UTR	Hyper
Lcn2	ENSMUSG00000026822	lipocalin 2	2	32384662	32384871	209	0	2.64	exon	Hyper
Slc38a10	ENSMUSG00000061306	solute carrier family 38, member 10	11	120104735	120106716	1,301,283	0	3.29	CDS	Hyper
Rpl41	ENSMUSG00000093674	ribosomal protein L41	10	128548143	128548497	30,822	0	1.11	exon	Hyper
Apcs	ENSMUSG00000026542	serum amyloid P-component	1	172894048	172895041	662,221	0	1.28	CDS	Hyper
Mup15	ENSMUSG00000096674	major urinary protein 15	4	61435819	61435969	150	0	-8.12	3′UTR	Hypo
Pigr	ENSMUSG00000026417	polymeric immunoglobulin receptor	1	130851592	130852249	657	0	-1.05	3′UTR	Hypo
Teddm2	ENSMUSG00000045968	transmembrane epididymal family member 2	1	153899900	153900228	328	0	-3.22	exon	Hypo
Oat	ENSMUSG00000030934	ornithine aminotransferase	7	132557925	132558254	329	0	-4.41	3′UTR	Hypo
Cyp8b1	ENSMUSG00000050445	cytochrome P450, family 8, subfamily b, polypeptide 1	9	121914355	121916095	1,740	0	-7.06	CDS	Hypo
Hrg	ENSMUSG00000022877	histidine-rich glycoprotein	16	22960759	22961536	777	0	-1.02	CDS	Hypo
Apoa1	ENSMUSG00000032083	apolipoprotein A-I	9	46229224	46230407	45,603	0	-1.38	CDS	Hypo
Glul	ENSMUSG00000026473	glutamate-ammonia ligase (glutamine synthetase)	1	153907866	153908376	510	0	-3.79	CDS	Hypo
Slc27a2	ENSMUSG00000027359	solute carrier family 27 (fatty acid transporter), member 2	2	126587765	126588035	270	0	-1.65	CDS	Hypo
Mup12	ENSMUSG00000094793	major urinary protein 12	4	60737382	60737562	180	0	-10.80	3′UTR	Hypo

expressed mRNA levels. Among these genes, there were 4 genes with m6A hypomethylation and downregulated mRNA expression, 51 genes with m6A hypermethylation and downregulated mRNA expression, 26 genes with m6A hypermethylation and upregulated mRNA expression and 9 genes with m6A hypomethylation and upregulated mRNA expression. The specific information on these genes is shown in **Supplementary Table 5**.

Subsequently, we confirmed the correlation between m6A modification and mRNA levels. The results in **Figure 6C** show that differential m6A-methylated transcripts do have different mRNA expression levels; that is, the mRNA expression level of hypomethylated transcripts is often higher than the mRNA expression level of hypermethylated transcripts. Based on interactions with combined scores ≥0.4, the PPI network analysis constructed interaction networks for these differential genes, as shown in **Figure 6D**.

The results of GO analysis showed that 670 GO terms were significantly enriched in biological processes (**Figure 6E**), 85 GO terms were significantly enriched in cellular components (**Figure 6F**), and 148 GO terms were significantly enriched in molecular functions (**Figure 6G**), particularly in lipid biosynthetic process, endoplasmic reticulum correlation, structural constituent of cytoskeleton, and more. Similarly, in **Figure 6H**, the results of KEGG analysis found that 29 pathways were significantly enriched, particularly steroid hormone biosynthesis, chemical carcinogenesis, gap junction, and more. The specific information of GO and KEGG pathway enrichment analyses is presented in **Supplementary Table 6**.

Levels of m6A Methylation and Methylase Expression in LF

To further explore the changes in m6A methylation in LF, we performed an m6A dot blot analysis. The results showed that compared with the control group, the m6A methylation abundance of the model group was significantly decreased (**Figures 7A,B**). Subsequently, considering that the difference in m6A levels in LF was probably caused by m6A regulatory enzymes, we focused on the methyltransferase WTAP, demethylase ALKBH5 and m6A binding protein YTHDF1. IGV visualization analysis was used to show the sequencing results intuitively. At the m6A methylation level, we found that the m6A levels of WTAP and ALKBH5 increased, while the YTHDF1 level decreased in LF (**Figures 7C–E**).

Likewise, at the mRNA level, we found that the expression of WTAP, ALKBH5 and YTHDF1 was reduced (**Figures 7F–H**) by IGV

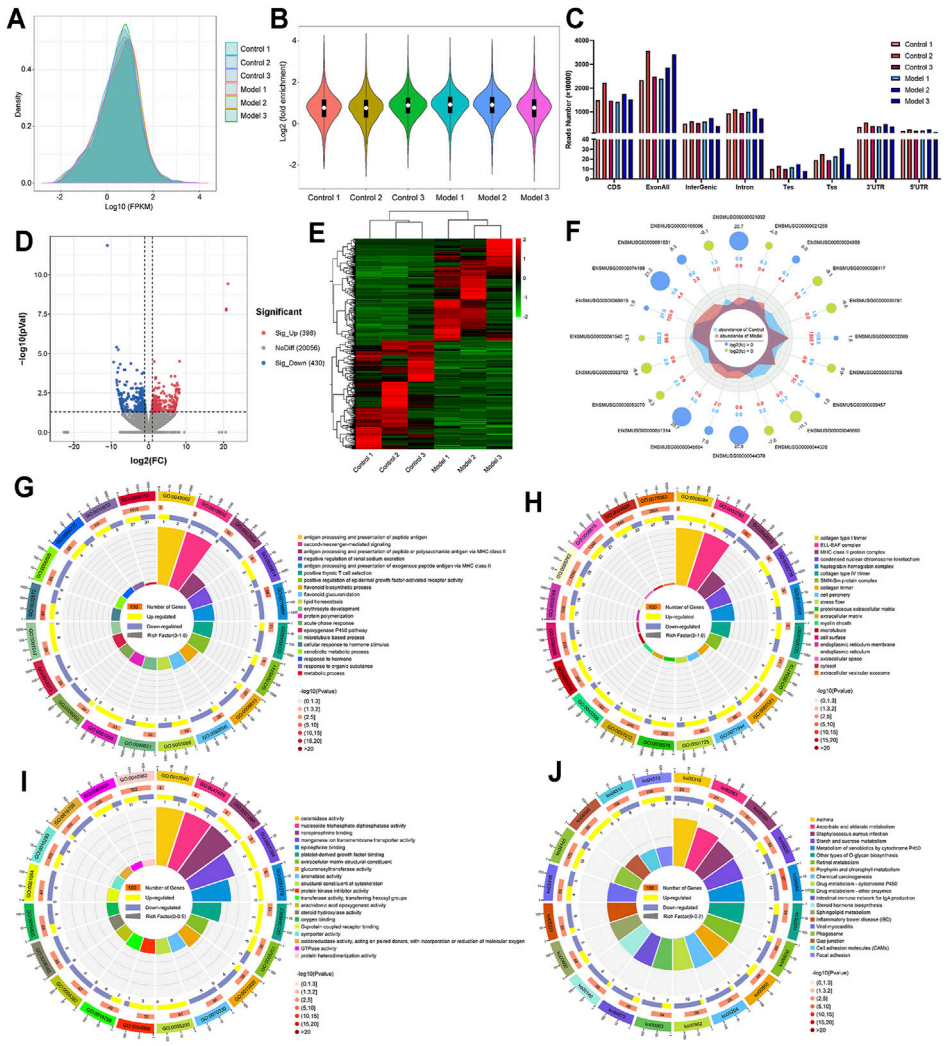


FIGURE 5 | The overall expression of mRNA and the description of differentially expressed mRNAs. **(A)** Metagene plots reveal the distribution intensity and abundance of mRNA expression after sequence alignment. **(B)** Violin plot of the relative abundance of mRNA expression in each sample. **(C)** Regional distribution of mRNA. **(D)** Volcano plot representation of microarray data on the differentially expressed mRNA genes. **(E)** Hierarchical cluster analysis of differentially expressed mRNA genes. **(F)** The radar map shows the top 10 upregulated genes and top 10 downregulated genes. **(G)** GO biological processes enrichment analysis. **(H)** GO cellular component enrichment analysis. **(I)** GO molecular function enrichment analysis. **(J)** KEGG enrichment analysis.

visualization analysis. Then, an RT-qPCR assay was utilized to examine the expression of the above genes. The results showed that the expression levels of WTAP, ALKBH5 and YTHDF1 in the model group were significantly lower than those in the control group, which was consistent with the IGV results (**Figures 7I–K**). Moreover, we also verified the protein expression levels of WTAP, ALKBH5 and YTHDF1 by Western blot and found that the protein levels of the three genes also decreased significantly in the model group (**Figure 7L–Q**).

Effects of Methyltransferase WTAP on Proliferation, Cell Cycle and Activation Markers of HSCs

As shown in **Figure 8A**, we analyzed the expression of WTAP in human LF samples through the GEO database (GSE33650) and found that the expression level of WTAP in high-fibrosis samples was significantly lower than the expression level of WTAP in low-fibrosis samples, which was consistent with our present experimental results. Furthermore, we designed and synthesized small interfering RNA targeting WTAP. As shown in **Figures 8B–D**, we screened the small interfering RNA sequences, durations and concentrations of WTAP small interfering RNA using RT-qPCR and found that the optimal interference sequence was si-WTAP-1, the optimum time of siRNA treatment for interference was 48 h, and the optimum concentration of siRNA for interference was 100 pmol. Follow-up experiments were carried out according to the above conditions.

As shown in **Figure 8E**, the CCK-8 assay results showed that compared with the control group, the proliferation of HSCs in the model group increased, while the proliferation of HSCs further increased after interfering with the expression of WTAP. Then,

TABLE 2 | the top 10 up-regulated genes and top 10 down-regulated genes.

Gene	ID	Description	Chromosome	Start	End	Sizes	*p* Value	Log_2FC	Up/ Down
Krtdap	ENSMUSG00000074199	keratinocyte differentiation associated protein	7	30487321	30490522	3,201	3.72E-10	21.21	Up
Slc15a5	ENSMUSG00000044378	solute carrier family 15, member 5	6	137960584	138056914	96330	1.45E-08	20.76	Up
Ffar2	ENSMUSG00000051314	free fatty acid receptor 2	7	30517773	30523200	5,427	1.74E-08	20.74	Up
Ngb	ENSMUSG00000021032	neuroglobin	12	87144305	87149313	5,008	1.74E-08	20.74	Up
Gm4707	ENSMUSG00000091831	predicted gene 4,707	17	71765298	71766913	1,615	3.13E-05	8.26	Up
Apoa4	ENSMUSG00000032080	apolipoprotein A-IV	9	4,6151994	46154757	2,763	3.22E-05	1.48	Up
Cdc42ep2	ENSMUSG00000045664	CDC42 effector protein (Rho GTPase binding) 2	19	5965664	5974844	9,180	0.000279,435	7.03	Up
Efemp2	ENSMUSG00000024909	epidermal growth factor-containing fibulin-like extracellular matrix protein 2	19	5523982	5532545	8,563	0.000280,346	5.99	Up
Hba-a1	ENSMUSG00000069919	hemoglobin alpha, adult chain 1	11	32233511	32234465	954	0.000320,964	1.90	Up
Ppl	ENSMUSG00000039457	periplakin	16	4904155	4950285	46130	0.000358,356	1.85	Up
Cyp2b9	ENSMUSG00000040660	cytochrome P450, family 2, subfamily b, polypeptide 9	7	25872836	25910086	37250	1.39416E-12	-11.05	Down
Slc5a2	ENSMUSG00000030781	solute carrier family 5 (sodium/ glucose cotransporter), member 2	7	127864829	127871602	6,773	3.95079E-06	-8.58	Down
Gbp10	ENSMUSG00000105096	guanylate-binding protein 10	5	105363565	105387399	23834	5.67824E-06	-8.14	Down
Nebl	ENSMUSG00000053702	nebulette	2	17348720	17736275	387,555	3.48814E-05	-9.35	Down
Cyp46a1	ENSMUSG00000021259	cytochrome P450, family 46, subfamily a, polypeptide 1	12	108300640	108328493	27853	4.29999E-05	-4.78	Down
Trp53i13	ENSMUSG00000044328	transformation related protein 53 inducible protein 13	11	77398925	77406806	7,881	4.80688E-05	-7.60	Down
Zap70	ENSMUSG00000026117	zeta-chain (TCR) associated protein kinase	1	36800879	3,6821899	21020	8.02432E-05	-8.09	Down
Nrxn2	ENSMUSG00000033768	neurexin II	19	6468761	6594199	125,438	0.000108,292	-6.52	Down
Cfap300	ENSMUSG00000053070	cilia and flagella associated protein 300	9	8021673	8042824	21151	0.000109,326	-6.33	Down

flow cytometry was used to detect differences in the HSC cell cycle under WTAP interference (**Figures 8F,G**). The results showed that the number of HSCs in the G0/G1 phase in the model group was significantly lower than that in the control group, while the number of HSCs in S phase and G2/M phase increased significantly. Compared with the model group, the number of HSCs in G0/G1 phase in the si-WTAP group further decreased, while the number of HSCs in the S phase and G2/M phase further increased. Interfering with WTAP promotes the proliferation of HSCs by inducing S phase and G2/M phase arrest.

Moreover, we also detected the expression of the HSC activation markers α-SMA and collagen Ⅰ. As shown in **Figure 8H**-8M, the mRNA and protein expression levels of α-SMA and collagen Ⅰ were significantly increased in the model group, while the mRNA and protein expression levels of α-SMA and collagen I were further increased after WTAP interference compared with expression in the model group, which also indicated that WTAP interference significantly promoted the activation of HSCs.

DISCUSSION

Modifications through m6A methylation modification, as a kind of RNA modification that exists widely in liver disease, has naturally received extensive attention (Wu et al., 2020; Pan et al., 2021). With regard to the effect of m6A methylation on the biological function of liver cells, existing studies have focused on the regulatory mechanism of genes and pathways (Zhang C. et al., 2020; Cao et al., 2021). A study by Zhu Y. et al. (2020) found that METTL3-mediated m6A methylation could be regulated by ASIC1a, which in turn affects the processing of miR-350, thus inducing the activation of HSCs and promoting the occurrence and development of LF. Unlike their studies, our study compared the difference in m6A methylation between the control and LF liver tissue, and confirmed that the m6A modification level changed significantly in LF.

Herein, we first constructed m6A-seq and RNA-seq libraries and investigated the changes in m6A methylation and the expression levels of genes in the liver of mice with hepatic fibrosis by methylated RNA immunoprecipitation combined with next-generation sequencing, and the results were analyzed by bioinformatics. We found 6,221 m6A modification genes in the control group and 6,982 m6A modification genes in the model group. Further analysis identified 3,315 different m6A methylation genes, of which 2,498 m6A hypermethylated genes and 817 m6A hypomethylated genes were identified, suggesting that there are some differences in the occurrence and development of m6A methylation in LF. Interestingly,

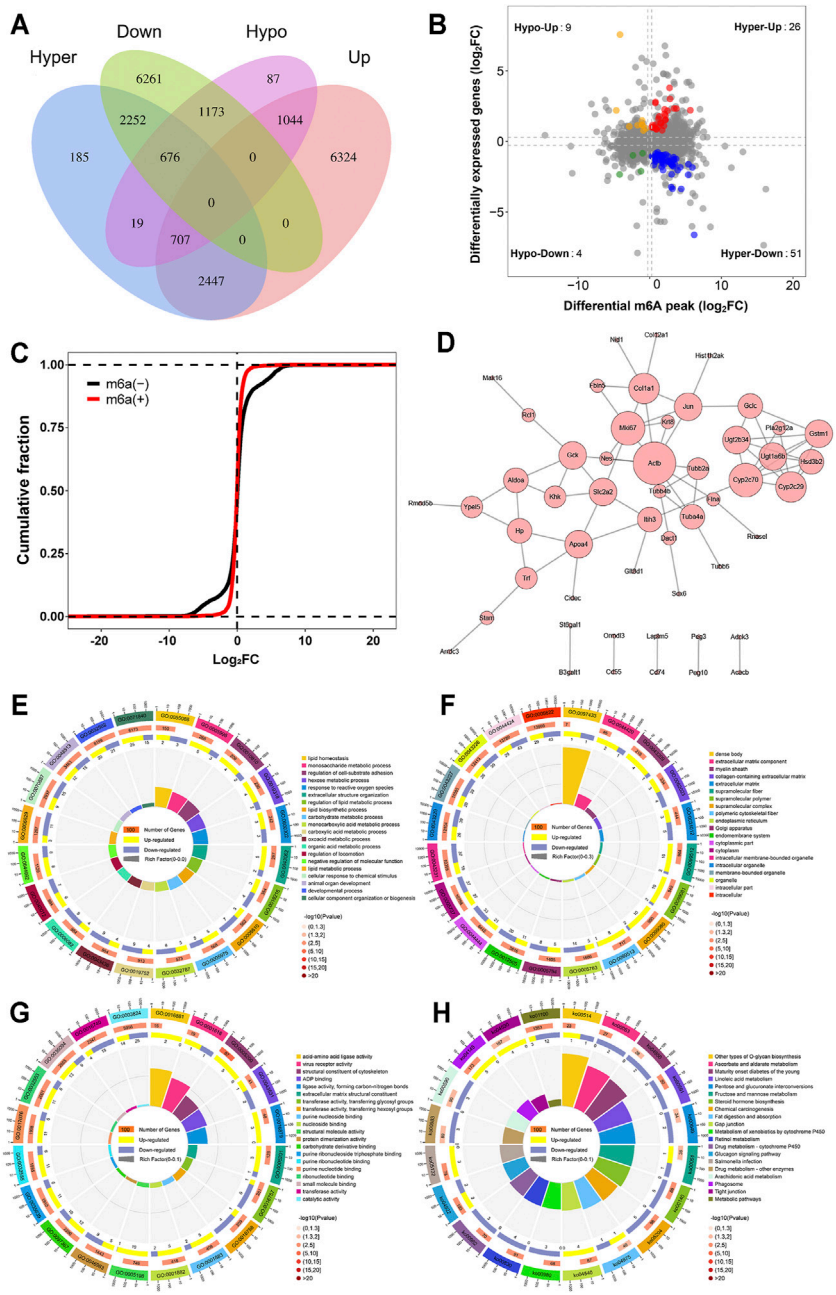


FIGURE 6 | Joint analysis of m6A methylation and mRNA expression. **(A)** Venn diagram of peaks with m6A methylation and mRNA. **(B)** Four quadrant graph of genes with differential m6A methylation and differentially expressed mRNA levels. **(C)** Cumulative frequency plot showing that there was a correlation between differential m6A methylation genes and mRNA levels. **(D)** PPI of genes with differentially expressed m6A methylation and differentially expressed mRNA. **(E)** GO biological processes enrichment analysis. **(F)** GO cellular component enrichment analysis. **(G)** GO molecular function enrichment analysis. **(H)** KEGG enrichment analysis.

although the m6A methylation of the gene was different, the distribution of m6A methylation in the control livers was similar to that in the model livers. We found that m6A methylation of most genes was distributed in CDS, 3′UTR and stop codon regions, accounting for 90% of the total. This is consistent with the report of Dominissini et al. (2012), who found that m6A methylation sites are mainly concentrated in long exons, stop codons and 3′UTR regions, and this distribution pattern is highly conserved between humans and mice. This distribution pattern may be related to the function of m6A methylation modification. Dynamic m6A modification in different regions affects biological functions such as splicing, output, stability and translation of mRNA (Wang et al., 2014; Wang and He, 2014; Maity and Das, 2016). Therefore, m6A modification may play an important role in regulating the expression of genes related to hepatic fibrosis.

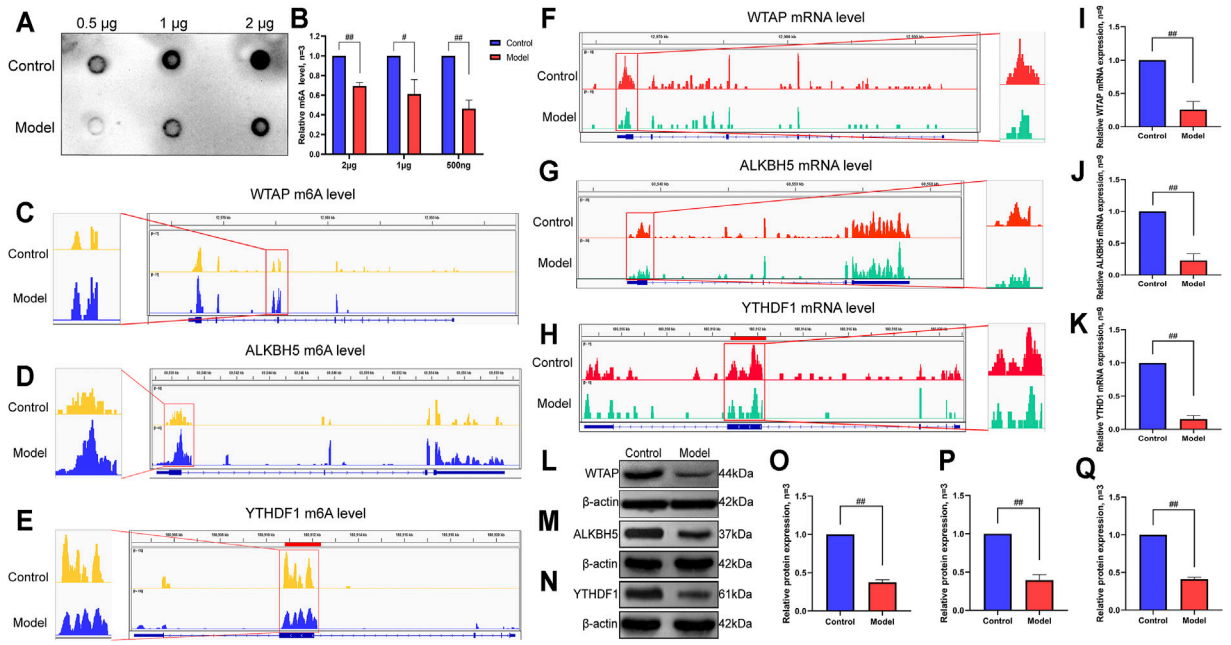


FIGURE 7 | Verification of m6A methylation level and methylase expression in LF. **(A)** The m6A methylation level in LF. **(B)** Semiquantitative analysis of m6A methylation. **(C)** IGV plots of the WTAP m6A level. **(D)** IGV plots of the ALKBH5 m6A level. **(E)** IGV plots of the YTHDF1 m6A level. **(F)** IGV plots of the WTAP expression level. **(G)** IGV plots of the ALKBH5 expression level. **(H)** IGV plots of the YTHDF1 expression level. **(I)** mRNA expression level of WTAP. **(J)** mRNA expression level of ALKBH5. **(K)** mRNA expression level of YTHDF1. **(L)** Protein expression levels of WTAP. **(M)** Protein expression levels of ALKBH5. **(N)** Protein expression levels of YTHDF1. **(O)** Semiquantitative analysis of WTAP protein. **(P)** Semiquantitative analysis of YTHDF1 protein. **(Q)** Semiquantitative analysis of ALKBH5 protein. $^{\#\#}p < 0.01$ compared with the control group, $^{\#}p < 0.05$ compared with the control group.

The m6A methylation site exists mainly in the RRACH motif, which is caused by the binding of m6A methyltransferase with the corresponding consensus sequence (Liu et al., 2018; Zhang Z. et al., 2019). The RNA binding motifs of METTL3, METTL14 and WTAP have been confirmed to be GGAC, GGAC and GACU, which are highly conserved between humans and animals (Liu et al., 2014). When the RRACH sequence is mutated, the single nucleotide polymorphism of the corresponding site changes, which affects m6A methylation. Kane et al. (Kane and Beemon, 1987) found that the mutation from GAC to GAU in the consensus sequence leads to the reversal of m6A methylation in Rous sarcoma virus mRNA transcripts. In the current study, we found many similar m6A consensus motifs in the control and LF tissues, but there were also some differences in the sequences, which further confirmed the emergence of specific m6A methylation sites in the process of LF. However, the RRACH consensus sequence is critical for m6A methylation, but not all RRACH sites in the body will have m6A modification (Gilbert et al., 2016), which corresponds to our results; that is, there are unmutated sequence sites, showing that m6A methylation modification is also regulated by other molecular mechanisms and needs further study.

To better understand the functions of these differentially expressed m6A methylated genes, GO and KEGG distribution analyses were conducted. We found that differential m6A genes were primarily involved in biological processes associated with the endoplasmic reticulum stress response, such as the unfolded protein response and the protein catabolic process, and were also related to the development and regeneration of liver organs. In addition, they were closely related to the PPAR signaling pathway, TGF-β signaling pathway and PI3K-Akt signaling pathway. Endoplasmic reticulum stress refers to the state of protein folding damage caused by the destruction of endoplasmic reticulum homeostasis, and some studies have confirmed that endoplasmic reticulum stress plays a role in the occurrence and development of various liver diseases (Huang et al., 2019; Wu et al., 2021). Virginia et al. (Hernández-Gea et al., 2013) found that oxidative stress disrupts endoplasmic reticulum homeostasis in stellate cells and causes the endoplasmic reticulum to enter a stressed state. To reduce the stress response, hepatic stellate cells initiate an unfolded protein response by limiting the accumulation of unfolded proteins during transient stress, which promotes cell activation and accelerates the development of LF. Peroxisome proliferation-activated receptor (PPAR) belongs to the nuclear hormone receptor family and plays an important role in many biological processes, such as adipogenesis (Lefterova et al., 2014), cell differentiation (Kim et al., 2019), cell growth regulation (Zhang X. et al., 2019) and inflammation (Bougarne et al., 2018). Previous studies have found that the activation of the PPAR pathway can delay the progression of hepatic fibrosis, and its activation can inhibit the transformation of HSCs from a resting state to an activated state (Guo et al., 2005; Anty and Lemoine, 2011). Liu and others have further found that the

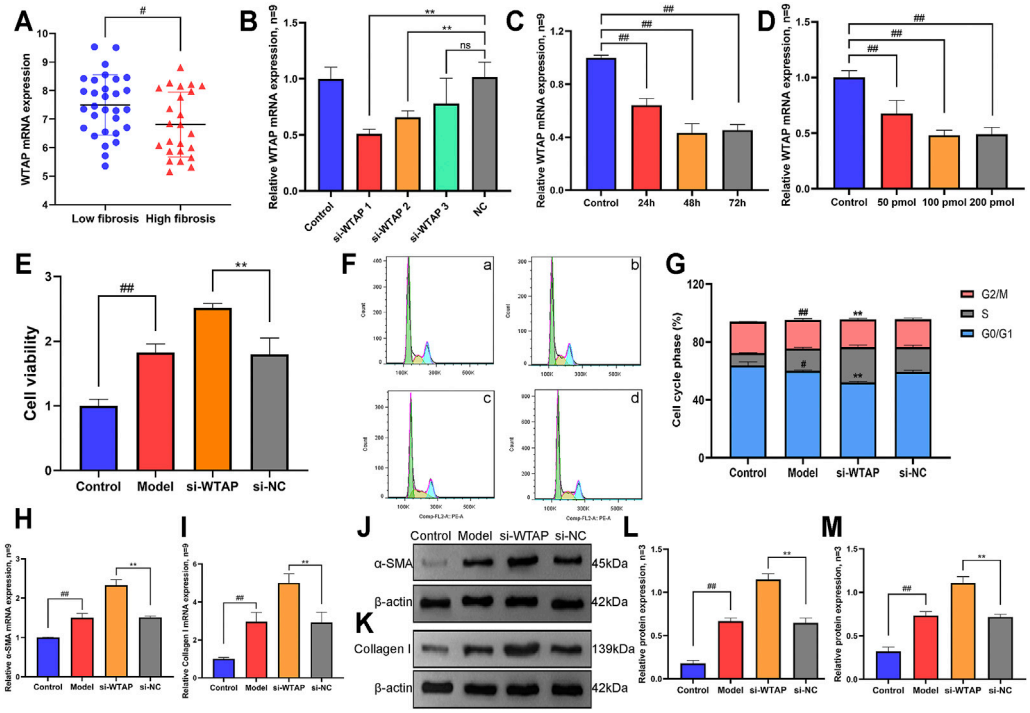


FIGURE 8 | Effects of methyltransferase WTAP on proliferation, cell cycle and activation markers of HSCs. **(A)** Expression levels of WTAP in low-fibrosis and high-fibrosis samples derived from the GEO database. **(B)** Small interfering RNA of WTAP was screened by RT-qPCR assay. **(C)** Optimal stimulation time of WTAP small interfering RNA was screened by RT-qPCR assay. **(D)** Optimal stimulation concentration of WTAP small interference RNA was screened by RT-qPCR assay. **(E)** Cell proliferation was detected by CCK8 assay. **(F)** The phase of the cell cycle was detected by flow cytometry. a, control group. b, model group. c, si-WTAP group. d, si-NC group. **(G)** Quantification of the cell cycle results. **(H)** mRNA expression level of α-SMA. **(I)** The mRNA expression level of collagen I. **(J)** Protein expression levels of α-SMA. **(K)** Protein expression levels of collagen I. **(L)** Semiquantitative analysis of α-SMA protein. **(M)** Semiquantitative analysis of collagen I protein.

activation of PPAR-γ can reduce the expression of α-SMA and collagen I in HSCs (Yang et al., 2006). Both the TGF-β and PI3K-Akt signaling pathways are one of the classical signaling pathways involved in the progression of LF. Abnormalities in TGF-β can stimulate HSCs to secrete excessive ECM, and the activity of the PI3K-Akt signaling pathway is significantly correlated with collagen production, HSC proliferation and apoptosis (Shah et al., 2013; Wu et al., 2017). Interestingly, the fibrogenic effects of TGF-β and PI3K-Akt are synergistic to some extent. Runyan et al. (2004) found that TGF-β can not only induce the activation of PI3K/Akt, but also enhance the transcriptional activity of Smad3, the target downstream of TGF-β signaling, thus enhancing the expression of collagen I.

By combining analyses of m6A-seq and RNA-seq data, we discovered 90 genes with differences in their m6A methylation peaks and synchronously differential mRNA expression in LF. The expression of these genes may be regulated by m6A modification of mRNAs. Among the genes with the highest differences, many have been identified to be closely related to the occurrence and development of LF, such as ApoA4 (apolipoprotein A4). Wang Y. et al. (2021) found that ApoA4 may reduce LF and liver injury by inhibiting LF mediators and inflammatory cytokines and suppressing proinflammatory hepatic M1 cell invasion. Although some genes have not been proven to be related to LF, they are involved in fibrosis in other tissues. For example, Ninj1 has been shown to promote the activation of macrophages by enhancing the interaction with epithelial cells, thus enhancing the inflammatory response of macrophages to participate in the occurrence and development of pulmonary fibrosis (Choi et al., 2018). These genes regulated by m6A modification may play key roles in the occurrence and development of LF and may also become an important target for the treatment of LF. However, the specific molecular mechanism of the effect of m6A methylation of these genes on LF is still unclear and needs further exploration and research in the future.

The most prominent finding in our data is that there is a significant difference in m6A modification between the LF and control tissues. The dot blot results also confirmed this significant difference, and we found that the overall level of m6A methylation in LF decreased significantly, which suggested that the modification of the m6A genes affected the progression of LF. A possible explanation for the global change in this m6A modification pattern may be the unique expression of the key m6A regulator or its own methylation modification. Considering that methylases play very important roles in regulating m6A methylation of liver fibrosis, we selected WTAP, ALKBH5 and YTHDF1 as the representative of methyltransferase, demethylase and m6A binding protein for further study, which verify the differences in mRNA and protein expression levels. Interestingly, not only did the expression of WTAP and YTHDF1 decrease in

LF, but the expression of the demethylase ALKBH5 also decreased significantly. Combined with the decrease in the overall level of m6A modification in LF, we speculated that the m6A level in the body involves the regulation of a variety of methylases, and the change in one or several methylation enzymes alone cannot be used as a decisive factor in determining the level of m6A methylation. The decrease in the m6A level in LF was because the overall degree of demethylation was greater than the decrease in the m6A level of methylation.

As an important component of the m6A methyltransferase complex, WTAP, unlike METTL3 and METTL14, does not have N6-methyladenine methyltransferase activity but is necessary for effective RNA methylation *in vivo* and for the localization of METTL3 and METTL14 in nuclear spots (Śledź and Jinek, 2016). WTAP has been proven to participate in some basic physiological processes, such as mRNA stability (Horiuchi et al., 2006), organ development (Anderson et al., 2014), cell proliferation, apoptosis and cell cycle regulation (Horiuchi et al., 2013). A recent study by Zhu B. et al. (2020) demonstrated that in a rat model of balloon injury-induced hyperplasia of vascular smooth muscle cells (VSMCs), the expression of WTAP decreased significantly. The suggested mechanism is that WTAP regulates p16INK4a through m6A modification and thus causing abnormal proliferation of VSMCs. Nevertheless, contrary to the above findings that WTAP can inhibit cell proliferation, some other studies have shown different results. A study by Chen et al. (2020) confirmed that WTAP could regulate the stability of HMBOX1 mRNA in an m6A methylation-dependent manner, thereby promoting the proliferation and metastasis of osteosarcoma cells. These studies confirmed that as a pivotal enzyme of m6A modification, WTAP can regulate the m6A methylation level in the body, thus fulfilling functionally different roles in different diseases.

Interestingly, in the present study, we found through sequencing that the m6A level of WTAP was significantly upregulated in LF mice, while the expression of mRNA was reduced. Further verification experiments showed that the mRNA and protein expression levels of WTAP decreased significantly, consistent with the sequencing results. Subsequently, we focused on the effect of WTAP interference on HSCs in LF and found that interfering with WTAP promoted the proliferation of HSCs and increased the expression of α-SMA, a marker of HSC activation and collagen I, the main component of extracellular matrix, which indicated that interfering with WTAP could promote the occurrence and development of LF. Therefore, based on the findings of the above study, we speculated that the possible mechanism of WTAP involved in the development of LF was that WTAP acted as a methyltransferase to affect the m6A level on downstream target genes related to cell proliferation and the cell cycle, thus regulating the mRNA expression levels of these genes and ultimately affecting the occurrence and development of LF. These findings may provide new thoughts and insights for other research on WTAP and m6A methylation in LF.

In summary, our findings established a m6A transcriptome map of LF mice, provided a comprehensive investigation of the potential relationship between m6A methylation and mRNA expression in LF, and revealed the key enzymes of m6A modification, especially WTAP, involved in the occurrence and development of LF.

DATA AVAILABILITY STATEMENT

The datasets presented in this study can be found in online repositories. The names of the repository/repositories and accession number(s) can be found below: BioProject: PRJNA761579, SRA accession: SRP336482.

ETHICS STATEMENT

The animal study was reviewed and approved by the Animal Ethics Committee of Anhui University of Chinese Medicine.

AUTHOR CONTRIBUTIONS

HJ made substantial contributions to the conception and design of the study. CF, YM, SC, and QZ performed the experiments. CF, HJ, JZ, and FW contributed to data acquisition, data analysis and interpretation. HJ revised the manuscript critically for important intellectual content. HJ, JZ and FW confirm the authenticity of all the raw data. All authors agreed to be accountable for all aspects of the work in ensuring that questions related to the accuracy or integrity of the work are appropriately investigated and resolved. All authors read and approved the final manuscript.

FUNDING

National Natural Science Foundation of China (grant no.81973648). National Natural Science Foundation of China (grant no. 82004139). Leading Talents Introduction and Cultivation Plan Project of Colleges in Anhui Province (gxfxZD2016118).

ACKNOWLEDGMENTS

We are grateful to Shanghai Bohao Biotechnology Corporation (Shanghai, China) for providing sequencing service. We thank AJE (www.aje.cn) for its linguistic assistance during the preparation of this manuscript.

SUPPLEMENTARY MATERIAL

The Supplementary Material for this article can be found online at: https://www.frontiersin.org/articles/10.3389/fcell.2021.767051/full#supplementary-material

REFERENCES

Anderson, A. M., Weasner, B. P., Weasner, B. M., and Kumar, J. P. (2014). The Drosophila Wilms′ Tumor 1-Associating Protein (WTAP) Homolog Is Required for Eye Development. *Develop. Biol.* 390 (2), 170–180. doi:10.1016/j.ydbio.2014.03.012

Anty, R., and Lemoine, M. (2011). Liver Fibrogenesis and Metabolic Factors. *Clin. Res. Hepatol. Gastroenterol.* 35 (Suppl. 1), S10–S20. doi:10.1016/s2210-7401(11)70003-1

Ashburner, M., Ball, C. A., Blake, J. A., Botstein, D., Butler, H., Cherry, J. M., et al. (2000). Gene Ontology: Tool for the Unification of Biology. *Nat. Genet.* 25 (1), 25–29. doi:10.1038/75556

Bataller, R., and Brenner, D. A. (2005). Liver Fibrosis. *J. Clin. Invest.* 115 (2), 209–218. doi:10.1172/jci24282

Berulava, T., Buchholz, E., Elerdashvili, V., Pena, T., Islam, M. R., Lbik, D., et al. (2020). Changes in m6A RNA Methylation Contribute to Heart Failure Progression by Modulating Translation. *Eur. J. Heart Fail.* 22 (1), 54–66. doi:10.1002/ejhf.1672

Bougarne, N., Weyers, B., Desmet, S. J., Deckers, J., Ray, D. W., Staels, B., et al. (2018). Molecular Actions of PPARα in Lipid Metabolism and Inflammation. *Endocr. Rev.* 39 (5), 760–802. doi:10.1210/er.2018-00064

Bushkin, G. G., Pincus, D., Morgan, J. T., Richardson, K., Lewis, C., Chan, S. H., et al. (2019). m6A Modification of a 3′ UTR Site Reduces RME1 mRNA Levels to Promote Meiosis. *Nat. Commun.* 10 (1), 3414. doi:10.1038/s41467-019-11232-7

Cao, X., Shu, Y., Chen, Y., Xu, Q., Guo, G., Wu, Z., et al. (2021). Mettl14-Mediated m6A Modification Facilitates Liver Regeneration by Maintaining Endoplasmic Reticulum Homeostasis. *Cell Mol. Gastroenterol. Hepatol.* 12 (2), 633–651. doi:10.1016/j.jcmgh.2021.04.001

Chen, S., Li, Y., Zhi, S., Ding, Z., Wang, W., Peng, Y., et al. (2020). WTAP Promotes Osteosarcoma Tumorigenesis by Repressing HMBOX1 Expression in an m6A-dependent Manner. *Cell Death Dis* 11 (8), 659. doi:10.1038/s41419-020-02847-6

Choi, S., Woo, J. K., Jang, Y.-S., Kang, J.-H., Hwang, J.-I., Seong, J. K., et al. (2018). Ninjurin1 Plays a Crucial Role in Pulmonary Fibrosis by Promoting Interaction between Macrophages and Alveolar Epithelial Cells. *Sci. Rep.* 8 (1), 17542. doi:10.1038/s41598-018-35997-x

Dominissini, D., Moshitch-Moshkovitz, S., Schwartz, S., Salmon-Divon, M., Ungar, L., Osenberg, S., et al. (2012). Topology of the Human and Mouse m6A RNA Methylomes Revealed by m6A-Seq. *Nature* 485 (7397), 201–206. doi:10.1038/nature11112

Du, Y., Hou, G., Zhang, H., Dou, J., He, J., Guo, Y., et al. (2018). SUMOylation of the m6A-RNA Methyltransferase METTL3 Modulates its Function. *Nucleic Acids Res.* 46 (10), 5195–5208. doi:10.1093/nar/gky156

Fan, C., Wu, F. R., Zhang, J. F., and Jiang, H. (2020). A Network Pharmacology Approach to Explore the Mechanisms of Shugan Jianpi Formula in Liver Fibrosis. *Evidence-Based Complement. Altern. Med.* 2020, 4780383. doi:10.1155/2020/4780383

Garsmeur, O., Droc, G., Antonise, R., Grimwood, J., Potier, B., Aitken, K., et al. (2018). A Mosaic Monoploid Reference Sequence for the Highly Complex Genome of Sugarcane. *Nat. Commun.* 9 (1), 2638. doi:10.1038/s41467-018-05051-5

Gilbert, W. V., Bell, T. A., and Schaening, C. (2016). Messenger RNA Modifications: Form, Distribution, and Function. *Science* 352 (6292), 1408–1412. doi:10.1126/science.aad8711

Gu, C., Wang, Z., Zhou, N., Li, G., Kou, Y., Luo, Y., et al. (2019). Mettl14 Inhibits Bladder TIC Self-Renewal and Bladder Tumorigenesis through N6-Methyladenosine of Notch1. *Mol. Cancer* 18 (1), 168. doi:10.1186/s12943-019-1084-1

Guo, Y.-T., Leng, X. S., Li, T., Peng, J. R., Song, S. H., Xiong, L. F., et al. (2005). Effect of Ligand of Peroxisome Proliferator-Activated Receptor γ on the Biological Characters of Hepatic Stellate Cells. *World J. Gastroenterol.* 11 (30), 4735–4739. doi:10.3748/wjg.v11.i30.4735

Heinz, S., Benner, C., Spann, N., Bertolino, E., Lin, Y. C., Laslo, P., et al. (2010). Simple Combinations of Lineage-Determining Transcription Factors Prime Cis-Regulatory Elements Required for Macrophage and B Cell Identities. *Mol. Cel* 38 (4), 576–589. doi:10.1016/j.molcel.2010.05.004

Hernández-Gea, V., Hilscher, M., Rozenfeld, R., Lim, M. P., Nieto, N., Werner, S., et al. (2013). Endoplasmic Reticulum Stress Induces Fibrogenic Activity in Hepatic Stellate Cells through Autophagy. *J. Hepatol.* 59 (1), 98–104. doi:10.1016/j.jhep.2013.02.016

Horiuchi, K., Umetani, M., Minami, T., Okayama, H., Takada, S., Yamamoto, M., et al. (2006). Wilms' Tumor 1-Associating Protein Regulates G2/M Transition through Stabilization of Cyclin A2 mRNA. *Proc. Natl. Acad. Sci.* 103 (46), 17278–17283. doi:10.1073/pnas.0608357103

Horiuchi, K., Kawamura, T., Iwanari, H., Ohashi, R., Naito, M., Kodama, T., et al. (2013). Identification of Wilms' Tumor 1-Associating Protein Complex and its Role in Alternative Splicing and the Cell Cycle. *J. Biol. Chem.* 288 (46), 33292–33302. doi:10.1074/jbc.M113.500397

Huang, H.-H., Lee, W.-J., Chen, S.-C., Chen, T.-F., Lee, S.-D., and Chen, C.-Y. (2019). Bile Acid and Fibroblast Growth Factor 19 Regulation in Obese Diabetics, and Non-Alcoholic Fatty Liver Disease after Sleeve Gastrectomy. *J. Clin. Med.* 8 (6), 815. doi:10.3390/jcm8060815

Jiang, X., Jiang, L., Shan, A., Su, Y., Cheng, Y., Song, D., et al. (2018). Targeting Hepatic miR-221/222 for Therapeutic Intervention of Nonalcoholic Steatohepatitis in Mice. *EBioMedicine* 37, 307–321. doi:10.1016/j.ebiom.2018.09.051

Kane, S. E., and Beemon, K. (1987). Inhibition of Methylation at Two Internal N6-Methyladenosine Sites Caused by GAC to GAU Mutations. *J. Biol. Chem.* 262 (7), 3422–3427. doi:10.1016/s0021-9258(18)61520-0

Kim, R. S., Hasegawa, D., Goossens, N., Tsuchida, T., Athwal, V., Sun, X., et al. (2016). The XBP1 Arm of the Unfolded Protein Response Induces Fibrogenic Activity in Hepatic Stellate Cells through Autophagy. *Sci. Rep.* 6, 39342. doi:10.1038/srep39342

Kim, Y.-H., Jang, W.-G., Oh, S.-H., Kim, J.-W., Lee, M. N., Song, J. H., et al. (2019). Fenofibrate Induces PPARα and BMP2 Expression to Stimulate Osteoblast Differentiation. *Biochem. Biophysical Res. Commun.* 520 (2), 459–465. doi:10.1016/j.bbrc.2019.10.048

Lefterova, M. I., Haakonsson, A. K., Lazar, M. A., and Mandrup, S. (2014). PPARγ and the Global Map of Adipogenesis and beyond. *Trends Endocrinol. Metab.* 25 (6), 293–302. doi:10.1016/j.tem.2014.04.001

Lin, Z., Niu, Y., Wan, A., Chen, D., Liang, H., Chen, X., et al. (2020). RNA M 6 A Methylation Regulates Sorafenib Resistance in Liver Cancer through FOXO 3-mediated Autophagy. *Embo j* 39 (12), e103181. doi:10.15252/embj.2019103181

Liu, J., Yue, Y., Han, D., Wang, X., Fu, Y., Zhang, L., et al. (2014). A METTL3-METTL14 Complex Mediates Mammalian Nuclear RNA N6-Adenosine Methylation. *Nat. Chem. Biol.* 10 (2), 93–95. doi:10.1038/nchembio.1432

Liu, N., Dai, Q., Zheng, G., He, C., Parisien, M., and Pan, T. (2015). N6-Methyladenosine-Dependent RNA Structural Switches Regulate RNA-Protein Interactions. *Nature* 518 (7540), 560–564. doi:10.1038/nature14234

Liu, B., Merriman, D. K., Choi, S. H., Schumacher, M. A., Plangger, R., Kreutz, C., et al. (2018). A Potentially Abundant Junctional RNA Motif Stabilized by m6A and Mg2+. *Nat. Commun.* 9 (1), 2761. doi:10.1038/s41467-018-05243-z

Liu, T., Wei, Q., Jin, J., Luo, Q., Liu, Y., Yang, Y., et al. (2020). The m6A Reader YTHDF1 Promotes Ovarian Cancer Progression via Augmenting EIF3C Translation. *Nucleic Acids Res.* 48 (7), 3816–3831. doi:10.1093/nar/gkaa048

Lu, J., Qian, J., Yin, S., Zhou, L., Zheng, S., and Zhang, W. (2020). Mechanisms of RNA N6-Methyladenosine in Hepatocellular Carcinoma: From the Perspectives of Etiology. *Front. Oncol.* 10, 1105. doi:10.3389/fonc.2020.01105

Ma, J. Z., Yang, F., Zhou, C. C., Liu, F., Yuan, J. H., Wang, F., et al. (2017). METTL14 Suppresses the Metastatic Potential of Hepatocellular Carcinoma by Modulating N 6 -Methyladenosine-Dependent Primary MicroRNA Processing. *Hepatology* 65 (2), 529–543. doi:10.1002/hep.28885

Maity, A., and Das, B. (2016). N6-Methyladenosine Modification inmRNA: Machinery, Function and Implications for Health and Diseases. *Febs j* 283 (9), 1607–1630. doi:10.1111/febs.13614

Mapperley, C., van de Lagemaat, L. N., Lawson, H., Tavosanis, A., Paris, J., Campos, J., et al. (2021). The mRNA m6A Reader YTHDF2 Suppresses Proinflammatory Pathways and Sustains Hematopoietic Stem Cell Function. *J. Exp. Med.* 218 (3), e20200829. doi:10.1084/jem.20200829

Meyer, K. D., and Jaffrey, S. R. (2014). The Dynamic Epitranscriptome: N6-Methyladenosine and Gene Expression Control. *Nat. Rev. Mol. Cel Biol* 15 (5), 313–326. doi:10.1038/nrm3785

Nishanth, G., Deckert, M., Wex, K., Massoumi, R., Schweitzer, K., Naumann, M., et al. (2013). CYLD Enhances Severe Listeriosis by Impairing IL-6/STAT3-

Dependent Fibrin Production. *Plos Pathog.* 9 (6), e1003455. doi:10.1371/journal.ppat.1003455

Ondo, K., Isono, M., Nakano, M., Hashiba, S., Fukami, T., and Nakajima, M. (2021). The N6-Methyladenosine Modification Posttranscriptionally Regulates Hepatic UGT2B7 Expression. *Biochem. Pharmacol.* 189, 114402. doi:10.1016/j.bcp.2020.114402

Pan, X.-Y., Huang, C., and Li, J. (2021). The Emerging Roles of m6A Modification in Liver Carcinogenesis. *Int. J. Biol. Sci.* 17 (1), 271–284. doi:10.7150/ijbs.50003

Robinson, J. T., Thorvaldsdóttir, H., Winckler, W., Guttman, M., Lander, E. S., Getz, G., et al. (2011). Integrative Genomics Viewer. *Nat. Biotechnol.* 29 (1), 24–26. doi:10.1038/nbt.1754

Runyan, C. E., Schnaper, H. W., and Poncelet, A.-C. (2004). The Phosphatidylinositol 3-Kinase/Akt Pathway Enhances Smad3-Stimulated Mesangial Cell Collagen I Expression in Response to Transforming Growth Factor-β1. *J. Biol. Chem.* 279 (4), 2632–2639. doi:10.1074/jbc.M310412200

Shah, R., Reyes-Gordillo, K., Arellanes-Robledo, J., Lechuga, C. G., Hernández-Nazara, Z., Cotty, A., et al. (2013). TGF-β1 Up-Regulates the Expression of PDGF-β Receptor mRNA and Induces a Delayed PI3K-, AKT-, and p70S6K-Dependent Proliferative Response in Activated Hepatic Stellate Cells. *Alcohol. Clin. Exp. Res.* 37 (11), 1838–1848. doi:10.1111/acer.12167

Śledź, P., and Jinek, M. (2016). Structural Insights into the Molecular Mechanism of the m6A Writer Complex. *Elife* 5, e18434. doi:10.7554/eLife.18434

Smith-Cortinez, N., van Eunen, K., Heegsma, J., Serna-Salas, S. A., Sydor, S., Bechmann, L. P., et al. (2020). Simultaneous Induction of Glycolysis and Oxidative Phosphorylation during Activation of Hepatic Stellate Cells Reveals Novel Mitochondrial Targets to Treat Liver Fibrosis. *Cells* 9 (11), 2456. doi:10.3390/cells9112456

Szklarczyk, D., Morris, J. H., Cook, H., Kuhn, M., Wyder, S., Simonovic, M., et al. (2017). The STRING Database in 2017: Quality-Controlled Protein-Protein Association Networks, Made Broadly Accessible. *Nucleic Acids Res.* 45 (D1), D362–d368. doi:10.1093/nar/gkw937

Vig, S., Talwar, P., Kaur, K., Srivastava, R., Srivastava, A. K., and Datta, M. (2015). Transcriptome Profiling Identifies P53 as a Key Player during Calreticulin Deficiency: Implications in Lipid Accumulation. *Cell Cycle* 14 (14), 2274–2284. doi:10.1080/15384101.2015.1046654

Wang, X., and He, C. (2014). Dynamic RNA Modifications in Posttranscriptional Regulation. *Mol. Cel* 56 (1), 5–12. doi:10.1016/j.molcel.2014.09.001

Wang, X., Lu, Z., Gomez, A., Hon, G. C., Yue, Y., Han, D., et al. (2014). N6-Methyladenosine-Dependent Regulation of Messenger RNA Stability. *Nature* 505 (7481), 117–120. doi:10.1038/nature12730

Wang, X., Zhao, B. S., Roundtree, I. A., Lu, Z., Han, D., Ma, H., et al. (2015). N6-Methyladenosine Modulates Messenger RNA Translation Efficiency. *Cell* 161 (6), 1388–1399. doi:10.1016/j.cell.2015.05.014

Wang, Q., Wei, S., Zhou, H., Li, L., Zhou, S., Shi, C., et al. (2020a). MicroRNA-98 Inhibits Hepatic Stellate Cell Activation and Attenuates Liver Fibrosis by Regulating HLF Expression. *Front. Cel Dev. Biol.* 8, 513. doi:10.3389/fcell.2020.00513

Wang, X., Liu, X., Liu, N., and Chen, H. (2020b). Prediction of Crucial Epigenetically-Associated, Differentially Expressed Genes by Integrated Bioinformatics Analysis and the Identification of S100A9 as a Novel Biomarker in Psoriasis. *Int. J. Mol. Med.* 45 (1), 93–102. doi:10.3892/ijmm.2019.4392

Wang, Y., Yang, Z., Wei, Y., Li, X., and Li, S. (2021a). Apolipoprotein A4 Regulates the Immune Response in Carbon Tetrachloride-Induced Chronic Liver Injury in Mice. *Int. Immunopharmacology* 90, 107222. doi:10.1016/j.intimp.2020.107222

Wang, Z., Gu, J., Yan, A., and Li, K. (2021b). Downregulation of Circ-RANBP9 in Laryngeal Cancer and its Clinical Significance. *Ann. Transl Med.* 9 (6), 484. doi:10.21037/atm-21-567

Wu, L., Zhang, Q., Mo, W., Feng, J., Li, S., Li, J., et al. (2017). Quercetin Prevents Hepatic Fibrosis by Inhibiting Hepatic Stellate Cell Activation and Reducing Autophagy via the TGF-β1/Smads and PI3K/Akt Pathways. *Sci. Rep.* 7 (1), 9289. doi:10.1038/s41598-017-09673-5

Wu, X., Zhang, X., Tao, L., Dai, X., and Chen, P. (2020). Prognostic Value of an m6A RNA Methylation Regulator-Based Signature in Patients with Hepatocellular Carcinoma. *Biomed. Res. Int.* 2020, 2053902. doi:10.1155/2020/2053902

Wu, S., Ye, S., Lin, X., Chen, Y., Zhang, Y., Jing, Z., et al. (2021). Small Hepatitis B Virus Surface Antigen Promotes Malignant Progression of Hepatocellular Carcinoma via Endoplasmic Reticulum Stress-Induced FGF19/JAK2/STAT3 Signaling. *Cancer Lett.* 499, 175–187. doi:10.1016/j.canlet.2020.11.032

Yang, L., Chan, C.-C., Kwon, O.-S., Liu, S., McGhee, J., Stimpson, S. A., et al. (2006). Regulation of Peroxisome Proliferator-Activated Receptor-γ in Liver Fibrosis. *Am. J. Physiology-Gastrointestinal Liver Physiol.* 291 (5), G902–G911. doi:10.1152/ajpgi.00124.2006

Yang, Y., Hsu, P. J., Chen, Y.-S., and Yang, Y.-G. (2018). Dynamic Transcriptomic m6A Decoration: Writers, Erasers, Readers and Functions in RNA Metabolism. *Cell Res* 28 (6), 616–624. doi:10.1038/s41422-018-0040-8

Yang, W., Tao, Y., Wu, Y., Zhao, X., Ye, W., Zhao, D., et al. (2019). Neutrophils Promote the Development of Reparative Macrophages Mediated by ROS to Orchestrate Liver Repair. *Nat. Commun.* 10 (1), 1076. doi:10.1038/s41467-019-09046-8

Zhang, W., Sargis, R. M., Volden, P. A., Carmean, C. M., Sun, X. J., and Brady, M. J. (2012). PCB 126 and Other Dioxin-like PCBs Specifically Suppress Hepatic PEPCK Expression via the Aryl Hydrocarbon Receptor. *PLoS One* 7 (5), e37103. doi:10.1371/journal.pone.0037103

Zhang, K., Han, X., Zhang, Z., Zheng, L., Hu, Z., Yao, Q., et al. (2017). The Liver-Enriched Lnc-LFAR1 Promotes Liver Fibrosis by Activating TGFβ and Notch Pathways. *Nat. Commun.* 8 (1), 144. doi:10.1038/s41467-017-00204-4

Zhang, X., Yao, J., Shi, H., Gao, B., and Zhang, L. (2019a). LncRNA TINCR/microRNA-107/CD36 Regulates Cell Proliferation and Apoptosis in Colorectal Cancer via PPAR Signaling Pathway Based on Bioinformatics Analysis. *Biol. Chem.* 400 (5), 663–675. doi:10.1515/hsz-2018-0236

Zhang, Z., Chen, L.-Q., Zhao, Y.-L., Yang, C.-G., Roundtree, I. A., Zhang, Z., et al. (2019b). Single-Base Mapping of M 6 A by an Antibody-Independent Method. *Sci. Adv.* 5 (7), eaax0250. doi:10.1126/sciadv.aax0250

Zhang, B., Wu, Q., Li, B., Wang, D., Wang, L., and Zhou, Y. L. (2020a). m6A Regulator-Mediated Methylation Modification Patterns and Tumor Microenvironment Infiltration Characterization in Gastric Cancer. *Mol. Cancer* 19 (1), 53. doi:10.1186/s12943-020-01170-0

Zhang, C., Huang, S., Zhuang, H., Ruan, S., Zhou, Z., Huang, K., et al. (2020b). YTHDF2 Promotes the Liver Cancer Stem Cell Phenotype and Cancer Metastasis by Regulating OCT4 Expression via m6A RNA Methylation. *Oncogene* 39 (23), 4507–4518. doi:10.1038/s41388-020-1303-7

Zhang, Z., Luo, K., Zou, Z., Qiu, M., Tian, J., Sieh, L., et al. (2020c). Genetic Analyses Support the Contribution of mRNA N6-Methyladenosine (m6A) Modification to Human Disease Heritability. *Nat. Genet.* 52 (9), 939–949. doi:10.1038/s41588-020-0644-z

Zhong, L., Liao, D., Zhang, M., Zeng, C., Li, X., Zhang, R., et al. (2019). YTHDF2 Suppresses Cell Proliferation and Growth via Destabilizing the EGFR mRNA in Hepatocellular Carcinoma. *Cancer Lett.* 442, 252–261. doi:10.1016/j.canlet.2018.11.006

Zhu, B., Gong, Y., Shen, L., Li, J., Han, J., Song, B., et al. (2020a). Total Panax Notoginseng Saponin Inhibits Vascular Smooth Muscle Cell Proliferation and Migration and Intimal Hyperplasia by Regulating WTAP/p16 Signals via m6A Modulation. *Biomed. Pharmacother.* 124, 109935. doi:10.1016/j.biopha.2020.109935

Zhu, Y., Pan, X., Du, N., Li, K., Hu, Y., Wang, L., et al. (2020b). ASIC1a Regulates miR-350/SPRY2 by N 6 -Methyladenosine to Promote Liver Fibrosis. *FASEB j.* 34 (11), 14371–14388. doi:10.1096/fj.202001337R

Conflict of Interest: The authors declare that the research was conducted in the absence of any commercial or financial relationships that could be construed as a potential conflict of interest.

Publisher's Note: All claims expressed in this article are solely those of the authors and do not necessarily represent those of their affiliated organizations, or those of the publisher, the editors and the reviewers. Any product that may be evaluated in this article, or claim that may be made by its manufacturer, is not guaranteed or endorsed by the publisher.

Copyright © 2021 Fan, Ma, Chen, Zhou, Jiang, Zhang and Wu. This is an open-access article distributed under the terms of the Creative Commons Attribution License (CC BY). The use, distribution or reproduction in other forums is permitted, provided the original author(s) and the copyright owner(s) are credited and that the original publication in this journal is cited, in accordance with accepted academic practice. No use, distribution or reproduction is permitted which does not comply with these terms.

frontiers in Cell and Developmental Biology

ORIGINAL RESEARCH
published: 22 November 2021
doi: 10.3389/fcell.2021.731365

LuHui Derivative, A Novel Compound That Inhibits the Fat Mass and Obesity-Associated (FTO), Alleviates the Inflammatory Response and Injury in Hyperlipidemia-Induced Cardiomyopathy

Ying Yu[1], Yumiao Pan[1], Ziyi Fan[1], Silun Xu[1], Zhiyuan Gao[1], Zijing Ren[1], Jie Yu[1], Wen Li[1], Fangtong Liu[1], Jintao Gu[1], Ye Yuan[1,2] and Zhimin Du[1,2,3]**

[1]Institute of Clinical Pharmacology, The Second Affiliated Hospital of Harbin Medical University (University Key Laboratory of Drug Research, Heilongjiang Province), Harbin, China, [2]Department of Clinical Pharmacology, College of Pharmacy, Harbin Medical University, Harbin, China, [3]State Key Laboratory of Quality Research in Chinese Medicines, Macau University of Science and Technology, Macau, China

OPEN ACCESS

Edited by:
Huilin Huang,
Sun Yat-sen University Cancer Center (SYSUCC), China

Reviewed by:
Huizhe Wu,
China Medical University, China
Chao Shen,
City of Hope National Medical Center, United States

***Correspondence:**
Ye Yuan
yuanye_hmu@126.com
Zhimin Du
dzm1956@126.com

Specialty section:
This article was submitted to Epigenomics and Epigenetics, a section of the journal Frontiers in Cell and Developmental Biology

Received: *27 June 2021*
Accepted: *25 October 2021*
Published: *22 November 2021*

Citation:
Yu Y, Pan Y, Fan Z, Xu S, Gao Z, Ren Z, Yu J, Li W, Liu F, Gu J, Yuan Y and Du Z (2021) LuHui Derivative, A Novel Compound That Inhibits the Fat Mass and Obesity-Associated (FTO), Alleviates the Inflammatory Response and Injury in Hyperlipidemia-Induced Cardiomyopathy. Front. Cell Dev. Biol. 9:731365. doi: 10.3389/fcell.2021.731365

Hyperlipidemia is a major risk factor for metabolic disorders and cardiovascular injury. The excessive deposition of saturated fatty acids in the heart leads to chronic cardiac inflammation, which in turn causes myocardial damage and systolic dysfunction. However, the effective suppression of cardiac inflammation has emerged as a new strategy to reduce the impact of hyperlipidemia on cardiovascular disease. In this study, we identified a novel monomer, known as LuHui Derivative (LHD), which reduced the serum levels of total cholesterol (TC), triglycerides (TG), low-density lipoprotein cholesterol (LDL-C), and reduced lipid deposition in cardiomyocytes. In addition, LHD treatment improved cardiac function, reduced hyperlipidemia-induced inflammatory infiltration in cardiomyocytes and suppressed the release of interleukin-6 (IL-6) and tumor necrosis factor-α (TNF-α). From a mechanistic perspective, cluster of differentiation 36 (CD36), an important cell surface receptor, was identified as a downstream target following the LHD treatment of palmitic acid-induced inflammation in cardiomyocytes. LHD specifically binds the pocket containing the regulatory sites of RNA methylation in the fat mass and obesity-associated (FTO) protein that is responsible for elevated intracellular m^6A levels. Moreover, the overexpression of the N6-methyladenosine (m^6A) demethylase FTO markedly increased CD36 expression and suppressed the anti-inflammatory effects of LHD. Conversely, loss-of-function of FTO inhibited palmitic acid-induced cardiac inflammation and altered CD36 expression by diminishing the stability of CD36 mRNA. Overall, our results provide evidence for the crucial role of LHD in fatty acid-induced cardiomyocyte inflammation and present a new strategy for the treatment of hyperlipidemia and its complications.

Keywords: hyperlipidemia, inflammation, LuHui derivative, FTO, CD36, m^6A

1 INTRODUCTION

Dyslipidemia causes damage to multiple tissues and organs and is a critical risk factor for atherosclerotic cardiovascular disease (Liu et al., 2017). Hyperlipidemia is characterized by the accumulation of total cholesterol (TC), triglycerides (TG), and low-density lipoprotein cholesterol (LDL-C). Increasingly, the evidence suggests that chronic systemic hyperlipidemia contributes to nonalcoholic fatty liver disease, diabetes, muscle and heart tissue damage, and the inflammatory response (Nicholls and Lundman, 2004; Ertunc and Hotamisligil, 2016; Healy et al., 2016; Ralston et al., 2017).

The heart is a non-adipose organ in which fatty acids mainly contribute to myocardial ATP production. The remaining ATP is provided by glucose and lactate, making the heart sensitive to lipotoxicity. Fatty acid metabolism disorders and lipid accumulation in cardiomyocytes result in the release of various cytokines, especially promoting the secretion of leukocyte adhesion molecules and chemokines, culminating in cardiomyocyte damaged and impaired diastolic and systolic functions (Schilling et al., 2012; Jia et al., 2016). Recent studies have examined the novel traditional Chinese medicines that may prevent the progression of hyperlipidemia (Bian et al., 2020; Chen et al., 2020; Su et al., 2020).

It has been recently reported that the dysregulation of m^6A methylation is associated with adipogenesis, the innate immune response, and many diseases (Liu et al., 2019; Wang L. et al., 2020). As the first regulatory factor of the m^6A modification, FTO was shown to exert a protective effect against alcohol-induced liver inflammation (Yu et al., 2020). FTO was also shown to play an essential role in the regulation of food intake and adipose synthesis (Hess et al., 2013; Ben-Haim et al., 2015). However, it has not been confirmed if FTO is a promising target for the treatment of hyperlipidemia-induced cardiomyocyte inflammation.

CD36 acts as a multifunctional membrane protein facilitating long-chain fatty acid uptake. It interacts with the membrane receptor Toll-like receptor 4 (TLR4), to co-regulate the oxidized low density lipoprotein (oxLDL)-induced inflammatory responses in the cardiac and skeletal muscle (Stewart et al., 2010; Sheedy et al., 2013). Owing to this functionality, CD36 has been confirmed as a promising candidate to alter the link between myocardial fatty acid utilization and the regulation of the inflammatory response, particularly in hyperlipidemia (Silverstein et al., 2010).

The aims of this study were to investigate the effect of a novel synthetic anthraquinone compound, LuHui Derivative (LHD, chemical name: 1,8-dihydroxy-3-(hydroxymethyl)-anthraquinone ethyl succinate), against hyperlipidemia-induced cardiomyocyte inflammation and to reveal the underlying molecular mechanisms of the modification of FTO and CD36. These results confirmed that LHD is a potential novel compound for the treatment of hyperlipidemia-induced cardiac inflammation.

2 MATERIALS AND METHODS

2.1 Chemicals and Reagents

The LHD monomer (purity > 95%) (**Figure 1A**), provided by the Department of Pharmaceutical and Chemical Research, Harbin Medical University, was dissolved in dimethyl sulfoxide (DMSO). Palmitic acid (PA) was purchased from Sigma (St. Louis, MO) and dissolved in 0.1 N sodium hydroxide and 15% bovine serum albumin (BSA), filtered, and then stored at -20°C. The high-fat diet (HFD) feed, consisting of 77.6% maintenance feed, 10% lard, 10% yolk powder, 2% cholesterol, 0.2% bile salt, and methylthiouracil 0.2%, were purchased from HuaFuKang Biotechnology (Beijing, China).

2.2 Animals

The animal procedures in this study were approved by the Animal Experimental Ethics Committee of Harbin Medical University. To avoid the complicating effects of estrogen on cardiovascular disease (Sabbatini and Kararigas, 2020; Meng et al., 2021), healthy male Wistar rats (180–220 g), purchased from the Experimental Animal Center of the Affiliated Second Hospital of Harbin Medical University (Harbin, China), were used in the study. The rats were maintained on a HFD for 4 weeks to establish hyperlipidemia, which was determined by analyzing the serum levels of TC, TG, LDL-C, and high-density lipoprotein cholesterol (HDL-C) in blood samples from orbital region of rats (**Supplementary Figure S1**). Following the method of previous studies (Su et al., 2020), the rats were divided into four groups: HFD, HFD with LHD 50 mg kg^{-1}, HFD with LHD 100 mg kg^{-1}, and HFD with atorvastatin 7.2 mg kg^{-1} (**Figure 1B**). In control (CTL) group, an equal volume of distilled water was administered. Heart tissue and serum samples were collected after 6 weeks of continuous daily intragastric administration for the corresponding follow-up experiments.

2.3 Cell Culture

Human cardiomyocyte AC16 cell line was kindly gifted by Prof. Ben-zhi Cai (Department of Pharmacy at The Second Affiliated Hospital) and grown in DMEM containing 10% fetal bovine serum (Biological Industries, Israel), 1% penicillin, and 1% streptomycin at 37°C in a humidified atmosphere containing 5% CO_2 (v v^{-1}). Cells were treated with LHD (25 μM) for 30 min and then added PA (500 μM) for 16 h to establish an *in vitro* model of inflammatory response induced by HFD.

2.4 Cell Transfection

For transfection, AC16 cells were grown to 60–70% confluence. We used Lipofectamine RNAiMAX Reagent (Thermo Fisher Scientific, CA, United States, 13778075) to transfect small interfering RNAs (siRNAs) and Lipofectamine 3,000 (Thermo Fisher Scientific, CA, United States, 3000015) to transfect plasmids for gene overexpression. The transfection was performed in accordance with the manufacturer's instructions (Han et al., 2021). Briefly, 2 μl targeting siRNA or negative control (NC) siRNA was mixed with 150 μl Opti-MEM (Thermo Fisher Scientific, CA, United States, 31985070) and 9 μl Lipofectamine RNAiMAX reagent was mixed with 150 μL Opti-MEM together at room temperature. For the overexpression analysis, the pHG-CMV-Kan2-FTO plasmid (Yingrun Biotechnology, Changsha, China, HG-HO080432) and pHG-CMV-Kan2-CD36 plasmid (Yingrun Biotechnology, Changsha, China, HG-HO000072) were diluted and transfected into AC16 cells. After 24 or 48 h

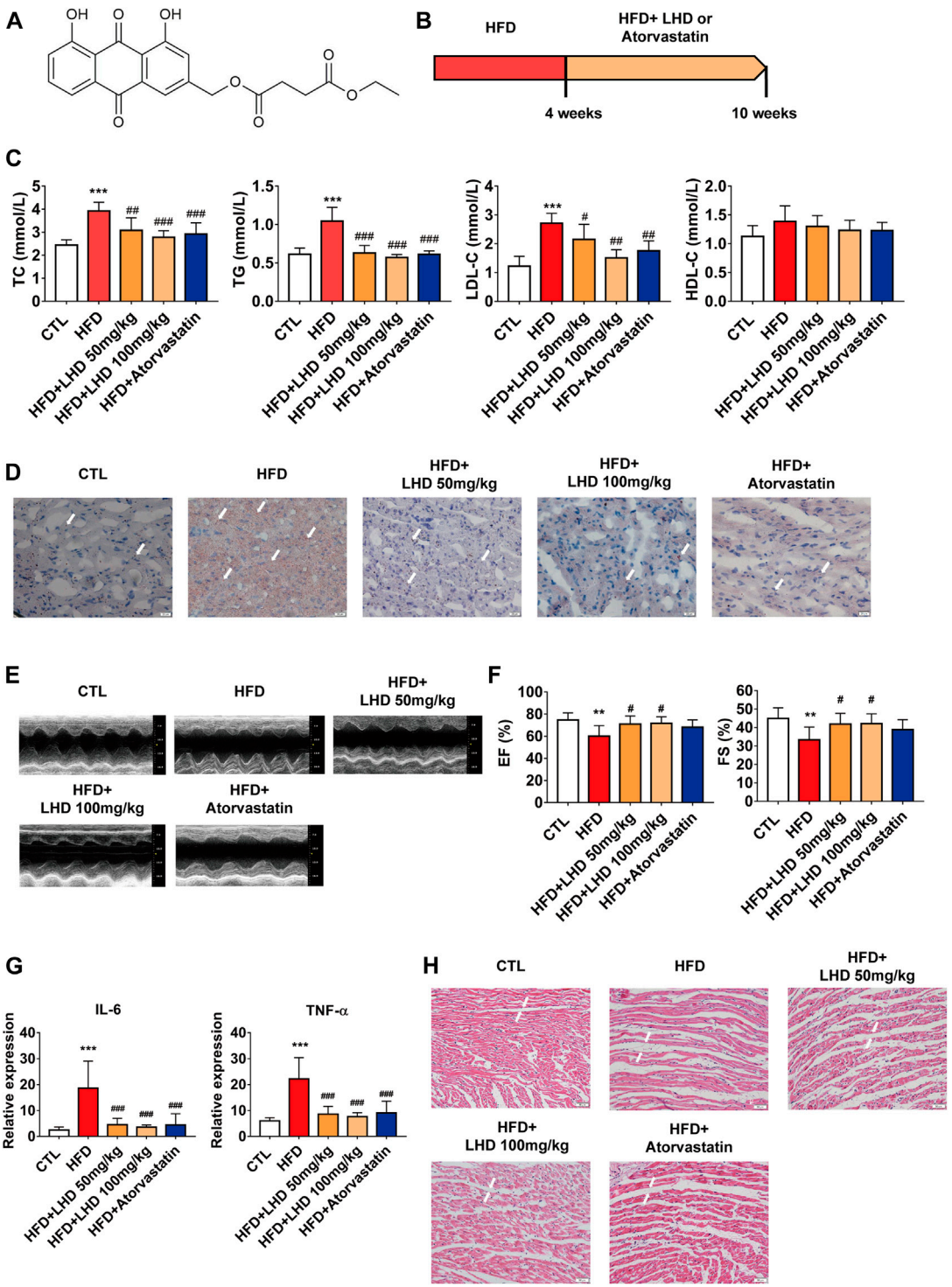


FIGURE 1 | LHD protects against hyperlipidemia-induced cardiac dysfunction. **(A)** Chemical structure of LHD. **(B)** Wistar rat feeding schedule. **(C)** Measurement of TC, TG, LDL-C, and HDL-C in the serum of rats fed a high-fat diet (HFD) for 10 weeks. $^{***}p < 0.001$, compared with the CTL group; $^{\#}p < 0.05$, $^{\#\#}p < 0.01$, $^{\#\#\#}p < 0.001$, compared with the HFD group, $n = 8$. **(D)** Oil Red O staining to identify lipid deposition in cardiac tissue (10× magnification). $n = 4$. **(E,F)** Echocardiographic analysis of left ventricular ejection fraction (EF%) and left ventricular shortening fraction (FS%) in rats fed with HFD for 10 weeks. $^{**}p < 0.01$, compared with the CTL group; $^{\#}p < 0.05$, compared with the HFD group, $n = 8$. **(G)** ELISA analysis of IL-6 and TNF-α in the serum. $^{***}p < 0.001$, compared with the CTL group; $^{\#\#\#}p < 0.001$, compared with the HFD group. $n = 8$. **(H)** H&E staining to identify infiltrative inflammation in cardiac tissue (10× magnification), $n = 4$.

of transfection, the cells were harvested for analysis. The siRNA sequences are shown in **Supplementary Table S1**.

2.5 Quantitative Real-Time Polymerase Chain Reaction (qRT-PCR)

Total RNA was isolated from the heart tissue and cells by using Trizol reagent (Invitrogen, Carlsbad, CA, United States); 0.5–1 μg of RNA was used to prepare cDNA using the Reverse Transcription Kit (Vazyme Biotech, Nanjing, China, R223-01) in accordance with the manufacturer's protocol. qRT-PCR was performed in a 10 μl volume with SYBR Green PCR Master Mix (Roche, Switzerland, RC-4913914001). The qRT-PCR analysis was performed on a LightCycler® 480 II (Roche, Switzerland) comprising initial denaturation, annealing, and extension steps. The real-time PCR conditions were: denaturation at 95°C for 10 s, followed by 40 cycles of 95°C for 10 s and 55°C for 30 s. The sequences of the specific primers used for qRT-PCR are shown in **Supplementary Table S2**.

2.6 Enzyme-Linked Immunosorbent Assay (ELISA)

Abdominal aortic blood was collected and centrifuged at 3,000 rpm for 15 min at 4°C to gather serum samples. To verify the protein expression of TNF-α and IL-6 in rat serum, the rat TNF-α ELISA kit (ABclonal, Wuhan, China, ab208348) and the rat IL-6 ELISA kit (ABclonal, Wuhan, China, ab100712), respectively, were used in accordance with the kit instructions. The supernatant was centrifuged at 1,000 rpm for 5 min prior to the analysis.

2.7 Cellular Thermal Shift Assay (CETSA)

The CETSA experiment was based on previously reported methods (Martinez Molina et al., 2013; Jafari et al., 2014). Briefly, after 100 μM LHD treatment for 3 h, the cells were collected in PBS and centrifuged at 300 g for 5 min, and the supernatant was discarded. Aliquots of the cells were transferred to separate Eppendorf tubes, subjected to a temperature gradient, and kept at room temperature for 3 min. After three freeze-thaw cycles, the supernatant was centrifuged and analyzed by sodium dodecyl sulfate-polyacrylamide gel electrophoresis (SDS-PAGE).

2.8 Drug Affinity Responsive Target Stability (DARTS) Assay

The DARTS assay was performed in accordance with a previously reported method (Lomenick et al., 2009; Pai et al., 2015). Briefly, we divided the cells into three groups: control (CTL), LHD, and input. First, we centrifuged the cells at 18,000 g for 10 min at 4°C in lysis solution. An appropriate volume of 10× TNC was added to the supernatant to detect the protein concentration using the bicinchoninic acid assay. Cell lysates were incubated with 83.4, 166.7, and 250.0 μM LHD at room temperature for 1 h before pronase digestion. Finally, the lysates were analyzed by western blotting to determine the binding between LHD and FTO.

2.9 Protein Extraction and Western Blotting

Western blotting analysis was performed as described in the previous report (Zhao et al., 2021). The cells were lysed in lysis buffer. After centrifugation, the supernatant was collected and the protein concentration was quantified by BCA assay kit. The samples were boiled at 95°C for 5 min and immediately frozen in a −80°C refrigerator. The primary antibodies were used as follows: anti-CD36 (ABclonal, Wuhan, China, A5792, 1: 1,000), anti-GAPDH (ABclonal, Wuhan, China, AC033, 1: 1,000), anti-FTO (ABclonal, Wuhan, China, A1438, 1:1,000), anti-P65-S536 (ABclonal, Wuhan, China, AP0475, 1:1,000), anti-IKB-α (Proteintech, Wuhan, China, 10268-1-AP, 1: 1,000), and anti-β-actin (ABclonal, Wuhan, China, AC026, 1: 1,000).

2.10 Echocardiography

The Wistar rats were anesthetized by intraperitoneal injection with avertin and the hair near the chest area was removed, as previously described (Cai et al., 2020). The cardiac function and heart dimensions were determined by two-dimensional echocardiography. Echocardiography was performed using a Vevo 1,100 VisualSonics device (VisualSonics, Toronto, ON, Canada). The left ventricular ejection fraction (EF%) and left fractional ventricular shortening (FS%) were calculated using M-mode images.

2.11 Histology

The heart tissue was fixed with 4% paraformaldehyde, embedded in paraffin, and sectioned into 5 μM coronal slides for further analysis. Hematoxylin eosin (H&E) staining (Solarbio, Beijing, China, g1260) was performed according to the method recommended by the manufacturer.

2.12 Oil Red O Staining

The tissues were fixed with paraformaldehyde and cryosectioned. The slides were first rinsed with PBS to wash off the embedding medium, and then soaked with 60% isopropyl alcohol. Staining with Oil Red O (Solarbio, Beijing, China, G1120) before washing with 60% isopropyl alcohol until the background was colorless. After counterstaining with hematoxylin, the slides were sealed with glycerol-gelatin.

2.13 Dot Blot

To determine the level of m^6A in cells, the dot blot assay were performed on total RNA or poly $(A)^+$ RNA, as described previously (Nagarajan et al., 2019). In brief, AC16 cells were treated with LHD (25 μM) for 16 h and transfected with FTO siRNA for 24 h before the dot blot assay. The RNA samples were diluted in RNase-free buffer, denatured at 95°C for 5 min, and immediately cooled, and then crosslinked by UV irradiation following stained with methylene blue (Solarbio, Beijing, China, G1300). After incubating with 5% skim milk, the membrane was detected with m^6A antibody (ABclonal, Wuhan, China, A19841, 1:1,000). Finally, the membrane was analyzed using an Odyssey (LICOR Biosciences, Lincoln, NE, United States).

2.14 Statistical Analysis

All data were expressed as mean ± standard deviation of mean unless otherwise noted. Data analysis was performed using GraphPad Prism 7.0 software. The significance of the differences was analyzed using Student's *t*-test or one-way analysis of variance ($^{*}p < 0.05$, $^{**}p < 0.01$, $^{***}p < 0.001$ compared with the CTL group, $^{\#}p < 0.05$, $^{\#\#}p < 0.01$, $^{\#\#\#}p < 0.001$ compared with the HFD or PA group). $p < 0.05$ was considered statistically significant.

3 RESULTS

3.1 LuHui Derivative Protects Against HFD-Induced Inflammation

To determine the role of LHD (**Figure 1A**) in hyperlipidemia and the associated cardiac function, we employed an HFD-induced rats model of hyperlipidemia. The *in vivo* experimental protocol is shown in **Figure 1B**. First, we analyzed the serum concentrations of TC, TG, LDL-C, and HDL-C in Wistar rats fed on a HFD for 4 weeks. Compared with the CTL group, the circulating concentrations of TC, TG, and LDL-C were higher in the HFD group (**Supplementary Figure S1**). After 6 weeks of continuous treatment with LHD, the serum levels of TC, TG, and LDL-C were significantly reduced, but there were no significant change in HDL-C levels. The same changes were observed in the atorvastatin treatment group (**Figure 1C**). Next, we performed Oil Red O staining to analyze lipid aggregation in the heart, and found that the administration with HFD for 10 weeks led to the accumulation of excess lipids in cardiomyocytes; however, treatment with LHD or atorvastatin significantly alleviated this accumulation (**Figure 1D**). Moreover, cardiac echocardiography showed that, compared with the CTL group, the administration of HFD clearly decreased the EF% and FS%; in contrast, LHD treatment significantly mitigated the hyperlipidemia-induced cardiac systolic and diastolic dysfunction (**Figures 1E,F**). These results indicated that LHD treatment altered the hyperlipidemia-associated changes in lipids and cardiac function *in vivo*.

Hyperlipidemia-induced dysfunction is usually accompanied by a spontaneous inflammatory response in cardiomyocytes (Wang Y. et al., 2017). Therefore, we performed an ELISA to detect the expression of pro-inflammatory cytokines. As shown in **Figure 1G**, hyperlipidemia resulted in higher serum concentrations of TNF-α and IL-6, but LHD and atorvastatin treatment significantly reduced the expression of inflammatory factors. Furthermore, H&E staining revealed that LHD and atorvastatin treatment reduced infiltrative inflammation in the heart of HFD-fed rats (**Figure 1H**). These results implied that LHD effectively reduced the inflammation associated with hyperlipidemia.

3.2 LuHui Derivative Protects Against Cardiomyocyte Inflammation *In Vitro*

Hyperlipidemia and other lipid metabolic diseases induce inflammation that are predominantly associated with saturated fatty acids. Of the various fatty acids, PA (16:0) plays an essential role in this process (Liu et al., 2017). To detect the anti-inflammatory effect of LHD *in vitro*, we stimulated AC16 cardiomyocytes with PA to mimic hyperlipidemia-induced inflammation. First, we observed the cell morphology after PA and LHD treatment. We found that, compared with the CTL group, PA treatment led to cardiomyocyte more rounded, but this was alleviated by PA treatment followed by LHD treatment (**Figure 2A**). Moreover, PA treatment stimulated the mRNA expression of the proinflammatory factors IL-6 and TNF-α, and LHD treatment significantly reduced this abnormal elevation (**Figure 2B**). However, LHD prevented the PA-induced phosphorylation and degradation of NF-κB P65 and IκB-α (**Figures 2C,D**).

Cardiomyocyte damage caused by hyperlipidemia disrupts the balance between metabolic enzymes and fatty acids (Son et al., 2018). To determine whether LHD rescued the hyperlipidemia-induced inflammatory phenotype by altering metabolism-related enzyme activity, we investigated the expression of oxidative phosphorylation-related enzymes and fatty acid metabolism enzymes in cardiomyocytes. The results showed that PA stimulation increased the expression of most metabolism-related enzymes; the most significant change occurred in CD36 expression and this increase was notably inhibited by LHD treatment (**Figures 2E,F**). Consistent with this, Western blot dected that CD36 expression was clearly suppressed in LHD-treated cells (**Figures 2G,H**). Collectively, these data indicate that CD36 may play an important role in the LHD-mediated regulation of the inflammatory response in cardiomyocytes.

3.3 CD36 Regulates PA-Induced Inflammation

To further investigate the effect of CD36 in PA-induced cardiomyocyte inflammation, we used siRNA to silence the expression of CD36 in AC16 cells. Two CD36 siRNA oligomers were tested and significant reductions were achieved in the mRNA and protein expression; siRNA2 was selected for subsequent studies (**Figures 3A,B**). As expected, the effect of silencing CD36 was similar to that of LHD treatment: the reduced expression of CD36 restored NF-κB phosphorylation and IκB-α expression in PA-treated cells (**Figures 3C,D**; **Supplementary Figure S2A**). Moreover, qRT-PCR results suggested that the expression of pro-inflammatory factors was markedly reduced by CD36 loss of function (**Figure 3E**). To further verify the important role of CD36 in LHD anti-PA-induced cardiac inflammation, we transfected the exogenous CD36 plasmid into AC16 cells. qRT-PCR analysis showed that CD36 overexpression significantly interfered with the mRNA expression of CD36, IL-6 and TNF-α rescued by LHD (**Supplementary Figure S2B–D**). These results suggest that CD36 is required for the LHD anti-PA stimulation of cardiomyocytes.

3.4 LuHui Derivative Binds to FTO and Inhibits its Activity

Next, to explore the underlying anti-inflammatory mechanism of LHD in cardiomyocytes, we used SwissTargetPrediction, a small

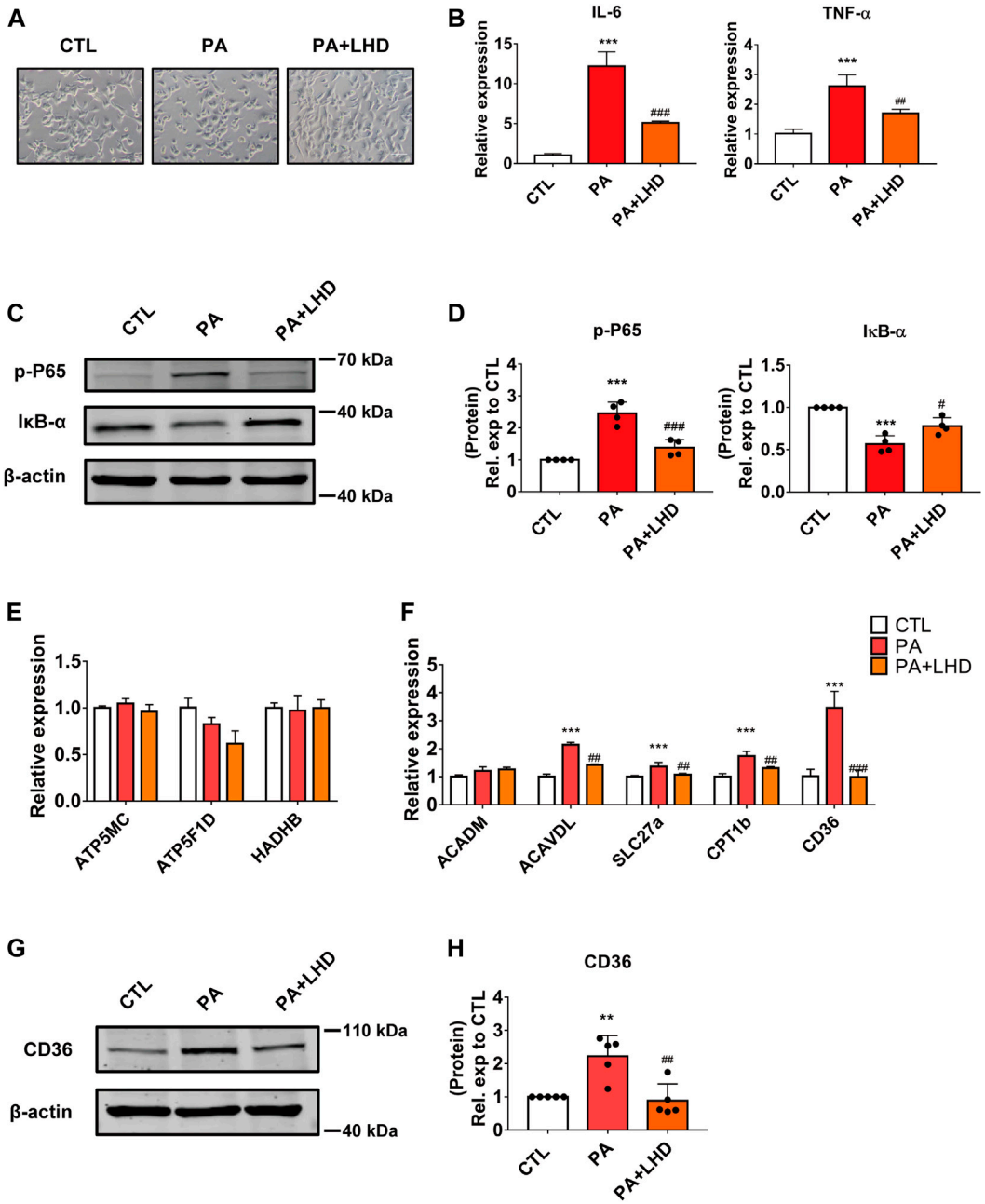


FIGURE 2 | LHD inhibits PA-induced cardiomyocyte inflammation *in vitro*. **(A)** Representative images of cell morphology captured by phase microscopy (20× magnification). $n = 3$. **(B)** Effect of LHD treatment on pro-inflammatory gene expression in AC16 cells treated with PA for 16 h. $^{***}p < 0.001$, compared with the CTL group, $^{\#\#}p < 0.01$, $^{\#\#\#}p < 0.001$, compared with the PA group, $n = 3$. **(C,D)** Changes in the intracellular inflammatory signaling pathway after LHD and PA treatment. **(C)** Western blotting analysis of the expression of the p-P65 and IκB-α inflammatory signaling proteins in human cardiomyocytes; **(D)** Statistical analysis of protein expression, $^{***}p < 0.001$, compared with the CTL group; $^{\#}p < 0.05$, $^{\#\#\#}p < 0.001$, compared with the PA group, $n = 4$. **(E,F)** Cardiac mRNA expression of **(E)** oxidative phosphorylation-related enzymes and **(F)** fatty acid metabolism-related genes. $^{***}p < 0.001$, compared with the CTL group; $^{\#\#}p < 0.01$, $^{\#\#\#}p < 0.001$, compared with the PA group, $n = 3$. **(G,H)** Western blotting analysis of the regulatory effect of LHD on CD36 expression. $^{**}p < 0.01$, compared with the CTL group; $^{\#\#}p < 0.01$, compared with the PA group, $n = 5$.

molecule compound and protein binding prediction website, to predict potential binding partners of LHD. We found that FTO, as an adiposity and obesity-related gene and an adipose metabolism-related gene (Wang et al., 2015), was the most promising LHD-binding candidate and may play a regulatory role in PA-induced inflammation process (**Figure 4A**; **Supplementary Table S3**). To understand the binding of LHD and FTO, we performed molecular docking studies of LHD and

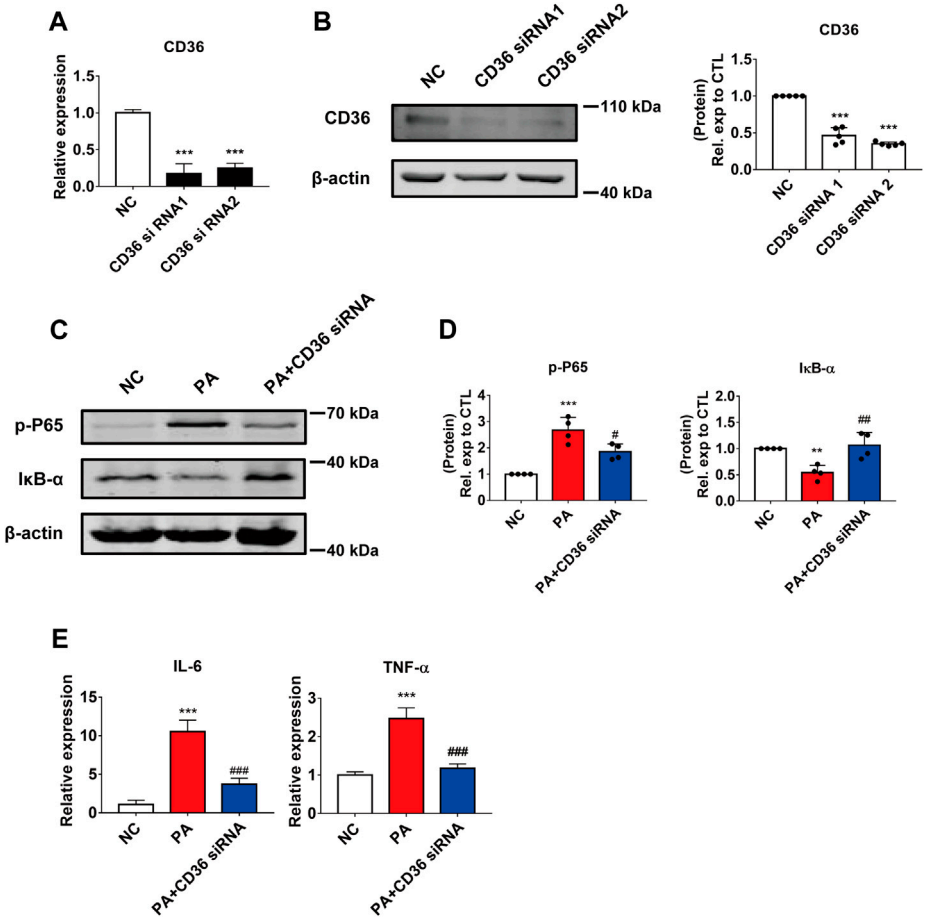


FIGURE 3 | The effect of CD36 in PA-induced cardiomyocyte inflammation. **(A,B)** Silencing efficiency of CD36. **(A)** qRT-PCR analysis of the effect of transfection of CD36 siRNA after 24 h in AC16 cells. ***$p < 0.001$, compared with the negative control (NC) group, $n = 3$. **(B)** Western blotting analysis of the effect of CD36 siRNA transfection after 48 h in AC16 cells. ***$p < 0.001$, compared with the NC group, $n = 5$. **(C,D)** Changes in the intracellular inflammatory signaling pathway after CD36 siRNA and PA treatment. **(C)** Western blotting analysis of the expression of the p-P65 and IκB-α proteins in human cardiomyocytes; **(D)** Statistical analysis of protein expression, **$p < 0.01$, ***$p < 0.001$ compared with the NC group; $^{\#}p < 0.05$, $^{\#\#}p < 0.01$, compared with the PA group, $n = 4$. **(E)** qRT-PCR analysis of the expression of the inflammatory genes IL-6 and TNF-α in CD36 siRNA and PA-treated cells. ***$p < 0.001$, compared with the NC group; $^{\#\#\#}p < 0.001$, compared with the PA group, $n = 4$.

the FTO protein using AutoDockTools 1.5.6 and PyMol 2.4 software. We found that LHD bound directly within the FTO catalytic pocket (**Figure 4B**). In addition, CETSA and DARTS assays were used to confirm the binding between LHD and FTO *in vitro*. As expected, the FTO protein resisted pronase activity in a dose-dependent manner in the presence of LHD (**Figure 4C**), and direct binding with LHD increased the thermal stability of the FTO protein (**Figure 4D**).

Notably, we found that expression of the FTO protein expression was not altered by the PA-induced inflammatory response or the anti-inflammatory effect of LHD (**Supplementary Figure S3A,B**). We then investigated whether LHD disrupted the enzymatic action of FTO. We observed the structure of LHD bound to FTO and found that LHD binds specifically to amino acids R96 and E234 of FTO (**Figure 4E**). The accumulated evidence shows that the N atom on the m^6A purine ring interacts with the R96 and E234 residues of the FTO protein via H-bonding, which locks the m^6A base in place (Zhang et al., 2019). To confirm these findings, we assessed whether LHD regulated FTO-mediated m^6A demethylation in cells. We performed a m^6A dot blot to analyze mRNA and found that m^6A methylation was increased in LHD-treated cells (**Figure 4F**; **Supplementary Figure S3C**). Overall, these results suggested that LHD effectively bonded with the FTO protein and inhibited m^6A demethylation by FTO.

3.5 FTO Regulates CD36 Expression in PA-Induced Cardiomyocyte Inflammation

To further investigate the effect of FTO on the PA-induced inflammatory response and CD36 expression, we used siRNA to silence intracellular FTO expression. The qRT-PCR and western blotting results showed that the two siRNAs tested, which targeted different regions of FTO, significantly reduced

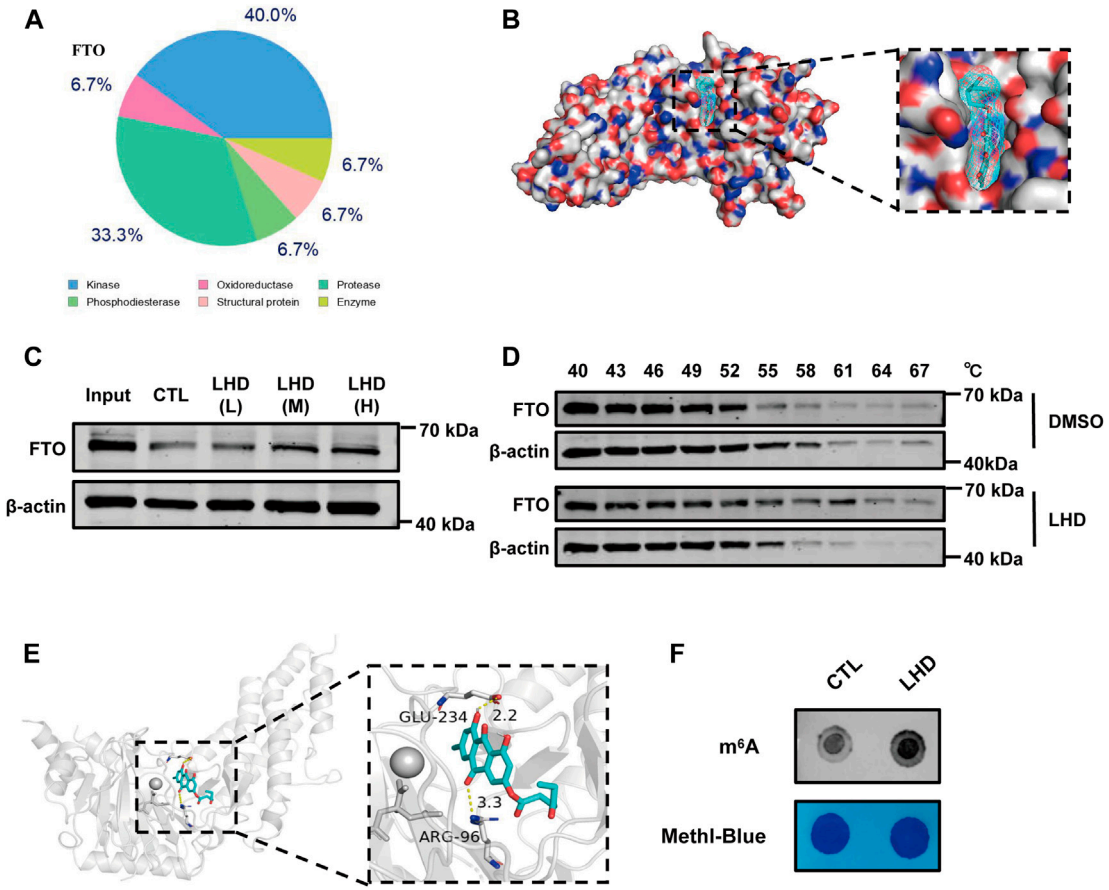


FIGURE 4 | LHD binds the FTO protein and regulates the level of m^{6}A modifications. **(A)** The top 15 compounds most likely to bind LHD. **(B)** Docking models simulating LHD binding into the FTO crystal structure (PDB ID: 3LFM). **(C)** Representative western blotting analysis of FTO from the DARTS assay. AC16 cells lysates with 83.4 (LHD L), 166.7 (LHD M), and 250.0 (LHD H) μM LHD were incubated for 1 h at room temperature before pronase digestion, $n = 3$. **(D)** Western blotting analysis of the thermal stability of FTO in LHD-treated cells, $n = 3$. **(E)** Structure of the complex of FTO bound with LHD; the yellow dotted lines indicate hydrogen bonding. **(F)** Determination of the abundance of the modification in 25 μM LHD-treated cells after 16 h, $n = 4$.

FTO expression, and the more effective siRNA, siRNA1, was selected for the subsequent experiments (**Figures 5A,B**; **Supplementary Figure S4A**). As reported in previous studies, FTO silencing significantly enhanced intracellular levels of the m^{6}A modification (**Supplementary Figure S4B**). The loss of function of FTO significantly enhanced the inhibitory effect of LHD in CD36 mRNA expression (**Figure 5C**), and the mRNA expression of IL-6 and TNF-α was markedly suppressed by FTO siRNA treated cells (**Figure 5D**; **Supplementary Figures S4C–E**).

To verify the effect of FTO in LHD against PA-induced cardiac inflammation, we transfected exogenous FTO plasmid and confirmed that the mRNA and protein expression of FTO was significantly increased (**Figures 5E,F**). From the qRT-PCR analysis, we found that the mRNA expression of CD36, IL-6 and TNF-α was significantly restored in LHD-treated cells. However, this was altered by FTO overexpression (**Figures 5G,H**), Moreover, the FTO overexpression plasmid significantly enhanced intracellular CD36 protein expression (**Supplementary Figure S4F**), which indicated that FTO is required to mediate the anti-inflammatory effects of LHD in PA-treated cardiomyocytes.

3.6 FTO-Dependent m^{6}A Modification Regulates CD36 Stability

It was shown that m^{6}A binding proteins selectively recognize the dynamic m^{6}A modification to regulate the stability of mRNA and the translation status (Wang et al., 2014). In combination with the above experiments showing that LHD, as an FTO inhibitor, regulates intracellular m^{6}A levels and mitigates the PA-induced increase in CD36 mRNA expression. Therefore, we hypothesized that the m^{6}A modification regulates the expression of CD36 in cardiomyocytes through its impact on mRNA transcription. To verify this hypothesis, we predicted the association between the m^{6}A modification sites and CD36 transcript by SRAMP, a sequence-based predictor of m^{6}A modification sites. The results showed that there were many m^{6}A modification sites on the CD36 transcript (**Figure 6A**). Next, we determined the stability of CD36

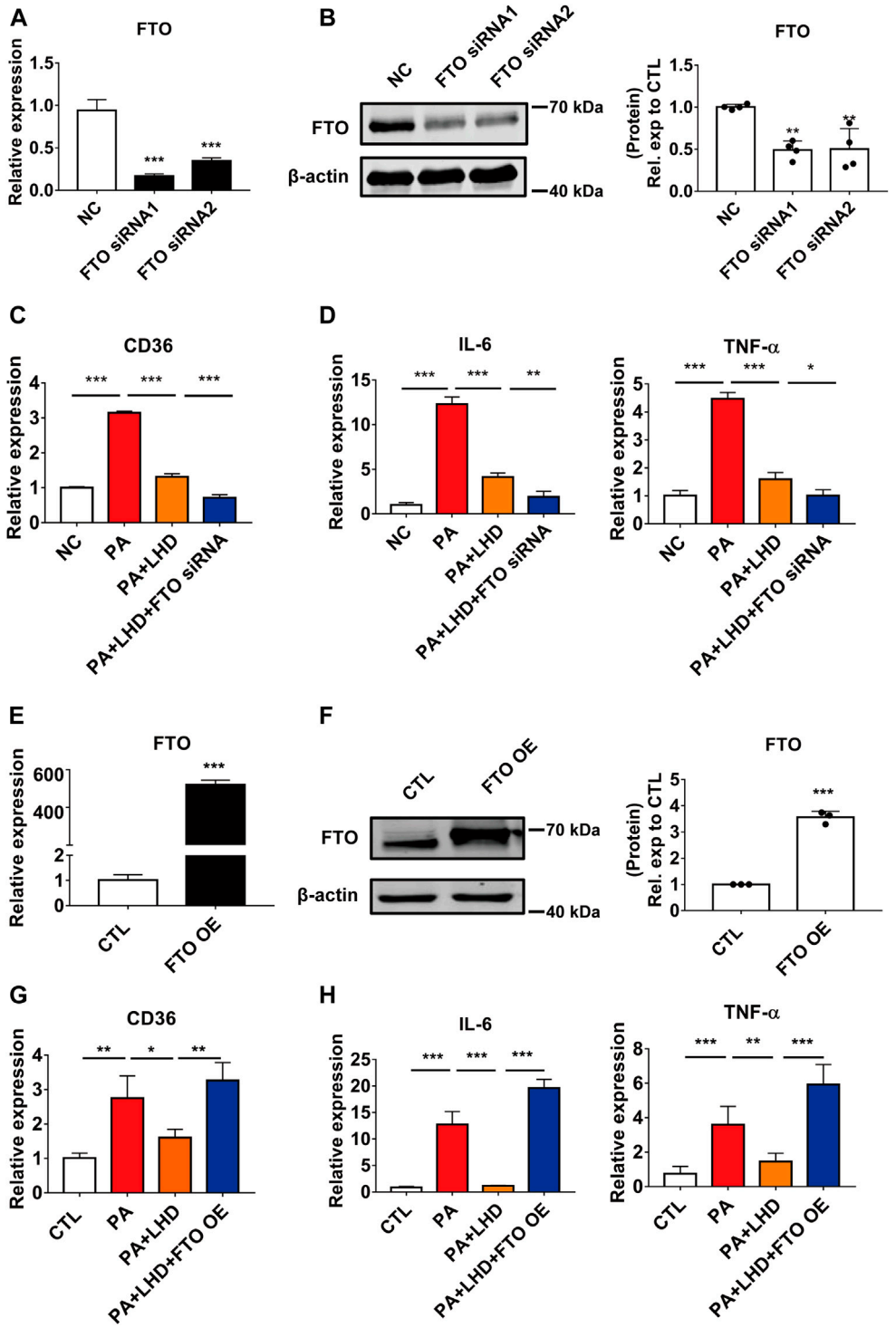


FIGURE 5 | FTO alters CD36 expression. **(A,B)** Silencing efficiency of FTO. **(A)** qRT-PCR analysis of the effect of transfection of FTO siRNA after 24 h in AC16 cells. ***$p < 0.001$, compared with the NC groups, $n = 3$. **(B)** Western blotting analysis of the effect of transfection of FTO siRNA after 48 h in AC16 cells. **$p < 0.01$, compared with the NC group, $n = 4$. **(C)** Effect of FTO loss of function and LHD co-treatment on CD36 expression in AC16 cells. ***$p < 0.001$, $n = 3$. **(D)** Effect of FTO loss of function and LHD co-treatment on IL-6 and TNF-α expression in AC16 cells. *$p < 0.05$, **$p < 0.01$, ***$p < 0.001$, $n = 3$. **(E,F)** Efficiency of FTO overexpression. **(E)** Expression of FTO mRNA after FTO overexpression for 24 h in AC16 cells. **(F)** Expression of FTO protein after FTO overexpression for 48 h in AC16 cells. ***$p < 0.001$, compared with the CTL group, $n = 3$. **(G)** Effect of FTO overexpression on the expression of CD36 in PA-treated AC16 cells. *$p < 0.05$, **$p < 0.01$, $n = 3$. **(H)** Effect of FTO overexpression on the expression of IL-6 and TNF-α in PA-treated AC16 cells. **$p < 0.01$, ***$p < 0.001$, $n = 3$.

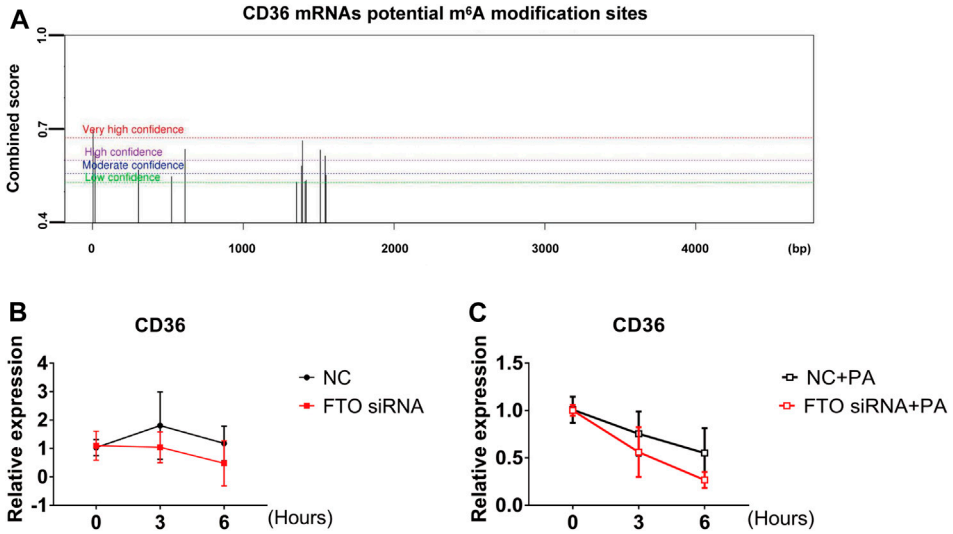


FIGURE 6 | FTO regulates CD36 expression through the m^{6}A modification. **(A)** The prediction of potential m^{6}A modification sites on CD36 mRNA. **(B)** Stability of CD36 mRNA in AC16 cells after FTO siRNA transfection for 24 h. **(C)** qRT-PCR analysis of CD36 mRNA stability after FTO silencing in PA-treated stimulation cells, $n = 3$.

mRNA after cells were transfected with FTO siRNA. We found that the half-life of CD36 mRNA was not significant change in FTO expression (**Figure 6B**). Thus, we examined the stability of CD36 mRNA following PA-induced inflammation. As expected, FTO silencing significantly decreased the half-life of CD36 mRNA compared with PA treatment (**Figure 6C**). Together, these results indicate that LHD/FTO-mediated m^{6}A demethylation impairs the stability of CD36 mRNA and protects against fatty acid-induced inflammation.

4 DISCUSSION

Herein, we have reported a novel chemically modified monomer, LHD, with protective effects against hyperlipidemia-induced cardiac injury, and determined the molecular mechanisms of these protective effects. Our results showed that LHD clearly reduced the lipid serum levels and alleviated cardiac inflammation *in vitro* and *in vivo* models of hyperlipidemia. Moreover, LHD decreased the expression of the inflammatory cytokines IL-6 and TNF-α *in vitro* model of PA stimulation (**Figure 7**).

Current knowledge suggests that the inflammation induced by a long-term HFD is directly associated with a range of metabolic diseases, including hyperlipidemia, insulin resistance, and type 2 diabetes (Goldberg et al., 2012). These diseases usually result in cardiac metabolic disorders, cardiomyocyte hypertrophy, apoptosis, fibrosis, inflammation, and systolic dysfunction (Palomer et al., 2013; Steven et al., 2018). Thus, maintaining of systemic metabolic homeostasis is a promising strategy to preserve heart function. In this study, we found that LHD had beneficial effects on cardiac function and alleviated inflammation by regulating CD36 expression and inhibiting the release of pro-inflammatory factors. In addition, this study provided persuasive evidence that LHD was an encouraging candidate for the treatment of cardiovascular-related metabolic diseases.

FTO is involved in the development of many metabolic diseases (Sun et al., 2020). In our study, we found that suppressing the expression of FTO inhibited the PA-induced inflammatory response in cardiomyocytes. The connection between FTO and cardiac disease has also been studied recently. Susmita demonstrated the importance of FTO-dependent m^{6}A methylation for cardiac systolic function and suggested that the overexpression of FTO reduced fibrosis in a mice model of myocardial infarction (MI) (Mathiyalagan et al., 2019). Moreover, Berulava et al. (2020) demonstrated that cardiac-specific FTO knockdown in transgenic mice delayed heart recovery and exacerbated heart failure. These experiments demonstrated the negative regulatory role of FTO in cardiomyocytes. However, these diseases were not associated with fatty acid metabolism or lipid accumulation. Clinical studies have confirmed fundamental differences in the mechanism of cardiometabolic disorders, obesity, and lipotoxicity-induced cardiovascular disease compared with ischemic cardiovascular disease (Obokata et al., 2017). In addition, research consistent with this finding showed that the endothelial cell-specific knockdown of FTO protected against obesity-induced metabolic disorders and insulin resistance, and improved cardiac functions (Kruger et al., 2020). The complex role of FTO in different cardiovascular diseases indicates that it has an essential role in fatty acid metabolism disorder-induced heart injury, as well as provides an effective therapeutic strategy for the utilization of FTO inhibitors in metabolic diseases.

Our research demonstrated that LHD was an FTO inhibitor and regulated the inflammatory responses in cardiomyocytes. This evidence supported further exploration of FTO inhibitors

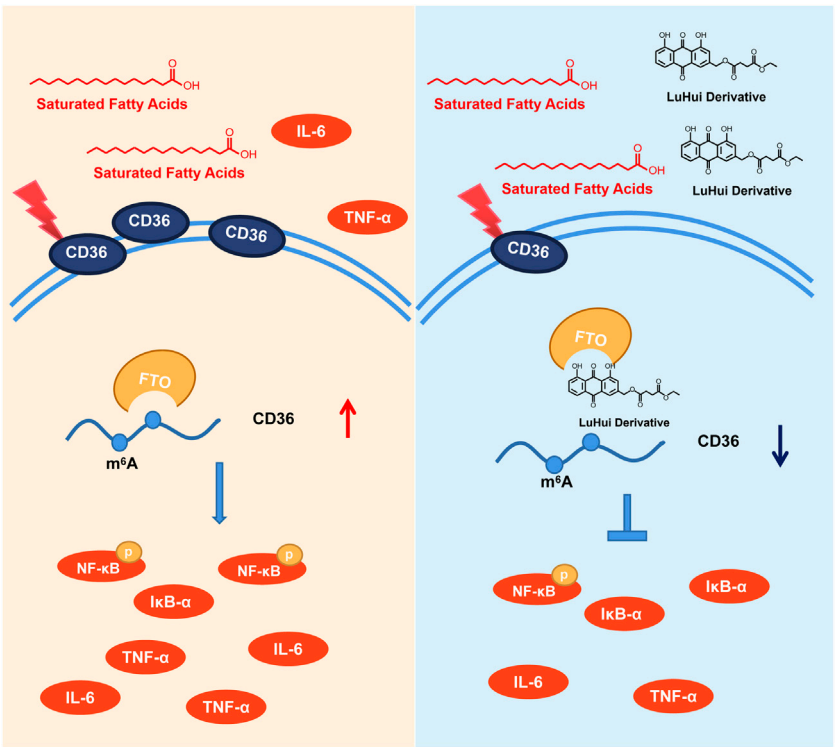


FIGURE 7 | Underlying mechanisms of the protective effect of LHD against hyperlipidemia-induced cardiomyocyte inflammation.

and expands the potential therapeutic applications for FTO. The non-steroidal anti-inflammatory drug meclofenamic acid (MA) binded specifically to FTO and inhibits FTO enzyme activity (Huang et al., 2015). Subsequently, Huang added a five-membered heterocycle to the structure of MA, showing that the novel compounds FB23 and FB23-2 were effective for the treatment of acute myeloid leukemia owing to their inhibition of the FTO methylesterase (Huang et al., 2019). Likewise, we showed that the chemically modified monomeric compound LHD could bind to FTO and interfere with the FTO-mediated m^6A modification, thereby ameliorating the hyperlipidemia- and PA-induced inflammatory responses in cardiomyocytes. These findings have enriched the body of knowledge concerning FTO inhibitors and provides a theoretical basis for further applications of FTO application.

Interestingly, we detected the expression of m^6A methylation modifying enzymes during PA pro-inflammatory and LHD anti-inflammatory processes. The results showed that PA treatment significantly reduced the changes in the expression levels of METTL3 and ALKBH5, but did not affect the intracellular expression levels of FTO and METTL14. During the anti-inflammatory process of LHD, the expression of m^6A methyltransferase (METTL3 and METTL14) and demethylase (ALKBH5 and FTO) did not change (**Supplementary Figure S3A,B**). This result suggested that LHD does not specifically affect the expression of methylation-modifying enzymes in PA-induced inflammation rescued by LHD. In regard to another FTO inhibitor, rhein, was shown to suppress FTO function in myogenic differentiation while not affecting FTO expression (Wang X. et al., 2017). Furthermore, FTO loss-of-function markedly affected intracellular m^6A modification and the release of inflammatory cytokines. The simultaneous overexpression of FTO enhanced the PA-induced inflammatory responses. Consistent with this finding, in the LPS-treated intestinal porcine epithelial J2 (IPEC-J2) cells and human dental pulp cells (HDPCs), FTO expression was not significantly altered during the inflammatory response, but the regulation of m^6A modification alleviated the inflammatory response (Feng et al., 2018; Zong et al., 2019). In atherosclerosis, a chronic inflammatory disease of arteries, FTO expression was not altered, but increased m^6A modification also influenced the development of atherosclerosis (Terpenning et al., 1987; Zhang et al., 2020). Based on these findings, we proposed several hypotheses: 1) The process of PA-induced inflammation is complex, and FTO may be sensitive to the substrates and mRNA maintain stability; 2) The binding of LHD in the FTO pocket only affects the m^6A demethylation ability of FTO, and does not induce FTO protein degradation; 3) The primary function of FTO is demethylation.

The m^6A modification, the most abundant type of mRNA modification, is involved in many processes, including mammalian development, immunity, stem cell renewal, fat differentiation, tumorigenesis, and metastasis (Geula et al., 2015; Zhao et al., 2017; Li et al., 2018; Weng et al., 2018; He et al., 2019; Winkler et al., 2019; Song et al., 2020). It has also been

shown that m^6A has an essential role in the formation and accumulation of fat. During these processes, the expression of CD36 decreases as the expression of FTO was decreased (Heng et al., 2020). Similarly, the level of m^6A modification was also affected by thermal stimulation, and CD36 was consistently elevated with FTO in pig abdominal fat. However, the regulatory relationship between FTO and CD36 has not previously been reported.

The m^6A methylation recognition protein, YTHDF2, has been shown to play essential roles, including the regulation of adipocyte autophagy, in a multitude of FTO-regulated diseases, such as alcohol-induced renal inflammation (Wu et al., 2018; Wang X. et al., 2020). The knockdown of YTHDF2 markedly increased the MAPK and NF-κB signaling pathways activity, increasing expression of pro-inflammatory cytokines and exacerbating inflammation in LPS-stimulated RAW 264.7 cells (Yu et al., 2019). Moreover, the knockdown of YTHDF2 in hepatoma cells inhibited the release of inflammatory cytokines and reduced macrophage clearance of hepatoma cells (Hou et al., 2019). These results demonstrated that YTHDF2 plays a critical role in the intracellular regulation of inflammatory factors. Therefore, it is reasonable to assume that FTO regulates the stability of CD36 mRNA via YTHDF2 dependent on the m^6A modification in hyperlipidemia and PA-induced cardiomyocyte inflammation.

Several studies indicated that CD36 may contribute to cardiac dysfunction and heart failure in metabolic disorders with an inflammatory background; the factors regulating CD36 expression were well studied. It was well established that peroxisome proliferator-activated receptor (PPAR) combines with retinoid X receptor (RXR) binding in the CD36 transcription region in ox-LDL or under transforming growth factor-β (TGF-β) stimulation (Han et al., 2000; Yu et al., 2016). Moreover, the promoter region of CD36 also could bind with a variety of regulators, including pregnane X receptor (PXR) reaction components, the liver X receptor (LXR), and the CCAAT/enhancer-binding protein (C/EBP) (Zhou et al., 2008). This observation was consistent with previous findings showing that signal transducer and activator of transcription 3 (STAT3) combine in an interferon-γ-activated sequence (GAS) in the CD36 promoter region to promote angiogenesis, tumor invasion, and metastasis (Sp et al., 2018). Similar outcomes, namely that microRNAs directly regulated CD36 expression, including miR-4668 and miR-26a, have been reported (Li et al., 2017; Ding et al., 2019). However, little is known regarding the contribution of the m^6A modification to CD36 expression. Our study found that the FTO-mediated m^6A modification alters CD36 expression by impairing the stability of CD36 mRNA. This finding will expand the known influence of m^6A and provide a basis for the further research into CD36.

However, the limitations of our study should be considered. First, we found the binding of LHD and FTO *in vivo* using published detection methods, but we could not conclusively determine whether LHD is involved in modifying proteins other than FTO. Second, the clinical development of hyperlipidemic cardiomyopathy requires prolonged exposure. Experimentally, although acute or short-term exposure to saturated fatty acids is adequate for research purposes, it may not encompass all the complications of abnormal lipid metabolism. In addition, owing to the availability of hyperlipidemic samples, we were unable to perform complete analyses of the experimental rats and cultured cells. Although essential measurements were collected in human cardiomyocytes for a better understanding of the clinical applications of LHD, further studies using samples from patients with hyperlipidemia would be necessary.

In the future, it is likely that research into inflammation will progress beyond conventional areas, to novel fields such as cardiomyocyte reprogramming. Our study has contributed to a deeper understanding of the inflammatory processes and provides a potential direction for the application of traditional Chinese anti-inflammatory medicines. With the continuous development of science and technology and the discovery of protein structures, the binding relationships and regulatory mechanisms between small molecule compounds and proteins can be studied in more depth. Such studies have led to clear progress in understanding the regulatory relationships between protein molecules and their applications in medicinal research.

5 CONCLUSION

Our study has demonstrated that LHD protects against hyperlipidemia-induced myocardial injury and PA-induced cardiomyocyte inflammation. Mechanistically, LHD binds to the FTO-specific m^6A binding site, inhibiting the demethylation modification of FTO, and suppressing the expression of the CD36, which consequently regulates myocardial metabolism and suppresses inflammation. This study has revealed the therapeutic effect of FTO on the heart and provides a platform to support the development of FTO inhibitors.

DATA AVAILABILITY STATEMENT

The original contributions presented in the study are included in the article/**Supplementary Material**, further inquiries can be directed to the corresponding authors.

ETHICS STATEMENT

The animal study was reviewed and approved by the Ethics Committee of Harbin Medical University.

AUTHOR CONTRIBUTIONS

YiY, YeY, and ZD supervised and performed the research, wrote the manuscript, and designed the experiments. YP and WL performed the cell-based experiments. ZF and SX performed

the protein-related experiments. YP and ZF provided a series of practical instructions. ZR and JY performed the data analysis. ZG, SX, JG, and FL performed the animal experiments. All authors approved the final version of the manuscript.

FUNDING

This work was supported by the National Natural Science Fund of China (82073838, 82161148007), and the Harbin Medical University Postgraduate Research and Practice Innovation Program (YJSKYCX2019-25HYD).

ACKNOWLEDGMENTS

Thanks to Prof. Benzhi Cai, Dr. ZhenBo Han, and Dr. Rui Gong for language help and writing assistance. Thanks to the other members of ZD's team for their help.

SUPPLEMENTARY MATERIAL

The Supplementary Material for this article can be found online at: https://www.frontiersin.org/articles/10.3389/fcell.2021.731365/full#supplementary-material

REFERENCES

Ben-Haim, M. S., Moshitch-Moshkovitz, S., and Rechavi, G. (2015). FTO: Linking m6A Demethylation to Adipogenesis. *Cell Res* 25 (1), 3–4. doi:10.1038/cr.2014.162

Berulava, T., Buchholz, E., Elerdashvili, V., Pena, T., Islam, M. R., Lbik, D., et al. (2020). Changes in m6A RNA Methylation Contribute to Heart Failure Progression by Modulating Translation. *Eur. J. Heart Fail.* 22 (1), 54–66. doi:10.1002/ejhf.1672

Bian, Y., Li, X., Pang, P., Hu, X.-l., Yu, S.-t., Liu, Y.-n., et al. (2020). Kanglexin, a Novel Anthraquinone Compound, Protects against Myocardial Ischemic Injury in Mice by Suppressing NLRP3 and Pyroptosis. *Acta Pharmacol. Sin* 41 (3), 319–326. doi:10.1038/s41401-019-0307-8

Cai, B., Ma, W., Wang, X., Sukhareva, N., Hua, B., Zhang, L., et al. (2020). Targeting LncDACH1 Promotes Cardiac Repair and Regeneration after Myocardium Infarction. *Cell Death Differ* 27 (7), 2158–2175. doi:10.1038/s41418-020-0492-5

Chen, Y., Feng, B., Yuan, Y., Hu, J., Zhao, W., Jiang, H., et al. (2020). Aloe Emodin Reduces Cardiac Inflammation Induced by a High-Fat Diet through the TLR4 Signaling Pathway. *Mediators Inflamm.* 2020, 1–12. doi:10.1155/2020/6318520

Ding, D., Ye, G., Lin, Y., Lu, Y., Zhang, H., Zhang, X., et al. (2019). MicroRNA-26a-CD36 Signaling Pathway: Pivotal Role in Lipid Accumulation in Hepatocytes Induced by PM2.5 Liposoluble Extracts. *Environ. Pollut.* 248, 269–278. doi:10.1016/j.envpol.2019.01.112

Ertunc, M. E., and Hotamisligil, G. S. (2016). Lipid Signaling and Lipotoxicity in Metaflammation: Indications for Metabolic Disease Pathogenesis and Treatment. *J. Lipid Res.* 57 (12), 2099–2114. doi:10.1194/jlr.R066514

Feng, Z., Li, Q., Meng, R., Yi, B., and Xu, Q. (2018). METTL 3 Regulates Alternative Splicing of MyD88 upon the Lipopolysaccharide-induced Inflammatory Response in Human Dental Pulp Cells. *J. Cell Mol Med* 22 (5), 2558–2568. doi:10.1111/jcmm.13491

Geula, S., Moshitch-Moshkovitz, S., Dominissini, D., Mansour, A. A., Kol, N., Salmon-Divon, M., et al. (2015). m 6 A mRNA Methylation Facilitates Resolution of Naïve Pluripotency toward Differentiation. *Science* 347 (6225), 1002–1006. doi:10.1126/science.1261417

Goldberg, I. J., Trent, C. M., and Schulze, P. C. (2012). Lipid Metabolism and Toxicity in the Heart. *Cell Metab.* 15 (6), 805–812. doi:10.1016/j.cmet.2012.04.006

Han, J., Hajjar, D. P., Tauras, J. M., Feng, J., Gotto, A. M., Jr., and Nicholson, A. C. (2000). Transforming Growth Factor-B1 (TGF-B1) and TGF-B2 Decrease Expression of CD36, the Type B Scavenger Receptor, through Mitogen-Activated Protein Kinase Phosphorylation of Peroxisome Proliferator-Activated Receptor-γ. *J. Biol. Chem.* 275 (2), 1241–1246. doi:10.1074/jbc.275.2.1241

Han, Z., Wang, X., Xu, Z., Cao, Y., Gong, R., Yu, Y., et al. (2021). ALKBH5 Regulates Cardiomyocyte Proliferation and Heart Regeneration by Demethylating the mRNA of YTHDF1. *Theranostics* 11 (6), 3000–3016. doi:10.7150/thno.47354

He, L., Li, H., Wu, A., Peng, Y., Shu, G., and Yin, G. (2019). Functions of N6-Methyladenosine and its Role in Cancer. *Mol. Cancer* 18 (1), 176. doi:10.1186/s12943-019-1109-9

Healy, N. P., Kirwan, A. M., McArdle, M. A., Holohan, K., Nongonierma, A. B., Keane, D., et al. (2016). A Casein Hydrolysate Protects Mice against High Fat Diet Induced Hyperglycemia by Attenuating NLRP3 Inflammasome-Mediated Inflammation and Improving Insulin Signaling. *Mol. Nutr. Food Res.* 60 (11), 2421–2432. doi:10.1002/mnfr.201501054

Heng, J., Wu, Z., Tian, M., Chen, J., Song, H., Chen, F., et al. (2020). Excessive BCAA Regulates Fat Metabolism Partially through the Modification of m6A RNA Methylation in Weanling Piglets. *Nutr. Metab. (Lond)* 17, 10. doi:10.1186/s12986-019-0424-x

Hess, M. E., Hess, S., Meyer, K. D., Verhagen, L. A. W., Koch, L., Brönneke, H. S., et al. (2013). The Fat Mass and Obesity Associated Gene (Fto) Regulates Activity of the Dopaminergic Midbrain Circuitry. *Nat. Neurosci.* 16 (8), 1042–1048. doi:10.1038/nn.3449

Hou, J., Zhang, H., Liu, J., Zhao, Z., Wang, J., Lu, Z., et al. (2019). YTHDF2 Reduction Fuels Inflammation and Vascular Abnormalization in Hepatocellular Carcinoma. *Mol. Cancer* 18 (1), 163. doi:10.1186/s12943-019-1082-3

Huang, Y., Su, R., Sheng, Y., Dong, L., Dong, Z., Xu, H., et al. (2019). Small-Molecule Targeting of Oncogenic FTO Demethylase in Acute Myeloid Leukemia. *Cancer Cell* 35 (4), 677–691. doi:10.1016/j.ccell.2019.03.006

Huang, Y., Yan, J., Li, Q., Li, J., Gong, S., Zhou, H., et al. (2015). Meclofenamic Acid Selectively Inhibits FTO Demethylation of m6A over ALKBH5. *Nucleic Acids Res.* 43 (1), 373–384. doi:10.1093/nar/gku1276

Jafari, R., Almqvist, H., Axelsson, H., Ignatushchenko, M., Lundbäck, T., Nordlund, P., et al. (2014). The Cellular thermal Shift Assay for Evaluating Drug Target Interactions in Cells. *Nat. Protoc.* 9 (9), 2100–2122. doi:10.1038/nprot.2014.138

Jia, G., DeMarco, V. G., and Sowers, J. R. (2016). Insulin Resistance and Hyperinsulinaemia in Diabetic Cardiomyopathy. *Nat. Rev. Endocrinol.* 12 (3), 144–153. doi:10.1038/nrendo.2015.216

Krüger, N., Biwer, L. A., Good, M. E., Ruddiman, C. A., Wolpe, A. G., DeLalio, L. J., et al. (2020). Loss of Endothelial FTO Antagonizes Obesity-Induced Metabolic and Vascular Dysfunction. *Circ. Res.* 126 (2), 232–242. doi:10.1161/CIRCRESAHA.119.315531

Li, B.-R., Xia, L.-Q., Liu, J., Liao, L.-L., Zhang, Y., Deng, M., et al. (2017). miR-758-5p Regulates Cholesterol Uptake via Targeting the CD36 3′UTR. *Biochem. Biophysical Res. Commun.* 494 (1-2), 384–389. doi:10.1016/j.bbrc.2017.09.150

Li, Z., Qian, P., Shao, W., Shi, H., He, X. C., Gogol, M., et al. (2018). Suppression of m6A Reader Ythdf2 Promotes Hematopoietic Stem Cell Expansion. *Cell Res* 28 (9), 904–917. doi:10.1038/s41422-018-0072-0

Liu, W., Ruiz-Velasco, A., Wang, S., Khan, S., Zi, M., Jungmann, A., et al. (2017). Metabolic Stress-Induced Cardiomyopathy Is Caused by Mitochondrial Dysfunction Due to Attenuated Erk5 Signaling. *Nat. Commun.* 8 (1), 494. doi:10.1038/s41467-017-00664-8

Liu, Y., You, Y., Lu, Z., Yang, J., Li, P., Liu, L., et al. (2019). N 6 -methyladenosine RNA Modification-Mediated Cellular Metabolism Rewiring Inhibits Viral Replication. *Science* 365 (6458), 1171–1176. doi:10.1126/science.aax4468

Lomenick, B., Hao, R., Jonai, N., Chin, R. M., Aghajan, M., Warburton, S., et al. (2009). Target Identification Using Drug Affinity Responsive Target Stability (DARTS). *Proc. Natl. Acad. Sci.* 106 (51), 21984–21989. doi:10.1073/pnas.0910040106

Mathiyalagan, P., Adamiak, M., Mayourian, J., Sassi, Y., Liang, Y., Agarwal, N., et al. (2019). FTO-dependent N 6 -Methyladenosine Regulates Cardiac Function during Remodeling and Repair. *Circulation* 139 (4), 518–532. doi:10.1161/CIRCULATIONAHA.118.033794

Meng, Q., Li, Y., Ji, T., Chao, Y., Li, J., Fu, Y., et al. (2021). Estrogen Prevent Atherosclerosis by Attenuating Endothelial Cell Pyroptosis via Activation of Estrogen Receptor α-mediated Autophagy. *J. Adv. Res.* 28, 149–164. doi:10.1016/j.jare.2020.08.010

Molina, D. M., Jafari, R., Ignatushchenko, M., Seki, T., Larsson, E. A., Dan, C., et al. (2013). Monitoring Drug Target Engagement in Cells and Tissues Using the Cellular thermal Shift Assay. *Science* 341 (6141), 84–87. doi:10.1126/science.1233606

Nagarajan, A., Janostiak, R., and Wajapeyee, N. (2019). Dot Blot Analysis for Measuring Global N6-Methyladenosine Modification of RNA. *Methods Mol. Biol.* 1870, 263–271. doi:10.1007/978-1-4939-8808-2_20

Nicholls, S., and Lundman, P. (2004). The Emerging Role of Lipoproteins in Atherogenesis: beyond LDL Cholesterol. *Semin. Vasc. Med.* 4 (2), 187–195. doi:10.1055/s-2004-835377

Obokata, M., Reddy, Y. N. V., Pislaru, S. V., Melenovsky, V., and Borlaug, B. A. (2017). Evidence Supporting the Existence of a Distinct Obese Phenotype of Heart Failure with Preserved Ejection Fraction. *Circulation* 136 (1), 6–19. doi:10.1161/CIRCULATIONAHA.116.026807

Pai, M. Y., Lomenick, B., Hwang, H., Schiestl, R., McBride, W., Loo, J. A., et al. (2015). Drug Affinity Responsive Target Stability (DARTS) for Small-Molecule Target Identification. *Methods Mol. Biol.* 1263, 287–298. doi:10.1007/978-1-4939-2269-7_22

Palomer, X., Salvadó, L., Barroso, E., and Vázquez-Carrera, M. (2013). An Overview of the Crosstalk between Inflammatory Processes and Metabolic Dysregulation during Diabetic Cardiomyopathy. *Int. J. Cardiol.* 168 (4), 3160–3172. doi:10.1016/j.ijcard.2013.07.150

Ralston, J. C., Lyons, C. L., Kennedy, E. B., Kirwan, A. M., and Roche, H. M. (2017). Fatty Acids and NLRP3 Inflammasome-Mediated Inflammation in Metabolic Tissues. *Annu. Rev. Nutr.* 37, 77–102. doi:10.1146/annurev-nutr-071816-064836

Sabbatini, A. R., and Kararigas, G. (2020). Menopause-Related Estrogen Decrease and the Pathogenesis of HFpEF. *J. Am. Coll. Cardiol.* 75 (9), 1074–1082. doi:10.1016/j.jacc.2019.12.049

Schilling, J. D., Machkovech, H. M., Kim, A. H. J., Schwedwener, R., and Schaffer, J. E. (2012). Macrophages Modulate Cardiac Function in Lipotoxic Cardiomyopathy. *Am. J. Physiology-Heart Circulatory Physiol.* 303 (11), H1366–H1373. doi:10.1152/ajpheart.00111.2012

Sheedy, F. J., Grebe, A., Rayner, K. J., Kalantari, P., Ramkhelawon, B., Carpenter, S. B., et al. (2013). CD36 Coordinates NLRP3 Inflammasome Activation by Facilitating Intracellular Nucleation of Soluble Ligands into Particulate Ligands in Sterile Inflammation. *Nat. Immunol.* 14 (8), 812–820. doi:10.1038/ni.2639

Silverstein, R. L., Li, W., Park, Y. M., and Rahaman, S. O. (2010). Mechanisms of Cell Signaling by the Scavenger Receptor CD36: Implications in Atherosclerosis and Thrombosis. *Trans. Am. Clin. Climatol Assoc.* 121, 206–220.

Son, N.-H., Basu, D., Samovski, D., Pietka, T. A., Peche, V. S., Willecke, F., et al. (2018). Endothelial Cell CD36 Optimizes Tissue Fatty Acid Uptake. *J. Clin. Invest.* 128 (10), 4329–4342. doi:10.1172/JCI99315

Song, T., Yang, Y., Jiang, S., and Peng, J. (2020). Novel Insights into Adipogenesis from the Perspective of Transcriptional and RNA N6-Methyladenosine-Mediated Post-Transcriptional Regulation. *Adv. Sci.* 7 (21), 2001563. doi:10.1002/advs.202001563

Sp, N., Kang, D., Kim, D., Park, J., Lee, H., Kim, H., et al. (2018). Nobiletin Inhibits CD36-dependent Tumor Angiogenesis, Migration, Invasion, and Sphere Formation through the Cd36/Stat3/Nf-Kb Signaling Axis. *Nutrients* 10 (6), 772. doi:10.3390/nu10060772

Steven, S., Dib, M., Hausding, M., Kashani, F., Oelze, M., Kröller-Schön, S., et al. (2018). CD40L Controls Obesity-Associated Vascular Inflammation, Oxidative Stress, and Endothelial Dysfunction in High Fat Diet-Treated and Db/db Mice. *Cardiovasc. Res.* 114 (2), 312–323. doi:10.1093/cvr/cvx197

Stewart, C. R., Stuart, L. M., Wilkinson, K., van Gils, J. M., Deng, J., Halle, A., et al. (2010). CD36 Ligands Promote Sterile Inflammation through Assembly of a Toll-like Receptor 4 and 6 Heterodimer. *Nat. Immunol.* 11 (2), 155–161. doi:10.1038/ni.1836

Su, Z.-l., Hang, P.-z., Hu, J., Zheng, Y.-y., Sun, H.-q., Guo, J., et al. (2020). Aloe-emodin Exerts Cholesterol-Lowering Effects by Inhibiting Proprotein Convertase Subtilisin/kexin Type 9 in Hyperlipidemic Rats. *Acta Pharmacol. Sin* 41 (8), 1085–1092. doi:10.1038/s41401-020-0392-8

Sun, L., Ling, Y., Jiang, J., Wang, D., Wang, J., Li, J., et al. (2020). Differential Mechanisms Regarding Triclosan vs. Bisphenol A and Fluorene-9-Bisphenol Induced Zebrafish Lipid-Metabolism Disorders by RNA-Seq. *Chemosphere* 251, 126318. doi:10.1016/j.chemosphere.2020.126318

Terpenning, M. S., Buggy, B. P., and Kauffman, C. A. (1987). Infective Endocarditis: Clinical Features in Young and Elderly Patients. *Am. J. Med.* 83 (4), 626–634. doi:10.1016/0002-9343(87)90890-4

Wang, C.-Y., Shie, S.-S., Wen, M.-S., Hung, K.-C., Hsieh, I.-C., Yeh, T.-S., et al. (2015). Loss of FTO in Adipose Tissue Decreases Angptl4 Translation and Alters Triglyceride Metabolism. *Sci. Signal.* 8 (407), ra127. doi:10.1126/scisignal.aab3357

Wang, L., Song, C., Wang, N., Li, S., Liu, Q., Sun, Z., et al. (2020a). NADP Modulates RNA m6A Methylation and Adipogenesis via Enhancing FTO Activity. *Nat. Chem. Biol.* 16 (12), 1394–1402. doi:10.1038/s41589-020-0601-2

Wang, X., Huang, N., Yang, M., Wei, D., Tai, H., Han, X., et al. (2017a). FTO Is Required for Myogenesis by Positively Regulating mTOR-PGC-1α Pathway-Mediated Mitochondria Biogenesis. *Cell Death Dis* 8 (3)–e2702. doi:10.1038/cddis.2017.122

Wang, X., Lu, Z., Gomez, A., Hon, G. C., Yue, Y., Han, D., et al. (2014). N6-methyladenosine-dependent Regulation of Messenger RNA Stability. *Nature* 505 (7481), 117–120. doi:10.1038/nature12730

Wang, X., Wu, R., Liu, Y., Zhao, Y., Bi, Z., Yao, Y., et al. (2020b). m6A mRNA Methylation Controls Autophagy and Adipogenesis by Targeting Atg5 and Atg7. *Autophagy* 16 (7), 1221–1235. doi:10.1080/15548627.2019.1659617

Wang, Y., Qian, Y., Fang, Q., Zhong, P., Li, W., Wang, L., et al. (2017b). Saturated Palmitic Acid Induces Myocardial Inflammatory Injuries through Direct Binding to TLR4 Accessory Protein MD2. *Nat. Commun.* 8, 13997. doi:10.1038/ncomms13997

Weng, H., Huang, H., Wu, H., Qin, X., Zhao, B. S., Dong, L., et al. (2018). METTL14 Inhibits Hematopoietic Stem/Progenitor Differentiation and Promotes Leukemogenesis via mRNA m6A Modification. *Cell Stem Cell* 22 (2), 191–205. doi:10.1016/j.stem.2017.11.016

Winkler, R., Gillis, E., Lasman, L., Safra, M., Geula, S., Soyris, C., et al. (2019). m6A Modification Controls the Innate Immune Response to Infection by Targeting Type I Interferons. *Nat. Immunol.* 20 (2), 173–182. doi:10.1038/s41590-018-0275-z

Wu, R., Liu, Y., Yao, Y., Zhao, Y., Bi, Z., Jiang, Q., et al. (2018). FTO Regulates Adipogenesis by Controlling Cell Cycle Progression via m6A-YTHDF2 Dependent Mechanism. *Biochim. Biophys. Acta (Bba) - Mol. Cell Biol. Lipids* 1863 (10), 1323–1330. doi:10.1016/j.bbalip.2018.08.008

Yu, J.-T., Hu, X.-W., Chen, H.-Y., Yang, Q., Li, H.-D., Dong, Y.-H., et al. (202110528). DNA Methylation of FTO Promotes Renal Inflammation by Enhancing m6A of PPAR-α in Alcohol-Induced Kidney Injury. *Pharmacol. Res.* 163, 105286. doi:10.1016/j.phrs.2020.105286

Yu, M., Jiang, M., Chen, Y., Zhang, S., Zhang, W., Yang, X., et al. (2016). Inhibition of Macrophage CD36 Expression and Cellular Oxidized Low Density Lipoprotein (oxLDL) Accumulation by Tamoxifen. *J. Biol. Chem.* 291 (33), 16977–16989. doi:10.1074/jbc.M116.740092

Yu, R., Li, Q., Feng, Z., Cai, L., and Xu, Q. (2019). m6A Reader YTHDF2 Regulates LPS-Induced Inflammatory Response. *Ijms* 20 (6), 1323. doi:10.3390/ijms20061323

Zhang, B. Y., Han, L., Tang, Y. F., Zhang, G. X., Fan, X. L., Zhang, J. J., et al. (2020). METTL14 Regulates M6A Methylation-Modified Primary miR-19a to Promote Cardiovascular Endothelial Cell Proliferation and Invasion. *Eur. Rev. Med. Pharmacol. Sci.* 24 (12), 7015–7023. doi:10.26355/eurrev_202006_21694

Zhang, X., Wei, L.-H., Wang, Y., Xiao, Y., Liu, J., Zhang, W., et al. (2019). Structural Insights into FTO's Catalytic Mechanism for the Demethylation of Multiple

RNA Substrates. *Proc. Natl. Acad. Sci. USA* 116 (8), 2919–2924. doi:10.1073/pnas.1820574116

Zhao, B. S., Roundtree, I. A., and He, C. (2017). Post-transcriptional Gene Regulation by mRNA Modifications. *Nat. Rev. Mol. Cell Biol* 18 (1), 31–42. doi:10.1038/nrm.2016.132

Zhao, W., Yuan, Y., Feng, B., Sun, Y., Jiang, H., Zhao, W., et al. (2021). Aloe-emodin Relieves Zidovudine-Induced Injury in Neonatal Rat Ventricular Myocytes by Regulating the P90rsk/p-Bad/bcl-2 Signaling Pathway. *Environ. Toxicol. Pharmacol.* 81, 103540. doi:10.1016/j.etap.2020.103540

Zhou, J., Febbraio, M., Wada, T., Zhai, Y., Kuruba, R., He, J., et al. (2008). Hepatic Fatty Acid Transporter Cd36 Is a Common Target of LXR, PXR, and PPARγ in Promoting Steatosis. *Gastroenterology* 134 (2), 556–567. doi:10.1053/j.gastro.2007.11.037

Zong, X., Zhao, J., Wang, H., Lu, Z., Wang, F., Du, H., et al. (2019). Mettl3 Deficiency Sustains Long-Chain Fatty Acid Absorption through Suppressing Traf6-dependent Inflammation Response. *J.I.* 202 (2), 567–578. doi:10.4049/jimmunol.1801151

Conflict of Interest: The authors declare that the research was conducted in the absence of any commercial or financial relationships that could be construed as a potential conflict of interest.

Publisher's Note: All claims expressed in this article are solely those of the authors and do not necessarily represent those of their affiliated organizations, or those of the publisher, the editors, and the reviewers. Any product that may be evaluated in this article or claim that may be made by its manufacturer is not guaranteed or endorsed by the publisher.

Copyright © 2021 Yu, Pan, Fan, Xu, Gao, Ren, Yu, Li, Liu, Gu, Yuan and Du. This is an open-access article distributed under the terms of the Creative Commons Attribution License (CC BY). The use, distribution or reproduction in other forums is permitted, provided the original author(s) and the copyright owner(s) are credited and that the original publication in this journal is cited, in accordance with accepted academic practice. No use, distribution or reproduction is permitted which does not comply with these terms.

frontiers in Cell and Developmental Biology

ORIGINAL RESEARCH
published: 25 November 2021
doi: 10.3389/fcell.2021.725764

Integrating m6A Regulators-Mediated Methylation Modification Models and Tumor Immune Microenvironment Characterization in Caucasian and Chinese Low-Grade Gliomas

Wangrui Liu[1,2†], Chuanyu Li[2†], Yuhao Wu[3†], Wenhao Xu[4†], Shuxian Chen[5], Hailiang Zhang[4*], Haineng Huang[2*], Shuai Zhao[1*] and Jian Wang[1*]*

[1] Department of Transplantation, Xinhua Hospital Affiliated to Shanghai Jiao Tong University School of Medicine, Shanghai, China, [2] Department of Neurosurgery, Affiliated Hospital of Youjiang Medical University for Nationalities, Guangxi, China, [3] School of Medicine, Tongji University, Shanghai, China, [4] Department of Urology, Fudan University Shanghai Cancer Center, Shanghai Medical College, Fudan University, Shanghai, China, [5] Department of Oncology, Xinhua Hospital Affiliated to Shanghai Jiao Tong University School of Medicine, Shanghai, China

Background: As an important epigenetic modification, m6A methylation plays an essential role in post-transcriptional regulation and tumor development. It is urgently needed to comprehensively and rigorously explore the prognostic value of m6A regulators and its association with tumor microenvironment (TME) infiltration characterization of low-grade glioma (LGG).

Methods: Based on the expression of 20 m6A regulatory factors, we comprehensively evaluated the m6A modification patterns of LGG after unsupervised clustering. Subsequent analysis of the differences between these groups was performed to obtain m6A-related genes, then consistent clustering was conducted to generate m6AgeneclusterA and m6AgeneclusterB. A Random Forest and machining learning algorithms were used to reduce dimensionality, identify TME characteristics and predict responses for LGG patients receiving immunotherapies.

Results: Evident differential m6A regulators were found in mutation, CNV and TME characteristics of LGG. Based on TCGA and CGGA databases, we identified that m6A regulators clusterA could significantly predict better prognosis (p = 0.00016) which enriched in mTOR signaling pathway, basal transcription factors, accompanied by elevated immune cells infiltration, and decreased IDH and TP53 mutations. We also investigated the distribution of differential genes in m6A regulators clusters which was closely associated with tumor immune microenvironment through three independent cohort comparisons. Next, we established m6Ascore based on previous m6A model, which accurately predicts outcomes in 1089 LGG patients ($p < 0.0001$) from discovering cohort and 497 LGG patients from testing cohort. Significant

OPEN ACCESS

Edited by:
Pengxu Qian,
Zhejiang University, China

Reviewed by:
Kunqi Chen,
Fujian Medical University, China
Manjari Kiran,
University of Hyderabad, India

***Correspondence:**
Shuxian Chen
csx_sjtu@163.com
Hailiang Zhang
071106248@alu.fudan.edu.cn
Haineng Huang
passpsycho@163.com
Shuai Zhao
zhaoshuai@xinhuamed.com.cn
Jian Wang
wangjian197906@126.com

† These authors have contributed equally to this work

Specialty section:
This article was submitted to Epigenomics and Epigenetics, a section of the journal Frontiers in Cell and Developmental Biology

Received: *15 June 2021*
Accepted: *11 October 2021*
Published: *25 November 2021*

Citation:
Liu W, Li C, Wu Y, Xu W, Chen S, Zhang H, Huang H, Zhao S and Wang J (2021) Integrating m6A Regulators-Mediated Methylation Modification Models and Tumor Immune Microenvironment Characterization in Caucasian and Chinese Low-Grade Gliomas. Front. Cell Dev. Biol. 9:725764. doi: 10.3389/fcell.2021.725764

TME characteristics, including genome heterogeneity, abidance of immune cells, and clinicopathologic parameters have been found between m6Ascore groups. Importantly, LGG patients with high m6Ascore are confronted with significantly decreased responses to chemotherapies, but benefit more from immunotherapies.

Conclusion: In conclusion, this study first demonstrates that m6A modification is crucial participant in tumorigenesis and TME infiltration characterization of LGG based on large-scale cohorts. The m6Ascore provides useful and accurately predict of prognosis and clinical responses to chemotherapy, immunotherapy and therapeutic strategy development for LGG patients.

Keywords: m6A, low-grade glioma, tumor environment, immunotherapy, prognosis, RNA modificatio

BACKGROUND

Low-grade glioma (LGG) is a progressive, invasive, and chronic central nervous system disease. LGGs are a group of heterogeneous neuroepithelial tumors that originate from the supporting glial cells in the central nervous system (Rueda et al., 2011; Duffau and Taillandier, 2015; Wesseling and Capper, 2018). Although the tumor progression is relative slow, and these tumors may undergo malignant transformation, leading to the development of high-grade gliomas. At present, the average survival time of LGG patients is generally less than 10 years (Wessels et al., 2003). The available treatment options for LGGs remain controversial and require further investigation. Regardless of the classic therapy strategy of resection followed by chemotherapy or novel developed personalized treatments based on specific molecular markers of tumors (Wessels et al., 2003; Duffau, 2007; Martino et al., 2009; Louis et al., 2014), the primary purpose is to extend the overall survival (OS) of the patients. Therefore, the development of a model that can evaluate the survival and prognosis of patients is urgently needed to assist clinicians in the effective treatment of LGG patients.

Although some cases showed remarkable clinical efficacy (Dunin-Horkawicz et al., 2006; Alarcón et al., 2015; Patil et al., 2016), most of patients did not benefit from immunotherapy, suggesting there are still unmet clinical needs in LGG treatment (Zhao et al., 2017). The tumor microenvironment (TME) is composed of cancer cells, stromal cells (cancer-associated fibroblasts and macrophages), and recruited immune cells that influence the development and progression of cancer. Tumor cells interact with the TME to modify the purity of the tumor, causing changes in various biological behaviors, such as the induction of immune tolerance, tumor proliferation, and angiogenesis and the inhibition of apoptosis (Wang et al., 2017). Determining the degree of TME cell infiltration and tumor purity to predict the blocking effect of immune checkpoint inhibitors is an essential step to improve the success rate of existing immunotherapies and develop new treatment strategies (Wang et al., 2017, 2018).

The methyltransferases (m6A "writers"), demethylases (m6A "erasers"), and m6A "reader" proteins coordinate in the process of m6A modification. m6A RNA methylation is considered to be the most important and abundant form of internal modification in eukaryotic cells (Granier et al., 2016; Cui et al., 2017; Pinello et al., 2018; Luo et al., 2021). According to previous reports, m6A regulatory factors play a vital role in RNA splicing, export, stability and translation et (Topalian et al., 2012; Helmy et al., 2013; Chen et al., 2021; Zheng et al., 2021). Recent studies have shown that m6A is associated with glioma (Topalian et al., 2012; Tu et al., 2020; Du et al., 2021), but its specific roles and mechanisms are still unknown.

In recent years, several studies have revealed that the TME is associated with m6A. It has been reported that m6A enhances the anti-cancer response of tumor-infiltrating CD8+ T cells, improves the therapeutic effect of anti-PDL1 receptor blockers (Wood et al., 2014; Wang et al., 2019). In addition, previous studies demonstrated that the abnormal expression of m6A regulators induces tumor proliferation and metastasis (Quail and Joyce, 2013). However, because of technical limitations, most p studies were limited to one or two m6A modulators and cell types, while the anti-tumor effect is characterized by several tumor suppressors interacting in a highly cooperative network. In summary, elucidating the mechanisms underlying TME cell infiltration mediated by multiple m6A regulatory factors will help to our further understanding of TME immune regulation. Furthermore, the potential role of m6A methylation modification in LGG remains unclear. Based on the expression of 21 m6A regulatory factors, this study comprehensively evaluated m6A modification patterns in LGG samples from The Cancer Genome Atlas (TCGA) and Chinese Glioma Genome Atlas (CGGA) databases and compared these results with data from the Affiliated Hospital of YouJiang Medical University for Nationalities (AHYMUN) for verification. Surprisingly, we found that evaluating the m6A modification pattern within a single LGG could predict patient prognosis and tumor progression. We also developed a comprehensive scoring system to quantify the m6A modification pattern in each LGG patient and enable the accurate prediction of specific prognosis and immunotherapy

Abbreviations: AUC, area under the curve; CGGA, Chinese Glioma Genome Atlas; CNV, Copy number variation; DEGs, Differential expressed genes; EMT, epithelial-mesenchymal transitions; GGI, Gene-gene interaction; GSVA, Gene set variation analysis; LGG, low grade glioma; OS, overall survival; ROC, Receiver operating characteristic; ssGSEA, single sample Gene Set Enrichment Analysis; TCGA, the Cancer Genome Atlas; TIDE, tumor immune dysfunction and exclusion; TME, tumor microenvironment.

efficacy. Significantly, we first demonstrated the function of m6A modification in facilitating LGG progression and provides promising target for prognostic or therapeutic prediction of LGG.

MATERIALS AND METHODS

Data

TCGA data: download the mRNA expression profile data and sample CNV (Copy number variation) information of low-grade glioma samples from https://xenabrowser.net/datapages/, clinical information using R package cgdsr, mutation data using R package TCGAbiolinks (Colaprico et al., 2016). In addition, we downloaded the expression profiles of two sets of low-grade glioma samples from http://www.cgga.org.cn/. Specific data information are shown in **Table 1**.

Data Preprocessing

In order to maintain data consistency, we used the Bioconductor -sva 1 package of R software (version 4.0.0) (Chan, 2018) to perform batch correction on low-level glioma transcriptome data downloaded from TCGA and CGGA databases.

Unsupervised Clustering Using 20 m6A Genes

Extract the expressions of 21 regulators from the TCGA and CGGA datasets to identify the different m6A modification patterns mediated by the m6A regulators, of which the expression of *IGF2BP1* is not detected in the CGGA dataset, so the last 20 extracted regulators the expression of the child. The 20 m6A regulatory factors include 8 writers (*METTL3*, *METTL14*, *RBM15*, *RBM15B*, *WTAP*, *KIAA1429*, *CBLL1*, *ZC3H13*), 2 erasers (*ALKBH5*, *FTO*), and 10 readers (*YTHDC1*, *YTHDC2*, *YTHDF1*, *YTHDF2*, *YTHDF3*, *HNRNPA2B1*, *HNRNPC*, *FMR1*, *LRPPRC*, *ELAVL1*). Using unsupervised cluster analysis, according to the expression of 20 m6A regulatory factors, identify different m6A modification patterns, and classify patients for further analysis. A consistent clustering algorithm is used to determine the number of clusters and their stability. We used the ConsensusClusterPlus (Wilkerson and Hayes, 2010) package for the operation. The distance used for clustering is the Euclidean distance, and repeated 1,000 times to ensure the stability of the classification.

TABLE 1 | Sample information form.

Data set	TCGA	CGGA
IDH		
Wild-type	33	144
Mutant	91	439
NA	375	0
Age		
≥60	68	28
<60	431	596
OS.Status		
Deceased	125	291
Living	374	309

Gene Set Variation Analysis and Single Sample Gene Set Enrichment Analysis

In order to study the difference of m6A modification patterns in biological processes, we used R package GSVA to perform GSVA enrichment analysis. GSVA is a non-parametric, unsupervised method that is mainly used to estimate changes in pathways and biological process activity in samples. Download the c2.cp.kegg.v6.2 gene set from the MSigDB database[1] for running GSVA analysis.

In order to evaluate the ratio and difference of 24 immune cells in different m6A regulators cluster, we used ssGSEA (single sample gene set enrichment analysis) analysis in the R package GSVA to obtain the infiltration ratio of 24 immune cells. Then use the Wilcox test to compare the differences between different m6A regulators cluster samples, and perform cox regression analysis on the different cells to compare the prognostic differences.

Identify the Differentially Expressed Genes Between Different m6A Regulators Cluster

Based on the expression of 20 m6A genes, we divided the low-grade gliomas in the TCGA and CGGA databases into two categories, and used the R package limma (Ritchie et al., 2015) to determine the DEGs between different groups. The significance standard for determining the difference gene is set as p-value < 0.05 (after BH correction), and the difference multiple is greater than 2 times or less than 0.5 times.

m6asocre Calculation

For the differential genes obtained in the previous analysis, use the random forest method to remove redundant genes, and then perform survival analysis on the remaining genes, filter out genes that are less related to survival (p-value < 0.05 is considered to be related to survival), and then use cox The regression model divides genes into two categories (coefficient is positive or negative). Refer to the Gene-gene interaction (GGI) score 4 to calculate m6Ascore using the following formula.

$$\text{m6Ascore} = \text{scale}(\sum \text{X} - \sum \text{Y})$$

X is the expression value of the gene set where Cox coefficient is positive, and Y is the expression value of the gene set where Cox coefficient is negative. Using the median of m6Ascore, the samples were then divided into m6Ascore-high and m6Ascore-low, and the correlation between these two types of samples and prognosis was further analyzed.

Correlation Between m6Ascore and Other Biological Processes

Mariathasan et al. (2018) constructed a set of genes to store genes related to certain biological processes, including immune

[1]https://www.gsea-msigdb.org/gsea/index.jsp

checkpoints; antigen processing and presentation; *EMT1*, *EMT2*, *EMT3* and other epithelial-mesenchymal transitions (*EMT*) Markers; DNA damage repair; mismatch repair; nucleotide excision repair and other pathways. We conducted a Pearson correlation analysis on m6Ascore and these biological processes, and further revealed the connection between m6Ascore and some related biological pathways.

Copy Number Variation Analysis

The GISTIC method was used to detect the common copy number change area in all samples based on SNP6 CopyNumber segment data. The parameters of the GISTIC method are set as: Q $\leq$ 0.05 as the change significance standard; when determining the peak interval, the confidence level is 0.95. The analysis is performed by the corresponding MutSigCV module in the online analysis tool GenePattern[2] developed by Broad Research Institute.

[2]https://cloud.genepattern.org/gp/pages/index.jsf

Tumor Immune Dysfunction and Exclusion Forecast and IC50 Estimate

Further, we use the R package pRRophetic to estimate the IC50 value of drugs (Cisplatin, Gemcitabine) based on the expression profile, and compare the differences in IC50 between m6Ascore high and low samples.

Researchers from Harvard developed the TIDE (tumor immune dysfunction and exclusion) tool[3] (Jiang et al., 2018) to evaluate the clinical effects of immune checkpoint suppression therapy, with higher tumor TIDE prediction scores and poorer immune checkpoint suppression the treatment effect is related, and it has a poor prognosis. Because of the five types of tumors with reliable tumor immune dysfunction and rejection characteristics that researchers can calculate, only melanoma has publicly available patient data on anti-PD1 or anti-CTLA4 treatment, so the prognosis of immune

[3]http://tide.dfci.harvard.edu/

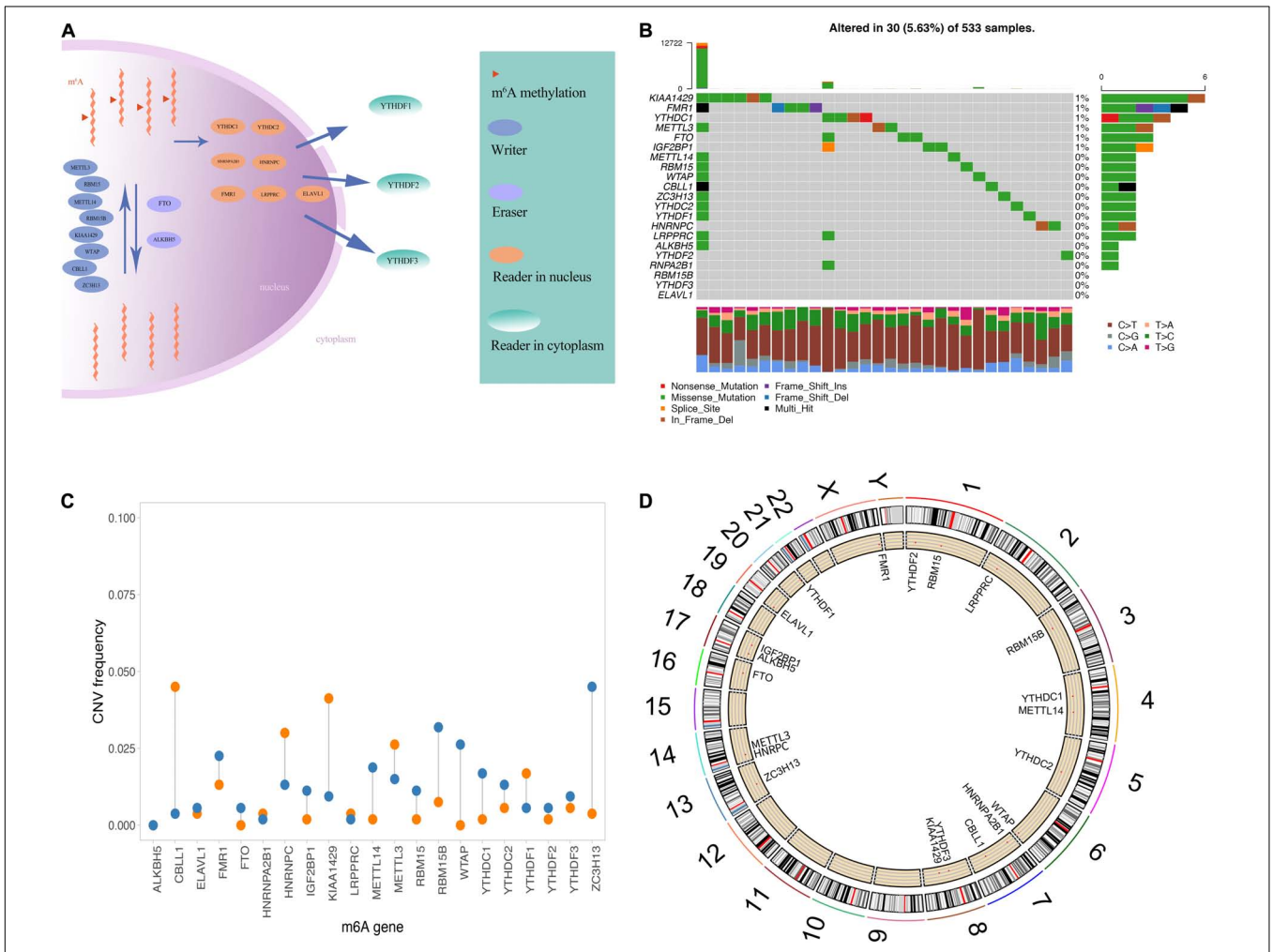


FIGURE 1 | Genetic variation of m6A regulatory factors. **(A)** Summary of the dynamic reversible process of m6A RNA methylation mediated by regulators ("writers," "erasers" and "readers") and their potential biological functions for RNA. **(B)** The distribution of m6A gene mutations and the distribution of different mutation types. **(C)** The frequency of CNV occurrence of m6A gene, blue indicates deletion, orange indicates amplification. **(D)** m6A gene is in Position on chromosome.

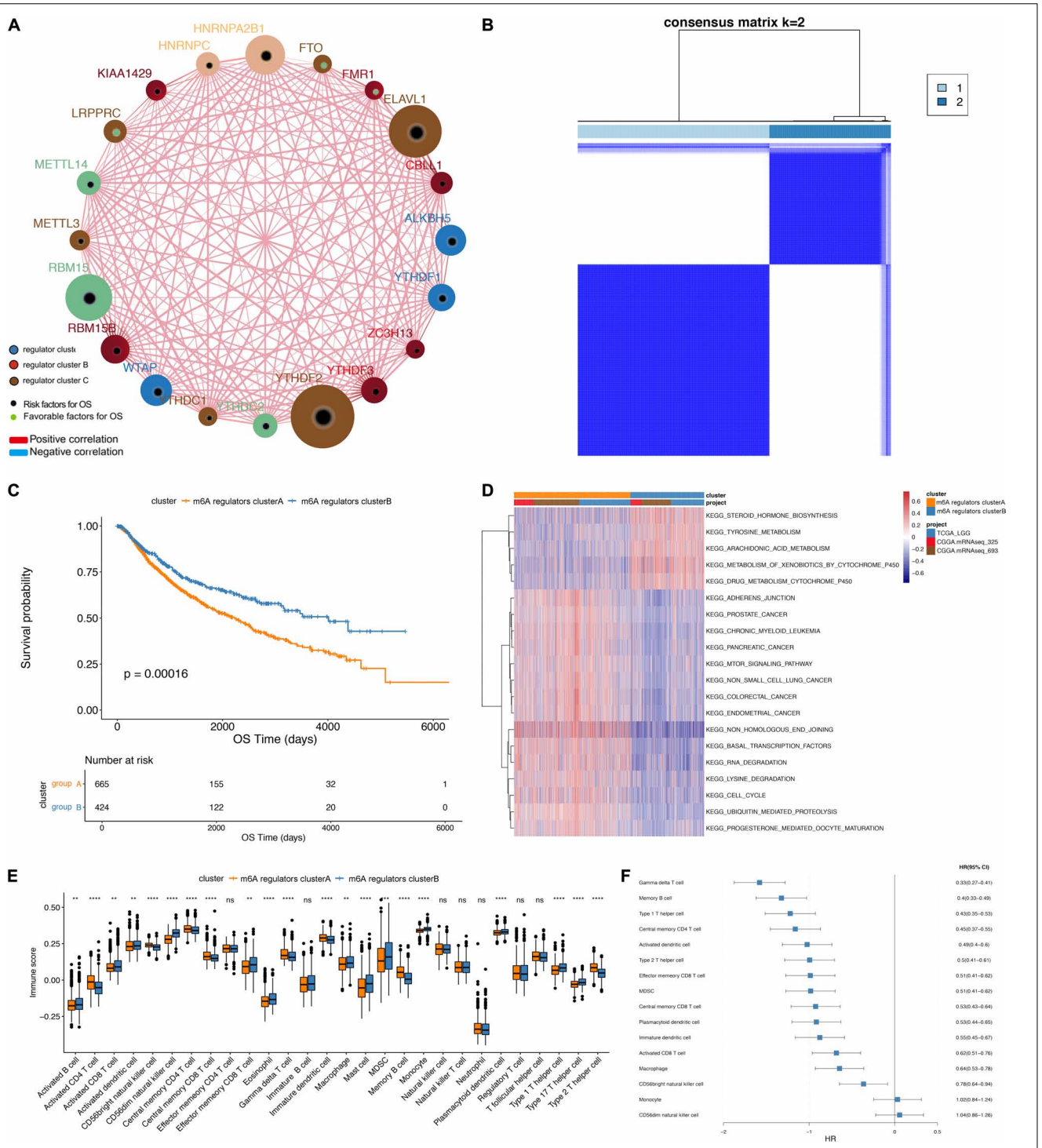


FIGURE 2 | Unsupervised clustering of m6A genes in low-grade glioma samples. **(A)** Interaction between m6A genes. The size of the circle indicates the impact of each gene on survival prediction, and the larger the expression, the more relevant the prognosis. In the circle the green dots in the circle indicate prognostic protective factors, and the black dots in the circle indicate prognostic risk factors. The lines connecting genes show their interactions. The negative correlations are marked in blue and positive correlations in red. Gene clusters ABC are marked in blue, respectively, color, red and brown. **(B)** Consistent clustering of m6A genes. **(C)** Kaplan-Meier curve showing significant survival differences in two m6A regulators clusters. **(D)** GSVA enrichment analysis, showing the biological pathways with different m6A regulators clusters Activation state. Heat map is used to visualize these biological processes, red means activation, blue means inhibition. **(E)** The distribution of immune infiltration of 22 immune cells in 2 m6A regulators clusters (**$p < 0.05$, ****$p < 0.001$). **(F)** Differential cell prognosis analysis.

checkpoint treatment in this analysis the prediction is done using TIDE score.

Statistical Analysis

In the significance analysis between various scores, the Wilcox test was used to compare the differences between the two groups of samples. In the drawing display, ns means $p > 0.05$, * means $p < = 0.05$, **: means $p < = 0.01$, *** means $p < = 0.001$, **** means $p < = 0.0001$. The Kaplan-Meier method was used to generate a survival curve for prognostic analysis, and the log-rank test was used to determine the significance of the difference. Receiver operating characteristic (ROC) curve is used to evaluate m6Ascore's prediction of immunotherapy, and the area under the curve (AUC) is quantified using R package pROC. When displaying mutation maps, use the R package maftools to present the mutation landscape of patients with m6Ascore high subtype and low subtype. The R package RCircos was used to plot the chromosome distribution of 21 m6A regulatory factors in 23 pairs of chromosomes.

RESULTS

Our research was divided into five steps. First, we downloaded three datasets from the TCGA and CCGA databases and performed m6A gene expression, mutation, and CNV analysis based on the collected data. Followed by unsupervised clustering of m6A genes, we performed GSVA enrichment, differential gene expression, mutation profiles, and clinical features analyses. Next, we verified and consistently clustered the m6A-related genes. We then identified characteristic genes through Random Forest and Cox regression analysis. Finally, we established the m6Ascore and identified its relationship with TME characteristics. The flow chart of study process is summarized in **Supplementary Figure 1**.

Genetic Variation in m6A Regulatory Factors of Low-Grade Glioma From the Cancer Genome Atlas and Chinese Glioma Genome Atlas Databases

A total of 21 m6A regulators analyzed in this study included 8 writers, 2 erasers, and 11 readers. Because there was no control sample in the TCGA data, it was not possible to compare the expression of these m6A regulatory factors between LGG and control samples. **Figure 1A** displays the dynamic process of m6A RNA methylation mediated by all known regulators.

In the experiments mentioned above, we observed that the expression of m6A regulatory factors was generally higher in the worse prognosis group. To explore the relationship between these regulatory factors and the prognosis of LGG, we compared TCGA and CGGA samples using the median expression of 20 regulatory factors, which was divided into two groups for Kaplan–Meier analysis (**Supplementary Figure 2**).

Then, we summarized the frequency of the copy number variations and somatic mutations of the 20 m6A regulatory factors in the LGG samples. Only a few mutations in the m6A regulators were observed in these samples, including *KIAA1429, FMR1, YTHDC1, METTL3, FTO, IGF2BO1,* and *METTL14* (**Figure 1B**). The CNV was generally different among the 21 regulatory factors, some of which showed copy number amplification, and the deletion frequency of genes was high, such as *FTO*, *RBM15B*, and *ZC3H13* (**Figure 1C**). In addition, we showed the position of the m6A regulator on the chromosome (**Figure 1D**). Overall, we analyzed genetic background and variation of 21 m6A regulators of LGG.

Unsupervised Clustering of m6A Genes in 1,089 Low-Grade Glioma Samples

As *IGF2BP1* was not expressed in the CGGA data set, we used the gene expression profile data of 20 m6A regulators and the survival data in TCGA and CGGA samples to

TABLE 2 | Proportion of immune cells in LGG.

Immune cells	*p*-value	HR	Low 95%CI	High 95%CI
Activated CD8 T cell	2.42E-06	0.623838	0.512717	0.759042
Activated dendritic cell	4.28E-12	0.49214	0.402692	0.601457
CD56bright natural killer cell	0.011365	0.777254	0.639479	0.944712
CD56dim natural killer cell	0.685581	1.040787	0.857652	1.263026
Central memory CD4 T cell	7.37E-15	0.447318	0.365237	0.547845
Central memory CD8 T cell	3.04E-10	0.527204	0.431959	0.643451
Effector memory CD8 T cell	1.91E-11	0.505114	0.413792	0.61659
Gamma delta T cell	2.82E-25	0.334964	0.272504	0.411739
Immature dendritic cell	2.82E-09	0.545516	0.44667	0.666235
Macrophage	8.03E-06	0.639708	0.525777	0.778326
MDSC	2.36E-11	0.506285	0.41465	0.61817
Memory B cell	1.44E-18	0.399784	0.325899	0.490421
Monocyte	0.814155	1.023477	0.843431	1.241957
Plasmacytoid dendritic cell	3.59E-10	0.530418	0.435062	0.646675
Type 1 T helper cell	3.88E-16	0.42936	0.350297	0.526267
Type 2 T helper cell	1.98E-11	0.502187	0.410632	0.614155

perform m6A gene consistency clustering and m6A gene single factor Cox regression analysis. The m6A regulatory network shown in **Figure 2A** describes the interactions between m6A regulatory factors, showing their correlation and predictive risk for OS. The impact of m6A regulators on the correlation in the interaction and the prognosis of LGG patients were shown in **Supplementary Table 1**. These results suggested that the interactions between m6A regulatory factors of different functional categories play a crucial role in the establishment of m6A modification patterns of LGG. Next, we determined the expression of 20 m6A regulators in LGG samples from the TCGA and CGGA databases and then used the R package

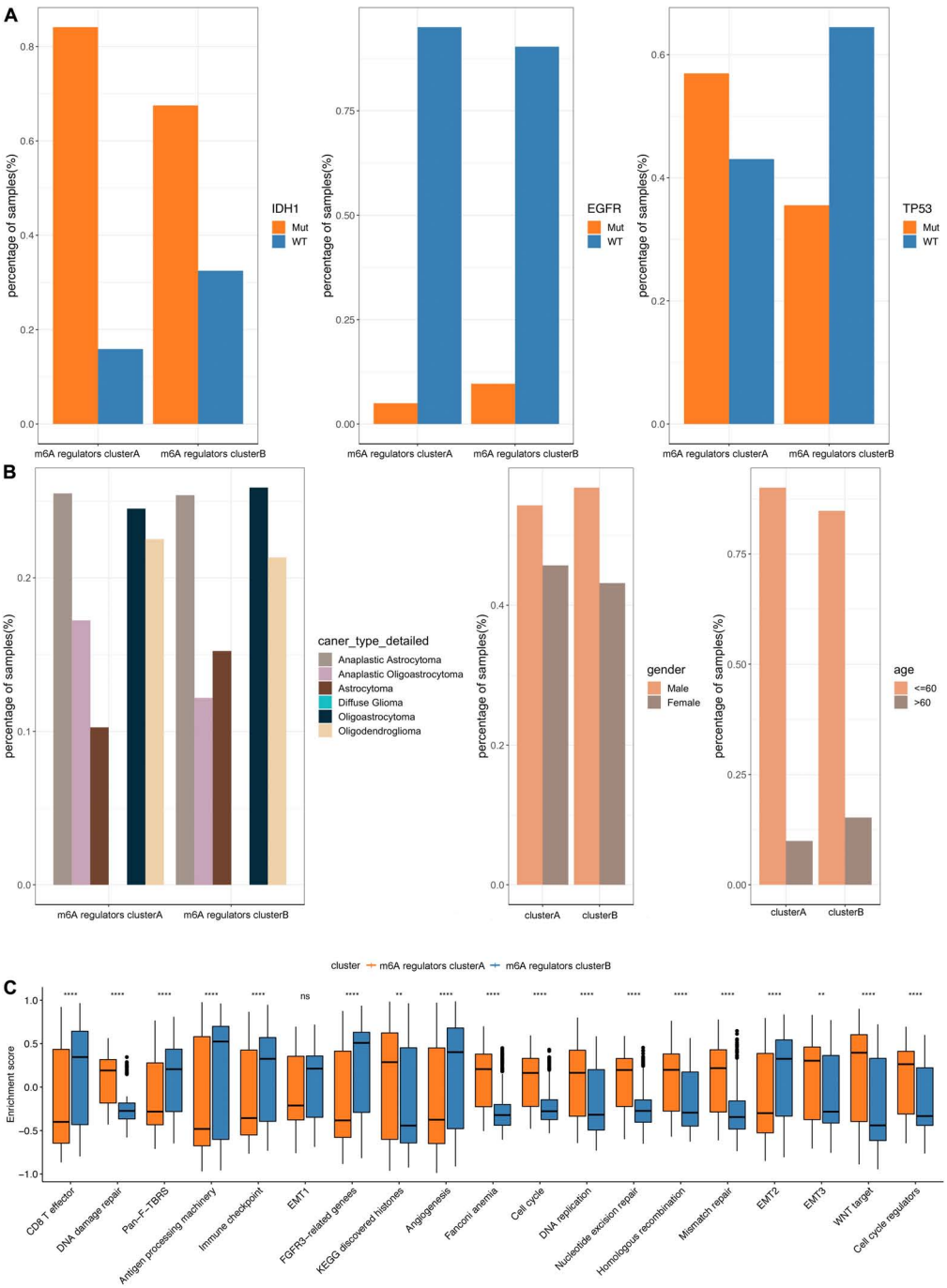


FIGURE 3 | Comparative analysis between m6A 4 regulators cluster in the TCGA dataset. **(A)** The distribution of IDH1, EGFR, TP53 mutations in the 2 m6A regulators clusters. **(B)** The distribution of cancer type, gender, and age in m6A regulators cluster. **(C)** The enrichment scores of different m6A regulators cluster groups difference (**$p < 0.05$, ****$p < 0.001$).

ConsensusClusterPlus to perform consistent clustering. Two significant subgroups, m6A regulators clusterA and m6A regulators clusterB were indicated (**Figure 2B**). Patients in m6A regulators clusterB showed significantly prolonged survival compared with m6A regulators clusterA patients (p = 0.00016, **Figure 2C**).

Functional Annotations and Tumor Microenvironment Infiltration Characterization Between m6A Regulators Clusters

Based on three datasets, we performed GSVA enrichment analysis to explore the differences in the biological behavior of the regulatory factors in two m6A modification subgroup, m6A regulators clusterA and m6A regulators clusterB. As shown in **Figure 2D**, m6A regulators clusterA was significantly enriched in biological processes, such as adhesion junctions, mTOR signaling, basal transcription factors and cancer-specific pathways. Nevertheless, m6A regulators clusterB was significantly enriched in differentiated processes, including steroid hormone biosynthesis, tyrosine metabolism, arachidonic acid metabolism and etc.

Furthermore, we performed ssGSEA analysis to obtain the proportion of immune cells infiltrations, like B memory cells, activated dendritic cells, M0 macrophages (**Figure 2E**). The results revealed significantly different distribution of immune cells abundance in the two subgroups. Next, we depict the results of univariate Cox regression analysis of immune cells with different proportions between the two m6A regulators clusters (**Figure 2F**). Proportion of immune cells infiltrated in different subgroups of LGG were listed in **Table 2**.

In TCGA dataset, we found that the *IDH1* (chi-square test, p = 2.31e-05) and *TP53* (chi-square test, p = 4.47e-06) mutation were significantly more frequently in m6A regulators clusterB, while *EGFR* (chi-square test, p = 0.065) mutation was relatively decreased compared with m6A regulators clusterA subgroup (**Figure 3A**). In terms of clinical characteristics, such as cancer types, gender and age, there was no significant difference in the two subgroups (**Figure 3B**). Subsequently, we performed GSVA analysis, and the enrichment scores in the m6A regulators cluster groups were significantly different (**Figure 3C**). Most m6A regulators were highly expressed in m6A regulators clusterB. Taken together, there are evident distributions of tumor microenvironment infiltration characterization, genetic variation and prognosis between m6A regulators clusters of LGG (**Figure 4**).

Differential Expressed m6A-Related Genes and Constructions of m6Agenecluster

To further study the potential biological behavior of the regulators in m6A regulators clusters, we exploited the "limma" R package and identified m6A phenotype-related DEGs and the clusterProfiler package to perform KEGG

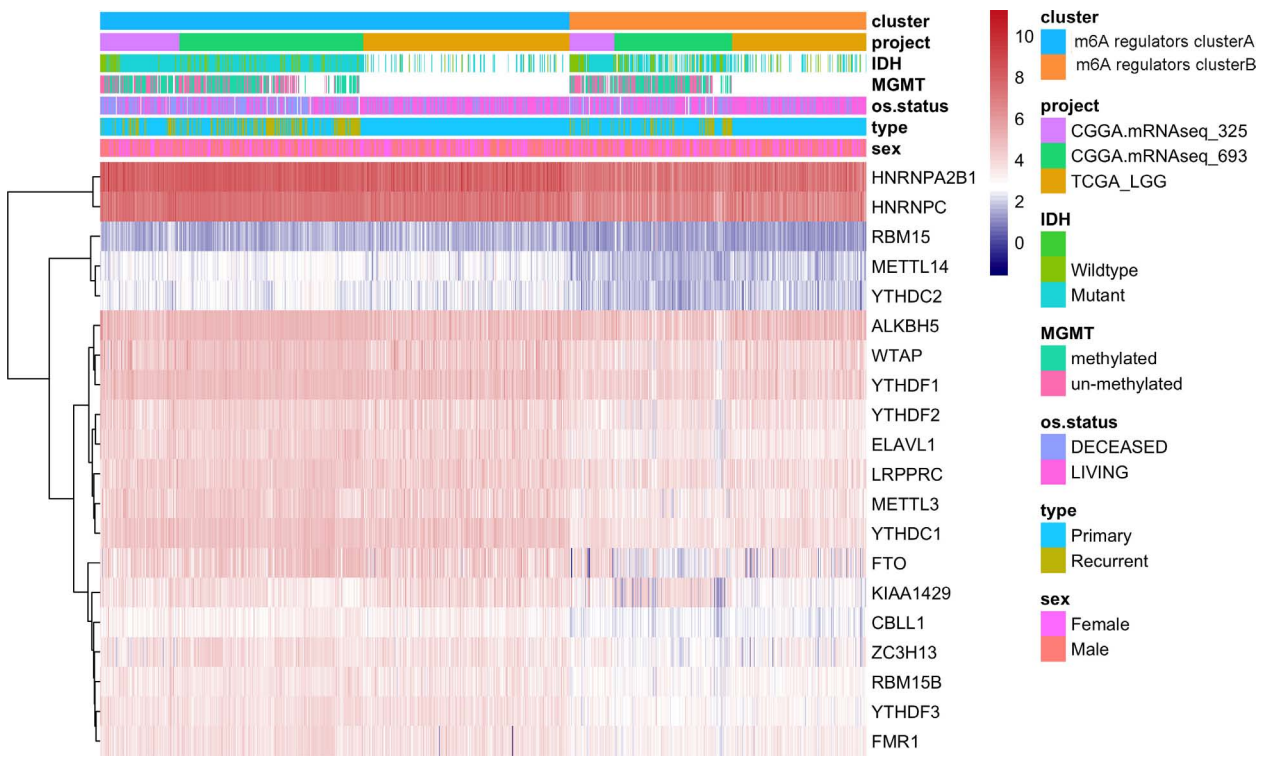


FIGURE 4 | The expression of m6A regulatory factors in m6A regulators cluster.

enrichment analysis on the DEGs. Next, we identified 238 DEGs, which were significantly enriched in the cell cycle pathway. Furthermore, we performed an unsupervised cluster analysis of the obtained m6A phenotype-related genes to group patients according to different genomic subtypes. Then, we obtained two different clusters of m6A-modified genome phenotypes, m6AgeneclusterA and m6AgeneclusterB (**Figure 5A**). It suggested that m6AgeneclusterA subgroup had significantly poor survival in 1,089 LGG patients (**Figure 5B**). In addition, the expression of most m6A regulatory factors in m6AgeneclusterA was significantly higher than that in m6AgeneclusterB (**Figure 5C**).

Establishment of m6Ascore and Its Association With Tumor Microenvironment Characterization in Chinese Glioma Genome Atlas Database

The Random Forest algorithm was used to remove the redundancy in the differentially expressed genes, and the characteristic genes most relevant to the classification were identified. A Cox regression model was then used to determine the relationship between these genes and the survival of LGG patients. Based on the coefficient value of the genes, the genes were divided into two categories, and the m6Ascore was calculated in all samples (**Figure 6A**). Finally, according to the median m6Ascore, the samples were divided into two groups: m6Ascore^{high} and m6Ascore^{low}. As presented in **Figure 6B**, the m6Ascore^{low} group showed significantly better prognosis than m6Ascore^{high} group ($p < 0.0001$), indicating that the calculation based on the m6Ascore provides an accurate characterization of patient prognosis.

The correlation analysis between m6Ascores and known gene features showed that the m6Ascore indicated significantly positive correlation with biological functions, such as DNA damage repair, DNA replication and cell cycle pathways (**Figure 6C** and **Table 3**). Importantly, m6Ascore^{high} subgroup was also highly enriched in immune cells infiltrations (CD8 T effector, immune checkpoint, antigen processing machinery), malignant biologic behaviors (EMT process, angiogenesis, WNT targets) and DNA processing (DNA damage repair, DNA replication, homologous recombination, cell cycle regulators, nucleotide excision repair, mismatch repair) (**Figure 6D**). The Wilcox test showed that m6A regulators clusters and m6Ageneclusters were significantly associated with different m6Ascores (**Figures 6E,F**). The m6Ascores in m6A regulators clusterA and m6AgeneclusterA were significantly higher than other groups.

Furthermore, from the testing TCGA cohort, our analysis revealed that the m6Ascore was significantly different among the classification subgroups (including *IDH1* mutation status, *TP53* mutation status, cancer subtype classification, gender and age) (**Figures 7A,B**). Additionally, the m6Ascore^{high} subgroup predicts significantly decreased outcomes of LGG compared with m6Ascore^{low} subgroup ($p < 0.0001$; **Figure 7C**). Then, we chose the CGGA database and GEO database (GSE107850) to verify the survival prediction ability of m6Ascore. We directly extracted the m6Ascore grouping of each sample from the CGGA database, and then plotted the KM curve. It can be seen that the survival results of patients in the m6Ascorehigh subgroup were significantly lower ($p < 0.0001$; **Figure 7D**). In GSE107850, we selected 195 samples and determined the best classification threshold according to the R function surv_cutpoint (cutoff = 1.233548). Through the KM curve, we found that the

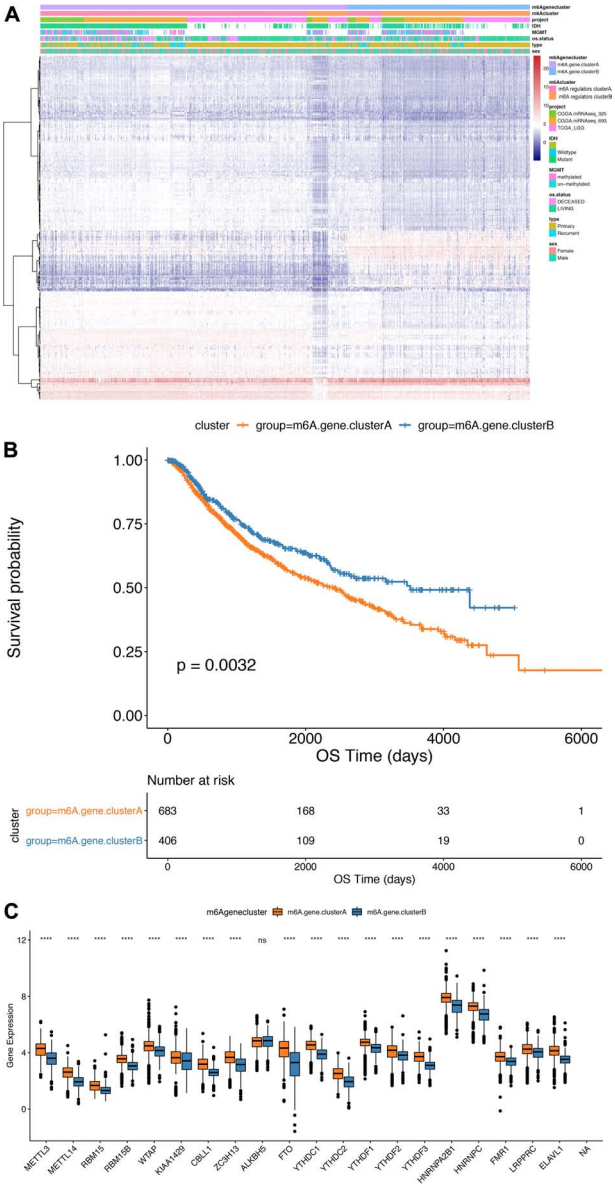


FIGURE 5 | Comparison between m6Agenecluster. **(A)** Unsupervised clustering of m6A phenotype-related genes in low-grade glioma samples. The samples are divided into different genomic subtypes, called m6AgeneclusterA and m6AgeneclusterB. **(B)** Kaplan-Meier curve indicates that m6A modifies the genome table type has an obvious relationship with overall survival rate. **(C)** Expression of 20 m6A genes in 2 gene clusters. The upper and lower ends of the box indicate the interquartile range of values. The line in the box indicates the median value, and the black dots indicate outliers. The *t*-test is used to test the statistical differences between gene clusters (***$p < 0.001$).

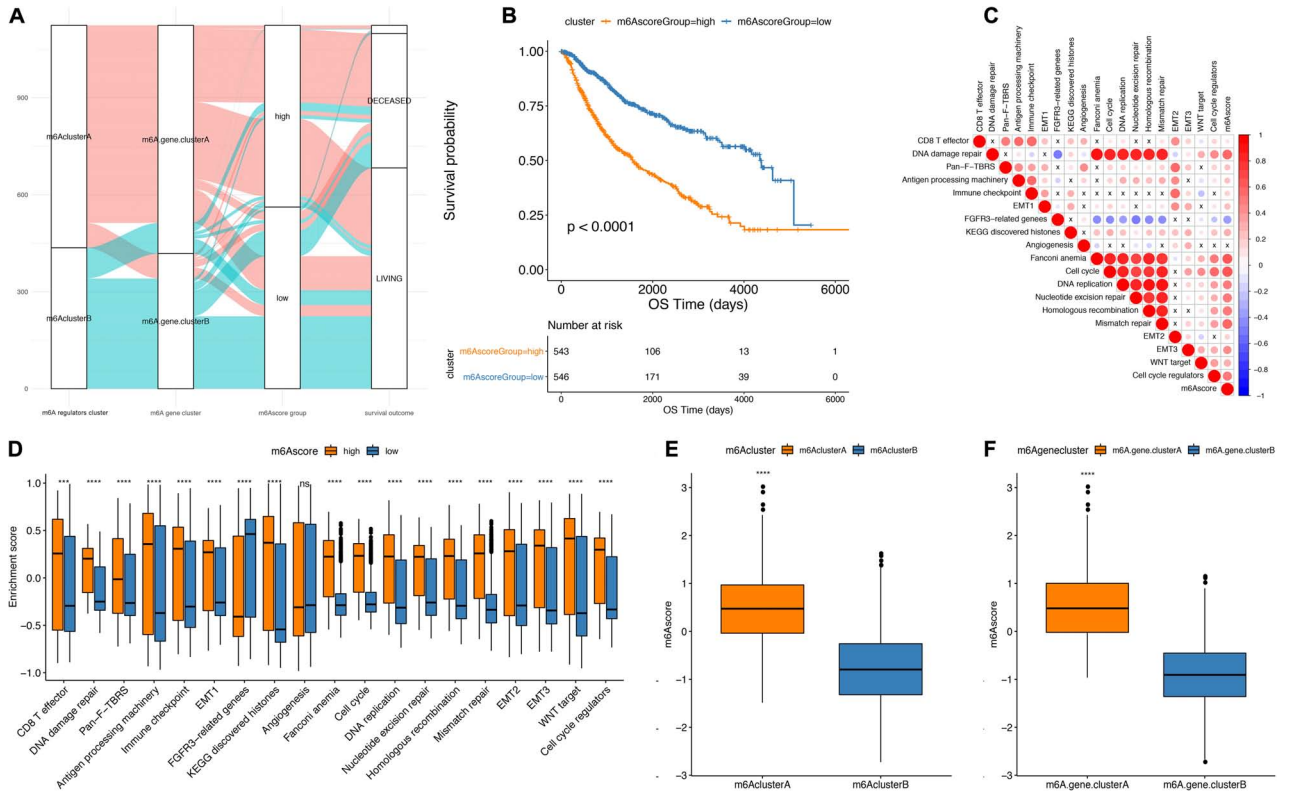


FIGURE 6 | Establishment of m6Ascore. **(A)** Alluvial plot showing the changes of m6A cluster, gene cluster and m6Ascore. **(B)** Kaplan-Meier curve shows that m6Ascore high and low grouping has a significant relationship with overall survival rate. **(C)** Using Pearson analysis, the correlation between m6Ascore and known gene features in low-grade gliomas. Negative correlation is marked in blue, and it is positively correlated with red. X in the figure indicates that the correlation is not significant, and the larger the circle, the more significant. **(D)** The distribution of the enrichment scores of known gene features in the m6Ascore high and low group samples in the TCGA+CGGA data set (***$p < 0.01$, ****$p < 0.001$). **(E)** The distribution of m6Ascore in m6A regulators cluster (****$p < 0.001$). **(F)** Distribution of m6Ascore in m6Agenecluster (****$p < 0.001$).

m6Ascorehigh subgroup predicted a significant decrease in LGG results ($p = 0.00017$; **Figure 7E**).

Differential Molecular Characteristics in m6Ascore^{high} and m6Ascore^{low} Group

Using the TCGA dataset, we further explored the differences between m6Ascore^{high} and m6Ascore^{low} groups. We used "maftools" R package to analyze the differences in somatic mutations between the samples in the m6Ascore^{high} and m6Ascore^{low} groups. As shown in **Figures 8A,B**, there are significant altered frequency of *IDH1* (69% in m6Ascore^{high}, 85% in m6Ascore^{low}), *TP53* (55% in m6Ascore^{high}, 42% in m6Ascore^{low}), *ATRX* (44% in m6Ascore^{high}, 32% in m6Ascore^{low}), CIC (12% in m6Ascore^{high}, 29% in m6Ascore^{low}) and FUBP1 (6% in m6Ascore^{high}, 13% in m6Ascore^{low}) genes. **Figures 8C,D** show the distribution of copy number variation regions in LGG samples in the m6Ascore^{high} and m6Ascore^{low} groups. In the m6Ascore^{high} group, the deletion regions of CCNA were mainly located in 4p16.1, 5q11.2, 6p21.32, 17q21.3, and 20p13; in the m6Ascore^{low} group, the deletion regions of CCNA were mainly in 1q21.3, 4p16.1, 5q11.2, 17q21.3, and 20p13.

m6Ascore Predicts Responses to Chemotherapy and Immunotherapy of Low-Grade Glioma

Based on 1,586 Chinese and Western LGG patients from TCGA and CGGA database, we used the "pRRophetic" R package to estimate the IC50 value of chemotherapy drugs (cisplatin and gemcitabine) based on the expression profiles and compared the IC50 values of these agents between m6Ascore^{high} and m6Ascore^{low} groups The results showed that the IC50 values in m6Ascore^{low} group was significantly higher than those in m6Ascore^{high} group, indicating that the m6Ascore^{high} patients exhibited poor prognosis and unfavorable responses to chemotherapies ($p < 2.2e\text{-}16$; **Figures 9A,B**).

Furthermore, Tumor Immune Dysfunction and Rejection (TIDE) scores was calculated to evaluate the clinical effects of immune checkpoint inhibitor therapy in m6Ascore^{high} and m6Ascore^{low} groups based on RNA-seq data. As shown in **Figure 9C**, the TIDE score in m6Ascore^{high} group was significantly higher than m6Ascore^{low} group. In addition, we analyzed the differential expression of immune checkpoint molecules. It suggested that *CD274*, *CXCL19*, and *HAVCR3* expression were significantly increased in m6Ascore^{high}

TABLE 3 | Correlation analysis between m6Ascore and known gene characteristics.

	CD8 T effector	DNA damage repair	Pan-F-TBRS	Antigen processing machinery	Immune checkpoint	EMT1	FGFR3-related genes	KEGG discovered histones	Angiogenesis	Fanconi anemia	Cell cycle	DNA replication	Nucleotide excision repair	Homologous recombination	Mismatch repair	EMT2	EMT3	WNT target	Cell cycle regulators	m6Ascore
CD8 T effector	1	−0.06623	0.494146	0.536072	0.598255	0.245074	0.029818	0.240562	0.269904	0.002989	0.082286	0.124355	0.016115	0.063399	0.112345	0.43682	0.199802	−0.11137	0.15242	0.10087
DNA damage repair	−0.06623	1	0.024836	0.116577	−0.13442	0.011223	−0.47825	0.146823	−0.12574	0.878726	0.813629	0.824877	0.836755	0.820814	0.820688	−0.16487	0.126626	0.309855	0.441637	0.584229
Pan-F-TBRS	0.494146	0.024836	1	0.438899	0.34292	0.28936	−0.05985	0.132219	0.406115	0.066112	0.196143	0.173792	0.092248	0.129053	0.174611	0.549272	0.224397	−0.01538	0.184433	0.212418
Antigen processing machinery	0.536072	0.116577	0.438899	1	0.541629	0.187812	−0.16389	0.072601	0.167215	0.064941	0.178006	0.281397	0.277245	0.247106	0.274653	0.415263	0.053926	−0.13306	0.125629	0.203783
Immune checkpoint	0.598255	−0.13442	0.34292	0.541629	1	0.356499	−0.02195	0.269656	0.068756	−0.07124	−0.04095	0.043847	0.022381	0.054325	0.058231	0.572692	0.142592	−0.24812	0.065915	0.176486
EMT1	0.245074	0.011223	0.28936	0.187812	0.356499	1	−0.08486	0.315416	0.016401	0.093048	0.15701	0.110437	0.065016	0.118769	0.119983	0.411339	0.327001	−0.02501	0.108318	0.23616
FGFR3-related genes	0.029818	−0.47825	−0.05985	−0.16389	−0.02195	−0.08486	1	−0.03991	0.132106	−0.41741	−0.40019	−0.37222	−0.48137	−0.43936	−0.40138	0.02771	0.006555	−0.09827	−0.21446	−0.39919
KEGG discovered histones	0.240562	0.146823	0.132219	0.072601	0.269656	0.315416	−0.03991	1	−0.06394	0.250681	0.292092	0.241739	0.119934	0.21112	0.255154	0.262104	0.280397	0.079615	0.237842	0.320571
Angiogenesis	0.269904	−0.12574	0.406115	0.167215	0.068756	0.016401	0.132106	−0.06394	1	−0.14645	−0.01328	−0.05129	−0.11277	−0.15947	−0.07124	0.17815	0.284032	0.036217	0.041066	−0.03072
Fanconi anemia	0.002989	0.878726	0.066112	0.064941	−0.07124	0.093048	−0.41741	0.250681	−0.14645	1	0.833289	0.803697	0.708281	0.847198	0.793349	−0.10502	0.182189	0.282467	0.481197	0.61288
Cell cycle	0.082286	0.813629	0.196143	0.175006	−0.04095	0.15701	−0.40019	0.292092	−0.01328	0.833289	1	0.821026	0.719566	0.751727	0.824546	0.004818	0.339261	0.404269	0.545496	0.660695
DNA replication	0.124355	0.824877	0.173792	0.281397	0.043847	0.110437	−0.37222	0.241739	−0.05129	0.803697	0.821026	1	0.839333	0.869693	0.915835	0.000474	0.168178	0.170521	0.345734	0.481268
Nucleotide excision repair	0.016115	0.836755	0.092248	0.277245	0.022381	0.065016	−0.48137	0.119934	−0.11277	0.708281	0.719566	0.839333	1	0.799102	0.852096	0.00519	0.100386	0.145031	0.294501	0.518847
Homologous recombination	0.063399	0.820814	0.129053	0.247106	0.054325	0.118769	−0.43936	0.21112	−0.15947	0.847198	0.751727	0.869693	0.799102	1	0.84498	0.022523	0.072592	0.123744	0.352855	0.533086
Mismatch repair	0.112345	0.820688	0.174611	0.274653	0.058231	0.119983	−0.40138	0.255154	−0.07124	0.793349	0.824546	0.915835	0.852096	0.84498	1	0.046523	0.196592	0.158169	0.384789	0.595633
EMT2	0.43682	−0.16487	0.549272	0.415263	0.411339	0.02771	0.262104	0.17815	−0.10502	0.000474	0.004818	0.000474	0.00519	0.022523	0.046523	1	0.155017	−0.16645	0.035051	0.174384
EMT3	0.199802	0.126626	0.224397	0.053926	0.142592	0.327001	0.006555	0.280397	0.284032	0.182189	0.339261	0.168178	0.100386	0.072592	0.196592	0.155017	1	0.315586	0.322768	0.408854
WNT target	−0.11137	0.309855	−0.01538	−0.13306	−0.24812	−0.02501	−0.09827	0.079615	0.036217	0.282467	0.404269	0.170521	0.145031	0.123744	0.158169	−0.16645	0.315586	1	0.386595	0.329243
Cell cycle regulators	0.15242	0.441637	0.184433	0.125629	0.065915	0.108318	−0.21446	0.237842	0.041086	0.481197	0.545496	0.345734	0.294501	0.352855	0.384789	0.035051	0.322768	0.386595	1	0.512414
m6Ascore	0.10087	0.584229	0.212418	0.203783	0.176486	0.23616	−0.39919	0.320571	−0.03072	0.61288	0.660695	0.481268	0.518847	0.533086	0.595633	0.174384	0.408854	0.329243	0.512414	1

compared with m6Ascore^{low} group ($p < 0.01$; **Figures 9D–F**). Overall, m6Ascore^{high} brings unfavorable responses for LGG patients received chemotherapies, but preferable responses for LGG patients received immunotherapy, suggesting the determined role of m6Ascore in effective treatment selection.

Validation of m6A Regulators and Prognostic Role of YTHDF2 in a Real-World Cohort

To further confirm the reliability and prognostic value of m6A-related genes, we selected six m6A regulators, including *ELAVL1*, *YTHDF2*, *RBM15*, *HNRNPA2B1*, *ALKBH5A*, and *RBM15B*, that exhibited the greatest effect on prognosis of LGG. Using immunohistochemistry, we detected protein expression of these genes in normal tissues and tumor tissues. The results showed that ELAVL1, YTHDF2, RBM15, HNRNPA2B1, ALKBH5A, and RBM15B expression was significantly upregulated in tumor tissues compared with normal tissues ($p < 0.05$; **Figure 10**).

DISCUSSION

In the past decade, new concepts for the treatment of LGG have emerged, including molecular and genotypic diagnosis, neuroplasticity, function-guided resection and supra-frontal resection (Duffau, 2005; Louis et al., 2016). These ideas have helped improve our understanding of the biological behavior of LGG. However, an important issue that remains to be addressed is that there is no accurate biomarker that can predict the prognosis and deterioration of LGG, which prevents the personalized treatment of these patients (Liu et al., 2020, 2021).

Traditionally, tumor metastasis and invasion were thought to be primarily mediated by genetic and epigenetic variations in tumor cells. Recent research shows that the microenvironment and purity of tumor cells also play a vital role in cancer development (Zhang et al., 2017). Therefore, by comprehensively analyzing the heterogeneity and complexity of the TME, it is possible to identify tumor immunophenotypes, accurate biomarkers, and novel therapeutic targets, thereby improving the ability to predict immunotherapy responses (Yoshihara et al., 2013; Rhee et al., 2018).

As an emerging research direction in oncology, the roles and mechanisms of m6A modification have been investigated by many researchers. Current research suggests that the aberrant expression of m6A regulatory factors is associated with several tumor-related processes, including abnormal cell death, abnormal proliferation, impaired development, tumor invasion, tumor deterioration and immune regulation dysfunction (Han et al., 2019; Wang H. et al., 2019; Zhang et al., 2020). There is an endless stream of research on the role of m6A in gliomas. The latest research combines LGG and GBM to study, and selects genes related to m6A for analysis. The study found that PDPN and TIMP1 can be used as prognostic factors for glioma. Potential biomarkers (Lin et al., 2020). In previous studies, we found that although LGG and GBM are both gliomas, their key markers and TME are not the same. Therefore, in this study,

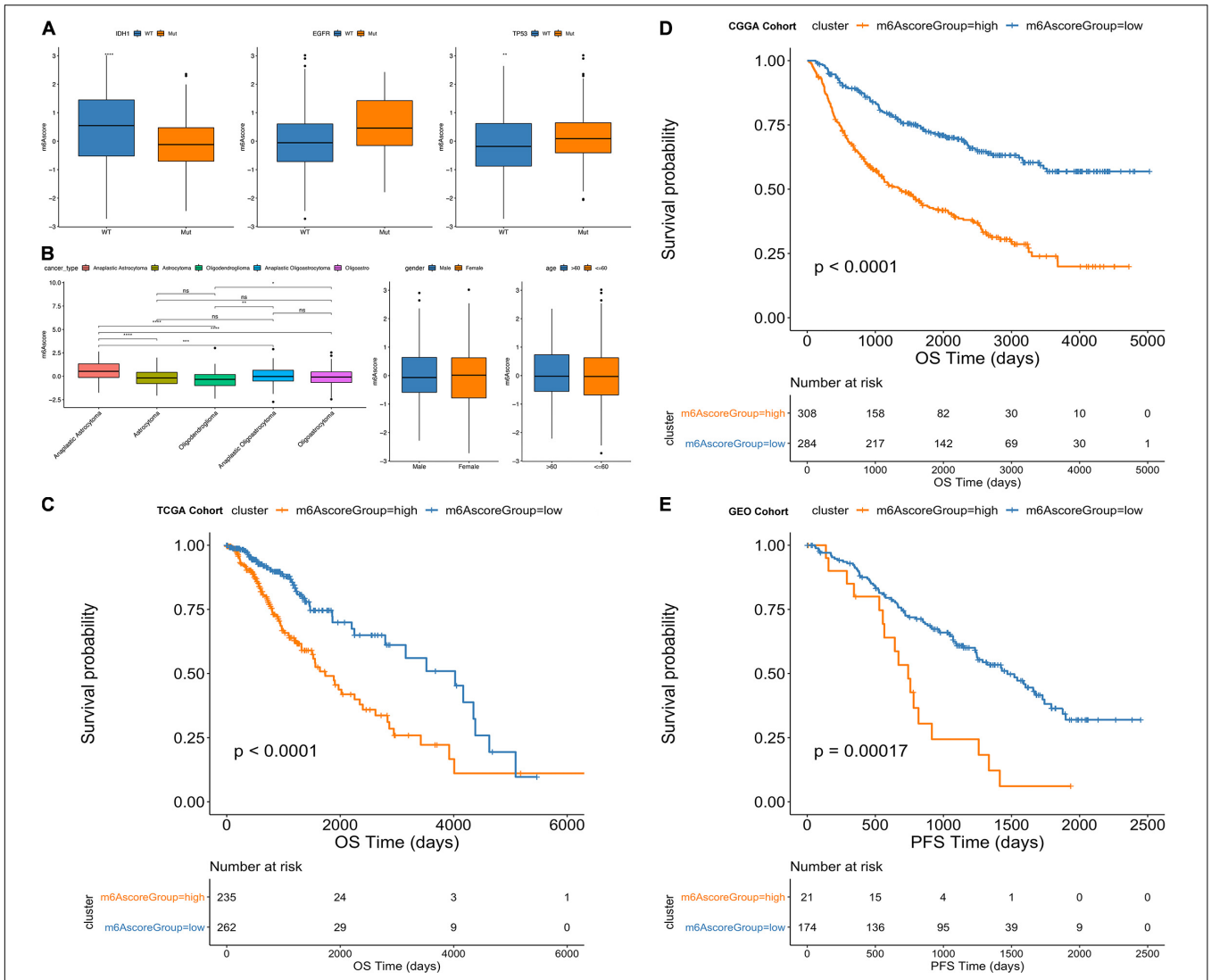


FIGURE 7 | Comparative analysis and model verification of m6Ascore in TCGA dataset. **(A–D)** Distribution of m6Ascore in different classification subgroups. **(A)** IDH1, EGFR, TP53. **(B)** Cancer type. **(C)** Gender. **(D)** Age. **(E)** Difference in survival between m6Ascore high and low groups in the TCGA samples. ($p < 0.0001$).

we only chose LGG for analysis. The analysis of GBM will be discussed in the next study. We have also innovatively established m6Ascore to predict the prognosis of LGG patients and the effect of immunotherapy. It is not a single biomarker. This has played a guiding role in revealing the cause of LGG and finding new personalized treatment methods.

Increasing evidence shows that the TME plays an important role in tumor invasion and metastasis. Previous studies have found that the TME-mediated regulation of tumor purity plays a key role in glioma (Fang and Declerck, 2013). Recent research suggests that m6A plays an indispensable role in inflammation, immune environment composition, and tumor progression by interacting with regulatory factors. However, most previous studies analyzed the effect of a single protein on the TME or performed a simple functional analysis of m6A. The investigation of the role of m6A in LGG is even less reported. Therefore, determining the effects of various m6A modification modes on the TME in LGG can improve our understanding of the TME anti-LGG immune response, identify more effective immunotherapy strategies, and lay the foundation for the personalized treatment of LGG patients.

Based on the expression of 21 m6A regulatory factors, we comprehensively evaluated the m6A modification pattern in LGG samples from the TCGA. The expression profiles of 20 m6A genes in LGG samples (no *IGF2BP1* gene expression in the CGGA data) were consistently clustered to obtain m6A regulators clusterA and m6A regulators clusterB. Subsequent analysis of the differences between these groups was performed to obtain m6A-related genes, and then consistent clustering was conducted to obtain m6AgeneclusterA and m6AgeneclusterB. Subsequently, the Random Forest algorithm was used to reduce dimensionality, and Cox regression analysis was performed to identify characteristic genes. We showed that evaluating m6A modification patterns within a single tumor could predict

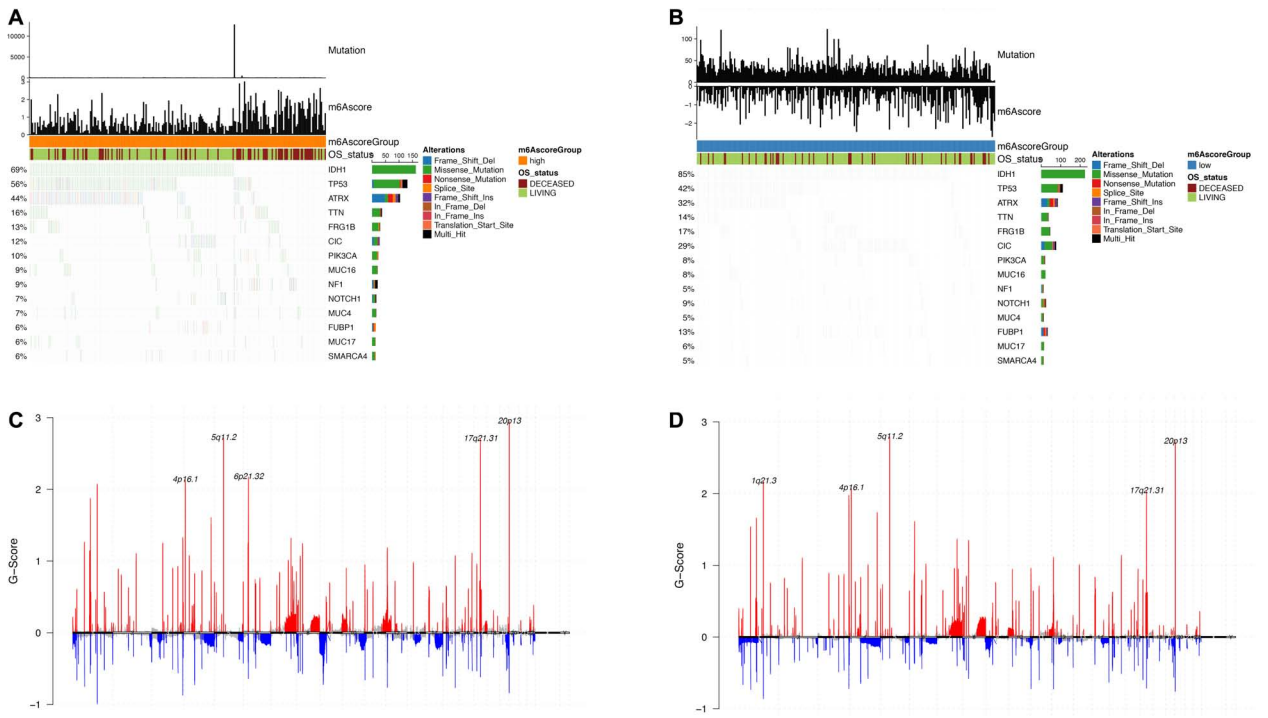


FIGURE 8 | Analysis of molecular characteristics of m6Ascore high and low groups. **(A,B)** Distribution of gene mutations in samples of m6Ascore high and low groups; **(C,D)** The distribution of copy number amplification and deletion regions in the sample set of m6Ascore high and low groups.

patient prognosis and tumor metastasis. The two clusters were dramatically enriched in different biological processes, specifically cancer-related pathways. We found that m6A regulators clusterA showed a significant immune carcinogenic status, including antigen processing pathways, CD8 T effectors, and immune checkpoints. Based on the infiltration characteristics of TME cells in each m6A regulators cluster, we confirmed that our immunophenotypic classification for different m6A modification patterns correct. Most genes and m6A regulatory factors were overexpressed in m6A regulators clusterA, and the prognosis of m6A regulators clusterA was poor.

Considering that the m6A modification pattern of each patient is unique, we need to quantify the m6A modification mode to enable individualized treatment. To achieve this, we developed an m6A scoring system to analyze the m6A modification pattern in each LGG patient. In our study, we found that the m6Ascores in m6A regulators clusterA and m6AgeneclusterA were significantly higher than those in the other groups, indicating that the m6Ascore can also reflect the TME in the patient. We also observed that the m6Ascore was significantly positively correlated with biological functions, such as DNA replication and cell cycle. Moreover, the m6Ascore exhibited significantly different among various groups of LGG samples depending on *IDH1* mutation, *TP53* mutation status or other LGG subtypes and showed significant association with the prognosis of LGG (Lehrer et al., 2019; Qi et al., 2020), suggesting that the m6Acore is a reliable and valuable tool for comprehensively evaluating the m6A modification pattern in single LGGs, and can be used to conduct a detailed analysis of the LGG immunophenotype in each patient, including the TME status and immune infiltration pattern. Our comprehensive analysis also showed that the m6Acore is an independent prognostic biomarker for LGG. Furthermore, our m6Acore showed a predictive advantage in LGG immunotherapy.

In our study, we found that m6A modification is related to DNA damage repair and DNA replication. Previous studies reported that DNA damage is closely related to autoimmune disorders that trigger inflammatory immune responses. We also found that the m6A modification pattern can affect the components of the LGG TME, such as CD8 T effector cells, or block immune checkpoints to increase treatment resistance (Weenink et al., 2019). Furthermore, a high m6Ascore will promote LGG invasion and infiltration because it may indicate that patients' angiogenesis, cell cycle changes will aggravate. These factors will likely affect precision immunotherapy in LGG patients. We also found that the m6A modification pattern can shape a variety of substrates and greatly affect the immune TME landscape of LGG. This indicates that m6A modification has an impact on the therapeutic effect of immune checkpoint blockade, highlighting its potential as a new target for immunotherapy. We also confirmed that patients with a high m6Ascore show increased drug resistance to immunotherapy, which may contribute to the variable treatment effects of temozolomide, a classic chemotherapy drug, in different patients. When we evaluated the effect of the TIDE score, the TIDE score in the high m6Ascore group was also higher, indicating that a decreased efficacy of immune checkpoint therapy was associated

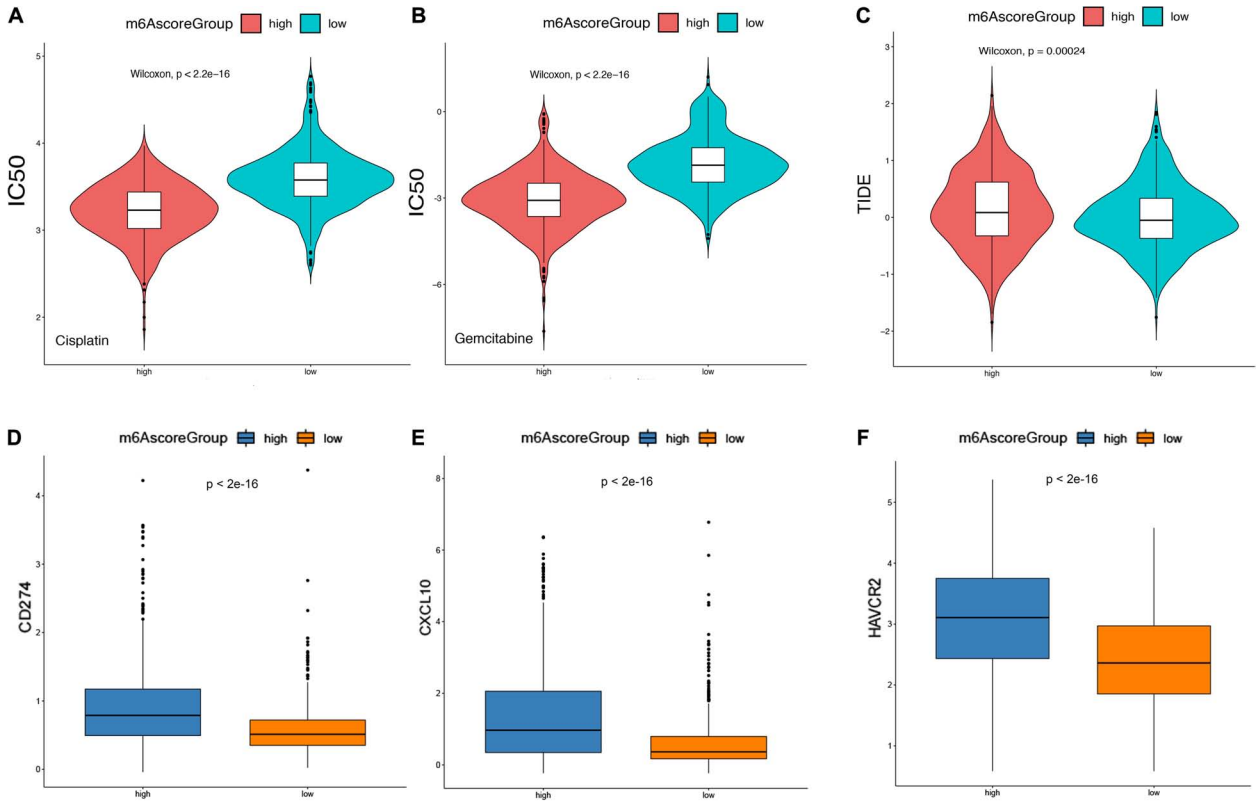


FIGURE 9 | m6Ascore provided predictive outcomes for LGG patients receiving immunotherapies. **(A,B)** The difference between the IC50 values of Cisplatin and Gemcitabine in the samples of the high-risk group and the low-risk group. **(C)** The difference of TIDE score between samples of high-risk group and low-risk group. **(D–F)** Analysis of the degree of correlation between the TIDE score in multiple cohorts and the differential expression of immune checkpoint molecules. **(D)** CD274, **(E)** CXCL10, **(F)** HAVCR2.

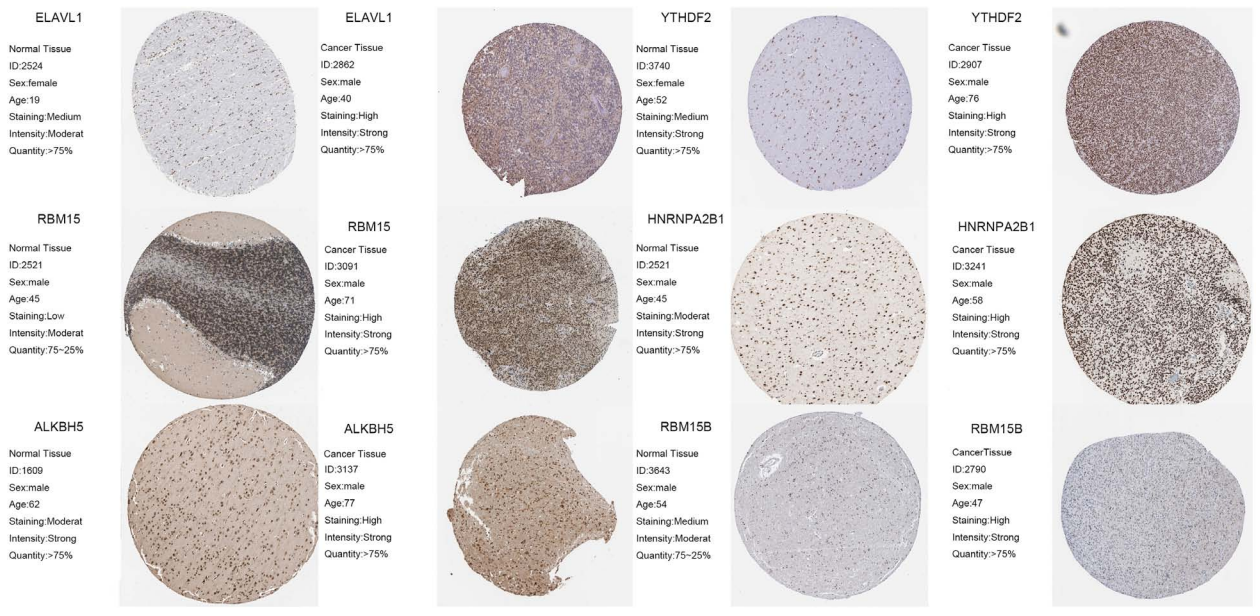


FIGURE 10 | The protein expression of m6A-related genes in normal tissues and tumor tissues.

with a lower survival rate of patients treated with anti-PD1 and anti-CTLA4 therapy.

CONCLUSION

In conclusion, this study first demonstrated that m6A modification plays an important role in tumorigenesis and TME infiltration characterization of LGG based on large-scale cohorts. The m6Ascore could accurately predict prognosis and clinical responses to chemotherapy and immunotherapy for LGG patients, which provides novel insights and directions for exploring underlying pathogenesis and identifying novel targets for the treatment of LGG patients.

DATA AVAILABILITY STATEMENT

The datasets presented in this study can be found in online repositories. The names of the repository/repositories and accession number(s) can be found in the article/ **Supplementary Material**.

AUTHOR CONTRIBUTIONS

The work presented here was carried out with the collaboration of all authors. SZ and JW defined the research topic and discussed the analyses and their interpretation, and presentation. WL, HZ, and HH developed the algorithm, found clinicopathological data, and performed the statistical analyses. WL and WX drafted the manuscript, recorded the clinical data, and interpreted the results. CL, YW, and SC participated in reviewing all clinical records and performed the associated data collection. All authors read and approved the final manuscript.

FUNDING

This study was supported by the Medical Engineering Cross Fund of Shanghai Jiaotong University (No. YG2021QN50), the National Natural Science Foundation of China (No. 82103520), 2020 Guangxi Zhuang Autonomous Region Health Committee self-funded scientific research project (contract no. Z20201157, project no. 20201558), in 2020, the general project of high-level talent scientific research project of the Affiliated Hospital of Youjiang Medical College for Nationalities (the young and middle-aged backbone talent project) (contract no. Y202011702), 2021 Guangxi University's young and middle-aged teachers' basic research ability improvement project (project no. 2021KY0542), and the self-financing project of Guangxi Medicine and Health (project no. Z20180200).

ACKNOWLEDGMENTS

We thank Melissa Crawford, Ph.D., from Liwen Bianji, Edanz Editing China (www.liwenbianji.cn/ac), for editing the English text of a draft of this manuscript.

SUPPLEMENTARY MATERIAL

The Supplementary Material for this article can be found online at: https://www.frontiersin.org/articles/10.3389/fcell.2021.725764/full#supplementary-material

Supplementary Figure 1 | The flowchart of our research.

Supplementary Figure 2 | The relationship between m6A regulators and the prognosis of LGG.

REFERENCES

Alarcón, C. R., Lee, H., Goodarzi, H., Halberg, N., and Tavazoie, S. F. (2015). N6-methyladenosine marks primary microRNAs for processing. *Nature* 519, 482–485. doi: 10.1038/nature14281

Chan, B. K. C. (2018). Data analysis using R programming. *Adv. Exp. Med. Biol.* 1082, 47–122.

Chen, K., Song, B., Tang, Y., Wei, Z., Xu, Q., Su, J., et al. (2021). RMDisease: a database of genetic variants that affect RNA modifications, with implications for epitranscriptome pathogenesis. *Nucleic Acids Res.* 49, D1396–D1404. doi: 10.1093/nar/gkaa790

Colaprico, A., Silva, T. C., Olsen, C., Garofano, L., Cava, C., Garolini, D., et al. (2016). TCGAbiolinks: an R/Bioconductor package for integrative analysis of TCGA data. *Nucleic Acids Res.* 44:e71. doi: 10.1093/nar/gkv1507

Cui, Q., Shi, H., Ye, P., Li, L., Qu, Q., Sun, G., et al. (2017). m(6)A RNA methylation regulates the self-renewal and tumorigenesis of glioblastoma stem cells. *Cell Rep.* 18, 2622–2634. doi: 10.1016/j.celrep.2017.02.059

Du, J., Ji, H., Ma, S., Jin, J., Mi, S., Hou, K., et al. (2021). m6A regulator-mediated methylation modification patterns and characteristics of immunity and stemness in low-grade glioma. *Brief Bioinform.* 22:bbab013. doi: 10.1093/bib/bbab013

Duffau, H. (2005). Lessons from brain mapping in surgery for low-grade glioma: insights into associations between tumour and brain plasticity. *Lancet Neurol.* 4, 476–486. doi: 10.1016/S1474-4422(05)70140-X

Duffau, H. (2007). Contribution of cortical and subcortical electrostimulation in brain glioma surgery: methodological and functional considerations. *Neurophysiol. Clin.* 37, 373–382. doi: 10.1016/j.neucli.2007.09.003

Duffau, H., and Taillandier, L. (2015). New concepts in the management of diffuse low-grade glioma: proposal of a multistage and individualized therapeutic approach. *Neuro Oncol.* 17, 332–342. doi: 10.1093/neuonc/nou153

Dunin-Horkawicz, S., Czerwoniec, A., Gajda, M. J., Feder, M., Grosjean, H., and Bujnicki, J. M. (2006). MODOMICS: a database of RNA modification pathways. *Nucleic Acids Res.* 34, D145–D149.

Fang, H., and Declerck, Y. A. (2013). Targeting the tumor microenvironment: from understanding pathways to effective clinical trials. *Cancer Res.* 73, 4965–4977.

Granier, C., Karaki, S., Roussel, H., Badoual, C., Tran, T., Anson, M., et al. (2016). [Cancer immunotherapy: rational and recent breakthroughs]. *Rev. Med. Interne.* 37, 694–700.

Han, D., Liu, J., Chen, C., Dong, L., Liu, Y., Chang, R., et al. (2019). Anti-tumour immunity controlled through mRNA m(6)A methylation and YTHDF1 in dendritic cells. *Nature* 566, 270–274.

Helmy, K. Y., Patel, S. A., Nahas, G. R., and Rameshwar, P. (2013). Cancer immunotherapy: accomplishments to date and future promise. *Ther. Deliv.* 4, 1307–1320. doi: 10.4155/tde.13.88

Jiang, P., Gu, S., Pan, D., Fu, J., Sahu, A., Hu, X., et al. (2018). Signatures of T cell dysfunction and exclusion predict cancer immunotherapy response. *Nat. Med.* 24, 1550–1558.

Lehrer, S., Rheinstein, P. H., Green, S., and Rosenzweig, K. E. (2019). von Willebrand factor gene expression in primary lower grade glioma: mutually co-occurring mutations in von willebrand factor, ATRX, and TP53. *Brain Tumor Res Treat* 7, 33–38. doi: 10.14791/btrt.2019.7.e20

Lin, S., Xu, H., Zhang, A., Ni, Y., Xu, Y., Meng, T., et al. (2020). Prognosis analysis and validation of m(6)A signature and tumor immune microenvironment in glioma. *Front. Oncol.* 10:541401. doi: 10.3389/fonc.2020.541401

Liu, W. R., Li, C. Y., Xu, W. H., Liu, X. J., Tang, H. D., and Huang, H. N. (2020). Genome-wide analyses of the prognosis-related mRNA alternative splicing landscape and novel splicing factors based on large-scale low grade glioma cohort. *Aging (Albany NY)* 12, 13684–13700. doi: 10.18632/aging.103491

Liu, W., Xu, W., Li, C., Xu, J., Huang, K., Hu, R., et al. (2021). Network pharmacological systems study of Huang-Lian-Tang in the treatment of glioblastoma multiforme. *Oncol .Lett.* 21:18. doi: 10.3892/ol.2020.12279

Louis, D. N., Perry, A., Burger, P., Ellison, D. W., Reifenberger, G., von Deimling, A., et al. (2014). International society of neuropathology–haarlem consensus guidelines for nervous system tumor classification and grading. *Brain Pathol.* 24, 429–435. doi: 10.1111/bpa.12171

Louis, D. N., Perry, A., Reifenberger, G., von Deimling, A., Figarella-Branger, D., Cavenee, W. K., et al. (2016). The 2016 World Health Organization classification of tumors of the central nervous system: a summary. *Acta Neuropathol.* 131, 803–820. doi: 10.1007/s00401-016-1545-1

Luo, X., Li, H., Liang, J., Zhao, Q., Xie, Y., Ren, J., et al. (2021). RMVar: an updated database of functional variants involved in RNA modifications. *Nucleic Acids Res.* 49, D1405–D1412. doi: 10.1093/nar/gkaa811

Mariathasan, S., Turley, S. J., Nickles, D., Castiglioni, A., Yuen, K., Wang, Y., et al. (2018). TGFβ attenuates tumour response to PD-L1 blockade by contributing to exclusion of T cells. *Nature* 554, 544–548. doi: 10.1038/nature25501

Martino, J., Taillandier, L., Moritz-Gasser, S., Gatignol, P., and Duffau, H. (2009). Re-operation is a safe and effective therapeutic strategy in recurrent WHO grade II gliomas within eloquent areas. *Acta Neurochir. (Wien)* 151, 427–36;discussion436. doi: 10.1007/s00701-009-0232-6

Patil, D. P., Chen, C. K., Pickering, B. F., Chow, A., Jackson, C., Guttman, M., et al. (2016). m(6)A RNA methylation promotes XIST-mediated transcriptional repression. *Nature* 537, 369–373. doi: 10.1038/nature19342

Pinello, N., Sun, S., and Wong, J. J. (2018). Aberrant expression of enzymes regulating m(6)A mRNA methylation: implication in cancer. *Cancer Biol. Med.* 15, 323–334.

Qi, C., Lei, L., Hu, J., Wang, G., Liu, J., and Ou, S. (2020). Serine incorporator 2 (SERINC2) expression predicts an unfavorable prognosis of low-grade glioma (LGG): evidence from bioinformatics analysis. *J. Mol. Neurosci.* 70, 1521–1532. doi: 10.1007/s12031-020-01620-w

Quail, D. F., and Joyce, J. A. (2013). Microenvironmental regulation of tumor progression and metastasis. *Nat. Med.* 19, 1423–1437. doi: 10.1038/nm.3394

Rhee, J. K., Jung, Y. C., Kim, K. R., Yoo, J., Kim, J., Lee, Y. J., et al. (2018). Impact of Tumor purity on immune gene expression and clustering analyses across multiple cancer types. *Cancer Immunol. Res.* 6, 87–97. doi: 10.1158/2326-6066.CIR-17-0201

Ritchie, M. E., Phipson, B., Wu, D., Hu, Y., Law, C. W., Shi, W., et al. (2015). limma powers differential expression analyses for RNA-sequencing and microarray studies. *Nucleic Acids Res.* 43:e47. doi: 10.1093/nar/gkv007

Rueda, E., Sierra, M., Infante, J., Berciano, J., Vázquez-Barquero, A., Ciordia, R., et al. (2011). [Controversial aspects in WHO grade II gliomas management: review of recent literature]. *Rev. Neurol.* 53, 747–757.

Topalian, S. L., Hodi, F. S., Brahmer, J. R., Gettinger, S. N., Smith, D. C., McDermott, D. F., et al. (2012). Safety, activity, and immune correlates of anti-PD-1 antibody in cancer. *N. Engl. J. Med.* 366, 2443–2454.

Tu, Z., Wu, L., Wang, P., Hu, Q., Tao, C., Li, K., et al. (2020). N6-methylandenosine-related lncRNAs are potential biomarkers for predicting the overall survival of lower-grade glioma patients. *Front. Cell Dev. Biol.* 8:642. doi: 10.3389/fcell.2020.00642

Wang, C. X., Cui, G. S., Liu, X., Xu, K., Wang, M., Zhang, X. X., et al. (2018). METTL3-mediated m6A modification is required for cerebellar development. *PLoS Biol.* 16:e2004880. doi: 10.1371/journal.pbio.2004880

Wang, H., Hu, X., Huang, M., Liu, J., Gu, Y., Ma, L., et al. (2019). Mettl3-mediated mRNA m(6)A methylation promotes dendritic cell activation. *Nat. Commun.* 10:1898. doi: 10.1038/s41467-019-09903-6

Wang, Q., Li, P., and Wu, W. (2019). A systematic analysis of immune genes and overall survival in cancer patients. *BMC Cancer* 19:1225.

Wang, S., Sun, C., Li, J., Zhang, E., Ma, Z., Xu, W., et al. (2017). Roles of RNA methylation by means of N(6)-methyladenosine (m(6)A) in human cancers. *Cancer Lett.* 408, 112–120. doi: 10.1016/j.canlet.2017.08.030

Weenink, B., Draaisma, K., Ooi, H. Z., Kros, J. M., Sillevis Smitt, P. A. E., Debets, R., et al. (2019). Low-grade glioma harbors few CD8 T cells, which is accompanied by decreased expression of chemo-attractants, not immunogenic antigens. *Sci. Rep.* 9:14643. doi: 10.1038/s41598-019-51063-6

Wesseling, P., and Capper, D. (2018). WHO 2016 Classification of gliomas. *Neuropathol. Appl. Neurobiol.* 44, 139–150. doi: 10.1111/nan.12432

Wessels, P. H., Weber, W. E., Raven, G., Ramaekers, F. C., Hopman, A. H., and Twijnstra, A. (2003). Supratentorial grade II astrocytoma: biological features and clinical course. *Lancet Neurol.* 2, 395–403. doi: 10.1016/s1474-4422(03)00434-4

Wilkerson, M. D., and Hayes, D. N. (2010). ConsensusClusterPlus: a class discovery tool with confidence assessments and item tracking. *Bioinformatics* 26, 1572–1573. doi: 10.1093/bioinformatics/btq170

Wood, S. L., Pernemalm, M., Crosbie, P. A., and Whetton, A. D. (2014). The role of the tumor-microenvironment in lung cancer-metastasis and its relationship to potential therapeutic targets. *Cancer Treat. Rev.* 40, 558–566. doi: 10.1016/j.ctrv.2013.10.001

Yoshihara, K., Shahmoradgoli, M., Martínez, E., Vegesna, R., Kim, H., Torres-Garcia, W., et al. (2013). Inferring tumour purity and stromal and immune cell admixture from expression data. *Nat. Commun.* 4:2612.

Zhang, B., Wu, Q., Li, B., Wang, D., Wang, L., and Zhou, Y. L. (2020). m(6)A regulator-mediated methylation modification patterns and tumor microenvironment infiltration characterization in gastric cancer. *Mol. Cancer* 19:53. doi: 10.1186/s12943-020-01170-0

Zhang, C., Cheng, W., Ren, X., Wang, Z., Liu, X., Li, G., et al. (2017). Tumor purity as an underlying key factor in glioma. *Clin. Cancer Res.* 23, 6279–6291. doi: 10.1158/1078-0432.CCR-16-2598

Zhao, B. S., Roundtree, I. A., and He, C. (2017). Post-transcriptional gene regulation by mRNA modifications. *Nat. Rev. Mol. Cell Biol.* 18, 31–42.

Zheng, J., Wang, X., Qiu, Y., Wang, M., Yu, H., Zhou, Z., et al. (2021). Identification of Critical m(6)a rna methylation regulators with prognostic value in lower-grade glioma. *Biomed. Res. Int.* 2021:9959212. doi: 10.1155/2021/9959212

Conflict of Interest: The authors declare that the research was conducted in the absence of any commercial or financial relationships that could be construed as a potential conflict of interest.

Publisher's Note: All claims expressed in this article are solely those of the authors and do not necessarily represent those of their affiliated organizations, or those of the publisher, the editors and the reviewers. Any product that may be evaluated in this article, or claim that may be made by its manufacturer, is not guaranteed or endorsed by the publisher.

Copyright © 2021 Liu, Li, Wu, Xu, Chen, Zhang, Huang, Zhao and Wang. This is an open-access article distributed under the terms of the Creative Commons Attribution License (CC BY). The use, distribution or reproduction in other forums is permitted, provided the original author(s) and the copyright owner(s) are credited and that the original publication in this journal is cited, in accordance with accepted academic practice. No use, distribution or reproduction is permitted which does not comply with these terms.

frontiers in Cell and Developmental Biology

REVIEW
published: 06 December 2021
doi: 10.3389/fcell.2021.772542

The Relationship Between the Network of Non-coding RNAs-Molecular Targets and N6-Methyladenosine Modification in Colorectal Cancer

Senxu Lu[1,2†], *Xiangyu Ding*[1,2†], *Yuanhe Wang*[3†], *Xiaoyun Hu*[1,2], *Tong Sun*[1,2], *Minjie Wei*[1,2,4*], *Xiaobin Wang*[5*] and *Huizhe Wu*[1,2*]

[1]*Department of Pharmacology, School of Pharmacy, China Medical University, Shenyang, China,* [2]*Liaoning Key Laboratory of Molecular Targeted Anti-tumor Drug Development and Evaluation, Liaoning Cancer Immune Peptide Drug Engineering Technology Research Center, Key Laboratory of Precision Diagnosis and Treatment of Gastrointestinal Tumors, Ministry of Education, China Medical University, Shenyang, China,* [3]*Department of Medical Oncology, Cancer Hospital of China Medical University, Shenyang, China,* [4]*Shenyang Kangwei Medical Laboratory Analysis Co. Ltd., Liaoning, China,* [5]*Center of Reproductive Medicine, Shengjing Hospital of China Medical University, Shenyang, China*

Recent accumulating researches implicate that non-coding RNAs (ncRNAs) including microRNA (miRNA), circular RNA (circRNA), and long non-coding RNA (lncRNAs) play crucial roles in colorectal cancer (CRC) initiation and development. Notably, N6-methyladenosine (m^6A) methylation, the critical posttranscriptional modulators, exerts various functions in ncRNA metabolism such as stability and degradation. However, the interaction regulation network among ncRNAs and the interplay with m^6A-related regulators has not been well documented, particularly in CRC. Here, we summarize the interaction networks and sub-networks of ncRNAs in CRC based on a data-driven approach from the publications (IF > 6) in the last quinquennium (2016–2021). Further, we extend the regulatory pattern between the core m^6A regulators and m^6A-related ncRNAs in the context of CRC metastasis and progression. Thus, our review will highlight the clinical potential of ncRNAs and m^6A modifiers as promising biomarkers and therapeutic targets for improving the diagnostic precision and treatment of CRC.

Keywords: long non-coding RNA, micro RNA, interaction network, colorectal cancer, N6-methyladenosine modification

OPEN ACCESS

Edited by:
Huilin Huang,
Sun Yat-sen University Cancer Center (SYSUCC), China

Reviewed by:
Guohui Wan,
Sun Yat-sen University, China
Ying Yang,
Chinese Academy of Sciences, China
Duo Liu,
Harbin Medical University Cancer Hospital, China

***Correspondence:**
Minjie Wei
mjwei@cmu.edu.cn
Xiaobin Wang
1657438092@qq.com
Huizhe Wu
wuhz@cmu.edu.cn

[†]*These authors contributed equally to this work.*

Specialty section:
This article was submitted to Epigenomics and Epigenetics, a section of the journal Frontiers in Cell and Developmental Biology

Received: *08 September 2021*
Accepted: *11 November 2021*
Published: *06 December 2021*

Citation:
Lu S, Ding X, Wang Y, Hu X, Sun T, Wei M, Wang X and Wu H (2021) The Relationship Between the Network of Non-coding RNAs-Molecular Targets and N6-Methyladenosine Modification in Colorectal Cancer. Front. Cell Dev. Biol. 9:772542. doi: 10.3389/fcell.2021.772542

INTRODUCTION

Background

Colorectal cancer (CRC) remains the third most common tumor worldwide with increasing incidence and mortality rates annually. The etiology of CRC is complicated and involves a variety of risk factors such as environmental exposure, genetic alterations as well as a variety of epigenetic modifications based on global molecular biomarkers such as mRNA, microRNA (miRNA), long non-coding RNA (lncRNA), circular RNA (circRNA), etc. Genomic studies show that human ncRNA transcripts that do not encode for proteins account for approximate 98% of the total human transcripts, which consist mainly of lncRNA, miRNA and circRNA, etc.

Among them, lncRNAs are non-coding RNAs longer than 200 nt, which play critical roles in regulating gene expression and chromatin dynamics (Bhan and Mandal, 2015). MiRNAs are ncRNAs with a length of 17–25 nt, which usually recognize the 3′UTR of mRNA and inhibit gene expression (Lee and Dutta, 2009). CircRNAs are single-stranded ncRNAs with a covalent closed loop structure, which play important biological functions by acting as miRNA inhibitors, protein "bait" or by encoding small peptides (Li et al., 2020). Notably, accumulating evidence shows that the dysregulated ncRNAs (such as lncRNAs, microRNAs, circRNAs, etc.) are involved in the pathological process of a variety of tumors such as prostate cancer, breast cancer, hepatic cancer, and CRC. Although several studies show that ncRNAs play critical regulatory roles in CRC by targeting different protein-coding transcripts or other ncRNAs to activate various signal pathways. However, the specific mechanism underlying the functions of ncRNAs in CRC remain unclear.

Accumulating researches show that ncRNAs are abnormally expressed in tissues, cells, exosomes, and blood of CRC patients (Barbagallo et al., 2018). These are identified as oncogenes or tumor suppressors that mediate CRC occurrence, metastasis, and resistance to radiotherapy and chemotherapy (Wang et al., 2017a; Luan et al., 2020; Meng et al., 2020). Although the regulatory mechanism of the biogenesis and function of ncRNAs remain unclear, existing studies show that ncRNAs play essential roles during tumorigenesis and progression through diverse mechanisms including action as miRNA sponges or baits, interaction with RNA binding proteins, translation to functional peptides as well as epigenetic modification mediated mechanisms (Ren et al., 2018a; Ni et al., 2019; Long et al., 2021). Notably, epigenetic modification of ncRNAs is a significant factor in the occurrence and development of CRC. Meanwhile, ncRNAs can also rely on epigenetic modification to regulate the expression of mRNA or ncRNAs and ultimately promote the progression of CRC. Among all epigenetic modifications, m^6A, as a research hotspot in recent years, exerted its critical functions in the progression and development of CRC. Specifically, the m^6A writers (METTL3, METTL14, WTAP, and other writers such as RBM15, VIRMA, CBLL1, ZC3H13) are responsible for "writing" m^6A modification. The m^6A erasers (FTO and ALKBH5) are responsible for "erasing" m^6A modification. Meanwhile, m^6A readers (YTHDC1-2, YTHDF1-3, IGF2BP1-3, HNRNPC and HNRNPA2B1) are responsible for "reading" m^6A modification. The writers, erasers and readers of m^6A modification can collaborate and directly participate in the progression of various types of tumors. In CRC, m^6A modification promotes CRC angiogenesis, metastasis, and chemical resistance by regulating lncRNA stability and degradation, miRNA biogenesis, and circRNA reverse splicing and translation (Dang et al., 2021; Liu et al., 2021; Xu et al., 2021). Recently, publications focused on that m^6A associated was supposed to regulate the expression of ncRNAs (Wu et al., 2019a; Chen et al., 2020a; Yang et al., 2020a). Yang et al. illustrated that knockdown of METTL14 enhanced the expression of long non-coding RNA XIST through YTHDF2 pathway (Yang et al., 2020a). Wu et al. clarified that m^6A-induced lncRNA RP11 triggered the metastasis of CRC cells through the post-translational up-regulation of Zeb1 (Wu et al., 2019a). Similarly, Peng et al. demonstrated that METTL14 promoted the expression of miR-375 in an m^6A-dependent pathway to promote the progression of CRC (Chen et al., 2020a). Furthermore, not only m^6A can regulate the expression of ncRNAs, ncRNAs are capable to regulate the m^6A level of RNA as well. For example, miR-96 downregulated AMPKα2, thereby blocking its m^6A modification and leading to increased FTO expression and subsequent upregulation of MYC expression (Yue et al., 2020); LNC00460 directly interacted with IGF2BP2 and DHX9 to bind to the 3′UTR of HMGA1 mRNA, thereby increasing the stability of HMGA1 mRNA (Hou et al., 2021); m^6A modified circNSUN2 stabilized HMGA2 mRNA and ultimately promoted liver metastasis of CRC by forming a circNSUN2/IGF2BP2/HMGA2 RNA-protein ternary complex. Thus, linking ncRNAs and m^6A modifications is essential for advancing future diagnostic and therapeutic inventions (Chen et al., 2019a). The correlation between ncRNAs and m^6A modification is shown in **Figure 1**.

The current researches on ncRNAs in CRC are limited on the selection of one or more representative ncRNAs in clinical genomics. In these studies, the CRC transcriptome is analyzed in cohort retrospectively and usually lacks a holistic approach. The current research is primarily based on miRNA as the representative of ncRNAs, which usually regulate biological functions and promote or inhibit the occurrence of tumors by affecting the expression of multiple direct or indirect targets in common biological networks. For each ncRNA, hundreds of mRNAs or other ncRNAs are generally enriched as direct or indirect targets, and the coordination of many of these can be regulated to produce a series of biological consequences. Using this functional feature to our advantage, we took a data-driven approach and collected all the articles on CRC-related ncRNAs and miRNAs from PubMed in the last 5 years, and set IF > as the threshold. Next, we combined text mining and network statistical analysis, and set all ncRNAs and their target genes that appeared more than twice in the collected literature as nodes, and finally obtained a ncRNA regulatory network as presented this review (All steps of our approach are represented in **Figure 2** and the ncRNA regulatory network thus obtained is shown in **Figure 3**). Next, based on the number of ncRNA targets and the citations of related ncRNAs, we speculated its potential importance in the gene regulatory network for cancer, determined the final priority. Thereafter, we examined the interaction between the star ncRNAs targets, and the potential biological functions of ncRNAs in CRC. Detailed information on the network composition is shown in **Table 1**. The filtered nodes, which represent the un-replicated findings, are shown in **Table 2**. Through this review, we aimed to investigate the role of ncRNA regulatory network in the initiation and progression of CRC. Our review may have implications in future research strategies using ncRNAs in the treatment of CRC and tackling multi-drug resistance.

Classification of ncRNA Networks in Colorectal Cancer

Through the ncRNA network of colorectal cancer, we can clearly observe that the entire network graph is mainly divided into three large sub-networks (Including the miR-34a/b/c/miR-194-5p/miR21 sub-network, the CRNDE/EZH2/miR214/UCA1 sub-network and the miR-149/150-5p/LINC00460/miR-19a/20a sub-network) and a series of small networks (Including small networks with LNC00152, YAP, miR-27a, miR-24, miR-31, miR-7

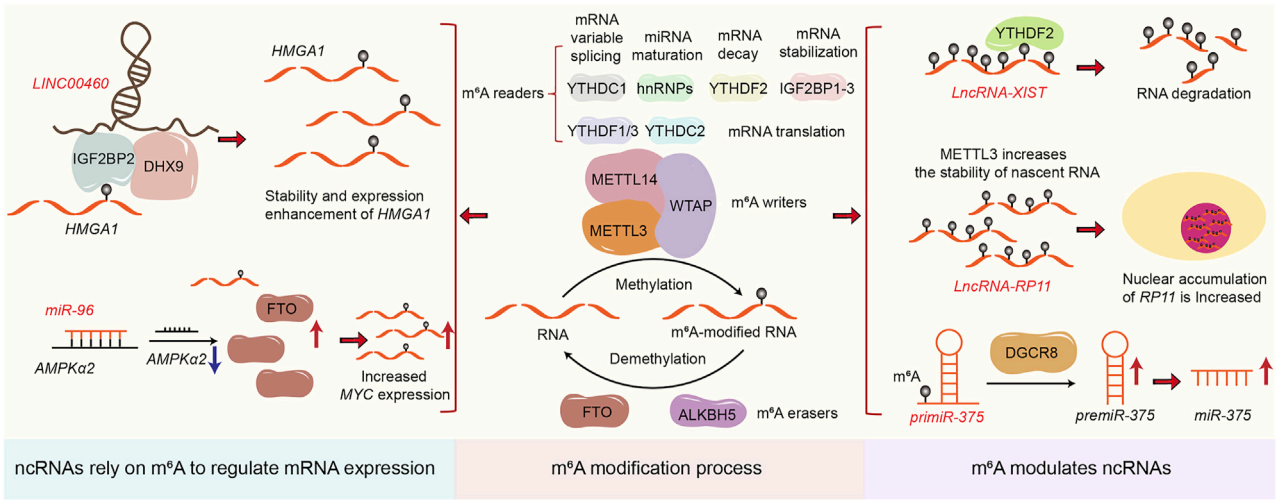


FIGURE 1 | The correlation between ncRNAs and m^{6}A modification. The figure shows how m^{6}A regulates ncRNAs expression and how ncRNAs rely on m^{6}A to regulate mRNA expression.

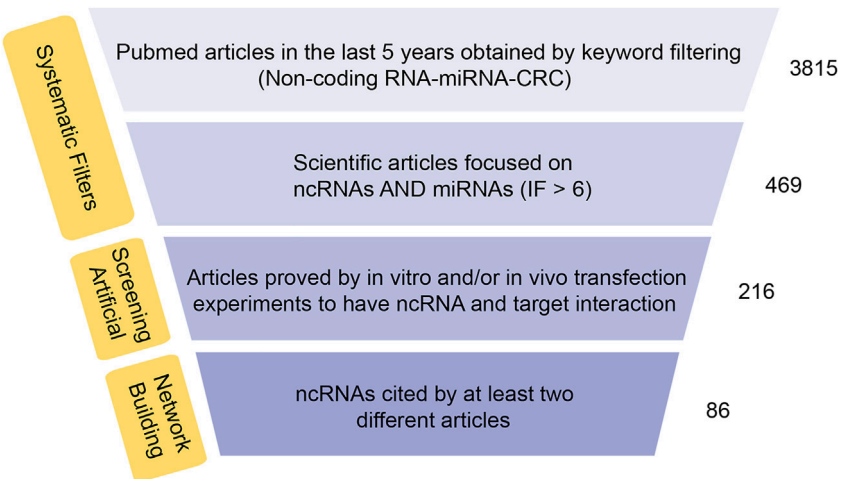


FIGURE 2 | Synthesis of data-approach used to build the network ncRNAs-target. Flow chart of RNA network construction.

as the core genes). Among these sub-networks, the miR-34a/b/c/miR-194-5p/miR21 sub-network and the LINC00152 network are mainly related to colorectal cancer chemotherapy resistance, which we call colorectal cancer chemotherapy resistance network; the CRNDE/EZH2/miR214/UCA1 sub-network, the YAP network and miR-24 network are mainly related to the metastasis of colorectal cancer, which we call the colorectal cancer metastasis network. These networks act synergistically and promote the progression of CRC (**Figure 4**; **Table 3**).

Chemotherapy Resistance Network of Colorectal Cancer

Chemotherapy resistance is one of the predominant reasons for the recurrence as well as poor prognosis of colorectal cancer (CRC) patients; ncRNAs reduce chemotherapy resistance of tumors by regulating signaling pathways in the initiation and progression of CRC. We integrated a variety of ncRNAs in CRC chemotherapy resistance and speculated that the combination of ncRNA-targeted inhibitors and chemotherapeutic drugs could be potential agents for improving the therapeutic effect of CRC.

The miR-34a/b/c/miR-194-5p/miR21 sub-network is the core chemotherapeutic resistance network in CRC treatment. The miR-34 family played a critical role in this sub-network by connecting multiple target proteins and lncRNAs. Furthermore, a number of reports show a reduced p53-induced miR-34 expression in CRC cells, and miR-34 can inhibit the occurrence and development of intestinal tumors. Moreover, miR-34 loss is related to tumor progression and chemotherapeutic resistance (Siemens et al., 2013). The mRNA

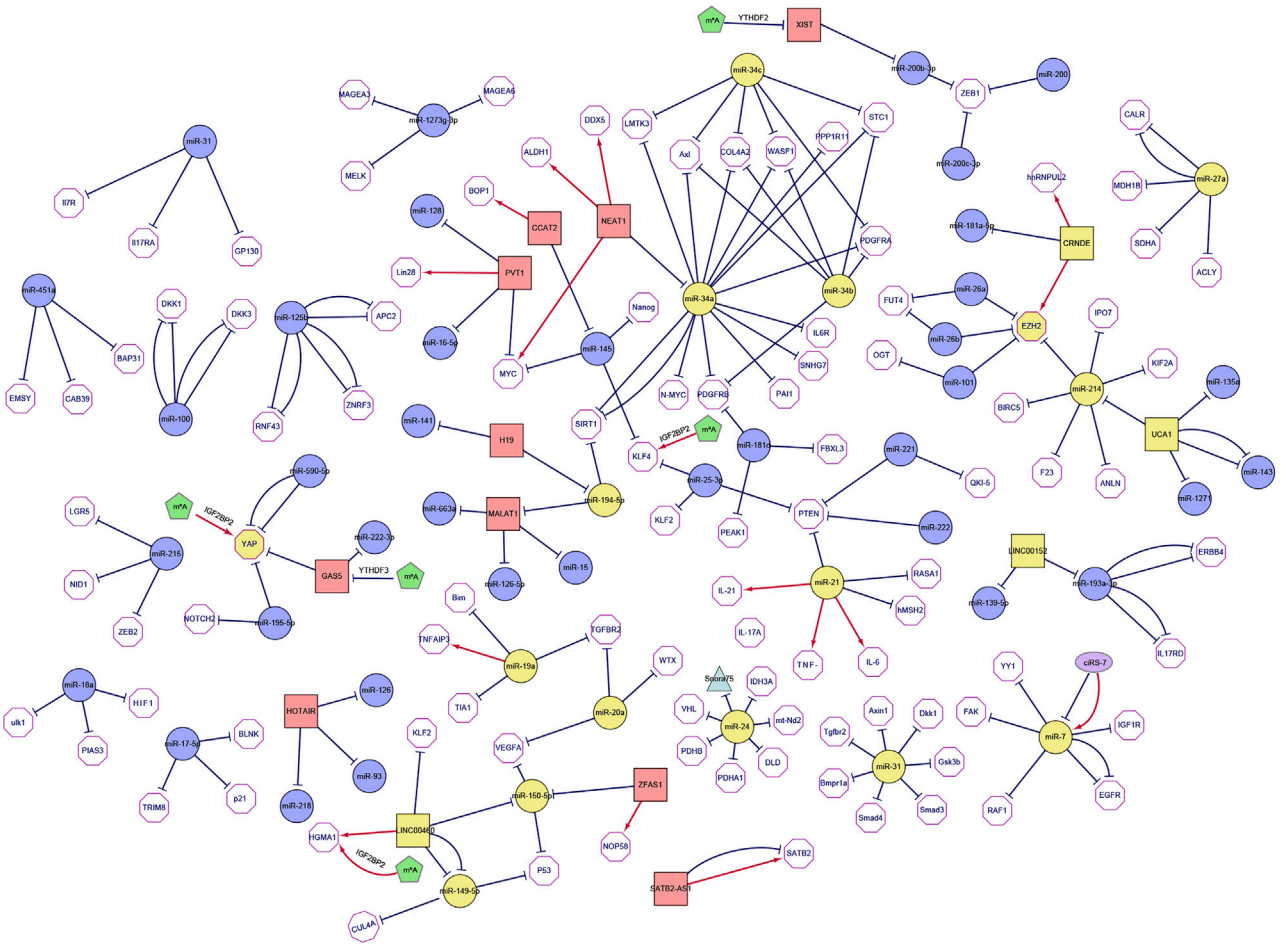


FIGURE 3 | The network of non-coding RNAs and its targets in colorectal cancer. The figure shows ncRNAs reported in at least two different literature sources (the squares represent long non-coding RNAs, the purple ellipses represent circular RNAs, the circles represent microRNAs, the triangles represent snoRNAs, the pentagon represents m^{6}A modification and yellow indicates core genes). The target mRNA of ncRNA is represented by a hexagon, and each target is reported in PUBMED. When the interaction is described in multiple articles, multiple line segments are drawn between the two nodes. The edges are directed (i.e., from the non-coding RNA to its target which could either be coding or non-coding). In the figure, red regular arrows indicate active links, and black flat arrows indicate inhibited links.

induction in miR-34a/b/c-deficient tumors was enriched in miR-34a/b/c seed-matching sites and mRNAs encoding proteins for Wnt signaling in epithelial-mesenchymal transition (EMT) and stemness such as INHBB, AXL, FGFR1 and PDFGRB, etc. This leads to a decrease in immune cell infiltration and down-regulation of barrier proteins, which in turn promote proliferation and inhibit apoptosis (Jiang and Hermeking, 2017). Meanwhile, studies show that miR-34 mimics can be utilized to stimulate target multiple key pathways, thereby preventing the emergence of drug resistance caused by mutations in a single pathway. The deletion of miR-34a also enhances the effects of TP53 deletion in the early or late stages during CRC initiation and progression. Additionally, miR-34a and TP53 can synergistically inhibit tumor initiation, invasion and metastasis in mouse models of CRC by increasing the levels of target proteins IL6R and PAI1 (Öner et al., 2018). PPP1R11 is also a target of miR-34a, and its product inhibits PP1. In p53-deficient CRC cells, PPP1R11 can activate the phosphorylation of STAT3, and simultaneously, high expression of PPP1R11 can induce EMT, invasion, migration and resistance to 5-fluorouracil under hypoxic conditions. Moreover, miR-34a can reduce the activation of STAT3 in p53-deficient CRC cells by decreasing the expression of PPP1R11, and ultimately inhibit EMT and metastasis of CRC cells (Li et al., 2017a). Thus, we speculate that inhibiting the expression of TP53 and miR-34a in CRC or using miR-34a/b/c replacement therapy may be a potential approach for CRC treatment. The antibodies or small molecule inhibitors to repress miR-34a targeting IL6R and PAI1 are potent promising treatment of CRC in the future.

Additionally, in this sub-network, we can find that KLF4 is significant related to miR-25-3p, and miR-25-3p, as an inhibitor of KLF4, has the effect of promoting the metastasis of CRC (Zeng et al., 2018a). A recent study further showed that MeCP2 bound to METTL14 and enhanced the m^{6}A level of KLF4, while m^{6}A-modified KLF4 was supposed to be stabilized by IGF2BP2 to increase the expression of KLF4, thereby

TABLE 1 | List of ncRNA-target and the type of interaction present in the network.

ncRNA	Direct target	Type of interaction	PMID	References
CCAT2	miR-145	neg	28964256	Yu et al. (2017a)
CCAT2	BOP1	pos	32805281	Chen et al. (2020c)
ciRS-7	miR-7	pos	32917870	Kristensen et al. (2020)
ciRS-7	miR-7	sponge	28174233	Weng et al. (2017)
CRNDE	EZH2	Pos	28796262	Ding et al. (2017a)
CRNDE	miR-181a-5p	Neg	28086904	Han et al. (2017)
CRNDE	hnRNPUL2	Shuttling neg	28594403	Jiang et al. (2017)
GAS5	YAP		31619268	Ni et al. (2019)
GAS5	miR-222−3p	Sponge	31400607	Liu et al. (2019a)
H19	miR-141	Sponge	30083271	Ren et al. (2018a)
H19	miR-194−5p	Sponge	30451820	Wang et al. (2018a)
HOTAIR	miR-218	Neg	28918035	Li et al. (2017b)
HOTAIR	miR-93	Sponge	32144238	Liu et al. (2020a)
HOTAIR	miR-126	Sponge	31974341	Jiang et al. (2020)
LINC00152	miR-193a-3p	Sponge	27633443	Yue et al. (2016)
LINC00152	miR-139−5p	Sponge	29180678	Bian et al. (2017)
LINC00460	miR-149−5p	Sponge	30092404	Lian et al. (2018)
LINC00460	miR-149−5p	Sponge	33251049	Meng et al. (2020)
LINC00460	miR-150−5p	Sponge	33251049	Meng et al. (2020)
LINC00460	KLF2	Neg	30092404	Lian et al. (2018)
MALAT1	miR-15	Sponge	31097689	Ji et al. (2019)
MALAT1	miR-126−5p	Sponge	30531836	Sun et al. (2019a)
MALAT1	miR-663a	Neg	30154407	Tian et al. (2018)
miR-100	DKK1	Neg	29035371	Lu et al. (2017)
miR-100	DKK3	Neg	29035371	Lu et al. (2017)
miR-100	DKK1	Neg	29094721	Thomas, (2017)
miR-100	DKK3	Neg	29094721	Thomas, (2017)
miR-101	OGT	Neg	30093632	Jiang et al. (2019)
miR-101	EZH2	Neg	30093632	Jiang et al. (2019)
miR-125b	ZNRF3	Neg	29035371	Lu et al. (2017)
miR-125b	RNF43	Neg	29035371	Lu et al. (2017)
miR-125b	APC2	Neg	29035371	Lu et al. (2017)
miR-125b	RNF43	neg	29094721	Thomas, (2017)
miR-125b	APC2	neg	29094721	Thomas, (2017)
miR-1273g-3p	MELK	neg	31358735	Zhao et al. (2019)
miR-1273g-3p	MAGEA3/6	neg	30056111	Wu et al. (2018)
miR-145	MYC	neg	29475734	Zhu et al. (2018a)
miR-145	KLF4	neg	29475734	Zhu et al. (2018a)
miR-145	Nanog	neg	29475734	Zhu et al. (2018a)
miR-149−5p	CUL4A	neg	30092404	Lian et al. (2018)
miR-149−5p	P53	neg	33251049	Meng et al. (2020)
miR-150−5p	P53	neg	33251049	Meng et al. (2020)
miR-150−5p	VEGFA	neg	30250022	Chen et al. (2018)
miR-17−5p	TRIM8	neg	28327152	Mastropasqua et al. (2017)
miR-17−5p	p21	neg	28327152	Mastropasqua et al. (2017)
miR-17−5p	BLNK	neg	30555542	Mai et al. (2018)
miR-181d	PDGFRB	neg	28363996	Jiang and Hermeking, (2017)
miR-181d	FBXL3	neg	28749470	Guo et al. (2017)
miR-181d	PEAK1	neg	29449544	Huang et al. (2018b)
miR-18a	ulk1	neg	28753429	Yu et al. (2017b)
miR-18a	PIAS3	neg	29896300	Ma et al. (2018)
miR-18a	HIF1α	neg	27080303	Ma et al. (2016a)
miR-193a-3p	IL17RD	neg	28600480	Pekow et al. (2017)
miR-193a-3p	ERBB4	neg	27633443	Yue et al. (2016)
miR-193a-3p	IL17RD	neg	28600480	Pekow et al. (2017)
miR-193a-3p	ERBB4	neg	27633443	Yue et al. (2016)
miR-194−5p	MALAT1	neg	31311811	Wu et al. (2019b)
miR-194−5p	SIRT1	neg	30451820	Wang et al. (2018a)
miR-195−5p	YAP	neg	28356122	Sun et al. (2017)
miR-195−5p	NOTCH2	neg	30808369	Lin et al. (2019a)
miR-19a	TGFBR2	neg	27080303	Ma et al. (2016a)
miR-19a	TIA1	neg	28257633	Liu et al. (2017a)
miR-19a	Bim	neg	32591507	Guo et al. (2020a)
miR-19a	TNFAIP3	pos	27991929	Wang et al. (2017a)

(Continued on following page)

TABLE 1 | (*Continued*) List of ncRNA-target and the type of interaction present in the network.

ncRNA	Direct target	Type of interaction	PMID	References
miR-200	ZEB1	neg	26455323	Barbáchano et al. (2016)
miR-200b-3p	ZEB1	neg	28837144	Chen et al. (2017a)
miR-200c-3p	ZEB1	neg	28535802	Rigoutsos et al. (2017)
miR-20a	TGFBR2	neg	27080303	Ma et al. (2016a)
miR-20a	VEGFA	neg	27080303	Ma et al. (2016a)
miR-20a	WTX	neg	30631060	Zhu et al. (2019)
miR-21	RASA1	neg	27876571	Yang et al. (2017)
miR-21	IL-6	pos	25994220	Shi et al. (2016)
miR-21	TNF-α	pos	25994220	Shi et al. (2016)
miR-21	IL-17A	pos	25994220	Shi et al. (2016)
miR-21	IL-21	pos	25994220	Shi et al. (2016)
miR-21	PTEN	neg	31918721	Liang et al. (2020a)
miR-21	hMSH2	neg	31918721	Liang et al. (2020a)
miR-214	EZH2	neg	30626446	Xu et al. (2019a)
miR-214	ANLN	neg	30195762	Barbagallo et al. (2018)
miR-214	F23	neg	30195762	Barbagallo et al. (2018)
miR-214	KIF2A	neg	30195762	Barbagallo et al. (2018)
miR-214	IPO7	neg	30195762	Barbagallo et al. (2018)
miR-214	BIRC5	neg	30195762	Barbagallo et al. (2018)
miR-215	NID1	neg	30831320	Rokavec et al. (2019)
miR-215	ZEB2	neg	29187907	Chen et al. (2017b)
miR-215	LGR5	neg	30790680	Ullmann et al. (2019)
miR-221	PTEN	neg	28986522	Antoniali et al. (2017)
miR-221	QKI-5	neg	31416845	Mukohyama et al. (2019)
miR-222	PTEN	neg	28986522	Antoniali et al. (2017)
miR-24	Snora75	neg	28500171	Michael et al. (2017)
miR-24	mt-Nd2	neg	28500171	Michael et al. (2017)
miR-24	VHL	neg	30393198	Jin et al. (2019)
miR-24	PDHB	neg	30393198	Jin et al. (2019)
miR-24	PDHA1	neg	30393198	Jin et al. (2019)
miR-24	DLD	neg	30393198	Jin et al. (2019)
miR-24	IDH3A	neg	30393198	Jin et al. (2019)
miR-25−3p	KLF2	neg	30568162	Zeng et al. (2018a)
miR-25−3p	KLF4	neg	30568162	Zeng et al. (2018a)
miR-25−3p	PTEN	neg	31931030	Wang et al. (2020a)
miR-26a	FUT4	neg	28640257	Li et al. (2017c)
miR-26a	EZH2	neg	30626446	Xu et al. (2019a)
miR-26b	FUT4	neg	28640257	Li et al. (2017c)
miR-26b	EZH2	neg	30626446	Xu et al. (2019a)
miR-27a	ACLY	neg	30393198	Jin et al. (2019)
miR-27a	MDH1B	neg	30393198	Jin et al. (2019)
miR-27a	SDHA	neg	30393198	Jin et al. (2019)
miR-27a	calreticulin	neg	26913599	Colangelo et al. (2016a)
miR-27a	calreticulin	neg	26913609	Colangelo et al. (2016b)
miR-31	Axin1	neg	28870287	Tian et al. (2017)
miR-31	Gsk3b	neg	28870287	Tian et al. (2017)
miR-31	Tgfbr2	neg	28870287	Tian et al. (2017)
miR-31	Bmpr1a	neg	28870287	Tian et al. (2017)
miR-31	Smad4	neg	28870287	Tian et al. (2017)
miR-31	Smad3	neg	28870287	Tian et al. (2017)
miR-31	Dkk1	neg	28870287	Tian et al. (2017)
miR-31	Il7R	neg	30779922	Tian et al. (2019)
miR-31	Il17RA	neg	30779922	Tian et al. (2019)
miR-31	GP130	neg	30779922	Tian et al. (2019)
miR-34a	IL6R	neg	30099074	Öner et al. (2018)
miR-34a	PAI1	neg	30099074	Öner et al. (2018)
miR-34a	PPP1R11	neg	28435028	Li et al. (2017a)
miR-34a	SNHG7	neg	29970122	Li et al. (2018a)
miR-34a	N-MYC	neg	28327152	Mastropasqua et al. (2017)
miR-34a	Pdgfra	neg	28363996	Jiang and Hermeking, (2017)
miR-34a	Axl	neg	28363996	Jiang and Hermeking, (2017)
miR-34a	COL4A2	neg	28363996	Jiang and Hermeking, (2017)
miR-34a	WASF1	neg	28363996	Jiang and Hermeking, (2017)
miR-34a	STC1	neg	28363996	Jiang and Hermeking, (2017)

(Continued on following page)

TABLE 1 | (*Continued*) List of ncRNA-target and the type of interaction present in the network.

ncRNA	Direct target	Type of interaction	PMID	References
miR-34a	PDGFRB	neg	28363996	Jiang and Hermeking, (2017)
miR-34a	SIRT1	neg	30312725	Luo et al. (2019)
miR-34a	SIRT1	neg	28943452	Fang et al. (2017)
miR-34a	LMTK3	neg	26739063	Jacob et al. (2016)
miR-34b	Pdgfra	neg	28363996	Jiang and Hermeking, (2017)
miR-34b	Axl	neg	28363996	Jiang and Hermeking, (2017)
miR-34b	COL4A2	neg	28363996	Jiang and Hermeking, (2017)
miR-34b	WASF1	neg	28363996	Jiang and Hermeking, (2017)
miR-34b	STC1	neg	28363996	Jiang and Hermeking, (2017)
miR-34b	PDGFRB	neg	28363996	Jiang and Hermeking, (2017)
miR-34c	LMTK3	neg	26739063	Jacob et al. (2016)
miR-34c	Pdgfra	neg	28363996	Jiang and Hermeking, (2017)
miR-34c	Axl	neg	28363996	Jiang and Hermeking, (2017)
miR-34c	COL4A2	neg	28363996	Jiang and Hermeking, (2017)
miR-34c	WASF1	neg	28363996	Jiang and Hermeking, (2017)
miR-34c	STC1	neg	28363996	Jiang and Hermeking, (2017)
miR-451a	EMSY	neg	28742699	Kelley et al. (2017)
miR-451a	CAB39	neg	28742699	Kelley et al. (2017)
miR-451a	BAP31	neg	30770794	Xu et al. (2019b)
miR-590−5p	YAP	neg	29912317	Yu et al. (2018a)
miR-590−5p	YAP	neg	29429755	Ou et al. (2018)
miR-7	EGFR	neg	28174233	Weng et al. (2017)
miR-7	RAF1	neg	28174233	Weng et al. (2017)
miR-7	FAK	neg	29549306	Zeng et al. (2018b)
miR-7	IGF1R	neg	29549306	Zeng et al. (2018b)
miR-7	EGFR	neg	29549306	Zeng et al. (2018b)
miR-7	YY1	neg	29549306	Zeng et al. (2018b)
NEAT1	ALDH1	pos	33168814	Zhu et al. (2020a)
NEAT1	MYC	pos	33168814	Zhu et al. (2020a)
NEAT1	miR-34a	sponge	30312725	Luo et al. (2019)
NEAT1	DDX5	pos	30185232	Zhang et al. (2018a)
PVT1	MYC	neg	33148262	Shigeyasu et al. (2020)
PVT1	miR-16−5p	neg	32276209	Wu et al. (2020a)
PVT1	Lin28	pos	30076414	He et al. (2019)
PVT1	miR-128	sponge	30076414	He et al. (2019)
SATB2-AS1	SATB2	neg	30858153	Wang et al. (2019a)
SATB2-AS1	SATB2	pos	31492160	Xu et al. (2019c)
UCA1	miR-143	sponge	31955010	Luan et al. (2020)
UCA1	miR-135a	sponge	30195762	Barbagallo et al. (2018)
UCA1	miR-143	sponge	30195762	Barbagallo et al. (2018)
UCA1	miR-214	sponge	30195762	Barbagallo et al. (2018)
UCA1	miR-1271	sponge	30195762	Barbagallo et al. (2018)
ZFAS1	NOP58	pos	32443980	Wu et al. (2020b)
ZFAS1	miR-150−5p	sponge	30250022	Chen et al. (2018)

inhibiting the metastasis of CRC (Wang et al., 2021). Therefore, the development of drugs that simultaneously target to promote the expression of IGF2BP2 and target to inhibit the expression of miR-25-3p may be also an important approach for the treatment of CRC.

SNHG7 (small nucleolar RNA host gene 7), miR-34a and GALNT7 also play an important role in the progression of CRC through the PI3K/AKT/mTOR pathway. SNHG7 can be used as a competitive endogenous RNA (ceRNAs). Along with the sponge miR-34a, it can regulate the level of GALNT7 in CRC and activate the PI3K/AKT/mTOR pathway to promote proliferation and metastasis (Li et al., 2018a). Mastropasqua et al. report that TRIM8 (tripartite motif containing 8) and its regulatory factors including miR-17-5p and miR-106b-5 participate in a feedback loop that controls cell proliferation in CRC by mutual regulation of p53, miR-34a, and N-Myc. In CRC, TRIM8 is a key target that triggers the sensitivity of CRC cells to chemotherapy. TRIM8 restores the function of the p53 tumor suppressor by inactivating the activity of oncoprotein N-Myc in chemotherapy-resistant tumors. Additionally, the silencing of miR-17-5p and miR-106b-5p restore the levels of TRIM8, and effectively promote the tumor suppressor activity of p53 and the transcription of miR-34a, thereby reducing the carcinogenic potential of miR-34a's target N-Myc. It restores the sensitivity of cells to chemotherapy (Mastropasqua et al., 2017). In addition, LMTK3 (lemur tyrosine kinase 3), an important node in the network diagram, plays an important role in the progression of a variety of cancers (breast cancer, lung cancer, CRC, etc.) (Xu et al., 2014; Xu et al., 2015). In CRC, nuclear LMTK3 interacts with DDX5 to target and regulate the expression of a group of

TABLE 2 | List of ncRNAs, their targets and the type of interactions, cited by only one scientific article.

ncRNA	Target	Type of interaction	PMID	References
ADAMTS9-AS2	miR-143−3p	sponge	30217729	Xie et al. (2018)
AK000053	miR-508	sponge	29374066	Yan et al. (2018)
AK036396	Ficolin B	neg	32102837	Tian et al. (2020)
ASBEL	ATF3	neg	27791078	Taniue et al. (2016a)
BC032913	TIMP3	pos	28918047	Lin et al. (2017)
BFAL1	miR-155−5p, miR-200a-3p	sponge	31515468	Bao et al. (2019)
BLACAT1	EZH2, p15	Cooperate, neg	28277544	Su et al. (2017)
CALIC	hnRNP-L, AXL	Cooperate, pos	31353791	Kawasaki et al. (2019)
CASC11	hnRNP-K	pos	27012187	Zhang et al. (2016a)
CCAL	AP-2α	neg	25994219	Ma et al. (2016b)
circ101555	miR-597−5p	sponge	31300733	Chen et al. (2019b)
circ5615	miR-149−5p	sponge	32393760	Ma et al. (2020)
circACC1	AMPK	pos	31155494	Li et al. (2019)
circCTNNA1	miR-149−5p	sponge	32699205	Chen et al. (2020b)
circHIPK3	miR-7	neg	29549306	Zeng et al. (2018b)
CYTOR	β-catenin	pos	29606502	Yue et al. (2018)
FARSA-AS1	miR-18b-5p	sponge	33318478	Zhou et al. (2020)
FEZF1-AS1	PKM2	pos	29914894	Bian et al. (2018)
FLANC	pSTAT3	pos	31988194	Pichler et al. (2020)
FOXC2-AS1	FOXC2	pos	32513911	Pan and Xie, (2020)
GLCC1	c-Myc	pos	31375671	Tang et al. (2019a)
GSEC	DHX36	neg	27797375	Matsumura et al. (2017)
HITT	HIF-1α	neg	31784651	Wang et al. (2020b)
HNF1A-AS1	miRNA-34a	sponge	28943452	Fang et al. (2017)
HOXA-AS2	p21, KLF2, EZH2	neg, neg, cooperate	28112720	Ding et al. (2017b)
HOXD-AS1	HOXD3	neg	30823921	Yang et al. (2019)
ITHI4-AS1	JAK1/2, FUS	pos	31557619	Liang et al. (2019a)
KRT7-AS	KRT7	pos	31910722	Chen et al. (2020d)
LDLRAD4-AS1	LDLRAD4	neg	32111819	Mo et al. (2020)
LINC00265	ZMIZ2	pos	31527801	Zhu et al. (2020b)
LINC00659	PI3K	pos	29523145	Tsai et al. (2018)
LINC00858	miR-4766−5p	sponge	31902050	Zhan et al. (2020)
LINC01106	miR-449b-5p	sponge	33067422	Guo et al. (2020b)
LINC01133	SRSF6	sponge	27443606	Kong et al. (2016)
LINC01234	miR-642a-5p	sponge	30755591	Lin et al. (2019b)
LINC01413	hnRNPK, ZEB1	cooperate, pos	31927328	Ji et al. (2020)
LINC01578	NFKBIB	neg	33040438	Liu et al. (2020b)
LINC02023	PTEN	pos	30849479	Wang et al. (2019b)
LINC02418	miR-1273g-3p	sponge	31358735	Zhao et al. (2019)
LINC-UFC1	β-catenin	pos	27195675	Yu et al. (2016)
LINRIS	IGF2BP2	pos	31791342	Wang et al. (2019c)
LNC34a	miR-34a	neg	27077950	Wang et al. (2016a)
LNC-C/EBPβ	Arg1, CYBB, NOS2, ptgs2	neg	30171135	Gao et al. (2018)
LNC-CMPK2	FUBP3	pos	32203166	Gao et al. (2020)
LNC-CRCMSL	HMGB2	shuttling	30575817	Han et al. (2019)
LNC-FAM84B-4	hnRNPK, DUSP1	cooperate, neg	32866608	Peng et al. (2020)
LNC-Gata6	Lgr4, Lgr5	pos	30224759	Zhu et al. (2018b)
LNC-RI	miR-4727−5p	sponge	32279126	Liu et al. (2020c)
LncRNA-APC1	Rab5b	pos	30511962	Wang et al. (2019d)
LNRRIL6	IL-6	pos	31246342	Wang et al. (2019e)
LUCAT1	NCL	binding	33097685	Wu et al. (2020c)
miR-342	FOXM1, FOXQ1	neg	27162244	Weng et al. (2016)
miR-101c	Tet1	neg	28249902	Tie et al. (2017)
miR-105	RAP2C	neg	29238068	Shen et al. (2017a)
miR-106a	WTX	neg	30631060	Zhu et al. (2019)
miR-106b-5p	TRIM8, p21	neg	28327152	Mastropasqua et al. (2017)
miR-10a	ACTG1, MMP14	neg	28383561	Liu et al. (2017b)
miR-124	iASPP	neg	29022915	Liu et al. (2017c)
miR-1249	HMGA2, VEGFA	neg	30755600	Chen et al. (2019c)
miR-125a-3p	FUT5, FUT6	neg	28771224	Liang et al. (2017)
miR-126	SCEL	neg	31974341	Jiang et al. (2020)
miR-126−5p	VEGFA, TWIST, SLUG	neg	30531836	Sun et al. (2019a)
miR-1271	ANLN, BIRC5, IPO7, KIF2A, F23	neg	30195762	Barbagallo et al. (2018)
miR-128	Lin28	neg	30076414	He et al. (2019)
miR-128−3p	Bmi1, MRP5	neg	30890168	Liu et al. (2019b)

(Continued on following page)

TABLE 2 | (*Continued*) List of ncRNAs, their targets and the type of interactions, cited by only one scientific article.

ncRNA	Target	Type of interaction	PMID	References
miR-130b-3p	PTEN	neg	31931030	Wang et al. (2020a)
miR-135a	ANLN, BIRC5, IPO7, KIF2A, F23	neg	30195762	Barbagallo et al. (2018)
miR-137	GLS1	neg	29730197	Li et al. (2018b)
miR137HG	mir-137	pos	29730197	Li et al. (2018b)
miR-139−5p	PDE4D	neg	27383270	Cao et al. (2016)
miR-141	β-catenin	neg	30083271	Ren et al. (2018a)
miR-141−3p	ZEB1	neg	28535802	Rigoutsos et al. (2017)
miR-143	ANLN, BIRC5, IPO7, KIF2A, F23	neg	30195762	Barbagallo et al. (2018)
miR-143−3p	ITGA6	neg	30217729	Xie et al. (2018)
miR-144	EZH2	neg	30770796	Shi et al. (2019)
miR-146a	c-met	neg	29133238	Bleau et al. (2018)
miR-148a	GP130, IL1R1, IKKα, IKKβ, TNFR2	neg	28960206	Zhu et al. (2017)
miR-149	CDK4/6, XIAP, BCLXL, cyclin D	neg	29061672	Lulla et al. (2017)
miR-149−3p	PDK2	neg	31597953	Liang et al. (2020b)
miR-15	LRP6	neg	31097689	Ji et al. (2019)
miR-150	ZEB1	neg	26455323	Barbáchano et al. (2016)
miR-153	IDO1	neg	29685162	Huang et al. (2018c)
miR-15b	DCLK1	Neg	30449704	Ji et al. (2018)
miR-16−5p	VEGFR1	Pos	32276209	Wu et al. (2020a)
miR17HG	miR-375	Sponge	31409641	Xu et al. (2019d)
miR-181a	SRCIN1	Neg	29739921	Sun et al. (2018)
miR-181a-5p	β-catenin, TCF4	Neg	28086904	Han et al. (2017)
miR-181b	PDCD4	Neg	27647131	Liu et al. (2016)
miR-182	LMTK3	Neg	26739063	Jacob et al. (2016)
miR-187	SOX4, PTK6, NT5E	Neg	26820227	Zhang et al. (2016b)
miR-18b-5p	FARSA	Neg	33318478	Zhou et al. (2020)
miR-193a	Caprin1	Neg	28211508	Teng et al. (2017)
miR-194	VAPA	Neg	29109785	Chang et al. (2017)
miR-195	WEE1, CHK1	Neg	29080751	Kim et al. (2018)
miR-196b-5p	HOXB7, GALNT5	Pos	28533224	Stiegelbauer et al. (2017)
miR-19b	Bim	Neg	32591507	Guo et al. (2020a)
miR-200a-3p	RHEB	Neg	31515468	Bao et al. (2019)
miR-203	BIRC5	Neg	31091026	Okugawa et al. (2019)
miR-205−5p	ZEB1	Neg	29352232	Gulei et al. (2018)
miR-206	Met	Neg	30250188	Xu et al. (2018a)
miR-214−3p	MyD88	Neg	30914411	Shang et al. (2019)
miR-215−5p	EREG, TYMS	Neg	31542354	Chen et al. (2019d)
miR-216b	GALNT1	Neg	29915311	Shan et al. (2018)
miR-218	VOPP1	Neg	28918035	Li et al. (2017b)
miR-22	HuR	Neg	29351796	Liu et al. (2018a)
miR-222−3p	PTEN	Neg	31400607	Liu et al. (2019a)
miR-223	FBX8	Neg	27916606	Wang et al. (2017b)
miR-224	SMAD4	Neg	25804630	Ling et al. (2016)
miR-23a	CS, PDHA1, IDH1, DLD	Neg	30393198	Jin et al. (2019)
miR-23b	LGR5	Neg	28487386	Viswanathan et al. (2017)
miR-301A	BTG1	Neg	28193514	He et al. (2017)
miR-302a	NFIB, CD44	Neg	31754405	Sun et al. (2019b)
miR-30a	ME1	Neg	28475173	Shen et al. (2017b)
miR-30a-5p	LDHA	Neg	28461244	Li et al. (2017d)
miR-320a	PKCγ	Neg	31515469	Aljagthmi et al. (2019)
miR-338−5p	IL-6	Neg	31208913	Xu et al. (2019e)
miR-372/373	SPOP, VDR, SETD7, RELA TRERF1, ZNF367, MTUS1	Neg	30171794	Wang et al. (2018b)
miR-375	RELA, MALT1, NFKBIE PPP3R1, MAP3K7, CBL	Neg	31409641	Xu et al. (2019d)
miR-425−5p	PTEN	Neg	31931030	Wang et al. (2020a)
miR-4260	MCC, SMAD4	Neg	28638476	Xiao et al. (2017)
miR-448	IDO1	Neg	31391111	Lou et al. (2019)
miR-449b-5p	Gli4	Neg	25961913	Wang et al. (2016b)
miR-4727−5p	LIG4	Neg	32279126	Liu et al. (2020c)
miR-4766−5p	PAK2	Neg	31902050	Zhan et al. (2020)
miR-4775	Smad7	Neg	28095858	Zhao et al. (2017)
miR-4802	ATG7	Neg	28753429	Yu et al. (2017b)
miR-486−5p	PLAGL2	Neg	30305607	Liu et al. (2018b)

(Continued on following page)

TABLE 2 | (*Continued*) List of ncRNAs, their targets and the type of interactions, cited by only one scientific article.

ncRNA	Target	Type of interaction	PMID	References
miR-487b-3p	GRM3	Neg	28114282	Yi et al. (2017)
miR-490−3p	FRAT1	Neg	27037061	Zheng et al. (2016)
miR-494	APC	Neg	29304823	Zhang et al. (2018b)
miR-500a-5p	HDAC2	Neg	30737378	Tang et al. (2019b)
miR-508	SALL4	Neg	29374066	Yan et al. (2018)
miR-514b-3p	FZD4, NTN1	Neg	29880874	Ren et al. (2018b)
miR-514b-5p	CDH1, CLDN1	Neg	29880874	Ren et al. (2018b)
miR-532−3p	ETS1	Neg	31570702	Gu et al. (2019a)
miR-532−5p	TGFBR1	Neg	29971498	Gu et al. (2019b)
miR-550a-3-5p	YAP	Neg	29844307	Choe et al. (2018)
miR-550a-5p	RNF43	neg	25961913	Wang et al. (2016b)
miR-5582−5p	GAB1, CDK2, SHC1	neg	27475256	An et al. (2016)
miR574−5p	APAF1	neg	32784109	Wu et al. (2020d)
miR-597−5p	CDK6, RPA3	neg	31300733	Chen et al. (2019b)
miR-625−3p	MAP2K6	neg	27526785	Rasmussen et al. (2016)
miR-642a-5p	SHMT2	neg	30755591	Lin et al. (2019b)
miR-655−3p	TGFBR2, ICK	neg	28457664	Oshima et al. (2017)
miR-663a	TGFB1, PIK3CD, P53, JUND, P21	neg	30154407	Tian et al. (2018)
miR-675−5p	TP53	neg	31734182	Cen et al. (2020)
miR-6883−5p	CDK4/6, XIAP, BCLXL, cyclin D	neg	29061672	Lulla et al. (2017)
miR-92a-3p	FBXW7, MOAP1	neg	31064356	Hu et al. (2019)
miR-93	ATG12	neg	32144238	Liu et al. (2020a)
miR-944	COP1, MDM2	neg	30393117	Kim et al. (2019b)
MYU	miR-16	neg	27568568	Kawasaki et al. (2016)
N-BLR	miR-141−3p, miR-200c-3p	neg	28535802	Rigoutsos et al. (2017)
OLA1P2	STAT3	neg	26898989	Guo et al. (2016)
Olfr29-ps1	miR-214−3p	sponge	30914411	Shang et al. (2019)
OVAAL	PTBP1	neg	30478051	Sang et al. (2018)
PiHL	RPL11, GRWD1	pos	31903119	Deng et al. (2020)
PINCR	Matrin3	neg	28580901	Chaudhary et al. (2017)
piR-1245	ATF3, BTG1, DUSP1, NFKBIA,FAS, UPP1, SESN2, TP53INP1,MDX1	neg	29382334	Weng et al. (2018)
pirl -54265	p-STAT3, BCL-XL,cleaved-CASP3/7/9	Pos, pos, neg	30555542	Mai et al. (2018)
RAMS11	CBX4	pos	32358485	Silva-Fisher et al. (2020)
RBM5-AS1	CMYC, CCND1, YAP1, SGK1	pos	27520449	Di Cecilia et al. (2016)
RPPH1	TUBB3	pos	31685807	Liang et al. (2019b)
SNHG1	miR-154−5p	sponge	30266084	Xu et al. (2018b)
SNHG5	SPATS2	pos	28004750	Damas et al. (2016)
SNHG6	miR-26a, miR-26b, miR-214	sponge	30626446	Xu et al. (2019a)
SNHG7	miR-216b	sponge	29915311	Shan et al. (2018)
SNHG11	HIF-1α	sponge	33060856	Xu et al. (2020a)
SNHG14	miR-186−5p, EZH2	sponge, pos	31273190	Di et al. (2019)
SNHG15	Slug	pos	29604394	Jiang et al. (2018)
SNORA42	SMAD2	pos	32127004	Xu et al. (2020b)
SNORD12C/78	EIF4A3, LAMC2	pos	32443980	Wu et al. (2020b)
tcon_00012883	MMP1	pos	33135346	Yang et al. (2020b)
TUG1	TWIST1	pos	1988275	Mosthaf et al. (1991)
u50535	CCL20	pos	29970882	Yu et al. (2018b)
UICLM	miR-215	sponge	29187907	Chen et al. (2017b)
UPAT	UHRF1	pos	26768845	Taniue et al. (2016b)
WiNTRLINC1	ASCL2	pos	27292638	Giakountis et al. (2016)
ZNFX1-AS1	miR-144	sponge	30770796	Shi et al. (2019)
δNp63α	miR-320a	pos	31515469	Aljagthmi et al. (2019)

miRNAs (miR-34a, miR-196a2, and miR-182). The tumor suppressor-like miRNAs, miR-34a and miR-182 directly bind to the 3′UTR of LMTK3 mRNA and inhibit its stability and translation, thereby inhibiting the proliferation, invasion, and migration in CRC (Jacob et al., 2016).

In addition to targeting some encoded proteins, miR-34a could also target long-chain non-coding RNAs, and played an important regulatory role in the progression of CRC. NEAT1 (nuclear paraspeckle assembly transcript 1), a long-chain non-coding RNA, is a known oncogene in CRC. For example, NEAT1 can directly interact with its target DDX5 and stabilizes its protein expression. DDX5, thus, activates the Wnt/β-catenin signaling pathway and promotes the progression of CRC (Zhang et al., 2018a). Additionally, some studies show that NEAT1 is associated with 5-FU resistance in CRC. NEAT1 increases H3K27ac enrichment at ALDH1 and c-Myc promoters by

altering chromatin remodeling, thereby up-regulating their expression, enhancing the stemness of CRC cells, and promoting 5-FU resistance (Zhu et al., 2020a). Thus, NEAT1 plays an important role in tumor resistance and tumorigenesis in CRC.

However, the effect of NEAT1 on the Wnt/β-catenin signaling pathway is not completely dependent on DDX5, and NEAT1 can also exert carcinogenic effects through miR-34a (Luo et al., 2019). In CRC, NEAT1 acts as a ceRNA that targets miR-34a and regulates its expression, thereby inhibiting the miR-34a/SIRT1 axis. It activates the Wnt/β-catenin signaling pathway, and inhibits miR-34a/SIRT1 feedback loop, which in turn promotes CRC progression, invasion, and metastasis, etc. The above studies show that NEAT1 can be used as a diagnostic marker and is a potential therapeutic target for CRC. Moreover, traditional chemotherapy combined with drugs targeting tumor stem cells provides a new strategy for the treatment of CRC patients CRC patients with high NEAT1 expression. More importantly, the combined network analysis showed that miR-34 may simultaneously target different genes and multiple core pathways in CRC, inhibit EMT, invasion, migration, and proliferation of cancer cells, and prevent the emergence of drug resistance caused by mutations in a single pathway. Therefore, miR-34 replacement therapy could also be a potential option for the treatment of CRC. In addition, targeting a certain pathway regulated by miR-34 for specific effects could also be a potential direction for further research in the treatment of CRC.

In addition to NEAT1, the network diagram also connects a series of other long non-coding RNAs through different target genes. Indeed, there are several studies confirming the role of these long non-coding RNAs in CRC. Therefore, the interaction of different lncRNAs in CRC and their target proteins in this network require in-depth analysis. For example, some studies show that H19 may be the main marker for predicting 5-FU chemotherapy resistance. H19 acts as a ceRNA to target miR-194-5p, and in turn regulates the SIRT1-dependent autophagy pathway which promotes 5-FU chemotherapy resistance in CRC (Wang et al., 2018a). Autophagy is triggered by the target protein of miR-34a, SIRT1 in this network diagram too. Some studies show that H19 acts as a ceRNA sponge of miR-141, activates the β-catenin pathway and promotes stemness as well as chemotherapy resistance of CRC by transferring H19 from exosomes (Ren et al., 2018a). The above studies suggest that conventional chemotherapy combined with targeted therapy can be a potential treatment for 5-FU resistant patients with elevated expression of H19. From the network diagram, we observe that the sub-network highlights another branch of miR-194-5p, which can directly target the lncRNAs-MALAT1 harboring the rs664589 G allele in the nucleus of CRC cells, thereby regulating the nuclear expression of MALAT1 and exerting a tumor suppressor effect (Ren et al., 2018a). Researchers indicate that in CRC, the rs664589 polymorphism of MALAT1 inhibits its affinity to miR-194-5p, resulting in its increased expression, and thus, promotes the development of CRC. Moreover, MALAT1 is primarily induced by YAP1 in CRC and YAP1 interacts with TCF4 and β-catenin to regulate the expression of MALAT1 (Sun et al., 2019a). MALAT1 also primarily functions as a competitive endogenous lncRNA in CRC, which targets and regulates the sponging of miR-126-5p, miR-663a, miR-15, and other microRNAs to exhibit a tumor suppressor effect. MALAT1 promotes the expression of VEGFA, SLUG, TWIST, and other metastasis-related molecules by regulating the sponge miR-126-5p; it regulates the angiogenesis and EMT of CRC cells and promotes metastasis (Sun et al., 2019a). Additionally, MALAT1 protects the targets of miR-663a from degradation. MiR-663a and MALAT1 may form a negative feedback loop and affect the progression of CRC (Tian et al., 2018). MALAT1 functions as a ceRNA to regulate the miR-15 family. MiR-15 family inhibits the expression of LRP6 and the activation of the downstream β-catenin signaling pathway. MALAT1 regulates the transcription of the proto-oncogene RUNX2 through the miR-15s/LRP6/β-catenin signaling pathway and thus, regulates the progression of CRC (Ji et al., 2019).

Thereafter, we focus on the last lncRNA-PVT1 of the network diagram. PVT1, a previously unknown transcriptional regulator in CRC, shows a significantly high enhancer activity controlled by epigenetic regulation due to abnormal methylation involved in the occurrence and development of CRC. Enhanced expression of PVT1 is associated with the poor survival in CRC patients with clinical stage II or III status. It also exerts its function as a novel epigenetic enhancer of MYC and responsible for regulating the expression of oncogenic MYC gene (Shigeyasu et al., 2020). Furthermore, PVT1 also functions as a ceRNA to regulate the expression of target genes in the cytoplasm. For example, it can promote the proliferation and invasion of CRC cells by stabilizing Lin28 and interacting with miR-128 (He et al., 2019). Another study reported that PVT1 also promoted the specific binding of RNA-binding proteins (Lin28 and Lin28B) to let-7 by the up-regulation of Lin28 for driving carcinogenic activity of CRC; PVT1 stabilizes and post-transcriptionally regulates Lin28, which targets the Lin28/let-7 axis and promotes tumorigenesis. It is also speculated that the low expression of PVT1 in CRC inhibits EMT and angiogenesis. PVT1 promotes the occurrence of CRC by stabilizing miR-16-5p targeting the VEGFA/VEGFR1/AKT axis. Vascular endothelial growth factor A (VEGFA) is the direct downstream target of miR-16-5p. In the absence of PVT1-miR-16-5p/VEGFA/VEGFR1/AKT, signaling pathway is inactive, thereby inhibiting the progression of CRC (Wu et al., 2020a). In sum, targeting PVT1 may be a potential treatment option for CRC patients.

MiR-21 is also observed as an important multi-target miRNA in this network. Fusobacterium activates the toll-like receptor 4 signaling pathway, which leads to the activation of nuclear factor kappa B (NFκb) and up-regulation of miR-21 expression. Up-regulation of miR-21 reduces the level RAS GTPase (RASA1) and promotes the occurrence and development of CRC (Yang et al., 2017). In mice, silencing miR-21 results in a significant decrease in the expression of pro-inflammatory and cancer-promoting factors (IL6, IL-23, IL-17a and IL-21) and inhibition of tumor proliferation. Studies show that the absence of miR-21 leads to the decrease in Ki67 expression and the inhibition of tumor growth in colitis-associated colon cancer (CAC) mouse, an up-regulation of E-cadherin, and the downregulation of β-catenin and SOX9. The deletion of miR-21 increases the expression of its target gene PDCD4,

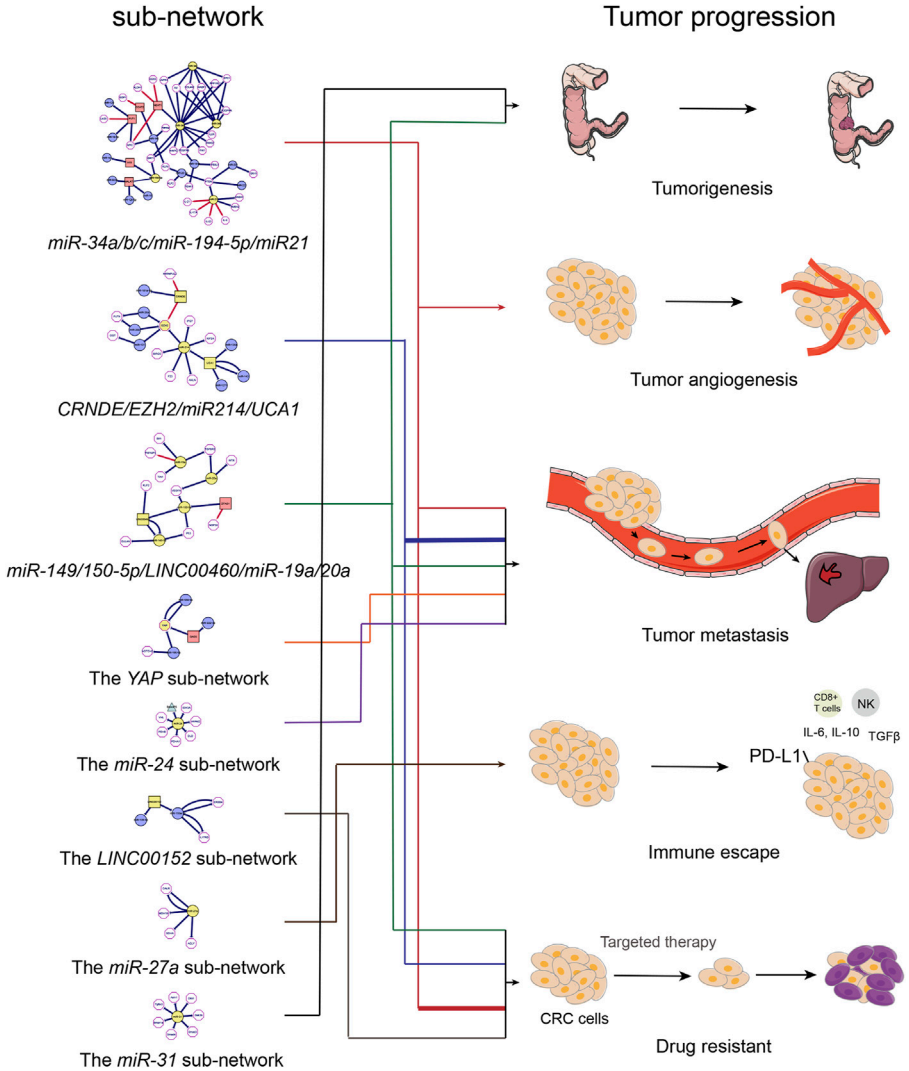


FIGURE 4 | The relationship between ncRNAs network and the progression of colorectal cancer. Diagram of the relationship between ncRNAs sub-network and colorectal cancer progression.

which in turn regulates the activation of NFκb. The deletion of miR-21 also inhibits the activation of STAT3 and Bcl-2 in CAC mice, leading to an increase in tumor cell apoptosis. These studies indicate the regulatory role of miR-21 in the development of CAC caused by colitis (Shi et al., 2016). Moreover, other studies show that miR-21 is correlated with chemotherapeutic resistance of CRC. MiR-21 regulates the expression of downstream targets PTEN and hMSH2, induces tumor cell cycle arrest, inhibits tumor cell proliferation, promotes cell apoptosis, and inhibits migration. MiR-21 targeted therapy can significantly enhance the cytotoxicity of 5-FU in resistant CRC cells and reverse the resistance in CRC just like the exosomal delivery of 5-FU (Liang et al., 2020a).

In the entire chemotherapy resistance network, LINC00152 acting as a ceRNA targets and regulates the expression of miR-193a-3p, antagonizes chemotherapy sensitivity, regulates erb-b2 receptor tyrosine kinase 4 (ERBB4), reduces the phosphorylation of AKT, and thereby reduces resistance to L-OHP (Yue et al., 2016). Similarly, it regulates the expression of NOTCH1 by inhibiting the activity of miR-139-5p, and increasing the resistance of CRC cells to 5-FU (Bian et al., 2017). These studies suggest that the Linc00152/miR-193a-3p/ERBB4/AKT and the LINC00152/miR-139-5p/NOTCH1 signaling axes may provide new insights into CRC resistance mechanisms. In addition, LINC00152 may also be a key tumor suppressor of ulcerative colitis-related CAC. Studies show that miR-193a-3p regulates the expression of IL17RD and controls the downstream EGFR signaling and inhibits the growth of colon cancer (Pekow et al., 2017). Thus, LINC00152 might be a novel potential target in the inflammation-driven CRC patients.

Metastasis Sub-network of Colorectal Cancer

The metastasis of CRC is the main reason for the poor clinical outcomes and high mortality for CRC patients. The CRNDE/

TABLE 3 | The relationship between ncRNAs network and the progression of colorectal cancer.

ncRNA network		Tumorigenesis	Tumor angiogenesis	Tumor metastasis	Immune escape	Drug resistant
The miR-34a/b/c/miR-194−5p/miR-21 sub-network	miR-34					PMID 24009080
	miR-194−5p					PMID 30451820
	miR-21					PMID 31918721
The CRNDE/EZH2/UCA1 sub-network	CRNDE					PMID 28086904
	EZH2			PMID 27638307		
	UCA1			PMID 31955010		
The miR-149/150−5p/LINC00460/miR-19a/20a sub-network	miR-149−5p		PMID 30531836			PMID 33251049
	miR-150−5p					PMID 33251049
	LINC00460					PMID 33251049
	miR-19a	PMID 27991929				
	miR-20a			PMID 30631060		
The YAP sub-network	YAP			PMID 28356122		
The miR-24 sub-network	miR-24			PMID 28500171		
The LINC00152 sub-network	LINC00152					PMID 27633443
The miR-27a sub-network	miR-27a				PMID 26913599	
The miR-31 sub-network	miR-31	PMID 28870287				

EZH2/UCA1 network is the main component of the metastasis network in CRC. The common target of multiple ncRNAs in this network was the oncogene EZH2 (enhancer of zeste2 polycomb repressive complex 2 subunits). The histone lysine N-methyltransferase encoded by the EZH2 gene is an important part of the PRC2/EED-EZH2 complex, which can methylate the "Lys-9" (H3K9me) and "Lys-27" (H3K27me) of histone H3 and inhibits the transcription of its downstream target genes (McCabe et al., 2012; Hübner et al., 2019). Mutation or over-expression of EZH2 is associated with many types of cancers (breast cancer, prostate cancer, melanoma, bladder cancer, etc.) (Bracken et al., 2003). Presently, many EZH2 targets have been identified. For example, the INK4B-ARF-INK4A tumor suppressor gene locus is a well-known target of EZH2 and its inhibition affects cancer growth and embryonic development (Kheradmand Kia et al., 2009); E-cadherin gene is another critical target of EZH2, and its down-regulation is essential for EMT and metastasis (Luo et al., 2016). Mu Xu et al. report that lncRNA SNHG6 acts as a molecular sponge of miR-26a/b and miR-214, and releases EZH2 by isolating the endogenous microRNA of CRC cells, which mainly regulates the expression of EZH2 in CRC (Xu et al., 2019a). Moreover, EZH2 and its targets H3K27me3, P14ARF, P15INK4b, P16INK4a and E-cadherin are involved in the carcinogenic effect of SNHG6 in CRC and regulate the EMT (Xu et al., 2019a).

In the sub-network of EZH2, O-glycosylation, is a unique post-translational modification (PTM), which participates in CRC metabolic reprogramming. The level of O-glycosylation increases in metastatic CRC tissues or cells. The expression of miR-101 reduces, while the expression of o-GlcNAc acyltransferase (OGT) and EZH2, which are regulated by miR-101, increases significantly. The down-regulation of miR-101 promotes O-GlcNAcylation, and the increased O-GlcNAcylation further enhances the stability and function of the EZH2 protein. O-GlcNAcylation and EZH2-mediated H3K27me3 modification of the miR-101 promoter region further reduce the expression of miR-101, consequently, miR-101/O-GlcNAcylation/EZH2 signals form a feedback loop that inhibits metastasis and eventually inhibits the invasion of CRC cells and regulate the EMT (Jiang et al., 2019). Thus, EZH2 has extremely high potential as a new target for CRC treatment.

Another important network node in the network diagram was CRNDE. CRNDE is located on human chromosome 16 and is highly expressed in a variety of cancers including CRC. CRNDE binds to EZH2, which in turn, can directly bind to DUSP5 and CDKN1A promoter regions, and induce histone H3 lysine 27 trimethylation (H3K27me3) modification in DLD1 and HCT116 cells (Ding et al., 2017a). This also inhibits dual specific phosphatase 5 (DUSP5) and CDKN1A expression and promotes the development of CRC (Ding et al., 2017a). In addition, CRNDE is also related to microRNAs. Han et al. found that miR-181a-5p could be used as the inhibitory target of CRNDE. β-catenin and TCF4 are inhibitory targets of miR-181a-5p and repress the Wnt/β-catenin signaling pathway. In CRC cell lines, CRNDE promotes CRC cell proliferation and chemotherapy resistance through the Wnt/β-catenin signaling pathway mediated by miR-181a-5p (Han et al., 2017). Thus, it warrants further studies to investigate the regulatory mechanism of CRNDE as a potential target in the therapy strategy and resistance of CRC.

Another ncRNA in the network diagram was the lncRNAs UCA1 (urothelial cancer associated 1). The presence of UCA1 in exosomes is verified, but its role and clinical applicability in CRC remain unclear. Barbagallo reported that UCA1 is upregulated in CRC biopsy (Barbagallo et al., 2018). In serum exosomes, the expression of UCA1 is regulated by an activating MAPK signal. UCA1 isolates miR-135a, miR-143, miR-214, and miR-1271 to protect ANLN, BIRC5, IPO7, KIF2A, KIF23 and other actin and cytoskeleton related proteins from miRNA-induced degradation, and thus, regulates their expression and promotes the progression of CRC and other key biological processes (Barbagallo et al., 2018). Luan et al. also demonstrate that UCA1 is upregulated in the serum exosomes of patients with CRC. UCA1 is packaged into exosomes which are transferred to CRC cells. As a ceRNA, UCA1 regulates the expression of MYO6 through miR-143, enhances cell proliferation and migration, and exerts essential functions in the tumor progression of CRC (Luan et al., 2020). Taken together, these reports suggest that UCA1 may be a potential new clinical biomarker for CRC.

From **Figure 4**, we observe that in addition to the CRNDE/EZH2/miR214/UCA1 network, the YAP sub-network and the miR-24 sub-network also play indispensable roles during the metastasis of CRC. YAP1 is upregulated through a variety of biological mechanisms and has a carcinogenic effect in a variety of tumors. As the core sub-network of CRC metastasis, YAP connected multiple ncRNAs such as GAS5, miR375, and circ1662, etc. The inactivation of YAP1 is required in cell-cell contact inhibition and act as a transcriptional co-activator to mediate the biological functions of the Hippo pathway (Zhao et al., 2007). It should be noted that lncRNA GAS5 (growth arrest-specific 5), a tumor suppressor in CRC as a ceRNA of miR-222-3p, regulates the expression of Beclin1, LC3B, and PTEN by targeting miR-222-3p/GAS5 phosphatase and PTEN signaling pathways, thereby inhibiting CRC cell migration and invasion, and promotes autophagy (Liu et al., 2019a). Notably, GAS5 as well as its target YAP are intently linked to m^6A modification. GAS5 directly interacts with the WW domain of YAP to promote the transfer of endogenous YAP from the nucleus to the cytoplasm, as well as its phosphorylation and its subsequent ubiquitin-mediated degradation which leads to tumor suppression (Ni et al., 2019). Interestingly, YTHDF3 selectively bound to GAS5 which was modified by m^6A and promoted the degradation of GAS5 in an m^6A-dependent manner. Meanwhile, GAS5 negatively regulated the expression of YAP, and YAP could bind to the promoter region of YTHDF3 to promote the transcription of YTHDF3, in other words, YTHDF3-GAS5-YAP-YTHDF3 formed a positive feedback loop and promoted the metastasis of CRC in an m^6A-dependent manner (Ni et al., 2019). Moreover, YAP not only regulated the expression of YTHDF3, m^6A modified YAP also directly bound to IGF2BP2, and stabilized YAP promoted the occurrence of CRC by up-regulating the expression of ErbB2 (Cui et al., 2021). In addition to directly regulating the expression of YAP mRNA, m^6A modification is supposed to indirectly regulate the expression of YAP1 protein. Chen et al. illustrated that the overexpression of METTL14 increased the m^6A level of primiR-375, and the m^6A-modified primiR-375 was transformed into premiR-375 under the action of DGCR8, thereby promoting the expression of miR-375 in CRC. Thereafter, elevated miR-375 suppressed the expression of YAP1, and ultimately inhibited the metastasis of CRC (Chen et al., 2020a). Interestingly, the expression of YAP1 protein is not only regulated by m^6A-modified miRNA, but also by m^6A-modified circRNA. Studies have shown that METTL3 induced the expression of circ1662 by installing m^6A modification in the circ1662 flanking reverse complement sequence. The overexpression of circ1662 promoted the transport of YAP1 protein to the nucleus and reduced the level of YAP1 protein in the cytoplasm and ultimately accelerated the metastasis of CRC (59).

MiR-590-5p inhibits the YAP expression by directly targeting its 3′UTR, thereby inhibiting intestinal inflammation and tumorigenesis of CRC cells (60). Ou et al., also validated the existence of the miR-590-5p/YAP axis. MiR-590-5p is a miRNA with density-sensitive property. The high density of CRC cells upregulates the expression of the RNase III endonuclease DICER1, which in turn promotes the biosynthesis of miR-590-5p and ultimately inhibits YAP expression (Ou et al., 2018). This also suggests that the miR-590-5p/YAP axis may be an important specific therapeutic target contributing to the pathogenesis of CRC. Furthermore, miR-590-5p itself may also serve as a therapeutic potential target for CRC patients. miR-590-5p is a hypoxia-sensitive miRNA and inhibits the expression of RECK, which promotes the invasion and metastasis of CRC cells by activating matrix metalloproteinases (MMPs) and filamentous processes in vitro, and consequently promotes tumor cell proliferation (Kim et al., 2019a). Moreover, Nuclear factor 90 (NF90), a direct target of miR-590-5p, is a positive regulator of vascular endothelial growth factor (VEGF) mRNA stability and protein synthesis. The NF90/VEGFA signaling axis can inhibit angiogenesis and metastasis in CRC (Zhou et al., 2016). In contrast, MiR-195, in the YAP sub-network, is an inhibitor of the Hippo-YAP signaling pathway. There are two conserved miR-195-5p homologous sites at the 3′UTR of YAP mRNA. MiR-195-5p inhibits EMT and blocks Hippo signaling, thereby inhibiting the proliferation, migration, invasion and epithelial-mesenchymal transition (EMT) of CRC cells (Sun et al., 2017). In addition, miR-195-5p can also regulate the expression of NOTCH2 in a post-transcriptional manner (Lin et al., 2019a).

Previous publications show that the miRNAs are usually organized in clusters (within 3 kb) in the genome and have the characteristics of a regulatory network that controls tumor metabolism. MiRNA clusters play essential roles in tumor progression by coordinating or inhibiting multiple target genes. The coordinated regulation of miRNA clusters may cause rapid switching of the metabolic signaling networks in CRC cells. Jin et al. report a cluster consisting of miR-23a, miR-27a and miR-24 induced by hypoxia conditions in CRC cells, which promotes glycolysis by regulating the related gene networks. Inhibition of miR-23a, miR-24, and miR-27a under hypoxic conditions weaken the stimulating effect of reduced oxygen on glycolysis-related genes along with the inhibitory effect on tricarboxylic acid cycle-related genes including PDHB, PDHA1, IDH2, DLD, and IDH3A. Moreover, miR-24 promotes the expression of HIF-1α by targeting VHL, forming a

double negative feedback loop and exhibits the strongest regulatory effect. Thus, it shows that the miR-23a/27a/24 cluster promotes the progression of CRC through metabolism reprogramming (Jin et al., 2019).

Other Sub-network in Colorectal Cancer

Among other sub-networks, miR-149/150-5p/LINC00460/miR-19a/20a occupies a major position. It covers tumorigenesis, metastasis and chemotherapy resistance of CRC. In the sub-network, LINC00460, acting as a vital ncRNA, linked multiple miRNAs such as miR-149-5p, miR-150-5p, etc. Studies show that LINC00460 has a carcinogenic effect on CRC. It recruits EZH2 (enhancer of zeste homolog 2, EZH2) and H3K27me3 to the tumor suppressor KLF2 promoter in the nucleus. Thereby, it epigenetically inhibits the expression and inactivation of KLF2 (Lian et al., 2018). LINC00460, as a molecular sponge of miR-149-5p, antagonizes its ability to inhibit the translation of cullin4A (CUL4A) protein and regulates the occurrence of CRC. Thereafter, LINC00460 directly interacted with IGF2BP2 and DHX9 and combined with m^{6}A-modified HGMA1 mRNA to enhance the stability of HGMA1 and ultimately promoted the metastasis of CRC (Hou et al., 2021). Notably, LINC00460 may also be a promising therapeutic target involved in chemotherapeutic resistance of CRC. Meng et al. found that LINC00460-miR-149/150-5p-mutant p53 feedback loop is associated with oxaliplatin resistance of CRC. Similarly, LINC00460 promotes oxaliplatin resistance by isolating miR-149-5p/miR-150-5p and upregulating the expression of the target p53 (Meng et al., 2020). In addition to LINC00460, the circCTNNA1 also acts as a ceRNA competitive sponging miR-149-5p to counteract its inhibitory effect on the downstream target FOXM1, thereby promoting the progression of CRC (Chen et al., 2020b). Similarly, circ5615 binds to miR-149-5p, exerting miR-149-5p sponge effect, upregulating TNKS, and subsequently promoting the progression of CRC through the Wnt/β-catenin signaling pathway (Ma et al., 2020). Thus, the carcinogenic functions of LINC00460 or circCTNNA1 as ceRNA in CRC were validated, which suggested that these indicators might be potential and valuable therapeutic targets in CRC treatment and multi-drug resistance.

Besides miR-149-5p, miR-150-5p, miR-19a/20 as critical parts of the sub-network, miR-200 family including miR-200, miR-200b-3p, and miR-200c-3p was found involved in the regulation of ZEB1 and XIST, etc. Interestingly, ZEB1 acted as one of the downstream targets of miR-200b-3p, the combination of XIST and miR-200b-3p disrupts the combination of miR-200b-3p and ZEB1. Meanwhile, XIST can also act as a sponge of miR-200b-3p to promote the expression of ZEB1 and thus promote the progression and metastasis of CRC (71). Importantly, recent report supports that METTL14 can increase the m^{6}A level of XIST and decrease the expression of XIST in a YTHDF2-dependent regulation manner. The decrease of XIST expression promotes the expression of miR-200b-3p by directly binding to miR-200b-3p (Yang et al., 2020a). Thus, these findings indicated that linking m^{6}A-modified XIST with miR-200 and miR-200c-3p might provide novel directions and approach for excavating the potential targets for CRC therapy.

Notably, another lncRNA, ZFAS1 is highly expressed in CRC tissues and cells. Moreover, as a miR-150-5p sponge, it targets and regulates the expression of its downstream VEGFA, and promotes the progression of CRC by promoting miR150-5p-mediated VEGFA/VEGFR2/Akt/mTOR signaling pathway and EMT (Chen et al., 2018). In addition, studies show that ZFAS1 promotes CRC by small nucleolar RNA-mediated 2′-O methylation through NOP58 recruitment and plays essential roles through the ZFAS1-NOP58-SNORD12C/78-EIF4A3/LAMC2 signaling axis (Wu et al., 2020b). Collectively, these researches broaden our spectrum and lay a solid foundation for further excavating the crosstalk functions between epigenetic modification and ncRNAs during the early prediction and therapy of CRC.

CONCLUSIONS AND PERSPECTIVES

During the past few decades, extensive promotions have been made to explore the biological functions of ncRNAs in the involvement of tumorigenesis and progression of various types of tumors including CRC. In this review, we analyzed the regulation network and sub-networks related to ncRNAs involved in the progression, metastasis and chemoresistance of CRC via transcriptional and post-transcriptional epigenetic modification levels. Among the networks, the miR-34a/b/c/miR-194-5p/miR21 sub-network showed a direct relationship with oxaliplatin resistance for CRC therapy. Meanwhile, the CRNDE/EZH2/UCA1 sub-network had a significant association with metastasis and progression of CRC. Furthermore, we analyzed the regulatory manner of the core m^{6}A regulators with m^{6}A-related ncRNAs as exemplified by YTHDF3-GAS5-YAP, IGF2BP2-YAP-ErbB2, METTL14-YTHDF2-XIST, MeCP2/METTL14-KLF4, LINC00460/IGF2BP2/DHX9-HMGA1 signaling axis in CRC progression.

Thus, the crosstalk and regulation network of m^{6}A modifications associated modulators and ncRNAs provide a novel direction for exploring the underlying regulatory mechanisms of gene expression in CRC development.

Until now, multiple ncRNAs associated epigenetic m^{6}A modification modulators has been found acting as potential biomarkers and targets for CRC therapeutic interventions. However, these indicators have not been effectively developed and applied for the CRC therapy, partly due to exceeding targets for each regulator. For example, IGF2BP1, IGF2BP2 and IGF2BP3 has an enrichment of 3747, 3211, and 3914 high confidence downstream targets, respectively (Huang et al., 2018a). These targets and cellular biological pathways were closely connected to form a huge ncRNAs regulatory network. Thus, targeting multiple dysregulated targets in the m^{6}A associated ncRNAs network holds an important potential direction contributing for CRC therapy. Developing highly specific and selective small-molecule inhibitors targeting m^{6}A regulators and associated ncRNAs demand urgently for inter-individual precision therapy of CRC. Overall, the regulatory network provides a foundation for further study of ncRNAs, which also provide critical possibilities for clinical treatment

through their associations with m^6A epigenetic modifications that warrants further investigations for CRC.

AUTHOR CONTRIBUTIONS

XD and HW contributed to the conception of this study. XD and SL drafted the manuscript. XD, SL, XH and TS made the diagrams and tables. XD, SL and YW conducted literature screening and data collection. HW, XW, MW and SL revised the manuscript. All authors read and approved the final manuscript.

FUNDING

This work was supported by grants from the National Natural Science Foundation of China (81872905, 82073884), Shenyang S&T Projects (20-204-4-22, 19-109-4-09), Liaoning Revitalization Talents Program (XLYC1807155), Science and Technology Innovative Foundation for Young and Middle-aged Scientists of Shenyang City (RC200382), Science and Technology Program of Liaoning Province (2017225036), Shenyang High Level Talent Innovation and Entrepreneurship Team (2019-SYRCCY-B-01), and Major Special S&T Projects in Liaoning Province (2019JH1/10300005).

REFERENCES

Aljagthmi, A. A., Hill, N. T., Cooke, M., Kazanietz, M. G., Abba, M. C., Long, W., et al. (2019). ΔNp63α Suppresses Cells Invasion by Downregulating PKCγ/Rac1 Signaling through miR-320a. *Cell Death Dis* 10 (9), 680. doi:10.1038/s41419-019-1921-6

An, H.-J., Kwak, S.-Y., Yoo, J.-O., Kim, J.-S., Bae, I.-H., Park, M.-J., et al. (2016). Novel miR-5582-5p Functions as a Tumor Suppressor by Inducing Apoptosis and Cell Cycle Arrest in Cancer Cells through Direct Targeting of GAB1, SHC1, and CDK2. *Biochim. Biophys. Acta (Bba) - Mol. Basis Dis.* 1862 (10), 1926–1937. doi:10.1016/j.bbadis.2016.07.017

Antoniali, G., Serra, F., Lirussi, L., Tanaka, M., D'Ambrosio, C., Zhang, S., et al. (2017). Mammalian APE1 Controls miRNA Processing and its Interactome Is Linked to Cancer RNA Metabolism. *Nat. Commun.* 8 (1), 797. doi:10.1038/s41467-017-00842-8

Bao, Y., Tang, J., Qian, Y., Sun, T., Chen, H., Chen, Z., et al. (2019). Long Noncoding RNA BFAL1 Mediates Enterotoxigenic Bacteroides Fragilis-Related Carcinogenesis in Colorectal Cancer via the RHEB/mTOR Pathway. *Cel Death Dis* 10 (9), 675. doi:10.1038/s41419-019-1925-2

Barbáchano, A., Fernández-Barral, A., Pereira, F., Segura, M. F., Ordóñez-Morán, P., Carrillo-de Santa Pau, E., et al. (2016). SPROUTY-2 Represses the Epithelial Phenotype of colon Carcinoma Cells via Upregulation of ZEB1 Mediated by ETS1 and miR-200/miR-150. *Oncogene* 35 (23), 2991–3003. doi:10.1038/onc.2015.366

Barbagallo, C., Brex, D., Caponnetto, A., Cirnigliaro, M., Scalia, M., Magnano, A., et al. (2018). LncRNA UCA1, Upregulated in CRC Biopsies and Downregulated in Serum Exosomes, Controls mRNA Expression by RNA-RNA Interactions. *Mol. Ther. - Nucleic Acids* 12, 229–241. doi:10.1016/j.omtn.2018.05.009

Bhan, A., and Mandal, S. S. (2015). LncRNA HOTAIR: A Master Regulator of Chromatin Dynamics and Cancer. *Biochim. Biophys. Acta (Bba) - Rev. Cancer* 1856 (1), 151–164. doi:10.1016/j.bbcan.2015.07.001

Bian, Z., Zhang, J., Li, M., Feng, Y., Wang, X., Zhang, J., et al. (2018). LncRNA-FEZF1-AS1 Promotes Tumor Proliferation and Metastasis in Colorectal Cancer by Regulating PKM2 Signaling. *Clin. Cancer Res.* 24 (19), 4808–4819. doi:10.1158/1078-0432.ccr-17-2967

Bian, Z., Zhang, J., Li, M., Feng, Y., Yao, S., Song, M., et al. (2017). Long Non-coding RNA LINC00152 Promotes Cell Proliferation, Metastasis, and Confers 5-FU Resistance in Colorectal Cancer by Inhibiting miR-139-5p. *Oncogenesis* 6 (11), 395. doi:10.1038/s41389-017-0008-4

Bleau, A.-M., Redrado, M., Nistal-Villan, E., Villalba, M., Exposito, F., Redin, E., et al. (2018). miR-146a Targets C-Met and Abolishes Colorectal Cancer Liver Metastasis. *Cancer Lett.* 414, 257–267. doi:10.1016/j.canlet.2017.11.008

Bracken, A. P., Pasini, D., Capra, M., Prosperini, E., Colli, E., and Helin, K. (2003). EZH2 Is Downstream of the pRB-E2f Pathway, Essential for Proliferation and Amplified in Cancer. *EMBO J.* 22 (20), 5323–5335. doi:10.1093/emboj/cdg542

Cao, B., Wang, K., Liao, J. M., Zhou, X., Liao, P., Zeng, S. X., et al. (2016). Inactivation of Oncogenic cAMP-specific Phosphodiesterase 4D by miR-139-5p in Response to P53 Activation. *Elife* 5. doi:10.7554/eLife.15978

Cen, B., Lang, J. D., Du, Y., Wei, J., Xiong, Y., Bradley, N., et al. (2020). Prostaglandin E2 Induces miR675-5p to Promote Colorectal Tumor Metastasis via Modulation of P53 Expression. *Gastroenterology* 158 (4), 971–984. doi:10.1053/j.gastro.2019.11.013

Chang, H.-Y., Ye, S.-P., Pan, S.-L., Kuo, T.-T., Liu, B. C., Chen, Y.-L., et al. (2017). Overexpression of miR-194 Reverses HMGA2-Driven Signatures in Colorectal Cancer. *Theranostics* 7 (16), 3889–3900. doi:10.7150/thno.20041

Chaudhary, R., Gryder, B., Woods, W. S., Subramanian, M., Jones, M. F., Li, X. L., et al. (2017). Prosurvival Long Noncoding RNA PINCR Regulates a Subset of P53 Targets in Human Colorectal Cancer Cells by Binding to Matrin 3. *Elife* 6. doi:10.7554/eLife.23244

Chen, B., Dragomir, M. P., Fabris, L., Bayraktar, R., Knutsen, E., Liu, X., et al. (2020). The Long Noncoding RNA CCAT2 Induces Chromosomal Instability through BOP1-AURKB Signaling. *Gastroenterology* 159 (6), 2146–2162. doi:10.1053/j.gastro.2020.08.018

Chen, C., Yuan, W., Zhou, Q., Shao, B., Guo, Y., Wang, W., et al. (2021). N6-methyladenosine-induced Circ1662 Promotes Metastasis of Colorectal Cancer by Accelerating YAP1 Nuclear Localization. *Theranostics* 11 (9), 4298–4315. doi:10.7150/thno.51342

Chen, D.-l., Chen, L.-z., Lu, Y.-x., Zhang, D.-s., Zeng, Z.-l., Pan, Z.-z., et al. (2017). Long Noncoding RNA XIST Expedites Metastasis and Modulates Epithelial-Mesenchymal Transition in Colorectal Cancer. *Cel Death Dis* 8 (8), e3011. doi:10.1038/cddis.2017.421

Chen, D.-l., Lu, Y.-x., Zhang, J.-x., Wei, X.-l., Wang, F., Zeng, Z.-l., et al. (2017). Long Non-coding RNA UICLM Promotes Colorectal Cancer Liver Metastasis by Acting as a ceRNA for microRNA-215 to Regulate ZEB2 Expression. *Theranostics* 7 (19), 4836–4849. doi:10.7150/thno.20942

Chen, P., Yao, Y., Yang, N., Gong, L., Kong, Y., and Wu, A. (2020). Circular RNA circCTNNA1 Promotes Colorectal Cancer Progression by Sponging miR-149-5p and Regulating FOXM1 Expression. *Cel Death Dis* 11 (7), 557. doi:10.1038/s41419-020-02757-7

Chen, R.-X., Chen, X., Xia, L.-P., Zhang, J.-X., Pan, Z.-Z., Ma, X.-D., et al. (2019). N6-methyladenosine Modification of circNSUN2 Facilitates Cytoplasmic export and Stabilizes HMGA2 to Promote Colorectal Liver Metastasis. *Nat. Commun.* 10 (1), 4695. doi:10.1038/s41467-019-12651-2

Chen, S., Su, T., Zhang, Y., Lee, A., He, J., Ge, Q., et al. (2020). Fusobacterium Nucleatum Promotes Colorectal Cancer Metastasis by Modulating KRT7-AS/KRT7. *Gut Microbes* 11 (3), 511–525. doi:10.1080/19490976.2019.1695494

Chen, S., Yue, T., Huang, Z., Zhu, J., Bu, D., Wang, X., et al. (2019). Inhibition of Hydrogen Sulfide Synthesis Reverses Acquired Resistance to 5-FU through miR-215-5p-EREG/TYMS axis in colon Cancer Cells. *Cancer Lett.* 466, 49–60. doi:10.1016/j.canlet.2019.09.006

Chen, X., Xu, M., Xu, X., Zeng, K., Liu, X., Sun, L., et al. (2020). METTL14 Suppresses CRC Progression via Regulating N6-methyladenosine-dependent Primary miR-375 Processing. *Mol. Ther.* 28 (2), 599–612. doi:10.1016/j.ymthe.2019.11.016

Chen, X., Zeng, K., Xu, M., Hu, X., Liu, X., Xu, T., et al. (2018). SP1-induced lncRNA-ZFAS1 Contributes to Colorectal Cancer Progression via the miR-150-5p/VEGFA axis. *Cel Death Dis* 9 (10), 982. doi:10.1038/s41419-018-0962-6

Chen, X., Zeng, K., Xu, M., Liu, X., Hu, X., Xu, T., et al. (2019). P53-induced miR-1249 Inhibits Tumor Growth, Metastasis, and Angiogenesis by Targeting VEGFA and HMGA2. *Cel Death Dis* 10 (2), 131. doi:10.1038/s41419-018-1188-3

Chen, Z., Ren, R., Wan, D., Wang, Y., Xue, X., Jiang, M., et al. (2019). Hsa_circ_101555 Functions as a Competing Endogenous RNA of miR-597-5p to Promote Colorectal Cancer Progression. *Oncogene* 38 (32), 6017–6034. doi:10.1038/s41388-019-0857-8

Choe, M. H., Yoon, Y., Kim, J., Hwang, S.-G., Han, Y.-H., and Kim, J.-S. (2018). miR-550a-3-5p Acts as a Tumor Suppressor and Reverses BRAF Inhibitor Resistance through the Direct Targeting of YAP. *Cel Death Dis* 9 (6), 640. doi:10.1038/s41419-018-0698-3

Colangelo, T., Polcaro, G., Ziccardi, P., Muccillo, L., Galgani, M., Pucci, B., et al. (2016). The miR-27a-Calreticulin axis Affects Drug-Induced Immunogenic Cell Death in Human Colorectal Cancer Cells. *Cel Death Dis* 7, e2108. doi:10.1038/cddis.2016.29

Colangelo, T., Polcaro, G., Ziccardi, P., Pucci, B., Muccillo, L., Galgani, M., et al. (2016). Proteomic Screening Identifies Calreticulin as a miR-27a Direct Target Repressing MHC Class I Cell Surface Exposure in Colorectal Cancer. *Cel Death Dis* 7, e2120. doi:10.1038/cddis.2016.28

Cui, J., Tian, J., Wang, W., He, T., Li, X., Gu, C., et al. (2021). IGF2BP2 Promotes the Progression of Colorectal Cancer through a YAP-dependent Mechanism. *Cancer Sci*.

Damas, N. D., Marcatti, M., Côme, C., Christensen, L. L., Nielsen, M. M., Baumgartner, R., et al. (2016). SNHG5 Promotes Colorectal Cancer Cell Survival by Counteracting STAU1-Mediated mRNA Destabilization. *Nat. Commun.* 7, 13875. doi:10.1038/ncomms13875

Dang, Q., Shao, B., Zhou, Q., Chen, C., Guo, Y., Wang, G., et al. (2021). RNA N6-Methyladenosine in Cancer Metastasis: Roles, Mechanisms, and Applications. *Front. Oncol.* 11, 681781. doi:10.3389/fonc.2021.681781

Deng, X., Li, S., Kong, F., Ruan, H., Xu, X., Zhang, X., et al. (2020). Long Noncoding RNA PiHL Regulates P53 Protein Stability through GRWD1/RPL11/MDM2 axis in Colorectal Cancer. *Theranostics* 10 (1), 265–280. doi:10.7150/thno.36045

Di Cecilia, S., Zhang, F., Sancho, A., Li, S., Aguiló, F., Sun, Y., et al. (2016). RBM5-AS1 Is Critical for Self-Renewal of Colon Cancer Stem-like Cells. *Cancer Res.* 76 (19), 5615–5627. doi:10.1158/0008-5472.can-15-1824

Di, W., Weinan, X., Xin, L., Zhiwei, Y., Xinyue, G., Jinxue, T., et al. (2019). Long Noncoding RNA SNHG14 Facilitates Colorectal Cancer Metastasis through Targeting EZH2-Regulated EPHA7. *Cel Death Dis* 10 (7), 514. doi:10.1038/s41419-019-1707-x

Ding, J., Li, J., Wang, H., Tian, Y., Xie, M., He, X., et al. (2017). Long Noncoding RNA CRNDE Promotes Colorectal Cancer Cell Proliferation via Epigenetically Silencing DUSP5/CDKN1A Expression. *Cel Death Dis* 8 (8), e2997. doi:10.1038/cddis.2017.328

Ding, J., Xie, M., Lian, Y., Zhu, Y., Peng, P., Wang, J., et al. (2017). Long Noncoding RNA HOXA-AS2 Represses P21 and KLF2 Expression Transcription by Binding with EZH2, LSD1 in Colorectal Cancer. *Oncogenesis* 6 (1), e288. doi:10.1038/oncsis.2016.84

Fang, C., Qiu, S., Sun, F., Li, W., Wang, Z., Yue, B., et al. (2017). Long Non-coding RNA HNF1A-AS1 Mediated Repression of miR-34a/SIRT1/p53 Feedback Loop Promotes the Metastatic Progression of colon Cancer by Functioning as a Competing Endogenous RNA. *Cancer Lett.* 410, 50–62. doi:10.1016/j.canlet.2017.09.012

Gao, Q., Zhou, R., Meng, Y., Duan, R., Wu, L., Li, R., et al. (2020). Long Noncoding RNA CMPK2 Promotes Colorectal Cancer Progression by Activating the FUBP3-C-Myc axis. *Oncogene* 39 (19), 3926–3938. doi:10.1038/s41388-020-1266-8

Gao, Y., Sun, W., Shang, W., Li, Y., Zhang, D., Wang, T., et al. (2018). Lnc-C/Ebpβ Negatively Regulates the Suppressive Function of Myeloid-Derived Suppressor Cells. *Cancer Immunol. Res.* 6 (11), 1352–1363. doi:10.1158/2326-6066.cir-18-0108

Giakountis, A., Moulos, P., Zarkou, V., Oikonomou, C., Harokopos, V., Hatzigeorgiou, A. G., et al. (2016). A Positive Regulatory Loop between a Wnt-Regulated Non-coding RNA and ASCL2 Controls Intestinal Stem Cell Fate. *Cel Rep.* 15 (12), 2588–2596. doi:10.1016/j.celrep.2016.05.038

Gu, C., Cai, J., Xu, Z., Zhou, S., Ye, L., Yan, Q., et al. (2019). MiR-532-3p Suppresses Colorectal Cancer Progression by Disrupting the ETS1/TGM2 axis-mediated Wnt/β-Catenin Signaling. *Cel Death Dis* 10 (10), 739. doi:10.1038/s41419-019-1962-x

Gu, D., Li, S., Du, M., Tang, C., Chu, H., Tong, N., et al. (2019). A Genetic Variant Located in the miR-532-5p-Binding Site of TGFBR1 Is Associated with the Colorectal Cancer Risk. *J. Gastroenterol.* 54 (2), 141–148. doi:10.1007/s00535-018-1490-y

Gulei, D., Magdo, L., Jurj, A., Raduly, L., Cojocneanu-Petric, R., Moldovan, A., et al. (2018). The Silent Healer: miR-205-5p Up-Regulation Inhibits Epithelial to Mesenchymal Transition in colon Cancer Cells by Indirectly Up-Regulating E-Cadherin Expression. *Cel Death Dis* 9 (2), 66. doi:10.1038/s41419-017-0102-8

Guo, H., Liu, J., Ben, Q., Qu, Y., Li, M., Wang, Y., et al. (2016). The Aspirin-Induced Long Non-coding RNA OLA1P2 Blocks Phosphorylated STAT3 Homodimer Formation. *Genome Biol.* 17, 24. doi:10.1186/s13059-016-0892-5

Guo, K., Gong, W., Wang, Q., Gu, G., Zheng, T., Li, Y., et al. (2020). LINC01106 Drives Colorectal Cancer Growth and Stemness through a Positive Feedback Loop to Regulate the Gli Family Factors. *Cel Death Dis* 11 (10), 869. doi:10.1038/s41419-020-03026-3

Guo, X., Zhu, Y., Hong, X., Zhang, M., Qiu, X., Wang, Z., et al. (2017). miR-181d and C-Myc-Mediated Inhibition of CRY2 and FBXL3 Reprograms Metabolism in Colorectal Cancer. *Cel Death Dis* 8 (7), e2958. doi:10.1038/cddis.2017.300

Guo, Y., Ye, Q., Deng, P., Cao, Y., He, D., Zhou, Z., et al. (2020). Spermine Synthase and MYC Cooperate to Maintain Colorectal Cancer Cell Survival by Repressing Bim Expression. *Nat. Commun.* 11 (1), 3243. doi:10.1038/s41467-020-17067-x

Han, P., Li, J.-w., Zhang, B.-m., Lv, J.-c., Li, Y.-m., Gu, X.-y., et al. (2017). The lncRNA CRNDE Promotes Colorectal Cancer Cell Proliferation and Chemoresistance via miR-181a-5p-Mediated Regulation of Wnt/β-Catenin Signaling. *Mol. Cancer* 16 (1), 9. doi:10.1186/s12943-017-0583-1

Han, Q., Xu, L., Lin, W., Yao, X., Jiang, M., Zhou, R., et al. (2019). Long Noncoding RNA CRCMSL Suppresses Tumor Invasive and Metastasis in Colorectal Carcinoma through Nucleocytoplasmic Shuttling of HMGB2. *Oncogene* 38 (16), 3019–3032. doi:10.1038/s41388-018-0614-4

He, C., Yu, T., Shi, Y., Ma, C., Yang, W., Fang, L., et al. (2017). MicroRNA 301A Promotes Intestinal Inflammation and Colitis-Associated Cancer Development by Inhibiting BTG1. *Gastroenterology* 152 (6), 1434–1448. doi:10.1053/j.gastro.2017.01.049

He, F., Song, Z., Chen, H., Chen, Z., Yang, P., Li, W., et al. (2019). Long Noncoding RNA PVT1-214 Promotes Proliferation and Invasion of Colorectal Cancer by Stabilizing Lin28 and Interacting with miR-128. *Oncogene* 38 (2), 164–179. doi:10.1038/s41388-018-0432-8

Hou, P., Meng, S., Li, M., Lin, T., Chu, S., Li, Z., et al. (2021). LINC00460/DHX9/IGF2BP2 Complex Promotes Colorectal Cancer Proliferation and Metastasis by Mediating HMGA1 mRNA Stability Depending on m6A Modification. *J. Exp. Clin. Cancer Res.* 40 (1), 52. doi:10.1186/s13046-021-01857-2

Hu, J. L., Wang, W., Lan, X. L., Zeng, Z. C., Liang, Y. S., Yan, Y. R., et al. (2019). CAFs Secreted Exosomes Promote Metastasis and Chemotherapy Resistance by Enhancing Cell Stemness and Epithelial-Mesenchymal Transition in Colorectal Cancer. *Mol. Cancer* 18 (1), 91. doi:10.1186/s12943-019-1019-x

Huang, H., Weng, H., Sun, W., Qin, X., Shi, H., Wu, H., et al. (2018). Recognition of RNA N6-Methyladenosine by IGF2BP Proteins Enhances mRNA Stability and Translation. *Nat. Cel Biol* 20 (3), 285–295. doi:10.1038/s41556-018-0045-z

Huang, L., Wen, C., Yang, X., Lou, Q., Wang, X., Che, J., et al. (2018). PEAK1, Acting as a Tumor Promoter in Colorectal Cancer, Is Regulated by the EGFR/KRas Signaling axis and miR-181d. *Cel Death Dis* 9 (3), 271. doi:10.1038/s41419-018-0320-8

Huang, Q., Xia, J., Wang, L., Wang, X., Ma, X., Deng, Q., et al. (2018). miR-153 Suppresses Ido1 Expression and Enhances CAR T Cell Immunotherapy. *J. Hematol. Oncol.* 11 (1), 58. doi:10.1186/s13045-018-0600-x

Hübner, J.-M., Müller, T., Papageorgiou, D. N., Mauermann, M., Krijgsveld, J., Russell, R. B., et al. (2019). EZHIP/CXorf67 Mimics K27M Mutated Oncohistones and Functions as an Intrinsic Inhibitor of PRC2 Function in Aggressive Posterior Fossa Ependymoma. *Neuro Oncol.* 21 (7), 878–889. doi:10.1093/neuonc/noz058

Jacob, J., Favicchio, R., Karimian, N., Mehrabi, M., Harding, V., Castellano, L., et al. (2016). LMTK3 Escapes Tumour Suppressor miRNAs via Sequestration of DDX5. *Cancer Lett.* 372 (1), 137–146. doi:10.1016/j.canlet.2015.12.026

Ji, D., Zhan, T., Li, M., Yao, Y., Jia, J., Yi, H., et al. (2018). Enhancement of Sensitivity to Chemo/Radiation Therapy by Using miR-15b against DCLK1 in Colorectal Cancer. *Stem Cel Rep.* 11 (6), 1506–1522. doi:10.1016/j.stemcr.2018.10.015

Ji, L., Li, X., Zhou, Z., Zheng, Z., Jin, L., and Jiang, F. (2020). LINC01413/hnRNP-K/ZEB1 Axis Accelerates Cell Proliferation and EMT in Colorectal Cancer via

Inducing YAP1/TAZ1 Translocation. *Mol. Ther. - Nucleic Acids* 19, 546–561. doi:10.1016/j.omtn.2019.11.027

Ji, Q., Cai, G., Liu, X., Zhang, Y., Wang, Y., Zhou, L., et al. (2019). MALAT1 Regulates the Transcriptional and Translational Levels of Proto-Oncogene RUNX2 in Colorectal Cancer Metastasis. *Cel Death Dis* 10 (6), 378. doi:10.1038/s41419-019-1598-x

Jiang, B., Tang, Y., Wang, H., Chen, C., Yu, W., Sun, H., et al. (2020). Down-regulation of Long Non-coding RNA HOTAIR Promotes Angiogenesis via Regulating miR-126/SCEL Pathways in Burn Wound Healing. *Cel Death Dis* 11 (1), 61. doi:10.1038/s41419-020-2247-0

Jiang, H., Li, T., Qu, Y., Wang, X., Li, B., Song, J., et al. (2018). Long Non-coding RNA SNHG15 Interacts with and Stabilizes Transcription Factor Slug and Promotes colon Cancer Progression. *Cancer Lett.* 425, 78–87. doi:10.1016/j.canlet.2018.03.038

Jiang, H., Wang, Y., Ai, M., Wang, H., Duan, Z., Wang, H., et al. (2017). Long Noncoding RNA CRNDE Stabilized by hnRNPUL2 Accelerates Cell Proliferation and Migration in Colorectal Carcinoma via Activating Ras/MAPK Signaling Pathways. *Cel Death Dis* 8 (6), e2862. doi:10.1038/cddis.2017.258

Jiang, L., and Hermeking, H. (2017). miR-34a and miR-34b/c Suppress Intestinal Tumorigenesis. *Cancer Res.* 77 (10), 2746–2758. doi:10.1158/0008-5472.can-16-2183

Jiang, M., Xu, B., Li, X., Shang, Y., Chu, Y., Wang, W., et al. (2019). O-GlcNAcylation Promotes Colorectal Cancer Metastasis via the miR-101-O-GlcNAc/EZH2 Regulatory Feedback Circuit. *Oncogene* 38 (3), 301–316. doi:10.1038/s41388-018-0435-5

Jin, F., Yang, R., Wei, Y., Wang, D., Zhu, Y., Wang, X., et al. (2019). HIF-1α-induced miR-23a~27a~24 Cluster Promotes Colorectal Cancer Progression via Reprogramming Metabolism. *Cancer Lett.* 440-441, 211–222. doi:10.1016/j.canlet.2018.10.025

Kawasaki, Y., Miyamoto, M., Oda, T., Matsumura, K., Negishi, L., Nakato, R., et al. (2019). The Novel lncRNA CALIC Upregulates AXL to Promote colon Cancer Metastasis. *EMBO Rep.* 20 (8), e47052. doi:10.15252/embr.201847052

Kawasaki, Y., Komiya, M., Matsumura, K., Negishi, L., Suda, S., Okuno, M., et al. (2016). MYU, a Target lncRNA for Wnt/c-Myc Signaling, Mediates Induction of CDK6 to Promote Cell Cycle Progression. *Cel Rep.* 16 (10), 2554–2564. doi:10.1016/j.celrep.2016.08.015

Kelley, K. A., Ruhl, R. A., Rana, S. R., Dewey, E., Espinosa, C., Thomas, C. R., Jr., et al. (2017). Understanding and Resetting Radiation Sensitivity in Rectal Cancer. *Ann. Surg.* 266 (4), 610–616. doi:10.1097/sla.0000000000002409

Kheradmand Kia, S., Solaimani Kartalaei, P., Farahbakhshian, E., Pourfarzad, F., von Lindern, M., and Verrijzer, C. P. (2009). EZH2-dependent Chromatin Looping Controls INK4a and INK4b, but Not ARF, during Human Progenitor Cell Differentiation and Cellular Senescence. *Epigenetics & Chromatin* 2 (1), 16. doi:10.1186/1756-8935-2-16

Kim, C., Hong, Y., Lee, H., Kang, H., and Lee, E. K. (2018). MicroRNA-195 Desensitizes HCT116 Human colon Cancer Cells to 5-fluorouracil. *Cancer Lett.* 412, 264–271. doi:10.1016/j.canlet.2017.10.022

Kim, C. W., Oh, E.-T., Kim, J. M., Park, J.-S., Lee, D. H., Lee, J.-S., et al. (2019). Hypoxia-induced microRNA-590-5p Promotes Colorectal Cancer Progression by Modulating Matrix Metalloproteinase Activity. *Cancer Lett.* 416, 3173–3241. doi:10.1016/j.canlet.2017.12.018

Kim, Y.-J., Lee, J. H., Jin, S., Kim, J. H., and Kim, S. H. (2019). Primate-specific miR-944 Activates P53-dependent Tumor Suppression in Human Colorectal Cancers. *Cancer Lett.* 440-441, 168–179. doi:10.1016/j.canlet.2018.10.029

Kong, J., Sun, W., Li, C., Wan, L., Wang, S., Wu, Y., et al. (2016). Long Non-coding RNA LINC01133 Inhibits Epithelial-Mesenchymal Transition and Metastasis in Colorectal Cancer by Interacting with SRSF6. *Cancer Lett.* 380 (2), 476–484. doi:10.1016/j.canlet.2016.07.015

Kristensen, L. S., Ebbesen, K. K., Sokol, M., Jakobsen, T., Korsgaard, U., Eriksen, A. C., et al. (2020). Spatial Expression Analyses of the Putative Oncogene ciRS-7 in Cancer Reshape the microRNA Sponge Theory. *Nat. Commun.* 11 (1), 4551. doi:10.1038/s41467-020-18355-2

Lee, Y. S., and Dutta, A. (2009). MicroRNAs in Cancer. *Annu. Rev. Pathol. Mech. Dis.* 4, 199–227. doi:10.1146/annurev.pathol.4.110807.092222

Li, H., Rokavec, M., Jiang, L., Horst, D., and Hermeking, H. (2017). Antagonistic Effects of P53 and HIF1A on microRNA-34a Regulation of PPP1R11 and STAT3 and Hypoxia-Induced Epithelial to Mesenchymal Transition in Colorectal Cancer Cells. *Gastroenterology* 153 (2), 505–520. doi:10.1053/j.gastro.2017.04.017

Li, J., Song, P., Jiang, T., Dai, D., Wang, H., Sun, J., et al. (2018). Heat Shock Factor 1 Epigenetically Stimulates Glutaminase-1-dependent mTOR Activation to Promote Colorectal Carcinogenesis. *Mol. Ther.* 26 (7), 1828–1839. doi:10.1016/j.ymthe.2018.04.014

Li, J., Sun, D., Pu, W., Wang, J., and Peng, Y. (2020). Circular RNAs in Cancer: Biogenesis, Function, and Clinical Significance. *Trends Cancer* 6 (4), 319–336. doi:10.1016/j.trecan.2020.01.012

Li, L., Kang, L., Zhao, W., Feng, Y., Liu, W., Wang, T., et al. (2017). miR-30a-5p Suppresses Breast Tumor Growth and Metastasis through Inhibition of LDHA-Mediated Warburg Effect. *Cancer Lett.* 400, 89–98. doi:10.1016/j.canlet.2017.04.034

Li, P., Zhang, X., Wang, L., Du, L., Yang, Y., Liu, T., et al. (2017). lncRNA HOTAIR Contributes to 5FU Resistance through Suppressing miR-218 and Activating NF-Kb/TS Signaling in Colorectal Cancer. *Mol. Ther. - Nucleic Acids* 8, 356–369. doi:10.1016/j.omtn.2017.07.007

Li, Q., Wang, Y., Wu, S., Zhou, Z., Ding, X., Shi, R., et al. (2019). CircACC1 Regulates Assembly and Activation of AMPK Complex under Metabolic Stress. *Cel Metab.* 30 (1), 157–173. doi:10.1016/j.cmet.2019.05.009

Li, Y., Sun, Z., Liu, B., Shan, Y., Zhao, L., and Jia, L. (2017). Tumor-suppressive miR-26a and miR-26b Inhibit Cell Aggressiveness by Regulating FUT4 in Colorectal Cancer. *Cel Death Dis* 8 (6), e2892. doi:10.1038/cddis.2017.281

Li, Y., Zeng, C., Hu, J., Pan, Y., Shan, Y., Liu, B., et al. (2018). Long Non-coding RNA-SNHG7 Acts as a Target of miR-34a to Increase GALNT7 Level and Regulate PI3K/Akt/mTOR Pathway in Colorectal Cancer Progression. *J. Hematol. Oncol.* 11 (1), 89. doi:10.1186/s13045-018-0632-2

Lian, Y., Yan, C., Xu, H., Yang, J., Yu, Y., Zhou, J., et al. (2018). A Novel lncRNA, LINC00460, Affects Cell Proliferation and Apoptosis by Regulating KLF2 and CUL4A Expression in Colorectal Cancer. *Mol. Ther. - Nucleic Acids* 12, 684–697. doi:10.1016/j.omtn.2018.06.012

Liang, C., Zhao, T., Li, H., He, F., Zhao, X., Zhang, Y., et al. (2019). Long Non-coding RNA ITIH4-AS1 Accelerates the Proliferation and Metastasis of Colorectal Cancer by Activating JAK/STAT3 Signaling. *Mol. Ther. - Nucleic Acids* 18, 183–193. doi:10.1016/j.omtn.2019.08.009

Liang, G., Zhu, Y., Ali, D. J., Tian, T., Xu, H., Si, K., et al. (2020). Engineered Exosomes for Targeted Co-delivery of miR-21 Inhibitor and Chemotherapeutics to Reverse Drug Resistance in colon Cancer. *J. Nanobiotechnol* 18 (1), 10. doi:10.1186/s12951-019-0563-2

Liang, L., Gao, C., Li, Y., Sun, M., Xu, J., Li, H., et al. (2017). miR-125a-3p/FUT5-FUT6 axis Mediates Colorectal Cancer Cell Proliferation, Migration, Invasion and Pathological Angiogenesis via PI3K-Akt Pathway. *Cel Death Dis* 8 (8), e2968. doi:10.1038/cddis.2017.352

Liang, Y., Hou, L., Li, L., Li, L., Zhu, L., Wang, Y., et al. (2020). Dichloroacetate Restores Colorectal Cancer Chemosensitivity through the p53/miR-149-3p/PDK2-Mediated Glucose Metabolic Pathway. *Oncogene* 39 (2), 469–485. doi:10.1038/s41388-019-1035-8

Liang, Z.-x., Liu, H.-s., Wang, F.-w., Xiong, L., Zhou, C., Hu, T., et al. (2019). LncRNA RPPH1 Promotes Colorectal Cancer Metastasis by Interacting with TUBB3 and by Promoting Exosomes-Mediated Macrophage M2 Polarization. *Cel Death Dis* 10 (11), 829. doi:10.1038/s41419-019-2077-0

Lin, C., Zhang, Y., Chen, Y., Bai, Y., and Zhang, Y. (2019). Long Noncoding RNA LINC01234 Promotes Serine Hydroxymethyltransferase 2 Expression and Proliferation by Competitively Binding miR-642a-5p in colon Cancer. *Cel Death Dis* 10 (2), 137. doi:10.1038/s41419-019-1352-4

Lin, J., Tan, X., Qiu, L., Huang, L., Zhou, Y., Pan, Z., et al. (2017). Long Noncoding RNA BC032913 as a Novel Therapeutic Target for Colorectal Cancer that Suppresses Metastasis by Upregulating TIMP3. *Mol. Ther. - Nucleic Acids* 8, 469–481. doi:10.1016/j.omtn.2017.07.009

Lin, X., Wang, S., Sun, M., Zhang, C., Wei, C., Yang, C., et al. (2019). miR-195-5p/NOTCH2-mediated EMT Modulates IL-4 Secretion in Colorectal Cancer to Affect M2-like TAM Polarization. *J. Hematol. Oncol.* 12 (1), 20. doi:10.1186/s13045-019-0708-7

Ling, H., Pickard, K., Ivan, C., Isella, C., Ikuo, M., Mitter, R., et al. (2016). The Clinical and Biological Significance of MIR-224 Expression in Colorectal Cancer Metastasis. *Gut* 65 (6), 977–989. doi:10.1136/gutjnl-2015-309372

Liu, J., Zhan, Y., Wang, J., Wang, J., Guo, J., and Kong, D. (2020). Long Noncoding RNA LINC01578 Drives colon Cancer Metastasis through a Positive Feedback

Loop with the NF-κB/YY1 axis. *Mol. Oncol.* 14 (12), 3211–3233. doi:10.1002/1878-0261.12819

Liu, K., Chen, W., Lei, S., Xiong, L., Zhao, H., Liang, D., et al. (2017). Wild-type and Mutant P53 Differentially Modulate miR-124/iASPP Feedback Following Pohotodynamic Therapy in Human colon Cancer Cell Line. *Cel Death Dis* 8 (10), e3096. doi:10.1038/cddis.2017.477

Liu, L., Wang, H.-J., Meng, T., Lei, C., Yang, X.-H., Wang, Q.-S., et al. (2019). lncRNA GAS5 Inhibits Cell Migration and Invasion and Promotes Autophagy by Targeting miR-222-3p via the GAS5/PTEN-Signaling Pathway in CRC. *Mol. Ther. - Nucleic Acids* 17, 644–656. doi:10.1016/j.omtn.2019.06.009

Liu, R., Zhang, Q., Shen, L., Chen, S., He, J., Wang, D., et al. (2020). Long Noncoding RNA Lnc-RI Regulates DNA Damage Repair and Radiation Sensitivity of CRC Cells through NHEJ Pathway. *Cell Biol Toxicol* 36 (5), 493–507. doi:10.1007/s10565-020-09524-6

Liu, T., Zhang, X., Du, L., Wang, Y., Liu, X., Tian, H., et al. (2019). Exosome-transmitted miR-128-3p Increase Chemosensitivity of Oxaliplatin-Resistant Colorectal Cancer. *Mol. Cancer* 18 (1), 43. doi:10.1186/s12943-019-0981-7

Liu, X., Chen, X., Zeng, K., Xu, M., He, B., Pan, Y., et al. (2018). DNA-methylation-mediated Silencing of miR-486-5p Promotes Colorectal Cancer Proliferation and Migration through Activation of PLAGL2/IGF2/β-Catenin Signal Pathways. *Cel Death Dis* 9 (10), 1037. doi:10.1038/s41419-018-1105-9

Liu, X., Su, K., Sun, X., Jiang, Y., Wang, L., Hu, C., et al. (2021). Sec62 Promotes Stemness and Chemoresistance of Human Colorectal Cancer through Activating Wnt/β-Catenin Pathway. *J. Exp. Clin. Cancer Res.* 40 (1), 132. doi:10.1186/s13046-021-01934-6

Liu, Y., Chen, X., Chen, X., Liu, J., Gu, H., Fan, R., et al. (2020). Long Non-coding RNA HOTAIR Knockdown Enhances Radiosensitivity through Regulating microRNA-93/ATG12 axis in Colorectal Cancer. *Cel Death Dis* 11 (3), 175. doi:10.1038/s41419-020-2268-8

Liu, Y., Chen, X., Cheng, R., Yang, F., Yu, M., Wang, C., et al. (2018). The Jun/miR-22/HuR Regulatory axis Contributes to Tumourigenesis in Colorectal Cancer. *Mol. Cancer* 17 (1), 11. doi:10.1186/s12943-017-0751-3

Liu, Y., Liu, R., Yang, F., Cheng, R., Chen, X., Cui, S., et al. (2017). miR-19a Promotes Colorectal Cancer Proliferation and Migration by Targeting TIA1. *Mol. Cancer* 16 (1), 53. doi:10.1186/s12943-017-0625-8

Liu, Y., Uzair-ur-Rehman, R., Guo, Y., Liang, H., Cheng, R., Yang, F., et al. (2016). miR-181b Functions as an oncomiR in Colorectal Cancer by Targeting PDCD4. *Protein Cell* 7 (10), 722–734. doi:10.1007/s13238-016-0313-2

Liu, Y., Zhang, Y., Wu, H., Li, Y., Zhang, Y., Liu, M., et al. (2017). miR-10a Suppresses Colorectal Cancer Metastasis by Modulating the Epithelial-To-Mesenchymal Transition and Anoikis. *Cel Death Dis* 8 (4), e2739. doi:10.1038/cddis.2017.61

Long, F., Lin, Z., Li, L., Ma, M., Lu, Z., Jing, L., et al. (2021). Comprehensive Landscape and Future Perspectives of Circular RNAs in Colorectal Cancer. *Mol. Cancer* 20 (1), 26. doi:10.1186/s12943-021-01318-6

Lou, Q., Liu, R., Yang, X., Li, W., Huang, L., Wei, L., et al. (2019). miR-448 Targets Ido1 and Regulates CD8+ T Cell Response in Human colon Cancer. *J. Immunotherapy Cancer* 7 (1), 210. doi:10.1186/s40425-019-0691-0

Lu, Y., Zhao, X., Liu, Q., Li, C., Graves-Deal, R., Cao, Z., et al. (2017). lncRNA MIR100HG-Derived miR-100 and miR-125b Mediate Cetuximab Resistance via Wnt/β-Catenin Signaling. *Nat. Med.* 23 (11), 1331–1341. doi:10.1038/nm.4424

Luan, Y., Li, X., Luan, Y., Zhao, R., Li, Y., Liu, L., et al. (2020). Circulating lncRNA UCA1 Promotes Malignancy of Colorectal Cancer via the miR-143/MYO6 Axis. *Mol. Ther. - Nucleic Acids* 19, 790–803. doi:10.1016/j.omtn.2019.12.009

Lulla, A. R., Slifker, M. J., Zhou, Y., Lev, A., Einarson, M. B., Dicker, D. T., et al. (2017). miR-6883 Family miRNAs Target CDK4/6 to Induce G1 Phase Cell-Cycle Arrest in Colon Cancer Cells. *Cancer Res.* 77 (24), 6902–6913. doi:10.1158/0008-5472.can-17-1767

Luo, H., Jiang, Y., Ma, S., Chang, H., Yi, C., Cao, H., et al. (2016). EZH2 Promotes Invasion and Metastasis of Laryngeal Squamous Cells Carcinoma via Epithelial-Mesenchymal Transition through H3K27me3. *Biochem. Biophysical Res. Commun.* 479 (2), 253–259. doi:10.1016/j.bbrc.2016.09.055

Luo, Y., Chen, J.-J., Lv, Q., Qin, J., Huang, Y.-Z., Yu, M.-H., et al. (2019). Long Non-coding RNA NEAT1 Promotes Colorectal Cancer Progression by Competitively Binding miR-34a with SIRT1 and Enhancing the Wnt/β-Catenin Signaling Pathway. *Cancer Lett.* 440-441, 11–22. doi:10.1016/j.canlet.2018.10.002

Ma, H., Pan, J.-S., Jin, L.-X., Wu, J., Ren, Y.-D., Chen, P., et al. (2016). MicroRNA-17~92 Inhibits Colorectal Cancer Progression by Targeting Angiogenesis. *Cancer Lett.* 376 (2), 293–302. doi:10.1016/j.canlet.2016.04.011

Ma, J., Yang, Y., Fu, Y., Guo, F., Zhang, X., Xiao, S., et al. (2018). PIAS3-mediated Feedback Loops Promote Chronic Colitis-Associated Malignant Transformation. *Theranostics* 8 (11), 3022–3037. doi:10.7150/thno.23046

Ma, Y., Yang, Y., Wang, F., Moyer, M.-P., Wei, Q., Zhang, P., et al. (2016). Long Non-coding RNA CCAL Regulates Colorectal Cancer Progression by Activating Wnt/β-Catenin Signalling Pathway via Suppression of Activator Protein 2α. *Gut* 65 (9), 1494–1504. doi:10.1136/gutjnl-2014-308392

Ma, Z., Han, C., Xia, W., Wang, S., Li, X., Fang, P., et al. (2020). circ5615 Functions as a ceRNA to Promote Colorectal Cancer Progression by Upregulating TNKS. *Cel Death Dis* 11 (5), 356. doi:10.1038/s41419-020-2514-0

Mai, D., Ding, P., Tan, L., Zhang, J., Pan, Z., Bai, R., et al. (2018). PIWI-interacting RNA-54265 Is Oncogenic and a Potential Therapeutic Target in Colorectal Adenocarcinoma. *Theranostics* 8 (19), 5213–5230. doi:10.7150/thno.28001

Mastropasqua, F., Marzano, F., Valletti, A., Aiello, I., Di Tullio, G., Morgano, A., et al. (2017). TRIM8 Restores P53 Tumour Suppressor Function by Blunting N-MYC Activity in Chemo-Resistant Tumours. *Mol. Cancer* 16 (1), 67. doi:10.1186/s12943-017-0634-7

Matsumura, K., Kawasaki, Y., Miyamoto, M., Kamoshida, Y., Nakamura, J., Negishi, L., et al. (2017). The Novel G-Quadruplex-Containing Long Non-coding RNA GSEC Antagonizes DHX36 and Modulates colon Cancer Cell Migration. *Oncogene* 36 (9), 1191–1199. doi:10.1038/onc.2016.282

McCabe, M. T., Graves, A. P., Ganji, G., Diaz, E., Halsey, W. S., Jiang, Y., et al. (2012). Mutation of A677 in Histone Methyltransferase EZH2 in Human B-Cell Lymphoma Promotes Hypertrimethylation of Histone H3 on Lysine 27 (H3K27). *Proc. Natl. Acad. Sci.* 109 (8), 2989–2994. doi:10.1073/pnas.1116418109

Meng, X., Sun, W., Yu, J., Zhou, Y., Gu, Y., Han, J., et al. (2020). LINC00460-miR-149-5p/miR-150-5p-Mutant P53 Feedback Loop Promotes Oxaliplatin Resistance in Colorectal Cancer. *Mol. Ther. - Nucleic Acids* 22, 1004–1015. doi:10.1016/j.omtn.2020.10.018

Michael, J. V., Wurtzel, J. G. T., Mao, G. F., Rao, A. K., Kolpakov, M. A., Sabri, A., et al. (2017). Platelet Microparticles Infiltrating Solid Tumors Transfer miRNAs that Suppress Tumor Growth. *Blood* 130 (5), 567–580. doi:10.1182/blood-2016-11-751099

Mo, S., Zhang, L., Dai, W., Han, L., Wang, R., Xiang, W., et al. (2020). Antisense lncRNA LDLRAD4-AS1 Promotes Metastasis by Decreasing the Expression of LDLRAD4 and Predicts a Poor Prognosis in Colorectal Cancer. *Cel Death Dis* 11 (2), 155. doi:10.1038/s41419-020-2338-y

Mosthaf, F. A., Gieseler, U., Mehmel, H. C., Fischer, J. T., and Gams, E. (1991). Left Bundle-branch Block and Primary Benign Heart Tumor. *Dtsch Med. Wochenschr* 116 (4), 134–136. doi:10.1055/s-2008-1063592

Mukohyama, J., Isobe, T., Hu, Q., Hayashi, T., Watanabe, T., Maeda, M., et al. (2019). miR-221 Targets QKI to Enhance the Tumorigenic Capacity of Human Colorectal Cancer Stem Cells. *Cancer Res.* 79 (20), 5151–5158. doi:10.1158/0008-5472.can-18-3544

Ni, W., Yao, S., Zhou, Y., Liu, Y., Huang, P., Zhou, A., et al. (2019). Long Noncoding RNA GAS5 Inhibits Progression of Colorectal Cancer by Interacting with and Triggering YAP Phosphorylation and Degradation and Is Negatively Regulated by the m6A Reader YTHDF3. *Mol. Cancer* 18 (1), 143. doi:10.1186/s12943-019-1079-y

Okugawa, Y., Toiyama, Y., Hur, K., Yamamoto, A., Yin, C., Ide, S., et al. (2019). Circulating miR-203 Derived from Metastatic Tissues Promotes Myopenia in Colorectal Cancer Patients. *J. Cachexia, Sarcopenia Muscle* 10 (3), 536–548. doi:10.1002/jcsm.12403

Öner, M. G., Rokavec, M., Kaller, M., Bouznad, N., Horst, D., Kirchner, T., et al. (2018). Combined Inactivation of TP53 and MIR34A Promotes Colorectal Cancer Development and Progression in Mice via Increasing Levels of IL6R and PAI1. *Gastroenterology* 155 (6), 1868–1882. doi:10.1053/j.gastro.2018.08.011

Oshima, G., Guo, N., He, C., Stack, M. E., Poon, C., Uppal, A., et al. (2017). *In Vivo* Delivery and Therapeutic Effects of a MicroRNA on Colorectal Liver Metastases. *Mol. Ther.* 25 (7), 1588–1595. doi:10.1016/j.ymthe.2017.04.005

Ou, C., Sun, Z., Li, X., Li, X., Ren, W., Qin, Z., et al. (2018). MiR-590-5p, a Density-Sensitive microRNA, Inhibits Tumorigenesis by Targeting YAP1 in Colorectal Cancer. *Cancer Lett.* 399, 53260–53263. doi:10.1016/j.canlet.2017.04.011

Pan, K., and Xie, Y. (2020). LncRNA FOXC2-AS1 Enhances FOXC2 mRNA Stability to Promote Colorectal Cancer Progression via Activation of Ca2+-FAK Signal Pathway. *Cel Death Dis* 11 (6), 434. doi:10.1038/s41419-020-2633-7

Pekow, J., Meckel, K., Dougherty, U., Huang, Y., Chen, X., Almoghrabi, A., et al. (2017). miR-193a-3p Is a Key Tumor Suppressor in Ulcerative Colitis-Associated Colon Cancer and Promotes Carcinogenesis through Upregulation of IL17RD. *Clin. Cancer Res.* 23 (17), 5281–5291. doi:10.1158/1078-0432.ccr-17-0171

Peng, W., Zhang, C., Peng, J., Huang, Y., Peng, C., Tan, Y., et al. (2020). Lnc-FAM84B-4 Acts as an Oncogenic lncRNA by Interacting with Protein hnRNPK to Restrain MAPK Phosphatases-DUSP1 Expression. *Cancer Lett.* 494, 94–106. doi:10.1016/j.canlet.2020.08.036

Pichler, M., Rodriguez-Aguayo, C., Nam, S. Y., Dragomir, M. P., Bayraktar, R., Anfossi, S., et al. (2020). Therapeutic Potential of FLANC, a Novel Primate-specific Long Non-coding RNA in Colorectal Cancer. *Gut* 69 (10), 1818–1831. doi:10.1136/gutjnl-2019-318903

Rasmussen, M. H., Lyskjær, I., Jersie-Christensen, R. R., Tarpgaard, L. S., Primdal-Bengtson, B., Nielsen, M. M., et al. (2016). miR-625-3p Regulates Oxaliplatin Resistance by Targeting MAP2K6-P38 Signalling in Human Colorectal Adenocarcinoma Cells. *Nat. Commun.* 7, 12436. doi:10.1038/ncomms12436

Ren, J., Ding, L., Zhang, D., Shi, G., Xu, Q., Shen, S., et al. (2018). Carcinoma-associated Fibroblasts Promote the Stemness and Chemoresistance of Colorectal Cancer by Transferring Exosomal lncRNA H19. *Theranostics* 8 (14), 3932–3948. doi:10.7150/thno.25541

Ren, L.-L., Yan, T.-T., Shen, C.-Q., Tang, J.-Y., Kong, X., Wang, Y.-C., et al. (2018). The Distinct Role of Strand-specific miR-514b-3p and miR-514b-5p in Colorectal Cancer Metastasis. *Cel Death Dis* 9 (6), 687. doi:10.1038/s41419-018-0732-5

Rigoutsos, I., Lee, S. K., Nam, S. Y., Anfossi, S., Pasculli, B., Pichler, M., et al. (2017). N-BLR, a Primate-specific Non-coding Transcript Leads to Colorectal Cancer Invasion and Migration. *Genome Biol.* 18 (1), 98. doi:10.1186/s13059-017-1224-0

Rokavec, M., Bouznad, N., and Hermeking, H. (2019). Paracrine Induction of Epithelial-Mesenchymal Transition between Colorectal Cancer Cells and its Suppression by a p53/miR-192/215/NID1 Axis. *Cell Mol. Gastroenterol. Hepatol.* 7 (4), 783–802. doi:10.1016/j.jcmgh.2019.02.003

Sang, B., Zhang, Y. Y., Guo, S. T., Kong, L. F., Cheng, Q., Liu, G. Z., et al. (2018). Dual Functions for OVAAL in Initiation of RAF/MEK/ERK Prosurvival Signals and Evasion of P27-Mediated Cellular Senescence. *Proc. Natl. Acad. Sci. USA* 115 (50), E11661–E11670. doi:10.1073/pnas.1805950115

Shan, Y., Ma, J., Pan, Y., Hu, J., Liu, B., and Jia, L. (2018). LncRNA SNHG7 Sponges miR-216b to Promote Proliferation and Liver Metastasis of Colorectal Cancer through Upregulating GALNT1. *Cel Death Dis* 9 (7), 722. doi:10.1038/s41419-018-0759-7

Shang, W., Gao, Y., Tang, Z., Zhang, Y., and Yang, R. (2019). The Pseudogene Olfr29-Ps1 Promotes the Suppressive Function and Differentiation of Monocytic MDSCs. *Cancer Immunol. Res.* 7 (5), 813–827. doi:10.1158/2326-6066.cir-18-0443

Shen, H., Xing, C., Cui, K., Li, Y., Zhang, J., Du, R., et al. (2017). MicroRNA-30a Attenuates Mutant KRAS-Driven Colorectal Tumorigenesis via Direct Suppression of ME1. *Cell Death Differ* 24 (7), 1253–1262. doi:10.1038/cdd.2017.63

Shen, Z., Zhou, R., Liu, C., Wang, Y., Zhan, W., Shao, Z., et al. (2017). MicroRNA-105 Is Involved in TNF-α-Related Tumor Microenvironment Enhanced Colorectal Cancer Progression. *Cel Death Dis* 8 (12), 3213. doi:10.1038/s41419-017-0048-x

Shi, C., Yang, Y., Xia, Y., Okugawa, Y., Yang, J., Liang, Y., et al. (2016). Novel Evidence for an Oncogenic Role of microRNA-21 in Colitis-Associated Colorectal Cancer. *Gut* 65 (9), 1470–1481. doi:10.1136/gutjnl-2014-308455

Shi, L., Hong, X., Ba, L., He, X., Xiong, Y., Ding, Q., et al. (2019). Long Non-coding RNA ZNFX1-AS1 Promotes the Tumor Progression and Metastasis of Colorectal Cancer by Acting as a Competing Endogenous RNA of miR-144 to Regulate EZH2 Expression. *Cel Death Dis* 10 (3), 150. doi:10.1038/s41419-019-1332-8

Shigeyasu, K., Toden, S., Ozawa, T., Matsuyama, T., Nagasaka, T., Ishikawa, T., et al. (2020). The PVT1 lncRNA Is a Novel Epigenetic Enhancer of MYC, and a Promising Risk-Stratification Biomarker in Colorectal Cancer. *Mol. Cancer* 19 (1), 155. doi:10.1186/s12943-020-01277-4

Siemens, H., Jackstadt, R., Kaller, M., and Hermeking, H. (2013). Repression of C-Kit by P53 Is Mediated by miR-34 and Is Associated with Reduced Chemoresistance, Migration and Stemness. *Oncotarget* 4 (9), 1399–1415. doi:10.18632/oncotarget.1202

Silva-Fisher, J. M., Dang, H. X., White, N. M., Strand, M. S., Krasnick, B. A., Rozycki, E. B., et al. (2020). Long Non-coding RNA RAMS11 Promotes Metastatic Colorectal Cancer Progression. *Nat. Commun.* 11 (1), 2156. doi:10.1038/s41467-020-15547-8

Stiegelbauer, V., Vychytilova-Faltejskova, P., Karbiener, M., Pehserl, A.-M., Reicher, A., Resel, M., et al. (2017). miR-196b-5p Regulates Colorectal Cancer Cell Migration and Metastases through Interaction with HOXB7 and GALNT5. *Clin. Cancer Res.* 23 (17), 5255–5266. doi:10.1158/1078-0432.ccr-17-0023

Su, J., Zhang, E., Han, L., Yin, D., Liu, Z., He, X., et al. (2017). Long Noncoding RNA BLACAT1 Indicates a Poor Prognosis of Colorectal Cancer and Affects Cell Proliferation by Epigenetically Silencing of P15. *Cel Death Dis* 8 (3), e2665. doi:10.1038/cddis.2017.83

Sun, L., Fang, Y., Wang, X., Han, Y., Du, F., Li, C., et al. (2019). miR-302a Inhibits Metastasis and Cetuximab Resistance in Colorectal Cancer by Targeting NFIB and CD44. *Theranostics* 9 (26), 8409–8425. doi:10.7150/thno.36605

Sun, M., Song, H., Wang, S., Zhang, C., Zheng, L., Chen, F., et al. (2017). Integrated Analysis Identifies microRNA-195 as a Suppressor of Hippo-YAP Pathway in Colorectal Cancer. *J. Hematol. Oncol.* 10 (1), 79. doi:10.1186/s13045-017-0445-8

Sun, W., Wang, X., Li, J., You, C., Lu, P., Feng, H., et al. (2018). MicroRNA-181a Promotes Angiogenesis in Colorectal Cancer by Targeting SRCIN1 to Promote the SRC/VEGF Signaling Pathway. *Cel Death Dis* 9 (4), 438. doi:10.1038/s41419-018-0490-4

Sun, Z., Ou, C., Liu, J., Chen, C., Zhou, Q., Yang, S., et al. (2019). YAP1-induced MALAT1 Promotes Epithelial-Mesenchymal Transition and Angiogenesis by Sponging miR-126-5p in Colorectal Cancer. *Oncogene* 38 (14), 2627–2644. doi:10.1038/s41388-018-0628-y

Tang, J., Yan, T., Bao, Y., Shen, C., Yu, C., Zhu, X., et al. (2019). LncRNA GLCC1 Promotes Colorectal Carcinogenesis and Glucose Metabolism by Stabilizing C-Myc. *Nat. Commun.* 10 (1), 3499. doi:10.1038/s41467-019-11447-8

Tang, W., Zhou, W., Xiang, L., Wu, X., Zhang, P., Wang, J., et al. (2019). The p300/YY1/miR-500a-5p/HDAC2 Signalling axis Regulates Cell Proliferation in Human Colorectal Cancer. *Nat. Commun.* 10 (1), 663. doi:10.1038/s41467-018-08225-3

Taniue, K., Kurimoto, A., Sugimasa, H., Nasu, E., Takeda, Y., Iwasaki, K., et al. (2016). Long Noncoding RNA UPAT Promotes colon Tumorigenesis by Inhibiting Degradation of UHRF1. *Proc. Natl. Acad. Sci. USA* 113 (5), 1273–1278. doi:10.1073/pnas.1500992113

Taniue, K., Kurimoto, A., Takeda, Y., Nagashima, T., Okada-Hatakeyama, M., Katou, Y., et al. (2016). ASBEL-TCF3 Complex Is Required for the Tumorigenicity of Colorectal Cancer Cells. *Proc. Natl. Acad. Sci. USA* 113 (45), 12739–12744. doi:10.1073/pnas.1605938113

Teng, Y., Ren, Y., Hu, X., Mu, J., Samykutty, A., Zhuang, X., et al. (2017). MVP-mediated Exosomal Sorting of miR-193a Promotes colon Cancer Progression. *Nat. Commun.* 8, 14448. doi:10.1038/ncomms14448

Thomas, H. (2017). miR-100 and miR-125b Induce Cetuximab Resistance in CRC. *Nat. Rev. Gastroenterol. Hepatol.* 14 (12), 691. doi:10.1038/nrgastro.2017.156

Tian, W., Du, Y., Ma, Y., Gu, L., Zhou, J., and Deng, D. (2018). MALAT1-miR663a Negative Feedback Loop in colon Cancer Cell Functions through Direct miRNA-lncRNA Binding. *Cel Death Dis* 9 (9), 857. doi:10.1038/s41419-018-0925-y

Tian, X., Zheng, Y., Yin, K., Ma, J., Tian, J., Zhang, Y., et al. (2020). LncRNAAK036396Inhibits Maturation and Accelerates Immunosuppression of Polymorphonuclear Myeloid-Derived Suppressor Cells by Enhancing the Stability of Ficolin B. *Cancer Immunol. Res.* 8 (4), 565–577. doi:10.1158/2326-6066.cir-19-0595

Tian, Y., Ma, X., Lv, C., Sheng, X., Li, X., Zhao, R., et al. (2017). Stress Responsive miR-31 Is a Major Modulator of Mouse Intestinal Stem Cells during Regeneration and Tumorigenesis. *Elife* 6. doi:10.7554/eLife.29538

Tian, Y., Xu, J., Li, Y., Zhao, R., Du, S., Lv, C., et al. (2019). MicroRNA-31 Reduces Inflammatory Signaling and Promotes Regeneration in Colon Epithelium, and Delivery of Mimics in Microspheres Reduces Colitis in Mice. *Gastroenterology* 156 (8), 2281–2296. doi:10.1053/j.gastro.2019.02.023

Tie, G., Yan, J., Khair, L., Messina, J. A., Deng, A., Kang, J., et al. (2017). Hypercholesterolemia Increases Colorectal Cancer Incidence by Reducing Production of NKT and γδ T Cells from Hematopoietic Stem Cells. *Cancer Res.* 77 (9), 2351–2362. doi:10.1158/0008-5472.can-16-1916

Tsai, K.-W., Lo, Y.-H., Liu, H., Yeh, C.-Y., Chen, Y.-Z., Hsu, C.-W., et al. (2018). Linc00659, a Long Noncoding RNA, Acts as Novel Oncogene in Regulating Cancer Cell Growth in Colorectal Cancer. *Mol. Cancer* 17 (1), 72. doi:10.1186/s12943-018-0821-1

Ullmann, P., Nurmik, M., Schmitz, M., Rodriguez, F., Weiler, J., Qureshi-Baig, K., et al. (2019). Tumor Suppressor miR-215 Counteracts Hypoxia-Induced colon Cancer Stem Cell Activity. *Cancer Lett.* 450, 32–41. doi:10.1016/j.canlet.2019.02.030

Viswanathan, V., Damle, S., Zhang, T., Opdenaker, L., Modarai, S., Accerbi, M., et al. (2017). An miRNA Expression Signature for the Human Colonic Stem Cell Niche Distinguishes Malignant from Normal Epithelia. *Cancer Res.* 77 (14), 3778–3790. doi:10.1158/0008-5472.can-16-2388

Wang, D., Wang, X., Si, M., Yang, J., Sun, S., Wu, H., et al. (2020). Exosome-encapsulated miRNAs Contribute to CXCL12/CXCR4-Induced Liver Metastasis of Colorectal Cancer by Enhancing M2 Polarization of Macrophages. *Cancer Lett.* 474, 36–52. doi:10.1016/j.canlet.2020.01.005

Wang, F.-W., Cao, C.-H., Han, K., Zhao, Y.-X., Cai, M.-Y., Xiang, Z.-C., et al. (2019). APC-activated Long Noncoding RNA Inhibits Colorectal Carcinoma Pathogenesis through Reduction of Exosome Production. *J. Clin. Invest.* 129 (2), 727–743. doi:10.1172/jci122478

Wang, F. F., Zhang, X. J., Yan, Y. R., Zhu, X. H., Yu, J., Ding, Y., et al. (2017). FBX8 Is a Metastasis Suppressor Downstream of miR-223 and Targeting mTOR for Degradation in Colorectal Carcinoma. *Cancer Lett.* 388, 85–95. doi:10.1016/j.canlet.2016.11.031

Wang, G., Fu, Y., Yang, X., Luo, X., Wang, J., Gong, J., et al. (2016). Brg-1 Targeting of Novel miR550a-5p/RNF43/Wnt Signaling axis Regulates Colorectal Cancer Metastasis. *Oncogene* 35 (5), 651–661. doi:10.1038/onc.2015.124

Wang, J., Zhou, J., Jiang, C., Zheng, J., Namba, H., Chi, P., et al. (2019). LNRRIL 6, a Novel Long Noncoding RNA , Protects Colorectal Cancer Cells by Activating the IL -6- STAT 3 Pathway. *Mol. Oncol.* 13 (11), 2344–2360. doi:10.1002/1878-0261.12538

Wang, L., Bu, P., Ai, Y., Srinivasan, T., Chen, H. J., Xiang, K., et al. (2016). A Long Non-coding RNA Targets microRNA miR-34a to Regulate colon Cancer Stem Cell Asymmetric Division. *Elife* 5. doi:10.7554/eLife.14620

Wang, L. Q., Yu, P., Li, B., Guo, Y. H., Liang, Z. R., Zheng, L. L., et al. (2018). miR-372 and miR-373 Enhance the Stemness of Colorectal Cancer Cells by Repressing Differentiation Signaling Pathways. *Mol. Oncol.* 12 (11), 1949–1964. doi:10.1002/1878-0261.12376

Wang, M., Han, D., Yuan, Z., Hu, H., Zhao, Z., Yang, R., et al. (2018). Long Non-coding RNA H19 Confers 5-Fu Resistance in Colorectal Cancer by Promoting SIRT1-Mediated Autophagy. *Cel Death Dis* 9 (12), 1149. doi:10.1038/s41419-018-1187-4

Wang, Q., Feng, Y., Peng, W., Ji, D., Zhang, Z., Qian, W., et al. (2019). Long Noncoding RNA Linc02023 Regulates PTEN Stability and Suppresses Tumorigenesis of Colorectal Cancer in a PTEN-dependent Pathway. *Cancer Lett.* 451, 68–78. doi:10.1016/j.canlet.2019.02.041

Wang, S., Gan, M., Chen, C., Zhang, Y., Kong, J., Zhang, H., et al. (2021). Methyl CpG Binding Protein 2 Promotes Colorectal Cancer Metastasis by Regulating N(6) -methyladenosine Methylation through Methyltransferase-like 14. *Cancer Sci.*

Wang, T., Xu, X., Xu, Q., Ren, J., Shen, S., Fan, C., et al. (2017). miR-19a Promotes Colitis-Associated Colorectal Cancer by Regulating Tumor Necrosis Factor Alpha-Induced Protein 3-NF-Kb Feedback Loops. *Oncogene* 36 (23), 3240–3251. doi:10.1038/onc.2016.468

Wang, X., Wang, Y., Li, L., Xue, X., Xie, H., Shi, H., et al. (2020). A lncRNA Coordinates with Ezh2 to Inhibit HIF-1α Transcription and Suppress Cancer Cell Adaption to Hypoxia. *Oncogene* 39 (9), 1860–1874. doi:10.1038/s41388-019-1123-9

Wang, Y.-Q., Jiang, D.-M., Hu, S.-S., Zhao, L., Wang, L., Yang, M.-H., et al. (2019). SATB2-AS1 Suppresses Colorectal Carcinoma Aggressiveness by Inhibiting SATB2-dependent Snail Transcription and Epithelial-Mesenchymal Transition. *Cancer Res.* 79 (14), 3542–3556. doi:10.1158/0008-5472.can-18-2900

Wang, Y., Lu, J.-H., Wu, Q.-N., Jin, Y., Wang, D.-S., Chen, Y.-X., et al. (2019). LncRNA LINRIS Stabilizes IGF2BP2 and Promotes the Aerobic Glycolysis in Colorectal Cancer. *Mol. Cancer* 18 (1), 174. doi:10.1186/s12943-019-1105-0

Weng, W., Liu, N., Toiyama, Y., Kusunoki, M., Nagasaka, T., Fujiwara, T., et al. (2018). Novel Evidence for a PIWI-Interacting RNA (piRNA) as an Oncogenic Mediator of Disease Progression, and a Potential Prognostic Biomarker in Colorectal Cancer. *Mol. Cancer* 17 (1), 16. doi:10.1186/s12943-018-0767-3

Weng, W., Okugawa, Y., Toden, S., Toiyama, Y., Kusunoki, M., and Goel, A. (2016). FOXM1 and FOXQ1 Are Promising Prognostic Biomarkers and Novel Targets of Tumor-Suppressive miR-342 in Human Colorectal Cancer. *Clin. Cancer Res.* 22 (19), 4947–4957. doi:10.1158/1078-0432.ccr-16-0360

Weng, W., Wei, Q., Toden, S., Yoshida, K., Nagasaka, T., Fujiwara, T., et al. (2017). Circular RNA ciRS-7-A Promising Prognostic Biomarker and a Potential Therapeutic Target in Colorectal Cancer. *Clin. Cancer Res.* 23 (14), 3918–3928. doi:10.1158/1078-0432.ccr-16-2541

Wu, F., Liu, F., Dong, L., Yang, H., He, X., Li, L., et al. (2018). miR-1273g Silences MAGEA3/6 to Inhibit Human Colorectal Cancer Cell Growth via Activation of AMPK Signaling. *Cancer Lett.* 435, 1–9. doi:10.1016/j.canlet.2018.07.031

Wu, H., Hu, X., Li, Y., Chen, Q., Sun, T., Qiao, Y., et al. (2020). LNC473 Regulating APAF1 IRES-dependent Translation via Competitive Sponging miR574 and miR15b: Implications in Colorectal Cancer. *Mol. Ther. - Nucleic Acids* 21, 764–779. doi:10.1016/j.omtn.2020.07.009

Wu, H., Qin, W., Lu, S., Wang, X., Zhang, J., Sun, T., et al. (2020). Long Noncoding RNA ZFAS1 Promoting Small Nucleolar RNA-Mediated 2′-O-Methylation via NOP58 Recruitment in Colorectal Cancer. *Mol. Cancer* 19 (1), 95. doi:10.1186/s12943-020-01201-w

Wu, H., Wei, M., Jiang, X., Tan, J., Xu, W., Fan, X., et al. (2020). lncRNA PVT1 Promotes Tumorigenesis of Colorectal Cancer by Stabilizing miR-16-5p and Interacting with the VEGFA/VEGFR1/AKT Axis. *Mol. Ther. - Nucleic Acids* 20, 438–450. doi:10.1016/j.omtn.2020.03.006

Wu, R., Li, L., Bai, Y., Yu, B., Xie, C., Wu, H., et al. (2020). The Long Noncoding RNA LUCAT1 Promotes Colorectal Cancer Cell Proliferation by Antagonizing Nucleolin to Regulate MYC Expression. *Cel Death Dis* 11 (10), 908. doi:10.1038/s41419-020-03095-4

Wu, S., Sun, H., Wang, Y., Yang, X., Meng, Q., Yang, H., et al. (2019). MALAT1 Rs664589 Polymorphism Inhibits Binding to miR-194-5p, Contributing to Colorectal Cancer Risk, Growth, and Metastasis. *Cancer Res.* 79 (20), 5432–5441. doi:10.1158/0008-5472.can-19-0773

Wu, Y., Yang, X., Chen, Z., Tian, L., Jiang, G., Chen, F., et al. (2019). m6A-induced lncRNA RP11 Triggers the Dissemination of Colorectal Cancer Cells via Upregulation of Zeb1A-Induced lncRNA RP11 Triggers the Dissemination of Colorectal Cancer Cells via Upregulation of Zeb1. *Mol. Cancer* 18 (1), 87. doi:10.1186/s12943-019-1014-2

Xiao, J., Lv, D., Zhou, J., Bei, Y., Chen, T., Hu, M., et al. (2017). Therapeutic Inhibition of miR-4260 Suppresses Colorectal Cancer via Targeting MCC and SMAD4. *Theranostics* 7 (7), 1901–1913. doi:10.7150/thno.19168

Xie, S., Yu, X., Li, Y., Ma, H., Fan, S., Chen, W., et al. (2018). Upregulation of lncRNA ADAMTS9-AS2 Promotes Salivary Adenoid Cystic Carcinoma Metastasis via PI3K/Akt and MEK/Erk Signaling. *Mol. Ther.* 26 (12), 2766–2778. doi:10.1016/j.ymthe.2018.08.018

Xu, J., Meng, Q., Li, X., Yang, H., Xu, J., Gao, N., et al. (2019). Long Noncoding RNA MIR17HG Promotes Colorectal Cancer Progression via miR-17-5p. *Cancer Res.* 79 (19), 4882–4895. doi:10.1158/0008-5472.can-18-3880

Xu, J., Shao, T., Song, M., Xie, Y., Zhou, J., Yin, J., et al. (2020). MIR22HG Acts as a Tumor Suppressor via TGFβ/SMAD Signaling and Facilitates Immunotherapy in Colorectal Cancer. *Mol. Cancer* 19 (1), 51. doi:10.1186/s12943-020-01174-w

Xu, K., Han, B., Bai, Y., Ma, X.-Y., Ji, Z.-N., Xiong, Y., et al. (2019). MiR-451a Suppressing BAP31 Can Inhibit Proliferation and Increase Apoptosis through Inducing ER Stress in Colorectal Cancer. *Cel Death Dis* 10 (3), 152. doi:10.1038/s41419-019-1403-x

Xu, K., Zhan, Y., Yuan, Z., Qiu, Y., Wang, H., Fan, G., et al. (2019). Hypoxia Induces Drug Resistance in Colorectal Cancer through the HIF-1α/miR-338-5p/IL-6 Feedback Loop. *Mol. Ther.* 27 (10), 1810–1824. doi:10.1016/j.ymthe.2019.05.017

Xu, L., Huan, L., Guo, T., Wu, Y., Liu, Y., Wang, Q., et al. (2020). LncRNA SNHG11 Facilitates Tumor Metastasis by Interacting with and Stabilizing HIF-1α. *Oncogene* 39 (46), 7005–7018. doi:10.1038/s41388-020-01512-8

Xu, M., Chen, X., Lin, K., Zeng, K., Liu, X., Pan, B., et al. (2018). The Long Noncoding RNA SNHG1 Regulates Colorectal Cancer Cell Growth through Interactions with EZH2 and miR-154-5p. *Mol. Cancer* 17 (1), 141. doi:10.1186/s12943-018-0894-x

Xu, M., Chen, X., Lin, K., Zeng, K., Liu, X., Xu, X., et al. (2019). lncRNA SNHG6 Regulates EZH2 Expression by Sponging miR-26a/b and miR-214 in Colorectal Cancer. *J. Hematol. Oncol.* 12 (1), 3. doi:10.1186/s13045-018-0690-5

Xu, M., Xu, X., Pan, B., Chen, X., Lin, K., Zeng, K., et al. (2019). LncRNA SATB2-AS1 Inhibits Tumor Metastasis and Affects the Tumor Immune Cell Microenvironment in Colorectal Cancer by Regulating SATB2. *Mol. Cancer* 18 (1), 135. doi:10.1186/s12943-019-1063-6

Xu, X., Huang, J., Ocansey, D. K. W., Xia, Y., Zhao, Z., Xu, Z., et al. (2021). The Emerging Clinical Application of m6A RNA Modification in Inflammatory Bowel Disease and its Associated Colorectal Cancer. *Jir* Vol. 14, 3289–3306. doi:10.2147/jir.s320449

Xu, Y., Zhang, H., Lit, L. C., Grothey, A., Athanasiadou, M., Kiritsi, M., et al. (2014). The Kinase LMTK3 Promotes Invasion in Breast Cancer through GRB2-Mediated Induction of Integrin β1. *Sci. Signal.* 7 (330), ra58. doi:10.1126/scisignal.2005170

Xu, Y., Zhang, H., Nguyen, V. T. M., Angelopoulos, N., Nunes, J., Reid, A., et al. (2015). LMTK3 Represses Tumor Suppressor-like Genes through Chromatin Remodeling in Breast Cancer. *Cel Rep.* 12 (5), 837–849. doi:10.1016/j.celrep.2015.06.073

Xu, Z., Zhu, C., Chen, C., Zong, Y., Feng, H., Liu, D., et al. (2018). CCL19 Suppresses Angiogenesis through Promoting miR-206 and Inhibiting Met/ERK/Elk-1/HIF-1α/VEGF-A Pathway in Colorectal Cancer. *Cel Death Dis* 9 (10), 974. doi:10.1038/s41419-018-1010-2

Yan, T.-T., Ren, L.-L., Shen, C.-Q., Wang, Z.-H., Yu, Y.-N., Liang, Q., et al. (2018). miR-508 Defines the Stem-like/Mesenchymal Subtype in Colorectal Cancer. *Cancer Res.* 78 (7), 1751–1765. doi:10.1158/0008-5472.can-17-2101

Yang, M.-H., Zhao, L., Wang, L., Ou-Yang, W., Hu, S.-S., Li, W.-L., et al. (2019). Nuclear lncRNA HOXD-AS1 Suppresses Colorectal Carcinoma Growth and Metastasis via Inhibiting HOXD3-Induced Integrin β3 Transcriptional Activating and MAPK/AKT Signalling. *Mol. Cancer* 18 (1), 31. doi:10.1186/s12943-019-0955-9

Yang, P., Li, J., Peng, C., Tan, Y., Chen, R., Peng, W., et al. (2020). TCONS_00012883 Promotes Proliferation and Metastasis via DDX3/YY1/MMP1/PI3K-AKT axis in Colorectal Cancer. *Clin. Transl Med.* 10 (6), e211. doi:10.1002/ctm2.211

Yang, X., Zhang, S., He, C., Xue, P., Zhang, L., He, Z., et al. (2020). METTL14 Suppresses Proliferation and Metastasis of Colorectal Cancer by Down-Regulating Oncogenic Long Non-coding RNA XIST. *Mol. Cancer* 19 (1), 46. doi:10.1186/s12943-020-1146-4

Yang, Y., Weng, W., Peng, J., Hong, L., Yang, L., Toiyama, Y., et al. (2017). Fusobacterium Nucleatum Increases Proliferation of Colorectal Cancer Cells and Tumor Development in Mice by Activating Toll-like Receptor 4 Signaling to Nuclear Factor−κB, and Up-Regulating Expression of MicroRNA-21. *Gastroenterology* 152 (4), 851–866. doi:10.1053/j.gastro.2016.11.018

Yi, H., Geng, L., Black, A., Talmon, G., Berim, L., and Wang, J. (2017). The miR-487b-3p/GRM3/TGFβ Signaling axis Is an Important Regulator of colon Cancer Tumorigenesis. *Oncogene* 36 (24), 3477–3489. doi:10.1038/onc.2016.499

Yu, M., Luo, Y., Cong, Z., Mu, Y., Qiu, Y., and Zhong, M. (2018). MicroRNA-590-5p Inhibits Intestinal Inflammation by Targeting YAP. *J. Crohns Colitis* 12 (8), 993–1004. doi:10.1093/ecco-jcc/jjy046

Yu, T., Guo, F., Yu, Y., Sun, T., Ma, D., Han, J., et al. (2017). Fusobacterium Nucleatum Promotes Chemoresistance to Colorectal Cancer by Modulating Autophagy. *Cell* 170 (3), 548–563. doi:10.1016/j.cell.2017.07.008

Yu, T., Shan, T.-D., Li, J.-Y., Huang, C.-Z., Wang, S.-Y., Ouyang, H., et al. (2016). Knockdown of Linc-UFC1 Suppresses Proliferation and Induces Apoptosis of Colorectal Cancer. *Cel Death Dis* 7, e2228. doi:10.1038/cddis.2016.124

Yu, X., Yuan, Z., Yang, Z., Chen, D., Kim, T., Cui, Y., et al. (2018). The Novel Long Noncoding RNA U50535 Promotes Colorectal Cancer Growth and Metastasis by Regulating CCL20. *Cel Death Dis* 9 (7), 751. doi:10.1038/s41419-018-0771-y

Yu, Y., Nangia-Makker, P., Farhana, L., and Majumdar, A. P. N. (2017). A Novel Mechanism of lncRNA and miRNA Interaction: CCAT2 Regulates miR-145 Expression by Suppressing its Maturation Process in colon Cancer Cells. *Mol. Cancer* 16 (1), 155. doi:10.1186/s12943-017-0725-5

Yue, B., Cai, D., Liu, C., Fang, C., and Yan, D. (2016). Linc00152 Functions as a Competing Endogenous RNA to Confer Oxaliplatin Resistance and Holds Prognostic Values in Colon Cancer. *Mol. Ther.* 24 (12), 2064–2077. doi:10.1038/mt.2016.180

Yue, B., Liu, C., Sun, H., Liu, M., Song, C., Cui, R., et al. (2018). A Positive Feed-Forward Loop between LncRNA-CYTOR and Wnt/β-Catenin Signaling Promotes Metastasis of Colon Cancer. *Mol. Ther.* 26 (5), 1287–1298. doi:10.1016/j.ymthe.2018.02.024

Yue, C., Chen, J., Li, Z., Li, L., Chen, J., and Guo, Y. (2020). microRNA-96 Promotes Occurrence and Progression of Colorectal Cancer via Regulation of the AMPKα2-FTO-m6A/MYC axis. *J. Exp. Clin. Cancer Res.* 39 (1), 240. doi:10.1186/s13046-020-01731-7

Zeng, K., Chen, X., Xu, M., Liu, X., Hu, X., Xu, T., et al. (2018). CircHIPK3 Promotes Colorectal Cancer Growth and Metastasis by Sponging miR-7. *Cel Death Dis* 9 (4), 417. doi:10.1038/s41419-018-0454-8

Zeng, Z., Li, Y., Pan, Y., Lan, X., Song, F., Sun, J., et al. (2018). Cancer-derived Exosomal miR-25-3p Promotes Pre-metastatic Niche Formation by Inducing Vascular Permeability and Angiogenesis. *Nat. Commun.* 9 (1), 5395. doi:10.1038/s41467-018-07810-w

Zhan, W., Liao, X., Chen, Z., Li, L., Tian, T., Yu, L., et al. (2020). LINC00858 Promotes Colorectal Cancer by Sponging miR-4766-5p to Regulate PAK2. *Cel Biol Toxicol* 36 (4), 333–347. doi:10.1007/s10565-019-09506-3

Zhang, F., Luo, Y., Shao, Z., Xu, L., Liu, X., Niu, Y., et al. (2016). MicroRNA-187, a Downstream Effector of TGFβ Pathway, Suppresses Smad-Mediated Epithelial-Mesenchymal Transition in Colorectal Cancer. *Cancer Lett.* 373 (2), 203–213. doi:10.1016/j.canlet.2016.01.037

Zhang, M., Weng, W., Zhang, Q., Wu, Y., Ni, S., Tan, C., et al. (2018). The lncRNA NEAT1 Activates Wnt/β-Catenin Signaling and Promotes Colorectal Cancer Progression via Interacting with DDX5. *J. Hematol. Oncol.* 11 (1), 113. doi:10.1186/s13045-018-0656-7

Zhang, Y., Guo, L., Li, Y., Feng, G.-H., Teng, F., Li, W., et al. (2018). MicroRNA-494 Promotes Cancer Progression and Targets Adenomatous Polyposis Coli in Colorectal Cancer. *Mol. Cancer* 17 (1), 1. doi:10.1186/s12943-017-0753-1

Zhang, Z., Zhou, C., Chang, Y., Zhang, Z., Hu, Y., Zhang, F., et al. (2016). Long Non-coding RNA CASC11 Interacts with hnRNP-K and Activates the WNT/β-catenin Pathway to Promote Growth and Metastasis in Colorectal Cancer. *Cancer Lett.* 376 (1), 62–73. doi:10.1016/j.canlet.2016.03.022

Zhao, B., Wei, X., Li, W., Udan, R. S., Yang, Q., Kim, J., et al. (2007). Inactivation of YAP Oncoprotein by the Hippo Pathway Is Involved in Cell Contact Inhibition and Tissue Growth Control. *Genes Dev.* 21 (21), 2747–2761. doi:10.1101/gad.1602907

Zhao, S., Sun, H., Jiang, W., Mi, Y., Zhang, D., Wen, Y., et al. (2017). miR-4775 Promotes Colorectal Cancer Invasion and Metastasis via the Smad7/TGFβ-Mediated Epithelial to Mesenchymal Transition. *Mol. Cancer* 16 (1), 12. doi:10.1186/s12943-017-0585-z

Zhao, Y., Du, T., Du, L., Li, P., Li, J., Duan, W., et al. (2019). Long Noncoding RNA LINC02418 Regulates MELK Expression by Acting as a ceRNA and May Serve as a Diagnostic Marker for Colorectal Cancer. *Cel Death Dis* 10 (8), 568. doi:10.1038/s41419-019-1804-x

Zheng, K., Zhou, X., Yu, J., Li, Q., Wang, H., Li, M., et al. (2016). Epigenetic Silencing of miR-490-3p Promotes Development of an Aggressive Colorectal Cancer Phenotype through Activation of the Wnt/β-Catenin Signaling Pathway. *Cancer Lett.* 376 (1), 178–187. doi:10.1016/j.canlet.2016.03.024

Zhou, Q., Zhu, Y., Wei, X., Zhou, J., Chang, L., Sui, H., et al. (2016). MiR-590-5p Inhibits Colorectal Cancer Angiogenesis and Metastasis by Regulating Nuclear Factor 90/vascular Endothelial Growth Factor A axis. *Cel Death Dis* 7 (10), e2413. doi:10.1038/cddis.2016.306

Zhou, T., Wu, L., Ma, N., Tang, F., Yu, Z., Jiang, Z., et al. (2020). SOX9-activated FARSA-AS1 Predetermines Cell Growth, Stemness, and Metastasis in Colorectal Cancer through Upregulating FARSA and SOX9. *Cel Death Dis* 11 (12), 1071. doi:10.1038/s41419-020-03273-4

Zhu, G.-f., Xu, Y.-w., Li, J., Niu, H.-l., Ma, W.-x., Xu, J., et al. (2019). Mir20a/106a-WTX axis Regulates RhoGDIa/CDC42 Signaling and colon Cancer Progression. *Nat. Commun.* 10 (1), 112. doi:10.1038/s41467-018-07998-x

Zhu, P., Wu, J., Wang, Y., Zhu, X., Lu, T., Liu, B., et al. (2018). LncGata6 Maintains Stemness of Intestinal Stem Cells and Promotes Intestinal Tumorigenesis. *Nat. Cel Biol* 20 (10), 1134–1144. doi:10.1038/s41556-018-0194-0

Zhu, Y., Gu, L., Li, Y., Lin, X., Shen, H., Cui, K., et al. (2017). miR-148a Inhibits Colitis and Colitis-Associated Tumorigenesis in Mice. *Cel Death Differ* 24 (12), 2199–2209. doi:10.1038/cdd.2017.151

Zhu, Y., Gu, L., Lin, X., Cui, K., Liu, C., Lu, B., et al. (2020). LINC00265 Promotes Colorectal Tumorigenesis via ZMIZ2 and USP7-Mediated Stabilization of β-catenin. *Cel Death Differ* 27 (4), 1316–1327. doi:10.1038/s41418-019-0417-3

Zhu, Y., Hu, H., Yuan, Z., Zhang, Q., Xiong, H., Hu, Z., et al. (2020). LncRNA NEAT1 Remodels Chromatin to Promote the 5-Fu Resistance by Maintaining Colorectal Cancer Stemness. *Cel Death Dis* 11 (11), 962. doi:10.1038/s41419-020-03164-8

Zhu, Y., Wang, C., Becker, S. A., Hurst, K., Nogueira, L. M., Findlay, V. J., et al. (2018). miR-145 Antagonizes SNAI1-Mediated Stemness and Radiation Resistance in Colorectal Cancer. *Mol. Ther.* 26 (3), 744–754. doi:10.1016/j.ymthe.2017.12.023

Conflict of Interest: Author MW was employed by Shenyang Kangwei Medical Laboratory Analysis Co. Ltd. The remaining authors declare that the review was conducted in the absence of any commercial or financial relationships that could be construed as a potential conflict of interest.

Publisher's Note: All claims expressed in this article are solely those of the authors and do not necessarily represent those of their affiliated organizations, or those of the publisher, the editors and the reviewers. Any product that may be evaluated in this article, or claim that may be made by its manufacturer, is not guaranteed or endorsed by the publisher.

Copyright © 2021 Lu, Ding, Wang, Hu, Sun, Wei, Wang and Wu. This is an open-access article distributed under the terms of the Creative Commons Attribution License (CC BY). The use, distribution or reproduction in other forums is permitted, provided the original author(s) and the copyright owner(s) are credited and that the original publication in this journal is cited, in accordance with accepted academic practice. No use, distribution or reproduction is permitted which does not comply with these terms.

frontiers in Cell and Developmental Biology

ORIGINAL RESEARCH
published: 19 January 2022
doi: 10.3389/fcell.2021.782636

A Broad m6A Modification Landscape in Inflammatory Bowel Disease

Kai Nie[1,2], Jun Yi[3], Yuanyuan Yang[1,2], Minzi Deng[1,2], Yan Yang[1], Tianyu Wang[1], Xuejie Chen[1], Zhaoyu Zhang[2,4] and Xiaoyan Wang[1,2]**

[1]Department of Gastroenterology, The Third Xiangya Hospital of Central South University, Changsha, China, [2]Hunan Key Laboratory of Nonresolving Inflammation and Cancer, Cancer Research Institute, Central South University, Changsha, China, [3]Department of Gastroenterology, The Xiangya Hospital of Central South University, Changsha, China, [4]Cancer Research Institute, Central South University, Changsha, China

Background and Aims: N6-Methyladenosine (m6A) is the most common post-transcriptional modification on eukaryotic mRNA, affecting the mRNA's fate. The role of m6A regulation in inflammatory bowel disease is unclear. Here, we investigated the m6A landscape in inflammatory bowel diseases (IBD).

Methods: Eleven human IBD microarray datasets were recruited from the Gene Expression Omnibus database and four were selected as discovery cohorts. An RNA-seq dataset from the Inflammatory Bowel Disease Multi'omics Database was used as a validation cohort. m6A regulators were measured in volunteers' colonic samples. Consensus clustering and immune scoring were used to estimate the characteristics of m6A regulation in IBD. m6A-related characteristics of different sub-phenotypes, sample sources, and biological therapeutic responses were determined using seven independent datasets.

Results: m6A modification involves methyltransferases (writers), demethylases (erasers), and methylation-reading proteins (readers). A wide interaction exists between m6A regulators and IBD risk genes. The IBD risk loci can also be modified by m6A modifications in the public m6A sequencing data. Furthermore, m6A regulators displayed extensive differential expression in four independent discovery cohorts that share common differential genes (IGF2BP2, HNRNPA2B1, ZCCHC4, and EIF3I). In the validated cohort and enrolled volunteers' colonic biopsy samples, the differential m6A regulators were reconfirmed. Two clusters of consensus clustering exhibit different immune phenotypes. m6A-modified positions exist in the core IBD immune cytokines. Another set of IBD datasets revealed m6A-related differences across clinical phenotypes, biological samples, and therapeutic response subgroups in IBD patients.

Conclusion: Regulation of m6A methylation is widely involved in IBD occurrence and development. m6A modifications in risk variants, core cytokines, immune cells, and other proteins may deeply influence the pathophysiology and clinical phenotypes. Further studies are needed to determine its role in IBD.

Keywords: N6-methyladenosine, inflammatory bowel diseases, RNA modifications, epigenetics, biologics response

OPEN ACCESS

Edited by:
Chengqi Yi,
Peking University, China

Reviewed by:
Abhijit Shukla,
Memorial Sloan Kettering Cancer Center, United States
Krishna Mohan Parsi,
University of Massachusetts Medical School, United States

****Correspondence:***
Zhaoyu Zhang
2511996036@qq.com
Xiaoyan Wang
wxy220011@163.com

Specialty section:
This article was submitted to Epigenomics and Epigenetics, a section of the journal Frontiers in Cell and Developmental Biology

Received: *24 September 2021*
Accepted: *16 December 2021*
Published: *19 January 2022*

Citation:
Nie K, Yi J, Yang Y, Deng M, Yang Y, Wang T, Chen X, Zhang Z and Wang X (2022) A Broad m6A Modification Landscape in Inflammatory Bowel Disease. Front. Cell Dev. Biol. 9:782636. doi: 10.3389/fcell.2021.782636

INTRODUCTION

N6-Methyladenosine (m6A) in mRNAs was first discovered in the 1970s (Desrosiers et al., 1974) and later implicated in mRNA instability. Being the most extensive and frequent mRNA modification, m6A modification has emerged as a major research topic in epitranscriptomics (Zaccara et al., 2019; Huang et al., 2020). m6A landscapes in humans and mice were not described until the development of m6A-seq (also known as methylated RNA immunoprecipitation with next-generation sequencing, MeRIP-Seq) in 2012 (Dominissini et al., 2012; Meyer et al., 2012). m6A RNA methylation influences all stages of RNA processing, including precursor mRNA (pre-mRNA) splicing and primary microRNA (pri-miRNA) processing, nuclear export, translation, and degradation (Liu L. et al., 2020; Han et al., 2020). m6A modifications affect physiology at, at least three levels: 1) organismal or tissue level, influencing various biological processes, including development, infertility, and carcinogenesis), 2) cell signaling pathway level, including p53 and Notch signaling, and 3) at the machinery level, including spliceosome and the nuclear export machinery (Fu et al., 2014). Writers, erasers, and readers are enzymes that add, remove, or preferentially bind to the chemical modifications at designated m6A nucleotides. These functional components constitute a complex post-transcriptional system of gene regulation (Zaccara et al., 2019). m6A has been implicated in various pathologies, including cancer, inflammation, autoimmune diseases, and infections (Li et al., 2017; Han et al., 2020). However, the role of m6A modifications in inflammatory bowel diseases (IBD) is poorly understood.

IBDs are chronic intestinal disorders that typically fall into two subtypes: Crohn's disease (CD) and ulcerative colitis (UC). Over 1 million residents in America and 2.5 million in Europe are estimated to have IBD, with substantial costs for health care (Kaplan, 2015). Moreover, IBD has emerged in newly industrialized countries in Asia, South America, and the Middle East and has evolved into a global disease with a rising prevalence in every continent (Kaplan, 2015). Several comorbid conditions have been proposed to be related to IBD, including cardiovascular disease, neuropsychological disorders, and metabolic syndrome with heavy disease burden (Argollo et al., 2019). UC is limited to the colon, with superficial mucosal inflammation that extends proximally in a contiguous manner and may cause ulcerations, severe bleeding, toxic megacolon, and fulminant colitis (Ungaro et al., 2017). In contrast, CD can affect any part of the digestive tract, often in a non-contiguous manner, and is characterized by transmural inflammation, which may cause complications such as fibrotic strictures, fistulas, and abscesses (Roda et al., 2020). It has been reported with respect to the potentially important pathophysiological signatures of UC and CD, such as differentially enriched immune-cell sub-populations and genetic variants (e.g., Nucleotide-binding oligomerization domain 2, NOD2). However, the mechanisms underlying IBD are not fully understood. Genome-wide association studies (GWASs) have identified risk variants, including NOD2, autophagy-related 16-like 1, interleukin 23 receptor, and interleukin 10 (Chang, 2020), but they are not clearly explained or mapped, and the genes commonly used to describe them are only putative. Moreover, in most cases, the biological functions of their products and interactions need delineation. Further understanding is required to determine the mechanism of specific variants affecting mRNA levels and consequently protein levels, so as to provide further insight into the mechanisms of IBD pathogenesis. However, many IBD variants may represent m6A modification loci that exert effects on gene expression. Immune dysfunction also influences IBD pathophysiological processes (Mitsialis et al., 2020). B-cells, dendrite cells (DCs), and T-cells are significantly involved in IBD, and strong evidence indicates global m6A modifications in innate and adaptive immune systems (Shulman and Stern-Ginossar, 2020). Several reports have linked m6A epigenetic modification to IBD indirectly. Studies support a single m6A regulator participating in the immune-associated colitis-like methyltransferase 14 (METTL14) deletion in T-cells trigger spontaneous colitis (Lu et al., 2020), and m6A reader ELAV-like RNA binding protein 1 (ELAVL1, also known as HuR) maintain colonic epithelial Paneth cells' function (Xiao et al., 2019; Xu et al., 2021; Zhang et al., 2021). However, m6A, as the major mRNA modification, and its systemic modifying landscape in IBD have not yet been described. The unknown truth is m6A regulators' network's role in IBD. There is a need to uncover the m6A's role in the pathogenesis, pathophysiology, clinical diagnosis, and treatment application of IBD. An important description of the missing link between IBD and m6A will bring new insights and directions for future studies. Here, we analyzed large-scale multi-IBD microarray and RNA-seq datasets to comprehensively describe the broad m6A modification landscape in IBD.

METHODS

Data Screening

To investigate the m6A landscape in IBD patients, data was retrieved from the gene expression omnibus (GEO) using the key words "(Inflammatory bowel disease OR IBD) AND microarray expression data AND Homo sapiens." Inclusion criteria: 1. IBD OR Crohn OR colitis; 2, Homo sapiens; 3, Expression profiling by array OR high throughput sequencing; 4, Sample size>50; 5, Submitting date<2020.10.31; 6, DataSets OR Series. Exclusion criteria: 1, Not coding-gene expression data; 2, Non-integral data with nonIBD samples (except for healthy controls); 3, Lack of healthy controls; 4, Nonstandard therapy; 5, Data not available or low data quality (i.e., no comparable subgroups or insufficient significant differential genes). For discovery cohorts, we also consider factors to uncover reliable findings, such as: 1, all colon samples; 2, shared platform and data-style; and, adult patients. We recruited cohorts with necessary information such as sample sources, patient group, disease state, and biologics' therapy response for subgroups' analysis. Detailed data processing and analysis flows were displayed in **Supplementary Figure S1A**.

TABLE 1 | Volunteers recruited in the experimental validation.

ID	Age	Gender	Diagnosis	Biopsy position	Sampling date
1	28	Male	Healthy control	Colon	16.11.2021
2	46	Male	Healthy control	Colon	17.11.2021
3	32	Male	Healthy control	Colon	16.11.2021
4	25	Male	Healthy control	Colon	16.11.2021
5	29	Female	Healthy control	Colon	16.11.2021
C1	33	Male	Crohn's disease	Colon	6.9.2021
C2	16	Male	Crohn's disease	Colon	27.8.2021
C3	26	Male	Crohn's disease	Colon	18.8.2021
U1	52	Male	Ulcerative colitis	Colon	12.7.2021
U2	37	Female	Ulcerative colitis	Colon	25.6.2021
U3	39	Male	Ulcerative colitis	Colon	4.7.2021
U4	34	Male	Ulcerative colitis	Colon	27.6.2021

Association Analysis Between IBD Risk Loci and m6A Regulation

Over 240 Single Nucleotide Polymorphisms (SNPs) have been identified as risk loci for IBD (de Lange et al., 2017), and genes at these risk loci have been collected and sorted out (Jostins et al., 2012; Liu et al., 2015; Huang et al., 2017; Park and Jeen, 2019). m6A regulatory genes, including writers, erasers, and readers, were collected by literature review. IBD risk genes and m6A regulatory genes were analyzed using the STRING database (https://string-db.org) and an interaction network developed (Szklarczyk et al., 2019). The interaction map of IBD risk genes and m6A regulatory genes based on the network was visualized using Cytoscape (version: 3.7.1) (Shannon et al., 2003). The RMVar database (a database of functional variants involved in RNA modification, http://rmvar.renlab.org) (Wang et al., 2020; Luo et al., 2021) was searched to identify m6A-regulated IBD-associated risk loci. Next, m6A regulatory genes closely related to IBD were obtained based on published data of m6A-label-seq, m6A individual-nucleotide-resolution cross-linking and immunoprecipitation seq (miCLIP-seq), and droplet-assisted RNA targeting by single-cell sequencing (DART-seq). These m6A methylation risk variants, SNP locations, transcriptome regulation, and risk genes were visualized on a Circos diagram (Gu et al., 2014).

The IBD m6A Signature in Discovery and Validated Cohorts

The GEO datasets GSE10616, GSE73661, GSE75214, and GSE126124 were used as discovery cohorts for analyzing differential m6A regulatory genes. All datasets were analyzed using the GEO2R online tool based on the R limma package (Ritchie et al., 2015). Overlapping gene expression profiles associated with m6A were obtained using Conway's UpSetR R package (Conway et al., 2017). Correlation analysis between the m6A gene group was done on the Inflammatory Bowel Disease Multi'omics Database (IBDMDB, http://ibdmdb.org) (Lloyd-Price et al., 2019) using the stats R package on Sangerbox tools (http://www.sangerbox.com/tool). A heatmap of m6A gene expression in IBD was validated using a validation cohort from IBDMDB. For example, validation cohort IBDMDB is part of the American National Institute of Health's integrative human microbiome project (HMP2/iHMP) (Lloyd-Price et al., 2019).

Volunteer Recruitment, Reverse Transcription-Quantitative Polymerase Chain Reaction Measure

From June to November 2021, we collected IBD patients' and healthy controls' colonic biopsy samples under coloscopy. These samples are from the cohort in research on Key Technologies of Comprehensive Prevention and Treatment of IBD in Hunan Province, China. The Ethics Institutional Review Board of China's Third Xiangya Hospital has approved this project's cohort. A total of twelve volunteers were enrolled, and their information is listed in **Table 1**. At least two biopsy samples were collected for each volunteer. Total RNA from colon tissue was isolated by using TRIzol® (Thermo Fisher Scientific, Inc.). The qPCR measure was conducted as previously described (Luo et al., 2019) (primer sequences are presented in **Table 2**).

Consensus Clustering in the IBD m6A Signature, Principal Component Analysis, Immune Scoring, and Clinical Correlation

Consensus clustering was performed to better distinguish the detailed m6A signature in IBDMDB subgroups using the consensus ClusterPlus R package (Swift et al., 2004). Heatmap and PCA were used to confirm m6A distinction between different m6A clusters in IBD. Furthermore, immune scoring results of 22 immune cells of different m6A clusters were analyzed using Xcell (https://xcell.ucsf.edu), an online tool that can be used for cell type enrichment analysis based on gene expression data from various immune cell types (Aran et al., 2017). C-reactive protein and erythrocyte sedimentation rate's data of different samples were obtained from IBDMDB and analyzed using a non-paired t-test.

The m6A Signature in IBDMDB

The IBDMDB validation cohort was used to analyze the correlation between IBD core cytokines and m6A regulatory genes using the stats R package (Team, 2013). Data on m6A methylation sites on IBD core cytokines were obtained from m6A-Atlas (www.xjtlu.edu.cn/biologicalsciences/atlas) (Tang et al., 2021). A detailed m6A expression profile was displayed for IBD and healthy controls in IBDMDB.

A Global Landscape of Different Phenotypes of IBD Patients

Based on previous search results, GSE75214 was introduced for analysis of differential m6A gene expression in UC vs. CD, inflamed (active tissues) vs. uninflamed (inactive tissues) biopsies, and adult IBD vs. healthy controls. Dataset GSE6989 was used for comparison between pediatric IBD and healthy adult controls, GSE119600 for comparison between IBD whole blood RNA and healthy controls, GSE33943 for comparison between IBD peripheral blood leukocytes (PBLs) and healthy controls, and

TABLE 2 | The primer sequences.

Gene	Forward	Reverse
IGF2BP2	TGTTGGTGCCATCATCGGA	TTCGGCTAGTTTGGTCTCATCT
HNRNPA2B1	AAGAGGAGGATATGGTGGTGGAG	GGACCGTAGTTAGAAGGTTGCTG
ZCCHC4	TCCGTTTGGTGGCTTGGTT	GGGAAAATCCAGAAAATGGGTAG
GAPDH	GGAAGCTTGTCATCAATGGAAATC	TGATGACCCTTTTGGCTCCC

TABLE 3 | The brief descriptions of the inclusive data series.

ID	Platform	Data	Sample	UC	CD	Control	Cohort
GSE10616	GPL5760	Microarray	Biopsy	10	32	11	Discovery
GSE73661	GPL6244	Microarray	Biopsy	167	0	11	Discovery
GSE75214	GPL6244	Microarray	Biopsy	74	75	22	Discovery
GSE126124	GPL6244	Microarray	Biopsy	20	39	39	Discovery
IBDMDB (GSE111889)	GPL11154	RNA-seq	Biopsy	73	86	49	Validation
GSE6989	GPL5760	Microarray	Biopsy	5	20	8	Pediatrics
GSE119600	GPL10558	Microarray	Blood	93	95	47	Blood
GSE33943	GPL570	Microarray	Blood	45 Unclassified IBDs		13	PBL
GSE3365	GPL96	Microarray	Blood	26	59	42	PBMC

TABLE 4 | GEO datasets involved in IBD's biologics response and m6A.

ID	Platform	Data	Sample	Biologics	Responder	Unresponder
GSE73661	GPL6244	Microarray	Biopsy	Infliximab	8	15
GSE73661	GPL6244	Microarray	Biopsy	Vedolizumab	22	37
GSE92415	GPL13158	Microarray	Biopsy	Golimumab	61	48
GSE112366	GPL13158	Microarray	Biopsy	Ustekinumab	132	113

GSE3365 for comparison between IBD peripheral blood mononuclear cells (PBMCs) and healthy controls. These differential analyses were done using GEO2R based on the limma R package. Another three datasets were analyzed for the differential m6A signature between different therapeutic response subgroups (i.e., GSE73661 for infliximab and vedolizumab, GSE92415 for golimumab, and GSE112366 for ustekinumab).

RESULTS

Data Searching and Processing

Finally, 11 datasets (GSE10616, GSE73661, GSE75214, GSE126124, GSE111889, GSE6989, GSE119600, GSE33943, GSE3365, GSE92415, and GSE112366) were screened out. Except for the microarray datasets, we also recruited a validatory RNA-seq dataset from IBDMDB (GSE111889) (**Table 3**). Of these datasets, GSE10616, GSE73661, GSE75214, and GSE126124 were analyzed as discovery cohorts, while GSE111889 was used as a validation cohort. GSE6989, GSE119600, GSE33943, GSE3365, GSE92415, and GSE112366 were further used to analyze the overall m6A landscape in IBD patients with various phenotypes (**Table 4**). To investigate the m6A's role in IBD, we further explored the interactions of m6A regulators by database and IBD data, aiming to describe the m6A's role in the pathogenesis, pathophysiology, and clinical outcome of IBD.

An Overview of m6A Regulation

We first confirmed the global interactions of m6A regulators in the gene function database and IBD data, revealing their close functional gene set's role. To better understand the m6A's role in IBD, we should first get impressions about m6A regulators' working mode and network. m6A modulators included writers (METTL3, METTL14, and METTL16), WTAP, RBM15, RBM15B, ZC3H13, KIAA1429, and ZCCHC4), erasers (FTO, ALKBH5, and ALKBH1), and readers (YTHDC1, YTHDC2, YTHDF1/2/3, IGF2BP1/2/3, HNRNPA2B1, HNRNPC/G, RBMX, ELAVL1, FMRP, PRRC2A, EIF3, and LRPPRC) (**Figure 1B**). Writers occur in a multicomponent m6A methyltransferase complex (MTC). The core MTC is comprised of METTL3 and METTL14. After deposition, the m6A methyl group can be removed by RNA demethylases (m6A erasers). m6A influences RNA fate by recruiting different m6A-binding proteins (m6A readers). MeRIP-seq relies on an antibody against m6A to immunoprecipitate fragmented RNA for subsequent deep sequencing (Meyer et al., 2012). Thus, m6A methylation peaks can be detected near the region between the coding DNA sequence (CDS) and the 3′ UTR, which is a common m6A methylation position that influences mRNA fate (**Figure 1A**). An interaction network between these m6A genes revealed a close relationship and mutual effect (**Figure 1C**). Further correlation analysis in IBDMDB revealed universal correlation between these m6A genes in IBD, and different m6A complexes exhibited

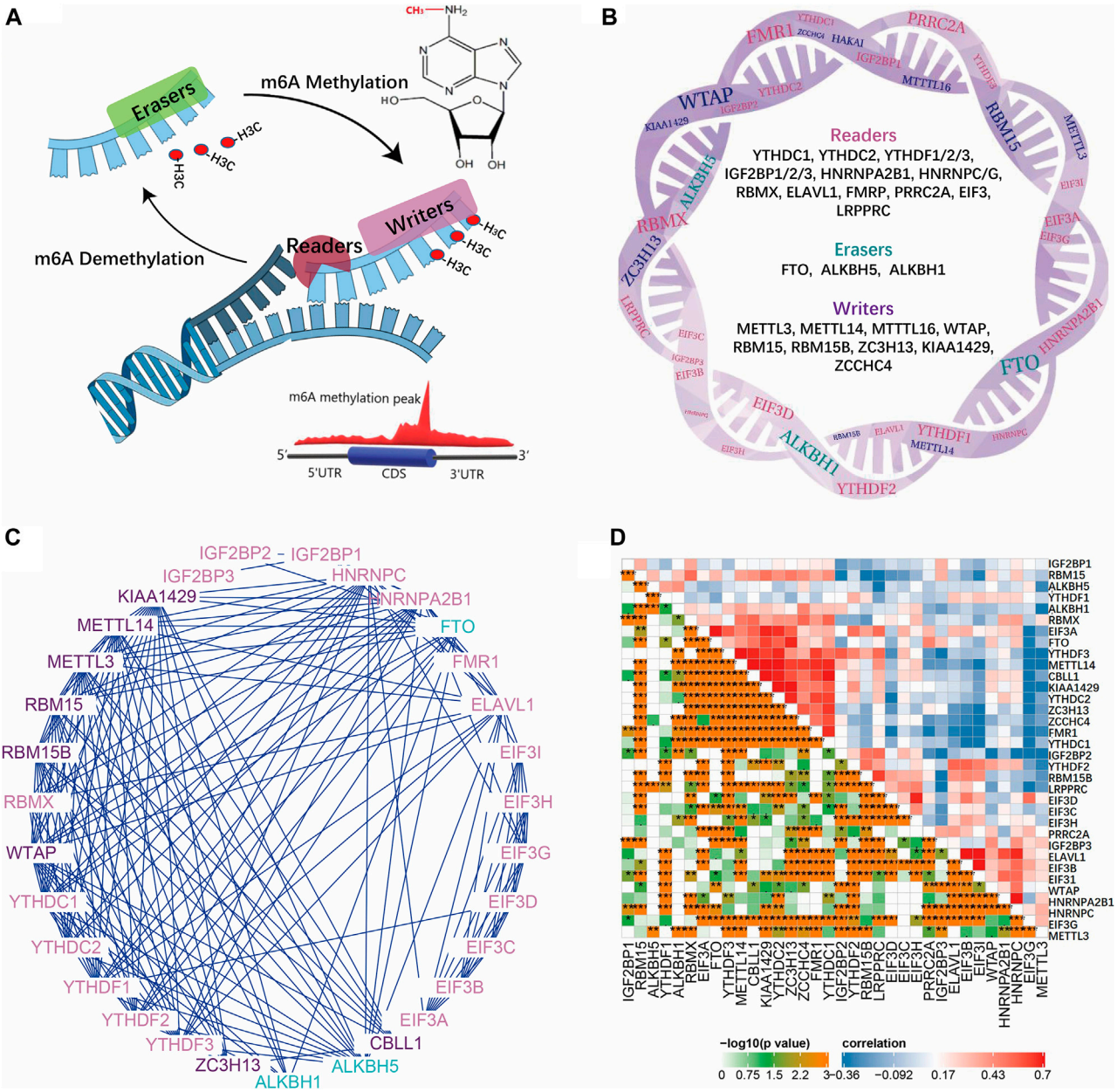


FIGURE 1 | Mechanism of m6A modifications and the interaction of regulating genes. **(A)** is the reversible process of methylation on adenine which is modified by reader, writer and eraser proteins. **(B)** is the detailed gene list of reader, writer and eraser proteins. **(C)** is the interaction network of reader, writer and eraser proteins. **(D)** is the correlation map of m6A reader, writer and eraser proteins in IBDMDB cohort.

clustering in the map (**Figure 1D**). These data indicate a close interaction between m6A genes.

The Emerging m6A Landscape in IBD

United Kingdom Biobank project analysis had identified 12.3 million variants that lead to changes in the encoded protein, and these variants were associated with human disease (Okada and Wang, 2021), and the IBD risk variants influenced the risk of IBD pathogenesis primarily as reported (Liu et al., 2015; de Lange et al., 2017). Moreover, m6A modifications usually read the specific SNPs as the signal label. To verify m6A's role in IBD pathogenesis and pathophysiology, we explored the connection between the IBD risk variants and m6A modifications and the universal differential m6A regulators in IBD patients. Methylations related to IBD risk loci were identified based on public m6A-label-seq, miCLIP &DART-seq, or miCLIP data from RMVar (Luo et al., 2021). This analysis revealed that 49 IBD risk SNPs had methylation m6A sites. Circos analysis revealed these m6A modification sites' chromosomal positions, transcriptome regulation, and risk genes (**Figure 2A**; **Supplementary Table**

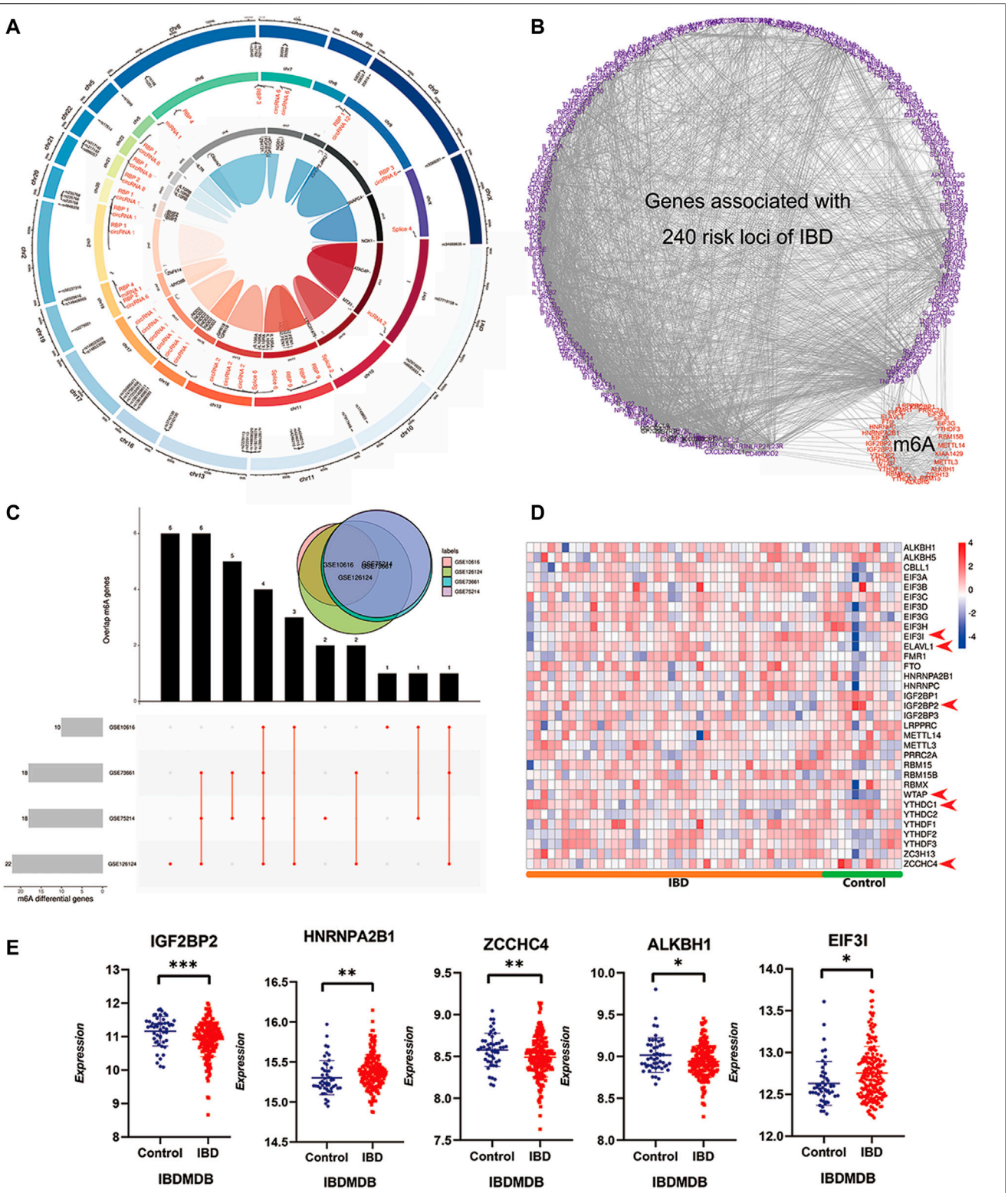


FIGURE 2 | A widespread interaction and participation of m6A modifications in IBD. **(A)** is the Circos diagram of known m6A modifications in IBD associated risk SNPs based m6A sequencing. The outer circle indicates the positions of m6A modified IBD associated risk SNPs in chromosome, the middle circle is transcriptome regulation of risk SNPs, the inner circle is the risk gene name. **(B)** is the interaction network of 240 known IBD risk genes and m6A reader, writer and eraser genes. **(C)** is the UpSet diagram of differential m6A regulators in four independent discovery IBD cohorts. The upper right venn displays the overlaps of differential genes in four cohorts together. **(D)** is the heatmap of m6A reader, writer and eraser in validatory IBDMDB cohort. **(E)** is the expressing profile of top differential m6A regulators in the validatory IBDMDB cohort (t test, $p < 0.05$).

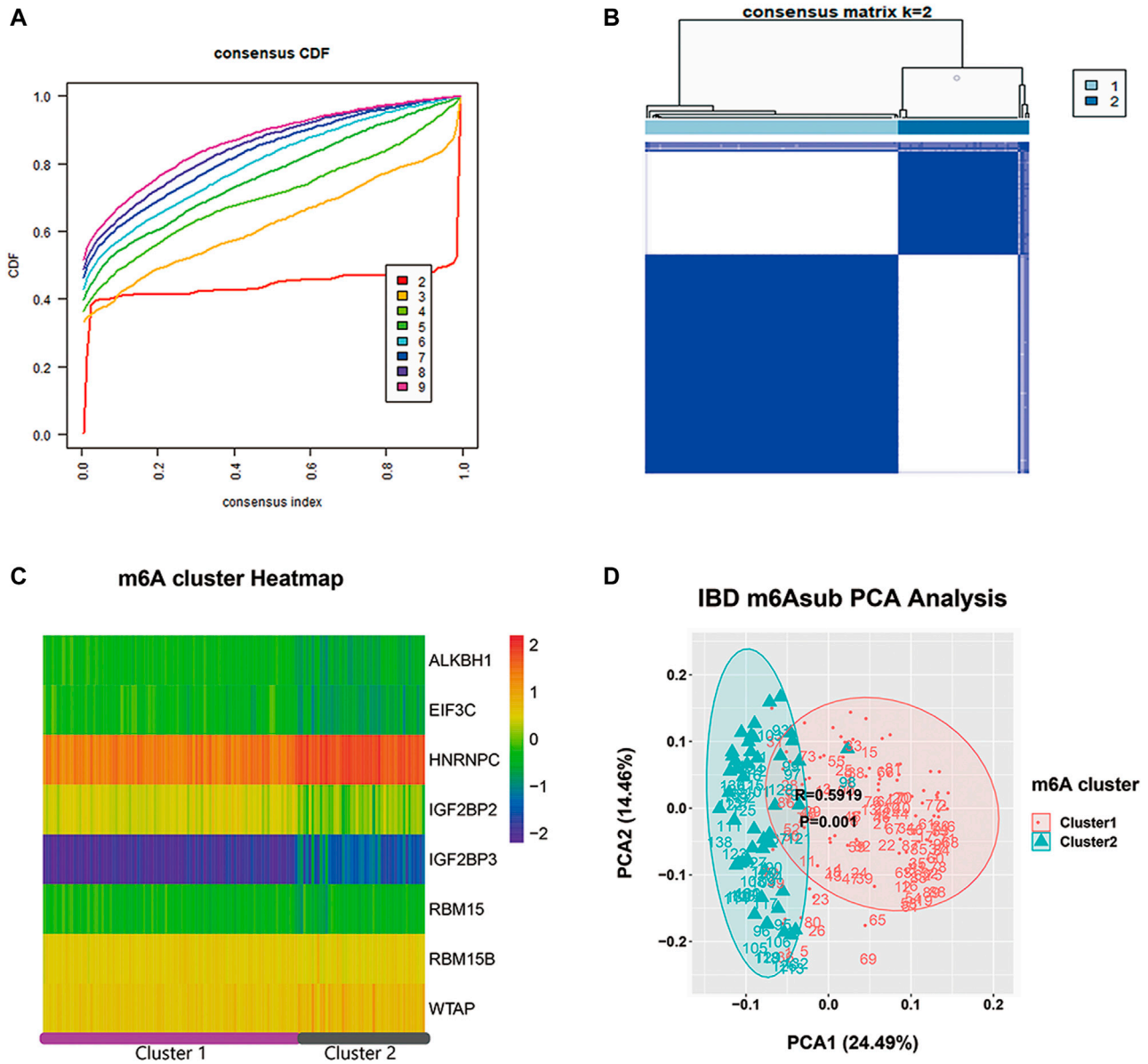


FIGURE 3 | The consensus clustering analysis of m6A regulators in IBDMDB cohort. **(A)** is the consensus CDF diagram which show a good clustering is obtained when k = 2. **(B)** is the different clusters after consensus clustering by k = 2, **(C)** is the heatmap of m6A reader, writer and eraser expression in different clusters. **(D)** is the PCA analysis that shows well discrimination between two clusters.

S1). An interaction network between 257 published IBD risk genes and m6A genes was used to elucidate high interactions (**Figure 2B**; **Supplementary Table S1**). Analysis of differential m6A gene expression between IBD patients and healthy controls using the aforementioned four discovery cohorts revealed 10, 18, 19, and 22 differentially expressed m6A genes in datasets GSE10616, GSE73661, GSE75214, and GSE126124, respectively (p = <0.05). The overlap map between these m6A genes in the discovery cohorts revealed universal and identical m6A methylation modifications in IBD patients (**Figure 2C**). Validation analysis using the IBDMDB cohort revealed expression differences between IBD patients and healthy controls (**Figure 2D**). Importantly, to achieve a better understanding of such changes, the expression profiles of partial m6A genes and differences were displayed in the IBDMDB validation cohort again (**Figure 2E**). We also enrolled twelve volunteers, including three Crohn's patients, four ulcerative colitis patients, and five healthy controls. Their colonic expression of m6A regulators was measured by qPCR. Reader insulin-like growth factor 2 mRNA binding protein 2 (IGF2BP2) was downregulated in IBD patients compared to healthy controls (**Supplementary Figure S1B**, non-paired test, p < 0.05). Zinc finger CCHC-type containing 4 (ZCCHC4) was also downregulated, although no significance exists (**Supplementary Figure S1B**). Heterogeneous nuclear ribonucleoprotein A2/B1

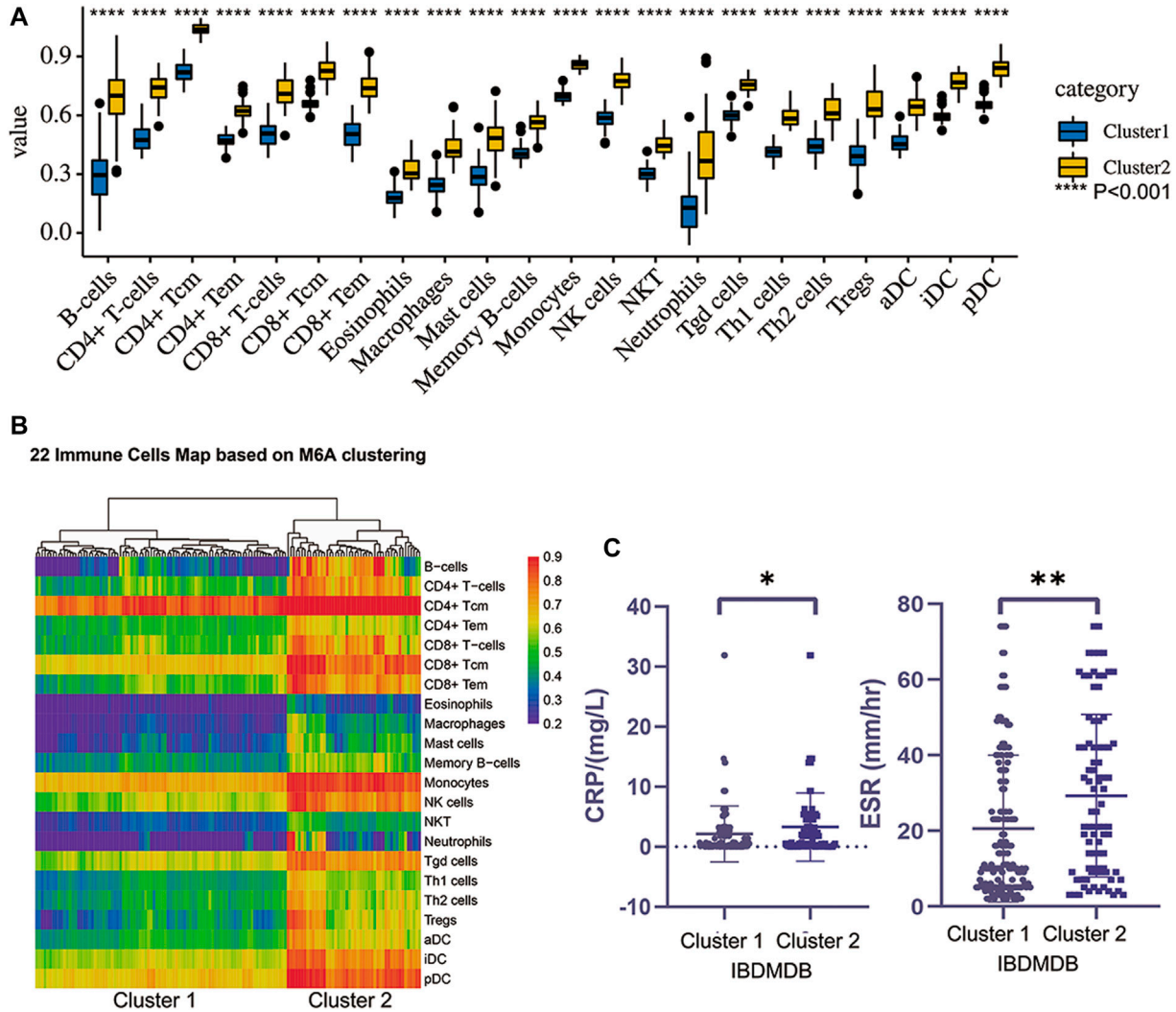


FIGURE 4 | The different immune landscape and clinical phenotypes of two clusters obtained by consensus clustering. **(A)** is the different immune scoring of major 22 immune cells in two clusters ($p < 0.01$). **(B)** is the heatmap of the two clusters' immune landscape. **(C)** is the difference of two clusters clinical indexes such as ESR and CRP (t test, $p < 0.05$).

(HNRNPA2B1) reached significance, but the tendency was not consistent (**Supplementary Figure S1B**, non-paired test, $p < 0.05$).

An Insight on m6A Landscape in IBD

To carefully understand the divergent roles of m6A modification in the IBD pathophysiology, we investigated m6A regulators' sub-phenotypes among IBD patients. m6A modification is a reversible biological process, and different groups of m6A genes have opposite effects on the fate of RNA. Consensus clustering was conducted based on the IBDMDB m6A matrix to explore m6A subgroups among IBD patients. The findings showed clusters of IBD patients' samples ($n = 198$), which appeared as "independent islands" in the map with K = 2, indicating that sub-clusters of samples exhibited common genomic m6A features (**Figures 3A,B**; **Supplementary Table S2**). In addition, the m6A expression profile of the sub-clusters was expressed as a heatmap, and PCA showed a distinction between two m6A clusters (**Figures 3C,D**; **Supplementary Table S2**). Dysregulation in the immune system plays an important role in IBD. Therefore, the immune scores of the different clusters were obtained from the Xcell website for 22 immune cell types for further analysis (Aran et al., 2017). Different m6A clusters displayed significant immune distance from each other, and the different immune phenotypes indicated different clinical features (**Figures 4A,B**; **Supplementary Table S2**). CRP and ESR are common clinical inflammation indexes for disease diagnosis and management. Moreover, the CRP and ESR data of these samples were retrieved from the IBDMDB database to further explore the clinical features of m6A clusters, and the analysis showed a significant difference (non-paired t-test; $p < 0.05$) between the two m6A clusters (**Figure 4C**; **Supplementary Table S2**). The sub-m6A-phenotypes' different clinical features will guide to better disease diagnosis and management.

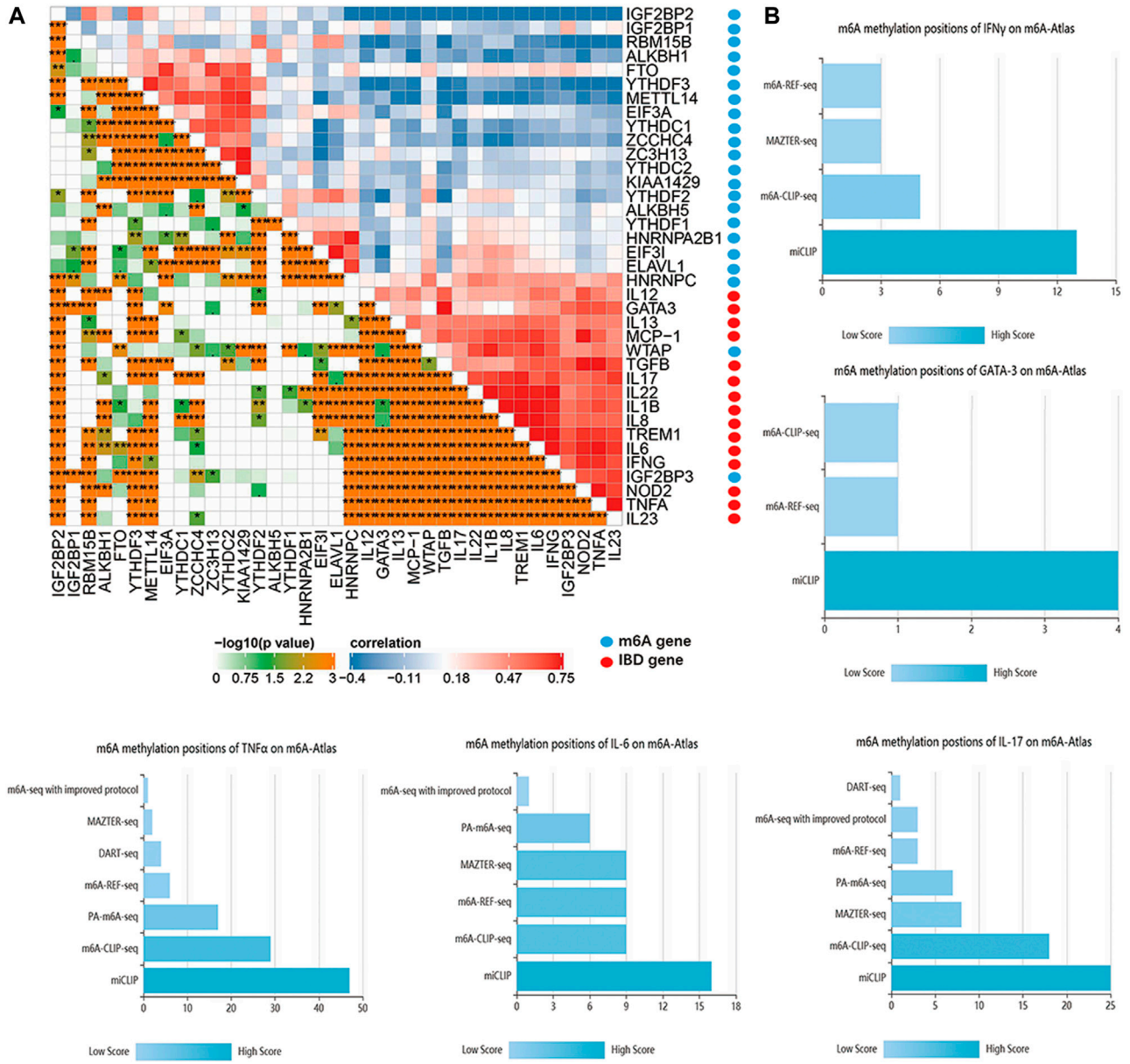


FIGURE 5 | The interaction of m6A regulators and IBD core cytokines. **(A)** is the correlation map of m6A regulators and IBD core cytokines. **(B)** is the m6A methylation positions of IBD core cytokines based on different m6A detecting technology.

Immune-Related m6A Methylation Landscape in IBD

Sub-m6A-phenotypes have different clinical features. With no doubt, the pathophysiology of IBD exhibits typical immune dysfunctions (Chang, 2020), and m6A modifications are known to influence immune cells a lot (Winkler et al., 2019; Shulman and Stern-Ginossar, 2020). Therefore, it is natural that we further explore the immune-related m6A methylation landscape in IBD. Immune cytokines play an important role in the pathogenesis and outcome of IBD. For example, IL2, IL4, GATA3, IL9, IL13, TGBβ, and TNFα are implicated in UC (Ungaro et al., 2017), whereas IL4, IL6, IL12, IL17, IL21, IL22, IL23, TNF, and IFNγ are involved in CD (Roda et al., 2020). Different m6A clusters exhibit differences in immune profiles. Therefore, correlation analysis was performed between IBD core cytokines and m6A genes in the IBDMDB. The findings showed significant correlations among m6A genes and immune cytokines (**Figure 5A**). Furthermore, m6A modification characteristics of these cytokines were obtained from the m6A-Atlas database (Tang et al., 2021). The N6-adenosine methylation sites on these cytokines were explored using high-quality sequencing analysis (such as miCLIP, m6A-CLIP-seq, m6A-REF-seq, MAZTER-seq, and PA-m6A-seq). Details on m6A

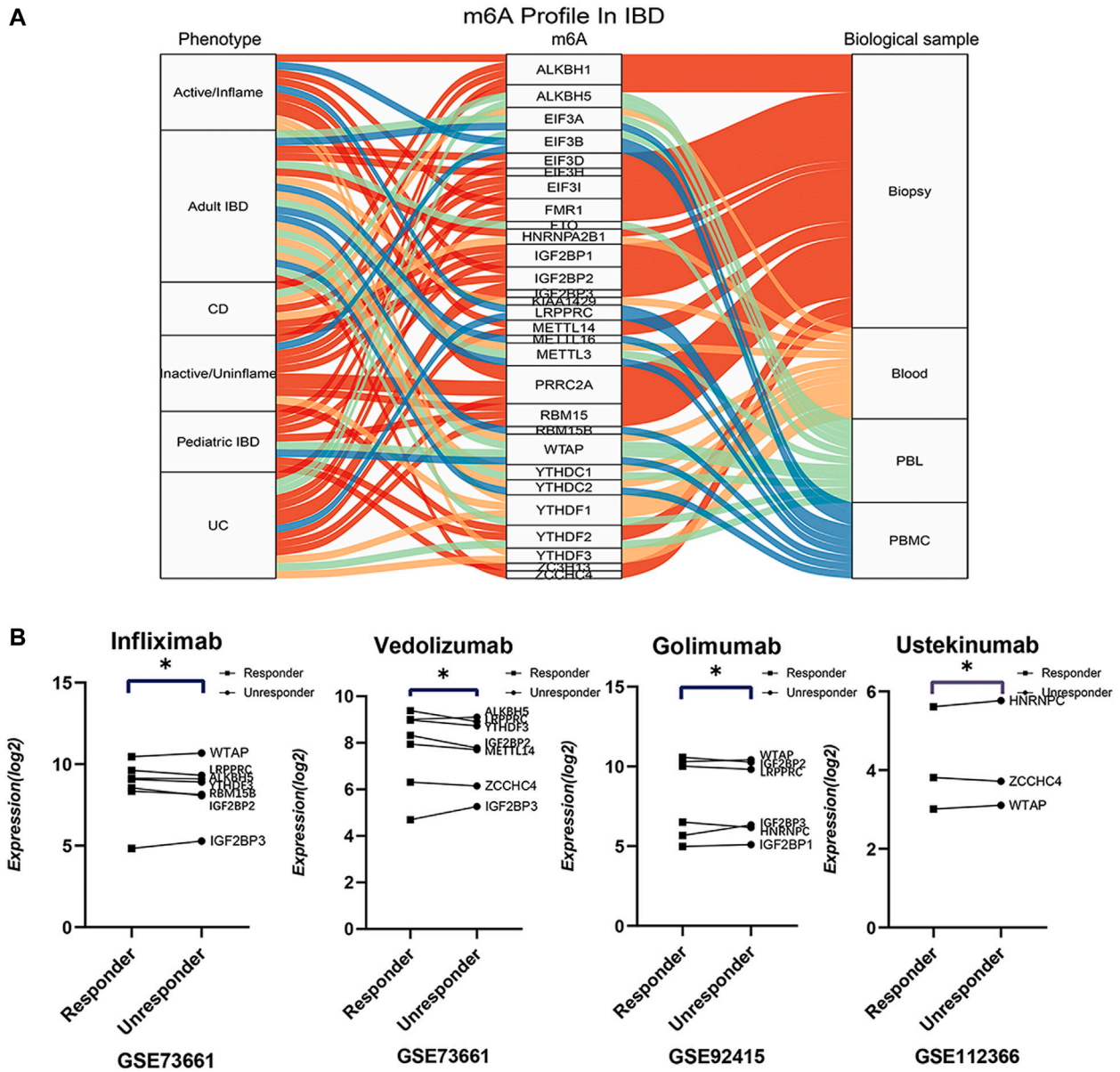


FIGURE 6 | The globally differential expressions of m6A readers, writers and erasers in different phenotypes, sample sources, patient groups, and therapeutic response subgroups. **(A)** is the sankey diagram of differential m6A regulators between different phenotypes, sample sources, patient groups. **(B)** is the top differential m6A regulators between responder and unresponder by biologics such as infliximab, vedolizumab, golimumab, and ustekinumab.

modifications of these immune cytokines are presented in **Figures 5B–F**; **Supplementary Table S2**.

Role of m6A Modifications in Different Phenotypes of IBD

Except for the pathogenesis and pathophysiology, the impressive m6A-IBD interactions reinforce us to further explore the effect of m6A modifications on clinical phenotypes and treatment of IBD. Global comparisons were carried out between UC and CD (GSE75214), inflamed and uninflamed tissues (GSE75214), adult IBD (GSE75214), pediatric IBD (GSE6989), IBD whole blood sample (GSE119600), IBD PBLs sample (GSE33943), and IBD PBMCs sample (GSE3365). The top five differentially expressed genes were obtained with $p < 0.05$. A Sankey diagram was generated to present the universal different m6A signatures among different clinical phenotypes (**Figure 6A**; **Supplementary Table S3**). In addition, m6A signatures were explored among different biological therapeutic response subgroups, and the findings showed differential expression of m6A genes among different response subgroups (**Figure 6B**; **Supplementary Table S4**). These findings indicate that m6A modifications have a significant effect on different IBD phenotypes.

DISCUSSION

Previous studies have not explored the integral role of m6A in IBD. For the first time, the current study explored a comprehensive landscape of m6A modifications in IBD. Analysis of the mechanism of m6A modifications shows that the multi-component m6A MTC (or "Writer") catalyzes adenosine methylation by binding S-adenosylmethionine. METTL3 and METTL14 combine to form a complex core methyltransferase domain. Notably, METTL16 functions without forming a complex, and targets U6 snRNA and MAT2A mRNA, which is independent of the m6A deposition DRACH motif (Meyer and Jaffrey, 2017; Zaccara et al., 2019; Huang et al., 2020). Other regulatory subunits, such as WTAP, RBM15/RBM15B, KIAA1429 (VIRMA) and ZC3H13, play roles in anchoring the "Writer" in regions adjacent to mRNAs' m6A sites. The common consensus m6A deposition motif is the DRACH motif (D = G, A, or U; R = G or A; and H = C, A, or U). MTC adds methyl to the adenosine within the DRACH motif (Linder et al., 2015). m6A is a reversible biological process modulated by several RNA demethylases (the "erasers"). For instance, FTO and ALKBH5 trigger demethylation of methylated adenosine (Frayling et al., 2007; Zaccara et al., 2019). Therefore, m6A modification is a dynamic RNA modification process involving m6A writers and erasers. Therefore, several RNA-binding proteins ("readers") can identify the m6A signal in mRNAs and modulate mRNA fate by affecting splicing, translocation, decay, stabilization, and translation processes (Zaccara et al., 2019). m6A has been reported its potential connections with IBD, METTL3 and METTL14 deficiency in immune cell induce colitis; m6A eraser FTO protects IBD patients from adverse reactions after thiopurine treatment (Xu et al., 2021). The current research on m6A and IBD is scarce, so the cognition of m6A on IBD is limited and frustratingly (Xu et al., 2021). Therefore, there is a strong need for relevant exploration to provide more possibilities for the pathogenesis, clinical diagnosis, and treatment applications in IBD (Xu et al., 2021; Zhang et al., 2021). A better understanding of primary RNA modification in IBD will undoubtedly provide a new direction for the occurrence, development, and clinical intervention of IBD.

In order to understand the role of m6A modification in the pathogenesis of IBD, our results show IBD-associated variants could be modified by m6A and their associated gene expression potential changed. Disease-associated SNPs affect disease state, and several IBD-associated SNPs have been detected by GWAS and other techniques (Liu et al., 2015; de Lange et al., 2017; Huang et al., 2017). One example of this mechanism is the NOD2 gene, mutations that generate a non-functional version of NOD2 are a risk factor for Crohn's disease, and NOD2 risk variants are associated with activated immune cells and fibrosis. Coding and noncoding variants could both influence the specific disease risk (Backman et al., 2021; Nasser et al., 2021). Correlations analysis of SNPs using m6A-seq showed an enrichment of SNPs in m6A-containing regions (Liu J.e. et al., 2020; Luo et al., 2021). Consequently, disease risk variants may modulate RNA fate and gene expression by RNA modification sensing. To explore the internal complex mechanism of IBD variants and their related genes, the current study performed bioinformatics analysis to offer a further insight on mechanisms of IBD pathogenesis. Out of the 232 IBD risk loci identified through GWAS, 122 were associated with a total of 157 genes (Furey et al., 2019). Genotypic variation can contribute to gene expression differences across individuals. Expression quantitative trait loci (eQTLs) are genomic regions with specific genetic variants, including SNPs, that are associated with levels of expression of one or more genes. Analysis of eQTL shows that IBD variants may represent m6A modification loci, which exert effects on the fate and expression of the risk gene (Furey et al., 2019). Moreover, risk genes exhibit several interactions with m6A genes. The RMVar database provides important IBD-related SNPs that are frequently modified by m6A through a combination of m6A-seq data and disease associated SNPs data (Luo et al., 2021). In addition, our provided network between IBD risk genes and m6A genes gives a direct impression of the potential role of m6A in IBD. These findings indicate that m6A plays a significant role in the pathogenesis of IBD, which would help with early screening and prevention of the disease. The specific testing panel targeting risk variants' m6A modifications might promote the prevention of IBD's occurrence.

The discussion of global m6A regulators' changes in IBD patients' colonic tissues puts the IBD-associated RNA modifications into a new state. Analysis of multiple independent data series showed that they shared differentially expressed m6A regulators in IBD cohorts, which indicated common phenomena of alterations of m6A-related genes implicated in the pathogenesis of IBD. A significant role in IBD was confirmed for the shared differentially expressed m6A genes in the IBDMDB validation cohort. The top common differential m6A regulator, IGF2BP2 (also known as IMP2, a m6A Reader), is a direct mTOR substrate that participates in glucose, lipid, protein, and energy metabolism (Dai, 2020), which are key events in the pathogenesis of IBD (Lloyd-Price et al., 2019; Ding et al., 2020). Pre-mRNA with m6A modifications detected by IGF2BP2 can be prevented from degradation in the P-body. In addition, IGF2BP2 can promote the export of premature mRNAs to the cytoplasm. IGF2BP2 protein in IGF2BP family promotes stability, inhibits decay and promotes storage of their target transcripts in a m6A-dependent manner, thus affecting mRNA fate and gene expression (Huang et al., 2018). The altered IGF2BP2 may modulate the stability, degradation, and storage of several important IBD genes, thus affecting IBD pathology. In addition, HNRNPA2B1 (Reader), another common m6A gene in IBD cohorts, promotes m6A modification and nucleocytoplasmic trafficking, thus facilitating effective production of interferons mediated by cyclic GMP-AMP synthase (cGAS)-STING (Wang L. et al., 2019). Dysbiosis of the gut virome is a common phenomenon in the process of IBD (Clooney et al., 2019). The cGAS-STING system is a vital virus-immune signaling pathway in which the gut virome dysbiosis deteriorates the impaired IBD innate immune system through cGAS-STING associated m6A modifications (Zheng et al., 2017; Wang L. et al., 2019). In addition to m6A readers, common IBD differential m6A writer ZCCHC4 plays an important role in methylating 28S rRNA, thus promoting ribosome assembly and translation, which in turn affects cell proliferation and growth

(Ren et al., 2019). ZCCHC4 determines the fate of IBD core cytokines. Furthermore, m6A in the 5′UTR is small and is recognized by a multi-subunit interface of eIF3 involving eIF3a, eIF3I and other subunits. eIF3 recruitment to mRNA is a general mechanism for promoting translational (Wang et al., 2013; Choe et al., 2018). The eIF3 complex can modulate several important IBD pathophysiological events. New evidence is emerging that m6A reader, ELAVL1, could directly interact with Atg16l1 mRNA via its 3′ untranslated region and enhance ATG16L1 translation without affecting Atg16l1 mRNA stability (Li et al., 2020). Intestinal mucosa from patients with IBD exhibited reduced levels of both ELAVL1 and ATG16L1 (Li et al., 2020), and ATG16L1 is a crucial autophagy-related gene in IBD (Murthy et al., 2014). Importantly, we validated the bioinformatic discoveries in our IBD colonic tissues. Therefore, the m6A regulators' dysfunction plays an unknown role in IBD, which needs to be explored further.

Immune dysfunction sustains an essential role in IBD. Immune cells such as T cells, macrophages, and dendrite cells exhibit differences between the m6A subgroups of IBD patients. Our results indicate that m6A modification influences the immune phenotypes and clinical inflammatory state of IBD. Several studies have explored the role of m6A modifications in the immune system (Han et al., 2019; Winkler et al., 2019; Shulman and Stern-Ginossar, 2020; Su et al., 2020; Wang et al., 2020). METTL3 is the core "writer" component of the MTC in m6A. A CD4-Cre loxP-flanked-METTL3 ($METTL3^{fl/fl}$) mouse model exhibited more circulating naive T lymphocytes and less abundant activated $CD4^+$ T cells, thus exerting a preventive role in the evolving colitis (Li et al., 2017). Moreover, T cells without METTL14, a m6A "writer" component of the MTC, showed similar phenomena (Lu et al., 2020). METTL3 and METTL4-deficient T helper cells do not induce colitis as they cannot differentiate into pathogenic effector T cells (Li et al., 2017). In addition to m6A writers, the m6A eraser ALKBH5 can modulate the naïve $CD4^+$T cells' infiltration and enhance the responses of $CD4^+$ T cells (Zhou et al., 2021). These studies indicate the critical roles of m6A genes in T-cell homeostatic proliferation and differentiation (Li et al., 2017). Mice with a specific METTL3 knockout from Tregs displayed a systematic loss of the suppressive function of Tregs and could not perform m6A RNA modification (Tong et al., 2018). m6A modifications mediate Tregs function by IL-2-STAT5 signaling pathway (Tong et al., 2018). A recent study reported that CD4-Cre $METTL14^{fl/fl}$ mice developed colitis, which was characterized by increased Th1 and Th17 cytokines and dysfunctional Tregs (Lu et al., 2020). Notably, a microbiome modulated by antibiotics alleviated colitis, indicating a microbiota-immune interaction in the model (Lu et al., 2020). Microbiota-immune dysfunction plays a key role in the development of IBD, thus m6A modifications may play a role in IBD-associated microbiota-immune dysfunction. DCs are innate immune cells that can stimulate T cells and present antigens, which is also a critical player in onset of IBD (Chang, 2020). Lipopolysaccharide (LPS) stimulating condition increases proliferation of DCs proliferated and upregulates its m6A modifications. METTL3-mediated m6A modification increases translation of immune cytokines, DC activation and DC-based T-cell response (Wang H. et al., 2019). Furthermore, macrophages can exert an extensive inflammation-modulating effect under m6A modifications (Yu et al., 2019). In addition, LPS can enhance the level and function of m6A Writer METTL3 in macrophages, and overexpression of METTL3 significantly alleviates the LPS-induced inflammatory response in an NF-κB signaling-dependent manner (Wang J. et al., 2019). IBD is an autoimmune disorder and presents significant dysregulation of innate and adaptive immune responses (Chang, 2020). The clustering findings showed different m6A gene signatures displaying different immune features owing to the reversible biological process of m6A modification. Different m6A gene clusters exhibited the landscape and state of distant immune cells, such as T lymphocytes, DCs, and macrophages. The m6A-related immune signature indicates different clinical indicators and phenotypes. Therefore, these key immune cells ($CD4^+$ T cells, Tregs, DCs and macrophages) may be implicated in occurrence and development of IBD, and m6A modification is involved in maintaining homeostasis and functions of these immune cells. However, the role of m6A modification in mediating T cells, DCs, and macrophages in the pathogenesis of IBD is not fully elucidated, and should be explored further. Our results support the m6A related immune dysfunction, which sets a basis of the m6A-induced effects in the pathophysiology of IBD. Further m6A-based prediction of prognosis will help with risk stratification and more precise management of patients.

In addition to immune cells, critical immune cytokines are the essential targets for m6A modifications. GATA3 and TNFα are important cytokines in the mucosa damaging and comorbidities of UC(Ungaro et al., 2017); whereas IL6, IL17, TNF, and IFNγ are deeply involved in the CD. Our results support the influence of critical cytokines by m6A modifications and their tight relationship with m6A regulators in IBD. Eraser ALKBH5 deficiency reduces levels of IFNβ and impairs the innate immune response (Liu et al., 2019). YTHDF3 suppresses interferon production by promoting FOXO3 translation (Zhang et al., 2019). HNRNPA2B1 promotes m6A modification and nucleocytoplasmic trafficking of cGAS-STING, a well-known virus sensing system (Wang L. et al., 2019). In addition, it facilitates effective induction of IFNα/β production mediated by cGAS, IFI16, and STING (Wang L. et al., 2019). The role of gut virome dysbiosis, a common feature in IBD, has not been fully elucidated (Clooney et al., 2019; Liang et al., 2020). The findings of the current study showed that HNRNPA2B1 was a common differential gene among IBD microarray data. Therefore, an impaired IBD innate immune and gut virome dysbiosis may play a role through an m6A-associated viral sensing signaling. Inflammatory cytokines such as GATA3 are modified by m6A for degradation by KIAA1429 (Lan et al., 2019). IL6 mRNA is demethylated by m6A eraser ALKBH5 to inhibit translocation from the nucleus, and the production of IL6 is suppressed by m6A modification (Zhao et al., 2020). Moreover, apoptosis involved in the pathogenesis of IBD may affect immune and gut barrier function (Pedersen et al., 2014; Lin et al., 2017). Notably, apoptosis can be significantly modulated by m6A modifications (Vu et al.,

2017; He et al., 2019). For example, m6A Writer METTL3 inhibits apoptosis (Vu et al., 2017; Cai et al., 2018), whereas its Eraser FTO and Reader YTHDF2 promote apoptosis (Huang et al., 2019; Zhong et al., 2019). Findings from the current study and previous studies indicate an extensive regulatory effect of m6A, not limited to apoptosis and immunity. Therefore, future IBD study design and therapy target development could focus on the m6A modifications.

Different phenotypes and therapeutic responses rely on genetic and environmental factors. m6A provides fundamental explanations of the different phenotypes such as flame and inflamed tissues, pediatric and adult patients; inconsistent biological differences including blood, PBLs, and PBMCs. m6A modifications induce genomic differential expression and distinct biological effects. Further studies on the m6A modification mechanism will further elucidate the pathophysiology of IBD. Another major concern is the clinical management of IBD, therapeutic agents should be well distributed to patients based on their different conditions. m6A accounts for an important part of biological response backgrounds of IBD patients. m6A modification provides a definition of the important distinctions between different biological response subgroups and offers a valuable basis for disease management.

As a primary mRNA modification, m6A contributes to a large group of disorders such as cancers, metabolism, immune, and others. Consequently, the progress of m6A's effect on IBD would be a breakthrough in understanding the disease. We want to contribute to the m6A modification's understanding of IBD's pathogenesis, pathophysiology, and clinical phenotypes. However, our analysis has several shortages, such as limited clinical sample validation, lack of detailed exploration, and more. Due to the COVID-19 epidemic, critical lockdown, and restricted admission, recruiting volunteers is complex, and colonic biopsy is usually limited. Further IBD-related m6A details need to be uncovered.

In conclusion, the current study performed comprehensive analysis on the significance of m6A in IBD. The findings showed a global m6A gene difference, m6A associated SNPs, m6A clusters and different clusters' immune signatures, and m6A features of different clinical phenotypes in IBD. The current study presents the IBD m6A modification network, including important immune cells, cytokines, and SNPs. This landscape provides information on the role of m6A modification in the progression of IBD. However, the specific m6A genes and corresponding modification mechanisms should be explored further, and their roles in IBD should be elucidated.

DATA AVAILABILITY STATEMENT

Publicly available datasets were analyzed in this study. This data can be found here: The recruited microarray date including GSE10616, GSE73661, GSE75214, GSE126124, GSE6989, GSE119600, GSE33943, GSE3365, GSE73661, GSE73661, GSE92415, and GSE112366 are available at the GEO database (https://www.ncbi.nlm.nih.gov/geo/). The validatory IBDMDB data and relevant participants' information are available at the IBDMDB database (http://ibdmdb.org). The functional variants involved in RNA modification are obtained from the RMVar database (http://rmvar.renlab.org). Data from m6A methylation sequencing is available at the m6A-Atlas (www.xjtlu.edu.cn/biologicalsciences/atlas).

ETHICS STATEMENT

All the human samples are from the cohort in Research on Key Technologies of Comprehensive Prevention and Treatment of IBD in Hunan Province, China. The Ethics Institutional Review Board of China's Third Xiangya Hospital has approved this project's cohort. We also have obtained the approve of sample use from the ethics institution.

AUTHOR CONTRIBUTIONS

KN formed the main conception and wrote the manuscript. KN performed all the data screening, analysis, and experiments. JY, YY, TW, and XC collected the biopsy samples in the cohort. ZZ helped form the conception and the consensus clustering analysis and m6A gene collection. MD and YYY reviewed the manuscript, discussed every part, and polished the language. XW funded the study and critically reviewed and edited our manuscript. All authors contributed to the article and approved the submitted version.

FUNDING

This project was supported by the National Natural Science Foundation of China (NSFC nos. 81970494 and 81800500); 81970494 was a grant to XW and 81800500 to YYY.

ACKNOWLEDGMENTS

We acknowledge the project entitled "Research on Key Technologies of Comprehensive Prevention and Treatment of Inflammatory Bowel Disease" (2019SK 2041), which is supported by the key research and development program of Hunan province, China. We also acknowledge FreeScience's language editing support.

SUPPLEMENTARY MATERIAL

The Supplementary Material for this article can be found online at: https://www.frontiersin.org/articles/10.3389/fcell.2021.782636/full#supplementary-material

Supplementary Figure 1 | (A) is the data processing procedure. **(B)** is the qPCR measure of some common m6A regulators in colonic tissues from three Crohn's patients, four ulcerative colitis patients, and five healthy controls (non-paired t-test, $^{*}p < 0.05$, ns $p > 0.05$).

REFERENCES

Aran, D., Hu, Z., and Butte, A. J. (2017). xCell: Digitally Portraying the Tissue Cellular Heterogeneity Landscape. *Genome Biol.* 18 (1), 220. doi:10.1186/s13059-017-1349-1

Argollo, M., Gilardi, D., Peyrin-Biroulet, C., Chabot, J.-F., Peyrin-Biroulet, L., and Danese, S. (2019). Comorbidities in Inflammatory Bowel Disease: a Call for Action. *Lancet Gastroenterol. Hepatol.* 4 (8), 643–654. doi:10.1016/s2468-1253(19)30173-6

Backman, J. D., Li, A. H., Marcketta, A., Sun, D., Mbatchou, J., Kessler, M. D., et al. (2021). Exome Sequencing and Analysis of 454,787 UK Biobank Participants. *Nature* 599, 628–634. doi:10.1038/s41586-021-04103-z

Cai, X., Wang, X., Cao, C., Gao, Y., Zhang, S., Yang, Z., et al. (2018). HBXIP-elevated Methyltransferase METTL3 Promotes the Progression of Breast Cancer via Inhibiting Tumor Suppressor Let-7g. *Cancer Lett.* 415, 11–19. doi:10.1016/j.canlet.2017.11.018

Chang, J. T. (2020). Pathophysiology of Inflammatory Bowel Diseases. *N. Engl. J. Med.* 383 (27), 2652–2664. doi:10.1056/NEJMra2002697

Choe, J., Lin, S., Zhang, W., Liu, Q., Wang, L., Ramirez-Moya, J., et al. (2018). mRNA Circularization by METTL3-eIF3h Enhances Translation and Promotes Oncogenesis. *Nature* 561 (7724), 556–560. doi:10.1038/s41586-018-0538-8

Clooney, A. G., Sutton, T. D. S., Shkoporov, A. N., Holohan, R. K., Daly, K. M., O'Regan, O., et al. (2019). Whole-Virome Analysis Sheds Light on Viral Dark Matter in Inflammatory Bowel Disease. *Cel. Host Microbe.* 26 (6), 764–778. doi:10.1016/j.chom.2019.10.009

Conway, J. R., Lex, A., and Gehlenborg, N. (2017). UpSetR: an R Package for the Visualization of Intersecting Sets and Their Properties. *Bioinformatics (Oxford, England)* 33 (18), 2938–2940. doi:10.1093/bioinformatics/btx364

Dai, N. (2020). The Diverse Functions of IMP2/IGF2BP2 in Metabolism. *Trends Endocrinol. Metab.* 31 (9), 670–679. doi:10.1016/j.tem.2020.05.007

de Lange, K. M., Moutsianas, L., Lee, J. C., Lamb, C. A., Luo, Y., Kennedy, N. A., et al. (2017). Genome-wide Association Study Implicates Immune Activation of Multiple Integrin Genes in Inflammatory Bowel Disease. *Nat. Genet.* 49 (2), 256–261. doi:10.1038/ng.3760

Desrosiers, R., Friderici, K., and Rottman, F. (1974). Identification of Methylated Nucleosides in Messenger RNA from Novikoff Hepatoma Cells. *Proc. Natl. Acad. Sci.* 71 (10), 3971–3975. doi:10.1073/pnas.71.10.3971

Ding, N. S., McDonald, J. A. K., Perdones-Montero, A., Rees, D. N., Adegbola, S. O., Misra, R., et al. (2020). Metabonomics and the Gut Microbiome Associated With Primary Response to Anti-TNF Therapy in Crohn's Disease. *J. Crohns Colitis* 14 (8), 1090–1102. doi:10.1093/ecco-jcc/jjaa039

Dominissini, D., Moshitch-Moshkovitz, S., Schwartz, S., Salmon-Divon, M., Ungar, L., Osenberg, S., et al. (2012). Topology of the Human and Mouse m6A RNA Methylomes Revealed by m6A-Seq. *Nature* 485 (7397), 201–206. doi:10.1038/nature11112

Frayling, T. M., Timpson, N. J., Weedon, M. N., Zeggini, E., Freathy, R. M., Lindgren, C. M., et al. (2007). A Common Variant in the FTO Gene Is Associated with Body Mass index and Predisposes to Childhood and Adult Obesity. *Science* 316 (5826), 889–894. doi:10.1126/science.1141634

Fu, Y., Dominissini, D., Rechavi, G., and He, C. (2014). Gene Expression Regulation Mediated through Reversible m6A RNA Methylation. *Nat. Rev. Genet.* 15 (5), 293–306. doi:10.1038/nrg3724

Furey, T. S., Sethupathy, P., and Sheikh, S. Z. (2019). Redefining the IBDs Using Genome-Scale Molecular Phenotyping. *Nat. Rev. Gastroenterol. Hepatol.* 16 (5), 296–311. doi:10.1038/s41575-019-0118-x

Gu, Z., Gu, L., Eils, R., Schlesner, M., and Brors, B. (2014). Circlize Implements and Enhances Circular Visualization in R. *Bioinformatics (Oxford, England)* 30 (19), 2811–2812. doi:10.1093/bioinformatics/btu393

Han, D., Liu, J., Chen, C., Dong, L., Liu, Y., Chang, R., et al. (2019). Anti-tumour Immunity Controlled through mRNA m6A Methylation and YTHDF1 in Dendritic Cells. *Nature* 566 (7743), 270–274. doi:10.1038/s41586-019-0916-x

Han, X., Wang, L., and Han, Q. (2020). Advances in the Role of m6A RNA Modification in Cancer Metabolic Reprogramming. *Cel. Biosci.* 10, 117. doi:10.1186/s13578-020-00479-z

He, L., Li, H., Wu, A., Peng, Y., Shu, G., and Yin, G. (2019). Functions of N6-Methyladenosine and its Role in Cancer. *Mol. Cancer* 18 (1), 176. doi:10.1186/s12943-019-1109-9

Huang, H., Fang, M., Fang, M., Jostins, L., Umićević Mirkov, M., Boucher, G., et al. (2017). Fine-mapping Inflammatory Bowel Disease Loci to Single-Variant Resolution. *Nature* 547 (7662), 173–178. doi:10.1038/nature22969

Huang, H., Weng, H., Sun, W., Qin, X., Shi, H., Wu, H., et al. (2018). Recognition of RNA N6-Methyladenosine by IGF2BP Proteins Enhances mRNA Stability and Translation. *Nat. Cel. Biol.* 20 (3), 285–295. doi:10.1038/s41556-018-0045-z

Huang, Y., Su, R., Sheng, Y., Dong, L., Dong, Z., Xu, H., et al. (2019). Small-Molecule Targeting of Oncogenic FTO Demethylase in Acute Myeloid Leukemia. *Cancer Cel.* 35 (4), 677–691.e10. doi:10.1016/j.ccell.2019.03.006

Huang, H., Weng, H., and Chen, J. (2020). The Biogenesis and Precise Control of RNA m6A Methylation. *Trends Genet.* 36 (1), 44–52. doi:10.1016/j.tig.2019.10.011

Jostins, L., Ripke, S., Weersma, R. K., Duerr, R. H., McGovern, D. P., Hui, K. Y., et al. (2012). Host-microbe Interactions Have Shaped the Genetic Architecture of Inflammatory Bowel Disease. *Nature* 491 (7422), 119–124. doi:10.1038/nature11582

Kaplan, G. G. (2015). The Global burden of IBD: from 2015 to 2025. *Nat. Rev. Gastroenterol. Hepatol.* 12 (12), 720–727. doi:10.1038/nrgastro.2015.150

Lan, T., Li, H., Zhang, D., Xu, L., Liu, H., Hao, X., et al. (2019). KIAA1429 Contributes to Liver Cancer Progression through N6-methyladenosine-dependent post-transcriptional Modification of GATA3. *Mol. Cancer* 18 (1), 186. doi:10.1186/s12943-019-1106-z

Li, H.-B., Tong, J., Zhu, S., Batista, P. J., Duffy, E. E., Zhao, J., et al. (2017). m6A mRNA Methylation Controls T Cell Homeostasis by Targeting the IL-7/STAT5/SOCS Pathways. *Nature* 548 (7667), 338–342. doi:10.1038/nature23450

Li, X.-X., Xiao, L., Chung, H. K., Ma, X.-X., Liu, X., Song, J.-L., et al. (2020). Interaction between HuR and circPABPN1 Modulates Autophagy in the Intestinal Epithelium by Altering ATG16L1 Translation. *Mol. Cel. Biol.* 40 (6), e00492–19. doi:10.1128/MCB.00492-19

Liang, G., Conrad, M. A., Kelsen, J. R., Kessler, L. R., Breton, J., Albenberg, L. G., et al. (2020). Dynamics of the Stool Virome in Very Early-Onset Inflammatory Bowel Disease. *J. Crohns Colitis* 14 (11), 1600–1610. doi:10.1093/ecco-jcc/jjaa094

Lin, W., Ma, C., Su, F., Jiang, Y., Lai, R., Zhang, T., et al. (2017). Raf Kinase Inhibitor Protein Mediates Intestinal Epithelial Cell Apoptosis and Promotes IBDs in Humans and Mice. *Gut* 66 (4), 597–610. doi:10.1136/gutjnl-2015-310096

Linder, B., Grozhik, A. V., Olarerin-George, A. O., Meydan, C., Mason, C. E., and Jaffrey, S. R. (2015). Single-nucleotide-resolution Mapping of m6A and m6Am throughout the Transcriptome. *Nat. Methods* 12 (8), 767–772. doi:10.1038/nmeth.3453

Liu, J. Z., van Sommeren, S., Huang, H., Ng, S. C., Alberts, R., Takahashi, A., et al. (2015). Association Analyses Identify 38 Susceptibility Loci for Inflammatory Bowel Disease and Highlight Shared Genetic Risk across Populations. *Nat. Genet.* 47 (9), 979–986. doi:10.1038/ng.3359

Liu, Y., You, Z., Yang, J., Li, P., Liu, L., Xu, H., et al. (2019). N 6 -methyladenosine RNA Modification-Mediated Cellular Metabolism Rewiring Inhibits Viral Replication. *Science* 365 (6458), 1171–1176. doi:10.1126/science.aax4468

Liu, J. e., Li, K., Cai, J., Zhang, M., Zhang, X., Xiong, X., et al. (2020a). Landscape and Regulation of m^6A and m^6Am Methylome across Human and Mouse Tissues. *Mol. Cel.* 77 (2), 426–440. doi:10.1016/j.molcel.2019.09.032

Liu, L., Wang, Y., Wu, J., Liu, J., Qin, Z., and Fan, H. (2020b). N6-Methyladenosine: A Potential Breakthrough for Human Cancer. *Mol. Ther. - Nucleic Acids* 19, 804–813. doi:10.1016/j.omtn.2019.12.013

Lloyd-Price, J., Arze, C., Arze, C., Ananthakrishnan, A. N., Schirmer, M., Avila-Pacheco, J., et al. (2019). Multi-omics of the Gut Microbial Ecosystem in Inflammatory Bowel Diseases. *Nature* 569 (7758), 655–662. doi:10.1038/s41586-019-1237-9

Lu, T. X., Zheng, Z., Zhang, L., Sun, H.-L., Bissonnette, M., Huang, H., et al. (2020). A New Model of Spontaneous Colitis in Mice Induced by Deletion of an RNA m6A Methyltransferase Component METTL14 in T Cells. *Cell Mol. Gastroenterol. Hepatol.* 10 (4), 747–761. doi:10.1016/j.jcmgh.2020.07.001

Luo, W., Shen, Z., Deng, M., Li, X., Tan, B., Xiao, M., et al. (2019). Roseburia Intestinalis Supernatant Ameliorates Colitis Induced in Mice by Regulating the Immune Response. *Mol. Med. Rep.* 20 (2), 1007–1016. doi:10.3892/mmr.2019.10327

Luo, X., Li, H., Liang, J., Zhao, Q., Xie, Y., Ren, J., et al. (2021). RMVar: an Updated Database of Functional Variants Involved in RNA Modifications. *Nucleic Acids Res.* 49 (D1), D1405–D1412. doi:10.1093/nar/gkaa811

Meyer, K. D., and Jaffrey, S. R. (2017). Rethinking m6A Readers, Writers, and Erasers. *Annu. Rev. Cel Dev. Biol.* 33, 319–342. doi:10.1146/annurev-cellbio-100616-060758

Meyer, K. D., Saletore, Y., Zumbo, P., Elemento, O., Mason, C. E., and Jaffrey, S. R. (2012). Comprehensive Analysis of mRNA Methylation Reveals Enrichment in 3′ UTRs and Near Stop Codons. *Cell* 149 (7), 1635–1646. doi:10.1016/j.cell.2012.05.003

Mitsialis, V., Wall, S., Liu, P., Ordovas-Montanes, J., Parmet, T., Vukovic, M., et al. (2020). Single-Cell Analyses of Colon and Blood Reveal Distinct Immune Cell Signatures of Ulcerative Colitis and Crohn's Disease. *Gastroenterology* 159 (2), 591–608.e10. doi:10.1053/j.gastro.2020.04.074

Murthy, A., Li, Y., Peng, I., Reichelt, M., Katakam, A. K., Noubade, R., et al. (2014). A Crohn's Disease Variant in Atg16l1 Enhances its Degradation by Caspase 3. *Nature* 506 (7489), 456–462. doi:10.1038/nature13044

Nasser, J., Bergman, D. T., Fulco, C. P., Guckelberger, P., Doughty, B. R., Patwardhan, T. A., et al. (2021). Genome-wide Enhancer Maps Link Risk Variants to Disease Genes. *Nature* 593 (7858), 238–243. doi:10.1038/s41586-021-03446-x

Okada, Y., and Wang, Q. S. (2021). A Massive Effort Links Protein-Coding Gene Variants to Health. *Nature* 599, 561–563. doi:10.1038/d41586-021-02873-0

Park, S. C., and Jeen, Y. T. (2019). Genetic Studies of Inflammatory Bowel Disease-Focusing on Asian Patients. *Cells* 8 (5), 404. doi:10.3390/cells8050404

Pedersen, J., LaCasse, E. C., Seidelin, J. B., Coskun, M., and Nielsen, O. H. (2014). Inhibitors of Apoptosis (IAPs) Regulate Intestinal Immunity and Inflammatory Bowel Disease (IBD) Inflammation. *Trends Mol. Med.* 20 (11), 652–665. doi:10.1016/j.molmed.2014.09.006

Ren, W., Lu, J., Huang, M., Gao, L., Li, D., Wang, G. G., et al. (2019). Structure and Regulation of ZCCHC4 in m6A-Methylation of 28S rRNA. *Nat. Commun.* 10 (1), 5042. doi:10.1038/s41467-019-12923-x

Ritchie, M. E., Phipson, B., Wu, D., Hu, Y., Law, C. W., Shi, W., et al. (2015). Limma powers Differential Expression Analyses for RNA-Sequencing and Microarray Studies. *Nucleic Acids Res.* 43 (7), e47. doi:10.1093/nar/gkv007

Roda, G., Chien Ng, S., Kotze, P. G., Argollo, M., Panaccione, R., Spinelli, A., et al. (2020). Crohn's Disease. *Nat. Rev. Dis. Primers* 6 (1), 22. doi:10.1038/s41572-020-0156-2

Shannon, P., Markiel, A., Ozier, O., Baliga, N. S., Wang, J. T., Ramage, D., et al. (2003). Cytoscape: a Software Environment for Integrated Models of Biomolecular Interaction Networks. *Genome Res.* 13 (11), 2498–2504. doi:10.1101/gr.1239303

Shulman, Z., and Stern-Ginossar, N. (2020). The RNA Modification N6-Methyladenosine as a Novel Regulator of the Immune System. *Nat. Immunol.* 21 (5), 501–512. doi:10.1038/s41590-020-0650-4

Su, R., Dong, L., Li, Y., Gao, M., Han, L., Wunderlich, M., et al. (2020). Targeting FTO Suppresses Cancer Stem Cell Maintenance and Immune Evasion. *Cancer Cel.* 38 (1), 79–96.e11. doi:10.1016/j.ccell.2020.04.017

Swift, S., Tucker, A., Vinciotti, V., Martin, N., Orengo, C., Liu, X., et al. (2004). Consensus Clustering and Functional Interpretation Of__gene-Expression Data. *Genome Biol.* 5(11), R94. doi:10.1186/gb-2004-5-11-r94

Szklarczyk, D., Gable, A. L., Lyon, D., Junge, A., Wyder, S., Huerta-Cepas, J., et al. (2019). STRING V11: Protein-Protein Association Networks with Increased Coverage, Supporting Functional Discovery in Genome-wide Experimental Datasets. *Nucleic Acids Res.* 47 (D1), D607–D613. doi:10.1093/nar/gky1131

Tang, Y., Chen, K., Song, B., Ma, J., Wu, X., Xu, Q., et al. (2021). m6A-Atlas: a Comprehensive Knowledgebase for Unraveling the N6-Methyladenosine (m6A) Epitranscriptome. *Nucleic Acids Res.* 49 (D1), D134–D143. doi:10.1093/nar/gkaa692

Team, R. C. (2013). *R: A Language and Environment for Statistical Computing*. Vienna, Austria: R Foundation for Statistical Computing. Available at: http://www.R-project.org/.

Tong, J., Cao, G., Zhang, T., Sefik, E., Amezcua Vesely, M. C., Broughton, J. P., et al. (2018). m6A mRNA Methylation Sustains Treg Suppressive Functions. *Cel. Res.* 28 (2), 253–256. doi:10.1038/cr.2018.7

Ungaro, R., Mehandru, S., Allen, P. B., Peyrin-Biroulet, L., and Colombel, J.-F. (2017). Ulcerative Colitis. *Lancet* 389 (10080), 1756–1770. doi:10.1016/S0140-6736(16)32126-2

Vu, L. P., Pickering, B. F., Cheng, Y., Zaccara, S., Nguyen, D., Minuesa, G., et al. (2017). The N6-Methyladenosine (m6A)-Forming Enzyme METTL3 Controls Myeloid Differentiation of normal Hematopoietic and Leukemia Cells. *Nat. Med.* 23 (11), 1369–1376. doi:10.1038/nm.4416

Wang, Y.-W., Lin, K.-T., Chen, S.-C., Gu, D.-L., Chen, C.-F., Tu, P.-H., et al. (2013). Overexpressed-eIF3I Interacted and Activated Oncogenic Akt1 Is a Theranostic Target in Human Hepatocellular Carcinoma. *Hepatology* 58 (1), 239–250. doi:10.1002/hep.26352

Wang, H., Hu, X., Huang, M., Liu, J., Gu, Y., Ma, L., et al. (2019a). Mettl3-mediated mRNA m6A Methylation Promotes Dendritic Cell Activation. *Nat. Commun.* 10 (1), 1898. doi:10.1038/s41467-019-09903-6

Wang, J., Yan, S., Lu, H., Wang, S., and Xu, D. (2019b). METTL3 Attenuates LPS-Induced Inflammatory Response in Macrophages via NF-Kb Signaling Pathway. *Mediators Inflamm.* 2019, 1–8. doi:10.1155/2019/3120391

Wang, L., Wen, M., and Cao, X. (2019c). Nuclear hnRNPA2B1 Initiates and Amplifies the Innate Immune Response to DNA Viruses. *Science* 365 (6454), eaav0758. doi:10.1126/science.aav0758

Wang, Y.-N., Yu, C.-Y., and Jin, H.-Z. (2020). RNA N6-Methyladenosine Modifications and the Immune Response. *J. Immunol. Res.* 2020, 1–6. doi:10.1155/2020/6327614

Winkler, R., Gillis, E., Lasman, L., Safra, M., Geula, S., Soyris, C., et al. (2019). m6A Modification Controls the Innate Immune Response to Infection by Targeting Type I Interferons. *Nat. Immunol.* 20 (2), 173–182. doi:10.1038/s41590-018-0275-z

Xiao, L., Li, X.-X., Chung, H. K., Kalakonda, S., Cai, J.-Z., Cao, S., et al. (2019). RNA-Binding Protein HuR Regulates Paneth Cell Function by Altering Membrane Localization of TLR2 via Post-transcriptional Control of CNPY3. *Gastroenterology* 157 (3), 731–743. doi:10.1053/j.gastro.2019.05.010

Xu, X., Huang, J., Ocansey, D. K. W., Xia, Y., Zhao, Z., Xu, Z., et al. (2021). The Emerging Clinical Application of m6A RNA Modification in Inflammatory Bowel Disease and its Associated Colorectal Cancer. *J.Inflamm. Res.* 14, 3289–3306. doi:10.2147/jir.S320449

Yu, R., Li, Q., Feng, Z., Cai, L., and Xu, Q. (2019). m6A Reader YTHDF2 Regulates LPS-Induced Inflammatory Response. *Ijms* 20 (6), 1323. doi:10.3390/ijms20061323

Zaccara, S., Ries, R. J., and Jaffrey, S. R. (2019). Reading, Writing and Erasing mRNA Methylation. *Nat. Rev. Mol. Cel. Biol.* 20 (10), 608–624. doi:10.1038/s41580-019-0168-5

Zhang, Y., Wang, X., Zhang, X., Wang, J., Ma, Y., Zhang, L., et al. (2019). RNA-binding Protein YTHDF3 Suppresses Interferon-dependent Antiviral Responses by Promoting FOXO3 Translation. *Proc. Natl. Acad. Sci. USA* 116 (3), 976–981. doi:10.1073/pnas.1812536116

Zhang, M. M., Yang, H., and Qian, J. M. (2021). Potential Mechanism of N6-Methyladenosine on Immune Modulation in Inflammatory Bowel Disease. *Zhonghua Nei Ke Za Zhi* 60 (4), 384–387. doi:10.3760/cma.j.cn112138-20200518-00489

Zhao, J., Han, D.-X., Wang, C.-B., and Wang, X.-L. (2020). Zbtb7b Suppresses Aseptic Inflammation by Regulating m6A Modification of IL6 mRNA. *Biochem. biophysical Res. Commun.* 530 (1), 336–341. doi:10.1016/j.bbrc.2020.07.011

Zheng, Q., Hou, J., Zhou, Y., Li, Z., and Cao, X. (2017). The RNA Helicase DDX46 Inhibits Innate Immunity by Entrapping m6A-Demethylated Antiviral Transcripts in the Nucleus. *Nat. Immunol.* 18 (10), 1094–1103. doi:10.1038/ni.3830

Zhong, L., Liao, D., Zhang, M., Zeng, C., Li, X., Zhang, R., et al. (2019). YTHDF2 Suppresses Cell Proliferation and Growth via Destabilizing the EGFR mRNA in Hepatocellular Carcinoma. *Cancer Lett.* 442, 252–261. doi:10.1016/j.canlet.2018.11.006

Zhou, J., Zhang, X., Hu, J., Qu, R., Yu, Z., Xu, H., et al. (2021). m 6 A Demethylase ALKBH5 Controls CD4 + T Cell Pathogenicity and Promotes Autoimmunity. *Sci. Adv.* 7 (25), eabg0470. doi:10.1126/sciadv.abg0470

Conflict of Interest: The authors declare that the research was conducted in the absence of any commercial or financial relationships that could be construed as a potential conflict of interest.

Publisher's Note: All claims expressed in this article are solely those of the authors and do not necessarily represent those of their affiliated organizations, or those of the publisher, the editors and the reviewers. Any product that may be evaluated in this article, or claim that may be made by its manufacturer, is not guaranteed or endorsed by the publisher.

Copyright © 2022 Nie, Yi, Yang, Deng, Yang, Wang, Chen, Zhang and Wang. This is an open-access article distributed under the terms of the Creative Commons Attribution License (CC BY). The use, distribution or reproduction in other forums is permitted, provided the original author(s) and the copyright owner(s) are credited and that the original publication in this journal is cited, in accordance with accepted academic practice. No use, distribution or reproduction is permitted which does not comply with these terms.

frontiers in Genetics

REVIEW
published: 28 January 2022
doi: 10.3389/fgene.2022.834413

The Basis and Promise of Programmable RNA Editing and Modification

Nicholas Lo[1†], *Xin Xu*[1†], *Fraser Soares*[1*] *and Housheng Hansen He*[1,2*]

[1]*Princess Margaret Cancer Center, University Health Network, Toronto, ON, Canada,* [2]*Department of Medical Biophysics, University of Toronto, Toronto, ON, Canada*

One key advantage of RNA over genomic editing is its temporary effects. Aside from current use of DNA-targeting CRISPR-Cas9, the more recently discovered CRISPR-Cas13 has been explored as a means of editing due to its RNA-targeting capabilities. Specifically, there has been a recent interest in identifying and functionally characterizing biochemical RNA modifications, which has spurred a new field of research known as "epitranscriptomics". As one of the most frequently occurring transcriptome modifications, N6-methyladenosine (m6A) has generated much interest. The presence of m6A modifications is under the tight control of a series of regulators, and the ability of fusing these proteins or demethylases to catalytically inactive CRISPR proteins have resulted in a new wave of programmable RNA methylation tools. In addition, studies have been conducted to develop different CRISPR/Cas and base editor systems capable of more efficient editing, and some have explored the effects of *in vivo* editing for certain diseases. As well, the application of CRISPR and base editors for screening shows promise in revealing the phenotypic outcomes from m6A modification, many of which are linked to physiological, and pathological effects. Thus, the therapeutic potential of CRISPR/Cas and base editors for not only m6A related, but other RNA and DNA related disease has also garnered insight. In this review, we summarize/discuss the recent findings on RNA editing with CRISPR, base editors and non-CRISPR related tools and offer a perspective regarding future applications for basic and clinical research.

Keywords: RNA editing, base editing, M6A, epitranscriptome, CRISPR

OPEN ACCESS

Edited by:
Chengqi Yi,
Peking University, China

Reviewed by:
Rui Zhang,
Sun Yat-sen University, China
Guan-Zheng Luo,
Sun Yat-sen University, China

***Correspondence:**
Fraser Soares
fraser.soares@utoronto.ca
Housheng Hansen He
Hansenhe@uhnresearch.ca

†These authors have contributed equally to this work

Specialty section:
This article was submitted to Epigenomics and Epigenetics, a section of the journal Frontiers in Genetics

Received: *13 December 2021*
Accepted: *07 January 2022*
Published: *28 January 2022*

Citation:
Lo N, Xu X, Soares F and He HH (2022) The Basis and Promise of Programmable RNA Editing and Modification. Front. Genet. 13:834413. doi: 10.3389/fgene.2022.834413

INTRODUCTION

Genome editing and modification technologies such as transcription activator-like effector nucleases (TALENs) and zinc-finger nucleases (ZFNs) originated from earlier nuclease technologies and other chemical techniques. However, these earlier methods were limited in terms of editing specificity and riddle with off-target side effects (Pattanayak et al., 2011). When the introduction of the bacteria-derived RNA-guided clustered regularly interspaced short palindromic sequences (CRISPR-Cas9) system was discovered, this new technique changed the versatility of genome editing (Gasiunas et al., 2020). An explosion of other CRISPR/Cas systems since then have been characterized and provided a molecular toolbox for basic and translational research. More recently, the application of systems such as CRISPR-Cas13—used by bacteria to degrade viral RNA, has opened a new area of exploration for editing techniques and is currently being adapted for uses in mammalian species (Cox et al., 2018).

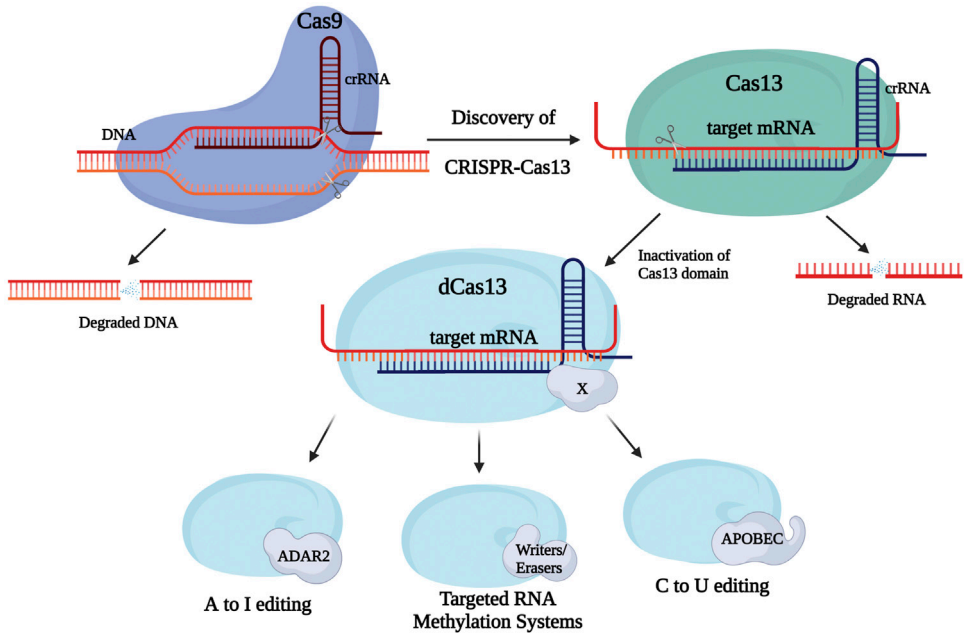


FIGURE 1 | Discovery and development of Clustered Regularly Interspaced Short Palindromic Repeats (CRISPR)/Cas systems for epitranscriptome editing. CRISPR-Cas9 is established as a tool capable of DNA targeting and modification, however, the rising implementation of RNA editing strategies led to the discovery of a natural RNA-targeting CRISPR system, Cas13. In turn, further modification of members of the Cas13 family in addition to fusions with different enzyme domains (e.g., writers, erasers) allows for performance of a variety of functions/modifications upon binding to its targets.

Base editing is a method currently used to introduce single nucleotide variants into DNA or RNA (Porto et al., 2020). Different components of CRISPR systems and other proteins (e.g., deaminases) come together to make point mutations without introducing double-strand breaks. The direct base changes limit the number of byproducts, making them a potential therapeutic option for future applications (Sun and Yu, 2019). The utility of these and other CRISPR/Cas systems to investigate the epitranscriptome has become an emerging area that aims to identify and functionally characterize biochemical modifications on RNA. Specifically, N6-methyladenosine (m6A) modifications appear abundantly on mRNA and non-coding RNA that are often involved in regulatory processes such as splicing, translation, and RNA stability (Chen et al., 2019). The effects and presence of m6A are mediated by three main classes of proteins: readers, erasers, and writers, which can be bound as an additional domain to existing Cas-related systems allowing for the development of programmable RNA methylation tools. Here, the characteristics of current base editing systems and a few CRISPR/Cas systems are analyzed in order to describe their utility for understanding RNA modifications such as m6A.

CRISPR/Cas Systems

When CRISPR systems emerged, the advantages over TALENs and ZFNs were observable. CRISPR-Cas9 is capable of editing with higher efficiency and precision on DNA at multiple loci simultaneously. It is able to target a given genome sequence through modifying the guide RNA sequence, whereas TALENs and ZFNs require the re-coding of proteins for each new target site (Gupta and Musunuru, 2014). Importantly, its smaller size allowed for easier cell delivery, as the bulky size of TALENs' cDNA showed to be a hindrance, limiting its therapeutic applications. One of the more notable advantages was the accessible design, allowing greater use at a lower price, and thus making it more practical for larger-scale applications such as screening.

However, CRISPR-Cas9 was still prone to relatively major off-target effects, even with the help of protospacers to increase specificity (Gupta and Musunuru, 2014). This became an increasing concern when considered for use in RNA-targeted manipulation. The retention of DNA-targeting activity itself would likely increase the chance of further unwanted off-target effects (Perculija et al., 2021). A possible solution to this dilemma would appear through the more recent investigations of RNA-targeting CRISPR-Cas13 systems (**Figure 1**).

Type VI (Cas13) systems are used in prokaryotes to target and ultimately cleave RNA. Systems such as Cas13a and Cas13b, which have different cleavage preferences, and guide CRISPR RNA (crRNA) structures (Perčulija et al., 2021), have been incorporated in several editing constructs (**Table 1**). For example, the RNA Editing for Programmable A to I Replacement, version 2 (REPAIRv2) tool—composed of inactive Cas13b (dCas13) and a mutant ADAR2 deaminase domain, edits adenosine to inosine, and making it potentially useful for treating diseases derived from G to A mutations (Cox et al., 2018). dCas13 with an APOBEC domain allows for cytidine to uridine edits, while a further modified version of REPAIRv2 called RESCUE edits C–U, while keeping the original ADAR2

TABLE 1 | Comparison of various RNA-targeting systems for base editing.

Name	Components	Function	Advantages	Relative efficiency	Off-target	References
REPAIRv2	dCas13b + mutant $ADAR2_{DD}$	A to I	AAV packaging for delivery	~30%	High	Perčulija et al. (2021)
RESCUE	dCas13b + $ADAR2_{DD}$	C to U	Original $ADAR2_{DD}$ activity maintained; can target any adenosine in genome	~70%	High	Cox et al. (2018); Abudayyeh et al. (2019)
Cas13bt	Cas13bt1 and Cas13bt3 + $ADAR2_{DD}$	A • I;C • U	Smaller size allows for AAV delivery	~40–50%	Medium	Kannan et al. (2021)
CasRx	dCas13X.1 + $ADAR2_{DD}$	A • I;C • U	Allow easier *in vivo* delivery	High	Low	Konermann et al. (2018)
CIRTS	Effector protein + RNA hairpin binding protein + ssRNA binding protein	Flexible	Small size; minimal immune response	High	Low	Rauch et al. (2019)
REWIRE	RNA-recognizing PUF domain + variable deaminase domain	A to I C to U	Target extranuclear genes *In vivo* AAV delivery Operate independently of endogenous repair pathways	~60–80%	Low	Han et al
λN–BoxB	ASO gRNA + λN proteins + $ADAR2_{DD}$	A to I	Improved *in vitro* editing with A•C mismatch	Medium	High	Montiel-Gonzalez et al. (2013)
RESTORE	Endogenous ADAR1 + ASO gRNA	A to I	Requires only oligonucleotide administration (for ADAR recruitment)	~75–85%	Low	Merkle et al. (2019)

deaminase activity intact (Cox et al., 2018; Abudayyeh et al., 2019). Interestingly, the REPAIR systems are able to encode an exact target site into its guide due to dCas13 having no targeting sequence restrictions, giving it the capacity to target any adenosine in the transcriptome. Even though efficiency is relatively high in these systems (up to 30% for REPAIRv2 and ~70% percent for RESCUE), off-target events are still substantially present (Abudayyeh et al., 2019). Nevertheless, rational mutagenesis has been able to increase the specificity dCas13b-$ADAR_{DD}$ complexes by more than 900-fold. A further subclass of Cas13b proteins known as Cas13bt has recently been constructed into variant REPAIR and RESCUE editors for transcript knockdown. Cas13bt′s smaller size permits packaging of the editor into an adeno-associated virus for delivery (Kannan et al., 2021).

Various Cas effector complexes have been shown to be proficient at targeting several other types of RNA modifications. CRISPR-Cas13d variants such as CasRx have been engineered for knocking down endogenous RNA as well as controlling RNA alternative splicing. Specifically, the inactivation of the HEPN-mediated RNase activity on dCasRx allows for flexible RNA-binding and specific targeting of RNA elements (Konermann et al., 2018). In addition, two compact families of Cas13 ribonucleases—Cas13X and Cas13Y—were identified from microbes. From these systems, Cas13X.1 was designed to perform RNA interference in mammalian cells with high levels of efficiency (Xu C et al., 2021). Furthermore, dCas13X.1 was combined with $ADAR2_{DD}$ in order to generate various RNA base editors, namely A to I (xABEs) and C–U (xCBEs) base editors, which were capable of editing at various mammalian loci. Subsequently, truncations of dCas13X.1 generating mxABEs and mxCBEs overcame the size limitations other Cas13 systems faced for *in vivo* delivery. The xABE and mxABE editors were found to perform A–I conversions more efficiently than the REPAIR systems when paired with a crRNA guide, and the mxCBE systems were found to outperform the RESCUE systems for C–U editing, demonstrating high transcriptome fidelity and reducing off-target edits (Xu C et al., 2021)

Emergence of Programmable CRISPR/Cas RNA Methylation Tools

mRNA is subject to several post-transcriptional modifications (e.g., capping, adenylation) before undergoing translation. To date, m6A modifications are observed to be the most abundant type of endogenous mRNA modification in eukaryotes (Wilson et al., 2020). Many m6A modifications often play a vital part in physiological processes and are involved in the progression of malignancies such as human cancers (Jiang et al., 2021). They undergo dynamic regulation and can be removed (erased) and installed (written) by RNA methylation complexes in order to observe the effects on specific pathways and systems (**Figure 2A**). Targeted RNA methylation (TRM) systems—composed of catalytically inactive Cas13 (dCas13) fused with a methyltransferase domain—are capable of highly specific m6A installation on transcripts, and through such changes, mediate processes such as alternative splicing, transcript abundance, and translational efficiency (**Figure 2B**). Recent studies have explored two main TRM m6a writing systems, dCas13-M3 (methyltransferase-like 3) and dCas13-M3M14 (methyltransferase-like 3 and methyltransferase-like 14). Each was designed to be localized to the nucleus via a nuclear localization signal (NLS) or exported for cytoplasmic function via a nuclear export signal (NES). While both dCas13-M3nls and dCas13-M3M14nes were shown to have high, comparable on-target m6A installation efficiency, dCas13-M3nls was observed to be less prone to off-target edits than dCas13-M3M14nes and another explored editor, M3M14-dCas9. This particular difference was attributed to a truncated methyltransferase domain within dCas13-m3nls resulting in a lack of a METTL14 RNA-binding domain (Wilson et al., 2020). Interestingly, the nuclear localization of dCas13-M3nls has also been shown to cause no loss of translation efficiency after

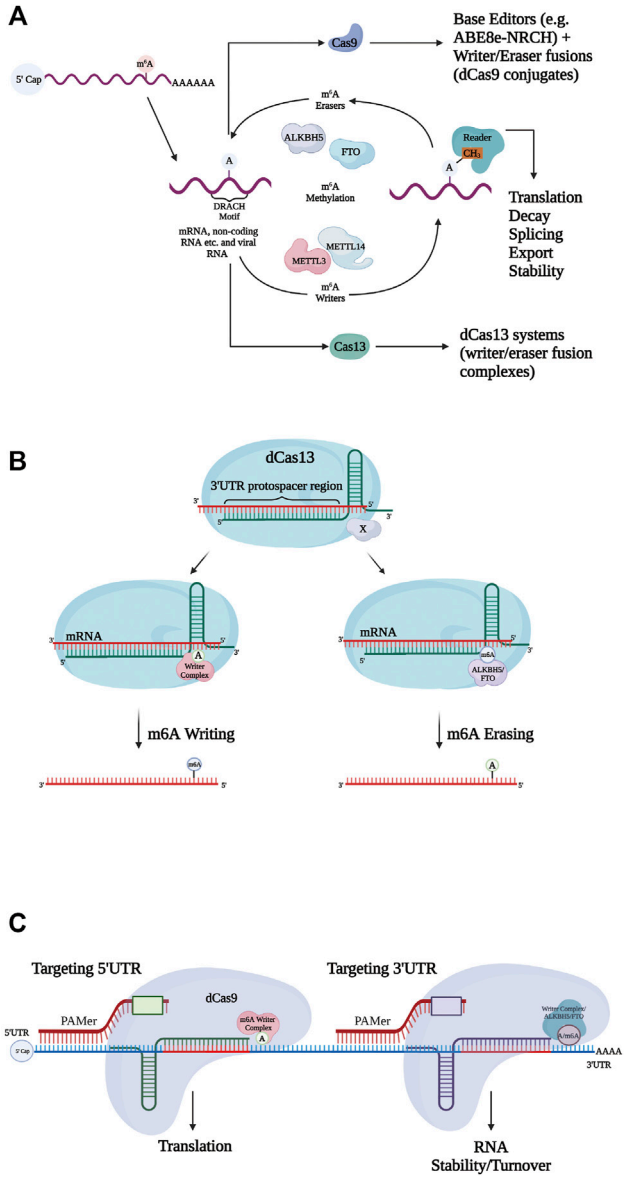


FIGURE 2 | Mechanisms for N6-methyladenosine (m6A) regulation. **(A)** Writers and erasers tightly regulate the presence of m6A on transcripts, by targeting the m6A motif (DRACH). m6A is recognized by readers, initiating steps regulating mRNA stability, translation etc. Modification systems can be expanded to include both Cas9 (base editors, writer/eraser fusions) and Cas13 ((de)methylation systems). **(B)** Catalytically inactive Cas13 (dCas13) fused to writer and eraser domains install and remove m6A modifications respectively. Single guide RNAs (sgRNAs) target specific sites (e.g., 3′UTR protospacer) for mRNA binding. **(c)** Catalytically inactive Cas9 (dCas9) conjugates fused to writer and eraser domains. Specific sgRNAs allow individual 5′UTR and 3′UTR targeting. Resulting effects of installing/ erasing at the different UTRs vary. PAMer provides the NGG PAM sequence.

targeting 5′UTRs, and transcripts can be further regulated by other writers after modification (Wilson et al., 2020). Therefore, dCas13-M3nls was deemed overall the most practical TRM system within the nucleus for inducing m6A-mediated phenotypes.

dCas13 effectors are not the only CRISPR systems capable of m6A modification. CRISPR-Cas9 conjugates were coupled with single-chain methyltransferase and ALKBH5/FTO in order to form writers and erasers, respectively. The target site specificity of these Cas9 editors was programmable through guide RNA (**Figure 2C**). Specifically, installation at the 5′UTR allowed for non-canonical translation, while erasure and installation at the 3′UTR influenced RNA turnover (Liu et al., 2019). It is still relatively unclear as to how the individual localization of the writer and eraser proteins (nucleus or cytosol) may affect TRM editing in different systems.

The reversibility of m6A modifications can be dynamically regulated by m6A demethylases such as ALKBH5 and FTO. It, too, is capable of targeting mRNA (for demethylation) when combined with dCas13 and targeted with an sgRNA in order to form a dm6ACRISPR system (Li et al., 2020). This construct has been used for *in vivo* manipulation of oncogenic targets on EGFR and MYC transcripts for controlling cell proliferation, while limiting the number of off-target edits. Demethylation efficiency was increased by calibrating the distance between the target sites and methylated sites to 100–300 nucleotides (Li et al., 2020). However, the effects of dm6ACRISPR demethylation vary due to the activity of different reader proteins, as it was observed that methylation of CYB5A and CTNNB1 transcripts resulted in increased mRNA stability, and thus increased expression. While this was one of the first systems set out to establish the role of m6A demethylation with respect to overall cell function (Li et al., 2020), more recent studies have explored a similar system with NLS CasRx, which is the smallest and most efficient of the Cas13 family for RNA knockdown. Thus, it was speculated that binding erasers (ALKBH5) and writers (e.g., METTL3) to dCasRx would allow for specific site manipulation on par with dCas13b (Li et al., 2020; Xia et al., 2021). In addition, its smaller size would allow for easier delivery into cells as a lentivirus, allowing for pooled screening approaches and widespread use in difficulty to transfect cell lines and primary cells (Li et al., 2020; Xia et al., 2021). We anticipate these programmable m6A tools will provide a functional platform to interrogate site-specific m6A RNA modifications that contribute to a wide range of physiological processes and complement existing m6A profiling studies.

Transcriptome and Epitranscriptome CRISPR Screening Approaches

The development of high-throughput technologies and genome-editing has revolutionized the field of functional genomics, which attempts to assess the function and interaction of genes in a systematic approach. Screening tools such as short interfering RNAs (siRNAs) were effective and consistent at silencing gene expression for genetic screens, however, both the cost, the short life of the siRNAs, and the lack of efficient delivery into primary cell cultures put limits on its application (Bernards et al., 2006). On the other hand, short-hairpin RNAs (shRNAs) were able to maintain constant levels of silencing after vector delivery, and

their compatibility with different types of vectors allowed for delivery into a greater variety of cells (Bernards et al., 2006). More recently, CRISPR-Cas13 has been explored as an alternative screening tool of shRNAs. Since Cas13 based TRM systems have only recently been characterized, screening has not been extensively applied towards evaluating m6A modifications. We anticipate TRM screening platforms to emerge in the near future, which will incorporate principles of Cas13-based screens that have investigated linear genes, and more recently non-coding RNAs such as circular RNAs (circRNAs).

Through the use of CRISPR-Cas13d in combination with improved designs of sgRNAs for circRNA back-splicing junction (BSJ) sites, circRNA silencing specificity is increased, indicating its effectiveness for high-throughput screening of functional circRNAs (Zhang et al., 2021). In a side-by-side comparison of Cas13d and shRNA functional screens, the read distribution for both gRNAs and shRNAs were found to both be highly correlated. However, non-targeting controls of shRNAs yielded more false-positive results compared to the gRNAs of Cas13d, indicating Cas13 to be a more refined method for circRNA targeting (Zhang et al., 2021). This difference was attributed to the off-target effects of shRNAs, while at the same time establishing on-target specificity of Cas13d. Like TRM systems, Cas13d (CasRx) is capable of being optimized for compartmental distribution. CasRx-NLS was observed to be optimal for circRNA targeting in the nucleus, while lack of the NLS signal optimized CasRx targeting of cytosolic circRNAs, allowing a further advantage over shRNAs (Zhang et al., 2021). This ability to compartmentalize allows CasRx systems to outperform RNAi. While efficiency between CasRx and RNAi is comparable, RNAi is not capable of compartmentalizing (Wessels et al., 2020), and is subject to more off-target effects (Zhang et al., 2021). CasRx is currently one of three main effector proteins—along with *Pgu*Cas13b and *Psp*Cas13b—that have been identified, however, CasRx was shown to be consistently more effective at target RNA knockdown, even more so when fused with an NLS (Wessels et al., 2020). CasRx-BSJ-gRNA systems are applicable for genome-wide screening, in particular for observing the loss-of-function effects of circRNAs originating from the gene's internal exons (Zhang et al., 2021). We envision similar approaches will utilize CRISPR/Cas programmable RNA modification tools (as discussed earlier and below) to study the epitranscriptome through pooled screening, which will serve as powerful tools to assess all types of RNA modifications.

Base Editors

Base editors usually indirectly modify RNA transcripts by modifying the DNA, thus, off-target edits are issues for which there are no possible solutions. It was hypothesized that embedding editing enzymes such as APOBEC1 and Tad-TadA into the middle of nCas9 instead of linking it to its N-terminus would reduce the off-target effects (Liu et al., 2020). Cas-embedding would introduce steric effects that could possibly block off-target editing. In combination with other techniques such as the usage of short-rigid linkers, the editing window can be narrowed for increased specificity (Liu et al., 2020). RNA base editors have been able to benefit from this technique as well. Off-target effects were found to be slightly reduced when the $ADAR2_{DD}$ was embedded into dCasRx's flexible loop instead of being linked at its terminal (Liu et al., 2020). Altering the structural components of the base editors has been shown to increase efficiency as well. Manipulating Cas9's secondary structure improved the interactions between the Cas9 endonuclease and the other base editor components in order to lower the level of off-target RNA editing. The same ABE variant was shown to behave differently with RNA and DNA through individual secondary structure changes (Nguyen Tran et al., 2020).

Some enhancements to base editor systems that seem to broaden their function could perhaps introduce a novel approach to future base editing techniques. Usually, CRISPR base editors are capable of modulating only one type of base modification (e.g., ABEs, CBEs). Grünewald and colleagues (Grünewald et al., 2020) were able to design a dual function base editor derived from miniABEmax-V82G and Target-AID deaminases called synchronous programmable adenine and cytosine editors (SPACE), capable of synchronous A-to-G and C-to-T edits (Grünewald et al., 2020). The editing window of SPACE is narrower compared to miniABEmax-V82G and Target-AID, however, it does not seem to provide an additional editing efficiency advantage. SPACE does have comparable (if not lower) efficiency capabilities to the individual base editors themselves, while minimizing off-target effects (Grünewald et al., 2020). This seems to be consistent with another set of designed dual-function editors. Target-ACE, Target-ACEmax and ABCEmax are composed of cytidine, and adenosine deaminases bound to nCas9 (Sakata et al., 2020). Like SPACE, Target-ACEmax was found to possess on and off-targeting capabilities like those of the single-function base editors. However, Target-ACEmax and ABCEmax were found to be useful as genome editing tools for applications such as therapeutics, which are capable of higher delivery efficiency. In particular, Target-ACEmax was able to mediate heterologous base editing more efficiently than current systems such as CRISPR-X (Sakata et al., 2020).

While *in vitro* studies were undertaken for optimizing base editor efficiency, there have been steps taken for using base editing *in vivo*, specifically in non-human primates and mice (Rothgangl et al., 2021). Through lipid nanoparticle-mediated (LNP) delivery, an ABE-encoding nucleoside-modified mRNA combined with modified gRNA was capable of editing PCSK9 in macaque livers (30 percent efficiency) with few off-target edits, resulting in lower LDL cholesterol. It was hypothesized that the efficiency rates mediated by LNP delivery would allow for treatment of other genetic liver diseases (Rothgangl et al., 2021). As an extended ABE presence was thought to eventually result in an increased number of off-target edits as well as induce an immune response, the treatments were delivered in doses. With each repeated dosage, the editing rates were found to increase in mice, but not the macaques (Rothgangl et al., 2021). Therefore, future adjustment of the dosage could possibly lead to increased editing rates in macaques, allowing this approach to eventually be applied in humans (Rothgangl et al., 2021).

Non-CRISPR based tools have shown promise for base editing in human cells with lower off-target effects. REWIRE (RNA editing with individual RNA-binding enzyme) is a gRNA independent system derived from human proteins (Han et al). It is a one-enzyme technique, which eliminates any complications that may arise from assembly. It can edit without involving endogenous repair pathways, which extends the possibility of personalized therapy to post-mitotic cells such as neurons. REWIRE is not only limited to nuclear compartments, as it was also found to be capable of targeting mitochondrial genes. Despite its capabilities, it is still subject to significant off-target effects due to the enzyme's PUF domain's naturally small target. However, this can be mitigated by increasing the number of PUF repeats or by modification to its other domains (e.g., deaminase). In theory, PUF can therefore also be applied for other purposes including RNA methylation with high specificity and increased targeting capabilities if associated with domains such as the methyltransferase domain of METTL3.

The principles of CRISPR-Cas systems have also been applied to the design of CIRTS (CRISPR/Cas inspired RNA targeting system). These endogenous transcriptome editing tools separate the main required functions (e.g., selective hairpin binding, gRNA complementary to the target and effector protein) that Cas13 holds in one protein domain into a complex of several different proteins, each one responsible for a single function (Rauch et al., 2019). There are advantages to separating the functions amongst several domains. First, the overall complex itself is smaller than the current CRISPR/Cas modification systems, allowing for easier direct protein delivery. As well, the individual proteins themselves do not have to be CRISPR/Cas derived, as human proteins can be substituted to engineer a CRISPR-Cas13 system. Importantly, from a therapeutic stance, it may be possible to edit RNA without inducing an immune response (Rauch et al., 2019).

Another practical method is the use of antisense oligonucleotide (ASO), which can modulate RNA expression, and have been under development as therapeutic tools for years. In systems such as recruiting endogenous ADAR to specific transcripts for oligonucleotide-mediated RNA editing (RESTORE), only delivery of the oligonucleotide is required. The RESTORE system has been found to achieve higher efficiency than its Cas13 counterparts with limited off-targeting (Merkle et al., 2019). On the other hand, systems such as the λN–BoxB RNA interaction requires binding between a λN protein and a BoxB hairpin loop containing the ASO (Montiel-Gonzalez et al., 2013). Base editing activity comes from the endogenous ADAR2 domain that binds to the λN protein. Potentially, ASO may be able to modulate RNA in the context of m6A methylation by blocking known sites where m6A readers and writers bind to.

Dissecting m6A Modifications With Base Editors

Due to the results and successes of base editor approaches, more recent studies have begun to utilize base editing technology to study m6A modifications. In order to observe the effects of m6A modifications on miRNA and long non-coding RNA, an adenine base editor system (ABE7.10) was used to induce single site base change. After the targeted mutation of an m6A site (T-A conversion) upstream of miR-675 in the H19 locus in HEK293T cells, miR-675, and H19 expression were observed to be suppressed, resulting in an increase in apoptosis (Hao et al., 2020). It was hypothesized that the reduced expression resulted in an increased presence of p53 protein, thus inducing cell death which indicates the role of m6A in regulating miR675 and H19 expression (Hao et al., 2020), and by extension, cell survival. As stated previously, m6A is highly involved in cancer development. This was further supported by (Lee et al., 2021), who showed the upregulation of METTL3 activity and m6A frequency commonly found in cancers. In particular, the methylation of homeobox containing 1 target mRNA has been linked to loss of p53 signaling and issues with telomere regulation (Lee et al., 2021).

Aside from direct RNA modifications and genome editing, base editors have been leveraged for genome-wide screening as well. Unlike canonical Cas9 knockout screens, iBARed cytosine base editing-mediated gene knockout (BARBEKO) systems do not utilize double-strand breaks for gene knockouts (Xu P et al., 2021). Instead, knockout methods are directed to the start codons and splice sites of target RNA, as well as stop codon introduction. Associated sgRNAs are designed to carry internal barcodes (iBARs), which assist with screening efficiency (Xu P et al., 2021). Another advantage found over Cas9-mediated cleaving is attributed to the absence of double-strand break activity. Inducing double-strand breaks in amplified regions often leads to false positives, however, BARBEKO is not subject to such copy-number effects. Along with being more cost and labour efficient, BARBEKO was found to be ideal for high-quality screening primary cells as well as *in vivo*, despite the usual risk of DNA damage and small sample sizes (Xu P et al., 2021). Currently, a method is being explored to mediate potential effects of BARBEKO screens with high multiplicity of infection, as the lentiviral transduction of several sgRNAs may cause cytotoxicity. It is quite likely that a similar system to BARBEKO could be used to study m6A through disrupting the canonical m6A RNA motif.

THERAPEUTIC OUTLOOK FOR CRISPR/CAS SYSTEMS AND M6A

Therapeutics

m6A has been shown to be associated with many physiological and pathological processes. However, it is only one of many different types of modifications which can be targeted. As such, the possible use of CRISPR and base editors as tools for therapeutic processes has been explored and is currently under promising development.

One of the fields of research is sickle cell disease. A customized base editor—ABE8e-NRCH - was developed in order to convert the sickle cell disease allele into a non-pathogenic form (Makassar beta-globin) (**Figure 3A**). Transplantation of human hematopoietic stem cells indicated long-lasting gene editing of up to 80% in mice, although it was shown that only about 20% was required for phenotypic rescue after autologous treatment

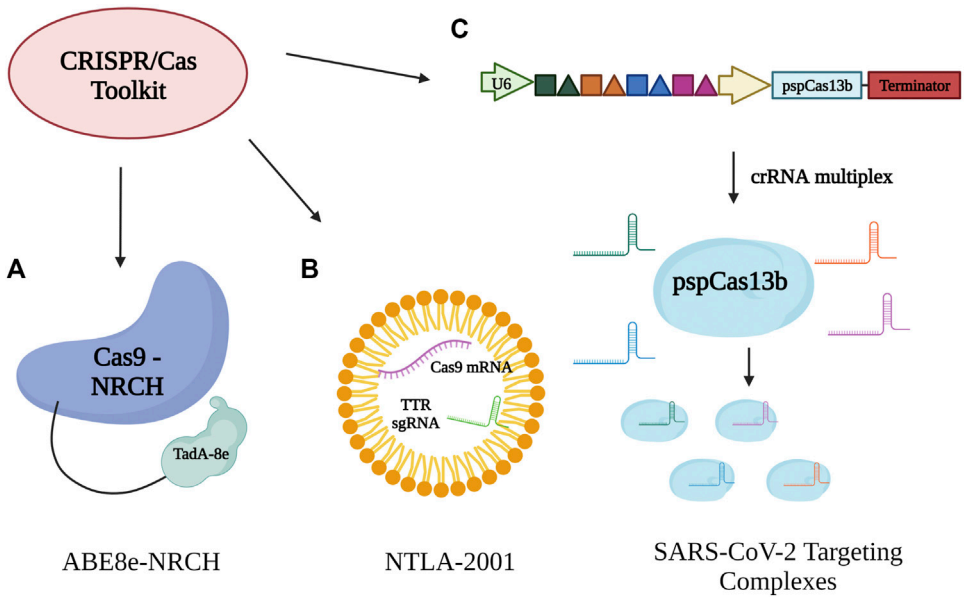


FIGURE 3 | Therapeutic applications for CRISPR/Cas systems. **(A)** A specialized adenine base editor composed of Cas9-NRCH bound to a TadA-8e domain. ABE8e-NRCH converts the pathogenic variant of the sickle cell disease allele into a non-pathogenic variant. **(B)** Lipid nanoparticle delivery of Cas9 mRNA and transthyretin-targeting (TTR) gRNA for treatment of ATTR amyloidosis with the goal of reducing both mutant and wildtype levels of transthyretin protein. **(C)** SARS-CoV-2 targeting complexes. A set of four targeting crRNAs is utilized in combination with pspCas13b in order to reduce the virus's chance for escape through mutation and daughter strain proliferation. Main targeted sites are conserved regions and sequences of coronaviruses.

(Newby et al., 2021). Using the base editor was ultimately more efficient than other techniques such as induction or lentiviral expression, which would have left the sickle cell allele untouched. It also avoids the possible faults of direct Cas9 application, such as larger genome deletions as well as possibly cell death through inappropriate p53 activation (Newby et al., 2021). An additional advantage of using base editing is the lack of requirement for DNA delivery, a usual component of other gene therapies which could lead to insertion mutations and other toxic effects. As the treatment is only required once, it also lowers the effects of double-strand breaks (Newby et al., 2021). The main concern regarding base editors is the possibility of off-target edits. However, these were kept to a minimum through a "CACC" PAM, and the changes to off-target sites were observed to be of little to no consequence. Possible methods for improving the safety and effectiveness of this base editor therapy involve pairing different Cas9 variants and deaminase domains in order to minimize off-target edits, as well as dose, and delivery optimization (Newby et al., 2021).

Though base editors seem to be ideal tools for therapy, CRISPR-Cas9 itself for *in vivo* gene editing is by no means an inferior method. LNP delivery of Cas9 endonuclease mRNA and transthyretin-targeting gRNA (NTLA-2001) (**Figure 3B**) was proposed as a treatment for ATTR amyloidosis. Current treatments require constant and long-term administration for RNA knockdown; however, the disease still progresses (Gillmore et al., 2021). The liposome–polycation–pDNA (LPD) method works through a dose-dependent effect, which is currently in the process of being escalated in order to reduce overall transthyretin (TTR) levels for both wild-type and mutant forms, with the hope of producing permanent knockdown after a single administration of treatment. As the liver cells are the main source of TTR, primary human hepatocytes were used for testing in order to increase efficiency and lower toxic effects (Gillmore et al., 2021). Cas9 off-target edits were not observed with NTLA-2001 and any induced genome variation through editing was deemed of little risk, thus setting precedent for predictable outcomes *in vivo* (Gillmore et al., 2021). Additional preclinical platforms are also being explored, such as prime editors which fuse a reverse transcriptase domain to dCas9, and thus facilite genome knock-in to rescue protein expression in mammalian cell lines (Anzalone et al., 2020).

METTL3-Mediation for Viral Detection

The detection of pathogens such as RNA viruses—in particular Vesicular Stomatitis Virus—is shown to have closely involved METTL3 methyltransferase. METTL3 was observed to translocate to the cytoplasm and increase m6A modification levels on viral transcripts (Qiu et al., 2021). This led to reshaping of the RNA, causing the reduction in double-stranded RNA formation—a key antiviral signal—thus lowering sensitivity and innate immune signaling and response. However, the identification of METTL3 as an innate suppressor has made it a possible target for reinstating immune response against viral infections and even curing patients. This would be a promising method especially for tumour suppression and immunogenicity, which is heavily dependent on innate immunity activation (Qiu et al., 2021).

Stopping SARS-CoV-2 Replication

In alignment with the current events of SARS-CoV-2, CRISPR-Cas13b has been modified in an attempt to prevent the virus's replication. One of the dangers of the virus is the development of strains with variation in transmissibility and pathogenic effects. CRISPR-pspCas13b was utilized along with two methods in order to account for the possibility of viral mutation. Multiple crRNAs were utilized (**Figure 3C**) in order to maximize accessibility to the viral RNA, as well as limit the virus's options for escape through mutation (Fareh et al., 2021), similar to that of a drug cocktail. Unlike other various viral inhibitors, generating the appropriate crRNAs for pspCas13b is a specific, and efficient process. As well, pspCas13b possesses a specific characteristic—a positively charged central channel—that allows it to function even with some mismatched nucleotide pairing. Ultimately, this increases the use of the associated crRNA to suppress both the parental virus and future variants (Fareh et al., 2021). Other technical strategies have been employed concurrently, such as targeting conserved regions for coronaviruses in order to further reduce the chance of mutational escape, even with only a single crRNA present. Targeting was also considerably calibrated in order to limit the possibility of off-target effects on human transcriptomes (Fareh et al., 2021). Due to its flexibility in design, it is expected that CRISPR-Cas13 will be an overall efficient tool against viral pathogenesis because it is more difficult for strains to evade compared to more traditional antiviral therapeutics.

Perspectives

CRISPR/Cas systems and base editors are shown to be overall useful and proficient modification tools. However, one of the persistent issues being faced is the level of off-target editing. Although the rate is observed to be lower than that of previous genome editing systems, improvements can be made; one of the major strategies involves combining variants of CRISPR/Cas systems with other editing domains and gRNAs to optimize targeting and binding efficiency for each system's purpose. Attaining accurate targeting should be one of the more important steps for further *in vivo* application of base editors and CRISPR/Cas systems in therapeutics. As m6A is an abundantly occurring modification as well as a common player in many pathological processes, one would expect that several editing therapies in the future will likely revolve around these sites.

In particular, RNA targeted methylation systems should be useful for treatment of viruses and pathogens. As methylation often plays a necessary role for the proliferation of RNA viruses, it thus provides a feasible target for treatment. For example, SARS-CoV-2 mRNA is methylated by an nsp16/nsp10 enzyme complex at the 2′-OH site of its first nucleotide in order to alter the composition of its cap, thus rendering it immune from surveillance (Viswanathan et al., 2021). Targeting this specific methylated site (perhaps with an eraser TRM system) would make a promising first step in a potential series of processes for treating SARS-CoV-2.

Although (CRISPR) RNA-targeting is the more current and popular methodology for phenotypic observation and novel therapeutic approaches, genome-targeting itself is still a very viable option. Recently, delivery of Cas9 mRNA with herpes simplex virus type 1 (HSV-1) erasing lentiviral particles (viral-targeting gRNA) stopped HSV-1 viral proliferation, as well as eradicated any latent viral reserves (Yin et al., 2021). An added advantage to this approach was the noted absence of off-target effects.

For industrial purposes, DNA and RNA targeting systems will likely play a prominent role in agricultural production. Like humans, m6A modifications are critical in plants. In early trials, it was shown that demethylation of m6A by FTO demethylase resulted in increased levels of yield and biomass for rice and potato crops (Yu et al., 2021). What m6A demethylation accomplished was elevating the amount of poly (A) RNA as well as the degree of open chromatin (thus influencing the levels of gene transcription). It is likely that m6A demethylation will be applicable for yield improvement in other agricultural plants in the future, but also will lead to exploring how m6A is involved in transcription in plants.

It is known that m6A modifications can affect RNA stability, and therefore increase or decrease the amount of translation that occurs as well as the longevity of the molecule itself. Therefore, introducing m6A modifications on individual RNA species could serve as an approach to fine-tune the stability of RNAs, which could have applications for RNA vaccine and RNAi therapeutics. In addition, engineering TRM systems for *in vitro* m6A detection of pathogenic transcripts will help preclinical research studies and serve as a blueprint for further extended research into other RNA modifications. We expect CRISPR-based approaches will allow the study of the modifications endogenously, as opposed to using conventional exogenous approaches that rely on luciferase reporter assays, which are currently used to measure the role of RNA modifications on protein stability. It is foreseeable that further exploration will bring us to the stage where we are eventually understanding the functions of individual m6A sites, by introducing a variety of writer and eraser fusions that assist with various biological studies, and optimizing CRISPR complexes for high quality pooled screens.

Costwise, current base editors, CRISPR, and techniques such as CIRTS and RESTORE are more economical than their predecessors. While base editors in general can be delivered in a variety of ways and provide an opportunity for the pursuit of personalized medicine, toxicity is still a concerning obstacle especially for systems such as BARBEKO that rely on sgRNA delivery. Overall, the major transition to Cas systems—especially CRISPR/Cas13—in search for a solution for programmable RNA editing was a fruitful process. Editing efficiency was improved and off-target effects were generally reduced, although they currently remain higher than desired. As more CRISPR proteins are being discovered, we expect that ones with smaller size and lower off-target efficiency will be available to address these shortcomings. With the right coupling, both Cas9 and Cas13 conjugates can target methylation sites for writing/erasing, and the same applies to PUF systems as well. PUF complexes are capable of targeting multiple subcellular compartments, although off-target effects need to be improved by modifying the PUF domain. On the other hand, off-target effects are less

of a pressing issue for ASO systems. By adjusting the ADAR domain of ASO systems, the editing efficiency can increase. However, the risk of off-target editing also increases, which is an area that requires further optimization.

AUTHOR CONTRIBUTIONS

Designed studies: FS and HH. Manuscript writing: NL, XX, FS, and HH.

REFERENCES

Abudayyeh, O. O., Gootenberg, J. S., Franklin, B., Koob, J., Kellner, M. J., Ladha, A., et al. (2019). A Cytosine Deaminase for Programmable Single-Base RNA Editing. *Science* 365, 382–386. doi:10.1126/science.aax7063

Anzalone, A. V., Koblan, L. W., and Liu, D. R. (2020). Genome Editing with CRISPR-Cas Nucleases, Base Editors, Transposases and Prime Editors. *Nat. Biotechnol.* 38, 824–844. doi:10.1038/s41587-020-0561-9

Bernards, R., Brummelkamp, T. R., and Beijersbergen, R. L. (2006). shRNA Libraries and Their Use in Cancer Genetics. *Nat. Methods* 3, 701–706. doi:10.1038/nmeth921

Chen, J., Fang, X., Zhong, P., Song, Z., and Hu, X. (2019). N6-methyladenosine Modifications: Interactions with Novel RNA-Binding Proteins and Roles in Signal Transduction. *RNA Biol.* 16, 991–1000. doi:10.1080/15476286.2019.1620060

Cox, D. B. T., Gootenberg, J. S., Abudayyeh, O. O., Franklin, B., Kellner, M. J., Joung, J., et al. (2018). RNA Editing with CRISPR-Cas13. *Espe* 358, 1019–1027. doi:10.1530/ey.15.14.11

Fareh, M., Zhao, W., Hu, W., Casan, J. M. L., Kumar, A., Symons, J., et al. (2021). Reprogrammed CRISPR-Cas13b Suppresses SARS-CoV-2 Replication and Circumvents its Mutational Escape through Mismatch Tolerance. *Nat. Commun.* 12, 4270. doi:10.1038/s41467-021-24577-9

Gasiunas, G., Young, J. K., Karvelis, T., Kazlauskas, D., Urbaitis, T., Jasnauskaite, M., et al. (2020). A Catalogue of Biochemically Diverse CRISPR-Cas9 Orthologs. *Nat. Commun.* 11, 5512. doi:10.1038/s41467-020-19344-1

Gillmore, J. D., Gane, E., Taubel, J., Kao, J., Fontana, M., Maitland, M. L., et al. (2021). CRISPR-Cas9 *In Vivo* Gene Editing for Transthyretin Amyloidosis. *N. Engl. J. Med.* 385, 493–502. doi:10.1056/NEJMoa2107454

Grünewald, J., Zhou, R., Lareau, C. A., Garcia, S. P., Iyer, S., Miller, B. R., et al. (2020). A Dual-Deaminase CRISPR Base Editor Enables Concurrent Adenine and Cytosine Editing. *Nat. Biotechnol.* 38, 861–864. doi:10.1038/s41587-020-0535-y

Gupta, R. M., and Musunuru, K. (2014). Expanding the Genetic Editing Tool Kit: ZFNs, TALENs, and CRISPR-Cas9. *J. Clin. Invest.* 124, 4154–4161. doi:10.1172/jci72992

Han, W., Huang, W., Mao, M., Wei, T., Ye, Y., and Wang, Z. Programmable RNA Base Editing with a Single gRNA-free Enzyme. *bioRxiv*. doi:10.1101/2021.08.31.458316

Hao, J., Li, C., Lin, C., Hao, Y., Yu, X., Xia, Y., et al. (2020). Targeted point Mutations of the m6A Modification in miR675 Using RNA-Guided Base Editing Induce Cell Apoptosis. *Biosci. Rep.* 40, BSR20192933. doi:10.1042/BSR20192933

Jiang, X., Liu, B., Nie, Z., Duan, L., Xiong, Q., Jin, Z., et al. (2021). The Role of m6A Modification in the Biological Functions and Diseases. *Sig Transduct Target. Ther.* 6, 74. doi:10.1038/s41392-020-00450-x

Kannan, S., Altae-Tran, H., Jin, X., Madigan, V. J., Oshiro, R., Makarova, K. S., et al. (2021). Compact RNA Editors with Small Cas13 Proteins. *Nat. Biotechnol.* doi:10.1038/s41587-021-01030-2

Konermann, S., Lotfy, P., Brideau, N. J., Oki, J., Shokhirev, M. N., and Hsu, P. D. (2018). Transcriptome Engineering with RNA-Targeting Type VI-D CRISPR Effectors. *Cell* 173, 665–676. doi:10.1016/j.cell.2018.02.033

Lee, J. H., Hong, J., Zhang, Z., de la Peña Avalos, B., Proietti, C. J., Deamicis, A. R., et al. (2021). Regulation of Telomere Homeostasis and Genomic Stability in Cancer by N 6 -adenosine Methylation (M 6 A). *Sci. Adv.* 7, eabg7073. doi:10.1126/sciadv.abg7073

Li, J., Chen, Z., Chen, F., Xie, G., Ling, Y., Peng, Y., et al. (2020). Targeted mRNA Demethylation Using an Engineered dCas13b-ALKBH5 Fusion Protein. *Nucleic Acids Res.* 48, 5684–5694. doi:10.1093/nar/gkaa269

Liu, X.-M., Zhou, J., Mao, Y., Ji, Q., and Qian, S.-B. (2019). Programmable RNA N6-Methyladenosine Editing by CRISPR-Cas9 Conjugates. *Nat. Chem. Biol.* 15, 865–871. doi:10.1038/s41589-019-0327-1

Liu, Y., Zhou, C., Huang, S., Dang, L., Wei, Y., He, J., et al. (2020). A Cas-Embedding Strategy for Minimizing Off-Target Effects of DNA Base Editors. *Nat. Commun.* 11, 6073. doi:10.1038/s41467-020-19690-0

Merkle, T., Merz, S., Reautschnig, P., Blaha, A., Li, Q., Vogel, P., et al. (2019). Precise RNA Editing by Recruiting Endogenous ADARs with Antisense Oligonucleotides. *Nat. Biotechnol.* 37, 133–138. doi:10.1038/s41587-019-0013-6

Montiel-Gonzalez, M. F., Vallecillo-Viejo, I., Yudowski, G. A., and Rosenthal, J. J. C. (2013). Correction of Mutations within the Cystic Fibrosis Transmembrane Conductance Regulator by Site-Directed RNA Editing. *Proc. Natl. Acad. Sci.* 110, 18285–18290. doi:10.1073/pnas.1306243110

Newby, G. A., Yen, J. S., Woodard, K. J., Mayuranathan, T., Lazzarotto, C. R., Li, Y., et al. (2021). Base Editing of Haematopoietic Stem Cells Rescues Sickle Cell Disease in Mice. *Nature* 595, 295–302. doi:10.1038/s41586-021-03609-w

Nguyen Tran, M. T., Mohd Khalid, M. K. N., Wang, Q., Walker, J. K. R., Lidgerwood, G. E., Dilworth, K. L., et al. (2020). Engineering Domain-Inlaid SaCas9 Adenine Base Editors with Reduced RNA Off-Targets and Increased On-Target DNA Editing. *Nat. Commun.* 11, 4871. doi:10.1038/s41467-020-18715-y

Pattanayak, V., Ramirez, C. L., Joung, J. K., and Liu, D. R. (2011). Revealing Off-Target Cleavage Specificities of Zinc-finger Nucleases by *In Vitro* Selection. *Nat. Methods* 8, 765–770. doi:10.1038/nmeth.1670

Perčulija, V., Lin, J., Zhang, B., and Ouyang, S. (2021). Functional Features and Current Applications of the RNA-Targeting Type VI CRISPR-Cas Systems. *Adv. Sci.* 8, 2004685. doi:10.1002/advs.202004685

Porto, E. M., Komor, A. C., Slaymaker, I. M., and Yeo, G. W. (2020). Base Editing: Advances and Therapeutic Opportunities. *Nat. Rev. Drug Discov.* 19, 839–859. doi:10.1038/s41573-020-0084-6

Qiu, W., Zhang, Q., Zhang, R., Lu, Y., Wang, X., Tian, H., et al. (2021). N6-methyladenosine RNA Modification Suppresses Antiviral Innate Sensing Pathways via Reshaping Double-Stranded RNA. *Nat. Commun.* 12, 1582. doi:10.1038/s41467-021-21904-y

Rauch, S., He, E., Srienc, M., Zhou, H., Zhang, Z., and Dickinson, B. C. (2019). Programmable RNA-Guided RNA Effector Proteins Built from Human Parts. *Cell* 178, 122–134. doi:10.1016/j.cell.2019.05.049

Rothgangl, T., Dennis, M. K., Lin, P. J. C., Oka, R., Witzigmann, D., Villiger, L., et al. (2021). *In Vivo* adenine Base Editing of PCSK9 in Macaques Reduces LDL Cholesterol Levels. *Nat. Biotechnol.* 39, 949–957. doi:10.1038/s41587-021-00933-4

Sakata, R. C., Ishiguro, S., Mori, H., Tanaka, M., Tatsuno, K., Ueda, H., et al. (2020). Base Editors for Simultaneous Introduction of C-To-T and A-To-G Mutations. *Nat. Biotechnol.* 38, 865–869. doi:10.1038/s41587-020-0509-0

Sun, H., and Yu, G. (2019). New Insights into the Pathogenicity of Non-synonymous Variants through Multi-Level Analysis. *Sci. Rep.* 9, 1667. doi:10.1038/s41598-018-38189-9

Viswanathan, T., Misra, A., Chan, S.-H., Qi, S., Dai, N., Arya, S., et al. (2021). A Metal Ion Orients SARS-CoV-2 mRNA to Ensure Accurate 2′-O Methylation of its First Nucleotide. *Nat. Commun.* 12, 3287. doi:10.1038/s41467-021-23594-y

Wessels, H.-H., Méndez-Mancilla, A., Guo, X., Legut, M., Daniloski, Z., and Sanjana, N. E. (2020). Massively Parallel Cas13 Screens Reveal Principles for Guide RNA Design. *Nat. Biotechnol.* 38, 722–727. doi:10.1038/s41587-020-0456-9

Wilson, C., Chen, P. J., Miao, Z., and Liu, D. R. (2020). Programmable m6A Modification of Cellular RNAs with a Cas13-Directed Methyltransferase. *Nat. Biotechnol.* 38, 1431–1440. doi:10.1038/s41587-020-0572-6

Xia, Z., Tang, M., Ma, J., Zhang, H., Gimple, R. C., Prager, B. C., et al. (2021). Epitranscriptomic Editing of the RNA N6-Methyladenosine Modification by dCasRx Conjugated Methyltransferase and Demethylase. *Nucleic Acids Res.* 49, 7361–7374. doi:10.1093/nar/gkab517

Xu, C., Zhou, Y., Xiao, Q., He, B., Geng, G., Wang, Z., et al. (2021). Programmable RNA Editing with Compact CRISPR-Cas13 Systems from Uncultivated Microbes. *Nat. Methods* 18, 499–506. doi:10.1038/s41592-021-01124-4

Xu, P., Liu, Z., Liu, Y., Ma, H., Xu, Y., Bao, Y., et al. (2021). Genome-wide Interrogation of Gene Functions through Base Editor Screens Empowered by Barcoded sgRNAs. *Nat. Biotechnol.* 39, 1403–1413. doi:10.1038/s41587-021-00944-1

Yin, D., Ling, S., Wang, D., Dai, Y., Jiang, H., Zhou, X., et al. (2021). Targeting Herpes Simplex Virus with CRISPR-Cas9 Cures Herpetic Stromal Keratitis in Mice. *Nat. Biotechnol.* 39, 567–577. doi:10.1038/s41587-020-00781-8

Yu, Q., Liu, S., Yu, L., Xiao, Y., Zhang, S., Wang, X., et al. (2021). RNA Demethylation Increases the Yield and Biomass of rice and Potato Plants in Field Trials. *Nat. Biotechnol.* 39, 1581–1588. doi:10.1038/s41587-021-00982-9

Zhang, Y., Nguyen, T. M., Zhang, X.-O., Wang, L., Phan, T., Clohessy, J. G., et al. (2021). Optimized RNA-Targeting CRISPR/Cas13d Technology Outperforms shRNA in Identifying Functional circRNAs. *Genome Biol.* 22, 41. doi:10.1186/s13059-021-02263-9

Conflict of Interest: The authors declare that the research was conducted in the absence of any commercial or financial relationships that could be construed as a potential conflict of interest.

Publisher's Note: All claims expressed in this article are solely those of the authors and do not necessarily represent those of their affiliated organizations, or those of the publisher, the editors and the reviewers. Any product that may be evaluated in this article, or claim that may be made by its manufacturer, is not guaranteed or endorsed by the publisher.

Copyright © 2022 Lo, Xu, Soares and He. This is an open-access article distributed under the terms of the Creative Commons Attribution License (CC BY). The use, distribution or reproduction in other forums is permitted, provided the original author(s) and the copyright owner(s) are credited and that the original publication in this journal is cited, in accordance with accepted academic practice. No use, distribution or reproduction is permitted which does not comply with these terms.

frontiers in Cell and Developmental Biology

ORIGINAL RESEARCH
published: 09 February 2022
doi: 10.3389/fcell.2022.822011

Diagnostic, Therapeutic, and Prognostic Value of the m^{6}A Writer Complex in Hepatocellular Carcinoma

Zongting Gu[1†], *Yongxing Du*[1†], *Xueping Zhao*[2†] *and Chengfeng Wang*[1*]

[1]*Department of Abdominal Surgery, National Cancer Center/Cancer Hospital, Chinese Academy of Medical Sciences and Peking Union Medical College, Beijing, China,* [2]*School of Life Science and Biopharmaceutical, Shenyang Pharmaceutical University, Shenyang, China*

Hepatocellular carcinoma (HCC) has poor prognosis and is usually diagnosed only at an advanced stage. Identification of novel biomarkers is critical to early diagnosis and better prognosis for HCC patients. N6-methyladenosine (m^{6}A) RNA methylation regulators play important roles in the development of many tumors. However, the m^{6}A writer complex, a key executor of m^{6}A methylation modification, has not been independently investigated, and its specific bioinformatics analysis has not yet been performed in HCC. In this study, we used multiple public databases to evaluate the diagnostic, therapeutic, and prognostic value of the m^{6}A writers in HCC. The results showed that expression levels of METTL3, VIRMA and CBLL1 were significantly increased, while expression levels of METTL14 and ZC3H13 were significantly decreased in HCC, which was closely related to clinicopathological factors, such as tumor stage and prognosis. Bioinformatics further explored the possible underlying mechanisms by which the m^{6}A writer complex are involved in activation of tumor-promoting pathways and/or inhibition of tumor-suppressing pathways, including apoptosis, cell cycle, DNA damage response and EMT. Furthermore, we showed that the m^{6}A writer complex is correlated with immune cell infiltration and immunoregulator expression in HCC. In conclusion, the m^{6}A writer complex may represent a promising biomarker and target that can guide targeted therapy or immunotherapy for HCC patients.

Keywords: M6A, RNA methylation, writer complex, methyltransferase, immune infiltration, hepatocellular carcinoma

OPEN ACCESS

Edited by:
Jianjun Chen,
City of Hope National Medical Center, United States

Reviewed by:
Zhicong Zhao,
Shanghai JiaoTong University, China
Lei Gu,
Max Planck Institute for Heart and Lung Research, Germany

***Correspondence:**
Chengfeng Wang
academicpaper@hotmail.com

[†]*These authors have contributed equally to this work*

Specialty section:
This article was submitted to Epigenomics and Epigenetics, a section of the journal Frontiers in Cell and Developmental Biology

Received: *25 November 2021*
Accepted: *25 January 2022*
Published: *09 February 2022*

Citation:
Gu Z, Du Y, Zhao X and Wang C (2022) Diagnostic, Therapeutic, and Prognostic Value of the m^{6}A Writer Complex in Hepatocellular Carcinoma. Front. Cell Dev. Biol. 10:822011. doi: 10.3389/fcell.2022.822011

INTRODUCTION

Globally, liver cancer is the fourth leading cause of cancer-related deaths, of which hepatocellular carcinoma (HCC) accounts for more than 80%, resulting in a heavy burden of disease (Global Burden of Disease Cancer et al., 2019). Over the past few decades, although considerable progress has been made in the epidemiology, risk factors, and molecular mechanisms of HCC, the incidence and cancer-specific mortality in many countries continue to increase, which is related to the fact that most HCC patients are diagnosed at an advanced stage and lack effective treatment options (Villanueva, 2019). Consequently, it is urgent to clarify the specific mechanism of HCC to develop novel biomarkers, improve the rate of early diagnosis, and identify new targets for molecular targeted therapy.

Epigenetic modifications are involved in the onset and progression of human diseases,especially cancer (Gu et al., 2015; Bauer et al., 2016). Various genetic and epigenetic alterations in hepatocytes

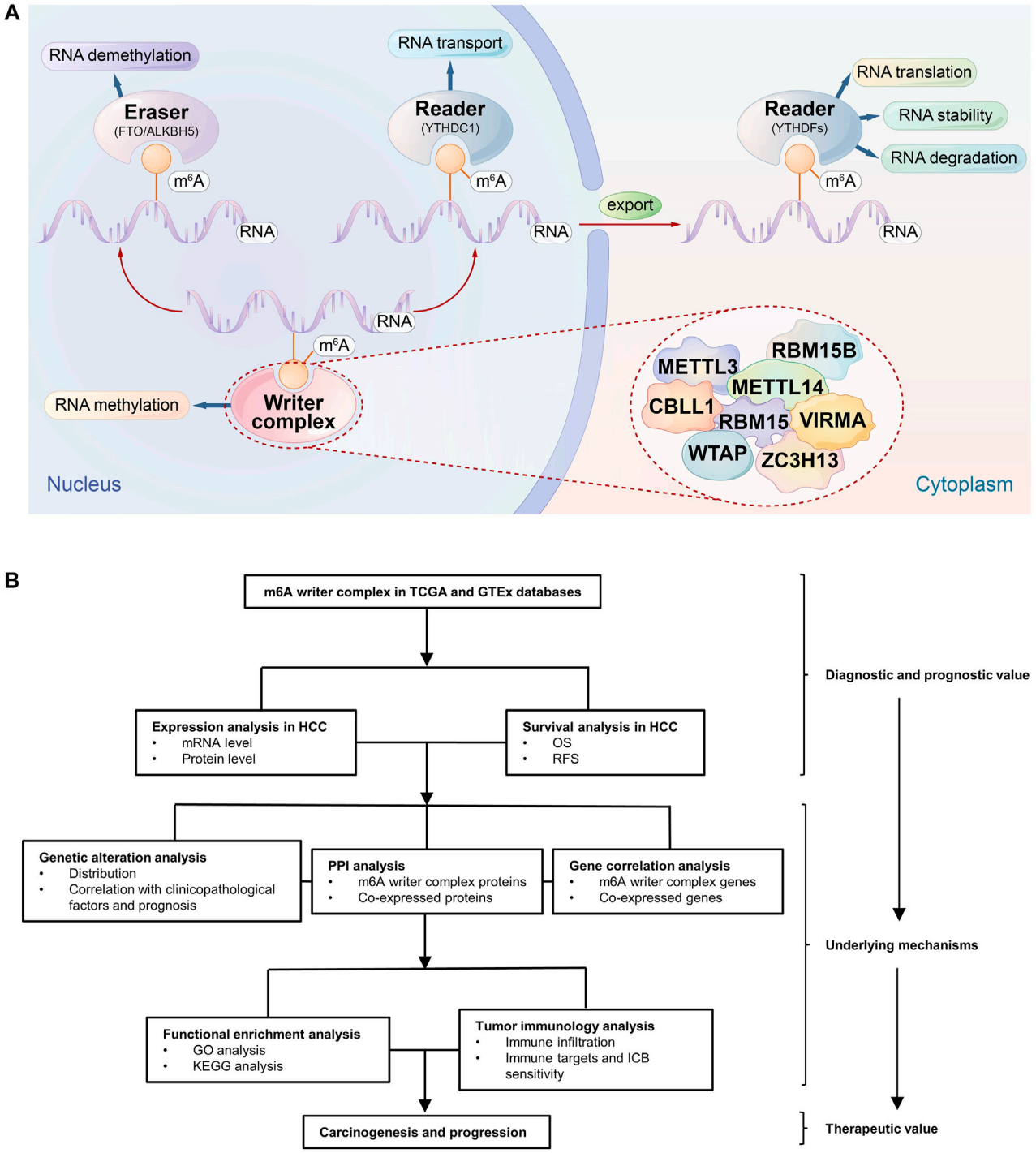


FIGURE 1 | Schematic diagram of the study. **(A)** The m^{6}A mRNA life cycle. m^{6}A methylation is a dynamic and reversible process involving methyltransferases (writers), removal by demethylases (erasers), and binding to specific reader proteins that affect the stability, translation and degradation of mRNA. The m^{6}A writer complex consists of METTL3, METTL14, WTAP, RBM15, METTL15B, VIRMA, ZC3H13, and CBLL1. **(B)** The flowchart of the study.

result in the conversion of proto-oncogenes into oncogenes and the loss of tumor suppressor genes, ultimately promoting carcinogenesis and progression of HCC (Shibata, 2021). The molecular mechanisms associated with genetics, including chromosomal translocations, single nucleotide polymorphisms and loss or deletion of targeted genes, and epigenetic modifications, including gene-specific DNA methylation modifications, aberrant histone modifications, have been

extensively explored in HCC (Shibata, 2021). However, as a novel epigenetic modification, the role of RNA methylation in cancer, especially in HCC, has not been fully defined, which has given rise to a new field of research called "epitranscriptomics" (Saletore et al., 2012).

N6-methyladenosine (m^6A) refers to the methylation modification of the sixth nitrogen (N) atom of adenine (A), which accounts for more than 60% of RNA modifications, especially the modification of eukaryotic mRNA, and affects the RNA metabolism, such as splicing, transport, translation, and degradation (Yu et al., 2018). Accumulating evidence suggests that dysregulated m^6A modification is involved in the carcinogenesis and progression of multiple cancers; for example, dysregulated m^6A modification in the transcripts of some oncogenes, such as Snail, or tumor suppressor genes, such as PHLPP2, is associated with tumor proliferation and metastasis (Liu et al., 2018a; Lin et al., 2019), and they have the potential for targeted therapies (Su et al., 2018). Notably, the current role of m^6A modification in cancer seems to be conflicting. Some genes promote tumor development after methylation, while others can promote tumor development after the removal of methylation (Ma et al., 2017; Chen et al., 2018). In addition, multiple studies have revealed a correlation between infiltrating immune cells in the tumor microenvironment (TME) and m6A modification (Li et al., 2020a; Zhang et al., 2020a), which may affect the response to immune checkpoint blocking (ICB) therapies (Xu et al., 2021). Therefore, m^6A modification may play a regulatory role in the tumorigenesis, progression and immune regulation of HCC. The m^6A modification in mRNA is reversible and dynamically regulated by methyltransferase (writer), demethylase (eraser), and binding protein (reader). However, the tumor-promoting or tumor-suppressive roles of these three regulators are not consistent (Melstrom and Chen, 2020). In fact, writers are a type of protein complex with m6A methyltransferase catalytic activity, i.e., a writer complex. Its components include METTL3, METTL14, WTAP, RBM15/15B, VIRMA, ZC3H13 and CBLL1, as well as other possible components (Gu et al., 2020), which catalyze m^6A formation in the mRNA of oncogenes or tumor suppressors and trigger a series of molecular biological effects, which in turn regulates the expression of cancer-related genes (Zaccara et al., 2019) (**Figure 1A**). Accordingly, as the initiator of methylation modification, the function and regulation of writer complex components will be key to understanding the nature and function of regulated m^6A sites. However, the relationship between the writer complex and HCC is still unclear, and relevant studies are also scarce.

Based on this background, our study focused on the analysis of m^6A writer complex-related genes (**Figure 1B**). Using TCGA and GTEx databases, we compared writer complex expression and prognosis differences between HCC samples and matched normal liver tissues. The possible mechanisms of these genes involved in the tumorigenesis and development of HCC were further explored by the analysis of gene alterations, protein interactions, functional enrichment and immune infiltration. Importantly, we validated the results in different databases to increase the credibility of the results. The findings of this study will help to identify potential diagnostic markers and novel targets for treatment, guide early clinical diagnosis and individualized treatment, and improve the prognosis of patients with HCC.

MATERIALS AND METHODS

Ethics Statement

This study was approved by the ethics committee of the National *Cancer* Center/*Cancer* Hospital, Chinese Academy of Medical Sciences (Beijing, China) and was performed in accordance with the principles of the Declaration of Helsinki. All datasets for this study are freely available from the published literature and do not involve any human or animal experiments.

Expression Analysis

Based on TCGA and GTEx databases, Oncomine (Rhodes et al., 2004) (https://www.oncomine.org/) and GEPIA (Tang et al., 2017) (http://gepia.cancer-pku.cn/) online tools were used to visualize differences in gene expression in the m^6A writer complex between HCC and adjacent normal tissues, and the two results were mutually verified. We used UALCAN (Chandrashekar et al., 2017) (http://ualcan.path.uab.edu/) and GEPIA online tools to compare the relationship between m^6A writer complex expression and HCC stage and pathological grade. We used R software (version 3.6.3) to evaluate the relationship between the m^6A writer complex and other clinicopathological features. We utilized the HPA(Asplund et al., 2012) (https://www.proteinatlas.org/) database to analyze protein expression levels of the m^6A writer complex in HCC.

Survival Analysis

We used the Kaplan–Meier Plotter (Győrffy et al., 2013) (www.kmplot.com) online tool to analyze the correlation between the expression of the m^6A writer complex genes and overall survival (OS) and relapse-free survival (RFS) in HCC. The split cutoff of low and high expression was set in the auto select best cutoff model, and biased arrays were excluded. The log-rank test was used to compute the p-value, and $p < 0.05$ was regarded as significant.

Genetic Alteration Analysis

We used the cBioPortal (Cerami et al., 2012) (https://www.cbioportal.org/) database to analyze genetic alterations in the m^6A writer complex and further determined the correlation between mutation and several important clinicopathological factors and survival (Gao et al., 2013).

Correlation and Interaction Analysis

We applied the TIMER (Li et al., 2017) (http://timer.cistrome.org/) database to analyze the correlation in gene expression between the m^6A writer-complex components in HCC and then plotted the heatmap based on the Pearson correlation coefficient. The volcano map of differentially expressed genes related to the m^6A writer complex in HCC and the heatmap of the top 50 genes positively/negatively correlated with the m^6A writer complex were drawn using the LinkedOmics (Vasaikar et al.,

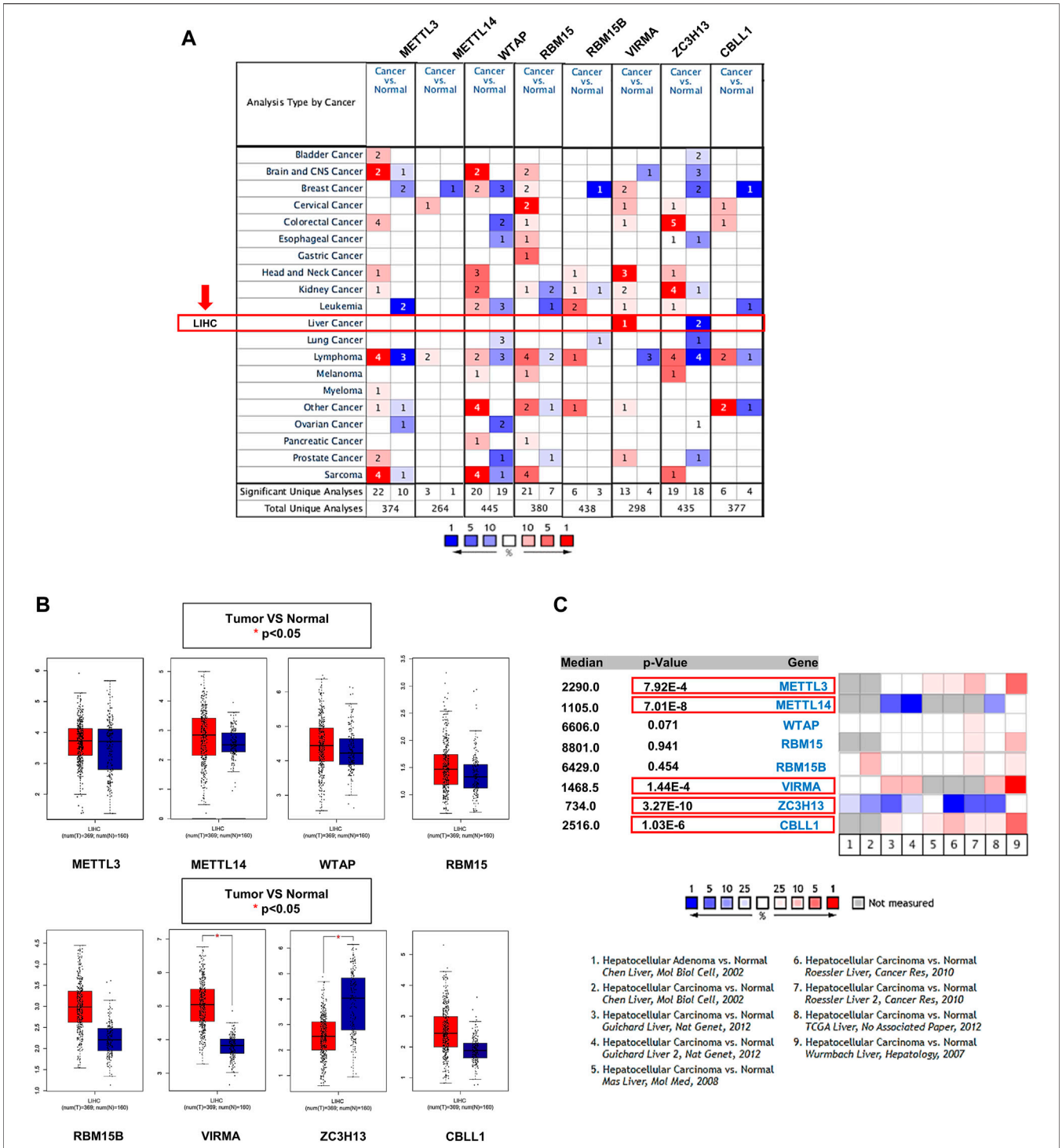


FIGURE 2 | Transcriptional levels of the m^{6}A writer complex in HCC. **(A)** mRNA expression levels of the m^{6}A writer complex (Oncomine). The box indicated by the red arrow shows liver hepatocellular carcinoma (LIHC). The colored squares represent the median rank of these genes (vs. normal tissue). Red represents high expression and blue represents low expression. Differences in transcriptional expression were compared using Student's t-test. The cutoff p-value and fold change were as follows: p-value: 0.01, fold change: 1.5, gene rank: 10%, data type: mRNA. **(B)** Box plot of m^{6}A writer complex expression in HCC (GEPIA). Red represents the expression in HCC tissue, and blue represents the expression in normal tissue. *$p < 0.05$. **(C)** Meta-analysis of the mRNA expression levels of the m^{6}A writer complex using the nine Oncomine datasets. The colored squares represent the median rank of these genes (vs. normal tissue) across the nine datasets. Red represents high expression and blue represents low expression. The significance level for the median rank analysis was set at $p < 0.05$.

2018) (http://www.linkedomics.org/) database. A heatmap of the correlation between the m^{6}A writer-complex components based on protein expression data was obtained by combined score analysis in the STRING (Mering et al., 2003) (https://string-db.org/) database. In addition, we used the igraph package (version 1.2.6) and ggraph package (version 2.0.5) of R software (version 3.6.3) to construct a network of the m^{6}A writer complex and the 10 most frequently altered coexpressed genes. The protein–protein interaction (PPI) network of the m^{6}A writer complex was constructed using the STRING database and visualized using Cytoscape software (Shannon et al., 2003; Doncheva et al., 2019) (v3.9.0), and then the cytoHubba plug-in (Chin et al., 2014) (http://apps.cytoscape.org/apps/cytohubba) was used to screen the top 10 hub genes based on degree value rank.

Functional Enrichment Analysis

We applied the Metascape (Zhou et al., 2019) (https://metascape.org) database to explore functional enrichment of the hub genes, while pathway enrichment was performed using the GSCALite (Liu et al., 2018b) (http://bioinfo.life.hust.edu.cn/web/GSCALite/) online tool. Gene Ontology (GO) and Kyoto Encyclopedia of Genes and Genomes (KEGG) analyses of the m^{6}A writer complex and coexpressed genes were performed using the ClusterProfiler package (Yu et al., 2012) (version 3.14.3) in R for functional annotation and pathway enrichment, respectively. GO analysis included biological process (BP), cellular component (CC) and molecular functions (MF).

Tumor Immunology Analysis

We applied R's GSVA package (Hänzelmann et al., 2013) (version 1.34.0) based on the TCGA database, combined with the TISIDB (Ru et al., 2019) (http://cis.hku.hk/TISIDB/index.php) database to analyze the relationship between the m^{6}A writer complex and immune cell infiltration in HCC. In addition, TISIDB was used to analyze the relationship between the m^{6}A writer complex and expression of immunomodulators in HCC. We analyzed the correlation between writer complex expression and drug sensitivity in immune or targeted therapies by applying the GSCALite online tool based on the GDSC database (Yang et al., 2013).

RESULTS

Transcriptional Levels of the m^{6}A Writer Complex in Hepatocellular Carcinoma

The Oncomine database showed that gene expression of the m^{6}A writer complex in cancer tissues is different from that in normal tissues, but not all components exhibited similar changes (**Figure 2A**). Among them, VIRMA and ZC3H13 exhibited increased and decreased transcription levels in HCC, respectively, compared to normal tissues (**Figure 2A**). Results from the GEPIA database also confirmed the differential expression of VIRMA and ZC3H13 in HCC (**Figures 2B,C**). Of concern, a subset of datasets in the Oncomine also exhibited significantly higher expression levels of METTL3 and CBLL1 and lower expression levels of METTL14 in HCC compared to normal tissues, although there was no significant difference in TCGA database (**Figure 2D**).

Tissue Levels of the m^{6}A Writer Complex in Hepatocellular Carcinoma

To explore the expression levels of writer complex proteins in HCC tissues, we analyzed immunohistochemistry (IHC) data using the HPA database and found that except for the missing METTL3 data, other complex proteins displayed different extents of expression in HCC compared to normal tissues. Among them, expression of METTL14 and ZC3H13 proteins was not significantly increased, while expression of other components, especially WTAP, RBM15 and CBLL1 proteins, was increased to varying extents (**Figure 3**), which was basically consistent with their changes at the transcriptional level.

Relationship Between the m^{6}A Writer Complex and Clinicopathological Parameters in Hepatocellular Carcinoma

The association between the m^{6}A writer complex and clinicopathological parameters was assessed based on an independent cohort of 424 patients with HCC from the TCGA database. Further analysis using the UALCAN database showed that the differences in writer complex expression between HCC and normal tissues might be related to tumor stage. The expression levels of METTL3, RBM15B, VIRMA, and CBLL1 in stages 1–4 were all significantly increased (ANOVA, $p < 0.01$) (**Figure 4A**), and expression levels of WTAP and RBM15 in stages 1–3 were significantly higher than those in adjacent tissues (ANOVA, $p < 0.01$), while expression of METTL14 and ZC3H13 was higher than that in adjacent tissues only in stage 3 (ANOVA, $p < 0.05$) (**Supplementary Figure S1A**). However, a stage plot from the GEPIA database (based on TCGA Project) showed that only expression of METTL3, RBM15, RBM15B and CBLL1 exhibited significant differences among HCC stages (ANOVA, $p < 0.05$) (**Figure 4B**; **Supplementary Figure S1B**). Furthermore, UALCAN revealed that the gene expression differences in METTL3, RBM15, RBM15B, VIRMA and CBLL1 may also be related to tumor grade (**Figure 4C**; **Supplementary Figure S1C**). The relationship between the m^{6}A writer complex and other clinicopathological features was shown in **Supplementary Table S1**.

Prognostic Value of the m^{6}A Writer Complex in Hepatocellular Carcinoma

Next, we used Kaplan–Meier Plotter tools to conduct survival analysis based on the TCGA database. The Kaplan–Meier curve and log-rank test analyses revealed that differences in the expression of the m^{6}A writer complex significantly affected OS in patients with HCC (log-rank test, $p < 0.05$) (**Figure 5A**). Upregulated expression of METTL3, WTAP, RBM15, RBM15B, VIRMA, and CBLL1 and downregulated expression of METTL14

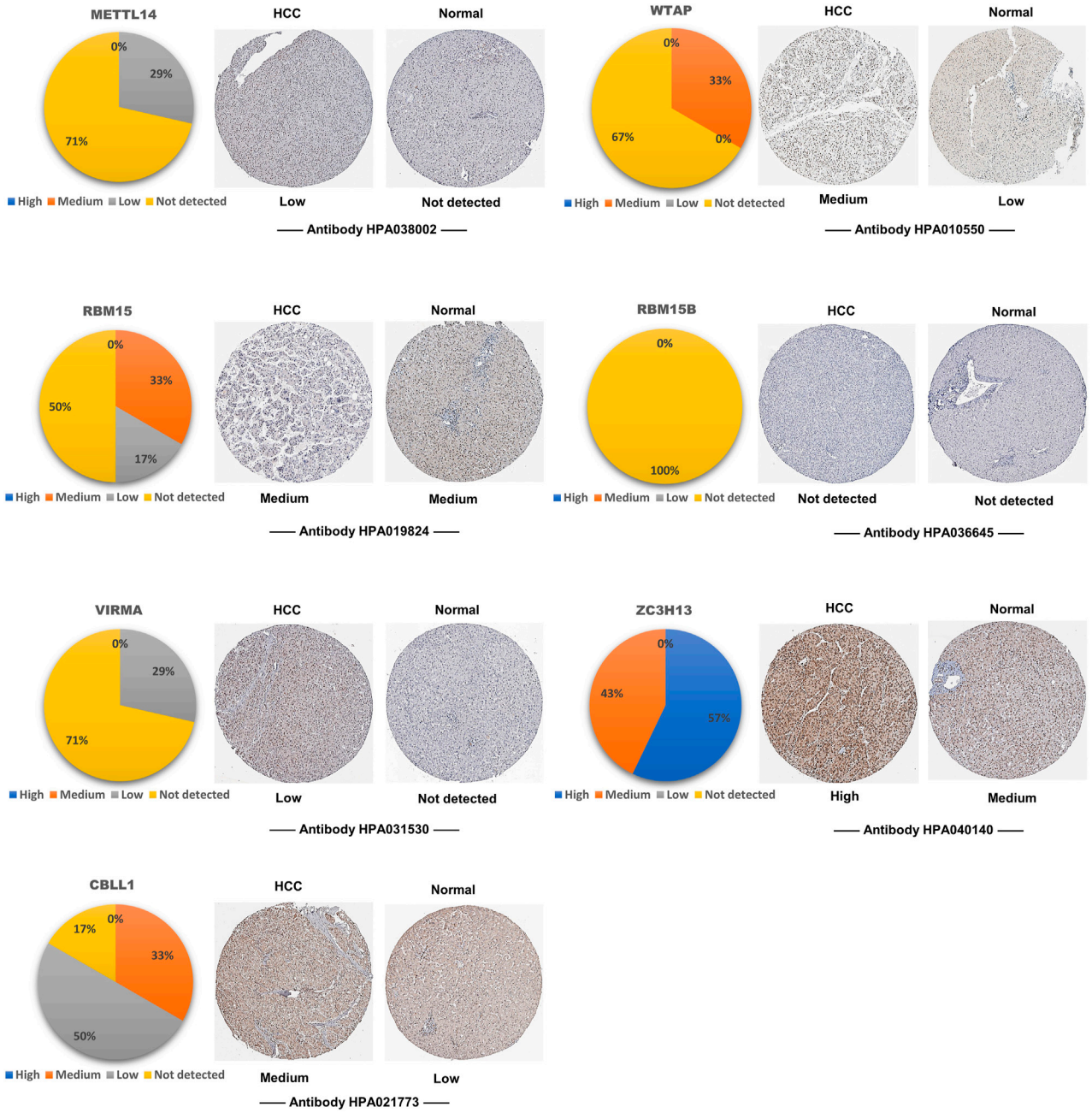


FIGURE 3 | Tissue levels of the m^{6}A writer complex in HCC (HPA). Representative immunohistochemistry (IHC) images of the m^{6}A writer complex in HCC tissues. METTL3 data is temporarily missing in HPA database. The pie chart shows the proportion of IHC staining differences in HCC tissues. Only images with the most prominent tissue expression are shown.

and ZC3H13 are markers of poor prognosis in HCC (**Figure 5A**), consistent with previous analytic results (**Figure 2D**). Moreover, the differential expression of other components of the writer complex was also significantly related to RFS in patients with HCC (log-rank test, $p < 0.05$), except for CBLL1 (**Figure 5B**), which may be related to the low number of HCC patients with CBLL1 upregulation in the TCGA database whose RFS was longer than 60 months, leading to statistical bias.

Genetic Alterations Related to the m^{6}A Writer Complex and Their Correlation With Clinicopathological Factors in Hepatocellular Carcinoma

To explore the possible underlying mechanisms of differential expression of the m^{6}A writer complex in HCC, we analyzed their gene alterations using the cBioPortal database. The

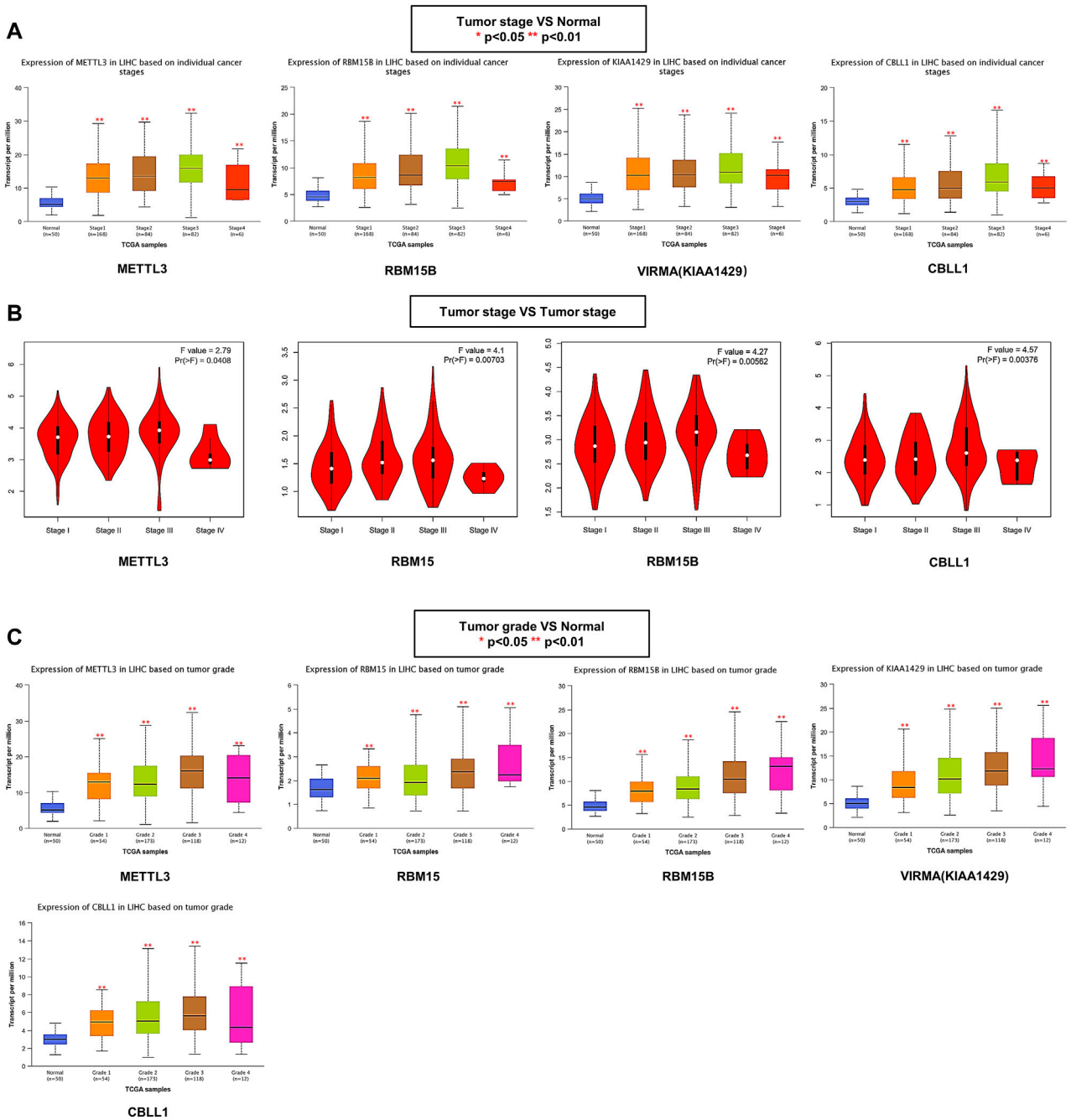


FIGURE 4 | Relationship between the m^{6}A writer complex and clinicopathological parameters in HCC. **(A)** Association of mRNA expression of the m^{6}A writer complex with individual cancer stages in HCC (UALCAN). **(B)** The correlation between m^{6}A writer complex expression and tumor stage in HCC (GEPIA). **(C)** Association of mRNA expression of the m^{6}A writer complex with tumor grades in HCC (UALCAN). ANOVA, $p < 0.05$ was regarded as statistically significant. *$p < 0.05$, **$p < 0.01$, ***$p < 0.001$.

results of the analysis revealed that two or more types of gene alterations were detected in 15% of cases (191/1267) (**Figures 6A,B**). Of these, amplification was more frequent in METTL3 (83%, 5/6), VIRMA (81%, 79/98) and CBLL1 (83%, 15/18), while WTAP (65%, 13/20), METTL14 (50%, 1/2) and ZC3H13 (50%, 14/28) were prone to deep deletions (**Figure 6A**). Further comparison with clinicopathological indicators revealed that altered the group was significantly associated with tumor type (**Figure 6C**), high Ishak fibrosis score (**Figure 6D**), high vascular invasion (**Figure 6E**), large tumor volume (**Figure 6F**) in male patients (**Figure 6G**) with high tumor grade (**Figure 6H**) and advanced tumor

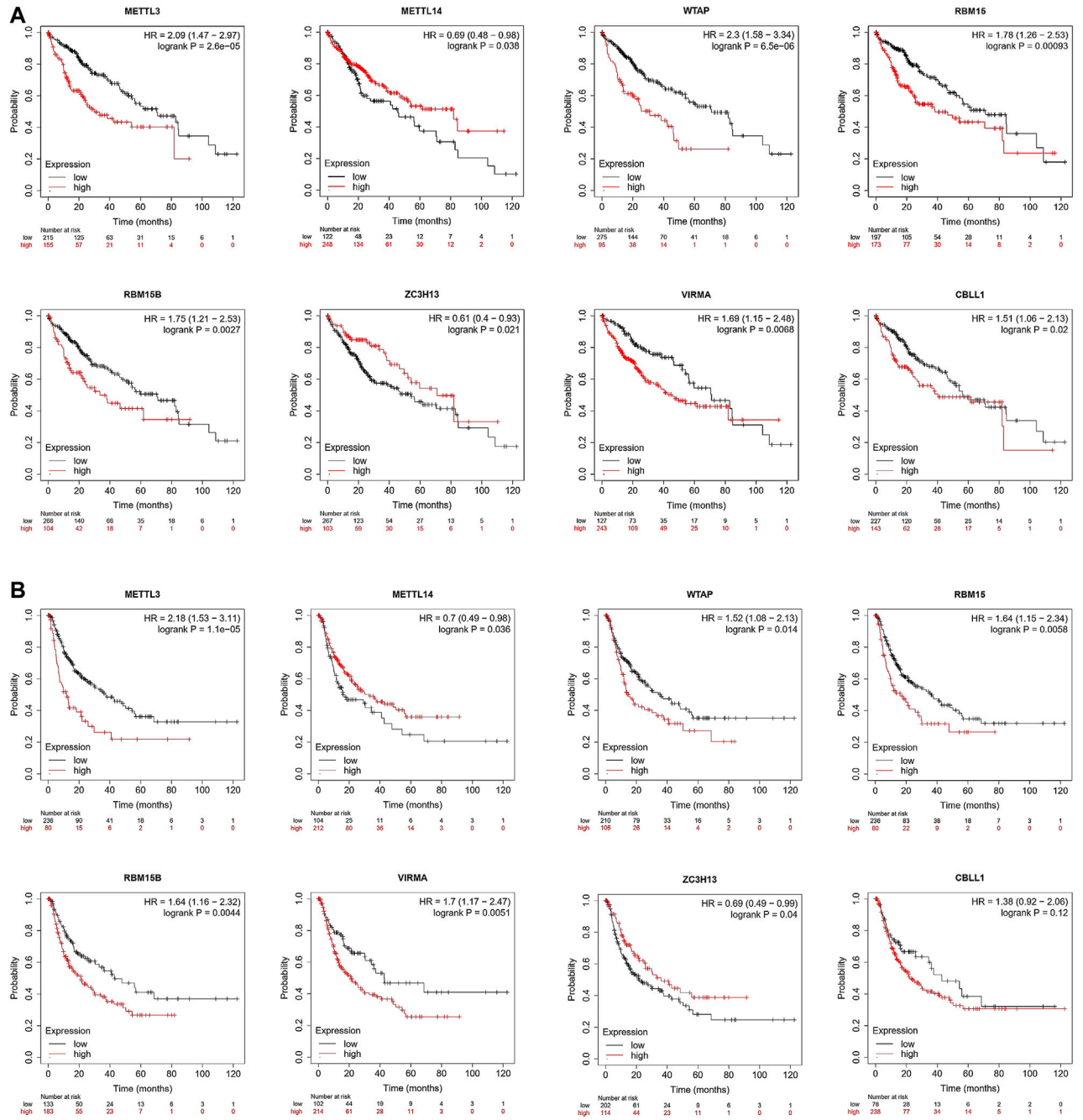


FIGURE 5 | Prognostic value of the m^{6}A writer complex in HCC (Kaplan–Meier Plotter). The correlation between expression of the m^{6}A writer complex genes and overall survival (OS) **(A)** and relapse-free survival (RFS) **(B)** in HCC. Data are shown as the hazard ratio with a 95% confidence interval. Log-rank $p < 0.05$ was regarded as statistically significant.

stage (**Figure 6I**) (Chi-Squared Test, $p < 0.05$). Unfortunately, the altered group did exhibit significantly altered OS (**Figure 6J**) or disease-free survival (DFS, **Figure 6K**) in patients with HCC (log-rank test, $p > 0.05$), which may be associated with their low mutation prevalence and multiple confounding factors.

Coexpressed Genes and Interactions of the m^{6}A Writer Complex in Hepatocellular Carcinoma

To explore the interaction between the m^{6}A writer complex genes and coexpressed genes in HCC, we first used the LinkedOmics

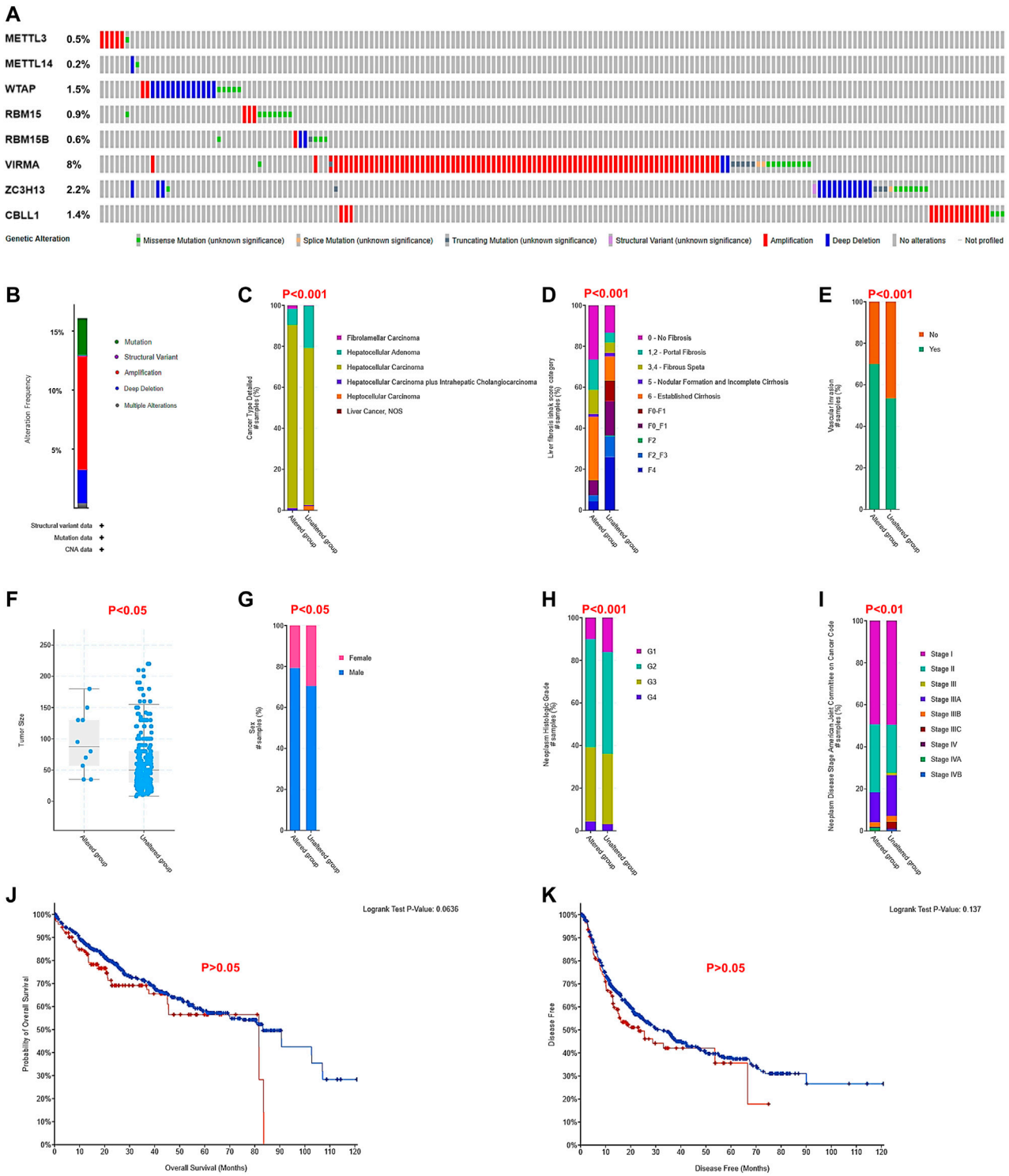


FIGURE 6 | Genetic alterations related to the m^{6}A writer complex and their correlation with clinicopathological factors in HCC (cBioPortal). **(A)** Amplification, deletion, and mutation of the m^{6}A writer complex in HCC. **(B)** Genetic alteration summary of the m^{6}A writer complex in HCC. The correlation between genetic alteration of the m^{6}A writer complex and tumor type **(C)**, Ishak fibrosis score **(D)**, vascular invasion **(E)**, tumor volume **(F)**, sex **(G)**, tumor grade **(H)**, and tumor stage **(I)**. Chi-squared test, $p < 0.05$ was regarded as statistically significant. The relationship between genetic alteration of the m^{6}A writer complex and OS **(J)** and DFS **(K)** of HCC patients. Log-rank $p < 0.05$ was regarded as statistically significant.

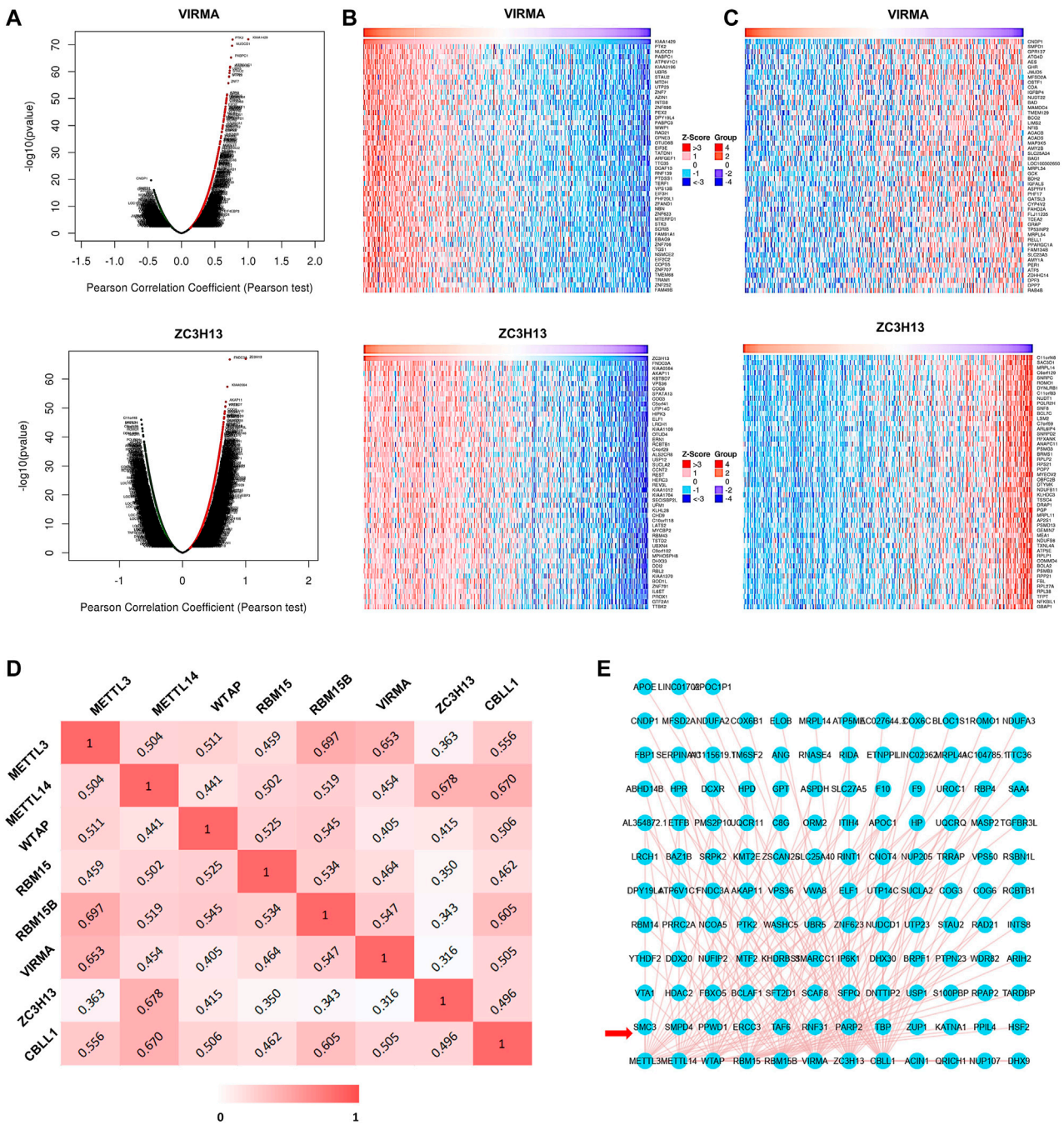


FIGURE 7 | Coexpressed genes and interactions of the m^{6}A writer complex in HCC. **(A)** Volcano plots show differentially expressed genes related to the m^{6}A writer complex in HCC (LinkedOmics). Heatmaps show the top 50 genes positively **(B)** and negatively **(C)** correlated with the m^{6}A writer complex in HCC (LinkedOmics). Red indicates positively correlated genes, and blue/green indicates negatively correlated genes. **(D)** Heatmap shows mRNA level correlation between the m^{6}A writer-complex components based on Pearson correlation coefficient. **(E)** Network for the m^{6}A writer complex and its 10 most frequently altered neighboring genes. The red arrow indicates the most frequently altered neighboring genes.

database to draw a volcano map of coexpressed genes related to the writer complex (**Figure 7A**; **Supplementary Figure S2A**). The top 50 positively (**Figure 7B**; **Supplementary Figure S2B**) and negatively (**Figure 7C**; **Supplementary Figure S2C**) regulated genes related to the writer complex are shown in the heatmap. We then applied the Timer database to analyze the Pearson correlation coefficient (r) between the complex components based on RNA-seq data and drew a heatmap (**Figure 7D**). The results showed that expression of each component was positively correlated (r > 0), of which the

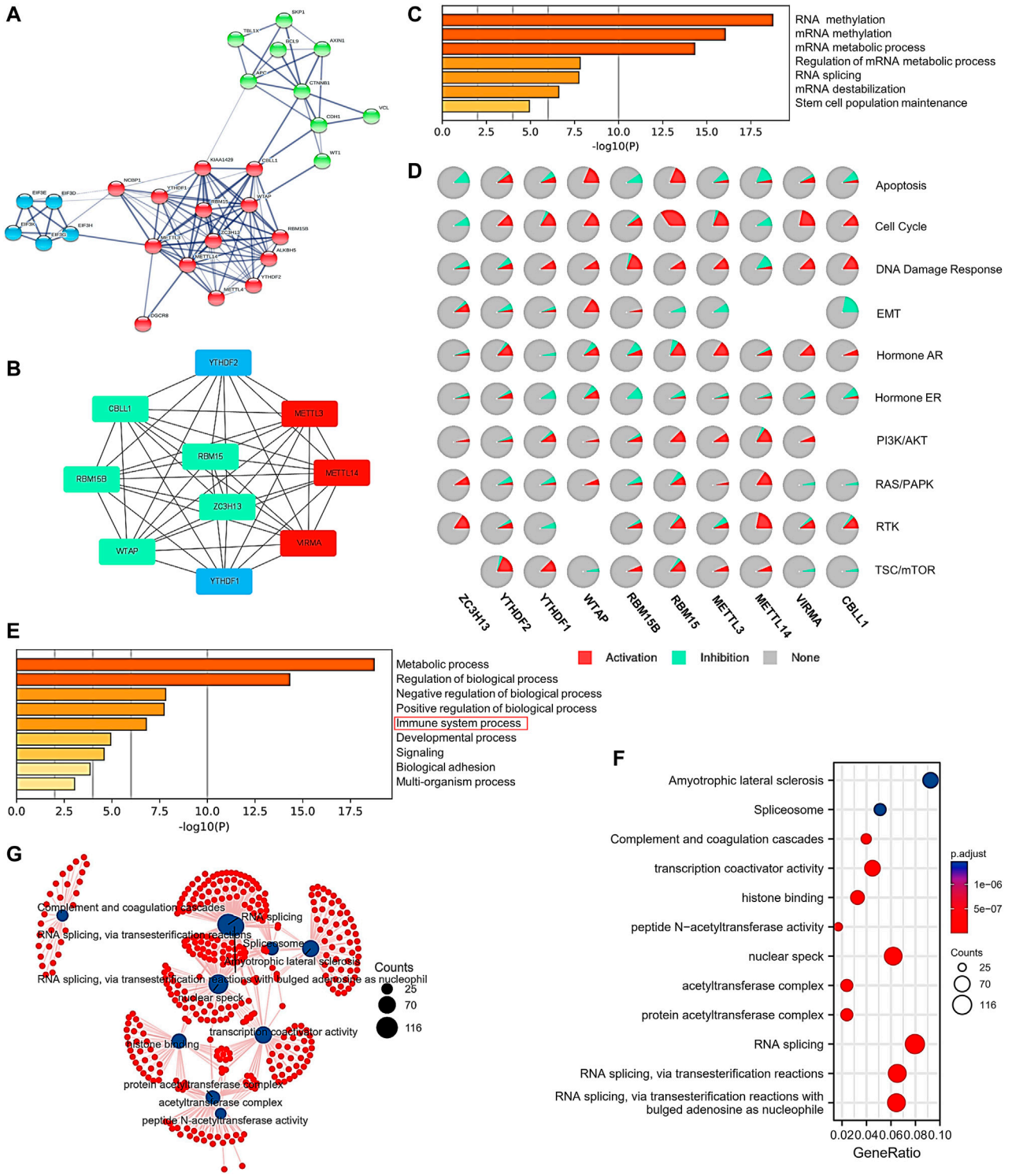


FIGURE 8 | Protein–protein interactions (PPIs) and functional enrichment analysis of the m^{6}A writer complex in HCC. **(A)** PPI network of the top 20 proteins related to the m^{6}A writer complex in HCC (STRING). **(B)** Ten hub genes selected by Cytoscape from the PPI network. Red represents high degree value of the gene. Blue represents the hub genes except for the writer complex components. **(C)** Molecular function enrichment of the hub genes (Metascape). **(D)** Pathway enrichment of the hub genes (GSCALite). **(E)** Biological process enrichment of the hub genes (Metascape). **(F)** Gene Ontology (GO) and Kyoto Encyclopedia of Genes and Genomes (KEGG) pathway enrichment analysis of the writer complex and the top 200 coexpressed genes. **(G)** Network for GO and KEGG pathway enrichment.

correlation between METTL3 and RBM15B was the strongest (r = 0.697), followed by METTL14 and ZC3H13 (r = 0.678) (**Figure 7D**). Next, we constructed a network of the m^6A writer complex and its 10 most frequently altered neighboring genes using the igraph package and the ggraph package in R software. The network revealed several genes significantly associated with the m^6A writer complex, including transcriptional regulators (TAF6, TBP), protein modification genes (PPWD1, RNF31) and DNA damage repair genes (PARP2, ERCC3) (**Figure 7E**).

Protein–Protein Interactions and Functional Enrichment Analysis of the m^6A Writer Complex in Hepatocellular Carcinoma

To explore the interactions of protein expression between writer complex components in HCC, we used the STRING database to analyze the combined score of each component and create a heatmap (**Supplementary Figure S3A**). The results showed that WTAP protein expression displayed the strongest relationship with VIRMA, ZC3H13 and CBLL1 (combined score = 0. 999), followed by METTL3 versus METTL14 and WTAP (combined score = 0.998) and METTL14 versus WTAP (combined score = 0.998) (**Supplementary Figure S3A**). We then analyzed the protein–protein interaction (PPI) network associated with the m^6A writer complex in HCC. We further used Cytoscape to map the hub gene network of the top 10 genes based on degree value rank (**Figure 8A**), and the results also showed that the protein interactions between the components of the writer complex were strong, especially between METTL3, METTL14 and VIRMA (**Figure 8B**). Notably, expression of the RNA-binding proteins YTHDF1 and YTHDF2 was also significantly associated with the m^6A writer complex (**Figure 8B**), consistent with their combined functions in methylation regulation (**Figure 1A**). Next, we conducted GO and KEGG analyses using Metascape, GSCALite and the clusterProfiler R package to explore the specific function and biological pathways of the m^6A writer complex identified in HCC. First, GO analysis of complex hub genes confirmed their ability to modify RNA methylation. Other functions may include RNA splicing, regulation of mRNA metabolism, and maintenance of stem cell function (**Figure 8C**). Pathway activity analysis suggested that the above functions were involved in activation of tumor-promoting pathways and/or inhibition of tumor-suppressing pathways, including apoptosis, cell cycle, DNA damage response and EMT (**Figure 8D**). Moreover, immune process regulation and signaling pathways were also involved, including AR/PR, PI3K/AKT, RAS/PAPK, RTK, and TSC/mTOR (**Figure 8E**; **Supplementary Figure S3B**). We then performed an extended GO and KEGG analysis by intersecting the top 200 coexpressed genes associated with each writer complex component. The results showed that the m6A writer complex may also involve histone binding, protein acetylation modification, transcription coactivator, and complement and coagulation cascades (**Figure 8F**; **Supplementary Figure S3C**). The function network is shown in **Figure 8G**.

Correlations Between the m^6A Writer Complex and Tumor Immunology in Hepatocellular Carcinoma

Immune cell infiltration is an important part of the tumor microenvironment and is closely related to the development of cancer (Gajewski et al., 2013). Therefore, we applied the GSVA R package and TISIDB database to analyze the relationship between the m^6A writer complex and immune cell infiltration in HCC (**Figure 9A**; **Supplementary Figures S4A,B**). Further intersection analysis of the results (**Supplementary Table S2**) revealed that METTL14 and ZC3H13 expression was positively correlated with Tcm, T helper cells, Th17 cells and eosinophil infiltration (**Figure 9B**). Expression of METTL3, WTAP, RBM15, RBM15B, VIRMA and CBLL1 was positively correlated with Tcm, T helper cell and Th2 cell infiltration (**Supplementary Figure S4C**). Interestingly, expression of all writer complex components was negatively correlated with the infiltration of pDCs, DCs and cytotoxic cells (**Figure 9C**; **Supplementary Figure S4D**). Furthermore, expression of the m^6A writer complex was significantly correlated with the immune subtypes of HCC (Kruskal–Wallis test, $p < 0.05$) (**Figure 9D**; **Supplementary Figure S4E**). Next, we analyzed the correlation between the m^6A writer complex and immunostimulators (**Figure 9E**), immunoinhibitors (**Figure 9F**), MHC molecules (**Supplementary Figure S4F**), chemokines (**Supplementary Figure S4G**) and chemokine receptors (**Supplementary Figure S4H**) of infiltrating immune cells in HCC. These results could provide important information for predicting potential therapeutic targets. Finally, we used the GSCALite online tool based on the GDSC database to analyze the relationship between the m^6A writer complex and drug sensitivity in immune or targeted therapies (**Figure 9G**). The results revealed that METTL3, WTAP and RBM15 expression was positively correlated with the sensitivity of several immune or targeted drugs, which might be potential biomarkers for drug screening.

DISCUSSION

Previous studies have reported that m^6A regulators are dysregulated in many cancers, including HCC, and may have prognostic value (8–10). However, the m^6A writer complex, which are responsible for m^6A installation, has not been independently examined, and a specific bioinformatics analysis of this complex has not yet been performed. In this study, we used multiple public databases to reveal that expression levels of METTL3, VIRMA and CBLL1 were significantly increased in the m^6A writer complex, while expression levels of METTL14 and ZC3H13 were significantly decreased in HCC, which was closely related to clinicopathological factors, such as tumor stage and prognosis, confirming their potential role as biomarkers for diagnosis and prognosis determination. In addition, we explored the possible underlying mechanisms of the m^6A writer complex involved in the carcinogenesis and progression of HCC and its relationship with the tumor immune response. This may provide potential targets for treatment with clinical translational implications.

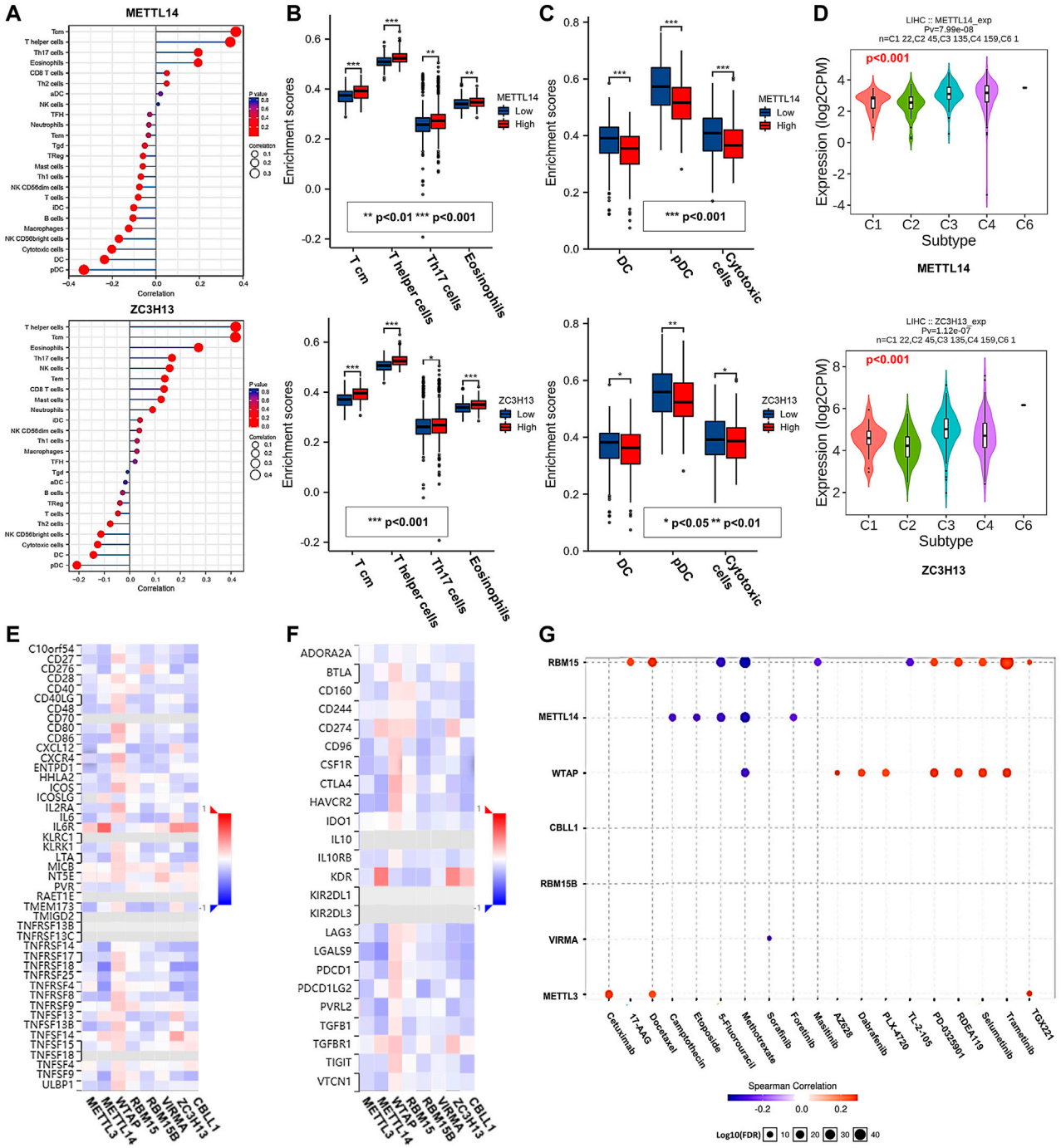


FIGURE 9 | Correlations between the m^{6}A writer complex and tumor immunology in HCC. **(A)** Relationship between the m^{6}A writer complex and immune cell infiltration in HCC. Box plots show immune cells positively **(B)** and negatively **(C)** correlated with the m^{6}A writer complex in HCC. **(D)** Correlations between the m^{6}A writer complex and immune subtypes in HCC (TISIDB). Kruskal–Wallis test, $p < 0.05$ was regarded as statistically significant. C1: wound healing, C2: IFN-γ dominant, C3: inflammatory, C4: lymphocyte depleted, C5: immunologically quiet, C6: TGF-β dominant. Heatmaps show correlations between the m^{6}A writer complex and the expression of immunostimulators **(E)** and immunoinhibitors **(F)** in HCC (TISIDB). **(G)** Correlations between the m^{6}A writer complex and drug sensitivity in immune or targeted therapies (GSCALite). Red and blue represent positive and negative correlations, respectively.

METTL3 is an S-adenosylmethionine (SAM)-binding protein that is the only component in the m^{6}A writer complex with methyltransferase catalytic activity (Śledź and Jinek, 2016). Recent studies have shown that METTL3 is upregulated and associated with poor prognosis in gastrointestinal malignancies, including liver cancer, pancreatic cancer and colorectal cancer (Li

et al., 2019). Subsequent *in vitro* and *in vivo* experiments have confirmed that downregulation of METTL3 inhibits tumor growth and metastasis (Li et al., 2019). Mechanistically, METTL3 increases methylation levels of suppressor of cytokine signaling 2 (SOCS2) mRNA, promotes its degradation through a m^6A-YTHDF2-dependent mechanism, and inhibits SOCS2 expression in HCC tissues, thereby promoting HCC progression (Chen et al., 2018). Moreover, METTL3 also accelerates HCC progression by methylating the transcription factor Snail of EMT and promoting its translation, a process that may involve the interaction between YTHDF1 and eukaryotic translation elongation factor 2 (eEF-2) (Lin et al., 2019). Therefore, METTL3 overexpression in HCC promotes the development of HCC by binding to the m^6A reader proteins YTHDF1 and YTHDF2 and subsequently regulating downstream signaling pathways, which is consistent with the finding that YTHDF1 and YTHDF2 are hub genes in this study. Further GO and KEGG analyses also confirmed the key biological processes involved, such as anti-apoptosis, promotion of proliferation, and EMT, suggesting that the writer complex plays a key role in regulating HCC cell proliferation and inducing chemotherapy resistance. Notably, the co-expressed gene network revealed that the expression of transcriptional regulatory factor (TBP) and DNA damage repair genes (PARP2, ERCC3) may also be significantly correlated with the m^6A writer complex in HCC, and recent studies have provided more evidence. A very recent study showed that TATA-binding protein (TBP) can positively regulate METTL3 transcription, which further upregulates PDK4 expression in HCC cells (Li et al., 2020b). PDK4 is one of the key factors involved in the regulation of glycolysis in cancer cells, which can promote tumor metabolic remodeling and contribute to chemoresistance (Li et al., 2020b). Therefore, the TBP/METTL3/PDK4 axis may be a novel mechanism involved in HCC progression. However, the specific mechanisms by which transcription factors regulate the m^6A writer complex remain to be further explored. Additionally, METTL3 can recruit the key DNA polymerase κ (Pol κ) to DNA damage sites through the PARP/METTL3/Pol κ axis, promoting ultraviolet (UV)-induced DNA damage repair and cell survival (Xiang et al., 2017). Moreover, METTL3-mediated upregulation of yes-associated protein (YAP) leads to DNA damage repair by upregulating the expression of downstream excision repair cross-complementing 1 (ERCC1) in NSCLC (Jin et al., 2019). DNA damage repair is one of the key mechanisms for cancer cells to survive chemotherapy. Therefore, METTL3-mediated recruitment or expression of key enzymes in DNA damage repair may facilitate tumor progression and chemoresistance in HCC. METTL14, an allosteric adapter of METTL3, forms a heterodimer with METTL3 to stabilize the writer complex and recruit substrate RNA ((Śledź and Jinek, 2016), (Wang et al., 2016)). The crystal structure and biochemical evidence suggested that METTL3, rather than METTL14, is the unique catalytic subunit (Wang et al., 2016). The different roles of METTL14 and METTL3 in methylation may underlie their conflicting expression changes in HCC. In addition, METTL3, but not METTL14, exerts the methyltransferase independent function to potentiate mRNA translation, which might also contribute to their divergent expression and biological function ((Lin et al., 2016), (Choe et al., 2018)). Our study confirmed reports that METTL14 acts as a tumor suppressor in HCC. *In vitro* experiments also demonstrated that METTL14 knockdown promotes tumor cell proliferation and invasion by activating PI3K/Akt signaling (Zhang et al., 2019), which is consistent with our pathway enrichment results. Analogous to METTL3, METTL14 combined with YTHDF1 can bind to the DNA damage-binding protein 2 (DDB2) transcript, regulating DDB2 m^6A methylation and translation, promoting UV-induced DNA damage repair and suppressing skin tumorigenesis (Yang et al., 2021). Consequently, these data suggest that METTL3 and METTL14 may serve as potential therapeutic targets and facilitate the development of new strategies to sensitize cancer cells to DNA-damaging agents in HCC. Interestingly, although METTL3 and METTL14 seem to play completely opposite roles in HCC progression, which may not be the case in other tumors, such as downregulated METTL3 expression detected in approximately 70% of endometrial cancers, which may be related to tumor heterogeneity (Liu et al., 2018a). VIRMA (also known as KIAA1429) interacts with WTAP to direct the writer complex to regionally selective methylation (Yue et al., 2018), and it is upregulated in HCC with poor prognosis (Lan et al., 2019), which is consistent with our study. Mechanistically, GATA3 is a direct downstream target of VIRMA-induced m^6A methylation modification, which leads to downregulation of GATA3 mRNA expression and promotes invasion and migration of HCC cells (Lan et al., 2019). CBLL1, or HAKAI, is a class of E3 ubiquitin ligases that interacts with E-cadherin (Fujita et al., 2002). CBLL1 has been reported to be overexpressed and associated with poor prognosis in non-small cell lung cancer (NSCLC) and esophageal cancer (EC) (Weng et al., 2019; Zhao et al., 2021). Recent studies have shown that CBLL1 interacts with E-cadherin phosphorylated by Src kinase to induce ubiquitination and endocytosis of E-cadherin in HCC, which is associated with the transformation of aggressive phenotypes of tumor cells (Lu et al., 2018). Targeted knockdown of CBLL1 inhibits the growth of tumor cells (Liu et al., 2018c), which may be the potential mechanism of CBLL1 overexpression that is related to poor prognosis in this study. ZC3H13 is a prototypical CCCH-type zinc finger protein that binds to RBM15/RBM15B and attaches to WTAP in the m^6A writer complex to improve catalytic potency (Zaccara et al., 2019). In contrast to its upregulation in cholangiocarcinoma and EC (Guo et al., 2021), we found that ZC3H13 acts as a tumor suppressor in HCC, consistent with the findings in breast and ovarian cancer (Zhang et al., 2020b; Wang et al., 2021a), suggesting functional diversity of ZC3H13 in different tumors. Very recently, an independent study indicated that ZC3H13 suppressed the progression of HCC through m^6A-PKM2-mediated glycolysis and sensitized HCC cells to cisplatin, which offered a novel insight into ZC3H13 downregulation in HCC (Wang et al., 2021b). Moreover, another study on colorectal cancer found that ZC3H13 inhibits tumor cell proliferation and invasion by downregulating the expression of Snail, cyclin D1 and cyclin E1 by inhibiting the RAS signaling pathway (Zhu et al., 2019). In addition, ZC3H13 levels are also positively correlated with ER and PR expression in breast cancer (Zhang et al., 2020b). These findings might explain our functional enrichment results. In addition, Wilms' tumor-associated protein acts as a key METTL3 adaptor and interacts with other components of the

writer complex to participate in specific m^6A methylation modification (Ping et al., 2014). However, the carcinogenic roles of WTAP and RBM15/15B in HCC remain controversial. For example, the study of Ma et al.(Ma et al., 2017) did not show that WTAP was overexpressed in HCC, but Chen et al. (Chen et al., 2019) found that WTAP expression was upregulated and promoted HCC progression through the HuR-ETS1-p21/p27 axis. These seemingly contradictory conclusions may be related to the adaptive stress of the m^6A writer complex in HCC.

Given the important role of intratumoral immune cells, we also evaluated the correlation between the m^6A writer complex and immune cell infiltration in HCC. Notably, expression of the tumor suppressors METTL14 and ZC3H13 was positively correlated with the infiltration of Tcm cells, Th17 cells, and eosinophils, consistent with previous findings that these cells are associated with a favorable prognosis of malignant tumors (Cua and Tato, 2010; Steel et al., 2010; Xu et al., 2019). Paradoxically, we found that tumor suppressors were negatively correlated with the infiltration of pDCs, DCs, and cytotoxic cells, and the tumor promoters METTL3, VIRMA, and CBLL1 were positively correlated with Tcm and Th2 cell infiltration. Infiltration of DCs, Tcm and their derived cytotoxic T cells, along with Th2 cells, are generally considered to be protective factors for HCC (Foerster et al., 2018; Lawal et al., 2021), which may be related to changes in the balance between DC subsets or T effector cells and regulatory T cells in tumors (Lawal et al., 2021; Gao et al., 2007), suggesting that stratification of immune cell infiltration is the key to achieving effective treatments. Therefore, the interplay between the m^6A writer complex and tumor microenvironment may be an important mechanism for the tumorigenesis and progression of HCC. However, more specific mechanisms remain to be clarified.

CONCLUSION

In conclusion, our study systematically illustrated the expression changes and prognostic value of the m^6A writer complex in HCC. Expression of several specific complex components correlates with pathways involved in carcinogenesis, tumor development, and tumor metastasis. Furthermore, the m^6A writer complex may be involved in the regulation of immune cell infiltration and immune targets. Therefore, our findings may help to provide new insights available to improve the diagnosis, improve treatment design, and ultimately improve the prognosis of HCC. However, further experimental studies are needed to confirm these conclusions.

DATA AVAILABILITY STATEMENT

The original contributions presented in the study are included in the article/**Supplementary Material**, further inquiries can be directed to the corresponding author.

AUTHOR CONTRIBUTIONS

ZG, YD and XZ conceived and designed the study. ZG, YD, XZ and CW performed the analyses. CW supervised the study. All authors contributed to the article and approved the submitted version.

FUNDING

This work was supported by CAMS Innovation Fund for Medical Sciences (CIFMS No. 2016-I2M-1-001) and National Natural Science Foundation of China (81972314 and 81802463).

SUPPLEMENTARY MATERIAL

The Supplementary Material for this article can be found online at: https://www.frontiersin.org/articles/10.3389/fcell.2022.822011/full#supplementary-material

REFERENCES

Asplund, A., Edqvist, P.-H. D., Schwenk, J. M., and Pontén, F. (2012). Antibodies for Profiling the Human Proteome-The Human Protein Atlas as a Resource for Cancer Research. *Proteomics* 12 (13), 2067–2077. Epub 2012/05/25PubMed PMID: 22623277. doi:10.1002/pmic.201100504

Bauer, T., Trump, S., Ishaque, N., Thürmann, L., Gu, L., Bauer, M., et al. (2016). Environment-induced Epigenetic Reprogramming in Genomic Regulatory Elements in Smoking Mothers and Their Children. *Mol. Syst. Biol.* 12 (3), 861. Epub 2016/03/26PubMed PMID: 27013061; PubMed Central PMCID: PMCPMC4812527. doi:10.15252/msb.20156520

Cerami, E., Gao, J., Dogrusoz, U., Gross, B. E., Sumer, S. O., Aksoy, B. A., et al. (2012). The cBio Cancer Genomics Portal: An Open Platform for Exploring Multidimensional Cancer Genomics Data: Figure 1. *Cancer Discov.* 2 (5), 401–404. Epub 2012/05/17PubMed PMID: 22588877; PubMed Central PMCID: PMCPMC3956037. doi:10.1158/2159-8290.CD-12-0095

Chandrashekar, D. S., Bashel, B., Balasubramanya, S. A. H., Creighton, C. J., Ponce-Rodriguez, I., Chakravarthi, B. V. S. K., et al. (2017). UALCAN: A Portal for Facilitating Tumor Subgroup Gene Expression and Survival Analyses. *Neoplasia* 19 (8), 649–658. Epub 2017/07/22PubMed PMID: 28732212; PubMed Central PMCID: PMCPMC5516091. doi:10.1016/j.neo.2017.05.002

Chen, M., Wei, L., Law, C.-T., Tsang, F. H.-C., Shen, J., Cheng, C. L.-H., et al. (2018). RNA N6-Methyladenosine Methyltransferase-like 3 Promotes Liver Cancer Progression through YTHDF2-dependent Posttranscriptional Silencing of SOCS2. *Hepatology* 67 (6), 2254–2270. Epub 2017/11/25PubMed PMID: 29171881. doi:10.1002/hep.29683

Chen, Y., Peng, C., Chen, J., Chen, D., Yang, B., He, B., et al. (2019). WTAP Facilitates Progression of Hepatocellular Carcinoma via m6A-HuR-dependent Epigenetic Silencing of ETS1. *Mol. Cancer* 18 (1), 127. Epub 2019/08/24PubMed PMID: 31438961; PubMed Central PMCID: PMCPMC6704583. doi:10.1186/s12943-019-1053-8

Chin, C.-H., Chen, S.-H., Wu, H.-H., Ho, C.-W., Ko, M.-T., and Lin, C.-Y. (2014). cytoHubba: Identifying Hub Objects and Sub-networks from Complex Interactome. *BMC Syst. Biol.* 8 (Suppl. 4), S11. Epub 2014/12/19PubMed PMID: 25521941; PubMed Central PMCID: PMCPMC4290687. doi:10.1186/1752-0509-8-S4-S11

Choe, J., Lin, S., Zhang, W., Liu, Q., Wang, L., Ramirez-Moya, J., et al. (2018). mRNA Circularization by METTL3-eIF3h Enhances Translation and Promotes Oncogenesis. *Nature* 561 (7724), 556–560. Epub 2018/09/21PubMed PMID:

30232453; PubMed Central PMCID: PMCPMC6234840. doi:10.1038/s41586-018-0538-8

Cua, D. J., and Tato, C. M. (2010). Innate IL-17-producing Cells: the Sentinels of the Immune System. *Nat. Rev. Immunol.* 10 (7), 479–489. Epub 2010/06/19PubMed PMID: 20559326. doi:10.1038/nri2800

Doncheva, N. T., Morris, J. H., Gorodkin, J., and Jensen, L. J. (2019). Cytoscape StringApp: Network Analysis and Visualization of Proteomics Data. *J. Proteome Res.* 18 (2), 623–632. Epub 2018/11/20PubMed PMID: 30450911; PubMed Central PMCID: PMCPMC6800166. doi:10.1021/acs.jproteome.8b00702

Foerster, F., Hess, M., Gerhold-Ay, A., Marquardt, J. U., Becker, D., Galle, P. R., et al. (2018). The Immune Contexture of Hepatocellular Carcinoma Predicts Clinical Outcome. *Sci. Rep.* 8 (1), 5351. Epub 2018/03/31PubMed PMID: 29599491; PubMed Central PMCID: PMCPMC5876395. doi:10.1038/s41598-018-21937-2

Fujita, Y., Krause, G., Scheffner, M., Zechner, D., Leddy, H. E. M., Behrens, J., et al. (2002). Hakai, a C-cbl-like Protein, Ubiquitinates and Induces Endocytosis of the E-Cadherin Complex. *Nat. Cel Biol* 4 (3), 222–231. Epub 2002/02/12PubMed PMID: 11836526. doi:10.1038/ncb758

Gajewski, T. F., Schreiber, H., and Fu, Y.-X. (2013). Innate and Adaptive Immune Cells in the Tumor Microenvironment. *Nat. Immunol.* 14 (10), 1014–1022. Epub 2013/09/21PubMed PMID: 24048123; PubMed Central PMCID: PMCPMC4118725. doi:10.1038/ni.2703

Gao, J., Aksoy, B. A., Dogrusoz, U., Dresdner, G., Gross, B., Sumer, S. O., et al. (2013). Integrative Analysis of Complex Cancer Genomics and Clinical Profiles Using the cBioPortal. *Sci. Signal.* 6 (269), pl1. Epub 2013/04/04PubMed PMID: 23550210; PubMed Central PMCID: PMCPMC4160307. doi:10.1126/scisignal.2004088

Gao, Q., Qiu, S.-J., Fan, J., Zhou, J., Wang, X.-Y., Xiao, Y.-S., et al. (2007). Intratumoral Balance of Regulatory and Cytotoxic T Cells Is Associated with Prognosis of Hepatocellular Carcinoma after Resection. *Jco* 25 (18), 2586–2593. Epub 2007/06/20PubMed PMID: 17577038. doi:10.1200/JCO.2006.09.4565

Global Burden of Disease Cancer, C., Fitzmaurice, C., Abate, D., Abbasi, N., Abbastabar, H., Abd-Allah, F., et al. (2019). Global, Regional, and National Cancer Incidence, Mortality, Years of Life Lost, Years Lived with Disability, and Disability-Adjusted Life-Years for 29 Cancer Groups, 1990 to 2017: A Systematic Analysis for the Global Burden of Disease Study. *JAMA Oncol.* 5 (12), 1749–1768. Epub 2019/09/29PubMed PMID: 31560378; PubMed Central PMCID: PMCPMC6777271. doi:10.1001/jamaoncol.2019.2996

Gu, L., Frommel, S. C., Frommel, S. C., Oakes, C. C., Simon, R., Grupp, K., et al. (2015). BAZ2A (TIP5) Is Involved in Epigenetic Alterations in Prostate Cancer and its Overexpression Predicts Disease Recurrence. *Nat. Genet.* 47 (1), 22–30. Epub 2014/12/09PubMed PMID: 25485837. doi:10.1038/ng.3165

Gu, L., Wang, L., Chen, H., Hong, J., Shen, Z., Dhall, A., et al. (2020). CG14906 (Mettl4) Mediates m6A Methylation of U2 snRNA in Drosophila. *Cell Discov* 6, 44. Epub 2020/07/09PubMed PMID: 32637152; PubMed Central PMCID: PMCPMC7324582. doi:10.1038/s41421-020-0178-7

Guo, T., Duan, H., Chen, J., Liu, J., Othmane, B., Hu, J., et al. (2021). N6-Methyladenosine Writer Gene ZC3H13 Predicts Immune Phenotype and Therapeutic Opportunities in Kidney Renal Clear Cell Carcinoma. *Front. Oncol.* 11, 718644. Epub 2021/09/10PubMed PMID: 34497769; PubMed Central PMCID: PMCPMC8420859. doi:10.3389/fonc.2021.718644

Győrffy, B., Surowiak, P., Budczies, J., and Lánczky, A. (2013). Online Survival Analysis Software to Assess the Prognostic Value of Biomarkers Using Transcriptomic Data in Non-small-cell Lung Cancer. *PLoS One* 8 (12), e82241. Epub 2013/12/25PubMed PMID: 24367507; PubMed Central PMCID: PMCPMC3867325. doi:10.1371/journal.pone.0082241

Hänzelmann, S., Castelo, R., and Guinney, J. (2013). GSVA: Gene Set Variation Analysis for Microarray and RNA-Seq Data. *BMC Bioinformatics* 14, 7. Epub 2013/01/18PubMed PMID: 23323831; PubMed Central PMCID: PMCPMC3618321. doi:10.1186/1471-2105-14-7

Jin, D., Guo, J., Wu, Y., Du, J., Yang, L., Wang, X., et al. (2019). m6A mRNA Methylation Initiated by METTL3 Directly Promotes YAP Translation and Increases YAP Activity by Regulating the MALAT1-miR-1914-3p-YAP axis to Induce NSCLC Drug Resistance and metastasisA mRNA Methylation Initiated by METTL3 Directly Promotes YAP Translation and Increases YAP Activity by Regulating the MALAT1-miR-1914-3p-YAP axis to Induce NSCLC Drug Resistance and Metastasis. *J. Hematol. Oncol.* 12 (1), 135. Epub 2019/12/11PubMed PMID: 31818312; PubMed Central PMCID: PMCPMC6902496. doi:10.1186/s13045-019-0830-6

Lan, T., Li, H., Zhang, D., Xu, L., Liu, H., Hao, X., et al. (2019). KIAA1429 Contributes to Liver Cancer Progression through N6-methyladenosine-dependent post-transcriptional Modification of GATA3. *Mol. Cancer* 18 (1), 186. Epub 2019/12/21PubMed PMID: 31856849; PubMed Central PMCID: PMCPMC6921542. doi:10.1186/s12943-019-1106-z

Lawal, G., Xiao, Y., Rahnemai-Azar, A. A., Tsilimigras, D. I., Kuang, M., Bakopoulos, A., et al. (2021). The Immunology of Hepatocellular Carcinoma. *Vaccines* 9 (10), 1184. Epub 2021/10/27PubMed PMID: 34696292; PubMed Central PMCID: PMCPMC8538643. doi:10.3390/vaccines9101184

Li, H., Su, Q., Li, B., Lan, L., Wang, C., Li, W., et al. (2020). High Expression of WTAP Leads to Poor Prognosis of Gastric Cancer by Influencing Tumour-associated T Lymphocyte Infiltration. *J. Cel Mol Med* 24 (8), 4452–4465. Epub 2020/03/17PubMed PMID: 32176425; PubMed Central PMCID: PMCPMC7176877. doi:10.1111/jcmm.15104

Li, T., Fan, J., Wang, B., Traugh, N., Chen, Q., Liu, J. S., et al. (2017). TIMER: A Web Server for Comprehensive Analysis of Tumor-Infiltrating Immune Cells. *Cancer Res.* 77 (21), e108–e110. Epub 2017/11/03PubMed PMID: 29092952; PubMed Central PMCID: PMCPMC6042652. doi:10.1158/0008-5472.CAN-17-0307

Li, T., Hu, P.-S., Zuo, Z., Lin, J.-F., Li, X., Wu, Q.-N., et al. (2019). METTL3 Facilitates Tumor Progression via an m6A-igf2bp2-dependent Mechanism in Colorectal Carcinoma. *Mol. Cancer* 18 (1), 112. Epub 2019/06/25PubMed PMID: 31230592; PubMed Central PMCID: PMCPMC6589893. doi:10.1186/s12943-019-1038-7

Li, Z., Peng, Y., Li, J., Chen, Z., Chen, F., Tu, J., et al. (2020). N6-methyladenosine Regulates Glycolysis of Cancer Cells through PDK4. *Nat. Commun.* 11 (1), 2578. Epub 2020/05/24PubMed PMID: 32444598; PubMed Central PMCID: PMCPMC7244544. doi:10.1038/s41467-020-16306-5

Lin, S., Choe, J., Du, P., Triboulet, R., and Gregory, R. I. (2016). The M 6 A Methyltransferase METTL3 Promotes Translation in Human Cancer Cells. *Mol. Cel* 62 (3), 335–345. Epub 2016/04/28PubMed PMID: 27117702; PubMed Central PMCID: PMCPMC4860043. doi:10.1016/j.molcel.2016.03.021

Lin, X., Chai, G., Wu, Y., Li, J., Chen, F., Liu, J., et al. (2019). RNA m6A Methylation Regulates the Epithelial Mesenchymal Transition of Cancer Cells and Translation of Snail. *Nat. Commun.* 10 (1), 2065. Epub 2019/05/08PubMed PMID: 31061416; PubMed Central PMCID: PMCPMC6502834. doi:10.1038/s41467-019-09865-9

Liu, C.-J., Hu, F.-F., Xia, M.-X., Han, L., Zhang, Q., and Guo, A.-Y. (2018). GSCALite: a Web Server for Gene Set Cancer Analysis. *Bioinformatics* 34 (21), 3771–3772. Epub 2018/05/24PubMed PMID: 29790900. doi:10.1093/bioinformatics/bty411

Liu, J., Eckert, M. A., Harada, B. T., Liu, S.-M., Lu, Z., Yu, K., et al. (2018). m6A mRNA Methylation Regulates AKT Activity to Promote the Proliferation and Tumorigenicity of Endometrial cancerA mRNA Methylation Regulates AKT Activity to Promote the Proliferation and Tumorigenicity of Endometrial Cancer. *Nat. Cel Biol* 20 (9), 1074–1083. Epub 2018/08/30PubMed PMID: 30154548; PubMed Central PMCID: PMCPMC6245953. doi:10.1038/s41556-018-0174-4

Liu, M., Jiang, K., Lin, G., Liu, P., Yan, Y., Ye, T., et al. (2018). Ajuba Inhibits Hepatocellular Carcinoma Cell Growth via Targeting of β-catenin and YAP Signaling and Is Regulated by E3 Ligase Hakai through Neddylation. *J. Exp. Clin. Cancer Res.* 37 (1), 165. Epub 2018/07/26PubMed PMID: 30041665; PubMed Central PMCID: PMCPMC6057013. doi:10.1186/s13046-018-0806-3

Lu, M., Wu, J., Hao, Z.-W., Shang, Y.-K., Xu, J., Nan, G., et al. (2018). Basolateral CD147 Induces Hepatocyte Polarity Loss by E-Cadherin Ubiquitination and Degradation in Hepatocellular Carcinoma Progress. *Hepatology* 68 (1), 317–332. Epub 2018/01/23PubMed PMID: 29356040; PubMed Central PMCID: PMCPMC6055794. doi:10.1002/hep.29798

Ma, J. z., Yang, F., Zhou, C. c., Liu, F., Yuan, J. h., Wang, F., et al. (2017). METTL14 Suppresses the Metastatic Potential of Hepatocellular Carcinoma by Modulating N 6 -methyladenosine-dependent Primary MicroRNA Processing. *Hepatology* 65 (2), 529–543. Epub 2016/10/25PubMed PMID: 27774652. doi:10.1002/hep.28885

Melstrom, L., and Chen, J. (2020). RNA N6-Methyladenosine Modification in Solid Tumors: New Therapeutic Frontiers. *Cancer Gene Ther.* 27 (9), 625–633. Epub 2020/01/21PubMed PMID: 31956264. doi:10.1038/s41417-020-0160-4

Mering, C. v., Huynen, M., Jaeggi, D., Schmidt, S., Bork, P., and Snel, B. (2003). STRING: a Database of Predicted Functional Associations between Proteins. *Nucleic Acids Res.* 31 (1), 258–261. Epub 2003/01/10PubMed PMID: 12519996; PubMed Central PMCID: PMCPMC165481. doi:10.1093/nar/gkg034

Ping, X.-L., Sun, B.-F., Wang, L., Xiao, W., Yang, X., Wang, W.-J., et al. (2014). Mammalian WTAP Is a Regulatory Subunit of the RNA N6-Methyladenosine Methyltransferase. *Cell Res* 24 (2), 177–189. Epub 2014/01/11PubMed PMID: 24407421; PubMed Central PMCID: PMCPMC3915904. doi:10.1038/cr.2014.3

Rhodes, D. R., Yu, J., Shanker, K., Deshpande, N., Varambally, R., Ghosh, D., et al. (2004). ONCOMINE: a Cancer Microarray Database and Integrated Data-Mining Platform. *Neoplasia* 6 (1), 1–6. Epub 2004/04/08PubMed PMID: 15068665; PubMed Central PMCID: PMCPMC1635162. doi:10.1016/s1476-5586(04)80047-2

Ru, B., Wong, C. N., Tong, Y., Zhong, J. Y., Zhong, S. S. W., Wu, W. C., et al. (2019). TISIDB: an Integrated Repository portal for Tumor-Immune System Interactions. *Bioinformatics* 35 (20), 4200–4202. Epub 2019/03/25PubMed PMID: 30903160. doi:10.1093/bioinformatics/btz210

Saletore, Y., Meyer, K., Korlach, J., Vilfan, I. D., Jaffrey, S., and Mason, C. E. (2012). The Birth of the Epitranscriptome: Deciphering the Function of RNA Modifications. *Genome Biol.* 13 (10), 175. Epub 2012/11/02PubMed PMID: 23113984; PubMed Central PMCID: PMCPMC3491402. doi:10.1186/gb-2012-13-10-175

Shannon, P., Markiel, A., Ozier, O., Baliga, N. S., Wang, J. T., Ramage, D., et al. (2003). Cytoscape: a Software Environment for Integrated Models of Biomolecular Interaction Networks. *Genome Res.* 13 (11), 2498–2504. Epub 2003/11/05PubMed PMID: 14597658; PubMed Central PMCID: PMCPMC403769. doi:10.1101/gr.1239303

Shibata, T. (2021). Genomic Landscape of Hepatocarcinogenesis. *J. Hum. Genet.* 66 (9), 845–851. Epub 2021/05/08PubMed PMID: 33958712. doi:10.1038/s10038-021-00928-8

Śledź, P., and Jinek, M. (2016). Structural Insights into the Molecular Mechanism of the m6A Writer Complex. *eLife* 5 (September), e18434. doi:10.7554/eLife.18434

Steel, J. L., Kim, K. H., Dew, M. A., Unruh, M. L., Antoni, M. H., Olek, M. C., et al. (2010). Cancer-related Symptom Clusters, Eosinophils, and Survival in Hepatobiliary Cancer: an Exploratory Study. *J. Pain Symptom Manage.* 39 (5), 859–871. Epub 2010/05/18PubMed PMID: 20471546; PubMed Central PMCID: PMCPMC3127169. doi:10.1016/j.jpainsymman.2009.09.019

Su, R., Dong, L., Li, C., Nachtergaele, S., Wunderlich, M., Qing, Y., et al. (2018). R-2HG Exhibits Anti-tumor Activity by Targeting FTO/m6A/MYC/CEBPA Signaling. *Cell* 172 (1-2), 90–105. Epub 2017/12/19PubMed PMID: 29249359; PubMed Central PMCID: PMCPMC5766423. doi:10.1016/j.cell.2017.11.031

Tang, Z., Li, C., Kang, B., Gao, G., Li, C., and Zhang, Z. (2017). GEPIA: a Web Server for Cancer and normal Gene Expression Profiling and Interactive Analyses. *Nucleic Acids Res.* 45 (W1), W98–W102. Epub 2017/04/14PubMed PMID: 28407145; PubMed Central PMCID: PMCPMC5570223. doi:10.1093/nar/gkx247

Vasaikar, S. V., Straub, P., Wang, J., and Zhang, B. (2018). LinkedOmics: Analyzing Multi-Omics Data within and across 32 Cancer Types. *Nucleic Acids Res.* 46 (D1), D956–D963. Epub 2017/11/15PubMed PMID: 29136207; PubMed Central PMCID: PMCPMC5753188. doi:10.1093/nar/gkx1090

Villanueva, A. (2019). Hepatocellular Carcinoma. *N. Engl. J. Med.* 380 (15), 1450–1462. Epub 2019/04/11PubMed PMID: 30970190. doi:10.1056/NEJMra1713263

Wang, Q., Xie, H., Peng, H., Yan, J., Han, L., and Ye, G. (2021). ZC3H13 Inhibits the Progression of Hepatocellular Carcinoma through m6A-PKM2-Mediated Glycolysis and Enhances Chemosensitivity. *J. Oncol.* 2021, 1–15. Epub 2022/01/11PubMed PMID: 35003256; PubMed Central PMCID: PMCPMC8736703 publication of this paper. doi:10.1155/2021/1328444

Wang, Q., Zhang, Q., Li, Q., Zhang, J., and Zhang, J. (2021). Clinicopathological and Immunological Characterization of RNA M 6 A Methylation Regulators in Ovarian Cancer. *Mol. Genet. Genomic Med.* 9 (1), e1547. doi:10.1002/mgg3.1547

Wang, X., Feng, J., Xue, Y., Guan, Z., Zhang, D., Liu, Z., et al. (2016). Structural Basis of N6-Adenosine Methylation by the METTL3-METTL14 Complex. *Nature* 534 (7608), 575–578. Epub 2016/06/10PubMed PMID: 27281194. doi:10.1038/nature18298

Weng, C.-H., Chen, L.-Y., Lin, Y.-C., Shih, J.-Y., Lin, Y.-C., Tseng, R.-Y., et al. (2019). Epithelial-mesenchymal Transition (EMT) beyond EGFR Mutations Per Se Is a Common Mechanism for Acquired Resistance to EGFR TKI. *Oncogene* 38 (4), 455–468. Epub 2018/08/17PubMed PMID: 30111817. doi:10.1038/s41388-018-0454-2

Xiang, Y., Laurent, B., Hsu, C.-H., Nachtergaele, S., Lu, Z., Sheng, W., et al. (2017). RNA m6A Methylation Regulates the Ultraviolet-Induced DNA Damage Response. *Nature* 543 (7646), 573–576. Epub 2017/03/16PubMed PMID: 28297716; PubMed Central PMCID: PMCPMC5490984. doi:10.1038/nature21671

Xu, X., Tan, Y., Qian, Y., Xue, W., Wang, Y., Du, J., et al. (2019). Clinicopathologic and Prognostic Significance of Tumor-Infiltrating CD8+ T Cells in Patients with Hepatocellular Carcinoma. *Medicine (Baltimore)* 98 (2), e13923. Epub 2019/01/1210.1097/MD.0000000000013923. PubMed PMID: 30633166; PubMed Central PMCID: PMCPMC6336640. doi:10.1097/md.0000000000013923

Xu, Y., He, X., Deng, J., Xiong, L., Li, Y., Zhang, X., et al. (2021). Comprehensive Analysis of the Immune Infiltrates and PD-L1 of m6A RNA Methylation Regulators in Hepatocellular Carcinoma. *Front. Cel Dev. Biol.* 9, 681745. Epub 2021/07/20PubMed PMID: 34277622; PubMed Central PMCID: PMCPMC8277965. doi:10.3389/fcell.2021.681745

Yang, W., Soares, J., Greninger, P., Edelman, E. J., Lightfoot, H., Forbes, S., et al. (2013). Genomics of Drug Sensitivity in Cancer (GDSC): a Resource for Therapeutic Biomarker Discovery in Cancer Cells. *Nucleic Acids Res.* 41 (Database issue), D955–D961. Epub 2012/11/28PubMed PMID: 23180760; PubMed Central PMCID: PMCPMC3531057. doi:10.1093/nar/gks1111

Yang, Z., Yang, S., Cui, Y.-H., Wei, J., Shah, P., Park, G., et al. (2021). METTL14 Facilitates Global Genome Repair and Suppresses Skin Tumorigenesis. *Proc. Natl. Acad. Sci. USA* 118 (35), e2025948118. Epub 2021/08/29PubMed PMID: 34452996; PubMed Central PMCID: PMCPMC8536359. doi:10.1073/pnas.2025948118

Yu, G., Wang, L.-G., Han, Y., and He, Q.-Y. (2012). clusterProfiler: an R Package for Comparing Biological Themes Among Gene Clusters. *OMICS: A J. Integr. Biol.* 16 (5), 284–287. Epub 2012/03/30PubMed PMID: 22455463; PubMed Central PMCID: PMCPMC3339379. doi:10.1089/omi.2011.0118

Yu, J., Chen, M., Huang, H., Zhu, J., Song, H., Zhu, J., et al. (2018). Dynamic m6A Modification Regulates Local Translation of mRNA in Axons. *Nucleic Acids Res.* 46 (3), 1412–1423. Epub 2017/12/01PubMed PMID: 29186567; PubMed Central PMCID: PMCPMC5815124. doi:10.1093/nar/gkx1182

Yue, Y., Liu, J., Cui, X., Cao, J., Luo, G., Zhang, Z., et al. (2018). VIRMA Mediates Preferential m6A mRNA Methylation in 3′UTR and Near Stop Codon and Associates with Alternative Polyadenylation. *Cel Discov* 4, 10. Epub 2018/03/07PubMed PMID: 29507755; PubMed Central PMCID: PMCPMC5826926 Scientific Advisory Committee. The remaining authors declare that they have no conflict of interest. doi:10.1038/s41421-018-0019-0

Zaccara, S., Ries, R. J., and Jaffrey, S. R. (2019). Reading, Writing and Erasing mRNA Methylation. *Nat. Rev. Mol. Cel Biol* 20 (10), 608–624. Epub 2019/09/15PubMed PMID: 31520073. doi:10.1038/s41580-019-0168-5

Zhang, B., Gu, Y., and Jiang, G. (2020). Expression and Prognostic Characteristics of M6 A RNA Methylation Regulators in Breast Cancer. *Front. Genet.* 11, 604597. Epub 2020/12/29PubMed PMID: 33362863; PubMed Central PMCID: PMCPMC7758326. doi:10.3389/fgene.2020.604597

Zhang, B., Wu, Q., Li, B., Wang, D., Wang, L., and Zhou, Y. L. (2020). m6A Regulator-Mediated Methylation Modification Patterns and Tumor Microenvironment Infiltration Characterization in Gastric cancerA Regulator-Mediated Methylation Modification Patterns and Tumor Microenvironment Infiltration Characterization in Gastric Cancer. *Mol. Cancer* 19 (1), 53. Epub 2020/03/14PubMed PMID: 32164750; PubMed Central PMCID: PMCPMC7066851. doi:10.1186/s12943-020-01170-0

Zhang, C., Zhang, M., Ge, S., Huang, W., Lin, X., Gao, J., et al. (2019). Reduced m6A Modification Predicts Malignant Phenotypes and Augmented Wnt/PI3K-

Akt Signaling in Gastric Cancer. *Cancer Med.* 8 (10), 4766–4781. Epub 2019/06/28PubMed PMID: 31243897; PubMed Central PMCID: PMCPMC6712480. doi:10.1002/cam4.2360

Zhao, H., Xu, Y., Xie, Y., Zhang, L., Gao, M., Li, S., et al. (2021). m6A Regulators Is Differently Expressed and Correlated with Immune Response of Esophageal Cancer. *Front. Cel Dev. Biol.* 9. doi:10.3389/fcell.2021.650023

Zhou, Y., Zhou, B., Pache, L., Chang, M., Khodabakhshi, A. H., Tanaseichuk, O., et al. (2019). Metascape Provides a Biologist-Oriented Resource for the Analysis of Systems-Level Datasets. *Nat. Commun.* 10 (1), 1523. Epub 2019/04/05PubMed PMID: 30944313; PubMed Central PMCID: PMCPMC6447622. doi:10.1038/s41467-019-09234-6

Zhu, D., Zhou, J., Zhao, J., Jiang, G., Zhang, X., Zhang, Y., et al. (2019). ZC3H13 Suppresses Colorectal Cancer Proliferation and Invasion via Inactivating Ras-ERK Signaling. *J. Cel Physiol* 234 (6), 8899–8907. Epub 2018/10/13PubMed PMID: 30311220. doi:10.1002/jcp.27551

Conflict of Interest: The authors declare that the research was conducted in the absence of any commercial or financial relationships that could be construed as a potential conflict of interest.

Publisher's Note: All claims expressed in this article are solely those of the authors and do not necessarily represent those of their affiliated organizations, or those of the publisher, the editors and the reviewers. Any product that may be evaluated in this article, or claim that may be made by its manufacturer, is not guaranteed or endorsed by the publisher.

Copyright © 2022 Gu, Du, Zhao and Wang. This is an open-access article distributed under the terms of the Creative Commons Attribution License (CC BY). The use, distribution or reproduction in other forums is permitted, provided the original author(s) and the copyright owner(s) are credited and that the original publication in this journal is cited, in accordance with accepted academic practice. No use, distribution or reproduction is permitted which does not comply with these terms.

frontiers in Cell and Developmental Biology

REVIEW
published: 08 March 2022
doi: 10.3389/fcell.2022.828683

Roles of RNA Modifications in Diverse Cellular Functions

Emma Wilkinson[1,2], *Yan-Hong Cui*[1] *and Yu-Ying He*[1,2]*

[1]Department of Medicine, Section of Dermatology, University of Chicago, Chicago, IL, United States, [2]Committee on Cancer Biology, University of Chicago, Chicago, IL, United States

Chemical modifications of RNA molecules regulate both RNA metabolism and fate. The deposition and function of these modifications are mediated by the actions of writer, reader, and eraser proteins. At the cellular level, RNA modifications regulate several cellular processes including cell death, proliferation, senescence, differentiation, migration, metabolism, autophagy, the DNA damage response, and liquid-liquid phase separation. Emerging evidence demonstrates that RNA modifications play active roles in the physiology and etiology of multiple diseases due to their pervasive roles in cellular functions. Here, we will summarize recent advances in the regulatory and functional role of RNA modifications in these cellular functions, emphasizing the context-specific roles of RNA modifications in mammalian systems. As m^6A is the best studied RNA modification in biological processes, this review will summarize the emerging advances on the diverse roles of m^6A in cellular functions. In addition, we will also provide an overview for the cellular functions of other RNA modifications, including m^5C and m^1A. Furthermore, we will also discuss the roles of RNA modifications within the context of disease etiologies and highlight recent advances in the development of therapeutics that target RNA modifications. Elucidating these context-specific functions will increase our understanding of how these modifications become dysregulated during disease pathogenesis and may provide new opportunities for improving disease prevention and therapy by targeting these pathways.

Keywords: m^6A, m^5C, m^1A, epitranscriptomics, cellular functions, therapeutics

OPEN ACCESS

Edited by:
Chengqi Yi,
Peking University, China

Reviewed by:
Zhe Liang,
Chinese Academy of Agricultural Sciences, China
Michael James Holmes,
Indiana University, United States
Adam Heck,
Fred Hutchinson Cancer Research Center, United States

***Correspondence:**
Yu-Ying He
yyhe@medicine.bsd.uchicago.edu

Specialty section:
This article was submitted to Epigenomics and Epigenetics, a section of the journal Frontiers in Cell and Developmental Biology

Received: *03 December 2021*
Accepted: *14 February 2022*
Published: *08 March 2022*

Citation:
Wilkinson E, Cui Y-H and He Y-Y (2022) Roles of RNA Modifications in Diverse Cellular Functions. Front. Cell Dev. Biol. 10:828683. doi: 10.3389/fcell.2022.828683

INTRODUCTION

Many RNA modifications are reversible modifications that are deposited onto RNA molecules, including mRNAs, tRNAs, rRNAs, and non-coding RNAs. To date, over 100 RNA modifications have been identified, including m^6A, m^5C, and m^1A on mRNA (Roundtree et al., 2017). Of these modifications, N^6-methyladenosine (m^6A) is the most abundant internal mRNA modification (Roundtree et al., 2017). Since m^6A is the best-studied mRNA modification, we will focus on the cellular functions of m^6A in mammalian systems in this review. Other RNA modifications, such as m^5C and m^1A, have been studied in the context of cellular processes as well, and will be summarized here. The role of m^6A and other RNA modifications in non-mammalian systems, including plants and yeast, is beyond the scope of this review and is detailed elsewhere (Schwartz et al., 2013; Shen et al., 2019; Yue et al., 2019).

RNA modifications are deposited onto, and erased from, RNA molecules through the actions of writer and eraser enzymes. m^6A writers and cofactors include METTL3, METTL14, WTAP, VIRMA/KIAA1429, RBM15/15B, ZC3H13, and METTL16 (Yang et al., 2018). Together,

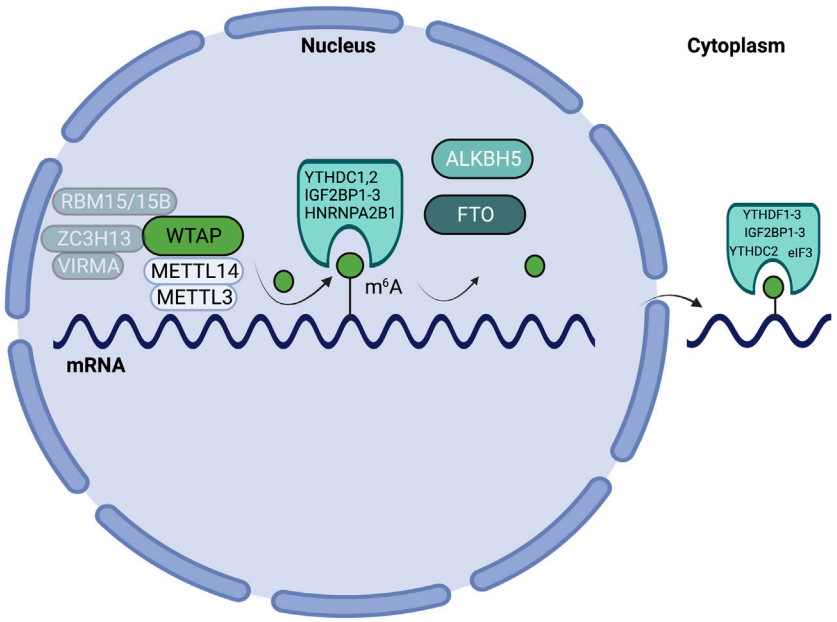


FIGURE 1 | Schematic highlighting m^{6}A writers, erasers, and readers on mRNA. m^{6}A patterning on mRNA is mediated by the actions of writers (METTL3, METTL14, WTAP, VIRMA/KIAA1429, RBM15/15B, ZC3H13), erasers (ALKBH5, FTO), and reader enzymes (YTHDF1-3, YTHDC1/2, IGF2BP1-3, HNRNPA2B1, and eIF3).

METTL3, METTL14, WTAP, VIRMA/KIAA1429, RBM15/15B, and ZC3H13 make up the methyltransferase complex (MTC) (Yang et al., 2018). Within the MTC, METTL3 serves as the catalytic subunit, while METTL14 serves as the RNA-binding subunit (Yang et al., 2018). m^{6}A erasers include FTO and ALKBH5 (Yang et al., 2018). RNA modifications influence various mechanisms of RNA metabolism, including nuclear processing, mRNA decay, and translation, through the action of reader enzymes (Roundtree et al., 2017). m^{6}A readers include YTHDF1-3, YTHDC1-2, IGF2BP1-3, HNRNPA2B1, and eIF3 (Meyer et al., 2015; Yang et al., 2018). m^{6}A mRNA writer, eraser and reader proteins are highlighted in **Figure 1**. While the writers and erasers can install or remove modifications in RNAs, it is the regulatory effect of the readers that ultimately controls the RNA fate and gene expression.

Another modification on mRNA, tRNA, and other non-coding RNAs, is 5-methylcytosine (m^{5}C). m^{5}C writers include DNMT2 and the NSUN (NSUN1-7) family proteins (Xue et al., 2020). The NSUN proteins contain an RNA recognition motif and a catalytic core that houses S-adenosylmethionine (SAM) (Bohnsack et al., 2019). Similarly, DNMT2 contains a catalytic site and a SAM binding site (Xue et al., 2020). The detailed biochemical mechanisms of how m^{5}C methyltransferases mediate methyl group transfers are discussed elsewhere (Bohnsack et al., 2019). m^{5}C readers, or m^{5}C binding-proteins, include ALYFREF and YBX1 (Xue et al., 2020). The TET family of enzymes have been hypothesized to serve as m^{5}C erasers (Xue et al., 2020). The function of m^{5}C in regulating RNA metabolism and expression is summarized elsewhere (Xue et al., 2020).

In addition to m^{6}A and m^{5}C, N^1-methyladenosine (m^{1}A) is another modification found on mRNA, tRNA, rRNA, and non-coding RNA (Xiong et al., 2018). m^{1}A writers include TRMT10C, TRMT6, TRMT61A, and TRMT61B (Xiong et al., 2018). TRMT6/TRMT61A form a heterotetrameric complex wherein TRMT61A functions as the catalytic subunit and TRMT6 is required for its methyltransferase function (Shi et al., 2020; Graille, 2022). m^{1}A erasers include ALKBH1 and ALKBH3 (Xiong et al., 2018).

Other RNA modification writer, eraser and reader enzymes are discussed elsewhere (Esteve-Puig et al., 2020). Elucidating the role of RNA modifications in mediating the RNA metabolism of diverse RNA species remains an active area of research.

RNA modifications, and their respective writer, eraser, and reader proteins, also play a role in a number of cellular functions. Here, we summarize the role of RNA modifications in such cellular processes as cell death, proliferation, differentiation, migration, metabolism, autophagy, and liquid-liquid phase separation in mammalian systems. Additionally, we also discuss the cell-type specific targets of these enzymes within these cellular processes.

Due to the pervasive roles of RNA modifications in numerous cellular functions, dysregulated RNA modifications have contributed to the pathogenesis of many diseases and can serve as attractive therapeutic targets due to the reversible nature of these modifications. The role of RNA modifications in diseases is covered in detail elsewhere (Wilkinson et al., 2021). Increasing our knowledge of RNA modifications in cellular processes will increase our understanding of the roles that RNA modifications play in disease etiology and will aid in

identifying new therapeutic targets. Clinical success of therapeutics targeting RNA modifications has not been reached and may reflect an incomplete understanding of the role that these modifications play in cellular functions.

THE ROLE OF m^{6}A IN DIVERSE CELLULAR FUNCTIONS

The writer, eraser, and reader proteins that regulate m^{6}A have been well studied in several cellular processes. Of the writer proteins, we will focus on the role of METTL3 and METTL14 in cellular functions, as they are best studied in cellular functions. The role of WTAP and VIRMA is summarized as well.

Cell Death

Apoptosis is a mechanism of programmed cell death (Elmore, 2007). This process involves coordination and communication across intracellular signaling pathways that ultimately result in the cellular decision to undergo cell death (Elmore, 2007). Apoptosis is initiated in response to pathogens or cellular stressors, immune stimulation, and within embryonic development (Elmore, 2007; Yan et al., 2020). While apoptosis is not the sole mechanism of cell death, it is the best-studied mechanism in the context of m^{6}A. The role of m^{6}A in specialized forms of cell death remains an active area of research.

Writers

The m^{6}A writer METTL3 can inhibit apoptosis, as several studies have shown that decreased *Mettl3* expression and methyltransferase activity resulted in increased apoptosis. As previously mentioned, coordinated apoptosis is required for embryonic development (Elmore, 2007; Yan et al., 2020). Accordingly, knockdown of *Mettl3* resulted in decreased m^{6}A levels, which increased the mRNA half-lives of neuronal apoptosis-associated genes, including *Dapk1*, *Fadd*, and *Ngfr*, in mouse cerebral granular cells (CGCs) (Wang C.-X. et al., 2018). Increased mRNA half-lives of these genes led to increased apoptosis in CGCs and contributed to severe developmental defects in mouse cerebella (Wang C.-X. et al., 2018).

Furthermore, several recent studies have established that METTL3 may play an oncogenic role in cell death by negatively regulating and reducing the translation of apoptosis-associated proteins, thereby promoting cell survival (Vu et al., 2017; Choe et al., 2018; Huang et al., 2020). Accordingly, knockdown of *Mettl3* resulted in increased expression of pro-apoptotic proteins in several cancer cell lines, emphasizing that METTL3 can function as a negative regulator of apoptosis (Vu et al., 2017; Zhou et al., 2020). In the MOLM-13 leukemia cell line, knockdown of *Mettl3* increased protein expression of pro-apoptotic proteins CASP3, CASP7, and BIM (Vu et al., 2017). Expression of CASP3 and BAX, other pro-apoptotic proteins, were also increased in *Mettl3* knockdown-osteosarcoma cell lines (Zhou et al., 2020). While it is unclear whether METTL3 regulates apoptosis in an m^{6}A-dependent manner, both studies provide evidence that METTL3 may inhibit apoptosis by regulating BCL-2 family proteins and caspase expression (Vu et al., 2017; Zhou et al., 2020). Knockdown of *Mettl3* in prostate cancer cells also increased protein expression of pro-apoptotic proteins BAK and BAX, CASP3 and CASP7 activity, and PARP cleavage (Cai et al., 2019). Additionally, knockdown of *Mettl3* in prostate cancer cells decreased protein expression of anti-apoptotic genes BCL-2 and BCL-XL (Cai et al., 2019). Furthermore, knockdown of *Mettl3* decreased expression of GLI1, a component of the Sonic hedgehog (SHH) signaling pathway, which prostate cancer cells are dependent on for survival (Regl et al., 2002; Chen et al., 2011; Cai et al., 2019). Due to prostate cancer cells' dependence on SHH signaling, decreased expression of GLI1 deprived prostate cancer cells of SHH signaling and forced apoptosis (Cai et al., 2019). METTL3 regulated the expression of GLI1 in an m^{6}A-dependent manner, as expression of GLI1 was rescued by the re-expression of wild-type, but not catalytically-inactive mutant, METTL3 (Cai et al., 2019). In gastric cancer, METTL3 promoted the mRNA stability of *Sec62*, which functions as a negative regulator of apoptosis, in an m^{6}A/IGF2BP1 -dependent manner (He et al., 2019). Increased *Sec62* mRNA stability and expression subsequently lead to decreased apoptosis and increased gastric cancer cell survival (He et al., 2019). The role of METTL3 in apoptosis is summarized in **Figure 2**.

In contrast, the role of METTL14 in mediating apoptosis is not as widely explored and presents an area of research that requires future study. One study found that knockdown of *Mettl14* promoted apoptosis in human AML cell lines (Weng et al., 2018). Mechanistically, METTL14 was found to promote cell survival by promoting the mRNA stability and translation of pro-survival proteins MYB and MYC in an m^{6}A-dependent manner (Weng et al., 2018). Therefore, in the absence of METTL14, MYB and MYC expression was decreased, leading to the induction of apoptosis (Weng et al., 2018).

Few studies have explored the role of m^{6}A writer-associated protein WTAP in cell death. One study found that WTAP expression was increased upon exposure to hypoxia/reoxygenation (H/R), resulting in the induction of ER stress and apoptosis in cardiomyocyte cells (Wang J. et al., 2021). Accordingly, H/R exposure in *Wtap* knockdown cells abrogated the induction of ER stress and apoptosis, suggesting that WTAP may regulate these processes upon H/R exposure (Wang J. et al., 2021). Mechanistically, WTAP was found to promote the mRNA stability of ER stress-response gene, *Atf4*, in an m^{6}A-dependent manner (Wang J. et al., 2021).

VIRMA, another m^{6}A writer-associated protein, has not been well-studied in the context of cell death. VIRMA has been found to serve an oncogenic role in several cancers, and was found to promote resistance to apoptosis in HCC (Lan et al., 2019). Mechanistically, VIRMA mediated the deposition of m^{6}A onto the 3′-untranslated region (UTR) of *Gata3*, a tumor suppressor, resulting in decreased GATA3 expression and promoted resistance to apoptosis (Lan et al., 2019). The oncogenic role of VIRMA in several cancers is covered elsewhere in detail (Zhu W. et al., 2021).

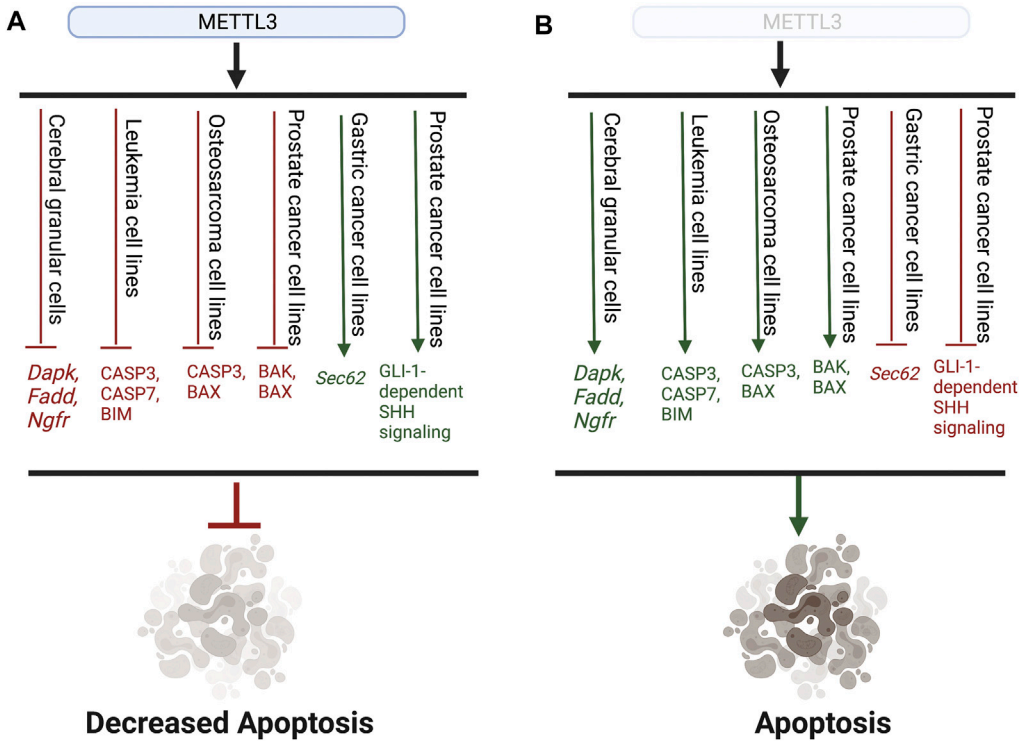


FIGURE 2 | Representative schematic highlighting the role of METTL3 in apoptosis. **(A)** METTL3 prohibits the expression of both pro-apoptotic genes and proteins (red) as well as promotes the expression of anti-apoptotic genes and pathways (green), leading to overall decreased apoptosis. **(B)** Without METTL3 expression, pro-apoptotic genes and proteins are expressed (green), while anti-apoptotic pathways are inhibited, leading to the induction of apoptosis.

Erasers

The role of the m^{6}A eraser ALKBH5 in apoptosis is cell-type dependent. *Alkbh5*-deficient mice exhibited increased apoptosis and developmental defects, potentially through a p53-mediated mechanism that is not entirely understood (Zheng et al., 2013). Conversely, *Alkbh5* knockdown in human ovarian granulosa (hGCs) cells had no effect on the apoptosis rate; rather, knockdown of *Fto* resulted in increased apoptosis in hGCs (Ding et al., 2018).

The role of FTO in apoptosis may also be cell-type-dependent. In leukemia, FTO is preferentially inhibited by R-2-hydroxyglutarate (R-2HG), an oncometabolite produced by mutant IDH1/2 enzymes (Ye et al., 2013; Su et al., 2018). *Fto* depletion decreased the mRNA stability and mRNA expression of downstream targets *Myc* and *Cebpa* through increased m^{6}A accumulation (Su et al., 2018). Decreased expression of *Myc* and *Cebpa* resulted in decreased expression of downstream MYC targets, including the E2F transcription factors, which are major regulators of cell cycle, thereby preventing cells from entering the cell cycle and forcing apoptosis or cell cycle arrest (Su et al., 2018). The trend wherein knockdown of *Fto* resulted in increased apoptosis was also seen in breast cancer and melanoma, suggesting that FTO may also serve an oncogenic function in these cancers by inhibiting apoptosis (Yang S. et al., 2019; Niu et al., 2019). In breast cancer, FTO mediated the demethylation of m^{6}A at the 3′-UTR of *Bnip3*, a pro-apoptotic gene, resulting in YTHDF2-mediated degradation of the *Bnip3* transcript (Niu et al., 2019). In melanoma, FTO promoted resistance to IFN γ-mediated cell death through m^{6}A demethylation of pro-tumorigenic genes *Pdcd-1*, *Cxcr4*, and *Sox10* (Yang S. et al., 2019). Demethylation of *Pdcd-1*, *Cxcr4*, and *Sox10* prevented downstream YTHDF2-mediated mRNA decay, resulting in increased expression of these melanoma-promoting genes (Yang S. et al., 2019).

Readers

Few studies have examined the role of only m^{6}A readers in mediating cell death. One study found that YTHDF2 negatively regulates apoptosis in TNBC (Einstein et al., 2021). Mechanistically, YTHDF2 was found to mediate the degradation of the *Prss23* mRNA transcript, a gene involved in translation, in an m^{6}A-dependent manner (Einstein et al., 2021). More generally, YTHDF2-mediated mRNA decay provides a mechanism by which to control the number of translated mRNAs by degrading mRNA transcripts, therefore resulting in translational control (Einstein et al., 2021). Knockdown of *Ythdf2* subsequently lead to an increase in PRSS23 expression and protein translation, triggering ER stress and inducing proteotoxic cell death (Einstein et al., 2021). Furthermore, in chondrocytes, YTHDF1 was found to negatively regulate apoptosis by promoting the mRNA stability of anti-apoptotic *Bcl-2* in a METTL3/m^{6}A-dependent manner (He et al., 2022).

While significant research efforts have been made to establish the role of RNA modifications in cell death, there remain significant gaps in knowledge surrounding this topic. Compelling evidence suggests a critical role of m^{6}A RNA methylation in other forms of cell death. For example, *Guo et al.* have recently established that m^{6}A may regulate macrophage pyroptosis, an inflammation-induced form of cell death, in circular RNAs in patients with acute coronary syndrome (Bergsbaken et al., 2009; Guo et al., 2020). However, the contribution of the m^{6}A machinery in this cellular process remains to be investigated.

Proliferation

The role of m^{6}A in regulating cellular proliferation has been best-studied in the context of cancer. Accordingly, m^{6}A writers, erasers, and readers may represent viable therapeutic targets for their role in promoting cell proliferation.

Writers

While the m^{6}A writer METTL3 has been well-studied within the context of apoptosis, METTL3 has been found to either promote or inhibit cellular proliferation, depending on the cellular context.

METTL3 was shown to inhibit cellular proliferation in endometrial cancer, as METTL3-mediated m^{6}A promoted the translation of PHLPP2, a negative regulator of pro-proliferative AKT signaling (Liu et al., 2018). Accordingly, knockdown of *Mettl3* resulted in increased cellular proliferation through decreased m^{6}A-dependent translation of PHLPP2, thereby promoting AKT signaling (Liu et al., 2018). Furthermore, in renal cell carcinoma (RCC), decreased *Mettl3* expression resulted in increased proliferation through induction of the PI3K/AKT/mTOR pathway (Li X. et al., 2017). Whether the activation of the PI3K/AKT/mTOR pathway upon *Mettl3* knockdown is m^{6}A-dependent was not explored (Li X. et al., 2017).

However, in several other cancer cell types, METTL3 was shown to promote cell proliferation. In colorectal cancer, METTL3 promoted GLUT1 translation in an m^{6}A-dependent manner, which resulted in downstream activation of mTORC1 and increased cell survival and proliferation (Chen et al., 2021). In hepatoblastoma cells, increased METTL3 activity resulted in increased m^{6}A deposition on *Ctnnb1*, leading to aberrant activation of the WNT/CTNNB1 pathway, which promoted hepatoblastoma cell growth (Liu et al., 2019). Another study in hepatocellular carcinoma (HCC) cells found that METTL3 promoted proliferation by inhibiting the expression of SOCS2, a transcription factor that can negatively regulate cell proliferation, through m^{6}A-dependent/YTHDF2-mediated mRNA degradation (Chen M. et al., 2018). Furthermore, in breast cancer cells, METTL3 was found to participate in a feedback loop with HBXIP, a co-factor of anti-apoptotic protein SURVIVIN, wherein HBXIP up-regulated METTL3 expression by suppressing METTL3 inhibitor *let-7g*, an miRNA (Garcia-Saez et al., 2011; Cai et al., 2018). Increased METTL3 expression then further promoted HBXIP expression in an m^{6}A-dependent manner and drove cell proliferation (Cai et al., 2018). However, whether METTL3-mediated m^{6}A on *Hbxip* promotes mRNA stability or translation was not explored (Cai et al., 2018). In bladder cancer, METTL3 promoted the m^{6}A-mediated maturation of pri-miR221/222, a PTEN antagonist, resulting in loss of cell cycle control and increased proliferation (Han et al., 2019). Similarly, METTL3 also drove proliferation in ovarian cancer through regulation of the receptor tyrosine kinase AXL; however, the regulatory mechanism by which METTL3 up-regulates AXL was not established (Hua et al., 2018). While the role of METTL3 in promoting proliferation in many cancer types has been well-established, the role of METTL3 in pancreatic cancer proliferation remains controversial as two independent studies found contrasting roles for METTL3 in promoting pancreatic cancer cell proliferation (Taketo et al., 2018; Xia et al., 2019). Authors of these studies reconcile differences in results based on differences in proliferation assays and cell lines used (Taketo et al., 2018; Xia et al., 2019).

Other m^{6}A writer co-factors have also been found to regulate cellular proliferation in a context-dependent manner. METTL14 expression was found to be decreased in colorectal cancer patients, and *Mettl14* knockdown *in vitro* resulted in decreased m^{6}A deposition on downstream target *Xist*, a long non-coding RNA (lncRNA) that has been found to promote proliferation (Yang et al., 2020). Decreased m^{6}A on *Xist* prevented YTHDF2-mediated mRNA degradation, resulting in increased *Xist* expression and increased cell proliferation (Yang et al., 2020). Similarly, in gastric cancer, METTL14 decreased cell proliferation by negatively regulating the pro-proliferative PI3K/AKT/mTOR pathway, emphasizing the cell-type-specific role of METTL14 in this cellular process (Liu X. et al., 2021). Whether METTL14 regulates the PI3K/AKT/mTOR pathway in an m^{6}A-dependent manner remains unclear (Liu X. et al., 2021). METTL14 can also promote cell proliferation. In breast cancer, METTL14 was recruited by oncogenic lncRNA *LINC00942* to increase the m^{6}A-mediated mRNA stability and protein expression of two downstream targets, CXCR4 and CYP1B1, which resulted in increased cell proliferation and tumorigenesis (Sun et al., 2020). In AML, METTL14 promoted cell survival and proliferation by regulating the mRNA stability and translation of two pro-proliferative downstream targets, MYB and MYC, in an m^{6}A-dependent manner (Weng et al., 2018). In skin cancer, METTL14 was also found to promote cell proliferation, as knockdown of *Mettl14* in human keratinocytes resulted in decreased cell proliferation; however, the mechanism by which METTL14 promotes proliferation in this context remains unclear (Yang Z. et al., 2021).

WTAP, another m^{6}A writer co-factor, has been found to promote proliferation. However, studies examining the role of WTAP in regulating proliferation do not detail whether WTAP promotes proliferation in an m^{6}A-dependent manner. In renal cell carcinoma (RCC), WTAP promoted the mRNA stability of *Cdk2*, a regulator of cell cycle control over the G1/S and S/G2 transition, by directly binding to the *Cdk2* transcript at the 3′-UTR (Tang et al., 2018). Furthermore, in primary AML patient samples and AML cell lines, reverse phase protein array (RPPA) analysis revealed that WTAP is positively associated with pro-proliferative cyclins and HSP90, as well as anti-apoptotic proteins, such as BCL-2 (Bansal et al., 2014). The mechanism by which WTAP regulates the expression of these pro-proliferative proteins, and whether this regulation is

m^{6}A-dependent, was not explored in this study (Bansal et al., 2014).

Additionally, VIRMA was found to promote non-small cell lung cancer (NSCLC) and increased NSCLC proliferation *in vitro* and *in vivo* (Xu et al., 2021). Mechanistically, VIRMA promoted the mRNA decay of tumor suppressor *Dapk3* through an m^{6}A-dependent YTHDF2/YTHDF3-mediated mechanism (Xu et al., 2021). Furthermore, VIRMA was found to promote breast cancer progression by promoting the mRNA stability of *Cdk1* in an m^{6}A-independent manner (Qian et al., 2019).

Erasers

The pro-proliferative role of the m^{6}A eraser FTO is well-studied within the context of cancer. In leukemia, FTO promoted the proliferation of AML cells by reducing m^{6}A levels at the 3′-UTR of *Asb2* and 3′ and 5′-UTR of *Rara*, two mediators of hematopoiesis and differentiation, resulting in decreased ASB2 and RARA protein expression (Li Z. et al., 2017). In melanoma, FTO promoted cell proliferation and overall tumorigenicity by demethylating m^{6}A on melanoma-promoting genes *Pdcd1*, *Cxcr4*, and *Sox10* (Yang S. et al., 2019). Furthermore, exposure to arsenic, a known human carcinogen, resulted in increased FTO stability and abundance in human keratinocytes, ultimately leading to increased proliferation and tumorigenesis (Cui et al., 2021). Furthermore, FTO and MYC have also been found to cooperate to drive cell proliferation in both pancreatic and cervical cancer (Tang et al., 2019; Zou et al., 2019). In pancreatic cancer, FTO mediated the m^{6}A demethylation of the *c-Myc* transcript, resulting in increased c-MYC expression (Tang et al., 2019). In cervical cancer, FTO was found to promote MYC translation; however, whether this mechanism was m^{6}A-dependent was not established (Zou et al., 2019). FTO also promoted the proliferation of NSCLC cells by demethylating and increasing the mRNA stability of the ubiquitinase *Usp7*, resulting in increased USP7 protein expression (Li et al., 2019). Future studies are needed to define the role of USP7 in mediating cell proliferation (Li et al., 2019).

In addition to FTO, m^{6}A eraser ALKBH5 drove proliferation in glioblastoma stem cells by demethylating nascent mRNA transcripts of *Foxm1*, a transcription factor involved in cell-cycle control and proliferation, resulting in increased FOXM1 expression and activity in an m^{6}A-dependent manner (Zona et al., 2014; Zhang S. et al., 2017).

Readers

The m^{6}A reader YTHDF2 promotes cell proliferation across different cell types and through distinct mechanisms. In pancreatic cancer, YTHDF2 promoted cell growth through activation of the AKT/GSK3β/CCND1 pathway (Chen et al., 2017). However, it is unclear whether YTHDF2 mediates pancreatic cancer growth in an m^{6}A-dependent manner (Chen et al., 2017). In leukemia, YTHDF2 increased cell proliferation by promoting the m^{6}A-dependent mRNA decay of *Wee1*, which regulates mitotic entry and serves as a negative cell-cycle regulator (Fei et al., 2020).

Additionally, PRRC2A, an m^{6}A-binding protein, promoted the proliferation of oligodendrocytes, a class of glial cells found in the brain and central nervous system, by binding and stabilizing the *Olig2* mRNA transcript in an m^{6}A-dependent manner (Wu et al., 2019).

While the role of m^{6}A in proliferation is widely studied in the context of cancer, cell proliferation is critical for other biological processes, such as wound repair and development, and is dysregulated in many diseases. Future studies are needed to address the role of m^{6}A in proliferation in these contexts.

Senescence

Senescence is a cellular mechanism wherein cells permanently undergo cell cycle arrest in response to cellular stress or other stimuli (Kumari and Jat, 2021). Intracellularly, senescent cells undergo metabolic and genomic changes that promote cell survival, yet in a growth-arrested state (Kumari and Jat, 2021). Extracellularly, senescent cells communicate with neighboring cells through a variety of secreted factors, including cytokines and chemokines, and assume a senescence-associated secretory phenotype (SASP) (Kumari and Jat, 2021). The role of m^{6}A in senescence has been studied in a variety of contexts, including tumorigenesis and aging, and is reviewed in detail elsewhere (Casella et al., 2019). In this section, we will summarize recent advances on the role of m^{6}A in senescence.

Writers

Liu et al. established that the m^{6}A writers METTL3 and METTL14 promoted SASP in lung embryonic fibroblasts in an m^{6}A-independent manner (Liu P. et al., 2021). During cellular senescence, METTL14 was found to localize to enhancer subunits, while METTL3 localized to promoters of SASP genes (Liu P. et al., 2021). Interestingly, WTAP was found to be required for the nuclear localization of METTL3 and METTL14 during senescence (Liu P. et al., 2021). However, METTL3 may function to inhibit senescence in human mesenchymal stem cells (hMSCs), as knockdown of *Mettl3* in hMSCs resulted in accelerated senescence (Wu et al., 2020). Overexpression of *Mettl3* in hMSCs reversed the phenotype seen in *Mettl3*-deficient hMSCs and delayed senescence induction through m^{6}A/IGF2BP2-mediated stabilization of the pro-proliferative gene *Mis12* (Wu et al., 2020). Furthermore, in human nucleus pulposus cells, METTL14 positively regulated TNFα-induced cellular senescence by promoting the maturation of *miR-34a-5p*, which inhibits SIRT1, a negative regulator of senescence (Zhu H. et al., 2021). However, the role of *miR-34a-5p* in senescence is not completely understood.

Erasers

The m^{6}A eraser FTO has been found to serve as a negative regulator of senescence in various contexts. Accordingly, FTO negatively regulated cellular senescence in granulosa-cell-induced ovarian aging in an m^{6}A-dependent manner (Jiang et al., 2021). In this context, expression of catalytically inactive mutant FTO, which lacks demethylase activity, increased m^{6}A on the 3′-UTR of *Fos*, a transcription factor that promotes aging, preventing the m^{6}A-mediated degradation of *Fos* mRNA and increasing FOS translation (Jiang et al., 2021). Similar deactivating mutations in FTO resulted in increased senescence in skin fibroblasts (Boissel

et al., 2009). While the mechanism by which FTO inhibits senescence was not delineated, these studies suggest that the demethylase activity of FTO is required to inhibit senescence (Boissel et al., 2009; Jiang et al., 2021).

Readers

The role of readers in cellular senescence is not well-studied. In human ovarian epithelial cells, RAS activation resulted in increases in Reactive Oxygen Species (ROS), which led to decreased expression of YTHDF2 (Zhu et al., 2020). Decreased expression of YTHDF2, which functions to mediate mRNA decay, resulted in downstream activation of the MAPK pathway and prevented the mRNA decay of *Map2k4* and *Map4k4* (Zhu et al., 2020). Activation of the MAPK pathway then led to downstream activation of NF-κB signaling pathways, resulting in the induction of SASP and senescence (Zhu et al., 2020).

A current gap in knowledge in this field revolves around our understanding of the m^{6}A machinery in cell fate decisions. Future studies should be centered on understanding the dynamic nature of m^{6}A in initiating cellular senescence and quiescence, as well as the changes in m^{6}A that are needed for the cell to re-enter the cell cycle. Elucidating the roles of m^{6}A machinery in cell fate decisions has broad-standing implications in understanding stem cell biology, cancer stem cell formation and maintenance, and cell cycle control.

Differentiation

Cell differentiation is the process of transformation into specialized cell types and is essential for development. The hematopoietic system is a well-established model which emphasizes the cell-type and stage-specific role of m^{6}A in differentiation. Outside of hematopoiesis, m^{6}A has been found to be a critical regulator in stem cell fate, neuronal development, and skin development. The role of m^{6}A in development and stem cell biology is reviewed extensively elsewhere (Frye et al., 2018; Malla et al., 2019; Rosselló-Tortella et al., 2020; Vasic et al., 2020; Song et al., 2021). Here we will summarize the role of m^{6}A in differentiation in several contexts.

Writers

The role of RNA modifications within hematopoietic differentiation is stage-specific. At early stages, m^{6}A is necessary for differentiation during the endothelial to hematopoietic transition (EHT), which mediates early-stage hematopoietic stem and progenitor cell (HSPC) differentiation (Zhang C. et al., 2017). The necessity of m^{6}A within EHT is demonstrated by *mettl3*$^{-/-}$ zebrafish, which display disrupted HSPC development (Zhang C. et al., 2017). Mechanistically, *mettl3*$^{-/-}$ zebrafish show continuous Notch activation, as depletion of m^{6}A on the *notch1a* transcript prevents Ythdf2-mediated *notch1a* mRNA decay (Zhang C. et al., 2017). Continuous Notch activation in *mettl3*$^{-/-}$ zebrafish promotes an endothelial cell lineage, thereby inhibiting EHT and preventing the HPSC generation (Zhang C. et al., 2017). In mice, conditional *Mettl3* knockout promoted hematopoietic stem cell (HSC) accumulation in the bone marrow, suggesting that HSC differentiation was unable to progress without METTL3 or m^{6}A (Lee et al., 2019). Mechanistically, METTL3-mediated m^{6}A is believed to promote the mRNA translation of downstream target *Myc*, which regulates differentiation; *Mettl3*$^{-/-}$ mice therefore display a differentiation block due to decreased MYC translation (Lee et al., 2019). Other independent studies have also noted blocks in HSC differentiation in *Mettl3*$^{-/-}$ mice, establishing a pervasive role for METTL3-mediated m^{6}A within differentiation (Cheng et al., 2019). However, knockdown of *Mettl3* in HSPCs resulted in increased cellular differentiation, emphasizing the stage-specific function of m^{6}A within differentiation (Vu et al., 2017). Furthermore, METTL3-mediated m^{6}A was found to inhibit differentiation in AML cells, which suggests that m^{6}A may have distinct functions upon oncogenic transformation in AML cell lines (Lee et al., 2019).

In embryonic stem cells, m^{6}A was found to be critical for mediating the mRNA decay and turnover of transcripts within differentiation (Batista et al., 2014). Similarly, in the context of neuronal development, *Yoon* et al. identified m^{6}A to be a critical factor in mediating neurogenesis, as m^{6}A was found to promote the mRNA decay of transcription factors involved in this process (Yoon et al., 2017). m^{6}A was also found to regulate embryonic neural stem cell renewal and differentiation through regulation of histone modifications, which may further influence the transcription or expression of transcription factors involved in neuronal development (Wang Y. et al., 2018). PRRC2A, an m^{6}A-binding protein, also promoted the fate determination of oligodendrocytes through stabilization of the *Olig2* mRNA transcript in an m^{6}A-dependent manner (Wu et al., 2019). Together, these studies establish the critical role of m^{6}A in mediating the coordination in gene expression events in stem cell differentiation.

Differentiation is a key process in skin development, homeostasis, and wound repair (Lopez-Pajares et al., 2013). Accordingly, *Lee* et al. determined that METTL14-dependent m^{6}A methylation on lncRNA *Pvt1* regulates stemness in epidermal progenitor cells, promoting both *Pvt1*-MYC interactions and MYC protein stabilization (Lee J. et al., 2021).

Furthermore, WTAP was found to be an essential factor for mediating the differentiation of endoderm and mesoderm as mouse embryos lacking *Wtap* failed to differentiate into endoderm and mesoderm and were embryonic lethal during the gastrulation phase of development (Fukusumi et al., 2008). *Horiuchi* et al. also found that loss of *Wtap* resulted in embryonic lethality at day 6.5 (Horiuchi et al., 2006). Mechanistically, this study found that WTAP promoted the stabilization of *Cyclin A2* mRNA, which regulates the G_2/M transition, and that loss of *Wtap* resulted in G_2 accumulation and subsequent lethality (Horiuchi et al., 2006).

Erasers

The m^{6}A eraser FTO may regulate differentiation across different cell types. However, the role of FTO in promoting, or inhibiting, differentiation is cell-type dependent. Knockout of *Fto* in adult neural stem cells (aNSCs) resulted in increased aNSC proliferation and differentiation through aberrant activation of the STAT3 pathway, resulting in inhibited neurogenesis and

dysregulated neuronal development (Cao et al., 2019). Mechanistically, the STAT3 pathway was activated through increased m^{6}A enrichment on *Pdgfrα* and *Socs5* mRNA transcripts, due to decreased FTO expression and activity (Cao et al., 2019). Interestingly, decreased FTO expression and activity resulted in increased PDGFRα protein expression and decreased SOCS5 protein expression, which, together, promote the phosphorylation and activation of STAT3 (Cao et al., 2019). The differences between m^{6}A-dependent regulation of PDGFR*α* and SOCS5 protein expression were not explored in this study (Cao et al., 2019).

FTO is also involved in adipogenic differentiation. Accordingly, decreased FTO demethylase activity resulted in decreased preadipocyte differentiation in an m^{6}A-dependent manner, and FTO-over-expressing mouse embryonic fibroblasts (MEFs) showed increased adipogenic differentiation (Merkestein et al., 2015; Zhang et al., 2015).

Readers

The m^{6}A reader YTHDF2 was identified to function as the main regulator of mRNA decay of transcriptional regulators involved in hematopoiesis and self-renewal (Li et al., 2018). *Ythdf2*$^{-/-}$ HSPCs resulted in increased expansion of HSCs and increased mRNA expression of transcription factors involved in self-renewal, such as *Gata2*, *Runx1*, *Tal1*, and *Stat5* (Li et al., 2018). Mechanistically, YTHDF2 is believed to negatively regulate HSC expansion by facilitating the mRNA decay of *Gata2*, *Runx1*, *Tal1*, and *Stat5* in an m^{6}A-dependent manner (Li et al., 2018). Furthermore, in *mettl3*$^{-/-}$ zebrafish, decreased m^{6}A resulted in decreased Ythdf2-mediated mRNA decay of *notch1a*, a transcription factor that represses HSPC formation (Zhang C. et al., 2017).

YTHDC1 also serves a role in differentiation as *Ythdc1* expression was increased in M0 undifferentiated acute myeloblastic leukemia cells, suggesting that YTHDC1 may be required to maintain an undifferentiated state (Cheng et al., 2021). Furthermore, knockdown of *Ythdc1* in the OCIAML3 cell line resulted in increased differentiation (Cheng et al., 2021). Mechanistically, YTHDC1 is believed to inhibit differentiation through downstream m^{6}A-dependent regulation of MYC (Cheng et al., 2021).

m^{6}A plays crucial roles in differentiation in the hematopoietic system, as well as in stem cell fate, neuronal development, and skin development. Expanded studies should be employed to specifically address the dynamic changes in m^{6}A machinery across totipotent, multipotent, and pluripotent stem cells.

Migration

Cell migration involves the coordination of biophysical and mechanical mechanisms that allow cells to migrate. Cell migration is also the major cellular process that drives wound healing, cancer progression, and metastasis.

Writers

METTL14 is the best-studied m^{6}A writer in the context of migration. Many studies have found that METTL14 may serve as either a positive or negative regulator of migration and metastasis, depending on cellular context. In gastric cancer and endometrial cancer, knockdown of *Mettl14* and decreased m^{6}A levels increased cell migration and invasiveness, establishing METTL14 as a negative regulator of migration and metastasis in these contexts (Liu et al., 2018; Zhang C. et al., 2019). Furthermore, in colorectal cancer, METTL14 inhibited migration and metastasis through m^{6}A/YTHDF2-mediated mRNA degradation of the epithelial-to-mesenchymal transition (EMT)-promoting transcription factor *Sox4* (Chen X. et al., 2020). Furthermore, in papillary thyroid cancer, METTL14 inhibited migration by binding, and decreasing the expression of, lncRNA *OIP5-As1*, which promotes proliferation and migration through downstream regulation of the MEK/ERK, EGFR, and PI3K pathways (Zhang et al., 2021). However, it is unclear whether this mechanism is m^{6}A-dependent (Zhang et al., 2021). Conversely, in keratinocytes and skin cancer cells, METTL14 promoted migration in an m^{6}A dependent manner, as knockdown of *Mettl14* decreased migration, while overexpression of wild-type, but not catalytically inactive mutant, *Mettl14* resulted in increased migration (Yang Z. et al., 2021).

Similarly, METTL3 may promote or inhibit migration depending on the cellular context. Several studies in melanoma have found that METTL3 induced migration by increasing expression of pro-migratory proteins, c-MET and MMP2, in an m^{6}A-dependent manner (Spina et al., 2015; Dahal et al., 2019; Luo et al., 2020). In lung cancer, METTL3 was increased during TGF-β-induced EMT (Wanna-Udom et al., 2020). Furthermore, in liver cancer, METTL3 was found to mediate increases in m^{6}A levels during EMT, including specific m^{6}A increases on the coding sequence (CDS) of EMT-associated transcription factor *Snail*, resulting in YTHDF1-mediated increases in SNAIL translation and EMT progression (Lin X. et al., 2019). Similarly, in bladder cancer, METTL3 deposited m^{6}A on the 3′-UTR of *Cdcp1*, which has been found to promote migration across several cancer types, resulting in YTHDF1-mediated increases in CDCP1 translation and increased cellular migration (Yang F. et al., 2019). In NSCLC and gastric cancer, METTL3 promoted migration through downstream activation of PI3K/AKT; however, whether this mechanism is m^{6}A-dependent is unclear (Lin S. et al., 2019; Wei et al., 2019). Interestingly, METTL3 expression in ovarian cancer also increased migration and induction of EMT through increased protein expression of the receptor tyrosine kinase AXL; however, while the *Axl* mRNA transcript contains fourteen m^{6}A sites, METTL3 regulation of AXL translation is believed to be m^{6}A-independent (Hua et al., 2018). The m^{6}A-independent mechanism by which METTL3 regulates AXL translation remains unclear (Hua et al., 2018). In contrast, in colorectal cancer cells, *Mettl3* over-expression resulted in decreased migration, while decreased *Mettl3* activated the p38/ERK pathways, resulting in increased migration (Deng et al., 2019). Whether regulation of p38/ERK by METTL3 is m^{6}A-dependent was not explored in this study (Deng et al., 2019).

Another m^{6}A writer-associated protein, WTAP, also induced migration and metastasis by increasing the mRNA expression of

migration-promoting genes, *Mmp7*, *Mmp28*, *Cathepsin H*, and *Muc1* in cholangiocarcinoma cells (Jo et al., 2013). However, this study did not investigate whether WTAP-mediated increases in *Mmp7*, *Mmp28*, *Cathepsin H*, and *Muc1* are m^{6}A-dependent (Jo et al., 2013).

Erasers

The role of the m^{6}A eraser FTO in migration is not well-established and requires further study. A study in cervical cancer suggested that FTO regulates migration by promoting the protein translation of E2F1 and MYC, two regulators of cell cycle and migration, in an m^{6}A-dependent manner (Zou et al., 2019). Furthermore, in melanoma cells, overexpression of FTO promoted migration and overall tumorigenicity in an m^{6}A-dependent manner, while knockdown of FTO inhibited migration (Yang S. et al., 2019).

Readers

The m^{6}A reader YTHDF2 may have inhibitory effects on migration. m^{6}A deposition on lncRNA THOR contributes to increased migration across many different cancer cell types (Liu H. et al., 2020). Interestingly, m^{6}A on THOR is read by YTHDF1 and YTHDF2, which can mediate the transcription or decay of THOR, respectively, and therefore influence migration through their respective effects on THOR RNA metabolism (Liu H. et al., 2020). In pancreatic cancer, YTHDF2 was involved in a "migration-proliferation dichotomy" wherein YTHDF2 promoted proliferation but inhibited migration by suppressing YAP signaling, an EMT-promoting signaling pathway (Chen et al., 2017). While YAP contains two m^{6}A sites, it is unclear whether YTHDF2 regulates YAP expression by directly regulating mRNA stability, or whether YTHDF2 regulates upstream regulators of YAP (Chen et al., 2017).

While many studies have reported the effects of RNA modification by writers, erasers and readers on regulating migration, the unique biophysical mechanisms that underlie these transitions are not well-elucidated and remain an active area of research. For example, future studies are needed to explore the potential role of RNA modifications in regulating cytoskeletal proteins.

Metabolism

m^{6}A mediates cellular metabolism in a cell-type dependent manner. The intersection of epitranscriptomics and metabolism remains an understudied area of research. The role of m^{6}A in mediating cancer metabolism is further reviewed elsewhere (Han et al., 2020).

Writers

The m^{6}A writer METTL3 promotes lipogenesis and adipogenesis across several different contexts. In HCC cell lines, METTL3-mediated m^{6}A promoted lncRNA *LINC00958* RNA stability in an m^{6}A-dependent manner (Zuo et al., 2020). With increased RNA stability, *LINC00958* promoted lipogenesis by regulating the *miR-3619-5p*/HDGF pathway, which, in turns, regulates lipogenesis enzymes such as SREB1, FASN, SCD1, and ACC1 (Zuo et al., 2020). As a result, increased *LINC0095* RNA stability resulted in increased cholesterol and triglyceride levels and lipid droplet formation (Zuo et al., 2020). Interestingly, FTO and METTL3 may communicate to coordinate adipogenesis and fat absorption, as visceral fat taken from offspring of high-fat diet-fed mice mothers exhibited decreased FTO expression, and increased METTL3 expression, at 3 weeks of age (Li et al., 2016). Increased m^{6}A levels were also noted at 3 weeks of age in the visceral fat of these offspring (Li et al., 2016). However, at 8 weeks of age, both FTO and METTL3 were increased in the visceral fat, despite their contradictory functions, with no changes in m^{6}A levels noted (Li et al., 2016). These results suggest a unique coordination between FTO and METTL3 in response to a high-fat diet and within development, but the mechanism remains unclear (Li et al., 2016). In addition to lipogenesis and adipogenesis, METTL3 was found to regulate glucose metabolism in colorectal cancer, as METTL3-mediated m^{6}A promoted the mRNA stability of *Hk2* and *Glut1* in an m^{6}A and IGF2BP2/3-dependent manner (Shen et al., 2020). Increased *Hk2* and *Glut1* mRNA stability subsequently led to the activation of glycolysis and promoted colorectal cancer cell progression (Shen et al., 2020).

Erasers

FTO serves a pivotal role in multiple metabolic processes, including fat metabolism, gluconeogenesis, metabolic stress, and lactate production. Several seminal studies were intrinsic to establishing the role of FTO in fat metabolism. However, because FTO was only recently established as an m^{6}A eraser, the contexts in which FTO promotes obesity in an m^{6}A-independent or dependent manner is not entirely clear. In humans, the FTO SNP rs9939609 was found to be linked to body mass index and is believed to be one of the strongest genetic determinants of obesity propensity (Frayling et al., 2007). Additionally, the FTO SNP rs8050136 in humans decreases the binding affinity of the CUX1 isoform P110, resulting in decreased expression of FTO and leptin signaling, preventing satiety, and promoting obesity (Stratigopoulos et al., 2011).

More recent studies have suggested that the demethylase activity of FTO is indispensable for its role in mediating fat metabolism, including lipogenesis and adipogenesis. Decreased m^{6}A levels, mediated by the demethylase activity of FTO, were found to increase triglyceride deposition in HepG2 hepatocyte cells (Kang et al., 2018). Additional studies in HepG2 cells show that FTO mediated an increase in the expression of SREBP1c and CIDEC, two transcriptional regulators of lipogenesis, by increasing their nuclear localization, thereby promoting lipogenesis (Wang Y. et al., 2015; Chen A. et al., 2018). Increases in SREBP1c protein expression were found to be m^{6}A-dependent, as mutant FTO was did not mediate changes in SREBP1c processing or protein expression (Chen A. et al., 2018). The mechanism by which FTO-mediated m^{6}A demethylation mediates CIDEC expression remains unclear (Chen A. et al., 2018). In 3T3-L1 preadipocytes, FTO promoted adipogenesis through regulation of cell cycle progression (Wu et al., 2018). Mitotic clonal expansion (MCE) is a pivotal prerequisite process required for adipocyte differentiation and adipogenesis (Tang et al., 2003). Within

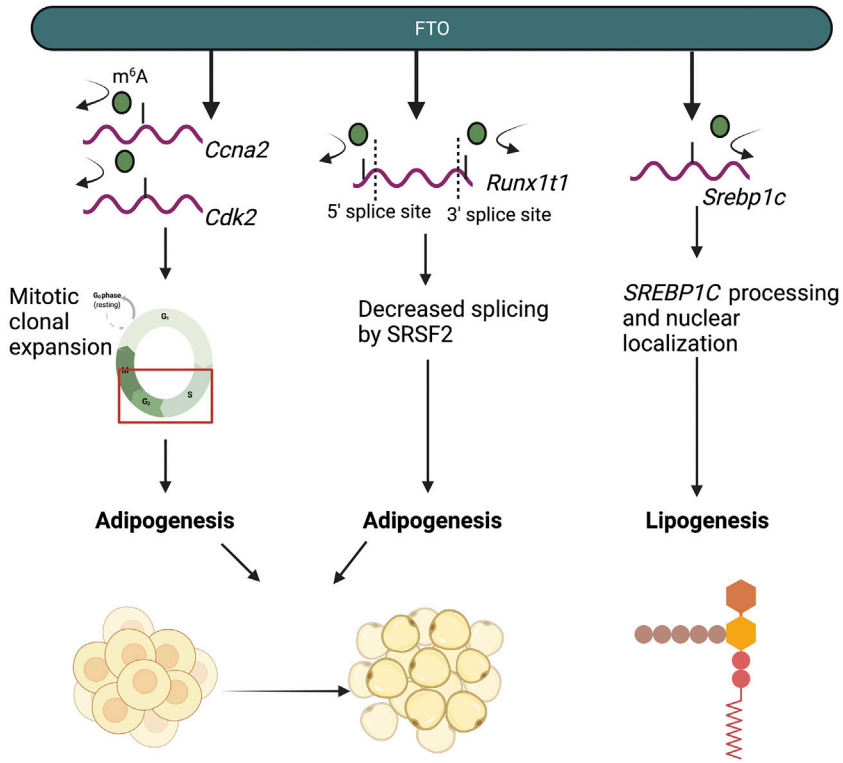


FIGURE 3 | The m^{6}A-dependent roles of FTO in adipocyte and lipid metabolism. FTO regulates and promotes adipogenesis and lipogenesis by demethylating mRNA transcripts of genes involved in adipogenesis (*Ccna2*, *Cdk2*, *Runx1t1*) and lipogenesis (*Srebp1c*).

this process, differentiating adipocytes are required to enter the cell cycle and proliferate (Tang et al., 2003). In 3T3-L1 cells with *Fto* knockdown, increased m^{6}A levels resulted in decreased mRNA expression of cell-cycle control genes *Ccna2* and *Cdk2*, which regulate the S to G2 transition (Wu et al., 2018). Subsequently, increased m^{6}A levels on *Ccna2* and *Cdk2* mRNA transcripts resulted in m^{6}A-dependent/YTHDF2-mediated decay of *Ccna2* and *Cdk2* mRNA and decreased CCNA2 and CDK2 protein expression (Wu et al., 2018). Decreased expression of CCNA2 and CDK2 resulted in the impairment of MCE and preadipocytes were unable to progress to the G2 phase, halting preadipocyte development (Wu et al., 2018). FTO has also been found to regulate RUNX1T1, an adipocyte transcription factor (Zhao et al., 2014). Within the *Runx1t1* mRNA transcript, m^{6}A was enriched at exonic regions near 5′ and 3′ splice sites; accordingly, increased m^{6}A levels, mediated through *Fto* knockdown, led to increased binding by the splicing protein SRSF2, which resulted in changes in exon splicing and inclusion in the *Runx1t1* transcript (Zhao et al., 2014; Zhang B. et al., 2020). The m^{6}A-dependent roles of FTO in lipid and adipocyte metabolism are highlighted in **Figure 3**.

FTO may also serve a role in regulating gluconeogenesis. Increased glucose uptake induced the expression of *Fto*, resulting in overall decreases in m^{6}A (Yang Y. et al., 2019). High FTO expression was also correlated with increased mRNA expression of genes involved in glucose and lipid metabolism, including *Foxo1*, *G6pc*, *Dgat2*, and *Fasn*, upon glucose stimulation (Jensen-Urstad and Semenkovich, 2012; Kousteni, 2012; Yang Y. et al., 2019). However, the mechanism by which FTO regulates the expression of *Foxo1*, *G6pc*, *Dgat2*, and *Fasn* was not explored in this study (Yang Y. et al., 2019). In another study, FTO was found to demethylate m^{6}A sites on *Foxo1*, resulting in increased FOXO1 expression, and increased gluconeogenesis (Peng et al., 2019). Interestingly, *Foxo1* mRNA expression was not changed by changes in FTO expression or activity (Peng et al., 2019). Rather, mutating an internal m^{6}A site on the *Foxo1* mRNA transcript prevented FTO-mediated increases in FOXO1, establishing that the internal m^{6}A site on the *Foxo1* mRNA transcript is required for the FTO-FOXO1 axis (Peng et al., 2019).

Furthermore, FTO and ALKBH5 may regulate metabolism in response to cellular stress through interactions with ATF4, a stress-response gene and major regulator of cellular metabolism. Under stress conditions, ATF4 expression increases (Zhou et al., 2018). However, upon *Fto* or *Alkbh5* knockdown in MEF and 293T cells, ATF4 expression failed to increase upon amino acid starvation (Zhou et al., 2018). Mechanistically, m^{6}A methylation on the 5′-UTR of *Atf4* is dynamically changed in response to stress; increased m^{6}A methylation on the *Atf4* mRNA transcript due to *Fto* or *Alkbh5* knockdown results in decreased ATF4 translation in response to amino acid starvation (Zhou et al., 2018). Conversely, *Mettl3* or *Mettl14* knockdown in this context

resulted in increased ATF4 translation upon amino acid starvation, suggesting that the ATF4 regulation in response to starvation is m^{6}A-dependent (Zhou et al., 2018).

Additionally, ALKBH5 was found to regulate lactate production in melanoma and colon cancer (Li et al., 2020). Knockdown of *Alkbh5* in melanoma and colon cancer cells resulted in m^{6}A-dependent decreases in the stability of *Mct4/Slc16a3* mRNA, a regulator of lactate secretion (Li et al., 2020). Accordingly, *Alkbh5* knockdown resulted in decreased lactate production in the tumor interstitial fluid of the tumor microenvironment in both melanoma and colon cancer (Li et al., 2020).

Readers

The role of readers in mediating metabolism requires future study. However, one study showed that m^{6}A on mitochondrial carrier homology 2 (*Mtch2*) mRNA resulted in increased MTCH2 protein expression, resulting in increased adipogenesis in longissimus dorsi muscle cells taken from both lean Landrace-breed pigs and obese Jinhua-breed pigs (Jiang et al., 2019).

The role of m^{6}A in metabolism is an exciting new field of interest. Few studies have addressed the role of other MTC proteins, such as WTAP and VIRMA, in regulating metabolism. Other potential directions the field could address include how the cellular microenvironment influences cell-intrinsic changes in m^{6}A and how changes in m^{6}A can contribute to changes in cancer cell metabolism.

Autophagy

Autophagy is a conserved cellular process that is mobilized during the stress response and within normal housekeeping functions. The autophagic process involves the removal and degradation of excessive or damaged organelles or proteins, as well as other biological molecules, into membrane-bound autophagosomes (Klionsky, 2007; Mizushima et al., 2008). m^{6}A has been found to regulate autophagy; however, the discrete mechanisms and cellular contexts with which m^{6}A influence autophagy remain unexplored (Frankel et al., 2017; Abildgaard et al., 2020).

Writers

The m^{6}A writer METTL3 has been found to negatively regulate autophagy across several contexts. In HCC, METTL3 inhibited autophagy by depositing m^{6}A at the 3′-UTR of *Foxo3a*, a negative regulator of autophagy (Lin et al., 2020). m^{6}A on the 3′-UTR of *Foxo3a* resulted in downstream YTHDF1-mediated *Foxo3a* mRNA stabilization and subsequently inhibited autophagy (Lin et al., 2020). Furthermore, in an ischemic heart model, METTL3-mediated m^{6}A on the 3′-UTR of *Tfeb*, which promotes autophagy and lysosome biogenesis, resulted in HNRNPD-mediated decreases in *Tfeb* mRNA expression and decreased autophagy (Song et al., 2019).

Autophagy can also promote therapeutic resistance and cell survival. Accordingly, METTL3 promoted resistance to gefitinib in NSCLC through regulation of two core autophagy genes, *Atg5* and *Atg7* (Glick et al., 2010; Liu S. et al., 2020). Accordingly, *Mettl3* knockdown in NSCLC cells resulted in decreased *Atg5* and *Atg7* mRNA expression (Liu S. et al., 2020). However, whether this regulation was m^{6}A-dependent is unclear (Liu S. et al., 2020).

Additionally, in human keratinocytes, METTL14 abundance was found to be down-regulated by UVB exposure through NBR1-mediated selective autophagy (Yang Z. et al., 2021). Furthermore, mTORC1, a negative regulator of autophagy, promoted the stabilization of the MTC consisting of METTL3, METTL14, WTAP, and RMB15/RBM15B (Tang et al., 2021). Mechanistically, mTORC1 promoted the stabilization of the MTC by regulating the chaperonin CCT, which facilitates protein folding and stabilization of the MTC in *Drosophila* S2R+ and human HEK293T cells (Tang et al., 2021). The mechanism by which mTORC1 regulates CCT is detailed further elsewhere (Tang et al., 2021). Increased stabilization of the MTC led to increased m^{6}A deposition and mRNA degradation of two downstream targets, autophagy genes *Atg1* and *Atg8a*, resulting in the suppression of autophagy (Tang et al., 2021).

Furthermore, one study found that WTAP could regulate autophagy by mediating the phosphorylation of the positive autophagy regulator, AMPK, in HCC cells (Li G. et al., 2021). Mechanistically, WTAP decreased the mRNA stability of *Lkb1*, the kinase upstream of AMPK which regulates AMPK phosphorylation, in an m^{6}A-dependent manner (Li G. et al., 2021). Subsequently, knockdown of *Wtap* resulted in increased autophagy (Li G. et al., 2021).

Erasers

The role of the m^{6}A eraser FTO as a regulator of autophagy has been studied in a variety of different contexts. In HeLa cells, knockdown of *Fto* decreased autophagic flux (Jin et al., 2018). Interestingly, only the catalytically active form of FTO was able to increase autophagic flux, evidenced by increased LC3B puncta in cells expressing wild-type, but not catalytically inactive mutant, FTO, which suggests that FTO regulates autophagy in an m^{6}A-dependent manner (Jin et al., 2018). RNA immunoprecipitation (RIP)-qPCR revealed that FTO binds to *Ulk1* mRNA, a gene involved in the initial stages of autophagy and is an important recruitment factor in autophagosome formation (Zachari and Ganley, 2017; Jin et al., 2018). The interaction between FTO and *Ulk1* was further elucidated as three m^{6}A sites were found in the 3′-UTR of the *Ulk1* transcript, which were subsequently targeted for degradation by YTHDF2 (Jin et al., 2018). FTO-mediated demethylation of *Ulk1* may therefore preserve *Ulk1* from YTHDF2-mediated degradation (Jin et al., 2018). In addition to ULK1, FTO may also preserve core autophagy genes, *Atg5* and *Atg7*, from YTHDF2-mediated degradation in adipocytes (Glick et al., 2010; Wang et al., 2020). Knockdown of *Fto* in 3T3-L1 cells increased m^{6}A levels across the *Atg5* and *Atg7* mRNA transcripts, resulting in YTHDF2-mediated degradation and inhibition of autophagy (Wang et al., 2020). Interestingly, knockdown of *Fto* in 3T3-L1 cells did not change m^{6}A levels on ULK1, emphasizing the cell-type dependent regulation of autophagy by FTO (Wang et al., 2020).

FTO has also been shown to be a target for p62-dependent selective autophagy. In human keratinocytes, FTO protein

expression was stabilized and up-regulated by arsenic exposure through inhibition of p62-mediated autophagy (Cui et al., 2021).

Furthermore, the m^{6}A eraser ALKBH5 was found to promote autophagy in Leydig cells (Chen Y. et al., 2020). Mechanistically, m^{6}A promoted the translation of PPM1A, a negative AMPK regulator, in a YTHDF1-dependent manner (Chen Y. et al., 2020). Furthermore, m^{6}A also reduced the mRNA stability of *Camkk2*, a positive AMPK regulator, in a YTHDF2-dependent manner, resulting in autophagy inhibition (Chen Y. et al., 2020). However, decreased m^{6}A methylation, mediated by ALKBH5, resulted in autophagy induction by preventing *Camkk2* mRNA decay (Chen Y. et al., 2020).

Readers

Few studies have examined the role of only m^{6}A readers in autophagy. YTHDC1 was found to regulate autophagy in human keratinocytes treated with high glucose, as knockdown of *Ythdc1* resulted in decreased autophagic flux (Liang et al., 2021). Mechanistically, YTHDC1 promoted mRNA stability of the autophagy receptor *Sqstm1* in an m^{6}A-dependent manner (Liang et al., 2021). Accordingly, knockdown of *Ythdc1* resulted in *Sqstm1* mRNA degradation, leading to decreased autophagic flux (Liang et al., 2021). Furthermore, in HCC, YTHDF1 was identified to positively regulate autophagy by promoting the translation of core autophagy proteins ATG2A and ATG14 under hypoxic conditions in an m^{6}A-dependent manner (Li Q. et al., 2021).

As this is a relatively new field of research, future studies are needed to identify the context-dependent role of m^{6}A at different stages in the autophagic process, from the formation of phagophore, autophagosome, and autolysosome, to cargo degradation in the lysosomes, and identify the different cellular stressors and stimuli that mediate dynamic m^{6}A changes within this process (Glick et al., 2010).

DNA Damage Response

Elucidating the communication between m^{6}A and DNA damage response (DDR) is an active area of study. The role of m^{6}A in modulating these pathways will add new insights into the DDR machinery.

Writers

In response to UVC or UVA radiation, m^{6}A and DNA Pol κ were rapidly recruited to sites of DNA damage (Xiang et al., 2017). While the detailed mechanism behind the role of DNA Pol κ in DDR is not fully understood, the catalytic activity of METTL3 was found to be required for DNA Pol κ recruitment to DNA damage sites (Xiang et al., 2017). Knockout of *Mettl3* in HeLa and U2OS cells exposed to UV radiation resulted in decreased cyclobutene pyrimidine dimer (CPD) removal, a major UV damage product, (Xiang et al., 2017). Knockout of *Mettl14* in human keratinocyte cell lines HaCaT and normal human epidermal keratinocytes (NHEK) cells also resulted in decreased CPD removal upon UVB irradiation (Yang Z. et al., 2021). Interestingly, another study found that m^{6}A was recruited to DNA damage lesions only in the presence of CPDs in response to UVA or UVB radiation, suggesting that m^{6}A and m^{6}A-associated enzymes may specifically recognize CPDs (Svobodová Kovaříková et al., 2020).

Furthermore, in response to UVA exposure, m^{6}A RNA modifications may serve in the nucleotide excision repair pathway, but not the non-homologous end-joining (NHEJ) pathway, as treatment with an inhibitor of SUV40H1/H2, which are NHEJ-specific enzymes, had no effect on m^{6}A recruitment (Svobodová Kovaříková et al., 2020). Interestingly, however, knockout of other NHEJ enzymes SUV39H1/H2, did decrease the recruitment of m^{6}A in response to UVA exposure, suggesting that the role of m^{6}A in NHEJ may be complex (Svobodová Kovaříková et al., 2020). In response to UVB exposure, METTL14 inhibited UVB-induced skin tumorigenesis by regulating global genome repair (GGR) in human keratinocyte cell lines (Yang Z. et al., 2021). Mechanistically, METTL14 regulated the m^{6}A deposition onto the DNA damage repair gene *Ddb2* and promoted YTHDF1-mediated DDB2 translation, and subsequent knockdown of *Mettl14* resulted in decreased DDB2 abundance in an m^{6}A-dependent manner (Yang Z. et al., 2021). The discrete epitranscriptomic mechanisms that underlie the DDR in response to UVA, UVB, and UVC exposure remains unclear.

Interestingly, in response to double-stranded breaks (DSBs), which were induced by X-ray radiation or Zeocin treatment, a chemical that induces DSBs, METTL3 was activated and phosphorylated at S43 by the key DDR kinase ATM, which then localized to DNA damage sites (Zhang C. et al., 2020). At these DNA-damage sites, METTL3 deposited m^{6}A onto DNA damage-associated RNA, forming a DNA-RNA hybrid (Zhang C. et al., 2020). Accordingly, knockdown of *Mettl3* resulted in decreased homologous recombination, a key process in the double-stranded break repair process (Zhang C. et al., 2020). YTHDC1 was also recruited to the DNA-RNA hybrid sites, potentially serving to preserve m^{6}A deposition on these RNA hybrids (Zhang C. et al., 2020). The DNA-RNA hybrids then recruited the DNA damage-associated proteins RAD51 and BRCA in order to initiate HR (Zhang C. et al., 2020).

Furthermore, in the NCCIT stem cell line, VIRMA was found to promote resistance to cisplatin through regulation of the DNA damage response (Miranda-Gonçalves et al., 2021). Accordingly, knockdown of VIRMA resulted in increased expression of DNA repair proteins, including γH2AX, GADD45A ,and GADD45B, and promoted sensitivity to cisplatin (Miranda-Gonçalves et al., 2021). Whether VIRMA mediates the DDR in an m^{6}A-dependent manner was not explored (Miranda-Gonçalves et al., 2021).

In addition to m^{6}A writers, METTL16, a methyltransferase that targets non-coding RNAs, including U6 small nuclear RNA, was also recruited to sites of DNA damage at a later time point (20–30 mins post UVA/UVC micro-irradiation) (Svobodová Kovaříková et al., 2020). However, the substrates of METTL16 in response to UV radiation were not explored in this study (Svobodová Kovaříková et al., 2020).

Erasers

In response to metabolic stress, UVC, and H_2O_2 treatment, the m^{6}A eraser FTO increased the mRNA stability of DNA repair

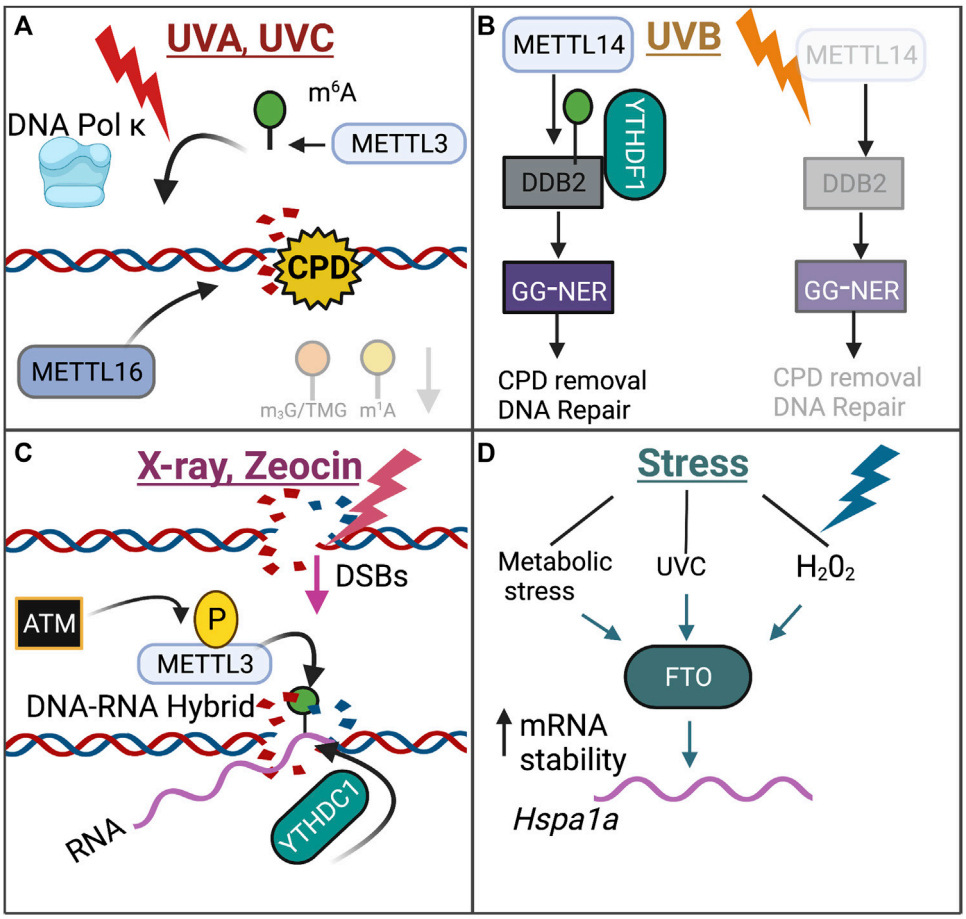


FIGURE 4 | Review of the role of m^{6}A within the DNA Damage Response. The role of m^{6}A with the DNA Damage Response is dependent on the DNA damaging agent, highlighted through the distinct mechanisms that are employed upon exposure to UVA/UVC **(A)**, UVB **(B)**, X-ray/Zeocin **(C)**, or Stress **(D)**.

pathway genes, including *Hspa1a* (*Hsp70*), in osteoblasts (Zhang Q. et al., 2019). Increased mRNA stability and expression of *Hspa1a* served to protect osteoblasts from NF-κ β-mediated apoptosis (Zhang Q. et al., 2019). While the *Hspa1a* mRNA transcript does contain m^{6}A sites, this study did not address whether FTO promotes *Hspa1a* mRNA stability in an m^{6}A-dependent manner (Zhang Q. et al., 2019).

The role of m^{6}A writers and erasers in the DNA damage response is highlighted in **Figure 4**.

The role of m^{6}A in mediating DNA damage response is an emerging field of interest. There are several gaps in this field that should be addressed accordingly. One major area of interest is elucidating the specific roles of m^{6}A readers in the DNA damage response. There is limited research on this topic. While m^{6}A readers have been implicated in DDR, it has only been in the context of their communication with the m^{6}A writers and erasers. Furthermore, another area of interest is to further elucidate the function of the m^{6}A machinery in response to chronic vs. acute DNA damage in response to genotoxic agents such as UV radiation, arsenic, chemotherapy, and ionizing radiation.

Liquid-Liquid Phase Separation

Liquid-liquid phase separation (LLPS) involves the formation of biological condensates containing aggregates of proteins or nucleic acids within the cell (Lyon et al., 2021). Biophysical mechanisms of liquid-liquid phase separation formation are discussed elsewhere (Lyon et al., 2021). Recent work has uncovered fascinating roles for these condensates in cellular functions, including involvement in stress responses, diseases, and aging (Alberti and Hyman, 2021; Lyon et al., 2021).

Readers

YTHDF readers YTHDF1 and YTHDF3 are believed to be critical in mediating LLPS as depletion of *Ythdf1* or *Ythdf3* prevented stress granule (SG) formation (Ries et al., 2019; Fu and Zhuang, 2020). There are contrasting reports on the role of YTHDF2 in LLPS and SG formation, as sodium-arsenite-induced SGs required YTHDF2, but not oxidative-stress-induced SG (Ries et al., 2019; Fu and Zhuang, 2020). These contrasting reports highlight that the role of YTHDF2 in LLPS and SG formation may be context-dependent (Ries et al., 2019; Fu and Zhuang, 2020). Biophysically, YTHDF1/3 are hypothesized to facilitate LLPS by

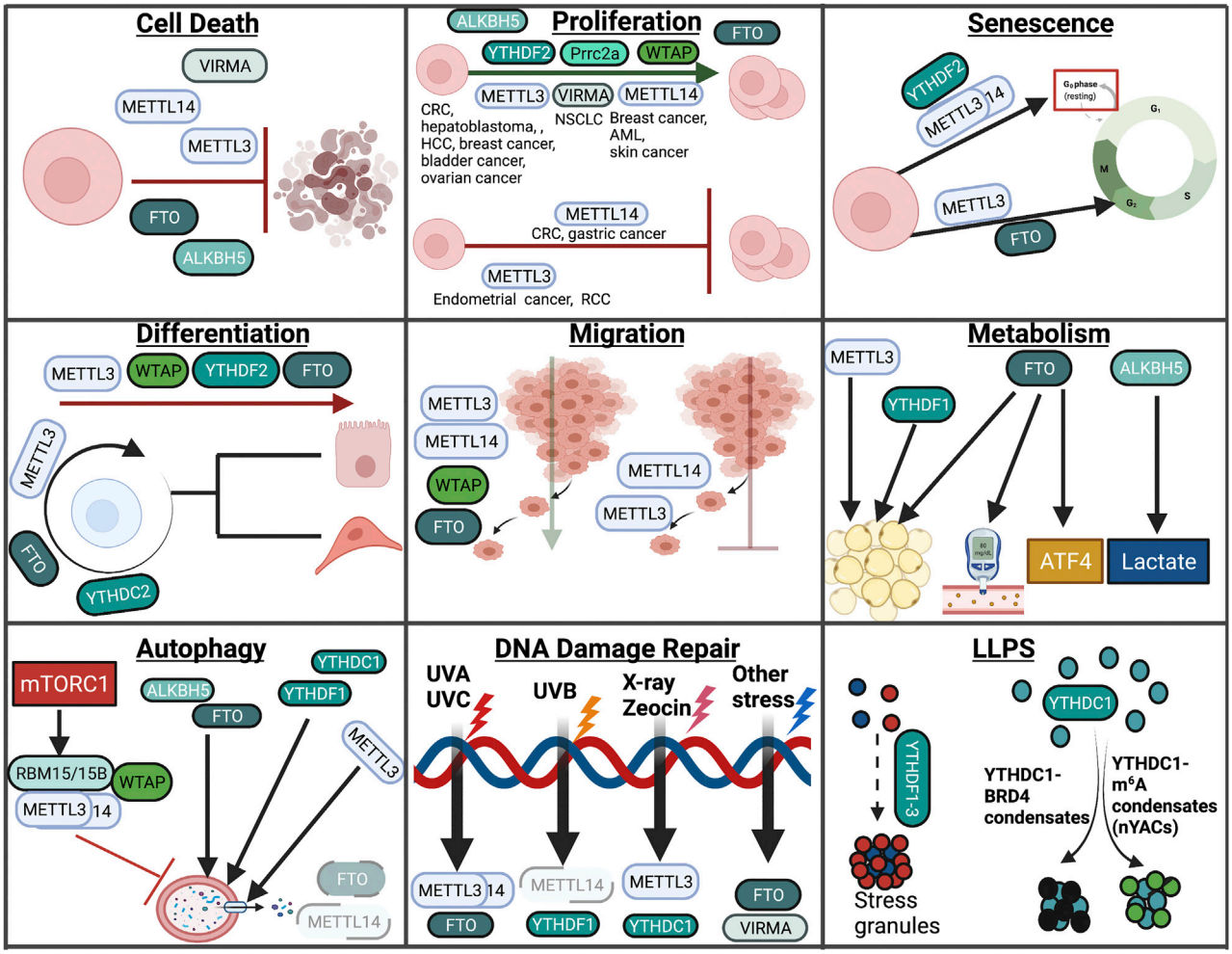


FIGURE 5 | Overview of m^{6}A in cellular processes. In this review, we highlight the role of RNA modifications in cellular processes such as cell death, proliferation, senescence, differentiation, migration, metabolism, autophagy, the DNA damage response, and LLPS. Within these processes, RNA modifications assume unique and context-dependent functions.

lowering the activation energy input needed for phase separation (Fu and Zhuang, 2020). Alternatively, another hypothesis states YTHDF1/3 may serve as shell proteins that promote SG formation (Fu and Zhuang, 2020). However, the mechanism by which YTHDF1 and YTHDF3 mediate LLPs and SG formation is unclear (Fu and Zhuang, 2020). Furthermore, YTHDF3 has also been found to promote triaging of mRNAs into SGs in response to oxidative stress (Anders et al., 2018). Under these conditions, mRNA transcripts are dynamically patterned with m^{6}A at the 5′-UTR and 5′-CDS regions and are partitioned into stress granules by YTHDF3, and are prevented from undergoing translation (Anders et al., 2018).

In addition to YTHDF1 and YTHDF3, two independent studies have established a role for YTHDC1 in LLPS. YTHDC1 is structurally made up of N or C-terminal internally-disordered regions (IDRs), which are believed to be necessary for YTHDC1's role in LLPS (Lee J.-H. et al., 2021; Cheng et al., 2021). In MEF, 293T, and HeLa cells, m^{6}A-eRNAs, which localize to active enhancer regions, recruited YTHDC1 to form YTHDC1-BRD4 condensates (Lee J.-H. et al., 2021). Additionally, YTHDC1 also formed m^{6}A-YTHDC1 condensates, termed nYACs, in AML cells (Cheng et al., 2021). In this context, the number of nYACs increased in AML cells, as compared to normal hematopoietic cells, and also promoted tumorigenesis by promoting an undifferentiated state and cell survival (Cheng et al., 2021). Furthermore, nYACs can influence mRNA metabolism by preventing m^{6}A-decorated mRNAs from being degraded by the PAXT-exosome complex (Cheng et al., 2021). The role of LLPS in tumorigenesis remains an emerging area of interest and is detailed further (Jiang et al., 2020).

It is important to note that whether m^{6}A is critical for LLPS and stress granule formation remains controversial. One study found that m^{6}A on mRNAs promoted YTHDF1-3 partitioning into phase-separated structures (Ries et al., 2019). However, a more recent study demonstrated that mRNAs, with or without

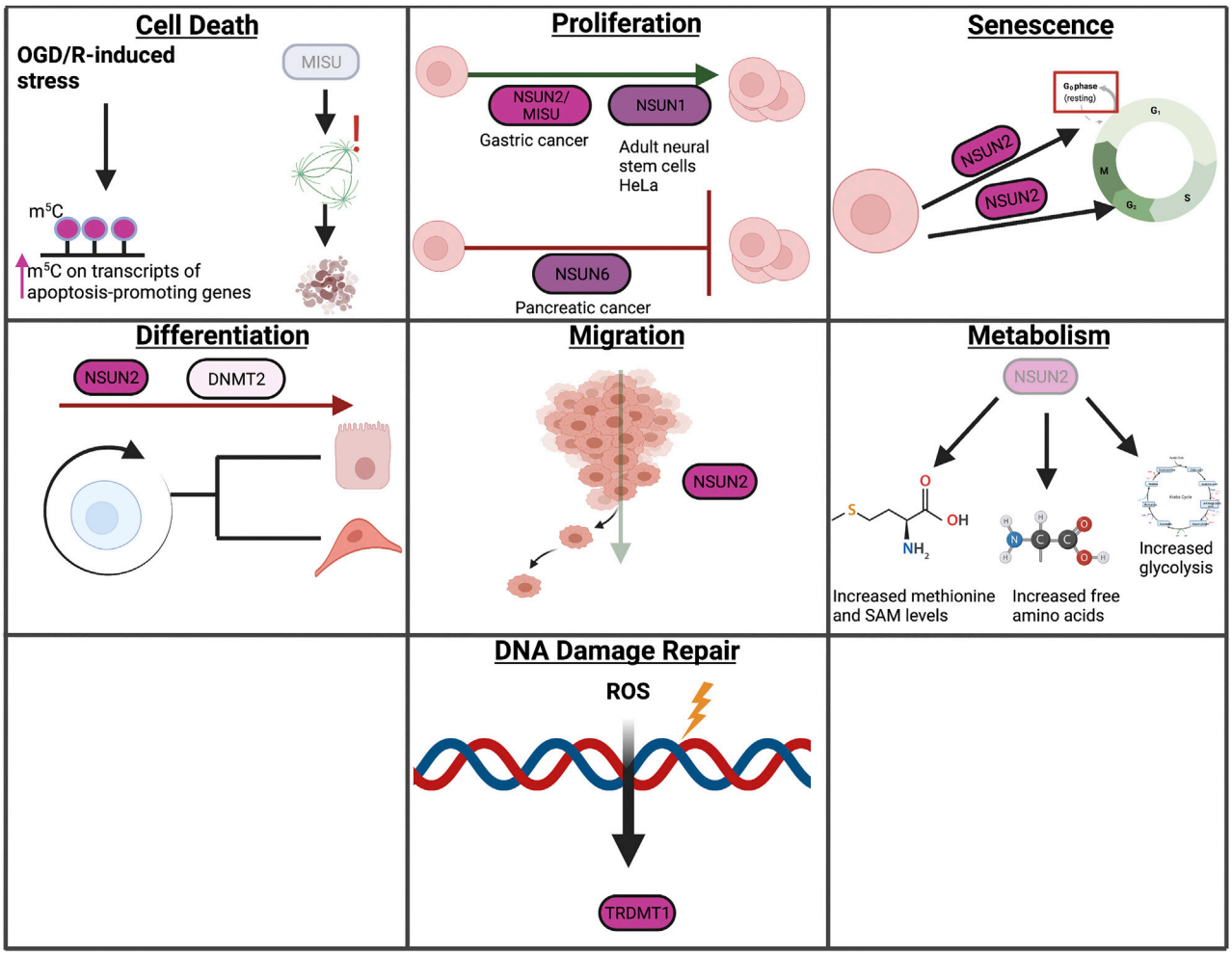


FIGURE 6 | Overview of m^{5}C in cellular processes. In this review, we highlight the role of RNA modifications in cellular processes such as cell death, proliferation, senescence, differentiation, migration, metabolism, and the DNA damage response. Within these processes, RNA modifications assume unique and context-dependent functions.

m^{6}A modifications, show minor differences in partitioning to stress granules and therefore argue that m^{6}A may only play a minor role in stress granule partitioning (Khong et al., 2021). The authors of this study hypothesize that it is not only m^{6}A-YTHDF interactions that promote stress granule partitioning, but rather, there may be several other RNA-protein interactions outside of m^{6}A-YTHDF that promote stress granule portioning (Khong et al., 2021). The identity and nature of these RNA-protein interactions remain unclear.

The field of LLPS is rapidly expanding and research into this topic breaches disciplines in biophysics, biochemistry, disease biology, as well as epitranscriptomics. Of the many gaps of knowledge within this field, expanding the role of m^{6}A machinery in LLPS, namely specific m^{6}A writers and erasers, remains paramount.

A summary of the role of m^{6}A modification in cellular responses covered in this review can be found in **Figure 5**.

THE ROLE OF m^{5}C in Diverse Cellular Functions

m^{5}C has been implicated in several cellular contexts, including cell death, proliferation, senescence, differentiation, migration, metabolism, and DDR (**Figure 6**). The role of m^{5}C in autophagy and LLPS has not been studied extensively and will therefore not be covered in this section. The role of m^{5}C in autophagy and LLPS represents a gap of knowledge within this growing field and therefore requires further studies.

Cell Death

Writers

The role of m^{5}C in cell death is not widely explored. Accordingly, one study employing an oxygen-glucose deprivation/reoxygenation (OGD/R) model in neurons found that m^{5}C-methylated sites were increased upon OGD/R (Jian et al., 2021). Furthermore, RNA bisulfite sequencing revealed that m^{5}C

hypermethylated transcripts after OGD/R were functionally involved in apoptosis (Jian et al., 2021). While the functional significance of these findings remains to be explored, these results suggest that m^5C methylation may be important in mediating apoptosis in response to cellular stress mediated by OGD/R (Jian et al., 2021). Furthermore, MISU, an NSUN2 homolog, was identified as a critical regulator of mitotic integrity; accordingly, MISU depletion resulted in apoptosis, potentially through decreased spindle integrity and induction of aneuploidy (Hussain et al., 2009).

Proliferation

Writers

m^5C RNA methylation may also have important roles in cell proliferation. Similar to trends seen with m^6A, the role of m^5C RNA modifications in cell proliferation have been studied primarily in the context of cancer.

Low expression of NSUN6, an m^5C methyltransferase, was found in pancreatic cancer patients, and may contribute to pancreatic cancer cell proliferation through regulation of CDK10 (Yang R. et al., 2021). While decreased NSUN6 expression was correlated with decreased CDK10 expression, resulting in increased cell proliferation, this study did not establish whether NSUN6 regulates CDK10 expression in an m^5C-dependent manner (Yang R. et al., 2021).

High levels of NSUN2, another m^5C methyltransferase, have been found in several different cancer types, but the functional role of NSUN2 in regulating proliferation was not clear (Okamoto et al., 2012). A recent study found in gastric cancer found that high NSUN2 levels were associated with worse overall survival, and that knockdown of *Nsun2* resulted in decreased proliferation in gastric cancer cells (Hu et al., 2021). NSUN2 protein stability was found to be regulated by SUMOylation, a post-translational modification (Hu et al., 2021). Interestingly, increased proliferation was also noted upon *Nsun2* overexpression in these cells, using both wild-type and catalytically inactive mutant NSUN2, suggesting that NSUN2 may have both m^5C-dependent and m^5C-independent functions in promoting proliferation (Hu et al., 2021). RNA bisulfite sequencing revealed that NSUN2-dependent m^5C methylated transcripts were involved in oncogenic pathways, including the RAP1 pathway, as well as pathways involved in drug resistance and cell cycle (Hu et al., 2021). Furthermore, NSUN2 promoted proliferation in U2OS cells by depositing m^5C onto *Cdk1* transcripts, resulting in increased CDK1 translation (Xing et al., 2015). The role of NSUN2 in promoting proliferation is further detailed elsewhere (Wang, 2016).

Interestingly, MISU, a NSUN2 homolog, was identified as a MYC target and mediated MYC-induced cell growth in human epidermis cells (Frye and Watt, 2006). However, the mechanism by which MISU regulates MYC-induced proliferation is unclear (Frye and Watt, 2006).

Furthermore, the expression of NSUN1, alternatively known as NOP2, was increased in adult neural stem cells after stroke and was positively correlated with adult neural stem cell proliferation, suggesting a potential role for NSUN1 in promoting recovery after stroke (Kosi et al., 2015). Additionally, NSUN1, also known as NOL1, promoted proliferation by binding to the *Ccnd1* promoter and promoting *Ccnd1* transcription in HeLa cells (Hong et al., 2016). Whether NSUN1 promoted the proliferation in an m^5C-dependent manner in these studies was not established.

Senescence

Writers

The m^5C writer NSUN2 has been found to promote senescence in a variety of contexts. In HeLa cells, METTL3/14 and NSUN2 cooperated to increase p21 translation in response to oxidative stress, ultimately leading to the induction of cellular senescence (Li Q. et al., 2017). NSUN2 also promoted oxidative-stress-induced cellular senescence in human umbilical vein endothelial cells through m^5C methylation of *Shc* mRNA, which led to increased SHC protein expression, activation of p38/MAPK, and increased ROS levels, thereby establishing a positive feedback loop (Cai et al., 2016). However, the role of NSUN2 in regulating senescence may be context and stimuli-dependent. In human diploid fibroblasts, NSUN2 negatively regulated senescence by methylating $p27^{KIP1}$, a CDK inhibitor, at the 5′-UTR, resulting in decreased p27 translation and increased CDK1 translation (Tang et al., 2015). By indirectly promoting CDK1 translation, NSUN2 served to promote cellular proliferation and inhibit cellular senescence (Tang et al., 2015).

Differentiation

Writers

NSUN2 levels are highly expressed in undifferentiated epidermal progenitor cells (Sajini et al., 2019). Vault tRNAs (vtRNAs) are RNA POLIII-derived transcripts that make up vault ribonucleoproteins, and can be processed into smaller regulatory RNAs (svRNAs) (Stadler et al., 2009; Sajini et al., 2019). Accordingly, *Sajini* et al. found that processing of vtRNA VTRNA1.1 is dependent on NSUN2-dependent m^5C methylation and is critical for proper epidermal cell development (Sajini et al., 2019). NSUN2-mediated m^5C on tRNAs is also believed to be required for epidermal stem cell, testis, and neural stem cell differentiation (Blanco et al., 2011; Hussain et al., 2013; Flores et al., 2017). Due to the important role of NSUN2 in promoting neural stem cell differentiation, loss of *Nsun2* is linked to several developmental disorders (Flores et al., 2017). DNMT2-mediated m^5C on tRNA is believed to be required for hematopoiesis, as *Dnmt2*-deficient mice showed decreased stem and progenitor cell populations (Tuorto et al., 2015). The role of m^5C in differentiation and development is summarized elsewhere (Song et al., 2021).

Migration

Writers

In addition to m^6A writers, the m^5C writer NSUN2 promoted the mRNA translation of autotaxin (*Atx*) in U87 glioma cells in an m^5C-dependent manner (Xu et al., 2020). NSUN2 deposited m^5C at the 3′-UTR of *Atx*, enhancing *Atx* translation and promoting the export of *Atx* from the nucleus to the cytoplasm through coordination with m^5C reader ALYREF (Xu et al., 2020). Downstream, ATX then converts lysophosphatidylcholine to

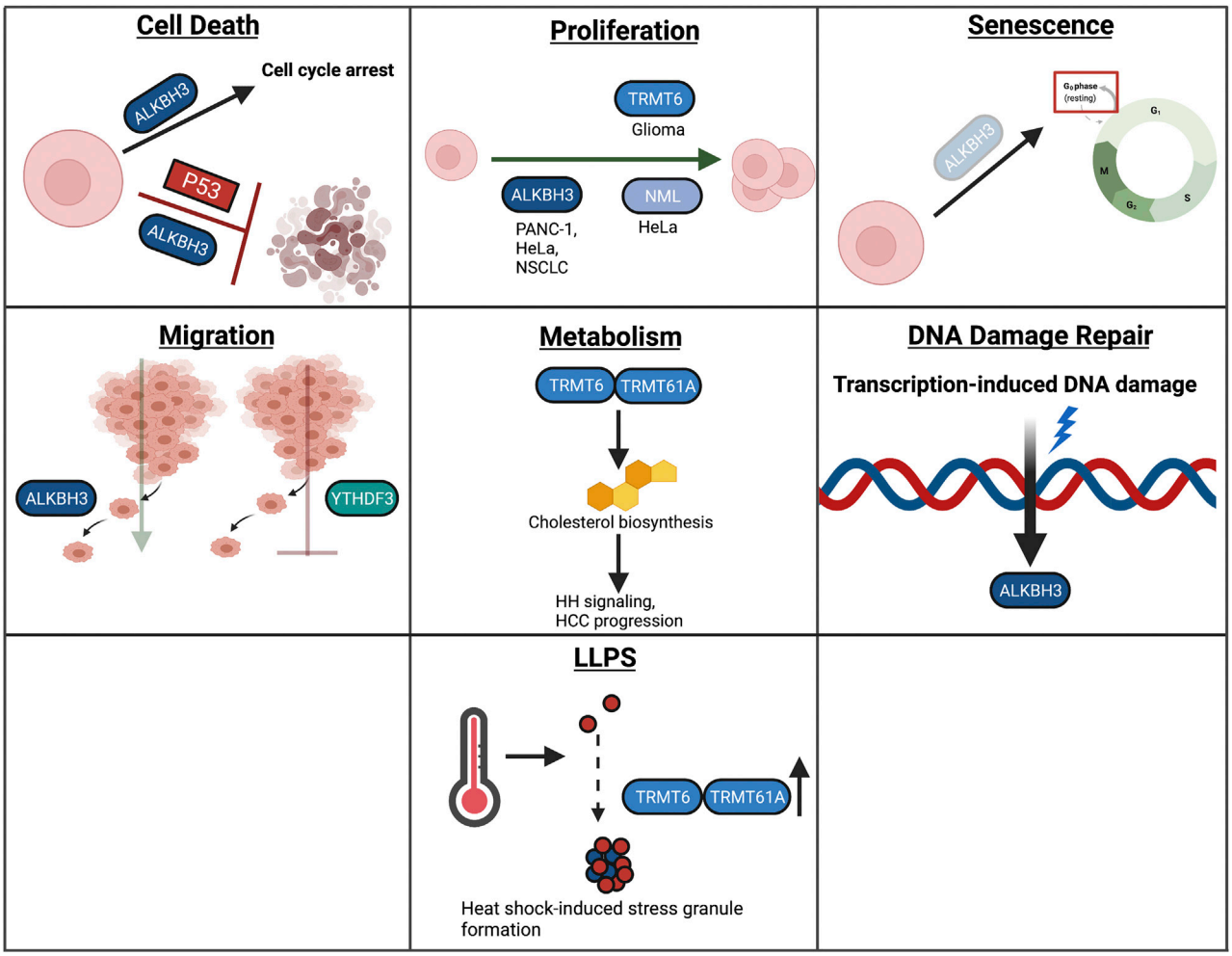


FIGURE 7 | Overview of m^1A in cellular processes. In this review, we highlight the role of RNA modifications in cellular processes such as cell death, proliferation, senescence, migration, metabolism, the DNA damage response, and LLPS. Within these processes, RNA modifications assume unique and context-dependent functions.

lysophosphatidic acid, a lipid that has been to promote migration and overall tumorigenicity (Valdés-Rives and González-Arenas, 2017; Xu et al., 2020). Furthermore, NSUN2 was also found to promote migration in gastric cancer cells (Hu et al., 2021).

Metabolism

Writers

Nsun2$^{-/-}$ mice resulted in changes in the metabolism of methionine and amino acids, and the TCA cycle (Gkatza et al., 2019). *Nsun2* deletion resulted in increased methionine and S-adenosyl-methionine (SAM) levels (Gkatza et al., 2019). Furthermore, free amino acid levels were increased upon loss of *Nsun2*, which was hypothesized to indicate overall decreases in translation (Gkatza et al., 2019). Additionally, *Nsun2* loss resulted in a metabolic shift towards glycolysis (Gkatza et al., 2019). Taken together, the authors hypothesized that *Nsun2* loss results in the induction of a catabolic state, and that NSUN2 functions to promote an anabolic fate (Gkatza et al., 2019).

DNA Damage Response

Writers

Interestingly, *Chen* et al. found that m^5C was localized to DSBs upon ROS-induced DNA damage, and is present at DNA-damage-induced DNA-RNA hybrids (Chen H. et al., 2020). Interestingly, tRNA methyltransferase TRDMT1 was also found to localize to DNA-damage-induced DNA-RNA hybrids and was hypothesized to serve as a damage-induced m^5C methyltransferase (Chen H. et al., 2020). Together, TRDMT1 and m^5C are believed to be necessary to mediate homologous recombination in response to DNA damage (Chen H. et al., 2020; Zhu X. et al., 2021).

THE ROLE OF m^1A in Diverse Cellular Functions

m^1A has been studied in several cellular contexts, including, cell death, proliferation, senescence, migration, metabolism, DDR,

and LLPS (**Figure 7**). The role of m^1A in differentiation in autophagy has not been studied extensively and will therefore not be covered in this section. The role of m^1A in differentiation and autophagy requires further study.

Cell Death

Erasers

In NSCLC, knockdown of the m^1A eraser *Alkbh3* promoted cell cycle arrest (Kogaki et al., 2017). Interestingly, knockdown of both *Alkbh3* and *Tp53* resulted in the induction of apoptosis, suggesting that TP53 may be critical for shifting cell fate from cell cycle arrest to undergoing apoptosis (Kogaki et al., 2017). However, whether ALKBH3 mediates this function as an RNA or DNA methyltransferase was not elucidated (Kogaki et al., 2017).

Proliferation

Writers

Many studies have found positive associations with m^1A regulators, such as the m^1A methyltransferase TRMT6, and cancer (Wang et al., 2019; Shi et al., 2020; Wang B. et al., 2021). However, few studies have established the biological mechanisms by which m^1A regulators assert their oncogenic function. Inhibition of *Trmt6* resulted in decreased proliferation in glioma cell lines, establishing a potential oncogenic role for TRMT6 in regulating proliferation (Macari et al., 2016; Wang B. et al., 2021). Furthermore, inhibition of *Alkbh3*, an m^1A demethylase, resulted in decreased proliferation in HeLa, PANC-1, and NSCLC cancer cells, suggesting a potential role for this demethylase in proliferation (Tasaki et al., 2011; Ueda et al., 2017; Chen et al., 2019). Furthermore, *Waku* et al. established that nucleomethylin (NML) can function as an m^1A 28S rRNA methyltransferase, and that inhibition of NML results in decreased proliferation (Waku et al., 2016).

Senescence

Erasers

Few studies have explored the role of m^1A in cellular senescence. One study, however, found that knockdown of *Alkbh3* in NSCLC cells resulted in senescence induction and cell cycle arrest, followed by increased expression of cell cycle arrest proteins, p27 and p21 (Tasaki et al., 2011).

Migration

Erasers

Few studies have investigated the role of m^1A and m^1A regulators in migration. One study found that knockdown of *Alkbh3* in HeLa cells resulted in decreased invasion (Chen et al., 2019). Furthermore, YTHDF3, serving as an m^1A reader, was found to inhibit invasion in HTR8/SVneo cells by promoting the mRNA decay of *Igf1r* (Zheng et al., 2020). IGF1R is upstream of the pro-migratory MMP9 signaling pathway, and subsequent knockdown of *Ythdf3* resulted in increased IGF1R and MMP9 expression, resulting in increased invasion and migration in these cells (Zheng et al., 2020).

Metabolism

Writers

As previously mentioned, TRMT6 has been found to be associated with oncogenesis in a variety of different cancers. In HCC, the TRMT6/TRMT61A m^1A methyltransferase complex was identified to mediate m^1A tRNA methylation, which resulted in increased PPARδ translation and cholesterol biosynthesis (Wang Y. et al., 2021). Increased cholesterol biosynthesis, in turn, activated Hedgehog signaling and promoted the formation of liver cancer stem cells and HCC tumorigenesis (Wang Y. et al., 2021).

DNA Damage Response

Erasers

Knockdown of *Alkbh3* in NSCLC resulted in increased phosphorylation of critical DDR factors ATM, ATR, and H2AX, suggesting that decreased ALKBH3 may promote single or double-stranded breaks (Kogaki et al., 2017). These DDR factors, as well as DNA-PKcs, were further upregulated in *p53/Alkbh3* dual-knockout cells, establishing that p53 may be a critical regulator of ALKBH3 in mediating DDR (Kogaki et al., 2017). Whether the role of ALKBH3 in DDR is mediated through its demethylase function was not explored in this study (Kogaki et al., 2017). ALKBH3 has also been suggested to function as a DNA repair protein in response to transcription-induced DNA damage (Liefke et al., 2015). Furthermore, levels of m^1A, found on small RNAs, were also noted to be decreased in UV-irradiated cells (Svobodová Kovaříková et al., 2020). However, the functional role of m^1A on small RNAs in response to UV exposure was not detailed in this study (Svobodová Kovaříková et al., 2020).

LLPS

Writers

m^1A methyltransferase TRMT61/61A and m^1A were increased in heat-shock-induced, stress-granule-sequestered mRNAs (Alriquet et al., 2020). In response to stress, mRNAs can form irreversible protein aggregates (Alriquet et al., 2020). Conversely, m^1A-patterned mRNAs were identified to be sequestered into reversible mRNA-protein aggregates, which can then undergo translation (Alriquet et al., 2020). Therefore, the authors hypothesize that m^1A serves a protective role on mRNAs in response to stress (Alriquet et al., 2020).

THERAPEUTICS TARGETING RNA MODIFICATIONS

Due to the pervasiveness of RNA modifications in disease, the development of targeted therapeutics remains critical and is an active area of research. Here, we will briefly summarize advances in the development of therapeutics targeting RNA modifications.

m^6A-Targeted Therapeutics

Yankova et al. recently identified a small molecule inhibitor (STM2457) for METTL3 using a high throughput drug screen (Yankova et al., 2021). STM2547 was identified to be specific to

METTL3 and did not disrupt the METTL3-METTL14 complex (Yankova et al., 2021). As METTL3 has been found to serve an oncogenic function in leukemia, the *in vitro* and *in vivo* efficacy of STM457 was explored as a therapeutic for AML (Vu et al., 2017). STM2457-treatment in AML cell lines resulted in decreased proliferation in a dose-dependent manner and decreased the colony forming capability of mouse AML cells (Yankova et al., 2021). Interestingly, STM2457 showed selectivity for AML cells, but did not affect $CD34^+$ cells, hematopoietic stem and progenitor cells, or non-leukemogenic cell lines (Yankova et al., 2021). STM2457 also decreased the protein expression of oncogenic METTL3 targets, SP1 and BRD4 (Yankova et al., 2021).

Many small molecule inhibitors for FTO have been discovered, including rhein, NCDPCB, meclofenamic acid, MO-I-500, and fluorescein derivatives, among others (Chen et al., 2012; Wang T. et al., 2015; He et al., 2015; Huang et al., 2015; Singh et al., 2016). While these inhibitors inhibit FTO, clinical efficacy of FTO inhibitors has remained unclear. FTO has been found to serve as an oncogene in AML (Li Z. et al., 2017). Accordingly, two studies have developed FTO inhibitors targeting AML (Huang et al., 2019; Su et al., 2020). *Huang* et al. identified FB23-2 as a potential inhibitor for FTO (Huang et al., 2019). Treatment of AML cell lines for FB23-2 slightly decreased AML proliferation and promoted apoptosis, as well as promoted myeloid differentiation (Huang et al., 2019). FB23-2 treatment also resulted in minimal changes in proliferation in bone marrow cells derived from a healthy donor (Huang et al., 2019). Furthermore, FB23-2 showed promising therapeutic efficacy in mice, targeting both AML and leukemia stem cell populations (Huang et al., 2019). Furthermore, using a high throughput screen, *Su* et al. reported the discovery of two small molecule inhibitors targeting FTO, CS1 and CS2, with efficacy in targeting AML (Su et al., 2020). Treatment of AML cell lines with CS1 and CS2 resulted in decreased proliferation, increased apoptosis, and prevented the self-renewal capabilities of leukemia stem cells and leukemia initiating cells (Su et al., 2020). Treatment of healthy control cells showed no change (Su et al., 2020). To date, neither FB23-2 or CS1/CS2 have been employed in clinical trials. While *Selberg* et al. have described the development of a potential ALKBH5 inhibitor, further studies are needed to reconcile the cell-type specific effect of ALKBH5 inhibition (Selberg et al., 2021).

m^5C-Targeted Therapeutics

m^5C-directed therapeutics have also been explored. Few studies have explored the therapeutic potential of targeting m^5C reader YBX1, but have only identified non-specific compounds that effectively target YBX1 (Shibata et al., 2020). *Shibata* et al. identified compounds, TAS0612 and everolimus, as potential compounds that target YBX1 phosphorylation (pYBX1) (Shibata et al., 2020). Increased YBX1 phosphorylation was found to be associated with resistance to fulvestrant, an antiestrogen commonly used to treat ER-positive breast cancer (Shibata et al., 2020). TAS0612 is a multi-kinase inhibitor that targets both the AKT/mTOR/p70S6K pathway, and pYBX1 was identified to be a downstream target of these pathways (Shibata et al., 2020). Everolimus is an mTORC1 inhibitor (Shibata et al., 2020). Accordingly, TAS0612 and everolimus treatment resulted in increased sensitivity to fulvestrant (Shibata et al., 2020). However, this study did not address whether changes in YBX1 phosphorylation changes m^5C regulation (Shibata et al., 2020). Azacytidine is a well-established drug targeting DNMT2 DNA methylation (Stresemann and Lyko, 2008). However, one study, using bisulfite sequencing, argued that azacytidine may also target DNMT2-mediated tRNA methylation (Schaefer et al., 2009). However, follow-up studies are needed to identify whether azacytidine-mediated changes in tRNA methylation are due to m^5C or other mechanisms (Schaefer et al., 2009).

m^1A-Targeted Therapeutics

Wang et al. recently identified thiram as a potential candidate compound that selectively inhibits m^1A writer complex TRMT6/TRMT61A (Wang Y. et al., 2021). Thiram treatment resulted in decreased oncosphere formation in HCC cell lines *in vitro*, and decreased tumor growth *in vivo* (Wang Y. et al., 2021). However, further pre-clinical studies are necessary to determine the safety of thiram treatment in patients, due to reported toxicities (Maita et al., 1991; Wang Y. et al., 2021).

Compound HUHS015 has been identified as an ALKBH3 inhibitor (Nakao et al., 2014). As previously mentioned, ALKBH3 has been found to serve an oncogenic role in many cancers, including prostate cancer (Liefke et al., 2015). HUHS015 has been found to decrease the growth of prostate cancer cell line DU145 and decreased tumor burden in xenograft models (Nakao et al., 2014; Mabuchi et al., 2015). To date, no clinical trial using HUHS015 has been employed.

PERSPECTIVES

While the roles of RNA modifications have been extensively studied for several cellular functions, there remain several areas of interest that are not well-established and require further examination.

Two areas of interest that remain open areas of research include evaluating the roles of RNA modifications in mediating specialized forms of cell death and within LLPS. In the area of cellular death, the role of RNA modifications has been well-studied in terms of apoptosis. However, emerging evidence suggests that RNA modifications may be important in mediating specialized forms of cell death including ferroptosis, pyroptosis, or other mechanisms of specialized cell death (Guo et al., 2020; Shen et al., 2021). Understanding the roles of RNA modifications in these specialized forms of cell death may lead to increased knowledge surrounding the cellular decisions that mediate these forms of cell death.

Furthermore, as previously mentioned, LLPS remains an emerging field of research. The field of LLPS encompasses the intersection of cell biology and biophysics; not only are the biophysical mechanisms by which these condensates form an active area of interest, but more recently, increased attention has been placed on detailing the role these condensates play within cellular processes. Increasing our understanding of RNA

modifications in this process will aid in understanding the function and necessity of LLPS in mediating cellular functions.

The roles of other RNA modifications, other than m^6A, within mammalian cellular processes is another gap of knowledge within the field of epitranscriptomics that remains critical to address. For example, while there are several studies that have identified cellular functions for pseudouridine in *Drosophila*, few studies have been done to explore the role of pseuoduridine in mammalian cellular functions (Vicidomini et al., 2015; Song et al., 2020).

Another area of interest that requires further study is understanding the cell-type specific function of the role of RNA modification in cellular functions. As demonstrated, not only do RNA modifications differ across cell types, but they can also differ across contexts, including across differentiation states and in response to stress. Understanding the relevance and pervasiveness of RNA modifications in these processes, and how different cell types adopt distinct mechanisms for RNA modifications across these functions, remains an important area of research.

In addition, due to the prevalence of RNA modifications in diverse cellular functions, the dysregulation of RNA modifications contributes to the etiology of several diseases. RNA modifications have been found to contribute to the pathologies of several diseases including cancer, diabetes, cardiovascular diseases, and developmental and neurological diseases. Increasing our understanding of the distinct roles that RNA modifications play in these cellular processes will allow for an increased understanding of disease etiology. While there are no therapeutics currently in clinical use that target RNA modifications, an increased understanding of their roles in disease etiology may contribute to the development of therapeutics that aim to selectively target this epitranscriptomic re-wiring.

AUTHOR CONTRIBUTIONS

EW, Y-HC, and Y-YH wrote the manuscript.

FUNDING

Work in the authors' laboratory was supported in part by NIH grants 5T32CA009594-33 (EW), ES031534 (Y-YH), ES024373 (Y-YH), ES030576 (Y-YH), the CACHET (NIH ES027792), the University of Chicago Comprehensive Cancer Center (NIH CA014599), the CTSA (NIH UL1 TR000430), and the University of Chicago Friends of Dermatology Endowment Fund.

ACKNOWLEDGMENTS

We apologize to those investigators whose work could not be directly referenced owing to space limitations. We thank Ann Motten for her critical reading of the manuscript. All figures were created with Biorender.com.

REFERENCES

Abildgaard, M. H., Brynjólfsdóttir, S. H., and Frankel, L. B. (2020). The Autophagy-RNA Interplay: Degradation and beyond. *Trends Biochem. Sci.* 45 (10), 845–857. doi:10.1016/j.tibs.2020.07.007

Alberti, S., and Hyman, A. A. (2021). Biomolecular Condensates at the Nexus of Cellular Stress, Protein Aggregation Disease and Ageing. *Nat. Rev. Mol. Cel Biol* 22 (3), 196–213. doi:10.1038/s41580-020-00326-6

Alriquet, M., Calloni, G., Martínez-Limón, A., Delli Ponti, R., Hanspach, G., Hengesbach, M., et al. (2020). The Protective Role of m1A during Stress-Induced Granulation. *J. Mol. Cel Biol.* 12 (11), 870–880. doi:10.1093/jmcb/mjaa023

Anders, M., Chelysheva, I., Goebel, I., Trenkner, T., Zhou, J., Mao, Y., et al. (2018). Dynamic m6A Methylation Facilitates mRNA Triaging to Stress Granules. *Life Sci. Alliance* 1 (4), e201800113. doi:10.26508/lsa.201800113

Bansal, H., Yihua, Q., Iyer, S. P., Ganapathy, S., Proia, D., Penalva, L. O., et al. (2014). WTAP Is a Novel Oncogenic Protein in Acute Myeloid Leukemia. *Leukemia* 28 (5), 1171–1174. doi:10.1038/leu.2014.16

Batista, P. J., Molinie, B., Wang, J., Qu, K., Zhang, J., Li, L., et al. (2014). m6A RNA Modification Controls Cell Fate Transition in Mammalian Embryonic Stem Cells. *Cell Stem Cell* 15 (6), 707–719. doi:10.1016/j.stem.2014.09.019

Bergsbaken, T., Fink, S. L., and Cookson, B. T. (2009). Pyroptosis: Host Cell Death and Inflammation. *Nat. Rev. Microbiol.* 7 (2), 99–109. doi:10.1038/nrmicro2070

Blanco, S., Kurowski, A., Nichols, J., Watt, F. M., Benitah, S. A., and Frye, M. (2011). The RNA-Methyltransferase Misu (NSun2) Poises Epidermal Stem Cells to Differentiate. *Plos Genet.* 7 (12), e1002403. doi:10.1371/journal.pgen.1002403

Bohnsack, K., Höbartner, C., and Bohnsack, M. (2019). Eukaryotic 5-methylcytosine (m5C) RNA Methyltransferases: Mechanisms, Cellular Functions, and Links to Disease. *Genes* 10 (2), 102. doi:10.3390/genes10020102

Boissel, S., Reish, O., Proulx, K., Kawagoe-Takaki, H., Sedgwick, B., Yeo, G. S. H., et al. (2009). Loss-of-function Mutation in the Dioxygenase-Encoding FTO Gene Causes Severe Growth Retardation and Multiple Malformations. *Am. J. Hum. Genet.* 85 (1), 106–111. doi:10.1016/j.ajhg.2009.06.002

Cai, J., Yang, F., Zhan, H., Situ, J., Li, W., Mao, Y., et al. (2019). RNA m6A Methyltransferase METTL3 Promotes the Growth of Prostate Cancer by Regulating Hedgehog Pathway. *Ott* 12, 9143–9152. doi:10.2147/OTT.S226796

Cai, X., Hu, Y., Tang, H., Hu, H., Pang, L., Xing, J., et al. (2016). RNA Methyltransferase NSUN2 Promotes Stress-Induced HUVEC Senescence. *Oncotarget* 7 (15), 19099–19110. doi:10.18632/oncotarget.8087

Cai, X., Wang, X., Cao, C., Gao, Y., Zhang, S., Yang, Z., et al. (2018). HBXIP-elevated Methyltransferase METTL3 Promotes the Progression of Breast Cancer via Inhibiting Tumor Suppressor Let-7g. *Cancer Lett.* 415, 11–19. doi:10.1016/j.canlet.2017.11.018

Cao, Y., Zhuang, Y., Chen, J., Xu, W., Shou, Y., Huang, X., et al. (2019). Dynamic Effects of Fto in Regulating the Proliferation and Differentiation of Adult Neural Stem Cells of Mice. *Hum. Mol. Genet.* 29 (5), 727–735. doi:10.1093/hmg/ddz274

Casella, G., Tsitsipatis, D., Abdelmohsen, K., and Gorospe, M. (2019). mRNA Methylation in Cell Senescence. *Wiley Interdiscip. Rev. RNA* 10 (6), e1547. doi:10.1002/wrna.1547

Chen, A., Chen, X., Cheng, S., Shu, L., Yan, M., Yao, L., et al. (2018a). FTO Promotes SREBP1c Maturation and Enhances CIDEC Transcription during Lipid Accumulation in HepG2 Cells. *Biochim. Biophys. Acta (Bba) - Mol. Cel Biol. Lipids* 1863 (5), 538–548. doi:10.1016/j.bbalip.2018.02.003

Chen, B., Ye, F., Yu, L., Jia, G., Huang, X., Zhang, X., et al. (2012). Development of Cell-Active N6-Methyladenosine RNA Demethylase FTO Inhibitor. *J. Am. Chem. Soc.* 134 (43), 17963–17971. doi:10.1021/ja3064149

Chen, G., Goto, Y., Sakamoto, R., Tanaka, K., Matsubara, E., Nakamura, M., et al. (2011). GLI1, a Crucial Mediator of Sonic Hedgehog Signaling in Prostate Cancer, Functions as a Negative Modulator for Androgen Receptor. *Biochem. Biophysical Res. Commun.* 404 (3), 809–815. doi:10.1016/j.bbrc.2010.12.065

Chen, H., Gao, S., Liu, W., Wong, C.-C., Wu, J., Wu, J., et al. (2021). RNA N6-Methyladenosine Methyltransferase METTL3 Facilitates Colorectal Cancer by Activating the m6A-GLUT1-mTORC1 Axis and Is a Therapeutic Target. *Gastroenterology* 160 (4), 1284–1300. doi:10.1053/j.gastro.2020.11.013

Chen, H., Yang, H., Zhu, X., Yadav, T., Ouyang, J., Truesdell, S. S., et al. (2020a). m5C Modification of mRNA Serves a DNA Damage Code to Promote Homologous Recombination. *Nat. Commun.* 11 (1), 2834. doi:10.1038/s41467-020-16722-7

Chen, J., Sun, Y., Xu, X., Wang, D., He, J., Zhou, H., et al. (2017). YTH Domain Family 2 Orchestrates Epithelial-Mesenchymal Transition/proliferation Dichotomy in Pancreatic Cancer Cells. *Cell Cycle* 16 (23), 2259–2271. doi:10.1080/15384101.2017.1380125

Chen, M., Wei, L., Law, C.-T., Tsang, F. H.-C., Shen, J., Cheng, C. L.-H., et al. (2018b). RNA N6-Methyladenosine Methyltransferase-like 3 Promotes Liver Cancer Progression through YTHDF2-dependent Posttranscriptional Silencing of SOCS2. *Hepatology* 67 (6), 2254–2270. doi:10.1002/hep.29683

Chen, X., Xu, M., Xu, X., Zeng, K., Liu, X., Pan, B., et al. (2020b). METTL14-mediated N6-Methyladenosine Modification of SOX4 mRNA Inhibits Tumor Metastasis in Colorectal Cancer. *Mol. Cancer* 19 (1), 106. doi:10.1186/s12943-020-01220-7

Chen, Y., Wang, J., Xu, D., Xiang, Z., Ding, J., Yang, X., et al. (2020c). m6A mRNA Methylation Regulates Testosterone Synthesis through Modulating Autophagy in Leydig Cells. *Autophagy*, 1–19. doi:10.1080/15548627.2020.1720431

Chen, Z., Qi, M., Shen, B., Luo, G., Wu, Y., Li, J., et al. (2019). Transfer RNA Demethylase ALKBH3 Promotes Cancer Progression via Induction of tRNA-Derived Small RNAs. *Nucleic Acids Res.* 47 (5), 2533–2545. doi:10.1093/nar/gky1250

Cheng, Y., Luo, H., Izzo, F., Pickering, B. F., Nguyen, D., Myers, R., et al. (2019). m6A RNA Methylation Maintains Hematopoietic Stem Cell Identity and Symmetric Commitment. *Cel Rep.* 28 (7), 1703–1716. doi:10.1016/j.celrep.2019.07.032

Cheng, Y., Xie, W., Pickering, B. F., Chu, K. L., Savino, A. M., Yang, X., et al. (2021). N6-Methyladenosine on mRNA Facilitates a Phase-Separated Nuclear Body that Suppresses Myeloid Leukemic Differentiation. *Cancer Cell* 39 (7), 958–972. doi:10.1016/j.ccell.2021.04.017

Choe, J., Lin, S., Zhang, W., Liu, Q., Wang, L., Ramirez-Moya, J., et al. (2018). mRNA Circularization by METTL3-eIF3h Enhances Translation and Promotes Oncogenesis. *Nature* 561 (7724), 556–560. doi:10.1038/s41586-018-0538-8

Cui, Y.-H., Yang, S., Wei, J., Shea, C. R., Zhong, W., Wang, F., et al. (2021). Autophagy of the m6A mRNA Demethylase FTO Is Impaired by Low-Level Arsenic Exposure to Promote Tumorigenesis. *Nat. Commun.* 12 (1), 2183. doi:10.1038/s41467-021-22469-6

Dahal, U., Le, K., and Gupta, M. (2019). RNA m6A Methyltransferase METTL3 Regulates Invasiveness of Melanoma Cells by Matrix Metallopeptidase 2. *Melanoma Res.* 29 (4), 382–389. doi:10.1097/cmr.0000000000000580

Deng, R., Cheng, Y., Ye, S., Zhang, J., Huang, R., Li, P., et al. (2019). m6A Methyltransferase METTL3 Suppresses Colorectal Cancer Proliferation and Migration through P38/ERK Pathways. *Ott* 12, 4391–4402. doi:10.2147/OTT.S201052

Ding, C., Zou, Q., Ding, J., Ling, M., Wang, W., Li, H., et al. (2018). Increased N6-methyladenosine Causes Infertility Is Associated with FTO Expression. *J. Cel Physiol* 233 (9), 7055–7066. doi:10.1002/jcp.26507

Einstein, J. M., Perelis, M., Chaim, I. A., Meena, J. K., Nussbacher, J. K., Tankka, A. T., et al. (2021). Inhibition of YTHDF2 Triggers Proteotoxic Cell Death in MYC-Driven Breast Cancer. *Mol. Cel* 81 (15), 3048–3064. doi:10.1016/j.molcel.2021.06.014

Elmore, S. (2007). Apoptosis: A Review of Programmed Cell Death. *Toxicol. Pathol.* 35 (4), 495–516. doi:10.1080/01926230701320337

Esteve-Puig, R., Bueno-Costa, A., and Esteller, M. (2020). Writers, Readers and Erasers of RNA Modifications in Cancer. *Cancer Lett.* 474, 127–137. doi:10.1016/j.canlet.2020.01.021

Fei, Q., Zou, Z., Roundtree, I. A., Sun, H.-L., and He, C. (2020). YTHDF2 Promotes Mitotic Entry and Is Regulated by Cell Cycle Mediators. *Plos Biol.* 18 (4), e3000664. doi:10.1371/journal.pbio.3000664

Flores, J. V., Cordero-Espinoza, L., Oeztuerk-Winder, F., Andersson-Rolf, A., Selmi, T., Blanco, S., et al. (2017). Cytosine-5 RNA Methylation Regulates Neural Stem Cell Differentiation and Motility. *Stem Cel. Rep.* 8 (1), 112–124. doi:10.1016/j.stemcr.2016.11.014

Frankel, L. B., Lubas, M., and Lund, A. H. (2017). Emerging Connections between RNA and Autophagy. *Autophagy* 13 (1), 3–23. doi:10.1080/15548627.2016.1222992

Frayling, T. M., Timpson, N. J., Weedon, M. N., Zeggini, E., Freathy, R. M., Lindgren, C. M., et al. (2007). A Common Variant in the FTO Gene Is Associated with Body Mass index and Predisposes to Childhood and Adult Obesity. *Science* 316 (5826), 889–894. doi:10.1126/science.1141634

Frye, M., Harada, B. T., Behm, M., and He, C. (2018). RNA Modifications Modulate Gene Expression during Development. *Science* 361 (6409), 1346–1349. doi:10.1126/science.aau1646

Frye, M., and Watt, F. M. (2006). The RNA Methyltransferase Misu (NSun2) Mediates Myc-Induced Proliferation and Is Upregulated in Tumors. *Curr. Biol.* 16 (10), 971–981. doi:10.1016/j.cub.2006.04.027

Fu, Y., and Zhuang, X. (2020). m6A-binding YTHDF Proteins Promote Stress Granule Formation. *Nat. Chem. Biol.* 16 (9), 955–963. doi:10.1038/s41589-020-0524-y

Fukusumi, Y., Naruse, C., and Asano, M. (2008). Wtap Is Required for Differentiation of Endoderm and Mesoderm in the Mouse Embryo. *Dev. Dyn.* 237 (3), 618–629. doi:10.1002/dvdy.21444

Garcia-Saez, I., Lacroix, F. B., Blot, D., Gabel, F., and Skoufias, D. A. (2011). Structural Characterization of HBXIP: the Protein that Interacts with the Anti-apoptotic Protein Survivin and the Oncogenic Viral Protein HBx. *J. Mol. Biol.* 405 (2), 331–340. doi:10.1016/j.jmb.2010.10.046

Gkatza, N. A., Castro, C., Harvey, R. F., Heiß, M., Popis, M. C., Blanco, S., et al. (2019). Cytosine-5 RNA Methylation Links Protein Synthesis to Cell Metabolism. *Plos Biol.* 17 (6), e3000297. doi:10.1371/journal.pbio.3000297

Glick, D., Barth, S., and Macleod, K. F. (2010). Autophagy: Cellular and Molecular Mechanisms. *J. Pathol.* 221 (1), 3–12. doi:10.1002/path.2697

Graille, M. (2022). Division of Labor in Epitranscriptomics: What Have We Learnt from the Structures of Eukaryotic and Viral Multimeric RNA Methyltransferases? *Wiley Interdiscip. Rev. RNA* 13 (1), e1673. doi:10.1002/wrna.1673

Guo, M., Yan, R., Ji, Q., Yao, H., Sun, M., Duan, L., et al. (2020). IFN Regulatory Factor-1 Induced Macrophage Pyroptosis by Modulating m6A Modification of Circ_0029589 in Patients with Acute Coronary Syndrome. *Int. Immunopharmacology* 86, 106800. doi:10.1016/j.intimp.2020.106800

Han, J., Wang, J.-z., Yang, X., Yu, H., Zhou, R., Lu, H.-C., et al. (2019). METTL3 Promote Tumor Proliferation of Bladder Cancer by Accelerating Pri-miR221/222 Maturation in m6A-dependent Manner. *Mol. Cancer* 18 (1), 110. doi:10.1186/s12943-019-1036-9

Han, X., Wang, L., and Han, Q. (2020). Advances in the Role of m6A RNA Modification in Cancer Metabolic Reprogramming. *Cell Biosci* 10 (1), 117. doi:10.1186/s13578-020-00479-z

He, H., Wu, W., Sun, Z., and Chai, L. (2019). MiR-4429 Prevented Gastric Cancer Progression through Targeting METTL3 to Inhibit m6A-Caused Stabilization of SEC62. *Biochem. Biophysical Res. Commun.* 517 (4), 581–587. doi:10.1016/j.bbrc.2019.07.058

He, W., Zhou, B., Liu, W., Zhang, M., Shen, Z., Han, Z., et al. (2015). Identification of A Novel Small-Molecule Binding Site of the Fat Mass and Obesity Associated Protein (FTO). *J. Med. Chem.* 58 (18), 7341–7348. doi:10.1021/acs.jmedchem.5b00702

He, Y., Wang, W., Xu, X., Yang, B., Yu, X., Wu, Y., et al. (2022). Mettl3 Inhibits the Apoptosis and Autophagy of Chondrocytes in Inflammation through Mediating Bcl2 Stability via Ythdf1-Mediated m6A Modification. *Bone* 154, 116182. doi:10.1016/j.bone.2021.116182

Hong, J., Lee, J. H., and Chung, I. K. (2016). Telomerase Activates Transcription of Cyclin D1 Gene through an Interaction with NOL1. *J. Cel Sci* 129 (8), 1566–1579. doi:10.1242/jcs.181040

Horiuchi, K., Umetani, M., Minami, T., Okayama, H., Takada, S., Yamamoto, M., et al. (2006). Wilms' Tumor 1-associating Protein Regulates G2/M Transition through Stabilization of Cyclin A2 mRNA. *Proc. Natl. Acad. Sci.* 103 (46), 17278–17283. doi:10.1073/pnas.0608357103

Hu, Y., Chen, C., Tong, X., Chen, S., Hu, X., Pan, B., et al. (2021). NSUN2 Modified by SUMO-2/3 Promotes Gastric Cancer Progression and Regulates

mRNA m5C Methylation. *Cell Death Dis* 12 (9), 842. doi:10.1038/s41419-021-04127-3

Hua, W., Zhao, Y., Jin, X., Yu, D., He, J., Xie, D., et al. (2018). METTL3 Promotes Ovarian Carcinoma Growth and Invasion through the Regulation of AXL Translation and Epithelial to Mesenchymal Transition. *Gynecol. Oncol.* 151 (2), 356–365. doi:10.1016/j.ygyno.2018.09.015

Huang, H., Weng, H., Deng, X., and Chen, J. (2020). RNA Modifications in Cancer: Functions, Mechanisms, and Therapeutic Implications. *Annu. Rev. Cancer Biol.* 4 (1), 221–240. doi:10.1146/annurev-cancerbio-030419-033357

Huang, Y., Su, R., Sheng, Y., Dong, L., Dong, Z., Xu, H., et al. (2019). Small-Molecule Targeting of Oncogenic FTO Demethylase in Acute Myeloid Leukemia. *Cancer cell* 35 (4), 677–691. doi:10.1016/j.ccell.2019.03.006

Huang, Y., Yan, J., Li, Q., Li, J., Gong, S., Zhou, H., et al. (2015). Meclofenamic Acid Selectively Inhibits FTO Demethylation of m6A over ALKBH5. *Nucleic Acids Res.* 43 (1), 373–384. doi:10.1093/nar/gku1276

Hussain, S., Benavente, S. B., Nascimento, E., Dragoni, I., Kurowski, A., Gillich, A., et al. (2009). The Nucleolar RNA Methyltransferase Misu (NSun2) Is Required for Mitotic Spindle Stability. *J. Cel Biol.* 186 (1), 27–40. doi:10.1083/jcb.200810180

Hussain, S., Tuorto, F., Menon, S., Blanco, S., Cox, C., Flores, J. V., et al. (2013). The Mouse Cytosine-5 RNA Methyltransferase NSun2 Is a Component of the Chromatoid Body and Required for Testis Differentiation. *Mol. Cel Biol* 33 (8), 1561–1570. doi:10.1128/MCB.01523-12

Jensen-Urstad, A. P. L., and Semenkovich, C. F. (2012). Fatty Acid Synthase and Liver Triglyceride Metabolism: Housekeeper or Messenger? *Biochim. Biophys. Acta (Bba) - Mol. Cel Biol. Lipids* 1821 (5), 747–753. doi:10.1016/j.bbalip.2011.09.017

Jian, H., Zhang, C., Qi, Z., Li, X., Lou, Y., Kang, Y., et al. (2021). Alteration of mRNA 5-Methylcytosine Modification in Neurons after OGD/R and Potential Roles in Cell Stress Response and Apoptosis. *Front. Genet.* 12. doi:10.3389/fgene.2021.633681

Jiang, Q., Sun, B., Liu, Q., Cai, M., Wu, R., Wang, F., et al. (2019). MTCH2 Promotes Adipogenesis in Intramuscular Preadipocytes via an M 6 A-YTHDF1-dependent Mechanism. *FASEB j.* 33 (2), 2971–2981. doi:10.1096/fj.201801393RRR

Jiang, S., Fagman, J. B., Chen, C., Alberti, S., and Liu, B. (2020). Protein Phase Separation and its Role in Tumorigenesis. *eLife* 9, e60264. doi:10.7554/eLife.60264

Jiang, Z.-x., Wang, Y.-n., Li, Z.-y., Dai, Z.-h., He, Y., Chu, K., et al. (2021). The m6A mRNA Demethylase FTO in Granulosa Cells Retards FOS-dependent Ovarian Aging. *Cel Death Dis* 12 (8), 744. doi:10.1038/s41419-021-04016-9

Jin, S., Zhang, X., Miao, Y., Liang, P., Zhu, K., She, Y., et al. (2018). m6A RNA Modification Controls Autophagy through Upregulating ULK1 Protein Abundance. *Cell Res* 28 (9), 955–957. doi:10.1038/s41422-018-0069-8

Jo, H.-J., Shim, H.-E., Han, M.-E., Kim, H.-J., Kim, K.-S., Baek, S., et al. (2013). WTAP Regulates Migration and Invasion of Cholangiocarcinoma Cells. *J. Gastroenterol.* 48 (11), 1271–1282. doi:10.1007/s00535-013-0748-7

Kang, H., Zhang, Z., Yu, L., Li, Y., Liang, M., and Zhou, L. (2018). FTO Reduces Mitochondria and Promotes Hepatic Fat Accumulation through RNA Demethylation. *J. Cel. Biochem.* 119 (7), 5676–5685. doi:10.1002/jcb.26746

Khong, A., Matheny, T., Huynh, T. N., Babl, V., and Parker, R. (2021). Limited Effects of m^6A Modification on mRNA Partitioning into Stress Granules. *bioRxiv*. doi:10.1101/2021.03.19.436090

Klionsky, D. J. (2007). Autophagy: from Phenomenology to Molecular Understanding in Less Than a Decade. *Nat. Rev. Mol. Cel Biol* 8 (11), 931–937. doi:10.1038/nrm2245

Kogaki, T., Ohshio, I., Kawaguchi, M., Kimoto, M., Kitae, K., Hase, H., et al. (2017). TP53 Gene Status Is a Critical Determinant of Phenotypes Induced by ALKBH3 Knockdown in Non-small Cell Lung Cancers. *Biochem. Biophysical Res. Commun.* 488 (2), 285–290. doi:10.1016/j.bbrc.2017.05.024

Kosi, N., Alić, I., Kolačević, M., Vrsaljko, N., Jovanov Milošević, N., Sobol, M., et al. (2015). Nop2 Is Expressed during Proliferation of Neural Stem Cells and in Adult Mouse and Human Brain. *Brain Res.* 1597, 65–76. doi:10.1016/j.brainres.2014.11.040

Kousteni, S. (2012). FoxO1, the Transcriptional Chief of Staff of Energy Metabolism. *Bone* 50 (2), 437–443. doi:10.1016/j.bone.2011.06.034

Kumari, R., and Jat, P. (2021). Mechanisms of Cellular Senescence: Cell Cycle Arrest and Senescence Associated Secretory Phenotype. *Front. Cel Developmental Biol.*9. doi:10.3389/fcell.2021.645593

Lan, T., Li, H., Zhang, D., Xu, L., Liu, H., Hao, X., et al. (2019). KIAA1429 Contributes to Liver Cancer Progression through N6-methyladenosine-dependent post-transcriptional Modification of GATA3. *Mol. Cancer* 18 (1), 186. doi:10.1186/s12943-019-1106-z

Lee, H., Bao, S., Qian, Y., Geula, S., Leslie, J., Zhang, C., et al. (2019). Stage-specific Requirement for Mettl3-dependent m6A mRNA Methylation during Haematopoietic Stem Cell Differentiation. *Nat. Cel Biol* 21 (6), 700–709. doi:10.1038/s41556-019-0318-1

Lee, J., Wu, Y., Harada, B. T., Li, Y., Zhao, J., He, C., et al. (2021a). N6 -methyladenosine Modification of lncRNA Pvt1 Governs Epidermal Stemness. *Embo j* 40 (8), e106276. doi:10.15252/embj.2020106276

Lee, J.-H., Wang, R., Xiong, F., Krakowiak, J., Liao, Z., Nguyen, P. T., et al. (2021b). Enhancer RNA m6A Methylation Facilitates Transcriptional Condensate Formation and Gene Activation. *Mol. Cel* 81 (16), 3368–3385. doi:10.1016/j.molcel.2021.07.024

Li, G., Deng, L., Huang, N., Cui, Z., Wu, Q., Ma, J., et al. (2021a). m6A mRNA Methylation Regulates LKB1 to Promote Autophagy of Hepatoblastoma Cells through Upregulated Phosphorylation of AMPK. *Genes* 12 (11), 1747. doi:10.3390/genes12111747

Li, J., Han, Y., Zhang, H., Qian, Z., Jia, W., Gao, Y., et al. (2019). The m6A Demethylase FTO Promotes the Growth of Lung Cancer Cells by Regulating the m6A Level of USP7 mRNA. *Biochem. Biophysical Res. Commun.* 512 (3), 479–485. doi:10.1016/j.bbrc.2019.03.093

Li, N., Kang, Y., Wang, L., Huff, S., Tang, R., Hui, H., et al. (2020). ALKBH5 Regulates Anti-PD-1 Therapy Response by Modulating Lactate and Suppressive Immune Cell Accumulation in Tumor Microenvironment. *Proc. Natl. Acad. Sci. USA* 117 (33), 20159–20170. doi:10.1073/pnas.1918986117

Li, Q., Li, X., Tang, H., Jiang, B., Dou, Y., Gorospe, M., et al. (2017a). NSUN2-Mediated m5C Methylation and METTL3/METTL14-Mediated m6A Methylation Cooperatively Enhance P21 Translation. *J. Cel. Biochem.* 118 (9), 2587–2598. doi:10.1002/jcb.25957

Li, Q., Ni, Y., Zhang, L., Jiang, R., Xu, J., Yang, H., et al. (2021b). HIF-1α-induced Expression of m6A Reader YTHDF1 Drives Hypoxia-Induced Autophagy and Malignancy of Hepatocellular Carcinoma by Promoting ATG2A and ATG14 Translation. *Sig Transduct Target. Ther.* 6 (1), 76. doi:10.1038/s41392-020-00453-8

Li, X., Tang, J., Huang, W., Wang, F., Li, P., Qin, C., et al. (2017b). The M6A Methyltransferase METTL3: Acting as a Tumor Suppressor in Renal Cell Carcinoma. *Oncotarget* 8 (56), 96103–96116. doi:10.18632/oncotarget.21726

Li, X., Yang, J., Zhu, Y., Liu, Y., Shi, X. e., and Yang, G. (2016). Mouse Maternal High-Fat Intake Dynamically Programmed mRNA m6A Modifications in Adipose and Skeletal Muscle Tissues in Offspring. *Ijms* 17 (8), 1336. doi:10.3390/ijms17081336

Li, Z., Qian, P., Shao, W., Shi, H., He, X. C., Gogol, M., et al. (2018). Suppression of m6A Reader Ythdf2 Promotes Hematopoietic Stem Cell Expansion. *Cel Res* 28 (9), 904–917. doi:10.1038/s41422-018-0072-0

Li, Z., Weng, H., Su, R., Weng, X., Zuo, Z., Li, C., et al. (2017c). FTO Plays an Oncogenic Role in Acute Myeloid Leukemia as a N 6 -Methyladenosine RNA Demethylase. *Cancer Cell* 31 (1), 127–141. doi:10.1016/j.ccell.2016.11.017

Liang, D., Lin, W.-J., Ren, M., Qiu, J., Yang, C., Wang, X., et al. (2021). m6A Reader YTHDC1 Modulates Autophagy by Targeting SQSTM1 in Diabetic Skin. *Autophagy*, 1–20. doi:10.1080/15548627.2021.1974175

Liefke, R., Windhof-Jaidhauser, I. M., Gaedcke, J., Salinas-Riester, G., Wu, F., Ghadimi, M., et al. (2015). The Oxidative Demethylase ALKBH3 marks Hyperactive Gene Promoters in Human Cancer Cells. *Genome Med.* 7 (1), 66. doi:10.1186/s13073-015-0180-0

Lin, S., Liu, J., Jiang, W., Wang, P., Sun, C., Wang, X., et al. (2019a). METTL3 Promotes the Proliferation and Mobility of Gastric Cancer Cells. *Open Med. (Wars)* 14, 25–31. doi:10.1515/med-2019-0005

Lin, X., Chai, G., Wu, Y., Li, J., Chen, F., Liu, J., et al. (2019b). RNA m6A Methylation Regulates the Epithelial Mesenchymal Transition of Cancer Cells and Translation of Snail. *Nat. Commun.* 10 (1), 2065. doi:10.1038/s41467-019-09865-9

Lin, Z., Niu, Y., Wan, A., Chen, D., Liang, H., Chen, X., et al. (2020). RNA M6 A Methylation Regulates Sorafenib Resistance in Liver Cancer through FOXO3-

Mediated Autophagy. *EMBO J.* 39 (12), e103181. doi:10.15252/embj.2019103181

Liu, H., Xu, Y., Yao, B., Sui, T., Lai, L., and Li, Z. (2020a). A Novel N6-Methyladenosine (m6A)-dependent Fate Decision for the lncRNA THOR. *Cel Death Dis* 11 (8), 613. doi:10.1038/s41419-020-02833-y

Liu, J., Eckert, M. A., Harada, B. T., Liu, S.-M., Lu, Z., Yu, K., et al. (2018). m6A mRNA Methylation Regulates AKT Activity to Promote the Proliferation and Tumorigenicity of Endometrial Cancer. *Nat. Cel Biol* 20 (9), 1074–1083. doi:10.1038/s41556-018-0174-4

Liu, L., Wang, J., Sun, G., Wu, Q., Ma, J., Zhang, X., et al. (2019). m6A mRNA Methylation Regulates CTNNB1 to Promote the Proliferation of Hepatoblastoma. *Mol. Cancer* 18 (1), 188. doi:10.1186/s12943-019-1119-7

Liu, P., Li, F., Lin, J., Fukumoto, T., Nacarelli, T., Hao, X., et al. (2021a). m6A-independent Genome-wide METTL3 and METTL14 Redistribution Drives the Senescence-Associated Secretory Phenotype. *Nat. Cel Biol* 23 (4), 355–365. doi:10.1038/s41556-021-00656-3

Liu, S., Li, Q., Li, G., Zhang, Q., Zhuo, L., Han, X., et al. (2020b). The Mechanism of m6A Methyltransferase METTL3-Mediated Autophagy in Reversing Gefitinib Resistance in NSCLC Cells by β-elemene. *Cel Death Dis* 11 (11), 969. doi:10.1038/s41419-020-03148-8

Liu, X., Xiao, M., Zhang, L., Li, L., Zhu, G., Shen, E., et al. (2021b). The m6A Methyltransferase METTL14 Inhibits the Proliferation, Migration, and Invasion of Gastric Cancer by Regulating the PI3K/AKT/mTOR Signaling Pathway. *J. Clin. Lab. Anal.* 35 (3), e23655. doi:10.1002/jcla.23655

Lopez-Pajares, V., Yan, K., Zarnegar, B. J., Jameson, K. L., and Khavari, P. A. (2013). Genetic Pathways in Disorders of Epidermal Differentiation. *Trends Genet.* 29 (1), 31–40. doi:10.1016/j.tig.2012.10.005

Luo, G., Xu, W., Zhao, Y., Jin, S., Wang, S., Liu, Q., et al. (2020). RNA M 6 A Methylation Regulates Uveal Melanoma Cell Proliferation, Migration, and Invasion by Targeting c-Met. *J. Cel Physiol* 235 (10), 7107–7119. doi:10.1002/jcp.29608

Lyon, A. S., Peeples, W. B., and Rosen, M. K. (2021). A Framework for Understanding the Functions of Biomolecular Condensates across Scales. *Nat. Rev. Mol. Cel Biol* 22 (3), 215–235. doi:10.1038/s41580-020-00303-z

Mabuchi, M., Shimizu, T., Ueda, M., Sasakawa, Y., Nakao, S., Ueda, Y., et al. (2015). Improving the Bioavailability and Anticancer Effect of the PCA-1/ALKBH3 Inhibitor HUHS015 Using Sodium Salt. *In Vivo* 29 (1), 39–43.

Macari, F., El-houfi, Y., Boldina, G., Xu, H., Khoury-Hanna, S., Ollier, J., et al. (2016). TRM6/61 Connects PKCα with Translational Control through tRNAiMet Stabilization: Impact on Tumorigenesis. *Oncogene* 35 (14), 1785–1796. doi:10.1038/onc.2015.244

Maita, K., Tsuda, S., and Shirasu, Y. (1991). Chronic Toxicity Studies with Thiram in Wistar Rats and Beagle Dogs. *Toxicol. Sci.* 16 (4), 667–686. doi:10.1016/0272-0590(91)90154-v10.1093/toxsci/16.4.667

Malla, S., Melguizo-Sanchis, D., and Aguilo, F. (2019). Steering Pluripotency and Differentiation with N6-Methyladenosine RNA Modification. *Biochim. Biophys. Acta (Bba) - Gene Regul. Mech.* 1862 (3), 394–402. doi:10.1016/j.bbagrm.2018.10.013

Merkestein, M., Laber, S., McMurray, F., Andrew, D., Sachse, G., Sanderson, J., et al. (2015). FTO Influences Adipogenesis by Regulating Mitotic Clonal Expansion. *Nat. Commun.* 6 (1), 6792. doi:10.1038/ncomms7792

Meyer, K. D., Patil, D. P., Zhou, J., Zinoviev, A., Skabkin, M. A., Elemento, O., et al. (2015). 5′ UTR m6A Promotes Cap-independent Translation. *Cell* 163 (4), 999–1010. doi:10.1016/j.cell.2015.10.012

Miranda-Gonçalves, V., Lobo, J., Guimarães-Teixeira, C., Barros-Silva, D., Guimarães, R., Cantante, M., et al. (2021). The Component of the m6A Writer Complex VIRMA Is Implicated in Aggressive Tumor Phenotype, DNA Damage Response and Cisplatin Resistance in Germ Cell Tumors. *J. Exp. Clin. Cancer Res.* 40 (1), 268. doi:10.1186/s13046-021-02072-9

Mizushima, N., Levine, B., Cuervo, A. M., and Klionsky, D. J. (2008). Autophagy Fights Disease through Cellular Self-Digestion. *Nature* 451 (7182), 1069–1075. doi:10.1038/nature06639

Nakao, S., Mabuchi, M., Shimizu, T., Itoh, Y., Takeuchi, Y., Ueda, M., et al. (2014). Design and Synthesis of Prostate Cancer Antigen-1 (PCA-1/ALKBH3) Inhibitors as Anti-prostate Cancer Drugs. *Bioorg. Med. Chem. Lett.* 24 (4), 1071–1074. doi:10.1016/j.bmcl.2014.01.008

Niu, Y., Lin, Z., Wan, A., Chen, H., Liang, H., Sun, L., et al. (2019). RNA N6-Methyladenosine Demethylase FTO Promotes Breast Tumor Progression through Inhibiting BNIP3. *Mol. Cancer* 18 (1), 46. doi:10.1186/s12943-019-1004-4

Okamoto, M., Hirata, S., Sato, S., Koga, S., Fujii, M., Qi, G., et al. (2012). Frequent Increased Gene Copy Number and High Protein Expression of tRNA (Cytosine-5-)-methyltransferase (NSUN2) in Human Cancers. *DNA Cel Biol.* 31 (5), 660–671. doi:10.1089/dna.2011.1446

Peng, S., Xiao, W., Ju, D., Sun, B., Hou, N., Liu, Q., et al. (2019). Identification of Entacapone as a Chemical Inhibitor of FTO Mediating Metabolic Regulation through FOXO1. *Sci. Translational Med.* 11, eaau7116. doi:10.1126/scitranslmed.aau7116

Qian, J.-Y., Gao, J., Sun, X., Cao, M.-D., Shi, L., Xia, T.-S., et al. (2019). KIAA1429 Acts as an Oncogenic Factor in Breast Cancer by Regulating CDK1 in an N6-methyladenosine-independent Manner. *Oncogene* 38 (33), 6123–6141. doi:10.1038/s41388-019-0861-z

Regl, G., Neill, G. W., Eichberger, T., Kasper, M., Ikram, M. S., Koller, J., et al. (2002). Human GLI2 and GLI1 Are Part of a Positive Feedback Mechanism in Basal Cell Carcinoma. *Oncogene* 21 (36), 5529–5539. doi:10.1038/sj.onc.1205748

Ries, R. J., Zaccara, S., Klein, P., Olarerin-George, A., Namkoong, S., Pickering, B. F., et al. (2019). m6A Enhances the Phase Separation Potential of mRNA. *Nature* 571 (7765), 424–428. doi:10.1038/s41586-019-1374-1

Rosselló-Tortella, M., Ferrer, G., and Esteller, M. (2020). Epitranscriptomics in Hematopoiesis and Hematologic Malignancies. *Blood Cancer Discov.* 1 (1), 26–31. doi:10.1158/2643-3249.Bcd-20-0032

Roundtree, I. A., Evans, M. E., Pan, T., and He, C. (2017). Dynamic RNA Modifications in Gene Expression Regulation. *Cell* 169 (7), 1187–1200. doi:10.1016/j.cell.2017.05.045

Sajini, A. A., Choudhury, N. R., Wagner, R. E., Bornelöv, S., Selmi, T., Spanos, C., et al. (2019). Loss of 5-methylcytosine Alters the Biogenesis of Vault-Derived Small RNAs to Coordinate Epidermal Differentiation. *Nat. Commun.* 10 (1), 2550. doi:10.1038/s41467-019-10020-7

Schaefer, M., Hagemann, S., Hanna, K., and Lyko, F. (2009). Azacytidine Inhibits RNA Methylation at DNMT2 Target Sites in Human Cancer Cell Lines. *Cancer Res.* 69 (20), 8127–8132. doi:10.1158/0008-5472.Can-09-0458

Schwartz, S., Agarwala, S. D., Mumbach, M. R., Jovanovic, M., Mertins, P., Shishkin, A., et al. (2013). High-Resolution Mapping Reveals a Conserved, Widespread, Dynamic mRNA Methylation Program in Yeast Meiosis. *Cell* 155 (6), 1409–1421. doi:10.1016/j.cell.2013.10.047

Selberg, S., Seli, N., Kankuri, E., and Karelson, M. (2021). Rational Design of Novel Anticancer Small-Molecule RNA m6A Demethylase ALKBH5 Inhibitors. *ACS omega* 6 (20), 13310–13320. doi:10.1021/acsomega.1c01289

Shen, C., Xuan, B., Yan, T., Ma, Y., Xu, P., Tian, X., et al. (2020). m6A-dependent Glycolysis Enhances Colorectal Cancer Progression. *Mol. Cancer* 19 (1), 72. doi:10.1186/s12943-020-01190-w

Shen, L., Liang, Z., Wong, C. E., and Yu, H. (2019). Messenger RNA Modifications in Plants. *Trends Plant Sci.* 24 (4), 328–341. doi:10.1016/j.tplants.2019.01.005

Shen, M., Li, Y., Wang, Y., Shao, J., Zhang, F., Yin, G., et al. (2021). N6-methyladenosine Modification Regulates Ferroptosis through Autophagy Signaling Pathway in Hepatic Stellate Cells. *Redox Biol.* 47, 102151. doi:10.1016/j.redox.2021.102151

Shi, Q., Xue, C., Yuan, X., He, Y., and Yu, Z. (2020). Gene Signatures and Prognostic Values of m1A-Related Regulatory Genes in Hepatocellular Carcinoma. *Sci. Rep.* 10 (1), 15083. doi:10.1038/s41598-020-72178-1

Shibata, T., Watari, K., Kawahara, A., Sudo, T., Hattori, S., Murakami, Y., et al. (2020). Targeting Phosphorylation of Y-Box-Binding Protein YBX1 by TAS0612 and Everolimus in Overcoming Antiestrogen Resistance. *Mol. Cancer Ther.* 19 (3), 882–894. doi:10.1158/1535-7163.Mct-19-0690

Singh, B., Kinne, H. E., Milligan, R. D., Washburn, L. J., Olsen, M., and Lucci, A. (2016). Important Role of FTO in the Survival of Rare Panresistant Triple-Negative Inflammatory Breast Cancer Cells Facing a Severe Metabolic Challenge. *PloS one* 11 (7), e0159072. doi:10.1371/journal.pone.0159072

Song, H., Feng, X., Zhang, H., Luo, Y., Huang, J., Lin, M., et al. (2019). METTL3 and ALKBH5 Oppositely Regulate m6A Modification of TFEB mRNA, Which Dictates the Fate of Hypoxia/reoxygenation-Treated Cardiomyocytes. *Autophagy* 15 (8), 1419–1437. doi:10.1080/15548627.2019.1586246

Song, P., Tayier, S., Cai, Z., and Jia, G. (2021). RNA Methylation in Mammalian Development and Cancer. *Cell Biol Toxicol* 37 (6), 811–831. doi:10.1007/s10565-021-09627-8

Song, W., Ressl, S., and Tracey, W. D. (2020). Loss of Pseudouridine Synthases in the RluA Family Causes Hypersensitive Nociception in Drosophila. *G3 (Bethesda, Md.* 10 (12), 4425–4438. doi:10.1534/g3.120.401767

Spina, A., De Pasquale, V., Cerulo, G., Cocchiaro, P., Della Morte, R., Avallone, L., et al. (2015). HGF/c-MET Axis in Tumor Microenvironment and Metastasis Formation. *Biomedicines* 3 (1), 71–88. doi:10.3390/biomedicines3010071

Stadler, P. F., Chen, J. J.-L., Hackermüller, J., Hoffmann, S., Horn, F., Khaitovich, P., et al. (2009). Evolution of Vault RNAs. *Mol. Biol. Evol.* 26 (9), 1975–1991. doi:10.1093/molbev/msp112

Stratigopoulos, G., LeDuc, C. A., Cremona, M. L., Chung, W. K., and Leibel, R. L. (2011). Cut-like Homeobox 1 (CUX1) Regulates Expression of the Fat Mass and Obesity-Associated and Retinitis Pigmentosa GTPase Regulator-Interacting Protein-1-like (RPGRIP1L) Genes and Coordinates Leptin Receptor Signaling. *J. Biol. Chem.* 286 (3), 2155–2170. doi:10.1074/jbc.M110.188482

Stresemann, C., and Lyko, F. (2008). Modes of Action of the DNA Methyltransferase Inhibitors Azacytidine and Decitabine. *Int. J. Cancer* 123 (1), 8–13. doi:10.1002/ijc.23607

Su, R., Dong, L., Li, C., Nachtergaele, S., Wunderlich, M., Qing, Y., et al. (2018). R-2HG Exhibits Anti-tumor Activity by Targeting FTO/m6A/MYC/CEBPA Signaling. *Cell* 172 (1-2), 90–e23. doi:10.1016/j.cell.2017.11.031

Su, R., Dong, L., Li, Y., Gao, M., Han, L., Wunderlich, M., et al. (2020). Targeting FTO Suppresses Cancer Stem Cell Maintenance and Immune Evasion. *Cancer cell* 38 (1), 79–96. doi:10.1016/j.ccell.2020.04.017

Sun, T., Wu, Z., Wang, X., Wang, Y., Hu, X., Qin, W., et al. (2020). LNC942 Promoting METTL14-Mediated m6A Methylation in Breast Cancer Cell Proliferation and Progression. *Oncogene* 39 (31), 5358–5372. doi:10.1038/s41388-020-1338-9

Svobodová Kovaříková, A., Stixová, L., Kovařík, A., Komůrková, D., Legartová, S., Fagherazzi, P., et al. (2020). N(6)-Adenosine Methylation in RNA and a Reduced m(3)G/TMG Level in Non-coding RNAs Appear at Microirradiation-Induced DNA Lesions. *Cells* 9 (2), 360. doi:10.3390/cells9020360

Taketo, K., Konno, M., Asai, A., Koseki, J., Toratani, M., Satoh, T., et al. (2018). The Epitranscriptome m6A Writer METTL3 Promotes Chemo- and Radioresistance in Pancreatic Cancer Cells. *Int. J. Oncol.* 52 (2), 621–629. doi:10.3892/ijo.2017.4219

Tang, H.-W., Weng, J.-H., Lee, W. X., Hu, Y., Gu, L., Cho, S., et al. (2021). mTORC1-chaperonin CCT Signaling Regulates m6A RNA Methylation to Suppress Autophagy. *Proc. Natl. Acad. Sci. USA* 118 (10), e2021945118. doi:10.1073/pnas.2021945118

Tang, H., Fan, X., Xing, J., Liu, Z., Jiang, B., Dou, Y., et al. (2015). NSun2 Delays Replicative Senescence by Repressing P27 (KIP1) Translation and Elevating CDK1 Translation. *Aging* 7 (12), 1143–1155. doi:10.18632/aging.100860

Tang, J., Wang, F., Cheng, G., Si, S., Sun, X., Han, J., et al. (2018). Wilms' Tumor 1-associating Protein Promotes Renal Cell Carcinoma Proliferation by Regulating CDK2 mRNA Stability. *J. Exp. Clin. Cancer Res.* 37 (1), 40. doi:10.1186/s13046-018-0706-6

Tang, Q.-Q., Otto, T. C., and Lane, M. D. (2003). Mitotic Clonal Expansion: a Synchronous Process Required for Adipogenesis. *Proc. Natl. Acad. Sci.* 100 (1), 44–49. doi:10.1073/pnas.0137044100

Tang, X., Liu, S., Chen, D., Zhao, Z., and Zhou, J. (2019). The Role of the Fat Mass and Obesity-Associated Protein in the Proliferation of Pancreatic Cancer Cells. *Oncol. Lett.* 17 (2), 2473–2478. doi:10.3892/ol.2018.9873

Tasaki, M., Shimada, K., Kimura, H., Tsujikawa, K., and Konishi, N. (2011). ALKBH3, a Human AlkB Homologue, Contributes to Cell Survival in Human Non-small-cell Lung Cancer. *Br. J. Cancer* 104 (4), 700–706. doi:10.1038/sj.bjc.6606012

Tuorto, F., Herbst, F., Alerasool, N., Bender, S., Popp, O., Federico, G., et al. (2015). The tRNA Methyltransferase Dnmt2 Is Required for Accurate Polypeptide Synthesis during Haematopoiesis. *Embo J.* 34 (18), 2350–2362. doi:10.15252/embj.201591382

Ueda, Y., Ooshio, I., Fusamae, Y., Kitae, K., Kawaguchi, M., Jingushi, K., et al. (2017). AlkB Homolog 3-mediated tRNA Demethylation Promotes Protein Synthesis in Cancer Cells. *Sci. Rep.* 7 (1), 42271. doi:10.1038/srep42271

Valdés-Rives, S. A., and González-Arenas, A. (2017). Autotaxin-Lysophosphatidic Acid: From Inflammation to Cancer Development. *Mediators Inflamm.* 2017, 9173090. doi:10.1155/2017/9173090

Vasic, R., Gao, Y., Liu, C., and Halene, S. (2020). The Role of RNA Epigenetic Modification in Normal and Malignant Hematopoiesis. *Curr. Stem Cel Rep* 6 (4), 144–155. doi:10.1007/s40778-020-00178-y

Vicidomini, R., Di Giovanni, A., Petrizzo, A., Iannucci, L. F., Benvenuto, G., Nagel, A. C., et al. (2015). Loss of Drosophila Pseudouridine Synthase Triggers Apoptosis-Induced Proliferation and Promotes Cell-Nonautonomous EMT. *Cel Death Dis* 6 (3), e1705. doi:10.1038/cddis.2015.68

Vu, L. P., Pickering, B. F., Cheng, Y., Zaccara, S., Nguyen, D., Minuesa, G., et al. (2017). The N6-Methyladenosine (m6A)-Forming Enzyme METTL3 Controls Myeloid Differentiation of normal Hematopoietic and Leukemia Cells. *Nat. Med.* 23 (11), 1369–1376. doi:10.1038/nm.4416

Waku, T., Nakajima, Y., Yokoyama, W., Nomura, N., Kako, K., Kobayashi, A., et al. (2016). NML-mediated rRNA Base Methylation Links Ribosomal Subunit Formation to Cell Proliferation in a P53-dependent Manner. *J. Cel Sci* 129 (12), 2382–2393. doi:10.1242/jcs.183723

Wang, B., Niu, L., Wang, Z., and Zhao, Z. (2021a). RNA m1A Methyltransferase TRMT6 Predicts Poorer Prognosis and Promotes Malignant Behavior in Glioma. *Front. Mol. Biosci.* 8, 692130. doi:10.3389/fmolb.2021.692130

Wang, C.-X., Cui, G.-S., Liu, X., Xu, K., Wang, M., Zhang, X.-X., et al. (2018a). METTL3-mediated m6A Modification Is Required for Cerebellar Development. *Plos Biol.* 16 (6), e2004880. doi:10.1371/journal.pbio.2004880

Wang, J., Zhang, J., Ma, Y., Zeng, Y., Lu, C., Yang, F., et al. (2021b). WTAP Promotes Myocardial Ischemia/reperfusion Injury by Increasing Endoplasmic Reticulum Stress via Regulating m6A Modification of ATF4 mRNA. *Aging* 13 (8), 11135–11149. doi:10.18632/aging.202770

Wang, T., Hong, T., Huang, Y., Su, H., Wu, F., Chen, Y., et al. (2015a). Fluorescein Derivatives as Bifunctional Molecules for the Simultaneous Inhibiting and Labeling of FTO Protein. *J. Am. Chem. Soc.* 137 (43), 13736–13739. doi:10.1021/jacs.5b06690

Wang, W. (2016). mRNA Methylation by NSUN2 in Cell Proliferation. *WIREs RNA* 7 (6), 838–842. doi:10.1002/wrna.1380

Wang, X., Wu, R., Liu, Y., Zhao, Y., Bi, Z., Yao, Y., et al. (2020). m6A mRNA Methylation Controls Autophagy and Adipogenesis by Targeting Atg5 and Atg7. *Autophagy* 16 (7), 1221–1235. doi:10.1080/15548627.2019.1659617

Wang, Y., Huang, Q., Deng, T., Li, B.-H., and Ren, X.-Q. (2019). Clinical Significance of TRMT6 in Hepatocellular Carcinoma: A Bioinformatics-Based Study. *Med. Sci. Monit.* 25, 3894–3901. doi:10.12659/msm.913556

Wang, Y., Li, Y., Yue, M., Wang, J., Kumar, S., Wechsler-Reya, R. J., et al. (2018b). N6-methyladenosine RNA Modification Regulates Embryonic Neural Stem Cell Self-Renewal through Histone Modifications. *Nat. Neurosci.* 21 (2), 195–206. doi:10.1038/s41593-017-0057-1

Wang, Y., Viscarra, J., Kim, S.-J., and Sul, H. S. (2015b). Transcriptional Regulation of Hepatic Lipogenesis. *Nat. Rev. Mol. Cel Biol* 16 (11), 678–689. doi:10.1038/nrm4074

Wang, Y., Wang, J., Li, X., Xiong, X., Wang, J., Zhou, Z., et al. (2021c). N1-methyladenosine Methylation in tRNA Drives Liver Tumourigenesis by Regulating Cholesterol Metabolism. *Nat. Commun.* 12 (1), 6314. doi:10.1038/s41467-021-26718-6

Wanna-Udom, S., Terashima, M., Lyu, H., Ishimura, A., Takino, T., Sakari, M., et al. (2020). The m6A Methyltransferase METTL3 Contributes to Transforming Growth Factor-Beta-Induced Epithelial-Mesenchymal Transition of Lung Cancer Cells through the Regulation of JUNB. *Biochem. Biophysical Res. Commun.* 524 (1), 150–155. doi:10.1016/j.bbrc.2020.01.042

Wei, W., Huo, B., and Shi, X. (2019). miR-600 Inhibits Lung Cancer via Downregulating the Expression of METTL3. *Cmar* 11, 1177–1187. doi:10.2147/CMAR.S181058

Weng, H., Huang, H., Wu, H., Qin, X., Zhao, B. S., Dong, L., et al. (2018). METTL14 Inhibits Hematopoietic Stem/Progenitor Differentiation and Promotes Leukemogenesis via mRNA m6A Modification. *Cell Stem Cell* 22 (2), 191–205. doi:10.1016/j.stem.2017.11.016

Wilkinson, E., Cui, Y. H., and He, Y. Y. (2021). Context-Dependent Roles of RNA Modifications in Stress Responses and Diseases. *Int. J. Mol. Sci.* 22. doi:10.3390/ijms22041949

Wu, R., Li, A., Sun, B., Sun, J.-G., Zhang, J., Zhang, T., et al. (2019). A Novel m6A Reader Prrc2a Controls Oligodendroglial Specification and Myelination. *Cel Res* 29 (1), 23–41. doi:10.1038/s41422-018-0113-8

Wu, R., Liu, Y., Yao, Y., Zhao, Y., Bi, Z., Jiang, Q., et al. (2018). FTO Regulates Adipogenesis by Controlling Cell Cycle Progression via m6A-YTHDF2

Dependent Mechanism. *Biochim. Biophys. Acta (Bba) - Mol. Cel Biol. Lipids* 1863 (10), 1323–1330. doi:10.1016/j.bbalip.2018.08.008

Wu, Z., Shi, Y., Lu, M., Song, M., Yu, Z., Wang, J., et al. (2020). METTL3 Counteracts Premature Aging via m6A-dependent Stabilization of MIS12 mRNA. *Nucleic Acids Res.* 48 (19), 11083–11096. doi:10.1093/nar/gkaa816

Xia, T., Wu, X., Cao, M., Zhang, P., Shi, G., Zhang, J., et al. (2019). The RNA m6A Methyltransferase METTL3 Promotes Pancreatic Cancer Cell Proliferation and Invasion. *Pathol. - Res. Pract.* 215 (11), 152666. doi:10.1016/j.prp.2019.152666

Xiang, Y., Laurent, B., Hsu, C.-H., Nachtergaele, S., Lu, Z., Sheng, W., et al. (2017). RNA m6A Methylation Regulates the Ultraviolet-Induced DNA Damage Response. *Nature* 543 (7646), 573–576. doi:10.1038/nature21671

Xing, J., Yi, J., Cai, X., Tang, H., Liu, Z., Zhang, X., et al. (2015). NSun2 Promotes Cell Growth via Elevating Cyclin-dependent Kinase 1 Translation. *Mol. Cel Biol* 35 (23), 4043–4052. doi:10.1128/MCB.00742-15

Xiong, X., Li, X., and Yi, C. (2018). N1-methyladenosine Methylome in Messenger RNA and Non-coding RNA. *Curr. Opin. Chem. Biol.* 45, 179–186. doi:10.1016/j.cbpa.2018.06.017

Xu, X., Zhang, Y., Zhang, J., and Zhang, X. (2020). NSun2 Promotes Cell Migration through Methylating Autotaxin mRNA. *J. Biol. Chem.* doi:10.1074/jbc.RA119.012009

Xu, Y., Chen, Y., Yao, Y., Xie, H., Lu, G., Du, C., et al. (2021). VIRMA Contributes to Non-small Cell Lung Cancer Progression via N6-methyladenosine-dependent DAPK3 post-transcriptional Modification. *Cancer Lett.* 522, 142–154. doi:10.1016/j.canlet.2021.08.027

Xue, C., Zhao, Y., and Li, L. (2020). Advances in RNA Cytosine-5 Methylation: Detection, Regulatory Mechanisms, Biological Functions and Links to Cancer. *Biomark Res.* 8 (1), 43. doi:10.1186/s40364-020-00225-0

Yan, G., Elbadawi, M., and Efferth, T. (2020). Multiple Cell Death Modalities and Their Key Features (Review). *World Acad. Sci. J.* 2 (2), 39–48. doi:10.3892/wasj.2020.40

Yang, F., Jin, H., Que, B., Chao, Y., Zhang, H., Ying, X., et al. (2019a). Dynamic m6A mRNA Methylation Reveals the Role of METTL3-m6A-CDCP1 Signaling axis in Chemical Carcinogenesis. *Oncogene* 38 (24), 4755–4772. doi:10.1038/s41388-019-0755-0

Yang, R., Liang, X., Wang, H., Guo, M., Shen, H., Shi, Y., et al. (2021a). The RNA Methyltransferase NSUN6 Suppresses Pancreatic Cancer Development by Regulating Cell Proliferation. *EBioMedicine* 63, 103195. doi:10.1016/j.ebiom.2020.103195

Yang, S., Wei, J., Cui, Y.-H., Park, G., Shah, P., Deng, Y., et al. (2019b). m6A mRNA Demethylase FTO Regulates Melanoma Tumorigenicity and Response to Anti-PD-1 Blockade. *Nat. Commun.* 10 (1), 2782. doi:10.1038/s41467-019-10669-0

Yang, X., Zhang, S., He, C., Xue, P., Zhang, L., He, Z., et al. (2020). METTL14 Suppresses Proliferation and Metastasis of Colorectal Cancer by Down-Regulating Oncogenic Long Non-coding RNA XIST. *Mol. Cancer* 19 (1), 46. doi:10.1186/s12943-020-1146-4

Yang, Y., Hsu, P. J., Chen, Y.-S., and Yang, Y.-G. (2018). Dynamic Transcriptomic m6A Decoration: Writers, Erasers, Readers and Functions in RNA Metabolism. *Cel Res* 28 (6), 616–624. doi:10.1038/s41422-018-0040-8

Yang, Y., Shen, F., Huang, W., Qin, S., Huang, J.-T., Sergi, C., et al. (2019c). Glucose Is Involved in the Dynamic Regulation of m6A in Patients with Type 2 Diabetes. *J. Clin. Endocrinol. Metab.* 104 (3), 665–673. doi:10.1210/jc.2018-00619

Yang, Z., Yang, S., Cui, Y. H., Wei, J., Shah, P., Park, G., et al. (2021b). METTL14 Facilitates Global Genome Repair and Suppresses Skin Tumorigenesis. *Proc. Natl. Acad. Sci. U S A.* 118. doi:10.1073/pnas.2025948118

Yankova, E., Blackaby, W., Albertella, M., Rak, J., De Braekeleer, E., Tsagkogeorga, G., et al. (2021). Small-molecule Inhibition of METTL3 as a Strategy against Myeloid Leukaemia. *Nature* 593 (7860), 597–601. doi:10.1038/s41586-021-03536-w

Ye, D., Ma, S., Xiong, Y., and Guan, K.-L. (2013). R-2-hydroxyglutarate as the Key Effector of IDH Mutations Promoting Oncogenesis. *Cancer cell* 23 (3), 274–276. doi:10.1016/j.ccr.2013.03.005

Yoon, K.-J., Ringeling, F. R., Vissers, C., Jacob, F., Pokrass, M., Jimenez-Cyrus, D., et al. (2017). Temporal Control of Mammalian Cortical Neurogenesis by m6A Methylation. *Cell* 171 (4), 877–889. doi:10.1016/j.cell.2017.09.003

Yue, H., Nie, X., Yan, Z., and Weining, S. (2019). N6-methyladenosine Regulatory Machinery in Plants: Composition, Function and Evolution. *Plant Biotechnol. J.* 17 (7), 1194–1208. doi:10.1111/pbi.13149

Zachari, M., and Ganley, I. G. (2017). The Mammalian ULK1 Complex and Autophagy Initiation. *Essays Biochem.* 61 (6), 585–596. doi:10.1042/ebc20170021

Zhang, B., Jiang, H., Dong, Z., Sun, A., and Ge, J. (2020a). The Critical Roles of m6A Modification in Metabolic Abnormality and Cardiovascular Diseases. *Genes Dis.* doi:10.1016/j.gendis.2020.07.011

Zhang, C., Chen, L., Peng, D., Jiang, A., He, Y., Zeng, Y., et al. (2020b). METTL3 and N6-Methyladenosine Promote Homologous Recombination-Mediated Repair of DSBs by Modulating DNA-RNA Hybrid Accumulation. *Mol. Cel* 79 (3), 425–442. doi:10.1016/j.molcel.2020.06.017

Zhang, C., Chen, Y., Sun, B., Wang, L., Yang, Y., Ma, D., et al. (2017a). m6A Modulates Haematopoietic Stem and Progenitor Cell Specification. *Nature* 549 (7671), 273–276. doi:10.1038/nature23883

Zhang, C., Zhang, M., Ge, S., Huang, W., Lin, X., Gao, J., et al. (2019a). Reduced m6A Modification Predicts Malignant Phenotypes and Augmented Wnt/PI3K-Akt Signaling in Gastric Cancer. *Cancer Med.* 8 (10), 4766–4781. doi:10.1002/cam4.2360

Zhang, M., Zhang, Y., Ma, J., Guo, F., Cao, Q., Zhang, Y., et al. (2015). The Demethylase Activity of FTO (Fat Mass and Obesity Associated Protein) Is Required for Preadipocyte Differentiation. *PLOS ONE* 10, e0133788. doi:10.1371/journal.pone.0133788

Zhang, Q., Riddle, R. C., Yang, Q., Rosen, C. R., Guttridge, D. C., Dirckx, N., et al. (2019b). The RNA Demethylase FTO Is Required for Maintenance of Bone Mass and Functions to Protect Osteoblasts from Genotoxic Damage. *Proc. Natl. Acad. Sci. USA* 116 (36), 17980–17989. doi:10.1073/pnas.1905489116

Zhang, S., Zhao, B. S., Zhou, A., Lin, K., Zheng, S., Lu, Z., et al. (2017b). m 6 A Demethylase ALKBH5 Maintains Tumorigenicity of Glioblastoma Stem-like Cells by Sustaining FOXM1 Expression and Cell Proliferation Program. *Cancer Cell* 31 (4), 591–606. doi:10.1016/j.ccell.2017.02.013

Zhang, X., Li, D., Jia, C., Cai, H., Lv, Z., and Wu, B. (2021). METTL14 Promotes Tumorigenesis by Regulating lncRNA OIP5-AS1/miR-98/ADAMTS8 Signaling in Papillary Thyroid Cancer. *Cel Death Dis* 12 (6), 617. doi:10.1038/s41419-021-03891-6

Zhao, X., Yang, Y., Sun, B.-F., Shi, Y., Yang, X., Xiao, W., et al. (2014). FTO-dependent Demethylation of N6-Methyladenosine Regulates mRNA Splicing and Is Required for Adipogenesis. *Cel Res* 24 (12), 1403–1419. doi:10.1038/cr.2014.151

Zheng, G., Dahl, J. A., Niu, Y., Fedorcsak, P., Huang, C.-M., Li, C. J., et al. (2013). ALKBH5 Is a Mammalian RNA Demethylase that Impacts RNA Metabolism and Mouse Fertility. *Mol. Cel* 49 (1), 18–29. doi:10.1016/j.molcel.2012.10.015

Zheng, Q., Gan, H., Yang, F., Yao, Y., Hao, F., Hong, L., et al. (2020). Cytoplasmic m1A Reader YTHDF3 Inhibits Trophoblast Invasion by Downregulation of m1A-Methylated IGF1R. *Cell Discov* 6, 12. doi:10.1038/s41421-020-0144-4

Zhou, J., Wan, J., Shu, X. E., Mao, Y., Liu, X.-M., Yuan, X., et al. (2018). N6-Methyladenosine Guides mRNA Alternative Translation during Integrated Stress Response. *Mol. Cel* 69 (4), 636–647. doi:10.1016/j.molcel.2018.01.019

Zhou, L., Yang, C., Zhang, N., Zhang, X., Zhao, T., and Yu, J. (2020). Silencing METTL3 Inhibits the Proliferation and Invasion of Osteosarcoma by Regulating ATAD2. *Biomed. Pharmacother.* 125, 109964. doi:10.1016/j.biopha.2020.109964

Zhu, H., Sun, B., Zhu, L., Zou, G., and Shen, Q. (2021a). N6-Methyladenosine Induced miR-34a-5p Promotes TNF-α-Induced Nucleus Pulposus Cell Senescence by Targeting SIRT1. *Front. Cel Developmental Biol.* 9. doi:10.3389/fcell.2021.642437

Zhu, R., Ji, X., Wu, X., Chen, J., Li, X., Jiang, H., et al. (2020). Melatonin Antagonizes Ovarian Aging via YTHDF2-MAPK-NF-Kb Pathway. *Genes Dis.* doi:10.1016/j.gendis.2020.08.005

Zhu, W., Wang, J.-Z., Wei, J.-F., and Lu, C. (2021b). Role of m6A Methyltransferase Component VIRMA in Multiple Human Cancers (Review). *Cancer Cel Int* 21 (1), 172. doi:10.1186/s12935-021-01868-1

Zhu, X., Wang, X., Yan, W., Yang, H., Xiang, Y., Lv, F., et al. (2021c). Ubiquitination-mediated Degradation of TRDMT1 Regulates Homologous Recombination and Therapeutic Response. *NAR Cancer* 3. doi:10.1093/narcan/zcab010

Zona, S., Bella, L., Burton, M. J., Nestal de Moraes, G., and Lam, E. W.-F. (2014). FOXM1: An Emerging Master Regulator of DNA Damage Response and

Genotoxic Agent Resistance. *Biochim. Biophys. Acta (Bba) - Gene Regul. Mech.* 1839 (11), 1316–1322. doi:10.1016/j.bbagrm.2014.09.016

Zou, D., Dong, L., Li, C., Yin, Z., Rao, S., and Zhou, Q. (2019). The m6A Eraser FTO Facilitates Proliferation and Migration of Human Cervical Cancer Cells. *Cancer Cel Int* 19, 321. doi:10.1186/s12935-019-1045-1

Zuo, X., Chen, Z., Gao, W., Zhang, Y., Wang, J., Wang, J., et al. (2020). M6A-mediated Upregulation of LINC00958 Increases Lipogenesis and Acts as a Nanotherapeutic Target in Hepatocellular Carcinoma. *J. Hematol. Oncol.* 13 (1), 5. doi:10.1186/s13045-019-0839-x

Conflict of Interest: The authors declare that the research was conducted in the absence of any commercial or financial relationships that could be construed as a potential conflict of interest.

Publisher's Note: All claims expressed in this article are solely those of the authors and do not necessarily represent those of their affiliated organizations, or those of the publisher, the editors and the reviewers. Any product that may be evaluated in this article, or claim that may be made by its manufacturer, is not guaranteed or endorsed by the publisher.

Copyright © 2022 Wilkinson, Cui and He. This is an open-access article distributed under the terms of the Creative Commons Attribution License (CC BY). The use, distribution or reproduction in other forums is permitted, provided the original author(s) and the copyright owner(s) are credited and that the original publication in this journal is cited, in accordance with accepted academic practice. No use, distribution or reproduction is permitted which does not comply with these terms.

frontiers | Frontiers in Cell and Developmental Biology

BRIEF RESEARCH REPORT
published: 27 April 2022
doi: 10.3389/fcell.2022.888279

Improved Methods for Deamination-Based m^{6}A Detection

Huanyu Zhu[1], *Xinhe Yin*[2], *Christopher L. Holley*[2,3] *and Kate D. Meyer*[1,4]*

[1]Department of Biochemistry, Duke University School of Medicine, Durham, NC, United States, [2]Department of Molecular Genetics and Microbiology, Duke University School of Medicine, Durham, NC, United States, [3]Department of Medicine, Duke University Medical Center, Durham, NC, United States, [4]Department of Neurobiology, Duke University School of Medicine, Durham, NC, United States

N^6-methyladenosine (m^{6}A) is a critical regulator of gene expression and cellular function. Much of our knowledge of m^{6}A has been enabled by the identification of m^{6}A sites transcriptome-wide. However, global m^{6}A profiling methods require high amounts of input RNA to accurately identify methylated RNAs, making m^{6}A profiling from rare cell types or scarce tissue samples infeasible. To overcome this issue, we previously developed DART-seq, which relies on the expression of a fusion protein consisting of the APOBEC1 cytidine deaminase tethered to the m^{6}A-binding YTH domain. APOBEC1-YTH directs C-to-U mutations adjacent to m^{6}A sites, therefore enabling single nucleotide-resolution m^{6}A mapping. Here, we present an improved version of DART-seq which utilizes a variant of the YTH domain engineered to achieve enhanced m^{6}A recognition. In addition, we develop *in vitro* DART-seq and show that it performs similarly to cellular DART-seq and can map m^{6}A in any sample of interest using nanogram amounts of total RNA. Altogether, these improvements to the DART-seq approach will enable better m^{6}A detection and will facilitate the mapping of m^{6}A in samples not previously amenable to global m^{6}A profiling.

Keywords: m^{6}A, epitranscriptome, DART-seq, RNA modification, RNA biology

OPEN ACCESS

Edited by:
Huilin Huang,
Sun Yat-sen University Cancer Center (SYSUCC), China

Reviewed by:
Guan-Zheng Luo,
Sun Yat-sen University, China
Joseph Mauro Calabrese,
University of North Carolina at Chapel Hill, United States

***Correspondence:**
Kate D. Meyer
kate.meyer@duke.edu

Specialty section:
This article was submitted to Epigenomics and Epigenetics, a section of the journal Frontiers in Cell and Developmental Biology

Received: *02 March 2022*
Accepted: *28 March 2022*
Published: *27 April 2022*

Citation:
Zhu H, Yin X, Holley CL and Meyer KD (2022) Improved Methods for Deamination-Based m^{6}A Detection. Front. Cell Dev. Biol. 10:888279. doi: 10.3389/fcell.2022.888279

INTRODUCTION

N^6-methyladenosine (m^{6}A) is the most abundant internal mRNA modification and plays important roles in multiple aspects of mRNA regulation, including translation, splicing, and stability (Meyer and Jaffrey, 2017; Zaccara et al., 2019). m^{6}A is deposited at RAC sites (R = A or G) by a methyltransferase complex composed of METTL3, METTL14, WTAP and other cofactors and is enriched in proximal 3′UTRs and in the vicinity of the stop codon (Meyer et al., 2012; Meyer and Jaffrey, 2017; Roundtree et al., 2017; Shi et al., 2019; Zaccara et al., 2019; He and He, 2021). Consistent with its broad roles in gene expression control, m^{6}A is important for several physiological processes, including stem cell fate decisions, learning and memory, and immune responses (Shi et al., 2018; Winkler et al., 2019; Zhang et al., 2020). Additionally, abnormal regulation of m^{6}A or its regulatory proteins contributes to a variety of human diseases, including several cancers (Chen et al., 2019; He et al., 2019; Gu et al., 2020; Wang et al., 2020). Thus, being able to identify the RNAs that contain m^{6}A in cells or tissues of interest is critical for enhancing our understanding of how this modification contributes to cellular function and for elucidating the impact that it has on human disease.

Traditional m^{6}A profiling approaches have used m^{6}A antibodies to immunoprecipitate methylated RNAs (Hafner et al., 2010; Dominissini et al., 2012; Meyer et al., 2012; Linder et al., 2015; Hsu and He, 2019). Such methods have been critical for our understanding of m^{6}A distribution and regulation, but they suffer from limitations that include cross-reactivity with other modifications

and the requirement for large amounts of RNA. Recently, a variety of antibody-free methods have been developed (Owens et al., 2021), but these also generally require large amounts of input material. To overcome these limitations, our group recently developed DART-seq (deamination adjacent to RNA modification targets), which utilizes a fusion protein consisting of the m^{6}A-binding YTH domain tethered to the cytidine deaminase APOBEC1 (hereafter APO1) to direct C-to-U editing at m^{6}A-adjacent cytidines (Meyer, 2019). DART-seq relies on a simple RNA-seq readout and can therefore identify m^{6}A sites at single-nucleotide resolution using low amounts of RNA, including in single cells (Tegowski et al., 2022a). However, one limitation of DART-seq is that it relies on expression of the APO1-YTH fusion protein in cells of interest, which may not always be possible or desirable. To address this, we previously developed an *in vitro* DART-seq approach (Meyer, 2019), but this strategy used a relatively crude APO1-YTH protein preparation and exhibited reduced sensitivity compared to cellular DART-seq. Thus, further optimization of the *in vitro* DART-seq approach is needed for it to be an effective tool for global m^{6}A mapping.

Here, we perform a systematic optimization of the major components of the DART fusion protein in an attempt to maximize m^{6}A detection sensitivity. We find that introducing a D422N mutation into the YTH domain of the DART protein leads to improved m^{6}A binding and m^{6}A detection transcriptome-wide. In addition, we find that substituting APO1 with the catalytic domain of ADAR containing a hyperactive E488Q mutation (ADARcd) characterized previously (Rahman et al., 2018) enables identification of methylated RNAs based on A-to-I editing and therefore provides an alternative approach for DART-seq-based m^{6}A profiling. Finally, we develop an improved version of *in vitro* DART-seq using the APO1-tethered DART protein and demonstrate its ability to identify m^{6}A sites with single-nucleotide resolution transcriptome-wide from ultra-low amounts of total RNA. Altogether, the tools developed here enhance the sensitivity of the original DART-seq approach and also provide new strategies for the detection of m^{6}A in virtually any sample of interest.

METHODS

Plasmids

DART protein variants used for cellular DART-seq (A3A-YTH, A3C-YTH, huAPO1-YTH, AID-YTH, rZDD-YTH, APO1-YTH^{DF1}, APO1-YTH$^{DF1(D401N)}$, and APO1-YTH^{D422N}), were cloned into the pCMV-APOBEC1-YTH plasmid (Addgene #131636) in place of APOBEC1 or the YTH domain as indicated using Gibson Assembly (NEB). ADARcd-YTH^{D422N} and ADARcd-YTH^{mut} plasmids were generated by replacing APOBEC1 from the pCMV-APOBEC1-YTH and pCMV-APOBEC1-YTH^{mut} plasmids (Addgene #131636 and #131637) with ADARcd containing a hyperactivating E488Q mutation (Addgene #139686) using Gibson Assembly (NEB). *In vitro* DART-seq proteins (APO1-YTH, APO1-YTH^{mut}, APO1-YTH^{D422N}, and APOBEC1 alone) were cloned into the PET-His6-MBP-TEV LIC plasmid (Addgene #29656) by ligation independent cloning using a T4 DNA Polymerase (NEB). YTH domain of human YTHDF2 was cloned into the PET-His6-MBP-TEV LIC cloning vector (Addgene #29656) with Gibson Assembly (NEB).

Cell Culture

HEK293T cells were obtained from the American Type Culture Collection (ATCC) and cultured in Dulbecco's Modified Eagle's Medium (DMEM) with 4.5 g/L glucose, L-glutamine, and sodium pyruvate (Corning) supplemented with 10% (v/v) fetal bovine serum (Avantor Seradigm) and Penicillin-Streptomycin (Gibco). Cells were cultured in a humidified incubator maintained at 37°C with 5% CO_2.

Cellular DART-Seq

Three independent plating and RNA isolation experiments were performed using HEK293T cells transiently expressing APO1-YTH, APO1-YTH^{mut}, A3A-YTH, A3C-YTH, huAPO1-YTH, AID-YTH, rZDD-YTH, APO1-YTH^{DF1}, APO1-YTH$^{DF1(D401N)}$, APO1-YTH^{D422N}, ADARcd-YTH^{D422N}, ADARcd-YTH^{mut}, and ADARcd. DART constructs were transiently transfected into HEK293T cells using Lipofectamine 2000 according to the manufacturer's protocol (Thermo Fisher). DART protein were expressed in HEK293T cells for 24 h. Cells were then briefly rinsed with cold 1X PBS and removed from the culture plate using a cell scraper. Total RNA was isolated using Trizol (Invitrogen) according to the manufacturer's instructions and subsequently treated with DNase I (NEB) for 15 min at 37°C to remove possible DNA contamination. RNA was then purified using ethanol precipitation and used for downstream analysis with either Sanger sequencing or next-generation sequencing.

Treatment of HEK293T Cells With STM2457

HEK293T cells were cultured to 40% confluency in Dulbecco's Modified Eagle's Medium (DMEM) as described above. 10 μM of STM2457 (WuXi AppTec) dissolved in water was then added to the culture media. Cells were incubated with this treatment for 72 h. Cellular DART-seq with ADARcd-YTH^{D422N} were conducted for STM2457 treated HEK293T cells through transient transfection 48 h after the start of 10 μM of STM2457. ADARcd-YTH^{D422N} construct was expressed in treated cells for 24 h, and the cells were cultured in media containing 10 μM of STM2457 for a total 72 h treatment.

In vitro DART-Seq

Purified APO1-YTH^{D422N}, APO1-YTH and APO1-YTH^{mut} proteins were purified as previously described (Tegowski et al., 2022b). DART proteins were expressed in One Shot™ BL21 (DE3) pLysE Chemically Competent *E. coli* (Invitrogen) through auto-induction. Bacterial lysate were then collected and processed using the Qproteome Bacterial Protein Prep Kit (Qiagen) following manufacturer protocol. DART protein was then affinity purified from lysate with Ni-NTA agarose beads (Gold Biotechnology) packed in a Poly-prep chromatography column (Biorad). The *In vitro* DART-seq assays were performed

by incubating 250 ng of purified DART protein with 50 ng of total HEK293T cell RNA in DART buffer (10 mM Tris-HCl (pH 7.4), 50 mM KCl, 0.1 μM $ZnCl_2$) and 1 μl RNaseOUT (Invitrogen) in a total volume of 50 μl for 4 h at 37°C. For *in vitro* DART-seq assays using the YTH blocking negative control, RNA was pre-incubated with 1 μg of purified YTH domain and 1 μl RNaseOUT in 30 μl volume in water at 37°C for 1 h with rotation. YTH blocked RNA samples were then incubated with 250 ng of purified APO1-YTH^{D422N} protein with 50 ng of total HEK293T cell RNA in DART buffer (10 mM Tris-HCl (pH 7.4), 50 mM KCl, 0.1 μM $ZnCl_2$) and 1 μl RNaseOUT (Invitrogen) in a total volume of 50 μl for 4 h at 37°C. RNA was isolated with the Qiagen RNeasy Plus Mini Kit (Qiagen) and stored at −80°C before thawed for downstream analysis with either Sanger sequencing or next generation sequencing.

Western Blotting

Cells were quickly rinsed with cold 1x PBS and scraped from culture plates. Cells were then pelleted by centrifugation at 1,000 × g for 3 min at 4°C. Cell pellets were resuspended in lysis buffer [25 mM Tris-HCl, pH7.4; NaCl 150 mM; Triton X-100 1% (v/v); sodium dodecyl sulfate 0.1% (v/v); complete proteinase inhibitor cocktail (Sigma-Aldrich)] and incubated on ice for 10 min. Lysates were then centrifuged at 13,000 × g for 15 min at 4°C. The supernatant was transferred to a new tube. Samples for SDS-PAGE were then prepared at a final concentration of 1 μg/μl total protein in 1 × NuPAGE LDS Sample Buffer (Invitrogen) and 0.1 M DTT (VWR). Samples were run on 4–12% SDS-PAGE gels (Invitrogen) and transferred for 60 min at 100 V in Towbin transfer buffer [25 mM Tris Base, 192 mM Glycine, 20% methanol (v/v)] to a PVDF membrane (GE Amersham). After transferring, the membrane was blocked in PBST [PBS with 0.1% Tween 20 (Sigma-Aldrich)] with 5% milk (w/v) (Quality Biological) for 1 h at room temperature. Primary antibodies, anti-βactin (Genscript), or anti-HA (Cell Signaling Technology) were incubated with the blots overnight at 4°C. The membrane was washed 3 times with PBST before the secondary antibody was added for 1 h at room temperature in PBST. Anti-rabbit-HRP secondary (Fisher Scientific) was used at 1:10,000 dilution, while anti-mouse-HRP secondary (Fisher Scientific) was used at 1:2,500. The membrane was then washed 3 times with PBST for 5 min. The western blot was visualized using Amersham ECL Prime Reagent (Amersham) and imaged on a Chemidoc MP (BioRad).

RNA Pulldown Assays

An appropriate volume of magnetic Streptavidin beads (Fisher), 20 μl per pulldown reaction was aliquoted, equilibrated with 480 μl of Binding Buffer [10 mM Tris, pH 7.5, 1.5 mM MgCl2, 150 mM KCl, 0.5 mM DTT, 0.05% (v/v) NP-40 substitute]. Magnetic Streptavidin beads was then further divided based on usage for each of the purified DART protein variants described above (Control: no RNA oligo, A: 5′-biotin unmodified RNA oligo, m^{6}A: 5′-biotin m^{6}A-modified RNA oligo). Magnetic Streptavidin beads were then batch-incubated with 2 μg of each RNA oligo in Binding Buffer + 100 U/ml RNase inhibitor for 1 h at 4°C on a rotator.

Concurrently, 500 ng of purified DART proteins variants (APO1-YTH, APO1-YTH^{DF1}, APO1-YTH$^{DF1(D401N)}$, and APO1-YTH^{D422N}) were resuspended in an 250 μl of Binding Buffer and kept on ice. 20 μl of the resuspension were taken as input for each sample for downstream Western blotting analysis.

After incubation, Streptavidin beads were washed twice with 360 μl of Binding Buffer (clearing with magnetic stand each time) to remove any unbound RNA oligo from solution (control/mock samples were treated and washed identically), and aliquoted and resuspeded in 20 μl/sample of Binding Buffer. Finally 20 μl of RNA bait attached Streptavidin beads were incubated with resuspended DART protein variants. Protein-RNA-bead complexes were incubated at room temperature for 30 min on a rotator, then moved to 4°C and incubated for 2 h with rotation.

Following the incubation period, RNA pulldown complexes were washed five times with 250 μl of Binding Buffer, each wash included a 3 min rotation at room temperature, to remove any unbounded purified DART protein, and supernatants were removed using a magnetic stand. Finally, 60 μl of Elution Buffer (50 mM Tris, pH 8, 200 mM NaCL, 2% (w/v) SDS, 1 mM Biotin) were added to each Protein-RNA-bead complex, mixed well by pipetting, and incubated at 60°C for 30 min. Eluents were collected following incubation using a magnetic stand. The eluents were then subjected to Western blotting for analysis.

Synthesis of cDNA and Sanger Sequencing

Total RNA isolated from cells expressing DART protein was treated with DNase I (NEB) for 15 min at 37°C to remove possible DNA contamination, then RNA was isolated using ethanol precipitation. For *in vitro* DART-seq, total RNA was column purified, after incubation with purified DART protein. In both cases, cDNA was made using iScript Reverse Transcription Supermix (Bio-Rad). PCR amplification of the region surrounding selected mRNAs was carried out with CloneAmp HiFi PCR Mastermix (Takara). The resulting PCR product was gel-purified on a 1% agarose gel and gel extracted using the Qiaquick Gel Extraction Kit (Qiagen). Samples were submitted for Sanger sequencing (Genewiz) and % C2U was quantified using EditR software (Kluesner et al., 2018).

Next-Generation Sequencing

All sequencing was performed by the Duke University Sequencing and Genomic Technologies Core facility. RNA samples purified from cellular DART-seq, and *in vitro* DART-seq as previously described were thawed on ice. For cellular DART-seq, 1 μg of RNA for each sample was used for sequencing library preparation using the NEBNext Ultra II Directional RNA Library Prep Kit for Illumina (NEB). For *in vitro* DART-seq, the entirety of RNA purified following incubation with purified DART protein was used for sequencing library preparation using the NEBNext Single Cell/Low Input RNA Library Prep Kit for Illumina (NEB). Before sequencing, all samples were barcoded using NEBNext Multiplex Oligos for Illumina (NEB), and their concentrations were quantified using Qubit Fluorometer (Thermo Fisher). Libraries were then sequenced on the NovaSeq 6,000.

Identification of m^{6}A Sites in Cellular DART-Seq

m^{6}A sites were identified using the Bullseye analysis pipeline (Tegowski et al., 2022a). Bullseye is available on GitHub (https://github.com/mflamand/Bullseye). Raw sequencing data in fastq format were downloaded, and adapter sequences were trimmed using Flexbar (3.0.3). Sequences were aligned to the hg19 genome using NovoAlign. PCR duplicates were removed from the BAM files using Samtools (1.11). Then, using Bullseye, the parseBAM.pl script was used to parse the BAM files and create a counts matrix of the number of reads for each nucleotide at all positions with coverage. The Find_edit_site.pl script was then used to find C-to-U (or A-to-I) mutations with at least 10 reads of coverage, an edit ratio of 5–95%, and an edit ratio at least 1.2-fold higher than mutant control samples (APO1-YTH^{mut} or ADARcd-YTH^{mut}), and at least 2 C-to-U (or A-to-I for cells expressing ADARcd-YTH^{D422N}) editing events at a given site. Sites that were only found in one replicate of each DART protein variant were removed. For cells expressing DART protein with APO1 variants, those sites were further filtered to include only those occurring in an RAC (G/A-A-C) motif. Editing events observed when APOBEC1 alone was over-expressed in HEK293T cells (Meyer, 2019) were removed.

Identification of m^{6}A Sites With *in vitro* DART-Seq

m^{6}A sites found by *in vitro* DART-seq were identified using Bullseye following a similar protocol as described above for cellular DART-seq. C-to-U mutations with at least 10 reads of coverage, an edit ratio of 5–95%, an edit ratio at least 1.2-fold higher than mutant control samples (APO1-YTH^{mut}), and at least 2 C-to-U editing events at a given site were selected. Sites that were only found in one replicate of the APO1-YTH^{D422N} or APO1-YTH sample were removed. The remaining sites were further filtered to include only those occurring in an RAC motif. Editing events observed in any of the three replicates of samples treated with APOBEC1 alone were removed.

Metagene Analysis

Metagene analysis was generated using metaPlotR (Olarerin-George and Jaffrey, 2017) with hg19 annotations as part of the computational pipeline in the Bullseye package.

Relative Distance Analysis

Relative distance plots comparing the relative distance of either C-to-U editing events detected in cellular or *in vitro* DART-seq, or A-to-I editing events identified in cellular DART-seq with ADARcd-YTH^{D422N} against m^{6}A sites called by miCLIP (Linder et al., 2015). Shuffle sites were generated using the Bullseye package. The program shuffle_sites.sh first finds all the exons of the transcripts containing edit sites. Then it shuffles the edit sites within these exons. The relative distance plots were generated in Rstudio using ggplot2 package.

Cumulative Distribution Analysis

Cumulative distribution function plot and corresponding box plot were generated by comparing the C-to-U (A-to-I) editing percentage of DART-seq samples in Rstudion using the ggplot2 and the tidyverse package. A Wilcoxon Rank-Sum test was conducted in Rstudio using the tidyverse package to access statistical significance.

Mass Spectrometry Analysis

Total RNA was isolated from either untreated or STM2457 treated (as described above) HEK293T cells using Trizol (Invitrogen) according to the manufacturer's instructions and subsequently treated with DNase I (NEB) for 15 min at 37°C to remove possible DNA contamination. mRNA was then isolated with two rounds of purification using Dynabeads mRNA Purification Kit (Thermo Fisher). 200 ng of mRNA was digested with 2 U of Nuclease P1 (Sigma) in 50 ul nuclease free water with 2.5 mM ZnCl and 25 mM NaCl for 2 h at 37°C. Subsequently, mRNA samples were treated with 5 U of antarctic phosphatase (NEB) for 2 h at 37°C. Samples were then processed using the Xevo TQ-S mass spectrometry system.

Comparison of Methylated Transcripts With REPIC Database

A text file containing the genomic coordinates, gene annotation, and dataset information for MeRIP peaks reported in HEK293T cells from 3 separate studies (Lichinchi et al., 2016; Meyer et al., 2012; Schwartz et al., 2014) was downloaded from the REPIC database. (https://repicmod.uchicago.edu/repic/download.php) (Liu et al., 2020). Gene names were then retrieved from the Ensembl Gene ID annotations. RNAs with called peaks in at least two of the three studies were then compared to the list of RNAs containing high-confidence m^{6}A sites in the cellular DART-seq or *in vitro* DART-seq.

RESULTS

Development of a DART Protein Variant With Improved m^{6}A Recognition

Accurate detection of m^{6}A sites by DART-seq relies on both m^{6}A recognition and efficient deamination of m^{6}A-adjacent cytidines. To achieve this, the DART fusion protein consists of the YTH domain of YTHDF2 tethered to the rat APOBEC1 cytidine deaminase (Meyer, 2019). However, it is possible that other variants of the YTH domain or alternative deaminase proteins may improve m^{6}A detection. To explore this, we first tested other deaminase enzymes. This included members of the AID/APOBEC family of proteins known to act on RNA, as well as the rat APOBEC1 deaminase domain alone (Salter et al., 2016; Smith, 2017; Jin S. et al., 2020) (**Supplementary Figure S1A**). Each deaminase was fused to the YTH domain and expressed in HEK293T cells, followed by assessment of C-to-U deamination adjacent to m^{6}A sites in a panel of mRNAs previously confirmed to contain m^{6}A (Linder et al., 2015; Meyer, 2019) (**Supplementary Figures S1B,C**). Surprisingly, most of these

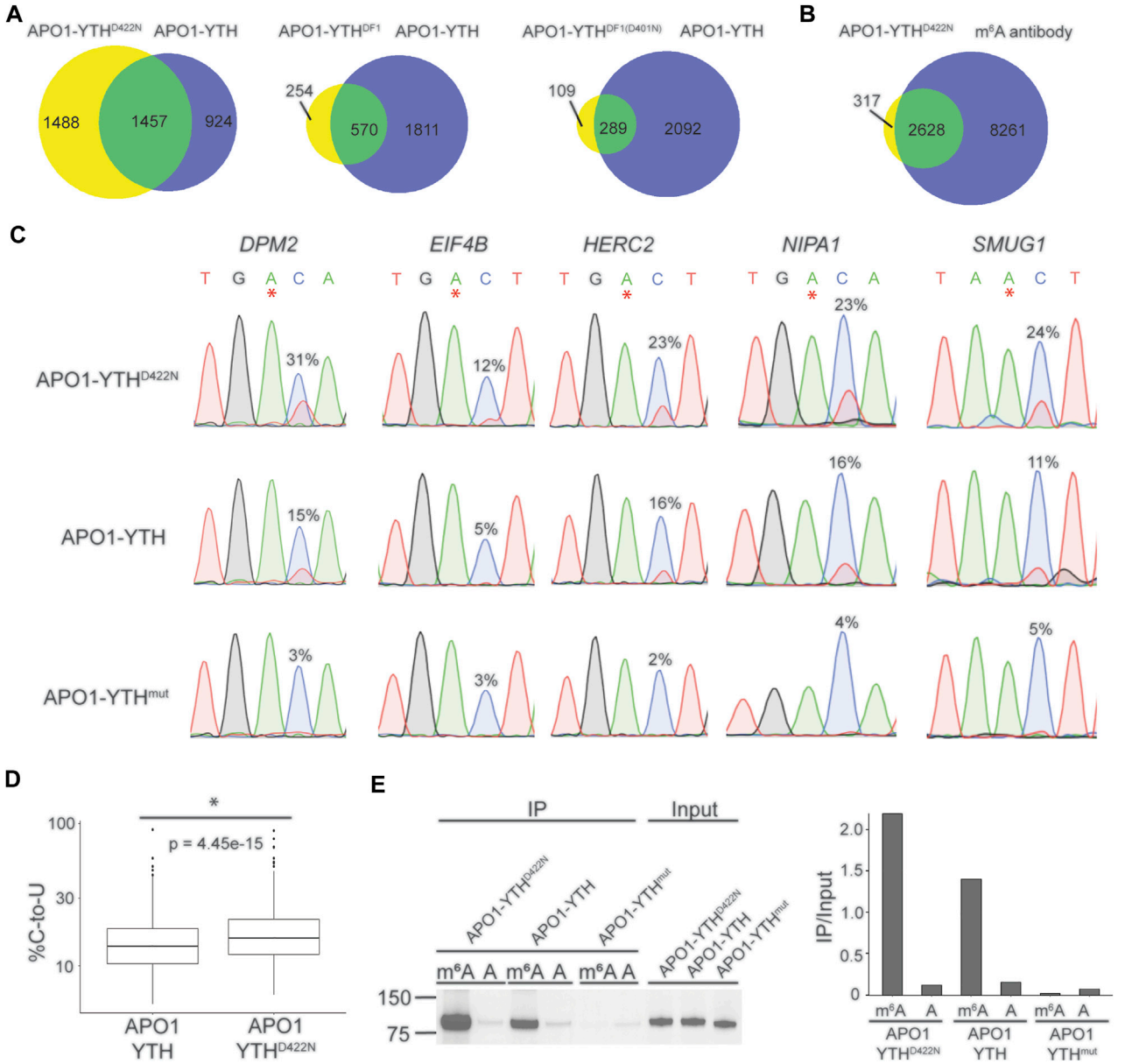


FIGURE 1 | Identification of an improved variant of the DART fusion protein. **(A)** Comparison of methylated RNAs identified by cellular DART-seq using expression of either APO1-YTH^{D422N}, APO1-YTH^{DF1}, or APO1-YTH$^{DF1(D401N)}$ in HEK293T cells. Venn diagrams compare each DART protein variant to the original APO1-YTH protein. **(B)** Overlap of methylated RNAs identified by cellular DART-seq using the APO1-YTH^{D422N} protein with those identified by antibody-based methods. **(C)** Sanger sequencing traces showing C-to-U editing adjacent to m^{6}A sites in cells expressing APO1-YTH^{D422N}, APO1-YTH, and APO1-YTH^{mut} for five mRNAs previously shown to contain m^{6}A: *DPM2*, *EIF4B*, *HERC2*, *NIPA1*, and *SMUG1*. m^{6}A sites are indicated by asterisks. C-to-U editing rate (%U) is indicated above the adjacent cytidine. Data are representative of three biological replicates. **(D)** Box plot showing the global C-to-U editing percentage of all sites common to HEK293T cells expressing APO1-YTH^{D422N} or APO1-YTH. **(E)** Western blot following RNA pulldown assays using purified DART proteins and bait RNAs. APO1-YTH^{D422N} exhibits improved binding to m^{6}A compared to APO1-YTH.

proteins failed to show editing above background, and none of the proteins led to improved m^{6}A detection compared to the original rat APO1-YTH fusion protein (**Supplementary Figure S1C**).

We next explored whether alternative YTH domains could improve DART-mediated detection of m^{6}A. We tested three variants of the YTH domain: 1) the YTH domain of YTHDF1 (YTH^{DF1}), which has a stronger affinity to some m^{6}A-containing RNAs compared to the YTH domain of YTHDF2 (Zhu et al., 2014; Xu et al., 2015); 2) the YTH^{DF1} domain engineered to contain the D401N mutation, which lies in the m^{6}A binding pocket and improves m^{6}A recognition by 16-fold (Xu et al., 2015) (YTH$^{DF1(D401N)}$); and 3) the YTH domain of YTHDF2 harboring an equivalent mutation, D422N (YTH^{D422N}) (**Supplementary Figure S1A**).

Each YTH variant was fused to rat APO1 and overexpressed in HEK293T cells. We then performed DART-seq to assess the ability of each DART protein variant to detect m^{6}A sites. C-to-U editing events in cells expressing each DART protein were enriched within the vicinity of the stop codon, consistent with the distribution of m^{6}A (**Supplementary Figure S1D**). We then identified m^{6}A sites from each dataset using Bullseye, a pipeline that we previously developed for analysis of DART-seq data (Tegowski et al., 2022a). Comparison of all DART protein variants showed that APO1-YTH^{D422N} identified the greatest number of methylated RNAs, which overlapped well with methylated RNAs identified by antibody-based approaches (**Figures 1A,B**, **Supplementary Table S1**). The sites that were identified by APO1-YTH^{D422N} but not by APO1-YTH exhibited a distribution in transcripts that matches that of m^{6}A and were found in RNAs identified by antibody-based methods, suggesting that these were not caused by false-positives (**Supplementary Figures S1E,F**). Additionally, C-to-U editing rates (% C2U) of m^{6}A sites identified by APO1-YTH^{D422N} were higher than those of the original DART protein in a panel of selected mRNAs, suggesting increased sensitivity of APO1-YTH^{D422N} for detecting m^{6}A (**Figures 1C,D**). Consistent with this, RNA pulldown assays revealed that APOBEC1-YTH^{D422N} has improved binding to methylated RNA compared to the wild type YTHDF2 YTH domain (**Figure 1E**). Thus, the YTH^{D422N} domain enables improved m^{6}A recognition and better sensitivity for m^{6}A detection using DART-seq.

ADARcd-Mediated DART-Seq Is an Alternative Method for Identifying Methylated RNAs

Using a cytidine deaminase as the catalytic protein in DART-seq enables nucleotide-resolution m^{6}A mapping since nearly all m^{6}A sites are followed by a cytidine (Wei and Moss, 1977; Dominissini et al., 2012; Meyer et al., 2012; Meyer, 2019). However, the adenosine deaminase ADAR offers an alternative approach for the identification of methylated RNAs through targeted A-to-I editing. This is analogous to the TRIBE method in which the ADAR catalytic domain (ADARcd) is fused to an RNA-binding protein of interest and RNA targets are identified by A-to-I editing (Mcmahon et al., 2016). The HyperTRIBE method, which utilizes ADARcd containing a hyperactivating E488Q mutation, further provides increased sensitivity (Rahman et al., 2018; Xu et al., 2018). We therefore wondered whether using the hyperactive ADARcd in place of APO1 would enable DART-seq to identify methylated RNAs with greater sensitivity.

To test this, we fused the hyperactive ADARcd to the YTH^{D422N} domain (ADARcd-YTH^{D422N}) and expressed it in HEK293T cells for 24 h followed by RNA-seq. In parallel, we expressed ADARcd alone and ADARcd-YTH^{mut} as controls. We then modified the Bullseye pipeline to identify A-to-I editing events which were absent in cells expressing ADARcd alone and which were enriched in ADARcd-YTH^{D422N}-expressing cells compared to ADARcd-YTH^{mut}-expressing cells (**Figure 2A**, **Supplementary Figure S2A**; Methods). Overall, we observed consistent A-to-I editing of RNAs across biological replicates, indicating the reproducibility of RNA targeting by ADAR-YTH^{D422N} (**Supplementary Figure S2B**). We identified a total of 21,717 A-to-I editing sites in 5,689 RNAs that were common to two out of three biological replicates and used these sites for downstream analyses (**Supplementary Table S3**). These sites were enriched in the vicinity of m^{6}A and had a distribution in mRNAs which matches that of m^{6}A, indicating that YTH^{D422N} can effectively target ADARcd to m^{6}A (**Figures 2B,C**). Additionally, there was a high degree of overlap between methylated RNAs identified by ADARcd-YTH^{D422N} and antibody-based methods (**Figure 2D**). To confirm that A-to-I editing events observed with ADARcd-YTH^{D422N} were m^{6}A dependent, we expressed ADARcd-YTH^{D422N} in HEK293T cells treated with the METTL3 inhibitor STM2457 (Yankova et al., 2021) (**Supplementary Figure S2C**). We then performed RNA-seq and examined the effect of STM2457 treatment on A-to-I editing transcriptome-wide. We found that STM2457 treatment led to a global reduction in the total number of A-to-I editing events (21,718 and 16,250 A-to-I sites for untreated and STM2457 treated samples, respectively), among common sites identified between treated and untreated samples, 75% of the same sites identified showed reduced %A-to-I editing.(**Figures 2E,F**, **Supplementary Table S3**). Altogether, these data confirm that A-to-I editing induced by ADAR-YTH^{D422N} is METTL3-dependent and indicate that ADAR can be used in place of APO1 to identify m^{6}A-containing RNAs by DART-seq.

We next compared the ability of ADARcd-YTH^{D422N} and APO1-YTH^{D422N} to identify methylated RNAs. Although there was high overlap of methylated RNAs identified by both methods, there were many more transcripts identified by ADAR-YTH^{D422N} (**Supplementary Figure S3A**). Consistent with this, there were also more A-to-I editing sites than C-to-U editing sites identified transcriptome-wide (21,718 and 6,042, for ADARcd-YTH^{D422N} and APO1-YTH^{D422N}, respectively) (**Supplementary Table S1**). The methylated RNAs uniquely identified by ADAR-YTHD^{422N} showed good agreement with those identified by antibody-based methods, and A-to-I editing sites in transcripts had a distribution that matches m^{6}A, suggesting that these sites were not caused by non-specific editing (**Supplementary Figures S3B,C**).

Since the majority of m^{6}A sites are found within the GAC consensus sequence, most A-to-I editing caused by ADAR-YTH^{D422N} does not occur adjacent to m^{6}A, and the Bullseye pipeline therefore does not filter sites based on the RAC consensus. In contrast, C-to-U editing caused by APO1-YTH^{D422N} can occur adjacent to m^{6}A, and Bullseye filters sites to include only those that occur in the RAC consensus. Removing this filter leads to a much greater number of C-to-U sites (12,129 sites compared to 6,042 sites), but it is still fewer than the number of A-to-I sites of ADAR-YTH^{D422N} (**Supplementary Table S3**). In addition, comparing the methylated RNAs identified by these non-RAC-filtered sites with those identified by ADAR-YTH^{D422N} shows a greater number of methylated RNAs identified by ADAR-YTH^{D422N} (5,689 compared to 4,083, respectively), suggesting that it has greater sensitivity for m^{6}A detection (**Supplementary Figure S3D**). Thus, both APO1-YTH^{D422N} and ADAR-YTH^{D422N} are effective methods for identifying

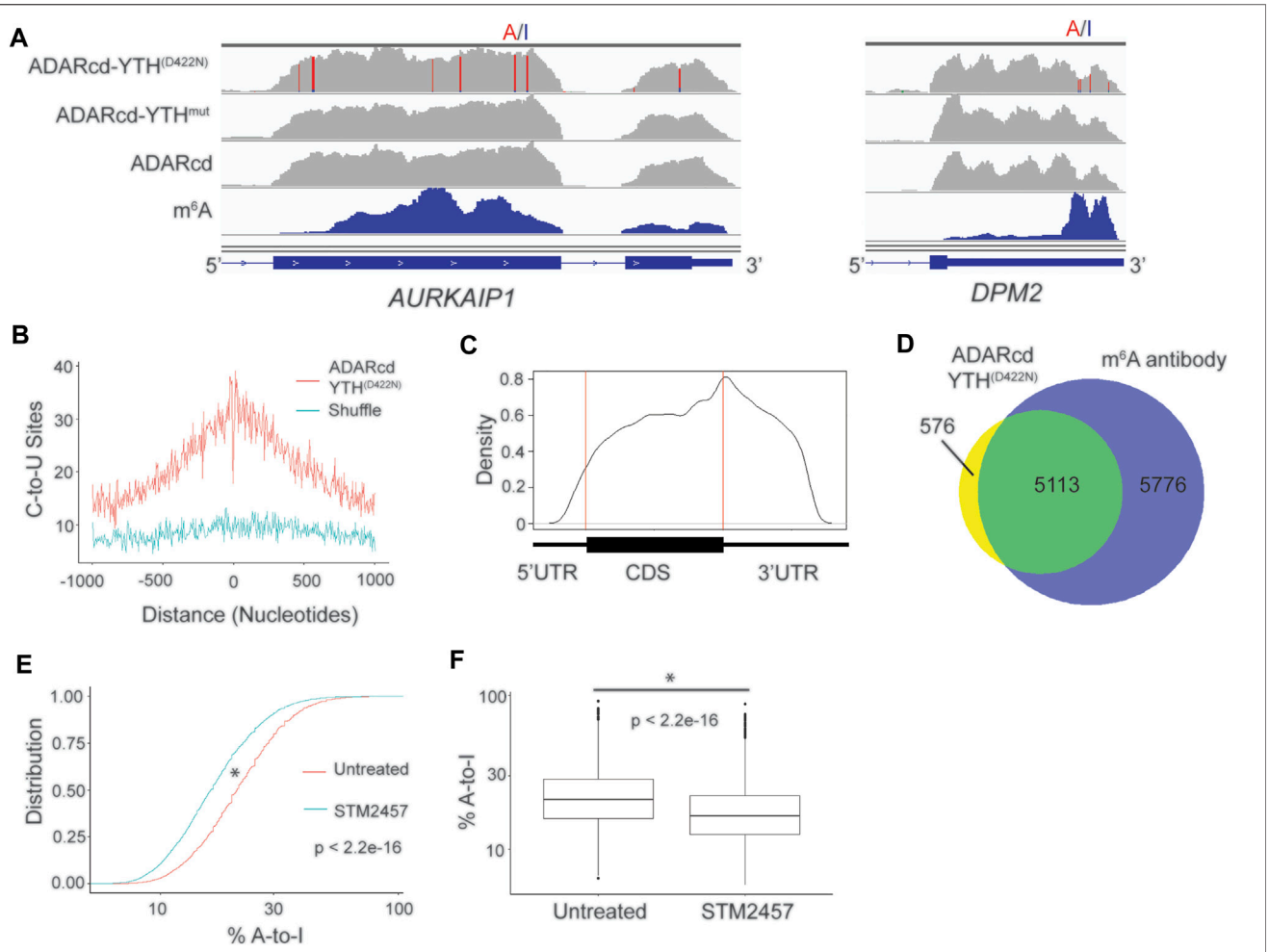


FIGURE 2 | ADARcd can be used as an alternative to APO1 to identify methylated RNAs with DART-seq. **(A)** Genome browser tracks showing two methylated mRNAs, *AURKAIP1* and *DPM2*, in HEK293T cells expressing ADARcd-YTH^{D422N}, ADARcd-YTH^{mut}, or ADARcd alone. A-to-I editing found in at least 10% of the reads are indicated by red/blue coloring. m^{6}A peaks identified by MeRIP (Meyer et al., 2012) is indicated in the bottom blue track. **(B)** Absolute distance plot showing the distance between A-to-I edit sites identified by ADARcd-YTH^{D422N} and m^{6}A sites identified by miCLIP (Linder et al., 2015). **(C)** Metagene plot showing the distribution of A-to-I edit sites found in cells expressing ADARcd-YTH^{D422N}. **(D)** Venn diagram showing overlap between methylated RNAs identified by cellular DART-seq from HEK293T cells expressing ADARcd-YTH^{D422N} and methylated RNAs identified by antibody-based profiling (Meyer et al., 2012; Schwartz et al., 2014; Lichinchi et al., 2016). **(E)** Cumulative distribution plot (left) of %A-to-I for sites identified by ADARcd-YTH^{D422N} in untreated and STM2457 treated HEK293T cells. **(F)** Box plot showing the global A-to-I editing percentage of all sites common to both untreated and STEM2457 treated HEK293T cells expressing ADARcd-YTH^{D422N}. A Wilcoxon Rank-Sum test was conducted to access statistical significance.

methylated RNAs in cells, with ADAR-YTH^{D422N} offering slightly increased sensitivity and APO1-YTH^{D422N} having the distinct advantage of identifying m^{6}A sites with single-nucleotide resolution.

In vitro DART-Seq Detects m^{6}A Transcriptome-Wide From Low Amounts of Input RNA

One limitation of DART-seq is that it requires expression of the DART fusion protein in cells or tissues of interest. This may not be desirable or even possible in some cell types, such as those from difficult-to-target tissues or human samples. To overcome this limitation, we previously demonstrated that *in vitro* DART-seq is capable of profiling m^{6}A transcriptome-wide (Meyer, 2019). However, this strategy used a crude preparation of the DART fusion protein and failed to identify m^{6}A sites with the same efficiency as cellular DART-seq.

We therefore sought to develop an improved version of *in vitro* DART-seq which can be used to profile m^{6}A in any sample of interest while maintaining the high sensitivity and low input requirements of cellular DART-seq. We first generated purified APO1-YTH^{D422N} and APO1-YTH^{mut} proteins using a bacterial expression system (**Supplementary Figure S4A**) (Tegowski et al., 2022b). We then performed *in vitro* DART assays with HEK293T cell RNA followed by RT-PCR and Sanger sequencing to assess

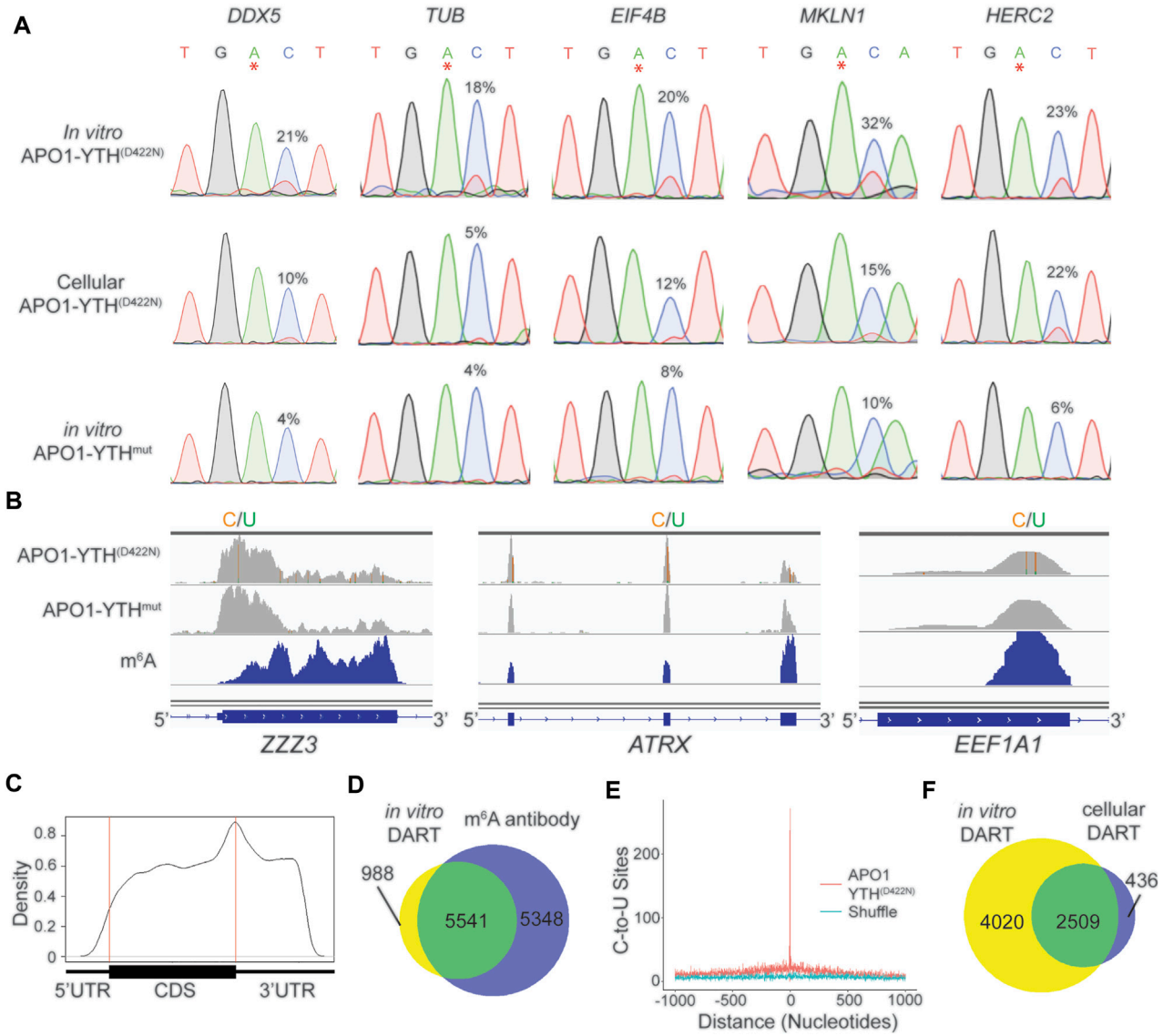


FIGURE 3 | *In vitro* DART-seq identifies m^{6}A transcriptome-wide. **(A)** Comparison of C-to-U editing rates in methylated mRNAs obtained by *in vitro* DART-seq and cellular DART-seq. Sanger sequencing traces show C-to-U editing adjacent to m^{6}A sites in a panel of five methylated mRNAs: *DDX5, TUB*, *EIF4B*, *MKLN1*, and *HERC2*. m^{6}A sites are indicated by asterisks. C-to-U editing rate (%U) is indicated above the adjacent cytidine. Data Representative of three biological replicates. **(B)** Genome browser tracks of *in vitro* DART-seq data showing C-to-U editing in three representative mRNAs: *ZZZ3, ATRX, and EEF1A1*. C-to-U editing found in at least 10% of the reads is indicated by green/yellow coloring. m^{6}A peaks identified by MeRIP (Meyer et al., 2012) is indicated in the bottom blue track. **(C)** Metagene analysis of m^{6}A sites identified by *in vitro* DART-seq using the APO1-YTH^{D422N} protein. **(D)** Venn diagram showing the overlap between methylated RNAs identified by *in vitro* DART-seq filtered against the APO1-YTH^{mut} negative control and methylated RNAs identified by antibody-based methods (Meyer et al., 2012; Schwartz et al., 2014; Lichinchi et al., 2016). **(E)** Absolute distance plot showing the distance of C-to-U editing sites identified by *in vitro* DART-seq relative to m^{6}A sites identified by miCLIP (Linder et al., 2015). m^{6}A sites are centered at position 0. **(F)** Venn diagram showing the overlap between methylated RNAs identified by *in vitro* DART-seq compared to methylated RNAs found by cellular DART-seq.

editing adjacent to m^{6}A sites in a panel of methylated mRNAs. APO1-YTH^{D422N} produced robust C-to-U editing adjacent to m^{6}A sites, an effect that was greatly reduced when APO1-YTH^{mut} was used (**Figure 3A**). Optimization of *in vitro* DART conditions showed that higher concentrations of APO1-YTH^{D422N} protein led to higher C-to-U editing rates but decreased enrichment in % C2U relative to APO1-YTH^{mut} samples, indicating that oversaturation with too much protein can likely increase the rate of false-positives (**Supplementary Figure S4B**). Similarly, longer incubation times led to higher editing rates but lower % C2U enrichment for APO1-YTH^{D422N} relative to APO1-YTH^{mut} (**Supplementary Figure S4C**). Thus, higher protein: RNA ratios and extended assay times may improve the detection of low-abundance m^{6}A sites, but careful calibration relative to the APO1-YTH^{mut} control condition is needed to avoid false-positives.

We next assessed the ability of *in vitro* DART-seq to identify m^{6}A sites transcriptome-wide. We performed *in vitro* DART-seq using 50 ng of total HEK293T cell RNA from three biological replicates. In parallel, we performed *in vitro* DART-seq using APO1-YTH^{mut} and then used Bullseye to identify m^{6}A sites that were enriched in APO1-YTH^{D422N} samples relative to APO1-YTH^{mut} samples (**Figure 3B**, **Supplementary Table S2**). There was high overlap of methylated RNAs identified among biological replicates, indicating the reproducibility of the *in vitro* DART-seq approach (**Supplementary Figure S4D**). Additionally, C-to-U editing sites showed a distribution within transcripts that matches m^{6}A, and methylated RNAs identified by *in vitro* DART-seq showed a high degree of overlap with those identified by antibody-based methods (**Figures 3C,D**). C-to-U editing sites from *in vitro* DART-seq were also found at C-to-T mutations in miCLIP data, indicating that *in vitro* DART-seq can successfully identify m^{6}A sites transcriptome-wide (**Figure 3E**).

We next compared the methylated RNAs identified by APO1-YTH^{D422N} with *in vitro* DART-seq to those of cellular DART-seq. The majority (85.2%) of methylated RNAs identified by cellular expression of APO1-YTH^{D422N} were also identified *in vitro*. However, *in vitro* DART-seq identified a much greater number of methylated RNAs (**Figure 3F**, **Supplementary Table S2**). C-to-U editing sites uniquely identified by *in vitro* DART-seq had a distribution that matches m^{6}A and occurred at C-to-T mutations sites previously called by miCLIP (**Supplementary Figures S4E,F**). This suggests that the greater number of methylated RNAs identified by *in vitro* DART-seq relative to cellular DART-seq is not caused by false positives and instead likely reflects greater sensitivity of the *in vitro* DART-seq approach.

Finally, to determine whether the increased sensitivity of APO1-YTH^{D422N} compared to APO1-YTH that we observed in cells was also recapitulated *in vitro*, we performed *in vitro* DART-seq using APO1-YTH. We found that APO1-YTH^{D422N} identified more m^{6}A sites and methylated RNAs than APO1-YTH (**Supplementary Figure S5A**, **Supplementary Table S2**), and C-to-U editing sites identified by APO1-YTH^{D422N} also had significantly higher % C2U values than sites identified by APO1-YTH (**Supplementary Figures S5B,C**). Similar to cellular DART-seq, the sites uniquely identified by APO1-YTH^{D422N} using *in vitro* DART-seq had a distribution that matches m^{6}A and were enriched at C-to-T mutations from miCLIP data (Linder et al., 2015), indicating that they are not due to false-positives (**Supplementary Figures S5D,E**). Altogether, we demonstrate *in vitro* DART-seq as a highly sensitive antibody-independent m^{6}A detection method.

YTH Domain Blocking Improves *in vitro* DART-Seq m^{6}A Detection Specificity

The use of APO1-YTH^{mut} to control for non-specific deamination helps ensure the identification of high-confidence m^{6}A sites. However, because the YTH^{mut} domain retains low-level m^{6}A binding (**Figure 1D**), it is possible that some m^{6}A sites are eliminated from DART-seq datasets when filtering against APO1-YTH^{mut} as a control. We therefore sought to develop alternative methods for eliminating false-positive site calls while minimizing false-negatives.

We tested whether blocking the DART protein from binding to m^{6}A sites could be an effective alternative to the use of APO1-YTH^{mut}. To do this, we purified the YTH domain (see Methods) and subjected HEK293T cell RNA to *in vitro* DART-seq using a modified protocol in which the RNA sample was pre-incubated with the YTH domain before addition of APO1-YTH^{D422N} (see Methods). m^{6}A sites were called by establishing a minimum editing enrichment threshold in the APO1-YTH^{D422N} condition relative to the YTH blocking condition, similar to what was done when using the APO1-YTH^{mut} control. C-to-U editing events that remained after YTH blocking showed a distribution distinct from that of m^{6}A and were enriched in the distal 3′UTR (**Figure 4A**). This was similar to the distribution of sites identified in the APO1-YTH^{mut} condition, suggesting that both methods can be used to identify false-negative sites.

We next assessed whether the YTH blocking strategy improves the m^{6}A detection accuracy of *in vitro* DART-seq compared to the APO1-YTH^{mut} control method. To do this, we filtered C-to-U editing sites in the APO1-YTH^{D422N} dataset by their % C2U enrichment relative to either the YTH blocking dataset or the APO1-YTH^{mut} dataset (see Methods). There was a high degree of overlap in the m^{6}A sites and methylated RNAs identified by both datasets and a similar distribution of m^{6}A sites within RNAs (**Figures 4B,C**). Interestingly, using APO1-YTH^{mut} as a negative control led to the exclusion of more sites (21,568 total sites identified when filtering against APO1-YTH^{mut} vs. 25,097 total sites identified when filtering against the YTH domain blocking dataset) (**Figure 4D**, **Supplementary Table S4**). Comparison of the sites unique to each filtering method showed a similar enrichment which matched that of m^{6}A, and the RNAs containing these sites were also identified by miCLIP, suggesting that these unique sites are not false-positives (**Supplementary Figures S6A,B**). Interestingly, the % C2U values of sites that were unique to the YTH blocking method of filtering were significantly lower than those of the APO1-YTH^{mut} method of filtering (**Supplementary Figures S6C,D**). This suggests that identifying sites by filtering against the YTH blocking dataset enables the detection of lower abundance m^{6}A sites compared to the APO1-YTH^{mut} method. This is consistent with the low-level m^{6}A binding of APO1-YTH^{mut}, which likely leads to editing adjacent to some m^{6}A sites and therefore their exclusion when using this method as a negative control. In addition, the unique sites identified with YTH blocking filtering showed an increased number of C-to-U edit sites adjacent to previously identified m^{6}A sites by miCLIP (**Supplementary Figure S6E**). Altogether, these data suggest that both APO1-YTH^{mut} and YTH domain blocking can serve as effective controls against which to filter *in vitro* DART-seq data for elimination of false-positives. Both strategies perform similarly well, but YTH domain blocking enables slightly more sites to be identified, which likely reflect low-abundance m^{6}A sites.

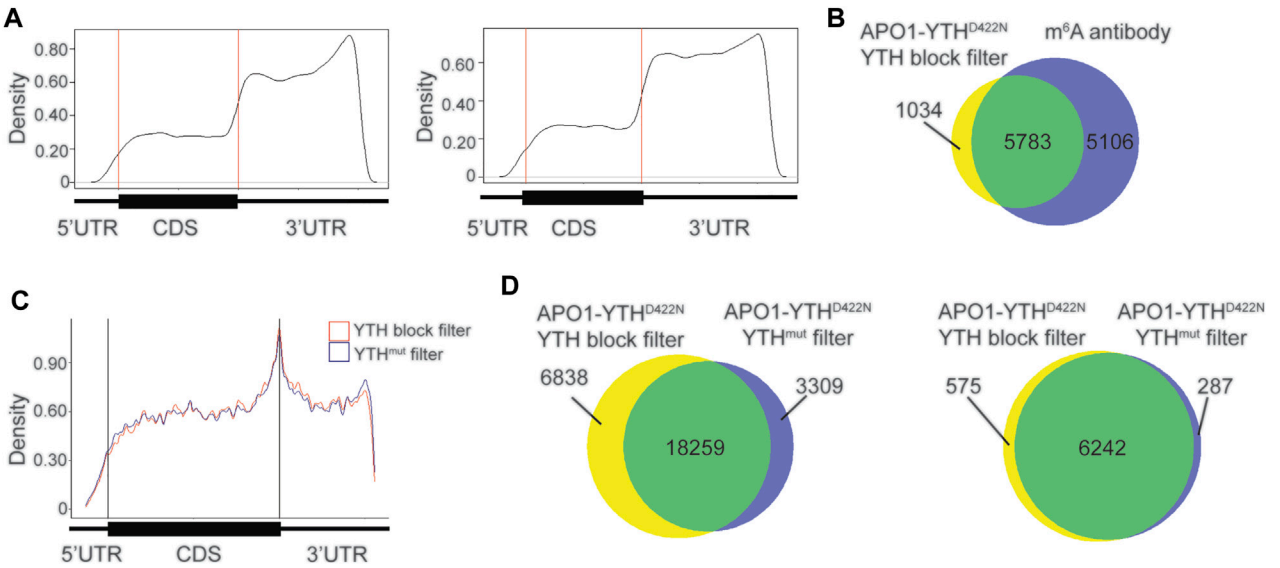


FIGURE 4 | Blocking with the YTH domain minimizes false positives with *in vitro* DART-seq. **(A)** Metagene analysis of C-to-U editing sites in mRNAs identified with *in vitro* DART-seq using the APO1-YTH^{D422N} protein after pre-incubation with the YTH domain (left) or the APO1-YTH^{mut} protein (right). **(B)** Venn diagram showing the overlap between methylated RNAs identified by *in vitro* DART-seq with APO1-YTH^{D422N} filtered by YTH blocking and methylated RNAs identified by antibody-based methods (Meyer et al., 2012; Schwartz et al., 2014; Lichinchi et al., 2016). **(C)** Metagene analysis showing the distribution of C-to-U editing sites in mRNAs after filtering of *in vitro* DART-seq data against by YTH blocking (blue) or by APO1-YTH^{mut} (red). **(D)** Venn diagram of C-to-U edit sites induced by *in vitro* DART-seq with APO1-YTH^{D422N}, filtered by use of either YTH blocking or APO1-YTH^{mut} (left). Venn diagram of methylated RNA identified by *in vitro* DART-seq with APO1-YTH^{D422N}, filtered by use of either YTH blocking or APO1-YTH^{mut} (right).

DISCUSSION

In this study, we present an improved version of DART-seq which utilizes a variant of the APO1-YTH fusion protein containing an engineered D422N mutation within the YTH domain. This variant exhibits improved m^{6}A recognition compared to the original APO1-YTH fusion protein and enables detection of m^{6}A transcriptome-wide with slightly greater sensitivity. Surprisingly, our attempts to optimize the editing domain of the DART fusion protein by using alternative cytidine deaminase proteins failed to identify a variant capable of editing RNAs adjacent to m^{6}A sites. This may reflect the requirement for a specific structural conformation of the fusion protein to permit access of the editing domain to m^{6}A-adjacent cytidines. Future studies examining the structure of APO1-YTH in complex with RNA would undoubtedly shed more light on how the fusion protein interacts with methylated RNA substrates to target cytidine residues that occur adjacent to m^{6}A.

Although the cytidine deaminase variants that we tested failed to improve DART protein editing, we discovered that swapping ADARcd for APO1 led to efficient deamination of adenosines in methylated RNAs. The resulting A-to-I editing sites are enriched near m^{6}A, although because m^{6}A occurs within a RAC consensus sequence, these sites are not immediately adjacent to m^{6}A. Thus, unlike APO1-YTH^{D422N}, ADARcd-YTH^{D422N} cannot identify m^{6}A sites with single-nucleotide resolution. However, direct comparison of both fusion proteins in cells indicated that ADARcd-YTH^{D422N} identifies a greater number of methylated RNAs, indicating that it has increased sensitivity for identifying methylated RNAs at the whole transcript level. However, one consideration when using this approach is that ADARcd is known to exhibit preferential editing of double-stranded RNA regions (Eggington et al., 2011; Jin H. et al., 2020); thus, ADARcd-YTH^{D422N} may miss some methylated RNAs that lack suitable double-stranded regions in near m^{6}A sites. Such issues will be important to consider for each individual study when deciding which DART fusion protein to use. In theory, it should also be possible to co-express both APO1-YTH^{D422N} and ADARcd-YTH^{D422N} at the same time in cells and identify transcripts with both A-to-I and C-to-U editing. Such a strategy would minimize the false-positives of both approaches and still provide single-nucleotide resolution m^{6}A mapping.

In addition to improving the cellular DART-seq method, we also developed an *in vitro* DART-seq approach which enables m^{6}A mapping from any sample of interest without the need for overexpression of the DART fusion protein. We demonstrate that *in vitro* DART-seq performs comparably to cellular DART-seq and that it can be used to accurately profile m^{6}A sites from low amounts of input material. Since a major limitation of m^{6}A mapping studies has been the requirement for large amounts of purified RNA, we anticipate that *in vitro* DART-seq will now enable m^{6}A mapping studies that were not previously possible, such as those that utilize human tissues or frozen samples.

An important component of both cellular and *in vitro* DART-seq is the use of controls to help eliminate false-positive sites. This includes identifying sites that are edited by the APO1 or ADARcd proteins alone and eliminating them from consideration. We have also traditionally used APO1-YTH^{mut} as a negative control. Although the YTH^{mut} domain exhibits reduced m^{6}A recognition, it still retains

some m^{6}A binding ability and therefore contributes to low-level C-to-U deamination when fused to APO1 (Meyer, 2019; Tegowski et al., 2022a). The Bullseye pipeline therefore uses thresholds based on % C2U enrichment relative to APO1-YTH^{mut} to identify high-confidence m^{6}A sites. However, this may lead to the elimination of some true m^{6}A sites which retain sufficient levels of editing by APO1-YTH^{mut}. We have mitigated this to some extent here by developing a YTH pre-blocking method for *in vitro* DART-seq, which eliminates the need for the APO1-YTH^{mut} control. We find that the YTH blocking approach enables the identification of slightly more m^{6}A sites which may otherwise be filtered out using the APO1-YTH^{mut} strategy as a control. Thus, for *in vitro* DART-seq, employing a pre-blocking step with the YTH domain alone may be preferred. Other methods for eliminating false-positives, such as the recently developed use of modification-free libraries (Zhang et al., 2021), are alternative strategies which may further increase the accuracy of the *in vitro* DART-seq method.

In summary, we have developed an improved version of the DART fusion protein and a suite of new methods related to the DART-seq approach which will facilitate more accurate and sensitive m^{6}A detection. The development of *in vitro* DART-seq in particular provides a method for transcriptome-wide m^{6}A mapping in nearly any sample of interest and overcomes the need for large amounts of input material that are required for most m^{6}A mapping approaches. Therefore, we anticipate that this method will enable future studies of m^{6}A in tissues or cell types that were otherwise not amenable to m^{6}A profiling.

DATA AVAILABILITY STATEMENT

The datasets presented in this study can be found in online repositories. The names of the repository/repositories and accession number(s) can be found below: NCBI's Gene Expression Omnibus (GEO) under accession code GSE196416.

AUTHOR CONTRIBUTIONS

KM and HZ designed the experiments. HZ performed experiments, collected data and performed data analysis. XY prepared samples for UPLC-MS/MS and analyzed results with guidance from CH. KM and HZ wrote the manuscript.

FUNDING

This work was supported by the National Institutes of Health (R01MH118366, DP1DA046584, R21MH119813, and RM1HG011563).

ACKNOWLEDGMENTS

We thank members of the Meyer laboratory for comments and suggestions.

SUPPLEMENTARY MATERIAL

The Supplementary Material for this article can be found online at: https://www.frontiersin.org/articles/10.3389/fcell.2022.888279/full#supplementary-material

Supplementary Figure S1 | Comparison of different DART protein variants. **(A)** Schematic showing the domain composition of all DART protein variants tested. **(B)** Western blot showing the expression of DART protein variants after expression in HEK293T cells. Results are representative of three biological replicates for each DART protein variant. **(C)** Sanger sequencing traces showing C-to-U editing adjacent to m6A sites found by cellular DART-seq with DART variants in panel **(A)** for five selected mRNAs: DPM2, EIF4B, HERC2, NIPA1, and SMUG1. Most variants failed to show editing above background (>5%). rZDD-YTH demonstrated C-to-U editing, but it was lower than that of APO1-YTHD422N. Results are representative of three biological replicates. **(D)** Metagene analysis of C-to-U editing sites identified by DART-seq in HEK293T cells expressing the indicated DART protein variant. **(E)** Metagene analysis of C-to-U editing events unique to APO1-YTHD422N that were not identified by cellular DART-seq with APO1-YTH. **(F)** Venn diagram showing the overlap between methylated RNAs identified by C-to-U editing events unique to APO1-YTHD422N that are not found in APO1-YTH, and methylated RNAs found by antibody-based profiling (Lichinchi et al., 2016, Meyer et al., 2012, Schwartz et al., 2014).

Supplementary Figure S2 | Validation of m6A-methylated RNAs identified by cellular DART-seq with ADARcd-YTHD422N. **(A)** Genome browser track showing the JUN mRNA in HEK293T cells expressing ADARcd-YTHD422N. A-to-I editing found in at least 10% of the reads are indicated by red/blue coloring (left). Expanded region of JUN (right) shows A-to-I editing (marked by arrow in both panels) in proximity to an m6A site previously identified by miCLIP (Linder et al., 2015). **(B)** Venn diagram of m6A-containing RNAs identified by each of the three biological replicates of cells expressing ADARcd-YTHD422N. **(C)** Mass spectrometry data examining the ratio between m6A/A in mRNA purified from untreated HEK293T cells or HEK293T cells treated with STM2457. The graph shows the average of two biological replicates in each condition and the error bar represents the standard deviation.

Supplementary Figure S3 | Validation of m6A-dependent editing by ADARcd-YTHD422N. **(A)** Venn diagram of methylated RNAs identified by cellular DART-seq with ADARcd-YTHD422N compared to those identified by APO1-YTHD422N. **(B)** Venn diagram of methylated RNAs identified uniquely by cellular DART-seq with ADARcd-YTHD422N and not identified by cellular DART-seq with APO1-YTHD422N, compared to methylated RNAs found by miCLIP (Linder et al., 2015). **(C)** Metagene analysis of A-to-I editing sites in methylated transcripts uniquely identified in ADARcd-YTHD422N DART-seq data and not in APO1-YTHD422N DART-seq data. **(D)** Venn diagram of methylated RNAs identified by cellular DART-seq with ADARcd-YTHD422N compared to those identified by APO1-YTHD422N without the RAC filter.

Supplementary Figure S4 | Optimization and validation of *in vitro* DART-seq as a global m6A profiling method. **(A)** Coomassie stain showing the purification of the APO1-YTHD422N (left) and APO1-YTH (right) proteins. **(B)** Quantification of Sanger sequencing data showing C-to-U editing rate ratio (APO1-YTHD422N/APO1-YTHmut) for cytidine residues adjacent to m6A sites in three representative mRNAs: ACTB, DPM2, and HERC2. *In vitro* DART assays were performed using x nanograms of total HEK293T cell RNA and 250 nanograms of APO1-YTHD422N incubated at 37°C for the indicated time points. *n*=2 biological replicates; error bars = standard deviation. **(C)** Quantification of Sanger sequencing data as in **(B)** for *in vitro* DART assays using the indicated concentration of APO1-YTHD422N and APO1-YTHmut protein incubated with 50 nanograms of total HEK293T cell RNA at 37°C for 4 h. *n*=2 biological replicates; error bars = standard deviation. **(D)** Overlap of methylated RNAs identified in each of the three biological replicates of *in vitro* DART-seq using APO1-YTHD422N. **(E)** Metagene plot of C-to-U editing sites in methylated transcripts uniquely found by *in vitro* DART-seq with APO1-YTHD422N compared to cellular DART-seq with the same protein variant. **(F)** Absolute distance plot showing the distance of C-to-U edit sites in methylated RNAs identified by APO1-YTHD422N that were not identified by cellular DART-seq with the same protein variant, and m6A sites identified by miCLIP (Linder et al., 2015).

Supplementary Figure S5 | Comparison of APO1-YTHD422N and APO1-YTH with *in vitro* DART-seq. **(A)** Comparison of methylated RNAs identified by *in vitro* DART-seq using APO1-YTHD422N or APO1-YTH. **(B)** Cumulative distribution of C-to-U editing rates for sites in *in vitro* DART-seq data using the APO1-YTHD422N

or APO1-YTH protein. **(C)** Box plot showing the editing percentage of C-to-U sites identified by *in vitro* DART-seq using APO1-YTHD422N or APO1-YTH both filtered by APO1-YTHmut. **(D)** Metagene analysis of C-to-U editing sites uniquely identified by APO1-YTHD422N but not identified by APO1-YTH. **(E)** Absolute distance plot showing the distance of C-to-U editing sites uniquely identified by APO1-YTHD422N compared to APO1-YTH from m6A sites identified by miCLIP (Linder et al., 2015). m^{6}A sites are centered at position 0.

Supplementary Figure S6 | Comparison of YTH blocking and APO1-YTHmut as controls for *in vitro* DART-seq. **(A)** Distribution of C-to-U editing sites in methylated RNAs identified by APO1-YTHD422N filtered by the YTH blocking dataset but not when filtered by APO1-YTHmut (left); vice-versa (right). **(B)** Venn diagram showing overlap of methylated RNAs identified by APO1-YTHD422N after filtering by YTH blocking (left) or APO1-YTHmut (right) with methylated RNAs identified by miCLIP (Linder et al., 2015). **(C)** Cumulative distribution of C-to-U editing rates of sites identified by *in vitro* DART-seq using APO1-YTHD422N and filtered by YTH blocking APO1-YTHmut. **(D)** Box plot showing C-to-U editing rates of sites identified by *in vitro* DART-seq using purified APO1-YTHD422N filtered by the YTH blocking dataset or by APO1-YTHmut dataset. **(E)** Absolute distance plot showing the distance of C-to-U editing sites identified by APO1-YTHD422N filtered by YTH blocking and not identified by APO1-YTHmut relative to m6A sites identified by miCLIP (Linder et al., 2015). m6A sites are centered at position 0.

Supplementary Table S1 | Sites identified by DART protein variants using cellular DART-seq in HEK293T cells. Listed are the genome coordinates of DART-seq C-to-U editing sites identified from cells expressing DART protein variants APO1-YTHD422N, APO1-YTH, APO1-YTH(DF1), and APO1-YTH(DF1-D401N). Also indicated is the proportion of C-to-U editing (U/C).

Supplementary Table S2 | Sites identified by APO1-YTH and APO1-YTHD422N with *in vitro* DART-seq. Listed are the genome coordinates of DART-seq C-to-U editing sites identified from *in vitro* DART-seq assay using purified APO1-YTH protein or purified APO1-YTHD422N protein. Also indicated are the proportion of C-to-U editing (U/C).

Supplementary Table S3 | A-to-I edit sites identified by cellular DART-seq with ADARcd-YTHD422N. Listed are the genome coordinates of m6A dependent A-to-I edit sites identified from HEK293T cells expressing ADARcd-YTHD422N and from HEK293T cells treated with STM2547 expressing ADARcd-YTHD422N. Also indicated are the proportion of A-to-I editing and the region of distribution of these sites.

Supplementary Table S4 | C-to-U editing events induced by APO1-YTHD422N *in vitro* DART-seq filtered by YTH blocking technique.

REFERENCES

Chen, X.-Y., Zhang, J., and Zhu, J.-S. (2019). The Role of m6A RNA Methylation in Human Cancer. *Mol. Cancer* 18, 103. doi:10.1186/s12943-019-1033-z

Dominissini, D., Moshitch-Moshkovitz, S., Schwartz, S., Salmon-Divon, M., Ungar, L., Osenberg, S., et al. (2012). Topology of the Human and Mouse m6A RNA Methylomes Revealed by m6A-Seq. *Nature* 485, 201–206. doi:10.1038/nature11112

Eggington, J. M., Greene, T., and Bass, B. L. (2011). Predicting Sites of ADAR Editing in Double-Stranded RNA. *Nat. Commun.* 2, 319. doi:10.1038/ncomms1324

Gu, C., Shi, X., Dai, C., Shen, F., Rocco, G., Chen, J., et al. (2020). RNA m6A Modification in Cancers: Molecular Mechanisms and Potential Clinical Applications. *The Innovation* 1, 100066. doi:10.1016/j.xinn.2020.100066

Hafner, M., Landthaler, M., Burger, L., Khorshid, M., Hausser, J., Berninger, P., et al. (2010). Transcriptome-wide Identification of RNA-Binding Protein and microRNA Target Sites by PAR-CLIP. *Cell* 141, 129–141. doi:10.1016/j.cell.2010.03.009

He, L., Li, H., Wu, A., Peng, Y., Shu, G., and Yin, G. (2019). Functions of N6-Methyladenosine and its Role in Cancer. *Mol. Cancer* 18, 176. doi:10.1186/s12943-019-1109-9

He, P. C., and He, C. (2021). m6 A RNA Methylation: from Mechanisms to Therapeutic Potential. *Embo j* 40, e105977. doi:10.15252/embj.2020105977

Hsu, P. J., and He, C. (2019). High-Resolution Mapping of N 6-Methyladenosine Using m6A Crosslinking Immunoprecipitation Sequencing (m6A-CLIP-Seq). *Methods Mol. Biol.* 1870, 69–79. doi:10.1007/978-1-4939-8808-2_5

Jin, H., Xu, W., Rahman, R., Na, D., Fieldsend, A., Song, W., et al. (2020a). TRIBE Editing Reveals Specific mRNA Targets of eIF4E-BP in *Drosophila* and in Mammals. *Sci. Adv.* 6, eabb8771. doi:10.1126/sciadv.abb8771

Jin, S., Fei, H., Zhu, Z., Luo, Y., Liu, J., Gao, S., et al. (2020b). Rationally Designed APOBEC3B Cytosine Base Editors with Improved Specificity. *Mol. Cel* 79, 728–740. doi:10.1016/j.molcel.2020.07.005

Kluesner, M. G., Nedveck, D. A., Lahr, W. S., Garbe, J. R., Abrahante, J. E., Webber, B. R., et al. (2018). EditR: A Method to Quantify Base Editing from Sanger Sequencing. *CRISPR J.* 1, 239–250. doi:10.1089/crispr.2018.0014

Lichinchi, G., Gao, S., Saletore, Y., Gonzalez, G. M., Bansal, V., Wang, Y., et al. (2016). Dynamics of the Human and Viral m6A RNA Methylomes during HIV-1 Infection of T Cells. *Nat. Microbiol.* 1, 16011. doi:10.1038/nmicrobiol.2016.11

Linder, B., Grozhik, A. V., Olarerin-George, A. O., Meydan, C., Mason, C. E., and Jaffrey, S. R. (2015). Single-nucleotide-resolution Mapping of m6A and m6Am throughout the Transcriptome. *Nat. Methods* 12, 767–772. doi:10.1038/nmeth.3453

Liu, S., Zhu, A., He, C., and Chen, M. (2020). REPIC: a Database for Exploring the N6-Methyladenosine Methylome. *Genome Biol.* 21, 100. doi:10.1186/s13059-020-02012-4

Mcmahon, A. C., Rahman, R., Jin, H., Shen, J. L., Fieldsend, A., Luo, W., et al. (2016). TRIBE: Hijacking an RNA-Editing Enzyme to Identify Cell-specific Targets of RNA-Binding Proteins. *Cell* 165, 742–753. doi:10.1016/j.cell.2016.03.007

Meyer, K. D. (2019). DART-seq: an Antibody-free Method for Global m6A Detection. *Nat. Methods* 16, 1275. doi:10.1038/s41592-019-0570-0

Meyer, K. D., and Jaffrey, S. R. (2017). Rethinking m6A Readers, Writers, and Erasers. *Annu. Rev. Cel Dev. Biol.* 33, 319–342. doi:10.1146/annurev-cellbio-100616-060758

Meyer, K. D., Saletore, Y., Zumbo, P., Elemento, O., Mason, C. E., and Jaffrey, S. R. (2012). Comprehensive Analysis of mRNA Methylation Reveals Enrichment in 3′ UTRs and Near Stop Codons. *Cell* 149, 1635–1646. doi:10.1016/j.cell.2012.05.003

Olarerin-George, A. O., and Jaffrey, S. R. (2017). MetaPlotR: a Perl/R Pipeline for Plotting Metagenes of Nucleotide Modifications and Other Transcriptomic Sites. *Bioinformatics* 33, 1563–1564. doi:10.1093/bioinformatics/btx002

Owens, M. C., Zhang, C., and Liu, K. F. (2021). Recent Technical Advances in the Study of Nucleic Acid Modifications. *Mol. Cel* 81, 4116–4136. doi:10.1016/j.molcel.2021.07.036

Rahman, R., Xu, W., Jin, H., and Rosbash, M. (2018). Identification of RNA-Binding Protein Targets with HyperTRIBE. *Nat. Protoc.* 13, 1829–1849. doi:10.1038/s41596-018-0020-y

Roundtree, I. A., Evans, M. E., Pan, T., and He, C. (2017). Dynamic RNA Modifications in Gene Expression Regulation. *Cell* 169, 1187–1200. doi:10.1016/j.cell.2017.05.045

Salter, J. D., Bennett, R. P., and Smith, H. C. (2016). The APOBEC Protein Family: United by Structure, Divergent in Function. *Trends Biochem. Sci.* 41, 578–594. doi:10.1016/j.tibs.2016.05.001

Schwartz, S., Mumbach, M. R., Jovanovic, M., Wang, T., Maciag, K., Bushkin, G. G., et al. (2014). Perturbation of m6A Writers Reveals Two Distinct Classes of mRNA Methylation at Internal and 5′ Sites. *Cel Rep.* 8, 284–296. doi:10.1016/j.celrep.2014.05.048

Shi, H., Wei, J., and He, C. (2019). Where, when, and How: Context-dependent Functions of RNA Methylation Writers, Readers, and Erasers. *Mol. Cel* 74, 640–650. doi:10.1016/j.molcel.2019.04.025

Shi, H., Zhang, X., Weng, Y.-L., Lu, Z., Liu, Y., Lu, Z., et al. (2018). m6A Facilitates Hippocampus-dependent Learning and Memory through YTHDF1. *Nature* 563, 249–253. doi:10.1038/s41586-018-0666-1

Smith, H. C. (2017). RNA Binding to APOBEC Deaminases; Not Simply a Substrate for C to U Editing. *RNA Biol.* 14, 1153–1165. doi:10.1080/15476286.2016.1259783

Tegowski, M., Flamand, M. N., and Meyer, K. D. (2022a). scDART-seq Reveals Distinct m^{6}A Signatures and mRNA Methylation Heterogeneity in Single Cells. *Mol. Cel* 82, 868. doi:10.1016/j.molcel.2021.12.038

Tegowski, M., Zhu, H., and Meyer, K. D. (2022b). "Detecting M6a with *In Vitro* Dart-Seq," in *Post-transcriptional Gene Regulation*. Editor E. Dassi (New York, NY: Springer US). doi:10.1007/978-1-0716-1851-6_20

Wang, T., Kong, S., Tao, M., and Ju, S. (2020). The Potential Role of RNA N6-Methyladenosine in Cancer Progression. *Mol. Cancer* 19, 88. doi:10.1186/s12943-020-01204-7

Wei, C.-M., and Moss, B. (1977). Nucleotide Sequences at the N6-Methyladenosine Sites of HeLa Cell Messenger Ribonucleic Acid. *Biochemistry* 16, 1672–1676. doi:10.1021/bi00627a023

Winkler, R., Gillis, E., Lasman, L., Safra, M., Geula, S., Soyris, C., et al. (2019). m6A Modification Controls the Innate Immune Response to Infection by Targeting Type I Interferons. *Nat. Immunol.* 20, 173–182. doi:10.1038/s41590-018-0275-z

Xu, C., Liu, K., Ahmed, H., Loppnau, P., Schapira, M., and Min, J. (2015). Structural Basis for the Discriminative Recognition of N6-Methyladenosine RNA by the Human YT521-B Homology Domain Family of Proteins. *J. Biol. Chem.* 290, 24902–24913. doi:10.1074/jbc.m115.680389

Xu, W., Rahman, R., and Rosbash, M. (2018). Mechanistic Implications of Enhanced Editing by a HyperTRIBE RNA-Binding Protein. *Rna* 24, 173–182. doi:10.1261/rna.064691.117

Yankova, E., Blackaby, W., Albertella, M., Rak, J., De Braekeleer, E., Tsagkogeorga, G., et al. (2021). Small-molecule Inhibition of METTL3 as a Strategy against Myeloid Leukaemia. *Nature* 593, 597–601. doi:10.1038/s41586-021-03536-w

Zaccara, S., Ries, R. J., and Jaffrey, S. R. (2019). Reading, Writing and Erasing mRNA Methylation. *Nat. Rev. Mol. Cel Biol* 20, 608–624. doi:10.1038/s41580-019-0168-5

Zhang, M., Zhai, Y., Zhang, S., Dai, X., and Li, Z. (2020). Roles of N6-Methyladenosine (m6A) in Stem Cell Fate Decisions and Early Embryonic Development in Mammals. *Front. Cel Dev. Biol.* 8, 782. doi:10.3389/fcell.2020.00782

Zhang, Z., Chen, T., Chen, H.-X., Xie, Y.-Y., Chen, L.-Q., Zhao, Y.-L., et al. (2021). Systematic Calibration of Epitranscriptomic Maps Using a Synthetic Modification-free RNA Library. *Nat. Methods* 18, 1213–1222. doi:10.1038/s41592-021-01280-7

Zhu, T., Roundtree, I. A., Wang, P., Wang, X., Wang, L., Sun, C., et al. (2014). Crystal Structure of the YTH Domain of YTHDF2 Reveals Mechanism for Recognition of N6-Methyladenosine. *Cell Res* 24, 1493–1496. doi:10.1038/cr.2014.152

Conflict of Interest: KM has filed a patent application for the DART-seq technology through Duke University.

The remaining authors declare that the research was conducted in the absence of any commercial or financial relationships that could be construed as a potential conflict of interest.

Publisher's Note: All claims expressed in this article are solely those of the authors and do not necessarily represent those of their affiliated organizations, or those of the publisher, the editors and the reviewers. Any product that may be evaluated in this article, or claim that may be made by its manufacturer, is not guaranteed or endorsed by the publisher.

Copyright © 2022 Zhu, Yin, Holley and Meyer. This is an open-access article distributed under the terms of the Creative Commons Attribution License (CC BY). The use, distribution or reproduction in other forums is permitted, provided the original author(s) and the copyright owner(s) are credited and that the original publication in this journal is cited, in accordance with accepted academic practice. No use, distribution or reproduction is permitted which does not comply with these terms.

frontiers | Frontiers in Cell and Developmental Biology

REVIEW
published: 01 June 2022
doi: 10.3389/fcell.2022.886642

tRNA Function and Dysregulation in Cancer

Tania Gupta[1], *Mark G. Malkin*[2,3] *and Suyun Huang*[3,4,5]*

[1]Virginia Commonwealth University, Richmond, VA, United States, [2]Department of Neurology, School of Medicine, Virginia Commonwealth University, Richmond, VA, United States, [3]VCU Massey Cancer Center, Virginia Commonwealth University, Richmond, VA, United States, [4]Department of Human and Molecular Genetics, School of Medicine, Virginia Commonwealth University, Richmond, VA, United States, [5]Institute of Molecular Medicine, School of Medicine, Virginia Commonwealth University, Richmond, VA, United States

Transfer RNA (tRNA) is a central component of protein synthesis and plays important roles in epigenetic regulation of gene expression in tumors. tRNAs are also involved in many cell processes including cell proliferation, cell signaling pathways and stress response, implicating a role in tumorigenesis and cancer progression. The complex role of tRNA in cell regulation implies that an understanding of tRNA function and dysregulation can be used to develop treatments for many cancers including breast cancer, colon cancer, and glioblastoma. Moreover, tRNA modifications including methylation are necessary for tRNA folding, stability, and function. In response to certain stress conditions, tRNAs can be cleaved in half to form tiRNAs, or even shorter tRNA fragments (tRF). tRNA structure and modifications, tiRNA induction of stress granule formation, and tRF regulation of gene expression through the repression of translation can all impact a cell's fate. This review focuses on how these functions of tRNAs, tiRNA, and tRFs can lead to tumor development and progression. Further studies focusing on the specific pathways of tRNA regulation could help identify tRNA biomarkers and therapeutic targets, which might prevent and treat cancers.

Keywords: tRNA, cancer, TRF, tiRNA, tumor, protein

OPEN ACCESS

Edited by:
Huilin Huang,
Sun Yat-sen University Cancer Center (SYSUCC), China

Reviewed by:
Shuibin Lin,
Sun Yat-sen University, China
Tao Pan,
The University of Chicago, United States

***Correspondence:**
Suyun Huang
suyun.huang@vcuhealth.org

Specialty section:
This article was submitted to Epigenomics and Epigenetics, a section of the journal Frontiers in Cell and Developmental Biology

Received: *28 February 2022*
Accepted: *05 May 2022*
Published: *01 June 2022*

Citation:
Gupta T, Malkin MG and Huang S (2022) tRNA Function and Dysregulation in Cancer. Front. Cell Dev. Biol. 10:886642. doi: 10.3389/fcell.2022.886642

INTRODUCTION

Cancer continues to be one of the leading causes of death in the world, accounting for 13% of all deaths (Zhao & Li, 2021). Cancer cells are characterized by rapid cell growth, which must be supported through the reprogramming of metabolic pathways. Unlike healthy cells which primarily use oxidative phosphorylation for energy production, tumor cells primarily rely on anabolic pathways including aerobic glycolysis, fatty acid synthesis, and the pentose phosphate pathway to absorb nutrients that can be used to build macromolecules in order to meet the demands of the rapidly proliferating cell (Zhao & Li, 2021). Because approximately 70% of cell dry weight is protein, cancer cells especially depend upon high levels of protein production (Dolfi et al., 2013). In fact, as the cell proliferation rate increases, so does the protein synthesis rate per cell volume (Dolfi et al., 2013).

Protein production begins when genetically coded, hardwired DNA is first transcribed into messenger RNA (Yu et al., 2021) in the nucleus, which is then transported into the cytoplasm to be translated into protein that can be used by the cell. In the cytoplasm, tRNA translates each three-base codon on the mRNA into an amino acid. These amino acids form a chain known as a polypeptide, which can be processed into a protein. Because of the critical role that tRNAs play in protein

production and cell survival, tRNA transcripts are tightly controlled before being post transcriptionally modified (Schaffer et al., 2019). These modifications are important for tRNA structure and function (Torres et al., 2014). The dysregulation of tRNAs and tRNA modifying enzymes has been implicated in a multitude of disorders such as neurodevelopmental disorders (Schaffer et al., 2019), type 2 diabetes, and the development and proliferation of many cancers including breast, bladder, and colorectal cancer (Torres et al., 2014). This is not surprising considering that tRNA synthesis is managed by many oncogenes and tumor suppressors (Huang et al., 2018). The understanding that we have regarding the role of tRNA in cancer cells suggests that there is at least a correlation, if not a causal relationship, between tRNA malfunction and cancer cell proliferation. This review will concentrate primarily on the association between tRNA methylation, tRNA fragments, and selenoproteins and cancer development.

TRNA STRUCTURE AND FUNCTIONS

tRNA structure and modifications play a dominant role in its function. During tRNA synthesis, tRNA precursors must be transcribed within the nucleus, before being modified and exported out of the nucleus (**Figure 1**). In eukaryotes, this process begins with RNA polymerase III and transcription factors TFIIIB and TFIIIC transcribing tRNA genes into pre-tRNAs (Santos et al., 2019). Post-transcription, tRNAs are processed to form mature tRNA. During procession, RNase P removes the 5′leader of the pre-tRNA transcript, La protein binds to the U tract of the 3′ end, and Rnase Z cleaves the discriminator nucleotide (Berg and Brandl). The basic structure of most tRNA molecules includes an acceptor stem and D-arm, which work together to recognize aminoacyl tRNA synthetase; the anticodon arm, which ensures that the correct amino acid is added to the peptide chain; the T-arm, which aides in ribosome interaction; and the variable loop (Lyons et al., 2018). However, despite this general structure, the positions of the anticodon and acceptor stems may differ among tRNAs, indicating a flexibility that is necessary for tRNA interaction with many different molecules within the cell (Kuhn, 2016). Upon development of the mature tRNA, modifying enzymes may then add modifications (Santos et al., 2019). Ninety-three tRNA modifications have been identified (Berg & Brandl, 2021), with tRNAs undergoing the most modifications of any RNA species at a median of thirteen modifications per tRNA in eukaryotes (Pan, 2018). Although the primary function of most tRNA modifications is to either stabilize the tertiary structure of the tRNA or influence the codon-anticodon recognition (Lyons et al., 2018), each modification has a different effect on tRNA function. Furthermore, the role of tRNA within the cell extends beyond the translation of mRNA. tRNA has been shown to be involved in many other cell processes including cell signaling pathways and the cellular response to stress.

TRNA MODIFICATIONS IN CANCER CELLS

tRNA modifications are epigenetic and can adjust the rate of translation to meet the cell's needs (Hou et al., 2015). Post-transcriptional modifications such as hydroxylation, acetylation, and deamination (Suzuki, 2021) can contradict the tRNA's

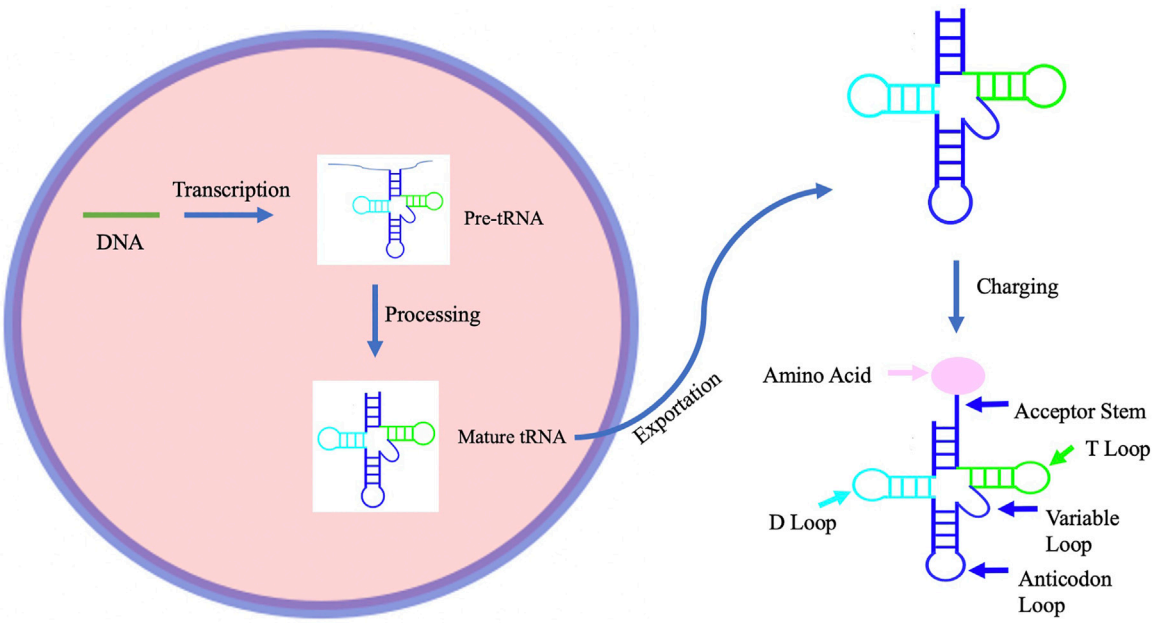


FIGURE 1 | A schematic representation of the process of tRNA biogenesis. tRNA biogenesis begins with transcription of tRNA to form pre-tRNA. This pre-tRNA is then processed to form a mature tRNA before being exported from the nucleus. The mature tRNA is then ready to be charged with an amino acid by an aminoacyltRNA synthetase.

default mode of reading codons using Watson-Crick base pairing rules through impacting the accuracy of translation, the efficiency of translation, or the abundance of certain tRNA species (Endres et al., 2019). For example, the N6-threonylcarbamoyladenosine (t^6A) tRNA modification, which is formed through addition of a Thr residue to the N^6 position of adenine aides in codon recognition, aminoacylation, and translocation, while queuosine, a hypermodified guanosine derivative, at position 34 can impact the rate of translation elongation (Suzuki, 2021). Additionally, tRNA methyltransferase ALKBH8 may impact mRNA translation through catalyzing the hydroxylation of cm^5U or mcm^5U into chm^5U or $mchm^5U$, respectively, in $tRNA^{Gly}$ (U*CC) (Fu et al., 2010). This function may be linked to cancer cell progression as ALKBH8 has been found to be upregulated in bladder cancer and increase ROS production in cancer cells (Fu et al., 2010). Some hypomodified tRNAs are degraded (Santos et al., 2019) by exonucleases and removed through a process known as rapid tRNA decay. However, some hypomodified tRNAs remain, indicating that tRNA modifications are not static and are dependent on cellular conditions (Suzuki, 2021). For example, although the transfer RNA guanine transglycosylase completely post transcriptionally modifies specific tRNAs to exchange guanine for queuine in terminally differentiated somatic cells, it incompletely modifies undifferentiated rapidly growing cells (Pathak et al., 2005).

Because of the abnormal cellular conditions in cancer cells, tRNA modifications are especially different. Due to the cancer cell's rapid proliferation rate, blood supply is often not enough to sustain the cancer cell, leading the cell to reach a state of hypoxia, or low oxygenation. This can cause oxidative stress. Oxidative stress can activate a multitude of tumor-activating signaling cascades, some of which may upregulate tRNA modifying enzymes. These modifying enzymes will catalyze tRNA modification, thus increasing translation of target tRNA molecules (Endres et al., 2019). This is supported by findings that anticodon wobble uridine tRNA modifications are upregulated in breast, bladder, and melanoma cancer cells (Hawer et al., 2018). Although the downstream effects of these modifications differed based on the cancer cell type, U34 modifications were shown to support the shift in translation in cancer cells and promote cancer cell growth (Hawer et al., 2018). Conversely, a decrease in wobble uridine modifications was demonstrated to be detrimental in hematopoiesis. In a mouse model, an inactivation of Elp3, the catalytic subunit of the elongator that modifies wobble uridine in tRNAs, led to p53 mutation-driven leukemia/lymphoma (Rosu et al., 2021). These functions of tRNA modification are further complicated by debate over whether these tRNA modifications directly impact the expression of stress-related proteins or act in stress signaling (Kirchner & Ignatova, 2014).

Dysregulation of some of these modifications can have serious consequences for protein synthesis and have been linked to certain cancers and genetic disorders (Lin et al., 2018) (**Figure 2**). For instance, hypomodification of tRNA by the transfer RNA guanine transglycosylase has been found to be associated with Dalton's Lymphoma ascites, lung cancer, ovarian cancer, and human leukemia (Pathak et al., 2005). Additionally, because of the importance of functioning protein synthesis for synapse development (Kirchner & Ignatova, 2014), neuronal cells may be particularly vulnerable to tRNA dysregulations.

Even the steps prior to tRNA modification can regulate gene expression. Aminoacyl-tRNA synthetase (Kim et al., 2012), a ligase which catalyzes the tRNA esterification to its cognate amino acid, has been shown to have other domains that are unrelated to this primary function, but can form complexes that are linked to cancers including glioblastoma (Kim et al., 2012). These interactions amongst ARSs may significantly impact the phenotype of glioblastoma, and thus influence the long-term survival of patients with glioblastoma (Kim et al., 2012). Aminoacylases such as Leucyl-tRNA synthetase and methionyl-tRNA synthetase, which charge tRNAs with leucine and methionine respectively, are associated with tumor formation or cell death (Rubio Gomez and Ibba, 2020). Additionally, misacylation by ARSs beyond the normal rate can cause changes in gene expression and may lead to cancer development, as these mistranslation errors can lead to polypeptide chains with unpredictable issues (Santos et al., 2019). These abnormal interactions of ARSs within the cell can change the prognosis of glioblastoma patients (Kim et al., 2012). These findings demonstrate the major effects of ineffective or mis-regulated tRNA modification on cell biology.

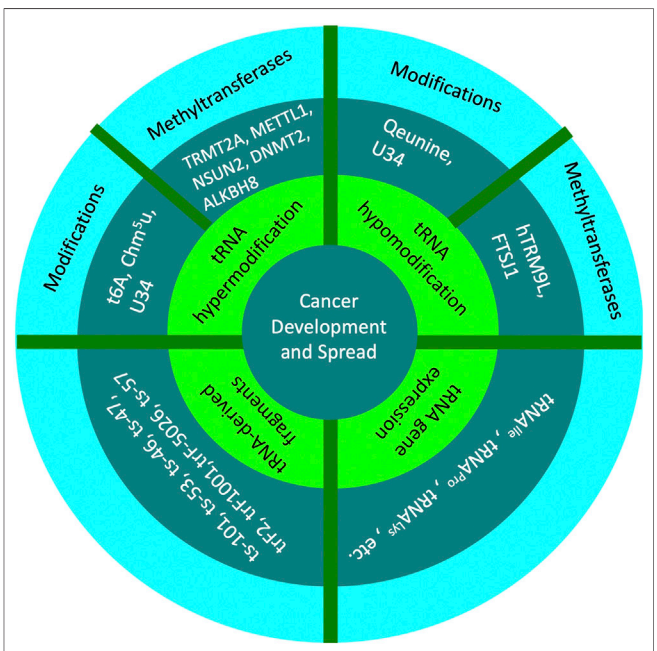


FIGURE 2 | This diagram lists examples of tRNA hypermodification, tRNA hypomodification, tRNA gene expression, and tRNA-derived fragments that can lead to cancer development and spread. For tRNA hypermodification and tRNA hypomodification, the diagram includes tRNA modifications and tRNA methyltransferases associated with cancer development and spread.

TRNA METHYLATION AND CANCER

The quantity and frequency of tRNA modifications varies, depending on factors such as chemical imbalances (Kimura et al., 2020) and cell cycle stage (Patil et al., 2012). A depletion of certain tRNA modifications can impact the rate of translation of cell cycle genes which are specifically coded by tRNAs (Lin et al., 2018). Many modifications play an active role in the cell's stress response in both healthy and diseased cells. One such modification, tRNA methylation is conducted by tRNA methyltransferases (Endres et al., 2019) and is necessary for tRNA folding, stability, and function (Lin et al., 2018). tRNA methylation is also an important modulator of cell proliferation and differentiation. Low tRNA methylation has been shown to decrease the global translation rate (Papatriantafyllou, 2012).

Although in healthy cells tRNA modifications can help prevent disease, changes in the rate of translation of cell cycle genes can disrupt cell cycle regulation and lead to tumorigenesis (**Figure 2**). In such cells, oxidative stress can activate the mitogen-activated protein kinase cascade (Li et al., 2021), which targets the human tRNA methyltransferase 9 like (*hTRM9L*) gene in order to suppress cell growth (Endres et al., 2019). The upregulation of *hTRM9L* has been shown to use different pathways to express tumor suppressive qualities in colon, lung, and ovarian cancers (Endres et al., 2019). However, a loss of the *hTRM9L* region on chromosome 8 has been found in breast, bladder, prostate, and colon cancer, and the hTMRM9L enzyme has been shown to downregulate the oncogene and cell cycle regulator, cyclin D1 (Endres et al., 2019). In lung cancer tissues, *hTRM9L* downregulation was also shown be associated with poor prognosis (Bian et al., 2021). Although *hTRM9L* has been shown to have different methods of tumor suppression of each of these cancers, it had a universal effect of reducing tumorigenesis (Da Ros et al., 2018).

The tRNA methyltransferase, FTSJ1, can mediate 2′O methylation of tRNA (He et al., 2020). It has been shown that FTSJ1 have a tumor-suppressor effect in healthy cells, but was downregulated in non-small cell lung cancers (Wang et al., 2022) (Bian et al., 2021). This downregulation of FTSJ1 resulted in fewer tRNA modifications, particularly of 2′-O-methyladenosine (Luchman et al.) modification, and an increase in tumor cell proliferation (Bian et al., 2021). In contrast, tRNA methyltransferase 1 (METTL1), which mediates the formation of N^7-methylguanine (m^7G) modification (Ying et al., 2021), has been shown to promote tumor cell proliferation and increase chemoresistance (Li et al., 2021). METTL1 levels were found to not only be higher in cancer patients, but also have an inverse relationship with survival for cancers such as bladder cancer (Li et al., 2021). Because METTL1 levels increased with increasing glioma grade, METTL1 expression levels may be able to be used to predict glioma prognosis (Li et al., 2021). METTL1 was also shown to promote hepatocarcinoma, lung cancer, and intrahepatic cholangiocarcinoma proliferation through catalyzing m^7G tRNA modification (Chen et al., 2021; Dai et al., 2021; Ma et al., 2021). Furthermore, depletion of METTL1 led to decreased m^7G tRNA modifications and the overall global translation rate, suggesting that METTL1 may be able to be used as an anti-cancer target (Orellana et al., 2021). High levels of METTL1 can also promote chemoresistance to cisplatin and docetaxel in advanced nasopharyngeal carcinoma through increasing m^7G tRNA modification and upregulating the WNT/β-catenin signaling pathway (Chen et al., 2022).

Additionally, the m^c5 tRNA methyltransferases NSUN2 and DNMT2, which also play a role in translation regulation, have been found to be overexpressed in many cancer types including oral, colon and breast cancer cells, respectively (Endres et al., 2019; Dong & Cui, 2020). The NSUN2 and METTL1 tRNA modification genes have been associated with resistance to anti-cancer therapy (Hawer et al., 2018). However, deletion of NSUN2 and METTL1 in HeLa cells increased sensitivity to the anti-cancer drug 5-fluorouracil (Suzuki, 2021). Previously mentioned, ALKBH8, can produce mcm^5 U tRNA modifications, has been shown to be upregulated in the event of DNA damage (Patil et al., 2012). Mcm^5 U levels have been shown to oscillate throughout the cell cycle and help regulate its progression (Patil et al., 2012). Mcm^5 U modifications have been shown to slow cell cycle progression in *S. cerevisiae*, and a similar result would be expected in humans in response to ALKBH8 upregulation (Patil et al., 2012). In contrast, ALKBH1, a member of the same AlkB family as ALKBH8 catalyzes the demethylation of N1 -methyladenosine (m^1A) in tRNAs in response to glucose availability (Liu et al., 2016). This decreases the use of tRNA in protein synthesis and the overall translation rate (Liu et al., 2016). The effects of ALKBH1 can differ based on cancer type. Although the upregulation of AlkBH1 was found to promote proliferation of gastric cancer cells, it was found to correlate to better survival in pancreatic cancer and lung cancer patients (Wang et al., 2022).

TRMT2A, another tRNA methyltransferase, is highly expressed in HER2+ breast cancer cells and may indicate a higher chance of relapse (Suzuki, 2021). Other tRNA modification genes such as TRIT1, TRMT12, and ELP1 are associated with lung cancer, breast cancer, and melanoma, respectively (Hawer et al., 2018). Although many modifications are upregulated in cancer cells, tRNA hypomodification is also often found in these diseased cells (Suzuki, 2021). Deficiencies of wybutosine, a nucleoside important for codon recognition and reading frame maintenance found on eukaryotic $tRNA^{Phe}$, has been detected in hepatoma, neuroblastoma, and colorectal cancer (Suzuki, 2021). This modification induces frame shifting and leads to nonsense-mediated RNA decay (Suzuki, 2021).

EFFECTS OF TRNA GENE EXPRESSION ON CANCER CELL REGULATION

Understanding tRNA gene expression may also provide insight regarding cell regulation. Close to half of the tRNA genes within the human population are constitutively silent or poorly expressed. These genes may have extra-transcriptional functions, such as acting as insulators, which can block gene expression (Torres, 2019). In another form of tRNA variation, tRNAs known as isodecoders, are associated with the same anticodon, yet differ elsewhere on the tRNA body (Czech

et al., 2010). These tRNA isodecoders vary in their efficiency of translational suppression despite having similar aminoacylation levels (Geslain & Pan, 2011), suggesting that some isodecoders may play a larger role in the regulation of gene expression (Czech et al., 2010). Evidence for the function of isodecoders in gene regulation can be seen in the differing translational efficiency rates of isodecoders despite their association with the same codon (Geslain & Pan, 2010). Specifically, Leu and Ser derived tRNA isodecoders have been shown to have varying levels of stop-codon suppression efficiencies, while all $tRNA^{Ala}$ have demonstrated low suppression activity (Geslain & Pan, 2010). Even the roles of aminoacyl tRNA synthetase extend beyond protein production. Some aminoacyl tRNA synthetases such as seryl tRNA synthetase have been shown to be associated with metabolism. In healthy cells, glucose mediates the acetylation of seryl tRNA synthetase, causing it to translocate into the nucleus and suppress *de novo* lipid biosynthesis. However, breast cancers inhibit this translocation leading to abnormal lipid biosynthesis (Zhao et al., 2021). These findings exhibit the complexity and variation within the roles of tRNA in the cell. Although the roles of silent tRNA and tRNA isodecoders are still being discovered, their ability to affect gene regulation suggests that misfunction can have detrimental effects on gene expression. tRNA gene expression most likely plays an important role in cell proliferation in both healthy and cancerous cells. Although the exact mechanism of tRNA regulation is unknown, the key role that tRNA regulation plays in cell proliferation suggests that the upregulation of tRNA can also induce the development of tumorigenesis.

As tumor cells rapidly proliferate, they require the necessary cellular components to maintain a high growth rate. Although most likely more of an effect than a cause of cancer proliferation, numerous tumor cells have been shown to have elevated levels of tRNAs (Gingold et al., 2014). For example, breast cancer cells have been shown to upregulate some tRNAs by up to ten times (Pavon-Eternod et al., 2009). Oncogenes play an important role in meeting the high level of gene transcription at the mRNA level. Through obstructing tumor suppressors ability to inhibit RNA polymerase III transcription in healthy cells, oncogenes can increase Pol III transcription, thus increasing tRNA transcription (Bian et al., 2021). Oncogenes are also able to selectively induce the expression of certain tRNAs and repress the expression of other tRNAs in order to aid in this rapid rate of cell proliferation (Santos et al., 2019). Specifically, the initiator methionine tRNA has been shown to be induced the most in proliferating cells (Pavon-Eternod et al., 2013), while the selenocysteine tRNA has been shown to be repressed in many cancerous and proliferating cells (Barroso et al., 2014) (Luchman et al., 2014) (Hudson et al., 2012). These induced tRNAs have been shown to prefer codons enriched in proliferation genes (Gingold et al., 2014). tRNA synthesis in glioblastoma has also been shown to be linked to *de novo* GTP biosynthesis caused by increased *Impdh2* expression (Kofuji et al., 2019). This upregulation of *Impdh2* has also been shown to be positively correlated with increased glioma malignancy and negatively correlated with patient survival (Kofuji et al., 2019). Similarly, high levels of $tRNA^{Ile}$, $tRNA^{Pro}$, $tRNA^{Lys}$ have been shown to be related to tumor differentiation in lung adenocarcinoma tissues and paracarcinoma tissues (Bian et al., 2021) (**Figure 2**). This tRNA upregulation may be linked not only to tumorigenesis, but may also to cancer patient prognosis, suggesting that it may be used as a marker of cancer development (Santos et al., 2019).

Conversely, the downregulation of tRNA can be used to limit cell growth and proliferation. Targeting certain tRNA genes that are necessary for mRNA translation will lead to cell cycle exit and decreased protein translation. This will decrease cell proliferation, acting as a tumor suppressant (Yang et al., 2020). One such gene is SOX4, a transcription factor that controls the expression of some tRNA genes. Although depending on the type of cancer SOX4 can act as a tumor suppressor or an oncogene, it has been shown to limit glioblastoma cell proliferation (Zhang et al., 2014). Through binding to certain tRNA genes, SOX4 can repress the expression of tRNAs and thus reduce protein synthesis (Yang et al., 2020). In fact, high SOX4 expression was found to be associated with better prognosis for glioblastoma patients (Zhang et al., 2014). Other pathways that decrease the rate of protein translation could be used to limit the spread of cancers. The drug Norcantharidin (Zhang et al., 2015) has demonstrated the capability to slow protein translation through targeting microRNA to treat cancer (Zhang et al., 2015). Norcantharidin has been used to treat certain malignant cancers and has been shown to suppress invasion by glioblastoma cells (Zhang et al., 2015). The success of Norcantharidin suggests the possibility that other drugs that reduce the rate of protein translation may be used as treatment (Zhang et al., 2015). Leucyl-tRNA synthetase, an aminoacyl tRNA synthetase that charges tRNA (Leu) with L-leucine, may also be targeted as an anticancer treatment partially due to its overexpression in cancer cells and association with the p21 protein, which may act as a tumor suppressor (Gao et al., 2015).

TRNA-DERIVED FRAGMENTS AND CANCER DEVELOPMENT

During times of stress, the cell has many measures in place to prevent long-term damage to the cell and conserve energy. Since protein translation has a high energy and resource demand, the cell takes measures to reduce protein production when resources are scarce. tRNA is often implicated in these measures due to its pivotal role in protein translation. Before protein translation, aminoacylation attaches an amino acid to a tRNA, thus charging it. However, under nutritional stress, aminoacylation levels of tRNAs within the cell can change (Raina & Ibba, 2014) and uncharged tRNAs can act as signaling molecules of cellular processes (Nunes et al., 2020). For example, uncharged tRNAs may activate the general amino acid control pathway during times of cellular stress (Zaborske et al., 2009). This pathway induces protein kinase Gcn2p to phosphorylate eukaryotic initiation factor-2 (Zaborske et al., 2009), a necessary factor for the start of translation, thus reducing its activity (Zaborske et al., 2009). Protein translation can also be rapidly inhibited through the

cleavage of the 3′CCA terminal sequence of tRNAs or the reuptake of cytoplasmic tRNAs into the nucleus during times of nutritional stress (Kirchner & Ignatova, 2014).

In mammalian cells under nutritional, biological, physicochemical, and oxidative stress conditions, tRNA's may be cut into fragments known as tRNA-derived small RNAs (tsRNAs). TsRNAs include half-tRNA molecules, called tiRNAs (Zhu et al., 2019), which are cleaved by the nuclease angiogenin (ANG), and are about 30–35 nucleotides in length (Yamasaki et al., 2009) (Ivanov et al., 2011). Certain tiRNAs have the ability to reduce protein production, induce stress granule formation, and interfere with siRNA-mediated silencing of stress-response genes in mammalian cells (Kirchner & Ignatova, 2014). Even shorter than tiRNAs molecules, are tRNA fragments (tRF) (Sobala & Hutvagner, 2013), which are between 13 and 20 nucleotides in length and are derived from the cleavage of mature or pre-tRNA by ANG (Raina & Ibba, 2014). There are five types of tRFs including tRF-1, tRF-2, tRF-3, tRF-5, and i-tRF (Zhang et al., 2020). Most tRFs are either induced in response to cellular stress of constitutively expressed (Lyons et al., 2018). Specific tRF functions include RNA silencing, translation regulation, and epigenetic regulation (Yu et al., 2020).

While tRFs make up only a fraction of the tRNA pool (Raina & Ibba, 2014), they can still have a major impact on the cell's survival and proliferation. For example, 3′U and 5′ tRFs can be found in very high levels in actively proliferating cells (Sobala & Hutvagner, 2013). Additionally, in response to stress conditions such as starvation, oxidative stress, and heat shock (Lyons et al., 2018), tRF levels tend to be upregulated. For example, sodium arsenite stress, has been shown to lead to the demethylation of tRNAs, which can make them more prone to cleavage by ANG, leading to the generation of tRFs (Yu et al., 2021). These tRFs can induce translation repression and stress-granule assembly (Sobala & Hutvagner, 2013). In certain cases, tRFs are able to inhibit protein translation by preventing peptide bond formation (Sobala, 2013) or acting as signal transducers (Czech et al., 2010). In almost all cancers, ANG expression is increased, potentially in order to increase tRF expression and, in turn, cancer proliferation (Zeng et al., 2020).

tRNA-derived fragments play a multitude of roles in both cancer development and suppression (**Figure 2**). tRFs have been shown to reduce cell progression through limiting kinase activity, impacting mRNA stability, regulating reverse transcription, and regulating apoptosis (Zhu et al., 2019). Some tRNA-derived fragments are known to be associated with certain cancers. For example, ts-101, ts-53, ts-46, and ts-47 have been found to be downregulated in lung cancer (Yu et al., 2020). Additionally, colon adenomas have been shown to downregulate ts-53 and ts-101, and chronic lymphocytic leukemia cancer cells have been shown to downregulate ts-46, ts-47, ts-49, ts-53, and ts-101 (Zeng et al., 2020). tRF-1001, which is derived from $tRNA^{Ser}$, has also been shown to promote cancer cell proliferation (Lyons et al., 2018). The upregulation of tRF-Leu-CAG in non-small cell lung cancers (NSCLCs) has also been shown to increase cell proliferation through upregulating the activity of aurora kinase A, an important kinase in mitosis (Bian et al., 2021). Mutations of tRNA fragments may also to cancer cell proliferation, such as ts-53 and ts-101 mutations found in chronic lymphocytic leukemia and lung cancer (Zeng et al., 2020).

tRFs may influence cancer progression through regulation of gene expression during cellular stress. During cellular stress, tRFs associate with RNA binding proteins that would otherwise bind oncogene transcripts and increase cell proliferation. This has been shown to hold true for the RNA binding protein Y-box binding protein (YBX1) in several cancers (Zhu et al., 2019). Specifically, in breast cancer cells, tRF-2s from $tRNA^{Glu}$, $tRNA^{Asp}$, $tRNA^{Gly}$ and $tRNA^{Tyr}$ have been shown to suppress metastasis through binding to YBX1, thus inhibiting its engagement with oncogenic mRNAs (Zeng et al., 2020). High YBX1 levels have been associated with poor prognosis of breast cancer patients and relapse following surgical resection (Shibata et al., 2018). YBX1 levels have also been directly correlated with poor prognosis for patients suffering from ovarian and prostate cancer (Shibata et al., 2018). Additionally, 5′-tRFs have been found to promote proliferation and migration of high-grade serous ovarian carcinoma cells through downregulation of HMBOX1 (Hu et al., 2022).

As another response to stress conditions, such as a change in cell pH or decrease in mitochondrial transmembrane potential, the cell may undergo apoptosis. Apoptosis is important for cell survival, as it can prevent the uncontrolled growth characteristic of cancer cells. tRNA may play a major role in this stress response process and the regulation of apoptosis. Apoptosis occurs through the release of cytochrome c from the mitochondria, which activates caspase-9 in the Apaf-1 apoptosome. Caspase-9 can then activate caspase-3, which will execute apoptosis. tRNA has been found to be able to directly inhibit apoptosis through scavenging for cytochrome c inside and outside the mitochondria (van Raam & Salvesen, 2010) and through repressing cytochrome c by binding to it (Huang et al., 2018). This suppression of cytochrome c prevents apoptosis and may lead to tumor proliferation (Mei et al., 2010). Further understanding of tRNA's anti-apoptotic function may be useful for cancer therapies (Mei et al., 2010). Such therapies may target these tRNAs in order to induce apoptosis and prevent cancer cell proliferation.

tRNA fragments may also be used as biomarkers for cancers. tRFs derived from $tRNA^{Phe(GAA)}$ and $tRNA^{Lys(CUU)}$ may act as biomarkers of progression-free disease survival in prostate tumors (Endres et al., 2019). Other tRNA fragments may be used as biomarkers for cancers, such as 5′-tiRNAs which have shown promise as potential noninvasive biomarkers for breast cancer and head and neck squamous cell carcinoma (Zeng et al., 2020). A better understanding of tRF biomarkers may help elucidate possible biomarkers. For example, tRF-5026a was shown to regulate PTEN/PI3/AKT signaling pathway and decrease gastric cancer cell proliferation, suggesting that tRF-5026 may be used as a biomarker for gastric cancer (Zhu et al., 2021).

Because of the strong association between cancer proliferation and tRFs, tRF regulation could be used to develop cancer treatment. The ability of tRF regulation to prevent cancer progression has been demonstrated in lung cancer cells, where the overexpression of tRNA signatures ts-46 and ts-47 inhibited

further growth and survival of two lung cancer cell lines (Yu et al., 2020). Additionally, tRFs have been identified as a therapeutic target in the treatment of hepatocellular carcinoma after blockage of tRF-3^{LeuCAG}, a tRNA fragment important for ribosome biogenesis, led to tumor cell apoptosis (Yu et al., 2021).

Conversely, tRFs and tiRNAs may impact cancer cell resistance to chemotherapeutics. For example, tRNA-derived fragments tDR-0009 and tDR-7336 were shown to be upregulated and increased chemoresistance of doxorubicin in triple-negative breast cancer (Zeng et al., 2020). Ts-57s and ts-46s were also found to be related to breast cancer chemoresistance to lapatinib (Zeng et al., 2020). tRNA-derived fragments may also increase chemoresistance through inhibition of the eukaryotic translation inhibiting factor 4 g (Zhu et al., 2019), which can block expression of the adenosine triphosphate-binding cassette (ABC) transporter. This transporter is important for effluxing anti-cancer drugs across cell membranes (Zhang et al., 2020). Additionally, tRFs and tiRNAs produce stress granules, which have been shown to make glioblastoma cells resistant to the anticancer drug bortezomib (Zhang et al., 2020). YBX1, as previously discussed, may also play a role in the drug resistance of breast cancer cells through promoting antiestrogen resistance, and decreasing the effectiveness of endocrine therapeutic drugs for estrogen receptor positive (ER-positive) breast cancer patients (Shibata et al., 2018). tiRNA-5s have also been shown to lead to phospho-eIF2α-independent stress granule assembly, which has been associated with chemotherapeutic resistance (Zeng et al., 2020).

SELENOPROTEIN EXPRESSION AND CANCER DEVELOPMENT

Selenium (Se) is an essential micronutrient that has been demonstrated to have many positive health benefits, including potentially preventing cancer cell differentiation (Murdolo et al., 2017). Selenoproteins (SEPs), which contain selenium, can differentially impact cancer development through antioxidant activity (Short & Williams, 2017). Selenoprotein development begins when dietary selenium in the form of selenomethionine undergoes metabolism in the liver to produce selenocysteine, which can then be degraded by selenocysteine lyase to yield selenide. These selenoproteins are formed when specialized tRNA translate the UGA site of mRNA as selenocysteine, rather than recognizing it as a termination signal (Jameson & Diamond, 2004). The tRNA is able to recognize this site due to the presence of the Sec insertion sequence (Jameson & Diamond, 2004) in the 3' untranslated region of the mRNA (Jameson & Diamond, 2004).

Although Selenoproteins are widely recognized for their antioxidant activity, they also may impact angiogenesis, growth factor signaling, and the inhibition of apoptosis, which may either support or repress tumorigenesis (Short & Williams, 2017). Selenoprotein expression may also effect DNA stability and oncogene activation (Murdolo et al., 2017).

The biological mechanism SEPs use to exert their anticancer effects is uncertain. However, SEPs such as selenoprotein P (SELP), glutathione peroxidases (Jameson & Diamond, 2004), thioredoxin reductases (TXNRD) and selenoprotein F (SEP15) have been shown to be able to regulate tumorigenesis through impacting cancer-related signaling proteins (Jia et al., 2020). The effect of stress-related (selenoproteins) SEPs on tumorigenesis differs depending on the organ and cancer type. Glutathione peroxidase 4 (GPX4) provides cell protection from oxidative stress-induced cell death (Becker et al., 2014) and may be found in high levels in cancer cells, causing resistance to chemotherapeutics (Yang et al., 2014). GPX4 has been shown to regulate ferroptosis in large B cell lymphoma cells, renal cell carcinomas (Yang et al., 2014), and head and neck cancer cell lines (Shin et al., 2018). Inhibition of transcription factor Nrf2 and silencing of p62 were found to sensitize head and neck cancer cells to GPX4 inhibitors, thus inducing ferroptosis and providing a potential treatment to overcome chemoresistance (Shin et al., 2018). Targeting GPX4 with dihydroartemisinin (Yi et al., 2020) treatment (Yi et al., 2020) was also shown to be successful in causing glioblastoma cell death through increasing cellular ROS levels and inducing ferroptosis (Yi et al., 2020). Single-nucleotide polymorphisms (SNPs) in selenoprotein genes such as SELNOP and GPX (Jia et al., 2020) may impact the efficiency of selenoprotein synthesis as well as the risk of disease. SNPs in selenoprotein S (SEPS) have been linked with lung, breast, prostate, colorectal, bladder, and thyroid cancers (Short & Williams, 2017).

Because selenoprotein expression is determined explicitly by the expression of Sec tRNA (Carlson et al., 2004), differing expression of Sec tRNA may be used to study the role of Se in cancer progression. For example, interbreeding of Sec tRNA transgenic mice with prostate cancer resulted in more high-grade lesions. However, Sec tRNA transgenic mice had no change in hepatocellular tumor number compared to wild type mice when crossed onto TGF-alpha transgenic background (Short & Williams, 2017).

Hypoxic conditions can reduce selenoprotein synthesis at the posttranscriptional level, through decreased Sec tRNA levels (Becker et al., 2014). The two isoforms of Sec tRNA are encoded on *Trsp* (Carlson et al., 2018), a single copy gene found in eukaryotes (Serrão et al., 2018). Deletion of the *Trsp* gene completely eliminates selenoprotein expression (Carlson et al., 2018) and was shown to increase oxidative stress and increase reactive oxygen species (ROS) accumulation in macrophages or the liver of mice with cancer (Serrão et al., 2018), while excision of *Trsp* in mammary glands led to increased mammary tumors and decreased survival (Serrão et al., 2018). Additionally, sec-tRNA^{sec} gene mutation or deletions have also been linked to cancers such breast, colon, and prostate cancer (Serrão et al., 2018).

DISCUSSION

tRNA structure, modification, upregulation, and downregulation not only change depending on cell type, but can also change in response to cell conditions and can impact cell proliferation. How and to what extent tRNAs are modified or cleaved can determine cell survival. The many functions of

tRNA and its derivatives contribute to the complex role tRNAs play within healthy cells, which only becomes further complicated in tumor cells. The unique roles tRNA derivatives play in different cancers (Huang et al., 2018) combined with tRNAs' secondary structure and chemical modifications, make tRNAs challenging to study (Schaffer et al., 2019). Because tRNA derivatives are often specific to certain cancers, they may be used as targets for chemotherapeutics or as biomarkers of disease. A more thorough understanding of how these aspects of tRNA impact tumor cell suppression, tumor cell activation, and treatment resistance can provide valuable information that is useful for the development of potential therapies for individuals diagnosed with cancer. However, barriers such as drug resistance and tumor heterogeneity continue to challenge the development of cancer treatments (Hu et al., 2022).

AUTHOR CONTRIBUTIONS

TG drafted the manuscript. MM and SH revised the article for content and approved the final version.

FUNDING

This work was supported in part by US NIH grants R01CA201327, and by Paul M. Corman, MD Chair in Cancer Research endowment fund.

REFERENCES

Barroso, M., Florindo, C., Kalwa, H., Silva, Z., Turanov, A. A., Carlson, B. A., et al. (2014). Inhibition of Cellular Methyltransferases Promotes Endothelial Cell Activation by Suppressing Glutathione Peroxidase 1 Protein Expression. *J. Biol. Chem.* 289 (22), 15350–15362. doi:10.1074/jbc.M114.549782

Becker, N.-P., Martitz, J., Renko, K., Stoedter, M., Hybsier, S., Cramer, T., et al. (2014). Hypoxia Reduces and Redirects Selenoprotein Biosynthesis. *Metallomics* 6 (5), 1079–1086. doi:10.1039/c4mt00004h

Berg, M. D., and Brandl, C. J. (2021). Transfer RNAs: Diversity in Form and Function. *RNA Biol.* 18 (3), 316–339. doi:10.1080/15476286.2020.1809197

Bian, M., Huang, S., Yu, D., and Zhou, Z. (2021). tRNA Metabolism and Lung Cancer: Beyond Translation. *Front. Mol. Biosci.* 8, 659388. doi:10.3389/fmolb.2021.659388

Carlson, B. A., Lee, B. J., Tsuji, P. A., Copeland, P. R., Schweizer, U., Gladyshev, V. N., et al. (2018). Selenocysteine tRNA[Ser]Sec, the Central Component of Selenoprotein Biosynthesis: Isolation, Identification, Modification, and Sequencing. *Methods Mol. Biol.* 1661, 43–60. doi:10.1007/978-1-4939-7258-6_4

Carlson, B. A., Novoselov, S. V., Kumaraswamy, E., Lee, B. J., Anver, M. R., Gladyshev, V. N., et al. (2004). Specific Excision of the Selenocysteine tRNA [Ser]Sec (Trsp) Gene in Mouse Liver Demonstrates an Essential Role of Selenoproteins in Liver Function. *J. Biol. Chem.* 279 (9), 8011–8017. doi:10.1074/jbc.M310470200

Chen, B., Jiang, W., Huang, Y., Zhang, J., Yu, P., Wu, L., et al. (2022). N7-methylguanosine tRNA Modification Promotes Tumorigenesis and Chemoresistance through WNT/β-catenin Pathway in Nasopharyngeal Carcinoma. *Oncogene* 41, 2239–2253. doi:10.1038/s41388-022-02250-9

Chen, Z., Zhu, W., Zhu, S., Sun, K., Liao, J., Liu, H., et al. (2021). METTL1 Promotes Hepatocarcinogenesis via M 7 G tRNA Modification-dependent Translation Control. *Clin. Transl. Med* 11 (12), e661. doi:10.1002/ctm2.661

Czech, A., Fedyunin, I., Zhang, G., and Ignatova, Z. (2010). Silent Mutations in Sight: Co-variations in tRNA Abundance as a Key to Unravel Consequences of Silent Mutations. *Mol. Biosyst.* 6 (10), 1767. doi:10.1039/c004796c

Da Ros, M., De Gregorio, V., Iorio, A., Giunti, L., Guidi, M., de Martino, M., et al. (2018). Glioblastoma Chemoresistance: The Double Play by Microenvironment and Blood-Brain Barrier. *Ijms* 19 (10), 2879. doi:10.3390/ijms19102879

Dai, Z., Liu, H., Liao, J., Huang, C., Ren, X., Zhu, W., et al. (2021). N7-Methylguanosine tRNA Modification Enhances Oncogenic mRNA Translation and Promotes Intrahepatic Cholangiocarcinoma Progression. *Mol. Cell* 81 (16), 3339–3355. e3338. doi:10.1016/j.molcel.2021.07.003

Dolfi, S. C., Chan, L. L.-Y., Qiu, J., Tedeschi, P. M., Bertino, J. R., Hirshfield, K. M., et al. (2013). The Metabolic Demands of Cancer Cells Are Coupled to Their Size and Protein Synthesis Rates. *Cancer Metab.* 1 (1), 20. doi:10.1186/2049-3002-1-20

Dong, Z., and Cui, H. (2020). The Emerging Roles of RNA Modifications in Glioblastoma. *Cancers* 12 (3), 736. doi:10.3390/cancers12030736

Endres, L., Fasullo, M., and Rose, R. (2019). tRNA Modification and Cancer: Potential for Therapeutic Prevention and Intervention. *Future Med. Chem.* 11 (8), 885–900. doi:10.4155/fmc-2018-0404

Fu, Y., Dai, Q., Zhang, W., Ren, J., Pan, T., and He, C. (2010). The AlkB Domain of Mammalian ABH8 Catalyzes Hydroxylation of 5-methoxycarbonylmethyluridine at the Wobble Position of tRNA. *Angew. Chem. Int. Ed.* 49 (47), 8885–8888. doi:10.1002/anie.201001242

Geslain, R., and Pan, T. (2010). Functional Analysis of Human tRNA Isodecoders. *J. Mol. Biol.* 396 (3), 821–831. doi:10.1016/j.jmb.2009.12.018

Geslain, R., and Pan, T. (2011). tRNA: Vast Reservoir of RNA Molecules with Unexpected Regulatory Function. *Proc. Natl. Acad. Sci. U.S.A.* 108 (40), 16489–16490. doi:10.1073/pnas.1113715108

Gingold, H., Tehler, D., Christoffersen, N. R., Nielsen, M. M., Asmar, F., Kooistra, S. M., et al. (2014). A Dual Program for Translation Regulation in Cellular Proliferation and Differentiation. *Cell* 158 (6), 1281–1292. doi:10.1016/j.cell.2014.08.011

Hawer, H., Hammermeister, A., Ravichandran, K., Glatt, S., Schaffrath, R., and Klassen, R. (2018). Roles of Elongator Dependent tRNA Modification Pathways in Neurodegeneration and Cancer. *Genes* 10 (1), 19. doi:10.3390/genes10010019

He, Q., Yang, L., Gao, K., Ding, P., Chen, Q., Xiong, J., et al. (2020). FTSJ1 Regulates tRNA 2′-O-Methyladenosine Modification and Suppresses the Malignancy of NSCLC via Inhibiting DRAM1 Expression. *Cell Death Dis.* 11 (5), 348. doi:10.1038/s41419-020-2525-x

Hou, Y.-M., Gamper, H., and Yang, W. (2015). Post-transcriptional Modifications to tRNA-A Response to the Genetic Code Degeneracy. *Rna* 21 (4), 642–644. doi:10.1261/rna.049825.115

Hu, Y., Cai, A., Xu, J., Feng, W., Wu, A., Liu, R., et al. (2022). An Emerging Role of the 5′ Termini of Mature tRNAs in Human Diseases: Current Situation and Prospects. *Biochimica Biophysica Acta (BBA) - Mol. Basis Dis.* 1868 (2), 166314. doi:10.1016/j.bbadis.2021.166314

Huang, S.-Q., Sun, B., Xiong, Z.-P., Shu, Y., Zhou, H.-H., Zhang, W., et al. (2018). The Dysregulation of tRNAs and tRNA Derivatives in Cancer. *J. Exp. Clin. Cancer Res.* 37 (1), 101. doi:10.1186/s13046-018-0745-z

Hudson, T. S., Carlson, B. A., Hoeneroff, M. J., Young, H. A., Sordillo, L., Muller, W. J., et al. (2012). Selenoproteins Reduce Susceptibility to DMBA-Induced Mammary Carcinogenesis. *Carcinogenesis* 33 (6), 1225–1230. doi:10.1093/carcin/bgs129

Ivanov, P., Villen, J., Gygi, S. P., Anderson, P., and Anderson, P. (2011). Angiogenin-induced tRNA Fragments Inhibit Translation Initiation. *Mol. Cell* 43 (4), 613–623. doi:10.1016/j.molcel.2011.06.022

Jameson, R. R., and Diamond, A. M. (2004). A Regulatory Role for Sec tRNA[Ser]Sec in Selenoprotein Synthesis. *RNA* 10 (7), 1142–1152. doi:10.1261/rna.7370104

Jia, Y., Dai, J., and Zeng, Z. (2020). Potential Relationship between the Selenoproteome and Cancer. *Mol. Clin. Oncol.* 13 (6), 1. doi:10.3892/mco.2020.2153

Kim, Y.-W., Kwon, C., Liu, J.-L., Kim, S. H., and Kim, S. (2012). Cancer Association Study of Aminoacyl-tRNA Synthetase Signaling Network in Glioblastoma. *PloS one* 7 (8), e40960. doi:10.1371/journal.pone.0040960

Kimura, S., Srisuknimit, V., and Waldor, M. K. (2020). Probing the Diversity and Regulation of tRNA Modifications. *Curr. Opin. Microbiol.* 57, 41–48. doi:10.1016/j.mib.2020.06.005

Kirchner, S., and Ignatova, Z. (2014). Emerging Roles of tRNA in Adaptive Translation, Signalling Dynamics and Disease. *Nat. Rev. Genet.* 16 (2), 98–112. doi:10.1038/nrg3861

Kofuji, S., Hirayama, A., Eberhardt, A. O., Kawaguchi, R., Sugiura, Y., Sampetrean, O., et al. (2019). IMP Dehydrogenase-2 Drives Aberrant Nucleolar Activity and Promotes Tumorigenesis in Glioblastoma. *Nat. Cell Biol.* 21 (8), 1003–1014. doi:10.1038/s41556-019-0363-9

Kuhn, C.-D. (2016). RNA Versatility Governs tRNA Function. *BioEssays* 38 (5), 465–473. doi:10.1002/bies.201500190

Li, D., Gao, G., Yao, Y., Li, K., Mashausi, D., Li, D., et al. (2015). A Human Leucyl-tRNA Synthetase as an Anticancer Target. *Ott* 8, 2933–2942. doi:10.2147/OTT.S88873

Li, L., Yang, Y., Wang, Z., Xu, C., Huang, J., and Li, G. (2021). Prognostic Role of METTL1 in Glioma. *Cancer Cell Int.* 21 (1), 633. doi:10.1186/s12935-021-02346-4

Lin, S., Liu, Q., Lelyveld, V. S., Choe, J., Szostak, J. W., and Gregory, R. I. (2018). Mettl1/Wdr4-Mediated m7G tRNA Methylome Is Required for Normal mRNA Translation and Embryonic Stem Cell Self-Renewal and Differentiation. *Mol. Cell* 71 (2), 244–255. e245. doi:10.1016/j.molcel.2018.06.001

Liu, F., Clark, W., Luo, G., Wang, X., Fu, Y., Wei, J., et al. (2016). ALKBH1-Mediated tRNA Demethylation Regulates Translation. *Cell* 167 (7), 1897. doi:10.1016/j.cell.2016.11.045

Luchman, H. A., Villemaire, M. L., Bismar, T. A., Carlson, B. A., and Jirik, F. R. (2014). Prostate Epithelium-specific Deletion of the Selenocysteine tRNA Gene Trsp Leads to Early Onset Intraepithelial Neoplasia. *Am. J. Pathology* 184 (3), 871–877. doi:10.1016/j.ajpath.2013.11.025

Lyons, S. M., Fay, M. M., and Ivanov, P. (2018). The Role of RNA Modifications in the Regulation of tRNA Cleavage. *FEBS Lett.* 592 (17), 2828–2844. doi:10.1002/1873-3468.13205

Ma, J., Han, H., Huang, Y., Yang, C., Zheng, S., Cai, T., et al. (2021). METTL1/WDR4-mediated m7G tRNA Modifications and m7G Codon Usage Promote mRNA Translation and Lung Cancer Progression. *Mol. Ther.* 29 (12), 3422–3435. doi:10.1016/j.ymthe.2021.08.005

Mei, Y., Stonestrom, A., Hou, Y.-M., and Yang, X. (2010). Apoptotic Regulation and tRNA. *Protein Cell* 1 (9), 795–801. doi:10.1007/s13238-010-0107-x

Murdolo, G., Bartolini, D., Tortoioli, C., Piroddi, M., Torquato, P., and Galli, F. (2017). "Selenium and Cancer Stem Cells," in *Selenium and Selenoproteins in Cancer*. Editor D. T. a. F. G. Kenneth (Academic Press), 136, 235–257. doi:10.1016/bs.acr.2017.07.006

Nunes, A., Ribeiro, D. R., Marques, M., Santos, M. A. S., Ribeiro, D., and Soares, A. R. (2020). Emerging Roles of tRNAs in RNA Virus Infections. *Trends Biochem. Sci.* 45 (9), 794–805. doi:10.1016/j.tibs.2020.05.007

Orellana, E. A., Liu, Q., Yankova, E., Pirouz, M., De Braekeleer, E., Zhang, W., et al. (2021). METTL1-mediated m7G Modification of Arg-TCT tRNA Drives Oncogenic Transformation. *Mol. Cell* 81 (16), 3323–3338. doi:10.1016/j.molcel.2021.06.031

Pan, T. (2018). Modifications and Functional Genomics of Human Transfer RNA. *Cell Res.* 28 (4), 395–404. doi:10.1038/s41422-018-0013-y

Papatriantafyllou, M. (2012). tRNA Methylation Controls Translation Rate. *Nat. Rev. Mol. Cell Biol.* 13 (9), 540. doi:10.1038/nrm3424

Pathak, C., Jaiswal, Y. K., and Vinayak, M. (2005). Hypomodification of Transfer RNA in Cancer with Respect to Queuosine. *RNA Biol.* 2 (4), 143–148. doi:10.4161/rna.2.4.2417

Patil, A., Dyavaiah, M., Joseph, F., Rooney, J. P., Chan, C. T. Y., Dedon, P. C., et al. (2012). Increased tRNA Modification and Gene-specific Codon Usage Regulate Cell Cycle Progression during the DNA Damage Response. *Cell Cycle* 11 (19), 3656–3665. doi:10.4161/cc.21919

Pavon-Eternod, M., Gomes, S., Geslain, R., Dai, Q., Rosner, M. R., and Pan, T. (2009). tRNA Over-expression in Breast Cancer and Functional Consequences. *Nucleic Acids Res.* 37 (21), 7268–7280. doi:10.1093/nar/gkp787

Pavon-Eternod, M., Gomes, S., Rosner, M. R., and Pan, T. (2013). Overexpression of Initiator Methionine tRNA Leads to Global Reprogramming of tRNA Expression and Increased Proliferation in Human Epithelial Cells. *RNA* 19 (4), 461–466. doi:10.1261/rna.037507.112

Raina, M., and Ibba, M. (2014). tRNAs as Regulators of Biological Processes. *Front. Genet.* 5, 171. doi:10.3389/fgene.2014.00171

Rosu, A., El Hachem, N., Rapino, F., Rouault-Pierre, K., Jorssen, J., Somja, J., et al. (2021). Loss of tRNA-Modifying Enzyme Elp3 Activates a P53-dependent Antitumor Checkpoint in Hematopoiesis. *J. Exp. Med.* 218 (3). doi:10.1084/jem.20200662

Rubio Gomez, M. A., and Ibba, M. (2020). Aminoacyl-tRNA Synthetases. *RNA* 26 (8), 910–936. doi:10.1261/rna.071720.119

Santos, M., Fidalgo, A., Varanda, A. S., Oliveira, C., and Santos, M. A. S. (2019). tRNA Deregulation and its Consequences in Cancer. *Trends Mol. Med.* 25 (10), 853–865. doi:10.1016/j.molmed.2019.05.011

Schaffer, A. E., Pinkard, O., and Coller, J. M. (2019). tRNA Metabolism and Neurodevelopmental Disorders. *Annu. Rev. Genom. Hum. Genet.* 20, 359–387. doi:10.1146/annurev-genom-083118-015334

Serrão, V. H. B., Silva, I. R., da Silva, M. T. A., Scortecci, J. F., de Freitas Fernandes, A., and Thiemann, O. H. (2018). The Unique tRNASec and its Role in Selenocysteine Biosynthesis. *Amino Acids* 50 (9), 1145–1167. doi:10.1007/s00726-018-2595-6

Shibata, T., Tokunaga, E., Hattori, S., Watari, K., Murakami, Y., Yamashita, N., et al. (2018). Y-box Binding Protein YBX1 and its Correlated Genes as Biomarkers for Poor Outcomes in Patients with Breast Cancer. *Oncotarget* 9 (98), 37216–37228. doi:10.18632/oncotarget.26469

Shin, D., Kim, E. H., Lee, J., and Roh, J.-L. (2018). Nrf2 Inhibition Reverses Resistance to GPX4 Inhibitor-Induced Ferroptosis in Head and Neck Cancer. *Free Radic. Biol. Med.* 129, 454–462. doi:10.1016/j.freeradbiomed.2018.10.426

Short, S. P., and Williams, C. S. (2017). Selenoproteins in Tumorigenesis and Cancer Progression. *Adv. Cancer Res.* 136, 49–83. doi:10.1016/bs.acr.2017.08.002

Sobala, A., and Hutvagner, G. (2013). Small RNAs Derived from the 5′ End of tRNA Can Inhibit Protein Translation in Human Cells. *RNA Biol.* 10 (4), 553–563. doi:10.4161/rna.24285

Sobala, A. (2013). Small RNAs Derived from the 5′ End of tRNA Can Inhibit Protein Translation in Human Cells. *RNA Biol.* 10, 553–563. doi:10.4161/rna.24285

Suzuki, T. (2021). The Expanding World of tRNA Modifications and Their Disease Relevance. *Nat. Rev. Mol. Cell Biol.* 22 (6), 375–392. doi:10.1038/s41580-021-00342-0

Torres, A. G., Batlle, E., and Ribas de Pouplana, L. (2014). Role of tRNA Modifications in Human Diseases. *Trends Mol. Med.* 20 (6), 306–314. doi:10.1016/j.molmed.2014.01.008

Torres, A. G. (2019). Enjoy the Silence: Nearly Half of Human tRNA Genes Are Silent. *Bioinform Biol. Insights* 13, 117793221986845–1177932219868454. doi:10.1177/1177932219868454

van Raam, B. J., and Salvesen, G. S. (2010). Transferring Death: A Role for tRNA in Apoptosis Regulation. *Mol. Cell* 37 (5), 591–592. doi:10.1016/j.molcel.2010.02.001

Wang, L., Feng, X., Jiao, Z., Gan, J., and Meng, Q. (2022). Characterization of the Prognostic and Diagnostic Values of ALKBH Family Members in Non-small Cell Lung Cancer. *Pathology - Res. Pract.* 231, 153809. doi:10.1016/j.prp.2022.153809

Yamasaki, S., Ivanov, P., Hu, G.-f., and Anderson, P. (2009). Angiogenin Cleaves tRNA and Promotes Stress-Induced Translational Repression. *J. Cell Biol.* 185 (1), 35–42. doi:10.1083/jcb.200811106

Yang, J., Smith, D. K., Ni, H., Wu, K., Huang, D., Pan, S., et al. (2020). SOX4-mediated Repression of Specific tRNAs Inhibits Proliferation of Human Glioblastoma Cells. *Proc. Natl. Acad. Sci. U.S.A.* 117 (11), 5782–5790. doi:10.1073/pnas.1920200117

Yang, W. S., SriRamaratnam, R., Welsch, M. E., Shimada, K., Skouta, R., Viswanathan, V. S., et al. (2014). Regulation of Ferroptotic Cancer Cell Death by GPX4. *Cell* 156 (1-2), 317–331. doi:10.1016/j.cell.2013.12.010

Yi, R., Wang, H., Deng, C., Wang, X., Yao, L., Niu, W., et al. (2020). Dihydroartemisinin Initiates Ferroptosis in Glioblastoma through GPX4 Inhibition. *Biosci. Rep.* 40 (6). doi:10.1042/BSR20193314

Ying, X., Liu, B., Yuan, Z., Huang, Y., Chen, C., Jiang, X., et al. (2021). METTL1-m 7 G-EGFR/EFEMP1 axis Promotes the Bladder Cancer Development. *Clin. Transl. Med* 11 (12), e675. doi:10.1002/ctm2.675

Yu, M., Lu, B., Zhang, J., Ding, J., Liu, P., and Lu, Y. (2020). tRNA-Derived RNA Fragments in Cancer: Current Status and Future Perspectives. *J. Hematol. Oncol.* 13 (1), 121. doi:10.1186/s13045-020-00955-6

Yu, X., Xie, Y., Zhang, S., Song, X., Xiao, B., and Yan, Z. (2021). tRNA-Derived Fragments: Mechanisms Underlying Their Regulation of Gene Expression and Potential Applications as Therapeutic Targets in Cancers and Virus Infections. *Theranostics* 11 (1), 461–469. doi:10.7150/thno.51963

Zaborske, J. M., Narasimhan, J., Jiang, L., Wek, S. A., Dittmar, K. A., Freimoser, F., et al. (2009). Genome-wide Analysis of tRNA Charging and Activation of the eIF2 Kinase Gcn2p. *J. Biol. Chem.* 284 (37), 25254–25267. doi:10.1074/jbc.M109.000877

Zeng, T., Hua, Y., Sun, C., Zhang, Y., Yang, F., Yang, M., et al. (2020). Relationship between tRNA -derived Fragments and Human Cancers. *Int. J. Cancer* 147 (11), 3007–3018. doi:10.1002/ijc.33107

Zhang, J., Jiang, H., Shao, J., Mao, R., Liu, J., Ma, Y., et al. (2014). SOX4 Inhibits GBM Cell Growth and Induces G0/G1 Cell Cycle Arrest through Akt-P53 axis. *BMC Neurol.* 14, 207. doi:10.1186/s12883-014-0207-y

Zhang, Y., Qian, H., He, J., and Gao, W. (2020). Mechanisms of tRNA-derived Fragments and tRNA Halves in Cancer Treatment Resistance. *Biomark. Res.* 8, 52. doi:10.1186/s40364-020-00233-0

Zhang, Z., Song, X., Feng, X., Miao, Y., Wang, H., Li, Y., et al. (2015). Norcantharidin Modulates miR-655-Regulated SENP6 Protein Translation to Suppresses Invasion of Glioblastoma Cells. *Tumor Biol.* 37, 15635–15641. doi:10.1007/s13277-015-4447-2

Zhao, H., and Li, Y. (2021). Cancer Metabolism and Intervention Therapy. *Mol. Biomed.* 2 (1), 5. doi:10.1186/s43556-020-00012-1

Zhao, J., Bai, H., Li, X., Yan, J., Zou, G., Wang, L., et al. (2021). Glucose-sensitive Acetylation of Seryl tRNA Synthetase Regulates Lipid Synthesis in Breast Cancer. *Sig Transduct. Target Ther.* 6 (1), 303. doi:10.1038/s41392-021-00714-0

Zhu, L., Ge, J., Li, T., Shen, Y., and Guo, J. (2019). tRNA-derived Fragments and tRNA Halves: The New Players in Cancers. *Cancer Lett.* 452, 31–37. doi:10.1016/j.canlet.2019.03.012

Zhu, L., Li, Z., Yu, X., Ruan, Y., Shen, Y., Shao, Y., et al. (2021). The tRNA-Derived Fragment 5026a Inhibits the Proliferation of Gastric Cancer Cells by Regulating the PTEN/PI3K/AKT Signaling Pathway. *Stem Cell Res. Ther.* 12 (1), 418. doi:10.1186/s13287-021-02497-1

Conflict of Interest: The authors declare that the research was conducted in the absence of any commercial or financial relationships that could be construed as a potential conflict of interest.

Publisher's Note: All claims expressed in this article are solely those of the authors and do not necessarily represent those of their affiliated organizations, or those of the publisher, the editors and the reviewers. Any product that may be evaluated in this article, or claim that may be made by its manufacturer, is not guaranteed or endorsed by the publisher.

Copyright © 2022 Gupta, Malkin and Huang. This is an open-access article distributed under the terms of the Creative Commons Attribution License (CC BY). The use, distribution or reproduction in other forums is permitted, provided the original author(s) and the copyright owner(s) are credited and that the original publication in this journal is cited, in accordance with accepted academic practice. No use, distribution or reproduction is permitted which does not comply with these terms.

frontiers | Frontiers in Cell and Developmental Biology

REVIEW
published: 01 June 2022
doi: 10.3389/fcell.2022.885133

The Key Role of RNA Modification in Breast Cancer

*Yang Liu, Tong Zhu, Yi Jiang, Jiawen Bu, Xudong Zhu and Xi Gu**

Department of Oncology, Shengjing Hospital of China Medical University, Shenyang, China

The modulation of the function and expression of epigenetic regulators of RNA modification has gradually become the hotspot of cancer research. Studies have shown that alteration of epigenetic modifications can promote the development and metastasis of breast cancer. This review highlights the progress in characterization of the link between RNA modification and the prognosis, carcinogenesis and treatment of breast cancer, which may provide a new theoretical basis for development of effective strategies for monitoring of breast cancer based on epigenetics.

Keywords: RNA modification, breast cancer, m^6A, carcinogenesis, treatment

OPEN ACCESS

Edited by:
Hengyou Weng, Guangzhou Regenerative Medicine and Health Guangdong Laboratory, China

Reviewed by:
Shuibin Lin, Sun Yat-sen University, China
Danny Misiak, Martin Luther University of Halle-Wittenberg, Germany

****Correspondence:***
Xi Gu
jadegx@163.com

Specialty section:
This article was submitted to Epigenomics and Epigenetics, a section of the journal Frontiers in Cell and Developmental Biology

Received: *27 February 2022*
Accepted: *25 April 2022*
Published: *01 June 2022*

Citation:
Liu Y, Zhu T, Jiang Y, Bu J, Zhu X and Gu X (2022) The Key Role of RNA Modification in Breast Cancer. Front. Cell Dev. Biol. 10:885133. doi: 10.3389/fcell.2022.885133

INTRODUCTION

Breast cancer is the most common female cancer in the world (Harbeck et al., 2019). Current treatments for breast cancer include surgery, chemotherapy, radiotherapy, hormone therapy and targeted therapy (Bray et al., 2018). However, comprehensive treatment strategies for breast cancer are still limited. Therefore, eradication of breast cancer remains a significant challenge, and there is an urgent need for new treatment strategies (Pedrosa et al., 2018). All biological macromolecules require post-synthesis and covalent modifications (Maresca and Wismayer, 2016). Over 100 different kinds of post-synthetic modifications have been identified to exist in RNA, and the four kinds of RNA bases and ribose can be targets for modification (He et al., 2019). Studies have shown that RNA can exert functional effects on the expression of gene in addition to acting as an effector of protein synthesis. Therefore, the importance of RNA modification has received increased attention, and studies have shown that dysregulation of RNA modification may be associated with human diseases, including breast cancer (Huang et al., 2020; Boccaletto et al., 2022). Herein, we review the progress of research focused on RNA modification and regulators of RNA modification in breast cancer.

RIBONUCLEIC ACID MODIFICATION REGULATORY PROTEINS IN BREAST CANCER

Eight different internal RNA modifications associated with a variety of cancers have been characterized: methylation of adenosine on position 6 on RNA to generate N 6-methyladenosine (m^6A); methylation of cytidine on position 5 to produce RNA with 5-methylcytosine (m^5C); methylation at position 1 of adenosine on tRNA to formN-1-methyladenosine (m^1A); 7-methylguanosine (m^7G); pseudouridylation of RNA to produce pseudouridine; editing of RNA adenosine to inosine; U34 modification of tRNA; N4-acetylcytidine (ac^4C) (Rong et al., 2021). Modification of RNA is a dynamic process that includes insertions, deletions, and recognition *via* specific cellular components called "writers," "erasers" and "readers" respectively.

N6-Methyladenosine Methyltransferases

Dynamic and reversible RNA modification plays a key role in maintaining RNA balance, and can affect splicing, translation, degradation, and localization of RNA, resulting in the regulation of various biological functions in human disease (Li and Mason, 2014). Ribosomal RNA (rRNA) and transport RNA (tRNA) are the two most abundant RNAs. Post-transcriptional modifications are very common on rRNA and tRNA (Frye et al., 2018). Continuous development of technology to detect RNA modifications has allowed for identification of post-transcriptional modifications of messenger RNA (mRNA) and non-coding RNA (ncRNA) (Zhao et al., 2017). N6-methyladenosine (m^6A) is the most common mRNA modification in mammals. In addition, m^6A was shown to play an important role in stem cell self-renewal, metabolism and metastasis in multiple cancers (Dong et al., 2021; Wood et al., 2021). The methyltransferase complex (MTC), also known as the m^6A "writer," catalyzes m^6A modification of adenylate on mRNA, and includes methyltransferase-like 3 (METTL3), methyltransferase-like 14 (METTL14), Wilms tumor 1 associated protein (WTAP), RNA binding motif protein 15/15B (RBM15/15B), Cbl proto-oncogene like 1 (CBLL1), zinc finger CCCH type containing 13 (ZC3H13), KIAA1429, CCHC-type zinc finger protein (ZCCHC4) and methyltransferase-like 16 (METTL16). METTL3 is a major catalytic enzyme in the N6-adenine methyltransferase system. The expression level of METTL3 is not consistent in each subtype of breast cancer (Yang et al., 2020). It was reported to play a tumor-suppressive role in triple-negative breast cancer (TNBC) while play an oncogenic role in other subtypes (Shi et al., 2020; He et al., 2021; Ruan et al., 2021). METTL14 stabilizes METTL3 and recognizes target RNA, which is found to be an oncogene or a tumor suppressor gene in breast cancer (Gong et al., 2020; Sun et al., 2020). WTAP is the main regulatory component of the m^6A methylation complex, and has mutual effects with METTL3 and METTL14 to aid in nuclear localization. The expression of WTAP varied in different in breast cancer studies (Wu et al., 2019; Wang et al., 2022). RBM15/RBM15B interacts with spliceosome components to participate in the modulation of m^6A modification in a WTAP-dependent manner. RBM15 was identified to be significantly high in TNBC (Yang et al., 2020). ZC3H13 is critical for anchoring regulatory complex in the nucleus. It was recognized as a tumorsupressor which positively related with tumor infiltrating lymphocytes (TILs) in the breast cancer (Gong et al., 2020). KIAA1429 is essential in the methylation process as a candidate new subunit in the methylase complex. High expression of KIAA1429 was associated with a poor prognosis in breast cancer (Zhang et al., 2022). CBLL1, as a co-regulator of m^6A methylation, was proved to promote the apoptosis in breast cancer (Zheng F. et al., 2021). ZCCHC4, a novel methyltransferase in the mediating of ribosome methylation, has a high expression in the breast lesion compared with pancancerous tissue (Pinto et al., 2020). METTL16 targets ncRNAs, lncRNAs and pre-mRNAs which is critical in splicing regulation (Su et al., 2022).

N6-Methyladenosine Demethylases

The demethylases ALKB homolog 5 (ALKBH5) and fat mass and obesity-related protein (FTO), also known as "m^6A erasers," remove m^6A using ferrous iron as a cofactor and α-ketoglutarate as a co-substrate (Jia et al., 2011; Zheng et al., 2013). ALKBH5 was higher in breast cancer tissue than in adjacent normal tissue of TNBC (Wang S. et al., 2020). FTO can oxidize m^6A to N6-hydroxymethylsalicylic acid and N6-formyl adenosine, which can be hydrolyzed to adenine (Fu et al., 2013). The expression of FTO varied in different breast cancer studies. Most of studies show that down-regulation of FTO enhanced the phenotype of invasiveness, migration and EMT in breast cancer (Jeschke et al., 2021). But in other cases, FTO played an oncogenic role with a high expression in breast cancer (Niu et al., 2019).

N6-Methyladenosine Readers

The "readers" mainly include the YTH domain family (YTHDF) and heterogeneous nuclear ribonucleoproteins (hnRNPs) family, Insulin-like growth factor 2 mRNA-binding proteins (IGF2BPs) and YTH domain-containing protein (YTHDC) increase the translation levels of modified RNAs which recognize m^6A, bind RNA and participate in regulatory functions (Huang et al., 2018; Xing et al., 2019; Dai X.-Y. et al., 2021). The YTHDF family includes three paralogs YTHDF1, YTHDF2 and YTHDF3, which can also be referred to as DF1, DF2, and DF3. DF1 promotes mRNA translation, DF2 promotes mRNA degradation, and DF3 promotes translation and degradation (Zaccara and Jaffrey, 2020). YTHDF1 and YTHDF3 were also found to overexpress in breast cancer (Chen et al., 2022; Lin et al., 2022). IGF2BP 2/3 and YTHDC2 were highly expressed in basal-like breast cancer (Yang et al., 2020). The overexpression of hnRNPc were related to poor prognosis in patients (Lv et al., 2021a), but hnRNPc A2/B1 was reported to negatively regulate the metastasis of breast cancer (Liu Y. et al., 2020). Although various readers, writers, and erasers may be independently associated with numerous changes in signaling pathways of cancer, there is evidence that writers, erasers and readers may have interplay with each other in cancer. Regulators in the same functional category show significant genetic changes and highly correlated expression patterns in cancer (Li et al., 2019). In addition, m^6A methylation was involved in regulation of the malignant phenotypes of tumors by controlling the expression of tumor-related genes in breast cancer (Barbieri and Kouzarides, 2020; Zhang et al., 2020). Recent studies have shown that m^5C, m^1A, m^7G, and recently discovered ac^4C modifications, also play important roles in RNA processing and metabolism. For example, m^5C could promote enucleation of mRNA through binding to its reader protein Aly/REF export factor (ALYREF) (Yang et al., 2017), m^1A can affect the translation efficiency of its modified mRNA (Li et al., 2017; Safra et al., 2017), and ac^4C stabilizes its modified mRNA and enhances translation efficiency (Arango et al., 2018).

5-Methylcytosine

The m^5C modification is involved in the metastasis and proliferation of cancer cells, and the development of cancer stem cells. The currently identified writers of m^5C genes include NOP2/Sun RNA methyltransferase 2 (NSUN2), NSUN6, tRNA aspartic acid methyltransferase 1 (TRDMT1), tRNA-specific methyltransferase 4B (TRM4B) and OsNSUN2

(Bujnicki et al., 2004; Moon and Redman, 2014; Liu et al., 2017; Muller et al., 2019; Tang et al., 2020; Li H. et al., 2021). The "readers" include ALYREF, DNA repair protein RAD52 homolog (RAD52) and Y-box binding protein 1 (YBX1) (Yang et al., 2017; Chen et al., 2020; Xue et al., 2021).

N1-Methyladenosine

The main modification of tRNA is m^1A, which has also been found in 28SrRNA. The tRNA methyltransferase 10 homologue A (TRM)-TRM61 complex is the only known methyltransferase that catalyzes m^1A modification (Saikia et al., 2010), and YTH protein family is a potential reader of m^1A modifications (Dai et al., 2018). In addition, ALKBH3 is an eraser of m^1A (Li et al., 2016).

7-Methylguanosine

The m^7G modification was illustrated as part of the type O' cap structure of mRNA and was also observed in rRNA and tRNA. The m^7G maintained the integrity of structure mediated by the METTL1-WDR4 complex (Dai Z. et al., 2021). In addition, the m^7G modification on rRNA is induced by Williams Beuren syndrome chromosome 22 region protein (WBSCR22) (Haag et al., 2015). Up-regulation of METTL1/WDR4 can promote the level of m^7G modification on tRNAs, which in turn promotes the stability of tRNAs and the translation of mRNAs (Katsara and Schneider, 2021).

Pseudouridine

Pseudouridine can maintain the structure and stability of tRNA. The most-studied regulatory factor related to pseudouridine modification is Dyskerin Pseudouridine Synthase 1 (DKC1), which is a component of a small nucleolar ribonucleoprotein complex, needs RNA guidance to exert its catalytic activity, is overexpressed in various types of cancer.

Adenosine-to-Inosine Editing

Adenosine deaminases targeting RNA (ADARs) are effective in RNA editing, and are particularly important in the process of converting adenosine residues in double stranded RNA to creatinine (Ota et al., 2013). The ADAR1p110 subtype can regulate the stability of the chromosome terminal genome, and is required for continuous proliferation of cancer cells (Shiromoto et al., 2021).

U34 on Transport Ribonucleic Acid

Establishment of the U34 modification results from three steps: modification of U34 with an extender complex to produce 5-carboxymethyluridine (cm5U), transformation of cm5u to 5-methoxycarbonylmethyluridine (mcm5U) mediated by ALKBH8. Finally, thiolase, cytoplasmic trna2 thiolated protein 1 (CTU1), and CTU2 promote the formation of 5-methoxycarbonylmethyl-2-thiouridine (mcm5s2U) on specific tRNA (tRNAUUULys, tRNArUCGlu and tRNAAUGln) (Rapino et al., 2017).

N4-Acetylcytidine

N4-acetylcytodine (ac^4C) is a conserved chemical modification in eukaryotes and prokaryotes. Early studies suggested that ac^4C modifications mainly occurred on tRNA and 18SrRNA. Recent studies showed extensive ac^4C modifications on mRNA, with similar abundance to the m^7G cap modification on mRNA. To date, N-acetyltransferase 10 (NAT10) is the only protein known to have both an acetylase domain and an RNA-binding domain, and is therefore considered an RNA ac^4C-modifying enzyme (Sas-Chen et al., 2020; Yang C. et al., 2021).

ASSOCIATION OF RIBONUCLEIC ACID MODIFICATION AND BREAST CANCER PROGNOSIS

Data from public databases and clinical studies have indicated that levels of RNA modification regulators have prognostic value for breast cancer (Zheng F. et al., 2021). Low expression of METTL3, METTL14, WTAP and FTO was shown to correlate with relapse-free survival in breast cancer (Wu et al., 2019). METTL3 was also demonstrated to be related with a poor survival rate in breast cancer (Wang H. et al., 2020). METTL14 and ZC3H13 were associated with favorable prognosis, and correlated with adenomatous polyposis coli (APC). Furthermore, ZC3H13, METTL14 and APC expression levels were positively related with the number of infiltrating immune cells in breast cancer (Gong et al., 2020). The regulators YTHDF1, YTHDF3 and KIAA1429 were found to be upregulated in breast cancer, and were associated with the metastasis of lymph nodes, breast cancer progression, and also were predictors of poor prognosis (Liu et al., 2019; Anita et al., 2020; He et al., 2021). The demethylase ALKBH5 was found to be associated with poor prognosis in patients with TNBC (Wang S. et al., 2020). FTO was associated with short survival in Her-2 positive breast cancer (Xu et al., 2020). Non-coding RNAs such as miRNA, lncRNA, and circRNA, can undergo m^6A modification, which regulates their expression and function. Ten m^6A-modified lncRNAs-LINC00571, ANKRD10- IT1, LINC00593, miR-205HG, CIRBP- AS1, BLACAT1, SUCLG2- AS1, SAMD12- AS1, BVES-AS1, a18SrRNA nd HOXB-AS1 were used to construct a prognostic score model, and may be potential predictors of survival in patients with TNBC (Wu et al., 2021). A prognostic risk model comprised of six m^6A-regulated lncRNAs-Z68871.1, AL122010.1, AL138724.1,OTUD6B-AS1, AC090948.3 and eosinophil granule ontogeny transcript (EGOT) for high-risk patients with tumor-infiltrating immune cells, indicated that m^6A-regulated lncRNAs may modulate the immune microenvironment in breast cancer (Lv et al., 2021b). High expression of the m^6A regulator hnRNPC, and low expression of hsa-miR-944, are associated with advanced stage breast cancer and poor prognosis (Lv et al., 2021a). Basal-like subtypes and other breast cancer subtypes are associated with the m^6A regulators YTHDC2, IGF2BP2, IGF2BP3 and RBM15, and luminal A and B subtypes are classified into two clusters according to the methylation status of these four regulators. In addition, cluster1 has been found to be associated with cell adhesion signaling pathways and immune-associated genes of TILs. Furthermore, cluster1 was related to poor prognosis among patients with stage II and luminal B of breast cancer. The accuracy

TABLE 1 | The main role of regulators of RNA modification related with prognosis of breast cancer.

Gene	Type of regulator	Type of Modification	Role in survival	Role in tumor	Expression in cancer	References
METTL3	Writer	m^6A	Poor favorable	Oncogene suppressor	Upregulated downregulated	Wang H et al. (2020), Wu et al. (2019)
METTL14	Writer	m^6A	Favorable	Suppressor	Downregulated	Wu et al. (2019); Gong et al. (2020)
WTAP	Writer	m^6A	Favorable	Suppressor	Downregulated	Wu et al. (2019)
RBM15	Writer	m^6A	Poor	Oncogene	Upregulated	Yang et al. (2020)
ZC3H13	Writer	m^6A	Favorable	Suppressor	Downregulated	Gong et al. (2020)
KIAA1429	Writer	m^6A	Poor	Oncogene	Upregulated	Liu et al. (2019); Zhang et al. (2022)
CBLL1	Writer	m^6A	Favorable	Suppressor	Downregulated	Zheng F et al. (2021)
ALKBH5	Eraser	m^6A	Poor	Oncogene	Upregulated	Wang S et al. (2020)
FTO	Eraser	m^6A	Poor Favorable	Oncogene suppressor	Upregulated Downregulated	Xu et al. (2020), Wu et al. (2019)
YTHDF1/3	Reader	m^6A	Poor	Oncogene	Upregulated	Anita et al. (2020); He et al. (2021)
hnRNPC	Reader	m^6A	Poor	Oncogene	Upregulated	Lv et al. (2021a)
hnRNPC A2B1	Reader	m^6A	Favorable	Suppressor	Downregulated	Liu Y et al. (2020)
IGF2BP2	Reader	m^6A	Poor	Oncogene	Upregulated	Yang et al. (2020)
IGF2BP3	Reader	m^6A	Poor	Oncogene	Upregulated	Yang et al. (2020)
YTHDC2	Reader	m^6A	Poor	Oncogene	Upregulated	Yang et al. (2020)
NSUN2	Writer	m^5C	Poor	Oncogene	Upregulated	Huang Z et al. (2021)
NSUN6	Writer	m^5C	Favorable	Suppressor	Downregulated	Huang Z et al. (2021)
DKC1	Writer	Pseudouri dine	Favorable	Suppressor	Downregulated	Elsharawy et al. (2020)
ELP3	Writer	U34	Poor	Oncogene	Upregulated	Delaunay et al. (2016)
CTU1	Writer	U34	Poor	Oncogene	Upregulated	Delaunay et al. (2016)
CTU2	Writer	U34	Poor	Oncogene	Upregulated	Delaunay et al. (2016)

of diagnosis and efficacy of treatment may be improved by using m^6A regulators as biomarkers of different subtypes (Yang et al., 2020). These studies indicated that METTL3, METTL14, WTAP, FTO, ALKBH5, and other N6-methyladenosine-related lncRNAs were associated with progression of breast cancer, and may be prognostic indicators. Changes in expression and activity of m^6A modulators may promote breast cancer progression (Chen and Du, 2019; Lv et al., 2021b; Zhang et al., 2021) (**Table 1**). Few studies have mentioned m^5C modifications and breast cancer, and most have focused on NSUN2. It was reported that NSUN2 expression was associated with tumor stage and pathological subtype of breast cancer. The m^5C RNA methylation regulators NSUN2 and NSUN6 were predictors of survival and affected the progression and tumor immune microenvironment in TNBC (Huang Z. et al., 2021). Low expression of DKC1, rRNA pseudouridine modification, and decreased intrinsic ribosomal activity are associated with better breast cancer prognosis (Elsharawy et al., 2020; Guerrieri et al., 2020). In addition, the U34 modification enzymes ELP3, CTU1, and CTU2 were shown to be upregulated in breast cancer (Delaunay et al., 2016) (**Table 1**). Determination of the predictive value of mRNA m^7G and m^1A modifications, editing of RNA adenosine to inosine, U34 modification of tRNA, or ac^4C-related effectors for tumor prognosis require further study.

ROLES OF THE RIBONUCLEIC ACID MODIFICATION IN THE CARCINOGENESIS OF BREAST CANCER

Previous studies have proven that m^6A levels were strongly associated with cancer, which indicated that m^6A may play a crucial role in the occurrence or inhibition of malignant tumors (Helm and Motorin, 2017; Mohammad et al., 2019; Gu et al., 2020).

Ribonucleic Acid Modification Regulators in the Proliferation, Invasion and Metastasis of Breast Cancer

The writer KIAA1429 promotes proliferation and metastasis of breast cancer by modulating cyclin-dependent kinase 1 (CDK1) (Qian et al., 2019). Studies showed that the increasing of METTL3 promoted proliferation and inhibited apoptosis in breast cancer by targeting Bcl-2 (Wang H. et al., 2020). Hepatitis B X-interacting protein (HBXIP) upregulated the expression of METTL3 by inhibiting the miRNA let-7g in another study. In addition, METTL3 activated HBXIP *via* m^6A modification, which promoted cell proliferation in breast cancer as part of a positive feedback loop (Cai et al., 2018). On the contrary, METTL3 played an anti-tumor role by COL3A1 and circMETTL3/miR-34c-3p in TNBC (Shi et al., 2020; Ruan et al., 2021). The expression of circMETTL3 was also found to be increased in breast cancer, and promoted migration, proliferation and invasion of breast cancer cells by targeting miR-31-5p/CDK1 (Li Z. et al., 2021). A further study showed that the m^6A levels were significantly upregulated in lung metastatic breast cancer cells, which promoted the translation, elongation, and mRNA stability of keratin 7 (KRT7), a key epithelial-to-mesenchymal transition (EMT)-associated protein, by targeting FTO and METTL3, thereby promoting lung metastasis of breast cancer cells. LINC00675 m^6A methylation was increased by METTL3, which resulted in the interaction with miR-513b-5p and inhibition of cancerous properties of breast cancer (Fan and Wang, 2021). LNC942 directly bound to METTL14 and

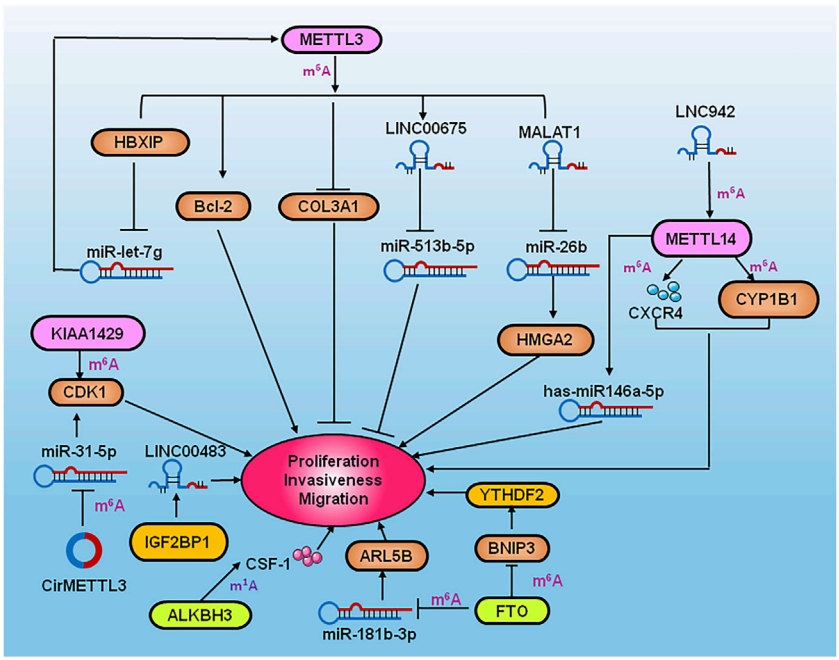


FIGURE 1 | Diagram of RNA modification regulators playing a vital role in the proliferation, invasion and metastasis of breast cancer. METTL3 promoted the proliferation, invasion and metastasis by targeting Bcl-2, while it reduced the expression of COL3A1 to inhibit the metastasis of breast cancer. LINC00675 m^6A methylation induced by METTL3 resulted in the inhibiting miR-513b-5p to suppress malignant phenotype breast cancer. LncMALAT1 increased/HMGA2 to facilitate the proliferation, invasion and metastasis of breast cancer cells by inhibiting miR-26b. LNC942 directly bound to METTL14 resulting in regulation of m^6A methylation of CXCR4 and CYP1B1 and mediate the onset and development of breast cancer. METTL14 also increased the expression of has-miR-146a-5p to promote invasion and migration of breast cancer. The writer KIAA1429 promoted the proliferation and metastasis of breast cancer by regulating CDK1, whereas circMETTL3 promoted the progression of breast cancer cells by targeting miR-31-5p/CDK1. FTO enhanced ARL5B by down-regulating miR-181b-3p to promote the invasion and migration of breast cancer. It also mediated m^6A demethylation by YTHDF2 to enhance the proliferation and metastasis of breast cancer *via* inhibiting BNIP3. IGF2BP1 promote proliferation of breast cancer by binding to LINC00483. ALKBH3 induced the decay of CSF-1 to promote breast cancer cell invasiveness.

promoted the expression of METTL14 protein through a specific binding domain (+176 to +265), resulting in the regulation of m^6A methylation of C-X-C motif chemokine receptor 4 (CXCR4) and cytochrome P450 family 1 subfamily B member 1 (CYP1B) to stabilize their expression and translation and mediate the onset and development of breast cancer (Sun et al., 2020). It was showed that METTL14 increased the expression of has-miR-146a-5p and promoted the invasion and migration of breast cancer (Yi et al., 2020). High level of FTO enhanced the expression of ARL5B by down-regulating miR-181b-3p to promote the invasion and migration of Her-2 positive breast cancer (Xu et al., 2020). FTO mediated m^6A demethylation in a YTHDF2-dependent manner and promoted the proliferation and metastasis of breast cancer *via* inhibiting BCL2 interacting protein 3 (BNIP3) (Niu et al., 2019). IGF2BP1 was shown to bind to LINC00483 and promote the proliferation of breast cancer cells (Qiao et al., 2021). Furthermore, the overexpression of NSUN2 induced by DNA hypomethylation promoted the proliferation, invasiveness and migration of breast cancer cells (Yi et al., 2017). Little is known about the functional mechanisms of m^1A-modified RNA. Therefore, epigenetic transcriptome research should focus on the function of m^1A-modified RNA. The up-regulation of m^1A demethylase ALKBH3 was shown to be involved in decay of macrophage-colony stimulating factor-1 (CSF-1) mRNA, which resulted in promoting breast cancer cell invasiveness (Woo and Chambers, 2019) (**Figure 1**).

Ribonucleic Acid Modification Regulators in the Breast Cancer Stem-Like Cells, Metastasis, Epithelial-to-Mesenchymal Transition, Glycosis and Immune Escape of Breast Caner

METTL3 was shown to methylate adenine 877 on the antisense nucleotide chain KRT7-AS of KRT7, which was recognized by IGF2BP1 and recruited the effector molecule HuR to increase the stability of the KRT7 and KRT7-AS complexes (Chen et al., 2021). METTL3 was demonstrated to upregulate PD-L1 expression *via* IGF2BP3 by m^6A-dependent manner to modulate immune surveillance in breast cancer (Wan et al., 2022). The high level of METTL3 induced EMT, invasion and migration by targeting MALAT1/miR-26b/HMGA2 axis (Li et al., 2022). DROSHA RNase III was upregulated in a number of cancers and interacted with β-catenin to activate stanniocalcin 1 (STC1) in an RNA cleavage-independent manner, which in turn contributed to the properties of breast cancer stem-like cells (BCSCs). Aurora kinase A (AURKA)-induced m^6A modification in BCSCs enhanced DROSHA mRNA stability.

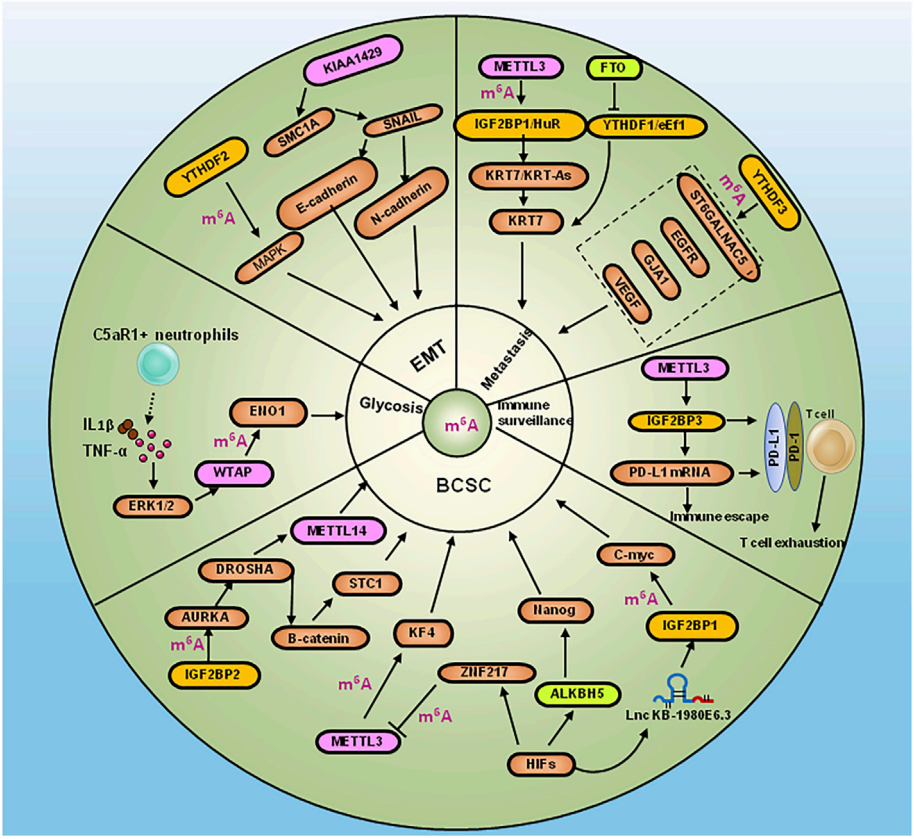


FIGURE 2 | Diagram summarizing RNA modification regulators in the pathogensis of BCSC, metastasis, EMT, glycosis and immune escape of breast caner. BCSC: Binding of AURKA to DROSHA transcripts induced by IGF2BP2 to enhance BCSC stemness, meanwhile DROSHA interacted with β-catenin to contribute to the BCSC property by activating STC1. ALKBH5 or ZNF21 increased Nanog and KLF4 mRNA expression by m^{6}A methylation, which led to pluripotency of breast cancer under hypoxic condition. The Lnc RNA KB-1980E6.3 facilitated BCSC self-renewal by IGF2BP1/c-Myc axis under hypoxic condition. Metastasis:YTHDF3 enhanced translation of ST6GALNAC5, GJA1, EGFR and VEFG to promote breast cancer metastasis to the brain. METTL3 and FTO promoted lung metastasis of breast cancer by KRT7 *via* suppressing YTHDF1/eEf1 complex and increasing IGF2BP1/HuR complex. EMT: YTHDF2 induced EMT by activating MAPK pathway. KIAA1429 promoted EMT by SMC1A/SNAIL in breast cancer. Glysosis: C5aR1-positive neutrophils secreted IL-1β and TNFα to synergistically activate ERK1/2, which resulted in the stabilizing WTAP to affect the glycolysis of breast cancer *via* ENO1. Immune surveillance: METTL3 upregulate PD-L1 *via* IGF2BP3 by m^{6}A-dependent manner to modulate immune escape and T cell exhausition in breast cancer.

In addition, AURKA stabilized METTL14 by inhibiting its ubiquitination and degradation, thereby promoting methylation of DROSHA mRNA. Furthermore, binding of AURKA to DROSHA transcripts induced by IGF2BP2 to stabilize m^{6}A-modified DROSHA, which enhanced BCSC stemness (Peng et al., 2021). Complement C5a receptor 1 (C5aR1)-positive neutrophils secreted IL (Interleukin) 1β and tumor necrosis factor α (TNFα) to synergistically activate ERK1/2, which resulted in phosphorylation of WTAP at serine 341, thereby stabilizing WTAP protein to promote RNA m^{6}A methylation of enolase 1 (ENO1) and affected the glycolysis of breast cancer cells (Ou et al., 2021). The overexpression of writer KIAA1429 was shown to bind the 3′-UTR of structural maintenance of chromosomes 1A (SMC1A) to promote EMT in breast cancer (Zhang et al., 2022). Down-regulation of FTO was shown to increase adenine methylation at position 950 on KRT7 mRNA, and enhanced the elongation efficiency of translation by recruiting the effector molecule eEF-1 through the recognition protein YTHDF1. The overexpression of FTO and knockdown of METTL3 and KRT7 reduced lung metastasis (Chen et al., 2021). ALKBH5 or ZNF217 mediated demethylation of m^{6}A in Nanog and KLF4 mRNA. The depleting of ALKBH5 reversed the pluripotency of breast cancer by inhibiting Nanog under hypoxic condition (Zhang et al., 2016). YTHDF3 enhanced the translation of m^{6}A-enriched transcripts of ST6 beta-galactoside alpha-2, 6-sialyltransferase 5 (ST6GALNAC5), gap junction protein alpha 1 (GJA1), epidermal growth factor receptor (EGFR) and vascular endothelial growth factor (VEGF), which promoted breast cancer metastasis to the brain (Chang et al., 2020). Apoptosis was shown to be triggered by the inhibition of YTHDF2-dependent mRNA degradation in TNBC through MAPK pathway-dependent induction of the EMT, and increased the global translation of mRNA synthesis in MYC-driven breast cancers (Einstein et al., 2021). The Lnc RNA KB-1980E6.3 facilitated BCSC self-renewal and carcinogenesis under hypoxic condition. In addition, IGF2BP1 was shown to be

recruited by LncRNA KB-1980E6.3 to strengthen the stability of c-Myc mRNA (Zhu et al., 2021). A study showed that CircBACH2 sponged hsa-miR-944, which resulted in MAPK signaling pathway-dependent up-regulation of hnRNPC expression and promotion of breast cancer cell proliferation (Lv et al., 2021a) (**Figure 2**).

The effects of RNA modification of target genes on progression of breast cancer depends on three factors: 1) the gene is a suppressor or an oncogene; 2) abnormal levels of RNA methylation in cancer; 3) Regulation of target mRNA modification. Taken together, the current study of m^6A RNA methylation in tumors is still at an early stage. RNA modification and its regulators seem to act as a "double-edged sword" in the tumor development, so it is challenging to rationally interpret the controversial findings. It is the functional versatility and tunability of this modification that underscores the important role of the environment in biological process. Therefore, the function of RNA modification may be more complex and extensive than the existing reports, and further exploration of its role in different cancers is expected to provide in-depth insights into tumorigenesis and development.

RIBONUCLEIC ACID MODIFICATIONS AS POTENTIAL DRUG TARGETS IN BREAST CANCER

Modification of RNA connects epigenetic transcriptomics with tumorigenesis and progression, and affects the processes of stem cell self-renewal and differentiation, proliferation and apoptosis, invasion and metastasis, drug resistance, and immunosuppression. Therefore, the key proteins involved in RNA modification are expected to become potential molecular targets for cancer diagnosis and treatment. To date, a number of small-molecule inhibitors that specifically target regulators of RNA methylation have shown great potential for suppression of carcinogenesis. For example, METTL3, METTL14 and WTAP were shown to be predictors of response to chemotherapy and hormone treatment (Song et al., 2021). S-adenosylhomocysteine (SAH) can be hydrolyzed to produce adenosine (adenine) and homocysteine, which can inhibit cellular methyltransferase activity through substrate inhibition, and regulates transmethylation through inhibition of METTL3-METTL14 activity (Eckert et al., 2019). The expression of MALAT1 was shown to be enhanced by METTL3 through recruitment of E2F transcription factor 1 (E2F1), resulting in transcription of anterior gradient 2 (AGR2), and subsequent adriamycin resistance in breast cancer (Li et al., 2022). In a further study, METTL3 also promoted maturation of miRNA-221-3p in an m^6A-dependent manner, which negatively regulated HIPK2, upregulated the target gene Che-1, and induced chemoresistance of breast cancer cells to doxorubicin (Pan et al., 2021).

Adenylate kinase 4 (AK4) and the m^6A writer METTL3 are highly expressed in tamoxifen-resistant breast cancer cell lines, and METTL3 was shown to promote tamoxifen resistance in breast cancer by promoting AK4 expression, reducing the production level of reactive oxygen species (ROS), and decreasing the activity of p38 (Liu X. et al., 2020). Metformin was found to inhibit the proliferation of breast cancer cells through upregulation of P21 in an m^6A-dependent manner *via* METTL3 (Cheng et al., 2021). STM2457 is an orally bioavailable small molecule METTL3 inhibitor that are slated for human clinical trials by targeting a novel mechanism for the treatment of acute myeloid leukemia and other solid and hematological cancers (Yankova et al., 2021). In addition, WTAP binds to the m^6A modified site of lncRNA DLGAP1 antisense RNA 1 (DLGAP1-AS1) to sponge miR-299-3p, resulting in adriamycin resistance in breast cancer (Huang T. et al., 2021). The inhibitor of 2-oxoglutarate oxygenase (OG) oxidase, IOX1, significantly inhibited ALKBH5 activity. Protein arginine methyltransferase 5 (PRMT5) inhibits doxorubicin-treated RNA m^6A modification by promoting nuclear translocation of ALKBH5 (Wu et al., 2022). The applying of PRMT5 inhibitor tadalafil improves the chemosensitivity of Doxorubicin in breast cancer by modulating RNA methylation (Wu et al., 2022). The most widely studied RNA methylation regulator is FTO (Chen and Du, 2019). A few potent inhibitors of FTO have been reported in the literature, namely FG-2216/IOX3, FB23-2, rhein, meclofenamic acid (MA), entacapone, bisantren and brequinar (Mcmurray et al., 2015; Van Der Werf and Jamieson, 2019; Su et al., 2020; Xiao et al., 2020; Yang B. et al., 2021; Lv et al., 2022). FTO was shown to promote tumor glycolysis and limit the response of T cells. The FTO inhibitor Dac51 increased CD8+ T cell infiltration and acted in synergy with anti-PD-L1 blockade (Liu Y. et al., 2021). MA is a highly selective FTO inhibitor relative to ALKBH5 by using high-throughput fluorescence polarization analysis (Zheng Q.-K. et al., 2021). The overexpression of m^6A reader hnRNPA2B1 (A2B1) resulted in tamoxifen and fulvestrant resistance, and decreased migration and invasion in TAM-resistant cells through activation of the protein kinase B (AKT) and mitogen-activated protein kinase (MAPK) signaling pathways (Petri et al., 2021). Transcription factor 3 (ATF3) was highly expressed in tamoxifen-resistant breast cancer, and was regulated by low expression of YTHDF2. Moreover, ATF3 enhanced the expression of ATP binding cassette subfamily B member 1 (ABCB1), which promotes tamoxifen resistance (Liu X. et al., 2021).

Through regulation by NSUN2, m^5C modifications were shown to be involved in the onset of various cancers, and may be potential targets for cancer treatment (Huang Z. et al., 2021; Hu et al., 2021). The expression of NSUN2 could be reduced by the inhibition of sphingosine kinase (SPHK), which is involved in sphingolipid metabolism in cell growth. Therefore, the SPHK1 inhibitor SK1 may be a latent drug for treatment through modulation of NSUN2 expression (Guo et al., 2021). In addition, the m^5C "reader" Y-box-binding-protein 1 (YBX1) is highly expressed in certain cisplatin-resistant cancers. A study showed that the YBX1 phosphorylation inhibitors including TAS0612 (multikinase inhibitor) and everolimus (rapamycin complex 1 inhibitor) mitigated antiestrogen resistance in breast cancer (Shibata et al., 2020).

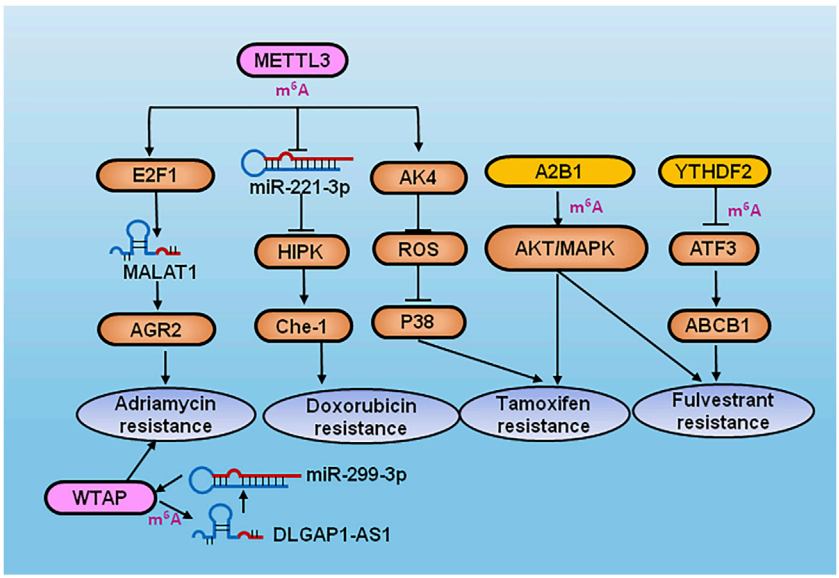


FIGURE 3 | Diagram of RNA modification regulators inducing drugs resistance in breast cancer. METTL3 increased the expression of MALAT1 to activate AGR2 by recruiting E2F1 and subsequent adriamycin resistance in breast cancer. METTL3 also promoted maturation of miRNA-221-3p in a m^{6}A-dependent manner and negatively regulated HIPK2 and upregulated Che-1 which induced chemoresistance of breast cancer cells to doxorubicin. METTL3 promoted tamoxifen resistance by promoting AK4 expression, reducing the production of ROS and decreasing the activity of p38. WTAP binds to DLGAP1-AS1 and sponged miR-299-3p to confer adriamycin resistance in breast cancer. A2B1 induced tamoxifen and fulvestrant resistance by AKT/MAPK signaling pathways. YTHDF2 downregulated ATF3 to activate ABCB1, resulting in tamoxifen resistance of breast cancer.

TABLE 2 | The potential drugs applied in the treatment of breast cancer based on the RNA modification.

Drug	Target regulators	Modification	Target	References
S-adenosylhomocysteine (SAH)	METTL3-METTL14	m^{6}A	Inhibit the activity of methyltransferase	Eckert et al. (2019)
Metformin	METTL3	m^{6}A	Inhibit the proliferation of breast cancer cell by upregulating P21	Cheng et al. (2021)
STM2457	METTL3	m^{6}A	Inhibit METTL3	Yankova et al. (2021)
Tadalafil	ALKBH5	m^{6}A	Inhibit doxorubicin-induced RNA methylation	Wu et al. (2022)
FB23-2	FTO	m^{6}A	Inhibit FTO	Van Der Werf and Jamieson, (2019)
FG-2216/IOX3	FTO	m^{6}A	Inhibit FTO	Yang B et al. (2021)
Rhein	FTO	m^{6}A	Inhibit FTO	Lv et al. (2022)
Entacapone	FTO	m^{6}A	Inhibit FTO	Mcmurray et al. (2015)
MA	FTO	m^{6}A	Inhibit FTO	Xiao et al. (2020)
Bisantren	FTO	m^{6}A	Inhibit FTO	Su et al. (2020)
Brequinar	FTO	m^{6}A	Inhibit FTO	Su et al. (2020)
Dac51	FTO	m^{6}A	Increased CD8+ T cell infiltration and synergistic effect with anti-PD-L1 blockade	Liu Y et al. (2021)
SPHK	NSUN2	m^{5}C	Maintained the metabolic balance of sphingolipids	Guo et al. (2021)
TAS0612	YBX1	m^{5}C	Overcome anti-estrogen resistance	Shibata et al. (2020)
Everolimus	YBX1	m^{5}C	Overcome anti-estrogen resistance	Shibata et al. (2020)

However, the effects of YBX1 inhibitors on drug resistance in breast cancer require further investigation (Jiang et al., 2022). Three inhibitors were developed based on the interaction between DKC1 and TERC to inhibit telomerase activity in breast cancer cell lines, which may aid in development of pseudouridine synthase inhibitors for treatment of cancer (Armando et al., 2018).

Modulating abnormal RNA modification levels can inhibit the occurrence and development of tumors (**Figure 3**). Although some RNA modification enzyme inhibitors have shown potential inhibitory effects in a variety of cancers (**Table 2**), more drugs and new therapeutic strategies related to RNA modification remain to be explored and requested in the clinical trials.

FUTURE DIRECTIONS

Research on tumor-related RNA modification is still in its infancy. Increasing number of novel RNA modifications are gradually discovered, such as RNA glycosylation modification, which is remarkably suggested that glycoRNA may play an important role in physiological and pathological processes including host immune defense, tumor immune escape, and autoimmune diseases (Flynn et al., 2021). It is also necessary to develop new technologies to discover new type of RNA modification. Further studies on the role of RNA methylation in the immune response will provide broader prospects for immunotherapy and prevention of tumor drug resistance. In terms of clinical application, it is of great significance to continue to explore whether RNA modification-related proteins could be potential diagnostic and therapeutic targets. Development of more specific and effective regulators of RNA modification is expected to result in new options for tumor treatment. In the context of disease treatment, small molecule inhibitors that can target RNA methylation-related effector proteins may have great promise. Demonstration of preclinical efficacy of these targeted drugs may result in future clinical use of RNA epigenetic drugs.

CONCLUSION

RNA methylation has been shown to exert tumor-promoting or tumor-suppressive activities, and is involved in the onset, development, and metastasis of breast cancer. The critical role of tumor-specific effects of RNA methylation provides insights into prognosis, pathogenesis, and treatment response in breast cancer. Design of novel therapeutics through targeted RNA modifications is an international research hotspot and may have profound implications in translational medicine application in breast cancer.

AUTHOR CONTRIBUTIONS

Conception and design: XG and YL. Drafting of the manuscript: TZ, YL and JB. Drawing of figures: YJ, JB, and XZ. Conceiving and Critical revision of the manuscript for important intellectual content: XG and YL. All authors read and approved the final manuscript.

FUNDING

This work was supported by the National Natural Science foundation of China (Grant No. 82103468 to YL), Natural Science foundation of Liaoning Province of China (Grant No. 2020-MS-178 to XG) and 345 Talent Project of Shengjing Hospital of China Medical University (M0961 to YL).

ACKNOWLEDGMENTS

We thank Charlesworth Author Service (https://www.cwauthors.com.cn/) for editing this manuscript.

REFERENCES

Anita, R., Paramasivam, A., Priyadharsini, J. V., and Chitra, S. (2020). The m6A Readers YTHDF1 and YTHDF3 Aberrations Associated with Metastasis and Predict Poor Prognosis in Breast Cancer Patients. *Am. J. Cancer Res.* 10, 2546–2554.

Arango, D., Sturgill, D., Alhusaini, N., Dillman, A. A., Sweet, T. J., Hanson, G., et al. (2018). Acetylation of Cytidine in mRNA Promotes Translation Efficiency. *Cell* 175, 1872–1886. e1824. doi:10.1016/j.cell.2018.10.030

Armando, R. G., Mengual Gómez, D. L., Juritz, E. I., Lorenzano Menna, P., and Gomez, D. E. (2018). Homology Model and Docking-Based Virtual Screening for Ligands of Human Dyskerin as New Inhibitors of Telomerase for Cancer Treatment. *Int. J. Mol. Sci.* 19, 3216. doi:10.3390/ijms19103216

Barbieri, I., and Kouzarides, T. (2020). Role of RNA Modifications in Cancer. *Nat. Rev. Cancer* 20, 303–322. doi:10.1038/s41568-020-0253-2

Boccaletto, P., Stefaniak, F., Ray, A., Cappannini, A., Mukherjee, S., Purta, E., et al. (2022). MODOMICS: a Database of RNA Modification Pathways. 2021 Update. *Nucleic Acids Res.* 50, D231–D235. doi:10.1093/nar/gkab1083

Bray, F., Ferlay, J., Soerjomataram, I., Siegel, R. L., Torre, L. A., and Jemal, A. (2018). Global Cancer Statistics 2018: GLOBOCAN Estimates of Incidence and Mortality Worldwide for 36 Cancers in 185 Countries. *CA A Cancer J. Clin.* 68, 394–424. doi:10.3322/caac.21492

Bujnicki, J. M., Feder, M., Ayres, C. L., and Redman, K. L. (2004). Sequence-structure-function Studies of tRNA:m5C Methyltransferase Trm4p and its Relationship to DNA:m5C and RNA:m5U Methyltransferases. *Nucleic Acids Res.* 32, 2453–2463. doi:10.1093/nar/gkh564

Cai, X., Wang, X., Cao, C., Gao, Y., Zhang, S., Yang, Z., et al. (2018). HBXIP-Elevated Methyltransferase METTL3 Promotes the Progression of Breast Cancer via Inhibiting Tumor Suppressor Let-7g. *Cancer Lett.* 415, 11–19. doi:10.1016/j.canlet.2017.11.018

Chang, G., Shi, L., Ye, Y., Shi, H., Zeng, L., Tiwary, S., et al. (2020). $YTHDF_3$ Induces the Translation of m^6A-Enriched Gene Transcripts to Promote Breast Cancer Brain Metastasis. *Cancer Cell* 38, 857–871. doi:10.1016/j.ccell.2020.10.004

Chen, F., Chen, Z., Guan, T., Zhou, Y., Ge, L., Zhang, H., et al. (2021). N^6-Methyladenosine Regulates mRNA Stability and Translation Efficiency of KRT7 to Promote Breast Cancer Lung Metastasis. *Cancer Res.* 81, 2847–2860. doi:10.1158/0008-5472.can-20-3779

Chen, H., Yang, H., Zhu, X., Yadav, T., Ouyang, J., Truesdell, S. S., et al. (2020). m^5C Modification of mRNA Serves a DNA Damage Code to Promote Homologous Recombination. *Nat. Commun.* 11, 2834. doi:10.1038/s41467-020-16722-7

Chen, H., Yu, Y., Yang, M., Huang, H., Ma, S., Hu, J., et al. (2022). YTHDF1 Promotes Breast Cancer Progression by Facilitating FOXM1 Translation in an m6A-Dependent Manner. *Cell Biosci.* 12, 19. doi:10.1186/s13578-022-00759-w

Chen, J., and Du, B. (2019). Novel Positioning from Obesity to Cancer: FTO, an m^6A RNA Demethylase, Regulates Tumour Progression. *J. Cancer Res. Clin. Oncol.* 145, 19–29. doi:10.1007/s00432-018-2796-0

Cheng, L., Zhang, X., Huang, Y.-Z., Zhu, Y.-L., Xu, L.-Y., Li, Z., et al. (2021). Metformin Exhibits Antiproliferation Activity in Breast Cancer via miR-483-3p/METTL3/m^6A/p21 Pathway. *Oncogenesis* 10, 7. doi:10.1038/s41389-020-00290-y

Dai, X.-Y., Shi, L., Li, Z., Yang, H.-Y., Wei, J.-F., and Ding, Q. (2021). Main N6-Methyladenosine Readers: YTH Family Proteins in Cancers. *Front. Oncol.* 11, 635329. doi:10.3389/fonc.2021.635329

Dai, Z., Liu, H., Liao, J., Huang, C., Ren, X., Zhu, W., et al. (2021). N^7-Methylguanosine tRNA Modification Enhances Oncogenic mRNA

Translation and Promotes Intrahepatic Cholangiocarcinoma Progression. *Mol. Cell* 81, 3339–3355. e3338. doi:10.1016/j.molcel.2021.07.003

Dai, X., Wang, T., Gonzalez, G., and Wang, Y. (2018). Identification of YTH Domain-Containing Proteins as the Readers for N1-Methyladenosine in RNA. *Anal. Chem.* 90, 6380–6384. doi:10.1021/acs.analchem.8b01703

Delaunay, S., Rapino, F., Tharun, L., Zhou, Z., Heukamp, L., Termathe, M., et al. (2016). Elp3 Links tRNA Modification to IRES-Dependent Translation of LEF1 to Sustain Metastasis in Breast Cancer. *J. Exp. Med.* 213, 2503–2523. doi:10.1084/jem.20160397

Dong, S., Wu, Y., Liu, Y., Weng, H., and Huang, H. (2021). N ^{6} -methyladenosine Steers RNA Metabolism and Regulation in Cancer. *Cancer Commun.* 41, 538–559. doi:10.1002/cac2.12161

Eckert, M. A., Coscia, F., Chryplewicz, A., Chang, J. W., Hernandez, K. M., Pan, S., et al. (2019). Proteomics Reveals NNMT as a Master Metabolic Regulator of Cancer-Associated Fibroblasts. *Nature* 569, 723–728. doi:10.1038/s41586-019-1173-8

Einstein, J. M., Perelis, M., Chaim, I. A., Meena, J. K., Nussbacher, J. K., Tankka, A. T., et al. (2021). Inhibition of YTHDF2 Triggers Proteotoxic Cell Death in MYC-Driven Breast Cancer. *Mol. Cell* 81, 3048–3064. e3049. doi:10.1016/j.molcel.2021.06.014

Elsharawy, K. A., Mohammed, O. J., Aleskandarany, M. A., Hyder, A., El-Gammal, H. L., Abou-Dobara, M. I., et al. (2020). The Nucleolar-Related Protein Dyskerin Pseudouridine Synthase 1 (DKC1) Predicts Poor Prognosis in Breast Cancer. *Br. J. Cancer* 123, 1543–1552. doi:10.1038/s41416-020-01045-7

Fan, S., and Wang, L. (2021). N^{6}-Methyladenosine-Regulated LINC00675 Suppress the Proliferation, Migration and Invasion of Breast Cancer Cells via Inhibiting miR-513b-5p. *Bioengineered* 12, 10690–10702. doi:10.1080/21655979.2021.2001905

Flynn, R. A., Pedram, K., Malaker, S. A., Batista, P. J., Smith, B. A. H., Johnson, A. G., et al. (2021). Small RNAs Are Modified with N-Glycans and Displayed on the Surface of Living Cells. *Cell* 184, 3109–3124. doi:10.1016/j.cell.2021.04.023

Frye, M., Harada, B. T., Behm, M., and He, C. (2018). RNA Modifications Modulate Gene Expression during Development. *Science* 361, 1346–1349. doi:10.1126/science.aau1646

Fu, Y., Jia, G., Pang, X., Wang, R. N., Wang, X., Li, C. J., et al. (2013). FTO-mediated Formation of N6-Hydroxymethyladenosine and N6-Formyladenosine in Mammalian RNA. *Nat. Commun.* 4, 1798. doi:10.1038/ncomms2822

Gong, P.-J., Shao, Y.-C., Yang, Y., Song, W.-J., He, X., Zeng, Y.-F., et al. (2020). Analysis of N6-Methyladenosine Methyltransferase Reveals METTL14 and ZC3H13 as Tumor Suppressor Genes in Breast Cancer. *Front. Oncol.* 10, 578963. doi:10.3389/fonc.2020.578963

Gu, C., Shi, X., Dai, C., Shen, F., Rocco, G., Chen, J., et al. (2020). RNA m6A Modification in Cancers: Molecular Mechanisms and Potential Clinical Applications. *InnovationInnovation (N Y)* 1, 100066. doi:10.1016/j.xinn.2020.100066

Guerrieri, A. N., Zacchini, F., Onofrillo, C., Di Viggiano, S., Penzo, M., Ansuini, A., et al. (2020). DKC1 Overexpression Induces a More Aggressive Cellular Behavior and Increases Intrinsic Ribosomal Activity in Immortalized Mammary Gland Cells. *Cancers (Basel)* 12, 3512. doi:10.3390/cancers12123512

Guo, G., Pan, K., Fang, S., Ye, L., Tong, X., Wang, Z., et al. (2021). Advances in mRNA 5-methylcytosine Modifications: Detection, Effectors, Biological Functions, and Clinical Relevance. *Mol. Ther. - Nucleic Acids* 26, 575–593. doi:10.1016/j.omtn.2021.08.020

Haag, S., Kretschmer, J., and Bohnsack, M. T. (2015). WBSCR22/Merm1 Is Required for Late Nuclear Pre-ribosomal RNA Processing and Mediates N7-Methylation of G1639 in Human 18S rRNA. *RNA* 21, 180–187. doi:10.1261/rna.047910.114

Harbeck, N., Penault-Llorca, F., Cortes, J., Gnant, M., Houssami, N., Poortmans, P., et al. (2019). Breast Cancer. *Nat. Rev. Dis. Prim.* 5, 66. doi:10.1038/s41572-019-0111-2

He, L., Li, H., Wu, A., Peng, Y., Shu, G., and Yin, G. (2019). Functions of N6-Methyladenosine and its Role in Cancer. *Mol. Cancer* 18, 176. doi:10.1186/s12943-019-1109-9

He, X., Tan, L., Ni, J., and Shen, G. (2021). Expression Pattern of m^{6}A Regulators Is Significantly Correlated with Malignancy and Antitumor Immune Response of Breast Cancer. *Cancer Gene Ther.* 28, 188–196. doi:10.1038/s41417-020-00208-1

Helm, M., and Motorin, Y. (2017). Detecting RNA Modifications in the Epitranscriptome: Predict and Validate. *Nat. Rev. Genet.* 18, 275–291. doi:10.1038/nrg.2016.169

Hu, Y., Chen, C., Tong, X., Chen, S., Hu, X., Pan, B., et al. (2021). NSUN2 Modified by SUMO-2/3 Promotes Gastric Cancer Progression and Regulates mRNA m5C Methylation. *Cell Death Dis.* 12, 842. doi:10.1038/s41419-021-04127-3

Huang, H., Weng, H., and Chen, J. (2020). m^{6}A Modification in Coding and Non-coding RNAs: Roles and Therapeutic Implications in Cancer. *Cancer Cell* 37, 270–288. doi:10.1016/j.ccell.2020.02.004

Huang, H., Weng, H., Sun, W., Qin, X., Shi, H., Wu, H., et al. (2018). Recognition of RNA N6-Methyladenosine by IGF2BP Proteins Enhances mRNA Stability and Translation. *Nat. Cell Biol.* 20, 285–295. doi:10.1038/s41556-018-0045-z

Huang, T., Cao, L., Feng, N., Xu, B., Dong, Y., and Wang, M. (2021). N^{6}-methyladenosine (m^{6}A)-Mediated lncRNA DLGAP1-AS1enhances Breast Canceradriamycin Resistance through miR-299-3p/WTAP Feedback Loop. *Bioengineered* 12, 10935–10944. doi:10.1080/21655979.2021.2000198

Huang, Z., Pan, J., Wang, H., Du, X., Xu, Y., Wang, Z., et al. (2021). Prognostic Significance and Tumor Immune Microenvironment Heterogenicity of m5C RNA Methylation Regulators in Triple-Negative Breast Cancer. *Front. Cell Dev. Biol.* 9, 657547. doi:10.3389/fcell.2021.657547

Jeschke, J., Collignon, E., Al Wardi, C., Krayem, M., Bizet, M., Jia, Y., et al. (2021). Downregulation of the FTO m^{6}A RNA Demethylase Promotes EMT-Mediated Progression of Epithelial Tumors and Sensitivity to Wnt Inhibitors. *Nat. Cancer* 2, 611–628. doi:10.1038/s43018-021-00223-7

Jia, G., Fu, Y., Zhao, X., Dai, Q., Zheng, G., Yang, Y., et al. (2011). N6-methyladenosine in Nuclear RNA Is a Major Substrate of the Obesity-Associated FTO. *Nat. Chem. Biol.* 7, 885–887. doi:10.1038/nchembio.687

Jiang, D., Qiu, T., Peng, J., Li, S., TalaRen, W., Yang, C., et al. (2022). YB-1 Is a Positive Regulator of KLF5 Transcription Factor in Basal-like Breast Cancer. *Cell Death Differ.* doi:10.1038/s41418-021-00920-x

Katsara, O., and Schneider, R. J. (2021). m^{7}G tRNA Modification Reveals New Secrets in the Translational Regulation of Cancer Development. *Mol. Cell* 81, 3243–3245. doi:10.1016/j.molcel.2021.07.030

Li, H., Zhu, D., Wu, J., Ma, Y., Cai, C., Chen, Y., et al. (2021). New Substrates and Determinants for tRNA Recognition of RNA Methyltransferase DNMT2/TRDMT1. *RNA Biol.* 18, 2531–2545. doi:10.1080/15476286.2021.1930756

Li, Z., Yang, H.-Y., Dai, X.-Y., Zhang, X., Huang, Y.-Z., Shi, L., et al. (2021). CircMETTL3, Upregulated in a m6A-dependent Manner, Promotes Breast Cancer Progression. *Int. J. Biol. Sci.* 17, 1178–1190. doi:10.7150/ijbs.57783

Li, S., Jiang, F., Chen, F., Deng, Y., and Pan, X. (2022). Effect of m6A Methyltransferase METTL3 -mediated MALAT1/E2F1/AGR2 axis on Adriamycin Resistance in Breast Cancer. *J. Biochem. Mol. Toxicol.* 36, e22922. doi:10.1002/jbt.22922

Li, S., and Mason, C. E. (2014). The Pivotal Regulatory Landscape of RNA Modifications. *Annu. Rev. Genom. Hum. Genet.* 15, 127–150. doi:10.1146/annurev-genom-090413-025405

Li, X., Xiong, X., Wang, K., Wang, L., Shu, X., Ma, S., et al. (2016). Transcriptome-wide Mapping Reveals Reversible and Dynamic N(1)-Methyladenosine Methylome. *Nat. Chem. Biol.* 12, 311–316. doi:10.1038/nchembio.2040

Li, X., Xiong, X., Zhang, M., Wang, K., Chen, Y., Zhou, J., et al. (2017). Base-Resolution Mapping Reveals Distinct m^{1}A Methylome in Nuclear- and Mitochondrial-Encoded Transcripts. *Mol. Cell* 68, 993–1005. doi:10.1016/j.molcel.2017.10.019

Li, Y., Xiao, J., Bai, J., Tian, Y., Qu, Y., Chen, X., et al. (2019). Molecular Characterization and Clinical Relevance of m^{6}A Regulators across 33 Cancer Types. *Mol. Cancer* 18, 137. doi:10.1186/s12943-019-1066-3

Lin, Y., Jin, X., Nie, Q., Chen, M., Guo, W., Chen, L., et al. (2022). YTHDF3 Facilitates Triple-Negative Breast Cancer Progression and Metastasis by Stabilizing ZEB1 mRNA in an m^{6}A-dependent Manner. *Ann. Transl. Med.* 10, 83. doi:10.21037/atm-21-6857

Liu, L., Liu, X., Dong, Z., Li, J., Yu, Y., Chen, X., et al. (2019). N6-methyladenosine-related Genomic Targets Are Altered in Breast Cancer Tissue and Associated with Poor Survival. *J. Cancer* 10, 5447–5459. doi:10.7150/jca.35053

Liu, R.-J., Long, T., Li, J., Li, H., and Wang, E.-D. (2017). Structural Basis for Substrate Binding and Catalytic Mechanism of a Human RNA:m5C Methyltransferase NSun6. *Nucleic Acids Res.* 45, 6684–6697. doi:10.1093/nar/gkx473

Liu, X., Gonzalez, G., Dai, X., Miao, W., Yuan, J., Huang, M., et al. (2020). Adenylate Kinase 4 Modulates the Resistance of Breast Cancer Cells to Tamoxifen through an m^{6}A-Based Epitranscriptomic Mechanism. *Mol. Ther.* 28, 2593–2604. doi:10.1016/j.ymthe.2020.09.007

Liu, Y., Li, H., Liu, F., Gao, L.-B., Han, R., Chen, C., et al. (2020). Heterogeneous Nuclear Ribonucleoprotein A2/B1 Is a Negative Regulator of Human Breast Cancer Metastasis by Maintaining the Balance of Multiple Genes and Pathways. *EBioMedicine* 51, 102583. doi:10.1016/j.ebiom.2019.11.044

Liu, X., Yuan, J., Zhang, X., Li, L., Dai, X., Chen, Q., et al. (2021). ATF3 Modulates the Resistance of Breast Cancer Cells to Tamoxifen through an N^6-Methyladenosine-Based Epitranscriptomic Mechanism. *Chem. Res. Toxicol.* 34, 1814–1821. doi:10.1021/acs.chemrestox.1c00206

Liu, Y., Liang, G., Xu, H., Dong, W., Dong, Z., Qiu, Z., et al. (2021). Tumors Exploit FTO-Mediated Regulation of Glycolytic Metabolism to Evade Immune Surveillance. *Cell Metab.* 33, 1221–1233. e1211. doi:10.1016/j.cmet.2021.04.001

Lv, D., Ding, S., Zhong, L., Tu, J., Li, H., Yao, H., et al. (2022). M(6)A Demethylase FTO-Mediated Downregulation of DACT1 mRNA Stability Promotes Wnt Signaling to Facilitate Osteosarcoma Progression. *Oncogene* 41 (12), 1727–1741. doi:10.1038/s41388-022-02214-z

Lv, W., Tan, Y., Xiong, M., Zhao, C., Wang, Y., Wu, M., et al. (2021a). Analysis and Validation of m6A Regulatory Network: a Novel circBACH2/has-miR-944/HNRNPC axis in Breast Cancer Progression. *J. Transl. Med.* 19, 527. doi:10.1186/s12967-021-03196-4

Lv, W., Wang, Y., Zhao, C., Tan, Y., Xiong, M., Yi, Y., et al. (2021b). Identification and Validation of m6A-Related lncRNA Signature as Potential Predictive Biomarkers in Breast Cancer. *Front. Oncol.* 11, 745719. doi:10.3389/fonc.2021.745719

Maresca, G., and Wismayer, P. S. (2016). DNA Methylation and Cancer: Identifying and Targeting Epigenetic Modifications May Be the Future of Cancer Therapy? *Gulf J. Oncol.* 1, 77–83.

Mcmurray, F., Demetriades, M., Aik, W., Merkestein, M., Kramer, H., Andrew, D. S., et al. (2015). Pharmacological Inhibition of FTO. *Plos One* 10, e0121829. doi:10.1371/journal.pone.0121829

Mohammad, H. P., Barbash, O., and Creasy, C. L. (2019). Targeting Epigenetic Modifications in Cancer Therapy: Erasing the Roadmap to Cancer. *Nat. Med.* 25, 403–418. doi:10.1038/s41591-019-0376-8

Moon, H. J., and Redman, K. L. (2014). Trm4 and Nsun2 RNA:m5C Methyltransferases Form Metabolite-dependent, Covalent Adducts with Previously Methylated RNA. *Biochemistry* 53, 7132–7144. doi:10.1021/bi500882b

Müller, M., Samel-Pommerencke, A., Legrand, C., Tuorto, F., Lyko, F., and Ehrenhofer-Murray, A. E. (2019). Division of Labour: tRNA Methylation by the NSun2 tRNA Methyltransferases Trm4a and Trm4b in Fission Yeast. *RNA Biol.* 16, 249–256. doi:10.1080/15476286.2019.1568819

Niu, Y., Lin, Z., Wan, A., Chen, H., Liang, H., Sun, L., et al. (2019). RNA N6-Methyladenosine Demethylase FTO Promotes Breast Tumor Progression through Inhibiting BNIP3. *Mol. Cancer* 18, 46. doi:10.1186/s12943-019-1004-4

Ota, H., Sakurai, M., Gupta, R., Valente, L., Wulff, B.-E., Ariyoshi, K., et al. (2013). ADAR1 Forms a Complex with Dicer to Promote microRNA Processing and RNA-Induced Gene Silencing. *Cell* 153, 575–589. doi:10.1016/j.cell.2013.03.024

Ou, B., Liu, Y., Yang, X., Xu, X., Yan, Y., and Zhang, J. (2021). C5aR1-positive Neutrophils Promote Breast Cancer Glycolysis through WTAP-dependent m6A Methylation of ENO1. *Cell Death Dis.* 12, 737. doi:10.1038/s41419-021-04028-5

Pan, X., Hong, X., Li, S., Meng, P., and Xiao, F. (2021). METTL3 Promotes Adriamycin Resistance in MCF-7 Breast Cancer Cells by Accelerating Pri-microRNA-221-3p Maturation in a m6A-dependent Manner. *Exp. Mol. Med.* 53, 91–102. doi:10.1038/s12276-020-00510-w

Pedrosa, R. M. S. M., Mustafa, D. A., Soffietti, R., and Kros, J. M. (2018). Breast Cancer Brain Metastasis: Molecular Mechanisms and Directions for Treatment. *Neuro Oncol.* 20, 1439–1449. doi:10.1093/neuonc/noy044

Peng, F., Xu, J., Cui, B., Liang, Q., Zeng, S., He, B., et al. (2021). Oncogenic AURKA-Enhanced N^6-Methyladenosine Modification Increases DROSHA mRNA Stability to Transactivate STC1 in Breast Cancer Stem-like Cells. *Cell Res.* 31, 345–361. doi:10.1038/s41422-020-00397-2

Petri, B. J., Piell, K. M., South Whitt, G. C., Wilt, A. E., Poulton, C. C., Lehman, N. L., et al. (2021). HNRNPA2B1 Regulates Tamoxifen- and Fulvestrant-Sensitivity and Hallmarks of Endocrine Resistance in Breast Cancer Cells. *Cancer Lett.* 518, 152–168. doi:10.1016/j.canlet.2021.07.015

Pinto, R., Vågbø, C. B., Jakobsson, M. E., Kim, Y., Baltissen, M. P., O'Donohue, M.-F., et al. (2020). The Human Methyltransferase ZCCHC4 Catalyses N6-Methyladenosine Modification of 28S Ribosomal RNA. *Nucleic Acids Res.* 48, 830–846. doi:10.1093/nar/gkz1147

Qian, J.-Y., Gao, J., Sun, X., Cao, M.-D., Shi, L., Xia, T.-S., et al. (2019). KIAA1429 Acts as an Oncogenic Factor in Breast Cancer by Regulating CDK1 in an N6-methyladenosine-independent Manner. *Oncogene* 38, 6123–6141. doi:10.1038/s41388-019-0861-z

Qiao, Y. S., Zhou, J. H., Jin, B. H., Wu, Y. Q., and Zhao, B. (2021). LINC00483 Is Regulated by IGF2BP1 and Participates in the Progression of Breast Cancer. *Eur. Rev. Med. Pharmacol. Sci.* 25, 1379–1386. doi:10.26355/eurrev_202102_24846

Rapino, F., Delaunay, S., Zhou, Z., Chariot, A., and Close, P. (2017). tRNA Modification: Is Cancer Having a Wobble? *Trends Cancer* 3, 249–252. doi:10.1016/j.trecan.2017.02.004

Rong, D., Sun, G., Wu, F., Cheng, Y., Sun, G., Jiang, W., et al. (2021). Epigenetics: Roles and Therapeutic Implications of Non-coding RNA Modifications in Human Cancers. *Mol. Ther. - Nucleic Acids* 25, 67–82. doi:10.1016/j.omtn.2021.04.021

Ruan, H.-g., Gu, W.-c., Xia, W., Gong, Y., Zhou, X.-l., Chen, W.-y., et al. (2021). METTL3 Is Suppressed by Circular RNA circMETTL3/miR-34c-3p Signaling and Limits the Tumor Growth and Metastasis in Triple Negative Breast Cancer. *Front. Oncol.* 11, 778132. doi:10.3389/fonc.2021.778132

Safra, M., Sas-Chen, A., Nir, R., Winkler, R., Nachshon, A., Bar-Yaacov, D., et al. (2017). The m1A Landscape on Cytosolic and Mitochondrial mRNA at Single-Base Resolution. *Nature* 551, 251–255. doi:10.1038/nature24456

Saikia, M., Fu, Y., Pavon-Eternod, M., He, C., and Pan, T. (2010). Genome-wide Analysis of N1-Methyl-Adenosine Modification in Human tRNAs. *RNA* 16, 1317–1327. doi:10.1261/rna.2057810

Sas-Chen, A., Thomas, J. M., Matzov, D., Taoka, M., Nance, K. D., Nir, R., et al. (2020). Dynamic RNA Acetylation Revealed by Quantitative Cross-Evolutionary Mapping. *Nature* 583, 638–643. doi:10.1038/s41586-020-2418-2

Shi, Y., Zheng, C., Jin, Y., Bao, B., Wang, D., Hou, K., et al. (2020). Reduced Expression of METTL3 Promotes Metastasis of Triple-Negative Breast Cancer by m6A Methylation-Mediated COL3A1 Up-Regulation. *Front. Oncol.* 10, 1126. doi:10.3389/fonc.2020.01126

Shibata, T., Watari, K., Kawahara, A., Sudo, T., Hattori, S., Murakami, Y., et al. (2020). Targeting Phosphorylation of Y-Box-Binding Protein YBX1 by TAS0612 and Everolimus in Overcoming Antiestrogen Resistance. *Mol. Cancer Ther.* 19, 882–894. doi:10.1158/1535-7163.mct-19-0690

Shiromoto, Y., Sakurai, M., Minakuchi, M., Ariyoshi, K., and Nishikura, K. (2021). ADAR1 RNA Editing Enzyme Regulates R-Loop Formation and Genome Stability at Telomeres in Cancer Cells. *Nat. Commun.* 12, 1654. doi:10.1038/s41467-021-21921-x

Song, Y., Zheng, C., Tao, Y., Huang, R., and Zhang, Q. (2021). N6-Methyladenosine Regulators Are Involved in the Progression of and Have Clinical Impact on Breast Cancer. *Med. Sci. Monit.* 27, e929615. doi:10.12659/msm.929615

Su, R., Dong, L., Li, Y., Gao, M., Han, L., Wunderlich, M., et al. (2020). Targeting FTO Suppresses Cancer Stem Cell Maintenance and Immune Evasion. *Cancer Cell* 38, 79–96. doi:10.1016/j.ccell.2020.04.017

Su, R., Dong, L., Li, Y., Gao, M., He, P. C., Liu, W., et al. (2022). METTL16 Exerts an m^{6}A-independent Function to Facilitate Translation and Tumorigenesis. *Nat. Cell Biol.* 24, 205–216. doi:10.1038/s41556-021-00835-2

Sun, T., Wu, Z., Wang, X., Wang, Y., Hu, X., Qin, W., et al. (2020). LNC942 Promoting METTL14-Mediated m^{6}A Methylation in Breast Cancer Cell Proliferation and Progression. *Oncogene* 39, 5358–5372. doi:10.1038/s41388-020-1338-9

Tang, Y., Gao, C.-C., Gao, Y., Yang, Y., Shi, B., Yu, J.-L., et al. (2020). OsNSUN2-Mediated 5-Methylcytosine mRNA Modification Enhances Rice Adaptation to High Temperature. *Dev. Cell* 53, 272–286. doi:10.1016/j.devcel.2020.03.009

Van Der Werf, I., and Jamieson, C. (2019). The Yin and Yang of RNA Methylation: An Imbalance of Erasers Enhances Sensitivity to FTO Demethylase Small-Molecule Targeting in Leukemia Stem Cells. *Cancer Cell* 35, 540–541. doi:10.1016/j.ccell.2019.03.011

Wan, W., Ao, X., Chen, Q., Yu, Y., Ao, L., Xing, W., et al. (2022). METTL3/IGF2BP3 axis Inhibits Tumor Immune Surveillance by Upregulating N^6-Methyladenosine Modification of PD-L1 mRNA in Breast Cancer. *Mol. Cancer* 21, 60. doi:10.1186/s12943-021-01447-y

Wang, C.-Q., Tang, C.-H., Wang, Y., Huang, B.-F., Hu, G.-N., Wang, Q., et al. (2022). Upregulated WTAP Expression Appears to Both Promote Breast Cancer Growth and Inhibit Lymph Node Metastasis. *Sci. Rep.* 12, 1023. doi:10.1038/s41598-022-05035-y

Wang, H., Xu, B., and Shi, J. (2020). N6-methyladenosine METTL3 Promotes the Breast Cancer Progression via Targeting Bcl-2. *Gene* 722, 144076. doi:10.1016/j.gene.2019.144076

Wang, S., Zou, X., Chen, Y., Cho, W. C., and Zhou, X. (2020). Effect of N6-Methyladenosine Regulators on Progression and Prognosis of Triple-Negative Breast Cancer. *Front. Genet.* 11, 580036. doi:10.3389/fgene.2020.580036

Woo, H.-H., and Chambers, S. K. (2019). Human ALKBH3-Induced m^1A Demethylation Increases the CSF-1 mRNA Stability in Breast and Ovarian Cancer Cells. *Biochimica Biophysica Acta (BBA) - Gene Regul. Mech.* 1862, 35–46. doi:10.1016/j.bbagrm.2018.10.008

Wood, S., Willbanks, A., and Cheng, J. X. (2021). The Role of RNA Modifications and RNA-Modifying Proteins in Cancer Therapy and Drug Resistance. *Ccdt* 21, 326–352. doi:10.2174/1568009621666210127092828

Wu, J., Cai, Y., Zhao, G., and Li, M. (2021). A Ten N6-Methyladenosine-Related Long Non-coding RNAs Signature Predicts Prognosis of Triple-Negative Breast Cancer. *J. Clin. Lab. Anal.* 35, e23779.

Wu, L., Wu, D., Ning, J., Liu, W., and Zhang, D. (2019). Changes of N6-Methyladenosine Modulators Promote Breast Cancer Progression. *BMC Cancer* 19, 326. doi:10.1186/s12885-019-5538-z

Wu, Y., Wang, Z., Han, L., Guo, Z., Yan, B., Guo, L., et al. (2022). PRMT5 Regulates RNA m6A Demethylation for Doxorubicin Sensitivity in Breast Cancer. *Mol. Ther.* S1525–0016 (22), 00160–00165. doi:10.1016/j.ymthe.2022.03.003

Xiao, L., Li, X., Mu, Z., Zhou, J., Zhou, P., Xie, C., et al. (2020). FTO Inhibition Enhances the Antitumor Effect of Temozolomide by Targeting MYC-miR-155/23a Cluster-MXI1 Feedback Circuit in Glioma. *Cancer Res.* 80, 3945–3958. doi:10.1158/0008-5472.can-20-0132

Xing, S., Li, Z., Ma, W., He, X., Shen, S., Wei, H., et al. (2019). DIS3L2 Promotes Progression of Hepatocellular Carcinoma via hnRNP U-Mediated Alternative Splicing. *Cancer Res.* 79, 4923–4936. doi:10.1158/0008-5472.can-19-0376

Xu, Y., Ye, S., Zhang, N., Zheng, S., Liu, H., Zhou, K., et al. (2020). The FTO/miR-181b-3p/ARL5B Signaling Pathway Regulates Cell Migration and Invasion in Breast Cancer. *Cancer Commun.* 40, 484–500. doi:10.1002/cac2.12075

Xue, C., Zhao, Y., Li, G., and Li, L. (2021). Multi-Omic Analyses of the m^5C Regulator ALYREF Reveal its Essential Roles in Hepatocellular Carcinoma. *Front. Oncol.* 11, 633415. doi:10.3389/fonc.2021.633415

Yang, B., Wang, J.-Q., Tan, Y., Yuan, R., Chen, Z.-S., and Zou, C. (2021). RNA Methylation and Cancer Treatment. *Pharmacol. Res.* 174, 105937. doi:10.1016/j.phrs.2021.105937

Yang, C., Wu, T., Zhang, J., Liu, J., Zhao, K., Sun, W., et al. (2021). Prognostic and Immunological Role of mRNA ac4C Regulator NAT10 in Pan-Cancer: New Territory for Cancer Research? *Front. Oncol.* 11, 630417. doi:10.3389/fonc.2021.630417

Yang, L., Wu, S., Ma, C., Song, S., Jin, F., Niu, Y., et al. (2020). RNA m^6A Methylation Regulators Subclassify Luminal Subtype in Breast Cancer. *Front. Oncol.* 10, 611191. doi:10.3389/fonc.2020.611191

Yang, X., Yang, Y., Sun, B.-F., Chen, Y.-S., Xu, J.-W., Lai, W.-Y., et al. (2017). 5-methylcytosine Promotes mRNA Export - NSUN2 as the Methyltransferase and ALYREF as an m^5C Reader. *Cell Res.* 27, 606–625. doi:10.1038/cr.2017.55

Yankova, E., Blackaby, W., Albertella, M., Rak, J., De Braekeleer, E., Tsagkogeorga, G., et al. (2021). Small-molecule Inhibition of METTL3 as a Strategy against Myeloid Leukaemia. *Nature* 593, 597–601. doi:10.1038/s41586-021-03536-w

Yi, D., Wang, R., Shi, X., Xu, L., Yilihamu, Y., and Sang, J. (2020). METTL14 Promotes the Migration and Invasion of Breast Cancer Cells by Modulating N6-methyladenosine and hsamiR146a5p Expression. *Oncol. Rep.* 43, 1375–1386. doi:10.3892/or.2020.7515

Yi, J., Gao, R., Chen, Y., Yang, Z., Han, P., Zhang, H., et al. (2017). Overexpression of NSUN2 by DNA Hypomethylation Is Associated with Metastatic Progression in Human Breast Cancer. *Oncotarget* 8, 20751–20765. doi:10.18632/oncotarget.10612

Zaccara, S., and Jaffrey, S. R. (2020). A Unified Model for the Function of YTHDF Proteins in Regulating m^6A-Modified mRNA. *Cell* 181, 1582–1595. doi:10.1016/j.cell.2020.05.012

Zhang, B., Gu, Y., and Jiang, G. (2020). Expression and Prognostic Characteristics of M^6 A RNA Methylation Regulators in Breast Cancer. *Front. Genet.* 11, 604597. doi:10.3389/fgene.2020.604597

Zhang, C., Zhi, W. I., Lu, H., Samanta, D., Chen, I., Gabrielson, E., et al. (2016). Hypoxia-inducible Factors Regulate Pluripotency Factor Expression by ZNF217- and ALKBH5-Mediated Modulation of RNA Methylation in Breast Cancer Cells. *Oncotarget* 7, 64527–64542. doi:10.18632/oncotarget.11743

Zhang, J., Shan, B., Lin, L., Dong, J., Sun, Q., Zhou, Q., et al. (2021). Dissecting the Role of N6-Methylandenosine-Related Long Non-coding RNAs Signature in Prognosis and Immune Microenvironment of Breast Cancer. *Front. Cell Dev. Biol.* 9, 711859. doi:10.3389/fcell.2021.711859

Zhang, X., Dai, X.-Y., Qian, J.-Y., Xu, F., Wang, Z.-W., Xia, T., et al. (2022). SMC1A Regulated by KIAA1429 in m6A-independent Manner Promotes EMT Progress in Breast Cancer. *Mol. Ther. - Nucleic Acids* 27, 133–146. doi:10.1016/j.omtn.2021.08.009

Zhao, B. S., Roundtree, I. A., and He, C. (2017). Post-transcriptional Gene Regulation by mRNA Modifications. *Nat. Rev. Mol. Cell Biol.* 18, 31–42. doi:10.1038/nrm.2016.132

Zheng F, F., Du, F., Qian, H., Zhao, J., Wang, X., Yue, J., et al. (2021). Expression and Clinical Prognostic Value of m6A RNA Methylation Modification in Breast Cancer. *Biomark. Res.* 9, 28. doi:10.1186/s40364-021-00285-w

Zheng, Q.-K., Ma, C., Ullah, I., Hu, K., Ma, R.-J., Zhang, N., et al. (2021). Roles of N6-Methyladenosine Demethylase FTO in Malignant Tumors Progression. *Onco Targets Ther.* 14, 4837–4846. doi:10.2147/ott.s329232

Zheng, G., Dahl, J. A., Niu, Y., Fedorcsak, P., Huang, C.-M., Li, C. J., et al. (2013). ALKBH5 Is a Mammalian RNA Demethylase that Impacts RNA Metabolism and Mouse Fertility. *Mol. Cell* 49, 18–29. doi:10.1016/j.molcel.2012.10.015

Zhu, P., He, F., Hou, Y., Tu, G., Li, Q., Jin, T., et al. (2021). A Novel Hypoxic Long Noncoding RNA KB-1980E6.3 Maintains Breast Cancer Stem Cell Stemness via Interacting with IGF2BP1 to Facilitate C-Myc mRNA Stability. *Oncogene* 40, 1609–1627. doi:10.1038/s41388-020-01638-9

Conflict of Interest: The authors declare that the research was conducted in the absence of any commercial or financial relationships that could be construed as a potential conflict of interest.

Publisher's Note: All claims expressed in this article are solely those of the authors and do not necessarily represent those of their affiliated organizations, or those of the publisher, the editors and the reviewers. Any product that may be evaluated in this article, or claim that may be made by its manufacturer, is not guaranteed or endorsed by the publisher.

Copyright © 2022 Liu, Zhu, Jiang, Bu, Zhu and Gu. This is an open-access article distributed under the terms of the Creative Commons Attribution License (CC BY). The use, distribution or reproduction in other forums is permitted, provided the original author(s) and the copyright owner(s) are credited and that the original publication in this journal is cited, in accordance with accepted academic practice. No use, distribution or reproduction is permitted which does not comply with these terms.

GLOSSARY

APC adenomatous polyposis coli
ABCB1 ATP binding cassette subfamily B member 1
ARL5B ADP ribosylation factor like GTPase5B
AGR2 anterior gradient 2
AK4 adenylate kinase 4
ADARs adenosine deaminases acting on RNA
ALKBH5 Demethylases ALKB homolog 5
ac^{4}C N4-acetylcytodine
AURKA aurora kinase a
ATF3 transcription factor 3
BNIP3 BCL2 Interacting Protein 3
C5aR1 C5a Receptor 1
COL3A1 collagen type III alpha 1 chain
CTU1 cytoplasmic trna2 thiolated protein 1
CDS coding sequence
CDK1 cyclin-dependent kinase 1
CYP1B1 cytochrome p450 family 1 subfamily B member 1
CSF-1 macrophage-colony stimulating factor-1
DLGAP1-AS1 lncRNA DLGAP1 antisense RNA 1
eIF3 eukaryotic initiation factor 3
EGFR epidermal growth factor receptor
EMT epithelial-to-mesenchymal transition
ENO1 enolase 1
EGOT eosinophil granule ontogeny transcript
E2F1 E2F transcription factor 1
FTO Fat mass and obesity-related protein
HBXIP hepatitis B X-interacting protein
hnRNP heterogeneous nuclear ribonucleoprotein
IL interlukin
IGF2BP1 insulin-like growth factor 2 mRNA-binding protein 1
KRT7 keratin 7
NSUN2 NOP2/sun RNA methyltransferase 2
GJA1 gap junction protein alpha 1
GRM3 glutamate metabotropic receptor 3
MALAT1 metastasis associated lung adenocarcinoma transcript 1
MTC methyltransferase complex
METTL3 methyltransferase-like 3
METT14 methyltransferase-like 14
MAPK mitogen-activated protein kinase
OG oxoglutarate oxygenase
rRNA ribosomal RNA
tRNA transport RNA
mRNA messenger RNA
ncRNA non coding RNA
m^{6}A N6-methyladenosine
3'UTR 3'untranslated region
mcm5s2U 5-methoxycarbonylmethyl-2-thiouridine
RBM15 RNA binding motif protein 15
STC1 stanniocalcin 1
TNBC triple-negative breast cancer
TNF tumor-necrosis-factor
ROS reactive oxygen species
SMC1A chromosomes 1a
ST6GALNAC5 ST6 beta-galactoside alpha-2,6-sialyltransferase
RAD52 DNA repair protein RAD52 homolog
SAH S-adenosylhomocysteine
SPHK sphingosine kinase
TRM tRNA methyltransferase 10 homologue A
WATP wilms tumor 1 associated protein
ZC3H13 zinc finger CCCHType Containing 13
METTL16 methyltransferase like 16
YTHDF YTH domain family
YTHDC YTH domain-containing protein
TRDMT1 tRNA aspartic acid methyltransferase 1
TRM4B tRNA-specific methyltransferase 4B
YBX1 Y-box binding protein 1
WBSCR22 Williams Beuren syndrome chromosome 22 region protein
YBX1 Y-box binding protein 1

frontiers | Frontiers in Cell and Developmental Biology

ORIGINAL RESEARCH
published: 07 July 2022
doi: 10.3389/fcell.2022.882994

The Maternal Microbiome Programs the m^{6}A Epitranscriptome of the Mouse Fetal Brain and Intestine

Zhuoyu Xiao[1†], Sun Liu[1†], Zengguang Li[1†], Jinru Cui[1], Hailan Wang[1], Zihan Wang[1], Qihuan Ren[1], Laixin Xia[1], Zhijian Wang[2]* and Yuan Li[1]**

[1]Department of Developmental Biology, School of Basic Medical Sciences, Southern Medical University, Guangzhou, China, [2]Department of Obstetrics and Gynecology, Nanfang Hospital, Southern Medical University, Guangzhou, China

OPEN ACCESS

Edited by:
Huilin Huang,
Sun Yat-sen University Cancer Center (SYSUCC), China

Reviewed by:
Huizhe Wu,
China Medical University, China
Pengze Yan,
Dana–Farber Cancer Institute, United States
Yu Hou,
Chongqing Medical University, China

***Correspondence:**
Laixin Xia
xialx@smu.edu.cn
Zhijian Wang
wzjnfyy@163.com
Yuan Li
gavin@smu.edu.cn

[†]These authors have contributed equally to this work

Specialty section:
This article was submitted to Epigenomics and Epigenetics, a section of the journal Frontiers in Cell and Developmental Biology

Received: 24 February 2022
Accepted: 06 June 2022
Published: 07 July 2022

Citation:
Xiao Z, Liu S, Li Z, Cui J, Wang H, Wang Z, Ren Q, Xia L, Wang Z and Li Y (2022) The Maternal Microbiome Programs the m^{6}A Epitranscriptome of the Mouse Fetal Brain and Intestine. Front. Cell Dev. Biol. 10:882994. doi: 10.3389/fcell.2022.882994

The microbiome exerts profound effects on fetal development and health, yet the mechanisms underlying remain elusive. N6-methyladenosine (m^{6}A) plays important roles in developmental regulation. Although it has been shown that the microbiome affects the mRNA m^{6}A modification of the host, it remains unclear whether the maternal microbiome affects m^{6}A epitranscriptome of the fetus so as to impact fetal development. Here, we found that loss of the maternal microbiome altered the expression of m^{6}A writers and erasers, as well as the m^{6}A methylome of the mouse fetal brain and intestine on embryonic day 18. From the m^{6}A profiles, we identified 2,655 and 2,252 m^{6}A modifications regulated by the maternal microbiome in the fetal brain and intestine, respectively, and we demonstrated that these m^{6}A-modified genes were enriched in the neuro/intestinal developmental pathways, such as the Wnt signaling pathway. Finally, we verified that antibiotic treatment mostly recapitulated changes in m^{6}A, and we further showed that the loss of heterozygosity of *Mettl3* rescued m^{6}A levels and the expression changes of some developmental genes in the fetal intestine that resulted from antibiotic treatment. Collectively, our data revealed that the maternal microbiome programs the m^{6}A epitranscriptome of the mouse fetal brain and intestine.

Keywords: maternal microbiome, m^{6}A, fetal development, Wnt signaling pathway, METTL3

INTRODUCTION

It is universally recognized that the microbiome exerts profound effects on host physiology and health, including host metabolism, circadian rhythm, intestinal morphology, and the development of the nervous system (Zhang et al., 2020; Brooks et al., 2021; Seki et al., 2021; Willyard, 2021; Wu J. et al., 2021; Wu Q. et al., 2021). Emerging studies have revealed that loss of the maternal microbiome impairs axonogenesis (Vuong et al., 2020), and that maternal exposure to antibiotics contributes to gut dysbiosis, immune dysfunction, and the occurrence of inflammatory bowel disease (IBD) in offspring (Miyoshi et al., 2017). These findings indicated that loss of the maternal microbiome impairs the fetal development and neonatal health in early life. However, the mechanisms underlying the actions of the maternal microbiome on the fetus remain elusive.

N6-methyladenosine (m^{6}A) has been shown to be the most abundant and a highly conserved modification on messenger RNAs (mRNAs) and lncRNAs in mammals (Dominissini et al., 2012; Zhao et al., 2017a; Liu et al., 2020; Shu et al., 2020; Deng et al., 2021). mRNA m^{6}A possesses a consensus motif of RRACH (R denoting G or A, and H reflecting A, C, or U) and it is principally found at stop codons, 3′untranslated regions (3′UTRs), and long exons (Dominissini et al., 2012;

Roundtree et al., 2017). m^{6}A is produced by the METTL3–METTL14 core methyltransferase complex (Liu et al., 2014; Liu X. et al., 2021), erased by demethylases FTO and ALKBH5 (Jia et al., 2011; Zheng et al., 2013; Roundtree et al., 2017), and recognized by readers such as the YTH family proteins (Dominissini et al., 2012; Wang X. et al., 2014; Alarcón et al., 2015). m^{6}A regulates various physiological processes, such as RNA stability (Dominissini et al., 2012; Wang X. et al., 2014; Alarcón et al., 2015; Huang et al., 2018), splicing (Xiao et al., 2016; Ke et al., 2017), translation (Meyer et al., 2015; Wang et al., 2015; Zhou et al., 2015; Shi et al., 2017), and signaling pathways (Li H.-B. et al., 2017; Huang H. et al., 2019; Uddin et al., 2021). Also, it occupies important roles in stem cell self-renewal (Li et al., 2018; Liu J. et al., 2021), embryonic development (Batista et al., 2014; Wang Y. et al., 2014; Chen et al., 2015; Geula et al., 2015; Vu et al., 2017; Bertero et al., 2018), tissue development (Zheng et al., 2013; Li H.-B. et al., 2017; Yoon et al., 2017; Zhao et al., 2017b; Wang et al., 2018), tumorigenesis (Ma et al., 2016; Li Z et al., 2017; Su et al., 2018; Huang Y et al., 2019; Su et al., 2020; Chen et al., 2021), and the progression of other human diseases (Fischer et al., 2009; Church et al., 2010; Mathiyalagan et al., 2019). It has been shown that the microbiome affects the mRNA m^{6}A modification on the host tissues, especially the brain, intestine, and liver (Wang et al., 2019; Jabs et al., 2020). However, it remains unclear whether the maternal microbiome affects m^{6}A epitranscriptome of the fetal brain, intestine, and liver so as to impact fetal development.

Herein, we demonstrated that the expression of m^{6}A writers and erasers in the brain and intestine of the mouse fetus is altered by the maternal microbiome. Using MeRIP-seq, we systematically investigated the transcriptome-wide m^{6}A methylome profiles of the mouse fetal brain and intestine, and we discovered that the maternal microbiome programs the fetal m^{6}A methylome, and that m^{6}A-modified genes regulated by the maternal microbiome are enriched in fetal neuro/intestine developmental pathways, such as the Wnt signaling. More importantly, antibiotic treatment recapitulated m^{6}A alterations in the mouse fetal intestine and brain, and loss of heterozygosity of *Mettl3* rescued this effect. Our findings collectively indicate that the maternal microbiome programs the m^{6}A epitranscriptome of the mouse fetal brain and intestine, and this may provide a promising basis to explore the mechanisms by which the maternal microbiome influences fetal development and diseases.

MATERIALS AND METHODS

Fetal Tissues Collection From SPF and GF Mice

Specific pathogen-free (SPF) pregnant mice ($n = 3$) and germ-free (GF) pregnant mice ($n = 3$) purchased from GemPharmatech Co., Ltd. were dissected on embryonic day 18 (E18), and the fetal tissues (brain, intestine, and liver) were collected and stored at −80°C for subsequent analyses.

PCR Amplification and qPCR Analysis of 16S rRNA Genes

A total of 40 mg mouse fecal pellets were suspended in 200 μl lysis buffer (5 mM EDTA, 0.2% SDS, 0.2M NaCl, and 0.1M Tris-HCl) supplemented with 4 μl of 20 mg/ml proteinase K. The mixtures were disrupted with a grinding rod and then incubated at 56 °C for 6 h. After centrifugation, the supernatant was used for 16S rRNA gene amplification, and the PCR products were visualized on a 2% agarose gel stained with ethidium bromide under UV light. The supernatant from CONV and ABX mice was used for the 16S rRNA gene qPCR analysis. The 16S rRNA gene was detected using two sets of universal bacterial primers: 27F and 1492R; 8F and 1541R. The primers are listed in **Supplementary Table S1**.

Tissues Lysate Preparation and Western Blots

Frozen tissues were homogenized and lysed in RIPA buffer (50 mM Tris-HCl pH 7.5, 1% Nonidet P-40, 0.5% sodium deoxycholate, 0.05% SDS, 1 mM EDTA, and 150 mM NaCl) with freshly added phosphorylase inhibitors and protease inhibitors, and then centrifuged for 20 min at 13,000 × g. The supernatant was aspirated and loaded for the Western immunoblotting analysis. The following antibodies are used: METTL3 (A8370, Abclonal, 1:1,000), METTL14 (HPA038002, Sigma-Aldrich, 1:1,000), FTO (27226-1-AP, Proteintech, 1:1,000), ALKBH5 (16837-1-AP, Proteintech, 1:1,000), and β-actin (66009-1-Ig, Proteintech, 1:5,000).

RNA Isolation and mRNA Purification

Fetal mouse tissues were homogenized in 1 ml of TRNzol Universal Reagent (TIANGEN) with glass beads using a LUKYM-I homogenizer, and total RNA was isolated following the manufacturer's protocol. mRNA was separated from total RNA using a Dynabeads mRNA purification kit (Thermo Fisher Scientific), with two rounds of purification.

LC-MS/MS Quantification of m^{6}A mRNA Modification

LC-MS/MS was performed essentially as described previously (Li et al., 2020). In brief, purified mRNA was digested to nucleosides by nuclease P1 and CIAP, and then it was diluted to 10 ng/μl using nuclease-free water. The samples were filtered and injected into an Agilent Poroshell 120 column coupled online to an AB SCIEX Triple Quad 5500 LC mass spectrometer (Applied Biosystems) in a positive electrospray ionization mode. Concentrations of m^{6}A and A were determined based on standard curves of the nucleosides, and the m^{6}A/A ratio was calculated.

RT-qPCR

Total RNA (5 μg) from fetal mouse tissues was reverse-transcribed using a GoScript Reverse Transcription System (Promega), and quantitative real-time PCR was executed using a 2 × RealStar Green Power Mixture (GenStar). The fluorescence intensity of the amplification process was monitored using a LightCycler96 system (Roche). The primers are listed in **Supplementary Table S2**.

Methylated RNA Immunoprecipitation Sequencing

MeRIP experiments were executed as previously reported (Xiao et al., 2019). In brief, approximately 90 μg of total RNA was fragmented into 100- to 300-nucleotide (nt)-long fragments by zinc acetate, followed by the addition of EDTA to terminate the reaction. Then, 5 μg of fragmented RNA was taken as the input control and the remainder was incubated with m^{6}A antibodies (4 μg, Abcam, ab151230) in IP buffer (150 mM NaCl, 0.05% NP-40, and 10 mM Tris-HCl) containing RNase inhibitor (Promega), and the mixture was subsequently bound to wash Dynabeads protein G (Invitrogen). After stringent wash, the m^{6}A-containing fragments were eluted by competition with 1 mg/ml N6-methyladenosine (Selleck Chemicals). Both the immunoprecipitated RNA fragments and the input RNA were ultimately extracted for library construction using a SMARTer Stranded Total RNA-Seq Kit v2 - Pico Input Mammalian (Takara) following the manufacturer's protocol. We then performed sequencing using an Illumina Nova platform.

MeRIP-Seq Data Processing and Mapping

Prior to mapping, all raw data were filtered to remove adapters, and low-quality reads using Trimmomatic (Bolger et al., 2014). Reads of all samples that mapped to rRNA FASTA sequences from UCSC gene annotation (mm10) using bowtie2 (Langmead and Salzberg, 2012) were discarded, and the remaining reads were aligned to the mouse reference genome (GRCm38) using HISAT2 (Pertea et al., 2016). Then mapped files were filtered to keep unique and high mapping quality reads for further analysis using Picard and SAMtools (Li et al., 2009).

m^{6}A Peak Calling

m^{6}A peaks were identified using MeTPeak. A custom transcriptome annotation file, assembled by StringTie (Pertea et al., 2016) using all sample reads, was created to include intronic and intergenic m^{6}A peaks. All other parameters were set to the default settings. The annotatePeaks.pl script from the Homer software suite (Heinz et al., 2010) was used for m^{6}A peak annotation.

Evaluation of the Similarity of m^{6}A Between Samples

m^{6}A peaks identified in all samples were merged, and featureCounts (Liao et al., 2014) was used to count the fragments that were mapped to the merged peaks. The normalized fragment counts of each peak in MeRIP-seq (MFPKM) were calculated using (methylated fragment counts mapped to the peak × 10^9)/(length of the peak × total counts of the mapped fragment), and the normalized fragment counts of each peak in input-seq (IFPKM) were calculated using (input fragment counts mapped to the peak × 10^9)/(length of the peak × total counts of mapped fragments). The methylation level was then calculated for each peak by dividing the MFPKM by the IFPKM. The Pearson correlation coefficient of log2-scaled m^{6}A levels across all samples was calculated using corrplot to represent the similarity of each sample.

Determination of m^{6}A Motif and Distribution Pattern

m^{6}A peaks were used for motif search using the findMotifsGenome.pl script from the Homer software suite, using "-rna" and "-len 5" parameters. The R package Guitar (Cui et al., 2016) was used to analyze and plot the distribution of m^{6}A on mRNA.

Identification of Differentially Methylated Regions

The regions in which the GF group mean m^{6}A level was 1.5 fold higher than the SPF group mean m^{6}A level were defined as GF group up regions. Also, the regions in which the GF group mean m^{6}A level was 1.5 fold lower than the SPF group mean m^{6}A level were defined as GF group down regions.

Gene Ontology Analysis of Differential m^{6}A-Methylated Genes

Differentially methylated regions were assigned to mouse genes using the annotatePeaks.pl script from the Homer software suite. The gene list was used for pathways and GO term enrichment using the clusterProfiler (Wu T. et al., 2021).

MeRIP-qPCR

The input RNA and the immunoprecipitated RNA fragments from mouse fetal tissues were reverse-transcribed using a GoScript Reverse Transcription System (Promega), and then they were analyzed using real-time qPCR. The ratio of immunoprecipitated RNA to the input of each peak was calculated and normalized to GAPDH. The primers are listed in **Supplementary Table S3**.

Cell Culture and Cell Line Generation

Mouse embryonic stem cell line E14TG2a (mES cells) was cultured with the N2B27 base medium supplemented with 1 mM glutamine (Invitrogen), 1% nonessential amino acids (Invitrogen), 0.15 mM 1-thioglycerol (Sigma), 100 U/ml of penicillin–streptomycin (Invitrogen), 25 μg/ml of BSA (Sigma), 1 μM MEK inhibitor PD0325901 (Selleck Chemicals), 3 μM GSK3β inhibitor CHIR99021 (Selleck Chemicals), 2% KOSR (Thermo Fisher), and 1000 U/ml of ESGRO leukemia inhibitory factor LIF (Millipore) on plates coated with 0.2% gelatin.

Mettl3$^{-/-}$ mES Cell Line Generation

The Mettl3$^{-/-}$ mES cell line was generated using CRISPR-Cas9 as described previously (Shalem et al., 2014) and the sgRNA sequences are shown in **Supplementary Table S4**. In brief, sgRNAs were designed on http://crispr-era.stanford.edu/and cloned into the pXPR_001 plasmid. Then, pXPR_001 plasmid was transfected into mES cells using Lipofectamine 3000 (Invitrogen, L3000015). After 12 h, 3 μg/ml of puromycin was added and resistant cells were plated for single colony isolation. Colonies with the desired mutation were identified by Sanger sequencing.

RNA Stability Assay

mES cells cultured in 12-well plates at 70–80% confluency were treated with actinomycin D (5 μg/ml final concentration, MCE, HY-17559) for 0, 2, 4, and 8 h before being collected for the extraction of total RNA. RNA was then reverse-transcribed using GoScript Reverse Transcriptase (Promega), and analyzed using real-time qPCR. Expression levels of RNA were calculated and normalized to *GAPDH* first, and then to the 0 h time point. The mRNA stability of genes was estimated by the half-life of mRNA and calculated using GraphPad Prism 5.0. The primers are listed in **Supplementary Table S3**.

Animals

All of the mice were group-housed in a temperature-controlled (22 ± 1 ˚C) room with a 12:12-h light:dark cycle, and they had free access to food and water. *Mettl3*$^{flox/+}$ mice were generated by Cyagen by inserting loxP sites with the same direction on both sides of exons 2 and 3 of the *Mettl3* gene. Male *Mettl3*$^{flox/+}$ mice were crossed with female *Mettl3*$^{flox/+}$ mice to obtain *Mettl3*$^{flox/flox}$ mice. Next, *Mettl3*$^{flox/flox}$ mice were first crossed with DDX4-Cre mice to generate *Mettl3*$^{flox/+}$; DDX4-Cre mice, and the latter were then crossed with wild-type mice to generate *Mettl3*$^{-/+}$ heterozygous mice. The genotype of each mouse was determined using the genomic DNA extracted from tail tissue.

Antibiotic Treatment of Mice

To mimic GF status, conventional mice (CONV) were treated with antibiotics (ABX), based on methods previously described (Vuong et al., 2020). In brief, 10- to 12 -weeks-old female mice were provided with a mixture of four antibiotics (vancomycin 0.5 g/L, neomycin 1 g/L, ampicillin 1 g/L, and amphotericin-B 0.1 g/L) in their water for 1 week. Female mice were then paired with male mice and gestational day 0.5 was determined by observation of a copulatory plug. Pregnant mice (n = 3) were maintained on ABX in their drinking water until embryonic day 18 (E18), and then dissected to obtain fetal tissues (brain and intestine).

Statistical Analysis

We expressed our measurement data as mean ± SEM. *T* tests were used for comparisons between two groups. Significant differences were represented by asterisks as follows: $^*p < 0.05$, $^{**}p < 0.01$, and $^{***}p < 0.001$, and ns, not significant.

RESULTS

Loss of the Maternal Microbiome Alters the Expression of m^{6}A Writers and Erasers in the Fetal Brain and Intestine

We initially collected fecal pellets from germ-free (GF, n = 3) and specific pathogen-free (SPF, n = 3) pregnant mice, and the absence of intestinal microbiota in the GF mice was confirmed by 16S rRNA gene amplification (**Supplementary Figure S1A**). We, then, examined the levels of m^{6}A regulators in the mouse fetal brain, intestine, and liver, including writers (METTL3 and METTL14), erasers (FTO and ALKBH5), and readers (YTH-domain family proteins). Using RT-qPCR, we determined that mRNA levels of m^{6}A writers and erasers are highly expressed in the fetal brain and intestine from GF pregnant mice (hereafter designated GFB and GFI, respectively) compared to the corresponding tissues from SPF pregnant mice (hereafter designated SPFB and SPFI, respectively). However, the differences in m^{6}A reader expression levels are much less marked (**Figures 1A,B**). Nevertheless, the expression of these proteins is similar in the fetal livers of these two types of mice (**Supplementary Figure S1B**). A similar tendency in the alteration of protein expression is also uncovered using the Western blotting analysis (**Figures 1C,D**). Taken together, these results indicated that loss of the maternal microbiome alters the expression of m^{6}A writers and erasers in the fetal brain and intestine.

m^{6}A Modification Profiles in the Fetal Brain and Intestine

To further investigate whether the maternal microbiome participates in modulating the m^{6}A epitranscriptome of offspring, we first detected total m^{6}A levels of mouse fetal tissues. We did not observe an apparent change in the global mRNA m^{6}A levels between SPF and GF mice as revealed by LC-MS/MS (**Supplementary Figure S2A**). We, thus, characterized m^{6}A methylomes of both mouse fetal brain and intestine (SPFB and GFB and SPFI and GFI—using two independent biological replicates for both) by an m^{6}A-immunoprecipitation sequencing (MeRIP-seq) analysis. The samples of the same tissue type were clustered well (**Figure 2A**) and the classic GGAC motif was observed in the fetal brain and intestine (**Figure 2B**). In agreement with previous studies (Dominissini et al., 2012; Roundtree et al., 2017), the distribution of m^{6}A signals around mRNA in the two types of fetal tissue samples was mostly presented in the CDS and 3'UTR, and to a lesser extent in the 5'UTR (**Figure 2C**). We identified the numbers of m^{6}A peaks from these fetal tissues (17,526 in SPFB, 16,885 in GFB, 14,436 in SPFI, and 13,781 in GFI), and we ascertained that approximately three-fourths of the m^{6}A peaks overlapped in both fetal brain and intestine (**Figure 2D**). Compared with SPFB, GFB showed some changes in patterns of m^{6}A peaks, with a relative elevation in exonic (SPF 26.81% vs. GFB 28%) and intronic regions (SPF 27.86% vs. GFB 29.38%), and a relative diminution in the 3'untranslated region

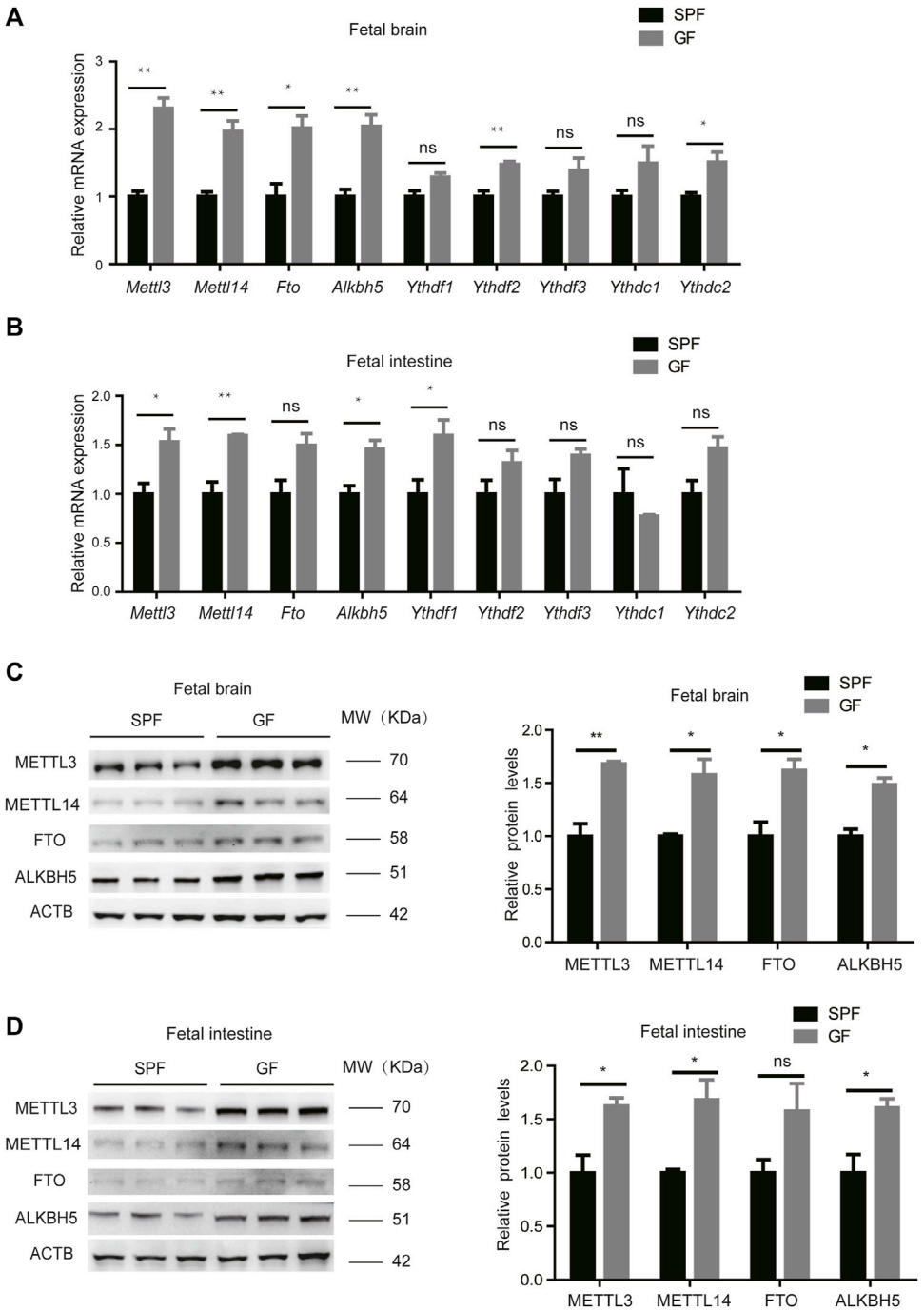


FIGURE 1 | Loss of the maternal microbiome alters the expression of m^{6}A writers and erasers in fetal mice. **(A,B)** Relative mRNA expression levels of m^{6}A writers, erasers, and readers in fetal brains **(A)** and intestines **(B)** of SPF and GF mice. **(C,D)** Western blots showing the protein expression of m^{6}A writers and erasers in fetal brains **(C)** and intestines **(D)** of SPF and GF mice, and relative protein expression levels were calculated based on the band density in Western blotting results.

(3'UTR) from 18 to 16.96% (**Figure 2E**). Compared with SPFI, the GFI also showed some alterations in patterns of m^{6}A peaks with a relative augmentation in exonic regions (SPFI 30.68% vs. GFI 32.5%), and a relative reduction in intronic regions from 30.12 to 29.18% and intergenic regions of 7.7–6.41% (**Figure 2F**).

The Maternal Microbiome Regulates the m^{6}A of Neurodevelopment Genes in the Mouse Fetal Brain

To investigate the dynamic characteristics of m^{6}A methylation, we further analyzed the differential m^{6}A peaks in mouse fetal

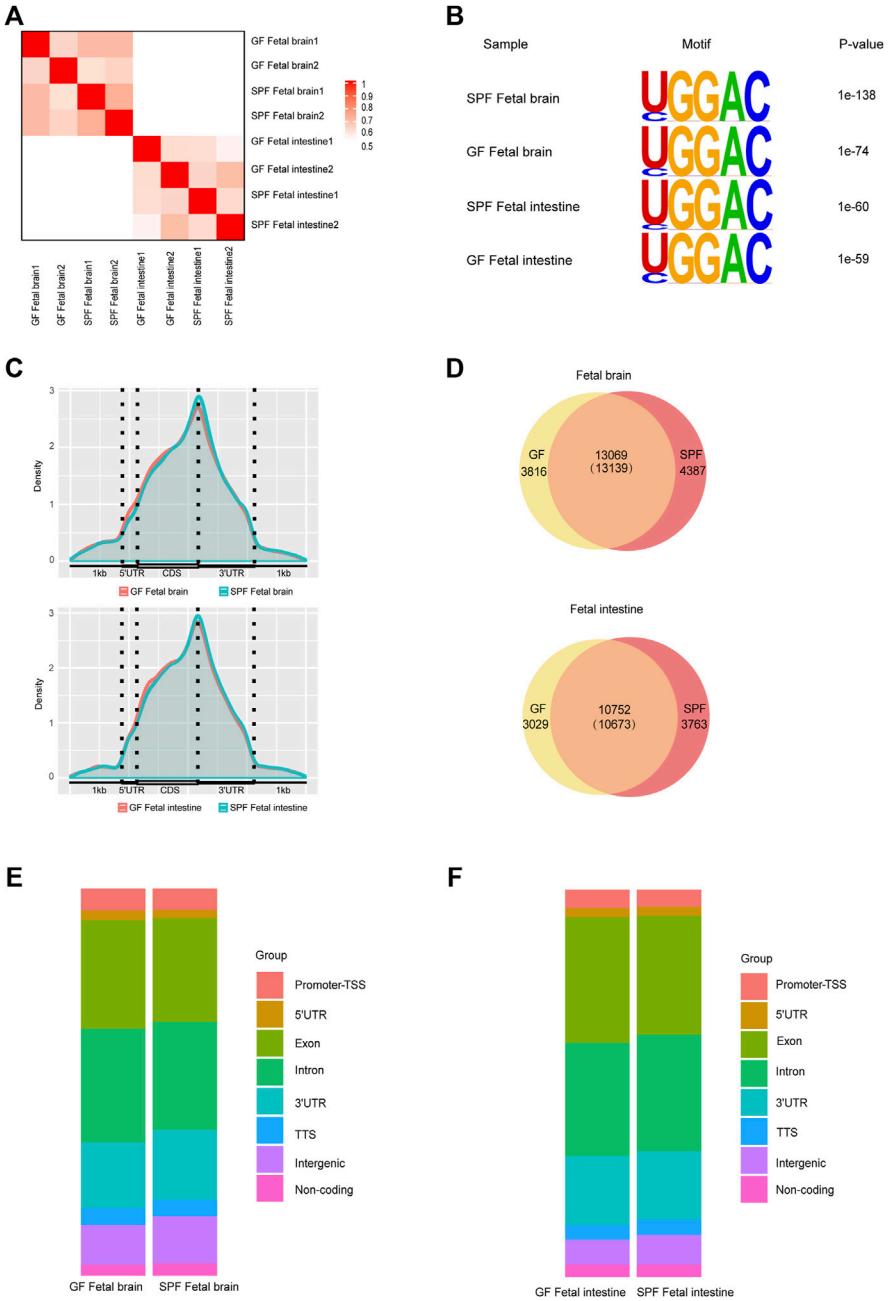


FIGURE 2 | Modification profiles of m^{6}A in the fetal brain and intestine. **(A)** Similarity (using Pearson's correlation) of m^{6}A peaks between each pair of samples. **(B)** Motif analysis of m^{6}A peaks in fetal brains and intestines of SPF and GF mice. **(C)** Pattern distribution of m^{6}A across the mRNA regions in the fetal brain and intestine. m^{6}A peaks were mapped back to the corresponding genes, and assigned as originating from the 5′-UTR, coding sequence (CDS), or 3′-UTR. **(D)** Venn diagram showing the overlap of m^{6}A peaks between fetal brains and intestines of SPF and GF mice. **(E,F)** Bar charts showing the distribution of m^{6}A peaks in the fetal brain **(E)** and intestine **(F)**.

tissues. As shown in **Figure 3A**, GFB manifested 2072 upregulated m^{6}A peaks and 583 downregulated m^{6}A peaks (with the criterion of fold-change ≥1.5). In further examination of the genomic distribution in all three mRNA regions of differential m^{6}A peaks, we demonstrated that a majority of the differential m^{6}A peaks were in CDS and 3'UTR (**Supplementary Figure S3A**). Mapping these reads of differential m^{6}A peaks to the genome, we identified 1147 genes with upregulated m^{6}A peaks and 496 genes with downregulated m^{6}A peaks (**Supplementary Figure S3B**). To further study the biological significance of dysregulated m^{6}A modifications in the fetal brain, we conducted GO analyses of differentially m^{6}A-methylated genes (**Figure 3B** and **Supplementary Figure S3C**). We concentrated on the function of m^{6}A-hypermethylated

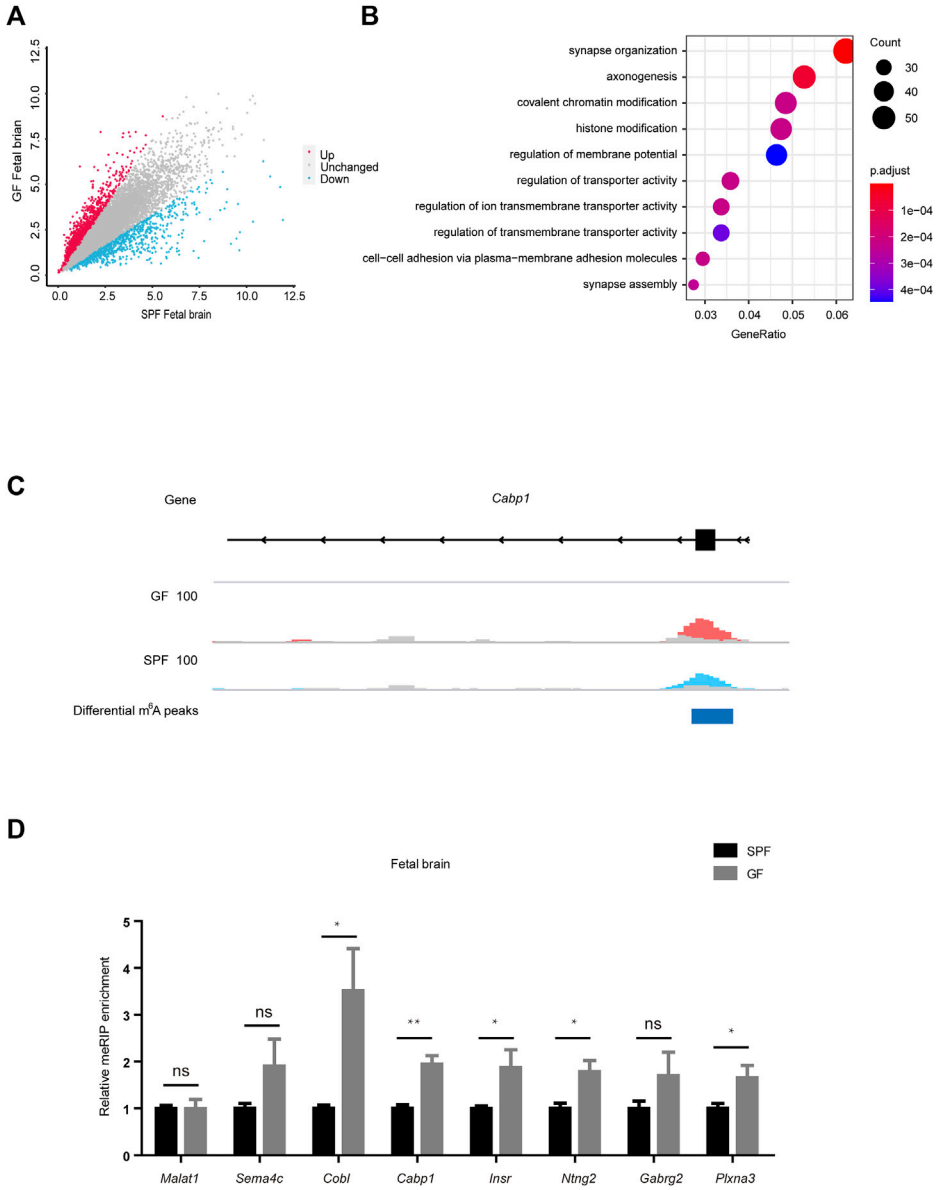


FIGURE 3 | Maternal microbiome regulates the m^{6}A of neurodevelopment genes in the mouse fetal brain. **(A)** Scatter diagram shows the number of differential m^{6}A peaks in the GF fetal brain. **(B)** Gene ontology-enrichment analysis of genes containing upregulated m^{6}A peaks in the GF fetal brain. **(C)** Integrated genome viewer (IGV) shows the distribution of representative differential m^{6}A peaks in *Cabp1*. GF IP, SPF IP, and input are shown in red, blue, and gray, respectively. **(D)** Validation of the relative m^{6}A enrichments of *Sema4c*, *Cobl*, *Cabp1*, *Insr*, *Ntng2*, *Gabrg2*, and *Plxna3* in SPF and GF fetal brains by m^{6}A-immunoprecipitation (IP)-qPCR.

genes and showed that these genes were significantly enriched in pathways related to neurodevelopment, such as synapse formation and axonogenesis. The read coverage plot of a representative gene *Cabp1* associated with neurodevelopment was depicted in **Figure 3C**, and the m^{6}A levels of genes (*Sema4c*, *Cobl*, *Cabp1*, *Insr*, *Ntng2*, *Gabrg2*, and *Plxna3*) were increased in GFB as revealed by using the MeRIP-qPCR analysis (**Figure 3D**). In addition, the transcript levels of these genes were confirmed by using the RT-qPCR analysis (**Supplementary Figure S3D**). Collectively, these data suggest that the maternal microbiome regulates the m^{6}A of neurodevelopment genes in the mouse fetal brain.

The Maternal Microbiome Regulates Fetal Intestinal m^{6}A-Modified Genes in the Wnt Signaling Pathway

As shown in **Figure 4A**, GFI reflected 2068 upregulated m^{6}A peaks and 184 downregulated m^{6}A peaks (with a fold-change ≥1.5). Further examination of the genomic distribution in all three mRNA regions of

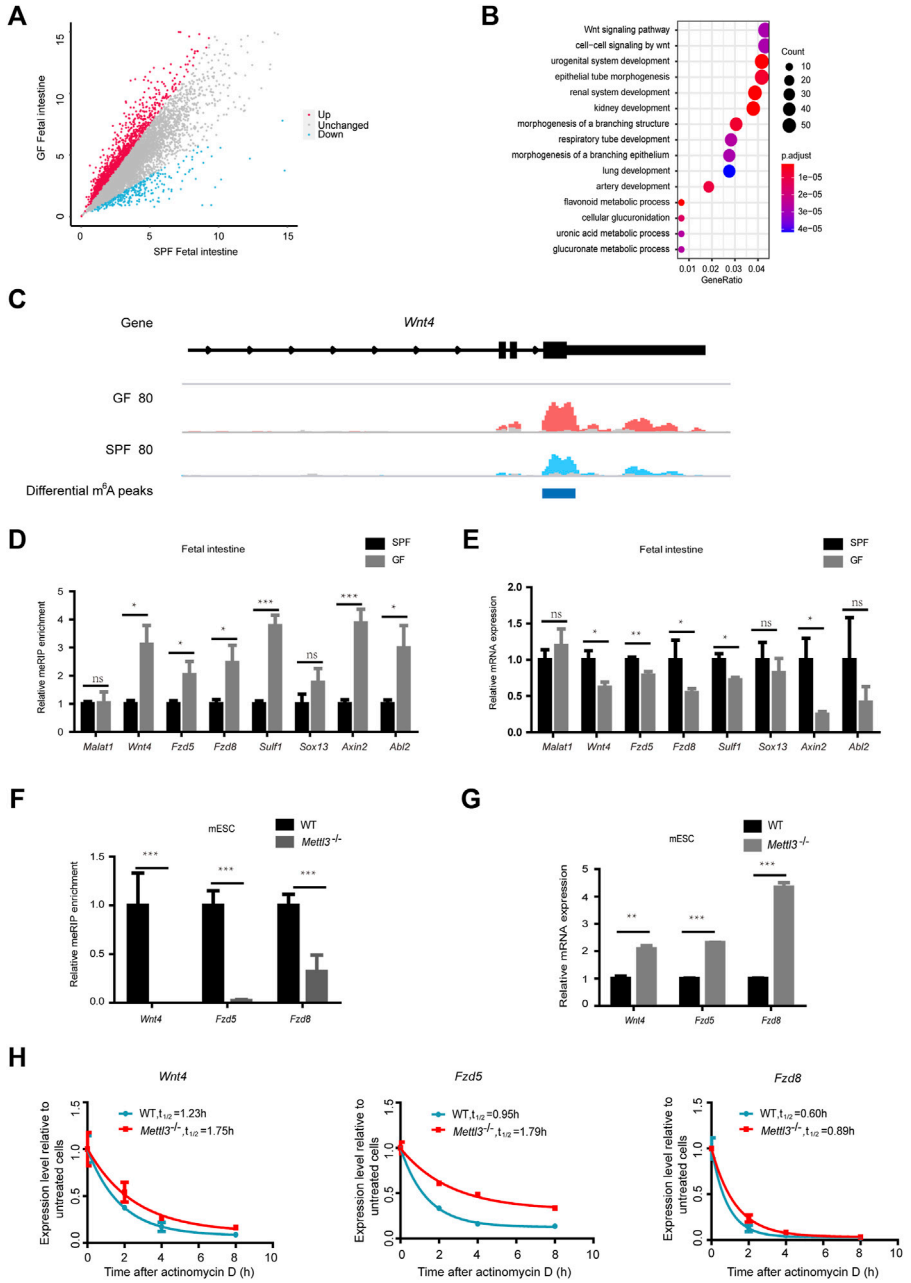


FIGURE 4 | Maternal microbiome regulates fetal intestinal m^{6}A-modified genes in the Wnt signaling pathway. **(A)** Scatter diagram shows the number of differential m^{6}A peaks in the GF fetal intestine. **(B)** Gene ontology-enrichment analysis of genes containing upregulated m^{6}A peaks in the GF fetal intestine. **(C)** IGV shows the distribution of representative differential m^{6}A peaks in *Wnt4*. GF IP, SPF IP, and input are shown in red, blue, and gray, respectively. **(D)** Validation of the relative m^{6}A enrichments of *Wnt4*, *Fzd5*, *Fzd8*, *Sulf1*, *Sox13*, *Axin2*, and *Abl2* in SPF and GF fetal intestines by m^{6}A-immunoprecipitation (IP)-qPCR. **(E)** Validation of the relative mRNA expression levels of *Wnt4*, *Fzd5*, *Fzd8*, *Sulf1*, *Sox13*, *Axin2*, and *Abl2* in SPF and GF fetal intestines. **(F)** Validation of the relative m^{6}A enrichments of *Wnt4*, *Fzd5*, and *Fzd8* in the WT and *Mettl3*$^{-/-}$ mouse embryonic stem cell line E14TG2a by m^{6}A-immunoprecipitation (IP)-qPCR. **(G)** Validation of the relative mRNA expression levels of *Wnt4*, *Fzd5*, and *Fzd8* in the WT and *Mettl3*$^{-/-}$ mouse embryonic stem cell line E14TG2a. **(H)** Half-life ($t_{1/2}$) of *Wnt4*, *Fzd5*, and *Fzd8* mRNA in the WT and *Mettl3*$^{-/-}$ mouse embryonic stem cell line E14TG2a after actinomycin D treatment.

the differential m^{6}A peaks revealed that most of the differential m^{6}A peaks were in CDS and 3′UTR (**Supplementary Figure S4A**). When we mapped these reads of differential m^{6}A peaks to the genome, we identified 1590 genes with upregulated m^{6}A peaks and 166 genes with downregulated m^{6}A peaks (**Supplementary Figure S4B**). To further assess the biological significance of dysregulated m^{6}A modification in the fetal intestine, we executed GO analysis of differentially m^{6}A-methylated genes (**Figure 4B** and **Supplementary Figure S4C**). When we concentrated on the functions of m^{6}A-hypermethylated genes, we found that they were significantly

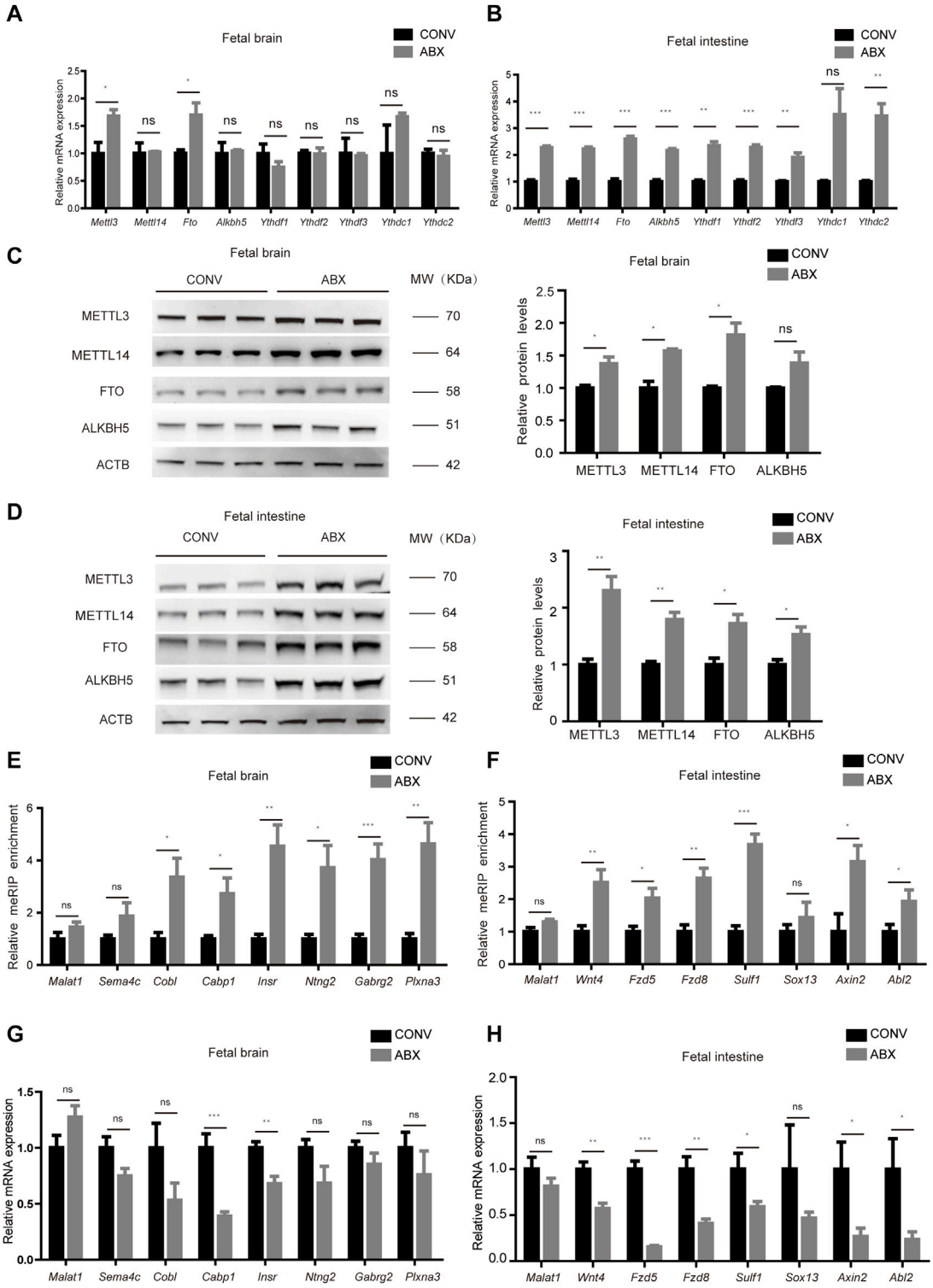


FIGURE 5 | Antibiotic treatment mostly recapitulates m^{6}A alterations in the mouse fetal intestine and brain. **(A,B)** Relative mRNA expression levels of m^{6}A writers and erasers in CONV and ABX fetal brains **(A)** and intestines **(B)**. **(C,D)** Western blot shows the protein expression levels of m^{6}A writers and erasers in fetal brains **(C)** and intestines **(D)** of CONV and ABX mice, and relative protein expression levels were calculated based on the band density in Western blotting results. **(E,G)** Validation of the relative m^{6}A enrichment of *Sema4c*, *Cobl*, *Cabp1*, *Insr*, *Ntng2*, *Gabrg2*, and *Plxna3* in CONV and ABX fetal brains **(E)** and of *Wnt4*, *Fzd5*, *Fzd8*, *Sulf1*, *Sox13*, *Axin2*, and *Abl2* in CONV and ABX fetal intestines **(G)** by m^{6}A-immunoprecipitation (IP)-qPCR. **(F,H)** Validation of the relative mRNA expression levels of *Sema4c*, *Cobl*, *Cabp1*, *Insr*, *Ntng2*, *Gabrg2*, and *Plxna3* in CONV and ABX fetal brains **(F)** and of *Wnt4*, *Fzd5*, *Fzd8*, *Sulf1*, *Sox13*, *Axin2*, and *Abl2* in CONV and ABX fetal intestines **(H)**.

enriched in the Wnt signaling pathway. The read coverage plot of a representative gene *Wnt4* is shown in **Figure 4C**. The differential m^{6}A levels of representative genes (*Wnt4*, *Fzd5*, *Fzd8*, *Sulf1*, *Sox13*, *Axin2*, and *Abl2*) were confirmed by the MeRIP-qPCR analysis (**Figure 4D**), and their transcript levels were all attenuated in GFI compared to SPFI as revealed by the RT-qPCR analysis (**Figure 4E**). This indicates that differential m^{6}A modifications in these two types of fetal intestines are correlated with the expression of genes enriched in the Wnt signaling pathways. Next, we knocked out *Mettl3* (*Mettl3*$^{-/-}$) in the mES cell line using CRISPR/Cas9, and we consistently found that *Mettl3* knockout significantly decreased m^{6}A levels of representative genes while increasing mRNA expression levels (**Figures 4F,G**). We further investigated whether the changes in m^{6}A methylation would affect mRNA levels of representative genes in mESC. We observed that in the presence of actinomycin D (an inhibitor of mRNA transcription), *Mettl3* knockout retards the degradation of representative genes mRNAs (**Figure 4H**). Collectively, these data suggest that the maternal microbiome regulates fetal intestinal m^{6}A-modified genes in the Wnt signaling pathway.

Antibiotic Treatment Mostly Recapitulates m^{6}A Change in the Mouse Fetal Intestine and Brain

To confirm the aforementioned results, we treated CONV pregnant mice with a mixture of four antibiotics (vancomycin, neomycin, ampicillin, and amphotericin-B) to mimic germ-free status (ABX mice) and validated that intestinal microbiota were almost exhausted by the 16S rRNA gene qPCR analysis (**Supplementary Figure S5A**). Similar to our previous experimental results, the mRNA expression levels of *Mettl3* and *Fto* in the ABX fetal brain were slightly higher than those in the CONV fetal brain (**Figure 5A**), while the mRNA expression levels of both m^{6}A writers and erasers in the ABX fetal intestine were significantly increased compared to the CONV fetal intestine (**Figure 5B**). In addition, the expression of these proteins remained unchanged in fetal livers from both CONV and ABX (**Supplementary Figure S5B**). As for the protein expression levels of m^{6}A writers and erasers, we noted a universal tendency for them to increase in the ABX fetal brain and intestine (**Figures 5C,D**). We then determined the m^{6}A levels and the expression of representative genes regulated by the maternal microbiome in the ABX and CONV fetal brain and intestine, and we found that the m^{6}A levels of these genes in the ABX brain and intestine were also increased relative to CONV (**Figures 5E,F**), and their transcript levels were confirmed by the RT-qPCR analysis (**Figures 5G,H**). Collectively, these data show that antibiotic treatment mostly recapitulates m^{6}A alterations in the mouse fetal intestine and brain.

Loss of Heterozygosity of *Mettl3* Inhibits the Susceptibility of the Mouse Fetal Intestine to the Maternal Microbiome

To further confirm that the expression of developmental genes was regulated by m^{6}A as programed by the maternal microbiome, we

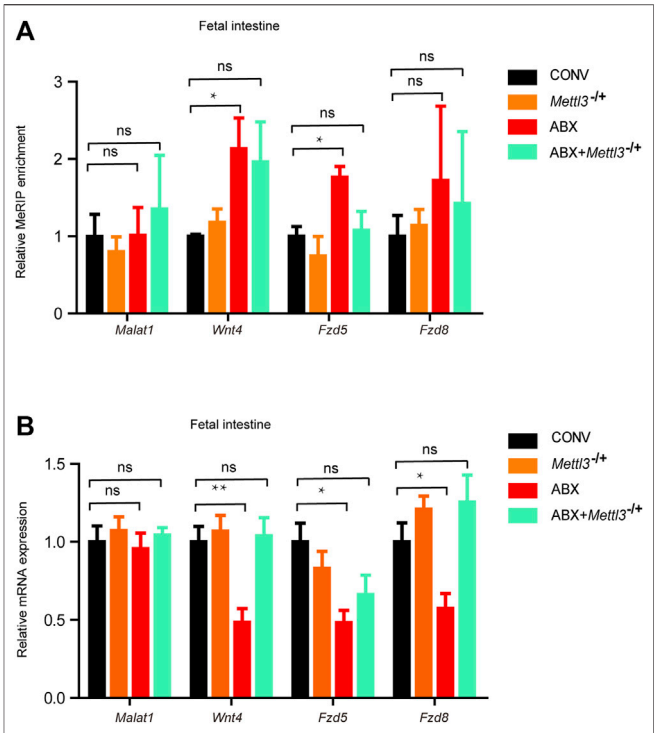


FIGURE 6 | Loss of heterozygosity of *Mettl3* inhibits the susceptibility of the mouse fetal intestine to the maternal microbiome. **(A)** Validation of the relative m^{6}A enrichments of *Wnt4*, *Fzd5*, and *Fzd8* in the intestines of CONV, *Mettl3*$^{-/+}$, ABX, and ABX + *Mettl3*$^{-/+}$ fetal mice by m^{6}A-immunoprecipitation (IP)-qPCR. **(B)** Validation of the relative mRNA expression levels of *Wnt4*, *Fzd5*, and *Fzd8* in the intestines of CONV, *Mettl3*$^{-/+}$, ABX, and ABX + *Mettl3*$^{-/+}$ fetal mice.

generated *Mettl3*$^{-/+}$ heterozygous mice (**Supplementary Figures S6A,B**). Because the homozygous knockout of *Mettl3* was embryonically lethal, we crossed *Mettl3* heterozygous knockout male mice (*Mettl3*$^{-/+}$) with wild-type (WT) female mice. The latter were provided with water (i.e., the offspring of CONV and *Mettl3*$^{-/+}$ mice) or ABX (i.e., the offspring of ABX and ABX + *Mettl3*$^{-/+}$mice). As expected, there were no significant differences in m^{6}A levels of representative genes between CONV and *Mettl3*$^{-/+}$ fetal intestines, however, m^{6}A levels of representative genes increased in the ABX fetal intestine but not in the ABX + *Mettl3*$^{-/+}$ fetal intestine, compared with the CONV fetal intestine (**Figure 6A**). Correspondingly, mRNA expression levels of representative genes showed no differences between CONV and *Mettl3*$^{-/+}$ fetal intestines, while they were significantly reduced in the ABX fetal intestine but not in the ABX + *Mettl3*$^{-/+}$ fetal intestine, compared with the CONV fetal intestine (**Figure 6B**). Our collective results, therefore, indicate that the maternal microbiome affects the developmental gene expression via m^{6}A modifications.

DISCUSSION

The microbiome and m^{6}A modifications are closely related to human health and disease, and previous studies have shown that host m^{6}A is strongly affected by the mouse microbiome (Wang et al., 2019; Jabs

et al., 2020). However, the impact of the maternal microbiome on the m^{6}A epitranscriptome of the mouse fetus has not yet been elucidated. In this study, we profiled the transcriptome-wide m^{6}A methylome of the mouse fetal brain and intestine, demonstrated the alterations in m^{6}A methylation caused by the maternal microbiome, identified differential m^{6}A peaks, and showed that genes with dysregulated m^{6}A peaks were potentially active in fetal development.

In a recent study, Wang et al. (2019)ascertained that both m^{6}A writers and erasers were highly overexpressed in the GF brain compared to the SPF brain regardless of RNA and protein levels. Intriguingly, our results also revealed that the maternal microbiome also altered the expression of m^{6}A writers and erasers in the mouse fetal brain and intestine, and that expression was recapitulated by antibiotic treatment.

Previous studies have depicted depletion of the maternal microbiome as impairing fetal thalamocortical axonogenesis (Vuong et al., 2020). Our results suggested that loss of the maternal microbiome contributed to m^{6}A-hypermethylated genes in GFB, and that these genes were significantly enriched in pathways related to neurodevelopment, including synapse formation and axonogenesis. Moreover, the mRNA expression levels of these m^{6}A-hypermethylated genes were commensurately altered, implying that m^{6}A plays a key role in effects engendered by the maternal microbiome on fetal neurodevelopment. It is worth noting that increasing evidence reveals a functional link between gut bacteria and neurodegenerative diseases such as Alzheimer's disease and Parkinson's diseases (Sampson et al., 2016; Bhattarai et al., 2021; Willyard, 2021), and the abnormality in m^{6}A is involved in neurological dysfunction and behavioral defects (Mitropoulos et al., 2017; Chen et al., 2019; Han et al., 2020; Huang et al., 2020). However, although it remains elusive whether the regulation of fetal neurodevelopment by the maternal gestational microbiome increases the risk of neurologic diseases in adulthood, we expect that the elucidation of such a mechanism will provide a foundation for future novel treatments of nerve diseases.

The Wnt signaling pathway is highly conserved from nematodes to mammals (Kohn and Moon, 2005; Clevers and Nusse, 2012) and is involved in many aspects of embryonic development (Clevers, 2006; MacDonald et al., 2009). Current evidence indicates that the Wnt signaling pathway regulates the self-renewal or differentiation of intestinal stem cells (Reya and Clevers, 2005; Böttcher et al., 2021). Our results showed that upregulated m^{6}A genes in GFI were enriched in the Wnt signaling pathway but that mRNA expression levels of these genes were downregulated compared with SPFI, the mechanism of which is that m^{6}A accelerates the degradation of these genes mRNA. These results reveal that the maternal microbiome regulates the gene expression in Wnt signaling by m^{6}A in the fetal intestine, and this may constitute a mechanism whereby loss of the maternal microbiome impairs fetal intestinal development. In addition, maternal exposure to antibiotics promotes gut dysbiosis and increases the risk of inflammatory bowel diseases in offspring (Miyoshi et al., 2017). Although such data suggest that the maternal gestational microbiome exerts a critical effect on the onset and progression of intestinal diseases in offspring, the precise role of m^{6}A in this action requires further clarification.

For further verification, we treated conventional mice (CONV) with antibiotics (ABX) to mimic GF status. Although antibiotic treatment mostly recapitulates m^{6}A change in mouse fetus, some differences in m^{6}A epitranscriptome between GF and ABX mouse still exist. For example, the mRNA expression levels of *Mettl14* and *Alkbh5* were increased in GFB but not in the ABX mouse fetal brain, which may be caused by some individual differences among different mice due to age, nutritional status, or other factors (Jabs et al., 2020). In addition, ABX treatments are unable to completely eradicate the microbiome so there still exists a small amount (about 5%) of the microbiome in ABX mice compared with GF mice, and the acute or subacute aseptic state simulated by antibiotic treatment is not exactly the same as the chronic rearing under an aseptic environment for a long time (Vuong et al., 2020), which may also be some important reasons why the m^{6}A epitranscriptome of GF mouse has some difference from the ABX mouse.

Collectively, our data reveal programing of the maternal microbiome on m^{6}A modifications in the mouse fetus and should assist in unveiling the underlying mechanisms by which gut dysbiosis precipitates human disease. With progressively maturing analyses and technical developments, we expect that m^{6}A will evolve into a potential therapeutic target of microbiota-directed disease.

DATA AVAILABILITY STATEMENT

The datasets presented in this study can be found in online repositories. The names of the repository and accession number can be found as follows: http://bigd.big.ac.cn/gsa, CRA006146.

ETHICS STATEMENT

The animal study was reviewed and approved by the Southern Medical University Experimental Animal Ethics Committee. Guangzhou. China.

AUTHOR CONTRIBUTIONS

YL, ZhW, and LX designed and supervised the project. ZX, SL, ZL, JC, HW, ZiW, and QR performed experiments. ZL and JC

conducted the bioinformatic analysis. YL and ZX wrote the manuscript with input from all authors.

FUNDING

This work was supported by the National Key R&D Program of China (grant nos. 2019YFA802303 and 2021YFA0805400), the Guangdong Basic and Applied Basic Research Foundation (grant no. 2022A1515011821), National Demonstration Center for Experimental Education of Basic Medical Sciences (Southern Medical University).

ACKNOWLEDGMENTS

We thank S. Xiao for discussion and critical reading of the manuscript.

SUPPLEMENTARY MATERIAL

The Supplementary Material for this article can be found online at: https://www.frontiersin.org/articles/10.3389/fcell.2022.882994/full#supplementary-material

REFERENCES

Alarcón, C. R., Goodarzi, H., Lee, H., Liu, X., Tavazoie, S., and Tavazoie, S. F. (2015). HNRNPA2B1 Is a Mediator of m^{6}A-dependent Nuclear RNA Processing Events. *Cell* 162 (6), 1299–1308. doi:10.1016/j.cell.2015.08.011

Batista, P. J., Molinie, B., Wang, J., Qu, K., Zhang, J., Li, L., et al. (2014). m^{6}A RNA Modification Controls Cell Fate Transition in Mammalian Embryonic Stem Cells. *Cell Stem Cell* 15 (6), 707–719. doi:10.1016/j.stem.2014.09.019

Bertero, A., Brown, S., Madrigal, P., Osnato, A., Ortmann, D., Yiangou, L., et al. (2018). The SMAD2/3 Interactome Reveals that TGFβ Controls m^{6}A mRNA Methylation in Pluripotency. *Nature* 555 (7695), 256–259. doi:10.1038/nature25784

Bhattarai, Y., Si, J., Pu, M., Ross, O. A., McLean, P. J., Till, L., et al. (2021). Role of Gut Microbiota in Regulating Gastrointestinal Dysfunction and Motor Symptoms in a Mouse Model of Parkinson's Disease. *Gut Microbes* 13 (1), 1866974. doi:10.1080/19490976.2020.1866974

Bolger, A. M., Lohse, M., and Usadel, B. (2014). Trimmomatic: A Flexible Trimmer for Illumina Sequence Data. *Bioinformatics* 30 (15), 2114–2120. doi:10.1093/bioinformatics/btu170

Böttcher, A., Büttner, M., Tritschler, S., Sterr, M., Aliluev, A., Oppenländer, L., et al. (2021). Non-canonical Wnt/PCP Signalling Regulates Intestinal Stem Cell Lineage Priming towards Enteroendocrine and Paneth Cell Fates. *Nat. Cell Biol.* 23 (1), 23–31. doi:10.1038/s41556-020-00617-2

Brooks, J. F., Behrendt, C. L., Ruhn, K. A., Lee, S., Raj, P., Takahashi, J. S., et al. (2021). The Microbiota Coordinates Diurnal Rhythms in Innate Immunity with the Circadian Clock. *Cell* 184 (16), 4154–4167. doi:10.1016/j.cell.2021.07.001

Chen, H., Gao, S., Liu, W., Wong, C.-C., Wu, J., Wu, J., et al. (2021). RNA N6-Methyladenosine Methyltransferase METTL3 Facilitates Colorectal Cancer by Activating the m^{6}A-GLUT1-mTORC1 axis and Is a Therapeutic Target. *Gastroenterology* 160 (4), 1284–1300. doi:10.1053/j.gastro.2020.11.013

Chen, T., Hao, Y.-J., Zhang, Y., Li, M.-M., Wang, M., Han, W., et al. (2015). m^{6}A RNA Methylation Is Regulated by MicroRNAs and Promotes Reprogramming to Pluripotency. *Cell Stem Cell* 16 (3), 289–301. doi:10.1016/j.stem.2015.01.016

Chen, X., Yu, C., Guo, M., Zheng, X., Ali, S., Huang, H., et al. (2019). Down-Regulation of m^{6}A mRNA Methylation Is Involved in Dopaminergic Neuronal Death. *ACS Chem. Neurosci.* 10 (5), 2355–2363. doi:10.1021/acschemneuro.8b00657

Church, C., Moir, L., McMurray, F., Girard, C., Banks, G. T., Teboul, L., et al. (2010). Overexpression of Fto Leads to Increased Food Intake and Results in Obesity. *Nat. Genet.* 42 (12), 1086–1092. doi:10.1038/ng.713

Clevers, H., and Nusse, R. (2012). Wnt/β-Catenin Signaling and Disease. *Cell* 149 (6), 1192–1205. doi:10.1016/j.cell.2012.05.012

Clevers, H. (2006). Wnt/β-Catenin Signaling in Development and Disease. *Cell* 127 (3), 469–480. doi:10.1016/j.cell.2006.10.018

Cui, X., Wei, Z., Zhang, L., Liu, H., Sun, L., Zhang, S.-W., et al. (2016). Guitar: An R/Bioconductor Package for Gene Annotation Guided Transcriptomic Analysis of RNA-Related Genomic Features. *BioMed Res. Int.* 2016, 1–8. doi:10.1155/2016/8367534

Deng, S., Zhang, H., Zhu, K., Li, X., Ye, Y., Li, R., et al. (2021). M6A2Target: A Comprehensive Database for Targets of m^{6}A Writers, Erasers and Readers. *Brief. Bioinform.* 22 (3), bbaa055. doi:10.1093/bib/bbaa055

Dominissini, D., Moshitch-Moshkovitz, S., Schwartz, S., Salmon-Divon, M., Ungar, L., Osenberg, S., et al. (2012). Topology of the Human and Mouse m^{6}A RNA Methylomes Revealed by m^{6}A-Seq. *Nature* 485 (7397), 201–206. doi:10.1038/nature11112

Fischer, J., Koch, L., Emmerling, C., Vierkotten, J., Peters, T., Brüning, J. C., et al. (2009). Inactivation of the Fto Gene Protects from Obesity. *Nature* 458 (7240), 894–898. doi:10.1038/nature07848

Geula, S., Moshitch-Moshkovitz, S., Dominissini, D., Mansour, A. A., Kol, N., Salmon-Divon, M., et al. (2015). m^{6}A mRNA Methylation Facilitates Resolution of Naïve Pluripotency toward Differentiation. *Science* 347 (6225), 1002–1006. doi:10.1126/science.1261417

Han, M., Liu, Z., Xu, Y., Liu, X., Wang, D., Li, F., et al. (2020). Abnormality of m^{6}A mRNA Methylation Is Involved in Alzheimer's Disease. *Front. Neurosci.* 14, 98. doi:10.3389/fnins.2020.00098

Heinz, S., Benner, C., Spann, N., Bertolino, E., Lin, Y. C., Laslo, P., et al. (2010). Simple Combinations of Lineage-Determining Transcription Factors Prime Cis-Regulatory Elements Required for Macrophage and B Cell Identities. *Mol. Cell* 38 (4), 576–589. doi:10.1016/j.molcel.2010.05.004

Huang, H., Camats-Perna, J., Medeiros, R., Anggono, V., and Widagdo, J. (2020). Altered Expression of the m^{6}A Methyltransferase METTL3 in Alzheimer's Disease. *eNeuro* 7 (5), 0125. doi:10.1523/ENEURO.0125-20.2020

Huang, H., Weng, H., Sun, W., Qin, X., Shi, H., Wu, H., et al. (2018). Recognition of RNA N6-Methyladenosine by IGF2BP Proteins Enhances mRNA Stability and Translation. *Nat. Cell Biol.* 20 (3), 285–295. doi:10.1038/s41556-018-0045-z

Huang H, H., Weng, H., Zhou, K., Wu, T., Zhao, B. S., Sun, M., et al. (2019). Histone H3 Trimethylation at Lysine 36 Guides m^{6}A RNA Modification Co-transcriptionally. *Nature* 567 (7748), 414–419. doi:10.1038/s41586-019-1016-7

Huang Y, Y., Su, R., Sheng, Y., Dong, L., Dong, Z., Xu, H., et al. (2019). Small-Molecule Targeting of Oncogenic FTO Demethylase in Acute Myeloid Leukemia. *Cancer Cell* 35 (4), 677–691. doi:10.1016/j.ccell.2019.03.006

Jabs, S., Biton, A., Bécavin, C., Nahori, M.-A., Ghozlane, A., Pagliuso, A., et al. (2020). Impact of the Gut Microbiota on the m^{6}A Epitranscriptome of Mouse Cecum and Liver. *Nat. Commun.* 11 (1), 1344. doi:10.1038/s41467-020-15126-x

Jia, G., Fu, Y., Zhao, X., Dai, Q., Zheng, G., Yang, Y., et al. (2011). N6-Methyladenosine in Nuclear RNA Is a Major Substrate of the Obesity-Associated FTO. *Nat. Chem. Biol.* 7 (12), 885–887. doi:10.1038/nchembio.687

Ke, S., Pandya-Jones, A., Saito, Y., Fak, J. J., Vågbø, C. B., Geula, S., et al. (2017). m^{6}A mRNA Modifications Are Deposited in Nascent Pre-mRNA and Are Not Required for Splicing but Do Specify Cytoplasmic Turnover. *Genes Dev.* 31 (10), 990–1006. doi:10.1101/gad.301036.117

Kohn, A. D., and Moon, R. T. (2005). Wnt and Calcium Signaling: B-Catenin-independent Pathways. *Cell Calcium* 38 (3-4), 439–446. doi:10.1016/j.ceca.2005.06.022

Langmead, B., and Salzberg, S. L. (2012). Fast Gapped-Read Alignment with Bowtie 2. *Nat. Methods.* 9 (4), 357–359. doi:10.1038/nmeth.1923

Li H. B, H.-B., Tong, J., Zhu, S., Batista, P. J., Duffy, E. E., Zhao, J., et al. (2017). m^{6}A mRNA Methylation Controls T Cell Homeostasis by Targeting the IL-7/STAT5/SOCS Pathways. *Nature* 548 (7667), 338–342. doi:10.1038/nature23450

Li, H., Handsaker, B., Wysoker, A., Fennell, T., Ruan, J., Homer, N., et al. (2009). The Sequence Alignment/Map Format and SAMtools. *Bioinformatics* 25 (16), 2078–2079. doi:10.1093/bioinformatics/btp352

Li, Y., Xia, L., Tan, K., Ye, X., Zuo, Z., Li, M., et al. (2020). N6-Methyladenosine Co-transcriptionally Directs the Demethylation of Histone H3K9me2. *Nat. Genet.* 52 (9), 870–877. doi:10.1038/s41588-020-0677-3

Li, Z., Qian, P., Shao, W., Shi, H., He, X. C., Gogol, M., et al. (2018). Suppression of m^{6}A Reader Ythdf2 Promotes Hematopoietic Stem Cell Expansion. *Cell Res.* 28 (9), 904–917. doi:10.1038/s41422-018-0072-0

Li Z, Z., Weng, H., Su, R., Weng, X., Zuo, Z., Li, C., et al. (2017). FTO Plays an Oncogenic Role in Acute Myeloid Leukemia as a N 6 -Methyladenosine RNA Demethylase. *Cancer Cell* 31 (1), 127–141. doi:10.1016/j.ccell.2016.11.017

Liao, Y., Smyth, G. K., and Shi, W. (2014). FeatureCounts: An Efficient General Purpose Program for Assigning Sequence Reads to Genomic Features. *Bioinformatics* 30 (7), 923–930. doi:10.1093/bioinformatics/btt656

Liu, J. E., Li, K., Cai, J., Zhang, M., Zhang, X., Xiong, X., et al. (2020). Landscape and Regulation of m^{6}A and m^{6}Am Methylome across Human and Mouse Tissues. *Mol. Cell* 77 (2), 426–440. doi:10.1016/j.molcel.2019.09.032

Liu J, J., Gao, M., He, J., Wu, K., Lin, S., Jin, L., et al. (2021). The RNA m^{6}A Reader YTHDC1 Silences Retrotransposons and Guards ES Cell Identity. *Nature* 591 (7849), 322–326. doi:10.1038/s41586-021-03313-9

Liu, J., Yue, Y., Han, D., Wang, X., Fu, Y., Zhang, L., et al. (2014). A METTL3-METTL14 Complex Mediates Mammalian Nuclear RNA N6-Adenosine Methylation. *Nat. Chem. Biol.* 10 (2), 93–95. doi:10.1038/nchembio.1432

Liu X, X., Wang, H., Zhao, X., Luo, Q., Wang, Q., Tan, K., et al. (2021). Arginine Methylation of METTL14 Promotes RNA N6-Methyladenosine Modification and Endoderm Differentiation of Mouse Embryonic Stem Cells. *Nat. Commun.* 12 (1), 3780. doi:10.1038/s41467-021-24035-6

Ma, J. Z., Yang, F., Zhou, C. C., Liu, F., Yuan, J. H., Wang, F., et al. (2016). METTL14 Suppresses the Metastatic Potential of Hepatocellular Carcinoma by Modulating N 6 -methyladenosine-dependent Primary MicroRNA Processing. *Hepatology* 65 (2), 529–543. doi:10.1002/hep.28885

MacDonald, B. T., Tamai, K., and He, X. (2009). Wnt/β-Catenin Signaling: Components, Mechanisms, and Diseases. *Dev. Cell* 17 (1), 9–26. doi:10.1016/j.devcel.2009.06.016

Mathiyalagan, P., Adamiak, M., Mayourian, J., Sassi, Y., Liang, Y., Agarwal, N., et al. (2019). FTO-dependent N 6 -Methyladenosine Regulates Cardiac Function during Remodeling and Repair. *Circulation* 139 (4), 518–532. doi:10.1161/CIRCULATIONAHA.118.033794

Meyer, K. D., Patil, D. P., Zhou, J., Zinoviev, A., Skabkin, M. A., Elemento, O., et al. (2015). 5′ UTR m^{6}A Promotes Cap-independent Translation. *Cell* 163 (4), 999–1010. doi:10.1016/j.cell.2015.10.012

Mitropoulos, K., Merkouri Papadima, E., Xiromerisiou, G., Balasopoulou, A., Charalampidou, K., Galani, V., et al. (2017). Genomic Variants in the FTO Gene Are Associated with Sporadic Amyotrophic Lateral Sclerosis in Greek Patients. *Hum. Genomics* 11 (1), 30. doi:10.1186/s40246-017-0126-2

Miyoshi, J., Bobe, A. M., Miyoshi, S., Huang, Y., Hubert, N., Delmont, T. O., et al. (2017). Peripartum Antibiotics Promote Gut Dysbiosis, Loss of Immune Tolerance, and Inflammatory Bowel Disease in Genetically Prone Offspring. *Cell Rep.* 20 (2), 491–504. doi:10.1016/j.celrep.2017.06.060

Pertea, M., Kim, D., Pertea, G. M., Leek, J. T., and Salzberg, S. L. (2016). Transcript-level Expression Analysis of RNA-Seq Experiments with HISAT, StringTie and Ballgown. *Nat. Protoc.* 11 (9), 1650–1667. doi:10.1038/nprot.2016.095

Reya, T., and Clevers, H. (2005). Wnt Signalling in Stem Cells and Cancer. *Nature* 434 (7035), 843–850. doi:10.1038/nature03319

Roundtree, I. A., Evans, M. E., Pan, T., and He, C. (2017). Dynamic RNA Modifications in Gene Expression Regulation. *Cell* 169 (7), 1187–1200. doi:10.1016/j.cell.2017.05.045

Sampson, T. R., Debelius, J. W., Thron, T., Janssen, S., Shastri, G. G., Ilhan, Z. E., et al. (2016). Gut Microbiota Regulate Motor Deficits and Neuroinflammation in a Model of Parkinson's Disease. *Cell* 167 (6), 1469–1480. doi:10.1016/j.cell.2016.11.018

Seki, D., Mayer, M., Hausmann, B., Pjevac, P., Giordano, V., Goeral, K., et al. (2021). Aberrant Gut-Microbiota-Immune-Brain axis Development in Premature Neonates with Brain Damage. *Cell Host Microbe* 29 (10), 1558–1572. doi:10.1016/j.chom.2021.08.004

Shalem, O., Sanjana, N. E., Hartenian, E., Shi, X., Scott, D. A., Mikkelsen, T. S., et al. (2014). Genome-Scale CRISPR-Cas9 Knockout Screening in Human Cells. *Science* 343 (6166), 84–87. doi:10.1126/science.1247005

Shi, H., Wang, X., Lu, Z., Zhao, B. S., Ma, H., Hsu, P. J., et al. (2017). YTHDF3 Facilitates Translation and Decay of N(6)-Methyladenosine-Modified RNA. *Cell Res.* 27 (3), 315–328. doi:10.1038/cr.2017.15

Shu, X., Cao, J., Cheng, M., Xiang, S., Gao, M., Li, T., et al. (2020). A Metabolic Labeling Method Detects m^{6}A Transcriptome-wide at Single Base Resolution. *Nat. Chem. Biol.* 16 (8), 887–895. doi:10.1038/s41589-020-0526-9

Su, R., Dong, L., Li, C., Nachtergaele, S., Wunderlich, M., Qing, Y., et al. (2018). R-2HG Exhibits Anti-tumor Activity by Targeting FTO/m^{6}A/MYC/CEBPA Signaling. *Cell* 172 (1-2), 90–105. doi:10.1016/j.cell.2017.11.031

Su, R., Dong, L., Li, Y., Gao, M., Han, L., Wunderlich, M., et al. (2020). Targeting FTO Suppresses Cancer Stem Cell Maintenance and Immune Evasion. *Cancer Cell* 38 (1), 79–96. doi:10.1016/j.ccell.2020.04.017

Uddin, M. B., Wang, Z., and Yang, C. (2021). The m^{6}A RNA Methylation Regulates Oncogenic Signaling Pathways Driving Cell Malignant Transformation and Carcinogenesis. *Mol. Cancer.* 20 (1), 61. doi:10.1186/s12943-021-01356-0

Vu, L. P., Pickering, B. F., Cheng, Y., Zaccara, S., Nguyen, D., Minuesa, G., et al. (2017). The N6-Methyladenosine (m^{6}A)-Forming Enzyme METTL3 Controls Myeloid Differentiation of Normal Hematopoietic and Leukemia Cells. *Nat. Med.* 23 (11), 1369–1376. doi:10.1038/nm.4416

Vuong, H. E., Pronovost, G. N., Williams, D. W., Coley, E. J. L., Siegler, E. L., Qiu, A., et al. (2020). The Maternal Microbiome Modulates Fetal Neurodevelopment in Mice. *Nature* 586 (7828), 281–286. doi:10.1038/s41586-020-2745-3

Wang, X., Li, Y., Chen, W., Shi, H., Eren, A. M., Morozov, A., et al. (2019). Transcriptome-wide Reprogramming of N6-Methyladenosine Modification by the Mouse Microbiome. *Cell Res.* 29 (2), 167–170. doi:10.1038/s41422-018-0127-2

Wang, X., Lu, Z., Gomez, A., Hon, G. C., Yue, Y., Han, D., et al. (2014). N6-methyladenosine-dependent Regulation of Messenger RNA Stability. *Nature* 505 (7481), 117–120. doi:10.1038/nature12730

Wang, X., Zhao, B. S., Roundtree, I. A., Lu, Z., Han, D., Ma, H., et al. (2015). N6-methyladenosine Modulates Messenger RNA Translation Efficiency. *Cell* 161 (6), 1388–1399. doi:10.1016/j.cell.2015.05.014

Wang, Y., Li, Y., Toth, J. I., Petroski, M. D., Zhang, Z., and Zhao, J. C. (2014). N6-methyladenosine Modification Destabilizes Developmental Regulators in Embryonic Stem Cells. *Nat. Cell Biol.* 16 (2), 191–198. doi:10.1038/ncb2902

Wang, Y., Li, Y., Yue, M., Wang, J., Kumar, S., Wechsler-Reya, R. J., et al. (2018). N6-methyladenosine RNA Modification Regulates Embryonic Neural Stem Cell Self-Renewal through Histone Modifications. *Nat. Neurosci.* 21 (2), 195–206. doi:10.1038/s41593-017-0057-1

Willyard, C. (2021). How Gut Microbes Could Drive Brain Disorders. *Nature* 590 (7844), 22–25. doi:10.1038/d41586-021-00260-3

Wu, J., Wang, K., Wang, X., Pang, Y., and Jiang, C. (2021). The Role of the Gut Microbiome and its Metabolites in Metabolic Diseases. *Protein Cell* 12 (5), 360–373. doi:10.1007/s13238-020-00814-7

Wu, Q., Liang, X., Wang, K., Lin, J., Wang, X., Wang, P., et al. (2021). Intestinal Hypoxia-Inducible Factor 2α Regulates Lactate Levels to Shape the Gut Microbiome and Alter Thermogenesis. *Cell Metab.* 33 (10), 1988–2003. doi:10.1016/j.cmet.2021.07.007

Wu, T., Hu, E., Xu, S., Chen, M., Guo, P., Dai, Z., et al. (2021). ClusterProfiler 4.0: A Universal Enrichment Tool for Interpreting Omics Data. *Innovation* 2 (3), 100141. doi:10.1016/j.xinn.2021.100141

Xiao, S., Cao, S., Huang, Q., Xia, L., Deng, M., Yang, M., et al. (2019). The RNA N6-Methyladenosine Modification Landscape of Human Fetal Tissues. *Nat. Cell Biol.* 21 (5), 651–661. doi:10.1038/s41556-019-0315-4

Xiao, W., Adhikari, S., Dahal, U., Chen, Y.-S., Hao, Y.-J., Sun, B.-F., et al. (2016). Nuclear m^{6}A Reader YTHDC1 Regulates mRNA Splicing. *Mol. Cell* 61 (4), 507–519. doi:10.1016/j.molcel.2016.01.012

Yoon, K.-J., Ringeling, F. R., Vissers, C., Jacob, F., Pokrass, M., Jimenez-Cyrus, D., et al. (2017). Temporal Control of Mammalian Cortical Neurogenesis by m^{6}A Methylation. *Cell* 171 (4), 877–889. doi:10.1016/j.cell.2017.09.003

Zhang, X., Chen, B.-d., Zhao, L.-d., and Li, H. (2020). The Gut Microbiota: Emerging Evidence in Autoimmune Diseases. *Trends Mol. Med.* 26 (9), 862–873. doi:10.1016/j.molmed.2020.04.001

Zhao, B. S., Roundtree, I. A., and He, C. (2017a). Post-transcriptional Gene Regulation by mRNA Modifications. *Nat. Rev. Mol. Cell Biol.* 18 (1), 31–42. doi:10.1038/nrm.2016.132

Zhao, B. S., Wang, X., Beadell, A. V., Lu, Z., Shi, H., Kuuspalu, A., et al. (2017b). m^{6}A-dependent Maternal mRNA Clearance Facilitates Zebrafish Maternal-To-Zygotic Transition. *Nature* 542 (7642), 475–478. doi:10.1038/nature21355

Zheng, G., Dahl, J. A., Niu, Y., Fedorcsak, P., Huang, C.-M., Li, C. J., et al. (2013). ALKBH5 Is a Mammalian RNA Demethylase that Impacts RNA Metabolism and Mouse Fertility. *Mol. Cell* 49 (1), 18–29. doi:10.1016/j.molcel.2012.10.015

Zhou, J., Wan, J., Gao, X., Zhang, X., Jaffrey, S. R., and Qian, S.-B. (2015). Dynamic m^{6}A mRNA Methylation Directs Translational Control of Heat Shock Response. *Nature* 526 (7574), 591–594. doi:10.1038/nature15377

Conflict of Interest: The authors declare that the research was conducted in the absence of any commercial or financial relationships that could be construed as a potential conflict of interest.

Publisher's Note: All claims expressed in this article are solely those of the authors and do not necessarily represent those of their affiliated organizations, or those of the publisher, the editors, and the reviewers. Any product that may be evaluated in this article, or claim that may be made by its manufacturer, is not guaranteed or endorsed by the publisher.

Copyright © 2022 Xiao, Liu, Li, Cui, Wang, Wang, Ren, Xia, Wang and Li. This is an open-access article distributed under the terms of the Creative Commons Attribution License (CC BY). The use, distribution or reproduction in other forums is permitted, provided the original author(s) and the copyright owner(s) are credited and that the original publication in this journal is cited, in accordance with accepted academic practice. No use, distribution or reproduction is permitted which does not comply with these terms.

frontiers | Frontiers in Cell and Developmental Biology

REVIEW
published: 13 July 2022
doi: 10.3389/fcell.2022.901510

The Pivotal Role of Chemical Modifications in mRNA Therapeutics

Albert Liu[1,2] *and Xiao Wang*[1,2]*

[1]Department of Chemistry, Massachusetts Institute of Technology, Cambridge, MA, United States, [2]Broad Institute of MIT and Harvard, Cambridge, MA, United States

After over a decade of development, mRNA has recently matured into a potent modality for therapeutics. The advantages of mRNA therapeutics, including their rapid development and scalability, have been highlighted due to the SARS-CoV-2 pandemic, in which the first two clinically approved mRNA vaccines have been spotlighted. These vaccines, as well as multiple other mRNA therapeutic candidates, are modified to modulate their immunogenicity, stability, and translational efficiency. Despite the importance of mRNA modifications for harnessing the full efficacy of mRNA drugs, the full breadth of potential modifications has yet to be explored clinically. In this review, we survey the field of mRNA modifications, highlighting their ability to tune the properties of mRNAs. These include cap and tail modifications, nucleoside substitutions, and chimeric mRNAs, each of which represents a component of mRNA that can be exploited for modification. Additionally, we cover clinical and preclinical trials of the modified mRNA platform not only to illustrate the promise of modified mRNAs but also to call attention to the room for diversifying future therapeutics.

Keywords: mRNA, chemical modifications, RNA modifications, mRNA therapeutics, mRNA vaccine, mocRNA, chimeric mRNA

OPEN ACCESS

Edited by:
Huilin Huang,
Sun Yat-sen University Cancer Center (SYSUCC), China

Reviewed by:
Jia Sheng,
University at Albany, United States
Yun Bai,
ShanghaiTech University, China
Yimeng Gao,
Yale University, United States

***Correspondence:**
Xiao Wang
xwangx@mit.edu

Specialty section:
This article was submitted to Epigenomics and Epigenetics, a section of the journal Frontiers in Cell and Developmental Biology

Received: *22 March 2022*
Accepted: *26 May 2022*
Published: *13 July 2022*

Citation:
Liu A and Wang X (2022) The Pivotal Role of Chemical Modifications in mRNA Therapeutics. Front. Cell Dev. Biol. 10:901510. doi: 10.3389/fcell.2022.901510

INTRODUCTION

mRNA has emerged as an important platform for gene therapies and vaccines, presenting a new opportunity to target previously challenging diseases. Although the concept of mRNA drugs was envisioned over 30 years ago (Wolff et al., 1990), they were considered too unstable and immunotoxic for clinical use (Weng et al., 2020). Nonetheless, research into the chemical modifications of mRNA has shown that it can be used as an effective therapeutic agent. Moreover, mRNA offers distinct advantages over traditional drugs (Sahin et al., 2014). Compared to DNA technology, mRNA avoids the risk of genomic integration, circumvents the need to enter the nucleus, and has a transient activity profile, desirable in many gene therapy applications. mRNA vaccines can also be developed rapidly, can produce high quantities of antigen with relatively low dosages, and are safer and more readily produced at scale than traditional vaccines. Such benefits have been showcased in the first clinically approved mRNA vaccines against SARS-CoV-2 (Dolgin, 2021a; Kis et al., 2021).

The use of unmodified mRNA as a therapeutic agent is presented with several challenges and risks. Exogenously delivered mRNA is intrinsically immunogenic, triggering several innate immune sensing pathways, which leads to the production of inflammatory cytokines and suppression of cellular translation, undesirable for the production of the therapeutic protein (Tatematsu et al., 2018). Although the immunostimulatory nature of RNA could provide adjuvant activity for vaccinations, the translational inhibition and directed degradation caused by unmodified exogenous mRNAs mitigate their success

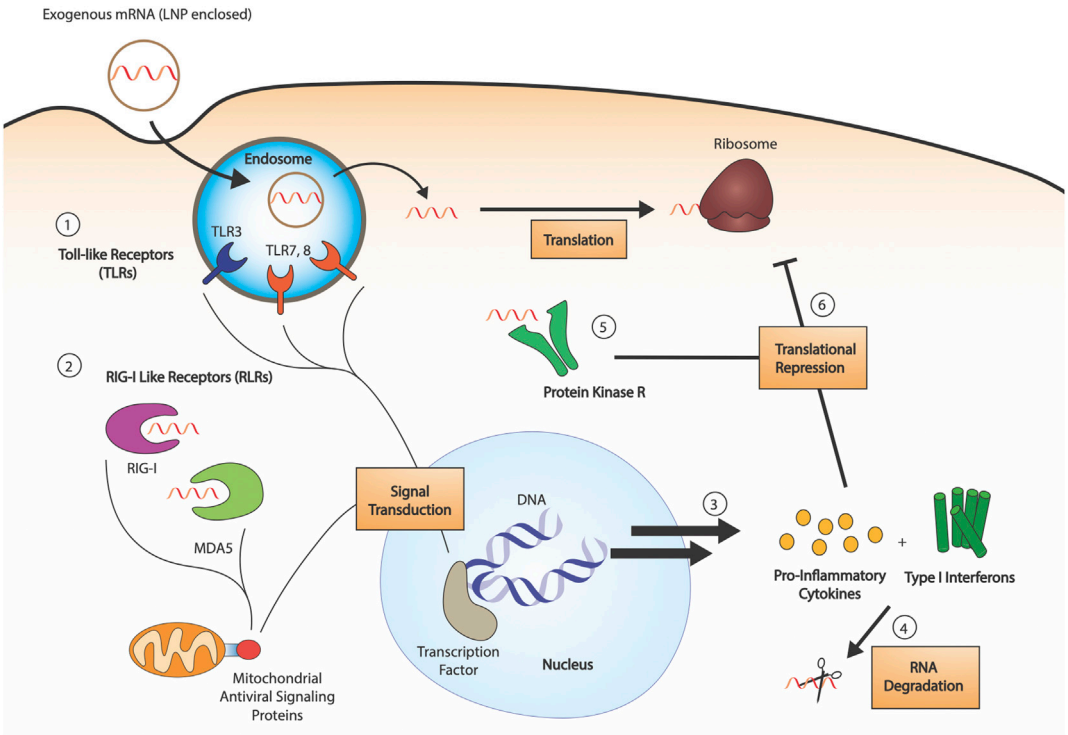


FIGURE 1 | RNA sensing by the innate immune system. 1) RNA sensing Toll-like receptors (TLR3, TLR7, TLR8) are endosomal compartment receptors in sentinel cells, which activate upon late-endosomal acidification. Exogenous RNA is endocytosed by the cell, and pathogen associated molecular patterns are detected by the TLRs (dsRNAs, uridine-rich ribonucleosides, etc.). 2) RIG-I like receptors (RLRs) are cytosolic receptors present in all cell types. Both RIG-I and MDA5 are 5′-triphosphate dependent sensors, with some affinity for both dsRNA and ssRNA. Their activation leads to signal transduction through mitochondrial antiviral signaling proteins. 3) Innate immune detection of exogenous RNA leads to production of pro-inflammatory cytokines and type I interferons, which activate RNA degradation 4). 5) Protein kinase R (PKR) is a cytosolic sensor also involved in dsRNA sensing, the activation of which leads to phosphorylation of eukaryotic initiation factor eIF2α. 6) The combined action of produced cytokines and PKR leads to translational repression.

(Morais et al., 2021). Other therapeutic strategies employing mRNAs, such as protein replacement therapy or regenerative therapy, are even less amenable to the strong stimulation of the immune system. The short half-life of mRNA, owing to its instability to degradation by ribonucleases, further obstructs the therapeutic application of mRNAs, limiting the protein production possible by delivered drugs. Improving both the lifespan and the translational efficiency of mRNA, in addition to removing its immune-activating nature, is thus necessary for successful therapeutics.

These technical challenges have been met by the development of mRNA modifications. Natural RNA contains many types of modifications, hundreds of which have been characterized (Boccaletto et al., 2018; Nachtergaele and He, 2018). Additionally, it has long been known that various viruses and bacteria decorate their genetic material with modifications to evade immune recognition by their host. With this motivation, several modified nucleotides have been incorporated during the *in vitro* transcription of RNA to make a synonymous modified transcript. Prominent among these substitutions is the replacement of uridine with pseudouridine (Ψ) and its methylated analog N1-methyl-pseudouridine ($m^1\Psi$), which have been shown to dramatically reduce the stimulation caused by transcripts carrying these modified nucleotides (Dolgin, 2021b; Morais et al., 2021). Other work focusing on the translational capacity of mRNA have yielded longer-lasting, more highly translated transcripts through both nucleotide substitutions as well as targeted modifications of the 5′-cap and poly(A) tail, important protective structures against mRNA degradation. This enhancement has been attributed to a combination of increased resistance to exonucleases, decreased immune-triggered repression of translation, and greater rates of initiation, giving rise to much more effective protein production per transcript, enabling the burgeoning field of mRNA therapeutics. In this Review, we provide an overview of mRNA modifications relevant to mRNA therapeutics, as well as the current state of modified mRNA in clinical and preclinical studies.

OVERVIEW OF mRNA THERAPEUTICS

Conceptually, mRNA therapeutics relies on the delivery of a synthetic transcript and subsequent translation of the encoded pharmacologically active protein product (Sahin et al., 2014). They are typically designed to be similar to natural mRNA, being able to harness the intracellular translational machinery in a functionally analogous or identical way. Natural mRNA is

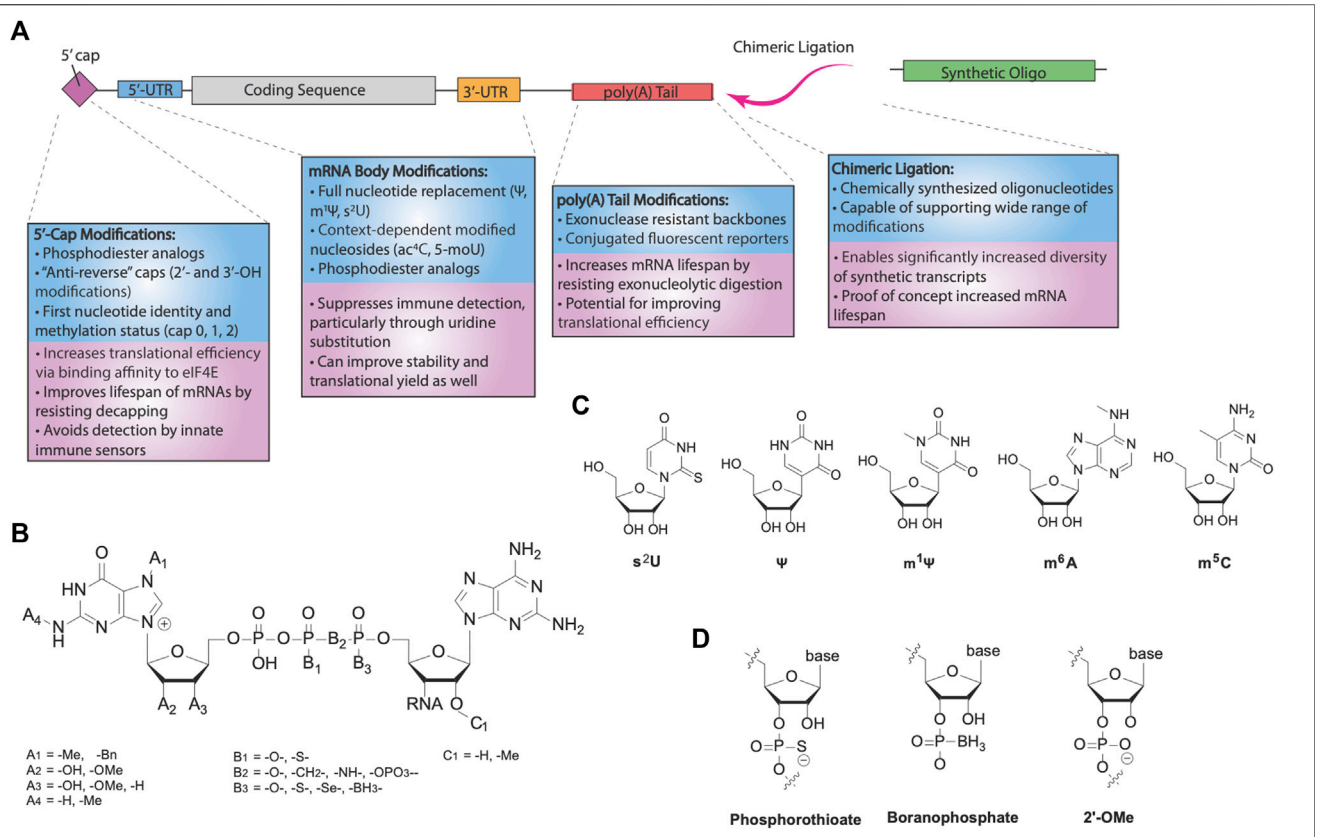


FIGURE 2 | RNA modifications for mRNA therapeutics. **(A)** Categories of different modifications for mRNA. Modification of the cap and nucleotide substitution of the mRNA body are important for innate immune avoidance. Translational efficiency and mRNA stability are further modulated by various modifications, *via* increased eIF4E binding and reduced hydrolysis by nucleases. Additionally, chimeric ligation is a separate class of modification enabling incorporation of highly modified synthetic oligonucleotides, forming chimeric mocRNAs. **(B)** Chemical structure of 5′-caps. Eukaryotic caps are typically modified on the first base (A's), triphosphate (B's), or second base (C's). **(C)** Common modified bases used for modification of mRNA. 2-thiouridine (s^2U), pseudouridine (Ψ), and N^1-methylpseudouridine ($m^1\Psi$) are uridine substitutes, whereas N6-methyladenosine (m^6A) is an adenosine substituent and 5-methylcytosine (m^5C) is a cytosine substituent. **(D)** Common backbone modifications used for modification of mRNA. The phosphate backbone and 2′-OH are frequently modified.

generally single-stranded, containing a coding sequence (CDS) which is translated to the protein product, flanked on either side by untranslated regions (UTRs). The 5′-end of mRNA in eukaryotes is marked with a 5′-cap, a modified 7-methyl-guanosine (m^7G) residue, which modulates mRNA stability and lifespan (Charenton and Graille, 2018). Ribosomal translation typically is also cap-dependent, beginning with the association of eukaryotic initiation factor eIF4E to the transcript, after which the remainder of the translational machinery assembles and translates the encoded protein (Jackson et al., 2010). At the 3′-end, a chain of adenosine residues termed the poly(A) tail buffers against 3′ degradation and further regulates mRNA stability.

The synthesis of mRNA drugs is predominantly achieved by *in vitro* transcription (IVT) from a DNA template, using T3, T7, or SP6 polymerase in the presence of cap precursor and free nucleoside triphosphates. The transcript can alternatively be capped and polyadenylated post-IVT to produce a functional mRNA (Weissman, 2015; Muttach et al., 2017). During these stages, mRNA modifications can be introduced enzymatically through the incorporation of modified nucleotides and cap analogs in the reaction mixture (as discussed below). After purification of the newly synthesized mRNA, it is delivered to target cells to produce the pharmacologically active protein product, which is post-translationally modified and processed naturally. Substantial research has gone into delivering mRNAs, given their large molecular weight and highly negatively charged nature (Kowalski et al., 2019; Hou et al., 2021). In some applications, including cancer immunotherapy and stem cell therapy, mRNA can be electroporated into cells *ex vivo*, after which the transfected cells can be returned to the patient. More commonly, mRNA is encapsulated in a shell of neutrally or positively charged lipids, termed a lipid nanoparticle (LNP), which is endocytosed and promotes the release of the mRNA drug into the cytosol. A wide variety of LNPs has been designed to shield mRNAs from degradation, enhance cell transfection, and facilitate endosomal escape, resulting in overall increased delivery efficiency in preclinical models and

demonstrating clinical success in the SARS-CoV-2 vaccines (Hou et al., 2021).

Once the mRNA drug reaches the site of interest, it begins producing of the desired protein, which can be used in a variety of therapeutic ways (Sahin et al., 2014). mRNA vaccines encode an antigenic-protein to stimulate the immune system. The vaccine can either be directly administered, through injection to intradermal, intramuscular, subcutaneous, and other locations; alternatively, *ex vivo* transfection of professional antigen-presenting cells, especially dendritic cells (DCs), has shown promise in treatments against cancer as a form of cell therapy. In either case, the translated protein is used to prime T cells and B cells in order to elicit protective immunity. Self-amplifying mRNAs, containing positive-sense RNA viral sequences that allow the mRNA to replicate, have also been tested for use in mRNA vaccines in order to increase the effective dose size and enable greater protein production (Bloom et al., 2021). Alternatively, mRNA can be used in protein replacement therapy to supplement the deficiency of a necessary protein or in regenerative medicine and gene therapy, reprogramming and gene-editing cells in order to restore function to target tissues and organs. The use of mRNA for remodeling otherwise untreatable tissues is promising for treating heart failure, neurodegeneration, etc. A more thorough description of mRNA therapeutic strategies is beyond the scope of this review and has been covered elsewhere (Sahin et al., 2014; Chandler, 2019; Zhang H.-X. et al., 2019; Damase et al., 2021).

IMMUNOGENICITY OF EXOGENOUS mRNA

Exogenously delivered, unmodified IVT mRNA is an inherent immunostimulant, which poses a challenge to the efficacy of exogenously delivered mRNA drugs. Innate immune sensor detection of mRNA leads to inhibition of the cellular translational machinery and increased degradation of the mRNA, preventing effective protein production (**Figure 1**). Studies outlined below have revealed not only the underlying pathways relevant to mRNA-induced activation of the immune system but also that modifications can suppress the immune response. Pathogen-associated molecular patterns recognized by immune sensors have been studied; double-stranded RNA and double-stranded secondary structures have been highly investigated (Chen and Hur, 2022). Meanwhile, single-stranded mRNA recognition patterns are still not well understood. The following sections summarize key pathways in mRNA-associated immune regulation and how modifications help synthetic mRNA escape immune activation.

Toll-Like Receptors

Toll-Like Receptors (TLRs) are a class of membrane-bound receptors present in sentinel cells of the immune system, such as dendritic cells and macrophages. Ten functional TLR family members have been identified in humans, four of which are responsible for the detection of nucleic acids: TLR9 recognizes unmethylated CpG DNA, TLR3 recognizes double-stranded RNA (dsRNA), and TLR7 and TLR8 recognize single-stranded RNA (ssRNA) (Kawasaki and Kawai, 2014). More specifically, TLR7 has shown to be activated by uridine-containing ribonucleosides, in addition to dsRNA (Diebold et al., 2006), whereas TLR8 responds to various ssRNA oligonucleotides and RNA degradation products. Nonetheless, the particular sequence preference of these ssRNA sensors is still unknown (Schlee and Hartmann, 2016). The four nucleic acid specific receptors are localized to the endosomal compartment and rely on endosomal acidification for activation (**Figure 1**). Upon TLR engagement, interferons (IFNs) and other inflammatory cytokines are secreted, causing the upregulation of a variety of interferon-stimulated genes (ISGs), including RNA degrading enzymes such as 2′-5′-oligoadenylate synthase (OAS) and RNase L (Anderson et al., 2011).

Various nucleotide modifications have been shown to be impactful in evading TLR activation. The replacement of all uridine residues with modified nucleotides, including pseudouridine (Ψ) and 2-thiouridine (s^2U), was shown by Karikó and coworkers to ablate the TLR immunogenicity of IVT mRNA (Karikó et al., 2005). Transcripts containing these modifications had decreased inflammatory signaling, corresponding to an enhanced translational capacity. Later work demonstrated that N^1-methyl-pseudouridine ($m^1\Psi$) substitution exhibited an even better performance, attributed to decreased activation of TLR3 compared to other modifications (Andries et al., 2015). Other modifications, such as 5-methylcytidine (m^5C), 5-methyluridine (m^5U), and N^6-methyladenosine (m^6A), have also been shown to have some immunosuppressive effects on TLR activity (Lou et al., 2021). Altogether, nucleotide replacement effectively suppresses TLR-associated immune signaling.

Retinoic Acid-Inducible Gene I Like Receptors

The retinoic acid-inducible gene I (RIG-I) like receptor family is a class of cytosolic pattern recognition receptors expressed in all cell types (Rehwinkel and Gack, 2020). This family consists of two primary receptors: the namesake RIG-I and melanoma differentiation-associated protein 5 (MDA5) (**Figure 1**). The two sensors are primarily associated with the detection of dsRNA: RIG-I senses short dsRNA segments containing 5′-triphosphates (Hornung et al., 2006), whereas MDA5 preferentially binds long dsRNAs. RIG-I can also detect 5′-triphosphate-containing ssRNAs, and the precise requirements for its activation are still being determined. MDA5 also has been suggested to detect the RNA of some ssRNA viruses, potentially due to the formation of secondary structures (Schlee, 2013). Despite the expanding understanding of their ligand range, the RIG-I-like receptors are a major part of the interferon response to RNA.

As a 5′-triphosphate is important for activation of RIG-I, the addition of a synthetic cap to IVT mRNA plays a critical role in evading RIG-I detection. The installation of an N^7-methylguanosine (m^7G) residue to the 5′ end of triphosphate mRNA decreases the RIG-I-dependent IFN secretion by synthetic transcripts (Hornung et al., 2006). Furthermore, modified nucleotide substitutions can also play an inhibitory role in

RIG-I signaling, with Ψ, s^2U, and 2′-O-methyluridine all reducing the total inflammatory cytokine-induced by 5′-triphosphate-containing mRNA (Karikó et al., 2008).

However, capping and nucleotide replacement are unable to fully abrogate the RIG-I dependent response to 5′-triphosphate mRNA (Schuberth-Wagner et al., 2015). Structural studies on RIG-I binding revealed that the receptor can accommodate the presence of an m^7G moiety without drastic disruption of its triphosphate recognition (Devarkar et al., 2016). On the other hand, methylation of the 5′-most nucleotide of capped mRNA strongly interferes with RIG-I binding, and methylation of the second nucleotide is also implicated in decreasing RIG-I's activation. Indeed, higher eukaryotic mRNA generally contain a 2′-O-methylated first nucleotide, termed a cap-1 structure in contrast with the unmethylated cap-0's, and coronaviruses and poxviruses have been shown to employ cap one modifications to evade the innate immune system (Daffis et al., 2010). MDA5, although also 5′-triphosphate dependent, induces IFN production even in the presence of cap-0 structures but is inactive in the presence of cap-1 mRNA (Züst et al., 2011). Moreover, IFIT1, a major interferon induced gene, further recognizes 5′-triphosphates and cap-0 mRNA, inhibiting translation by competing with eIF4E, a cap-binding translation initiation factor (Habjan et al., 2013). Cap-1 demonstrated decreased IFIT1 binding activity, further assisting immune system evasion of modified mRNAs.

Protein Kinase R and eIF2α Phosphorylation

Protein kinase R (PKR) is an interferon-induced protein kinase (**Figure 1**), capable of being activated by either dsRNA (>33 bp) or ssRNA containing an exposed 5′-triphosphate (Nallagatla and Bevilacqua, 2008). Upon activation and autophosphorylation, PKR then phosphorylates the α-subunit of eIF2, the GTP-dependent translation initiation factor responsible for mediating binding of the first aminoacyl-tRNA (Met-tRNA) to the ribosome. Phosphorylation enhances the binding affinity of eIF2 for its GTP exchange factor, eIF2B, causing sequestration which results in impaired translation. Substitution of uridine using Ψ, s^2U, 2′-dU, and other modifications are able to inhibit PKR signaling (Anderson et al., 2010). Notably, $m^1\Psi$ exhibited strong repression of PKR activation, outperforming Ψ and other modifications (Svitkin et al., 2017).

Future Directions

Much progress has been made in understanding the immune mechanisms and modifications relevant to mRNA therapeutics. Nonetheless, multiple confounding factors have complicated the research. Indeed, dsRNA contaminants cause residual stimulation of multiple innate immune sensors, and multiple purification methods have been developed to counteract this, including HPLC (Karikó et al., 2011) and RNase III digestion (Foster et al., 2019). Differences in the manufacturing process, such as the ratio of modified to unmodified nucleotides present in the IVT reaction mixture, also lead to differences in dsRNA byproduct formation (Nelson et al., 2020). Additionally, the immune response to mRNAs is highly dependent on the system under study, with variable results depending on target cell type, temperature, etc. (Uchida et al., 2015; Li et al., 2016) For example, whereas RNAs containing both $m^1\Psi$ substitution for uridine and m^5C for cytidine had a higher translational yield *in vitro*, mRNA with only $m^1\Psi$ demonstrated higher performance *in vivo* in mice (Andries et al., 2015). As such, more investigation with standardized conditions and preparation is necessary to comprehensively understand the effects of mRNA modifications on immune responses.

STABILITY AND TRANSLATIONAL EFFICIENCY OF mRNA

The effectiveness of mRNA therapeutics depends highly on the amount of protein that can be produced from a given transcript. This translational yield is dependent both on the lifespan of mRNA as well as the rate of translational initiation. Years ago, significant doubt arose over the capability of mRNA as a drug, primarily due to its instability from both immune-induced degradation and its intrinsically shorter half-life from other therapeutic modalities. However, chemical modifications of mRNA targeted at decreasing its susceptibility to enzymatic degradation have been able to greatly increase the lifetime of IVT RNAs (**Figure 2A**). Additionally, the same modifications also affect the translational efficiency of delivered transcripts, leaving further potential for increasing the protein yield of mRNA drugs. Here, we review various modification strategies in order to improve the translational capacity of IVT mRNA.

The 5′-Cap

The degradation of mRNA is mediated primarily through two pathways: 5′ → 3′ and 3′ → 5′ degradation. In the 5′ → 3′ pathway, decapping of the 5′-end *via* cleavage of the α-β phosphodiester bond by the Dcp1/2 decapping complex precedes exonucleolytic degradation of the mRNA, primarily by the ribonuclease Xrn1 (Charenton and Graille, 2018). Thus, the stability of the 5′-cap is essential for controlling the lifespan of mRNA. The 5′-cap also exerts an effect on translational yield through modulating translational efficiency (Jackson et al., 2010). Translation is typically rate limited by the initiation step, a generally cap-dependent process reliant on binding of initiation factor eIF4E to the 5′-cap. Given its significance in both translational efficiency and mRNA stability, optimizing the 5′-cap of mRNA is crucial for designing more effective mRNA drugs (**Figure 2A**).

Two strategies are generally employed to cap synthetic mRNAs (Muttach et al., 2017). Recombinant viral capping enzymes, such as the vaccinia virus capping enzyme (VCE), can be used in conjunction with a methyltransferase in the presence of GTP and the 5′-triphosphate IVT mRNA to add a cap-1 structure. More commonly, however, co-transcriptional capping can be performed using a cap dinucleotide in the presence of the IVT polymerase mixture. The 3′-OH of the cap dinucleotide nucleophilically attacks the α phosphate of the next nucleotide, and elongation by the polymerase continues onwards. However, due to the similarity between the two 3′-OH's present in the dinucleotide, capping with unmodified dinucleotides results in the wrong orientation at least half of the time, reducing the translational efficiency of the product mRNAs (Stepinski et al., 2001). To address this, Rhoads and others designed anti-reverse cap analogs (ARCAs), modified dinucleotides containing a 3′-O, 7′-dimethylguanosine

or 3′-deoxy-7-methylguanosine, preventing incorrect incorporation into synthetic transcripts and more than doubling their translational efficiencies relative to unmodified cap dinucleotides. Alternative modifications were also shown to enforce the correct orientation, including 2′-O-methylation (Jemielity et al., 2003) and N^7-benzyl-N^2-methyl- dual modification (Grudzien et al., 2004). In all, the use of ARCAs allows for improved synthesis and function of mRNA drugs.

A series of ARCAs have since been synthesized and explored to improve the performance of synthetic transcripts while maintaining the anti-reverse function of these analogs (**Figure 2B**). For example, tetraphosphate analogs of the first-generation ARCA dinucleotides improved the translational yield of mRNAs, associated with the higher binding affinity for eIF4E (Muttach et al., 2017). Surprisingly, pentaphosphate counterparts did not recapitulate this trend, with a lower translational efficiency despite even higher binding affinities for eIF4E. This effect was attributed to slower release kinetics of eIF4E after initiation, indicating the strength of eIF4E binding does not directly imply higher translational efficiency. Meanwhile, modifications targeted towards improving IVT mRNA stability to decapping focused on altering the phosphodiester moiety. Grudzien et al. (2006) demonstrated that Dcp1/2 acts primarily on the α, β phosphodiester bond and replacement of the bridging oxygen with a methylene group (-CH_2) blocked 5′ → 3′ degradation, albeit with some cost towards translational efficiency. Motivated by evidence that phosphorothioate modification of the mRNA backbone could also increase stability, later generations of cleavage-resistant caps used modifications of either the α or β phosphates with a phosphorothioate (Grudzien et al., 2007). Phosphorothioate modified caps yielded higher translational efficiencies than unmodified ARCAs, while simultaneously greatly improving the half-life of synthetic transcripts. Polysome profiling studies revealed that a greater rate of initiation is responsible for the increased translation rate, and phosphorothioate cap analogs have also been demonstrated to be effective in dendritic cells and *in vivo* in mice for vaccination and immune system priming (Kuhn et al., 2010). 1,2-dithiodiphosphates were also tested and demonstrated even higher stability profiles than phosphorothioate caps (Strenkowska et al., 2016).

A slew of other analogs have been explored as well, including phosphorothiolate (Wojtczak et al., 2018), phosphoroselenoate (Kowalska et al., 2009), boranophosphate (Kowalska et al., 2014), imidodiphosphate modified caps (Rydzik et al., 2012), etc. (Warminski et al., 2013; Shanmugasundaram et al., 2016; Dülmen et al., 2021; Wojcik et al., 2021) Locked nucleic acid (LNA) caps have also been investigated, in which the ribose is locked in an C3′-endo conformation by a bridging methylene group between the 2′ oxygen and 4′ carbon (Kore et al., 2009). Although LNAs have primarily been used in oligonucleotides, mRNAs capped by an LNA analog have recently been demonstrated to have increased translational efficiency and stability (Senthilvelan et al., 2021). Given the promise many of these modifications have demonstrated in *in vitro* experiments, the optimization of capped mRNAs using these analogs *in vivo* and in clinical applications holds promise for even more effective future drugs.

mRNA Body Modifications

Nucleoside and backbone modifications of the DNA encoded mRNA body are critical to enhance the protein production of mRNAs (**Figures 2A,C,D**). Ψ and $m^1Ψ$ are the most widely used body modifications for mRNA therapeutics. When incorporated as 100% replacement for U, they significantly increase the translational efficiency of mRNAs by turning off the innate immune-triggered eIF2α phosphorylation-dependent inhibition of translation (Karikó et al., 2008; Svitkin et al., 2017). Moreover, in comparison with Ψ, $m^1Ψ$ showed further enhancement of translational capacity, which has been linked to its capability of increasing ribosome density on the mRNA. Specifically, the additional methyl group on $m^1Ψ$ blocks hydrogen bonding at the N1 position, despite resulting in ribosome pausing, dramatically increasing the ribosome loading per mRNA (Svitkin et al., 2017), which may potentially increase translation initiation and prevent mRNA from entering degradation pathways. Thus, full-length body modifications using immunosuppressive and translation-enhancing modified nucleosides can generate mRNA drugs with greatly improved translational capacity.

Earlier attempts of backbone modification *via* IVT incorporation of phosphorothioates showed successful translation in reconstituted *E. coli in vitro* translation system (Ueda et al., 1991; Tohda et al., 1994). A recent study further uncovered that introduction of phosphorothioates to the 5′-UTR at either cytidine or both cytidine and uridine increases translational efficiency *via* faster initiation, even at the expense of elongation processivity (Kawaguchi et al., 2020). Other familiar modifications, including m^6A and s^2U, can increase RNA stability by decreased activation of the 2′-5′-oligoadenylate synthetase system (OAS), an interferon associated pathway that leads to RNase L activation (Anderson et al., 2011). In addition, some modifications have been revealed to exert a context-dependent effect on mRNA translational yield. The first nucleotide after the 5′-cap appears to play an important role in protein production (Sikorski et al., 2020). Adenosine and m^6A residues at this site demonstrate higher translational yields, and 2′-O-methylation of the first nucleotide modulates protein production based on the identity of the first nucleotide. N^4-acetylcytidine (ac4C) also increases transcript stability and translational yield in a position specific manner, increasing the speed of mRNA decoding when positioned at a wobble site (Arango et al., 2018). Another study revealed that 5-methoxyuridine (5-moU) is also capable of increasing mRNA stability, though further research is required to unravel the underlying mechanism of its enhancement (Li et al., 2016). In all, the diversity of potential chemical modifications gives substantial promise for even better-performing mRNA therapeutics.

The poly(A) Tail

The poly(A) tail is a chain of adenosine residues at the 3′-end of mRNA, which buffers it from degradation in a length-dependent fashion. Poly(A) shortening is catalyzed by the Pan2-Pan3 deadenylation complex, preceding both 3′ → 5′ and 5′ → 3′ degradation. Moreover, the tail and cap of actively translated mRNA interact, providing a mechanism by which the poly(A) tail can affect translational efficiency (Gallie, 1991; Goss and Kleiman, 2013). Although earlier works attempting to modify the poly(A) tail were met with disappointment (Rabinovich et al., 2006), more recent studies have indicated that there is still potential for improving stability and translational yield through poly(A) tail modifications (**Figure 2A**). Indeed, initial efforts to modify the poly(A) tail employed 3′-

deoxyadenosine (cordycepin) or 8-aza-adenosine, which were shown to stabilize mRNA similarly to lengthening of the poly(A) tail, but were unable to outperform them in translational assays. Nonetheless, phosphorothioate modification of the poly(A) tail was able to exhibit increased stability and translational yield in some systems (Strzelecka et al., 2020). Boranophosphate substitution has also been tested, but underperformed compared to phosphorothioate functionalization. Interestingly, attachment of sulforhodamine B (SRB), a fluorescent small-molecule label, using click chemistry with incorporated 2′-azido-2′-dATP was able to substantially increase translational efficiency, though the mechanism of such enhancement has yet to be determined (Anhäuser et al., 2019). In all, despite the rather limited exploration of poly(A) tail modifications, future research into the poly(A) tail can likely further improve mRNA therapeutics.

Chimeric RNA

Recently, our group has demonstrated the generation of chimeric mRNAs, formed by the enzymatic ligation of an IVT synthesized mRNA transcript with a chemically synthesized oligonucleotide (Aditham et al., 2022) (**Figure 2A**). Termed mRNA-oligonucleotide conjugated RNA (mocRNA), this platform presents a novel method of circumventing translational restrictions on incorporating modified nucleotides and expands the possible space of synthetic transcripts for therapeutics. In our work, nuclease-resistant oligonucleotides were ligated to the poly(A) tail, resulting in 3–10 folds higher expression in human HeLa cells and rat primary neurons. The programmable and modular nature of mocRNAs enabled engineering mRNAs without interfering with the coding region. Future work into diversifying the ligated oligonucleotides will likely further illustrate the potential of chimeric RNAs.

CLINICAL AND PRECLINICAL EXAMPLES OF MODIFIED RNA

Various candidate mRNA therapeutic drugs have been examined both preclinically and clinically in the past years and have been reviewed extensively. Here, we highlight a number of these which employed modified mRNAs.

Vaccines

A number of vaccines based on modified mRNA have been developed (Zhang C. et al., 2019). Most prominent of the modified mRNA vaccines are those against SARS-CoV-2, advanced by Moderna (mRNA-1273) and BioNTech in partnership with Pfizer (BNT-162b2). Both vaccines encode the prefusion conformation of spike glycoprotein using N^1-methyl-pseudouridine encoding mRNAs containing a 5' cap-1 (Corbett et al., 2020; World Health Organization 2020). mRNA modifications proved to be critical for the success of these vaccines, with similar products with unmodified mRNAs underperforming expectations (Morais et al., 2021; Nance and Meier, 2021). Moreover, the use of mRNA as a platform for a vaccine during the COVID-19 pandemic proved advantageous, owing to the rapid development and manufacturing speed of mRNA (Kis et al., 2021). Indeed, both vaccines were able to be produced within 10 months after the sequencing of the SARS-CoV-2 genome and proved to be over 90% effective (Polack et al., 2020; El Sahly et al., 2021). mRNA is also easily adaptable to new strains and mutations. The prefusion spike protein encoded in the aforementioned vaccines uses missense mutations at two loci in the original sequence to enforce the proper immunogenic conformation. As the SARS-CoV-2 virus continues to evolve, the adjustability of the mRNA vaccine platform will be critical.

Various influenza virus vaccines using modified mRNA have also been under development (Dolgin, 2021c). A vaccine candidate against H10N8 and H7N9 entered phase I trials in 2015 (Feldman et al., 2019), and two other candidates (mRNA-1010 and PF-07252220) entered phase I trials in late 2021. mRNA-1010 is a quadrivalent vaccine against the H1N1, H3N2, Yamagata, and Victoria strains, whereas the PF-07252220 is currently a monovalent vaccine, which is planned to be combined into a bivalent or quadrivalent product in the future. A slew of other mRNA influenza vaccine candidates have also undergone preclinical testing. The advent of mRNA vaccines against the flu is particularly exciting, as traditional flu vaccines are often ineffective and inconsistently manufactured (Wu et al., 2017). Additionally, due to constraints on the time necessary to develop traditional vaccines, the yearly influenza vaccines are often disappointingly ineffective. On the other hand, mRNA can easily be adjusted to encode antigens for the precise strain of influenza relevant, and its scalability bypasses the error-prone egg-based method for producing traditional vaccines. Altogether, the growing interest in modified mRNA vaccines holds promise for flu vaccinations in the future.

Clinical trials have also been initiated for a number of other diseases, which have posed a challenge for traditional vaccines. Phase III trials for a modified mRNA vaccine against cytomegalovirus (CMV) began late in 2021, after promising early results (John et al., 2018). Phase I trials of a modified mRNA vaccine against HIV have also recently begun in January 2022. Preclinical studies have also been performed for modified mRNA vaccine candidates against Ebola (Meyer et al., 2018), Zika (Pardi et al., 2017) human metapneumovirus (hMPV) (Shaw et al., 2019), etc.

Due to the highly polymorphic nature of cancer profiles, effective therapeutic vaccines against cancer often require individualization. Modified mRNA has been used in multiple preclinical and clinical applications against cancer, primarily in direct vaccine injections. LNP encapsulated modified mRNAs encoding bispecific antibodies (Stadler et al., 2017), cytokines (Hewitt et al., 2019; Kranz et al., 2019; Vormehr, 2019), or chimeric antigens (Foster et al., 2019) have been investigated. A full coverage of mRNA in cancer therapeutics can be found in other reviews (Beck et al., 2021; Miao et al., 2021).

Replacement and Gene Therapy

Protein production from mRNA has also been investigated as a tool for replacement and gene therapies. As opposed to DNA-based therapies, modified mRNAs demonstrate a pulse-like expression profile and do not risk genomic integration - problems that hindered previous efforts in such therapeutic approaches.

Potential use of modified mRNA as a vector for reprogramming and regenerative medicine was first demonstrated in 2010, when Warren and others used repeated transfections of reprogramming factor-encoding mRNAs to generate pluripotent stem cells (iPSCs) from fibroblasts with relatively high efficiency (Warren et al., 2010).

These mRNAs were modified with m^5C and Ψ substitutions for C and U, respectively, reducing the innate immune response against ectopic mRNA, and improving viability of targeted cells. Interestingly, evidence suggests that some residual inflammatory signaling may actually play a role in assisting reprogramming (Lee et al., 2012), but the presence of immunosuppressive modification nonetheless helped avoid translational silencing of the transcripts and overstimulation of the immune system. Indeed, the repeated transfection regime was only made possible by suppression of the innate immune system, indicating an essential role for mRNA modifications. The use of mRNA reprogramming for iPSC generation therapeutically has been covered elsewhere (Shi et al., 2017; Warren and Lin, 2019).

In addition to reprogramming, modified mRNAs have significant therapeutic potential in regenerative medicine, especially in organs and tissues with little regenerative capacity. In the heart, VEGF-A expression from modified mRNA resulted in healthy regeneration of cardiac vasculature after myocardial infarction in mice and swine (Zangi et al., 2013; Carlsson et al., 2018). In contrast, DNA-based expression was prolonged and resulted in edema and death. Additionally, Phase II a trials of a modified mRNA encoding VEGF-A have also been performed in patients with coronary artery disease, with generally positive results (Anttila et al., 2020). Expression of other proteins, including PKM2, FSTL1, and IGF-1 were used to promote cell survival and cardiomyocyte regeneration *in vivo*, improving general pathophysiology (Kaur and Zangi, 2020). VEGF-A mRNA has also been tested for the treatment of type II diabetes, yielding enhancements in skin blood flow in a phase I trial (Gan et al., 2019). Thus, mRNA holds potential as a platform for VEGF-A induced revascularization.

Modified mRNAs have been used in a variety of other regenerative medicinal applications. Attempts to prevent cell death in neuronal tissue after ischemic attack (Fukushima et al., 2021), to induce regeneration following liver damage (Rizvi et al., 2021), etc. have been successful preclinically. Delivery of gene editing enzymes through the expression of modified mRNAs have also presented an opportunity for gene therapies, circumventing many previous challenges of such strategies (Zhang H.-X. et al., 2019). Finally, modified mRNAs may also be used for direct replacement therapies for deficient proteins, including surfactant protein B (SP-B) (Kormann et al., 2011), arginase 1 (ARG1) (Asrani et al., 2018), cytochrome c oxidase (SCO2) (Miliotou et al., 2021), etc. In all, modified mRNA-based gene therapies provide an opportunity to treat many previously challenging diseases.

CONCLUSION AND PERSPECTIVES

With the increasing popularity and maturation of mRNA therapeutics, significant progress has been made in understanding the role of mRNA modifications in attuning their immunogenicity, stability, and translational efficiency. Nucleotide substitutions and cap modifications play important parts in reducing innate immune sensing of IVT mRNA. Furthermore, modifications promoting translational initiation increase the translational yield of modified RNAs, and modifications resisting degradation by decapping or deadenylation increase the half-life of mRNA drugs for more sustained expression. Research into mRNA modifications has yielded multiple candidate mRNA therapeutics undergoing clinical or preclinical trials, as well as effective SARS-CoV vaccines.

However, mRNA modifications have yet to be fully employed in therapeutics. The diversity of known modifications has not been reflected in current mRNA drug candidates, which primarily focus on substitutions of uridine with N^1-methyl-pseudouridine and cap methylation state. Given the evidence that phosphodiester modifications, labeling of the poly(A) tail, and other nucleoside substitutions are capable of increasing the stability and translational yield of mRNA, many optimizations can likely be made to future mRNA therapeutics. Indeed, in addition to altering the necessary dosage of mRNA drugs, modifications could also foreseeably increase their shelf-life, which is currently one of the major criticisms of their practicality. Nonetheless, the sensitivity and context-dependence of modified mRNAs' performance requires further efforts to parse the precise effects of mRNA modifications on immunosuppression, translation, and stability.

Additionally, further insight into biological pathways relevant to mRNA therapeutics may motivate the targeted use of modifications. The importance of poly(A) tail modifications on translational initiation have yet to be fully understood and leaves room for potential improvements. Similarly, advances and new techniques in sequencing technology have enabled the discovery of new therapeutically relevant modifications. Surveying the effects of these new modifications and the mechanisms underlying them could lead the way to even more effective therapeutics. Finally, on a more cautionary note, further research into the long-term effects of highly modified mRNAs (including downstream byproducts of modified bases) are desired for the safe use in mRNA therapeutics. Nonetheless, given recent advances in modified mRNAs, future mRNA therapies will likely be shaped by progress in RNA modifications and have unlimited potentials in treating other diseases beyond mRNA vaccines.

AUTHOR CONTRIBUTIONS

Conceptualization, AL and XW; writing, review, and editing, AL and XW. Both authors have read and agreed to the published version of the manuscript.

FUNDING

The research performed in the Wang lab is funded by the Searle Scholars Program, Thomas D. and Virginia W. Cabot Professorship, Edward Scolnick Professorship, Merkin Institute Fellowship, Ono Pharma Breakthrough Science Initiative Award, and NIH DP2 New Innovator Award.

ACKNOWLEDGMENTS

We thank Huilin Huang and Chenqi Yi for handling our manuscript. We also thank the reviewers for their constructive feedback during the revision.

REFERENCES

Aditham, A., Shi, H., Guo, J., Zeng, H., Zhou, Y., Wade, S. D., et al. (2022). Chemically Modified mocRNAs for Highly Efficient Protein Expression in Mammalian Cells. *ACS Chem. Biol. Artic. ASAP.* doi:10.1021/acschembio.1c00569

Anderson, B. R., Muramatsu, H., Jha, B. K., Silverman, R. H., Weissman, D., and Kariko, K. (2011). Nucleoside Modifications in RNA Limit Activation of 2'-5'-oligoadenylate Synthetase and Increase Resistance to Cleavage by RNase L. *Nucleic Acids Res.* 39 (21), 9329–9338. doi:10.1093/nar/gkr586

Anderson, B. R., Muramatsu, H., Nallagatla, S. R., Bevilacqua, P. C., Sansing, L. H., Weissman, D., et al. (2010). Incorporation of Pseudouridine into mRNA Enhances Translation by Diminishing PKR Activation. *Nucleic Acids Res.* 38 (17), 5884–5892. doi:10.1093/nar/gkq347

Andries, O., Mc Cafferty, S., De Smedt, S. C., Weiss, R., Sanders, N. N., and Kitada, T. (2015). N1-methylpseudouridine-incorporated mRNA Outperforms Pseudouridine-Incorporated mRNA by Providing Enhanced Protein Expression and Reduced Immunogenicity in Mammalian Cell Lines and Mice. *J. Control. Release* 217, 337–344. doi:10.1016/j.jconrel.2015.08.051

Anhäuser, L., Hüwel, S., Zobel, T., and Rentmeister, A. (2019). Multiple Covalent Fluorescence Labeling of Eukaryotic mRNA at the Poly(A) Tail Enhances Translation and Can Be Performed in Living Cells. *Nucleic Acids Res.* 47 (7), e42.

Anttila, V., Saraste, A., Knuuti, J., Jaakkola, P., Hedman, M., Svedlund, S., et al. (2020). Synthetic mRNA Encoding VEGF-A in Patients Undergoing Coronary Artery Bypass Grafting: Design of a Phase 2a Clinical Trial. *Mol. Ther. - Methods & Clin. Dev.* 18, 464–472. doi:10.1016/j.omtm.2020.05.030

Arango, D., Sturgill, D., Alhusaini, N., Dillman, A. A., Sweet, T. J., Hanson, G., et al. (2018). Acetylation of Cytidine in mRNA Promotes Translation Efficiency. *Cell* 175 (7), 1872–1886. doi:10.1016/j.cell.2018.10.030

Asrani, K. H., Cheng, L., Cheng, C. J., and Subramanian, R. R. (2018). Arginase I mRNA Therapy - a Novel Approach to Rescue Arginase 1 Enzyme Deficiency. *RNA Biol.* 15 (7), 914–922. doi:10.1080/15476286.2018.1475178

Beck, J. D., Reidenbach, D., Salomon, N., Sahin, U., Türeci, Ö., Vormehr, M., et al. (2021). mRNA Therapeutics in Cancer Immunotherapy. *Mol. Cancer* 20, 69. doi:10.1186/s12943-021-01348-0

Bloom, K., van den Berg, F., and Arbuthnot, P. (2021). Self-amplifying RNA Vaccines for Infectious Diseases. *Gene Ther.* 28, 117–129. doi:10.1038/s41434-020-00204-y

Boccaletto, P., Machnicka, M. A., Purta, E., Piątkowski, P., Bagiński, B., Wirecki, T. K., et al. (2018). MODOMICS: a Database of RNA Modification Pathways. 2017 Update. *Nucleic Acids Res.* 46, D303–D307. doi:10.1093/nar/gkx1030

Carlsson, L., Clarke, J. C., Yen, C., Gregoire, F., Albery, T., Billger, M., et al. (2018). Biocompatible, Purified VEGF-A mRNA Improves Cardiac Function after Intracardiac Injection 1 Week Post-myocardial Infarction in Swine. *Mol. Ther. - Methods & Clin. Dev.* 9, 330–346. doi:10.1016/j.omtm.2018.04.003

Chandler, R. J. (2019). Messenger RNA Therapy as an Option for Treating Metabolic Disorders. *Proc. Natl. Acad. Sci. U.S.A.* 116 (42), 20804–20806. doi:10.1073/pnas.1914673116

Charenton, C., and Graille, M. (2018). mRNA Decapping: Finding the Right Structures. *Philos. Trans. R. Soc. Lond B Biol. Sci.* 373. doi:10.1098/rstb.2018.0164

Chen, Y. G., and Hur, S. (2022). Cellular Origins of dsRNA, Their Recognition and Consequences. *Nat. Rev. Mol. Cell Biol.* 23, 286–301. doi:10.1038/s41580-021-00430-1

Corbett, K. S., Edwards, D. K., Leist, S. R., Abiona, O. M., Boyoglu-Barnum, S., Gillespie, R. A., et al. (2020). SARS-CoV-2 mRNA Vaccine Design Enabled by Prototype Pathogen Preparedness. *Nature* 586, 567–571. doi:10.1038/s41586-020-2622-0

Daffis, S., Szretter, K. J., Schriewer, J., Li, J., Youn, S., Errett, J., et al. (2010). 2′-O Methylation of the Viral mRNA Cap Evades Host Restriction by IFIT Family Members. *Nature* 468, 452–456. doi:10.1038/nature09489

Damase, T. R., Sukhovershin, R., Boada, C., Taraballi, F., Pettigrew, R. I., and Cooke, J. P. (2021). The Limitless Future of RNA Therapeutics. *Front. Bioeng. Biotechnol.* 9, 628137. doi:10.3389/fbioe.2021.628137

Devarkar, S. C., Wang, C., Miller, M. T., Ramanathan, A., Jiang, F., Khan, A. G., et al. (2016). Structural Basis for m7G Recognition and 2′-O-Methyl Discrimination in Capped RNAs by the Innate Immune Receptor RIG-I. *Proc. Natl. Acad. Sci. U.S.A.* 113 (3), 596–601. doi:10.1073/pnas.1515152113

Diebold, S. S., Massacrier, C., Akira, S., Paturel, C., Morel, Y., and Reis e Sousa, C. (2006). Nucleic Acid Agonists for Toll-like Receptor 7 Are Defined by the Presence of Uridine Ribonucleotides. *Eur. J. Immunol.* 36 (12), 3256–3267. doi:10.1002/eji.200636617

Dolgin, E. (2021c). CureVac COVID Vaccine Let-Down Spotlights mRNA Design Challenges. *Nature* 594, 483. doi:10.1038/d41586-021-01661-0

Dolgin, E. (2021a). How COVID Unlocked the Power of RNA Vaccines. *Nature* 589, 189–191. doi:10.1038/d41586-021-00019-w

Dolgin, E. (2021b). mRNA Flu Shots Move into Trials. *Nat. Rev. Drug Discov.* 20, 801–803. doi:10.1038/d41573-021-00176-7

Dülmen, M., Muthmann, N., and Rentmeister, A. (2021). Chemo-enzymatic Modification of the 5'-cap Maintains Translation and Increases Immunogenic Properties of mRNA. *Angew. Chem. Int. Ed.* 60, 13280–13286.

El Sahly, H. M., Baden, L. R., Essink, B., Doblecki-Lewis, S., Martin, J. M., Anderson, E. J., et al. (2021). Efficacy of the mRNA-1273 SARS-CoV-2 Vaccine at Completion of Blinded Phase. *N. Engl. J. Med.* 385, 1774–1785. doi:10.1056/nejmoa2113017

Feldman, R. A., Fuhr, R., Smolenov, I., Ribeiro, A., Panther, L., Watson, M., et al. (2019). mRNA Vaccines against H10N8 and H7N9 Influenza Viruses of Pandemic Potential Are Immunogenic and Well Tolerated in Healthy Adults in Phase 1 Randomized Clinical Trials. *Vaccine* 37 (25), 3326–3334. doi:10.1016/j.vaccine.2019.04.074

Foster, J. B., Choudhari, N., Perazzelli, J., Storm, J., Hofmann, T. J., Jain, P., et al. (2019). Purification of mRNA Encoding Chimeric Antigen Receptor Is Critical for Generation of a Robust T-Cell Response. *Hum. Gene Ther.* 30 (2), 168–178. doi:10.1089/hum.2018.145

Fukushima, Y., Uchida, S., Imai, H., Nakatomi, H., Kataoka, K., Saito, N., et al. (2021). Treatment of Ischemic Neuronal Death by Introducing Brain-Derived Neurotrophic Factor mRNA Using Polyplex Nanomicelle. *Biomaterials* 270, 120681. doi:10.1016/j.biomaterials.2021.120681

Gallie, D. R. (1991). The Cap and Poly(A) Tail Function Synergistically to Regulate mRNA Translational Efficiency. *Genes Dev.* 5 (11), 2108–2116. doi:10.1101/gad.5.11.2108

Gan, L.-M., Lagerström-Fermér, M., Carlsson, L. G., Arfvidsson, C., Egnell, A.-C., Rudvik, A., et al. (2019). Intradermal Delivery of Modified mRNA Encoding VEGF-A in Patients with Type 2 Diabetes. *Nat. Commun.* 10, 871. doi:10.1038/s41467-019-08852-4

Goss, D. J., and Kleiman, F. E. (2013). Poly(A) Binding Proteins: Are They All Created Equal? *WIREs RNA* 4 (2), 167–179. doi:10.1002/wrna.1151

Grudzien, E., Kalek, M., Jemielity, J., Darzynkiewicz, E., and Rhoads, R. E. (2006). Differential Inhibition of mRNA Degradation Pathways by Novel Cap Analogs. *J. Biol. Chem.* 281 (4), 1857–1867. doi:10.1074/jbc.m509121200

Grudzien, E., Stepinski, J., Jankowska-anyszka, M., Stolarski, R., Darzynkiewicz, E., and Rhoads, R. E. (2004). Novel Cap Analogs for *In Vitro* Synthesis of mRNAs with High Translational Efficiency. *RNA* 10 (9), 1479–1487. doi:10.1261/rna.7380904

Grudzien-Nogalska, E., Jemielity, J., Kowalska, J., Darzynkiewicz, E., and Rhoads, R. E. (2007). Phosphorothioate Cap Analogs Stabilize mRNA and Increase Translational Efficiency in Mammalian Cells. *RNA* 13 (10), 1745–1755. doi:10.1261/rna.701307

Habjan, M., Hubel, P., Lacerda, L., Benda, C., Holze, C., Eberl, C. H., et al. (2013). Sequestration by IFIT1 Impairs Translation of 2'O-Unmethylated Capped RNA. *PLoS Pathog.* 9 (10), e1003663. doi:10.1371/journal.ppat.1003663

Hewitt, S. L., Bai, A., Bailey, D., Ichikawa, K., Zielinski, J., Karp, R., et al. (2019). Durable Anticancer Immunity from Intratumoral Administration of IL-23, IL-36γ, and OX40L mRNAs. *Sci. Transl. Med.* 11 (477), eaat9143. doi:10.1126/scitranslmed.aat9143

Hornung, V., Ellegast, J., Kim, S., Brzozka, K., Jung, A., Kato, H., et al. (2006). 5'-Triphosphate RNA Is the Ligand for RIG-I. *Science* 314, 994–997. doi:10.1126/science.1132505

Hou, X., Zaks, T., Langer, R., and Dong, Y. (2021). Lipid Nanoparticles for mRNA Delivery. *Nat. Rev. Mater* 6, 1078–1094. doi:10.1038/s41578-021-00358-0

Jackson, R. J., Hellen, C. U. T., and Pestova, T. V. (2010). The Mechanism of Eukaryotic Translation Initiation and Principles of its Regulation. *Nat. Rev. Mol. Cell Biol.* 11, 113–127. doi:10.1038/nrm2838

Jemielity, J., Fowler, T., Zuberek, J., Stepinski, J., Lewdorowicz, M., Niedzwiecka, A., et al. (2003). Novel "Anti-reverse" Cap Analogs with Superior Translational Properties. *RNA* 9 (9), 1108–1122. doi:10.1261/rna.5430403

John, S., Yuzhakov, O., Woods, A., Deterling, J., Hassett, K., Shaw, C. A., et al. (2018). Multi-antigenic Human Cytomegalovirus mRNA Vaccines that Elicit Potent Humoral and Cell-Mediated Immunity. *Vaccine* 36 (12), 1689–1699. doi:10.1016/j.vaccine.2018.01.029

Karikó, K., Buckstein, M., Ni, H., and Weissman, D. (2005). Suppression of RNA Recognition by Toll-like Receptors: The Impact of Nucleoside Modification and the Evolutionary Origin of RNA. *Immunity* 23, 165–175. doi:10.1016/j.immuni.2005.06.008

Karikó, K., Muramatsu, H., Ludwig, J., and Weissman, D. (2011). Generating the Optimal mRNA for Therapy: HPLC Purification Eliminates Immune Activation and Improves Translation of Nucleoside-Modified, Protein-Encoding mRNA. *Nucleic Acids Res.* 39 (21), e142. doi:10.1093/nar/gkr695

Karikó, K., Muramatsu, H., Welsh, F. A., Ludwig, J., Kato, H., Akira, S., et al. (2008). Incorporation of Pseudouridine into mRNA Yields Superior Nonimmunogenic Vector with Increased Translational Capacity and Biological Stability. *Mol. Ther.* 16 (11), 1833–1840. doi:10.1038/mt.2008.200

Kaur, K., and Zangi, L. (2020). Modified mRNA as a Therapeutic Tool for the Heart. *Cardiovasc Drugs Ther.* 34, 871–880. doi:10.1007/s10557-020-07051-4

Kawaguchi, D., Kodama, A., Abe, N., Takebuchi, K., Hashiya, F., Tomoike, F., et al. (2020). Phosphorothioate Modification of mRNA Accelerates the Rate of Translation Initiation to Provide More Efficient Protein Synthesis. *Angew. Chem. Int. Ed.* 59 (40), 17403–17407. doi:10.1002/anie.202007111

Kawasaki, T., and Kawai, T. (2014). Toll-like Receptor Signaling Pathways. *Front. Immunol.* 5, 461. doi:10.3389/fimmu.2014.00461

Kis, Z., Kontoravdi, C., Shattock, R., and Shah, N. (2021). Resources, Production Scales and Time Required for Producing RNA Vaccines for the Global Pandemic Demand. *Vaccines* 9, 3. doi:10.3390/vaccines9030205

Kore, A. R., Shanmugasundaram, M., Charles, I., Vlassov, A. V., and Barta, T. J. (2009). Locked Nucleic Acid (LNA)-modified Dinucleotide mRNA Cap Analogue: Synthesis, Enzymatic Incorporation, and Utilization. *J. Am. Chem. Soc.* 131 (18), 6364–6365. doi:10.1021/ja901655p

Kormann, M. S. D., Hasenpusch, G., Aneja, M. K., Nica, G., Flemmer, A. W., Herber-Jonat, S., et al. (2011). Expression of Therapeutic Proteins after Delivery of Chemically Modified mRNA in Mice. *Nat. Biotechnol.* 29 (2), 154–157. doi:10.1038/nbt.1733

Kowalska, J., Lukaszewicz, M., Zuberek, J., Darzynkiewicz, E., and Jemielity, J. (2009). Phosphoroselenoate Dinucleotides for Modification of mRNA 5′ End. *ChemBioChem* 10, 2469–2473. doi:10.1002/cbic.200900522

Kowalska, J., Wypijewska del Nogal, A., Darzynkiewicz, Z. M., Buck, J., Nicola, C., Kuhn, A. N., et al. (2014). Synthesis, Properties, and Biological Activity of Boranophosphate Analogs of the mRNA Cap: Versatile Tools for Manipulation of Therapeutically Relevant Cap-dependent Processes. *Nucleic Acids Res.* 42 (16), 10245–10264. doi:10.1093/nar/gku757

Kowalski, P. S., Rudra, A., Miao, L., and Anderson, D. G. (2019). Delivering the Messenger: Advances in Technologies for Therapeutic mRNA Delivery. *Mol. Ther.* 27 (4), 710–728. doi:10.1016/j.ymthe.2019.02.012

Kranz, L. M., Vormehr, M., Diesckmann, J., Lindemann, C., Eisel, D., Muik, A., et al. (2019). *Complementary Effects of RNA Encoded, Extended Half-Life IL2 and IL7 Synergize in Modulating T Cell Responses and Anti-tumoral Efficacy*. SITC. Abstract P620.

Kuhn, A. N., Diken, M., Kreiter, S., Selmi, A., Kowalska, J., Jemielity, J., et al. (2010). Phosphorothioate Cap Analogs Increase Stability and Translational Efficiency of RNA Vaccines in Immature Dendritic Cells and Induce Superior Immune Responses *In Vivo*. *Gene Ther.* 17, 961–971. doi:10.1038/gt.2010.52

Lee, J., Sayed, N., Hunter, A., Au, K. F., Wong, W. H., Mocarski, E. S., et al. (2012). Activation of Innate Immunity Is Required for Efficient Nuclear Reprogramming. *Cell* 151, 547–558. doi:10.1016/j.cell.2012.09.034

Li, B., Luo, X., and Dong, Y. (2016). Effects of Chemically Modified Messenger RNA on Protein Expression. *Bioconjugate Chem.* 27 (3), 849–853. doi:10.1021/acs.bioconjchem.6b00090

Lou, X., Wang, J.-J., Wei, Y.-Q., and Sun, J.-J. (2021). Emerging Role of RNA Modification N6-Methyladenosine in Immune Evasion. *Cell Death Dis.* 12, 300. doi:10.1038/s41419-021-03585-z

Meyer, M., Huang, E., Yuzhakov, O., Ramanathan, P., Ciaramella, G., and Bukreyev, A. (2018). Modified mRNA-Based Vaccines Elicit Robust Immune Responses and Protect Guinea Pigs from Ebola Virus Disease. *J. Infect. Dis.* 217 (3), 451–455. doi:10.1093/infdis/jix592

Miao, L., Zhang, Y., and Huang, L. (2021). mRNA Vaccine for Cancer Immunotherapy. *Mol. Cancer* 20, 41. doi:10.1186/s12943-021-01335-5

Miliotou, A. N., Pappas, I. S., Spyroulias, G., Vlachaki, E., Tsiftsoglou, A. S., Vizirianakis, I. S., et al. (2021). Development of a Novel PTD-Mediated IVT-mRNA Delivery Platform for Potential Protein Replacement Therapy of Metabolic/genetic Disorders. *Mol. Ther. - Nucleic Acids* 26, 694–710. doi:10.1016/j.omtn.2021.09.008

Morais, P., Adachi, H., and Yu, Y. T. (2021). The Critical Contribution of Pseudouridine to mRNA COVID-19 Vaccines. *Front. Cell Dev. Biol.* 9, 789427. doi:10.3389/fcell.2021.789427

Muttach, F., Muthmann, N., and Rentmeister, A. (2017). Synthetic mRNA Capping. *Beilstein J. Org. Chem.* 13, 2819–2832. doi:10.3762/bjoc.13.274

Nachtergaele, S., and He, C. (2018). Chemical Modifications in the Life of an mRNA Transcript. *Annu. Rev. Genet.* 52, 349–372. doi:10.1146/annurev-genet-120417-031522

Nallagatla, S. R., and Bevilacqua, P. C. (2008). Nucleoside Modifications Modulate Activation of the Protein Kinase PKR in an RNA Structure-specific Manner. *RNA* 14 (6), 1201–1213. doi:10.1261/rna.1007408

Nance, K. D., and Meier, J. L. (2021). Modifications in an Emergency: the Role of N1-Methylpseudouridine in COVID-19 Vaccines. *ACS Cent. Sci.* 7, 748–756. doi:10.1021/acscentsci.1c00197

Nelson, J., Sorensen, E. W., Mintri, S., Rabideau, A. E., Zheng, W., Besin, G., et al. (2020). Impact of mRNA Chemistry and Manufacturing Process on Innate Immune Activation. *Sci. Adv.* 6 (26), eaaz6893. doi:10.1126/sciadv.aaz6893

Pardi, N., Hogan, M. J., Pelc, R. S., Muramatsu, H., Andersen, H., DeMaso, C. R., et al. (2017). Zika Virus Protection by a Single Low-Dose Nucleoside-Modified mRNA Vaccination. *Nature* 543, 248–251. doi:10.1038/nature21428

Polack, F. P., Thomas, S. J., Kitchin, N., Absalon, J., Gurtman, A., Lockhart, S., et al. (2020). Safety and Efficacy of the BNT162b2 mRNA Covid-19 Vaccine. *N. Engl. J. Med.* 383, 2603–2615. doi:10.1056/nejmoa2034577

Rabinovich, P. M., Komarovskaya, M. E., Ye, Z.-J., Imai, C., Campana, D., Bahceci, E., et al. (2006). Synthetic Messenger RNA as a Tool for Gene Therapy. *Hum. Gene Ther.* 17 (10), 1027–1035. doi:10.1089/hum.2006.17.1027

Rehwinkel, J., and Gack, M. U. (2020). RIG-I-like Receptors: Their Regulation and Roles in RNA Sensing. *Nat. Rev. Immunol.* 20, 537–551. doi:10.1038/s41577-020-0288-3

Rizvi, F., Everton, E., Smith, A. R., Liu, H., Osota, E., Beattie, M., et al. (2021). Murine Liver Repair via Transient Activation of Regenerative Pathways in Hepatocytes Using Lipid Nanoparticle-Complexed Nucleoside-Modified mRNA. *Nat. Commun.* 12, 613. doi:10.1038/s41467-021-20903-3

Rydzik, A. M., Kulis, M., Lukaszewicz, M., Kowalska, J., Zuberek, J., Darzynkiewicz, Z. M., et al. (2012). Synthesis and Properties of mRNA Cap Analogs Containing Imidodiphosphate Moiety-Fairly Mimicking Natural Cap Structure, yet Resistant to Enzymatic Hydrolysis. *Bioorg. Med. Chem.* 20 (5), 1699–1710. doi:10.1016/j.bmc.2012.01.013

Sahin, U., Karikó, K., and Türeci, Ö. (2014). mRNA-based Therapeutics - Developing a New Class of Drugs. *Nat. Rev. Drug Discov.* 13, 759–780. doi:10.1038/nrd4278

Schlee, M., and Hartmann, G. (2016). Discriminating Self from Non-self in Nucleic Acid Sensing. *Nat. Rev. Immunol.* 16, 566–580. doi:10.1038/nri.2016.78

Schlee, M. (2013). Master Sensors of Pathogenic RNA - RIG-I like Receptors. *Immunobiology* 218 (11), 1322–1335. doi:10.1016/j.imbio.2013.06.007

Schuberth-Wagner, C., Ludwig, J., Bruder, A. K., Herzner, A.-M., Zillinger, T., Goldeck, M., et al. (2015). A Conserved Histidine in the RNA Sensor RIG-I Controls Immune Tolerance to N1-2′o-Methylated Self RNA. *Immunity* 43, 41–51. doi:10.1016/j.immuni.2015.06.015

Senthilvelan, A., Vonderfecht, T., Shanmugasundaram, M., Pal, I., Potter, J., and Kore, A. R. (2021). Trinucleotide Cap Analogue Bearing a Locked Nucleic Acid Moiety: Synthesis, mRNA Modification, and Translation for Therapeutic Applications. *Org. Lett.* 23 (11), 4133–4136. doi:10.1021/acs.orglett.1c01037

Shanmugasundaram, M., Charles, I., and Kore, A. R. (2016). Design, Synthesis and Biological Evaluation of Dinucleotide mRNA Cap Analog Containing Propargyl Moiety. *Bioorg. Med. Chem.* 24 (6), 1204–1208. doi:10.1016/j.bmc.2016.01.048

Shaw, C., Lee, H., Knightly, C., Kalidindi, S., Zaks, T., Smolenov, I., et al. (2019). Phase 1 Trial of an mRNA-Based Combination Vaccine against hMPV and PIV3. *Open Forum Infect. Dis.* 6 (Suppl. 2), S970.

Shi, Y., Inoue, H., Wu, J. C., and Yamanaka, S. (2017). Induced Pluripotent Stem Cell Technology: a Decade of Progress. *Nat. Rev. Drug Discov.* 16, 115–130. doi:10.1038/nrd.2016.245

Sikorski, P. J., Warminski, M., Kubacka, D., Ratajczak, T., Nowis, D., Kowalska, J., et al. (2020). The Identity and Methylation Status of the First Transcribed Nucleotide in Eukaryotic mRNA 5′ Cap Modulates Protein Expression in Living Cells. *Nucleic Acids Res.* 48 (4), 1607–1626. doi:10.1093/nar/gkaa032

Stadler, C. R., Bähr-Mahmud, H., Celik, L., Hebich, B., Roth, A. S., Roth, R. P., et al. (2017). Elimination of Large Tumors in Mice by mRNA-Encoded Bispecific Antibodies. *Nat. Med.* 23, 815–817. doi:10.1038/nm.4356

Stepinski, J., Waddell, C., Stolarski, R., Darzynkiewicz, E., and Rhoads, R. E. (2001). Synthesis and Properties of mRNAs Containing the Novel "Anti-reverse" Cap Analogs 7-Methyl(3'-O-methyl)GpppG and 7-methyl (3'-deoxy)GpppG. *RNA* 7 (10), 1486–1495.

Strenkowska, M., Grzela, R., Majewski, M., Wnek, K., Kowalska, J., Lukaszewicz, M., et al. (2016). Cap Analogs Modified with 1,2-dithiodiphosphate Moiety Protect mRNA from Decapping and Enhance its Translational Potential. *Nucleic Acids Res.* 44 (20), 9578–9590. doi:10.1093/nar/gkw896

Strzelecka, D., Smietanski, M., Sikorski, P. J., Warminski, M., Kowalska, J., and Jemielity, J. (2020). Phosphodiester Modifications in mRNA Poly(A) Tail Prevent Deadenylation without Compromising Protein Expression. *RNA* 26 (12), 1815–1837. doi:10.1261/rna.077099.120

Svitkin, Y. V., Cheng, Y. M., Chakraborty, T., Presnyak, V., John, M., and Sonenberg, N. (2017). N1-methyl-pseudouridine in mRNA Enhances Translation through eIF2α-dependent and Independent Mechanisms by Increasing Ribosome Density. *Nucleic Acids Res.* 45 (10), 6023–6036. doi:10.1093/nar/gkx135

Tatematsu, M., Funami, K., Seya, T., and Matsumoto, M. (2018). Extracellular RNA Sensing by Pattern Recognition Receptors. *J. Innate Immun.* 10, 398–406. doi:10.1159/000494034

Tohda, H., Chikazumi, N., Ueda, T., Nishikawa, K., and Watanabe, K. (1994). Efficient Expression of E. coli Dihydrofolate Reductase Gene by an *In Vitro* Translation System Using Phosphorothioate mRNA. *J. Biotechnol.* 34 (1), 61–69. doi:10.1016/0168-1656(94)90166-x

Uchida, S., Kataoka, K., and Itaka, K. (2015). Screening of mRNA Chemical Modification to Maximize Protein Expression with Reduced Immunogenicity. *Pharmaceutics* 7 (3), 137–151. doi:10.3390/pharmaceutics7030137

Ueda, T., Tohda, H., Chikazumi, N., Eckstein, F., and Watanabe, K. (1991). Phosphorothioate-containing RNAs Show mRNA Activity in the Prokaryotic Translation Systemsin Vitro. *Nucl. Acids Res.* 19 (3), 547–552. doi:10.1093/nar/19.3.547

Vormehr, M. (2019). *Substantial Improvement of Cancer Immunotherapy by an RNA Encoded Extend-Ed Half-Life Interleukin-2 Variant*. SITC. Abstract P626.

Warminski, M., Kowalska, J., Buck, J., Zuberek, J., Lukaszewicz, M., Nicola, C., et al. (2013). The Synthesis of Isopropylidene mRNA Cap Analogs Modified with Phosphorothioate Moiety and Their Evaluation as Promoters of mRNA Translation. *Bioorg. Med. Chem. Lett.* 23 (13), 3753–3758. doi:10.1016/j.bmcl.2013.05.001

Warren, L., and Lin, C. (2019). mRNA-based Genetic Reprogramming. *Mol. Ther.* 27 (4), 729–734. doi:10.1016/j.ymthe.2018.12.009

Warren, L., Manos, P. D., Ahfeldt, T., Loh, Y.-H., Li, H., Lau, F., et al. (2010). Highly Efficient Reprogramming to Pluripotency and Directed Differentiation of Human Cells with Synthetic Modified mRNA. *Cell Stem Cell* 7 (5), 618–630. doi:10.1016/j.stem.2010.08.012

Weissman, D. (2015). mRNA Transcript Therapy. *Expert Rev. vaccines* 14 (2), 265–281. doi:10.1586/14760584.2015.973859

Weng, Y., Li, C., Yang, T., Hu, B., Zhang, M., Guo, S., et al. (2020). The Challenge and Prospect of mRNA Therapeutics Landscape. *Biotechnol. Adv.* 40, 107534. doi:10.1016/j.biotechadv.2020.107534

Wojcik, R., Baranowski, M. R., Markiewicz, L., Kubacka, D., Bednarczyk, M., Baran, N., et al. (2021). Novel N7-Arylmethyl Substituted Dinucleotide mRNA 5' Cap Analogs: Synthesis and Evaluation as Modulators of Translation. *Pharmaceutics* 13 (11). doi:10.3390/pharmaceutics13111941

Wojtczak, B. A., Sikorski, P. J., Fac-Dabrowska, K., Nowicka, A., Warminski, M., Kubacka, D., et al. (2018). 5′-Phosphorothiolate Dinucleotide Cap Analogues: Reagents for Messenger RNA Modification and Potent Small-Molecular Inhibitors of Decapping Enzymes. *J. Am. Chem. Soc.* 140 (18), 5987–5999. doi:10.1021/jacs.8b02597

Wolff, J. A., Malone, R. W., Williams, P., Chong, W., Acsadi, G., Jani, A., et al. (1990). Direct Gene Transfer into Mouse Muscle *In Vivo*. *Science* 247, 1465–1468. doi:10.1126/science.1690918

World Health Organization (2020). *International Nonproprietary Names Programme. Messenger RNA Encoding the Full-Length SARS-CoV-2 Spike Glycoprotein*, 11889.

Wu, N. C., Zost, S. J., Thompson, A. J., Oyen, D., Nycholat, C. M., McBride, R., et al. (2017). A Structural Explanation for the Low Effectiveness of the Seasonal Influenza H3N2 Vaccine. *PLoS Pathog.* 13 (10), e1006682. doi:10.1371/journal.ppat.1006682

Zangi, L., Lui, K. O., von Gise, A., Ma, Q., Ebina, W., Ptaszek, L. M., et al. (2013). Modified mRNA Directs the Fate of Heart Progenitor Cells and Induces Vascular Regeneration after Myocardial Infarction. *Nat. Biotechnol.* 31, 898–907. doi:10.1038/nbt.2682

Zhang, C., Maruggi, G., Shan, H., and Li, J. (2019). Advances in mRNA Vaccines for Infectious Diseases. *Front. Immunol.* 10, 594. doi:10.3389/fimmu.2019.00594

Zhang, H.-X., Zhang, Y., and Yin, H. (2019). Genome Editing with mRNA Encoding ZFN, TALEN, and Cas9. *Mol. Ther.* 27 (4), 735–746. doi:10.1016/j.ymthe.2019.01.014

Züst, R., Cervantes-Barragan, L., Habjan, M., Maier, R., Neuman, B. W., Ziebuhr, J., et al. (2011). Ribose 2'-O-Methylation Provides a Molecular Signature for the Distinction of Self and Non-self mRNA Dependent on the RNA Sensor Mda5. *Nat. Immunol.* 12, 137–143.

Conflict of Interest: XW is an inventor of chimeric-RNA related patent application.

The remaining author declares that the research was conducted in the absence of any commercial or financial relationships that could be construed as a potential conflict of interest.

Publisher's Note: All claims expressed in this article are solely those of the authors and do not necessarily represent those of their affiliated organizations, or those of the publisher, the editors and the reviewers. Any product that may be evaluated in this article, or claim that may be made by its manufacturer, is not guaranteed or endorsed by the publisher.

Copyright © 2022 Liu and Wang. This is an open-access article distributed under the terms of the Creative Commons Attribution License (CC BY). The use, distribution or reproduction in other forums is permitted, provided the original author(s) and the copyright owner(s) are credited and that the original publication in this journal is cited, in accordance with accepted academic practice. No use, distribution or reproduction is permitted which does not comply with these terms.

frontiers | Frontiers in Cell and Developmental Biology

TYPE Original Research
PUBLISHED 01 November 2022
DOI 10.3389/fcell.2022.999351

Check for updates

OPEN ACCESS

EDITED BY
Huilin Huang,
Sun Yat-sen University Cancer Center (SYSUCC), China

REVIEWED BY
Tuan Anh Nguyen,
Hong Kong University of Science and Technology, Hong Kong SAR, China
Banhi Biswas,
Johns Hopkins University, United States

*CORRESPONDENCE
Viviana Simon,
viviana.simon@mssm.edu
Tao Pan,
taopan@uchicago.edu

SPECIALTY SECTION
This article was submitted to Epigenomics and Epigenetics, a section of the journal Frontiers in Cell and Developmental Biology

RECEIVED 20 July 2022
ACCEPTED 26 September 2022
PUBLISHED 01 November 2022

CITATION
Katanski CD, Alshammary H, Watkins CP, Huang S, Gonzales-Reiche A, Sordillo EM, van Bakel H, Mount Sinai PSP study group, Lolans K, Simon V and Pan T (2022), tRNA abundance, modification and fragmentation in nasopharyngeal swabs as biomarkers for COVID-19 severity.
Front. Cell Dev. Biol. 10:999351.
doi: 10.3389/fcell.2022.999351

COPYRIGHT
© 2022 Katanski, Alshammary, Watkins, Huang, Gonzales-Reiche, Sordillo, van Bakel, Mount Sinai PSP study group, Lolans, Simon and Pan. This is an open-access article distributed under the terms of the Creative Commons Attribution License (CC BY). The use, distribution or reproduction in other forums is permitted, provided the original author(s) and the copyright owner(s) are credited and that the original publication in this journal is cited, in accordance with accepted academic practice. No use, distribution or reproduction is permitted which does not comply with these terms.

tRNA abundance, modification and fragmentation in nasopharyngeal swabs as biomarkers for COVID-19 severity

Christopher D. Katanski[1], Hala Alshammary[2,3], Christopher P. Watkins[1], Sihao Huang[1], Ana Gonzales-Reiche[4,5], Emilia Mia Sordillo[6], Harm van Bakel[4,7], Mount Sinai PSP study group, Karen Lolans[8], Viviana Simon[2,3,5,6,9]* and Tao Pan[1]*

[1]Department of Biochemistry and Molecular Biology, University of Chicago, Chicago, IL, United States, [2]Department of Microbiology, Icahn School of Medicine at Mount Sinai, New York, NY, United States, [3]Center for Vaccine Research and Pandemic Preparedness (C-VARPP), Icahn School of Medicine at Mount Sinai, New York, NY, United States, [4]Department of Genetics and Genomic Sciences, Icahn School of Medicine at Mount Sinai, New York, NY, United States, [5]The Global Health and Emerging Pathogens Institute, Icahn School of Medicine at Mount Sinai, New York, NY, United States, [6]Department of Pathology, Molecular and Cell-Based Medicine, Icahn School of Medicine at Mount Sinai, New York, NY, United States, [7]Icahn Genomics Institute, Icahn School of Medicine at Mount Sinai, New York, NY, United States, [8]Department of Medicine, University of Chicago, Chicago, IL, United States, [9]Division of Infectious Diseases, Department of Medicine, Icahn School of Medicine at Mount Sinai, New York, NY, United States

Emerging and re-emerging respiratory viruses can spread rapidly and cause pandemics as demonstrated by the recent severe acute respiratory syndrome coronavirus 2 (SARS-CoV-2) pandemic. The early human immune responses to respiratory viruses are in the nasal cavity and nasopharyngeal regions. Defining biomarkers of disease trajectory at the time of a positive diagnostic test would be an important tool to facilitate decisions such as initiation of antiviral treatment. We hypothesize that nasopharyngeal tRNA profiles could be used to predict Coronavirus Disease 19 (COVID-19) severity. We carried out multiplex small RNA sequencing (MSR-seq) on residual nasopharyngeal swabs to measure simultaneously full-length tRNA abundance, tRNA modifications, and tRNA fragmentation for the human tRNA response to SARS-CoV-2 infection. We identified distinct tRNA signatures associated with mild symptoms versus severe COVID-19 manifestations requiring hospitalization. These results highlight the utility of host tRNA properties as biomarkers for the clinical outcome of SARS-CoV-2.

KEYWORDS

tRNA, modification, fragmentation, biomarker, SARS-CoV-2, COVID-19 severity

Introduction

A major response of biological systems to environmental change is regulated protein synthesis where transfer RNA (tRNA) plays a key role in decoding genetic information on-demand. tRNAs are small non-coding RNAs (74–95 residues) that read the genetic code and provide amino acids in protein synthesis. A human cell has several hundred tRNA sequences, up to 100 million tRNA transcripts, and each human tRNA contains on average 13 modifications (Chan and Lowe, 2016; Boccaletto et al., 2022). Modifications in tRNAs are dynamically regulated during cellular stress (Begley et al., 2007; Gu et al., 2014; Zhang et al., 2022) and can affect decoding speed and accuracy of translation. Hypo-modified tRNAs can also become better substrates for RNase cleavage leading to tRNA fragment generation (Huang and Hopper, 2016; Oberbauer and Schaefer, 2018). tRNA fragments are a family of small RNAs that participate in many regulatory processes at the cellular and organismal levels (Anderson and Ivanov, 2014; Schimmel, 2018; Pandey et al., 2021). In the context of viral infections, tRNAs as well as tRNA fragments may facilitate viral replication (Jin and Musier-Forsyth, 2019; Nunes et al., 2020).

Understanding the determinants of severity of viral infections is important for selecting the appropriate level of clinical care including initiation of therapeutic interventions aimed at preventing severe outcomes. In the case of emerging viral pathogens such as severe acute respiratory syndrome coronavirus-2 (SARS-CoV-2), a major challenge is the wide range of Coronavirus Disease 19 (COVID-19) severities. Many viral and host factors influence the symptom severity upon infection, including age, co-morbidities, host genetics and possibly SARS-CoV-2 variant. However, it remains difficult to predict which COVID-19 patients will develop mild or severe symptoms at the time of diagnosis.

Activated immune cells known as granulocytes secrete RNases as part of the innate immune response. In humans, eight secreted RNase genes have been identified, each with a range of antiviral, antibacterial and/or cytotoxic functions (Koczera et al., 2016; Lu et al., 2018). We propose that tRNAs, due to their high abundance and RNase resistance, represent one of the best opportunities to detect early immune activation in the context of viral infection by measuring their ongoing fragmentation, alteration in abundance and in modification levels. These measurements can be made directly from virally lysed or apoptotic epithelial tissues, which often represent the sites of initial respiratory viral infection.

Here we apply Multiplex Small RNA-seq [MSR-seq, (Watkins et al., 2022)] to identify tRNA-based biomarkers to predict SARS-CoV-2 infection severity at the time of a positive test. MSR-seq simultaneously measures tRNA abundance, fragmentation and modifications in a single sequencing library generated directly from RNA isolated from the viral transport media of the diagnostic nasopharyngeal swab. Our results show that multiple tRNA properties vary significantly among individuals with COVID-19 who develop no/mild versus severe symptoms, thus indicating the biomarker potential of human nasal tRNA responses to an infectious disease such as COVID-19.

Materials and methods

Ethics statement

The Mount Sinai Pathogens Surveillance Program (MS-PSP) systematically collected residual nasopharyngeal swab samples that tested positive for respiratory pathogens (e.g., SARS-CoV-2, Influenza A virus) after clinical testing was completed. A subset of representative specimen was selected for viral genome sequencing in the context of precision surveillance (Gonzalez-Reiche et al., 2020; Javaid et al., 2021) and remaining RNA was included in this study. The residual diagnostic specimen used in this study were collected during the first wave of the pandemic (March–May 2020) when ancestral SARS-CoV-2 variants were circulating (Gonzalez-Reiche et al., 2020). The Institutional Review Board of the Icahn School of Medicine at Mount Sinai reviewed and approved MS-PSP (13-00981) as well as this study (21-01934).

Total RNA extraction from viral transport media

Total RNA was extracted from viral transport media (VTM) of the nasopharyngeal swabs using high-throughput specimen processing (KingFisher Flex Purification System, ThermoFisher, cat. 5400610). The MagMax mirVana Total RNA Isolation Kit (ThermoFisher, cat. A27828) was used to extract total RNA from 250 µL of viral transport medium, as per the manufacturer's protocol. The total nucleic acid concentration measured by nanodrop absorbance ranged from 4–40 ng/µL.

RNA sample selection

We selected for this study 56 RNA samples extracted from nasopharyngeal swabs that tested positive for SARS-CoV-2, four RNA samples from nasopharyngeal swabs that tested positive for Influenza A, and five RNA samples from individuals without any known viral infection (uninfected control). All SARS-CoV-2 tested samples were collected during the first wave of the SARS-CoV-2 pandemic in New York City (March–May 2020). Thirty-five RNA samples were extracted from VTM of nasopharyngeal swabs collected from individuals who tested positive for SARS-CoV-2 but did not require hospitalization

at the time of testing (Group I) while 21 RNA samples were extracted from VTM of nasopharyngeal swabs collected from individuals who were admitted to the hospital due to severe COVID-19 manifestations at the time of testing (Group II).

Multiplex small RNA sequencing library construction

MSR-seq library construction followed the same procedure as described previously (Watkins et al., 2022). A total of 10 µL of each extracted sample described above were used for sequencing library construction. The key features of MSR-seq are to first ligate total RNA with a bar-coded capture hairpin oligonucleotide which enables pooling of up to 12 bar-coded samples for all subsequent steps. The specific design of the capture hairpin oligo allows for all subsequent steps to be carried out on magnetic streptavidin beads. The basic steps of library construction include 1) deacylation to remove charged amino acids to tRNA; 2) 3' end repair to remove all 3' phosphate/cyclic phosphate; 3) first ligation of the barcoded hairpin oligonucleotide; 4) sample pooling, mix with streptavidin beads, wash; 5) remove 3' phosphate of the capture hairpin oligo; wash; 6) reverse transcription using a thermophilic RT and overnight extension; 7) remove RNA; 8) periodate oxidation to block unligated hairpin oligonucleotide; 9) second ligation of PCR primer; 10) PCR using Illumina index primers.

For low abundant RNA samples, a gel purification step of the final PCR products was added to remove the excess primer only products as follows. After PCR, amplicons were concentrated using the Zymo DNA Clean & Concentrate spin columns (7 equivalents of DNA binding buffer to 1 equivalent of PCR reaction; e.g. 350 µL of DNA binding buffer to 50 µL PCR reaction). Samples were eluted in 12 µL of deionized, autoclaved water.

After eluting off the column, samples were mixed with 2.5 µL of 6x TriTrack gel loading dye and loaded onto a 6% Novex TBE gel. Samples, together with dsDNA size markers were electrophoresed at 180 V for approximately 40 min. After electrophoresis, the gel was incubated for 10 min in 1x SYBR Gold and then imaged on a blue light box. Samples were cut from approximately 170–300 bp, whereas the primer alone products containing barcodes and indexes were approximately 140–145 bp.

After cutting, gel fragments were crushed using a 1 ml pipette tip and then 500 µL of gel elution buffer (200 mM KCl, 50 mM KOAc, pH 7). Gel fragments were incubated overnight (12 + hours). After overnight incubation, samples were centrifuged for 10 min at room temperature at 10,000 g^{-1}. The supernatant was then collected and the samples were then centrifuged again to remove any remaining gel fragments. Next, 1 µL of GlycoBlue and 500 µL of isopropanol were added to each tube and the tubes were then placed in a −80°C freezer for a minimum of 1 h.

After cold incubation, the samples were centrifuged at 4°C for 1 h at 17,000 g^{-1}. The supernatant was then removed and the remaining pellet was resuspended in 20 µL of deionized, autoclaved water.

Data analysis

Read processing and mapping: Libraries were sequenced on Illumina Nova-seq S(1)-200) platform, 100 bp paired-end. First, paired end reads were split by barcode sequence using Je demultiplex with options BPOS = BOTH BM = READ_1 LEN = 4:6 FORCE = true C = false 6. Next read 2 files were used to map with bowtie2 with the following parameters: q -p 10 --local—no-unal. Reads were mapped to curated hg19 list of non-redundant tRNA genes with tRNAScan score >40 (Lowe and Chan, 2016). Bowtie2 output sam files were converted to bam files, then sorted using samtools (Danecek et al., 2021). Next IGV was used to collapse reads into 1 nt window. IGV output. wig files were reformatted using custom python scripts (available on GitHub at https://github.com/ckatanski/MSR-seq). The bowtie2 output Sam files were also used as input for a custom python script using PySam, a python wrapper for SAMTools (https://github.com/pysam-developers/pysam) to sum all reads that mapped to each gene. Data was visualized with custom R scripts (available on GitHub at https://github.com/ckatanski/CovidNasalSwabs_2022ck).

tRNA fragmentation: tRNA fragments were identified as previously described (Watkins et al., 2022). Briefly, the precise 3' end of the read in the MSR-seq procedure represents the 3' end of the RNA present in the sample. We binned the ends with 3' ends mapped to the individual tRNA genes between nucleotides 20–30, 30–40, 40–50, 50–60 and >60 (full-length). These bins roughly correspond to the stem loops in tRNA structure and can be used to characterize the broad types of tRNA fragment. The fraction of a fragment was calculated by comparing the number of reads in one bin compared to all the reads in every bin for a particular gene from a particular patient. To summarize the data, the number of reads that sort to each bin among all genes was summed for each patient.

tRNA abundance: Relative abundance of individual tRNA isodecoders was normalized to the 5.8S rRNA reads within each sample. This normalized abundance was then compared between patient groups.

tRNA modification: Mutation rates from bowtie mapping at individual sites were used to estimate modification rates. Analysis focused on well characterized sites with known modifications. Mutation rate is not a 1-to-1 output for modification fraction, but it is known to vary linearly. Thus relative changes are a reliable metric for relative changes in modification levels. Analysis was limited to sites and samples with >50 reads and a >2% mutation rate. After initial site selection, the 2% mutation filter was relaxed for individual site

analysis so as to include samples which may have been excluded from initial screening.

p-value calculations: To identify differentially expressed, fragmented, or modified tRNAs, patient group comparisons for individual genes were performed with pairwise two-sided t-tests with no correction. To normalize tRNA abundance reads among patients, all abundances were normalized to the well detected 5.8S rRNA reads within the same sample. This normalized abundance was calculated for every tRNA gene using all sense-mapped reads. Comparing abundance of an individual gene between patient groups was done with a two-sided pairwise *t*-test with no correction. Analysis was restricted to isodecoders and samples with >10 reads for the respective tRNA sequence. To compare tRNA fragmentations, reads were subdivided based on the position of the 3' end mapping. With MSR-seq, this is a faithful representation of the biological 3' end of the tRNA and can separate fragments from full length tRNAs. Calculation was restricted to only sense reads, and fragments with >10 reads. Notably, similar analysis cannot be done for the 5' end since truncated 5' ends could reflect biological fragments or premature termination of reverse transcription in sequencing library preparation. To compare tRNA modifications among patient groups, we calculated the mutation rate at every base for every gene between patient groups using a two-sided pairwise *t*-test with no correction, at a filter of >50 reads per site.

Logistic regression (LR) models and ROC curves: The samples with non-NULL values in the selected features were used to build the LR models (McKinney, 2010; Pedregosa et al., 2011; Harris et al., 2020). The data were shuffled and normalized. Then, 3-fold cross-validation was performed with abundance (rpm/5.8S rpm) of $tRNA^{iMet}$-c1t32, mutation rate at position 9 for mitochondrial $tRNA^{Val}$, fragmentation calculated with $tRNA^{Arg}$(ACG) isoacceptor family in the 30–40 bin or a combination of the three biomarkers and the scores of each sample are predicted. Specificity, sensitivity and AUC (area under curve) were calculated (Pedregosa et al., 2011) and the ROC curves drawn (Hunter, 2007) with python.

Clustering heatmap: The biomarkers with non-NULL values in at least 50% of the mild symptom samples and 50% of the severe symptom samples were selected. For the 68 selected biomarkers, NULL values were filled by the median of all the samples in the mild or severe groups respectively. Then, the data were normalized. The samples were ordered by their 3-fold cross validation scores in the LR model (McKinney, 2010; Pedregosa et al., 2011; Harris et al., 2020) with 68 selected biomarkers in the heatmap (Michael Waskom et al., 2017). The selected biomarkers were clustered in the heatmap.

Results and discussion

We analyzed the tRNA profile (abundance, modification and fragmentation) using total RNA extracted from residual diagnostic specimen collected from individuals with symptoms suggestive of upper respiratory tract infection who tested positive for SARS-CoV-2. These samples were collected during the first wave of the pandemic when only ancestral SARS-CoV-2 variants were circulating. These biospecimen are of low-biomass and contain only very small amounts of RNA. Using a new library construction technology for tRNA sequencing that uses total RNA from any biological source and on-bead library construction (Watkins et al., 2022), we obtained tRNA-seq data informing simultaneously on full-length tRNA abundance, certain tRNA modifications, as well as 5' tRNA fragments (5'tRF). After library construction and sequencing we found that RNAs could be mapped to tRNA and other small RNAs at appreciate rates (Supplementary Table S1) with average mapped read counts of 1,006,000, 131,000, 1,102,500 for all small RNA and 397,500, 77,100, 285,000 for tRNA of the uninfected, influenza, and SARS-CoV-2 infected samples, respectively. While these rates are lower than tRNA-seq from cell cultures, they still reveal the potential to obtain high quality small RNA sequencing data from viral transport media of nasopharyngeal swabs used for diagnostic nucleic acid amplification testing (NAAT). Ultimately RNA-seq would be too costly and time-consuming to serve as a practical tool for triage, however our goal was to identify potential prognostic biomarkers for further development using scalable nucleic acid technologies such as qPCR.

We first analyzed 5'tRF differences among the SARS-CoV-2, influenza, and uninfected groups by binning the tRNA reads with the 3' end in different tRNA positions [(Watkins et al., 2022), Figure 1A]. Approximately 85% of the tRNA reads had 3' ends past nucleotide 60 which roughly corresponded to the full-length tRNAs in our analysis. tRNA fragmentation occurred extensively in all samples, compared to well-controlled samples from cell culture (Watkins et al., 2022). Globally, fragmentations of tRNAs were present with cleavage sites in all tRNA regions. As expected, cleavage in the anticodon loop region (3' ends within position 30–40 of tRNA, anticodon positions approximately 34–36) generated the highest amount of tRF products. Since fragmentation was not evenly distributed among accessible loop regions, this suggests some level of biological specificity. Influenza-infected patients showed a much greater degree of fragmentation compared to healthy subjects, though only 4 samples were available for analysis, limiting the strength of this observation. SARS-CoV-2 infected patients also showed greater fragmentation compared to healthy subjects. Interestingly, SARS-CoV-2 patients who developed mild symptoms showed a significantly higher degree of global tRNA fragmentation compared to patients who developed severe symptoms (Figure 1B). We speculate that this could reflect the strength of an innate immune response to viral infection, which is known to include secretion of human genome-encoded RNases. In such a narrative, patients with weaker immune responses might secrete less defensive

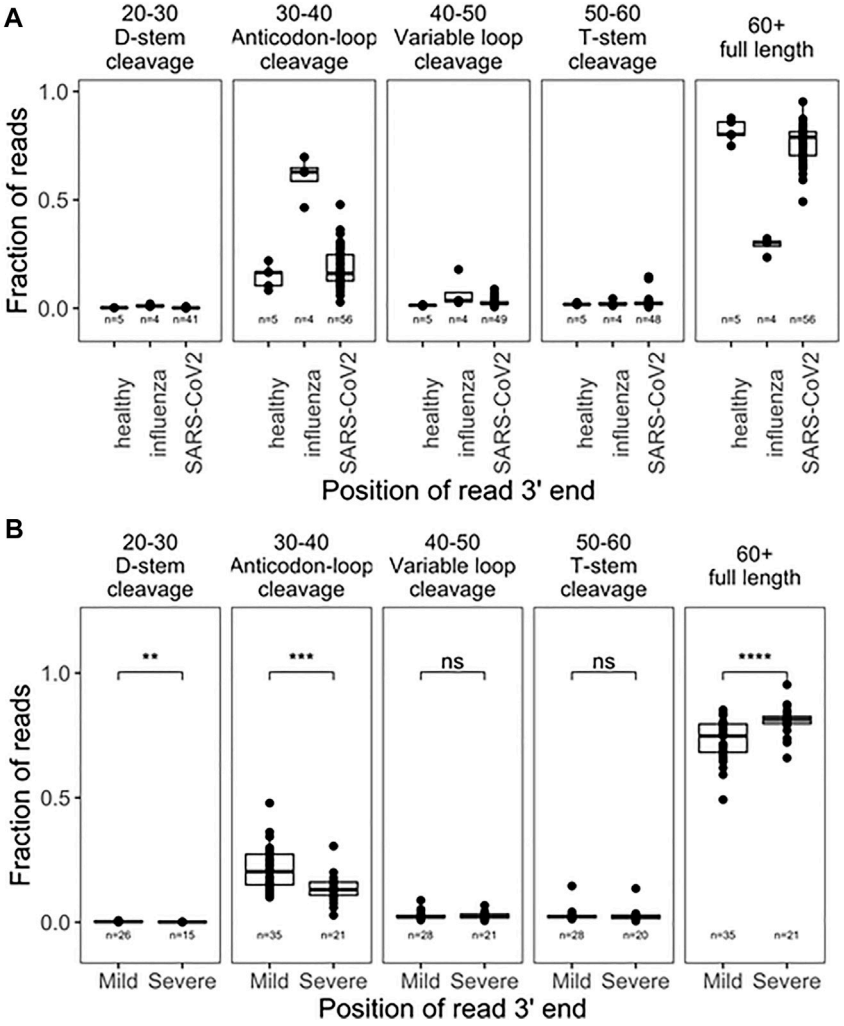


FIGURE 1
Global tRNA fragmentation pattern among nasopharyngeal swab samples. **(A)** Fraction of reads mapped to different tRNA fragments are shown for uninfected control (n = 5), influenza infected (n = 4), and SARS-CoV-2 in fected (n = 56) individuals. All tRNA species are pooied together to reflect global levels of tRNA fragmentation. **(B)** Comparison of global tRNA fragmentation between SARS-CoV-2 infected patients who go on to develope either mild or severe COVID19 symptoms. All tests are two-side-test with the number of samples passing filters indicated on that plot,p-values: *<0.05; **<10^{-2};***<10^{-3};****<10^{-4}.

RNases, experience less tRNA fragmentation, and develop more severe symptoms.

We further analyzed the tRF products of specific tRNAs among all pairwise comparisons of patient groups; samples were filtered for fragments with >10 reads (Figure 2A; Supplementary Table S2). Due to limited cohort sizes, we restricted further analysis to the SARS-CoV-2 positive biospecimen. For this analysis, reads from individual isodecoders were pooled among isoacceptor families. This was done because fragment reads often cannot be distinguished among related isodecoder sequences, since the distinguishing bases were cleaved away. Further, RT-qPCR-base assays that can distinguish closely related isodecoders represent an additional challenge, so pooled analysis may yield more transferable insights. Among tRFs of isoacceptor families, we found statistically significant differences among 20 distinct fragments ($p < 0.05$), including fragments for the anticodon loop, variable loop, and T-stem loop (Supplementary Table S2). Fragments from the anticodon loop tend to be more abundant and thus better candidates for development into prognostic qPCR tests. Top candidates include $tRNA^{Ala}$(AGC), $tRNA^{Arg}$(ACG), $tRNA^{Pro}$(AGG), and $tRNA^{Gln}$(CTG) (Figure 2B). For these tRNA isoacceptors, patients who developed mild COVID-19 symptoms produced more tRFs than patients who developed severe COVID-19 symptoms. Again, these results may potentially be associated with the differential activities of immune response in the

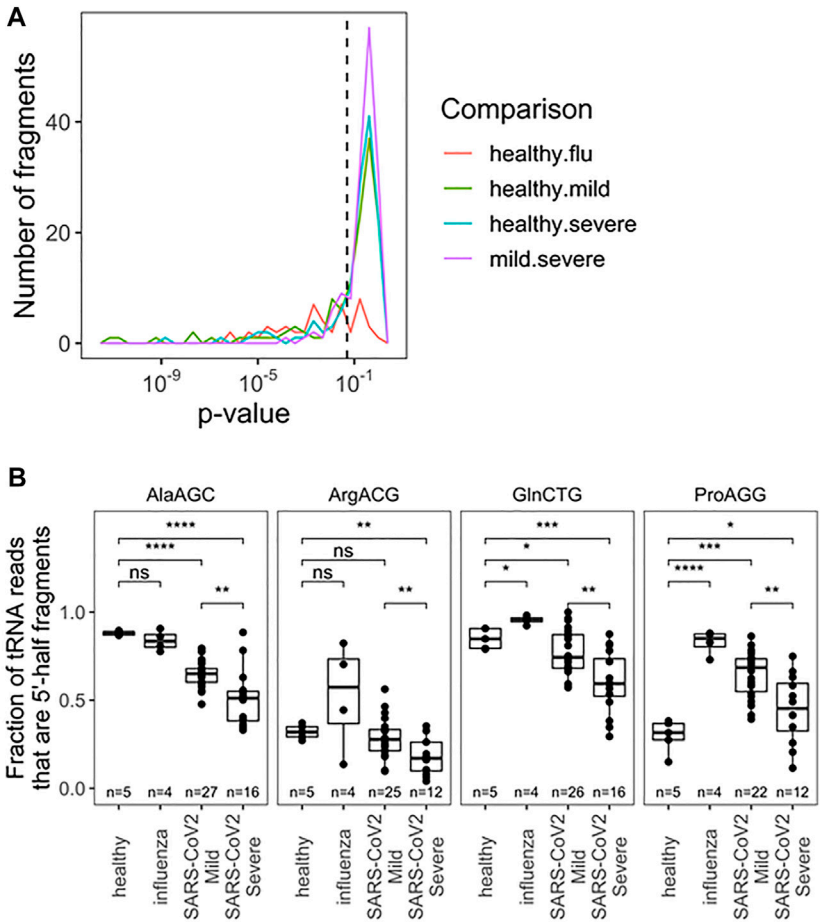


FIGURE 2
Fragmentation profile of specific tRNA Isoacceptor families allows for seperation of RNA obtained from nasophary swabs collected from SARS-CoV-2 infected individuals who developed mild or severe symptoms. **(A)** Uncorrected *p*-Values for pairwise two-sided t-tests indicate several notable differences in fragmentation amoung specific tRNA isoacceptor families. Precise values are indicated in table S2. **(B)** Fragmentation profies for top anticdon-cleaved tRNAs are hightlighted:$tRNA^{Ala}$, $tRNA^{Arg}$(ACG), $tRNA^{pro}$(AGG), and $tRNA^{Gln}$(CTG). In addition to distinguising among SARS-CoV-2 patients, fragmentation can provide diagnostic insight which compared to healthy patients. *p*-values:*<0.05; **$<10^{-2}$;***$<10^{-3}$; ****$<10^{-4}$. Two-side t-tests with the number of samples passing a 10 read fliter indicated in each plot.

nasopharyngeal region, for example, the amount of RNase released upon SARS-CoV-2 infection.

Next, we analyzed the abundance of full-length tRNAs at the isodecoder level. Abundance was measured relative to 5.8S rRNA, a very abundant small rRNA present in all samples; isodecoders were limited to samples with >10 reads. This choice was made with development of scalable prognostics in mind, where normalization must be done verses a specific, measurable RNA species, as opposed to a "reads per million" approach for typical of RNA-seq analysis. The abundance of all tRNA reads, summed together, compared with 5.8S rRNA was different between uninfected, influenza and SARS-CoV-2 infected groups, though not between SARS-CoV-2 patients (Supplementary Figure S1). This may reflect global changes in translation activity within cells or differences in the nature of collected material (e.g., lytic cell debris vs. shed cells). This result also highlights the critical importance of choosing normalization standards. We found significantly different levels of specific tRNA isodecoders in all pairwise comparisons, but restricted our analysis to the two SARS-CoV-2 groups with the most biospecimen and no global differences in total tRNA abundance. Here 53 isodecoders showed significant abundance differences between the mild and severe SARS-CoV-2 groups (Figure 3A; Supplementary Table S3). We highlight three tRNAs that can distinguish between mild and severe SARS-CoV-2 patient groups (Figure 3B): $tRNA^{Ala}$(AGC)c2t3, $tRNA^{Met}$(CAT)c1t32, and $tRNA^{Leu}$(CGG)c1t34. Further, we highlight $tRNA^{Pro}$(CGG)c1t52 which can be used to distinguish SARS-CoV-2 patients from healthy controls. Interestingly $tRNA^{Leu}$(CGG)c1t34 is not well suited as a

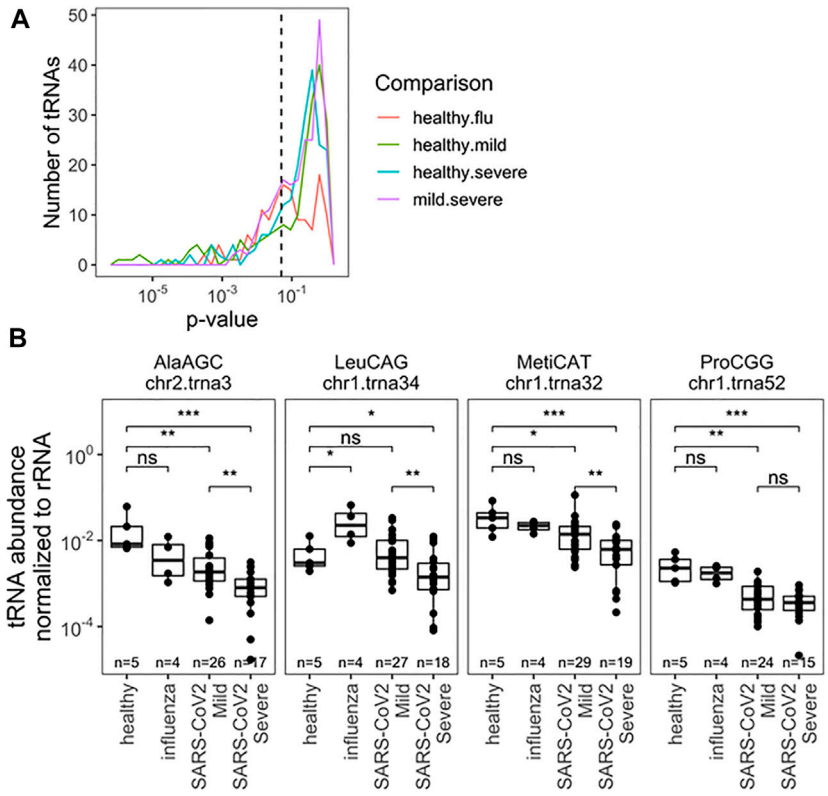


FIGURE 3
Relative abundance of specific tRNA isodecoders to 5.8S rRNA in the same RNA samples allowes for separation by infection status (uninfected, influenza and SARS-CoV-2 infected individuals). **(A)** Uncorreced *p*-Values for pairwise two-sided t-tests indicate several notable differences in rRNA-normalized abundance among specific. tRNA isodecoders. Analysis inciudes all sense-mapped reads for each isodecoders. Precisee values are indicated in Supplementary Table S3. **(B)** rRNA-normalized abundance for notable abundance tRNAs are highlighted tRNA^{Ala}(ACG),c2t3tRNA^{Mct}(CAT), and tRNA^{Leu}(CGG)c1t34. In addition to distinguisting among SARS-Cov-2 patients, normalized abundance of tRNA^{Pro}(CGG)c1t52. amoung others, can provide diagnostic insight which compared to healthy patients.*<0.05; **<10^{-2};***<10^{-3};****<10^{-4}. Two-side *t*-tests with the number of samples passing a 10 read fliter indicated in each plot.

general SARS-CoV-2 marker, despite discriminating between symptom groups, demonstrating a diversity of behaviors. Of note, tRNA^{Met}(CAT)c1t32 is the main initiator tRNA isodecoder in human cells (Chan and Lowe, 2016) and the observed differences in its abundance may reflect the translation activity of the human nasal cells upon SARS-CoV-2 infection.

The final parameter we obtained from our sequencing data was the comparison of tRNA modification levels through RT mutation signatures (Helm and Motorin, 2017). Briefly, certain modifications interfere with reverse transcription during library preparation, leading to enzymatic misincorporation of bases, which is measured as a "mutation" during sequencing. These signatures do not represent DNA-level mutations, but misincorporation by reverse transcriptase. The mutation rate at specific site can be quantitatively compared to access the differences between modification changes between any two samples. This analysis is particularly sensitive to tRNA modifications with the added chemical group at the Watson-Crick face of the nucleobase, for example, N1-methyladenosine [m^{1}A, (Cozen et al., 2015; Clark et al., 2016)] which is among the most widespread human tRNA modification types. Using the differences in mutation fractions, we found specific tRNA modifications that can distinguish all pairwise patient groups (Figure 4A). Analysis was limited to sites with a mutation rate >2% and more than 50 reads to limit spurious differences arising from noise at sites known to be unmodified. Again we restrict our analysis to SARS-CoV-2 patients with a greater number of patients sampled. Together, 33 different modification sites showed significant ability to distinguish patient groups, with examples in the D-loop, anticodon loop, and T-stem loop (Figure 4A; Supplementary Table S4). *A priori*, it is not obvious what effect changes in modification level can have on changes in tRNA biology, including abundance and fragmentation. For example, we previously reported that different modifications can either stimulate or protect from tRNA fragmentation

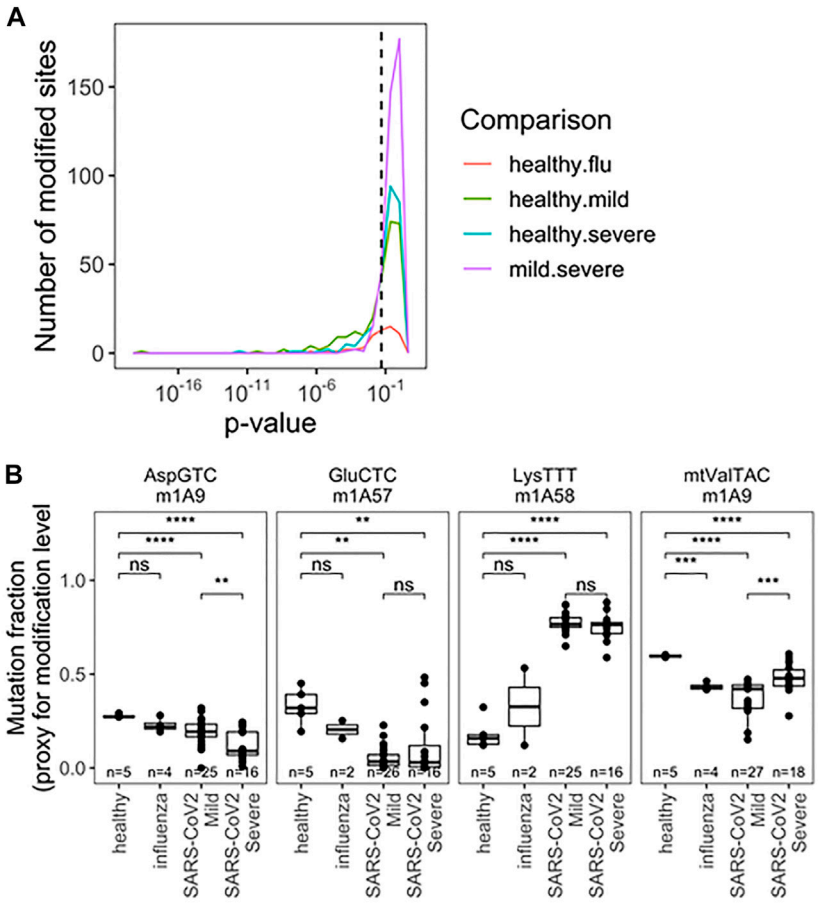


FIGURE 4
Rspecific tRNA modification profile in RNA obtained fromnasopharyngeal swabs allows for seperation of uninfected, influenza and SARS-CoV-2 infected individuals with mild or severe Covid -19 symptoms). **(A)** Uncorreced *p*-Values for pairwise two-sided *t*-tests indicate differences amoung specific tRNA modifications. Modifications are detected as a "muation" derived from reverse transcriptase disincorporation when reading modified bases. Analysis includes sites with >2% mutation rate and >50 mapped reads. Precise values are indicated in table S4. **(B)** Modifications exhibiting notable patterns are highlighted m^1A9 on $tRNA^{Asp}$(GTC), m1A58 on $tRNA^{Glu}$(CTC), m1A58 on $tRNA^{Lys}$(TTT),m^1A9 on mt-$tRNA^{Val}$(TAC). *p*-values.*<0.05; **<10^{-2};***<10^{-3};****<10^{-4}. Two-side *t*-tests with the number of samples passing a 50 read fliter indicated on each plot-the 2% mutation rate filter was relaxed after individual sites were chosen.

(Watkins et al., 2022). Here we observed a variety of behaviors from different modifications relating to SARS-CoV-2 infection (Figure 4B). First, m^1A9 on $tRNA^{Asp}$(GTC) showed progressive reduction of methylation from healthy, to mild symptoms, to severe symptoms patients. Similarly, methylation of m^1A58 on $tRNA^{Glu}$(CTC) was reduced drastically in all SARS-CoV-2 positive biospecimen compared to those from healthy controls. This site is not suitable to distinguish between SARS-CoV-2 severity groups, likely because the methylation levels are already fully reduced. The opposite behavior was observed for $tRNA^{Lys}$(TTT) where methylation at m^1A58 dramatically increased upon SARS-CoV-2 infection, but again, methylation cannot distinguish among SARS-CoV-2 patients. Finally, methylation of m^1A9 of mt-$tRNA^{Val}$(TAC) followed a pattern remittent of fragmentation: methylation was significantly reduced in samples obtained from healthy controls compared to samples from patients with mild COVID-19. This response was further muted in biospecimen from patients with severe COVID-19. Of note, mitochondrial $tRNA^{Val}$ plays a dual role in mitochondrial translation. It not only works as a tRNA in translation but is also an essential component of the human mitochondrial ribosome (Amunts et al., 2015). M^1A9 in mt-$tRNA^{Val}$ may, thus, modulate its activity either as a tRNA and/or its ribosomal function. This could plausibly be related to global changes in translation reflected in Supplementary Figure S1.

Based on the findings described above, we perceive that these tRNA features could be used as biomarkers. Clustering 68 selected tRNA biomarkers from 60 samples show that the two SARS-CoV-2 groups are markedly separated (Supplementary Figure S2). As a consideration for future

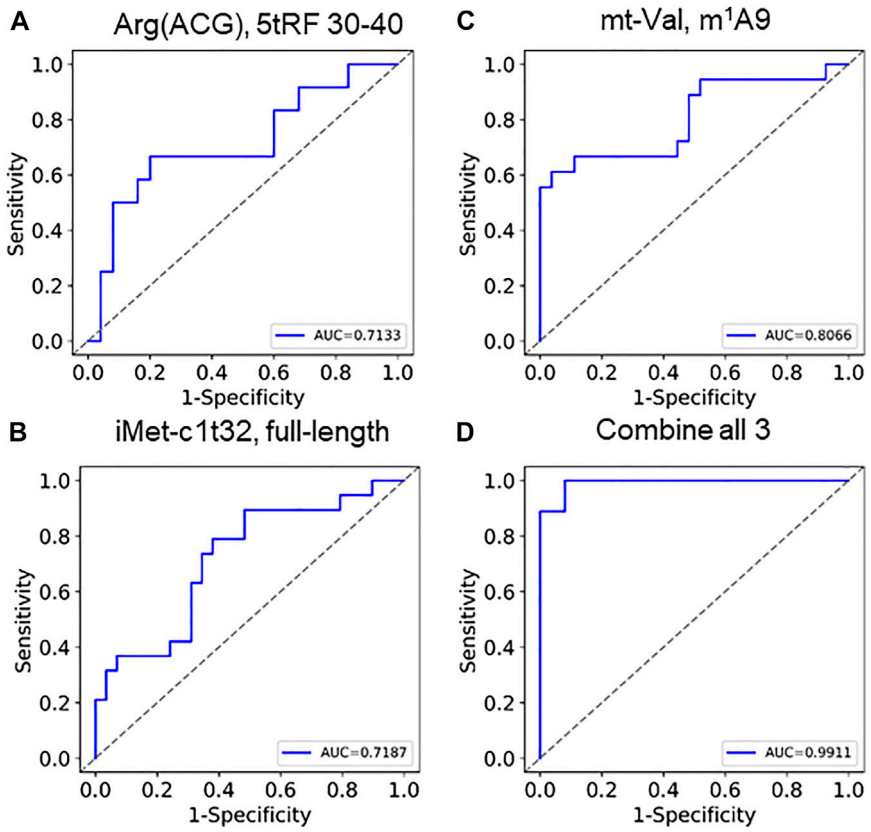


FIGURE 5
ROC curves of using tRNA abundance, modification, and fragmentation as biomarkers Individual curves of **(A)** fragmentation ($tRNA^{Arg}$(ACG),5′tRF), **(B)** abundance ($tRNA_i^{Met}$(CAT)c1t32), **(C)** modification (tmitochondrial $tRNA^{Val}$,m^1A9) show AUC between 0.71 and 0.81. **(D)** Combining these 3 generates an AUC of 0.99.

qPCR type biomarker assays, we selected one specific tRNA for fragmentation, abundance, and modification for statistical calculation of COVID-19 severity (Figures 5A–C; Supplementary Figures S3A–C). Each of the three individual parameters produced an area under curve (AUC) value of 0.71–0.81. We developed a combine metric using a linear combination of individual measurements of tRNA abundance, modification, and fragmentation. Using these three tRNA properties, we obtained an AUC value of 0.99 (Figures 5D, Supplementary Figure S3D), indicating the power of using multiple tRNA properties for accurate prediction of SACS-CoV-2 infection symposium severity.

In summary, we were able to generate good quality tRNA-seq results from residual diagnostic nasopharyngeal biospecimen. tRNA profiles of these RNA samples, taken at the time of initial SARS-CoV-2 diagnosis, may provide new information that can be used to predict COVID-19 symptom severity. These results represent a distinct approach in defining biomarkers of infectious disease severity which may allow for the identification of patients at high risk for complication from respiratory virus infection. Future work will test our hypothesis that these tRNA signatures are related to the nasal innate immune RNase secretions and represent non-genetic factors contributing to viral pathogenesis. Future studies are also needed to independently validate these findings and to develop assays to allow for rapid testing in the setting of clinical applications, free from the cost and time constrains of the sequencing-based approach used here. Notably, developing methods scalable that can distinguish tRNA fragments from intact tRNAs are sorely lacking. The best current approaches require gel-based size selection which is labor and bio-mass intensive, and thus not scalable. Similarly, qPCR methods to measure tRNA modifications with a useful dynamic range will be crucial for this nuanced biology to become clinically impactful. Current tRNA-focused RT-qPCR approaches measure an uninterpretable amalgam of full length tRNA, RT-induced stops, and tRNA fragmentation. Here, we articulate the

value of developing more precise methods for clinical deployment.

Mount Sinai Pathogen Surveillance Program (PSP) study group

Shelcie Fabre, Jose Polanco, Matthew M. Hernandez, Alberto Paniz-Mondolfi.

Data availability statement

The datasets presented in this study can be found in online repositories. The names of the repository/repositories and accession number(s) can be found below: All sequencing data have been deposited to NCBI GEO under the accession GSE208612.

Ethics statement

The studies involving human participants were reviewed and approved by The Mount Sinai Pathogen Surveillance Program. The patients/participants provided their written informed consent to participate in this study.

Author contributions

CK and SH. analyzed sequencing data, CW built sequencing libraries, KL extracted RNA from nasopharyngeal swabs of uninfected people, HA extracted RNA from clinical biospecimen, AG-R and HB maintain the Mount Sinai Pathogen Surveillance Database, AG-R, ES, HB, and VS reviewed the metadata and selected samples for this study, the Mount Sinai PSP study group banked and provided the specimen. CK, VS, and TP conceived the project, designed the experiments, and wrote the manuscript. All authors approved the final version of the manuscript.

Funding

This work was supported by grants from NIAID R21 AI169280 (to TP and VS), Keck Foundation (to TP), NHGRI (RM1HG008935 to TP), and NIAID 75N93021C00014 and HHSN272201400008C (to VS and HB). The Mount Sinai Pathogen Surveillance Program is also supported by institutional funds from the hospital as well as the school.

Conflict of interest

The authors declare that the research was conducted in the absence of any commercial or financial relationships that could be construed as a potential conflict of interest.

Publisher's note

All claims expressed in this article are solely those of the authors and do not necessarily represent those of their affiliated organizations, or those of the publisher, the editors and the reviewers. Any product that may be evaluated in this article, or claim that may be made by its manufacturer, is not guaranteed or endorsed by the publisher.

Supplementary material

The Supplementary Material for this article can be found online at: https://www.frontiersin.org/articles/10.3389/fcell.2022.999351/full#supplementary-material

References

Amunts, A., Brown, A., Toots, J., Scheres, S. H. W., and Ramakrishnan, V. (2015). Ribosome. The structure of the human mitochondrial ribosome. *Science* 348, 95–98. doi:10.1126/science.aaa1193

Anderson, P., and Ivanov, P. (2014). tRNA fragments in human health and disease. *FEBS Lett.* 588, 4297–4304. doi:10.1016/j.febslet.2014.09.001

Begley, U., Dyavaiah, M., Patil, A., Rooney, J. P., DiRenzo, D., Young, C. M., et al. (2007). Trm9-catalyzed tRNA modifications link translation to the DNA damage response. *Mol. Cell* 28, 860–870. doi:10.1016/j.molcel.2007.09.021

Boccaletto, P., Stefaniak, F., Ray, A., Cappannini, A., Mukherjee, S., Purta, E., et al. (2022). Modomics: A database of RNA modification pathways. 2021 update. *Nucleic Acids Res.* 50, D231–D235. doi:10.1093/nar/gkab1083

Chan, P. P., and Lowe, T. M. (2016). GtRNAdb 2.0: An expanded database of transfer RNA genes identified in complete and draft genomes. *Nucleic Acids Res.* 44, D184–D189. doi:10.1093/nar/gkv1309

Clark, W. C., Evans, M. E., Dominissini, D., Zheng, G., and Pan, T. (2016). tRNA base methylation identification and quantification via high-throughput sequencing. *RNA* 22, 1771–1784. doi:10.1261/rna.056531.116

Cozen, A. E., Quartley, E., Holmes, A. D., Hrabeta-Robinson, E., Phizicky, E. M., and Lowe, T. M. (2015). ARM-Seq: AlkB-facilitated RNA methylation sequencing reveals a complex landscape of modified tRNA fragments. *Nat. Methods* 12, 879–884. doi:10.1038/nmeth.3508

Danecek, P., Bonfield, J. K., Liddle, J., Marshall, J., Ohan, V., Pollard, M. O., et al. (2021). Twelve years of SAMtools and BCFtools. *Gigascience* 10, giab008. doi:10.1093/gigascience/giab008

Gonzalez-Reiche, A. S., Hernandez, M. M., Sullivan, M. J., Ciferri, B., Alshammary, H., Obla, A., et al. (2020). Introductions and early spread of SARS-CoV-2 in the New York City area. *Science* 369, 297–301. doi:10.1126/science.abc1917

Gu, C., Begley, T. J., and Dedon, P. C. (2014). tRNA modifications regulate translation during cellular stress. *FEBS Lett.* 588, 4287–4296. doi:10.1016/j.febslet.2014.09.038

Harris, C. R., Millman, K. J., van der Walt, S. J., Gommers, R., Virtanen, P., Cournapeau, D., et al. (2020). Array programming with NumPy. *Nature* 585, 357–362. doi:10.1038/s41586-020-2649-2

Helm, M., and Motorin, Y. (2017). Detecting RNA modifications in the epitranscriptome: Predict and validate. *Nat. Rev. Genet.* 18, 275–291. doi:10.1038/nrg.2016.169

Huang, H. Y., and Hopper, A. K. (2016). Multiple layers of stress-induced regulation in tRNA biology. *Life (Basel)* 6, 16. doi:10.3390/life6020016

Hunter, J. D. (2007). Matplotlib: A 2D graphics environment. *Comput. Sci. Eng.* 9, 90–95. doi:10.1109/mcse.2007.55

Javaid, W., Ehni, J., Gonzalez-Reiche, A. S., Carreno, J. M., Hirsch, E., Tan, J., et al. (2021). Real-time investigation of a large nosocomial influenza A outbreak informed by genomic epidemiology. *Clin. Infect. Dis.* 73, e4375–e4383. doi:10.1093/cid/ciaa1781

Jin, D., and Musier-Forsyth, K. (2019). Role of host tRNAs and aminoacyl-tRNA synthetases in retroviral replication. *J. Biol. Chem.* 294, 5352–5364. doi:10.1074/jbc.REV118.002957

Koczera, P., Martin, L., Marx, G., and Schuerholz, T. (2016). The ribonuclease A superfamily in humans: Canonical RNases as the buttress of innate immunity. *Int. J. Mol. Sci.* 17, 1278. doi:10.3390/ijms17081278

Lowe, T. M., and Chan, P. P. (2016). tRNAscan-SE On-line: integrating search and context for analysis of transfer RNA genes. *Nucleic Acids Res.* 44, W54–W57. doi:10.1093/nar/gkw413

Lu, L., Li, J., Moussaoui, M., and Boix, E. (2018). Immune modulation by human secreted RNases at the extracellular space. *Front. Immunol.* 9, 1012. doi:10.3389/fimmu.2018.01012

McKinney, W. (2010). Data structures for statistical computing in python. *Proc. 9th Python Sci. Conf.* 445, 51–56.

Waskom, M., Botvinnik, O., O'Kane, D., Hobson, P., Lukauskas, S., Gemperline, D. C., et al. (2017). *mwaskom/seaborn: v0.8.1* Zenodo. doi:10.5281/zenodo.883859

Nunes, A., Ribeiro, D. R., Marques, M., Santos, M. A. S., Ribeiro, D., and Soares, A. R. (2020). Emerging roles of tRNAs in RNA virus infections. *Trends biochem. Sci.* 45, 794–805. doi:10.1016/j.tibs.2020.05.007

Oberbauer, V., and Schaefer, M. R. (2018). tRNA-Derived small RNAs: Biogenesis, modification, function and potential impact on human disease development. *Genes (Basel)* 9, 607. doi:10.3390/genes9120607

Pandey, K. K., Madhry, D., Ravi Kumar, Y. S., Malvankar, S., Sapra, L., Srivastava, R. K., et al. (2021). Regulatory roles of tRNA-derived RNA fragments in human pathophysiology. *Mol. Ther. Nucleic Acids* 26, 161–173. doi:10.1016/j.omtn.2021.06.023

Pedregosa, F., Varoquaux, G., Gramfort, A., Michel, V., Thirion, B., Grisel, O., et al. (2011). Scikit-learn: Machine learning in Python. *J. Mach. Learn Res.* 12, 2825–2830.

Schimmel, P. (2018). The emerging complexity of the tRNA world: Mammalian tRNAs beyond protein synthesis. *Nat. Rev. Mol. Cell Biol.* 19, 45–58. doi:10.1038/nrm.2017.77

Watkins, C. P., Zhang, W., Wylder, A. C., Katanski, C. D., and Pan, T. (2022). A multiplex platform for small RNA sequencing elucidates multifaceted tRNA stress response and translational regulation. *Nat. Commun.* 13, 2491. doi:10.1038/s41467-022-30261-3

Zhang, W., Foo, M., Eren, A. M., and Pan, T. (2022). tRNA modification dynamics from individual organisms to metaepitranscriptomics of microbiomes. *Mol. Cell* 82, 891–906. doi:10.1016/j.molcel.2021.12.007

Frontiers in
Cell and Developmental Biology

Explores the fundamental biological processes of life, covering intracellular and extracellular dynamics.

The world's most cited developmental biology journal, advancing our understanding of the fundamental processes of life. It explores a wide spectrum of cell and developmental biology, covering intracellular and extracellular dynamics.

Discover the latest Research Topics

See more →



Frontiers

Avenue du Tribunal-Fédéral 34
1005 Lausanne, Switzerland
frontiersin.org

Contact us

+41 (0)21 510 17 00
frontiersin.org/about/contact